HYDRO POWER

The Design, Use, and Function of Hydromechanical, Hydraulic, and Electrical Equipment

Professor Dr.-Ing. Joachim Raabe

For Bertl

All my thoughts that I have,
they are with you ...
(Old German folk-song)

Prefatory Note

The appearance of this new book is doubly welcome, firstly because, being in English, it is available to a very large number of readers and, secondly, because it is an up to date and largely rewritten account of the subject on which the author has already made an international reputation. Professor *Raabe*'s four previous books on hydraulic machinery and installations published by the VDI-Verlag were available to readers of the German language but are now out of print. Although there has also been a translated Russian version his valuable account of hydroelectric practice have not therefore been easily accessible to the vast number of potential readers familiar with English. This has been particularly unfortunate recently because of the world-wide resurgence of the long established hydro power industry. Because of economic problems caused by rising fuel costs and expendable fossil fuels the interest in hydro power has greatly increased in most countries, not only for large schemes but also for mini and micro installations where power can be used locally for agricultural and industrial use. This new definitive work by Professor *Raabe* will therefore meet with even wider acclaim internationally than his previous publications.

The author is a distinguished hydraulic expert who has travelled widely and lectured in many countries on hydraulic machines and hydro power equipment. He has had extensive industrial, research and academic experience and is well known on international technical committees for his valued contributions. This monograph represents his accumulated wisdom over many years together with accounts of recent researches and advanced course lecture material. The result is a valuable treatise which will help engineers, teachers, advanced students, and many others concerned with the creation and management of hydroelectric installations.

I am most grateful for the opportunity to introduce this comprehensive new book and wish both it and its readers all success in helping to make the world a better place by the skilful application of hydro power.

S. P. Hutton

Preface

Water is one of nature's gifts. The mere chance of creation has made water vapour lighter than the surrounding atmosphere, so that sunshine can raise it from the ocean, while sun-born winds carry it to those regions where it condenses again and then falls down to the earth, from which gravity makes it flow downhill back towards the ocean, thus closing its earthly cycle.

Ancient civilizations were fluvial and their members already managed to lift water for irrigation by machines equipped with pails and driven by water mills of the undershot type.

In 1831 when the French engineer *B. Fourneyron* had already built the first reliable water turbine, the famous German poet *Goethe* finished the second part of his tragedy *Faust*. At death's door *Faust* wins his wager with the devil (to be redeemed if there came a moment of which he could say, "linger you now you are that fair"), when he has the following vision of the harnessing of the tidal powers of the ocean.

"A paradise our closed-in land provides,
Though to its margin rage the blustering tides;
When they eat through, in fierce devouring flood,
All swiftly join to make the dammage good.
Ay, in this thought I pledge my faith unswerving.
Here wisdom speaks its final word and true,
None is of freedom or of life deserving,
Unless he daily conquers it anew.
With dangers thus begirt, defying fears,
Childhood, youth, age shall strive through strenuous years.
Such busy, teeming throngs I long to see,
Standing on freedom's soil, a people free.
Then to the moment could I say:
Linger you now, you are that fair!"

The hard *Stachanovite* hand labour of *Goethe*'s vision of liberty would today be thought of as an unbelievable slavery in the face of a graceless nature to which men were delivered up when they had not the powerful tools of today's electrotechnology.

The inventions of engineers in the last century and a half since the death of our famous *Goethe* are the main factors which have relieved the average man from laborious slave-like work.

This has been done by harnessing the energy resources offered by nature in the form of fuel and, last but not least, in the form of hydro power. Even if hydro power covers at present in West Germany only a modest portion of the electric energy demand, hydro-electricity has made in our country, and especially in its more waterpower blessed southern part, a decisive contribution to the momentum that electrification brought into our daily economical life during the last century.

To understand this manifestation, a glance at the historical development of electrification should be made. Two key events have stimulated the consumption and production of electricity.

One was the invention of the self-exciting dynamo (1869) by *W. von Siemens* in Berlin and the induction motor by *M. von Dolivo Dobrovolsky* in 1890 also in Berlin. The other was the invention of the light bulb by the German-American *Göbel* 1859 in New York. *Edison* made the vital contribution of reinventing this 25 years later and illuminating a quarter of New York by these means with the aid of the first thermo-electric power plant erected 1882 in New York.

With the invention of electric illumination a large consumer market was stimulated to install electricity in homes. These consumers were concentrated in big towns whereas the usable waterpower was in far remote areas. Therefore power transmission of hydro power from sites to the consumer became an urgent need.

In 1891 the crucial step forward was made by the Germans *O. von Miller*, the promoter, and *M. von Dolivo Dobrovolsky*, the constructor, by the transmission of 300 hp over 175 km between Heilbronn and Frankfurt using a 15 000 Volt three phase AC power line. After this breakthrough experiment, which was successful, the USA started with the erection of the first huge power station on the Niagara Falls with 10 · 5000 hp in 1892. Another advance for harnessing waterpower was achieved by the German professor *Fink* in Berlin, who obtained a patent on adjustable wicket gates. In 1873 the German manu-facturer *Voith* equipped for the first time a Francis turbine with these gates. Only this combination made the Francis turbine an effective tool for harnessing waterpower.

The way was shown for the development of low head river power plants by the patent of the German-Austrian *V. Kaplan* in 1913 for axial turbines with adjustable runner vanes. To harness river power of the lowest head, the German *A. Fischer* together with the Escher Wyss firm have built, since 1936, tubular turbines with rim generators after Harza's patent from 1919, and the first bulb turbine. In the compact design of a rim generator plant, all the components have to be adapted to each other with respect to their purpose and the small space available. In this context the pioneer work of the German *H. Fentzloff* must be mentioned. Pumped storage plants have been developed by the Swiss firm Sulzer and Escher Wyss and the German firm Voith since the turn of the century, culminating in 1928 in the Herdecke plant with 4 · 27 MW tandem sets. In 1932 and 1936 Escher Wyss and Voith built the first axial and radial pump turbines in the German Baldeney plant and the Brazilian Pedreira plant.

Recent corner stones in the West German development of hydro power are as follows. Firstly the African plant Cabora Bassa in Mozambique: There 5 · 415 MW were installed for power transmission over 1400 km by 1 million volt DC using dry thyristor technique; the turbines were manufactured by a consortium of the West German firm Voith and the French firm Neyrpic.

Both firms are now erecting the turbines for the 18 · 715 MW Francis turbine sets of Itaipú in Brazil, at the moment the hydro power station with the largest installed capacity. In this context it may also be mentioned, that the West German firm Ossberger has logically developed from the Michell type turbine the most reliable and simple small turbine of the Ossberger type, especially for developing countries.

Camerer, the founder of the author's institute, formulated in 1905 the specific speed as the generally adopted most important criterion to distinguish types of hydroturbines. In 1922 my predecessor *Thoma* introduced the now internationally used cavitation index σ.

X

In the past decade I have had the privilege of holding lecture courses on hydro power for advanced post-graduate students in the following centres of recent water power development: The Indian Institute of Technology Madras, India; The University of São Paulo, Brazil; The Laval University, Quebec and Hydro Quebec, Montreal, Canada: The Central University Caracas, Venezuela; The Polytechnic Institute Timisoara, Rumania; The Huazhong Institute of Technology, Wuhan, People's Republic of China.

This has stimulated me to publish this book, which can be considered as the outcome of these lectures, some rewritten chapters of a former book of mine in German, and the many papers and findings made over the past 15 years in the Teaching Chair and Laboratory headed by me at The Technical University of Munich, Federal Republic of Germany.

In this context the names of Dr.-Ing. *W. Kühnel*, Dr.-Ing. *D. Castorph*, Dr.-Ing. *E. Bär*, Dr.-Ing. *M. Vötter*, Dr.-Ing. *G. Schlemmer*, Dr.-Ing. *G. Mollenkopf*, Dr.-Ing. *R. Gerich*, Dr.-Ing. *M. Lotz* (deceased), Dr.-Ing. *R. Kirmse*, Dr.-Ing. *J. Korcian*, Dr.-Ing. *N. Furtner*, Prof. Dr.-Ing. *R. Jahn*, Dr.-Ing. *E. Hartner*, Dipl.-Ing. *H. Pfoertner*, Dr.-Ing. *E. Walter*, Dr.-Ing. *J. Klein*, Prof. Dr.-Ing. *F. El Reffaie*, Professor Dr. *Engng Ravindran*, and Mr. *D. Lauria* may be mentioned for their valuable help, their suggestions, and contributions in connection with scientific papers presented at international or national congresses, or in connection with work for theses made at the Lehrstuhl und Laboratorium für Hydraulische Maschinen und Anlagen der Technischen Hochschule München.

For many neatly drawn figures my thanks are due to Mr. *M. Ring*. In connection with the erection of reliable test stands but mainly for his valuable contribution of building quick response vector probes, the name of Mr. *H. Kriegl*, head of our lab's workshop should be mentioned.

Many firms have supported the publication of this book monetarily in a liberal manner. They are

> Allis Chalmers, Milwaukee, Wisconsin, USA
> Ing.-Büro Freisl, Garmisch-Partenkirchen, F. R. Germany
> Hydroart, Milano, Italy
> KaMeWa, Kristineham, Sweden
> Kvaerner Brugg, A. S., Oslo, Norway
> Neyrpic, Grenoble, France
> Ossberger, Weissenburg, F. R. Germany
> Sulzer Escher Wyss, Zürich, Switzerland
> Tampella, Tampere, Finland
> Vevey-Charmilles Engineering Works, Vevey, Switzerland
> Voest Alpine, Linz, Austria
> Zahnradfabrik Friedrichshafen, Friedrichshafen, F. R. Germany

The library of the Technical University Munich an organization of the Bavarian State Ministry of Education and Kultus headed by Dr. *Schweigler* contributed in a similar manner.

Moreover thanks should be given to the VDI-Verlag as the publisher, who undertook the venture of publishing a book directed to all the specialists and students in the world engaged in the development of hydro power.

The work would not have been succeeded if Mr. *T. B. Ferguson*, Senior Lecturer at the Department of Mechanical Engineering of the University of Sheffield, a well-known author of a book on turbomachinery, versed in treating technical terms and also versed

XI

This book may show how scientific work can bridge the frontiers between countries of different cultures. May Hydro Power, which to date is used only by about ten percent of its potential, flourish also in future under the motto: vivat, floreat, crescat!

Munich, autumn 1984   *Joachim Raabe*

XII

Hints to the reader

In decimal fractions, the decimal point is replaced by a comma, e.g., 8,6 is used instead of the Anglo American 8 · 6.

In products, multiplication mark ' × ' is replaced by a point e.g., 8 · 23 is used instead of the Anglo American 8 × 23. The multiplication mark ' × ' is reserved for vector products $a \times b$, b) multipliers that extend over one line, c) output of 3 equal sets thus $P = 3 \times 30$ MW occasionally used.

Abbreviations: Machines types are usually abbreviated as follows: Kaplan turbine = KT (plural KTs), Francis turbine = FT, Pelton (impulse) turbine = PT, pump-turbine = PuT, tubular turbine = TT, bulb turbine = BT, pump = P, Straflo turbine = ST.

The vorticity rot c is denoted by curl c.

The inverse functions of sin x, cos x, tan x, cotan x are denoted by arcsin x, arccos x, arctan x, arccotan x, instead of $\sin^{-1} x$, $\cos^{-1} x$, $\tan^{-1} x$, $\cotan^{-1} x$.

How to use the references in the text: All references within the text are put in square brackets and can be found in a reference list at the end of the last chapter. There they are arranged by chapters and within the chapters in the sequence they are quoted in the respective chapters. The first number points to the chapter, the second number to the reference. For example [9.18] quotes reference 18 in chapter 9. More references can be quoted by [9.18; 9.19], [9.18 to 9.30] or [8.5; 9.18]. References which are not quoted in the book are found in the second list of reference at the end of the book, arranged in alphabetical order of the author's names. At its end, the latter is supplemented by same references, that came out during the production of this book.

Equations are quoted by numbers put in round brackets and placed behind the number of the subchapter in which the equation appears, e.g. (10.2−4) refers to equation 4 in subchapter 10.2.

Hints at subchapters are quoted by cap, and the number of the subchapter behind it, e.g. cap. 9.3.1 hints at subchapter 9.3.1.

The figures are numbered through consecutively, subchapter by subchapter, the number of which precedes that of the figure, e.g. Fig. 9.2.1 hints at figure 1 in the subchapter 9.2.

Contents

XVI

XX

XXII

XXVI

Nomenclature

a) Roman letters

a celerity ($=$ velocity of sound); thermal diffusivity; distance, distance between adjacent towers; direction from shroud to hub along the rotor vane, and along lines of approximately constant moment of momentum.

a' projection of the a-line in the meridian
revenue factor.

a^x capital recovery factor $= 1/\alpha$.

A constant, e.g., due to the bound vortex distribution γ_A
surface area, cross sectional area.

A_{re} real wetted cross sectional area of channel.

A_s cross sectional area of a rotor vane's intersection with an axisymmetric flow plane.

A_s' projection of A_s onto a plane normal to the rotor axis.

AC   alternating current.

A cost term due to dam section (4.3–16).

b width (i.e. of river valley); span (width) of a blade (vane); depth of flow layer or elementary turbine; minimum distance of conductor from ground; acceleration; rotor breadth.

Δb axial thickness of shroud and crown (hub) at external diameter.

b_P length of power house normal to flow direction.

b_s width of excavated ground volume per set.

B barometric head H_A-critical head h_{cr} (due to cavitation);
constant, i.e. due to the bound vortex distribution γ_B.

c absolute velocity; specific heat.

c_m meridional component of c.

c_u whirl component of c.

c_a axial component of c.

C constant, due to the bound vortex distribution γ_C; gas concentration of solved gas (kg/m^3), iron utilization factor of alternator (Esson number).

d damping coefficient; diameter of pipe; diameter of conductor
diameter.

d_0 jet diameter (impulse turbine).

d_e depth of excavated ground volume.

d_R original depth of river bed below minimum tailwater level.

D Nominal rotor diameter (reaction machines: outmost diameter of rotor passage; impulse turbines: jet circle diameter); mass diffusivity; diameter of vortex tube.

$D_{op\,\eta}$ optimum diameter D with respect to efficiency of axial turbine.

$D_{op\,NPSH}$ optimum diameter D with respect to $NPSH$ of axial turbine.

$D_{1aop\eta}$ optimum diameter of rotor eye (throat diameter) D_{1a} with respect to efficiency at semiaxial or radial pump-turbine.

$D_{1aopNPSH}$ optimum diameter of rotor eye (throat diameter) D_{1a} with respect to NPSH at semiaxial or radial pump-turbine.

DC direct current.

e internal energy; distance from neutral axis in a certain cross sectional area.

E Young's modulus (modulus of elasticity), internal effective voltage of alternator; cost factor due to excavation (4.3–12).

$E(\pi/2, k)$ complete elliptic integral of the first order

E_L bulk modulus.

$\dot{E}$ energy flux.

Eu Euler (pressure) number.

f deflection of the shaft centre line; line frequency; spacing of opposite rotor shroud (hub) and casing wall.

f_x, f_y influence functions of velocity induced by a whirl row.

$F(\pi/2, k)$ complete elliptic integral of the second order.

Fr Froude number.

g acceleration due to gravity; total pressure.

G cost term due to dam section (4.3–17).

h altitude; vane thickness; elementary length along the contour of a profile; order of harmonics; number of days per year; $= \Delta H/H$ nondimensional small fluctuations of pressure head.

h' nondimensional loss.

h_s suction head.

h_i insulator length.

Δh drop in river level; backwater effect.

H head; delivery head.

i imaginary unit; enthalpy; number of sets; number of wheels; number of stages; runaway speed to rated speed ratio.

I investment; electric (effective) current; cost due to fabrication and assembly of sets (4.3–18); elliptic integrals.

j imaginary unit.

J moment of inertia due to cross sectional area; cost factor due to cash value of loss during useful life (4.3–22).

k design bound stress concentration factor (11.4–12).

k_1 critical to undisturbed speed ratio; design bound parameter due to start up time of set (11.4–15); excavated width per set to diameter D ratio.

k_s streamwise excavated length to diameter D ratio.

k_{s1} cost factor due to accessories of one set.

k_P cost per unit volume of power house superstructure.

k_{ex} cost per unit volume of excavation.

k_e electricity rate.

k_R roughness.

k_i cost factor; gas constant.

K $= a c_N/(gH)$ penstock parameter due to water hammer, cost term.

K_D cost of dam.

K_{Qn} $= (n_N/Q_{11})(\partial Q_{11}/\partial n)_m$ for turbine.

2

K_{Qm}	$= (m_M/Q_{11})\,(\partial Q_{11}/\partial m)_n$ for turbine.
$K_{\eta n}$	$= (n_N/\eta)\,(\partial\eta/\partial n)_m$ for turbine.
$K_{\eta m}$	$= (m_M/\eta)\,(\partial\eta/\partial m)_n$ for turbine.
K_e	$= 1 + u + K_{\eta n} + K_{Qn}$ self regulation parameter of grid and turbine.
Kc_i	$= c_i/\sqrt{2gH}$ velocity coefficient, by which velocity c_i is referred to the spouting velocity under the head.

l	lever of force; distance of critical point from stagnation point.
L	chord length; pipe length; conductor length; streamwise length of excavation; loss parameter (4.3–21).

m	mass; dimensionless deviation of servomotor piston $\Delta m/m_M$; Poisson's ratio (0,3).
m_M	servomotor-piston stroke.
M	torque; moment.
M_1, M_c	scale of length and velocity under conformal mapping.

n, n'	rotational speed (rpm) or (rps); integer number; exponent of cost term; direction normal to meridional streamline in the meridian; direction normal to arbitrary surface, polytropic exponent.
n'_q	nondimensional specific speed (type number) $= \omega Q^{1/2}(gH)^{-3/4}$.
n_s	specific speed $= n(\text{rpm})\,P(\text{kW})^{1/2}\,H(\text{m})^{-5/4}$.
n_q	specific speed $= n(\text{rpm})\,Q(\text{m}^3/\text{s})^{1/2}\,H(\text{m})^{-3/4}$.
$n'_{q\,\eta\,NPSH}$	best type number of axial turbine or semiaxial pump-turbine $NPSH$.
n_{11}	unit speed $n(\text{rpm})\,D(\text{m})\,H(\text{m})^{-1/2}$.
N, N_1	hub to tip ratio in axial turbines or in the throat of semi axial machine.
$NPSH$	net positive suction head.

p	pressure; interest rate.
p_A	atmospheric pressure.
p_i	impact pressure due to bubble implosion.
p_P	number of pole pairs.
P	power (input, output).
P_i	internal output (input).
P_u	peripheral output (input).
P_{sh}	shaft output (input).
P_b, P_n	gross output, net input ϱQgH.

q	interest factor $1 + p$; dimensionless flow fluctuation $\Delta Q/Q_N$; flow ratio of pump turbine $= Q_P/Q_T$; Weinig factor $(\pi/2)\,(L/t)\,\varkappa\,\sin\beta_0$.
Q	flow (discharge).
Q_{op}	flow at bep.
Q_{11}	unit flow $Q(\text{m}^3/\text{s})\,D(\text{m})^{-2}\,H(\text{m})^{-1/2}$.

r	radius, distance from axis.
R	bubble radius; distance between space points; ohmic resistance radius of curvature of meridional streamline.
R_t	radius of curvature of streamline in an axisymmetric stream plane.
Re	Reynolds number.

s	streamwise length; pipe wall thickness; entropy.
S	surplus; cost factor due to fabrication and erection of set (4.3–19).
Sr	Strouhal number.

3

t	time elapsed; time period; pitch; depth of flow layer (7.3–71).
T	peak load period (4.5–11); absolute temperature.
T_l	travel time of pressure pulse along penstock.
T_r	reflection time of pressure pulse in penstock.
T_i	reset (isodrome) time of governor.
T_b	rate (acceleration) time of governor.
T_a	start up time of sets.
T_{sp}	start up time of penstock.
T_0	opening time of distributor.
T_s	closing time of distributor.
u	$= r\omega$ blade speed; voltage drop along a line $\Delta U/U$; exponent of generator torque due to certain kinds of grid load (11.3–7); blade speed at rotor diameter D.
U	voltage; voltage at generator terminals (effective v.).
U_0	undisturbed velocity outside of wake.
U_{re}	wetted circumference of real channel.
v	specific volume; velocity component normal to wall.
v_{ax}	particle velocity normal to fringes due to laser measurement.
V	volume.
V_t	volume due to seepage, evaporation, precipitation.
ΔV	live storage volume.
w	relative velocity (in the rotating frame of reference); velocity component in secondary flow direction; weight of conductor.
w_h	velocity induced by the deficit of relative eddy within the interior of the vane of a mixed flow rotor.
W	internal friction; annual work; sectional modulus.
x	coordinate in main flow direction; unknown variable; coordinate in the direction of the undisturbed velocity from the midchord; dummy variable; nondimensional speed deviation $\Delta n/n_M$; meridional coordinate.
x'	coordinate of point considered.
X	meridional coordinate in axisymmetric flow plane.
y	coordinate normal to wall; coordinate in peripheral direction of cascade; coordinate normal to undisturbed flow; sagging coordinate of high voltage transmission line.
y_0	length of critical zone referred to l.
Y	specific head (delivery head) gH.
Y_a	mechanical flow energy per unit mass $= p/\varrho + c^2/2 + gh$.
Y_r	mechanical rothalpy per unit mass $= p/\varrho + w^2/2 - u^2/2 + gh$.
z	coordinate in the direction of secondary flow; coordinate in the direction of rotor axis; number of years of useful life (depreciation), Gaussian complex coordinate of point considered on the contour of profile, at which the kinematic boundary condition is satisfied; vane number; number of stages in a labyrinth.

4

b) Greek letters

α acute angle between absolute velocity and periphery; interest factor during useful life $[(1 + p)^z - 1]/[p(1 + p)^z]$; stagger angle of cascade $= \pi/2 - \beta$; heat transfer coefficient.

α' guide vane (gate) position angle.

β acute angle between relative velocity and circumference.

β' acute angle between pattern making vane section and circumference.

β_∞ acute angle between undisturbed flow and circumference.

β_0 acute angle between zero lift direction and circumference.

γ longitudinal dihedral angle of vane; strength of bound vortex, continuously distributed along the contour of the profile, and referred to unit length of contour.

Γ circulation around a profile or a vortex tube; cost ratio $\Delta K_T/K_P$ due to pumping of tidal power plant (10.2–34).

δ angle of attack between chord and undisturbed flow; boundary layer thickness; parameter of rotor diameter (4.4–3).

δ_0 physical angle of attack between zero lift direction and undisturbed velocity.

$\delta(F_A = 0)$ zero angle of attack between chord and zero lift direction.

δ_i boundary layer parameter.

δ_P permanent speed droop, proportional band.

δ_T temporary speed droop, transient proportional band.

Δ difference; Laplace operator.

ε angle of glide; angle between resultant velocity close to the wall and main flow direction in consequence of secondary flow; liquid property during cavitation $1 - \varrho_v/\varrho_L$; orientation angle of a vortex tube within a duct (7.2–9).

ζ complex contour coordinate.

ζ_i loss coefficient due to i; lift coefficient ($i = A$).

η efficiency; dynamic viscosity; dummy variable in y direction.

η_i internal efficiency.

η_u circumferential (peripheral) efficiency.

η_{sh} shaft (coupling) efficiency.

η_s draft tube (diffuser) efficiency.

ϑ angle of a' line and radius in the meridian.

ϑ_i angle between skeleton and chord at Birnbaum point x_i.

ϑ_{11} momentum thickness of the boundary layer.

Θ angle of radial vane section to radius; rotor's moment of inertia.

$\varkappa$ isentropic coefficient $= c_p/c_v$ (c_p and c_v being the specific heats at constant pressure and volume respectively); cascade coefficient $= |\zeta_{AG}/\zeta_{AE}|_{\delta_{UG} = \delta_{OE}}$; speed ratio: n_P/n_T of pump-turbine with pole changing alternator.

λ pressure number of critical point.

λ_L wave length of laser beam.

Λ latent heat; breaking length.

μ angle of meridional streamline to radius; exponent of (8.2–4).

ν kinematic viscosity; angle of a-direction to circumference.

$\Delta\nu$ frequency of scattered light of laser beam.

ξ	dummy variable in x-direction.
Π	Coles' wake function.
ϱ, ϱ_i	density of water, density of material or medium i.
ϱ^0	specific resistance of conductor.
σ	surface tension in liquid-gas interface; cavitation index.
σ_{ad}	admissible tensile stress.
σ_{ij}	stress in plane with normal in i-direction, acting in j-direction.
Σ	sum.
τ	time period, shear stress.
φ	azimuth; flow coefficient $= c_m/r\omega$; load factor of plant.
$\cos\varphi$	power factor.
Φ	contraction coefficient; potential; excavated cross section of penstock to unobstructed section; $= \psi k_1 k_3$ (see excavation).
χ	head ratio H_p/H_T; angle of a to n-direction; rotor parameter (4.4–8).
ψ	pressure coefficient $= 2gH/u^2$; streamfunction; excavation depth parameter.
ω	angular velocity.
Ω	form parameter of rotor (10.4–13) or (4.4–5).
Ω_i	vorticity in i-direction.

Subscripts

1	low pressure edge of rotor vane.
2	high pressure edge of rotor vane.
3	low pressure edge of diffuser (guide) vane.
1/1	full load.
$+(-)$	on positive (negative) characteristic in the $x(t)$ plane for an observer, moving with $a + c(-a+c)$ in x-direction.
A	lift; due to bound vortex distribution γ_A.
a	active cascade; axial direction; external; alternator.
ad	admissible value.
b	admissible variable depth of flow layer; bending.
B	admissible bound vortex density γ_B.
C	admissible bound vortex density γ_C.
cr	critical (cavitation); critical (speed).
D	diffuser, drag.
Dm	diffuser, meridional velocity.
Du	diffuser, whirl velocity.
Df	disk friction.
e	relating to electricity rate.
ex	relating to excavation.
E	relating to single profile.
G	relating to profile in cascade.
g	gas.
h	hydraulic; relating to diffuser, rotor, guide apparatus and suction pipe.
in	inlet.

6

i	internal; instantaneous; due to Birnbaum point P_i.
l	loss.
M	mean value; channel centre line.
m	mixed; meridional.
min	minimum.
max	maximum.
n	nozzle.
N	nominal value.
op	best point (bep).
out	outlet.
P	point P on contour; pumping; pressure face; power house; permanent.
p	pipe; passive cascade.
pl	plate.
Q	volumetric loss (leakage).
r	rated; radial; roughness.
res	resulting.
ra	runaway.
R	rotor; residual cascade.
S	rotor blade; suction face; saturation point.
s	draft tube; streamwise direction; longitudinal.
st	stagnation point.
sh	shaft.
u	circumferential.
v	loss, vapour.
w	windage; wheel.
x, y, z	in x, y, z-direction, respectively.

Other symbols

$\mathbf{n}$	vector in n direction.
$\mathbf{n}^0$	unit vector.
$\bar{c}$	time-averaged velocity c.
c'	velocity fluctuation.
h'	nondimensional value of h.
$\dot{R}$	time derivative of R.
Δ	deviation; Laplace operator.

1. The origin of hydro power, its potential and its use in a world wide context

1.1. Introduction

The main sources of hydro power are the large river systems of the world with their vast catchment areas. A survey of the characteristic features of some river systems shows that the usable potential increases more with the catchment area than with the mean altitude of the system. The usable potential is usually greater in the downstream areas than in the upstream ones. In general the potential does not only depend on such obvious figures as the total river length or the discharge at the river mouth.

The topography of the continents together with the climate and the rainfall rate may favour the damming of a river even of low gradient provided the valley has a sufficient depth. This and the collection of water creates head and discharge as the basic requirements of hydro power. The theoretical potential of the world can be predicted from hydrographs, precipitation and the gradient of the river. It is always related to the usable potential. This depends on the theoretical potential and results from the technical possibilities available, from the feasibility of electric power transmission over a long distance and from the power demand in the neighbourhood of a certain scheme. Any development requires a usable potential, a certain demand for power and a reasonable electricity rate due to hydro power. Therefore the usable potential has to be considered in the context of the total power production at least of the total electricity production in the area of a certain site. For these reasons the harnessable potential of the river power does not only change with the system of rivers and their topography, but differs also from one country to another depending on their economies. When compared with other sources of primary energy it has its merits, e.g., its regeneration and availability for nearly nothing in addition to the absence of pollution. It can be generated by run-of-river, storage, diversion, depression and tidal power plants. It may easily be stored by damming and pumping to cover peak load economically and with flexibility.

1.2. Water from rivers, its causes and features

1.2.1. The rivers

1.2.1.1. Large sources of water power

Mountain regions are more gifted with water power than the plains. They usually combine the advantages of water courses and inclined surfaces and are therefore important as prerequisites of water power. However because of their larger surface area the plains may surpass mountain regions in their energy potential. Hence the biggest supplies

of "white coal" are obtained from the large rivers of the plains and not from mountain torrents, e.g., the catchment area of the river Paraná at Itaipú at its exit from Brazil is four times the surface area of West Germany, see [1.1].

1.2.1.2. Characteristics and classification of well-known rivers

Some features of the largest rivers are tabulated in Tab. 1.2.1. Whereas Tab. 1.2.2 is for rivers of large hydroelectric potential. Here the harnessable potential after Cotillon [1.1] is subdivided into 1) already harnessed 2) in construction and 3) to be harnessed.

The harnessed potential of the Columbia river in the USA is actually the greatest of all and it may keep this position for a considerable period. The additional schemes under construction, possible by the regulation of the Columbia by new Canadian catchment areas will increase its annual output to 92 TWh. According to Cotillon [1.1] the Paraná will precede this figure with 96 TWh, when the power schemes of Yacyreta Apipe and Itaipú are inaugurated between 1980 and 1990 [1.2].

The harnessable potential of a river depends not only on its discharge, and the slope of its bed, but also on the topography of the river, because without any slopes adjacent to

Table 1.2.1. Classification of large rivers.
From Cotillon [1.1].

Continent	river	Catchment area		Average discharge*)		Length	
		10^3 km^2	rank	m^3/s	rank	km	rank
Europe	Volga	1385	12	8000	19	3701	15
North-america	Mississippi	3222	3	18000	6	4200	11
	Mackenzie	1805	11	7200	21	4600	7
	St. Lawrence	1030	19	10300	16	3800	14
South america	Amazon	6150	1	185000	1	7025	1
	Paraná	2343	8	16000	8	3300	18
	Orinoco	1085	15	31000	4	2062	47
	Tocantins	840	23	9500	17	2698	30
Africa	Zaire (Congo)	3800	2	42000	2	4667	5
	Nile	3000	4	2500	41	6607	2
	Zambezi	1330	13	3500	34	2660	31
	Niger	1100	14	7000	22	4184	12
Asia	Yenissei	2600	5	17400	7	4506	9
	Ob	2485	6	12500	13	5150	3
	Lena	2245	7	15500	10	4506	8
	Yangtse	1960	9	34500	3	4989	4
	Amoor	1845	10	11000	15	4667	6
	Ganga	1075	16	14000	11	2478	36
	Sikiang	435	40	12000	14	2655	33
	Brahmaputra**)	632	32	19000	5	2704	28
	Mekong	795	27	15500	9	4023	13
	Irrawadi	430	41	13300	13	2012	48
	Hwang Ho	800	26	1600	53	4345	10

*) At river mouth
**) Chinese: Yarlung Zangbu Jiang

Table 1.2.2. Some river courses with large hydro potential.
From [1.1].

River	Potential in TWh				m³/s Average mouth discharge
	Used in 1977	Under erection in 1977	Rest to be used	Total usable	
Zaire	2,4	9,6	700	700	42 000
Yangtse				< 500	35 000
Orinoco				?	31 000
Brahmaputra*)				500?	19 000
Paraná	21	75	78	174	16 000 (73 000 crest)
Yenissei	20	25	95	140	17 400
Zambezi	24	0	106	130	3 500
Columbia	83	3,5	5,5	92	7 500
Angara	26	42	16	84	3 600
La Grande	0	68	0	68	3 500
Tocantins	0	21,5		64	9 200
São Francisco	13	12	37	62	3 000 (100 000 crest)
St. Lawrence	52	0	6	58	10 300
Churchill	34	12	0	46	1 600
Danube	19,3	9,75	14	43	6 400
Volga	30	?	10?	40	8 000
Rhine	14,7	0,008	0,8	15,5	2 200

*) Chinese: Yarlung Zangbu Jiang

the river banks any construction of a dam as a prerequisite for the exploitation of hydro power founders. Therefore the Amazon and the Mississippi have only a small harnessable potential. Any damming of the latter would lead to a considerable inundation along the river banks submerging much densely populated or arable land; see Garstka [1.3].

In the case of the Amazon, which has a drop of only 60 m in level during the long course of 3000 km from its mouth to Manaus, an inundation of the virgin woods along its valley would deprive the world of one of its main sources of oxygen.

Contrary to this the southern tributaries of the Amazon offer great possibilities for better use: The Tocantin, the Xaigu, the Tapajos and the Madeira being the large energy-ful arteries of to-morrow.

A similar situation exists with the first rivers of China. The Yarlung Zangbu Kiang (the Brahmaputra in India) with its estimated total harnessable potential of about 500 TWh, is too far from the next Chinese consumer centre, and moreover its decisive reach is also claimed by India. Information about China's hydro development are given by Cao Weigong [1.4], and Smil [1.5]. V. Smil [1.6] has also reported, that the hydro potential of the Yangtse and its tributaries represents 2/5th of the harnessable potential of China of the order of 500 TWh. The 2800 MW scheme Gezhouba as the first on the Changjiang (the official name for the Yangtse) with a head of 27 m is now erected and may be considered as the first step of starting the 25 000 MW scheme of Sanxia (the Three Gorges), upstream of Gezhouba, with a head of about 130 m, which is now under study [1.7].

1.2.1.3. Depth and slope of a river

The crest height of a dam as a necessary component of any river power plant depends on the depth of the river valley. The latter is usually independent of the slope of the river. Thus the crest height often reaches 100 m in the case of the Russian Angara even if its

slope of 1 : 5000 is about half of that of the Columbia, which reaches this height only once at Grand Coulee. Also the Volga occasionally provides heads of 11 to 24 m, the same as the Tennessee has, even though the slope of the latter is three times larger. The small slope of the Volga explains the enormous length of its storage basins which reaches 530 km in Volgograd (formerly Stalingrad). The surface area being 3100 km². See *Gubin* [1.8], *Borovoi* [1.9], and *Cotillon* [1.1].

If the river bed is only slightly cut in, dikes of small height are necessary for distances of tens and sometimes hundreds of km. Thus on the Argentine Paraná, to exploit two 16 TWh stations, 245 km of dikes are needed in a reach of 600 km, having a mean slope of 0,006 %. But often the deep cut of the river bed dispenses with the need of a dike. Thus on the Dnjepr a dike was built only for 50 km out of 185 km on the left river bank near Kiev, see [1.1].

Contrary to this, damming dikes are needed for the French-German Rhine and the Danube in the neighbourhood of Vienna; see *Lefoulon* [1.10], *Götz* [1.11], and *Cotillon* [1.1].

1.2.1.4. High head and large discharge

These favourable circumstances exist in general where the river leaves the large plane of its main catchment area through a series of rapids, usually located in a strongly sloping gorge. The Churchill Falls on the Churchill river in Labrador, Itaipú on the Paraná in the south of Brazil, the Inga Rapids on the Zaire (formerly Congo) and the Victora Falls on the Zambezi are some of the most characteristic examples [1.1].

Sometimes the cut in of the river bed with a strong slope may be long and the level drop large. In this case many power plants in cascades are needed. This holds true for the rivers Manicouagan, Aux Outardes and La Grande as tributatires of the St. Lawrence and the Hudson Bay respectively. A plateau may have steps, the accompanying river then has some natural falls, sometimes at large distance from each other. This is the case of the St. Lawrence in Canada (e.g., Niagara Falls).

The exceptional aspects of some river sites result from considerations of topography and climate.

1.2.2. Topography

1.2.2.1. The elements of the continents

The continents are formed by three essential elements: The plateaus, the ranges and the basins. The plateaus are the platforms, which originated from the formation of planes due to erosion of the mountain ranges of the Primary Earth Period. They cover the largest portion of the continental surface.

The ranges are nearly all formed in the Alpine folding period, e.g., the Alps, the Himalaya and the Andes. As a whole they occupy the smallest portion of the continent.

The basins originate from sedimentation of the material eroded from ranges and plateaus. They correspond to the low regions of the continent, progressively lowered by the rising weight of marine or river sedimentation. Due to their different origin their age may be very distinct and even of the Primary Period of the earth like the Toungouza in the North-East of Siberia. They cover the second largest part of the surface area of continents, less than the plateaus and greater than the ranges. Examples may be the North American belt of the Prairies, the Western Amazon basin and the Rio Plata basin of Brazil and Paraguay.

12

1.2.2.2. Topography and water circulation

The topography creates slopes, rapids and falls and collects the water in river beds. This is possible because of the earth's surface water [1.12], the sun's radiation, and the resulting evaporation of water, which rises in a heavier atmosphere (the troposphere) up to the outer edge of the latter and is transported by winds. When this water drops down from clouds only a very small portion of its original potential energy relative to the ocean level remains for the potential of the rivers. A large portion seeps into the ground, and another evaporates again.

The downstream gravity component of a river with a sloping bed is the origin of the kinetic energy of a stream. This is finally converted into heat by dissipation. The local water circulation, investigated in [1.13] may be considered as a part of the global one mentioned above. The latter is also the base of our terrestrial life [1.14].

1.2.2.3. Topography as the origin of falls and water collection

– The falls: The steps in the slopes of a river bed creating falls or steep slopes of the river bed, with rapids, are always linked to rocky elements sometimes in the form of a chain. They may result from an elevated plateau being adjacent to the lower basin of sedimentary or marine origin. The connection of both by the river is made usually by a drop in level ranging from 1 to 10% or also by a fall if the boundary of the plateau is sufficiently resistant or perhaps by a series of subsequent falls. This passage from the plateau to the basin is illustrated by the Paraná in its southern part leaving the Brazilian plateau at the falls of Sete Quedas 1700 km from the river mouth [1.1].

The transition from the plateau to the ocean by an inclined profile of the river bed, is given in the cases of the Canadian rivers Churchill (Labrador), Aux Outardes, Manicouagan and La Grande [1.1].

If the river is barred by the plateau it is diverted there in several arms or cuts towards the ocean. The Zaire downstream of Kinshaha-Brazzaville is an example of the diversion type and the Dnjepr of the cutting type.

When the plateau emerges from a sedimentary ground in the form of a barrier this determines a break of the slope. The Yenissei at Krasnoyarsk illustrates this. The same occurs, when a mountain range crosses the location of a basin. This is the case at the Iron Gate, where the Danube crosses a spur of the Carpathians.

The short-circuiting of a river bend may enlarge considerably the slope in the diversion thus created (Diversion power plant). The most famous cut of a river bend, only an idea to date, is located in China at Yarlung Zangbu (Brahmaputra): The length of the short-circuited reach between Timpa and Yortong is of the order of 200 km, the level drop 2200 m, the time-averaged discharge is 2000 m³/s, the power produced could attain 240 TWh annually. The distance between Timpa and Yortong is 40 km, but only an underground diversion of 16 km is needed, see *Cotillon* [1.1].

– The collection of water: According to *Cotillon* [1.1] river systems are partly elementary and partly of an hierarchic order. In the first case we have rivers following the line of the greatest slope. The rivers of the Baie James (La Grande), also the Manicouagan and Aux Outardes are good examples.

The other limiting system is that of a network around one final collector. Here the catchment area, feeding the main river assures the concentration of the discharge in various ways. Because of their small resistance to crossing, the sedimentary basins result into this concentration (Zaire, Yenissei). But this may occur also above a plateau (Paraná)

or as in the Alpine ranges, where they have been formed by capture often due to regressive erosion, see *Cotillon* [1.1].

Tremendous regions may be drained by one single collector. The large Siberian rivers (Yenissei, Ob, Lena) have catchment areas, each of which is ten times that of West Germany and in the case of Zaire (Congo) this figure would be 14, and 22 times for the Amazon. The catchment area is not limited always by mountainous ranges forming the horizon. Sometimes especially in Jurrasic ground subterranean streams connect adjacent catchment areas, e.g. that of the upper Danube with that of the Rhine by the Ache.

1.2.3. Climate

The climate also determines the nature of a hydro power site. Outside the equatorial zone with its high rainfall and its arid boundary zones the depth of annual rainfall grows as the ocean is approached. On the other hand rising continental character reduces the precipitation rate.

Rivers of large discharge may have on the one side a large catchment area together with a small precipitation or vice versa. Thus the Siberian Angara and La Grande (Hudson Bay) have the same mean discharge at their river mouth, but the precipitation rate of the catchment area is five times larger on the La Grande than on the Angara [1.15].

Exceptionally large discharges like those of the Amazon and the Zaire (Congo) result from a combination of an immense catchment area and a high equatorial precipitation rate. The hydro electric Inga site on the Zaire is unique, because the topography and the climate are cumulative in contributing all the possible factors for water power production: Large discharge from equatorial rainfall rate and a large catchment area near the river mouth and rapids and hence high available head there, where the river possesses its final flow rate, [1.16].

1.3. The potential and its distribution

1.3.1. Theoretical, harnessable, harnessed potential

The potential of a certain river system is defined by the annual work that the surface water of the system produces in the average year. Table 1.3.1 shows the distribution of the theoretical and harnessable potential and installable capacity over the different regions of the world. Table 1.3.2 shows the same for the main producers of hydro power, supplemented also by the harnessed potential and the installed capacity [1.1].

The theoretical potential T, can be calculated from averaged hydrographical records or estimates and level drop measurements along the river course in the following way. For every river the distribution of the time-averaged discharge Q and the level drop is taken along its course from the source to the mouth or confluence point. From this is known for a section i of the river between the confluences of two subsequent tributaries the time-averaged discharge Q_i. The drop in level Δh_i of this section is also known. This then yields the theoretical power of the section considered $\Delta P_i = g \, \Delta h_i \varrho \, Q_i$. Summing up this figure over the whole length of all the rivers in the area considered, the theoretical potential T is obtained as annual work in a mean year (ϱ being the density of water)

$$T = \Sigma g \, \Delta h_i \varrho \, Q_i \, 10^{-3} \, 8760 \, \text{kWh}.$$

A more simple estimate of T results from the relation: T = mean drop in level in the catchment area × catchment area × precipitation rate per unit area and year × 9,81/3600.

14

Table 1.3.1. Distribution of Hydro Potential over the world.
After *Cotillon* [1.1].

Zone	Surface area in 10^6 km^2	Theoretical potential T in TWh	Usable potential H in TWh	Installable capacity P in GW	Load factor (φ) $H/(8760\ P)$
Europe without USSR	4,9	3 400	700	215	0,37 ·
USSR	22	4 000	1100	269	0,465
USA, Canada, Greenland	21	6 100	1300	200	0,740
Japan, China	10	9 000	1450	380	0,435
Middle and South America	20,5	5 400	1850	328	0,642
Africa	30	6 300	2000	437	0,52
Asia (without Japan, China, Siberia)	21	?	1200	309	0,443
Oceania and Australia	8,5	1 500	200	38	0,60
Antarctis	14	200	?	?	—
Total	153	36 000	9800	2266	0,485

The error in using formulas like this results from the fact that usually the relevant mean drop in level lies far below the mean value given by the highest difference in altitude of the mountains of this area. Thus in Europe mountainous areas with an altitude range of 2500 m possess one third of their area at altitudes below one tenth of 2500 m. Therefore the simplified formula leads usually to an over estimation of the theoretical potential.

The harnessable potential H depends on the one hand on the theoretical potential and, on the other hand it depends on the power demand, on the technical tools for river power development, on the distance of the site envisaged from the next consumer and hence also on the state of the art of power transmission. Therefore the harnessable potential is a figure varying with time.

The same holds on a larger scale for the potential harnessed. This figure naturally increases continuously as long as it falls short of the harnessable potential H.

Table 1.3.1 shows, that for 1974, for example, the harnessable potential of 9800 TWh is 27% of the theoretical potential of 36000 TWh [1.1]. This comes close to a recent estimate of 44 000 TWh [1.17], and falls short of an earlier estimate of *Slebinger* [1.18] and includes also Greenland, the theoretical potential of which is deemed to be 100 TWh.

The harnessed potential will reach 2200 TWh in 1985 being then 22,4% of the harnessable potential. In the above, the harnessable potential is taken as 9800 TWh [1.19].

Strictly speaking, the work and not the capacity installed is significant for the development of hydro power. Nevertheless the installed capacity is often used. It depends on the presence of a storage basin, on the distance of the site from the next consumer centre, and on the peak load demands of the electric grid. However, naturally the maker of hydromechanical and electric equipment is more interested in the development of the capacity installed.

Table 1.3.2. Main producers of water power in 1974 [1.1] and 1980 [1.77]

Area	Theor. pot. (TWh)	Harnessable pot. (TWh)	Harnessable pot. output (GW)	Harnessed pot. (TWh) 1974	Harnessed pot. (TWh) 1980	Installed capacity (GW) 1974	Installed capacity (GW) 1980	Load factor 1974	Load factor 1980	Harnessed pot. (TWh) 1985	% of harnessable pot. 1985
World	36000	9800	2266,0	1426,5	1750,4	340,0	459,9	0,479	0,434	2200	22
USA	6100	700	186,7	304,9	277,7	64,0	76,6	0,542	0,414	652	53
Canada		535	94,5	210,0	251,0	36,7	45,4	0,625	0,631		21
USSR	4000	1095	269,0	132,0	180,0	36,9	51,2	0,408	0,401	230	23
Brazil	658	519	46,1	66,9	126,9	13,7	27,3	0,557	0,531	120	90
Japan	670	130	49,6	82,3	92,1	23,5	29,3	0,400	0,359	117	83
Norway	500	121	29,6	76,5	83,5	16,0	18,8	0,546	0,507	102	90
France	266	65	21,0	56,8	69,9	16,6	19,3	0,391	0,413	65	100
Sweden	196	100	20,1	57,2	61,7	12,3	14,6	0,531	0,423	66	66
China	5870	1320	301,0	35,0	55,6	?	21,0	?	0,302	?	?
Italy	341	50	19,2	38,8	49,6	17,2	15,8	0,258	0,358	50	100
India	?	280	70,0	27,4	46,9	7,5	12,3	0,417	0,381	?	?
Switzerland	144	32	11,0	28,9	33,6	9,8	11,1	0,336	0,346	29	90
Spain	155	67	29,3	30,6	31,2	11,5	13,5	0,304	0,264	48	72
Austria	153	44	12,3	22,6	29,1	6,0	7,9	0,430	0,420	32	72
Yugoslavia	110	64	17,0	20,6	28,2	4,5	6,3	0,523	0,511	?	?
West Germany	33	22	4,4	17,8	18,4	4,8	6,4	0,423	0,328	18	81
Australia	33	24	8,6	13,5	17,1	2,8	6,5	0,550	0,300		44
New Zealand	500	55	10,0	15,4	16,3	4,3	3,9	0,409	0,477	35	
Mexico	?	100	20,3	16,7	16,1	3,6	5,3	0,530	0,347	?	?
Argentine	?	191	43,6	5,0	15,2	?	3,3	?	0,526	?	?
Total	19740	5514	1263,3	1258,0	1500,7	291,7	395,8	0,450	0,410	1564	39,2
% of world value	55	56	56	88	86	86	86			71	

16

Therefore Tables 1.3.1 and 1.3.2 contain also this capacity and its development. The tables contain also the load factor φ, as the portion of full load hours the plant makes in the average year.

From Table 1.3.2 it is seen that the installed capacity tends to be relatively larger in areas with a low precipitation, e.g. Australia, or large catchment areas, e.g. USSR, USA, or with an irregular hydrograph varying with time due to, snow fall, melting period or monsoon (Spain, China, India). It will be smaller in regions with smaller storing facilities, more continuous rainfall, smaller reliability of peak load demand on hydro power (Norway, Canada). In general an increased capacity installed may lead to a smaller load factor φ. In storage plants this factor may drop down to 0,1.

1.3.2. Distribution of harnessed and harnessable potential

Table 1.3.3. Countries with the biggest usable potential (estimate in 1974) from *Cotillon* [1.1] and their potential actually used in 1980 from the Yearbook of World Energy Statistics, United Nations [1.77].

Country	Usable potential TWh	Used potential TWh	Percentage of usable pot.
1 China	1320	55,6	4,22
2 USSR	1095	180,0	16,45
3 USA	701,5	277,7	39,60
4 Zaire	660	4,30	0,65
5 Canada	535,2	251,0	46,90
6 Brazil	519,3	126,9	24,45
7 Malaysia	320	1,25	0,39
8 Columbia	300	13,8	4,60
9 India	280	46,87	16,70
10 Burma	225	0,87	0,39
11 Vietnam and Laos	192	0,70	0,36
12 Argentina	191	15,20	7,95
13 Indonesia	150	2,60	1,73
14 Japan	130	92,14	70,9
15 Ecuador	126	0,94	0,74
16 New Guinea	121,7	4,00	3,29
17 Norway	121	83,5	69,00
18 Cameroon	114,8	1,25	1,09
19 Peru	109,2	7,62	6,98
20 Pakistan	105	10,38	9,89
21 Sweden	100,3	61,70	61,50
22 Mexico	99,4	16,15	16,15
23 Venezuela	98	14,60	14,90
24 Chile	88,6	7,42	8,37
25 Gaboon	87,6	0,35	0,40
26 Spain	67,5	31,2	46,2
27 France	65	69,87	107,5
28 Yugoslavia	63,6	28.16	44,2
Sum	7986,7 (81,5%)	1405,87 (80,8%)	17,8
Other countries	1815,7 (18,5%)	344,53 (19,2%)	19,0
Total	9802,4	1750,40	17,8

Table 1.3.3 shows the distribution of harnessed and harnessable potential of the 28 countries that posses 81,5% of the harnessable potential *H*. From this it is seen, that the People's Republic of China, the country with the largest harnessable potential in the world of 1320 TWh, in 1974 has harnessed only 4,22% of this. According to *Cotillon*'s estimate [1.1] with growth rates of 14,2% up to 1985 and then 8%, China should have harnessed roughly 26% of *H* by the year 2000. This would need the installation of nearly 4600 MW per year of new hydro power, a figure that Chinese turbine makers cannot cope with and that water turbine makers of countries other than China should be prepared for.

Table 1.3.2 gives an idea of hydro power development of the actual main producers of hydro power during the period 1974 to 1980 according to *Cotillon* [1.1] and UNO report [1.77]. Assuming a mean load factor of 0,4, it indicates in this decade a mean annual growth of installed capacity in hydro power of 11 500 MW for the whole world.

The following authors describe this development in some countries, namely *Garstka* [1.3] and *Gillette* [1.20] in the USA. *Borovoi* [1.9] in the Soviet Union, *Weber* [1.21; 1.23] and *Goldsmith* [1.22] in Switzerland, *Smil* [1.5; 1.6] and *Koh* [1.24] in the People's Republic of China, *Fällström* [1.25] and *Angelin* [1.26] in Sweden, *Aalto* [1.27] in Finnland, *Morariu* [1.28] in Peru, *Oramas* [1.29] in Columbia, *Bichon* [1.30] in France. *Domercq* [1.31] in Spain, *Jeganathan* [1.32] and *Datta* [1.33] in India, and *Götz*, and *Schiller* [1.11] in Austria [1.34].

Recently also small hydro power has gained interest, which is shown by the publications of *Goubet* [1.35], *Francou* [1.36], *Cuinat* and *Roussel* [1.37], *Rouyer* and *le Plomb* [1.38], *Kössler* [1.39], *Gordon*

Table 1.3.4. Distribution and development of harnessed potential referred to harnessable potential over the large geographic zones of the world [1.1].

Zone	Harnessable potential a TWh	Harnessed potential b TWh 1974	% of a c	Harnessed potential d TWh 1985	% of a e	Harnessed potential f TWh 2000	% of a g
Europe without USSR	700	402,3	65%	520	73%	560	80%
USSR	1100	132	12%	230	21%	550	50%
Greenland	65	0	0	?	?	?	?
Canada	535 }1235	212,5	39,2%	299	56% }53%	900	73%
USA	700	304	43,5%	353,6	50%		
Japan	130	82,3	63,4%	117	.90%	117	90%
China	1320	35	2,6%	153	11%	350	26,5%
Latin America	1850	123,6	6,6%				
Africa	2000	34,3	1,7%				
Asia without Japan, China and Siberia	1200 }5250	74,6 }261	6,2% }5%	528	10%	1523	30%
Oceania and Australia	200	28,2	14%				
Total	9800	1426,5	14,5%	2200	22,4%	4000	41%

and *Penman* [1.40], *King* [1.41] and *Cotillon* [1.42]. For more information about small hydro power schemes see cap. 2.5. In this context *Nair's* paper on the development potential for low head hydro is of interest [1.43], and the paper of *Warnick* on the hydro potential of irrigation schemes [1.44]. The prediction of hydrograph and flow duration line is discussed by *Tomasino* [1.45] and *Plate* [1.46]. In this connection also *Press's* book [1.47] dealing with electronic computation in hydrology and his tables for the solution of such problems [1.49] and the computer program for a river development presented by *Murry* and *Weissbeck* [1.48] are of interest.

Table 1.3.4 shows according to *Cotillon* [1.1] the developement of hydro power in 1974, 1985 and 2000 over the large geographic zones.

Table 1.3.5 from [1.1] and [1.77] refers to the annual electric energy production *H* to the total electric energy production *E* in 1974 and 1980 for the most important countries with

Table 1.3.5. Hydro electric annual energy production *H* referred to total energy production *E* of the most important countries with respect to *H* in 1974 [1.1] and in 1980 [1.77].

State	H (TWh)		E (TWh)		H/E (%)	
	1974	1980	1974	1980	1974	1980
Canada	210,0	251,0	279,0	366,7	75	68
USA	304,0	277,7	1967,0	2356,0	15	12
USSR	132,0	180,0	975,0	1295,0	13	14
Brazil	67,0	127,0	70,5	137,4	95	92
Japan	82,0	92,1	460,0	612,0	18	15
Norway	76,0	83,5	76,0	83,9	100	99,5
France	56,8	69,9	180,4	257,7	31	27
Sweden	57,0	61,8	75,0	96,2	76	64
China	35,0	55,6	118,0	300,6	30	18
Italy	39,0	49,0	147,0	186,3	26	26
India	27,0	46,9	75,4	116,3	36	40
Switzerland	29,0	33,6	38,0	48,2	77	70
Spain	31,2	31,0	81,0	110,0	38	28
Austria	23,0	29,1	34,0	42,0	68	69
Yugoslavia	21,0	28,2	40,0	58,9	52	48
North Korea	?	22,5	?	35,0	?	64
West Germany	18,0	18,4	311,0	368,7	6	5
Australia	14,0	17,1	70,0	95,9	19	18
New Zealand	15,4	16,3	18,0	22,0	86	74
Mexico	17,0	16,2	41,0	64,2	41	25
Finland	12,0	16,0	26,0	38,6	47	41
Argentina	5,0	15,2	28,0	40,6	17	37
Venezuela	7,0	14,7	18,0	31,0	40	47
Columbia	8,2	13,8	12,0	20,7	68	67
Mozambique	0,3	13,5	0,6	14,0	50	96
Turkey	3,3	11,4	13,5	23,3	25	49
Pakistan	4,6	10,4	8,7	16,1	53	65
Egypt	5,2	9,6	8,2	18,5	63	52
Zambia	5,5	8,8	5,5	8,9	100	99
Portugal	8,0	8,0	11,0	15,0	74	53
Peru	6,0	7,6	8,0	9,8	75	78
Chile	6,0	7,4	9,0	11,5	67	64
Great Britain	4,8	5,2	273,0	285,1	1,7	1,8
Czechoslovakia	4,0	4,2	56,0	74,1	7	6
Zimbabwe	5,2	4,0	5,5	4,5	95	89
Zaire	4,0	4,0	4,0	4,4	100	91

respect to H. Citing the ratio H/E of this table in brackets, the following countries are saturated in H. Their harnessed potential nearly equals their harnessable potential: Switzerland (0,70), France (0,27), Italy (0,26), Spain (0,28).

The following countries show a continuous growth in hydro power: ($H/E = 0,995$), Sweden (0,64), Austria (0,69), Yugoslavia (0,48), Finland (0,41), Portugal (0,53), USSR (0,14), India (0,4), China (0,18), Brazil (0,92), Mexico (0,25), Venezuela (0,47), Columbia (0,67), Chile (0,64), Argentine (0,37), Australia (0,18), Canada (0.68), Peru (0,78), Pakistan (0,65), Mozambique (0,96), Zimbabwe (0,89), Zaire (0,91), Turkey (0,49).

The following countries have a very low water power H/E: Denmark ($H/E = 0.001$) Hungary (0,008), Belgium (0,011). German Democratic Republic (0,014), Great Britain (0,018), Czechoslovakia (0,07), Federal Republic of Germany (0,05), Bulgaria (0,097), Ireland (0,10).

According to the estimate of a West German firm the degree of exploitation expressed by the ratio of installed hydro power to installable power has actually a world mean value of 8,6%, of which 62% are in the open market. For the individual regions of the world this exploitation degree reads as follows: Europe 39,9%, Asia 5,5%, Africa 0,8%, Latin America 3,9%, North America 26,5%, Australia, Oceania 4,6%.

1.4. Hydroelectricity, its development

1.4.1. Past and future of hydro power in the context of other power

Table 1.4.1 shows the development of primary energy, electricity and hydroelectricity consumption during the past 60 years and its prediction for the next 15 years on the base of a 5% growth rate within the world. In this context the ton equivalent of coal TE = 3000 kWh is used under an assumption of 33% efficiency of the generating cycle and using pit coal.

Hence there has been during the past 60 years a population growth of 2,45 times, a growth of primary energy consumption of 8,55 times, a growth of produced electricity of 60 times, a growth of hydroelectricity produced of 28 times, a growth of kWh consumption per inhabitant per year by a factor of 24,1 and a growth of energy consumption per inhabitant per year by a factor 3,46. This shows a strong development over the whole world combined with a shift towards electricity consumption, see [1.1].

Table 1.4.1. Development of primary energy, electricity and hydroelectricity consumption of the world between 1925 and 2000.
From *Cotillon* [1.1].

Item	Unit	1925	1950	1963	1974	1985	2000
Primary energy e	10^9 TEC	1,56	2,66	5	8,64	13,3	24
Produced electricity E	10^9 TEC	0,067	0,32	0,96	2,08	4	9,6
	TWh	200	959	2880	6246	12000	28800
E/e	%	4,3%	12,1%	19,2%	24%	30%	40%
Hydroelectricity H	TWh	78,7	342,8	802,7	1426	2200	4000
H/E	%	40%	35,8%	27,8%	23%	18,4%	14%
$H/e = H/E \cdot E/e$	%	1,7%	4,3%	5,3%	5,5%	5,5%	5,5%
World population	10^6	1965	2486	3160	3890	4800	6200
kWh per inhabitant	kWh/inh	104	386	911	1613	2500	4650
TEC per inhabitant	TEC/inh	0,8	1,06	1,58	2,28	2,77	3,88

1.4.2. Cost and social problems due to electrification

Table 1.4.1 reveals the availability of nearly 5000 kWh annually in every man's hand in 2000. According to the tests of occupational physiologists, the average male worker between 25 and 45 years of age may perfom during the 8 working hours of a day a continuous output of 50 W. Hence the annual work over 220 working days, the West German year, becomes $W = 50 \cdot 8 \cdot 220 \cdot 10^{-3} = 88$ kWh. The corresponding female worker may perform 66 % of this work. Assume the duration of the remaining average life to be 40 years, during which only 50 % of the specific work mentioned above is performed, and imagine the population to consist only of 30 % of blue collar workers. Hence the average work per inhabitant and year is $W = 88\,[(0,5 + 0,66 \cdot 0,5)(0,33 + 0,3 \cdot 0,66)] \cdot 0,3 = 14,5$ kWh. This is for the year 2000 a fraction of $14,5/5000 = 1/345$ of what is offered per inhabitant by the electric grid. Imagine 345 workers are then available for every person from birth to death by a mere touch of an electric switch.

Following an undesirable but convenient trend, it may be imagined, that in the year 2000 two thirds of electric energy are used for heating, especially in the chemical industry. Hence the average person in 2000 has roughly "only" 115 men available as mechanical helpers. Obviously this is a key for understanding the wealth produced in an electrified world.

For a drastic example of the cheapness of electricity, assume a consumption of 8800 kWh per inhabitant per year, a figure some of the developed states have at present. Maintaining this figure needs the installation of 1 kW continuously available per inhabitant. The blue collar working population is possibly 25 % of the whole. Electricity may be supplied by thermal power plants with a load factor of 0,5. Thus the monetary equivalent for a working inhabitant would be that of 8 installed kW. 30 % of this might produce mechanical work.

Assume that the first and fuel cost per year are raised by the sale of energy. Hence in the above plant, an electricity rate of 0,04 US$/kWh would result in an annual cost of 1400 US$. This figure is to be compared with the annual wages of 800 blue collar workers as equivalent to the $4 \cdot 8800$ kWh.

Assuming now an annual salary of 9000 US$ for the blue collar labour, this yields $800 \cdot 9000/1400 = 5140$ times more than the total cost of the equivalent electric energy. Moreover electricity creates wealth made otherwise by 5140 workers. This procedure leads on the one hand to the production of things never done in the era before electrification. On the other hand it feeds a growing number of people in the less productive service sector.

1.4.3. The future of hydroelectricity

As shown in Table 1.4.1, hydroelectricity H referred to total electricity E is slowly decreasing from 20 % to 14 % in the period of 1980 to 2000. During this period H has reached a nearly constant portion of 5,5 % of primary energy. This has something to do with the rising transfer of heating by fuel to electric heating.

It is seen from the above table that the annual energy production of hydroelectricity should rise during the period of 1974 to 2000 by 2500 TWh. With an average load factor of $\varphi = 0,5$ this would mean that the hydro turbine manufacturers of the world need to enlarge their workshops for the production of machines with an output of 570 000 MW. What this means may be highlighted by the fact that in the foregoing 15 years from 1970 to 1985 hydro power production has been increased by 1100 TWh, namely, less than half the value it will increase over the following 15 years.

Certain problems arising from this may be eliminated when the fabrication of large hydroturbines is transferred from the workshop to the site. But nevertheless large machine tools and transportation

facilities must be provided for this increase. Some centres of gravity of water power like South America may insists that a home industry for water power equipment is erected in their own countries. But this can be done only with the continued help of developed countries.

Since the not harnessed potential is often in areas having neither power demand nor political stability, the development of large schemes there suffers mainly from a lack of obvious utility and immediate profit.

1.5. Hydro power, its actual dimensions, development and features

1.5.1. The largest structures found in hydro power at present

In Table 1.5.1 the figures of some important features of the largest water power plants in the world are mentioned.

Table 1.5.1. Some important features of the world's largest hydro power plants. From *Cotillon* [1.1].

The highest dams in service (crest height)	
Nourek in Tadshigiskan near Tashkent (USSR): earth dam	317 m
Grande Dixence (Switzerland near Rhone valley) gravity dam	285 m
Mauvoisin (Switzerland) arch dam	236 m
Daniel Johnson dam (Manicouagan 5, Canada), multiple arch dam	220 m
Greatest storage capacities	
Tarbela on Indus (Pakistan), earth dam	142 hm³
Fort Peck (USA)	96 hm³
The highest heads harnessed for water power	
Reisseck (Austria)	1772 m
Grand Dixence (Switzerland)	1748 m
Portillon (France)	1420 m
The largest man-built storage lakes	
– in total capacity	
Bratsk (Angara. Siberia, USSR) 5500 km² surface	169 km³
Aswan (Egypt, Nil) 3900 km² surface	164 km³
Kariba (Rhodesia, Zambesi) 5180 km²	160 km³
Akosombo (Ghana, Volta) 8470 km²	148 km³
Manicouagan 5 (Canada, Manicouagan)	137 km³
Luchia Gorge (Hoangho, China) Barrage with 213 m	130 km³
– in surface	
Akosombo on Volta	8470 km²
Kouibichev on Volga	6450 km²
Bratsk	5500 km²
For comparison: Lake of Geneva	580 km²

The most productive power plants (In service or under erection[+])		
– In the world	Head	Production
Itaipú (Paraná, Brazil)	120 m	70 TWh
LG 2 (La Grande, Canada)[+]	135 m	38,8 TWh
Churchill Falls (Churchill, Canada)	310 m	34,4 TWh
Sayano Suchensk (Yenissei, USSR)[+]	220 m	34,4 TWh
Bratsk (Angara, USSR)	106 m	23 TWh
Tucuri (Tocantins, Brazil)[+]	68 m	21,5 TWh
Ust Ilim (Angara, USSR)[+]	90 m	21,9 TWh

Table 1.5.1. Continuation

Krasnoyarsk (Yenissei, USSR)	101 m	20,4 TWh
Grand Coulee I-II-III (Columbia, USA)	105 m	20,3 TWh
Bogoutchany (Angara, USSR)[+]	76 m	19,8 TWh
Cabora-Bassa (Zambezi, Mozambique)	105 m	18 TWh
Yacyreta-Apipe (Paraná, Argentine)[+]	30 m	18 TWh
LG 4 (La Grande, Canada)[+]	112 m	14,3 TWh
Niagara (St. Lawrence, USA)	27 m	14,2 TWh
Cornwall (St. Lawrence, USA-Canada)	24 m	14 TWh
— In Europe		
Iron Gate (Danube, Rumania, Yugoslavia)	30 m	11,4 TWh
Volgograd (Now XXII th Congress) (Volga, USSR)	20 m	11 TWh ·
Kouibichev (Now Lenin) (Volga, USSR)	20 m	11 TWh
Saratov (Volga, USSR)	9,7 m	7 TWh
Dnieprostroy (Now Dniepro) (Dniepr, USSR)	36,3 m	3,6 TWh
— In Spain		
Aldeadavila (Douro-International, Portugal, Spain)	139,5 m	2,4 TWh
— In France		
Donzère (Rhône)	25 m	2,1 TWh

The most powerful plants (In service or under erection[+])		Planned value
— In the world		
Sanxia (Three-Gorges) (Yangtse, PR China)		25 000 MW
Itaipú (Paraná, Brazil)	12 870 MW	21 500 MW
Guri (Caroni, Venezuela)	6 525 MW	8 000 MW
Grand Coulee (Columbia, USA)[+]	6 480 MW	10 230 MW
Sayano Suchensk (Yenissei, USSR)[+]	6 360 MW	
Krasnoyarsk (Yenissei, USSR)	6 000 MW	
LG 2 (La Grande, Canada)[+]	5 328 MW	
Churchill Falls (Churchill, Canada)	5 225 MW	
Ust Ilim (Angara, USSR)	4 320 MW	
Bratsk (Angara, USSR)	4 050 MW	4 500 MW
Bougatchany (Angara, USSR)	4 000 MW	
Paulo Afonso I-II-III-IV (São Francisco, Brazil)	3 675 MW	6 650 MW
Tucuri (Tocantins, Brazil)	3 000 MW	5 700 MW
John Day (Columbia, USA)	2 700 MW	
Nurek (Vakhsh, USSR, Tadchikistan)	2 700 MW	
Revelstoke (Canada, Rocky Mountains)[+]	2 700 MW	
Ilha Solteira (Paraná, Brazil)	3 200 MW	
XXII th Congress, ex Volgograd (Volga, USSR)	2 530 MW	
Chicoasén (Grijalva)[+]	2 400 MW	
Cabora Bassa (Zambezi, Mozambique)	2 040 MW	3 672 MW
— In Europe		
XXII th Congress, late Volgograd (Volga, USSR)	2 530 MW	
Lenin, ex Kouibichev (Volga, USSR)	2 300 MW	
Iron Gate (Danube, Rumania, Yugoslavia)	2 050 MW	
Saratov (Volga, USSR)	1 290 MW	
— In Spain		
Aldeadavila (Duero-International, Spain-Portugal)	762 MW	
— In Federal Republic of Germany		
Wehr (Ternary pumped storage plant)	2 000 MW	
— In France		
Roselend	520 MW	
Genissiat	405 MW	
Mont-Cenis	360 MW	
Rance (Tidal power plant)	240 MW	

1.5.2. Survey of historical development

Hydro power as the production of hydroelectricity started in 1880 by a small DC generating plant in Wisconsin USA. But it began on a large modern scale, when economical transmission of high voltage AC was initiated in the Frankfurt exhibition in 1891 (see preface).

Corner stones of turbine development may be seen in the inventions of *Fourneyron* 1827 (centrifugal reaction turbine), *Howd* 1837 (centripetal reaction turbine), *Henschel* 1837 (axial reaction turbine, draft tube), *Boyden* 1848 (diffuser), *Francis* 1848 (Lowell experiments on Howd turbine), *Fink* 1855 (adjustable guide vane), *Swain* 1869 (radial axial reaction runner), *Voith* 1873 (*Francis* turbine with adjustable gate) mainly made with respect to the semi axial or *Francis* turbine.

For the impulse turbine this was done mainly by *Girard* 1863 (axial tangential action turbine), *Pelton* 1880 (bucket jet action turbine), *Breuer* 1890 (needle valve) and *Abner Doble* 1900 (bucket cutout). For the cross-flow turbine the essential inventions have been made by *Michell* 1903, *Banki* 1918 and *Ossberger* 1922.

For axial turbines *Kaplan* in 1913 made the decisive step (adjustable runner vane), followed by *Fischer* together with Escher Wyss in 1936 (bulb turbine, turbine with rim generator), *Gibrat* in 1942 (tidal power turbine) and again Escher Wyss 1875 (Straflo turbine). Further historical hints are given by *Raabe* [1.50] and *Moser* [1.51].

Pumped storage was started by Sulzer Brothers in 1891 (ternary set), followed by Escher Wyss 1930 (axial pumpturbine) and Voith 1934 (radial pumpturbine).

The development of modern water turbines and storage pumps cannot be separated from the names of world reknowned firms engaged in this work. To mention only a few: Sulzer Escher Wyss (Switzerland); J. M. Voith, Heidenheim (Federal Republic Germany); Neyrpic, Grenoble (France); Hydroart, Milano (Italy); Allis Chalmers, Milwaukee, Wisc. (USA), Ateliers de Constructions Méchanique de Vevey (Switzerland), Tampella Tampere (Finland), Ossberger Weissenburg (F. R. Germany), Karlstads Mekaniska Werkstaden Kristineham (Sweden), Dominion Engineering Montreal (Canada), LMZ Leningrad (USSR), Voest Alpine Linz (Austria), Mitsubishi and Hitachi Works (Japan), Kvaerner Brugg (Norway), Andritz Graz (Austria), Litostroj Lubljana (Yugoslavia), Resita Works (Rumania), Harbin Generator Works (China), Blansko Works (Czechoslovakia), Heavy Indian Electric, Hardware (India), Boving, London and Mc Lellan, Newcastle upon Tyne, both England.

The development of heavy electric and high voltage equipment has been stimulated by the inventions of *Siemens* (DC dynamo by residual magnetism), *Hefner von Alteneck* (drum armature), *Ferraris* (induction motor), *Brown* (oil insulated heavy current transformer) and *Dolivo von Dobrovolsky* (three phase induction motor and high voltage power transmission) in connection with enterprises like Siemens, AEG, BBC, Westinghouse, Edison, Alsthom, General Electric, ASEA, Fuji Electric and Toshiba.

To this should be added the progress made in high voltage transmission. After the initiative of Oskar von Miller and Deprez in 1868 this was started on an industrial scale by Dolivo von Dobrovolsky in 1891 with a voltage of 15 kV and reached in the years 1906, 1920, 1930, 1960, 1968, 1972 and 1983 the levels of 100, 200, 360, 500, 735, 1000 and 1200 kV, respectively both the last with DC transmission.

A lively impression of how fast development of hydro power goes foreward can be obtained by the development in Brazil during 1963 to 1971, where the mean growth rate was 12,6% with extreme values of 27% in 1969 and 2,4% in 1966. At the moment this development stagnates.

24

1.5.3. The features of water power plants

These are listed in Table 1.5.2. It may be added to this table, that the initial cost especially of low head plants may be much higher than those in thermal power plants. Nevertheless, the present value of total cost, including also those of fuel, is in general lower in a water power plant.

Table 1.5.2. The features of water power plants.

Advantages	Disadvantages
From the technical point of view	
Excellent availability if cavitation pitting is kept within limits by sufficient submergence. Technology simple and proven. Long useful life. Short time requirements of starting and loading, if pressure surges are kept within limits by adequate devices. Thermal phenomena restricted to bearings and generator. High efficiency.	Number of favourable sites limited and only occurring in some countries. Sites of interest more and more distantly located from the consumer centres due to progress in power transmission techniques. Cavitation, water hammer.
From the economical point of view	
Small operating, maintenance and replacement costs (10 to 15% of the financial charges) even if the annual revenues from them are retained (profit due to inflation). Harnessable as base and peak load energy. Resources are gratuitously renewed. May contribute to the advantages of other fields: agriculture (irrigation, reduction of inundated areas) navigation, mastering of inundations, zones of leisure, drinking water reservoirs. The access to the site may open also the road for the development and exploitation of other wealth. It may permit access to new countries for their improvement.	High initial investments especially for low head plants in comparison to thermal power plants but not more than that of a nuclear power plant, particularly when the cost of removal of waste material and environmental protection against dammage are included. Indemnification for submerged land. Rebuilding of roads railroads and townships occasionally submerged.
From the ecological and social point of view	
No air pollution. No thermal pollution of water. (Contrary to many thermal power plants).	Inundations of the reservoirs. Displacement of population. Loss of arable land by growing salination. Spreading of tropical diseases (Bilharziosis). Facilitating sedimentation upstream and erosion downstream of a barrage. Interrrupting the aquatic food chain. Possible induction of landslide and earthquake at high head. Black out of long transmission lines by pressure groups may undermine social order.

1.6. Survey of types of hydro power plants

1.6.1. Plants for conversion of hydraulic primary energy

1.6.1.1. General remarks on conversion of primary energy

In these plants primary energy in the form of water potential obtained from river, depression, gas washer and tidal power plants is converted into electric energy.

In general a hydraulic machine converts the available specific energy of fluid into work done by the shaft work (but also on a smaller scale into waste heat) and hence into electric energy between the terminals of its generator. Strictly speaking this available energy is the difference of total enthalpy between inlet II and exit I of the machine and referred to the unit mass of the fluid according to

$$\Delta i_t = \Delta (p/\varrho + e + gh + c^2/2)_I^{II},\qquad\qquad(1.6-1)$$

where Δ indicates the difference of the values in the brackets between the pressure flange (II) and the suction flange (I) of the machine. Their location depends on the type of machine as shown in Table 1.6.1. The values of p and c are understood as mass-flow-averaged at the respective cross sections II and I.

Table 1.6.1. Localization of cross section II and I with regard to machine type and according to the rules of the international electric commision (IEC).

Machine type	Section II	Section I
Reaction type with admission through open flume	Intake of chamber	Draft tube exit
Ditto with admission by semi spiral casing	Intake of semi spiral	Ditto
Ditto with admission by full spiral casing	Inlet flange of spiral case	Ditto
Impulse or cross flow type	Before jet needle, or inlet valve	Past turbine chamber, or on contact point of jet circle and jet centre line

In the above p is the pressure, ϱ the density and hence p/ϱ the specific positive displacement work, e the specific internal energy, $c^2/2$ the specific kinetic energy and gh the specific potential energy per unit mass of fluid resulting from its height h above a reference altitude, and g the gravitational acceleration.

In general the difference of specific kinetic energy $c^2/2$ is relatively small, excepting the rare case of a free stream or rapids turbine using only $c^2/2$ by diffusing the flow in a river rapid. In low head plants the term Δgh is relatively large, in high head plants the term $\Delta p/\varrho$ is relatively large compared with the residual terms.

Excepting gas purification plants, the pressure term $\Delta p/\varrho$ has its origin in a difference of altitudes Δh between head and tail water levels and hence in the gravity field of the earth. g may vanish, e.g. in a space missile. In a rocket, accelerated by b, $-b$ must be added vectorially to g.

1.6.1.2. River power plants

Here the higher potential energy of water gh at an arbitrary station of the river compared with another station downstream the same river, with its lower elevation h above sea level, is used. This difference in level of both the stations is a consequence of the slope of river level to overcome wall friction on the river bed and the dissipation of adjacent turbulent flow laminae.

This potential energy gh is utilized by retarding the flow by means of a barrage. Thus the dissipation of the river and hence the gradient of its slope decrease. This enables the

generation of a difference in level upstream of the dam and downstream of it. This level difference is nearly the net head. The high head thus created generates then the economical high velocity of the fluid to drive a turbine of economically high speed.

In the case of a run-of-river and barrage power plant, including submersible power plants the tail water lies adjacent to the dam. In the case of a diversion power plant a loop of the river is short-circuited by a canal or closed duct. Thus the tailwater now is far away from the dam. The same holds for a transition power plant with the difference that now the diversion joins another river system, or a tributary of the original river from which the diversion has been branched off, see [1.52 to 1.54].

In the exceptional case of a plant with free stream turbines no damming device is needed. There only the head $\Delta c^2/2$ is harnessed by diffusion in the draft tube of turbine, Cap. 10.2.

1.6.1.3. Depression power plants

In these plants the water is diverted from the ocean into a depression of the continent, located near the sea and below the sea level in a hot desert for example, so that the water evaporates from the surface of this tailwater reservoir to such a degree that its level is retained in altitude. A project will probably be made in the Cattara depression in Egypt near the Mediterranean Sea and Cairo, potential 5.7 TWh [1.50; 1.53; 1.55a]. Another project exists for the Dead Sea also fed from the Mediterranean Sea.

A similar kind of depression can be created, if an estuary of an ocean, surrounded by a continent and hence heated more and evaporating more quickly than the adjacent ocean, is separated artificially from the latter by closing the straits with a barrage. Such a project, e.g. in the strait of Gibraltar, would lead, owing to unbalance between inflow by rivers, rainfall and evaporation to a lowering of the level of the Mediterranean Sea relative to the Atlantic Ocean.

The same would result from a barrage in the strait of Bab el Mandeb, which separates the Red Sea from the Indian Ocean. According to *E. Mosonyi* [1.53] in this case the level of the Red Sea would come down relative to that of the Indian Ocean by 2,5 m annually. Within 20 years this would create a head of 50 m. After this period, supplying the plant with annually evaporated water, an annual output of about 130 TWh could be generated, that is, sufficient for Italy in 1974. However, the estimated dam volume of about $2 \cdot 10^9 \, \mathrm{m}^3$ and the environmental impact of such a project, with consequences on the adjacent coast which are not clearly known and the absence of local energy demand, make such a project castles in the air.

1.6.1.4. Wave energy

Wave power is a form of wind power when the waves result from the effect of wind. According to *Simeons* [1.55 a] the total available energy within the United Kingdom's territorial waters has been estimated to be greater than twice the present installed capacity of British power stations. Fortuitously the seasonal peak matches electrical demand.

In Sweden, the theoretical wave power potential along the 2200 km coastline is estimated at 45 TWh annually. The percentage time, when conditions permit extraction of wave energy varies from 60 % in the north of Sweden to 100 % in the south. According to *Simeons* [1.55 a], a wave power plant in Sweden is assumed to consists of 6700 concrete buoys each with a diameter of 3 m, some 3 km from shore and at a depth of some 30 m. Each generator produces AC which is immediately converted into DC and led to a converter on the shore. Interest rates have been assumed at 10 % with 25 years write off time giving a price per kWh of 0,14 to 0,23 Swedish crowns.

A comparison between a 20 MW Diesel plant and a 20 MW wave power plant shows that the capital cost per kW in the wave power plant is about 3 times higher than in the Diesel plant, whereas the operating cost of the latter is 50 % higher than in the wave power plant.

To date larger wave power plants exist only as projects. The safe and efficient design of wave energy systems requires a solution of the following problems:

1) Accurate prediction of the wave-induced motions and loads, mooring forces, extreme loads, likely fatigue damages.
2) Evaluating structural responses which may include destructive testing.
3) Simulating structural designs, reliability and minimum life.

Countries involved are Australia, Canada, China, Egypt, Finland, Japan, Mauritius, Norway, South Africa, Sweden, United Kingdom, USA, USSR.

Over the years, many devices have been patented with the object of extracting energy from the waves. These includes converging channels, flaps, floats and ramps, but many of them have failed because they did not operate on the principle that, in a wave, each particle of water approximately moves at a constant speed in a circle.

The effectiveness of a float or other device depends on its shape. A fixed body will prevent waves from developing behind, the waves being reflected almost totally after impact. However, if free movement is permitted with the waves, the reflection no longer occurs, a wave being transmitted behind the float. In neither case will power be extracted. The approaching waves must be absorbed coupled with the absence of any wave behind the device if power is to be recovered.

For this purpose a rocking beam was proposed by *Salter* [1.55 a]. Here the float (*Salter's* duck) has a front surface which moves with the water of the oncoming wave and a back surface that does not disturb the water behind. Thus the float rocks about its axis and this motion relative to a neighbouring body, not rocking, has to be converted into electric energy.

There are numerous ways in which power can be derived from the slow oscillation caused by waves. One means to consider is converting the motion of waves into uni-directional high pressure water pulses by means of a reversing pump.

One of the problems is the means by which the power generated is to be brought ashore. This could be achieved through the use of flexible submarine cables or alternatively water might be pumped at high pressure from floats at sea, with the electricity then being generated on land.

Masuda in Japan [1.55 a] has developed an air pressure ring buoy. This is open at its bottom from which air is displaced rhythmically by the wave action. The air flow is rectified by Flap valves and used to produce power through a low pressure air turbine.

Another device, Russel's rectifier [1.55 a] is composed of a series of high level and low level reservoirs both of which are exposed to waves. The reservoirs are separated from the sea by a set of vertical return flaps so that waves drive sea water into the high level reservoir and extract it from those at the lower level. A turbine is installed between both the reservoirs.

In Mauritius wave energy is extracted on the principle of a wave run-up over a contoured wall sloping 30°, behind which the water becomes entrapped to a head water reservoir.

The Lancaster flexible bag has a number of cells which are formed in a long tube of flexible material. The tube is open along its lower side and sealed to a rigid and moored beam, in which two air mains are formed. When a wave rises around a cell, it forces the air from it into the high pressure main of the beam. As the surface in the vicinity of the cell falls, the pressure within it drops until air flows into it from the low pressure main. Air then returns from the high pressure main to the low pressure main via an air turbine, [1.55 a].

The Vickers energy converter [1.55 a] is a fully submerged device likely to be mounted on the sea bed. This arrangements avoids the problems of mooring normally associated with floating devices. Here a resonantly oscillating mass of water is excited by the changing static head of the wave passing over it. The function of this device does not depend on the direction of wave propagation.

28

Whittington and *Wilson* [1.56] have developed a model for generation of steady DC output from variable wave power by means of an induction machine and a synchronous machine, both coupled electrically.

Besides the wind-induced waves, there exist also tide-induced waves and sea-quake-induced waves. In general, the wind-induced waves have the shortest wave length. All these waves are superimposed to each other.

In the Pacific Ocean e.g. along the Japanese coast occasionally sea-quake-induced waves, the so called Tsunamis may attain amplitudes up to 35 m. By the impact pressure of such Tsunamis waves on steeply inclined coasts the water due to the wave may be lifted into artificial reservoirs. From these the water then may propel a water turbine.

1.6.1.5. Tidal power plants

These plants harness the tidal range of the oceans between ebb and flood. This effect is caused mainly by the mutual attraction of moon and earth when rotating with a nearly monthly period around an axis 'a' (see Fig. 1.6.1) through their common centre of gravity S, orientated normal to the plane of the lunar orbit. S being accidentally underneath the earth surface.

Fig. 1.6.1. Generation of flood humps. E earth, M moon; S common centre of gravity moon-earth; h_ω flood hump due to centrifugal force; h_G flood hump due to gravity force; a axis of rotation of the earth-moon system; e earth axis; l plane of lunar orbit and approximately also that of the earth orbit; − − − imaginary spherical earth surface; F_W weight; F_ω centrifugal force; F_G gravity force of moon; F_r resulting force on body on the earth normal to the sea surface; AB parallel to axis a, La latitude.
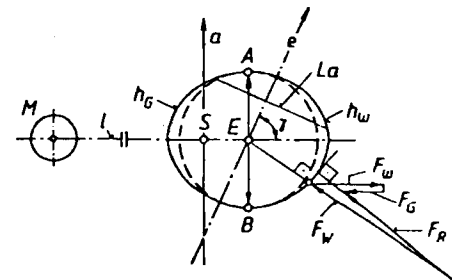
Along an earth diameter parallel to 'a' (see Fig. 1.6.1) the centrifugal force induced by rotation around the above axis 'a' and the lunar gravitational attraction are balanced. Therefore the resulting force on a fluid element at the ends A and B of this earth diameter points towards the centre of the earth E. Hence a fluid element at these stations remains with its surface parallel to the earth's surface. For a liquid element on the side away from the moon the centrifugal force due to rotation around the axis 'a' is stronger than the lunar gravitational attraction.

Hence by static equilibrium the ocean surface there deviates slightly from the nearly spherical original form, creating a hump oriented away from the moon. On the opposite side of the earth oriented towards the moon the more influential gravitational attraction of moon forms as a whole a liquid hump, pointing towards the moon (see Fig. 1.6.1).

As a whole the surface of the oceans has an oval deformation along the connecting line of earth and moon. The earth itself rotates around its spatially fixed axis once a day. Therefore every point on its liquid surface passes within approximately one day the flood hump, caused by the gravity of the moon and then 12 hours later the hump caused by rotation of the earth around the axis 'a' (see Fig. 1.6.1). From this it is also seen that these two flood humps usually cause at any instant at a point of a certain latitude on the earth a special tidal range. This depends also on the angle γ, the earth's axis makes with the connecting line l of earth and moon, see Fig. 1.6.1.

29

When this angle becomes 90° we have the equinox[1]. Now the stations on an average latitude cross twice daily nearly the summit of both the flood humps. Consequently this frequent excitation of the oceans during the equinox in connection with the eigen-frequency of the large water masses at the Atlantic coast of Europe and Southern Canada results into the highest tidal range. In the polar region, especially in summer or winter, this model gives only one flood daily, which is what happens.

A similar interaction exists between earth and sun. Here the common centre of gravity of the system is in the sun. For the same effects, as described above, two flood humps are generated at the ocean in the direction towards the sun and away from it. They are naturally smaller than the two due to interaction of earth and moon. Both pairs of humps have to be added when earth and moon are along a straight line during new moon and full moon. Then the highest tidal range occurs, the spring tide. When the earth is on the corner of a rectangle formed by sun, moon and earth, then both the humps have to be subtracted from each other. Now the lowest tidal range occurs, the neap tide.

Considering only the action of the moon, the highest tide-conditioned sea level has to occur, according to the static consideration made so far, when the moon passes the meridian. This in fact is retarded owing to the inertia of the large water masses by about six hours in our latitude.

Adding the information given in [1.55 a], the usable potential of tidal power may be estimated in the order of 1000 TWh. The average tidal range in the open ocean is very small below one metre. The effect becomes remarkable by the impact of a tidal wave on estuaries and straits as for example the Channel between France and Britain. In the latter case, the tide-conditioned flow between the Atlantic Ocean and the German Sea at the instant the tidal flood wave enters the Channel, causes a Coriolis force. This lifts the water additionally at the English coast and lowers it at the French. The additional ram effect in a convergent estuary adequately oriented may lift the tidal range during spring tide at the equinox up to 13,5 m in the river mouth of the French Rance and up to 17 m in the Canadian Fundy Bay at the North Atlantic coast, see *Shaw* [1.57] and *de Lory* [1.58]. There the largest tidal power unit is installed in the power station Annapolis (see Fig. 10.2.21, 22). It is of the Straflo design with rim generator, which is genuinely best fitted for harnessing tidal power, and built after the designs of Sulzer Escher Wyss the patentee, see *Douma, Steward* and *Meier* [1.59].

Also Indian tidal power projects were discussed by *Sharma* [1.60] and *Subrahmanyan* [1.61]. Problems and benefits of tidal power stations are considered by *Benn* [1.62].

A tidal power plant may be equipped with one or two basins. The one basin type which is the only type built to date (see Fig. 1.6.2) may have one flow direction (single effect) as, e.g. in Annapolis. This guarantees highest efficiency with the slight disadvantage of either a great storage volume or limited working period. More see Cap. 10.2.

Therefore the French firm Neyrpic, Grenoble, has developed, for the Rance tidal power plant (see Fig. 10.2.15), and axial bulb turbine that operates with one basin in both the flow directions both as a turbine and as a pump (double effect scheme).

The action of such a tidal power plant as the Rance with one basin and double action (reversal of turbine flow) is considered more in detail (see Fig. 1.6.2). Owing to the tides, the ocean level 0 moves nearly harmoniously vs time. At its highest level it is connected with the basin by a sluice then opened. When the ocean level begins to lower, the sluice gates are closed. At a reasonable difference of height of water levels in basin and ocean, the set starts turbining from the basin to the ocean, period 3. Before ebb the set is shut down. The sluice gates, then opened equalize the level of the ocean and basin.

---

[1]) Strictly speaking this holds true only if the planes of the orbits of sun and moon are coincident.

Fig. 1.6.2. Time sequence of operating mode in a tidal power plant with double effect: 1 waiting; 2 filling; 3 direct turbining; 4 reversed turbining; 5 emptying (sluicing); o ocean level; b basin level; c basin level with pumping.
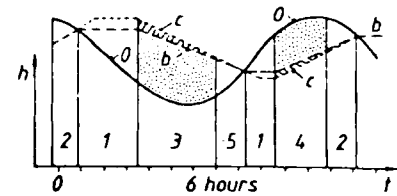
When a reasonable head between the rising level of the ocean and that of the basin for the second cycle of power generation (period 4) has been reached, the machine begins to operate as a turbine with reversed flow direction from the ocean to the basin. For more details see Cap. 10.2.

1.6.1.6. Hydro power from gas washers

The principle of these plants can be seen in Fig. 1.6.3. Pressurized waste gas charged with pollutants is exhausted from a process. For the purification of this gas and the use of its energy, the gas flows into a closed vessel and is sprinkled with pressurized water circulated by an impeller pump. By this and Raschig-rings, the gas is adsorbed by water. This then operates a turbine. Past the runner in the low pressure zone the gas comes out of solution. The clean gas then is removed from the top of the tailwater tank and its impurities from the bottom of the latter. The surplus of turbine output over the impeller pump's input drives a generator [1.50].
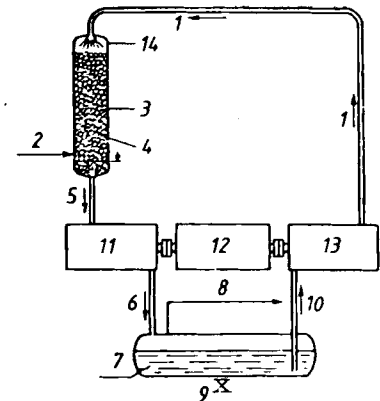
Fig. 1.6.3. Scheme of a gas washer: 1 purified water pressurized; crude gas polluted and pressurized; 3 Raschig rings; 4 washing line; 5 polluted water pressurized; 6 polluted water pressure-relieved; 7 separator; 8 purified gas; 9 sludge pocket; 10 clean water pressure-relieved; 11 turbine; 12 alternator; 13 impeller pump; 14 sprinkler; (Scheme courtesy Vevey Engineering Works, Switzerland).

1.6.2. Plants for conversion of secondary energy

These so called pumped-storage plants use secondary energy in the form of electric energy for storing it as potential energy in an elevated artificial reservoir. In these plants cheap base load energy from a plant converting primary energy (e.g. run-of-river or thermal power plant) is used to pump water from a tail water basin into an artificial head water basin. The water potential thus generated is used, to cover expensive peak load demand.

European aspects of pumped storage were discussed by *Angelini* [1.63], the Japanese by *Okada* [1.64], some Swiss aspects by *Stürzinger* [1.65] and *Rochat* [1.66]. Hernan considers Dinorwic, Great Britain's biggest binary plant [1.67]. *Meier, Müller, Grein* and *Jaquet* [1.68] give information about recent binary and ternary sets in Western Europe. Similar projects in Italy are reported by *Magnago* and *Bortolan* [1.69].

Pumped storage plants were equipped originally by ternary (or tandem) sets with a special impeller pump, turbine and motor-generator along the shaft (see Fig. 1.6.4 a). As a consequence of rises in wages and hence in initial cost of the power house and its equipment, nowadays binary sets are preferred with pump-turbines as the only hydraulic

31
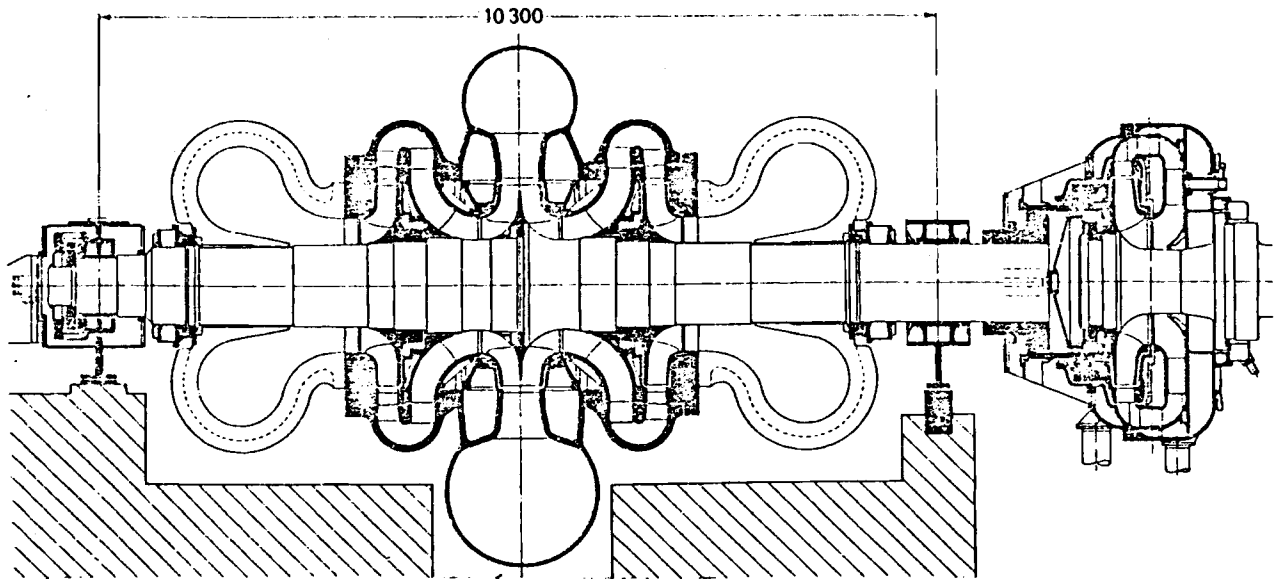
Fig. 1.6.4. a) Double flow 2-stage storage pump, horizontal shaft, and torque converter for synchronizing and speeding up the water filled pump of pumped storage plant with ternary sets, Wehr, Wehra, Federal Republic of Germany (West Germany) (Owner Schluchsee AG, Freiburg) built by J. M. Voith, Heidenheim. Data of pump: $H_m = 640$ m, $Q = 36$ m³/s, $n = 600$ rpm, $P_m = 248$ MW; torque converter $P = 150$ MW (water filled). Pumps belong to 4 ternary sets with Francisturbines shown in Fig. 10.3.10 built by Sulzer Escher Wyss. To date the most powerful plant with ternary sets (Drawing courtesy Voith).

machine on the shaft of a set (see Fig. 1.6.4 b). Also plants for the harnessing of water power potential have been equipped subsequently with pumped-storage sets (see Fig. 1.6.9).

A ternary 100 MW set of about 300 m head now may reach a storing cycle efficiency of 77% (see Fig. 1.6.5). As a corresponding binary set shows a drop of this efficiency by about 2 to 4% and hence a shortage of revenue corresponding to the capital expenditure of 2 to 4 sets, efforts have been made to reach greater compactness with the ternary set (see Fig. 1.6.6).

Greatest compactness in ternary sets is effected by the so called "Isogyre" design (Fig. 1.6.7 [1.70]). Invented by the firm Ateliers de Charmilles, this design is now exclusively built by Vevey Engineering Works Ltd, one of the oldest turbine makers of Switzerland, who many years ago were affiliated to B. Fourneyron, the pioneer of modern hydroturbine engineering. Also Girard, inventor of the first useful impulse turbine, worked there.

Fig. 1.6.4. b) Elevation of pump-turbine set at Kühtai, Austria (owner Tiroler Wasserkraftwerke), built by J. M. Voith, West Germany. Data $n = 600$ rpm; $H = 319$ to 440 m. With one set: turbine mode $P = 87,5$ to 151,3 MW, pump mode: $P = 124$ to 109,4 MW; with 2 sets: turbine mode $P = 82,5$ to 143,5 MW, pump mode $P = 123,7$ to 108,5 MW. Spiral casing free of external forces by means of a Sulzer Escher Wyss type load compensator (see Fig. 3.4.44) and by embedding it in sponge rubber. Gates operated by single servo motors, electro hydraulic controlled; welded spiral casing with a stay ring of nearly parallel plate design, 3 guide bearings. Thrust bearing supported on a spider above the alternator. Start up into pump mode with dewatered rotor in air by means of a pony motor within 90 s. Pony motor $P = 15$ MW. Total weight of the set 940 tons, weight of the rotating parts 287 tons, fly wheel moment $GD^2 = 1195$ Mpm² (drawing courtesy J. M. Voith).

32

184760

1834.00

15832

T 450

33
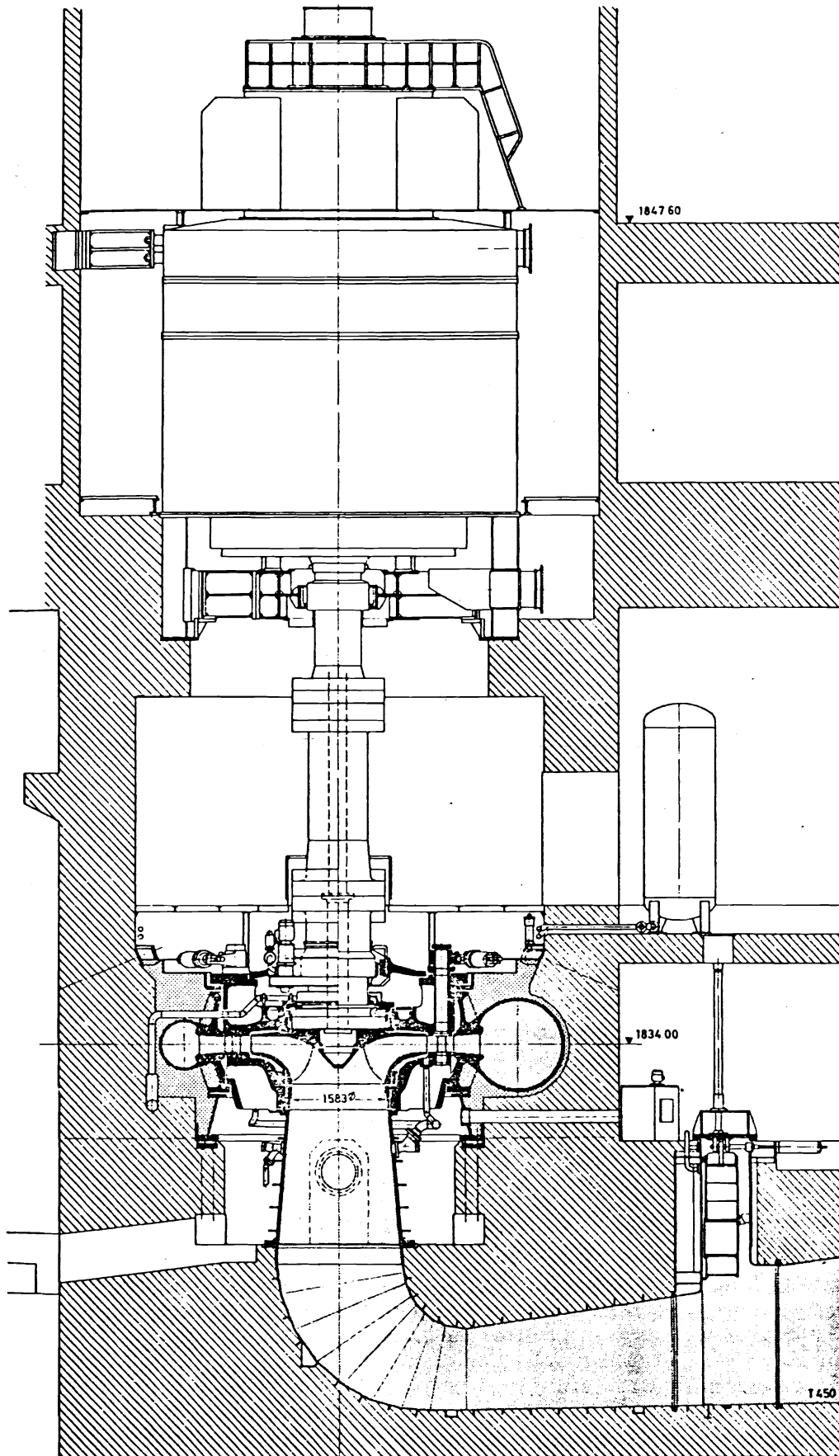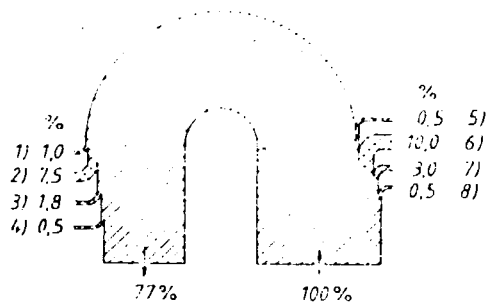
Fig. 1.6.5. Losses and efficiencies of a ternary (tandem) set in a pumped-storage plant; example Vianden, Luxemburg (owner Société d'Electricité d'Our); 9 sets: turbines H – 287 m; n = 428.6 rpm; P = 105 MW; pumps H – 287 m; P = 68 MW. Losses during turbining: 1 penstock, 2 turbine, 3 generator, 4 transformer. Losses during pumping: 5 penstock; 6 pump; 7 motor; 8 transformer (Drawing Société d'Electricité d'Our)
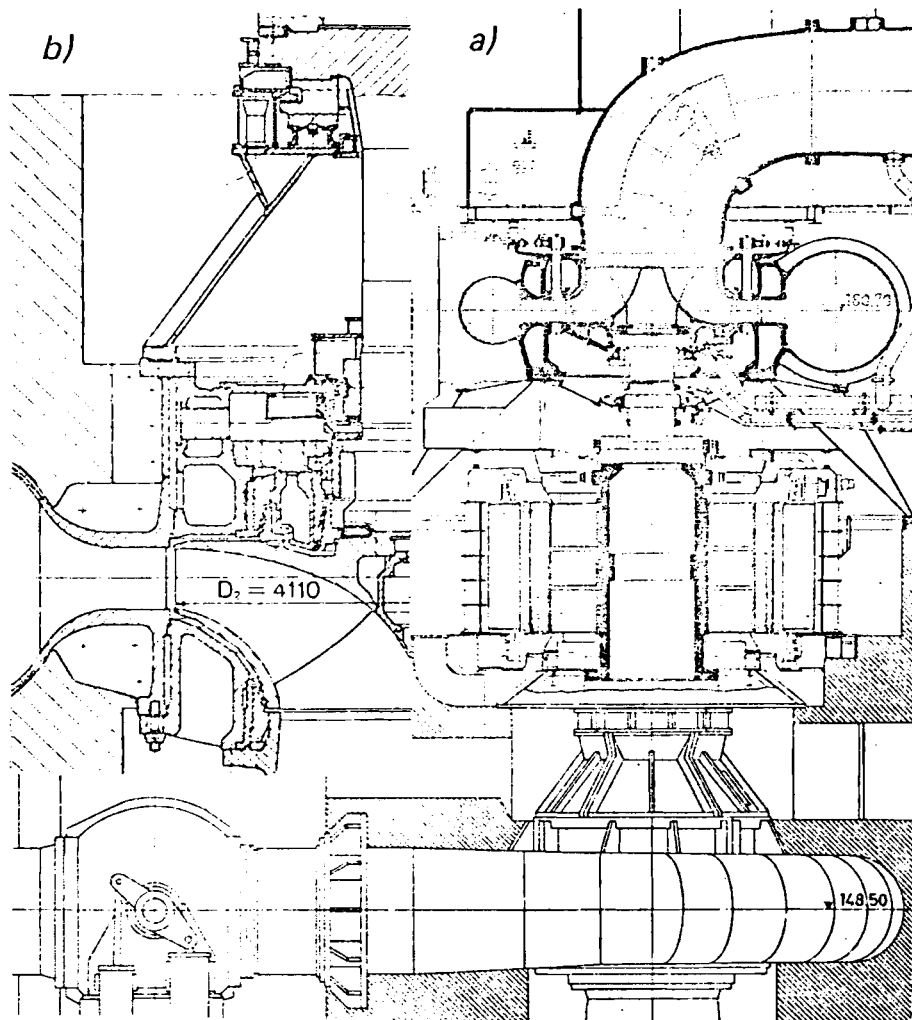
Fig. 1.6.6. a) Elevation of a vertical shaft ternary pumped storage set, Waldeck 2 (owner Preussenelektra-Wasserkraftanlagen GmbH Hannover); 2 sets: Francisturbine (FT), built by Voith: H = 336 m; n = 375 rpm; P = 239 MW; 1-stage pump (P) built by Sulzer Escher Wyss: H = 330 m, P = 230 MW. For higher submergence the pump should be underneath the turbine. Overhung design of both rotors lowers cost. To eliminate disk friction of labyrinth rings on emptied pump impeller, radial clearance of staircase labyrinth is increased by lifting stationary labyrinth ring hydraulically. Axial thrust bearing on pump head cover. Motor generator badly accessible.
b) Detail of pump section (Drawings courtesy Sulzer Escher Wyss, and J. M. Voith).

34

Fig. 1.6.7. Elevation of vertical shaft "Isogyre" of Austrian Malta scheme (owner Österreichische Draukraftwerke AG, Klagenfurt), upper stage, also provided for pumped-storage. 2 sets. Runner (above) and impeller (below) in back to back arrangement with 1 spiral casing give the most compact ternary set. Flow reversal in the toroidal diffuser of a pump. Built by Vevey Charmilles Engineering Works. Pole changing motor generator built by Brown Boveri. Data: turbining with $n = 500$ rpm: $H = 129$ to 220 m; $P = 36,4$ to 83 MW; with $n = 375$ rpm: $H = 60$ to 129 m; $P = 11,3$ to $36,3$ MW; pumping with $n = 500$ rpm: $H = 109,5$ to 200 m; $P = 46,7$ to 46 MW; with $n = 375$ rpm: $H = 50$ to $109,5$ m; $P = 18,4$ to $19,9$ MW; $D = 2$ m (Drawing courtesy Vevey Charmilles Engineering Works).
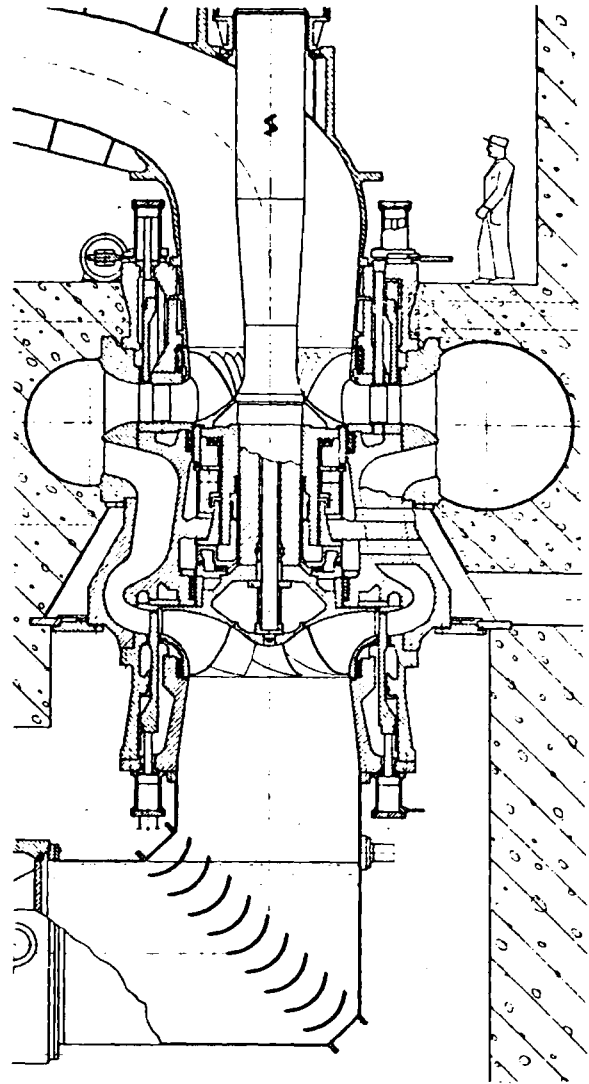
The Isogyre design has a pump and turbine rotor back-to-back. For economical reasons both are connected alternately with the same spiral casing and suction flange by means of cylindrical gates. A retention of speed direction during both the modes of operation guarantees a short transition period. Hence a given sense of the spiral casing requires a reversal of flow by 180° for one of these services. This is done very effectively on the pump side by means of a bladed toroidal diffuser channel so known from the multistage impeller pump.

A symposium was dedicated to the Isogyre [1.71]. The latter was described by *Fauconnet* [1.72]. The owner's view on this design is revealed by *Widmann* et al. [1.73], and *Hautzenberg* [1.74].

A certain disadvantage of pumped storage plants lies in the fact, that peak load demand exists usually in the densely populated industrialized areas, mostly located in flat regions. On the other hand the storage volume of the upper, usually artifical, reservoir for a certain work per cycle becomes smaller with increasing head and with it also the cost per kW.

The head range at present is between 20 and 1600 m (San Fiorano in Italy, see Figs. 1.6.8 and 1.6.9). In West Germany many of these pumped storage schemes, some dating back
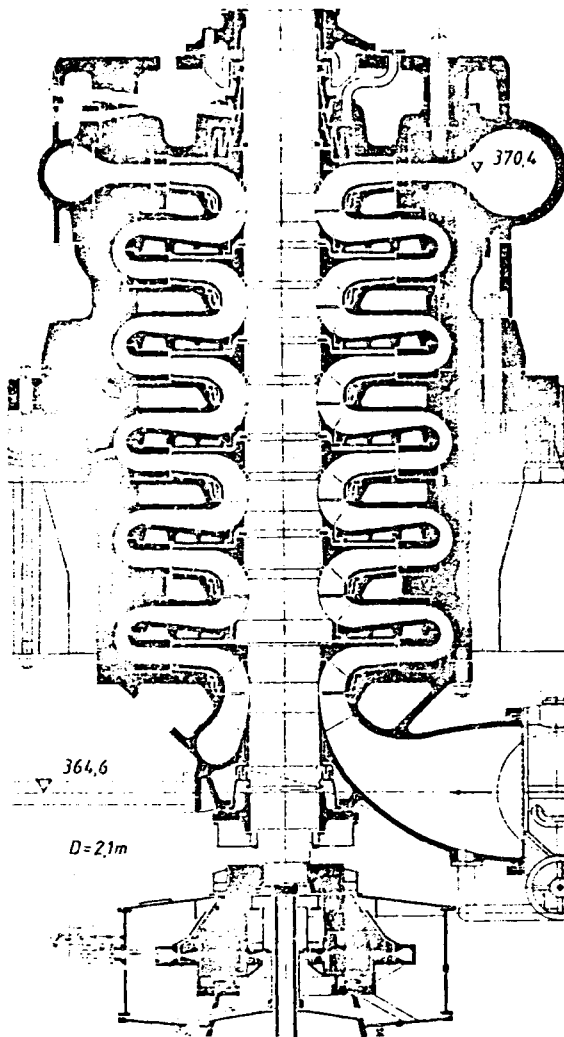
Fig. 1.6.8. Elevation of a 6-stage storage P of 2 ternary pumped-storage sets, San Fiorano, Italy (owner Italian Electricity power board ENEL) built by de Pretto Escher Wyss. Data: $H_m = 1483,7$ m; $n = 600$ rpm, $P_m = 105,8$ MW, $D = 2,1$ m. To date highest delivery head of pumped-storage (Drawing courtesy Sulzer Escher Wyss, Switzerland).

to 1910 (Brunnenmühle), are located in a mountainous southern area far from the large consumers of the northern Rhine Ruhr region. They need therefore a long and expensive high voltage line of about 800 km at 360 kV.

To save such expenses and for making these pumped-storage plants independent of the topography of industrialized areas, it has been proposed to use subterranean caverns as tail water basins, e.g., abandoned coal mines. In the West German Ruhr region the latter may have a depth of 1000 m or more.

1.6.3. Hydro power in transmission drives (torque converter)

These gears are an invention of the German *H. Föttinger*, 1905. They consists of a turbine and impeller pump short-circuited with a guide apparatus in between. This enables the differential torque between the input and output shaft to be led into the ground. Because of the absence of a diffuser the efficiency is quite high but below that of a toothed wheel gearing. Therefore the use is limited to gear changing. The high density of fluid and heads up to 50 bar per stage enable a high power density. For example the water-operated synchronizing torque converter of a 250 MW ternary set at Wehr (West Germany) has a turbine part with a centrifugal runner (after Fourneyron) with about 2.3 m tip diameter and up to 160 MW output (see Fig. 1.6.4).

36
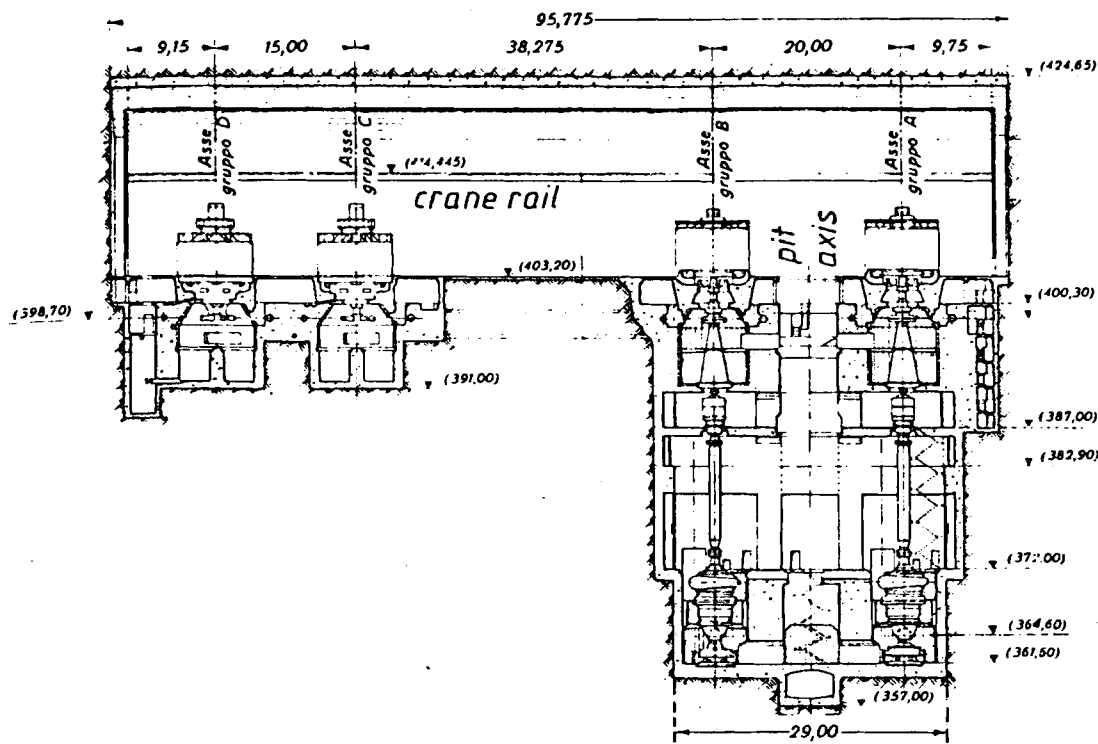
Fig. 1.6.9. Longitudinal section of the power house at San Fiorano, Italy (owner ENEL). Mixed plant with 2 ternary sets for pumped-storage. Pelton turbine (PT) built by Hydroart, Milan, Italy. Data: $H_m = 1403$ m; $n = 600$ rpm; $P_m = 140$ MW. To date the highest nHP in a storage P (Drawing courtesy ENEL).

Such gears are widely used now as hydromatic drives in cars and with an output up to 2000 kW for Diesel hydraulic locomotives. Because of their low specific weight, these gears are extremely suitable for Diesel locomotives. Such locomotives are the backbone of traction power of the unelectrified lines of the West German federal railroads. With their low specific weight, for a certain limit they are superior in output to Diesel electric locomotives.

1.6.4. Hydro power plants with respect to their availability

– Run-of-river power stations operate fairly continuously and supply base load. Most of run-of-river power plants have a low reservoir storage capacity and usually low head. Together with thermal and nuclear power plants, they cover the base load of an electric grid. These sets usually have a speed control (if any), which cares for a small variation of output within the permitted range of frequency (provided the grid is an AC one) and hence of speed from n_{min} to n_{max}.

This is effected by a rather high permanent speed droop defined by $\delta_P = (n_{max} - n_{min})/n_{mean}$ (see also Cap. 11.2) in the range of $\delta_P = 0,03$ to $0,04$.
– Storage plants with a small storage volume (weekend reservoir). Usually a chain of river power plants, which has a certain storing capacity in its terminating highest and lowest reservoirs. In West Germany, rivers without navigation, e.g. the Lech or the upper Danube between Ulm and Regensburg have such a chain of power stations to cover smaller peak load demand (e.g. electric traction power) by the so called "swell" operation. With this a certain water quantity passes through the chain to the reservoir on the chain's

37

lower end. From there on downstream a certain target relief has to be delivered into the river, see Fig. 1.6.10 and Grüner [1.75]. Having the covering of peak load in mind, the set needs a characteristic, in which the output drops more vs speed than in a base load plant. Hence the permanent speed droop $\delta_p = 0.02$. At the Danube this service will quitted.
- Storage plants with a large storage volume (annual reservoir). Usually the upper reservoir is located in the mountains to store melted snow and ice (see Fig. 1.6.11). As
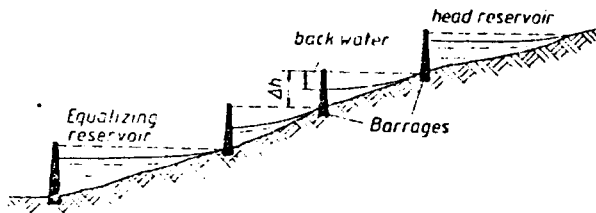
Fig. 1.6.10. Section along a river with head reservoir and flow equalizing reservoir at its ends, and chain of power stations between for swell operation.
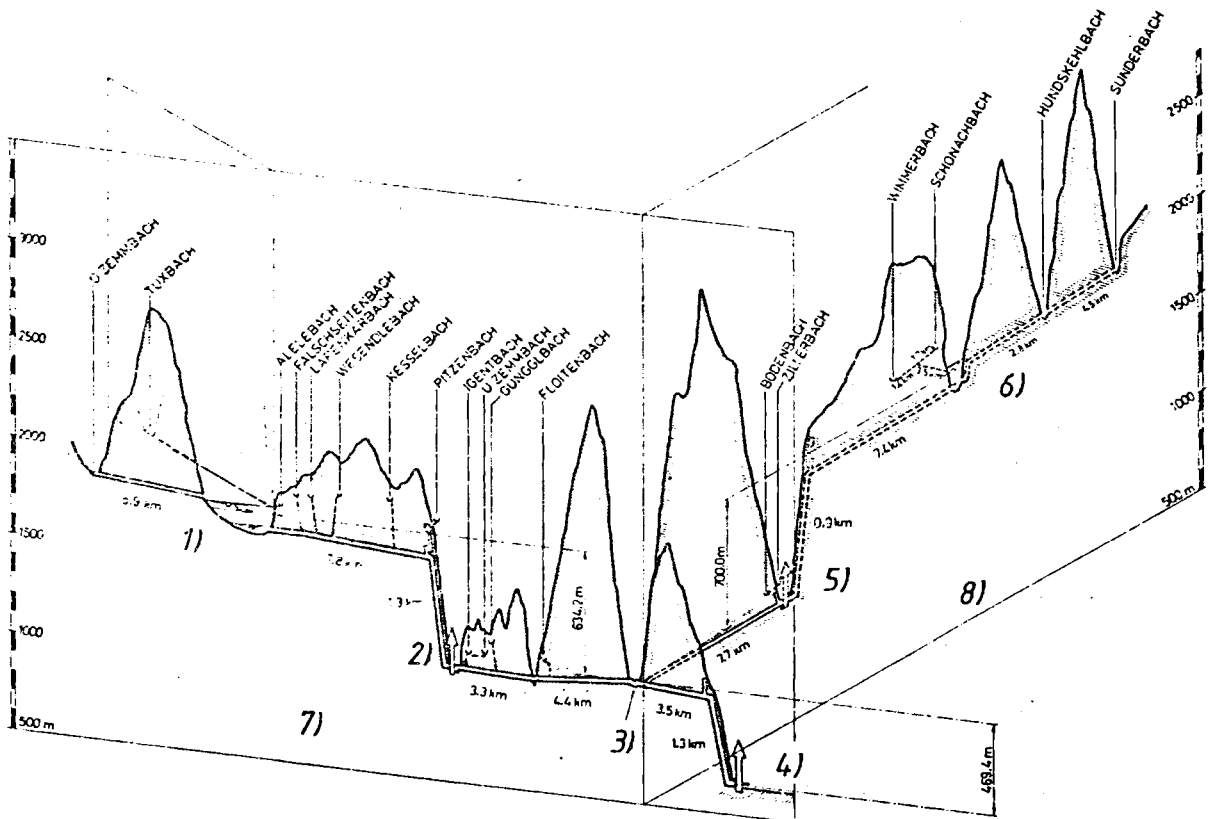
Fig. 1.6.11. Schematic perspective view of combined peak load storage and pumped-storage plants Ziller and Zemm, Austria (owner Tauernkraftwerke AG, Salzburg). Annual productivity 1072,9 GWh: annual consumption by pumping 758 GWh. 1) Schlegeis reservoir, levels at altitudes h_{max} = 1782 m: h_{min} = 1680 m; live storage volume ΔV = 127,7 · 10^6 m^3 2) Rosshaag powerhouse: 4 ternary sets, Francisturbines (Fig. 10.3.9) with H_{max} = 672 m (to date highest head of a Francis turbine operating, here since 1970) built by Sulzer Escher Wyss Andritz: n = 750 rpm; P = 58 MW. 2-stage pumps started up filled by Föttinger torque converter, all built by Voith. P = 62,5 MW. 3) Stillup reservoir: h_{max} = 1120 m; h_{min} = 1106 m; ΔV = 6,9 · 10^6 m^3; 4) Mayerhofen power house, H = 469 m: $P_{r,s}$(Only turbining) = 345 MW; 5) Häusling power house (under erection) 2 ternary sets with Francis turbines of then highest head H_{max} = 744 m, P_m = 180 MW (see Fig. 10.3.11) 6) Zillergründl reservoir h_{max} = 1850 m: h_{min} = 1740 m; ΔV = 89 · 10^6 m^3. 7) Zemm scheme operating. 8) Ziller scheme under erection. From Widmann [1.76].

38

these plants have, in the main, also to cover peak load demand, their permanent speed droop is small δ_p = 0,01 to 0,015. *Widmann* desribes a recent scheme of this type [1.76].

− Tidal power plants: for the usual type of plant made to date with one basin, the availability of its power depends on the date, the moment, and especially on the related position of moon and sun (see Fig. 1.6.2).

− Pumped storage plants: these plants meet the daily peak load demand (see Fig. 1.6.12).
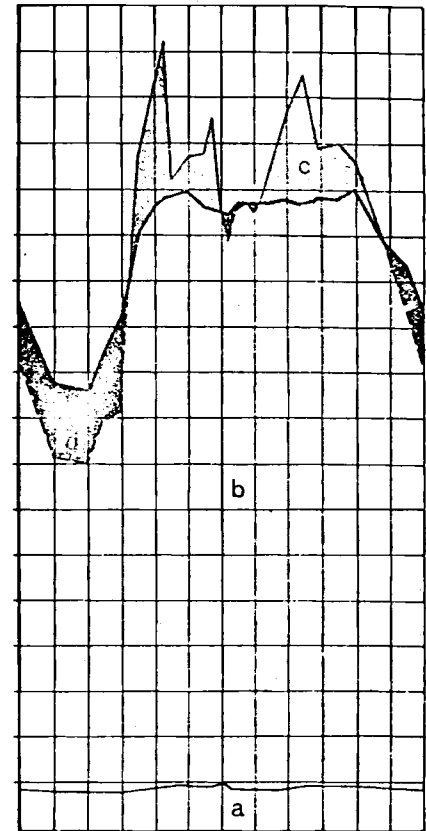
Fig. 1.6.12. Variation of grid load of West German power board (RWE) during a winter working day a) base load of run-of-river sets b) the same for thermal power plants c) peak load of storage and pumped-storage plants d) consumption by pumping of pumped-storage plants.

1.6.5. Hydromechanical equipment of outstanding plants

Table 1.6.2 shows a compilation of the important dates and features of the hydro turbomachines of some important plants.

Table 1.6.2. Compilation of hydroturbomachinery of large water power plants

Plant/river (country)	Number of sets	Head (m)	Output (MW)	D(m)
Kaplan turbines				
22nd Congress/Volga (USSR)	22	22	120	9,3
Iron Door/Danube (Rumania-Jugoslavia)	12	35,5	178	9,5
Porto Primavera (Brazil)	18	18,3	103	.
Jupia/Rio Paraná (Brazil)	14	25,2	107	8,4
Rocky Reach (Columbia)	11	29	118	7,3
Tres Marias/Rio São Francisco (Brazil)	6	55	75	4,65
Gezhouba 1 (China)	2	25	180	11,3

Table 1.6.2. Continuation.

Palmar (Uruguay)	3	32,3	113,4	7,6
Aschach/Danube (Austria)	4	17	75 .	8,4
Orlik/Vultava (Czecho-Slovakia)	3	72	91	
Prittikoski (Finland)	2	27	66,3	5,8
Solbergfoss (Norway)	1	20	106,7	8,3
Otori (Japan)	1	51	100	6,15

Francis turbines

Itaipú/Rio Paraná (Brazil-Paraguay)	18	126,7	740	8,1
Guri II (Venezuela)	10	146	730	7,17
Sajansk/Ycnissei (USSR)	12	230	600	
Krasnojarsk/Yenissei (USSR)	12	101	507	7,5
Churchill Falls (Canada)	11	312	483	4,34
Bratsk/Angara (USSR)	18	102	230	5,5
Ust Ilim/Angara (USSR)	18	100	220	
Ilha Solteira/Rio Paraná (Brazil)	16	46	193,5	6,8
Tucuri/Tocantin (Brazil)	8	67,6	369	8,15
La Grande 2 (Canada)	8	137,2	338,5	
Itaparica/Rio São Francisco (Brazil)	10	53,2	264	7,925
Cabora Bassa/Zambesi (Mozambique)	5	113,5	485,3	6,96
Grand Coulee III/Columbia (USA)	3	87	700	9,26

Pelton turbines

Chivor (Columbia)	8	803,5	151
Sy Sima (Norway)	3	885	350
Grand Maison-L'Eau d'Olle (France)	4	922,4	157
Paute (Ecuador)	5	667	120,4
Lotru (Rumania)	3	788	187,5
Silz (Austria)	2	1238,5	264,8
Lago Delio (Italy)	4	732	127,3
Roselend (France)	6	1201	83
El Toro (Chile)	4	545	116,2
Idikki (India)	3	660	134,4
Villarodin-Mont Cenis (France)	2	870	200
Chandoline (Switzerland)	5	1740	36,6
Reißeck (Austria)	3	1765,3	22,8

Pumped storage plants	PuT Pumpturbine	TS Ternary set	
Bath County (USA)	6	329	457 PuT
Cornwall (USA)	8	350	295 PuT
Dinorwic (Great Britain)	6	536	317 PuT
Racoon (USA)	4	305	382 PuT
Helms (USA)	3	531,6	414 PuT
Grand Maison-L'Eau d'Olle (France)	8	955	152,5 PuT
Okukiyotsu (Japan)	4	490	260 PuT
Wehr (West Germany)	4	645(max)	257,5 TS with FT
Vianden (Luxemburg)	9	287	105 TS with FT
Montezic (France)	4	419,1	230 PuT
Malta/Drau (Austria)	4	1030	208 TS with PT
Coo 2 (Belgium)	3	275	234 PuT
Caplijna (Jugoslavia)	2	237	250 PuT
San Fiorano (Italy)	2	1438,6	105,8 TS with PT
Häusling (Austria)	2	744(max)	180 TS with FT

2. Economical and other aspects of hydro power and actual examples

2.1. Introduction

The economical aspect is certainly important in determining whether any hydro power project comes to fruition. Since nobody is an island, the engineer, the economist or the politician, whilst seeing a certain project as progress in their own eyes must be aware that it may not be so in the mind of the ecologist, sociologist or even the ordinary man affected by the project.

The mere size of a hydro power project especially the largest ones, and its environmental and sociological impact turns it from a business alone between the engineer and economist or the business men into a political affair.

What is one man's meat is another man's poison, and any project has three aspects: Yours, mine and the facts. Usually engineers and economists claim to concern themselves only with facts (but who knows them perfectly with all their consequences?). Putting aside the impossibility of reconciling the many conflicting opinions, it has to be realized that most public opinion is determined not by reasoning but by emotions; e.g. when deciding on the justification of a nuclear plant many people associate this with the bomb. On the contrary in the case of a hydro power plant, only an infinitesimal minority associates this with the casualities of dam disasters, of dam-induced earthquakes, spreading of bilharziosis, the distress of displaced people, the calamity of rising ground salination, sinking water table, rising erosion, interrupted transport of fertilizing sediments and aquatic food to the detriment of fauna and flora, etc.

This situation should not seduce the planner to dispose of imaginable objections. He should meet them with public consense and by means of studies based on the actual state of knowledge. The latter should not fall short of the planner's responsability range.

A hydro power plant is an investment with relatively high specific initial cost and usually also high total initial cost. The decision to build a plant has to be based on a reasonable purpose, since it absorbs working power or its monetary equivalent for the relatively long period of its useful life in the order of about 40 years.

From the capitalistic point of view a hydro power plant is an investment that has to be remunerative. Once the demand for power and the feasibility of power transmission are given, the investment is usually always lucrative, because of the rising energy demand in the world. Even if the initial cost of a hydro power plant are relatively high especially in the low head range, the balance may be reached by a rather long depreciation period, revenues by an adequate electricity rate, low operating, maintenance and replacement cost, and often by the multipurpose profitability of the plant, such as improvement of navigation, fishery, flood protection, storing water for industry, home and farms and creation of leisure zones, building access roads and exposing an originally unaccessible and remote area to economical development.

The specific initial cost of a hydro power plant depends mainly on the head and size and hence on the rotational speed of the unit. The cost of civil engineering works, architecture, power transmission line, mechanical and electrical equipment depends both on the head and on the type of plant (i.e., whether river run, pumped storage etc.). The actual state of art is reflected by discussing the development of some important rivers.

2.2. Economical aspects of hydro power plants

2.2.1. General remark about feasibility of a project

In general the planning of a hydro power plant has to be based on the principle that the plant has to be economically viable. Strictly speaking this means that the cost of the plant's equipment (i.e., turbines, alternators, transformers, switchgear, high voltage transmission, control rooms) its buildings (i.e., barrage, tunnel, pressure shaft, surge tank, spillway, power house) its erection and assembly, its ground acquisition, indemnification and water easement, its maintainance, repair and service during its useful life and the loan and interest on it during its depreciation period (not to forget the salaries for a reasonable board of directors), must be equal to the earning by sale of energy and other improvements.

The implementation of a hydro power plant withdraws available funds, one of the most scarce goods, from the money market for the rather long period of a plant's useful economical life. Raising the expenses of a plant by borrowing money is the usual practice [2.1 to 2.4]. Bonds and assurance provide for financial safety [2.5].

2.2.2. The electricity rate

In a free market the electricity rate depends on the demand. Therefore it is usual for energy to be much cheaper during the hours of low demand, (e.g. night) than during the peak load hours (usually during the day). Usually certain power stations are designed to meet base load demand, others to meet peak load demand. As the duration of peak load demand is shorter than that of base load and as the cost of a plant has to be covered by revenues during a certain depreciation period, the electricity rate depends mainly on the duration of full load service per year (see Table 2.2.1). Setting the electricity rate implies evaluation of the plant's uses [2.6 to 2.10]. On the other hand in a free market economy, the electricity rate has to cover the initial cost inclusive of interest, and the operating, maintenance and repair. In a multi purpose plant this has to be set with due consideration of earnings due to other benefits, see Table 2.2.1 and [2.11 to 2.17].

2.2.3. The specific investment cost per installed kW

The specific investment cost/installed kW is also an essential factor in planning. Even if this depends on local circumstances, in general, it is lowered by increasing the power installed, and for a given plant with a certain number of sets of a given type (e.g. Francis turbines of a certain specific speed and head), it is also lowered by increasing the speed and hence the specific speed of the set. For the small number of sets which are normally involved, any economic benefit due to quantity production ·by increasing the number of sets may be excluded.

On the contrary for sets which are usually of large size, increasing the number of sets increases also the number of large machine members to be fabricated on large machine tools only available in limited numbers. Moreover it increases the number of accessories, manifolds, control mechanism, the concrete forms necessary for the draft tube, spiral casing and pit. Hence usually the specific cost is lowered by lowering the number of sets in a certain plant.

42

Table 2.2.1. Energy production cost of today, according to Bohn.

Comparison of electricity rates	Hydroelectricity		Thermoelectricity		Nuclear power plant
Duration of service per year (hours)	Lower limit	Upper limit	Lower limit	Upper limit	Mean value
	US $/kWh		US $/kWh		US $/kWh
3000	0,0125	0,04	0,083	0,0923	0,07
5000	0.008	0,03	0,063	0,072	0,05
7000	0,006	0,022	0,057	0,065	0,038

Typical figures of hydro power:

Cabora Bassa, Mozambique:	2 100 MW;	8000 h/year;	0,002 US $/kWh
Inga I + II, Zaire:	1 760 MW;	6800 h/year;	0,0024 US $/kWh
Itaipú, Brazil:	12 870 MW;	5000 h/year;	0,014 US $/kWh
West German Lech:	20 MW;	4700 h/year;	0,02 US $/kWh

Trends in electricity rates:

Year	Hydroelectric multi purpose scheme (irrigation, storing, navigation, protection against inundation) without weighing these purposes	Hydroelectric plants for energy production only	Thermal plant using pit coal (subsidized by government, here West Germany)	Nuclear plant	Year
1975	100%	100%	100%	100%	1975
1981	110%	122%	144%	154%	1981
1984	116%	135%	175%	193%	1984

Once the fabrication of large machine parts on site is excluded, the lower limit for the number of sets results from the transport facilities in the factory and on the roads near the site. In the special case of a plant in a rather broad valley, requiring a large submergence into difficult ground, increasing the number of sets may lower the specific cost. This may apply in the mean head range of 10 to 30 m.

For a given power installed, a certain number of sets of definite type, the specific cost per kW decreases with increase in head up to $H = 800$ m, because the resulting increasing pressure difference on the rotor vane makes the plant more compact.

Hence tidal power plants with the lowest heads down to $H = 1,5$ m (in the case of the Sovjet Russian plant Kislogubskaja in the Mersenj Bay of the Ice Sea) are the most expensive in specific cost reaching in former reports a figure of 10 000 US $/kW in the case of Fundy Bay. Nevertheless in a recent study of A. Douma, G. D. Stewart (Annapolis Straflo turbine will demonstrate Bay of Fundy tidal project, issued by Sulzer Escher Wyss), the so-called B 9 project of the Fundy Bay with 3800 MW was suggested to have a specific cost of only 960 US $/kW.

From about 800 m head on upwards the specific cost rises with the head. Then the power station usually is fed from a reservoir in a remote mountainous area. This requires the building of long and often difficult access roads with longer tunnels (up to 15 km) and pressure shafts or penstocks.

To give further details about specific cost some actual examples of hydro power plants are mentioned in the following.

1) Pumped storage plant with pump-turbines for the generation of railroad traction power (16⅔ Hertz). Langenprozelten, owner Rhein-Main-Donau AG, Munich, Fed. Rep. of Germany, completed in 1977. Head $H = 300$ m, 2 pump-turbines of 75 MW each

with a booster Francis turbine of 30 MW each for starting pumping. Specific cost 400 US$/kW.

2) Low head run-of-river power station with small output Geisling on the upper Danube, owner Rhein-Main-Donau AG, Munich, Fed. Rep. of Germany. Completed in 1983. Head $H = 5,9$ m, 3 Kaplan turbines of 8,5 MW each. Specific cost 1400 US $/kW.

3) The most powerful hydro power (and power) plant of the world with spillway for 58 000 m³/s, built on rocky ground, used as quarry for concrete. 800 km long, 1200 kV DC transmission line for 13 000 MW power block. "Itaipú" on the river Paraná near where it forms the frontier between Brazil and Paraguay both of which share the output. 18 Francis turbines of 718 MW rated output each (12 900 total) at a rated head of 110 m to be completed between 1985 and 1990. Estimate of specific cost: In 1975: 160 US $/kW; in 1979: 1000 US $/kW; in 1984: 1500 US $/kW. Two ± 600 kV DC transmission lines, 1600 km enlarge this about 40%. Builder: International consortium.

4) The largest power plant with a higher head range (300 m) with the largest annual power production of 34,5 TWh (1 TWh $= 10^9$ kWh) up to 1980 (then followed by La Grande, Hudson Bay) located in the "Taiga" of the Labrador plateau with annual average temperature of $- 2\,^{\circ}$C, at a distance of 1200 km from the nearest consumer (Montreal), transmission by 735 kV AC. This plant is 200 km from the nearest railroad station. "Churchill Falls", Labrador, Canada, 11 Francis turbines of 483 MW each (5330 MW total) at $H = 312$ m head. Operated by Churchill Falls Labrador Corporation (CFLC). Specific first cost 200 US $/kW including the 1200 km long AC 135 kV transmission line. Completed in 1970.

In Table 2.2.2, the costs of the above 4 plants are subdivided into the shares due to civil engineering works, reservoir, power house, mechanical and electrical equipment etc. From this it can be seen that these shares depend on the head as well as on the type of plant. For example in a low head run-of-river power station the spillway requires 35%

Table 2.2.2. Cost of components for several types of hydro power plants*).

1) Pumped storage plant Langenprozelten, Federal Republic of Germany built by Rhein-Main-Donau AG Munich:
$H = 300$ m; $P = 2 \cdot 75$ MW.

Parts	Percentage of total cost
Upper storage basin	11,1 %
Pressure shaft without reinforcement	7,5 %
Power house (Underground type)	10,9 %
Tail race basin	13,8 %
Retaining basin	2,56%
Power house architecture and intake structure	2,27%
Total civil engineering	48,13%
Pump-turbines, 2 sets	9,3 %
Main valves, valve-operated booster Francis turbines for speeding up water filled machine to pumping mode, needing up to 40% of rated power. which cannot be supplied from limited Federal German grid for tractive power with single phase AC and 16⅔ Hz.	7,3 %
Piping	0,61%
Lining of pressure shaft	6,35%
Trash rack rake, intake gate, cooling system	1,1. %
Cranes, elevators	0,73%
Total mechanical equipment	25,39%

Table 2.2.2. Continuation.

Alternators (for traction power with single phase AC of 16⅔ Hertz, since 1905 in Germany for reduction of commutator sparking, when using high voltage supply from overhead wire and transformer regulation). | 13,5 %
Transformers | 2,73%
Switch plant and distributing board | 10,25%

Total electrical equipment | 26,48%

---

2) Low head run-of-river power plant Geisling on the upper Danube, Rhein-Main-Donau München: $H = 5,9$ m; $P = 3 \cdot 8,5$ MW; $D = 5,35$ m.

Parts	Percentage of total cost
Architecture of power house	3,8 %
Civil engineering work head water reservoir	20,8 %
Total architecture and civil engineering	24,6 %
3 Turbines (Kaplan turbines)	23,9 %
Cranes	0,648 %
Stop logs	1,07 %
Intake trash rack	0,435 %
thrash rack rake	0,912 %
Covers for grids etc.	0,152 %
Transportation of trash	0,054 %
Workshop for assembly and repairs	0,736 %
Total mechanical equipment	27,907 %
Spillway steel structure	12,2 %
Civil engineering for spillway including stilling basin	21,2 %
Architecture of spillway	0,457 %
Electrical equipment of spillway	0,766 %
Total spillway equiment	34,623 %
Electric installation	0,335 %
Alternator and exciting devices	9,2 %
Switchyard	2,16 %
Transformer	0,683 %
Telephone operating plant	0,16 %
Emergency alarm plant	0,030 %
Inventory	0,31 %
Electrical equipment	12,870 %

---

3) Plant Itaipú, Rio Parana (Brazil, Paraguay):
$P = 18 \cdot 715$ MW; $H = 82,9 - 126,7$ m; DC transmission 1200 kV over 800 km.

Estimated cost in 1979 in millions of US $:

Infrastructure	926	9 %
Civil engineering work	2725	28 %
Diversion of river		4,4%
Barrages, intakes		16,8%
Spillways		4,5%
Power house architecture		2,3%
Mechanical and electrical equipment	1753	17 %
Administration, engineering and supervision	1144	11 %
Interests during construction (10 years)	3476	35 %
Total	10024	

Table 2.2.2. Continuation.

4) Plant-Churchill Falls, Labrador, Canada, Churchill River:
$H = 312$ m; $P = 11 \cdot 483$ MW.

Funds required for	In million US$	Percentage of total cost
Reservoirs	115	12,3%
Power plant and generators	168	17,9%
Switchyard and transmission	100	10,7%
Permanent support facilities	25	2,7%
Temporary facilities and services	83	8,8%
Management and engineering	31	3,3%
Escalation	102	10,9%
Contingency	41	4,3%
Direct construction cost	665	71,0%
Interest during construction	189	20,1%
Administration, overheads, miscellaneous	82	8,9%
Total	936	
Funds originally available:		
Equity paid	83	7,7%
Mortgage bonds	690	64,3%
Retained earnings during construction	150	14,0%
Bank financing available	150	14,0%
Total	1073	

*) For detailed informations on item 1) and 2) the author is greatly indebted to Mr. *J. Grüner*, superintendent of Electromechanic Equipment, Rhein-Main-Donau AG, München, Federal Republic of Germany. Informations on item 3) from different Brazilian and West German sources. Informations on item 4) from a special publication of Churchill Falls Labrador Corporation, New Foundland, Canada.

of cost, in a medium head giant plant like Itaipú only 4,5%. But there instead of the gates and the power house in the low head plant, the barrage appears which takes 17% of the cost. This seems to be comparable with 21% needed in a low head plant for civil engineering work at the head water reservoir mainly consisting in the erection of side dikes, which function as a dam just as the barrage does at Itaipú.

2.2.4. Economic appraisal of the projects[2])

2.2.4.1. The present value method

To establish the economic feasibility of a project, the assets and liabilities which occur during its planning, construction and useful life have to be accounted for. By way of comparison, the cash flow of the project has to be expressed by its present values.

A hydro-power project is an investment. To realize it, the owner has to invest capital at a certain interest rate. This involves his intention to obtain monetary benefits during the useful life of the project. The latter generally differs from the pay-off period, determined by the moment at which the sum of cash flow surmounts the sum of investment.

[2]) This subchapter was stimulated by a lecture Prof. *E. Mosonyi* held about this topic in November 1981 in Haus der Technik in Essen, Federal Republic of Germany. On this occasion the author would like to thank Prof. *E. Mosonyi* for having reviewed this section.

The earnings made by the sales of energy or other benefits derived from the plant, mentioned in Cap. 2.2.2 are expected at such a level that, by good economy, the proprietor will obtain revenues from his capital investment [2.18; 2.19].

The interest rate p depends on the conditions of the loan, such as securities, inflation rate, period of amortization, etc. In this context it may be mentioned that a hydro power plant offers great economic safety for the following reasons. 1) It cannot be removed. 2) Energy is in an ever rising demand.

The planning (P) and erection (e) of the plant usually require various investments, I_p over the $P + e$ years of planning and erection. At the end of this period, i.e., when the energy production begins (instant $t = 0$), the present value of the investment grows up to

$$I = \sum_{t = -(P + e)}^{0} I_p q^t, \tag{2.2-1}$$

where $q = 1 + p$. Similarly all benefits and costs occurring during the financial life time of the project are discounted to this instant. Let us denote by B_j the benefit obtained by sales of energy in any arbitrary year j. In the same year let the annual expenses amount to C_j. They consist of the so-called OMR costs, operation, maintenance and replacement.

At the end of the 'z' years of its useful life, the plant may still have a remaining cash value: R. This corresponds at least to the ground value of the site. Discounting to the instant $t = 0$, i.e., to the beginning of the year in which energy production starts, the present value of the entire cash flow of the project is

$$PV = -I + \sum_{j=1}^{z} (B_j - C_j)/q^j + R/q^j. \tag{2.2-2}$$

In this formula the interest rate p and consequently $q = 1 + p$ may change during the z years of useful life.

A project is defined as profitable if $PV \geq 0$. It is considered as non profitable if $PV < 0$. Sometimes a project characterized by $PV < 0$, is accepted as profitable, if it yields further benefits besides power generation, such as equalization of flow-off, improvement of irrigation, or navigability of the river etc. (Naturally the economic appraisal of such multi-purpose projects is much more complicated: an accurate analysis requires the allocation of the investment costs too.)

2.2.4.2. Internal rate of return method

In this case a constant interest rate $p_0 = q_0 - 1$ results from (2.2-2), under the condition that the present value of the project cash flow PV equals zero. The value of p_0 can be split into an economically acceptable minimum p_1, and an additional value p_2 (profit and/or risk). The profitableness results from p_2. According to *Mosonyi* [2.19], the most economical variant of a project usually is not that one which is indicated by the highest value of p_2.

2.2.4.3. The annuity method

This procedure assumes the terms in (2.2-2) to be: $B_j = B = $ const, $C_j = C = $ const, $R = 0$, $p = $ const, $q = $ const, and $PV = 0$. Introducing the annual balance $A = B - C$, Eq. (2.2-2) yields the investment $I = A \sum_{j=1}^{z} q^{z-j}$ or

$$Iq^z = A \sum_{j=1}^{z} q^{z-j} = A(q^z - 1)/(q - 1). \qquad (2.2-3)$$

This results in an annual balance $A = B - C = a^x I$ or

$$A = a^x I, \qquad (2.2-4)$$

where

$$a^x = q^z[(q - 1)/(q^z - 1)] \qquad (2.2-5)$$

is the so-called capital recovery factor of the investment. It indicates the portion of the present value I of the investment which corresponds to the annual balance A. That means in other words (according to the well-known calculation method for repayment of loans in banking mathematics) those annual net benefits (annual revenues minus annual costs) of constant value A will balance the value of investment accumulated at the end of the project's life time.

2.2.4.4. The benefit-cost ratio

In this procedure, the ratio of all the benefits to the total expenditures is calculated. It can be derived from the present value method or when the case can be simplified, expressed as an average annual ratio by using the terms of annuity computation.

In the first case, by separating the benefit and expenditure terms from Eq. (2.2-2), the benefit-cost ratio of the project is

$$r = \left(\sum_{j=1}^{z} B_j/q^j + R/q^z \right) \Big/ \left(I + \sum_{j=1}^{z} C_j/q^j \right). \qquad (2.2-8)$$

Sometimes this formula is simplified by assuming $R = 0$.

Under the simplified conditions, assumed earlier in 2.2.4.3 the benefit-cost ratio reads

$$r = B/(a^x I + C) = B/(A + C). \qquad (2.2-9)$$

Not in every case, is the cost-benefit factor an economic parameter of the project. Occasionally the annual costs (OMR costs) are split according to $C = C_0 + C'$, where C_0 is the direct cost of operation, maintenance and replacement and C' an expenditure which is not closely linked to power generation (e.g. central administration, marketing and advertising, costs of power distribution, taxes, or even civil engineering expenditures, as dredging of sediments, etc.).

Sometimes this splitting induces planner or owner to consider the annual expenditure C' as a loss in the benefit and not a real cost. Consequently the correct magnitude of cost-benefit ratio is assumed to be

$$r_1 = (B - C')/(a^x I + C_0). \qquad (2.2-10)$$

However this is not true and may be misleading. Obviously $r_1 > r$, when $r > 1$. Consequently, this distortion of r involves the temptation for manipulation. The following example illustrates this situation.

Given: $B = 3000$ US$ per annum, $a^x I = A = 1000$ US$/a, $C_0 = 250$ US$/a and $C' = 250$ US$/a. Hence the proper relation yields $r = 3000/(1000 + 500) = 2,0$, whereas r_1 results in an unrealistic high value $r_1 = (3000 - 250)/(1000 + 250) = 2,2$, which is 10% higher than the true value r.

48

However, the benefit cost ratio should not be completely abandoned in the planning, since it may be a useful figure for "screening" alternative solutions of a certain project.

2.2.4.5. Production cost of energy unit, electricity rate

The specific investment cost of a plant is defined as $I_s = I/P$, where P is the installed capacity. Using the above terms, the total annual cost related to 1 kW capacity is $a^x I_s + C/P$. On the other hand, with a load factor φ, the annual utilization time under rated load P equals $8760\,\varphi$ hours. Accordingly the unit power produces $8760\,\varphi$ kWh per annum. Thus the production cost per kWh equals

$$k_e = (a^x I_s + C/P)/8760\,\varphi \text{ US\$/kWh.} \tag{2.2-11}$$

If the annually produced and saleable energy is known as E kWh, the unit production cost results

$$k_e^x = (a^x I + C)/E \text{ US\$/kWh.} \tag{2.2-12}$$

k_e^x is mainly used in the first phases of planning, when a decision on installed capacity is still open. In this case, it is also common to relate C/P, i.e., the OMR costs, to the specific investment cost I_s by a rough estimate on the basis of experience and statistical data. Hence from (2.2-11) the electricity rate

$$k_e = (a^x + a_0)\,I_s/8760\,\varphi = a\,I_s/8760\,\varphi. \tag{2.2-13}$$

For a preliminary calculation of the energy unit cost, the annual utilization hours have to be assessed. In many cases, this can be done to a fairly good approximation by evaluating the hydrological conditions and by estimating the power demand.

Numerical example: $I_s = 1000$ US\$/kW, $a^x = 0{,}082$ (presuming $p = 0{,}08$ and $z = 50$ years), $a_0 \approx 0{,}018$ (estimate), $\varphi = 0{,}6$ (run-off-river, base load plant). Accordingly, the utilization time is $0{,}6 \cdot 8760 = 5256$ hours, and the unit energy production cost, or the electricity rate is

$$k_e = (0{,}08 + 0{,}018) \cdot 1000/5256 = 0{,}019 \text{ US\$/kWh.}$$

2.3. The hydro power development of some large rivers

2.3.1. The Tennessee (USA)

Cotillon [1.1] says that the valley of the Tennessee is rather small compared to the other great arteries of hydro electricity. But this is the first complete exploitation of a river for power production, flood regulation, improvement of navigability, enlarged water supply for irrigation and industrialization. The development of its main course was accomplished between 1936 and 1945 by nine power plants with a head range from 12 to 27 m. Its productivity is 9,6 TWh. (1 TWh = 10^9 kWh). Its discharge of 1900 m³/s is the fifth largest for a river in the USA. The Tennessee is really formed in Knoxville near the confluence points of Holston, French River and Petit-Tennessee. From there to its meeting with the Ohio, it has a length of 1050 km with a drop in elevation of 145 m.

2.3.2. The Columbia (USA, Canada)

The Columbia flows from the Canadian Rockies to the Pacific with a length of 2000 km. Its course within the USA is 1100 km length with a drop in altitude of 386 m and consists

of two distinct parts. The upstream reach where the gradient is large (0,05%) and the enclosed valley has seven barrage power plants with heads generally between 22 and 54 m with a highest value of 105 m (crest height) at Grand Coulee and the lowest of 12 m at Rock Islands, the power station with the most powerful existing bulb turbines, see Cap. 10.2 and [1.1].

The downstream reach with a mean slope of 0,025% contains four schemes with heads between 18 and 32 m, and a fifth site of 13 m head which is not as yet completed. The regulation of the water is effected by two Canadian Reservoirs (19,2 km^3 capacity). The production attained is 75 TWh with an installed output of 11 700 MW in 1975. After putting into service the two Canadian reservoirs, the installed output will attain 26 000 MW and the productivity 92 TWh. In 1975, the catchment area of the Columbia with 24 plants of an installed capacity of 20 000 MW was producing 112 TWh (42% of the USA's hydroelectricity).

The most powerful hydroelectric groups in operation in the world namely Grand Coulee III with 3 · 600 and 3 · 700 MW rated output together with Grand Coulee I and II each of 1125 MW and a pump station with 350 MW comprise an installed rated capacity to date at Grand Coulee of 6480 MW.

Sirman describes the turbines of Grand Coulee III from the point of view of the planner [2.20], Pfafflin [2,21] from that of the maker, and Engström [2.22] from that of the owner.

Fig. 2.3.1 shows the 700 MW runner (weight 450 tons) on weld positioner. The whole was welded from cast pieces of shroud, hub and vanes on site, then stress-relieved in a furnace placed over the welded runner by a smaller crane and statically balanced and refined by grinding the labyrinth and shaft flange faces. The runner has an outside diameter of nearly 10 m and an overload output of 837 MW (= 1,135 million hp!). The shaft of this turbine (see Fig. 2.3.2 and 10.3.1) is welded together from rolled liners of 190 mm thickness, 3,2 m diameter (see Chacour [2.23] and Cap. 10.3.1).

A ductile electrode was used for the butt welds joining the runner vanes to the hub and shroud. This was then stress-relieved at 650 °C for 30 hours. The welded material had a yield point of 3600 bar, a tensile strength of 5100 bar and a percentage elongation after fracture (British = U.T.S. strain) of 42%. The spiral casing (see Fig. 2.3.3 and Cap. 10.3.1) was welded on site from 42 mm thick plates rolled earlier at the manufacturer's works (Allis Chalmers, Milwaukee, Wisconsin, USA, see [2.24]).

The outer diameter of this parallel plate spiral casing was reduced to transmit its meridionally directed pull towards the innermost diameter of the water passage wall of the head and bottom cover of the stay vanes. Any flow disturbance caused by the extension of the stay ring's parallel plates into the spiral casing was eliminated by toroidal metal sheet guides. They also deflect the secondary flow of the spiral casing from the inlet of the gate channel (see Fig. 2.3.2). The stay vane and their rings were constructed so as to equalize the highest combined tensile and bending stress (caused by the meridional pull of the spiral casing) on the midspan of all the stay vanes. Thus the highest stressed point was moved from the outside edge of the largest vane at the spiral tongue to the inside edge of the smallest vane [2.23].

The head cover uplift was entirely balanced by the download of the hydraulic thrust introduced from the thrust bearing via a spider into the concrete surrounding the stay vane crown.

The wicket gate of cast carbon steel has two bearings (see Fig. 10.3.1). According to Chacour [2.23], this presents several advantages over the usual three bearing arrangement, namely:

50
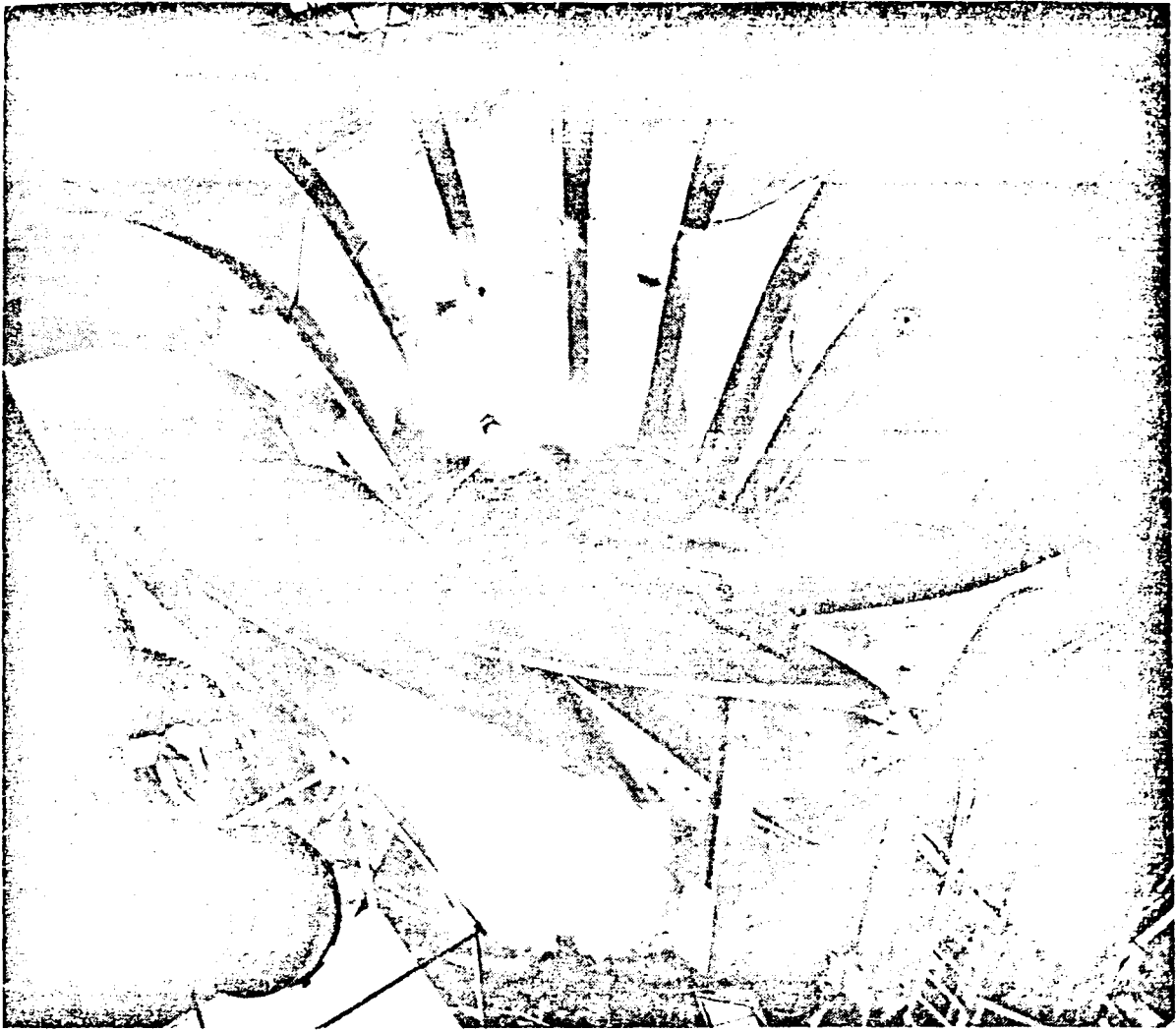
Fig. 2.3.1. 800 MW runner of Grand Coulee III, Columbia river, Washington, USA (owner Bureau of Reclamation). 3 sets: $H = 87$ m, $n = 85,7$ rpm; originally rated as 700 MW, but actually uprated as $P_{max} = 837$ MW ($= 1,123$ million hp!), built by Allis Chalmers. Runner on a weld positioner on site, weight 450 t. (Photograph courtesy Allis Chalmers Corp., Milwaukee, Wisconsin, USA.)

1) In a three bearing system a high bending moment is induced at the junction of the gate stem and blade by the differential pressure across the gate. This moment combined with a large torque produced by the servomotor during the squeezing of the gate acts at a point with very high changes in area and sectional modulus, thus creating a fatigue problem. In a two bearing system the maximum bending moment acts at the midspan of the blade, which provides a large sectional modulus and is insulated from the above torsional moment.

2) Bearing loads on two bearings are substantially lower than on three bearings resulting in a reduction of servomotor capacity.

3) The shorter stem of the gate increases its torsional rigidity.

4) The axial depth and hence the rigidity of the head cover can be increased independent of the gate stem length.

5) The machining of the head cover is greatly reduced to a single setting on a boring mill.

6) The stresses in the blade of the gate do not depend on the deformation of the head cover (see Fig. 2.3.2).

To avoid any clamping of the gate mechanism by deformation of the head cover, the joints on both ends of the link were made spherical. The four double acting gate servomotors are accomodated in

51
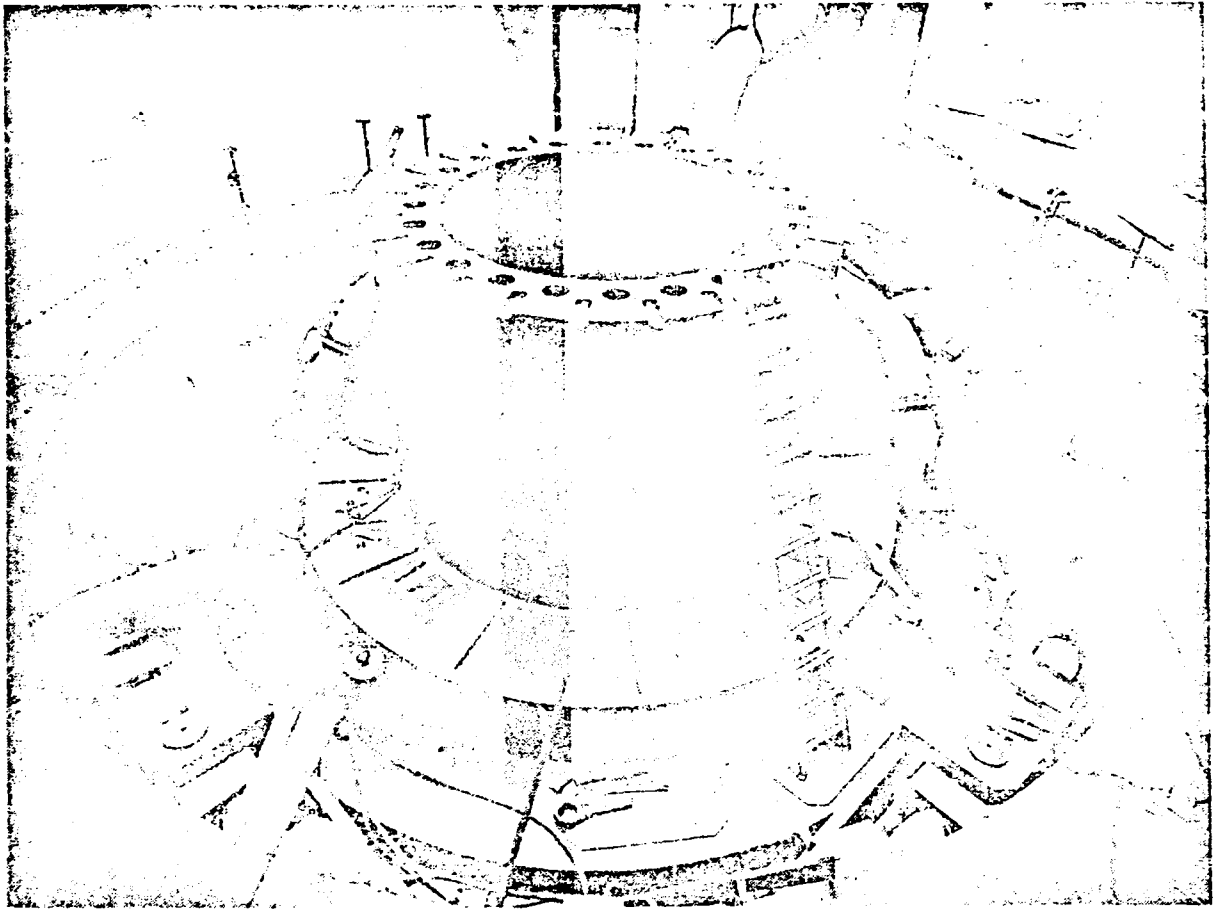
Fig. 2.3.2. Head cover. gate servomotor, shaft of a Grand Coulee III FT. Note drive of gates is housed in the head cover. Thus its upper plate can be used as an inspection platform, and also gives high rigidity, only 2 gate bearing, a saving of height on the machine pit. (Photograph courtesy Allis Chalmers Corp., Milwaukee, Wisconsin, USA).

the head cover which is axially deep and thus rigid. This arrangement facilitates preassembly and keeps the concrete free of servomotor load. Moreover the cover plate of the head cover can be used as an inspection platform (Fig. 2.3.2).

The high head cover also enables the radial pull from the stay vane crown to turn the cover about a tangential axis against a sense in which the uplift on the inner head cover would turn the cover. This inner head cover also supports (see Figs. 2.3.2 and 10.1) the shoe type lower journal bearing, the gate shifting ring and the floating shaft seal.

In smaller machines, the head cover's uplift is usually balanced by leading the axial thrust onto the head cover instead of leading via a spider on the concrete of the pit of the set. This also counteracts the pressure in the spiral casing.

The bell form of the shaft at this bearing also provides lubrication at start-up. The machining of this bell shaped part of shaft located very close to the lower shaft flange was made possible by the inward orientation of the shaft flange. This also brings the bearing centre very close to that of the runner.

The rolled plate tubular shaft design provided excellent torsional and lateral rigidity versus weight ratio. The torsional buckling resistance greatly exceeds the maximum stalling torque imposed by a locked rotor. The large shaft diameter (Fig. 2.3.3) provides sufficient peripheral speed for the pads. It also allows the torque to be transmitted through friction, although radial dowel pins provided added safety, e.g. in case of short-circuit-induced torque. In this context also general experiences of field welding are of interest, as reported by *Akhtar* [2.25].

52
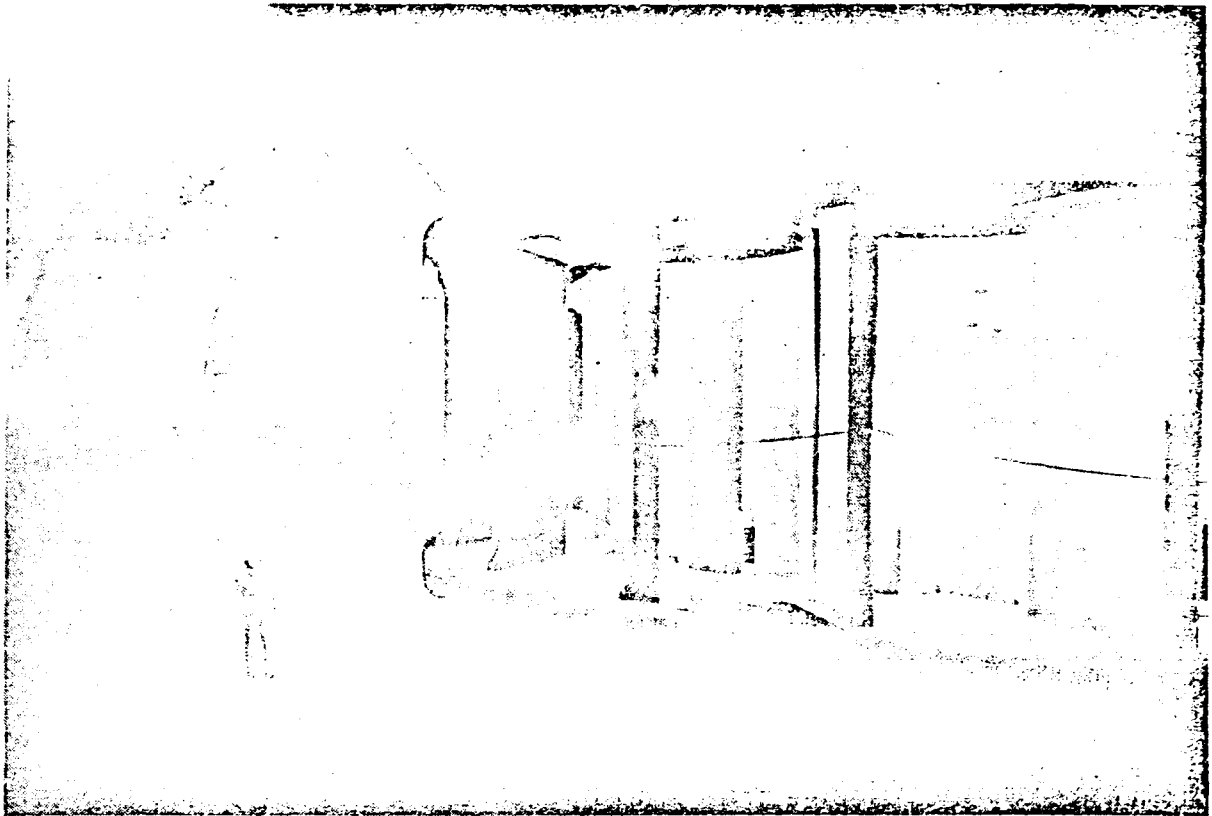
Fig. 2.3.3. Spiral casing, parallel plate type stay ring with smooth toroidal intake nozzle, stay and guide vanes of Grand Coulee III FT (Courtesy Allis Chalmers Corp., Milwaukee, Wisconsin. USA).

2.3.3. The Paraná (Brazil, Paraguay, Argentine)

The Paraná is formed by the confluence of the Rio Grande (1000 km) and the Paranaiba (900 km). Its total length inclusive of Rio Grande is 3300 km. Its average discharge of 16000 m³/s is double that of the Volga. Its drop in elevation is 350 m as compared to the Volga's 140 m. The precipitation rate of 7 l/s/km² in its catchment area is 17 % above that of the Volga [1.1].

The Paraná crosses first the southern part of Brazil then it forms the frontier between Paraguay and Brazil and then between Argentina and Paraguay. At the point where it starts crossing Argentina, the Paraguay flows in. Both rivers have the same length (2500 km) from source to confluence point and catchment areas of nearly the same size (1 100 000 km² the Paraguay and 840 000 km² the Paraná). But as it drains a dryer basin the Paraguay reaches only 40% of the average discharge of the Paraná.

The Paraná then enters Argentina at an elevation of 50 m in a vaste alluvial plain. There it is complete and receives only insignificant tributaries; moreover the banks of the river are very low (Cap. 1.2.1.3).

Three divisions may be distinguished along the course of the Paraná. (2100 km with 330 m level drop.) After the first 500 km with an average slope of 0,025% the slope changes quickly to 0,16% along the 60 km of the Sete Quedas falls when it enters the frontier section between Brazil and Paraguay. Here the Paraná leaves the Brazilian plateau, it retains a slope of 0,015% over the following 130 km. Here is Itaipú, the site

53

of the largest power plant in the world under erection. Downstream its slope is reduced to only 0.005% along a distance of 1410 km.

The harnessable drop of river level is 300 m and the potential due to it 172 TWh. This potential of the proper Paraná has to be added to the 85 TWh of its mother rivers, yielding in 1985 an installed power of 14 000 MW. Moreover in Brazil the Tiete and the Paranápanema, tributaries on the left river bank of the Paraná are nearly entirely developed with power plants of 15 000 MW capacity. Thus the basin of the Paraná will have in 1985 an annual production of 200 TWh realized by 65 000 MW installed capacity, of which 14 200 are due to Argentina. Table 2.3.1 gives information about its 9 power stations [1.1].

Table 2.3.1. Data of power stations along the Paraná river.

Plant	Head m	Output MW	Work TWh	Number	Type	State
Ilha Solteira	49	3 200	15	20	Francis T	operating
Jupia	24	1 400	6	12	Kaplan T	operating
Porto Primavera	17	1 750	8		Kaplan T	
Ilha Grande	18	2 600	8		Kaplan T	
Itaipú	95	12 840	57	18	Francis T	under erection
Corpus	45	4 500	30		?	
Yacyreta Apipe	30	4 000	18		Kaplan T	under erection
Argentine plant 1	12	3 400	16		Bulb T	under erection
Argentine plant 2	13	2 300	16		Bulb T	under erection

Of these Ilha Solteira is the largest operating plant as to power capacity within the southern hemisphere. It has Francis turbines (FT) with a rated head of 49 m, rather low for a FT. The reader may be surprised to read that since 1962 Kaplan turbines (KT) of 50 m rated head and 70 MW output have been working in the Brazilian plant Tres Marias (Fig. 10.2.8). One argument in favour of FT in the above case is the large number of sets (20). This enables then to work near the bep even with the rather narrow working range around the bep of such a high specific speed FT by switching on and off the appropriate number of sets to meet the changing demand. A KT here would have required a larger runner diameter and hence a more expensive set. Further the relative small head fluctuations of Ilha Solteira would not have justified a KT. Moreover fatigue cracks in runner vanes of KTs have warned the planning staff about possible troubles with a KT of 160 MW which up to the present has not been built for 49 m head.

Itaipú (see Figs. 2.3.4 and 2.3.5) which has been under erection since 1975, and should probably be completed in 1985 with a capacity of 12 840 MW and provision for additional 8000 MW [2.26] will for a long time thereafter be the largest power plant in the world. For its completion the neighbouring states Brazil and Paraguay, signed a treaty in 1966 by which, according to the international law they agreed that the energy delivered by Itaipú should be divided into equal portions between the countries.

The plant will operate with 18 FTs. 715 MW each built by a consortium consisting of the French firm Neyrpic, Grenoble in collaboration with the affiliated Brazilian firm Mecanica Pesada, Taubate and the West German firm J. M. Voith, Heidenheim and her subsidiary company in São Paulo, Brazil. ·

Since the Paraguayan 50 cycle grid has only a capacity of about 300 MW to date, the first FT coming into service for Paraguay has to be equipped with a sophisticated aeration device, [2.27] to facilitate as smooth as possible operation even under an abnormal low part load of about 10%. Moreover
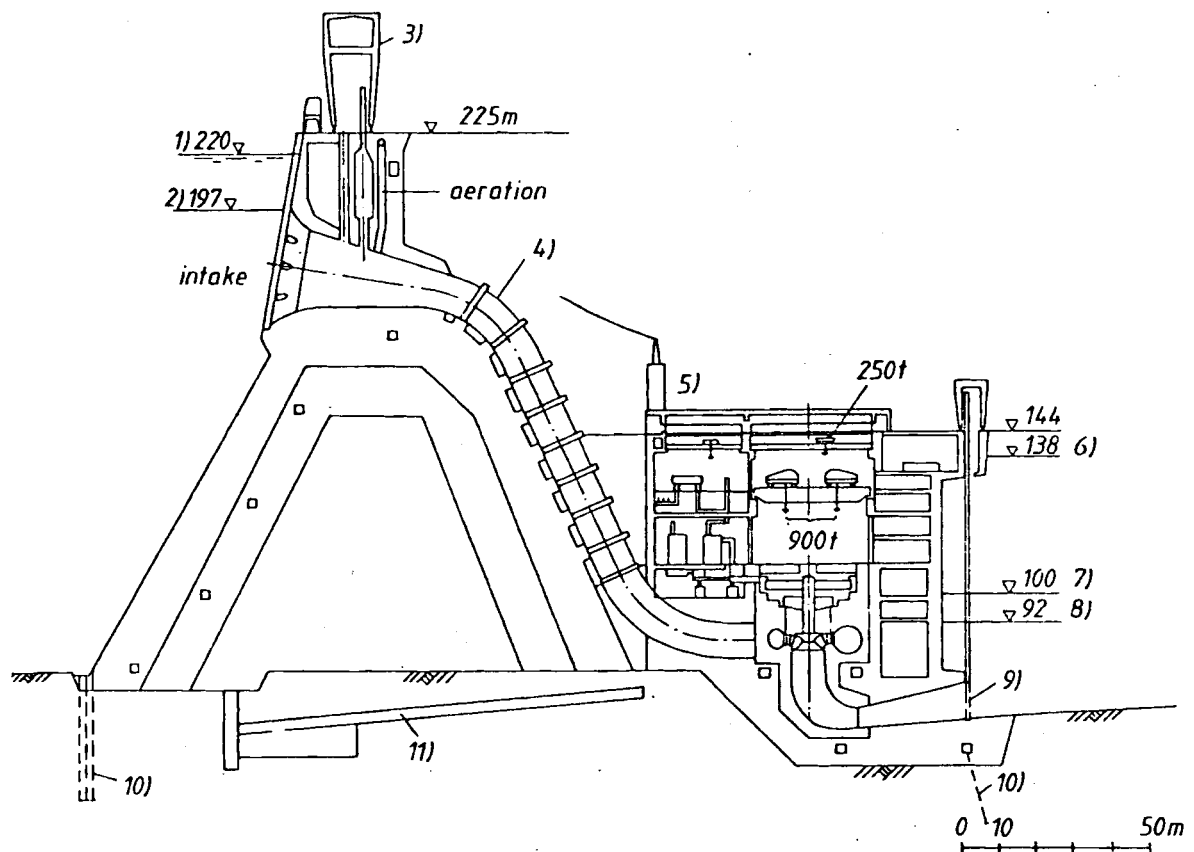
Fig. 2.3.4. Sectional view of a hollow dam and power house, Itaipú, Rio Paraná, Brazil, Paraguay (owner Itaipu Binacional). Under erection: 18 sets with FTs P_t = 715 MW, P_m = 740 MW. Largest hydropower plant: n = 92,3 rpm (60 Hz) of 9 Brazilian sets; n = 90 rpm (50 Hz) of 9 Paraguayan sets. Turbines designed in close collaboration by Neyrpic, Grenoble, France and J. M. Voith, Heidenheim, West Germany, and manufactured partly by Brazilian subsidiary companies. Runner weight 350 tons, throat diameter (see next figure) = 8,1 m. Generator rated at 900 MVA, rotor diameter 16 m, weight 2000 tons, gap clearance 29 mm. Designed by Siemens, Erlangen, West Germany in close collaboration with Brown Boverie & Cie. Baden, Switzerland and manufactured partly by the Brazilian subsidiary companies. The semi water-cooled generator has the same weight and size as the similar generator of the 507 MW Krasnojarsk set (H = 101 m) built 20 years earlier in the USSR, having only 66% of the iron utilization factor of Itaipú. 1) maximum head water level 2) minimum head water level 3) stop log main crane 4) penstock (10,5 m diamcter) 5) main transformer 400 kV 6) maximum tail water level 7) normal tail water level 8) minimum tail water level 1), 2), 6), 7), 8) yield a head range H = 82,9 to 126,7 m. Hence the output range P = 400 to 740 MW. 9) stop log 10) grout curtain, 11) control tunnel. (Drawing courtesy Neyrpic, Grenoble, France)

provision is made that the Paraguayan sets supply preliminarily the Argentine and Brazilian grid with 60 cycles by means of converters and in the case of Brazil also via a high voltage DC transmission line of 1200 kV to the next consumer centre São Paulo 600 km distant [2.26].

For design data of Itaipú see Table 2.3.2.

The turbines with 8647 mm outermost diameter and 350 Mp runner weight were finished in the shops and then transported complete to the site [2.29]. The reported initial cost of 1000 US $/kW of the power station with an estimated annual production of 70 TWh enables a rather low electricity rate estimated at 0,014 US $/kW (estimate 1979).

55
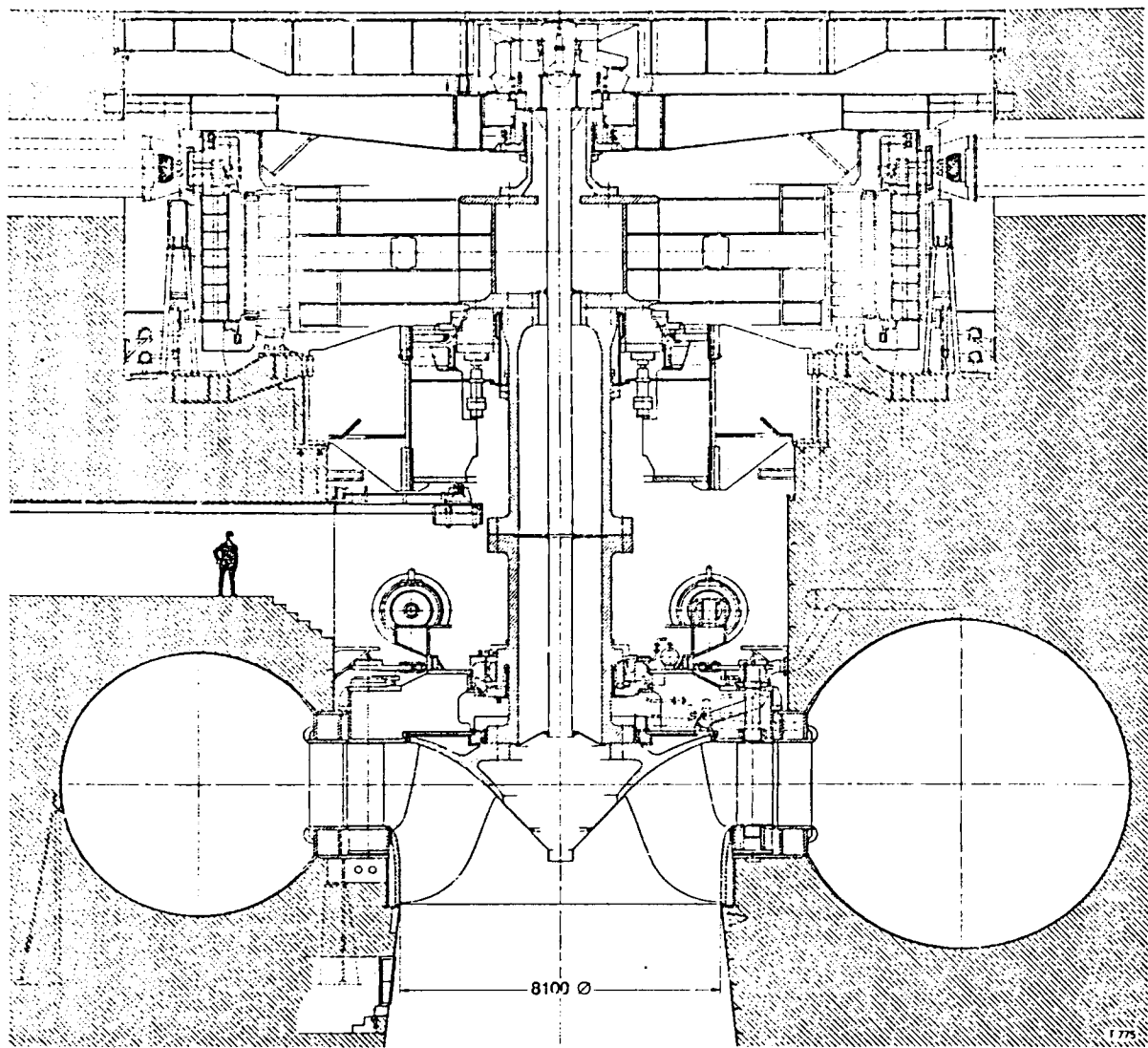
Fig. 2.3.5. Elevation of Francis turbine Itaipú, Rio Paraná, Brazil, Paraguay (owner Itaipú Binacional) built by Neyrpic, Grenoble, France in close collaboration with J. M. Voith, Heidenheim, West Germany. Data: $n = 90(92,3)$ rpm (see Fig. 2.3.4.), $H = 126,7 - 118,4 - 112,9 - 98,7$ m; $P = 740 - 740 - 715 - 560$ MW. 18 sets. (Drawing courtesy J. M. Voith, Heidenheim, West Germany)

A transfer of technical know how and drawings to the Brazilian subsidiary companies Voith São Paulo and Mecanica Pesada engaged in the construction was urged by the World Bank. Naturally it has been urged also with respect to fabrication. Thus the runners have to be made from Brazilian steel, to be fabricated in the workshops of European subsidiary firms in Brazil.

In this context it may be mentioned, that, at the moment, Brazil, Argentina, and Mexico are the only Latin American countries in which heavy hydro electric equipment can be fabricated with foreign assistance. In this respect, Venezuela, where Guri, the world's second most powerful plant is being erected, relies on foreign imports [2.30 to 2.36].

2.3.4. The Yenissei (USSR, Siberia)

1) Generally: The Yenissei has the third highest discharge in Asia after the Yangtse and Brahmaputra (Yarlung Zangbu) and has the highest catchment area, discharge and

Table 2.3.2. Design data of Itaipú [2.28; 2.27].

Number of sets: 18.
Head range: 82,9 m–126,7 m; output range: 400 MW–740 MW; rated output: 715 MW; runner tip diameter 8,75 m (this because of the larger head is somewhat smaller than in Grand Coulee with 9,9 m). Largest axial extension of runner 4,5 m; rotational speeds 92,3 and 90,9 rpm for 60 and 50 Hertz respectively. Runaway speed 175 rpm. Distance of adjacent sets 35 m. Diameter of spiral inlet 10,5 m. Alternators 18 · 765 MW nominal output. Length of power house 900 m (this size takes care of the 18 sets envisaged at first and 8 additional sets).

Catchment area for the plant: 820 000 km². Average discharge per year: 9070 m³/s.

Storage basin: Surface area: 1355 km². Length: 200 km (this rather modest figure for a power plant with 100 m head in contrast to Bratsk with 550 km results from the extraordinarily steep slope of 0,16% over 60 km river length; for comparison 0,02% on the Angara around Bratsk). Live storage volume with 23 m level drop: 19 km³. Barrage: Length: 1643 m. Maximum crest head: 170 m. (Taller than the towers of the cathedral of Cologne). Lateral rock dikes: Length: 2800 m. maximum height: 60 m, lateral earth dikes: Length: 3700 m, maximum height: 30 m. Type: Hollow gravity dam. Bottom outlet: Number: 8, total discharge 6000 m³/s. Spillways: Number: 14, dimension: 20 · 20 m, total discharge: 58 000 m³/s (this is 45 times greater than the Danube has on at least 100 days before it leaves West Germany). Penstocks: Number: 26, mean diameter: 12,2 m.

Civil engineering work: Excavation: Diversion channel (to be blasted in the rocky underground): 12 · 10⁶ m³, for barrage: 2 · 10⁶ m³, dikes: 3,8 · 10⁶ m³, spillways: 14,7 · 10⁶ m³, power house: 4,25 · 10⁶ m³. Concrete (to be obtained by blasting the rocky ground at site): Barrage: 7,9 · 10⁶ m³, spillway: 0,75 · 10⁶ m³, power house: 2 · 10⁶ m³, total structure: 10,75 · 10⁶ m³. Rock and earth: Total volume of excavated rock: 3,4 · 10⁶ m³, volume of lateral rock filled dikes: 16,65 · 10⁶ m³, total volume of earth filled dikes: 3,2 · 10⁶ m³. Material for construction: Cement: 1,85 · 10⁶ Mp, sand: 4,3 · 10⁶ m³, mixture of concrete: 8,6 · 10⁶ m³. Reinforcement: 71 400 Mp.

length of the four large Siberian rivers Yenissei, Ob, Lena and Amoor. After the Zaire (Congo), Brahmaputra, Yangtse and Paraná, it is also the river with the largest harnessable potential in the world.

Along the 1250 km of its upper course three plants are projected: Chevelig, Seybinsk and Ouyouk. For the following section of 900 km where its slope is still steep (0,04 %), three plants are in service or being developed. 1) Sayano Shushensk under erection since 1963 (23,8 TWh); 2) Mainsk probably under erection (3,4 TWh); 3) Krasnoyarsk, in service since 1978 (20,4 TWh) [1.1].

These stations are remarkable also for their large installed output. Sayano Shushensk has 12 FT with 222 m head and a total rated output of 6360 MW (the fourth largest after Itaipú, Guri II and Grand Coulee I-II-III). They were built in the Leningrad Metal works (Leningradskij Metaliceskij Zavod = LMZ) the greatest maker of hydro and steam turbines in the USSR. During a visit to the LMZ in Leningrad (11 years since his previous visit at which he saw the runner of Krasnoyarsk in the LMZ) the author saw the model runner of Sayano Shushensk with about 600 mm outmost diameter equipped with strain gauges for stress measurements. Simultaneous tests then had been carried out on the model of the plant's ski jump spillway above the power house at the base of the dam.

Lenin who, by the way, spent some years in Sayano Shushensk in his Siberian exile, tried later to make up for Russian backwardness by coining the slogan "Socialism is Soviet power plus electrification", which now can be read in the interior of many power houses in the USSR.

2) Krasnoyarsk: 12 FTs each of 507 MW at 101 m rated head. These turbines (Fig. 10.3.2) which have been in operation since 1978 also were made at the LMZ and were for a long time the most powerful water turbines and well known for their advanced cast-welded construction, and for the

water cooled rotor and stator of the alternator. A rather small runner tip diameter resulted in a nearly hook-formed runner vane with a rather thick and round nose and an inlet angle of nearly 90°. The runner of 250 Mp weight, welded together from cast steel hub and shroud sections with stumps for the 14 vanes, was transported by a special ship via the Lenin canal, Ice Ocean and upstream the lower course of the Yenissei. Contrary to the usual recommendations, the number of gates is an integer multiple, namely twice the runner vane number. This together with the rather blunt runner vane inlet edge parallel to the shaft may cause a noisy operation of the sets; which was also reported.

Another feature is that the welded spiral casing has 2 intakes (Dwuchnaja spiralnaja kamara) which should obviously lower transportation weights, but also may reduce radial force and secondary flow in the volute casing. The welded shaft of 2,3 m diameter has a water lubricated lower journal bearing. The Mitchell thrust bearing rated at 3400 tons is supported by a conical trunk on the head cover. The gates are operated by two pairs of opposite plunger servomotors, mounted on the head cover, [2.35].

The exploitation of the middle Yenissei is yet to be carried out. The development of the lower Yenissei (1250 km with 0,006% slope) has been made in two steps: Ossinov and Igarka.

Speaking of the harnessable potential of the Yenissei proper, has excluded its greatest tributary the Angara. This famous and only outflow of the Baikal Lake has a length of 1850 km and a drop in level of 378 m between Baikal and its confluence with the Yenissei. The average slope of the Angara is 0,02%, but the depth of the valley permits development at three sites having 76 to 106 m head and at four other sites with smaller head.

The first plant in service is Irkutsk with 31 m head and 8 KT of 82,5 MW each with vibrating oil heads above the alternators. Irkutsk serves partly as an outflow regulator for the huge 700 km long reservoir of the Baikal Lake. In a typical Soviet manner the spillways were built here as by-pass outlets around the semi-spiral casing and draft tube of each machine and act during spillage as a head enlarger by virtue of the hydraulic jump then formed past the draft tube outlet (see Fig. 3.3.2). This facilitates also the deflection of ice floes during the very cold (temperature drops down to − 50 °C) and long lasting winter in this region of nearly 0° average temperature.

On account of the large specific heat of water, the heat insulation of the ice sheet and the heat flow from the interior of the earth, all the great northwardly flowing Siberian streams crossing about 1500 km of perma-frost-soil do not freeze completely even in winter time whilst at the river mouth there are zones with − 17 °C average temperature.

3) Bratsk: This is the next station in service downstream of Irkutsk with an annual production of 22 TWh. This was the greatest station output before the inauguration of Churchill Falls in 1970. After commissioning Grand Coulee III in 1979, La Grande 2 in 1980, Sayano Shushensk and Itaipú (between 1985 and 90) Bratsk then will be the fifth largest plant on the basis of annual energy production. With respect to its output of 4050 MW Bratsk was the most powerful station from 1962 until 1968 when Krasnojarsk started. Now it is the fourth largest after Krasnojarsk, Gran Coulee I-II-III and Churchill Falls.

Also the high voltage transmission of 500 kV built with the assistance of Savoisienne (France) was the first of this type. The 220 MW FTs once were amongst the most powerful, consisting of integrally cast runner halves, bolted together on site with welded shaft, and having 14 runner vanes.

The reservoir of Bratsk with a capacity of 169 km³ remains however the largest artificial lake located in the midst of the nearly everlasting virgin needle forest of Siberia, the so-called Taiga.

It is closed by a 1500 m long and 110 m high gravity dam with a 400 m long power house on its base (Fig. 3.4.49). Owing to the time taken to fill the reservoir, energy production of Bratsk started with a half filled basin. This caused a rather noisy stalling cavitation in

the midst of the rotor channel, which was eliminated by injecting air at the rotor vane's inlet edge [2.36].

A symbol of Soviet power, "victory of men over nature in concrete, the New Jerusalem song of the poet Yevtushenko, the shop window of Siberia, Bratsk has been all of these for the pioneers of its period of construction" says *Hendrick Smith* [2.37]. But now other giants have appeared.

In the north of Bratsk begins the perma-frost soil. In this zone such work as tunnelling and digging the foundation of dams and buildings becomes extremely difficult. Any larger construction in the course of time melts the upper layer of the soil by heat transfer, destabilizing its foundation. Such troubles were envisaged at the northern sites of the Angara like Ust Ilim and Bougatchany, the first of which is being put to work the second probably yet under erection.

2.3.5. The Volga (USSR, European part)

With its length (3700 km) its catchment area (1 385 000 km^2) and its average discharge (8000 m^3/s), this is the twelveth river in catchment area and the fifteenth in length [1.1]. Its slope within the harnessed section varies between 0,012 and 0,002%. With a mean value of 0,04% it is one tenth of that of the Columbia. Its development will be made by nine barrage power plants with heads between 11 and 24 m of which two remain up to the moment only as projects. Its actual annual output is 29,5 TWh at 7100 MW installed capacity and its final values will be 39,5 TWh and 10 270 MW.

The plant "22nd Congress" at Volgograd (formerly Stalingrad) with a head of 23 m is the third low head plant ($H < 30$ m) in annual output (11,1 TWh). The reservoir of Kouibishev is the second largest artificial lake in surface area (6450 km^2).

Inaugurated in 1960 with its 22 KTs of 116 MW and 9,4 m runner diameter, the 22nd Congress plant has had for a long time the largest Soviet manufactured huge KTs with the largest runner diameter. In Western KT plants the runner diameter is only up to 8,4 m, e.g. in the 4 · 70 MW plant "Asch-ach", Danube, Austria. The actual largest runner diameter in the world of a KT is 11,3 m at the Chinese Changjiang plant Gezhouba ($P = 2 · 178$ MW, rated head 18 m, maximum head 27 m). These machines are similar to Western design (e.g., runner servomotor with movable cylinder underneath the blades) and operate smoothly. Moreover Gezhouba has KT sets with 10,3 m runner.

The original Volga plants were provided with fish passes about 9 m in length in its casings, to enable the migration at spawning time of the big Volga sturgeon, the Beluga (Accipenser huso), which reached a length of 9 m [2.38]. This is the producer of the Beluga Malasol (mildly salted) Caviar, a valuable export for foreign currency. But now, when the size of runners has grown up to 9 m the Beluga when ready to spawn is reduced to 2 m. (Note animals inversely proportional to machines!)

2.3.6. The Zambesi (Zimbabwe, Mozambique, Africa)

The Zambesi has the third largest catchment area (1 330 000 km^2) and discharge (3500 m^3/s) in Africa, and is the forth longest there (2660 km). Its catchment area is at rather high altitude half of its course being above 500 m. But it lies also in an area with 26% less rainfall than the Russian Angara, namely 2,8 l/s/km^2. Downstream of the steeply inclined reach following the Victoria Falls (0,16% along 250 km) it has a mean slope larger than 0,04%.

The slope is even 0,07% over the 250 km long reach now submerged by the reservoir of Cabora Bassa. There are two large barrages: Kariba (125 m crest height) in Zimbabwe

(formerly Rhodesia) and Cabora Bassa (160 m crest height) in Mozambique forming two of the largest artificial storage basins in volume, surface area and length, namely:

Kariba: 160 km³, 5180 km², 280 km. Cabora Bassa: 60 km³, 2700 km², 250 km [1.1].

The harnessable potential of the Zambesi (130 TWh) is of the same order as that of the Yenissei (140 TWh) because of its highly elevated area. But the development of these resources has numerous political problems.

The Cabora Bassa station which is shown in Fig. 3.4.55, and whose energy is mainly exported to the South African Republic, has to date been constructed in its first phase only (power house on the southern river bank) with 5 sets of 415 MW resulting in a capacity of 2075 MW. The rated discharge is 1974 m³/s (average discharge there 2750 m³/s). Hence the spillway of the ski jump type is to operate nearly continuously. The 18 TWh annual output is the largest in the southern hemisphere and Africa. The specific initial cost in 1974 was 180 US$/kW.

The Francis turbines (FT) of the first phase were assigned to a French German syndicate (Neyrpic Grenoble, France and J. M. Voith, Heidenheim Fed. Rep. of Germany). They are, by their rated output of 415 MW, the most powerful turbines ever built in a West German workshop. At a rated head of 113,5 m, their runner diameter of 6,56 m is relatively small. This results in a runner weight of 165 Mp, modest compared with the 1000 Mp of its alternator rotor (see Fig. 3.4.16).

Nevertheless these weights and dimensions were beyond the transportation facilities in Mozambique. Therefore the runner made in the workshop of a European firm, was split along a plane normal to the axis (see Fig. 2.3.6). The upper vaned part was integrally cast with the hub from stainless steel (17% chrome, 4% nickel). The shroud was welded from integrally cast pieces made of stainless steel (13% chrom, 14% nickel). The lower part of the runner vanes was cast from the same stainless steel as the shroud.
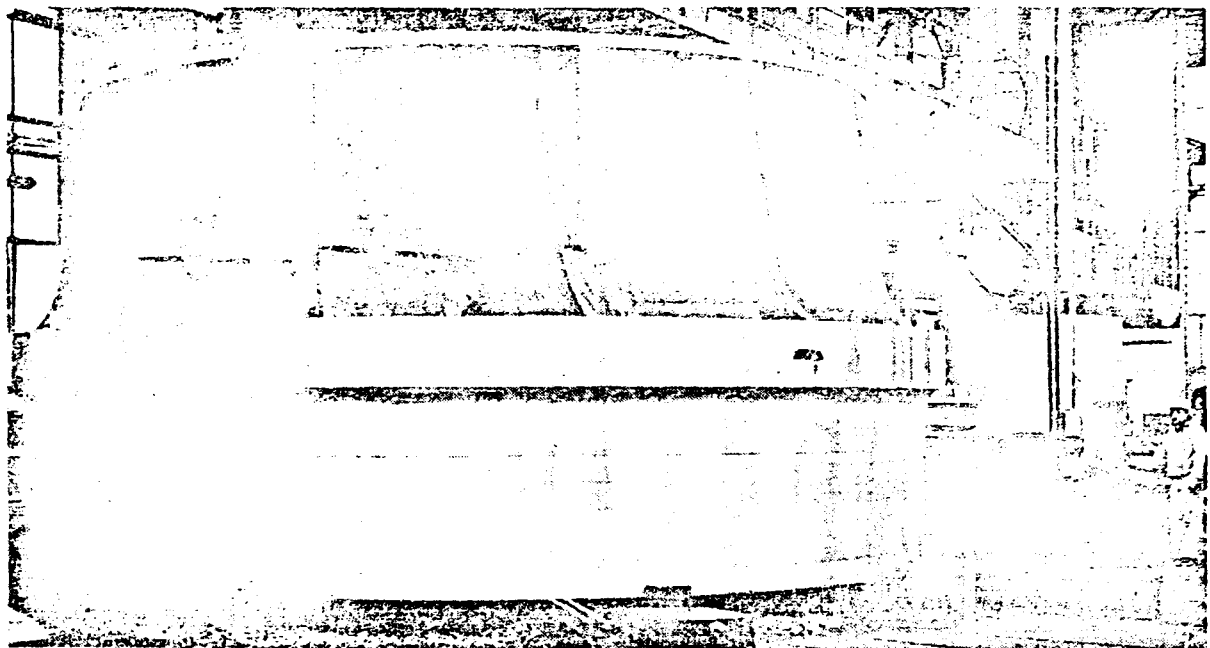
Fig. 2.3.6. 415 MW Francis runner of Cabora Bassa. Zambezi, Mozambique, Africa, on two column lathe in Voith works. Heidenheim, West Germany, split into two halves for transporting. Note flaps to retain good alignment. Runner: weight 165 tons, throat diameter (see also Fig. 3.4.16) 6,56 m. Designed and manufactured in close collaboration by J. M. Voith, Heidenheim West Germany and Neyrpic, Grenoble. France. (Photograph courtesy J. M. Voith, Heidenheim, West Germany).

After finishing, it was welded to the shroud. For assembly before and after transport, the vane at the joint of both sections were equipped with flaps, later removed. The welding of the two halves of the runner on site was followed by static balance and finish. Normalizing was not required.

Because of the long distance of 1400 km to the main consumer in Pretoria (South African Republic) a high voltage DC transmission of 1000 kV was provided, based on thyristor technique. Strictly speaking, a DC of 1000 kV has ± 500 kV against earth.

On account of the cost of converters at both ends of the line the application of DC transmission is only economical for lines longer than 500 km without an intermediate consumer. Therefore the transmission of Cabora Bassa can be considered as typical for the further development of water power in remote areas [2.39; 2.40].

2.3.7. The Danube

In harnessed potential (43 TWh), length (2850 km), average discharge at its mouth (6400 m³/s), the Danube ranks second in Europe, behind the Volga (for comparison: Rhine, 14,7 TWh, 1300 km, 2200 m³/s). Its harnessed potential is about 30 TWh. Its catchment area is 817000 km² (only 13,5 % of the Amazone's).

The Danube comes from the confluence of the two small rivers Breg and Brigach (which have their sources in the German Black Forest) at an altitude of 680 m near Donaueschingen (Federal Republic of Germany). It starts passing the Jura mountains at Tuttlingen where at low water it seeps completely into the ground then feeding the catchment area of the Rhine by the Ache at Lake Constance (altitude 390 m). Through its passage through the Jura (about 200 km long) it continues to lose water up to its confluence point with the Iller near Ulm. In consequence of the seepage into Jurassic ground, the first 269 km long reach of the German Danube with its available head of 335 m cannot be economically exploited. This is reflected by the small installed capacity of only 7 MW along this reach.

Here the Iller, its first Alpine tributary has a much larger discharge than the Danube. Hence any effective harnessing of the Danube starts from here at an altitude of 477 m.

Over the next 378 km of the German and finally the mixed German-Austrian section up to Jochenstein, the Danube has a mean slope of 0,045 % and a drop in level of 175,2 m. A cascade of 24½ power stations with an annual output of 2,64 TWh and an installable capacity of 430 MW is planned along this reach. 19½ stations are already in service.

In the following Austrian and finally mixed Austrian and Czechoslovakian section of 330 km length the Danube has a mean slope of 0,043 % and a drop in level of 149 m. 12 power stations are planned with an annual output of 14,6 TWh and an installable capacity of 2402 MW. To date 3½ of them, namely Jochenstein (by ½ of its production), Aschach and Wallsee Mitterkirchen and Ybbs Persenbeug are equipped with vertical shaft Kaplan turbines and the residual plants with bulb turbines. Altogether they have an annual production of 8,75 TWh and an installed capacity of 1450 MW.

In the following mixed Czechoslovakian-Hungarian section the river's slope falls to 0,006 %. Therefore any passage of the Danube at low water becomes difficult. To improve the navigability, the river is diverted into a 142 km long channel. A drop in level of 51 m is used by 2 channel power stations now under erection: Gabcikovo and Nagymaros with an installed capacity of 850 MW and an annual output of 3,98 TWh.

The following Yugoslav section of the mean Danube of 436 km length with an average slope of 0,006 % and a drop in level of 27 m will be used by the plant Novi Sad with

1.5 TWh and P = 250 kW, already projected. In the next mixed Rumanian and Yugoslav section of the mean Danube, 402 km long, the drop in level is 42,5 m, and the slope rises occasionally up to 0.03 % at the site of the Iron Gate I (Yugoslavia's Djerdap, Rumania's Porte Ferile). The Iron Gate I plant, equipped with vertical shaft Kaplan turbines, has been operating since 1970. The Iron Gate II plant equipped with bulb turbines, is now under erection.

The following 480 km long mixed Yugoslav, Bulgarian and Rumanian section with a level drop of 21 m will have 3 plants equipped with bulb turbines only projected, with 9.2 TWh annual output and 1560 MW installed capacity altogether, [2.41]. The last section cannot be harnessed. It borders on the USSR.

The site of the Iron Gate I [2.42] with an annual output of 11,4 TWh and an installed capacity of 2140 MW, is the biggest river power plant in Europe with the world's most powerful Kaplan turbines of 178 MW unit output.

This turbine has a runner diameter of 9,5 m. It is the 3rd largest in the world after the Chinese Gezhouba turbines (11.3 m) and the Russian Saratov turbines (10,3 m). It was designed by LMZ (Leningradskij metaliceskij zavod = Leningrad Metal Works). Three of the 6 Rumanian units were fabricated in the Reşiţă Works I, Rumania. According to the author's impression the turbines
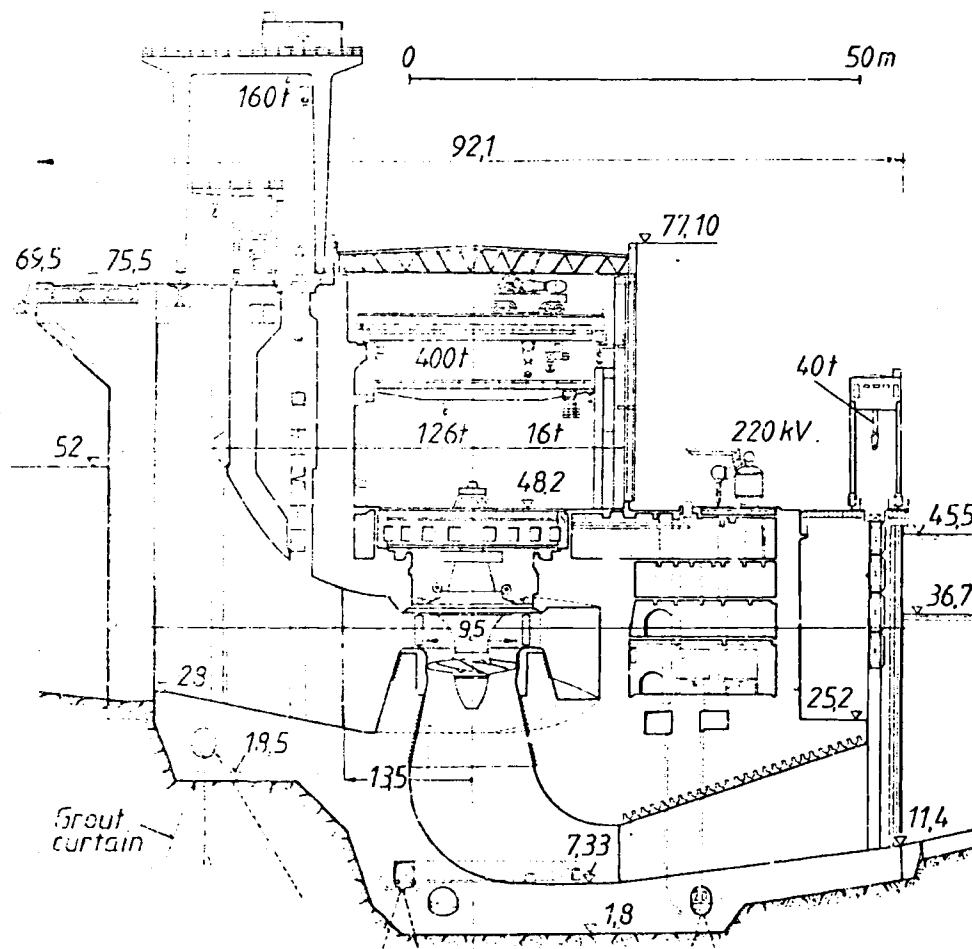

Fig. 2.3.7. Longitudinal section of the power house and Kaplan turbine set at the Iron Gate, Danube. Rumania. Yugoslavia (owner 6 sets Rumanian state power board, 6 sets Yugoslavian state power board) H = 21.6 to 35.46 m; n = 71,5 rpm; P_r = 178 MW; 12 sets designed by Leningrad metal works (LMZ). 3 sets manufactured by Resita Works, Rumania (Drawing courtesy Resita Works, Rumania).

operate rather smoothly, but some of the Rumanian units suffered badly from cavitation pitting after one year of full load operation, see Fig. 10.2.7.

The power houses on each river bank each have 6 vertical shaft sets with Kaplan turbines of 6 runner blades [2.42], (see Fig. 2.3.7 and Table 2.3.3).

Table 2.3.3. Data of the Iron Gate plant (Rumania, Yugoslavia).

Mechanical equipment: Designed by LMZ Leningrad. 3 sets machined at Resita Works Rumania. The power house on each river bank has each 6 vertical sets with Kaplanturbines each with 6 runner vanes.

largest net head	35,46 m	
rated head	27,16 m	
smallest head	21,6 m	
head for temporary operation	10–18m	
rated discharge	732	m^3/s
rated output	178	MW
rotational speed	71,5	rpm
runaway speed	180	rpm
guaranteed efficiency	94	%
runner tip diameter	9,5	m
total weight	1400	t
control system oil pressure	40	bar
maximum crane capacity	$2 \cdot 400 + 2 \cdot 160$ t	
Generators (three phase, 50 Hz)		
rated output	190	MVA
voltage	15,75 kV	
power factor	0,9	
guaranteed efficiency	98,2	%
total weight	1300	t
transformer voltages	15,75/220 kV and 220/400 kV	

Spillway:
14 Double hook sluice gates for discharging 15 500 m³/s width 25 m height 14,8 m. Volume 620 000 m³ concrete, separation abutment thickness: 7 m.
Maximum width: 440 m. Maximum height 60,60 m.
Barrage:
Type: Gravity dam. Length of whole barrage inclusive of power house 1100 m.
Power house type: Tall hall. Number: 2. Length 210 m. Maximum height inclusive draft tubes: 84,2 m
Storage basin:
Maximum length: approximately 200 km (backwater reaching upstream of Belgrad).
Inundated area 101 km². Reconstructed roads: 160 km.
Reconstructed railroads: 24 km.
Historical sites such as the table of Trajan, the city of the Island Ada Kaleh have been conserved in a museum.

Volumes:

Excavation of alluvial soil	18 000 000 m³
Rock excavations	5 000 000 m³
Concrete simple reinforced	3 200 000 m³
Earth dam	5 000 000 m³
Rock dam	2 500 000 m³
Electromechanic equipment	68 000 t
Costs at European level	395 million US$

*) From a special issue on the Iron Gate Plant of the Resita Works, Rumania.

A remarkable feature of this plant is the rather large area of 101 km² of mainly arable and inhabited land, which was inundated by damming the Danube. New houses had to be built for 22 934 persons, 160 km roads, 24 km railroad lines mainly in tunnels and on bridges, and 7 harbours had to be reconstructed. 18 % of the total cost of 395 millions of US$ had to be paid for indemnification and ground acquisition. On the Danube see also [2.46 to 2.49].

2.4. Exceptional sites

2.4.1. Churchill Falls (Churchill River, Labrador, Canada)

Nearly the whole plateau of Labrador is drained by the Churchill River. At a distance of 300 km from its mouth it eats into the plateau over 35 km as a deep gorge with a mean slope of 0,9 %. This contains the Churchill Falls with a drop of 75 m. For this latitude the precipitation is remarkably high (20 l/s/km²).

According to Cotillon [1.1] for this catchment area of 79 000 km² only the Italian Po has a greater figure namely 22 l/s/km². The mean discharge (1600 m³/s) is modest. In drop of level along the developed river section (323 m) the Columbia, Paraná and Angara are nearly equal.

The discharge and spillway operation of the Churchill Falls is nearly completely regulated by numerous lakes of glacial origin regrouped into one lake of nearly five times the original surface area by the construction of small earth-filled dikes of 10 m average crest height and a total length of 64 km. Under this the Smallwood reservoir (28 300 hm³) can be distinguished, mainly constructed to divert the drainage of many of these original lakes from the Goosebay river system into the Churchill. The exploitation of the available head of 323 m is made by one single power station. The energy production started in 1970.

With its annual output (34,5 TWh), Churchill Falls headed until 1982 all the power stations in the world. Now La Grande 2 heads with 35,8 TWh. Work has also started on another development, Gull Island (1800 MW, 12 TWh) 200 km downstream of Churchill Falls.

In the words of Cotillon [1.1] the high head of 312 m, the elevated precipitation rate, the nearly complete regulation of the discharge by one tremendous reservoir, the topographic conditions which reduce nearly all the civil engineering work of storing and collection render Churchill Falls an exceptional site [2.43].

– Data of site: Annual precipitation 765 mm. Temperatures: Range – 48 °C to 30 °C, average annual – 4 °C. Topography: 396 m to 580 m altitudes. Hills rise 150 m above the plateau level. Water level lower Churchill River gorge at power site 129 m. Vegetation: Shallow muskeg and irregular spruce forest. Surface Geology: Irregular deposit of silty sand, gravel and boulders in random thickness up to 12 m.
– Data of plant: Dikes: Number 88, average height 9 m, maximum height 36 m, longest 6041 m total volume of material used 20 · 10⁶ m³, largest volume of a single dam 1,95 · 10⁶ m³. Reservoirs: Smallwood and Ossokmanuan with 65 000 km² surface, 31 100 hm³ storage volume, 6510 m³/s discharge capacity, 88 800 m³ concrete.

– Power installations: Gross head 323 m, 11 units with P_r = 475 MW. Vertical FT, spiral casing embedded in concrete without shut off valve on the inlet except for the gate at the penstock intake (see Fig. 2.4.1). Wicket gates operated by a pair of servomotors opposite each other on the pit wall. Thrust bearing supported by conical trunk on head cover. Two journal bearings. Runners from Dominion Engineering with vane leading inlet edges parallel to the shaft, from Marine Engineering (licensee of Neyrpic) with dihedral angle to cut more smoothly the wakes past the gates.
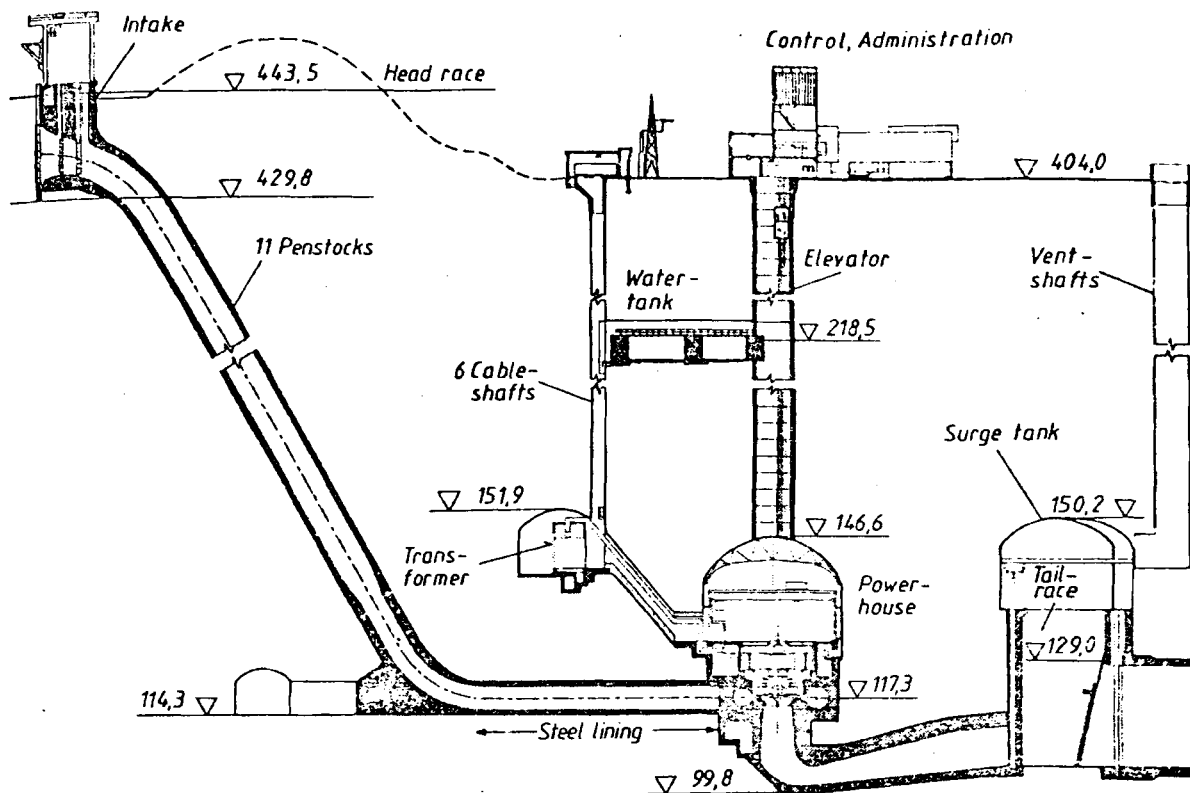
64

Fig. 2.4.1. Schematic longitudinal section of plant and power house Churchill Falls, Churchill River, Labrador, Canada (owner Churchill Falls corp.) 11 sets with FTs designed by Neyrpic Grenoble, France and manufactured by Marine Engineering Canada and Dominion Engineering, $H = 312$ m, $n = 200$ rpm, $P = 483$ MW. (Drawing from Public relation office Churchill Falls Co.)

According to tests carried out by Netsch, the design with inlet edges parallel to the shaft is noisy [2.44]. The compact design, the elastic response of its stationary welded parts to wakes past the spiral tongue, stay and guide vanes, and then cut by the runner vanes, the concentration of losses on a cylinder of about 6 m diameter, first of all due to vortex generation, these altogether create such a noise in the turbine pit, that the use of ear plugs is imperative and hence a special noise, caused by damage, is hidden from the human ear.

Other details are the gate levers with breaking bolts. This is a rather risky device in a turbine with no shut off valve with such a long penstock. The obvious saving of this omission has been balanced by the planning staff against the possible damage under a sudden load rejection, simultaneous reaction of breaking bolts and subsequent runaway.

The bottom of the elbow draft tube is 3 times the runner throat diameter underneath the throat to prevent the entrance of air from the surge chamber downstream by a level drop under a sudden load decrease. The whole machine is a very compact design. Pertinent data see Table 2.4.1. Elevation see Fig. 10.3.3.

Energy transmission: By transformers in two stages from 15 to 220 kV in underground transformers and then by transformers in the outdoor switch yard up to 735 kV for the 1200 km distance to the next consumer. In unpopulated areas the towers have only one abutment on the earth kept in upright position by anchored cables.

– Townsite: The remote area needed the erection of a townsite with an airport offering a regular air service to Montreal, 1200 km distant. The permanent town site, which was

Table 2.4.1. Design data of Churchill Falls power plant.*)

Turbines:			Generators:		
Rated net head	312	m	Rated capacity	500 000	kVA
Rated output	483	MW	Rated voltage	15	kV
Rated speed	200	rpm	Power factor (overexcited)	0,95	
Runaway speed	330	rpm	Synchronous reactance	100	%
Scroll case inlet diameter	4,45 m		Transient reactance	33	%
Runner inlet diameter	5,82 m		Inertia constant	3,47 min	
Runner throat diameter	4,30 m		Rotor diameter	9,11 m	
Runner weight	77,1 t		Rotor weight	576	t
Total weight	907,0 t		Stator core depth	2,98 m	
			Total weight	1020	t

Penstocks:
Number: 11. Length 426 m. Internal diameter-concrete lined: 6,1 m. Internal diameter – steel lined: 4,45 m.

Powerhouse:
Maximum length: 296 m. Maximum width: 24,7 m. Maximum height: 45,1 m.

Surge chamber:
Length: 233 m. Width (varying): 12,2 to 19,5 m. Height: 45,1 m.

Vent shaft:
Diameter: 6,1 m. Depth: 253 m.

Tailrace tunnels (unlined):
Number: 2. Width: 13,7 m. Height: 18,3 m. Average length: 1692 m.

Transformer gallery:
Length: 261 m. Width: 15,2 m. Height: 11,9 m.

Cable shafts:
Number 6. Internal diameter: 2,13 m. Average depth: 264 m.

*) From a special publication of the Churchill Falls Labrador Corporation, New Foundland, Canada.

utilized by construction staff initially, provides housing, shopping, medical and security services for the residents. Accommodation is provided. For the population and the public a conservation programme was implemented to preserve and protect the natural environment.

Permanent residents number about 900. Of these one third are for the maintainance of the access roads, the roads to the airport and the airport itself, another third are employed in plant operation. The remaining third are employed in the service sector and on the plant as white collar workers. It seems advisable to operate in such a remote area even a highly automated plant with a staff of white collar men capable of operating the plant by themselves in an emergency.

– Financing: Cost estimates established the capital required to complete the development at 936 · 10⁶ US $. To meet this requirement the largest financial assistance ever undertaken for a single industrial enterprise was negotiated.

2.4.2. Inga (Zaire, Congo) Africa

Due to its second largest catchment area (3 800 000 km²) the rather high altitude of this area even in its lower course and the high precipitation (30 l/s/km²) the Zaire (Congo) has the largest harnessable potential (700 TWh).

In Kinshaha-Brazzaville the Zaire is completely formed even though it has an altitude of 300 m. The following section constitutes the Inga Rapids with 100 m level drop along 15 km (see Fig. 2.4.2). Taking into account the considerable average discharge (42 000 m³/s) these rapids are the site, where the biggest harnessable hydroelectric potential in the world of 300 TWh is concentrated. This is about the annual electricity production of West Germany in 1973.
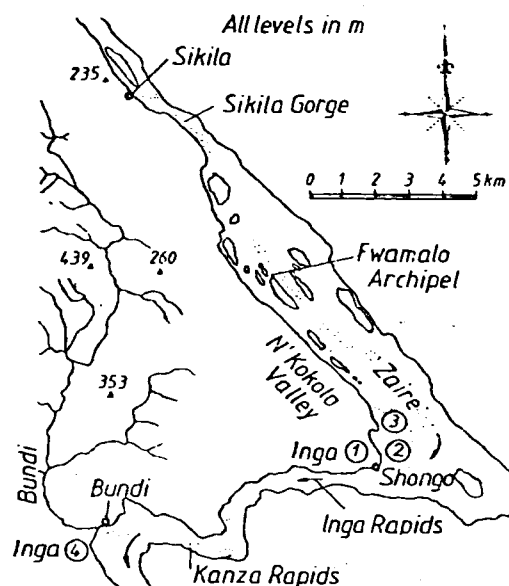

Fig. 2.4.2. Location of the sites of the Inga schemes 1, 2, 3, 4 on the Zaire River (late Congo), Zaire, Africa. Schemes 1 and 2 operating. Large scheme 3, in the planning stage, will short-circuit the schemes 1 and 2. Usable potential of scheme 3 : 300 TWh. (For comparison: 1973 electricity consumption of West Germany (the world's forth largest consumer after USA, USSR, Japan): 369 TWh in 1983.) 4: large project.

According to *Cotillon* [1.1] the development of the site could be accomplished in the following two ways.

The first consists of a diversion of part of the discharge without a barrage through a gap on the right river bank into the dead valley of N'Kokolo (formerly van Deuren) where the barrage of Shongo creates a head of some 60 m: Annual output 26 TWh. The second way consists of a diversion of the whole river under low water conditions into the valley of Bundi tributary (see Fig. 2.4.2), at whose mouth a barrage of 150 m crest height was built earlier. Annual output: 300 TWh achieved by a number of convenient stages for the development of the power house. The large project shortcircuits the small project.

In the small project which has been preliminarily chosen, the completion could be done in two or three stages, namely Inga 1 (in service) 350 MW; 2,4 TWh; Inga 2 (in construction) 1350 MW; 9,6 TWh; Inga 3 (in project) 2000 MW; 14 TWh. Hence the small project could attain a final output of 3700 MW at 26 TWh [2.45].

As for the large project, to date its implementation fails because of a lack of power demand in a distance, which facilitates an economic power transmission.

2.5. Small hydro power schemes

On account of widely varying topography and hydrographs, the hydro power schemes show a great variety of designs. To be competitive with large hydro power schemes, small schemes as their opposites have some special features.

Small hydro power schemes may range as "micro plants" from 0,02 to 1 MW installed capacity, and as "mini plants" from 1 to 10 MW. Contrary to the limited number of large

plants, small hydro power schemes exist in great number. Sometimes they are the first step in using a site of larger harnessable potential; see [1.34 to 1.42].

Most small plants mainly of "micro power" type are located in remote areas of the Third World with a low population density, usually near to a smaller township with a grid, or near to a village without any electrification. In the first case, the consumer may be a factory or a hospital etc., in the second case the village itself. In both cases no essential and long electric transmission line has to be installed, which favours the economical feasibility of the plant. When the small plant is connected with an existing relatively larger AC grid the speed control can be omitted. In the absence of a larger grid the small plant supplies a grid by itself. Then some speed control becomes necessary.

In countries with a large usable potential not yet harnessed, small hydro power plants may be erected first on the more economical sites. In countries with largely exploited hydro potential, the small hydro power plants usually are using the less economical small rivers with their strongly varying duration line.

In the case of economically feasible sites with falls, rapids or great slopes of the river, the latter is usually by-passed through a simple diversion, or a simple run-of-river scheme as possibly rapids turbines (Cap. 10.2). On a small river with irregular supply and a flood flow relatively high compared with the rated flow of the plant, again a simple diversion should be applied. Any diversion has the economical advantage that it saves the cost of barrage and spillway at net head and also the cost of dams along the river itself. Thus the civil engineering works, which normally account for two third to one half of the total initial cost, may be considerably reduced.

Intakes are the Achilles heel of small hydro power schemes and their design is of crucial importance. For very small intakes of about 0,5 m^3/s, a skip design has been developed, where water and sediments jump right over the intake during flood flow. Combined with a riprap-lined stilling basin, this device has developed into cheap and effective intakes for maintenance-free operation. At any rate sedimentation in the intake channel has to be prevented. Usually the intake has a screen and a stop log, which at low head may save the installation of any gate or valve before the turbine inlet.

There is a continuous debate over the merits of maintenance-free versus ease-of-maintenance for small hydro equipment. The first reduces the labour requirements and the servicing cost, the second requires personal visits and then reduces the possibilities of break downs through lack of regular visual inspection. The second should be preferred when skilled labour is readily available in the supporting community, but the first has many advantages when building small schemes in underdeveloped countries, neighbouring the region in which the plant is manufactured.

The usual low head and the low installed capacity of small hydro power schemes make their specific investment cost/installed kW extremely high. Therefore the initial costs of the scheme's components have to be reduced. They are the cost of:

1) transmission line,
2) civil engineering works,
3) speed governor and other control devices,
4) power house,
5) accessories of each sets such as main, valve, device for starting, synchronizing, shut down, limiting overspeed etc.,
6) generator,
7) turbine.

68

The absence of a transmission line, a simple diversion or run-of-river design, and the absence of any submergence meet the requirements of both the first cost terms.

The elimination of conventional turbine speed governor, not only because the governor of small machines is itself an expensive constructional member, but also its removal, permits further simplifications to the turbine (removal of gate, needle or runner blade adjustment equipment), particularly when high efficiency is not a dominant concern.

The conventional speed governor may be eliminated if the turbine is operated, e.g. at constant flow and constant load. To achieve this also when the machine supplies a grid by itself, some designs have used hydraulic or eddy current brakes. But recently, a strong interest has been in the control of speed by rapid adjustment of electrical load. This can be done, e.g. by switching frequency-controlled separate dummy resistors across the alternator terminals. The energy dissipated may be used to heat water or to produce hydrogen by electrolysis. In plants connected to a larger AC grid, the speed is retained by the magnetic force between the armature and the rotary field of its stator. Here the load can be set at will by means of an opening limiter (Cap. 11.2).

In a not too cold and rainy climate, the cost 4) of the power house may be considerably reduced by locating the whole set or its generator (S-tube turbines or bulb turbines with bevel gear) in the open air, there possibly protected by a box or a dry shelter.

The cost 5) of accessories for each set can be reduced by installing one generating unit. This is only compatible with varying demand if the turbine has a flat curve of efficiency versus its load, as for example with multi-cell cross flow turbines of the *Michell-Ossberger* type, inclined-jet impulse turbines of the "Turgo" type, ordinary impulse turbines or any kind of action turbine, and double, or runner-blade-adjusted reaction turbines (usually axial turbines); but both the latter are rather expensive.

If efficiency is no dominant concern, e.g. when the plant uses a river with a wealth of hydro potential, then the multi-cell cross flow or the inclined-jet impulse turbine should be preferred for their simplicity (cylindrical plates as rotor vanes).

The cost 6) of the generator can be substantially reduced by a simple step up spur gear or a less simple bevel gear (bulb turbine). This is usually possible in low and medium head plants. It may be remembered (Cap. 10.5) that any gear can be converted into an over-speed protection of the generator (which also makes the generator cheaper) by means of a speed-operated clutch between the gear casing and its base.

The major characteristics of a cheap direct coupled small generator are:

a) In vertical sets, the axial thrust is carried by a generator bearing.

b) The set has a greater propensity to overspeed. In the predominant low head range the rotary parts may be not overstressed during runaway. Here runaway may correspond more to an idling of the set. This holds especially for very small low head units where countermeasures against runaway, after an alarm signal, occasionally are released by hand operation of the inspection personal.

c) The generator requires an extra inertia usually in form of a separate fly wheel to reduce overspeed at sudden load rejection.

d) Cooling is effected by means of air from outdoors. Moreover roller bearings prevail in the smallest units.

When the output is below 6 MW, the exciter can be saved by applying an induction (asynchronous) generator. This requires reactance compensation from extra capacity in associated synchronous machines, or from special capacitors if the set supplies a grid by itself (so called isolated operation).

The cost to the manufacturer of skilled labour at far distant sites can be reduced considerably or eliminated if turbine and generator are mounted on a common base plate in the manufacturer's factory. This is an easy procedure for small sets with a horizontal shaft equipped with cross flow or impulse turbines, see Figs. 3.4.9 and 10.

To reduce the cost 7) of the turbine, a simplified design should be preferred, e.g. flow admission through a pit at the end of a flume, removal of any adjusting mechanism, low number of stay and guide vanes, linkage for gate adjusting mechanism in water, self or water lubricated bearings of shaft and trunnions, roller bearings, conical hub or plane disk hub, cylindrical shroud, removal of shroud, cylindrical forms for vanes and buckets, avoidance of any submergence. Such a design may lend itself to large volume production at low unit cost, or it may be manufactured in a Third World workshop using local labour and readily available materials.

According to *Bachmann* [2.50] standardization is justified in the output range from 0,1 to 2 MW and for heads from 2 to 800 m. Reducing this only to the geometry of the turbine, the runner diameter should be tailored to the working data of the site, especially in countries with scarce energy resources.

3. Survey and classification of essential devices of a hydro power plant

3.1. Introduction and survey

The various machines and devices, which are found in hydro power plants can be imagined to exist in a river diversion power plant. This simplifies the introduction of all the possible structural members, their variety, their purposes, their falling out of use and eventual omissions. For example, in the case of a run-of-river power plant the diversion section is reduced to the turbine.

Fig. 3.1.1 shows the elements of a diversion power plant in elevation and plan. Most of these members exist in special forms due to the particular requirements of an individual plant but mainly depending on the head.
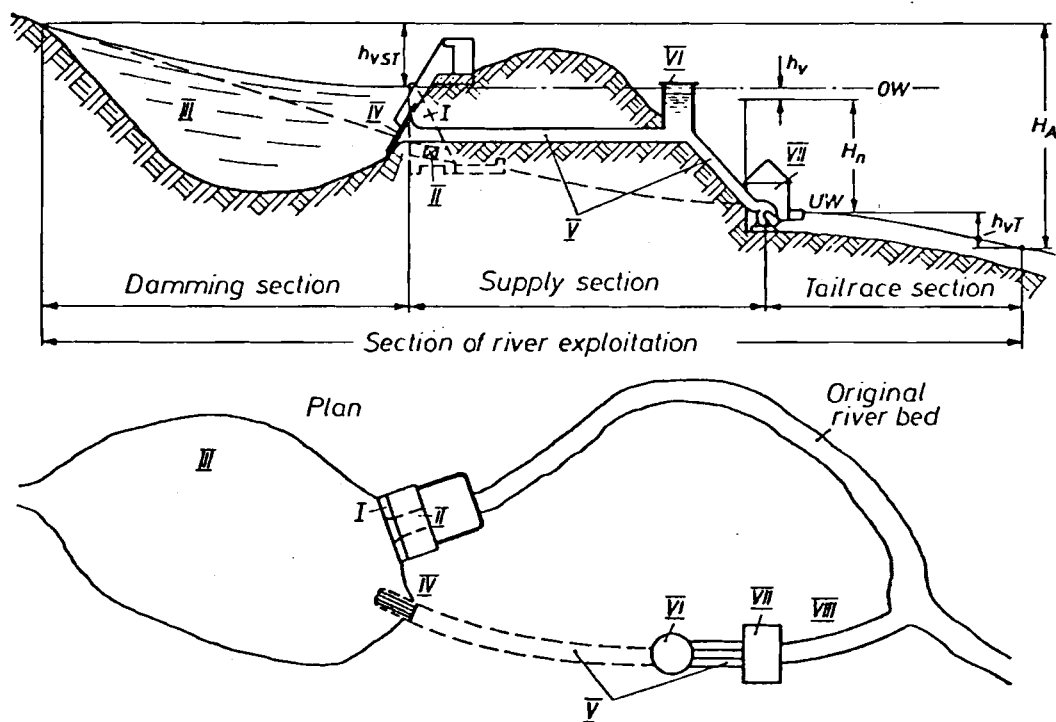
Fig. 3.1.1. Elevation and plan of characteristic components of diversion river power plant along its section of exploitation. I damming device II spillway III upper reservoir IV Inlet structure V supply (admission) or piping (as the head section of the diversion duct) VI surge discharging device VII power house VIII tail race; h_{vst} level drop in the damming section, h_v level drop in the supply section; h_{vT} level drop in the tail race section, H_n net head $H_A - h_{vst} - h_v - h_{vT}$; H_A = available head = drop in the river level along the exploited section.

– The damming device I blocks the downstream end of the upper basin (reservoir). In storage plants for heads above about 30 m it consists of a barrage usually assisted by dikes. In a run-of-river plant with heads below 30 m the power house and weir, assisted by long dikes along the river banks, replace the barrage. In diversion plants this device is reduced to a weir, in channel plants it consists of dikes power house and weir.

– The spillway or flood discharging device II firstly controls the maximum permissible head water level by means of barrage crest, fixed or adjustable weirs with movable or rotary gates, by syphons or by-pass outlets. Secondly it must enable the passage of high water which could be catastrophic.

In the case of a run-of-river and barrage power plant the spillage occurs under the plant's head. In diversion plants the head at spillway is smaller and hence also the bad effects of spillage to be controlled. For the controlled dissipation of spilled discharge a stilling basin at the foot of spillway is used. The latter can be omitted in the case of a ski jump spillway.

– The fish protecting device (if a fishery act exists) consists of an inlet screen at least at the intake of machines but if possible also before weirs with a width small enough to prevent the passage of finger-thick young fishes. Otherwise a large mortality rate occurs, caused by shock or cavitation damage, to the fish. This ranges up to 80% at a head of 100 m [3.1; 3.2]. In rivers with species such as salmon and sturgeon, which migrate at spawning time, a fish pass must be provided with cases according to the length of fish (e.g. the "Beluga" of the Volga (Accipenser huso) reaches 9 m in length).

–The upper basin (reservoir) III is formed by the damming device. If needed especially in diversion plants, the basin contains a sand separator. This cares for sedimentation of silt by flow retardation and turbidity artificially created upstream of the intake structure.

– The intake structure IV for the working fluid is always underneath the lowest head water level, protected by a screen and usually cleaned by a trash rack [3.3]. Care must be taken that the inlet is free of vortices [3.4]. In run-of-river plants the inlet is in front of the power house. In high head plants it may be within the barrage or a separate structural member, sometimes in a tower within the reservoir. In diversion plants the sedimentation of silt may be eased, according to Mosonyi [3.5], if the structure lies on the hollow side of the flow caused by the spillage.

– The supply (piping) V runs from the intake structure to the turbines. In the case of a high head diversion plant this device consists in the upper reach between intake and surge tank (when it exists) of a tunnel or a tunneled or open channel of small slope. In the latter case the surge tank is replaced by a swell weir. In the downstream reach, the so called "power drop", the water is conveyed to the power house either underground by a pressure shaft or outdoor by a penstock [3.6; 3.7]. In front of the power house the main may form branches to the individual machines [3.8]. In a barrage river plant the supply crosses the dam (barrage).

In a low head plant, the supply consists either of a longer channel (channel power plant) or it shrinks to the bell mouth of the turbine's intake.

– The surge relieving device VI is provided in the supply V, the hydraulic machine or the tail water tunnel. It should lessen the surges of pressure or water level induced by the regulation of the machine at least in the longer ducts. For high head plants it usually consists of a surge tank between the upper and downstream reach of supply (see Fig. 3.1.2) [3.9 to 3.15].

Underground power stations with a vertical or steeply inclined and hence short supply with heads up to 600 m may omit the surge tank upstream of the machine. This usually requires a surge tank at the inlet of the tail water tunnel which is then very long [3.16].

72

Fig. 3.1.2. Special construc-
tions of surge tanks as a
possible means of a surge
discharging device (except
the simple vertical shaft
surge tank). a) Two chamber
design. b) Throttle design;
throttle usually with a lower
resistance in the upwards
orientated flow direction
than in the reversed direc-
tion, implemented, e.g., by
the backflow throttle of
Thoma. c) Differential design with the throttle in the side tank and the overflow weir between this
and the upper extension of the penstock. d) Johnson design where the standpipe as the upper
extension of the penstock in c) is surrounded by a throttled tank.
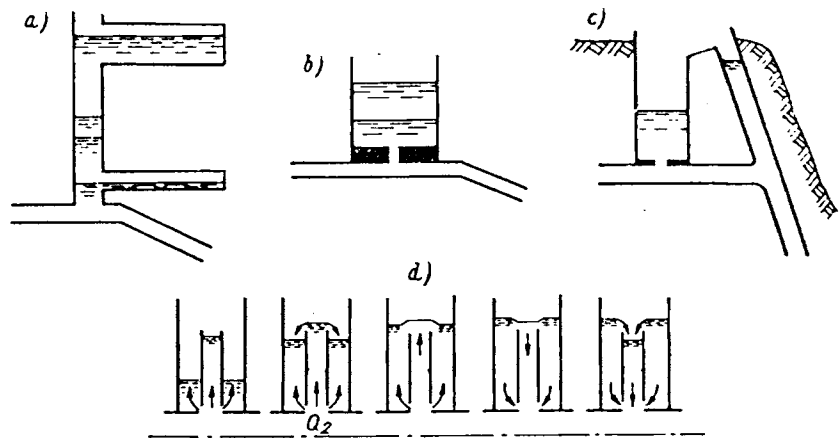
In badly accessible areas and to save excavation costs the surge tank with an open air
level may be substituted by an air chamber filled with compressed air [3.17].

In FT plants especially of higher head or on longer penstocks the surge relieving device
consists of a by-pass outlet, controlled by the gate operating ring in the case of a rapid
shut down. In reaction turbines also controlled ventilation past the gates or the rotor may
relieve the machine from pressure surges. In PTs a jet deflector is provided as a surge
relieving device. Surge on the level of navigable rivers caused by a sudden shut down
[3.18] may be prevented by means of a swell cutting cam replacing the usual cam between
the control loop of gates and the runner vanes of a double regulated KT.

At the end of long channels i.e. in channel plants the surge of level is prevented by a swell
weir.

– The power house proper VII. Here can be distinguished:

1) The power house which is designated according to its structure: a) Hall design also
containing the main crane in the interior of a tall hall. b) Chamber design only containing
an auxiliary crane in the interior (see also E. Mosonyi [3.18]). c) Pit design with generator
or its removable cover in the open air. b) and c) have the main crane outdoor.
2) Power house designated according to its location relative to the river course, the river
level, the barrage and the surface of the earth: a) Underground power house as an earth
covered building or pit, an artificial or natural cave. b) Semi-underground power house
as a pit or building, earth covered against land slides or avalanches at the base of a slope.
c) Outdoor power house at the bottom of a slope. d) Power house at the base or interior
of a barrage. e) Submersible power house in a dam. f) Power house on a river, as a unit
in a bay or split into two halves on both the river banks. g) Power house compounded
with the spillway to form a submersible power house, a power house underneath a ski
jump, an abutment power house [3.19].
– The tail water section VIII, the reach that connects the turbine outlet with the original
river (the usual case of a diversion power plant), but sometimes also with a river of
another catchment area (a transition plant) depends greatly on the location of the power
house (underground or outdoor) on the type of turbine (requiring a submergence and
hence a pressurized tailwater duct or not), the topography of the valley possibly ending
the diversion (circuiting a large river reach) and the degree of exploitation of the scheme.
For a long valley the more lucrative reaches were developed first.

For a run-of-river plant with a power house in a bay this section becomes as long as the spillway abutment that borders upon the power house. For a barrage plant on a river it shrinks to zero

3.2. Dams

3.2.1. Classification of dams

The denomination "dam" includes here only fixed damming devices excluding a power house and spillway used as a damming device in run-of-river power plants. Dams create a constant obstacle to the river whereas weir gates permit a varying level obstruction allowing therefore regulation of head water level. With the first device a large reservoir is made, whereas with the second, whose height rarely exceeds 30 m, only a daily or weekly reserve would be made.

A dam or a barrage consists of
a) a solid or hollow body of masonry, concrete, earth- or rock-filled, made water tight,
b) a crest carrying usually a road,
c) a foundation on the river bed and a support on the slopes of its valley. Usually either on the crest or in the concrete part of the body, there is a spillway.

Dams are classified according to the principle of resistance against hydraulic thrust as
I)   Gravity dam (designated as dike or embankment when earth- or rock-filled)
II) Arch dam with single or double curvature
III) Multiple arch dam with buttresses as supports
IV) Mixed dams consisting of a mixture of the types previously mentioned
V)   Hollow dams with reinforced flat or arched decks of concrete as external walls, supported by buttresses partly filling the dam section.

The crest height of the dam: This is given by the depth of the valley. It should be as high as possible to catch the largest possible volume of water due to the catchment area and with respect to the fact that any subsequent increase of height is extremely difficult and expensive. For this purpose an adequate site (if there is one) has to be selected.

3.2.2. The foundation of a dam and related problems

The foundation of a dam includes not only that part on the bottom of the valley but also the part on the valley slope. The foundation type depends mainly on the quality of soil. It has to transmit the hydraulic thrust of the barrage and the loads related to it from the base of the dam into the adjacent soil, taking care that this is not overloaded with respect to its permissible pressure, normal tensile stress and shear stress to avoid slippage [3.20] and landslide [3.21]. Soil and dam are also stressed by seepage-induced uplift.

Moreover the ground should be as tight as possible against seepage [3.22]. If possible a dam should base on rocky ground. In some sites, e.g. that of the Aswan high dam [3.23] the ground is formed by a sand deposit more than 100 m underneath the river bed. In these cases one has to be satisfied with the injection of a grout curtain through pipes down to the upper face of the rock or by compressing the ground in the best possible way to avoid undermining the dam foundation. To prevent seepage, blankets [3.24] and other means are used [3.25].

During the filling of a reservoir the danger of slippage of the slopes of valley is increased. In valleys with a steep slope, a slippage of soil there, originated by the basin being filled too fast, may cause

by displacement of water in the reservoir, a surge of level, overtopping the dam crest with possible terrible consequences. The most spectacular accident induced in this way by landslide occured at the Vajont dam in Northern Italy with about 2000 casualities [3.26].

Other severe accidents occured as a consequence of slippage of soil in the abutment of the dam and the valley slope resulting in a barrage bursting. In this way the dam of Malpasset Frejus in France was damaged destroying the village downstream of the dam site [3.27].

To predict a dam failure, the body of the dam and its foundation are equipped with inspection galleries to control the seepage and to control displacement and strain by continuously gauging them. They are also used for drainage (Fig. 2.3.4) [3.28 to 3.32].

It seems advisable to inform the population threatened by a dam failure in advance that in the case of emergency a certain signal would be given to them urging them to flee to a station sufficiently elevated above the valley ground, as to be out of the reach of a possible flood wave. Naturally such a point has to be provided.

However, the problem exists how to set the point at which an alarm should be made. A signal which was too early and hence too often would lose its credibility. Lifting the threshold of tripping too much, could be too late to prevent a disaster. According to experiences, mentioned by *Fanelli* [3.33, 3.34] dams may undergo without any danger large gradual deformation, much higher than that fixed before as the disaster limit. There remains the problem how to relate the above measurement to the tripping of alarm.

Latest experience with dams, e.g. Aswan dam in Egypt, located in regions originally not effected by earthquakes, demonstrate that such events may be caused by lifting and lowering the level of a reservoir. This seismic activity can be traced to inactive faults in the relatively thin SiAl crust of the earth (Si from SiO_2 = quartz and Al from Al_2O_3 = pure clay as the essential component parts of it) [3.35; 3.36]. Hence forced vibrations are also used to test dams [3.37].

It seems likely that the effect of added forces by the weight of water in the reservoir liberates greater tensions in this crust. It also appears in this context that the crest height of the dam is more important than the volume stored. This seismic activity becomes pronounced once the height exceeds 100 m. Here are the crest heights of some earthquake, landslide affected dams: Nurek 317 m, Vajont 262 m, Hoover 226 m, Contra 220 m, Canelles 150 m, Kremasta 147 m, Monteynard 130 m, Cariba 130 m, Pieve de Cadore 112 m, Aswan 111 m, Konya 103 m, [3.38 to 3.41].

The Konya disaster of 1967, in the Indian Peninsula which resulted in a heavy loss of lives and considerable property damage, was due to an earthquake whose epicentre coincided with the dam itself [3.42]. Hence stability control is required [3.43]. Insurance against dam risks is discussed [3.44]. The crest height of the highest dams is listed in Table 3.2.1.

3.2.3. Gravity dams

Gravity dams may exist as masonry, concrete, rockfilled or earthfilled dams. The gravity dam is a barrage which resists the hydraulic thrust by its own weight with respect to its moment about the tilting edge on the downstream heel of the dam and with respect to its friction on the ground. A slight curvature of the dam in its plan convex to the reservoir, sometimes found in masonry dams, balances a part of the thrust by internal wall pressure instead of friction.

An embankment is made of stones, gravel and sand, consisting in its core of concrete, earth and clay or loam against seepage with an asphalt coating against water action on its water facing side. A dam of concrete is usually erected at first in separate blocks to avoid internal stresses due to the release of the heat of combination and the subsequent thermal expansion of concrete [3.45 to 3.47].

Table 3.2.1. Crest height of dams higher than 200 m.

Name	Country	Type	crest height (in m)
Nurek	USSR	Rockfill dam	317
Grand Dixence	Suisse	Gravity dam, concr.	285
Inguri	USSR	Arch dam	272
Vajont	Italy	Arch dam	262
Mica	Canada	Rockfill dam	242
Sayano Sushensk	USSR	Arch dam	242
Mauvoisin	Switzerland	Arch dam	237
Oroville	USA	Earth dam	236
Chirkey	USSR	Arch dam	233
Bakkra	India	Gravity dam, concr.	230
Hoover (Boulder)	USA	Arch dam	226
Mratinje	Yugoslavia	Arch dam	221
Contra	Suisse	Arch dam	220
Dworshak	USA	Gravity dam, concr.	219
Glen Canyon	USA	Arch dam	216
Toktogul	USSR	Arch dam	215
Daniel Johnson	Canada	Multiple arch dam	214
Auburn	USA	Arch dam	209
Luzzone	Switzerland	Arch dam	208
Keban	Turkey	Rockfill dam	207
Mohamed Reza Chan Pahlevi	Iran	Arch dam	203
Almendra	Spain	Arch dam	202
Reza Chan Kabir	Iran	Arch dam	200
Kölbrein	Austria	Arch dam	200

The problem whether a gravity dam is built of masonry or concrete or as an embankment of gravel. clay etc., depends on the one hand on the material found in the neighbourhood and the transportation facilities for cement. On the other hand it depends on the reliability and existence of a rocky ground, that is needed for a concrete dam, and the dam volume [3.48].

If there is locally no material for making it watertight such as clay or loam, then concrete is used to build the dam, or masonry of hewn rock found in the neighbourhood of the site. In general a dam of concrete or masonry needs a reliable rocky foundation. An embankment is preferred for smaller crest heights or where it is built on deep sandy soil (see Aswan dam, Fig. 3.2.1 [3.23]).

In regions of greater earthquake probability a concrete dam is preferred. Nevertheless the world's highest dam in the Nurek power plant, Tadschikistan, USSR, being in such an endangered region, is an embankment [2.17]. Occasionally a gravity dam of concrete is continued at both its ends as an embankment. In the case of exclusively rocky soil at the site of dam, the gravel needed has to be quarried (Itaipú [2.28]).

With the following list of symbols: H_0 = crest height, b = wall thickness at root, l_c = crest length, the characteristic dimensions of some important gravity dams are: Nurek, Tadschikistan. USSR, H_0 = 317 m, b = 1200 m; Hoover (Boulder), Colorado river, USA, H_0 = 226 m, b = 170 m, l_c = 385 m; Grand Coulee, Columbia River, USA, H_0 = 168 m, b = 90 m, l_c = 1592 m; Grand Dixence, Dixence river, Switzerland, H_0 = 285 m, b = 200 m, l_c = 750 m (Fig. 3.2.2) [3.49 to 3.52].
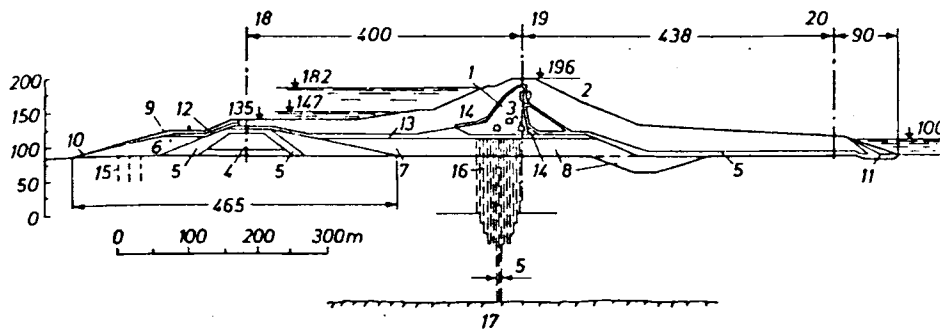
Fig. 3.2.1. Cross section of an earth and rock filled gravity dam, Assuan power plant, Nile. Egypt. Africa (owner Egyptian state power board). Design and erection of dam by Hydro Project Moscow, USSR. Power station equipped with 12 sets of 180 MW FTs built by LMZ, Leningrad. $H = 75$ m. Only grout curtain 5) prevents seepage between rocky ground 17) and loam core 1). 2) rockfilling 3) control galleries in the loam core; 4) upstream dam; 5) grout curtain; 6) gravel; 7) compressed gravel; 8) coarse gravel; 9) rubble stone layer; 10) slurry deposit; 11) boulder; 12) clay layer; 13) compressed slurry and rubble bed layer between layers of sand and boulder; 14) soft clay; 15) sealing blanket of upper dam; 16) main sealing grout curtain; 17) rock; 18) axis of upper dam; 19) axis of main dam; 20) axis of downstream dam. From the Moscow Hydro Project.

3.2.4. Arch dams

This has an arch structure with a convex curve towards the basin originally only with a curvature in its horizontal section, but sometimes varying over the width and height. Nowadays designs have also a curvature, usually varying with height, in the vertical cross section, sometimes leading to an overhanging crest at the top of dam. The wall thickness rises towards the piers and the base, sometimes designed as a hinge for reducing stresses there [3.53 to 3.56].

Here the hydraulic thrust is aimed to be transmitted only by wall pressure into the supports and foundation. Sometimes the wall thickness is enlarged above the value needed for maintenance of permissible pressure. Thus the additional weight contributes to greater stability (mixed gravity-arch dam). To eliminate tensile stresses, the Bureau of Reclamation (USA) has tentatively introduced the prestressing of an arch dam. This was achieved by embedding flat jacks within the dam wall and inflating them for prestressing [3.57].

In consequence of its thin wall, the arch dam is more susceptible to vibrations [3.58]. Creeping may influence the stresses [3.59].

The material used for an arch dam decreases with rising pressure admitted. For a design, which requires the minimum of material the latter increases with crest length l_c being about the width of valley. Below a certain value of l_c ranging actually about 600 m, the material required for an arch dam is smaller than that for a gravity dam [3.60].

The latter results from the different laws the wall thickness has to follow for an arch dam or a gravity dam. Assuming for simplicity a cylindrical arch dam with a radius of curvature in the plan proportional to the dam width l and an admissible pressure in the wall p_{ad} the wall thickness is $s_a \sim l \ p_w/p_{ad}$ in which p_w is the water pressure. Assuming p_w to be proportional to the crest height h, the wall thickness of an arch dam is $s_a \sim l h/p_{ad}$. Contrary to this, the equilibrium of a gravity dam requires a wall thickness proportional to the crest height $s_g \sim h$. Hence the material required, proportional to $h l s$, is for an arch

dam. $m_u \sim l^2 h^2 p_{ad}$ and for a gravity dam, $m_g \sim l h^2$. Hence the ratio of material used for an arch dam to a gravity dam is proportional to the width l. This leads to the above result.

The construction of a simple arch dam is not advisable, when the width of valley is more than 5 to 6 times larger than its depth. In any case the ground has to be rocky and the soil of the valley at site must offer good support on the slopes. Otherwise it has to be strengthened by injection of concrete and by reinforcement. In any case the economy in working time of an arch dam is less than that of a gravity dam because of the complicated shuttering.

The arch dam of Vajont, the second highest in the world, having survived the disastrous landslide in its reservoir, has the following characteristics: $H_0 = 262$ m, $b = 23$ m, $l_c = 190$ m. The Figs. 3.2.2 and 3 show cross sections of some arch dams.
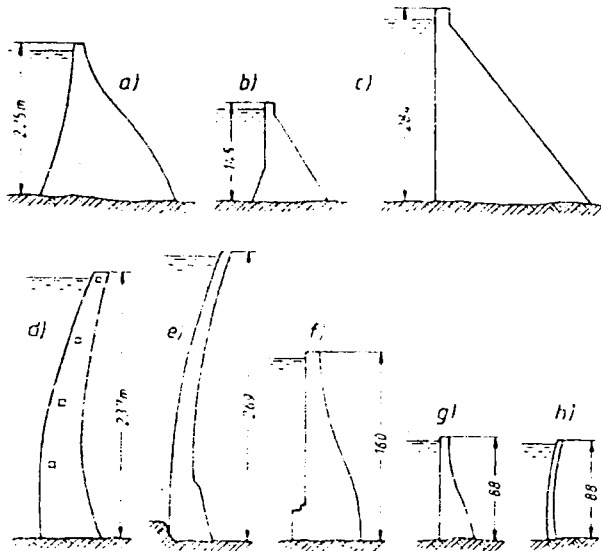
Fig. 3.2.2. Schematic elevation of remarkable dams. Gravity dams: a) Hoover d. b) Grand Coulee d. c) Grand Dixence d. Arch dams: d) Mauvoisin d. e) Vajont d. f) Tignes d. g) Cap Delong d. h) Tolla d.
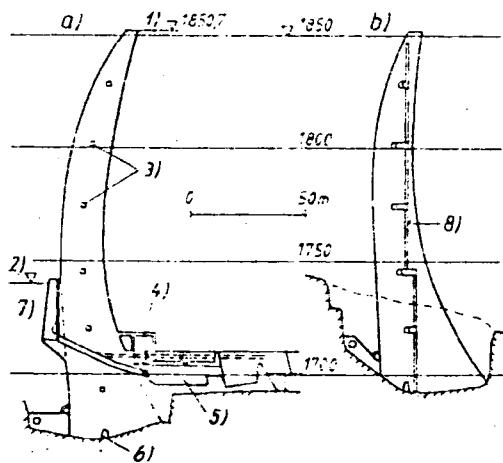
Fig. 3.2.3. Cross sections of Zillergründl arch dam, Ziller, Austria (owner Tauernkraftwerke AG Salzburg) a) cross section through bottom discharge b) section of the right side with plumb shaft 1) maximum permissible water level 1850 m; 2) minimum permissible water level 1740 m; 3) control passage; 4) valve chamber; 5) stilling basin; 6) brim passage; 7) bottom discharge; 8) plumb shaft rockdrilled, diameter 0,3 m, depth 60 m.

3.2.5. Multiple arch dams

This dam can be used, if the width of the valley is more than 5 to 6 times its depth and if the foundation of a concrete structure can be built on rock [3.61].

78

It consists usually of a large number (up to 40) of parabolic cylindrical shells normally of concrete, which make an angle of about 45° with the ground level and whose upper obliquely cut ends are covered by a horizontal plate-like cantilever forming the crest. The lateral ends of each arch are supported by abutments.

One of the most notable multiple arch dams is the Daniel Johnson dam in the valley of Manicouagan river, Canada, for the power station Manicouagan 5 (1768 MW, 7,36 TWh, H = 150 m, 8 FTs) built between 1960 and 70 in the Virgin forest of the province Quebec (Fig. 3.2.4). Its characteristics: H_0 = 214 m, central arch l_c = 161 m, 12 side arches each l_c = 76,5 m.
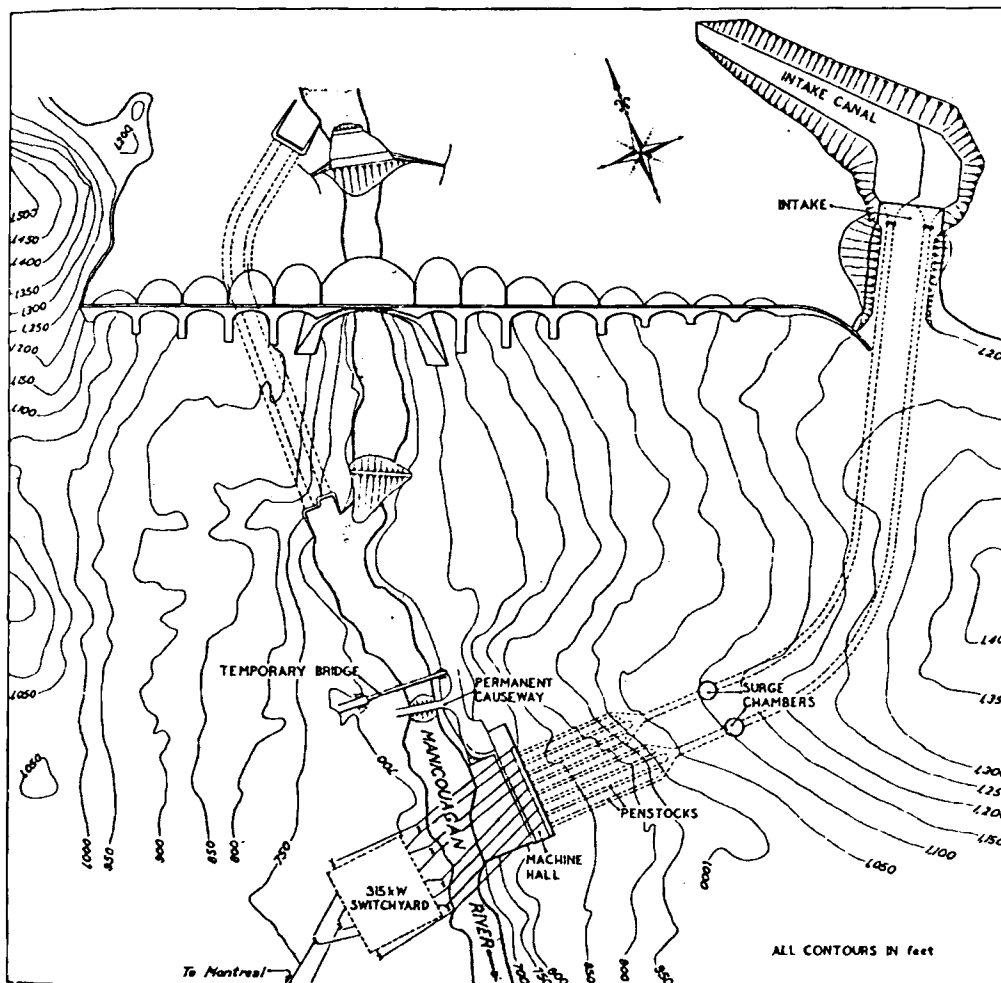
Fig. 3.2.4. Plan of Manicouagan 5 multiple arch dam (Daniel Johnson dam), Manicouagan, Quebec, Canada (owner Hydro Quebec, Montreal, Canada), crest height 214 m, tallest multiple arch dam. (From Water Power 16 (1964), no. 10 p. 410; no. 11; p. 463).

Constructional details see Table 3.2.2.

Increasing capacity of a power station at the heel of a dam is facilitated by the angular dam [3.62]. A survey of dams is presented by *Mackintosh* [3.63]. Research activities are listed in [3.64].

Table 3.2.2. Details of design, material, reservoir, power house, and labour for the example of Daniel Johnson multiple arch dam (Canada)*)

Weight of concrete: $6 \cdot 10^6$ tons. To obtain complete security of the dam on its foundation, it was necessary to excavate below the central arch a gorge 49 m deep and 20 m wide. To secure and control the safety of the foundation and the supporting soil, inspection galleries have been drilled in the adjacent rock. Similar provision has been made in the concrete. Moreover, any displacement of the dam is continuously controlled by land surveying.
Total volume of concrete used: $2.25 \cdot 10^6$ m³. Compression resistance: 316 bar over 91 days.

Composition of concrete
Cement 230 kg/m³, Welding sand 360 kg/m³
Stones in the range 75–150 mm diameter 360 kg/m³
Stones in the range 37,5–75 mm diameter 535 kg/m³
Stones in the range 18,8–37,5 mm diameter 232 kg/m³
Stones in the range 9,4–18,8 mm 148 kg/m³
Water 113 kg/m³, additives for absorption of air 3,6 kg/m³

Reservoir of the Daniel Johnson dam:
Surface: 2100 km², length 200 km, total volume 139 km³,
storage volume 36 km³, catchment area 29 000 km².
Spillway: Height 21,3 m, width 440 m, number of gates 3.
Volume of concrete 58 500 m³, flood flow 2830 m³/s.
Power station: Installed power capacity 1768 MW, annual work 7,36 TWh,
number of sets 8, Francis turbines, net head 150 m,
rated discharge 642 m³/s, power station load factor 0,635.
Voltages: terminal 13,8 kV, transmission to switchyard 315 kV,
long distance transmission 735 kV, (the first power station in the world using this voltage at the time of its inauguration in 1970).
Admission: 4 gates, dimension 11 m · 6,1 m;
number of galleries 2, diameter of galleries 11 m, length 1100 m, maximum discharge 960 m³/s.

Production of concrete during the erection:
Monthly 105 000 m³, weekly 25 500 m³, daily 4900 m³ (maximum values reached).
Pressure shaft: number 8, diameter 4860 mm, length of liner 176 m.
Labour involved: Man hours during construction of the dam 31 350 000,
total number of workers 12 900, number of workers during peak of construction 3544 in 1964,
number of men, women children living at site at peak of construction 4700.

*) From special issue of Hydro Quebec, Montreal, Canada

3.2.6. Response of present society to social and ecological impacts of dams

There is no doubt that the primary effects of the vast majority of dams have been beneficial. Equally, however, there is no doubt, that many of these dams have contributed to unanticipated adverse secondary effects, many of which could have been eliminated by a proper planning process [3.42]. In addition, there seems to be a considerable difference of opinion in judging the success or failure of some projects.

The environmental damages arising from the construction of dams are many, and they have far reaching effects, their interactions are often so complex and so little understood that ecologists and environmentalists cannot predict them with certainty. Our current knowledge of the eco-system of manmade lakes leaves much to be desired. According to Biswas [3.42], e.g. low water levels caused by the construction of a dam may result in serious consequences to the local fauna and flora.

Ecologists and sociologists, who often seriously question a certain project, find it impossible to influence and convince engineers, economists and politicians, hailing this project as a technological triumph, because of the lack of hard facts or solid scientific evidence.

3.2.7. Environmental consequences of large dams

– On the physical system: Dams invariably change the river and eco-system regime and thus the real question is not whether a dam will affect the environment but how much change is acceptable to society as a whole and what countermeasures should be taken to keep the changes to a minimum and within an acceptable range.

For example, the Assuan dam in Egypt has reduced the fish population of the Mediterranean by abruptly breaking the aquatic food chain in the eastern Mediterranean. Nile sediments and organic micro organism are now trapped in the reservoir. Erosion has become a major problem, and the fertility of the Nile valley has been lowered by lack of sediments. Salinity in middle and in upper Egypt is increasing rapidly [3.42].

Since practically all the dams built for hydropower in recent years have also been used for other purposes, notably irrigation, they also have contributed to the deterioration of soil fertility and the resulting loss of good agricultural land due to salinity and alkalinity [3.42].

– Earthquakes: Several recent studies indicate, that observed seismic activity can be attributed directly to the creation of dams and storage reservoirs [3.42]. See also under 3.2.2.

– Disease propagation: One of the most serious effects in tropical climates is the spreading of water-born diseases, and the consequent suffering of millions of human beings and animals. The relationship between increasing use of irrigation and the spread of bilharziosis (carried by snails) has been conclusively demonstrated in several countries in the world.

– Resettlement problems: Some of the dams have also created problems by the displacement of population. The Kariba dam on the Zambesi dispiaced about 57 000 Tonga tribesmen. What the planners there, often from outside Africa, did not realize was the enormously complex relationship between tribes and their land. In the above case it took two years to clear sufficient land to meet their subsistence needs and the government of Great Britain had to step in to avert famine. Approximately 100 000 people had to be relocated for the Aswan high dam without adequate planning, and the World Food Programme had to rush in famine relief for the Nubians [3.42].

3.3. The spillway, gates and shut off devices

3.3.1. The spillway in connection with other members of the plant

The spillway as the structural member for by-passing the turbines may be located separately from the power house or even from the barrage. In low head run-of-river power plants, the power house and the spillway gates serve together with the embankment as a damming device and thereby constitute a unit together with the power house (see Fig. 3.3.1). This unit is very compact, when the sets and spillway are located in a common block of concrete in the case of a plant with ejector by-pass outlet (see Fig. 3.3.2), e.g., in the USSR to facilitate the transport of floes during the long winter. Also submersible plants (see Fig. 3.3.3.), abutment power stations (see Fig. 3.3.4) and certain designs
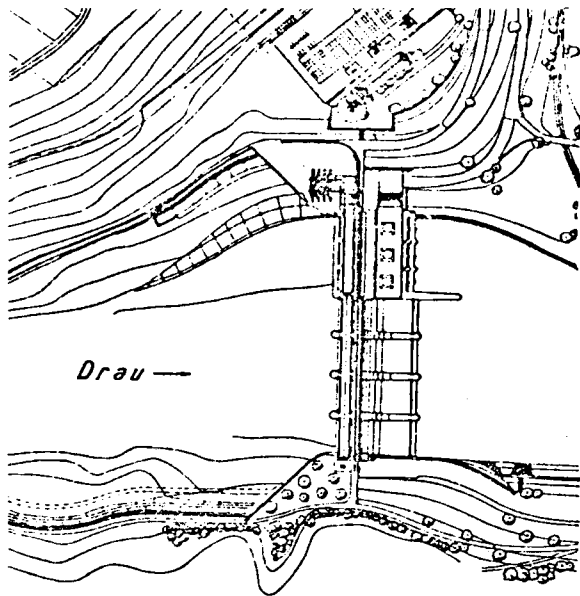
Fig. 3.3.1. The Schwabeck run-of-river power plant, Drau, Austria. Power house in bay, and spillway across the stream course as a structural unit form the damming device.

Drau →
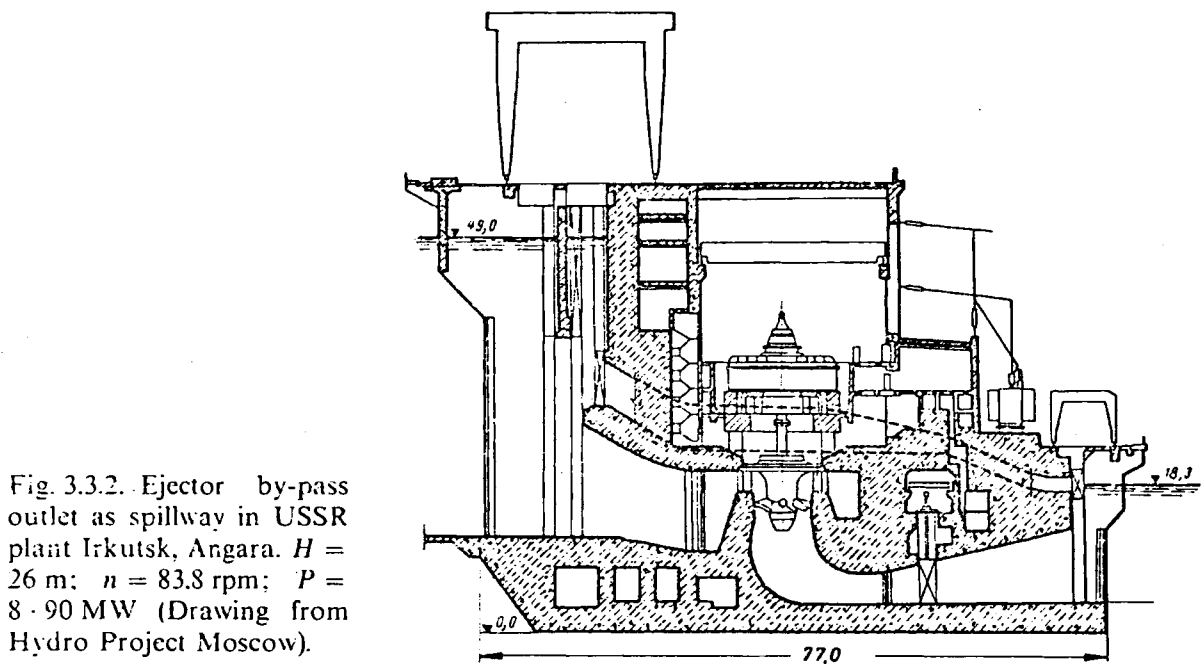
Fig. 3.3.2. Ejector by-pass outlet as spillway in USSR plant Irkutsk, Angara. $H =$ 26 m; $n = 83.8$ rpm; $P =$ $8 \cdot 90$ MW (Drawing from Hydro Project Moscow).

Axis of power house
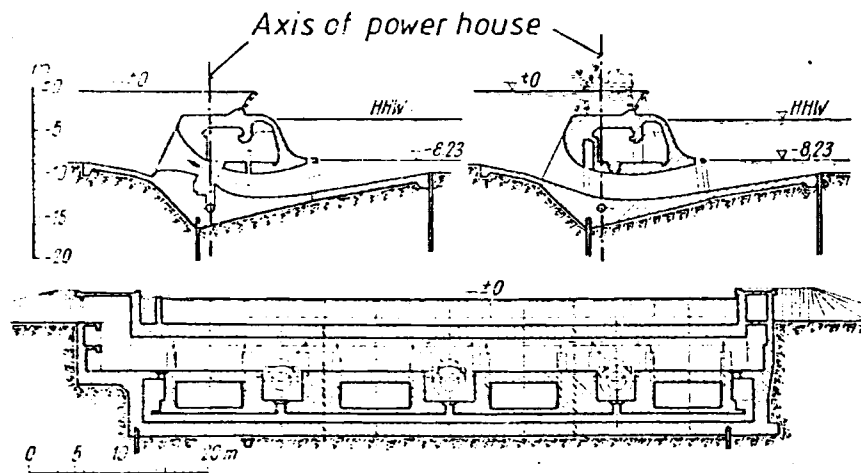
Fig. 3.3.3. Longitudinal and cross section of set (left) and sluice (right) of submersible plant. Rott-Freilassing, Saalach, West Germany. $H =$ 8,5 m; $P = 4 \cdot 1$ MW. From *Mosonyi* [1.53].

82

a)

24,00   20,00

9,00

4,34

13,41   3,25   6,70   4,60   7,17   10,54

2,17/51   2,32,5/51

51   7/51   51

b)

0   50   100 m

100 kV

to Draubrücke
to Schwabeck
100 kV

355,75

354,75

Control house

350,50

144,00

DRAU

Fish ladder

LAVAMÜND

c)

16,0

1,2

1,2

5,1   5,1

d)

6500 Ø
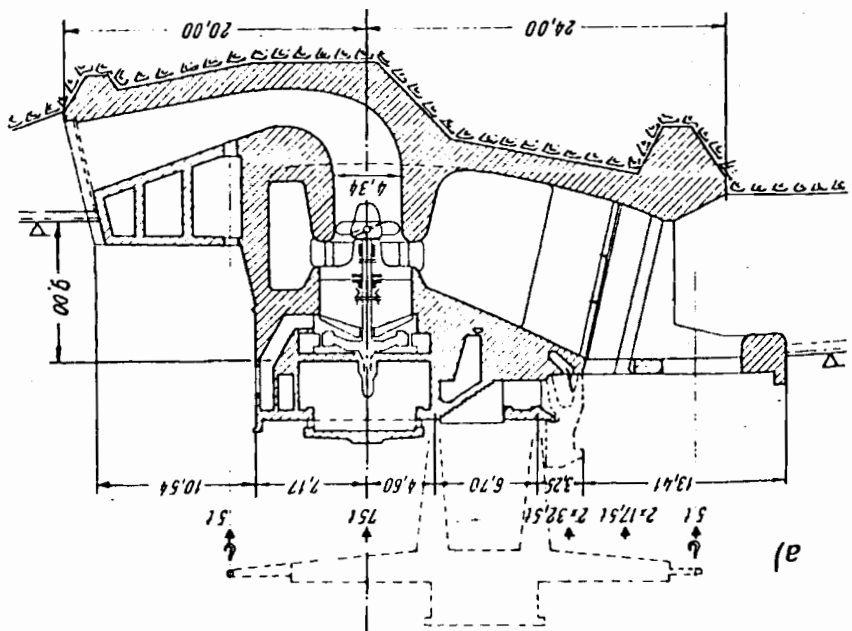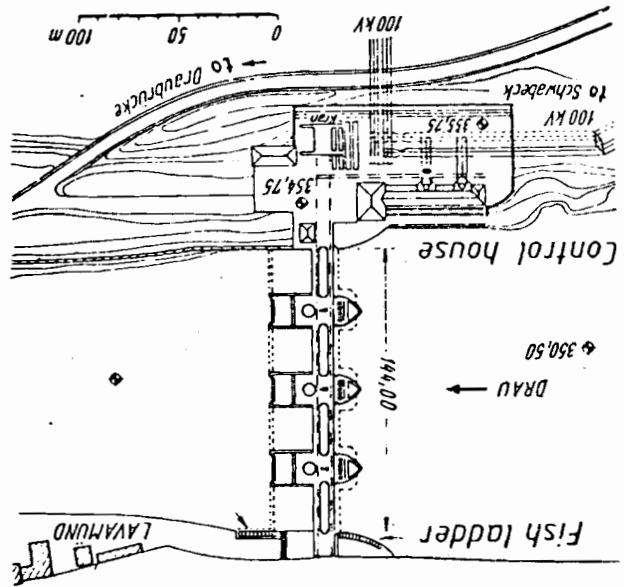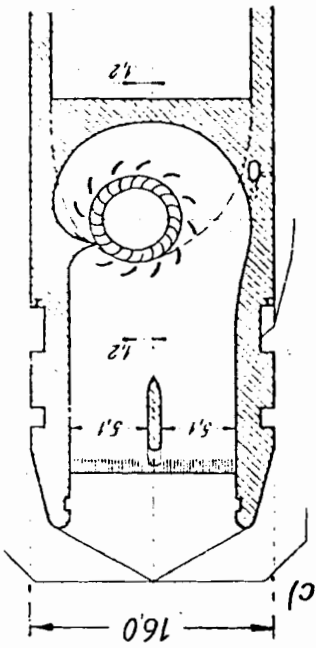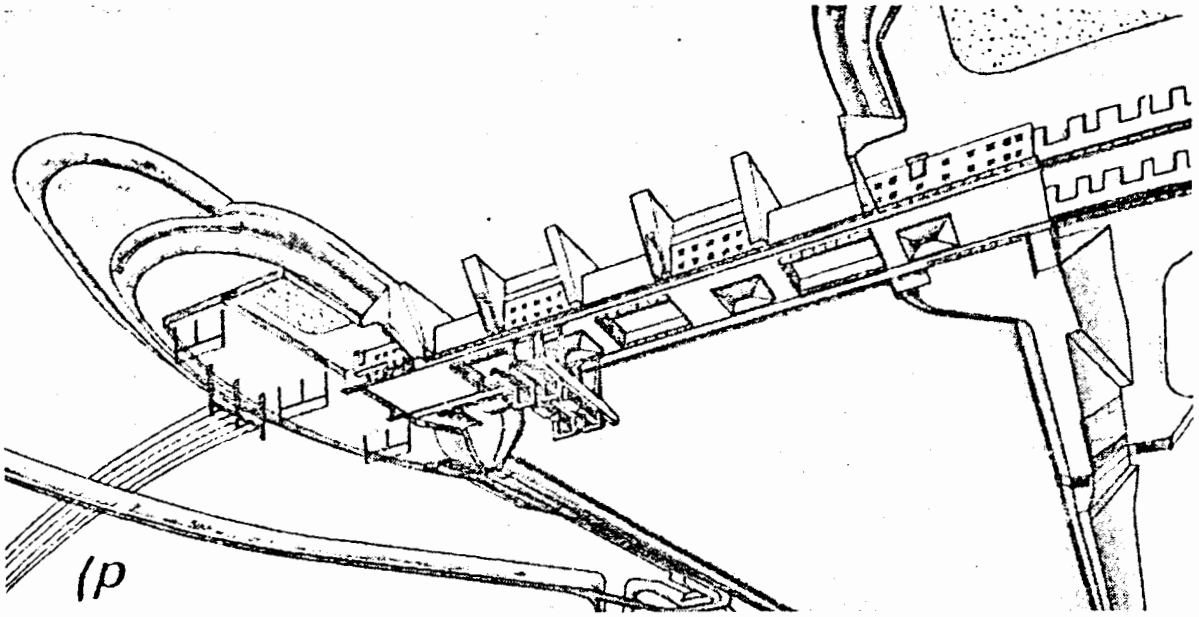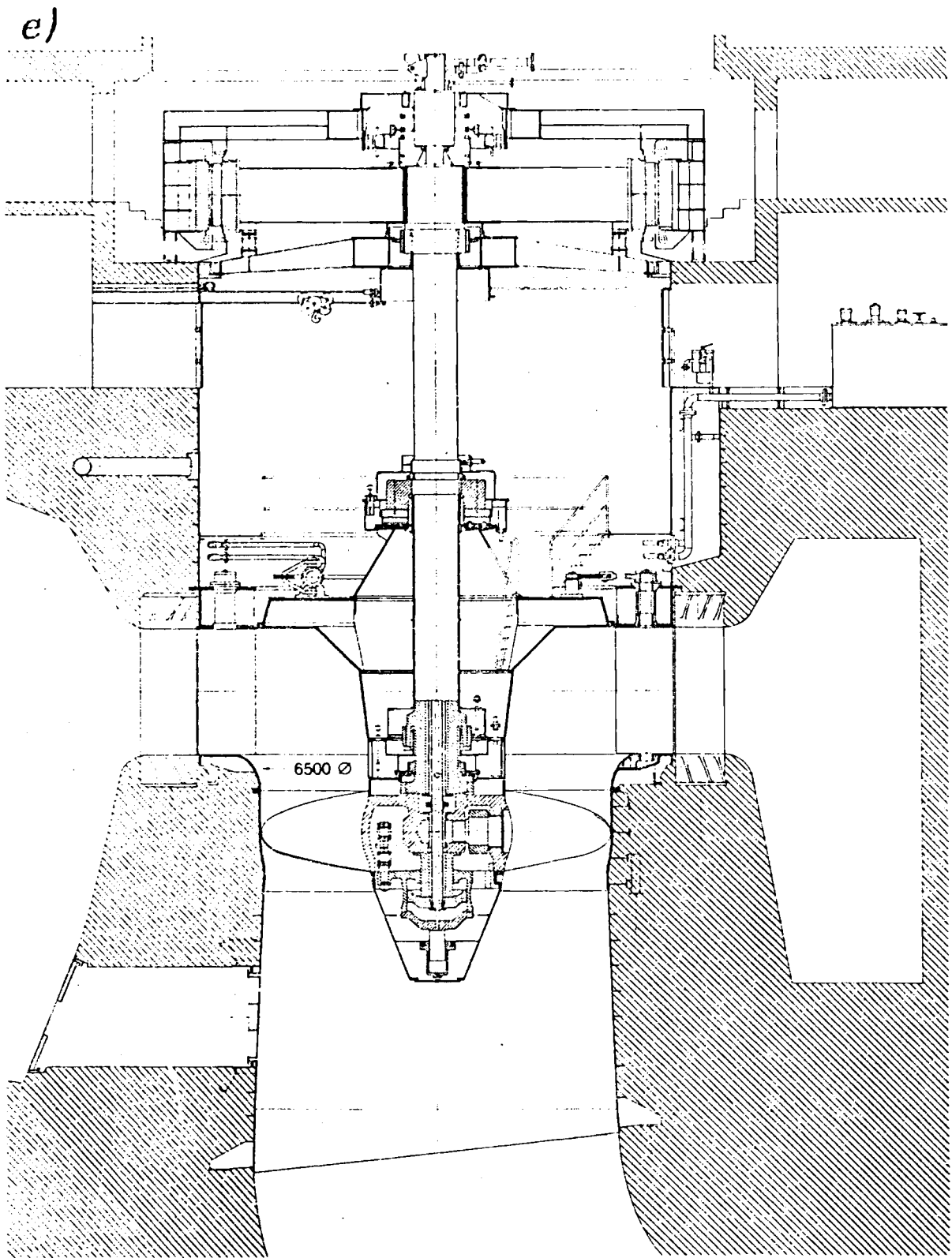
Fig. 3.3.4. Abutment power plants. a) through c) show Lavamünd, Drau, Austria. $H = 9$ m, $P = 3 \cdot 7.5$ MW a) elevation and longitudinal section c) plan of the power house in the abutment of the spillway: b) plan. From *H. Lauffer* and *H. Grengg.* d) Perspective view of abutment power plant Nußdorf, Inn. West Germany (owner Innkraftwerke Töging). 2 welded gantry cranes built by Noell. (Drawing courtesy Innkraftwerke Töging) e) Sectional drawing of KT Nußdorf, Inn, West Germany (owner Innkraftwerke Töging). $H = 10,1$ m, $n = 75$ rpm, $P = 2 \cdot 24,9$ MW. KT built by J. M. Voith. This type may yield the most uniform inflow of all the sets (Drawing courtesy Voith).

of barrage power houses with a ski jump spillway above them have this compact form (see Fig. 3.3.5).

Here by a skillful arrangement of draft tube outlet upstream of the hydraulic jump due to spillage, the head can be increased compared with plants in which the spillway is situated separately from the power house [3.18]. This is valid during spillage.

Fig. 3.3.5. Elevation of the Karakaya dam and power house, Euphrat, Turkey (owner State water authority of Turkey). Ski jump spillway, operated by tainter gate at the crest of the dam. 1) butterfly valve; 2) machine hall; 3) transformer hall; 4) penstock; 5) draft tube; 6) high water spillway. From *Howald* et al.: Karakaya, a hydro electric power plant in Turkey. BBC review 67 (1980) no 2, p. 100/107.
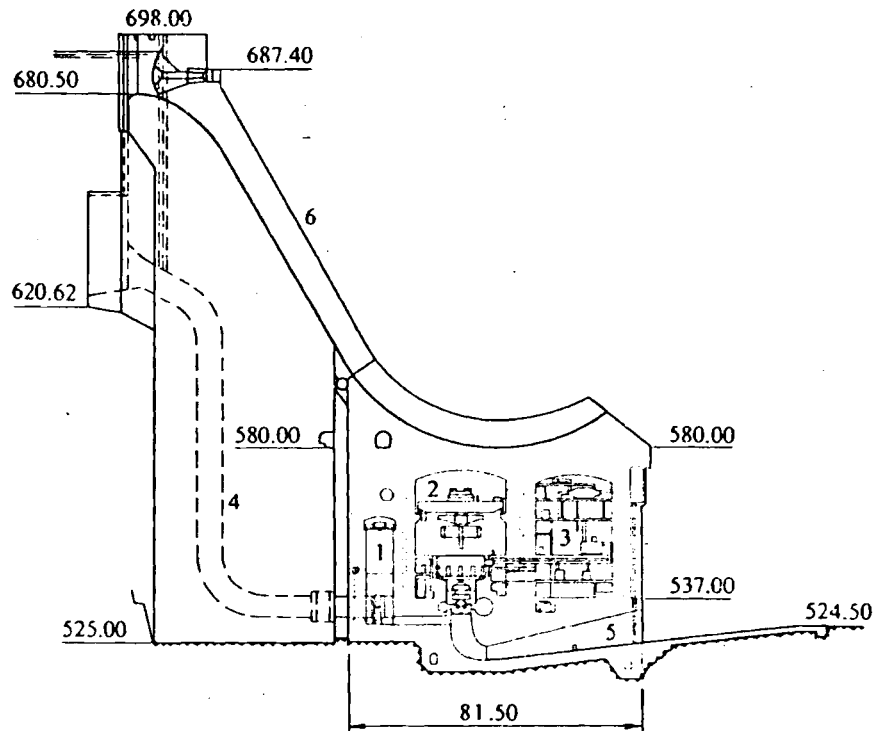
This unit of spillway and power house disappears in the case of a diversion power plant. Here the power house lies at a distance from the spillway. Now the spillway may be reduced in size as spillage occurs with a spillway head usually rather small compared with the plant head under which spillage occurs in barrage or run-of-river plants.

Sometimes in such diversion plants a sophisticated spillway is omitted, as the flood flow here is left to the original river reach which has been short-circuited and which is capable of receiving this flow (e.g. a deep gorge). Hence, e.g., a riprap flume may fit.

3.3.2. The spillway

3.3.2.1. The duties of the spillway

1) Maintenance of maximum permissible water level in the head water reservoir.
2) Dewatering of this reservoir so as not to be detrimental to the foundations and construction of the plant in the case of catastrophic high water with closed turbines. The discharge due to the latter is usually a multiple of rated discharge. As an example, the lower Inn along the West German-Austrian border has, downstream of its confluence point with the Salzach at Simbach-Braunau, a catastrophic high water of 6000 m³/s, 6 times the rated flow. But there may exist cases in which the latter is a nearly vanishing portion of the flood flow whereby the power house is degraded more or less to a small

appendix of the spillway. Such a situation exists. e.g. in the first stage of the development of a huge river in a developing country (see Fig. 3.3.6) [3.65 to 3.71].
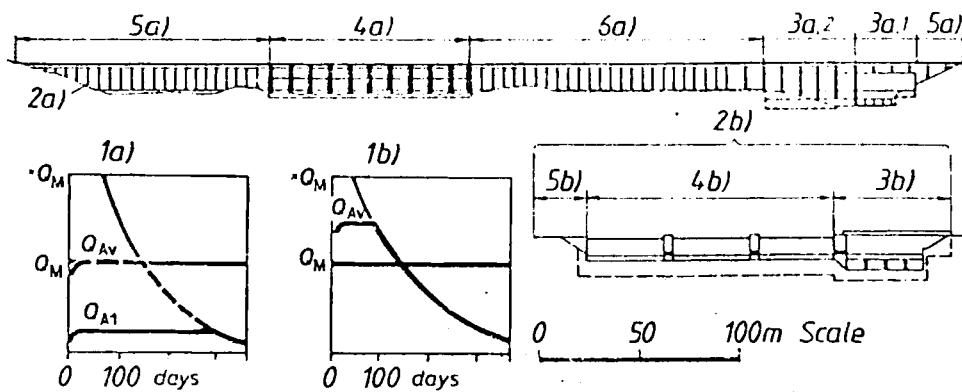
Fig. 3.3.6. Example of the difference in the method of river development a) in a developing country, St. Paul river, Liberia, Africa, and b) in a developed country. here Trier. Mosel, West Germany. 1) Flow duration curve; 2) river-bed; 3) power house. 3 a. 1) 1st stage; 3 a. 2) 2nd stage; 3 b) final stage; 4) spillway; 5) side barrage; 6) main barrage. Q_M mean flow rate. Q_{A1} rated flow after 1st stage of development. Q_{Av} rated flow, xQ_M mean maximum flow rate. (Drawing and graph courtesy Messrs Siemens, Erlangen)

3.3.2.2. Survey of flood discharging devices

The flood discharging device may be of a fixed structure (weir on the crest of the dam, pits, syphons) or a movable structure (gate) of the translational or rotary type. Gates may be actuated manually, through servomotors and automatically, by means of electric, hydraulic or pneumatic devices. Imperative is the reliability of a spillway.

3.3.2.3. Fixed flood discharging devices

I. Weirs on the crest of the dam: The utilization of the crest of the dam as a flood discharging device is a common practice, especially for concrete or masonry gravity dams. Its advantage exists in the availability of the whole width of the dam. thus facilitating a spilled flow lamina, combining a large capacity with a small depth of lamina [3.72].

II. Weirs within the structure of a dam, located laterally (see Fig. 3.3.7). Such a design leaves the central part of dam free for other purposes. Thus the power house can be constructed there. In other cases a spillway of the ski jump type is laid above the power house in the dam's centre [3.73].

III. Pit type weirs, (drop shaft, morning glory): In this case (see Fig. 3.3.8) the weirs are arranged around the circular crest of a pit. This structure may be far away from the dam and may dewater into a tunnel. Such a design is recommended for example with a thin-walled arch dam, releasing the construction of the dam from possible vibratory loads under spillage. It may also be fitted to an earth- or rock-filled embankment to avoid erosion. It is preferable also for very large flows [3.74].

IV. Syphons: This design (see Fig. 3.3.9) consists of one or more syphons in parallel united at their upper end with the head water and at their lower end with the tail water.

When the head water reaches the inner crest of the syphon, the water commences flowing. Then the air within the syphon, now separated by means of a trip baffle is spilled downstream. Hence the

Fig. 3.3.7. Spillway on the side of the main dam.
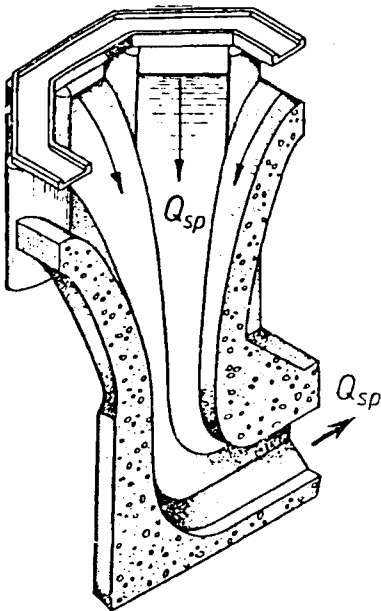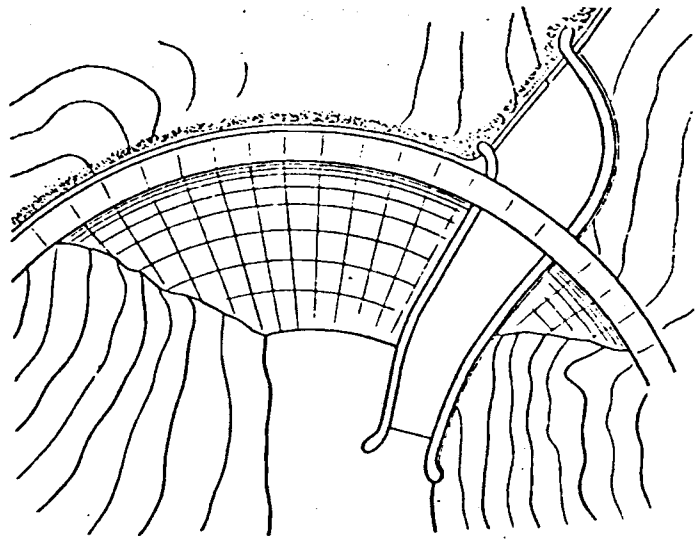
Fig. 3.3.8. Pit type spillway (morning glory).
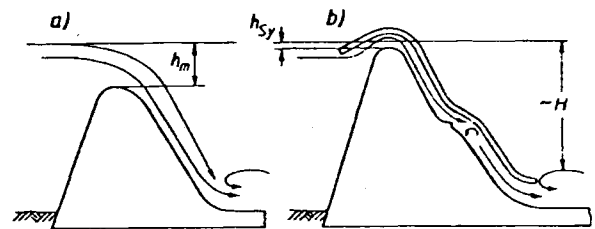
Fig. 3.3.9. Comparison between siphon a) and b) spillway with overflow weir on the crest of a dam.

discharge increases finally propelled by the head on the weir, nearly coinciding with the head of the plant in case of a river power plant. This is contrary to the weir at the crest of a dam or a gate, where only the relatively small head on the crest h_m does this (see Fig. 3.3.9).

When the head water level falls short of the inner crest of the syphon, the latter is aerated, thereby cutting suddenly the flow. Thus the head water level is automatically controlled without any sophisticated movable device, within the range of vertical distance, h_{sy} of the ceiling of the intake and the inner crest. This is of the order of a few cm (see Fig. 3.3.9).

On the contrary the crest of an ordinary weir must be at a vertical distance h_{vm} underneath the maximum permissible head water level, in which h_{vm} is the head on the crest needed for spilling catastrophic flood flow Q_{max}. According to the known weir formulas [1.53] Q is proportional to $bh_{vm}^{3/2}$, b being the width of the crest. Consider a syphon of the same width and the same cross sectional area bh_{vm} of the spilled flow lamina at the weir crest. This needs only $(h_{vm}/H)^{1/2}$ times the crest length of a common weir to discharge Q_{max}, H being about the plant's head.

Hence a syphon is reasonable, if 1) the level of head water must be maintained accurately, 2) this level control shall be simple and automatic, 3) the width b of the dam crest is limited, 4) the catastrophic high water flow is very large.

3.3.2.4. Weir gates as an adjustable flood discharging device

1. Gates with translational motion: These are sluice gates. For micro power plants and small heads they consist of a frame of steel cantilevers filled with wooden planks and operated by a rack. For larger plants they are fabricated from a framework of steel cantilevers, covered by a steel liner on the side of head water. They may be composed of simple or multiple sluices.

The spillage may occur 1) between the upper and lower sluice, 2) underneath the gate, 3) above the upper gate usually either along a nozzle shaped guide face or a rounded backed weir.

The procedure 3) has the advantage of spilling easily floating bodies like driftwood and leaves. For high water usually the gates are lifted thus allowing the flow to pass underneath the lowest gate [3.75 to 3.77].

The gate adjustment, eased by counterweights and guide rollers (see Fig. 3.3.10) may be effected mechanically, electrically, hydraulically or pneumatically. When the width of the water way is large or the hydraulic thrust excessive, the spillway is subdivided by abutments into more openings.
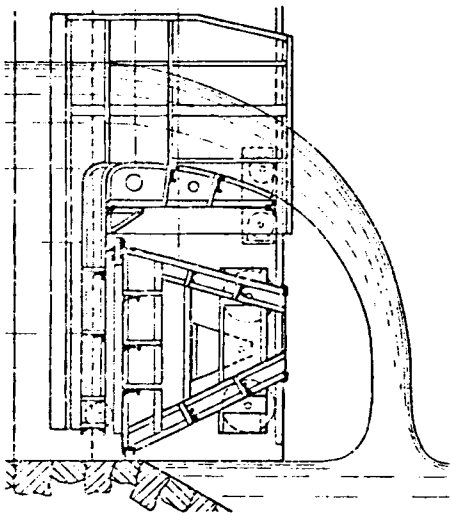
Fig. 3.3.10. Double hook gate (MAN). Spillage of medium discharge with the upper gate lowered. For catastrophic high water both gates lifted

In a gate of only one sluice the flow discharges usually underneath the gate. Sometimes it is also convenient to discharge above the gate, not only for cleaning but also for preventing excessive velocities along the walls of abutment, bottom, or the sluice, possibly causing erosion, cavitation and excessive vibration of the weir. However, to reduce the cross section of the spilled flow, catastrophic flood flow is preferrably spilled underneath the lowest gate.

All the possibilities are unified by a design with various gates, e.g., double hook sluice gate (see Fig. 3.3.10). Here the upper gate is used to retain the head water level in case of small spillage. For large spillage both the gates are encased and then lifted together. The lifting of gates may be induced automatically by a float, which actuates synchronized electro motors moving both ends of the gate by chains. The actuation of the motor then is neutralized by a feedback linkage between float and gate.

Contrary to the rotary gates of the sector and segmental type the streamwise extension of sluice gate is small and its height rather unlimited. Contrary to the below mentioned rotary gates and the roller weir the plate-like structure of the sluice gate yields a rather high weight to load ratio. Hence these

gates are predestined for flood control in low head run-of-river plants, where the width of river provides sufficient place, e.g. Kuibisheff, Volga, USSR, Q_{max} = 64 000 m^3/s, 38 openings of 20 m width.

II. Gates with rotary motion: By rotating about an axis, friction and wear is lower than in sliding gates. This feature also limits the height of the individual gate and its stroke and makes the streamwise length of the gate larger than in case 1. Moreover a multiple arrangement of gates as in case I is rarely found. The cylindrical shell type of these weirs yields a lower weight to load ratio as type I.

– Fishbelly flaps: These are mainly used as an attachement to other weirs and then exclusively applied to head water level regulation (see Figs. 3.3.11 and 3.3.12 b, [3.76]).

– Segmental barrage type tainter: Here (see Fig. 3.3.12 a and b) a water-loaded cylindrical surface eliminates the torque of the hydraulic thrust and usually also that of the weight about its fulcrum. This fits the gate also for medium heads. The flow is underneath the gate and the torque due to the gate's weight is usually hydraulically balanced by shifting the segment's centre away from its fulcrum (Fig. 3.3.12 b). Operation by one or two oilhydraulic servomotors, whose swiveling cylinders are supported by a cross beam downstream.

– Submersible tainter gate dam (see Fig. 3.3.13 a). Its wetted surface consists of a complete watertight sector, which is turned (and thus submerges) into a suitable pit, water tight along the sliding face of gate. The flow is discharged above the upper edge. Instead of only the two fulcrums of the tainter type, it is supported by many of them. This enables a larger clear width. Hence this weir is predestined for large flow in low head run-of-river plants.

Here in the floating type (see Fig. 3.3.13 b) not only the torque due to water load disappears, but also that owing to weight is compensated by hydrostatic uplift of the floating sector (so called drum barrage dam).

The regulation may be effected automatically by a float on the head water level. Its linkage actuates simultaneously two valves that connect or disconnect respectively the head water with the pit and the pit with the tailwater, stabilized by a feedback from the gate.

– Bear trap dam: This gate consists of two rotary parts (see Fig. 3.3.14). One first part downstream rests on water by means of a float. The flow is discharged above its crest.
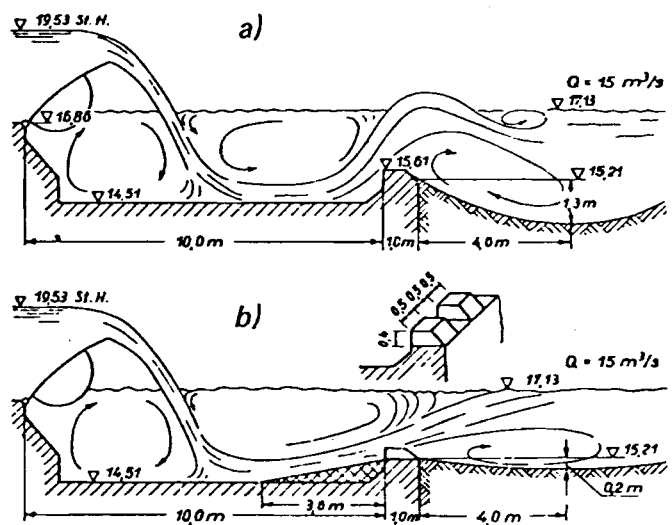
Fig. 3.3.11. Schematic view of fishbelly flap and stilling basin under spillage a) scour past stilling basin favoured by ford at the downstream end b) scour past stilling basin diminished by indentation of a ford (From MAN).

89
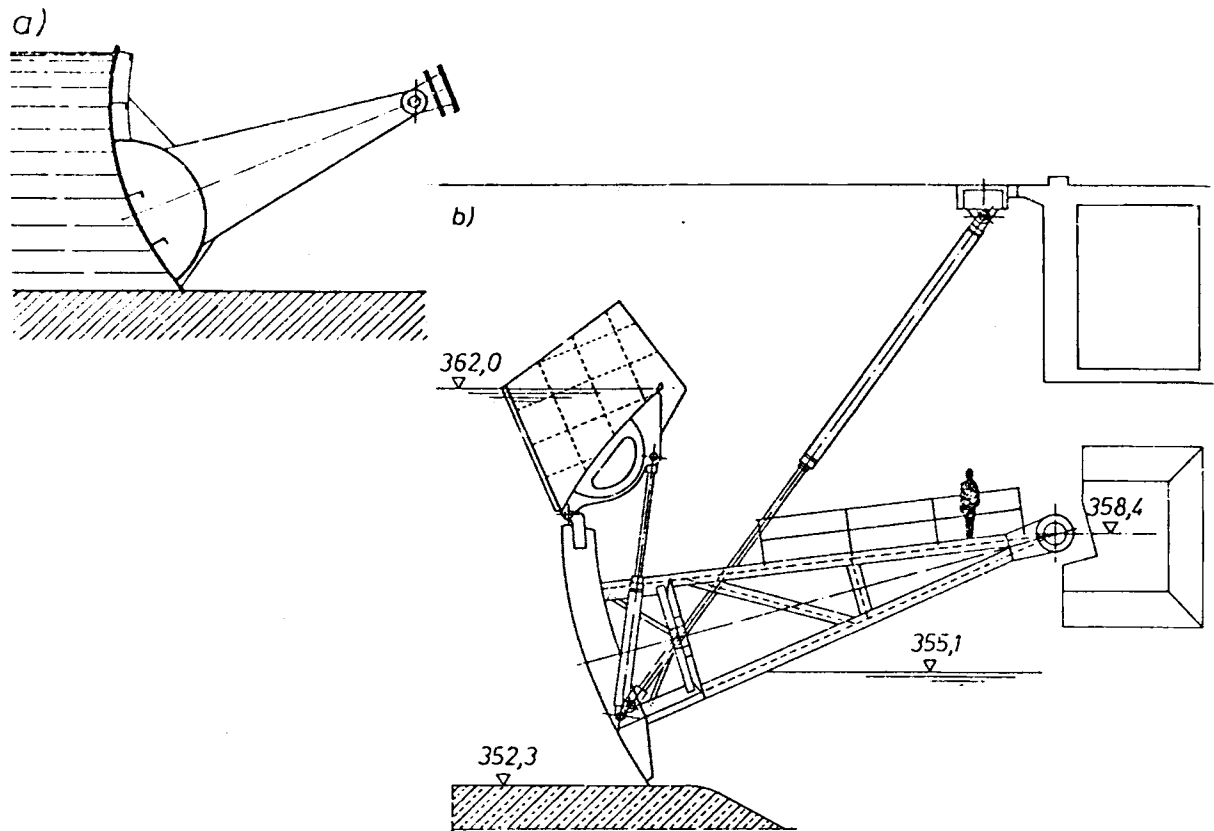
Fig. 3.3.12. a) Segmental barrage of the tainter type. Inclination of the segment towards the horizontal facilitates the balance of weight-induced torque about the fulcrum and also by that of the hydrostatic lift. The gate is moved either by synchronized chain drive on both sides or by a swivelling oil operated servomotor in the median plane. b) Tainter gate with fishbelly flap on crest of abutment power plant Perach. Inn, West Germany (owner Innkraftwerke Töging). Built by Noell, Würzburg. Clear width 4 · 18 m. height of closure 9,7 m with 2,9 m for the flap. Tainter gate operated by swivelling oil hydraulic servomotor on both sides. Additional servomotor for flap. (Drawing courtesy Noell, Würzburg).
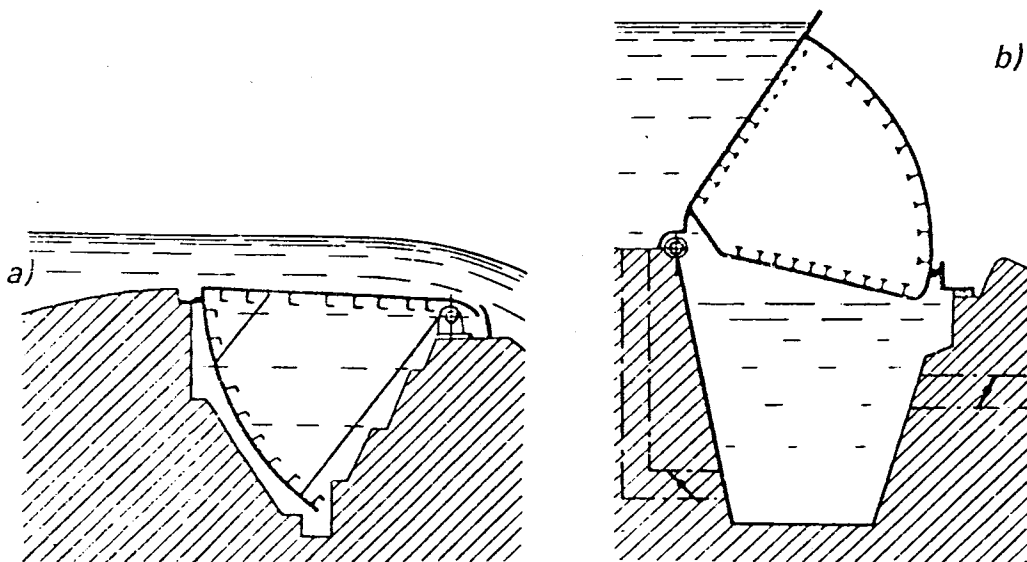
Fig. 3.3.13. a) Submergible tainter gate dam, in the lowered position b) Floating type of a) (drum barrage dam) in the elevated position (From MAN).

90

Fig. 3.3.14. Bear trap dam. Automatic control by float, actuating a valve, from upstream.
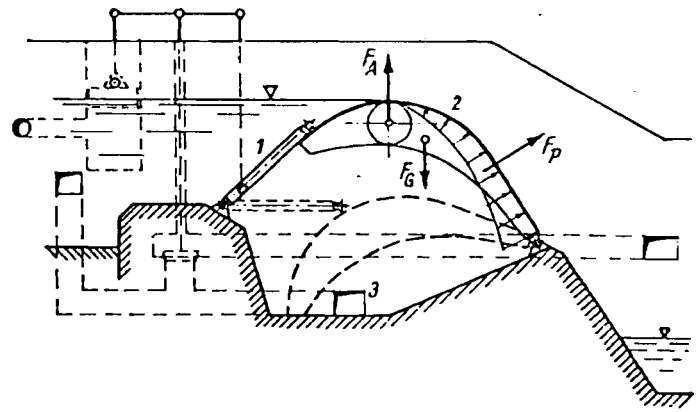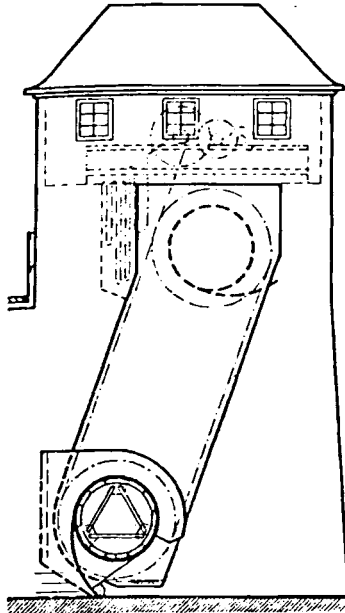
Fig. 3.3.15. Roller weir in extreme positions, specifically light construction (After MAN).

To enable control, by watering or dewatering respectively, the pit of this body, and the pit's upper end are made watertight by a second rotary gate upstream and sealed against the first in addition to the seals at the walls. A hook at this gate limits the stroke. Automatic control by float-actuated valves.

- Roller weirs: They comprise a tight steel cylinder (see Fig. 3.3.15) whose front disks are driven by a gear wheel at both ends. These engage with an inclined rack. This mechanism provides for the lift of the weir by means of a cable wrapped around it and pulled by a motor. The discharge is underneath. A shield on the upstream front of weir provides for water tightness of lowered gate. This type is deemed to be especially frost resistant.

3.3.2.5. Dynamic behaviour of spillways

Any spillage is usually connected with high overcritical velocities in the lamina spilled and then with the conversion of them into subcritical speed. The first may be connected with high wear and tear at the gate walls in the case of a bottom outlet or at least on the bottom of the stilling basin. This is in connection with silt transport.

If passing a wall projection, which is too sharply curved or sharply edged towering in the through-flow section of a bottom outlet, the spilled flow may cavitate and cause pitting. Spilled flow requires attention to its hydro elastic effects (Naudascher [3.78 to 3.80]). For its low velocity at crest and the respective low inertia forces, a nappe tends to start flutter there [3.81]. This may be damped by ventilation, and excited by hydro-elastic response of elastic guide walls but mainly of air pockets formed by the bottom impact of the nappe.

Often streamwisely orientated vortices moving across the back of weir during spillage may amplify these effects. To prevent this cross motion the back of the weir is usually equipped with guide plates in the streamwise direction [3.82]. Also other kinds of vibrations may occur at gates [3.83].

91

3.3.3. The stilling basin

The flow spilled, flows against the stilling basin with a major resonant speed due to the depth of the tailwater [3.18]. Then in the stilling basin the flow again is converted into subcritical flow with respect to channel depth via a hydraulic jump. This conversion is connected with the dissipation of head at the spillway into heat.

Without a properly designed stilling basin the foundations of the spillway and its neighbouring structures would be undermined by erosion in consequence of shock and wall shear stress due to this energy conversion [3.84]. Hence scour has to be prevented.

The conversion of kinetic energy into heat and dissipation results essentially from shear flow layers due to vortices. In order not to damage the walls too much, vortices are artificially created by means of prisms of concrete, so called Rehbock teeth on the stilling basin's bottom (see Fig. 3.3.11).

The axes of these vortices should be mainly inclined into the free flow of a stilling basin, that is sufficiently deep. Thus the dissipation expands into a large volume of water.

In low head plants with by pass-outlets around the sets or spillways above the sets (submersible power plant) the design of the stilling basin should be such as to favour the formation of a hydraulic jump downstream of the turbine's exit, thus enlarging the head by the hydraulic jump's height [1.53] when spillage is occurring.

Ski jump spillways (see Fig. 3.3.5) may save the expenditure of the stilling basin [3.86]. Here the kinetic energy of the jetlike flow lamina spilled is dissipated in the tailwater sufficiently far away from the plant's foundation. If the ski jump spillway orients the individual jets somewhat against each other, the spilled flow lamina dissipates a portion of its energy by this interaction before it reaches the tailwater level.

Further references on spillway design see [3.85 to 3.90].

3.3.4. Valves

I. General remarks: Valves may serve different purposes. In general a valve located upstream of the entrance of the turbine should interrupt the flow and stop the turbine, thus permitting inspection. Hence a valve usually is used for higher pressures than a gate. Therefore the cross section blocked by a valve is smaller than that closed by a weir gate. To save rather expensive valves at the inlet of large high head turbines, these highly loaded valves have been omitted in favour of a low loaded gate at the inlet of the penstock in Churchill Falls, see also 2.4.

Another purpose of a valve may be that of a locking or a regulated closing apparatus of a bottom outlet assisting a spillway or substituting for it. Further valves are found in FTs as by-pass outlet against water hammer-induced pressure surges. In both the last cases the valve serves as an energy dissipator (in the first cases assisted by a stilling basin or at least the tail water) [3.76, 3.91].

II. Wedge valves: Advantages: Short and simple, for the case of a design with wetted spindle, also small height, unlimited pressure, no loss under full load. Disadvantages: No part load opening, closure may provoke vibration by stall and cavitation, tightness needs careful finish, a cheap and well accessible drive via a dry spindle of carbon steel needs a spacious casing.

III. Ring (needle) valve: Designed either with a drive inside the hub or outside with a rod crossing a bend (see Fig. 3.3.16). Advantages: Partial opening possible, high head, small

92

Fig. 3.3.16. Ring (needle) valve in bend with
external drive.
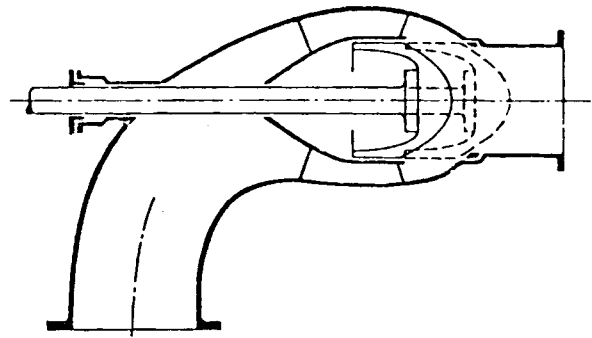
adjusting power. Disadvantages: Expensive, demands large space, also small loss during full opening, bad vibrations and cavitation possible under small openings, limited in size [3.92].

To save expenses the FTs of La Grande 2 (Canada) have been equipped with spindle-operated ring valves or cylindrical gates between stay vanes and guide vanes, as a watertight shut down device [3.93]. It may be hinted that the joint between stay ring and head cover usually in a FT has to transmit large forces and moments, which need an absolutely tight seal close to the guide vane channel. The above arrangement spreads this joint and loads it in the critical case of sudden shut down with control-induced forces [3.83].

The conical valve may be considered as a related design, diffusing the flow instead of contracting it [3.94], especially used as by-pass outlet of FTs in North America and known there under the designation Howell-Bunger valve.

IV. Spherical valve: (see Fig. 3.3.17). Occasionally equipped with a locking apparatus for revision (see Fig. 3.3.17 c). Advantages: No losses in the opened position, small opening power, if equipped with a filling device for the pipe between the valve and the turbine's control mechanism (needle valve, gate), then closed; suitable for highest head [3.95; 3.96].

Disadvantages: Expensive, somewhat space consuming, large adjusting power for shut down under full load flow, then also cavitating and badly vibrating, no part load operation, limited size.

V. Butterfly valve: (see Fig. 3.3.18). Advantages: Cheap and space saving for heads up to 400 m, losses under full opening can be reduced by the biplane disk design. Disadvantages: Part load operation is not steady and may lead to cavitation.
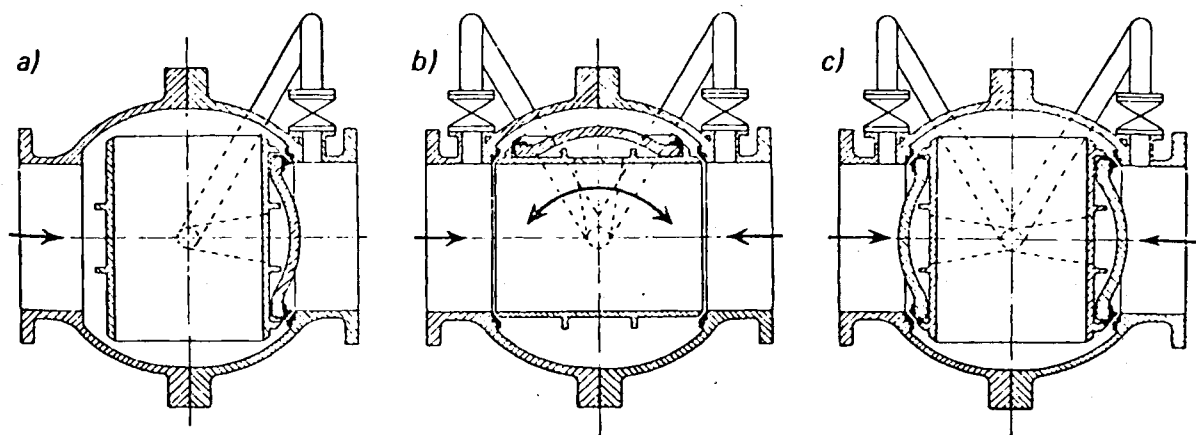
Fig. 3.3.17. Spherical valve a) closed b) opened c) with additional revision seal. In a recent design the short stroke piston on the rotor is replaced by a pressure loaded elastic ring plate, clamped at its tip diameter (Drawing courtesy Sulzer Escher Wyss).
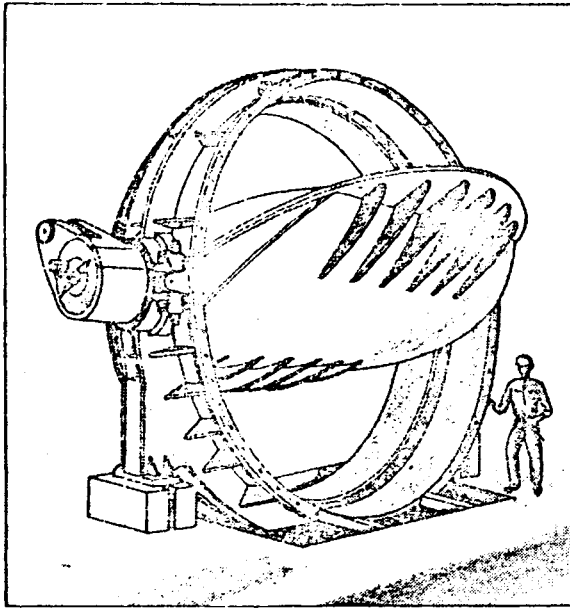
The dynamic behaviour of butterfly valves also under cavitation was described by *Grein* and *Osterwalder* [3.97 to 3.103]. For any case, the dynamic behaviour of valves, their cavitation, their adjustment forces versus stroke have been carefully investigated [3.103; 3.104], also under natural pressure heads and under penstock failure [3.105 to 3.109].

3.4. The power house and its equipment.

3.4.1. The constituent elements of a power house

3.4.1.1. General remarks

The main purpose of the power house design is the proper location of the electrical and hydro mechanical equipment of plant.

In installations with vertical shafts (which predominate in the head range up to about 1300 m, except the majority of pumped storage plants with ternary sets) the structure of the power house can be divided vertically into three zones from the bottom to the top. They are: 1) The zone of the draft tube and tailrace tunnel, 2) the zone of turbines, their pit and penstock, 3) the zone of generator and building construction.

In installations with a horizontal shaft, zones 2) and 3) are at the same level. The zone 1) along with the foundation of machinery and its possible draft tubes dominate the "substructure", and zone 2) and 3) the "superstructure". In plants with vertical shaft, large submergence, and ternary sets with one thrust bearing underneath, also zone 2) may be included in zone 1).

Even if the vertical arrangement is common practice with large sized sets, a comparison will be made between some features of a power house due to vertical sets and horizontal sets with respect to floor required, rectilinearity of flow passage, ease of assembly, revision and dismantling.

Vertical sets have the smallest floor space requirement. This may be important in narrow valleys and densely populated areas but also if only to a lesser degree in underground

94

stations as then the expensive roof of the gallery is shortest. Any vertical plant with reaction turbines requires a bend in the draft tube, a source of additional loss. In high head plants also the admission duct shows two bends in series in different planes, a cause for secondary flow.

During assembly the alignment of rotor and stator with its small gap clearance is eased because of the absence of shaft deflection. However, dismantling the lowest parts may be more difficult. Servicing becomes more difficult especially in peak load or pumped storage plants, often changing their modes. The axial thrust misplaces rotor vs stator.

The horizontal set requires more floor space. It guarantees the smallest deflection of flow especially in tubular turbines and in plants fed by one penstock, that is in the same plane as the shaft. The assembly is rendered difficult by shaft deflection especially caused by the heavy alternator rotor of large high head machines. To keep the clearance of turbine labyrinths, e.g. shin plates are required. Servicing on one floor and accessibility of all parts (e.g. dismantling) is eased.

3.4.1.2. The superstructure of the power house

The superstructure consists mainly of the machinery (the sets, the main crane, the repair shop, the erection bay, the control room, the offices, sometimes as in underground stations also the transformers, the high voltage switch plant with high capacity circuit breaker, disconnector). Usually the latter equipment is installed in an open air switch yard.

I. Impulse turbines, PT: 1) With horizontal shaft, with up to two wheels, overhung, on both sides of the alternator (Fig. 3.4.1) with 1 nozzle pipe, curved and passed by the needle rod or straight for the highest head, with 2 nozzle pipes in the "tongs design" (Fig. 3.4.2) [3.110] with needle servomotor inside or outside the nozzle pipe. 2) With vertical shaft, up to 6 nozzles, with spiral distributor (see Fig. 3.4.3), or other arrangement of manifolds, e.g. the "pine-tree-design" (see Fig. 3.4.4).

A price comparison shows the advantage of a supply by multiple branches. This solution, in spite of its apparent complexity, results in considerable savings for the penstock equipment, when at the same time the single spherical valve for each turbine is replaced by one for two sets. First of all, according to Vevey-Charmilles, a large bus-pipe distributor can be avoided. Then the reduction of
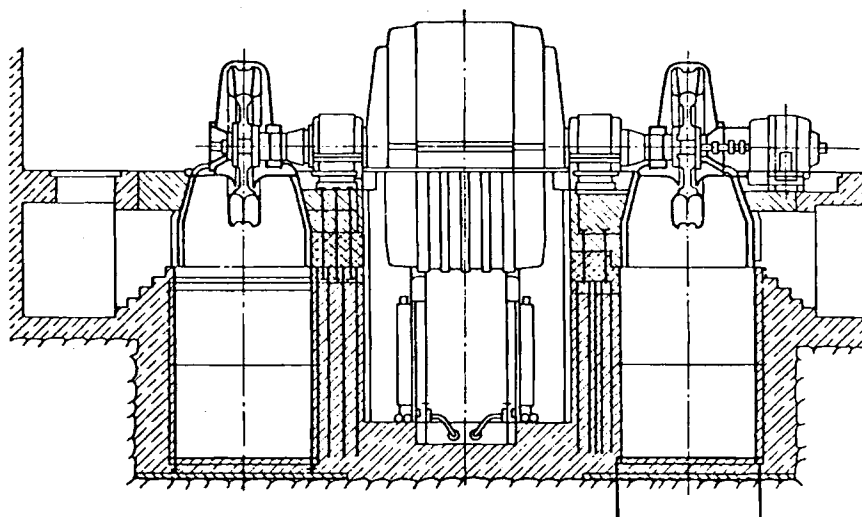
Fig. 3.4.1. Elevation of horizontal shaft, 2-wheel PT of Biasca, Ticino, Switzerland, overhung design, 1 nozzle per wheel, $H = 707$ m, $P = 4 \cdot 79$ MW (Drawing Courtesy Sulzer Escher Wyss).
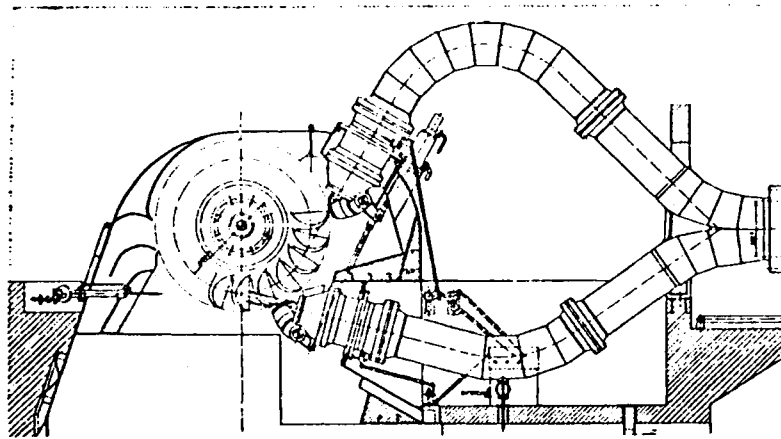
Fig. 3.4.2. Cross section of horizontal shaft, 2-nozzle, 2-wheel PT at Kops, Austria (owner Vorarlberg Illwerke, Bregenz). $H = 780$ m, $n = 500$ rpm. $P = 3 \cdot 76{,}6$ MW, runner weight 7,7 tons. Admission pipes in the so-called tongs design. Large space requirement for reduced curvature of pipes (Drawing courtesy Voith).
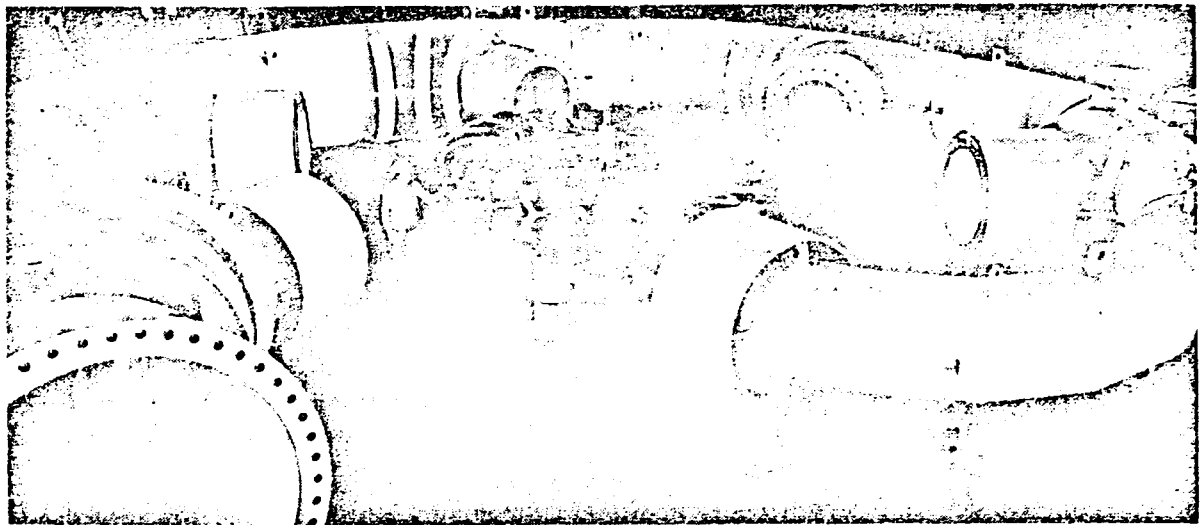
Fig. 3.4.3. Spiral distributor of 6-nozzle PT for Restitucion, Peru in Hydroart Works, Milan, Italy. $H = 255$ m; $Q = 32$ m^3/s; $P = 75$ MW; $n = 200$ rpm. Integrally cast whell of 13/4 Cr/Ni steel; $D = 4190$ mm, 33 tons. bucket width 1000 mm; 20 buckets. Distributor inlet diameter 2400 mm. Note guide rib in nozzle pipe inlet. (Photograph courtesy Hydroart, Milan, Italy).

the pipe diameters occurs much sooner than is the case with a conventional spiral, thus reducing the dimensions of the branch pipes as well as the thickness of steel plate and the amount of welding [3.111].

According to their high head, PTs are usually located in underground stations (see Fig. 3.4.5), or in an open house on the base of a slope (see Fig. 3.4.6). For horizontal sets, the power house volume is smallest (see Fig. 3.4.5). Vertical sets have the smallest floor space requirement [3.112].

To avoid flow disturbance, the needle servomotor is housed within the nozzle pipe (see Fig. 3.4.7) usually equipped with coil springs to balance the hydraulic force on the needle.

To protect the environment from the noise of the jet if cut by the buckets, the tail water tunnel needs a "ducking wall" as a short immersion ceiling between the wheel chamber and the surroundings.

96
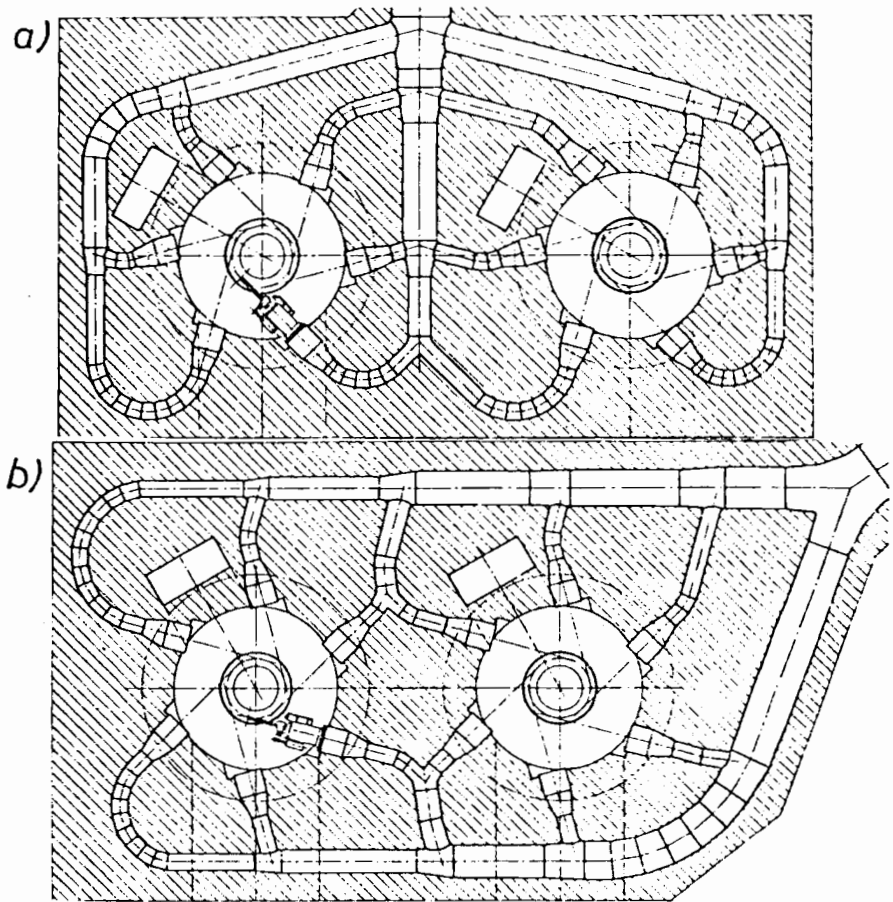
Fig. 3.4.4. Alternatives to spiral distributor of vertical multi-nozzle PTs a) Pine-tree-design, plant El Toro, Chile. $H = 545$ m; $n = 333,3$ rpm; $P = 116,2$ MW. b) Ramification of 2 branches in parallel, plant Mauranger, Norway. $H = 825$ m; $n = 500$ rpm; $P = 126.8$ MW. Note only 1 shut down valve for 2 neighbouring sets (Drawing courtesy Vevey Charmilles Engineering Works).

Fig. 3.4.5. Cross section of the underground power house and valve chamber at Nendaz, Rhone, Switzerland. Horizontal 2-wheel, 1-nozzle PT. $H = 1004$ m; $n = 500$ rpm; $P = 6 \cdot 64$ MW. Space required per set 8250 m^3 (Drawing Vevey Charmilles Engineering Works).
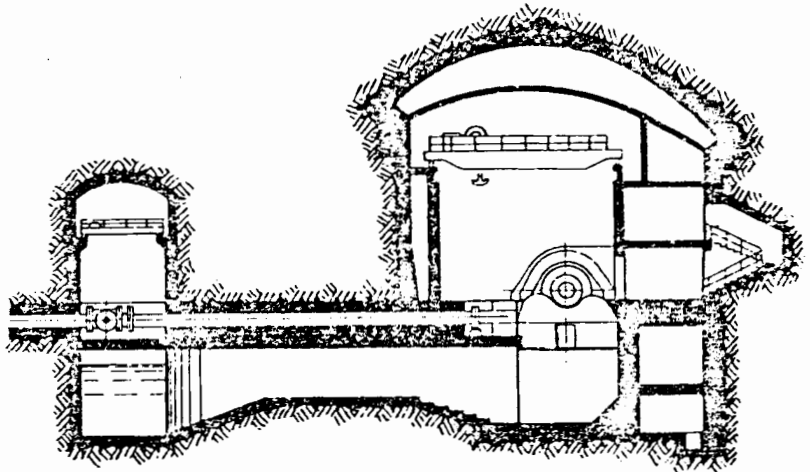
In some rare cases of a hydropneumatized Pelton T with a wheel chamber submerged under a changing tail water level (e.g. the ocean by tides), the then pressurized tail water tunnel has a ceiling that descends in streamwise direction. This is made with the aim of separating and then returning the air into the wheel chamber as much as possible by virtue of buoyancy. This is found in the Norwegian plant Tysso, built by Sulzer Escher Wyss [3.113; 3.114].

97
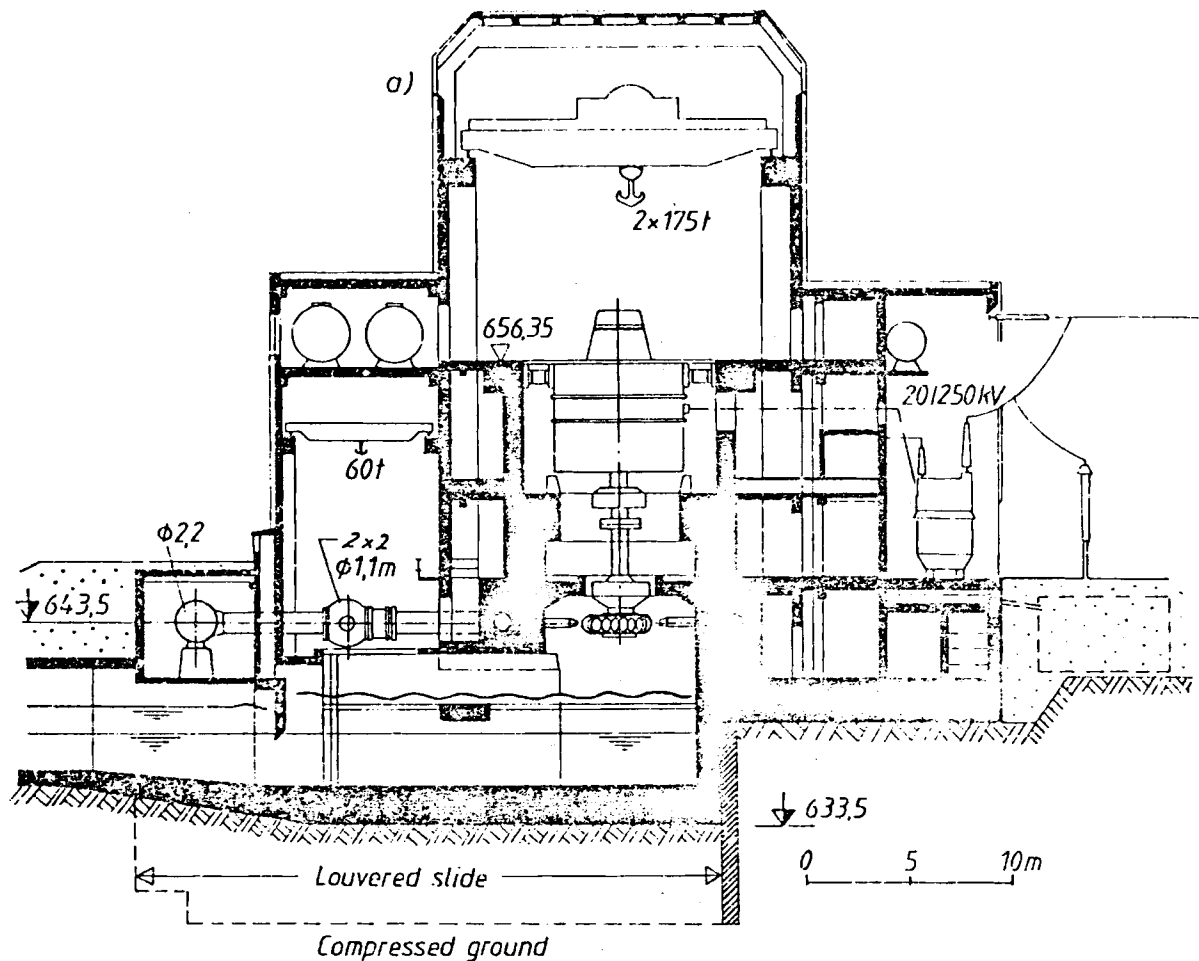
Fig. 3.4.6. a) Cross section of outdoor power house Silz, Austria (owner Tiroler Wasserkraftwerke. Innsbruck). Two vertical, 6-nozzle PTs. Power house of tall hall design with the main crane in the interior. Total weight of the rotating parts of one set 366 tons, total weight of one set 1022 tons.

II. Cross flow turbines type Michell-Banki: Preferably in Micro Power plants (see Cap. 2.5). To date mainly existing as the Ossberger design, with heads below 100 m and using rivers with often strongly varying discharge and hence also largely varying tail water level.

To use also the then varying elevation of the rotor above the tailwater level, the wheel chamber of this impulse turbine is equipped with a draft tube according to Ossberger (see Fig. 3.4.8). By means of a "snifting valve" the water level in the draft tube is automatically kept at a distance from the wheel so as to avoid immersion of the lower wheel edge in the water and hence to prevent disk friction. Now the jet passing the bladed wheel twice underneath the shaft, expands against a pressure, that is below that on the tail water by the draft tube water column [3.115]. Thus the suction head of this column is not lost.

Dividing the wheel chamber by disks into seprate sections, into which the water is admitted by differently adjusted guide vanes, the discharge may change in a wide range due to optimum efficiency.

The design is noted for great simplicity of construction (cylindrical runner vanes from plates, all welded).

98
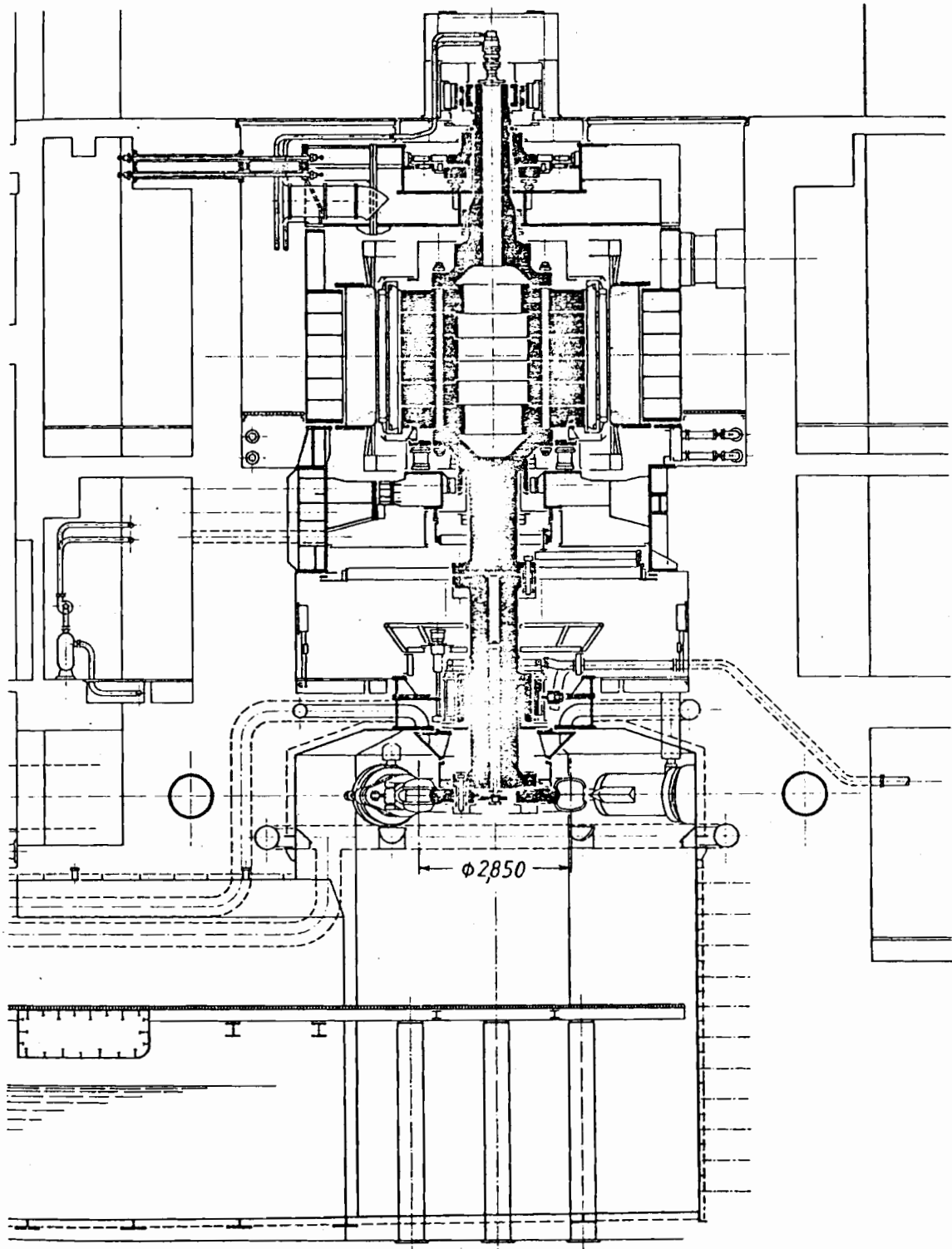
b) Elevation of one set, $n = 500$ rpm, $H = 1238,5$ to $1257,5$ m, with 2 sets $P = 233,3$ to $244,3$ MW, with 1 set $P = 259,9$ to $264,8$ MW (in consequence of penstock loss, a smaller output with 2 sets operating) wheel, $D = 2,85$ m, flow admission similar Fig. 3.4.4.b. PT built by Sulzer Escher Wyss. Fully water cooled alternator. (Drawing courtesy Tiroler Wasserkraftwerke, Innsbruck).
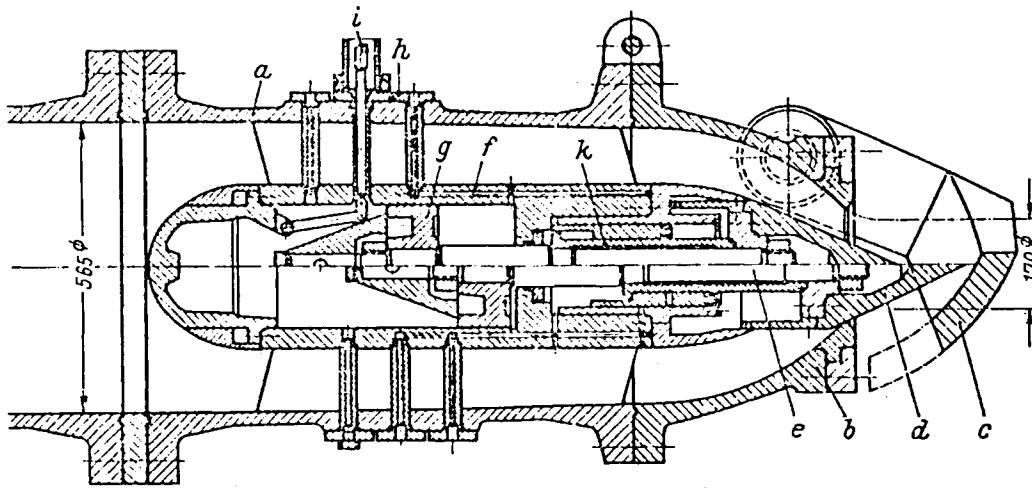
Fig. 3.4.7. PT needle drive inside nozzle. No external linkage. No reaction force on the pipe wall or surrounding concrete. No disturbance of the needle control by rod elasticity. 2-stage compensation piston without a spring to equalize the adjusting force along the needle travel. Sulzer Escher Wyss design. a nozzle pipe with guide fins. b nozzle; c jet deflector; d needle head detachable; e needle rod; f servomotor cylinder; g piston; h oil head; i feed back; k relieving piston (Courtesy Sulzer Escher Wyss).
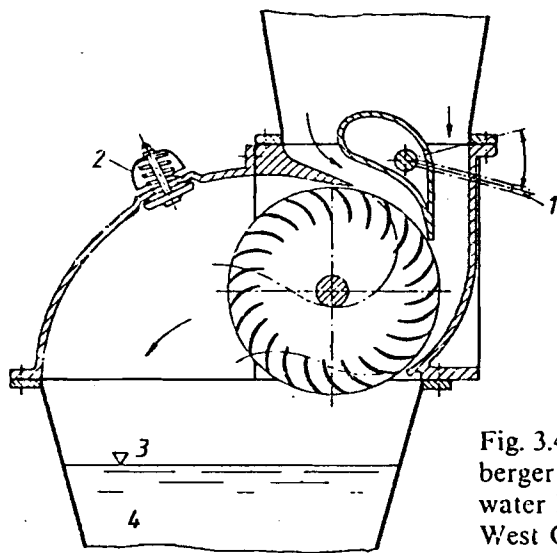
Fig. 3.4.8. Cross section of a Michell-Banki turbine of Ossberger design; 1 control vane; 2 snifting valve; 3 draft tube water level; 4 draft tube (Courtesy Ossberger Weissenburg, West Germany).

Typical superstructures of the Ossberger turbine are shown in the Figs. 3.4.9 and 10.

III. Reaction turbines. Here the following types are used: Kaplan turbines (KT), tubular turbines (TT) with their variant of bulb turbine (BT) and Straflo turbine (ST) or turbine with rim generator, Francis turbine (FT), diagonal turbine (DT) after *Deriaz* and *Kviatkovsky* [3.116; 3.117]. There the following typical designs of superstructure and machinery may be distinguished.

a) Wall turbine with horizontal shaft (in general FT) in a free surface chamber (see Fig. 3.4.11 a), flow admission without spiral casing with inside regulation of gates. Overhung design of runner, elbow draft tube traversing the head tank [3.118; 3.119].

Fig. 3.4.9. Superstructure of larger Mini power plant equipped with Banki-Ossberger turbines. Drouet, Haiti; 3 sets: $H = 9,7$ m; $n = 120$ rpm; $P = 0,55$ MW; 2 sets: $H = 12.15$ m; $n = 135$ rpm; $P = 0,69$ MW. Belt-driven speed governor with control linkage; step up spur gear; high speed alternator (Photograph courtesy Ossberger, Weissenburg, West Germany).
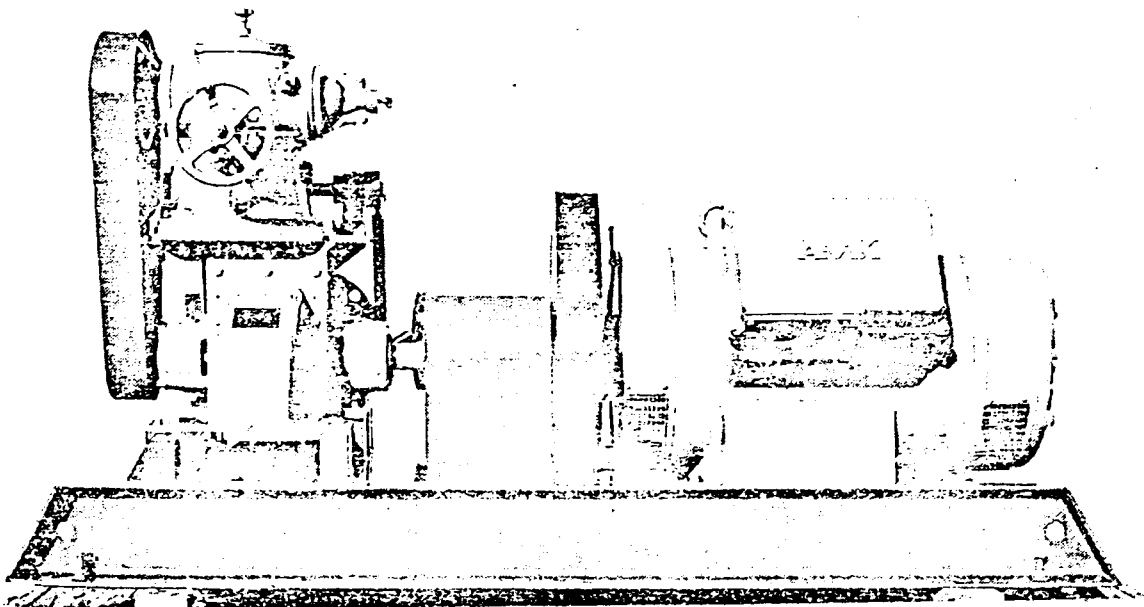
Fig. 3.4.10. External view of a high head Ossberger turbine. Totora-Epizana (Bolivia). $H = 150$ m; $n = 1500$ rpm; $P = 95$ kW. The size of governor and direct coupled generator in relation to the turbine casing reveals the power density of the "high head" crossflow turbine type Ossberger. (Drawing courtesy Ossberger, W. Germany).

101
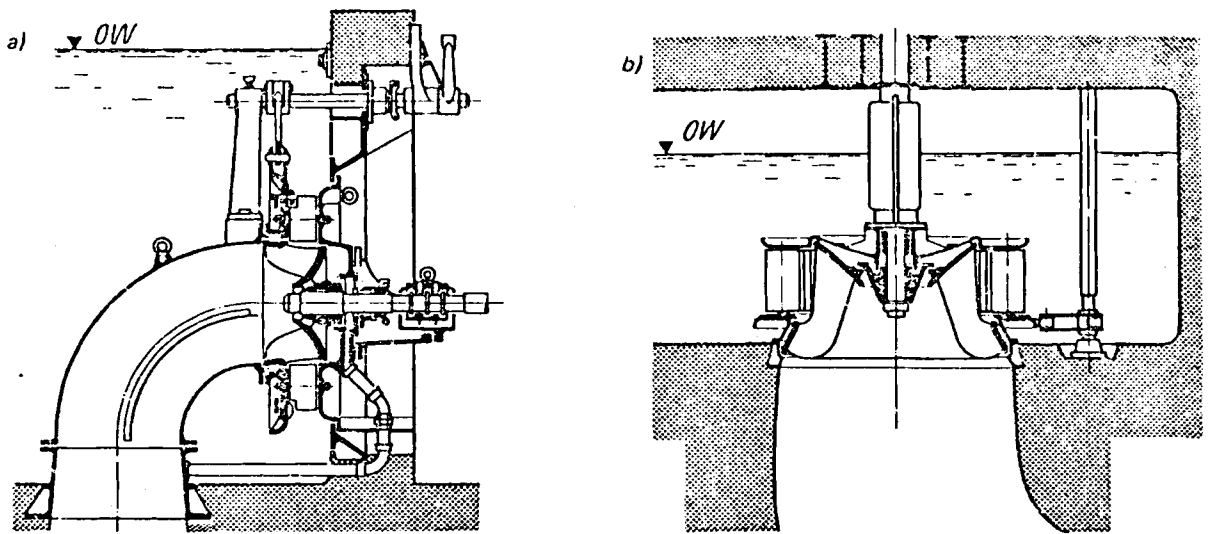
Fig. 3.4.11. a) Francis wall-turbine with horizontal shaft b) Francis pit-turbine with vertical shaft. Both supplied by open head race tank. (Drawing courtesy Voith)

b) Pit turbines with vertical shaft (see Fig. 3.4.11 b), admission, regulation and runner as a), elbow draft tube in concrete, FT or KT [3.120; 3.121]. a) and b): Cheap but bad inflow.

c) Turbine with vertical shaft, runner as a), admission by semi-spiral casing in concrete (see Fig. 3.4.12) with underground power house (see Fig. 3.4.13) or open air power house (see Fig. 3.4.14), external gate regulation. Usually KT.

d) Turbine with vertical shaft, admission by spiral casing of concrete, steel-lined, riveted or welded and embedded in reinforced concrete or made of cast iron. For high head KT, FT or DT (see Figs. 3.4.15 to 3.4.16).

e) Turbine with horizontal shaft, admission by spiral casing of cast iron or steel, welded or riveted. For high head KT or FT of wide head range (see Figs. 3.4.17; 18).

f) TT with rim generator, horizontal or slightly inclined shaft, traversing the power house of a submersible plant (see Fig. 3.3.3), recently as the Straflo turbine (ST). In the original version with an axial distributor and normally fixed runner vanes (see Fig. 3.4.19). In the
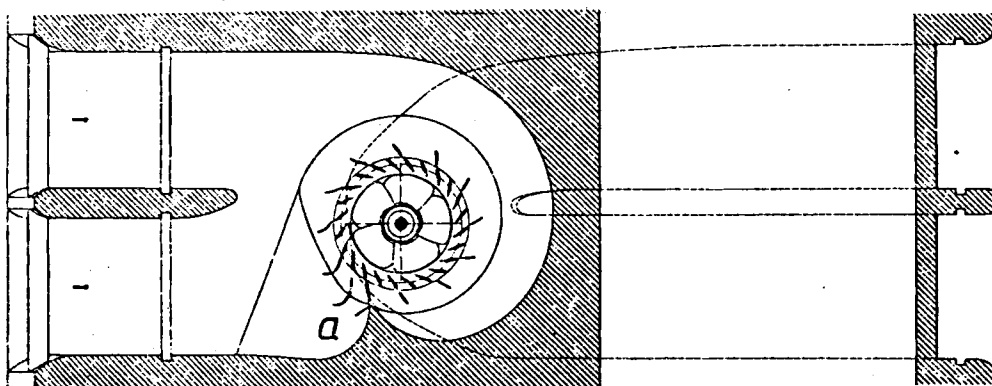
Fig. 3.4.12. Plan of semi-spiral casing and elbow draft tube of vertical shaft KT. Plane joint of neighbouring concrete blocks. Excentric flow admission in spiral compensated by curved draft tube centre line. Tongue about 30° upstream of turbine axis. Before tongue generation of cirulation only by stay vanes a. (From Voith)

102

Fig. 3.4.13. High head KT Pirttikoski, Finland in underground power house (A Scandinavian feature). $H = 27$ m; $n = 115.4$ rpm; $P = 2 \cdot 66$ MW. KTs built by Sulzer Escher Wyss. Stop logs in draft tube. Higher head stresses stay vanes by tension, which is transmitted into concrete by tie rods. 1 maximum, 2 minimum tailrace level (Drawing courtesy Sulzer Escher Wyss).
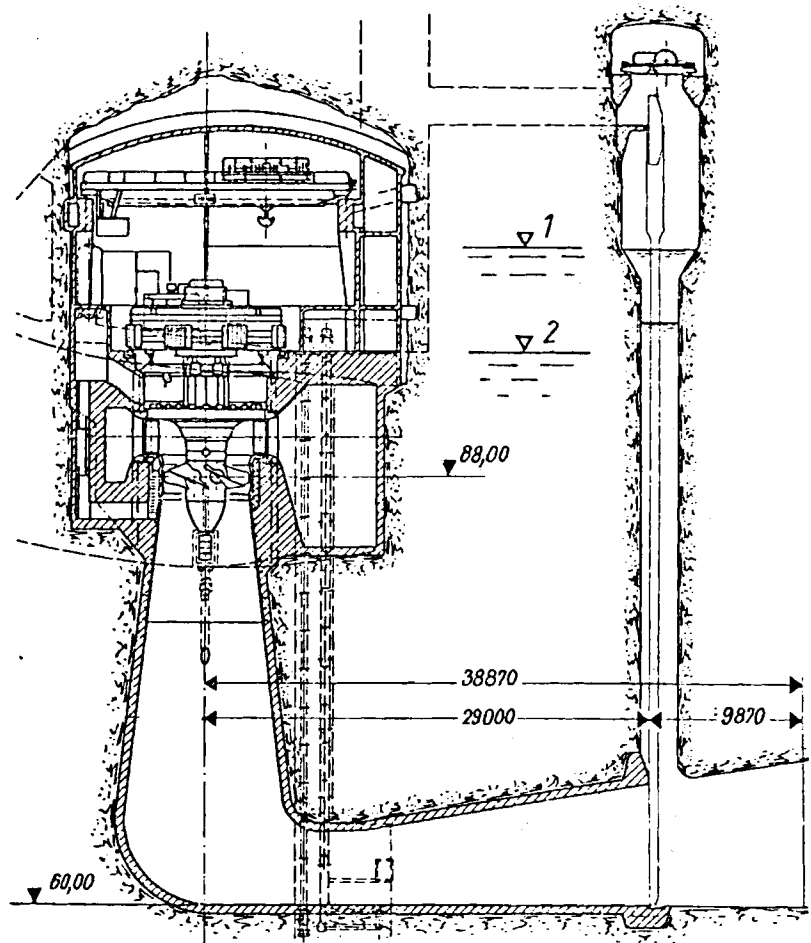
ST version mainly with adjustable runner vanes and a conical distributor, also useful for tidal power (see Fig. 3.4.20) [3.122].

g) BT with alternator in a bulb upstream of the runner and directly coupled to it, double regulated. To mount the generator rotor, diameter D_r, the following possibilities exist:
1) The bulb in an open flume accessible by a portal crane, a possibility for river and tidal plants in the open air (see Fig. 3.4.21). Generator easily accessible, rarely found.
2) The bulb with a hatch on its top for the generator rotor (Fig. 10.2.11). Expensive but easy access to the generator.
3) The bulb with access through a bore from the side of the runner, diameter $D > D_r$, (regular case). Then only one hatch, accessible by the main crane, is required for the runner and the generator rotor (Fig. 3.4.22) [3.123], generator badly accessible.

The design 2) and 3) result in 2 guide bearings for an output $P < 40$ MW (Fig. 3.4.23), and in 3 guide bearings for an output up to 60 MW (Fig. 10.2.10). Both the last types 2) and 3) can also be used in tidal power plants (Fig. 3.4.24).

h) BT, usually double regulated and with conical distributor, alternator with high ratio planetary gear, the shaft horizontal or inclined. The alternator may be dismantled and assembled or access obtained to it through a hollow stream-lined access shaft to the bulb; the draft tube crosses the power house, split into pieces, hence the runner is accessible and may be dismantled by a crane within or outside the power house, for river power plants (see Fig. 3.4.25) and for tidal power plants (see Fig. 3.4.26), especially suitable for the

a)

b)
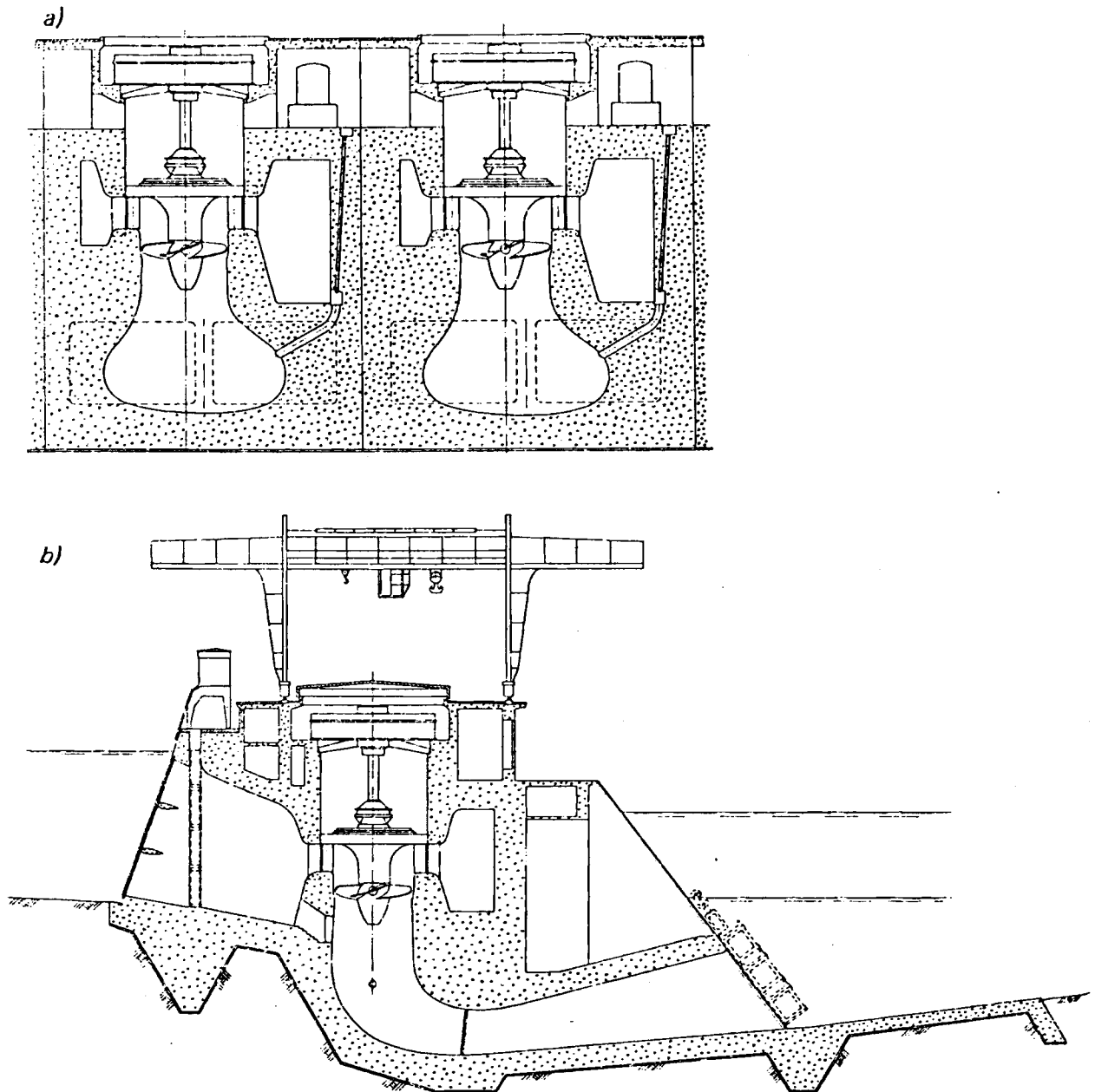
Fig. 3.4.14. a) Lateral section of adjacent blocks of vertical KTs, Feldkirchen, West German-Austrian Inn. (German owner Innkraftwerke AG, Töging) $H = 9$ m; $n = 90,9$ rpm; $P = 3 \cdot 38$ MW; KT built by Voith. Asymmetric draft tube for plane joint of neighbouring sets. b) Longitudinal section. Outdoor pit power house. Main crane outdoors, also for stoplogs. Trash rack rake. Access door to draft tube from spiral. Supporting pillar in the draft tube past the bend. Once stoplogs inserted, the drainage of the spiral into the draft tube and then into the sump of the drainage pumps. (Drawing courtesy Voith)

lowest head range and output up to 15 MW, according to the abilities of the gear manufacturers [3.124].

i) TT, single or double regulated, with a horizontal or inclined shaft crossing the draft tube bend, the generator directly coupled or gear – driven in the power house (Fig. 3.4.27), or, as the cheapest variant, in the open air (see Fig. 3.4.28), so called S-turbine. This type

104
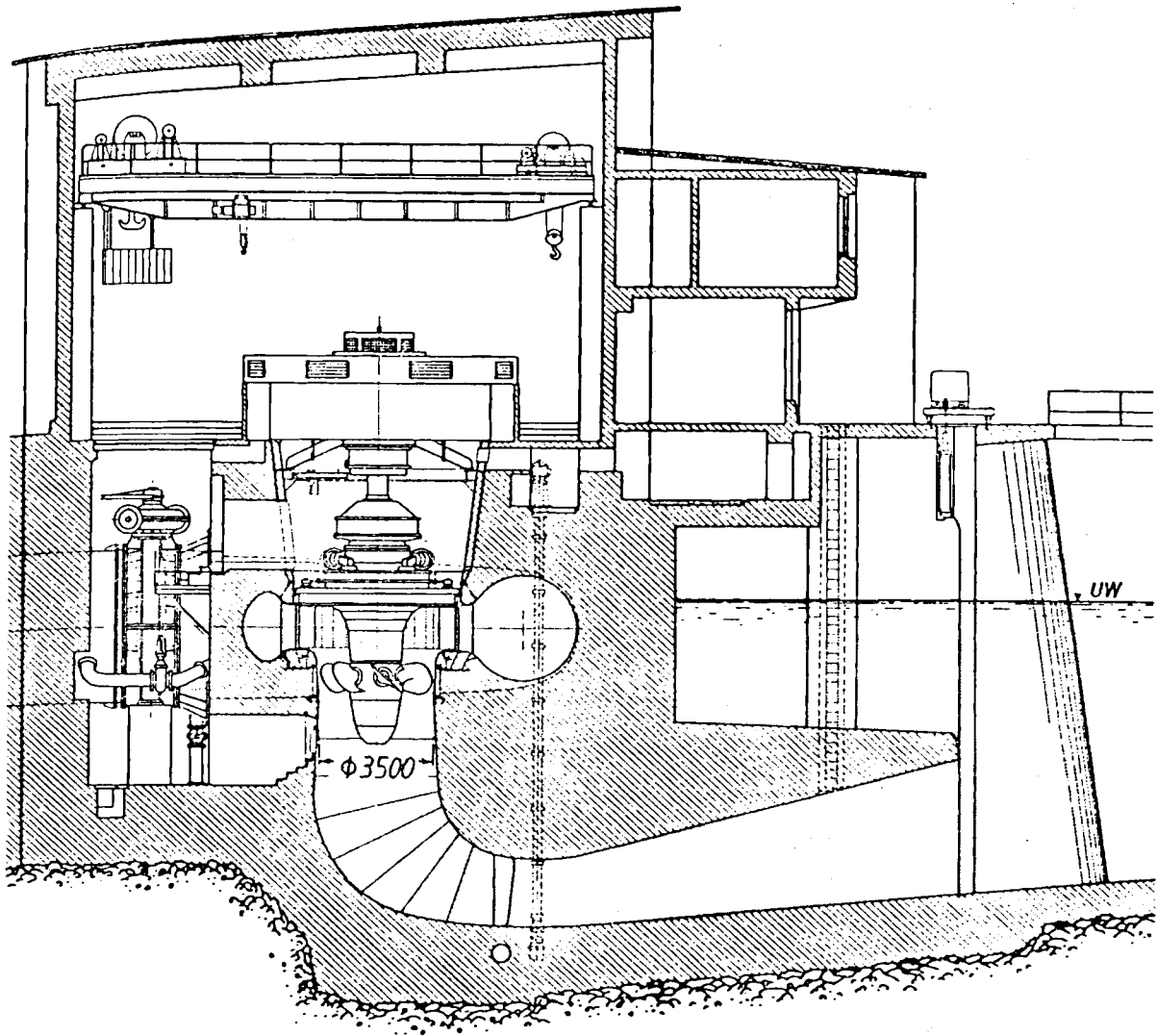
Fig. 3.4.15. Longitudinal section of power house and set, Rosshaupten, Lech, West Germany (owner Bayerische Wasserkraft AG BAWAG, München). Vertical KT with its spiral casing in concrete, steel-lined. At inlet a butterfly valve and y-fitting. $H_m = 40$ m; $n = 200$ rpm; $P = 2 \cdot 24$ MW. Runner 7 blades. (Drawing courtesy Voith)

of machine may also have a vertical shaft, passing a bend or an open flume before the runner inlet. The bend in the draft tube reduces the efficiency.

j) TT, non adjustable, with inclined shaft and draft tube bend as a siphon for convenient shut down and a head below 3 m, also useful as a free stream turbine to diffuse the kinetic energy of river rapids (see Fig. 3.4.29). For small units.

k) TT with a horizontal shaft of the BT design, the generator outside and driven by a bevel gear and a shaft passing through a hollow stay vane (see Fig. 3.4.30) (gear limits output).

l) KT with a vertical shaft, admission by a semi-spiral chamber of siphon design, the generator directly coupled, or with spur gear (see Fig. 3.4.31), or bevel gear. (Output limit gear-conditioned.)

m) Turbine with conical distributor as a diagonal turbine after Deriaz (Fig. 3.4.32), a vertical shaft KT (Fig. 3.4.33), or a tubular turbine of different design (BT, Straflo, S-turbine).

105
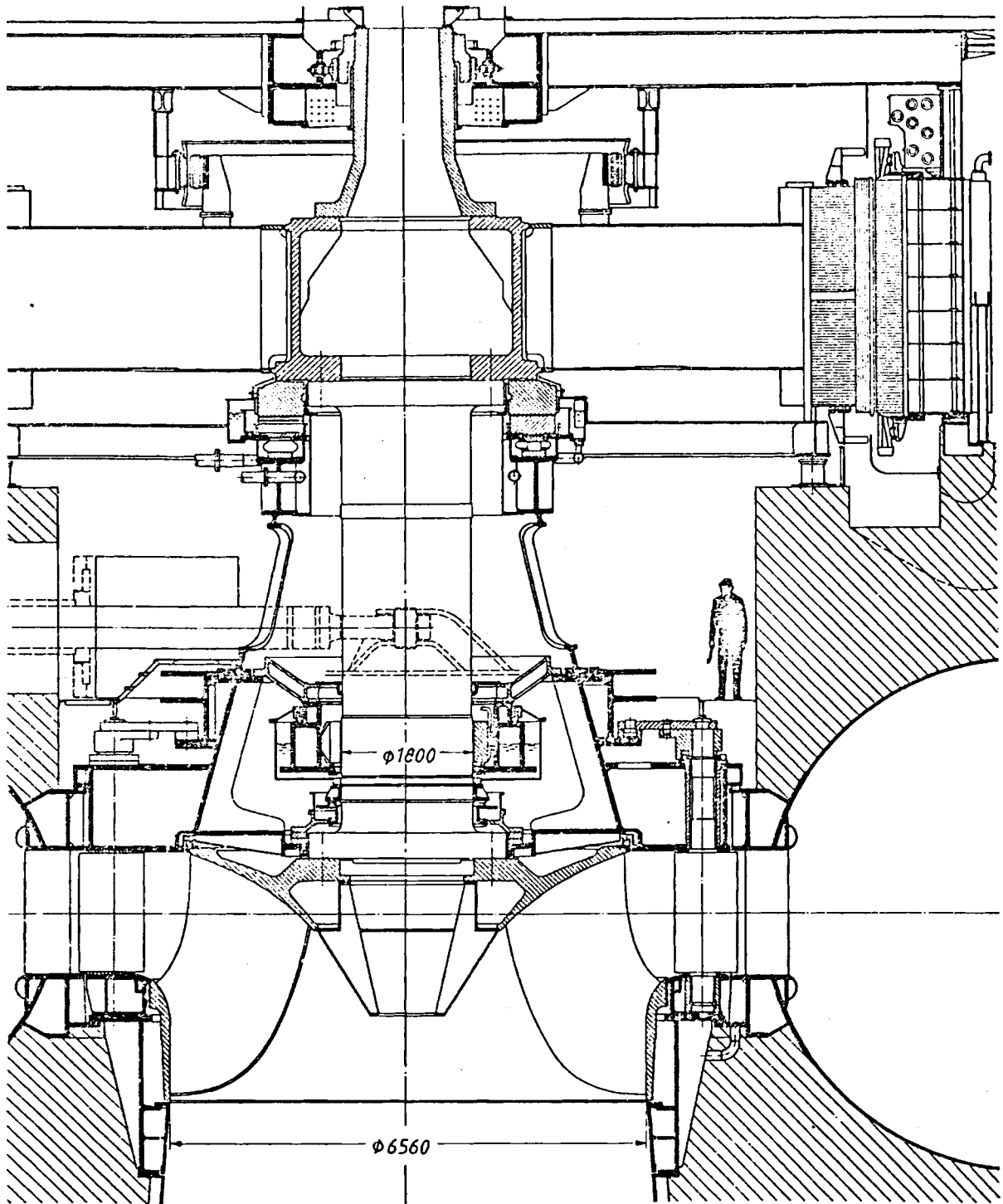
Fig. 3.4.16. Sectional view of vertical FT Cabora Bassa, Zambesi, Mozambique, Africa (owner State power board of Mozambique). $H = 113,5$ m, $n = 107$ rpm; $P = 5 \cdot 415$ MW. One of the most powerful FT sets ever built in Western Europe by the collaboration of Neyrpic, Grenoble, France and Voith, Heidenheim, West Germany. Parallel plate stay ring with guide rolls. Hence reduced outermost diameter of the spiral casing. Concrete around the spiral reinforced in the meridian between the stay rings (Drawing courtesy Voith).

Fig. 3.4.17. Elevation of a horizontal KT with a spiral casing St. Leonhard, Austria. $H_m = 74,5$ m; $n = 610$ rpm; $P = 11,05$ MW. High-head KT; 8 blades. (Drawing courtesy Voith)
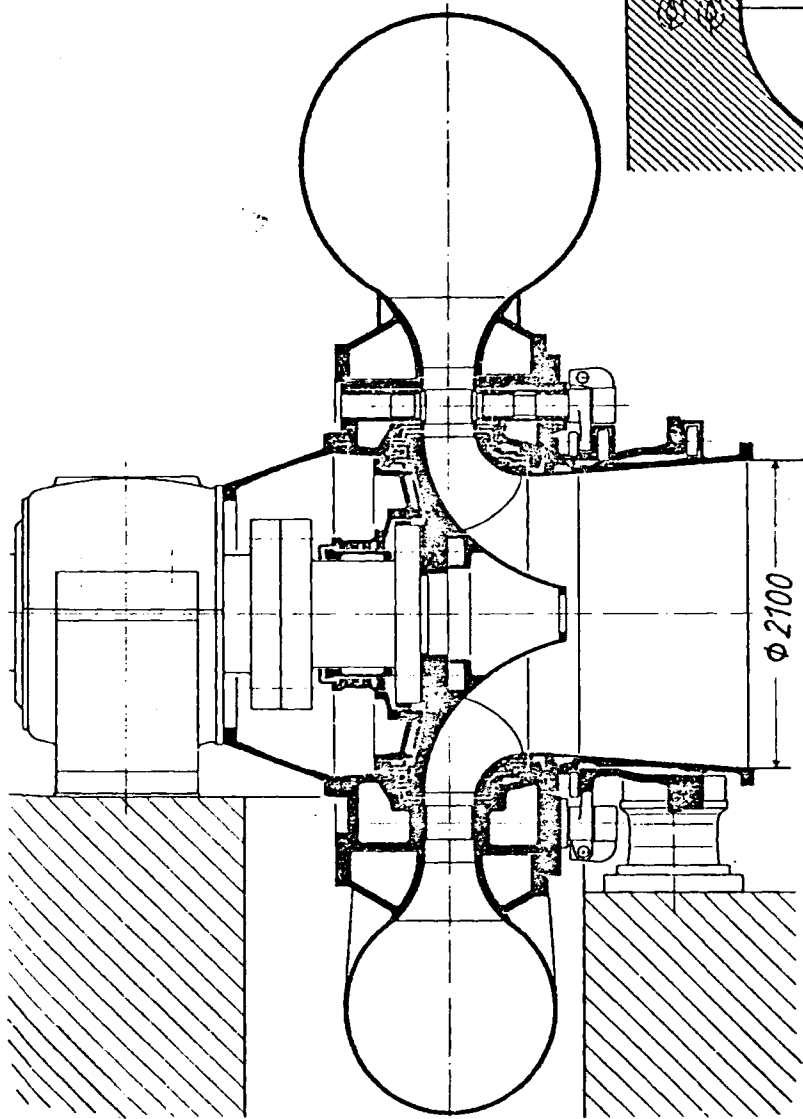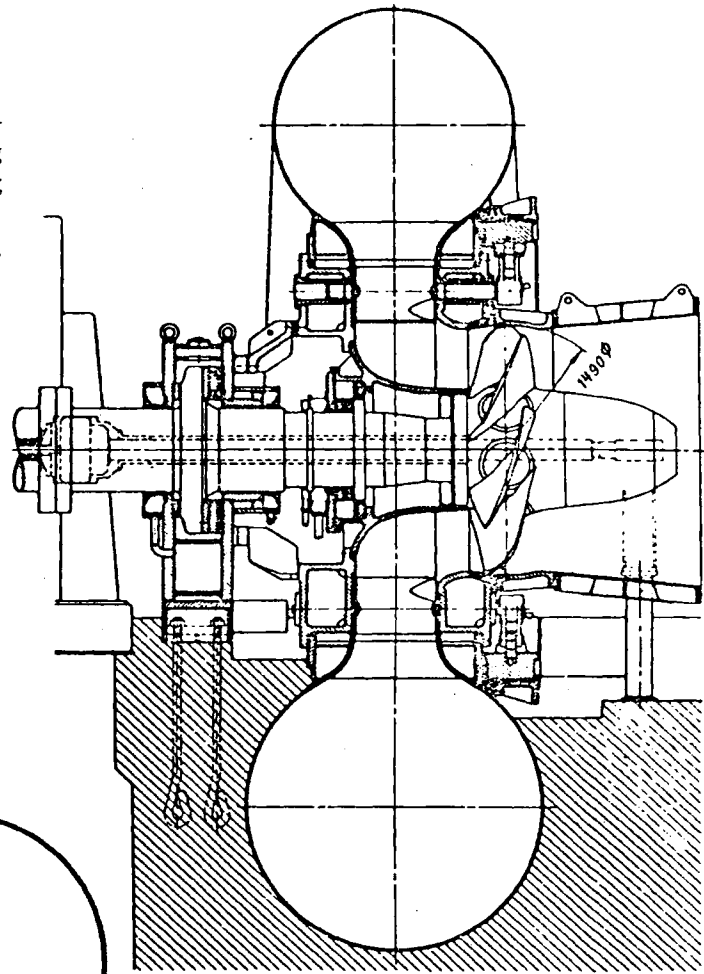
Fig. 3.4.18. Elevation of a horizontal FT of a ternary set, the pumped storage plant at Vianden, Luxemburg (owner Société d'Électricité d'Our). $H = 287$ m; $n = 428,7$ rpm; $P = 105$ MW. $D = 2,4$ m. Runner of overhung design. Combined guide and thrust bearing, supported by a truncated cone on the head cover, facilitates the smallest clearance of the runner labyrinths, and relieves the surrounding concrete of bearing force (thrust). Spiral casing, welded of fine grained steel with high yield point (3600 bar), stress relieved in the shop. For transportation split into 2 halves screwed together. Spiral inlet above the shaft requires a Sulzer Escher Wyss type load compensator. (Drawing courtesy Sulzer Escher Wyss, Switzerland)
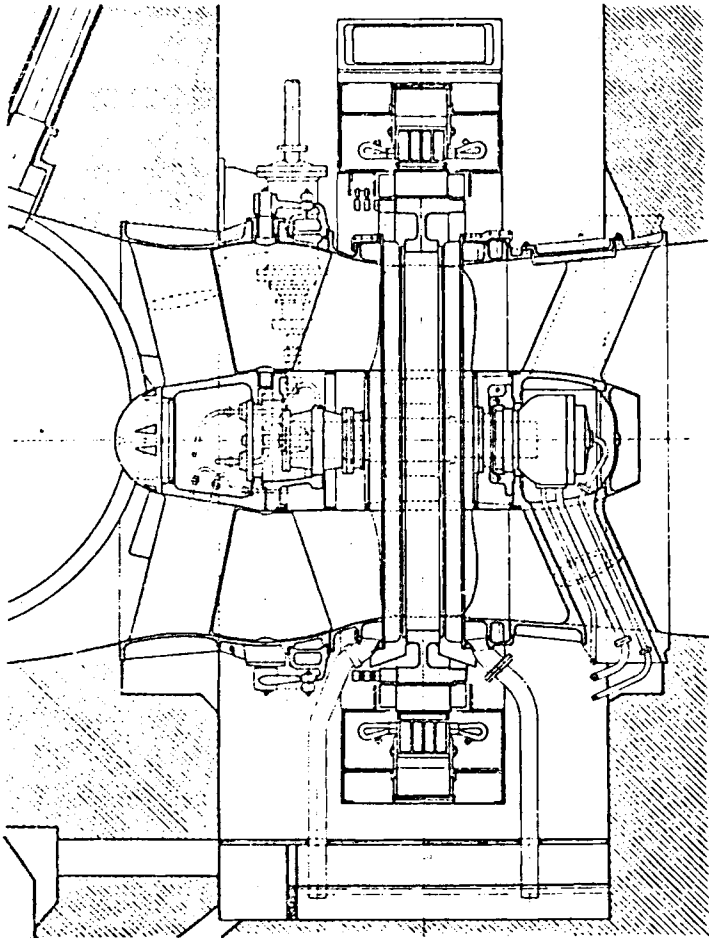
Fig. 3.4.19. Horizontal shaft tubular turbine with a rim generator. According to Harza's patent, first built by Sulzer Escher Wyss under the instruction of *A. Fischer* in 1936 for a German Iller plant. 73 turbines have been built for West German plants at Iller, Lech, Saalach. Working data in a typical case: $H = 8.5$ m; $n = 214.3$ rpm; $P = 1.4$ MW; $D = 1.8$ m. Usually only regulated by axial guide vanes, in one case also by adjustable runner vanes. (Courtesy Sulzer Escher Wyss)
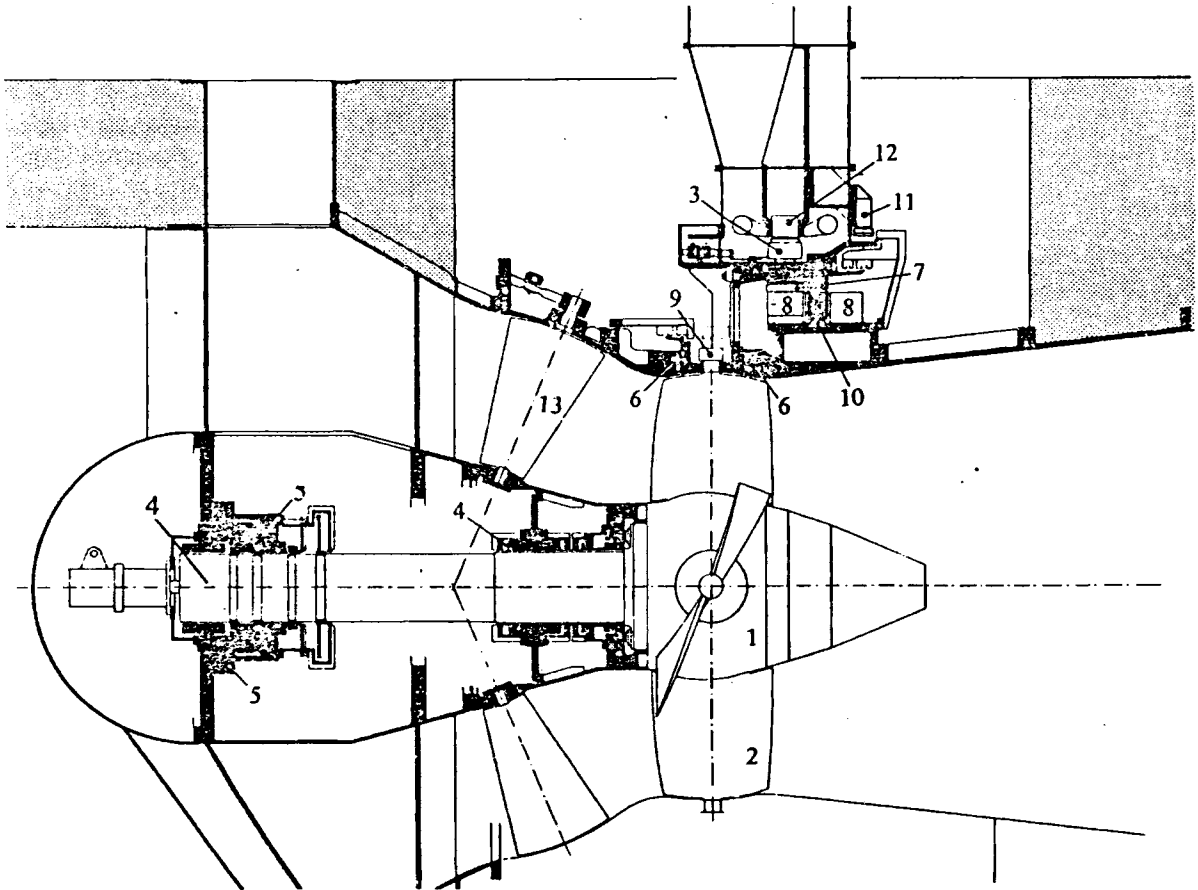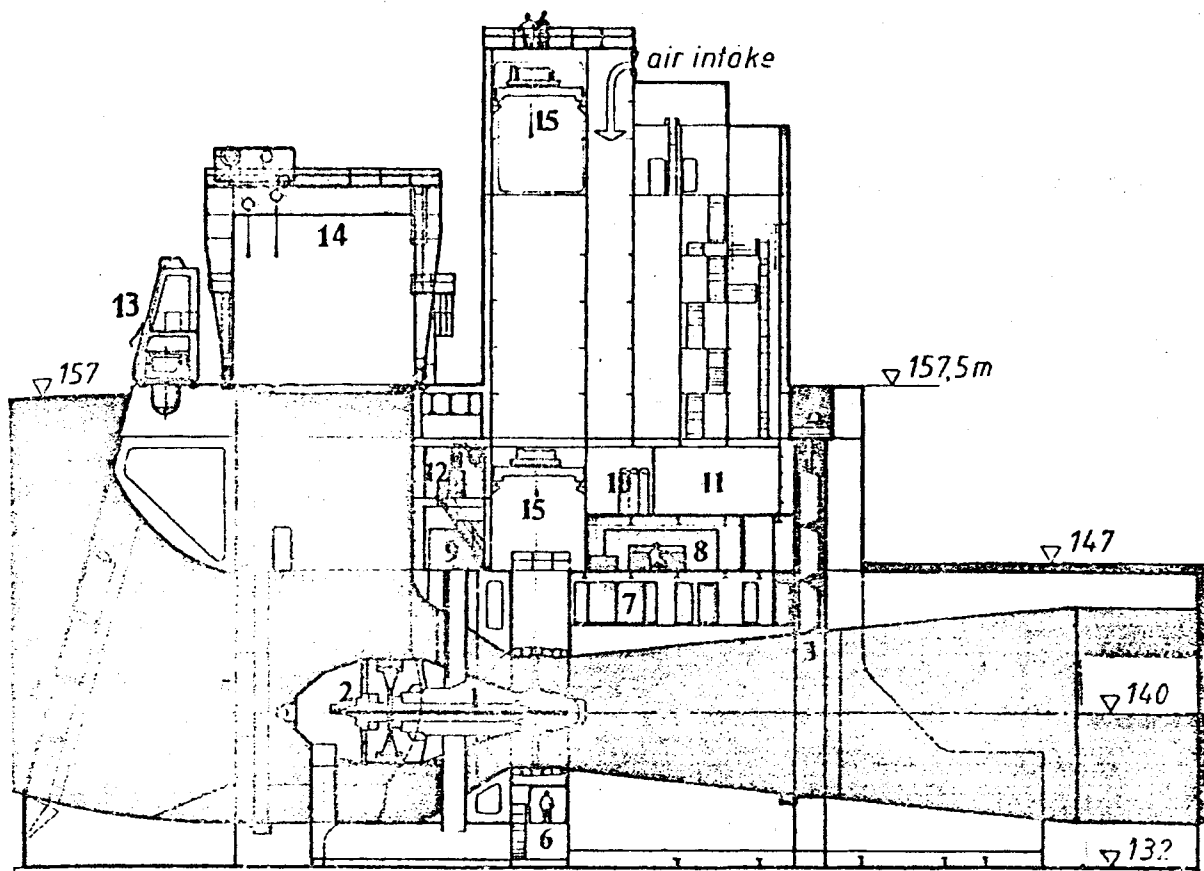
Fig. 3.4.21. Longitudinal section of power house and set, Greenup dam, Ohio river, USA (owner City of Vanceburg, Kentucky, Ohio.) built by Alsthom Atlantic Neyrpic. Horizontal open flume bulb turbine (BT) $H = 8.4$ m; $n = 90$ rpm; $P = 2 \cdot 24.3$ MW; $H_{min} = 1.5$ m. Runner: $D = 6.1$ m; 4 blades. 1 turbine; 2 generator; 3 downstream gate; 4 trash rack; 5 upstream stoplog; 6 water pump and turbine auxiliaries, 7 transformers; 8 control room; 9 turbine and generator auxiliaries; 10 fire-proof room; 11 air conditioned room; 12 standby Dieselgenerator; 13 thrash rack rake; 14 gantry crane; 15 overhead travelling cranes. Access tower: altitude level from 154 m to 176 m (Drawing courtesy Neyrpic, Grenoble, France).

Fig. 3.4.20. High power Straflo turbines (ST) built by Sulzer Escher Wyss, patentee. 1 hub; 2 runner blades; 3 generator poles; 4 radial bearing of turbine; 5 thrust bearing of turbine; 6 runner seal; 7 radial bearing of generator rotor; 8 axial bearing of generator rotor; (bearings 7 and 8 are of water-lubricated, self-adjusting, supporting water head type and facilitate good guidance of the shroud and hence also runner blade adjustment); 9 tangential load compensator of bearings 7; 10 emergency bearing; 11 brake; 12 generator stator; 13 guide vanes. (Drawing courtesy Sulzer Escher Wyss, Switzerland)

109

n) Isogyre [1.70] with the pump and turbine rotor in back-to-back arrangement, connected with a common spiral casing and suction flange, waterways by adjustabel ring gates, with vertical (Fig. 1.6.7) or horizontal shaft (Fig. 3.4.34).

o) One-stage pump turbine with horizontal or vertical shaft (see Fig. 3.4.35).

p) Double stage pump turbine with adjustable gates in series (see Fig. 3.4.36).

q) Multistage pump turbine with fixed gates (Fig. 3.4.37) [3.125].

r) Ternary set (tandem set) with a special multistage and double or single flow impeller pump and a FT, with a horizontal shaft (Fig. 3.4.38), or vertical shaft (Figs. 3.4.39 and 1.6.6).

s) The same as r) but equipped with PT (see Fig. 3.4.40; 41).

In general the application of a siphon in the admission chamber (see Fig. 3.4.31) is limited to heads up to 4 m. A siphon in the admission pipe is a convenient shut down device also for higher heads.

Tubular turbines of the bulb or rim generator type (see Figs. 3.4.19 and 3.4.23) are limited to the head range of up to 17 m, exceptionally 30 m (BT Sylvenstein, Isar, West Germany). Turbines with step up gear are for heads between 2 to 15 m, exceptionally up to 30 m.

Admission by open chamber up to $H = 7$ m, by semi-spiral casing up to $H = 30$ m, by spiral casing in reinforced concrete with steel lining up to $H = 50$ m, by welded spiral casing nowadays up to 740 m, and by spherical casing, according to W. Meier possible up to 1000 m head [3.126]. For double stage machines according to Hamish the head may attain 1800 m.
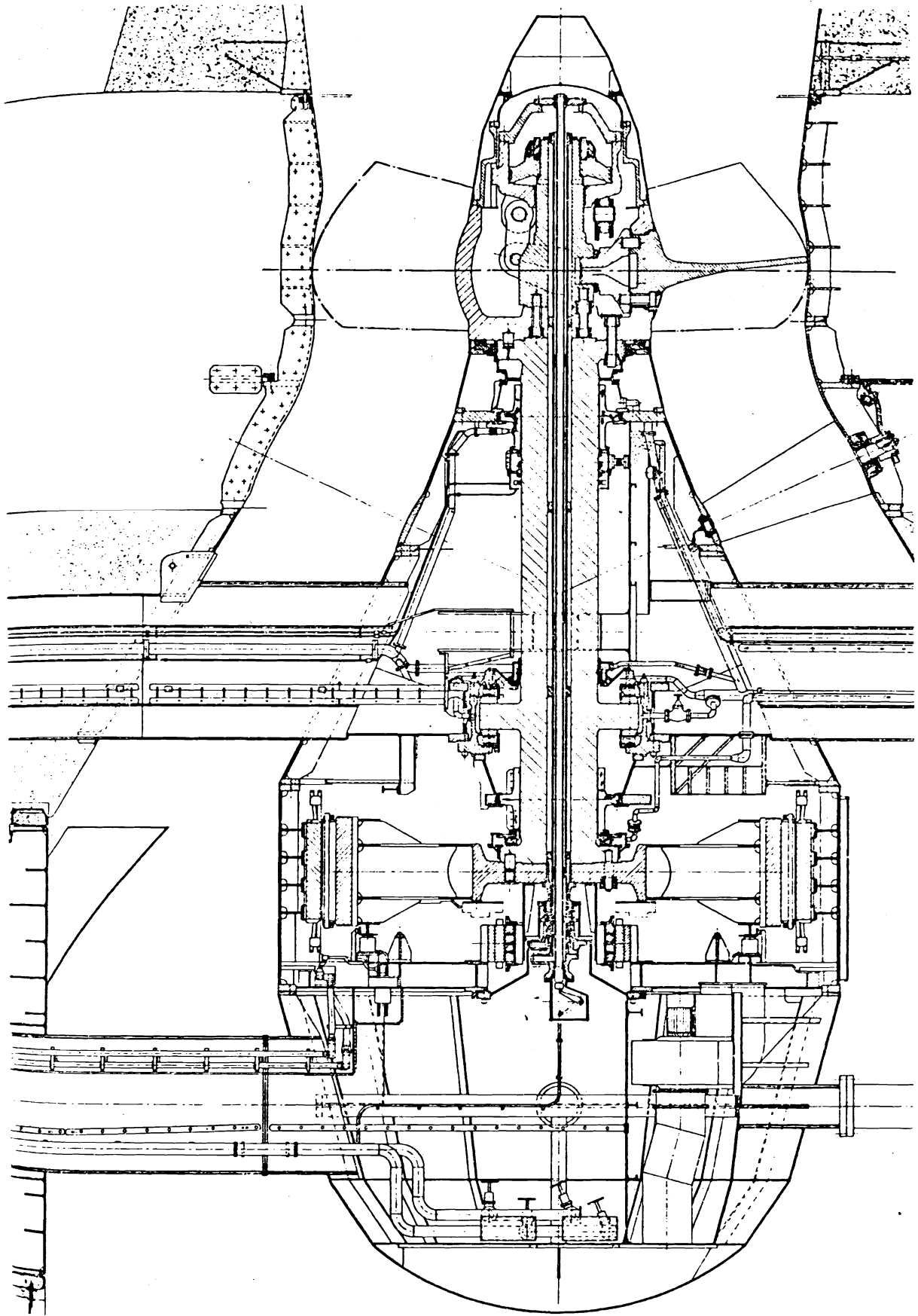
Fig. 3.4.23. Longitudinal section of horizontal bulb turbine Crestuma, Portugal (owner Electricidade de Portugal) $H=12.3$ m; $n=83.3$ rpm; $P=43$ MW. Runner $D=6.8$ m. Neyrpic design. 2 radial bearings, alternator rotor overhung. Runner servomotor with piston bolted on the hub by screws. Oil head on the free shaft end. Assembly of the generator through the draft tube and a bore at the turbine end of bulb. Access to runner by axially split draft tube crossing a trench in the power house. (Drawing courtesy Neyrpic, Grenoble, France)

111
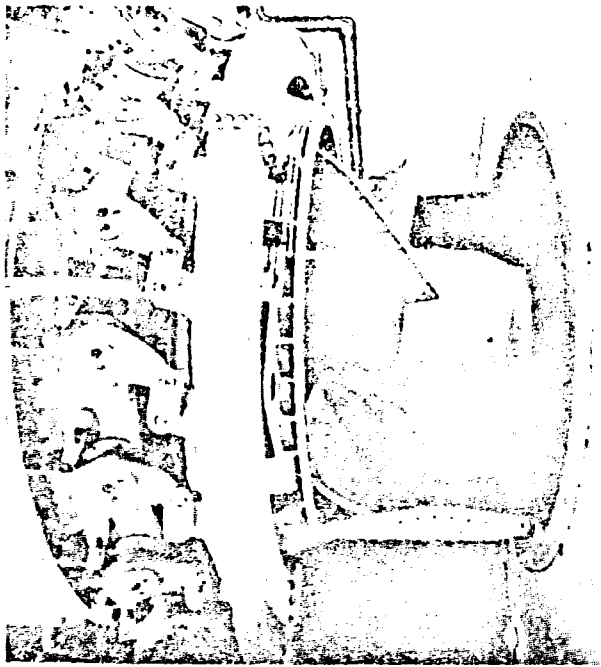
Fig. 3.4.24. Runner and gate drive of horizontal, reversible axial bulb pump-turbine for tidal power plant, with double effect Rance, France (owner Électricité de France EdF). Neyrpic design in collaboration with EdF. Net annual productivity 544 · 10⁶ kWh. 24 sets. Turbining: $H = 11 - 7 - 3$ m; direct (basin-sea = distributor runner) $P = 10 - 10 - 3.2$ MW; reversed (sea-basin) $P = 10 - 9.5 - 2$ MW. Pumping sea-basin $H = 1 - 2 - 3 - 6$ m; $P = 10 - 10 - 10 - 10$ MW. $n = 93.75$ rpm; $n_{ra} = 260$ rpm. Rotor: 4 blades; $D = 5.35$ m. Blade angle from $-5°$ to $+35°$, the first for braking, therefore $t/L > 1$. Double-cambered blades. Distance of adjacent sets 13,3 m. Basin left side. (Photograph courtesy Électricité de France)
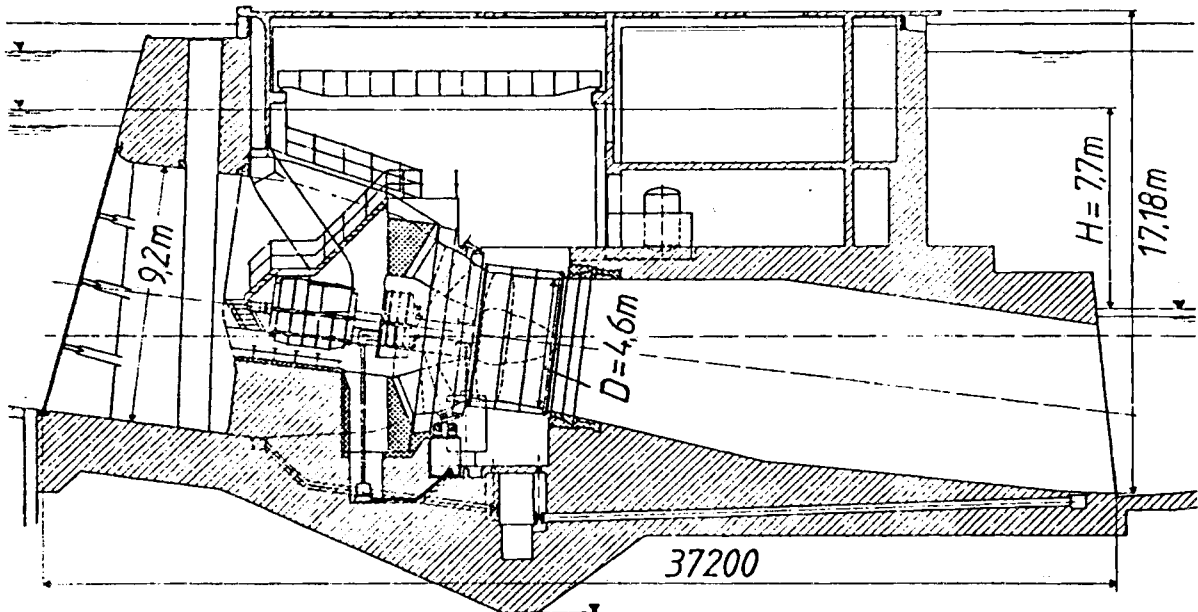
Fig. 3.4.25. Longitudinal section of power house and inclined shaft BT Trier, Mosel, West Germany (owner Rheinisch Westfälisches Elektrizitätswerk AG, Essen RWE). Turbine built by Sulzer Escher Wyss. $H = 7.7$ m; $n_T/n_G = 78/750$ (stepped up by Krupp Stoeckicht planetary gear); $P = 4 \cdot 4.4$ MW. Gear reduces size of generator, then assembled through streamlined access pit. Conical gates, closed by weight. Axial thrust transmitted into the concrete by long stays on the stay vane ring. Runner assembly through split draft tube crossing a trench in the power house accessible by crane. Stuffing box at the lower draft tube end facilitates thermal expansion. (Drawing courtesy Sulzer Escher Wyss)

Fig. 3.4.26. Elevation of horizontal BT of tidal power plant Kislogubs-kaja, Ice Sea, USSR, built by Neyr-pic, with planetary step up gearing of Krupp Stoeckicht type. $H = 1 - 2$ m; $n = 72,600$ rpm; $P_m = 0,29$ MW. Runner 4 blades, $D = 3,3$ m. Power house of pre-fabricated concrete blocks, built in Leningrad dockyard, made float-able by means of flushing tanks, then pulled via North Cape to the site, where it was sunk to the sea bed. (Drawing courtesy Neyrpic, Grenoble, France)
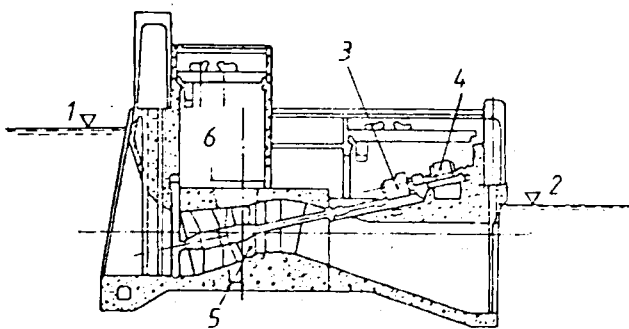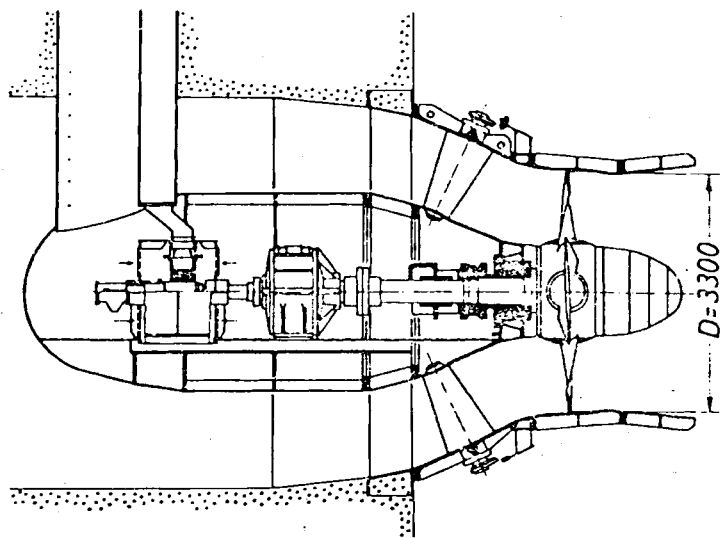
Fig. 3.4.27. Tubular turbine (TT), so-called S-turbine, with inclined shaft, passing the draft tube bend. Alternator in the power house gear driven. 1 head pond level; 2 tailrace level; 3 spur-gear; 4 generator; 5 runner; 6 hatch for assembly by crane. From J. Cottilon

Fig. 3.4.28. Tubular turbine (S-type) with horizontal shaft. Outdoor alternator di-rectly driven. Modified Tampella design. Lowest investment cost, but at the expense of highest efficiency. (Drawing courtesy Tampella, Tampere, Finland)

113
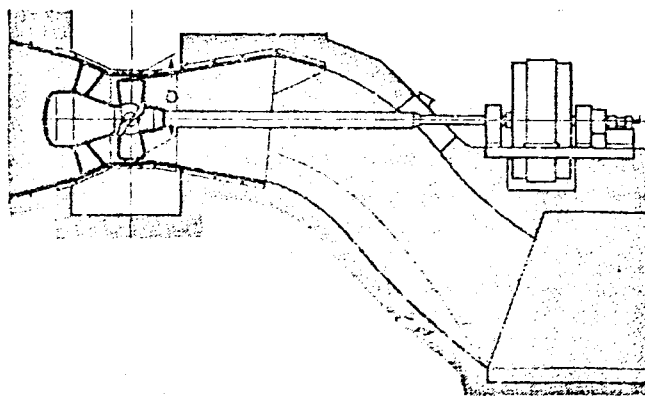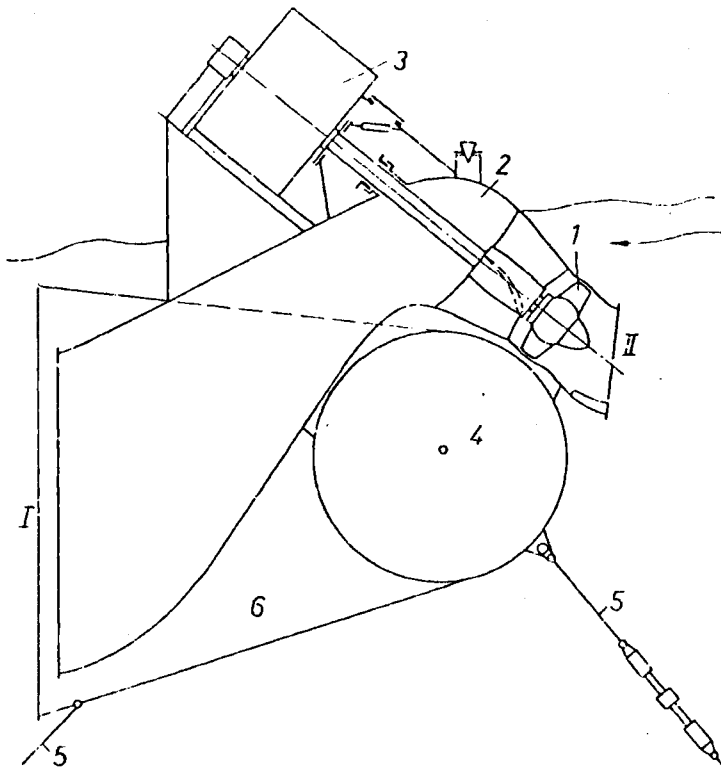
Fig. 3.4.29. Tubular turbine with siphon in bend, non-adjustable. According to a proposal by the author also useful for river rapids, and then as in the figure, mounted on a moored float. 1 runner; 2 draft tube with bend as siphon; 3 generator; 4 float; 5 stay cable anchored; 6 stabilizing fin.
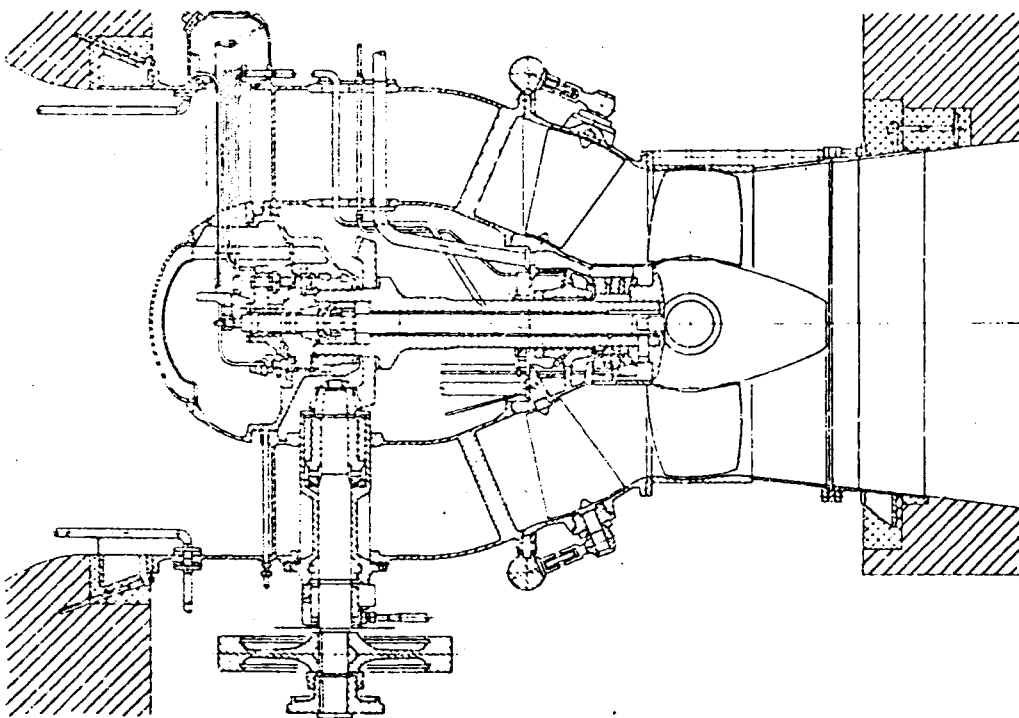
Fig. 3.4.30. Bulb turbine with tail flange at bevel pinion drive, shaft passing through a streamlined hollow stay vane. Very small hub diameter. Gear not easily accessible and needs to be carefully adjusted under load. (Drawing courtesy Sulzer Escher Wyss)

114
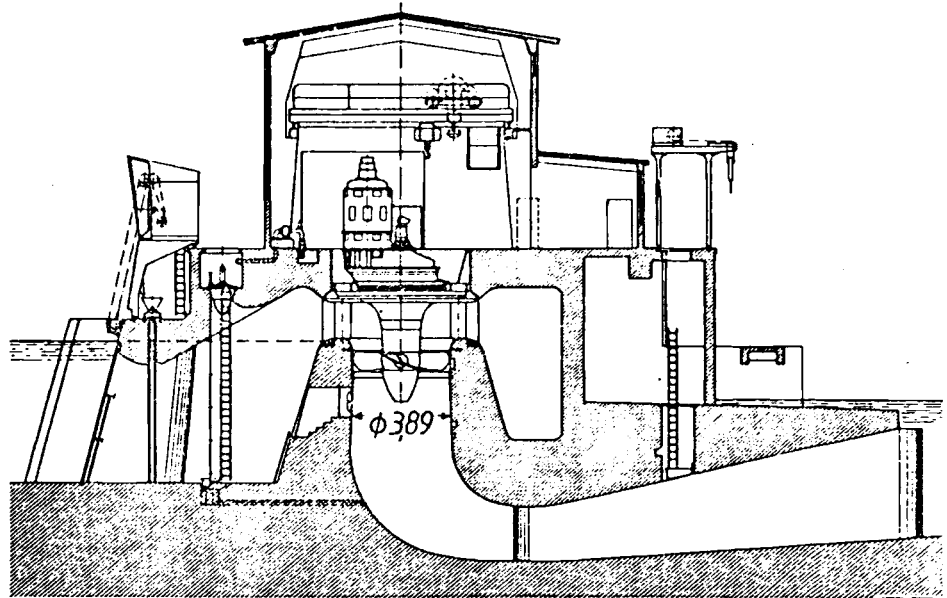
Fig. 3.4.31. Vertical shaft KT with semi spiral casing of siphon design. Marktbreit, Main, West Germany (owner, Rhein Main Donau AG, München). $H = 2.5$ m; $n = 68.2$ rpm; $P = 1100$ kW. Siphon saves stop log for draining the machine, but is limited to small heads. Step up spur gear for generator. (Drawing courtesy Voith)
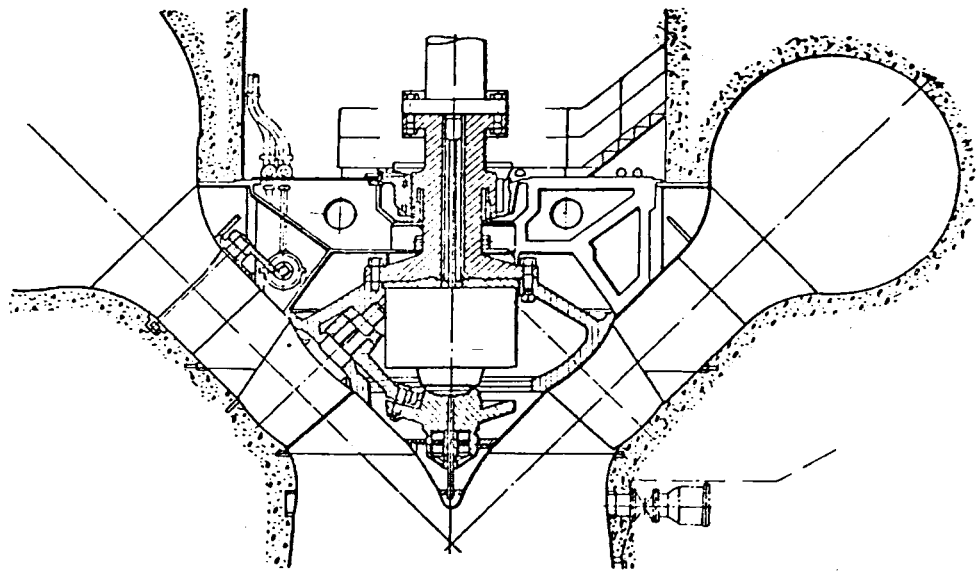
Fig. 3.4.32. Mixed flow reaction turbomachine with conical distributor or diffuser and vertical shaft. The pump-turbine of Deriaz type in the pumped storage plant at Sir Adam Beck, St. Lawrence (Niagara Falls), Canada (owner Hydroelectric Power Comission of Ontario) built by English Electric, Liverpool, England. $H = 25$ m; $n = 92.3$ rpm; $P = 33$ MW. Adjustable blades moved by wing servomotor (Deriaz patent) via block and link drive. Blades tightly closing in flow direction, hence low loss if working against closed valve at start of pumping. At standstill leakage through tip and hub clearance reduced by lowering bottom of the thrust bearing hydrostatically. Ingenious design. If turbining competitive with a high head Kaplan turbine. (Photograph courtesy English Electric Co.)

115
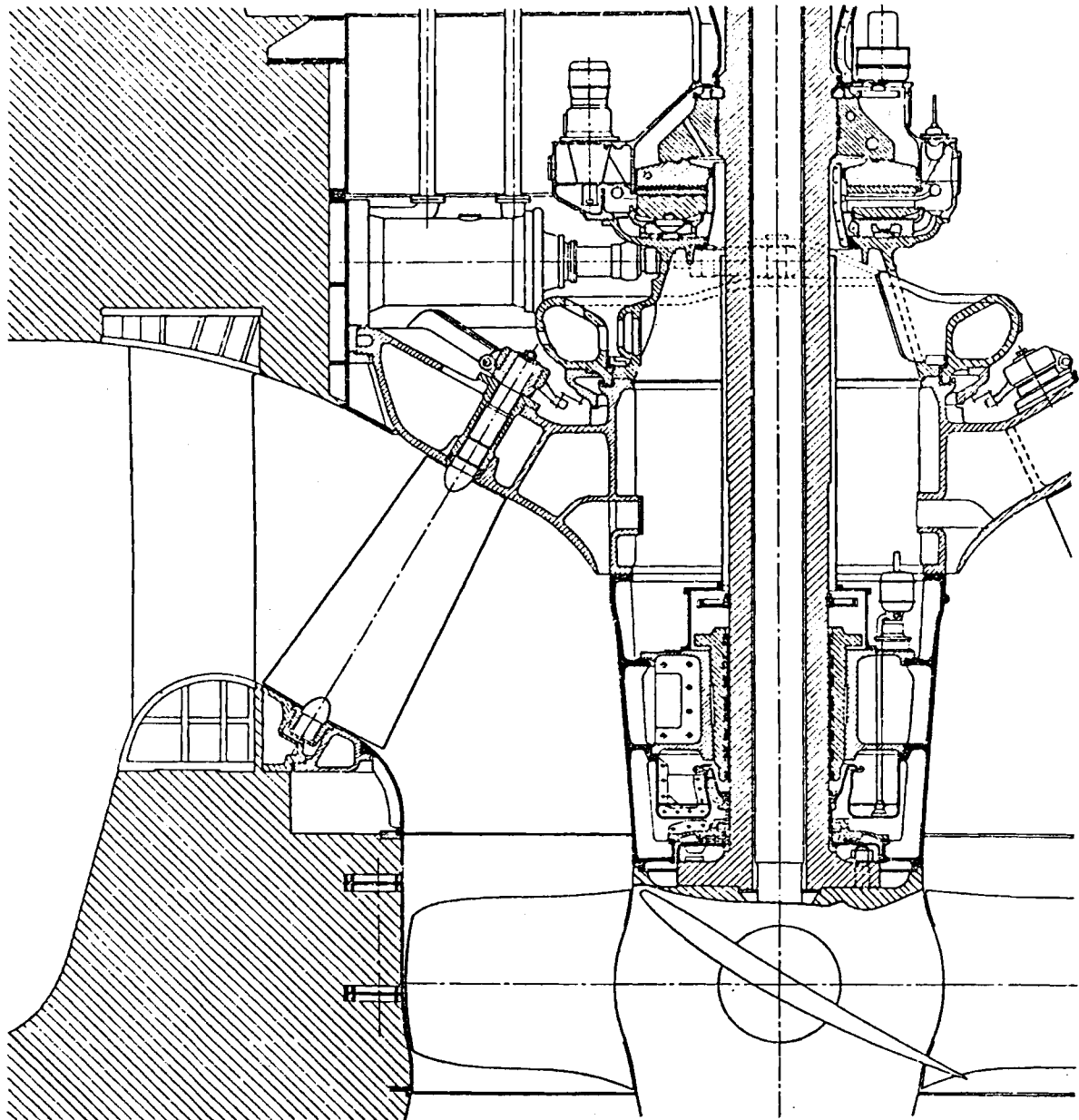
Fig. 3.4.33. Vertical shaft KT with conical guide apparatus. Obernberg, West German-Austrian Inn. (Owner on German side Innwerke AG, Töging) $H = 10,3$ m; $n = 96,7$ rpm; $P = 6 \cdot 14$ MW. Possible reduction of head cover diameter to that of the runner. Spherical articulations in the gate drive. Meridional streamline curvature near the bottom ring reduced. Lower rearward corner of opened gate not disturbing the flow reduces cavitation sensitivity of outmost runner parts. (Drawing courtesy Sulzer Escher Wyss)

For a compact design, the semi-spiral casing is formed of trapezoidal cross sections. radially "squeezed" and stretched downward. Its tongue tends to be shifted from a radius making an angle of 135° with the flow direction to an angle of only 45° (see the KTs of the USSR plant "22nd Congress" [3.127]).

Embedding the elastic spiral casing of high head pump turbines in sponge rubber and providing a self supporting erection, releases the surrounding concrete from alternating strain when frequently varying the mode of operation.

116
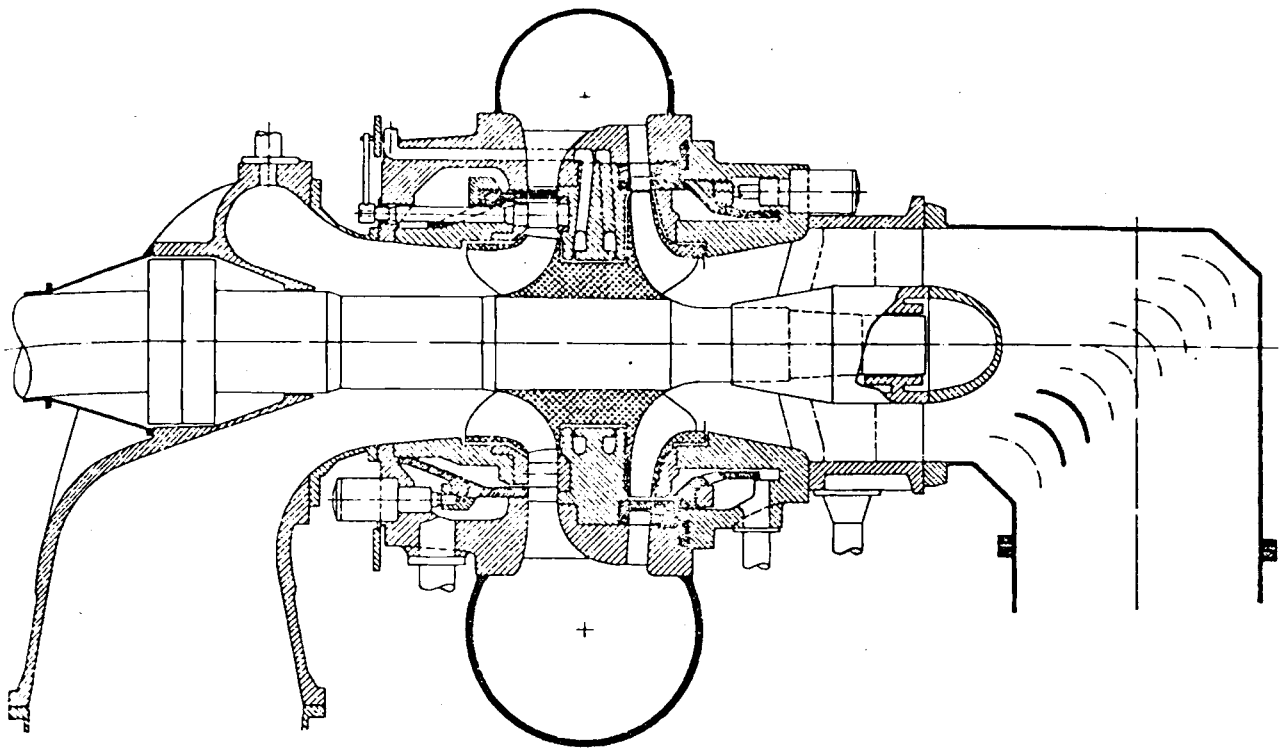
Fig. 3.4.34. Isogyre. The horizontal Isogyre of the pumped storage plant Handeck III, at Aare, Switzerland (owner Oberhasli AG, Innertkirchen) built by Vevey Charmilles Engineering works. $n = 1000$ rpm; $n_{ra} = 1600$ rpm. Turbining: $H = 310$ to 400 m; $P_m = 55$ MW. Pumping: $H = 475$ m. $P = 55$ MW. The large rotor-generator distance in this design decreases the critical speed. Hence overcritical runaway speed. (Drawing courtesy Vevey Charmilles Engineering Works, Switzerland)

For heads below 450 m, the spiral casing with vertical axis may have a retracted outer diameter with parallel plate stay ring, according to Piguet [3.128], see Fig. 3.4.16. Above a head of 15 m, smaller FTs may have a spiral casing. At lower head this is made of cast iron with prestressed bolts through the stay vanes. With rising head and size the casing is made of steel, cast, riveted or welded.

In horizontal Francis turbines the admission flange of the casing can be above the shaft (see Fig. 3.4.42) or underneath it (see Fig. 3.4.43). Owing to the long moment arm via which any load from the penstock may attack the casing support, an Escher Wyss load compensator (see Fig. 3.4.44) seems advisable for admission above the shaft [3.129].

The distance between neighbouring groups depends on the type of turbines and guide apparatus.

Typical values are: (2 to 2,5) · D, (D = runner tip diameter) for TT, 3 · D for turbines with semi-spiral casing, 4 · D for turbines with spiral casing (Fig. 3.4.45).

The main crane of the plant must be capable of lifting the heaviest continuous part. This is the generator rotor in a direct driven set. To avoid the shaft being out of round, the latter should have as few couplings as possible. Hence for a not too large-sized machine [3.130], ($D < 6$ m) the shaft is in one pice. For a vertical set the shaft length gives the elevation of the crane hook above the upper face of the generator rotor. The main crane must be capable of lifting the shaft from the stator bore by means of a diagonal pull, which lowers the elevation of the crane runway [3.130].

In the classical tall hall design of power house the interior has to be sufficiently high, to house a crane of this capability in its walls (see Fig. 3.4.46).
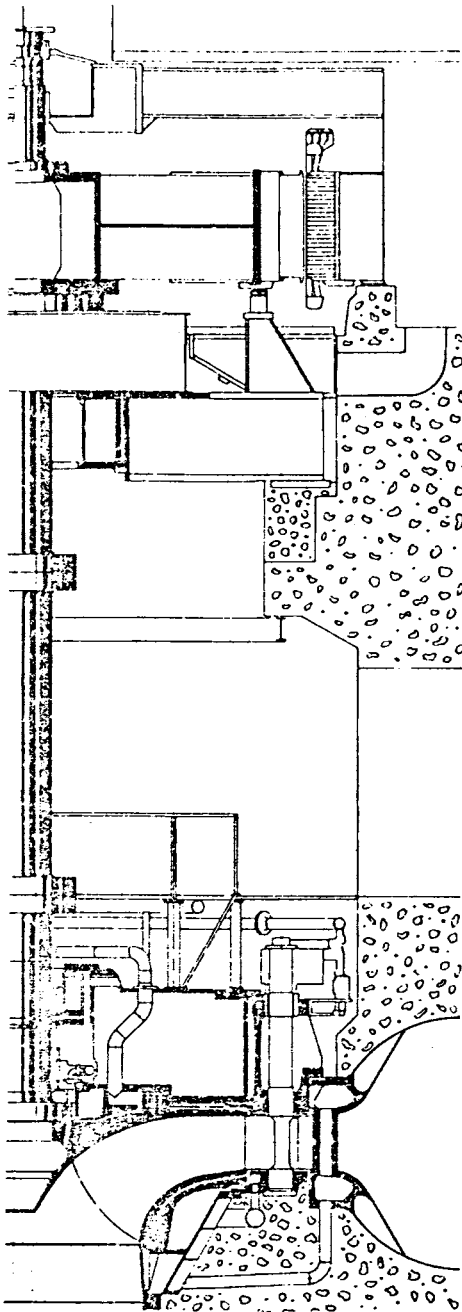
117

Fig. 3.4.35. Vertical pump-turbine of the pumped storage plant at Vouglans, France (owner Electricité de France) built by Vevey Charmilles. $n = 150$ rpm. Turbining: $H = 99,5$ m; $P = 65$ MW. Pumping: $H = 100,2$ m; $P = 60$ MW. (Drawing courtesy Vevey Charmilles Engineering Works, Switzerland.)
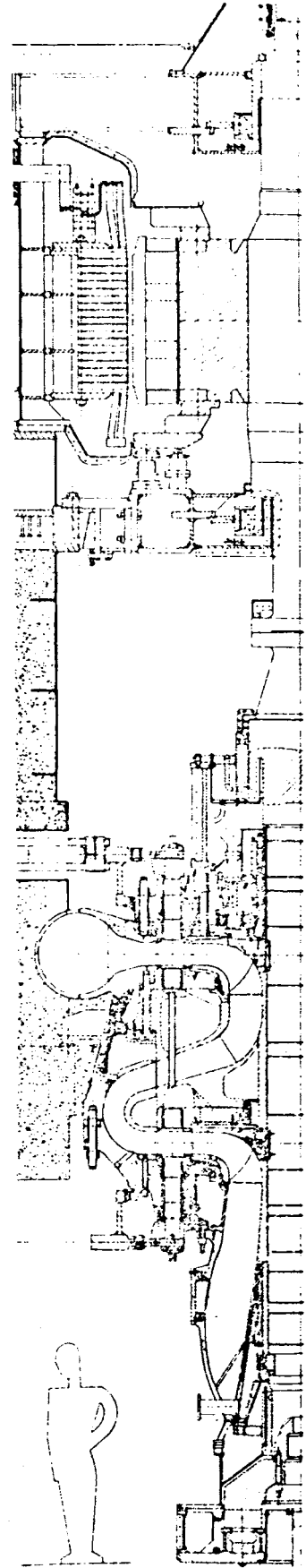
Fig. 3.4.36. 2-stage, gate adjusted reaction machine. The vertical pump-turbine of pumped storage plant Truel, France (owner Électricité de France), design Neyrpic. $n = 750$ rpm; $H_T = 438$ m; $P_T = 38$ MW; $H_P = 440$ m. Contrary to the multistage non adjustable pump-turbine, this type requires access to the head and bottom cover for the linkage of both gates. Highly stressed design. If gate of the 2nd stage is closed and that of the 1st stage leaks, the whole casing is subjected to the maximum total pressure of machine. For a wider high efficiency characteristic. Prototype with relative modest head, since design seems to fit into H up to 1500 m. (Drawing courtesy Neyrpic, Grenoble, France)

118

Fig. 3.4.37. Non-adjustable vertical multistage radial pump-turbine. Here 3-stage-machine of the pumped storage plant at Chiotas, Italy (owner Italian state power board ENEL), de Pretto Sulzer Escher Wyss design. A similar set was built by Hydroart, Milano. $n = 600$ rpm. Turbining: $H_m = 1047$ m; $P_m = 149.5$ MW. Pumping: $H_p = 1070$ m; $P_m = 151.7$ MW. (Drawing courtesy Sulzer Escher Wyss, Switzerland)
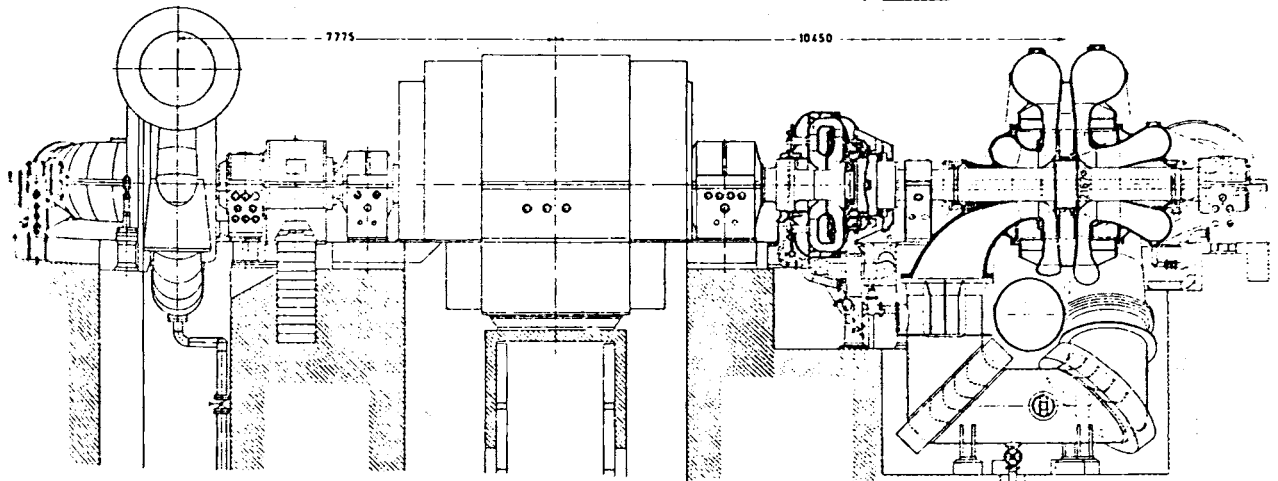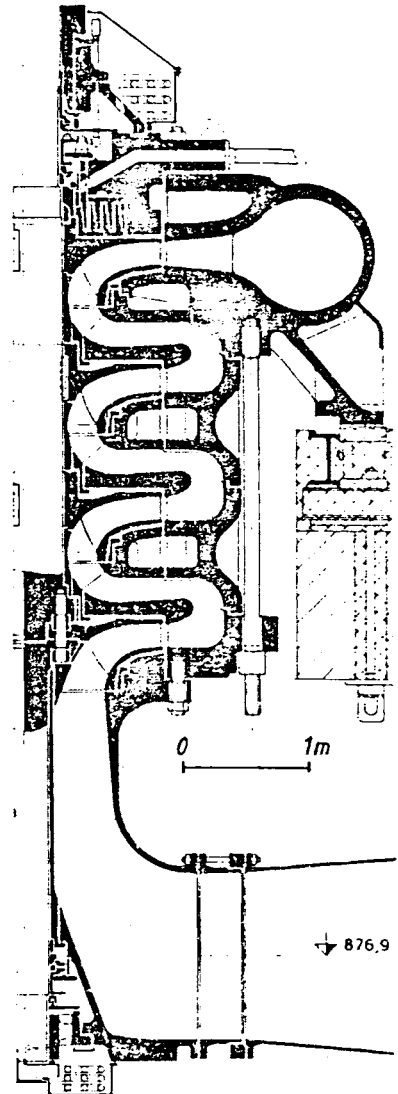

0   1m

876,9

Fig. 3.4.38. Elevation of horizontal ternary set in pumped storage plant Säckingen, West Germany (owner Schluchsee AG Freiburg). 4 FT (Sulzer Escher Wyss): $H = 408$ m; $n = 600$ rpm; $P = 92.8$ MW. 2-guide bearings enable detachment under pumping. Four 2-stage storage pumps. $H = 408$ m; $P = 70.6$ MW (Voith); filled start by torque converter (Voith). Back to back arrangement of pump impeller compensates axial thrust. Hence high efficiency. (Drawing courtesy Voith)

119
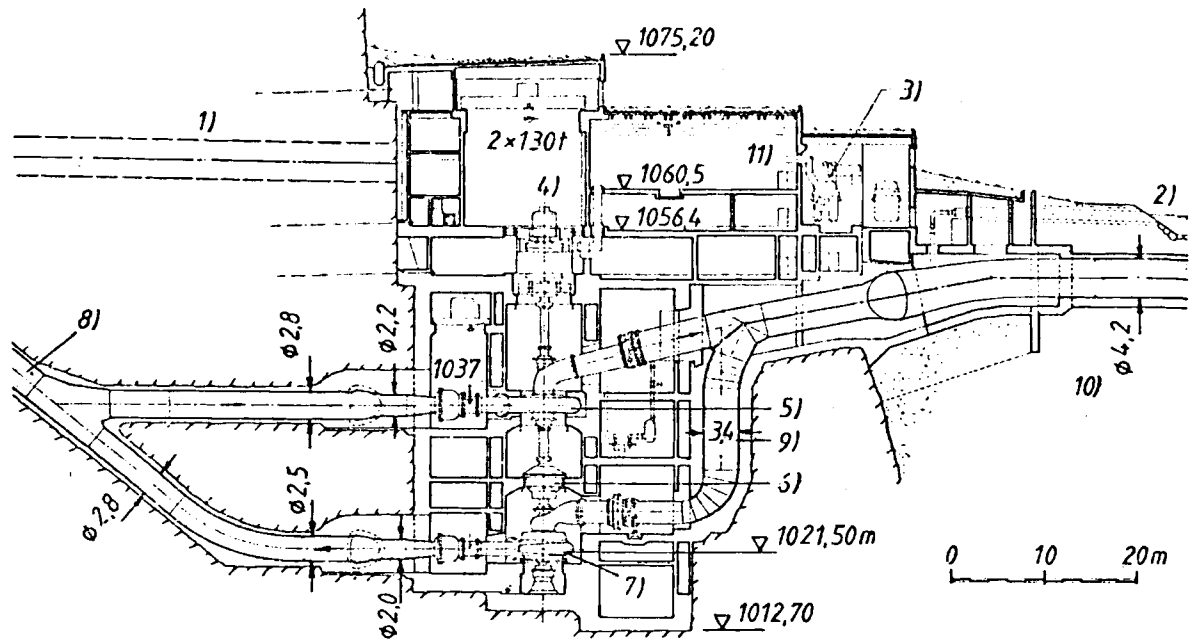
Fig. 3.4.39. Sectional view of power house with vertical ternary sets of combined peak load and pumped storage plant Häusling, Ziller, Austria (owner Tauernkraftwerke AG Salzburg). 2 FTs: $H = 620$ to 744 m (to date the highest head for a FT), $n = 600$ rpm; $P = 2 \cdot 180$ MW (Sulzer Escher Wyss). 2-stage single flow pumps: $P = 2 \cdot 180$ MW; $Q = 2 \cdot 22,5$ m³/s, filled start up by torque converter (Voith). 1 access tunnel from the horizontal section of the main tunnel; 2 Ziller; 3 transformer; 4 motor generator; 5 turbine; 6 torque converter; 7 pumps; 8 penstock; 9 suction line 10 Ziller undercrossed by levelled tunnel; 11 20 kV station. Annual productivity 175,6 GWh. Annual consumption by pumping 508 GWh. From *Widmann* [1.76].

In the so-called chamber design, due to *Mosonyi* [1.53] (see Fig. 3.4.47) the main crane is located outside the power house, which consequently is reduced in height. A removable and split hatch on the chamber roof facilitates also transportation of heavy parts through the opening.

In the so-called pit design with a removable cover or the generator in the open air this chamber is reduced to the pit of the set (see Fig. 3.4.48).

For plants needing a large submergence, because of cavitation, in unreliable ground at site the "pit" power house (see Fig. 3.4.49) may be an economical solution [3.131].

The main part of the set, the runner, must be made easily to assemble, dismantle and transport by crane. This can be achieved for high head FTs by providing a door in the draft tube wall (see Fig. 3.4.50). This door gives access to the runner and if repair is required enables it to be dismantled. It is then transported by means of a special rail car to a workshop with a suitable crane.

For reasons of submergence a reaction turbine is always put underneath the alternator when the shaft is vertical. Since the weight ratio of the alternator to the turbine rotor increases rapidly with the head, it seems advisable to support the thrust bearing in different ways according to the head For the highest head and medium sized sets, the alternator stator is usually located on a separate floor, capable of carrying this extremely heavy load (see Fig. 1.6.4 b). The thrust bearing is supported here by a spider on the top of the alternator stator.

120

Fig. 3.4.40. 1) Vertical ternary set of combined peak load and pumped storage plant Malta, Austria (owner Draukraftwerke Klagenfurt). 6-nozzle PT: $H = 1030$ m; $n = 500$ rpm; $P = 4 \cdot 208$ MW; $n_{ra} = 890$ rpm. 4-stage storage pumps; $H_m = 1100\,m$; $P_m = 2 \cdot 145$ MW; spiral casing shrunk onto the diffuser ring. Synchronizing torque converter (75 MW) for starting with filled pump. Air suspension of impulse wheel and suction requirement of pump lead to extremely long shaft. Hydraulic equipment Voith. Motor-generator and alternator $4 \cdot 220$ MVA; 13,8 kV; cos φ = 0,9; $GD^2 = 2100$ tm^2. Stator and rotor water cooled, built by BBC. Elevation of set, axially shortened. (Drawing courtesy Voith and Draukraftwerke Klagenfurt).

2 m
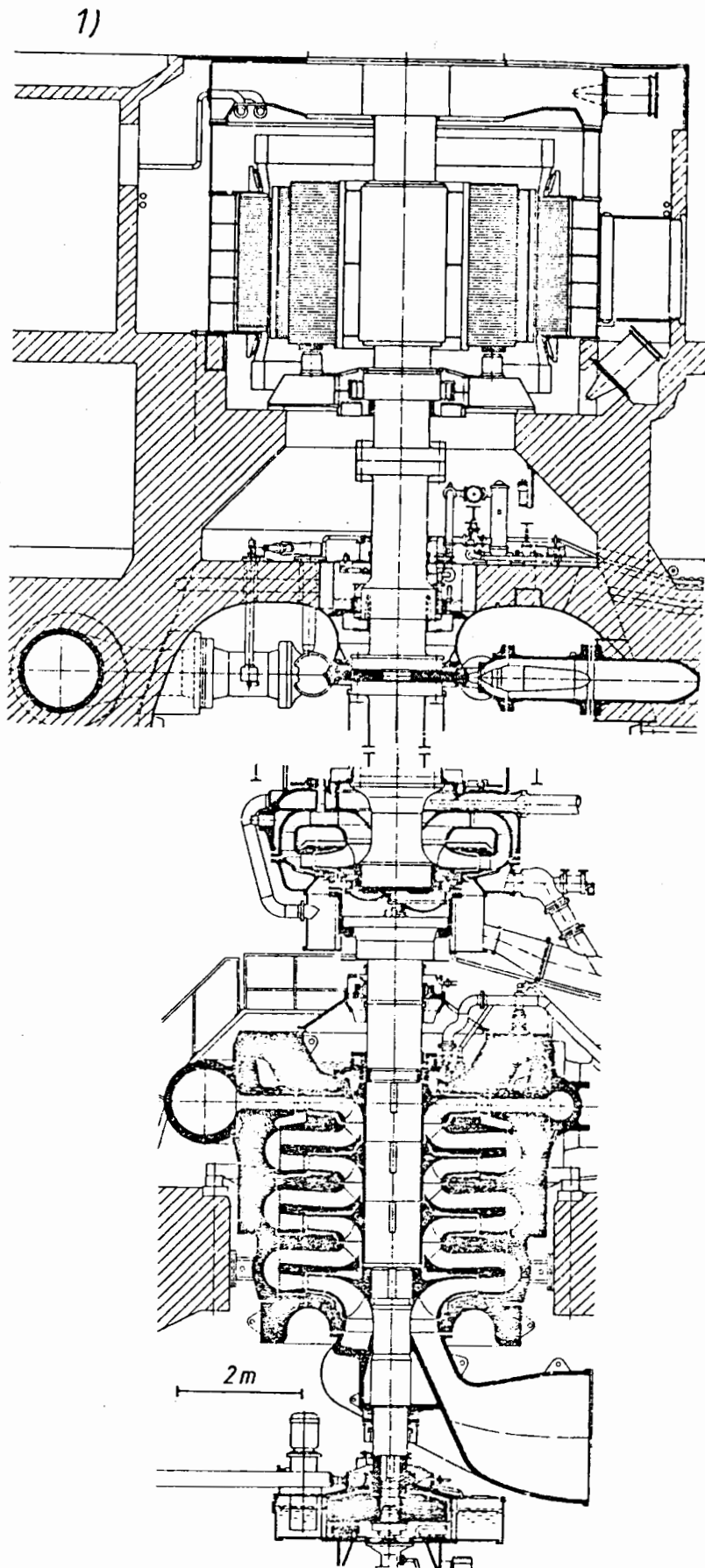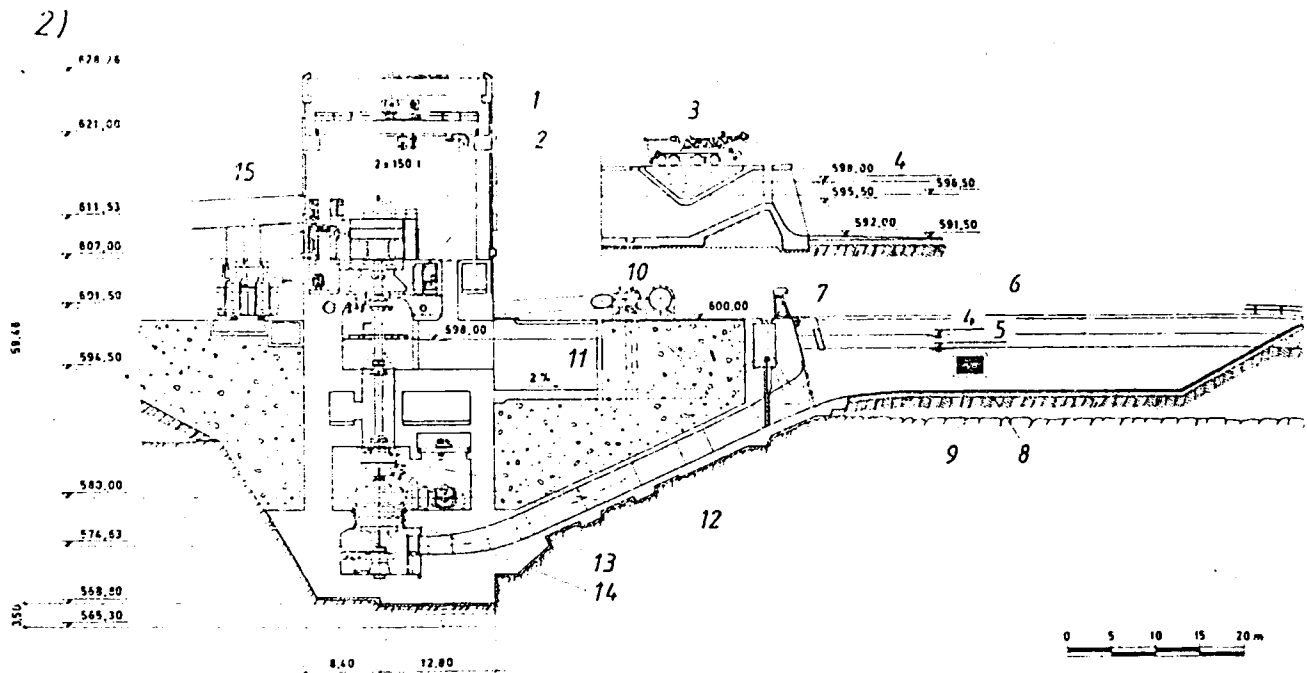
Fig. 3.4.40. 2) Longitudinal section of power house, ternary (tandem) pumped-storage set, tailwater intake and forebay, Rottau, Drau, Austria, main stage of Malta scheme (owner: Draukraftwerke, Klagenfurt, Austria). Outdoor power house of tall hall design with the main crane in its interior, located at the base of the valley slope, founded on mica and sericite slate. 2 ternary pumped-storage sets as shown in the figure, 2 sets without storage pump. The rather long vertical extension of the ternary sets results on the one hand from the need to place the impulse wheel above the maximum tailwater level and on the other hand from the needed submergence of the lowest first pump stage (here 21.1 m) underneath the minimum tailwater level. 1 220 MVA alternator, Stator and rotor, directly water cooled; 2 6-nozzle impulse turbine; 3 tailwater channel exit; 4 maximum permissible tailwater level; 5 minimum permissible tailwater level; 6 forebay; 7 trash rack; 8 relieve zone; 9 cooling water intake; 10 distributor main; 11 tailwater channel; 12 torque converter; 13 pump intake; 14 1-flow, 4-stage storage pump, 144 MW; 15 main transformer 220 MVA. (Drawing courtesy Draukraftwerke, Klagenfurt, Austria)

The runner of these turbines is accessible after removal of the head cover. Then the shaft needs an intermediate and removable piece to facilitate the dismantling of the runner without moving the heavy rotor of the alternator (Fig. 1.6.4 b).

In the case of lower heads and larger sets the thrust bearing is preferably supported underneath the alternator by a spider, on the concrete of pit. This also prestresses the concrete around the spiral casing. For heads below 300 m the thrust bearing in Europe-influenced designs is usually supported on the head cover, which then is released from its uplift.

Usually in plants with a penstock the valve chamber with its manifolds, bifurcations and bends, is upstream of the power house, see Figs. 3.4.51 and 3.4.52.

At larger submergence, such a valve chamber is also down-stream of the power house (Fig. 3.4.52). The usual bifurcations have stiffeners in the form of external or internal ribs (see Fig. 3.4.53 a and 53 b), or a spherical shell (see Fig. 3.4.53 c) to transmit the tensile stress along the periphery of the pipe into a solid support with a sufficient sectional modulus. These bifurcations and the adjacent penstock have been carefully investigated with respect to stress and flow loss [3.132 to 3.139].

Fig. 3.4.41. Horizontal ternary set with impulse turbine, plant S. Massenza, Italy (owner ENEL). Suspension of impulse wheel in the air, and suction requirements of storage pump needs application of a mixed flow booster pump. $H = 596$ m, $n = 600$ rpm; $P = 4 \cdot 32$ MW, $D = 1,7$ m. Turbine 1-nozzle twin PT with a runner overhung at both ends of the shaft. $H = 528,5$ m; $P = 4 \cdot 32,5$ MW. All built by Hydroart, Milan. (Drawing courtesy Hydroart, Milan).
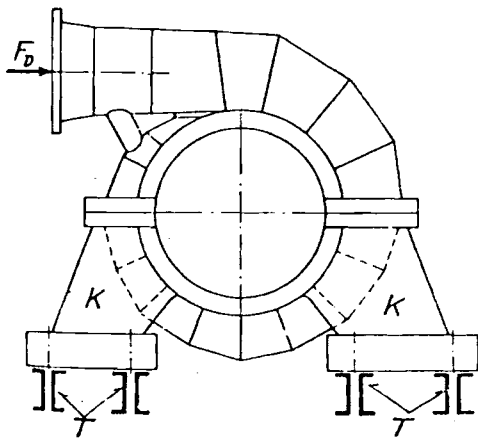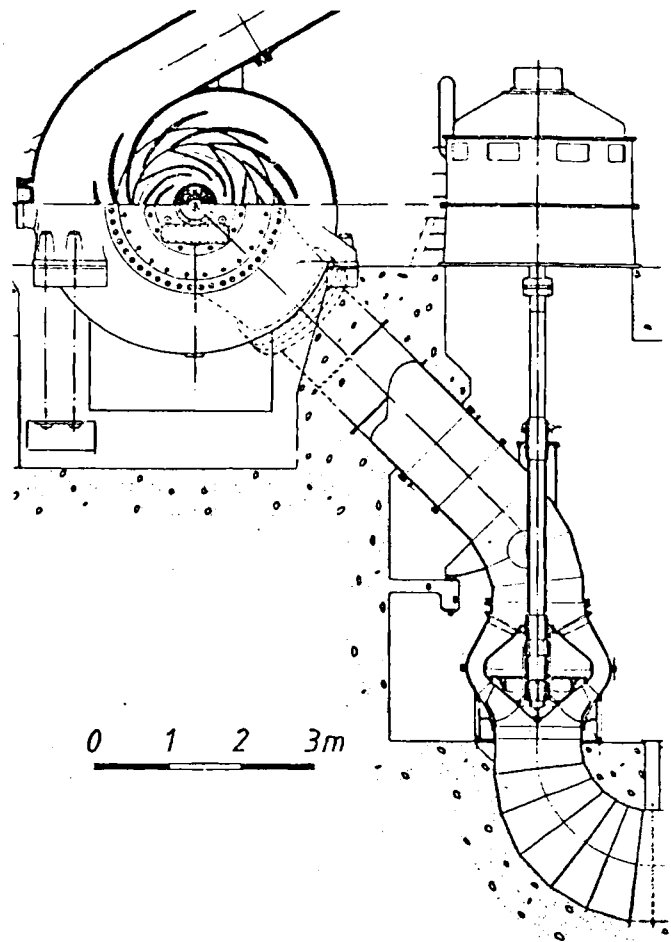

Fig. 3.4.42. Welded spiral casing for a horizontal machine. Flow admission above shaft requires load compensator (see Fig. 3.4.44). Without this device, force F_D, induced by pressure and thermal expansion of the penstock attacks spiral casing by a long moment arm against its supporting points, and hence would deform spiral casing.

In the power houses at the base of a dam (see Fig. 3.4.54) the flow admission is usually perpendicular to the axis of the power house. In underground stations, or in power houses at the base of a slope, along which the penstock comes down, the admission of water may be perpendicular to or along the axis of the power house. The first may protect an open air power house against a pipe failure on the line as the pipe jet (in case of a rupture) would not strike the power house.
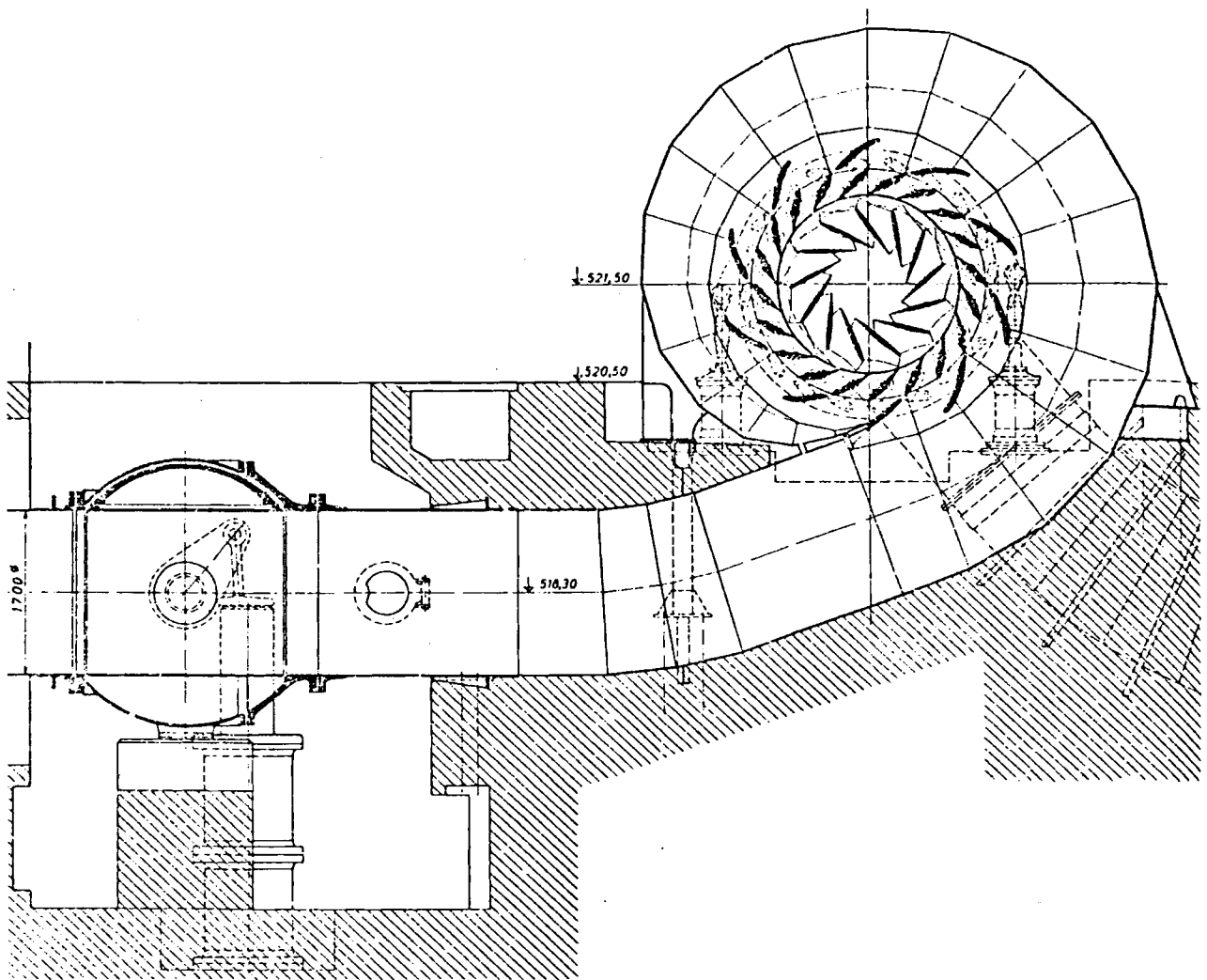
Fig. 3.4.43. Spiral casing for a horizontal machine. Flow admission underneath the shaft requires the introduction of a force F_D (see Fig. 3.4.42) at spiral inlet into the surrounding concrete, correspondingly reinforced. Spiral inlet needs interruption and thus weakening of the casing's supporting beam. Here the storage pump of a ternary set in a pumped storage plant at Leitzach, West Germany (owner Stadtwerke München) $H = 126$ m; $n = 428,6$ rpm; $P = 2 \cdot 24$ MW, design Sulzer Escher Wyss. (Drawing courtesy Sulzer Escher Wyss)
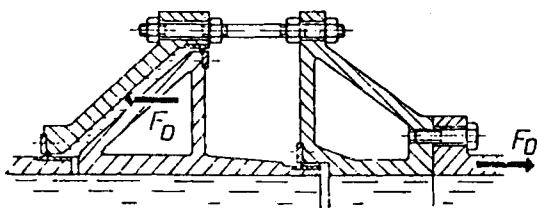
Fig. 3.4.44. Escher Wyss type load compensator, if the inlet of the spiral casing is not embedded in concrete, the casing is liberated from the penstock force induced by pressure and thermal expansion.

Fig. 3.4.46. Run-of-river power plant Birsfelden, Swiss German Rhine with main crane accommodated in the power house (tall hall design). $H = 4$ to 8 m; $P = 4 \cdot 15,6$ MW, KTs. 1 fish ladder; 2 Rhine; 3 boat harbour; 4 lock; 5 inclined elevator for boats; 6 maximum permissible head water level; 7 power house. From *E. Mosonyi*: Die neueste Entwicklung im Bau von Niederdruckwasserkraftanlagen. Wasserwirtschaft 54 (1964) No 7, p. 186.
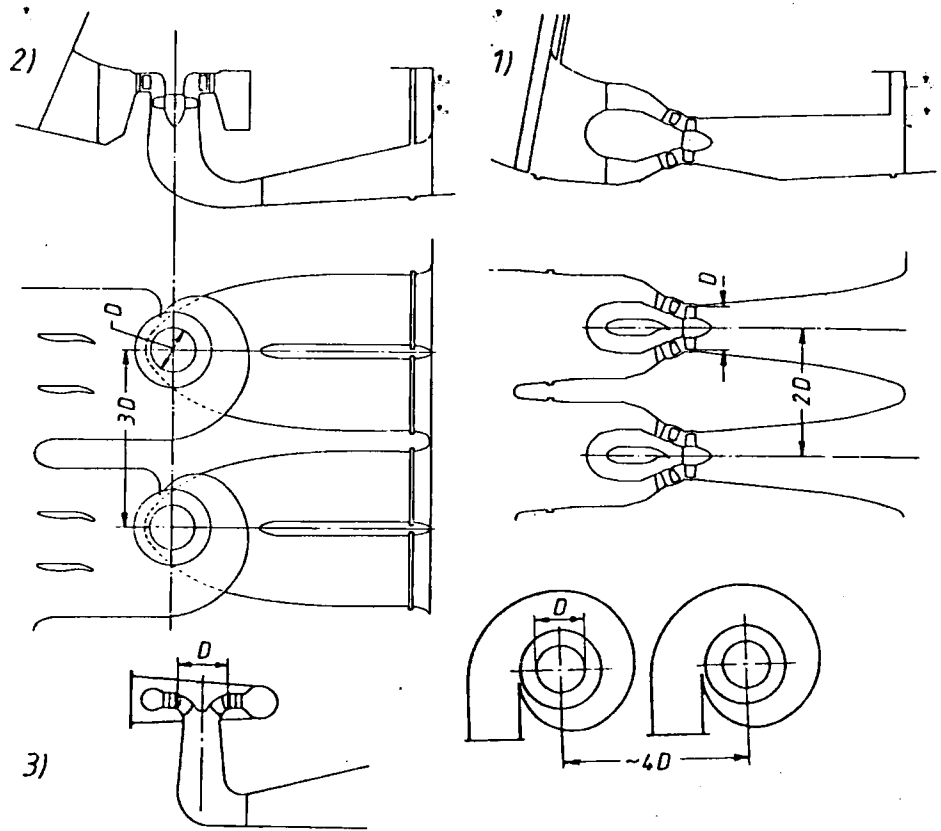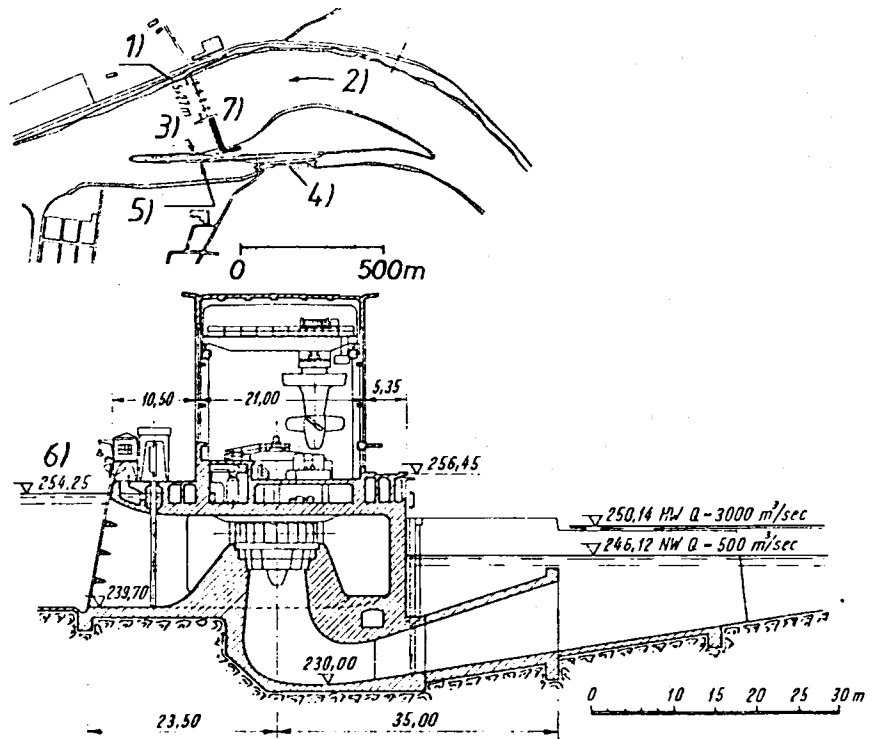
124

Fig. 3.4.45. Distance of adjacent sets in relation to the runner diameter in plan and space requirement in the elevation: 1 tubular turbine; 2 turbine with admission by semispiral casing; 3 turbine with admission by spiral casing. D runner diameter. (Drawing partly from Sulzer Escher Wyss)
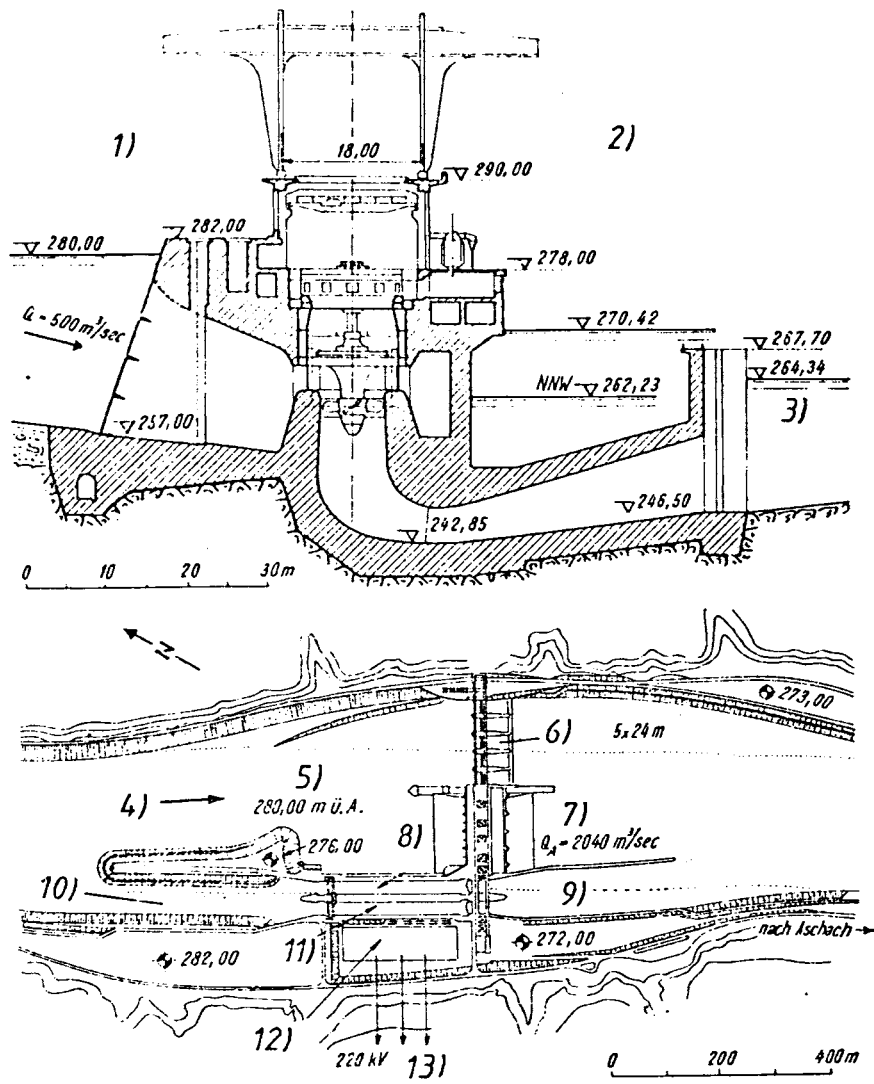
Fig. 3.4.48. Perspective view of outdoor pumped storage plant with pump-turbines. By-pass outlet as a surge relieving device. (Drawing courtesy Allis Chalmers, Milwaukee, Wisconsins, USA)

Fig. 3.4.47. Run-of-river power plant at Aschach, Danube, Austria (owner Österreichische Donau-kraftwerke AG). $H = 10$ to 18 m; $n = 68,2$ rpm; $P = 4 \cdot 68$ MW (2 sets Voith, 2 sets Andritz – Sulzer Escher Wyss) Runner: 5 blades; $D = 8,4$ m. 1 head water; 2 tail-race; 3 mean tail-race level; 4 Danube; 5 normal head water level; 6 spillway: 7 power house; 8 northern lock; 9 lower port; 10 upper port; 11 southern lock; 12 outdoor switch plant; 13 transmission line. Small machine hall, access from main crane outdoor by hatch. From E. Mosonyi, see Fig. 3.4.47.
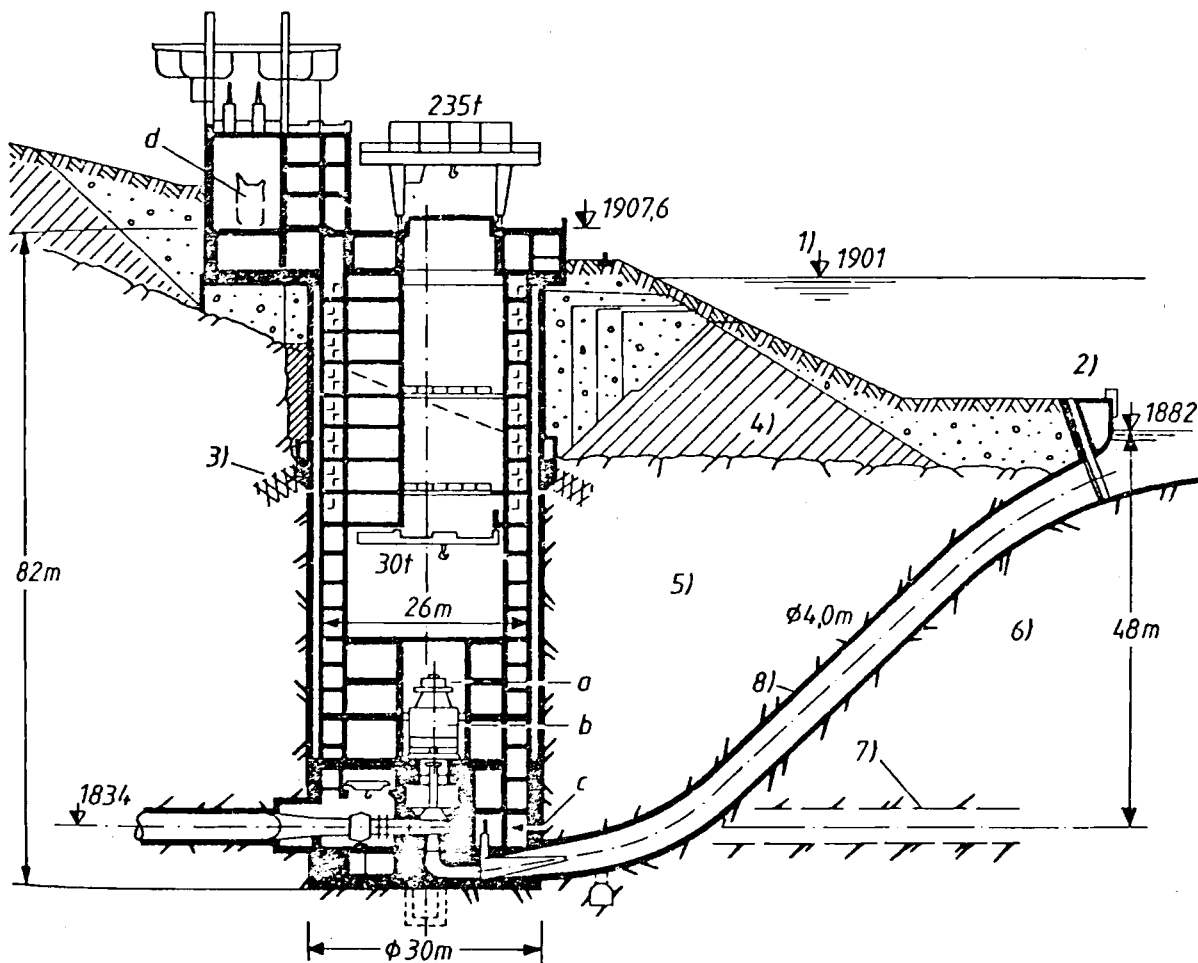

Fig. 3.4.49. Pit power house with elliptic plan of binary pumped storage plant Kühtai, Austria (owner Tiroler Wasserkraftwerke, Innsbruck). Two sets with vertical pump-turbines (Voith design) consisting of a pony motor, 15 MW, 90 s start up time, b motor generator 160 kVA, 18 kV, c pump-turbine, $n = 600$ rpm, $H = 394$ to 440 m, $T: P = 115,5$ to 139 MW, $Pu: P = 112$ to 119 MW, maximum submergence — 50 m; spiral casing self supporting, with Escher Wyss type load compensator at the inlet, embedded in sponge rubber. Gates operated by single servomotors, electro hydraulic controlled, electro hydraulic braking down to stand still; alternator air cooled, d = transformer. 160 kVA, 18/220 kV. 1 maximum tailrace level, 2 minimum tailrace level, 3 grout curtain, 4 moraine, 5 amphibolite, 6 slated gneiss, 7 drainage gallery, 8 2 tailrace shafts. (Drawing courtesy Tiroler Wasserkraftwerke, Innsbruck, Austria)

127
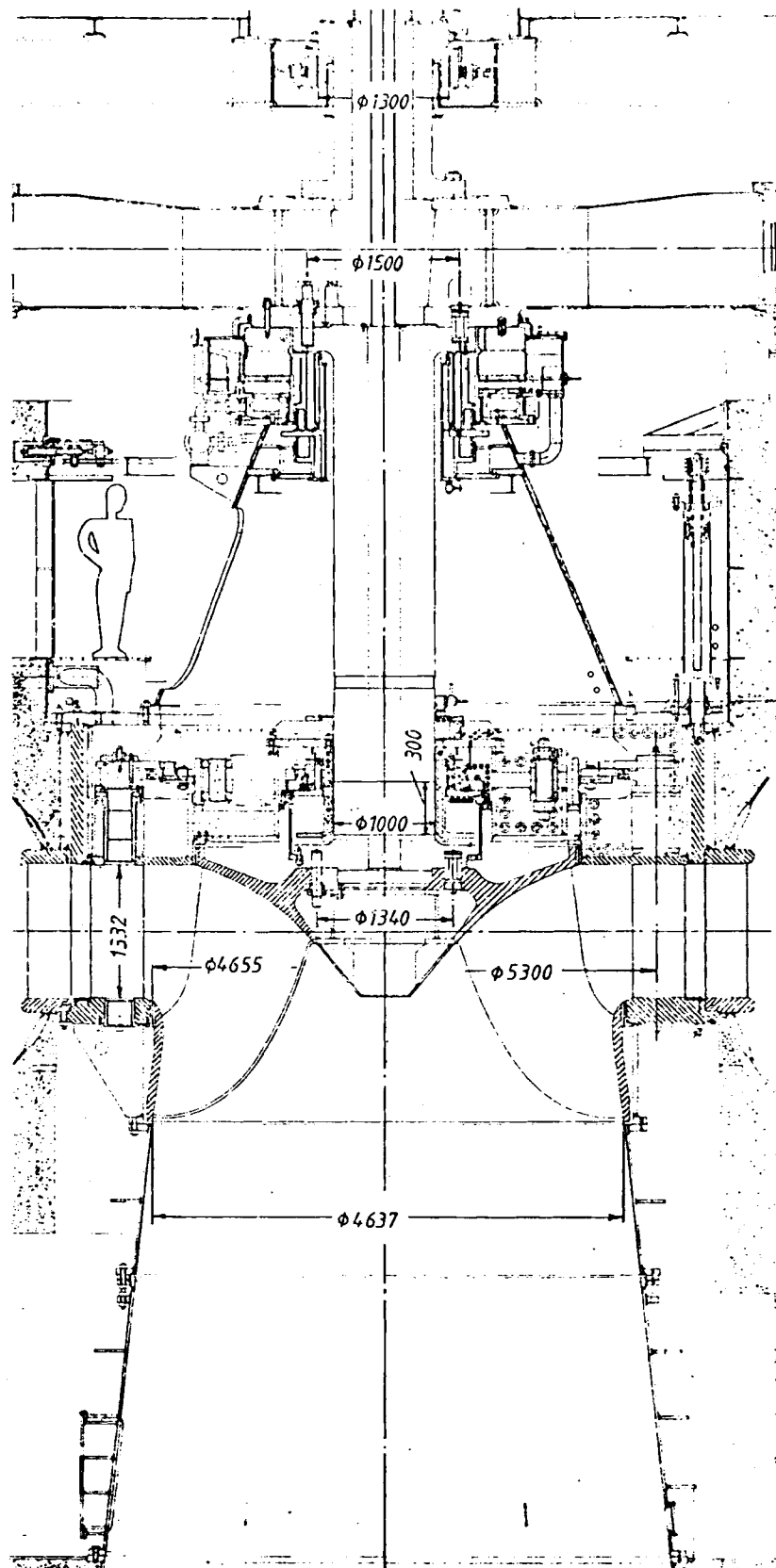
The compact design of Fig. 3.4.50 is only restricted to low head machines with parallel plate spiral casing. At high head machines, the stay vane with streamwisely varying span tends to increase the clearance of the ring gate's lower seal. Moreover in consequence of its relatively high rotor weight, the axial thrust of a vertical high head machine is not induced into the head cover. Hence the moment of the hydraulic uplift about the bolt circle on the stay vane crown, additionally widens the clearance of the ring gate's lower seal. Thereby pressurized water leaks through the seal and also loads the outer cylindrical wall of the head cover and the inner cylindrical wall of the stay vane crown. Relieving the ring valve chamber from the pressure of this leakage may squeeze the seal into this chamber and hence provoke a dangerously high leakage in a power house usually underground. For the reasons mentioned above, the radial sections of stay vane crown and head cover are subject to high bending moments about their radial neutral axes. Hence high tensile sresses in tangential direction occur in the water guide walls which usually have a high wear.

Fig. 3.4.50. Vertical FT at Aigle, France (owner EdF). Example of a ring gate between stay and guide vanes instead of shut down valve at the lower penstock end. (Because of highly stressed joint between stay ring and head cover, this design is limited to smaller heads) $H = 79,5$ m; $n = 143$ rpm; $P = 133$ MW (design Neyrpic). Runner: $D = 4,65$ m; dismantled from underneath. (Drawing courtesy Neyrpic, Grenoble, France)
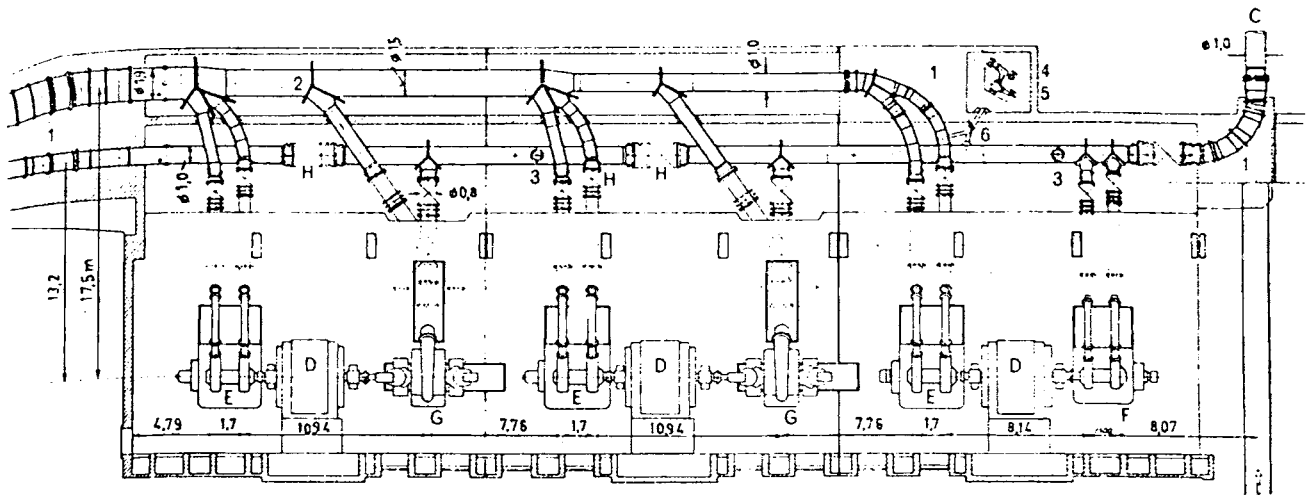
128

Fig. 3.4.51. Distribution chamber for penstock bifurcations separated from power house at Lanoux and Besines, France, at power house Hospitalet, France, with PTs and storage pumps (Riva-Jeumont). A distributor main Lanoux in separate chamber; B distributor main Besines; C joint for penstock Sisca-Baldarques; D motor generators; E twin PTs; G storage pumps; H spherical valves; 1 Fix point massive concrete; 2 supporting pedestal; 3 manholes; 4 corner nozzle valve; 5 wedge valve; 6 drainage duct; F low head impulse turbines.
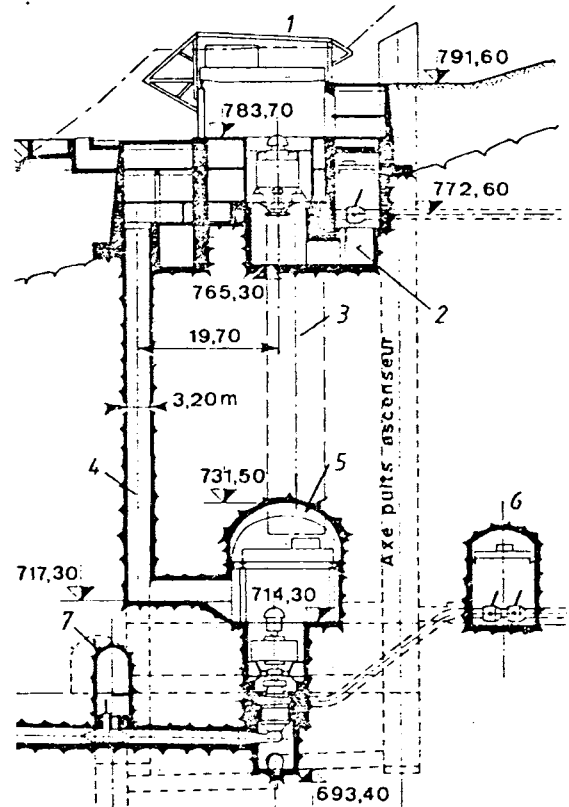

Fig. 3.4.52. Valve chambers up- and downstream of power house, at Grand Maison, l'Eau d'Olles, France (owner EdF). 1 power house upper stage; 4 vertical 5-nozzle PT (Neyrpic). $H = 817.4$ to 922.4 m; $n = 428.7$ rpm; $P_m = 4 \cdot 157$ MW; 2 valve chamber: 4 penstocks, 4 spherical valves; 3 transport shaft; 4 cable shaft; 5 underground power house for a pumped storage plant with eight 4-stage pumpturbines. $n = 600$ rpm; $H_T = 949$ m; $P_{Tm} = 8 \cdot 152$ MW; $H_P = 826$ m; $P_{Pm} = 8 \cdot 160$ MW (Neyrpic design); 6 valve chamber, 2 spherical valves in series; 7 downstream valve chamber with wedge valve. (Drawing courtesy EdF)

3.4.1.3. The substructure of the power house

The substructure is determined by the type of tailrace conduit. The following arrangements are usually employed for reaction turbines:

1) Elbow draft tubes for each turbine. Frequently applied in plants with KTs and FTs of low and medium head (see Fig. 3.4.14), especially for those with vertical shaft. Here
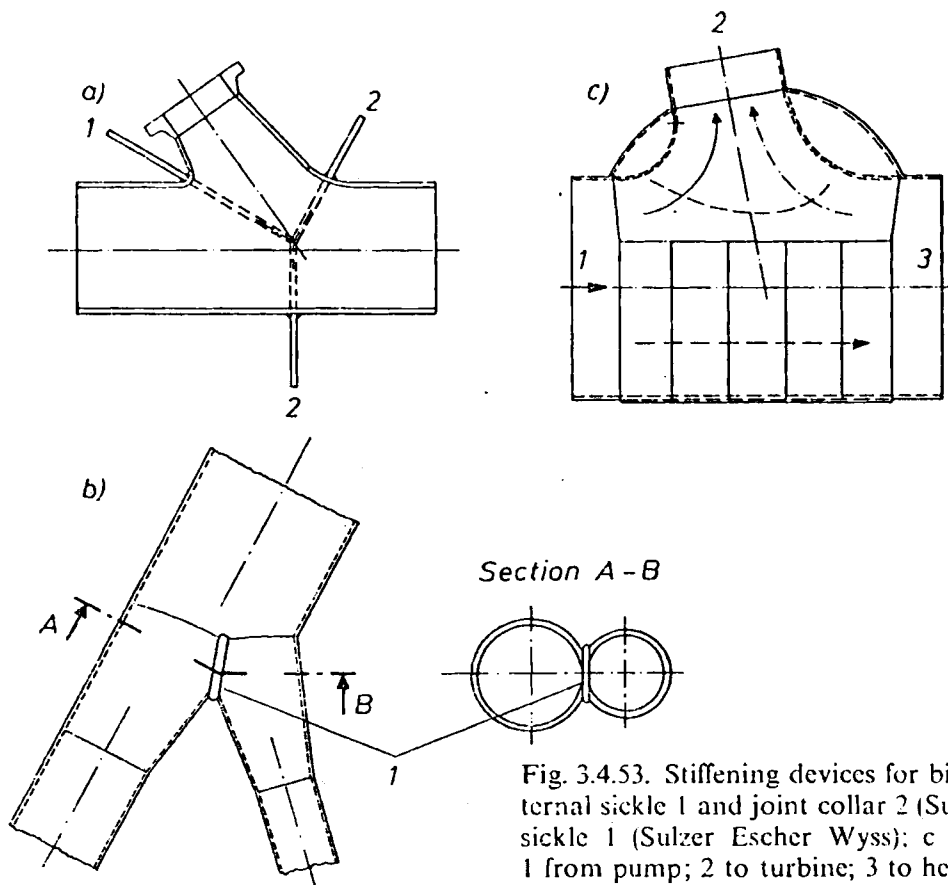
Fig. 3.4.53. Stiffening devices for bifurcations a with external sickle 1 and joint collar 2 (Sulzer); b with internal sickle 1 (Sulzer Escher Wyss); c with spherical shell; 1 from pump; 2 to turbine; 3 to head pond.
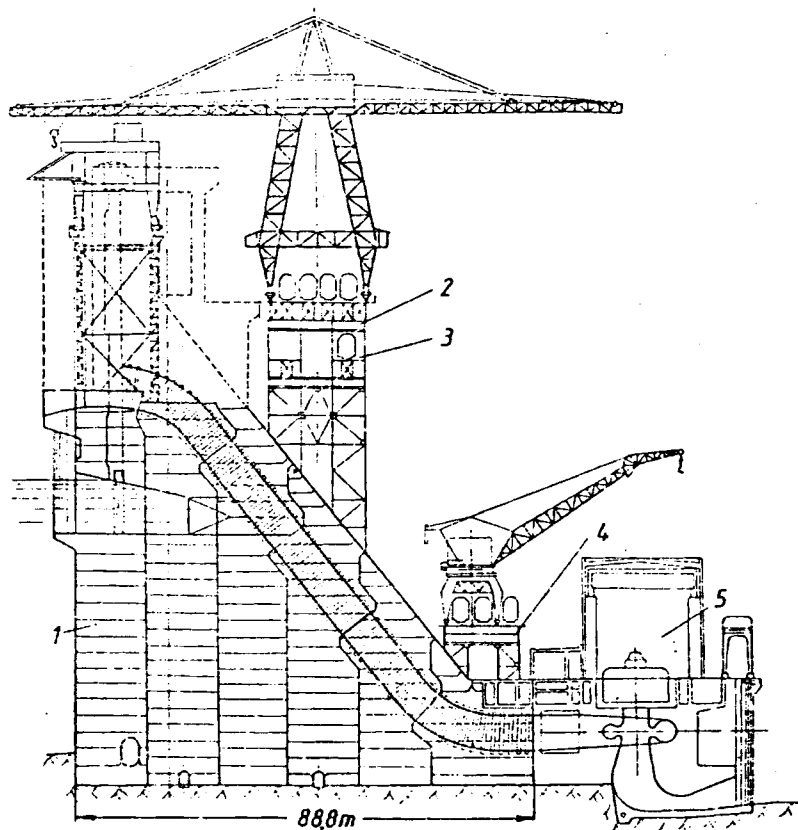
Section A-B

Fig. 3.4.54. Power house at base of gravity dam, at Bratsk, Angara, USSR (owner Sowjet State Power Board). Vertical FTs (LMZ design) $H = 102$ m; $n = 125$ rpm; $P = 18 \cdot 230$ MW. Runner: $D = 5,5$ m; z 14 vanes; integrally cast in 2 halves bolted together. Welded shaft. Welded spiral casing. Water-lubricated guide bearing. 1 barrage; 2 main crane (hammer head crane); 3 Baikal Amoor railroad; 4 auxiliary crane; 5 power house. (Drawing from Hydro Project Moscow).

888m

130

especially in the case of KTs. the large kinetic energy at runner exit requires a long draft tube (7 to 8 · D) and a considerable distance of the bottom of the inner draft tube from the runner exit (up to 3 · D). Effective pressure recovery requires the largest possible draft tube exit, whose width is given by the distance of adjacent sets.

Since such turbines usually are located along the base of the dam normal to the flow direction, the flow in the draft tube outlet continues the flow direction of the admission to the set. To obtain a plane face separating the adjacent blocks due to sets, the draft tube centre line must be slightly off-centred in its plan, thus compensating the eccentric inflow of the spiral casing (see Fig. 3.4.14).

II) Straight draft tube for each set: applied in tubular turbines with a straight centre line in elevation and plan, thus facilitating a plane separation face of adjacent concrete blocks from set to set (Fig. 3.4.45).

III) Draft tubes of FT with low specific speed and high head. Owing to the relatively low kinetic energy at runner exit, the draft tubes can be kept shorter than above. Here the flow usually discharges into a common tail water duct. This may be oriented in the original flow direction at turbine inlet or at 90° to it according to the requirements of the site's topography. In consequence of the submergence required, the duct is a pressurized tunnel. In the usual plant with PT this duct is not pressurized with a ducking wall to protect the surroundings from the noise.

3.4.2. Power house design with respect to distance from dam

I. Power house close to or within the dam: In low head run-of-river power plants, the power house forms together with the spillway part of the damming device and hence is close to the dam or incorporated within it. Proximity of the dam exists in the case of a plant with power house on the base of a dam (Figs. 2.3.4 and 3.4.54), or with an underground power house in the slopes of the valley (see Fig. 3.4.55). The incorporation of the power house into the damming device exists in the case of plant on a river bay (see Fig. 3.3.1), on both of the river banks, and in an abutment type power plant (see Fig. 3.3.4). The erection of a power house in the interior of the dam appears in submersible power plants (Fig. 3.3.3) and in barrages containing the power house, especially those underneath a spillway of the ski jump type (see Fig. 3.3.5).

II. Power house at greater distance from the dam: In this type of power station the diversion section in the form of a channel (see Fig. 3.3.1) or an extended system of tunnel, penstock or pressure shaft is very long. Here the power house may be an open air building at the end of the channel or at the base of a slope (see Fig. 3.4.56), linked to the penstock. Or it may be an underground power house (see Figs. 3.4.52; 55; 57) connected with the steel-lined pressure shaft at the lower end of the so-called "power drop" of the penstock.

Several varieties of the underground power house exist. The first is the pit power house (see Fig. 3.4.49). It is preferred for high head reaction machines needing large submergence. Another type is the earth-covered power house (Fig. 3.4.39). Both are usually located at the base of a slope, where they are now well protected against avalanches or rock fall. Both types of power house may be located in boulders or gravel.

The proper underground power house is usually within an artificial cave in rocky ground or within a natural cave that may exist, e.g. in Jurrasic ground.

The advantages of an underground power station especially in rock are the following:

1) No need for an outdoor area which is often both expensive and in short supply, especially in mountainous and densely populated areas, e.g. Switzerland.
2) No need for the maintenance of the exterior as it exists in an outdoor power house.
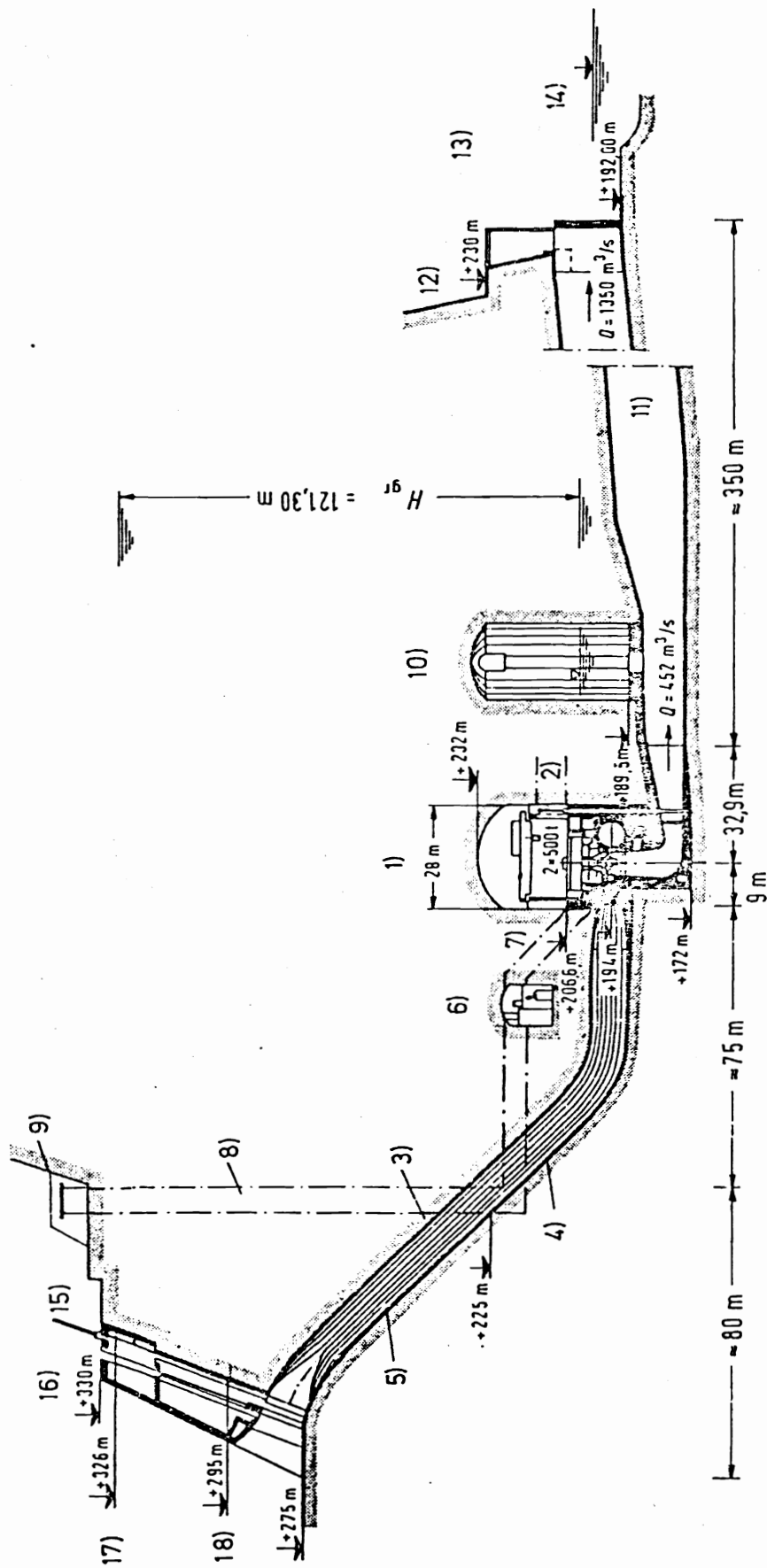
Fig. 3.4.55. An underground power house (cavern) close to a barrage in a river slope. Cabora Bassa, Zambesi, Mozambique, Africa (owner State Power Board Mozambique). 5 sets with vertical Francis turbincs. $H_m = 113.5$ m, $n = 107.1$ rpm; $P = 5 \cdot 415$ MW, (built by Ncyrpic, France, and Voith, West Germany). 1) power house cavern, area $A = 1380$ m^2, 2) access tunnel, 3) penstock, $\varnothing$ 9.7 m, 4) steel lining, 5) concrete lining, 6) transformer gallery, 7) bus bar, 13.5 kV, 8) cable shaft 220 kV, 9) platform 220 kV with an AC transmission line to converter station where 220 kV is converted into $\pm$ 530 kV DC covering 1400 km distance to the next consumer in the South African Republic, 10) tail water surge tank, $A = 350$ m^2, 11) tail race gallery, 12) exit structure, 13) Zambesi, 14) tailwater, 15) admission road, 16) intake and thrash rack, 17) maximum permissible head water level, 18) minimum permissible head water level.
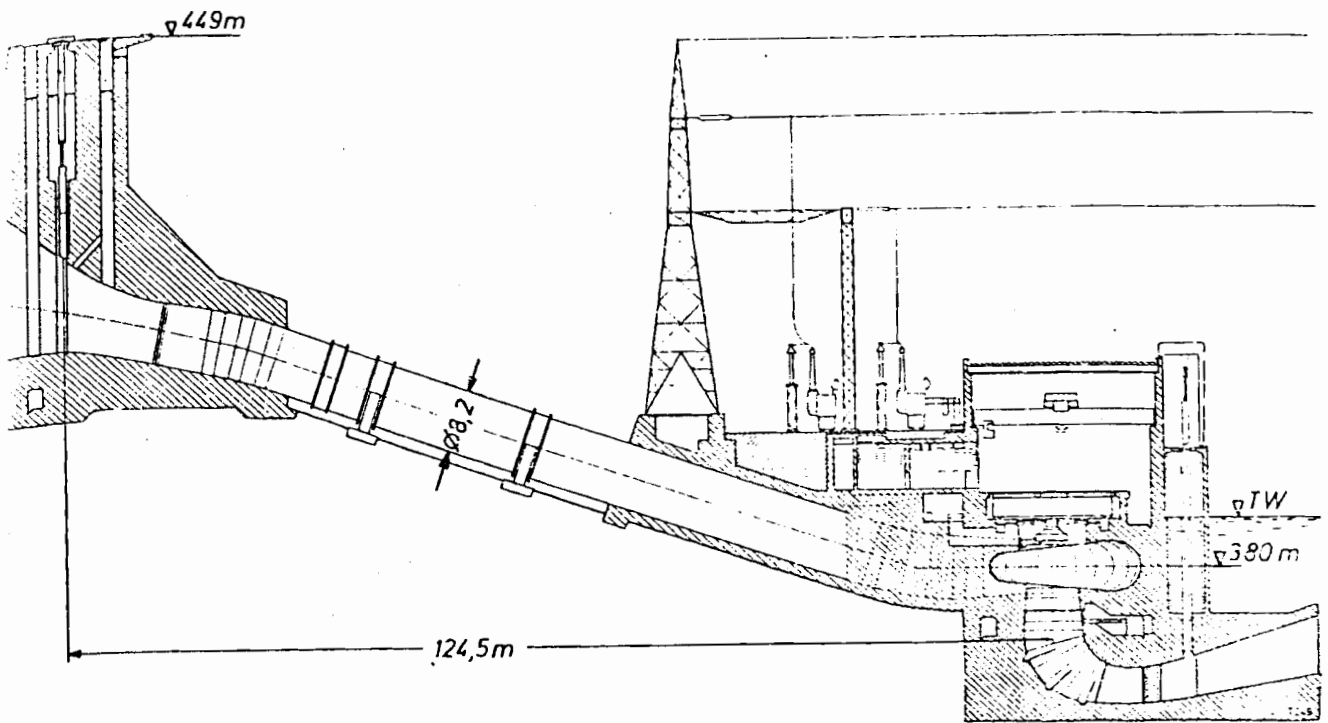
132

Fig. 3.4.56. Longitudinal section of a penstock and power house at the base of a slope. Marimbondo, Rio Grande, Brazil (owner Furnas Centrais Eletricas SA). $H = 62$ m; $n = 100$ rpm; $P = 8 \cdot 185$ MW (Voith design). (Drawing courtesy Voith)

g. 3.4.57. Underground power house of : Montezic pumped storage plant vner Electricité de France) with 4 pump-rbines (design Neyrpic) $n = 428,6$ rpm. irbining: $H = 378,9$ to 419 m; $P = 193$ MW; $\eta_{Tm} = 0,888$ (guaranteed). imping: $H = 384,5$ to 423 m; $P = 218$ to 2 MW; $\eta_{Pm} = 0,909$ (guaranteed). Rotor: $= 4,01$ m; $n_{ra} = 685$ rpm, 1 cavern; surge tank shaft. 2 a upper expansion amber of the surge tank, 3 access tunnel the cavern with an inspection tunnel to : suction line, 4 suction line, 5 lined sec-'n of the suction line, covered with stell ites, 6 admission pit, 7 access tunnel to : surge tank and the pit 6, 8 drainage !!ery, 9 drainage pit, 10 tunnel for inspec-'n of drainage facilities, 11 ground floor ·el of the machine hall. (Drawing courte-EdF)

133
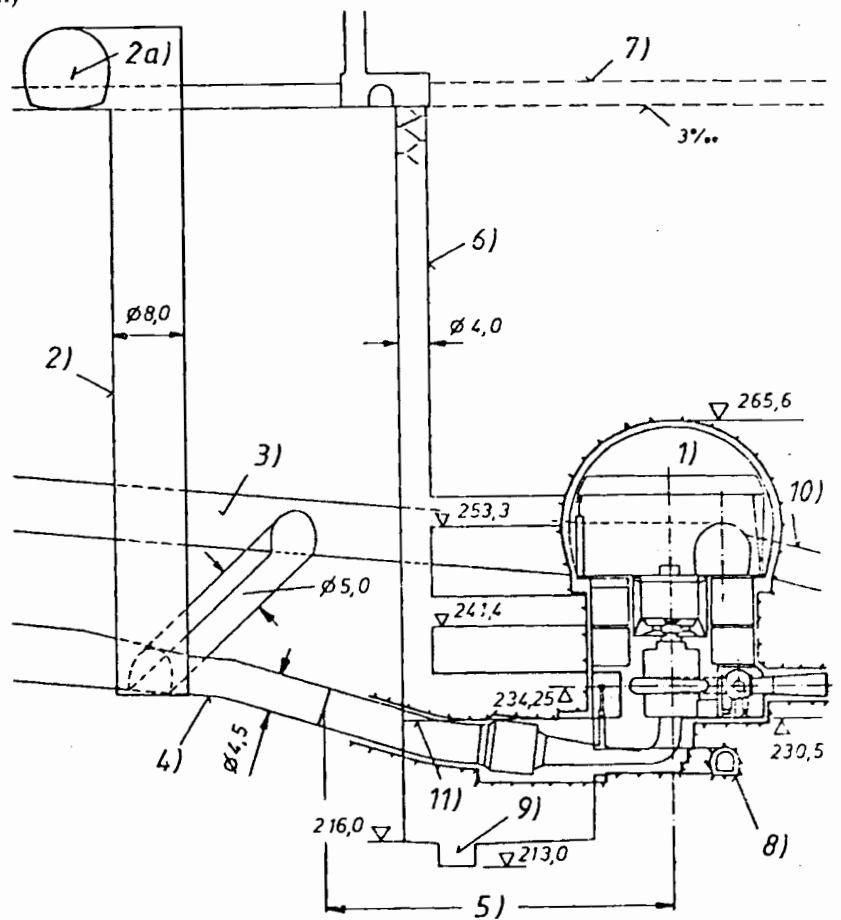
3) Saving of heating especially in the case of a severe climate. e.g Sweden or mountainous area.
4) Protection against avalanches and rockfall.
5) No destruction of the landscape.
6) Protection against air raids and nuclear war.
7) The rock extracted from the cavity can be used for other purposes, e.g. dam construction [1.54].

Notes on the Solidity of the structures in a hydro power plant:

For reasons of good economy, the water retention devices e.g., the upper reservoir, the dam, the spillway, possibly also the powerhouse, and the waterways have to be watertight. Hence on Jurassic ground, a channel or a reservoir cannot be erected easily. Under the deteriorating influence of the climate (e.g., frost, perma frost soil, and sun radiation), this water tightness has to be maintained during the useful life of the plant.

Nevertheless any realistic stress calculation has to be based on the assumption of a certain seepage and the resulting uplift on the structure.

Since seepage may enlarge the danger of soil slippage at the foundation and hence may threaten the stability of any structure, any seepage of the waterways and the damming devices like dam, spillway, and possibly also powerhouse. has to be controlled (e.g., by galleries or by ditches occasionally equipped with pumping stations to evacuate them).

In unreliable ground the seepage should be limited by special devices (grout curtain, sheet pile). These means have to be applied especially during the erection of the plant's components like powerhouse, dam, waterways and spillway.

The soil deformation of a structure, in consequence of seepage- or load-induced slippage, should be continuously controlled by the methods of land survey.

To complete the above note on dams in relation to this topic, some considerations must be also given to the loads and their corresponding stresses on spillway, powerhouse and their foundations.

The spillway and possibly also the powerhouse have to transmit the hydraulic thrust from the head water into the foundations, the abutment, and the soil without endangering the stability of the structure. Simultaneously, spillway and powerhouse are subject to reaction forces and moments from the soil, (e.g., uplift by seepage).

As a consequence, the admissible values of stress, pressure and strain between soil and the concrete of the foundations of both components have to be accounted for.

Moreover, the powerhouse receives the weight of its electro-mechanic and hydraulic equipment. For the location of the latter and the resulting stresses, the state of erection and repair has to be considered also. The powerhouse is further loaded by the reaction force and moment of the turbine distributor, its servomotor and valve and by the corresponding loads of the draft tube.

This superposes the pressure- and temperature-induced steady loads of the penstock (if any), of the spiral casing, and the draft tube, the water-hammer-, and surge-induced unsteady loads of these elements, and the vibratory reaction torque of the alternator stator, especially in case of short circuit. Also to be accounted for are weight-, hydraulic thrust-, and temperature-induced loads of the bearings on the powerhouse, loads due to flexural and torsional shaft vibrations, especially at start up and runaway of the set. The unsteady loads due to the impact of wind and possibly of water waves and ice floes, must be added.

A powerhouse on the base of a slope, possibly has also to resist the impact of rockfall and avalanches. In this case an earth-covered construction or a pit powerhouse may fit best.

The static and dynamic response of the powerhouse structure to the above loads, and the corresponding stresses and strains, also in the foundations and in the adjacent soil, have to be kept in admissible limits. An eventual tensile stress, e.g., due to a bending moment in the wall, requires a corresponding reinforcement of the concrete. In the case of a dangerous resonance, e.g., at a power swing, the elastic properties of the power house structure, but also its mass of concrete, have to be tuned so as to keep the vibratory wall amplitude within admissible limits. These limits have to be set with respect to load changes during the useful life of the plant, and with respect to the fatigue effects combined herewith.

134

4. The layout of river-run and storage plants with respect to optimized figures such as rated discharge, number of sets and their diameter, storage volume, hydraulic radius of the water way and dimensions of the electric transmission line

4.1. Introduction

The layout of a hydro power plant has to start from its character whether it is a run-of-river and a base load plant or a storage and peak load plant, or of mixed character. It has to be based, as the case may be, on hydrological data such as the flow duration line of a river, the catastrophic high water, the topography of the site, the width of the river bed, the head and hence the machine type, the eventual length of diversion by channel or pipe or both, the electricity rate, amount and structure of demand and the distance of the next consumer from the site and the geology of the site.

In developing countries with large rivers the exploitation has to start with the erection of the barrage and spillway, huge constructions compared with the orignal small energy demand. Hence the main problem then arising is the question, how to develop in smaller stages, e.g., by using side valleys to by-pass the main river in steps. If this is not feasible, the river must be diverted temporarily during the erection period of the barrage, the spillway and the power house.

Contrary to this in the following chapter the layout is discussed under the assumption that the demand exists. Then from the economical point of view the question arises how to set the operating data of the plant and the dimensions of its structural members so as to make a maximum the surplus of revenue over initial cost mainly due to the sale of electricity during the depreciation period of the plant.

Assuming the site, its topography and hydrology and hence also head and type of machines to be given, an attempt is here made, to ascertain the optimum value of a certain device, or an operating figure of a plant, so as to satisfy the requirement above mentioned.

Such an optimization may be attained with respect to rated discharge in a run-of-river hydro power plant, with respect to size and number of sets, with respect to the coefficient of rotor blade speed, the hydraulic radius of the waterway (if there is one) such as channel or pipeline, the diameter of the electric conductor for power transmission and the distance between adjacent towers on this line.

This optimization includes many cost terms, e.g. fabrication, earth excavation, super-structure and substructure of the power house and spillway costs and accounting for the losses of the hydraulic machine, and, in case of a reaction machine, for its ground excavation required due to cavitation, as a function of the machine's size.

For the layout of a storage plant on a river, the topography of the site, the target release due to the river and the power demand are assumed as known values. For the case of a

pumped storage plant, which only consumes electric energy, the problem arises how to set the electricity rate during base load and peak load hours so as to make a surplus by sale of peak load energy.

The break down of a plant economy into linearly interrelated components is admittedly difficult and remains often only an estimate. To obtain, e.g. the specific cost of the components from a real scheme, scale effects, often unknown due to size, position, inflation, degree of development, local state of the art, and imponderabilities such as the political ambition of the planner or owner, have to be separated, to obtain actual information [4.1].

In this chapter the assignment of the electric machine and the hydraulic machine to each other with respect to the limits of output and speed (see chapter 11.4) is ignored. In any plant, it is expected that, at least for a sufficient and reasonable number of days in the average year, the plant operates with rated head and rated discharge at the bep of the machines.

It is important to know that the operating point of a machine results from the intersection of two curves. The one is the head as function of the river flow that results from the hydrograph, the topography of the site, and the geometry of the water way, which is often influenced by sedimentation. The other curve is the head as a function of the flow, which passes the machine at a certain speed and a certain gate opening.

If the intersection point of both the curves misses the bep of the machine, then there may be litigation to seek for the person responsible. The only thing a court can do in this case is to obtain the opinion of a consultant on the base of careful research and field tests.

On the one hand, the faulty construction may result from wrong surveying, or a faulty reading of the hydrograph by the planner. Also a wrong evaluation of the friction in the water ways, or an erroneous estimation of the depositing sediments may have led the planner to wrong conclusions about back water effects etc.

On the other hand the maker of the machine can make a mistake either in designing, machining, or controlling the machine he has supplied.

In general the maker has an interest to meet the bep, as a bad efficiency would be a bad recommendation for his business. But also the user of the plant, which is usually also the planner, must be interested in a high revenue. On no account can the maker be made responsible for having adopted a wrong hydrograph or head since such measurements are too time-consuming, in this respect he must trust the planner. This holds true especially for the manufacturer of the set.

The planning of a hydro power plant is also made difficult by the fact, that two random effects must coincide with the best efficiency point of the machine characteristics.

One is the available annual output of the plant, which can be predicted (especially in a run-of-river plant) only as a time-averaged value. This results from observations over many years.

The other is the prediction of the annual output of the plant during its useful life. This can be only derived from the preceding development and may undergo unpredictable variations in the future. The consequences of this uncertainty may be further complicated when the plant supplies a grid by itself or when its annual output is relatively large compared to that of the interlinked grid. Finally the planning of a hydropower plant in the way described here is characterized by the fact that its rated capacity which equals the energy demand, exists only at a certain moment during its useful life.

To overcome this discrepancy, the plant may be developed either in stages, or certain limiting working data, e.g. the current density or the velocity in the water way, are reached at the end of its useful life. In this chapter, the concept of the capitalized cash value of energy loss is applied. This needs some comment, since this cost term is neither an asset nor a liability in the usual economic

136

sence. It is an imaginary cost term, depending on the loss of a component considered during its useful life. Thereby it is a function of the components's size. This facilitates an optimization of this size also depending on the investment, the income by sales of energy, and other benefits of the plant.

The above capitalized cash value of loss is a part of what is here called resulting cost. It is here assumed that the later does not contain the OMR cost (due to operation, maintenance, and replacement). The OMR cost is deemed to be independent of the component's size, and hence irrelevant for optimization. Strictly speaking, it depends also on this size. Therefore the first cost (investment for planning, construction and erection of the plant) could be imagined to include the OMR cost. Here the cash value is identical with the present value at starting power production.

In the following text a "set" denotes a generating unit consisting of a turbine and its generator. Moreover the cost of electric energy is referred to as electricity rate. Finally the initial investment cost of a plant is also referred to as first cost.

4.2. Optimization of rated discharge of a run-of-river plant

4.2.1. General remarks and assumptions

An exploitable reach of a river with an available head, that results from the river's drop along this reach, is considered [4.2; 4.3]. This available head Δh is assumed to equal the available drop of maximum permissible water levels in the reservoirs existing after the completion of the development.

The flow duration curve of the average hydraulic year may be known for this reach. The development is based on a plan according to which the river, without any flow regulation, is developed in subsequent reaches having available head. From the topography of the river bed, the back water effect as a function of the known hydrograph for the subsequent plant is also known and accounted for (Fig. 4.2.1 a).

For this scheme the rated discharge as a function of turbine arrangement is to be optimized with respect to a maximum surplus of earnings from the sale of energy over the initial cost of plant for the economic life of the facilities. For simplicity the net earnings
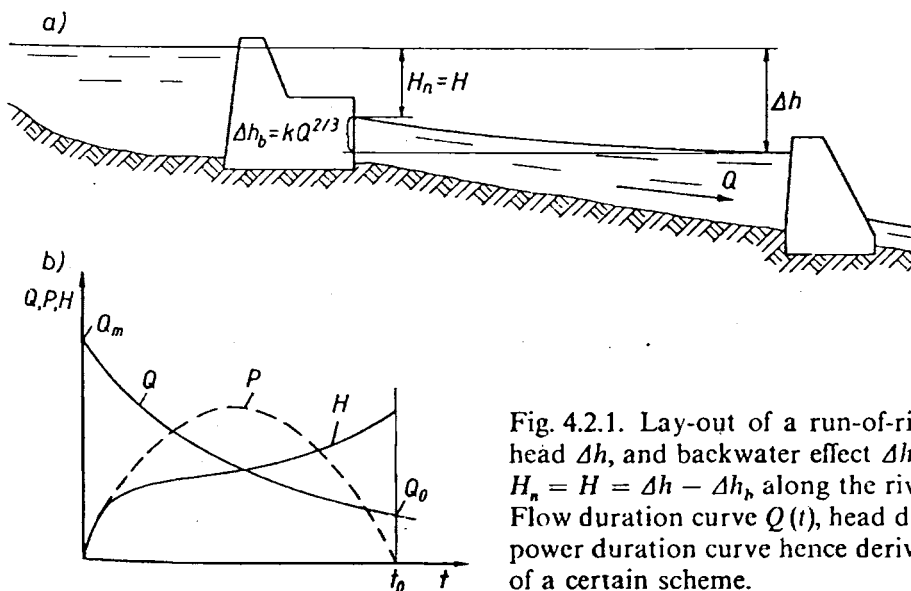

Fig. 4.2.1. Lay-out of a run-of-river plant. a) Available head Δh, and backwater effect Δh_b, yielding the net head $H_n = H = \Delta h - \Delta h_b$ along the river section exploited. b) Flow duration curve $Q(t)$, head duration curve $H(t)$, and power duration curve hence derived for the average year of a certain scheme.

considered are obtained by subtracting the OMR cost from the gross earning. The electricity rate is assumed constant during the period of depreciation.

The live storage volume of the reservoir is assumed so small, that it can be neglected. Hence the plant considered always operates under its maximum permissible head water level. To obtain the net head H from this, Δh has to be diminished by the flow-induced level drop due to the back water effect $\Delta h(Q)$. Hence the net head $H = \Delta h - \Delta h(Q)$. For practical purposes and in accordance with experience $\Delta h(Q)$ is assumed to equal the head computed by a weir formula $\Delta h(Q) = k Q^{2/3}$, Q being the discharge and k an empirical constant parameter [4.4].

As the live storage volume is negligible, any river flow that passes over the rated flow Q_r of the turbines at rated gate has to be spilled to limit cavitation pitting.

It is assumed that all the machines installed are available for operation, when the river offers this discharge. Moreover the electric grid is assumed to be large enough to consume the energy offered by the plant. The number of sets is assumed to be of a size so as to allow (by switching on and off an adequate number of sets) the sets to operate at their bep under the available river flow. Hence $\eta = \eta_{op}$ depends only on the net head H.

Since the spillway is designed for the maximum flood discharge, it absorbs a constant amount of the initial cost and therefore does not affect the surplus. The same holds for the cost of high voltage transmission – if required – with its outdoor switchyard.

The cost term for the barrage (if any at all) may be slightly affected by that of the power house, if the latter forms a part of the damming device. However in a run-of-river plant like the one considered, the main cost of the damming device is due to the embankment along the developed reach of the river. Assuming this, the cost of dam may be considered as independent of rated discharge. In the following chapter 4.3 an attempt is made to account for the influence of capacity and hence of the power house on the cost of a dam that crosses a river of given width.

The cost term for the power house is split here into one term, K_P, for its superstructure and another term for its substructure, mainly owing to excavation for the draft tube and the spiral casing, K_{ex}.

The remaining first cost of the sets consisting of turbines, alternators and a portion of the transformer K_s are assumed to vary with the rated discharge and hence with the size of machine which is assumed to determine the cost of fabrication.

As opposed to Cap. 4.3., in this section the cost of the accessories per set are assumed to be proportional to that of the set, and consequently can be included in the aforementioned cost term K_s.

The net head is computed from the known available head Δh and the backwater effect $kQ^{2/3}$ as $H = \Delta h - kQ^{2/3}$, where clearly H is a function of the flow Q. Since the latter is given by the flow duration curve as a function of time (here taken in hours over a year with t_0 hours), a net head duration curve is also given $H = H(Q) = H(Q(t)) = H(t)$ and hence $\eta = \eta(H) = \eta(t)$ [4.5] (Fig. 4.2.1 b), where η denotes the efficiency of the set.

For a comparison with the initial cost, the present value of earnings during the z years of depreciation under a constant electricity rate k_e and interest rate p, denoted by K_e is computed for the time, when energy production starts.

The optimization of rated discharge Q_r relative to a surplus of earnings K_e over the initial cost terms K_P, K_{ex} and K_s due to the power house, excavation and fabrication of sets, depending on Q_r, is made under the following alternative cases.

138

In the first case the nominal runner diameter D might be given. Naturally this is done with consideration of the number of sets i, assumed large, and, of course, an integer.

In the second case the number of sets, i, is given. This must be done, however, to conform with the feasibility imposed by the resulting runner diameter D. Turbines with vertical shafts are assumed.

4.2.2. Specialization of the problem

4.2.2.1. The case of a given runner diameter D and desired i

From the assumptions made, the flow duration curve $Q(t)$, the net head duration curve $H(t)$ and the efficiency duration curve $\eta(t)$ are given (see Fig. 4.2.1 b). Hence the "power duration" curve is $P(t) = \varrho g H(t) Q(t) \eta(t) 10^{-3}$ kW. During the $t = t_r$ days of a year (measured in hours from now on) the rated discharge required to make a maximum surplus is $Q_r = Q(t_r)$. Hence and from the assumption, the rated head H_r due to Q_r is [4.4]

$$H_r = H(t_r) = \Delta h - k Q_r^{2/3}. \tag{4.2-1}$$

The unknown quantity is t_r. According to the assumptions, during the period t_r the discharge exceeding Q_r under H_r must be spilled. During t_r the turbines consume, according to the similarity laws (Cap. 9.2) at an arbitrary instant, the flow

$$Q(t) = Q(t_r)[H(t)/H(t_r)]^{1/2} = Q_r[H(t)/H_r]^{1/2}.$$

The work done in the period t is $W(t) = \int_0^t P(\tau) d\tau$ and the associated earnings $K_e = k_e W(t)$. Then the capitalized cash value of earnings at a constant electricity rate k_e and interest rate p during the z years of depreciation at the instant of starting energy production is obtained as

$$K_e = 10^{-3} \varrho g k_e \left[(Q_r/H_r^{1/2}) \int_0^{t_r} \eta(\tau) H(\tau)^{3/2} d\tau + \int_{t_r}^{t_0} Q(\tau) \eta(\tau) H(\tau) d\tau \right] \alpha \tag{4.2-2}$$

with $t_0 = 8760$ annual hours and the factor α due to interest

$$\alpha = [(1 + p)^z - 1]/[p(1 + p)^z] \tag{4.2-3}$$

$$\lim_{p \to 0} \alpha = z. \tag{4.2-4}$$

The cost of the superstructure of the power house with i units of diameter D is approximately

$$K_p = i k_p k_1 k_5 D^2 (H_0 + k_6 D) \chi, \tag{4.2-5}$$

where k_p is the cost per unit volume of the power house superstructure, k_5 the streamwise extension of the superstructure related to D, H_0 the height of the pit (usually of the order of $(2$ to $3) \cdot D)$, k_6 a design parameter for the power house, being about 0 for an open air plant and reaching about 3 for a tall hall design, containing the main crane in its interior, k_1 a parameter depending on the lateral size of the block of the set related to D and being $k_1 = 2$ for a TT, $k_1 = 3$ for a semi-spiral casing, $k_1 = 4$ for a spiral casing, χ the ratio of the average height of power house in relation to $H_0 + k_6 D$ (height due to the crane runway above the turbine pit), where $\chi < 1$.

The cost due to excavation K_{ex} now considered requires the volume excavated of one set

$V_e = d_e L b_s$ (see Fig. 4.3.1 b). This is composed of the depth d_e, which follows from the figure above by

$$d_e = (k_2 D_1 - h_s - d_R) \psi = [k_2(D_1/D_2)D - h_s - d_R] \psi, \qquad (4.2-6)$$

where D_1 is the runner throat diameter $[D_1 = (D_1/D_2)D$ and D_1/D_2 is roughly determined by the head and hence the type number], $k_2 = 1,0$ to 1,5 or 2,6 to 3,2 for a straight or elbow draft tube, h_s is the suction head (Fig. 4.3.1 b), d_R the original depth of river bed below the tailwater level (see Fig. 4.3.1 b), $\psi < 1$ accounts for the varying depth of excavation.

The streamwise length of the excavation is (Fig. 4.3.1 b)

$$L = k_3 D_1 = k_3 (D_1/D_2) D, \qquad (4.2-7)$$

where $k_3 = 5$ to 6, or 7 to 10 for an elbow, or horizontal straight draft tube. Finally the excavated volume consists of the width per set (see Fig. 4.3.1.c)

$$b_s = k_1 D, \qquad (4.2-8)$$

where k_1 is from (4.2-5).

The suction head in (4.2-6) depends on the $NPSH$ required (Cap. 8.2) by $h_s = B - NPSH$, where B depends on the altitude h of the plant and its critical pressure h_{cr}

$$B = 10,33 - 0,0012 h - h_{cr}. \qquad (4.2-9)$$

According to cap. 8.2, $NPSH$ as function of the pressure number λ of the critical point in the rotor and the draft tube efficiency η_s for the bep (with $c_{u1} = 0$) is

$$2g\, NPSH = (\lambda + \eta_s) c_{m1}^2 + \lambda u_1^2, \qquad (4.2-10)$$

where c_{m1} is the meridional speed and u_1 the peripheral rotor blade speed at station 1 (rotor throat diameter [3]).

The above relation can also be used for the general case, where the rated point has a whirl c_{u1} past the runner. Then under the assumptions leading to (4.2-10), $NPSH$ is given by $2g\, NPSH = \lambda w_1^2 + \eta_s c_1^2$, w_1 and c_1 being the relative and absolute speed at point 1. From the velocity triangle there, the following relations can be obtained: $c_1^2 = c_{m1}^2 + c_{u1}^2$, with the whirl $c_{u1} = u_1 - c_{m1} \cot \beta_1 = u_1 (1 - \varphi_1 \cot \beta_1)$, $\varphi_1 = c_{m1}/u_1$, $c_{m1} = Q_r/(A_1 i)$ due to the rated flow Q_r, β_1 being the runner vane angle at station 1 and A_1 the rotor's cross section there. Hence

$$2g\, NPSH = (\lambda/\sin^2 \beta_1 + \eta_s) c_{m1}^2 + \eta_s (1 - \varphi_1 \cot \beta_1)^2 u_1^2. \qquad (4.2-11)$$

It can be seen that the structure of relation (4.2-10) corresponds to the more general case of (4.2-11), if $(\lambda/\sin^2 \beta_1 + \eta_s)$ is substituted for $\lambda + \eta_s$, and $\eta_s(1 - \varphi_1 \cot \beta_1)^2$ is substituted for λ. Obviously, λ in (4.2-11) and (4.2-10) are different.

The peripheral blade speed $u_1 = (\omega/2)(D_1/D_2)D$ where D_2/D_1 is a design-conditioned value following from the type number n_q as a non dimensional specific speed defined according to cap. 9.2 by $n_q = \omega (Q_r/i)^{1/2}/(g H_r)^{3/4}$. Hence $\omega = n_q (i/Q_r)^{1/2} (g H_r)^{3/4}$, $u_1 = D(D_1/D_2) n_q (g H_r)^{3/4} [i/(4 Q_r)]^{1/2}$. Inserting this, and c_{m1} from continuity $c_{m1} = \{4 Q/[\pi i (1 - N^2)]\} (D_2/D_1)^2/D^2$ in (4.2-10), putting $NPSH$ in $h_s = B - NPSH$, and this in d_e (4.2-6), the cost due to excavation of i sets with rotor diameter D becomes with respect to submergence required and the cost per unit volume k_{ex}

---

[3] Strictly speaking, rotor throat diameter (here and elsewhere) defines the largest diameter of the rotor exit edge in a turbine.

140

$$K_{ex} = \psi\, i\, k_{ex} k_1 k_3 DD_1 \{k_2 D_1 - B - d_R$$
$$+ 8(\lambda + \eta_s) Q_r^2 / \langle g\,[i(1 - N^2)\pi(D_1/D_2)^2]^2\, D^4\rangle$$
$$+ \lambda n_q^2 g^{3/2} H_r^{3/2} D^2 (D_1/D_2)^2\, i/(8\,g\,Q_r)\}\,. \tag{4.2-12}$$

The cost of fabrication, transport and assembly of the i units with the runner diameter D is assumed as [4.6]

$$K_s = i\, k_s D^n, \tag{4.2-13}$$

where k_s is an empirical cost factor, $n = 2{,}3$ to $2{,}5$. For i sets with Q_{11} as unit discharge (Cap. 9.2), the rated discharge of the station reads $Q_r = i\, Q_{11} D^2 (g\,H_r)^{1/2}$. Hence i becomes the following function $i(t_r)$ of the unknown time t_r by which also $Q_r = Q(t_r)$ and $H_r = H(t_r)$ are determined

$$i = (Q_r/H_r^{1/2})(Q_{11} D^2 g^{1/2})^{-1} = i(t_r). \tag{4.2-14}$$

Inserting this in (4.2–5), (4.2–12), (4.2–13) the individual terms are obtained as functions of the unknown time t_r, namely

$$K_{ex} = \psi\, k_{ex} k_1 k_3 D_1 D \{k_2 D_1 - B - d_R$$
$$+ \langle 8(\lambda + \eta_s) Q_{11}^2 /[\pi(1 - N^2)(D_1/D_2)^2]^2$$
$$+ \lambda n_q^2 (D_1/D_2)^2/(8\,Q_{11})\rangle H_r\} i(t_r), \tag{4.2-15}$$

$$K_P = k_P k_1 k_5 D^2 (H_0 + k_6 D)\chi\, i(t_r), \tag{4.2-16}$$

$$K_s = k_s D^n i(t_r). \tag{4.2-17}$$

Expressing the suction head h_s in (4.2–6) according to cap. 8.2. by the cavitation index σ as $h_s = B - \sigma H$, K_{ex} (4.2–15) yields

$$K_{ex} = \psi\, k_{ex} k_1 k_3 (D_1/D_2) D^2 [k_2(D_1/D_2)D - B - d_R + \sigma H_r] i(t_r). \tag{4.2-18}$$

The earnings given in (4.2–2) are already expressed as functions of t_r taking into account that H_r and Q_r are also such functions according to $Q_r = Q(t_r)$ and (4.2–1). The surplus of profit reads

$$S = K_e - K_s - K_P - K_{ex}. \tag{4.2-19}$$

Its desired maximum follows by putting its differential coefficient with respect to time t_r, correlated to the rated discharge Q_r, to zero. Accordingly $dS(t_r)/dt_r = 0$.

With the simplifications: $dH_r/dt_r = \dot{H}_r$, $dQ_r/dt_r = \dot{Q}_r$, then from the extremum condition, from (4.2–19), (4.2–2), (4.2–16) through (4.2–18), the following equation is obtained

$$0 = (\dot{Q}_r H_r - Q_r \dot{H}_r/2)\left[A_1 \int_0^{t_r} \eta(\tau) H(\tau)^{3/2}\, d\tau - (A_2 + A_3 + A_4 A_5 + A_4 \sigma H_r)\right]$$
$$- A_4(\sigma + H_r\, d\sigma/dH)\dot{H}_r H_r Q_r, \tag{4.2-20}$$

where the parameters A_i read as follows

$$A_1 = 10^{-3} k_e \varrho g^{3/2} Q_{11} D^2 \alpha, \tag{4.2-21}$$

$$A_2 = k_s D^n, \tag{4.2-22}$$

$$A_3 = k_P k_1 k_5 D^2 (H_0 + k_6 D)\chi, \tag{4.2-23}$$

$$A_4 = \psi\, k_{ex} k_1 k_3 (D_1/D_2) D^2, \tag{4.2-24}$$

$$A_5 = k_2(D_1/D_2)D - B - d_R. \tag{4.2-25}$$

141

The cavitation index σ and hence also its derivative $d\sigma/dH$ are known as functions of head from Table 9.2.1. For (4.2–20) this head is found by trial and error.

The relation (4.2–20) can be evaluated only if the functions $H(t)$ and $Q(t)$ and subsequently H_r, Q_r, η_r, $\dot{H}_r$, $\dot{Q}_r$, and then the integral in (4.2–20) are known and approximated by polynomials in t_r. In this case (4.2–20) is an equation for t_r, the solutions of which are the values making the surplus a maximum. They can be found by Newton's approximation. The solution of interest is that due to largest surplus S. The time t_r leads to the rated discharge $Q_r = Q(t_r)$ of the plant's flow duration line and hence by (4.2–1) also the rated head H_r. The required number of sets i follows from (4.2–14), and has to be adapted to an integer [4.7]. For the adaptation of the generator's speed and output see chapter 11.4. Obviously the time t_r has to be smaller than t_0 due to one year.

4.2.2.2. The case of a given number i of sets and runner diameter D to be estimated

Equation (4.2–14) gives the diameter D as a function of t_r, namely

$$D = (Q_r^{1/2} H_r^{1/4})/(Q_{11}^{1/2} i^{1/2} g^{1/4}) = D(t_r). \tag{4.2–26}$$

Inserting this into (4.2–5), (4.2–13), (4.2–18), the optimum condition $dS/dt_r = 0$ for the surplus after (4.2–19) gives

$$
\begin{aligned}
0 = {}& 10^{-3} k_v \varrho \, g \, \alpha (\dot{Q}_r H_r^{-1/2} - Q_r \dot{H}_r H_r^{-3/2}) \int_0^{t_r} \eta(\tau) H(\tau)^{3/2} \, d\tau \\
& - i\{k_s n D^{n-1} + D^2 (3 k_p k_1 k_5 k_6 \chi + 3 k_{ex} k_1 k_2 k_3 (D_1/D_2)^2 \psi) \\
& + 2D[k_p k_1 k_5 \chi H_0 - k_{ex} k_1 k_3 \psi (D_1/D_2)(B + d_R) \\
& + k_{er} k_1 k_3 \psi (D_1/D_2) \sigma H_r]\} \dot{D} \\
& - i k_{ex} k_1 k_3 \psi (D_1/D_2) D^2 \dot{H}_r (H_r \, d\sigma/dH + \sigma),
\end{aligned} \tag{4.2–27}
$$

where $\dot{D} = dD(t_r)/dt_r$ and $D = D(t_r)$ depend on t_r.

4.2.3. Example of the estimation of runner diameter D

The flow duration curve is assumed to be linear, $Q(t) = Q_m - (Q_m - Q_0)(t/t_0)$ with Q_m and Q_0 as maximum and minimum flow rates. Hence with $x = t_r/t_0$ as the unknown figure

$$Q_r = Q_m - (Q_m - Q_0)x, \tag{4.2–28}$$

$$H_r = \Delta h - k[Q_m - (Q_m - Q_0)x]^{2/3}. \tag{4.2–29}$$

Moreover the efficiency is assumed as constant. Hence the integral in (4.2–20) $\int_0^{t_r} H^{3/2} \, d\tau$ can be strictly solved by the substitution $k[Q_m - (Q_m - Q_0)\tau/t_0]^{2/3} = \Delta h \sin^2 u$. This brings $d\tau = -\{3 \Delta h^{3/2} t_0/[(Q_m - Q_0) k^{3/2}]\} \sin^2 u \cos u \, du$ and

$$\int_0^{t_r} H^{3/2} \, d\tau = -3 \Delta h^3 t_0/[k^{3/2}(Q_m - Q_0)] \int_0^{t_r} \cos^4 u \sin^2 u \, du.$$

Making use of the abbreviations

$$k Q_m^{2/3}/\Delta h = q, \tag{4.2–30}$$

$$[1 - (1 - Q_0/Q_m)x]^{2/3} = s, \tag{4.2–31}$$

the integral in (4.2–20) has the solution

$$\int_0^{t_r} \eta\, H^{3/2}\, d\tau = \frac{\eta\, t_0\, \Delta h^{3/2}}{q^{3/2}(1 - Q_0/Q_m)} \left\{ \frac{17}{30}\, q^{5/2}\, [(1 - qs)^{1/2}\, s^{5/2} - (1 - q)^{1/2}] \right.$$

$$- \frac{7}{24}\, q^{3/2}\, [(1 - qs)^{1/2}\, s^{3/2} - (1 - q)^{1/2}]$$

$$- \frac{1}{16}\, q^{1/2}\, [(1 - qs)^{1/2}\, s^{1/2} - (1 - q)^{1/2}]$$

$$\left. - \frac{1}{16}\, [\arcsin(qs)^{1/2} - \arcsin q^{1/2}] \right\}. \tag{4.2-32}$$

From (4.2−28), (4.2−29), (4.2−30), (4.2−31) the t_r-dependent parameters in (4.2−27) can be reduced to s, with $x = t_r/t_0$, which is also a t_r-dependent parameter, as follows

$$H_r = \Delta h(1 - sq); \qquad \dot{H}_r = -2\Delta h q/(3 t_0 s^{1/2}), \qquad \dot{Q}_r = -(Q_m - Q_0)/t_0,$$

$$\dot{D} = (2 H_r \dot{Q}_r - Q_r \dot{H}_r)/[4 (i Q_{11} Q_r)^{1/2} (g H_r^5)^{1/4}]. \tag{4.2-33}$$

Inserting (4.2−32) and (4.2−33) in the governing relation (4.2−27) yields an equation for s and hence also for t_r, whose numerical solution makes the profit S a maximum. Obviously here the absolute maximum is desired under the side condition $t_r < t_0$, according to the assumptions. Inserting this in (4.2−26) gives the required runner diameter D, which naturally has to be suitable for the facilities of machining and transportation.

4.2.4. Reasons for the number of sets relating to the turbines

Disregarding the transportation and fabrication facilities and contrary to the introductory assumptions, now attention is directed to a plant with a low number of sets i. With respect to eventual repair of the turbines, the lowest number of sets is $i = 2$. This also fits the usual run-of-river plant with its strongly varying flow and head, in consequence of the flow duration curve [4.5].

More generally, in a run-of-river plant with strongly varying head and flow, i must lie above a certain minimum. This results from the similarity laws and the type of turbine. In the following it is assumed that all the turbines are of the same size D.

Under a head H_{op} corresponding to the bep, lying between the maximum and minimum head H_{max} and H_{min} of the flow duration curve, i_{op} sets are assumed to take a flow Q_{op}. This lies between Q_{max} and Q_{min} of this curve. If the machine with its unit discharge $Q_{11\,op}$ at bep (Cap. 9.2) is to operate with Q_{op} at its bep, its runner diameter follows from similarity laws (Cap. 9.2.) as $D = \{Q_{op}/[i_{op} Q_{11\,op} (g H_{op})^{1/2}]\}^{1/2}$.

The known rated discharge Q_r at the rated head H_r changes, at maximum flow Q_{mcx} and corresponding head H_{min} (from the similarity laws), to the following flow: $Q_r (H_{min}/H_r)^{1/2}$.

It is assumed that the maximum number of sets installed i_{max} is provided for this case. Contrary to Q_{op} the sets now operate with fully opened gates (corresponding to the unit discharge $Q_{11\,max}$ or $Q_{11\,1/1}$). Then the flow Q_{op}/i_{op} passing through a turbine at bep under Q_{op} and H_{op} now changes into the total flow passing the i_{max} sets: $Q_{op}(i_{max}/i_{op})(H_{min}/H_{op})^{1/2}(Q_{11\,max}/Q_{11\,op})$. Equating both the flow rates last mentioned yields

$$i_{max}/i_{op} = (H_{op}/H_r)^{1/2}(Q_r/Q_{op})(Q_{11\,op}/Q_{11\,max}). \tag{4.2-34}$$

A certain flow and head duration curve has $H_{op}/H_r = 2$, $Q_r/Q_{op} = 3$. Using a high specific speed Francis turbine with $Q_{11\ max}/Q_{11\ op} = 1,1$ the last relation gives $i_{max}/i_{op} = 3,86 \sim 4$. The bep (Q_{op}, H_{op}) may be connected with an efficiency curve vs Q such that one set can cover the range between Q_{op} and Q_{min}. In this case only one set is needed for Q_{op}. The whole plant then requires at least four sets.

For the case of Kaplan turbines with $Q_{11\ max}/Q_{11\ op} = 2,5$ the maximum number of sets $i_{max} = 1,70\,i_{op}$. Here for the same plant at least $i_{max} = 2$ sets are needed [4.7; 4.8].

4.3. The optimum size (D) and number of sets for a river power plant with given rated discharge and rated head

4.3.1. Introduction to the problem and assumptions

The resulting rated discharge Q_r and rated head H of a river power plant are assumed known, e.g., from a calculation as in the previous section. Also the load factor φ, the proportion of hours per annum under rated load, is known. Now the problem arises of finding either the number of sets i or their size, here represented by the runner diameter D.

For this purpose a certain site with given topography of river bed, namely its width b (see Fig. 4.3.1 a) is considered. The width of spillway required, across the river, is assumed not to constrain placement of the power house also across the river either as a part of the damming device or situated on the base of the dam. Subsequently the case of a forebay dam is also dealt with (see Fig. 4.3.1 d).

Only reaction turbines are considered, needing some submergence and hence excavation of the ground. From the rated head H, the specific speed or the nondimensional type
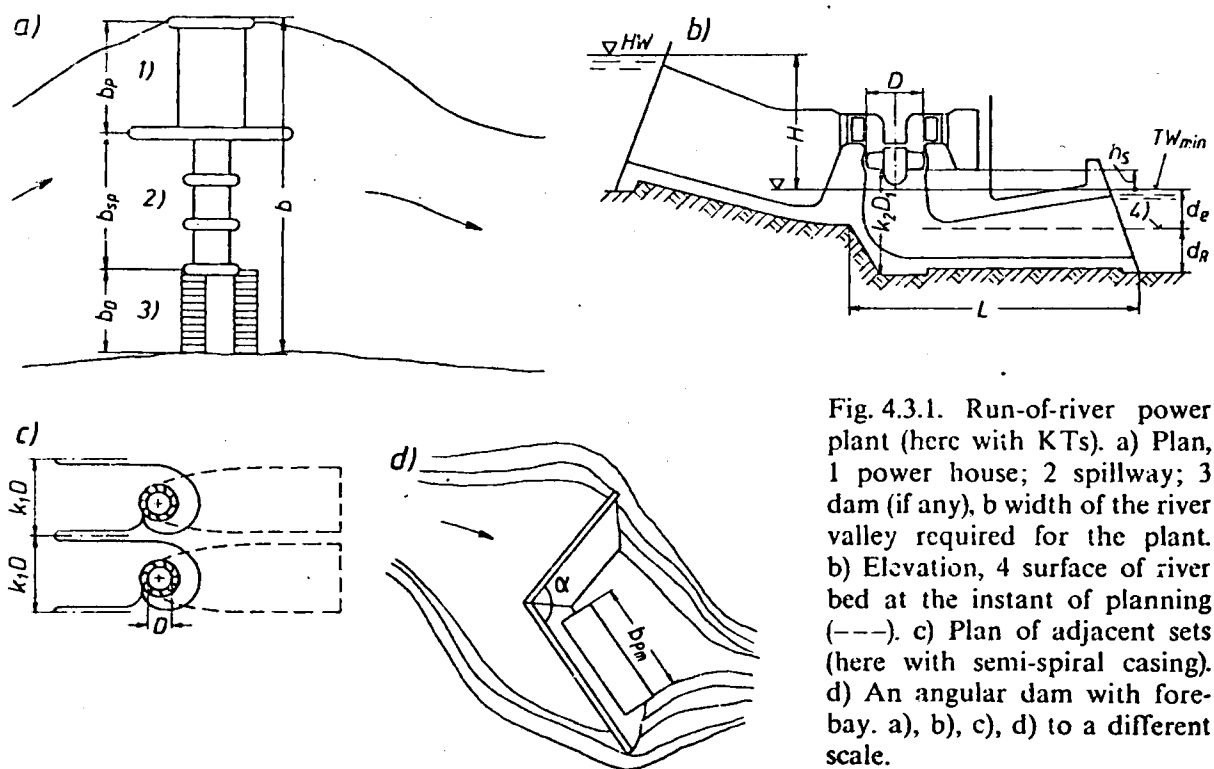
Fig. 4.3.1. Run-of-river power plant (here with KTs). a) Plan, 1 power house; 2 spillway; 3 dam (if any), b width of the river valley required for the plant. b) Elevation, 4 surface of river bed at the instant of planning (---). c) Plan of adjacent sets (here with semi-spiral casing). d) An angular dam with forebay. a), b), c), d) to a different scale.

number is known (Cap. 9.2.) as: $n_q = \omega Q^{1/2}/(g H)^{3/4}$, where $Q = Q_r/i$ is the flow of one set and ω its angular velocity. Once i is set, ω follows mainly from H, n_q, Q_r, leaving aside the adaptation of ω to the grid frequency (which is of minor importance, when the consideration is limited to large multipole generators) but leaving also aside the dependence of the unit output on the speed. For limiting generator design this dependence follows from the restrictions on the electric machine due to the space for the conductor and pole shoes and due to the requirements of fly wheel moment and cooling, see Cap. 11.4.

Now i or D, alternatively required are set such as to make the surplus of revenues during the depreciation period a maximum compared with the initial cost of the plant. Hence the initial cost of fabrication and erection of the sets and their accessories, due to earth excavation (substructure of the power house), the superstructure of power house, the spillway, the residual dam plus the monetary equivalent of the losses during the depreciation of plant at the instant of starting power production are made a minimum. The calculation starts from the runner diameter as a function of turbine type and working data.

4.3.2. The runner diameter as a function of working data

4.3.2.1. Kaplan turbines (KTs)

I. Assumptions: The flow downstream of the runner exit has zero whirl ($c_{u1} = 0$) at bep. For an arbitrary number of sets working under varying head and flow this assumption requires a KT with at least adjustable runner vanes.

II. Optimum diameter with respect to efficiency: According to Cap. 10.2 after C. Keller [4.9]

$$D = D_{op\,\eta} = 1,155\,\{(1 - \eta_s)/(K_0\,\omega\,\varepsilon\,gH)\}^{1/7}\,[Q/(1 - N^2)]^{3/7}, \qquad (4.3-1)$$

where Q is the rated flow, H the rated head, ω the angular velocity, N the hub to tip diameter ratio, ε the glide angle of the runner blade, $K_0 = (2/3)(1 - N^3)/(1 - N^2)$, η_s the draft tube efficiency.

III. Optimum diameter with respect to $NPSH$ and thereby ground excavation: According to Cap. 10.2 and reflecting the relation $D \sim Q^{1/3}$ first mentioned by *Ahlfors* [4.10; 4.11]:

$$D = D_{op\,NPSH} = 2\,[2\,(\eta_s + \lambda)/\lambda]^{1/6}\,\{Q/[\pi\,\omega\,(1 - N^2)]\}^{1/3}, \qquad (4.3-2)$$

where λ is the pressure number of the critical rotor point with respect to cavitation. This is also valid for FTs at $D = D_1$.

It may be mentioned that contrary to expectation, especially in large low head sets with vertical shafts $D_{op\,NPSH}$ requires a larger earth excavation than $D_{op\,\eta}$ ($D_{op\,NPSH} > D_{op\,\eta}$).

4.3.2.2. Francis turbines (FTs)

Here the calculation starts from an economical optimization of the runner tip speed coefficient $Ku_{op} = u_{op}/(2\,gH)^{1/2}$ shown in Cap. 4.4. Hence the peripheral blade speed $u_1 = u(D_1/D)$ follows from the diameter ratio $D_1/D_2 = D_1/D$, which is known from H via the resulting type number n_q, by the relation $u_1 = (D_1/D_2)\,Ku_{op}\,(2\,gH)^{1/2}$.

Continuity in the runner throat with its hub to tip diameter ratio N_1 gives the constant assumed meridional speed by $c_{m1} = 4Q/[\pi D_1^2(1 - N_1^2)]$. As is well known from C. *Pfleiderer* [4.12] the runner vane angle at the outlet at the tip section β_1 can be

optimized with respect to minimum susceptibility to cavitation. Hence $\tan \beta_{1\,op}$ $= \{\lambda/[2(\eta_s + \lambda)]\}^{1/2}$. For the whirl-free absolute flow assumed: $\tan \beta_{1\,op} = c_{m1}/u_1$. Hence the optimum runner tip diameter $D = D_{op}$ (where from now on the index 2 is omitted for convenience) via $D = (D_2/D_1)D_1$ is obtained as

$$D_{op} = 2[2(\eta_s + \lambda)/\lambda]^{1/4}\{Q(D_2/D_1)^3/[\pi(1 - N_1^2)Ku_{op}(2gH)^{1/2}]\}^{1/2}. \quad (4.3\text{--}3)$$

4.3.3. The runner diameter as a function of the number of sets

The given rated discharge Q_r of the plant and of one set Q (and the number of sets i) are related by $Q = Q_r/i$. To limit the submergence, the type number $n_q = \omega Q^{1/2}/(gH)^{3/4}$ is mainly given by the rated head H. Hence according to the assumptions, the angular velocity for a plant with given rated flow Q_r and i sets results from $\omega = n_q(gH)^{3/4}Q_r^{-1/2}i^{1/2}$. Inserting this in the relations (4.3-1), (4.3-2) or inserting $Q = Q_r/i$ in (4.3-3) the respective throat diameter D_1 (coinciding for a KT with D) as a function of the number of sets reads

$$D_1 = C\,i^{-1/2}, \quad (4.3\text{--}4)$$

where C reads as follows as a function of the turbine type or advances in design:

For a KT, designed on lines optimizing η:

$$C = C_0 = 1,155\,\{(1 - \eta_s)/[K_0\,n_q\,\varepsilon(gH)^{7/4}]\}^{1/7}\,Q_r^{1/2}(1 - N^2)^{-3/7}. \quad (4.3\text{--}5)$$

For a KT or FT (then $N = N_1$) designed on lines optimizing $NPSH$:

$$C = C_0^* = 2[2(\eta_s + \lambda)/\lambda]^{1/6}Q_r^{1/2}/[\pi\,n_q\,(gH)^{3/4}(1 - N^2)]^{1/3}. \quad (4.3\text{--}6)$$

For a FT, but in general also for a KT, designed on lines optimizing as well the overall economy by Ku_{op} and $NPSH$

$$C = C_0^{**} = 2[(\lambda + \eta_s)/\lambda]^{1/4}\{Q_r(D_2/D_1)^3/[\pi(1 - N_1^2)Ku_{op}(2gH)^{1/2}]\}^{1/2} \quad (4.3\text{--}7\,\text{a})$$

With the unit flow Q_{11}, known by H, the similarity law from Cap. 9.2 gives another C:

$$C_0^{***} = (D_1/D_2)Q_{11}^{-1/2}Q_r^{1/2}(gH)^{-1/4}. \quad (4.3\text{--}7\,\text{b})$$

4.3.4. The NPSH as a function of the working data and type

Inserting in $NPSH$ according to (4.2-10) the peripheral blade speed at the throat diameter $u_1 = \omega D_1/2$, the meridional speed from continuity $c_{m1} = \{4Q_r/[\pi(1 - N_1^2)]\}/(i\,D_1^2)$ and using the angular velocity ω from the type number n_q, mainly given by H, and the rated flow Q_r of plant with i sets as $\omega = n_q(i/Q_r)^{1/2}(gH)^{3/4}$, then $NPSH$ results as a function of the type number n_q (according to turbine type), the rated flow of plant Q_r, the number of sets i, the throat diameter D_1, the design feature N_1 and the parameters λ and η_s due to cavitational susceptibility in the form

$$2gNPSH = \{16(\lambda + \eta_s)Q_r^2/[\pi(1 - N_1^2)]^2\}\,i^{-2}D_1^{-4}$$
$$+ (\lambda/4)n_q^2(gH)^{3/2}Q_r^{-1}i\,D_1^2. \quad (4.3\text{--}8)$$

Inserting D_1 from (4.3-4) reconfirms the well known fact that $NPSH$ as a parameter of cavitational sensitivity of a certain machine cannot depend on the number of sets i.

4.3.5. The cost of ground excavation, power house and dam

According to the assumptions, the width of the river at site b, and the width of spillway required for spillage of flood flow b_{sp} differ by a figure $b_{Pm} = b - b_{sp}$, corresponding to the maximum length of power house located across the river. The plant considered needs a power house of a length b_P smaller than b_{Pm}. Hence the calculation is based on the relations

$$b_{Pm} = b - b_{sp}, \tag{4.3-9}$$

$$b_P \leqq b_{Pm}. \tag{4.3-10}$$

In the general case of a Francis turbine with a runner throat diameter D_1 (see Fig. 10.3.18), the excavation of ground for the substructure of the power house has a depth $d_e = k_2 D_1 - h_s - d_R$, a length $L = k_3 D_1$ and a width per set $b = k_1 D = k_1 (D_2/D_1) D_1, k_1$ being defined after (4.2-5), h_s being the suction head, d_R the depth of river bed underneath the tail water level, (D_2/D_1) a figure given from the head H. With a factor $\psi < 1$, due to the lateral variation of depth, the volume excavated of i sets becomes $V_e = \psi k_1 k_3 (D_2/D_1) \cdot i D_1^2 (k_2 D_1 - h_s - d_R)$. Inserting here D_1 from (4.3-4), with k_{ex} being the specific cost per volume excavated, the excavation cost of i sets becomes

$$K_{ex} = k_{ex} V_e = E(k_2 C i^{-1/2} - h_s - d_R), \tag{4.3-11}$$

$$E = k_{ex} \psi k_3 k_1 (D_2/D_1) C^2. \tag{4.3-12}$$

Since the task of the spillway is not affected by the number i of sets, which is the variable of interest, the cost of the spillway is a constant, hence set aside.

The cost of the power house superstructure from (4.2-5) may be reduced to the throat diameter D_1 by $D = (D_2/D_1) D_1$, where the diameter ratio D_2/D_1 is given by the head. Hence $K_P = i k_P k_1 k_5 (D_2/D_1)^2 D_1^2 [H_0 + k_6 (D_2/D_1) D_1] \chi$. Putting here D_1 from (4.3-4) gives, $K_P = \chi k_P k_1 k_5 (D_2/D_1)^2 C^2 [H_0 + k_6 (D_2/D_1) C i^{-1/2}]$. From this only the cost term, that varies with i, is taken from now on as cost due to the power house superstructure, namely,

$$K_P = F i^{-1/2}, \tag{4.3-13}$$

$$F = \chi k_P k_1 k_5 k_6 (D_2/D_1)^3 C^3. \tag{4.3-14}$$

The cost of the proper dam section (if any at all) K_D is valid for a dam of length b_D, resulting from $b_D = b - b_{sp} - b_P$, in which b is the width of the river valley, b_{sp} that of spillway and b_P that occupied by the length of the power house. According to (4.2-8) $b_P = i k_1 D$. Reducing D to the throat diameter by the diameter ratio D_2/D_1 which is known from H and putting D_1 from (4.3-4) gives the length of the power house as $b_P = k_1 (D_2/D_1) C i^{1/2}$.

Introducing the cross sectional area of the dam as $\varkappa H^2$ with $\varkappa$ as a form factor, the volume of the proper dam section is $V_D = \varkappa H^2 b_D = \varkappa H^2 [b - b_{sp} - k_1 (D_2/D_1) C i^{1/2}]$, H denoting the rated head. With the specific cost k_D per m^3 of the proper dam section, the cost of this section becomes

$$K_D = G(b - b_{sp} - A i^{1/2}), \tag{4.3-15}$$

$$A = k_1 (D_2/D_1) C, \tag{4.3-16}$$

$$G = \varkappa k_D H^2. \tag{4.3-17}$$

Strictly speaking, the barrage can be subdivided into the proper barrage portion and into a part, which corresponds in its base to the substructure of the power house (for heads below 20 to 40 m), or which contains the power house (when it is within the dam), or finally, is supported downstream by the power house, but also perforated by the penstocks or pressure shafts. Attributing these elements to the upper part of the power house, for simplicity it is assumed here that the cost of this dam portion linked to the power house is charged to the cost of the power house.

4.3.6. The cost of fabrication and erection of sets

The cost for fabrication, transport and assembly of one set contains a term which is proportional to D^n, where $n = 2,3$ to $2,5$. This shows that part of this procedure is proportional to the face to be machined (D^2) and another part is proportional to the volume of material to be bought and transported (D^3). Introducing an empirical cost factor k_s, the head-linked diameter ratio D_2/D_1 and the throat diameter D_1 from (4.3–4) give one cost term for i sets as $I_1 = k_s(D_2/D_1)^n C^n i^{-n/2}$ [4.6].

To this a term has to be added, proportional to the number of units, namely $I_2 = k_{s1} i$, where k_{s1} again is an empirical cost factor. This term accounts for the fact that at least a portion of the cost due to the machines increases in consequence of the number of accessories (i.e., piping, valves, bearings, control mechanism, casings needed to encase the pit, scroll casing and draft tube wall) and the number of large pieces to be transported and to be machined on machine tools, e.g. large boring mills or lathes, only available in limited number and due to each of the i sets. Therefore the cost of fabrication and erection of the i sets is

$$I = I_1 + I_2 = S i^{-n/2} + k_{s1} i, \qquad (4.3-18)$$

$$S = k_s(D_2/D_1)^n C^n. \qquad (4.3-19)$$

4.3.7. The cash value of energy loss during useful life

It is assumed that the dimensionless loss here is composed of a portion h'_0 independent of the size D of the set and another portion decreasing according to the known functional dependence of loss and Reynolds number of the machine (see Cap. 9.3) by $a D^{-1/m}$ with rising size D of set. Here m is about 5 and 'a' about 0,3 to 0,7 according to the type of machine. Reducing D to the throat diameter D_1 by the head-linked diameter ratio D_2/D_1 and D_1 to i by (4.3–4) gives the dimensionless loss

$$h' = h'_0 + a(D_2/D_1)^{-1/m} C^{-1/m} i^{1/2m}. \qquad (4.3-19\,b)$$

The capitalized cash value of energy loss during the period of z years, for depreciation at an interest rate p, with the electricity rate k_e per kWh for a hydro power station with an annual output W in kWh at the instant when power production starts, is with the interest-linked function α from (4.2–3)

$$K'_e = J(h'_0 + Li^{1/2m}), \qquad (4.3-20)$$

$$L = a(D_2/D_1)^{-1/m} C^{-1/m}, \qquad (4.3-21)$$

$$J = \alpha k_e W. \qquad (4.3-22)$$

148

The annual work W produced follows from the rated discharge Q_r and head H, the load factor φ, as the share of annual hours under rated load, the mean resulting efficiency of the generator η and the grid efficiency η_{gr} (the ratio of consumed to generated output) by $W = 8,76 \, \varrho \, \varphi \, \eta \, Q_r \, gH \, \eta_{gr}$.

4.3.8. The resulting cost as a function of the number of sets i

For $m = 5$ and $n = 2,4$ the resulting first cost together with cash value of energy loss during depreciation $K_{res} = K_{ex} + K_P + K_D + K'_e + I$ is as function of set number

$$K_{res} = E(k_2 C i^{-0.5} - h_s - d_R) + F i^{-0.5} + S i^{-1.2} + k_{s1} i$$
$$+ G(b - b_{sp} - A i^{0.5}) + J(h'_0 + L i^{0.1}). \tag{4.3-23}$$

From this it is seen that the resulting cost of a plant with given rated head and discharge decreases with a rising number of sets i in terms of: a) ground excavation due to depth of the draft tube $k_2 CE$, b) the upper part of the power house (F), c) the fabrication, transportation and assembly of the sets (S), d) the dam part due to the power house (G).

Contrary to the above the resulting cost increases with a rising number of sets i: e) in consequence of the accessories and the processing due to each set (k_{s1}), f) in consequence of the then higher cash value of energy loss (JL). The optimum number of sets corresponds to the minimum of K_{res}, determined graphically or analytically and expressed in integers. The usually observed predominance of the term due to e) makes it advisable to set the number of sets as small as possible. This has to be done within the frame of given facilities due to the transportation and machining of the largest parts eventually on site. Cost estimates are discussed in [4.13].

4.3.9. Reasons for setting unit size as large as possible

In some cases the assumption (4.3-10) of sufficient space at site for the required power house is not satisfied. With regard to growing peak load demand in future and the profit to be made by rising electricity rate for peak load, the power installed should often be as large as possible. This raises the question of maximum power capacity that could be installed under a given rated head H within a power house of a certain length b_{Pm} in a valley of given width at a certain site.

According to (4.2-8) the length of a power house with i sets of the same diameter becomes $b_{Pm} = i k_1 D$. With P_{11} as the head-linked unit power, i can be expressed by gH, D, and the resulting power installed P_{res} as follows $i = P_{res}/(P_{11} D^2 (gH)^{3/2})$. Hence the resulting power as function of the runner diameter:

$$P_{res} = (P_{11}/k_1)(gH)^{3/2} b_{Pm} D. \tag{4.3-24}$$

From this it is seen that for a given width of valley and hence given length of power house across it b_{Pm}, the installed capacity increases with the runner diameter. Escaping this constraint in the case of given D and b_{Pm}, consists in splitting the power house into underground locations of the valley slopes, provided the geology and topography allow this (Cabora Bassa).

Another solution is to arrange the power house at the foot of a forebay dam (Fig. 4.3.1 d). This has been done, e.g. in Grand Coulee III [4.14].

- The specific cost of excavation per unit output: The cost of excavating the power house with $b_P = b_{P_m}$, using the head-linked diameter ratio D_1/D_2 and the considerations yielding (4.3–11) $K_{ex} = \psi\, k_{ex}\, k_3 (D_1/D_2)\, D b_{P_m} [k_2 (D_1/D_2)\, D - h_s - d_R]$. Substituting here $b_{P_m} D$ from (4.3–24) the specific cost of excavation per unit output is

$$K_e^* = K_{ex}/P_{res} = \psi\, k_{ex}\, k_3 (D_1/D_2)[k_2 (D_1/D_2)\, D - h_s - d_R]/[(P_{11}/k_1)(gH)^{3/2}].$$
(4.3–25)

Obviously K_e^* rises with the runner diameter.

- The specific cost of sets due to fabrication and erection per unit output: According to the considerations leading to (4.3–19), the cost for the fabrication and erection of i sets is $I = (k_s/k_1)\,i\,k_1\, D\, D\, D^{n-2} + (k_{s1}/k_1)\,i\,k_1\, D\, D\, D^{-2}$. Substituting now from (4.2–8) $i\,k_1\,D = b_{P_m}$ and then expressing this from (4.3–24) gives the following specific cost per unit power

$$I^* = I/P_{res} = [k_s D^{n-2} + k_{s1} D^{-2}]/[P_{11}(gH)^{3/2}].$$
(4.3–26)

Since $n = 2{,}3$ to $2{,}5$ and since the second term in the numerator usually is much bigger than the first, it is seen that the specific cost of fabrication and erection per unit power installed falls with a rising runner diameter and decreasing number of sets i.

The reason for this results from the rising number of accessories, plankings and large parts, to be machined on machine tools, available in limited number, and the more complicated assembly, repair and inspection due to a rising number of sets. Here the feasibility of mass production vanishes.

In the important speed range, a limiting alternator design shows a drop of output P_a vs speed ω (Cap. 11.4) about $P_a \sim \omega^{-2}$. Using $\omega \sim D^{-1}$ and assuming the spiral casing to determine the lateral distance of adjacent sets, the capacity of a power house of length b_{P_m} becomes $P_{res} \sim D\, b_{P_m}$. Hence for a maximum capacity the alternator also requires a maximum possible diameter D.

Obviously the size of a set should be set with respect to the power installed in the grid. The arguments in favour of a minimum number of sets are also limited by the load gauge of access roads to the site, by the capacity of cranes on site and in the workshop and by the load capacity of bridges to be passed. Such obstacles exist mainly in remote and mountainous areas. They can be overcome to a certain degree by applying fabrication of large pieces on site by modern welding techniques [2.21].

4.4. The optimum coefficient of peripheral blade speed Ku

4.4.1. Introduction to the problem

From the similarity laws (Cap. 9.2) it is known that the type number n_q (here used in its nondimensional form $n_q = \omega\, Q^{1/2}/(gH)^{3/4}$) rises roughly with the 1,5th power of the blade speed coefficient $Ku = u_1/(2\,gH)^{1/2}$ at the runner tip diameter D of a reaction turbine. To limit the submergence n_q depends on the rated head H according to Tables 9.2.1 or 10.3.1.

It is known, that different values of Ku may be assigned to a certain type number n_q. This depends on the purpose of the machine (pump, pump turbine or turbine) but also on the rotor blade form chosen. For example backward curved vanes also applied in turbines give a higher Ku. Therefore the problem will be reflected by the following question: What value of Ku would yield the lowest resulting cost when the rated head H and discharge of the turbine are known and the rated point coincides with the bep with vanishing whirl $c_{u1} = 0$ past the runner? Strictly speaking the answer should be given so as to minimize

the initial cost and the capitalized cash value of the loss during the useful life of the turbine, where the loss is split into its components.

This problem was treated by the author for a FT [4.15]. In the following an attempt is made to determine Ku by limiting the economic aspect to the following items: a) cost K_s due to fabrication, erection and assembly of the turbine, see (4.2−13); b) cost due to superstructure of power house K_P, see (4.2−5) of one set; c) the same due to excavation, see (4.2−18); d) cost due to capitalized loss, see (4.3−20−22).

4.4.2. Assumptions

− Simplifications in the cost terms: Assuming the term $H_0 + k_6 D$ in (4.2−5) to be proportional to D, the cost of the power house superstructure per set is now

$$K_P = k_{A1} D^3, \qquad\qquad (4.4-1)$$

k_{A1} being a specific cost factor per unit volume.

The volume excavated per turbine has, (Fig. 4.3.1 b) and (10.3.18), the streamwise length $k_3 D_1$, see (4.2−7), the depth underneath the bed of tailwater, see (4.2−6), $d_e = (k_2 D_1 - h_s - d_R)\psi$, ($d_R$ being the depth of tailwater bed below the lowest tailwater level, h_s the suction head) and a width $b_s = k_1 D$, see (4.2−8). Using the head-linked diameter ratio D_1/D_2 and $\Phi = \psi k_1 k_3 D_2/D_1$, this value may be expressed by the rotor tip diameter D ($D = D_2$) as follows $V_e = \Phi D^2 [k_2 (D_1/D_2)D - h_s - d_R]$, D_1 being the throat diameter.

Expressing the suction head (Cap. 8.2.) by $h_s = B - NPSH$ with B from (4.2−9), and splitting $NPSH$ according to (4.2−10) (see also Cap. 8.2), the excavation cost reads

$$K_{ex} = k_{ex}\,\Phi D^2 [k_2 (D_1/D_2)D - B - d_R + [(\lambda + \eta_s)Kc_{m1}^2 + \lambda Ku_1^2]H], \qquad (4.4-2)$$

where $Kc_{m1} = c_{m1}/\sqrt{2gH}$, $Ku_1 = u_1/\sqrt{2gH}$, and k_{ex} is a specific cost factor per unit volume.

− Steps, to reduce the runner diameter D to the coefficient Ku:
a) Rated head H and rated discharge Q are given at the bep.
b) The nondimensional type number n_q results from the working data H and Q in a) according to the state of the art, Cap. 10.3, especially with respect to $n_q(H)$ (see Table 9.2.1).
c) With n_q known, the geometry of the runner and distributor with their essential features is also known, i.e.: b_2/D_2, D_1/D_2 in which D_2 is the runner tip diameter at inlet (see Table 9.2.1), b_2 the inlet breadth of the runner, D_1 the runner throat diameter. In the following for convenience $D_2 = D$ (without index).
d) With the reservations made in Cap. 4.3.1, the angular velocity ω of the set results from the type number n_q, the head H and the rated flow by $\omega = n_q(gH)^{3/4}/Q^{1/2}$.

With ω known, the diameter D as a function of Ku follows via the relation $D = 2u/\omega$ as

$$D = \delta Ku, \qquad\qquad (4.4-3)$$

$$\delta = 2^{3/2} Q^{1/2}/[n_q(gH)^{1/4}]. \qquad\qquad (4.4-4)$$

e) From the known relation between n_q, Ku and Kc_{m2} (Cap. 9.2) at b_2/D given $n_q = 2^{7/4} \pi^{1/2} (b_2/D_2)^{1/2} Ku\,Kc_{m2}^{1/2}$ it is also possible to express Kc_{m2} in terms of the non-dimensional runner inlet breadth b_2/D_2, given according to c) and hence

151

$$\Omega = 2^{7/4} \pi^{1/2} (b_2/D_2)^{1/2},$$ (4.4-5)

as a function of the type number n_q and the speed coefficient Ku

$$Kc_{m2} = (n_q/\Omega)^2 Ku^{-2}.$$ (4.4-6)

By means of continuity and assuming constant meridional velocity across the flow passages at runner entrance and exit and introducing the figure χ defined below and also known from c), the coefficient of meridional velocity at the runner exit Kc_{m1} may be expressed in terms of that at the runner inlet Kc_{m2} as (b_1 = rotor exit breadth)

$$Kc_{m1} = \chi Kc_{m2},$$ (4.4-7)

$$\chi = 4(D_2/D_1)(b_2/b_1).$$ (4.4-8)

4.4.3. Expressing the cost terms as a function of Ku

- The fabrication and erection cost of one set: They are with respect to (4.2-13) and (4.4-3) and (4.4-4)

$$K_s = k_s \delta^n Ku^n.$$ (4.4-9)

The cost of the power house superstructure of one set is according to (4.4-1) and (4.4-3) and (4.4-4)

$$K_p = k_{A1} \delta^3 Ku^3.$$ (4.4-10)

The cost of excavation of one set becomes from (4.4-2) with Kc_{m1} from (4.4-6), (4.4-7), (4.4-3) and $Ku_1 = (D_1/D_2) Ku$

$$K_{ex} = k_{ex} \Phi \delta^2 Ku^2 [k_2(D_1/D_2)\delta Ku + E_1 Ku^{-4} + E_2 Ku^2 - B - d_R],$$ (4.4-11)

where

$$E_1 = (\eta_s + \lambda)\chi^2 (n_q/\Omega)^4 H,$$ (4.4-12)

$$E_2 = \lambda(D_1/D_2)^2 H.$$ (4.4-13)

- The cost of capitalized loss during the depreciation period: Following the considerations leading to (4.3-20), the cash value of loss during the depreciation period at the instant of starting energy production becomes with respect to (4.3-4) and with D from (4.4-3)

$$K'_e = J(h'_0 + a \delta^{-1/m} Ku^{-1/m}).$$ (4.4-14)

4.4.4. The resulting cost of the turbine during its useful life

Adding the cost terms K_s, K_p, K_{ex} and K'_e, the resulting cost of a set during its depreciation becomes as a function of $Ku = x$

$$K_{res} = Jh'_0 + C_4 x^4 + C_3 x^3 + C_n x^n - C_2 x^2 + C_{-2} x^{-2} + C_{-1/m} x^{-1/m},$$ (4.4-15)

where

$$C_4 = k_{ex} \Phi \delta^2 E_2,$$ (4.4-16)

$$C_3 = \delta^3 (k_{ex} k_2 \Phi(D_1/D_2) + k_{A1}),$$ (4.4-17)

152

$$C_n = k_s \delta^n, \tag{4.4-18}$$

$$C_2 = k_{ex} \Phi \delta^2 (B + d_R), \tag{4.4-19}$$

$$C_{-2} = k_{ex} \Phi \delta^2 E_1, \tag{4.4-20}$$

$$C_{-1/m} = J a \delta^{-1/m}. \tag{4.4-21}$$

The cost K_{res} has a constant term due to a portion of the capitalized loss $J h_0'$. It contains the term C_4 due to excavation, C_3 due to fabrication and erection, both rising with Ku, C_n due to fabrication and erection all rising with Ku. Then K_{res} contains the terms C_2 and C_{-2} both due to excavation and $C_{-1/m}$ due to capitalized loss all decreasing with Ku. Hence

$$dK_{res}/dx = 0. \tag{4.4-22}$$

From this follows an optimum of the speed coefficient $x = x_{op}$ or $Ku = Ku_{op}$.

According to experience this can be obtained rather easily after a first estimate by Newton's approximation, e.g. for a FT with a head of 300 m this is about $Ku = 0,72$.

More details are given in reference [4.15].

4.5. Problems due to the layout of the reservoir

4.5.1. Basic considerations concerning a reservoir

4.5.1.1. Introduction

A reservoir or basin as a water storing device is the necessary counterpart of a dam or other damming devices such as dikes. It is the prerequisite of any peak load and hence storage or pumped storage plant, but it is also necessary for any run-of-river plant. As such it may be arranged in a chain of river power plants and thus be used simultaneously as head and tailwater basin.

In the following a reservoir in a narrover sense is understood as a basin used as head water with a large, live storage volume and hence a considerable change in level usually generating a head in a range of at least 20 m.

Excluding the rare cases of reservoirs in natural caves or in abandoned mines, the reservoir considered is located in a valley, usually that of a river. Its erection depends on the topography and the geology of the neighbourhood, the water tightness of the ground, the economic facility of building dams as an enclosure.

Excluding a pump storage plant, any reservoir also needs a catchment area with an adequate precipitation rate.

The benefits of a reservoir in its widest sense can be briefly listed as follows:
a) Prevention of floods especially in mountainous and monsoon areas.
b) Irrigation especially in rural areas with irregular precipitation.
c) Power generation especially for peak load demand or in a pumped storage plant.
d) Equalization and regulation of run-off into a certain river.
e) Improvement of navigation.
f) Tourism.
g) Fisheries.
h) Climatic benefits through damping temperature fluctuations.
i) Social and cultural changes by enlarging social communications.

4.5.1.2. Assumptions for basic relations of layout

In the following a reservoir is considered filled by a river with a large catchment area and a known hydrograph $Q(t)$ for the average year, which is considered as the operational cycle of the reservoir. Gains by precipitation on the surfaces of the reservoir and losses by seepage and evaporation are neglected.

The cycle for the operation is given by the fact, that the altitude h of its level returns to its initial value h_0 after the period considered. This value coincides with the dead storage of the reservoir determining the minimum head of the turbines supplied by it. The turbine type depends also on the maximum of this level, due to the maximum head. This results from the topography of the site, the crest height of the barrage and the flood storage capacity eventually needed at the instant of h_{max}. The topography of the reservoir also gives its surface area A as a function of the altitude h of its level. Thus $A = A(h)$.

For irrigation and other purposes a minimum flow target release $Q_R = Q_R(t)$ must be delivered as a function of time t into the river downstream of the reservoir. Also adequately timed, with respect, to power demands $P(t)$ (especially for peak load), to the target release $Q_R(t)$, to the hydrograph $Q(t)$, and to the basin's geometry $A(h)$, a flow rate for power generation has to be delivered by the reservoir: $Q_P = Q_P(t)$.

Downstream of the reservoir a gauging station monitors the river for permissible level. This may be reached by appropriate regulating devices. Measuring any altitude from this level, specifically the tail water level of the barrage can be assumed to follow a "head on weir" flow relation

$$h_T = k_2 (Q_P(t) + Q_R(t))^{2/3}, \tag{4.5-1}$$

in which k_2 is a constant.

A power station may be at the base of the barrage, receiving its discharge $Q_P(t)$ by a duct separate from that for $Q_R(t)$. This power supply may have a head loss $k_1 Q_P^2(t)$. Then the net head is obtained from the instantaneous altitude $h(t)$ of the reservoir as a function of time

$$H(t) = h(t) - k_2 (Q_P(t) + Q_R(t))^{2/3} - k_1 Q_P^2(t). \tag{4.5-2}$$

4.5.1.3. The basic relation for the layout and its problems

Under the assumptions made, $h(t)$ results from continuity

$$Q(t) = Q_P(t) + Q_R(t) + A[h(t)] \, dh(t)/dt. \tag{4.5-3}$$

Counting the time t from the instant at which $h = h_0$, it follows that

$$h(t) = h_0 + \int_0^t \{1/A[h(\tau)]\} [Q(\tau) - Q_P(\tau) - Q_R(\tau)] d\tau. \tag{4.5-4}$$

The turbine output required may be given as a function of time as $P = P(t)$. $P(t)$ depends on the net head $H(t)$, the power-linked flow rate $Q_P(t)$ and the efficiency η of the turbines. Joint regulation of all the sets may facilitate operation of all the sets around their bep. Thus efficiency depends only on the head according to $\eta = \eta(H)$. Hence the power-linked flow

$$Q_P(t) = P(t)/[\varrho g H(t) \eta(H(t))], \tag{4.5-5}$$

where $H(t)$ results from (4.5-2) and (4.5-4). One problem consists in fixing the live storage volume according to $\Delta V = \int_{h_0}^{h_{max}} A(h) dh$. If flood storage is also needed and the

154

flood is considered, as usual, as a random effect not belonging to the average year, the level h_{max} must also allow for additional flood storage whose volume then may be added as a benefit to Q_R or (and) Q_P.

The solution of ΔV for a given geometric parameter $A(h)$ of the valley, a given hydrograph $Q(t)$, k_2 and k_1, can be reached only by trial and error.

The inverse problem of setting $Q_R(t)$ and $P(t)$ or $Q_P(t)$ for a given live storage volume ΔV can also be reached only by trial and error.

Therefore in the following section an approximate treatment of the problem will be discussed. In this treatment the figure $Q(t) - Q_R(t)$ is replaced by a power flow duration curve $Q_P(t)$ of simple form. The function $A(h)$ is replaced by a mean surface area of the reservoir, H by a mean head H_m, and the power requirement $P(t)$ by a simple sinusoidal power duration curve of daily peak load demand.

The optimization and adaptation of a reservoir has been treated in detail by *Seus* [4.16; 4.17].

4.5.2. An approach to the layout of a peak load storage plant

4.5.2.1. Basic relations of the reservoir and the river feeding it

Instead of the compatibility of the momentary level of reservoir $h(t)$, and the power-linked flow rate $Q_P(t)$ within the permissible limits of the level and the momentarily available head, it is now assumed that at constant efficiency, the stored electric potential energy within one storing cycle equals the electric energy demand, which is generated during this time interval.

The live storage volume is approximated by the minimum and the maximum head H_{min} and H_{max}, respectively, during the storing cycle and the average surface area of the reservoir A_m by

$$\Delta V = A_m H_{max}(1 - \chi),\tag{4.5-6}$$

$$\chi = H_{min}/H_{max}.\tag{4.5-7}$$

The electric energy of the stored volume is approximately with an overall efficiency η_m and a mean head $H_m = (H_{max} + H_{min})/2$

$$E_{pot} = \varrho \Delta V g H_m \eta_m = (1/2)\eta_m g \varrho A_m H_{max}^2(1 - \chi^2).\tag{4.5-8}$$

It is assumed that the reservoir has to supply this energy during a definite time interval t_1, e.g. one year.

A river used to fill the reservoir may have the following flow duration curve for the average year

$$Q = Q_m - 2(Q_m - Q_0)(t/t_1) + (Q_m - Q_0)(t/t_1)^2,\tag{4.5-9}$$

in which Q_m and Q_0 are the maximum and minimum "flow remaining" respectively within the average year. The "flow remaining" means here the surplus of flow over the legally prescribed minimum flow-off, the so called minimum target release.

The live storage volume ΔV of the reservoir has to be released into the river during the time interval t_1 (now one year). Expressing the surplus of seepage and evaporation over

rainfall (see [4.18; 4.19]) by the term V_v, continuity gives $\int_0^{t_1} Q\,dt = V_t + \Delta V$. Inserting (4.5-9) and (4.5-6) results in

$$t_1(Q_m + 2Q_0)/3 = V_v + A_m H_{max}(1 - \chi).$$ (4.5-10)

4.5.2.2. Load demand and its balance with energy stored

The demand of the consumer may be approximated by the following periodical function over the daily time interval T and with P_m as peak load: $P = P_m[1 - \cos(2\pi t/T)]/2$. Hence the daily energy consumption $E_d = P_m T/2$. Imagine this is needed during h days of the average year then the annual power demand becomes

$$E_v = P_m Th/2.$$ (4.5-11)

Contrary to a run-of-river plant, delivering base load, the power capacity P_m is independent of the "flow remaining" offered by the river. The energy E_{pot} from (4.5-8) stored during the period t_1 has to be equated to the simultaneous energy demand E_v (4.5-11). Hence

$$\varrho g A_m \eta_m H_{max}^2(1 - \chi^2) = h P_m T.$$ (4.5-12)

The elimination of the mean area A_m from (4.5-10) results in the peak load as a function of the river parameters Q_m, Q_0, the max head H_{max}, the head ratio χ, the time parameters t_1, T, h and the surplus V_v of seepage and evaporation over precipitation:

$$P_m = [(Q_m + 2Q_0)t_1/3 - V_v]\varrho g \eta_m H_{max}(1 + \chi)/(h T).$$ (4.5-13)

H_{max} is given by the topography, Q_m, Q_0 by the flow duration curve of the river, while η_m and $\chi = H_{min}/H_{max}$ depend mainly on the design of the turbine. Hence a given H_{min}/H_{max} indicates the type of turbine to be installed.

When the annual consumption period $h T$ and the peak load are prescribed by the consumers then only the turbine design conditioned by the head ratio χ may help to satisfy the last relation.

4.5.2.3. Storage volume required, also for pumped storage

Squaring (4.5-13) and substituting H_{max}^2 from (4.5-12) gives the peak load as a function of the hydrological data Q_m, Q_0, the time parameters h, T, t_1, the head ratio χ and the surface A_m of reservoir required:

$$P_m = \varrho g \eta_m[(Q_m + 2Q_0)t_1/3 - V_v]^2(1 + \chi)/[(1 - \chi)A_m h T].$$ (4.5-14)

Changing the places of P_m and A_m and then multiplying by the head range $H_{max}(1 - \chi)$ yields the live storage volume ΔV

$$\Delta V = A_m H_{max}(1 - \chi)$$

$$= \varrho g \eta_m H_{max}[(Q_m + 2Q_0)t_1/3 - V_v]^2(1 + \chi)/(P_m h T).$$ (4.5-15)

The last relation could also be applied to a mere pumped storage scheme, whose live storage volume circulates e.g., daily. Here the values Q_0 and Q_m may vanish, as only a small water source is needed to fill the system and cover seepage and evaporation. Remember that V_v in the above relation was the surplus of seepage and evaporation over rainfall. Hence V_v can be replaced by a negative live storage volume, if the latter is imagined to be filled by precipitation only. Hence $\Delta V = - V_v$.

156

Inserting this into the right hand side of (4.5 - 15) and then reducing to ΔV yields the live storage volume of a pumped storage plant to cover a certain peak load P_m

$$\Delta V = \{P_m(1 - \chi)A_m h T/[(1 + \chi)\varrho g \eta_m]\}^{1/2}.$$ (4.5 – 16)

4.5.2.4. Economical aspects of the layout of a pumped storage plant

The economical background of a pumped storage plant is based on the fact that peak load can be sold at a higher electricity rate and hence a higher earning than the generation of the pumped storage needed for this peak load would cost at the low electricity rate of base load.

During the period t_P the flow Q_P is pumped into an upper reservoir. During the period t_T the flow Q_T passes the turbine from the head water to the tailwater reservoir.

In the following , target release, rainfall, seepage and evaporation are neglected. Hence the volume pumped into the upper basin during the working cycle $V_P = \int_0^{t_P} Q_P dt$ has to be equal to the volume $V_T = \int_0^{t_T} Q_T dt$ passing through the turbines during this cycle.

The instantaneous output or input power with respect to head H, discharge Q and efficiency η whilst turbining (T) and whilst pumping (P) respectively, is

$$P_T = \varrho g \eta_T H_T Q_T, \qquad P_P = \varrho g H_P Q_P/\eta_P.$$ (4.5 – 17)

With k_{eT} and k_{eP} as the electricity rates during turbining (T) and pumping (P) respectively, the net balance per working cycle is obtained as

$$S = \int_0^{t_T} P_T k_{eT} dt - \int_0^{t_P} P_P k_{eP} dt.$$ (4.5 – 18)

This surplus should be above a limit, which has to cover the OMR cost of the plant and its annuity due to its initial cost. Including in the efficiencies also those of the penstock, the motor-generator and the grid (as the domestic consumer often pays the lion's share), the surplus now reads $(\Delta V = V_T = V_P)$

$$S = \eta_T' \Delta V k_{eT} H_T [1 - k_{eP}/(k_{eT} \eta_P' \eta_T')] \cdot \varrho g$$ (4.5 – 19)

where the efficiencies with the prime are supposed to include all the losses within the corresponding operating mode. From this it is seen, that the economy of a pumped storage plant rises with

a) Rising storage volume ΔV.
b) Rising efficiency due to turbining η_T'.
c) Rising head due to turbining H_T. Usually the head is given with the topography in the neighbourhood of the plant. As a rough rule it can be said that the product of head and volume in simple storage plants does not vary as much in nature as the head itself does.
d) Rising ratio of electricity rate due to turbining to that due to pumping, ranging always above "one".

The positive values within the bracket of (4.5 – 19) lead to the essential criterion for the economical feasibility of a pumped storage scheme: $k_{eP}/k_{eT} < \eta_T' \eta_P'$. Example: $\eta_T' = 0{,}91$, $\eta_P' = 0{,}865$. This gives $k_{eP}/k_{eT} < 0{,}787$.

Mühlemann treats the economic details of machines used in pumped storage systems [4.20], *Panicelli* [4.21] their planning.

Usually when making, as in the above, profit the guide line of planning, the capitalist economy appeals to the power of given conditions. However, in many pumped storage plants these conditions

are no longer convincing at present. For example the majority of pumped storage plants in West Germany, once one of the pioneers of this idea, are degraded to an emergency status to be used in the case of accidental failure of one of the big nuclear power plants.

At least in developed countries the benefits and possibility of pumping by means of cheap and excessive base load seem to disappear more and more. This may be a consequence of the rising application of electricity to night heating, to operate chemical plants around the clock etc.

Those plants in which pumped storage sets (binary or ternary ones) have been installed as supplementary devices, apply their sets nearly exclusively to turbining.

Countries like the USSR which probably for ideological reasons don't have different electricity rates between base and peak load supply, nevertheless now install pumped storage plants, probably as a quick substitute for a deficient thermal power plant.

4.6. The problems of optimizing the cross section of water ways

4.6.1. General remarks

Water way means here the structural member of a diversion or channel power plant, required to convey the water from the upper reservoir or the intake structure to the power house and from the latter to the tail water of the river.

Strictly speaking the surge tank must also be included into this consideration. Its main designs are: a) the double chamber design (Fig. 3.1.2), b) the differential surge tank with throttle (Fig. 3.1.2), c) the surge tank with throttle (Fig. 3.1.2), the latter now mainly applied in Austria in the form of Thoma's return flow throttle [4.22], and the Johnson design (Fig. 3.1.2), which brings together the advantages and devices of the differential and throttle designs, namely cutting and damping the amplitudes of level oscillations in the surge tank. In remote areas according to Brekke [3.17] air chambers excavated in the rock are used to an increasing degree.

The dimensioning of the cross sectional area of such a surge relief device does not follow that of the common water way but results from consideration of dynamic stability in the utmost critical cases of regulation. Starting with the early work of Thoma, who made the first statement of the minimum cross sectional area of a simple surge tank [1.50], much research work and theoretical considerations have been published in this respect, from which the papers of Seeber [4.23], Tagwerker [4.24], Brekke [3.17], and the book of E. Mosonyi about high head plants [1.54] may be mentioned. For calculating surge tank motion, see Cap. 11.3.8.

However, in the following, consideration exclusively concentrates on the dimensioning of the cross sectional area of the channel, penstocks (or pressure shafts), tunnel or tailwater gallery at stationary rated flow.

To approximate real conditions, a difference is made between full running closed ducts such as penstocks, pressure shafts or tunnels and partly filled, unpressurized ducts such as channels or tail water galleries.

The basic principle now applied to the optimum dimensioning of cross sectional area runs as follows: Imagine a given rated flow through the water way. For a very small available cross sectional area the first cost of the water way resulting from materials used, construction and ground acquisition (if needed at all), is small. As then the velocity and the loss linked to it are high, the capitalized cost due to it during the depreciation period is also high. On the other hand the initial cost increases with cross sectional area and the loss dependent cost decreases with increased cross sectional area.

Hence the resulting cost must have a minimum, which yields the optimum size of the water way, as calculated below.

158

4.6.2. The optimization of the channel section

4.6.2.1. The rectangular channel section as a model and the resulting loss

The real unpressurized tunnel or open channel considered now may be trapezoidal, horse-shoe-shaped or rectangular with real wetted cross section A_{re} and a real wetted periphery U_{re} [4.25]. Hence the real hydraulic diameter is: $d_{h\,re} = 4\,A_{re}/U_{re}$. The real channel is now replaced by a rectangular channel with the same wetted cross sectional area $A = A_{re}$ and hence the same mean flow velocity $c = Q/A$ for the given rated flow Q and with the same hydraulic diameter $d_h = d_{h\,re}$ as the real channel.

The imaginary rectangular channel now serving as a model has a width b and a wetted depth d. Hence the hydraulic diameter d_h of the rectangular channel is $d_h = 4\,bd/(2\,d + b)$. Inserting $b = A/d$ gives $d_h = 4\,A/(2\,d + A/d)$. Making this equal the hydraulic diameter of the real channel $d_{h\,re} = 4\,A_{re}/U_{re}$, and with $A = A_{re}$, the following relation is obtained for the wetted circumference U_{re} of the real channel as a function of the rectangular channel's depth d: $U_{re} = 2d + A/d$. Usually $A = A_{re}$ is fixed for a given rated flow Q via continuity $A = Q/c$, using a certain mean velocity c, which limits sedimentation or erosion. Once the optimum depth of the rectangular model channel has been found as d_{op} the above gives the optimum of the real channel's wetted periphery (perimeter)

$$U_{re\,op} = 2\,d_{op} + A/d_{cp}.$$ (4.6-1)

Finding d_{op} will be the following task. According to the above the hydraulic diameter of the rectangular channel becomes, if the width is reduced to d by $b = A/d$

$$d_h = 4\,A/(2\,d + A/d),$$ (4.6-2)

in which d is the depth and A the cross section of the channel.

4.6.2.2. The cash value of energy loss

In general the drop in level h_v of a channel results from

$$h_v = \lambda\,Lc^2/(2\,g\,d_h),$$ (4.6-3)

in which c is the mean velocity in the channel, L its length, and λ its resistance coefficient. The latter depends, according to Bazin, on the wall roughness k_R and the hydraulic diameter d_h as follows:

$$\lambda = 0{,}01037\,(1 + 2\,k_R/d_h^{1/2})^2,$$ (4.6-4)

in which the wall roughness, k_R, has the following values as a function of the wall material after *Kutter* [3.18]; 0,06 for planed wooden planks; 0,16 for unplaned wooden planks or hewn stones (asher masonry); 0,47 for rock masonry walls; 1,3 for pure earthen masonry of regular structure; 1,75 for boulders.

For a hydro power plant the head loss from (4.6-3) must be treated like a head loss of a machine, having efficiency η. Then the power loss results from the given rated flow Q as $P = 10^{-3}\,\varrho\,Q\,g\,h_v\eta$ kW.

The cash value of energy loss during the depreciation period of z years at the instant when operation starts becomes

$$K_e = 8{,}76\,\varrho\,Q\,g\,h_v\,\alpha\,\eta\,\varphi\,k_e,$$ (4.6-5)

159

in which k_v is the electricity rate, $\alpha = 1/a^*$ the reciprocal of the capital recovery factor a^* (see (2.2–5) and (4.2–3)). φ the load factor as the share of annual hours under rated load, ϱ the density, and η the overall efficiency of plant and grid.

Inserting h_v from (4.6–3) with the hydraulic diameter from (4.6–2) into (4.6–5) gives the capitalized energy loss

$$K_e = (8,76/8)\,\lambda\,\varrho\,k_e\,\alpha\,\varphi\,\eta\,LQ^3(2\,d/A + 1/d)/A^2\,. \tag{4.6–6}$$

4.6.2.3. The initial cost of the channel

The initial cost of a channel is assumed to consist of the following terms: a) K_m, the cost due to the wall material, excavation and construction, b) K_g, the cost for ground acquisition and indemnities.

K_m is assumed to be proportional to the volume of the channel material. Hence with respect to $b = A/d$: $K_m = k'_1(2\,d + A/d)\,Lt$, where t is the mean wall thickness of the channel and k'_1 the specific cost of the wall material per unit volume including the construction of an excavation for the channel. The thickness t of channel wall is taken as a mean value. Assuming the channel wall acts as a gravity dam, the stability condition between the dam-weight-induced- and the water-pressure-induced tilting moment yields $t \sim d(\varrho/\varrho_D)^{1/2}$, ϱ_D being the dam's density. Hence

$$K_m = k_1(\varrho/\varrho_D)^{1/2}(2\,d + A/d)\,Ld\,. \tag{4.6–7}$$

The cost K_g for the ground is assumed to be proportional to the channel's ground surface. Thus

$$K_g = k_2\,Lb = k_2\,LA/d\,. \tag{4.6–8}$$

Strictly speaking k_2 is split into a ground rate and an indemnity rate.

4.6.2.4. The resulting cost and the optimum depth d_{op}

The resulting cost of a channel from (4.6–6) through (4.6–8) is

$$K_{res} = C_0 + C_1/d + C_2\,d + C_3\,d^2\,, \tag{4.6–9}$$

where

$$C_0 = k_1\,AL(\varrho/\varrho_D)^{1/2}\,, \tag{4.6–10}$$

$$C_3 = 2\,k_1(\varrho/\varrho_D)^{1/2}\cdot L\,, \tag{4.6–11}$$

$$C_1 = k_2\,LA + (8,76/8)\,\lambda\,\varrho\,\varphi\,\eta\,\alpha\,Lk_e\,Q^3/A^2\,, \tag{4.6–12}$$

$$C_2 = (8,76/4)\,\lambda\,\varphi\,\alpha\,\eta\,\varrho\,Lk_e\,Q^3/A^3\,. \tag{4.6–13}$$

The condition $\partial K_{res}/\partial d = 0$, gives the following third degree equation for the optimum depth $d_{op} = d$:

$$d^3 + e\,d^2 + f = 0\,, \qquad e = C_2/(2\,C_3)\,, \qquad f = -\,C_1/(2\,C_3)\,. \tag{4.6–14}$$

Introducing $d = x - e/3$, this reduces to $x^3 + 3px + 2q = 0$, where

$$p = -\,e^2/9\,, \qquad q = e^3/27 + f/2\,. \tag{4.6–15}$$

Obviously equation (4.6–14) has only one real root. Hence the original case of Cardano's solution is given [4.26]. With the discriminant

$$\Delta = q^2 + p^3\,, \tag{4.6–16}$$

the solution of (4.6–14) reads

$$d_{op} = (-q + \Delta^{1/2})^{1/3} + (-q - \Delta^{1/2})^{1/3} - e/3.$$ (4.6–17)

Because of the topography, this proposed optimization may be limited by site conditions, e.g. a given limitation of the channel width b.

4.6.3. The optimization of the diameter of a pressurized duct

4.6.3.1. The duct with cylindrical cross section as a model

For closed pressurized ducts, a pipe with a cylindrical cross section may serve as a model. Following the directions in Cap. 4.6.2.1, the model is assumed to have the same cross sectional area A as the real duct with A_{re} and the same hydraulic diameter $d_h = d$ as the real duct with $d_{h\,re}$. Hence the optimized wetted periphery of the real duct may be obtained by the relation (4.6–1).

4.6.3.2. The loss, its cash value, initial cost

Consider a developed turbulent pipe flow in a straight pipe of length L and diameter d. With the mean velocity c depending on the given rated discharge Q and the pipe's cross section A, the pressure drop along this pipe reads [4.26] (with λ as the loss coefficient mainly depending on the Reynolds number and the roughness, but occasionally also on the fluid [4.27; 4.28; 4.30])

$$\Delta p = \lambda \varrho (L/d) c^2/2.$$ (4.6–18)

Following the considerations which lead to (4.6–5), the cash value of energy loss during the depreciation period in the instant the plant starts operating reads now per unit length

$$K_e = (8,76/2)(4/\pi)^2 \eta \varphi \alpha k_e \varrho \lambda Q^3 d^{-5},$$ (4.6–19)

with the meanings of symbols corresponding to those due to (4.6–5), except that d now is the pipe diameter.

The first cost is proportional to the mass of pipe per unit length namely, $m = \pi \varrho_P ds$, s being the wall thickness, assumed as small compared to d. s results as follows from the admissible tensile stress σ_{ad} in the longitudinal pipe section $s = p\,d/(2\sigma_{ad})$. A certain minimum pipe wall thickness s is advisable [4.31]. By experiment, *Surber* [4.32] determined s for a lining of a pressure shaft. *Matt* [4.33] considered prestressed walls of concrete. In the above, p is the maximum internal pressure inclusive water hammer.

With a specific cost factor k_1 that includes also transportation and erection, the pipe cost is $k_1 \varrho_P \pi d^2 p/(2\sigma_{ad})$, ϱ_P being the density of the pipe wall material. The excavation of a pressure shaft or a tunnel but also that of a penstock within a ditch along a slope is expressed by the volume of a cylinder larger in diameter than the pipe $\Phi(\pi/4)d^2$ and a specific cost factor k_3. Thus the initial cost of the pipe's unit length

$$K_{1P} = \pi d^2 [k_1 \varrho_P p/(2\sigma_{ad}) + \Phi k_3/4].$$ (4.6–20)

4.6.3.3. The resulting cost and optimum diameter

From (4.6–19) and (4.6–20), the resulting cost of pipe is

$$K_{res\,P} = E_1 d^2 + E_2 d^{-5},$$ (4.6–21)

161

where

$$E_1 = \pi\,[k_1\,\varrho_p\,p/(2\,\sigma_{ad}) + \Phi\,k_3/4]\,,$$ (4.6–22)

$$E_2 = (8,76/2)(4/\pi)^2\,\eta\,\varphi\,\alpha\,k_v\,\varrho\,Q^3\,\lambda\,.$$ (4.6–23)

The minimum cost results from $\partial K_{res}/\partial d = 0$. Hence the optimum pipe diameter $d_{op} = [(5/2)\,E_2/E_1]^{1/7}$ or

$$d_{op} = 1{,}414\,\{\lambda\,\varphi\,\eta\,\alpha\,\varrho\,Q^3\,k_v/[\Phi\,k_3/2 + \varrho_p\,k_1\,p/\sigma_{ad}]\}^{1/7}\,,$$ (4.6–24)

where φ is the load factor as the share of annual hours under rated load, η the overall efficiency of the set and grid up to the terminals of the consumer, α the factor due to interest rate p over the z years of depreciation, see (4.2–3), λ the loss coefficient of the pipe as a function of Reynolds number, preliminarily fixed as a function of d, and relative pipe wall roughness (see Fig. 4.6.1), k_v the electricity rate, k_3 the cost per m³ of excavated volume due to the pipe, k_1 the specific pipe cost per kg inclusive of transport and erection but without excavation, Φ the ratio of excavated cross sectional area to that of the pipe $\pi d^2/4$, and p the maximum internal pressure.

From the last relation is seen. that the optimum pipe diameter decreases with increasing internal pressure p. Hence for heads above about 500 m the penstock diameter is staged according to the requirements of the last relation.
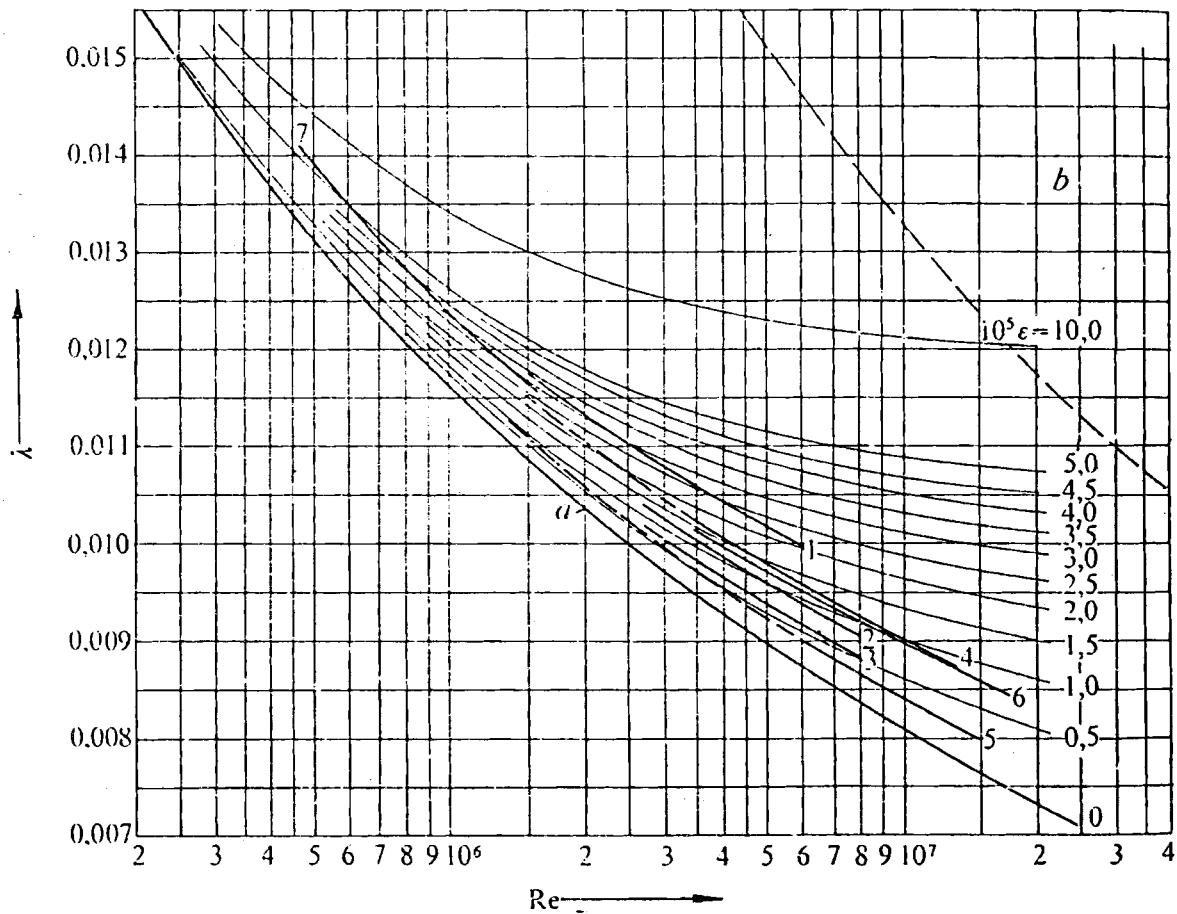
Fig. 4.6.1. Pipe loss friction coefficient λ based on tests, carried out by Sulzer on Swiss penstocks. a hydraulically smooth wall; b hydraulically rough wall. 1 Lucendro; 2, 3 Riddes, penstock 1, 2; 4, 5 Luenersee penstock. pressure shaft; 6 experimental penstock of Dauphinois, Grenoble. From *W. Müller, H. Stratmann.* Technische Rundschau Sulzer 1964, no 3.

The economic diameter of a pipe is also treated by *Sarkaria* [4.34]. A survey of penstocks, already in use, is presented by *Mühlemann* [4.35].

For peak load plants, with frequent water hammer-induced stress changes in the penstock walls, fatigue effects have to be accounted for, before determining the wall thickness. Any resonance of machine-induced pressure fluctuations with the natural frequency of the penstock should be avoided. This holds good especially in the case of an outdoor penstock. Here resonance may cause considerable noise, undesirable in a mountain recreation area. A rather extreme remedy against this consists in wrapping a sound-proof blanket around the penstock. Another remedy could be avoiding resonance by means of a change in the penstock support.

4.7. Problems of optimization of electric power transmission

4.7.1. Historical survey

Long range power transmission has proved the most reliable means for nearly one century of harnessing hydro power in sites far from the consumer. Thus electric power transmission is one of the most essential prerequisites for developing the potential in remote areas especially in developing countries.

Historically, hydroelectricity started with a hydroelectric plant in Wisconsin in 1883. By generating DC this could only supply its immediate neighbourhood. Power supply to consumers in places far from the plant started with high voltage AC power transmission in 1891. This was for a 3-phase AC

Table 4.7.1. Survey of actual high voltage transmissions.

Plant River Country Continent	year	Power supplied in MW (final value)	Next consumer Town Country	Distance in km	Voltage in kV (between poles in case of DC, delta voltage in case of AC)	System
Cabora Bassa Sambesi Mozambique Africa	1974	2075 (3672)	Pretoria Union of South Africa	1450	1050	High tension DC transmission. Converted by thyristor
Churchill Falls Labrador Canada North America	1971	5225 (7000)	Hydro-Quebec Montreal Canada	1200	735	AC transformed 15/220 and 220/735
LG 2, La Grande Quebec Canada North America	1982	5328	Hydro-Quebec Montreal Canada	1200	735	AC
Itaipú Paraná Paraguay Brazil South America	1985 – 1990	12870	São Paulo Brazil	800	1200	DC

transmission of 220 kW and 15 kV over a distance of 175 km between Heilbronn upon Neckar and Frankfurt on Main in West Germany.

Meanwhile for reasons discussed later, also DC high voltage transmission by means of thyristor converters has proved to be successful for distances up to 1500 km, using voltages up to 1200 kV [4.36 to 4.38].

The Table 4.7.1 shows the recent development in this scope.

4.7.2. The cost of 1% loss in relation to that of power transmission

Assume the power station operates h hours annually during z years of depreciation. Without interest and with an electricity rate of k_e, the monetary equivalent of 1% of 1 kW installed is $10^{-2} h z k_e$. Assume the initial cost per installed kW to be k_1 and the cost of electric power transmission in proportion to k_1 to be γk_1. Hence the cost ratio of 1% output (lost or gained) to the initial cost of the power transmission is $K_T = 10^{-2} h z k_e/(\gamma k_1)$. The compilation of terms due to initial cost in 2.2.2 shows that γ may reach the order 0,1. In a special example: $k_e = 0,05$ US \$/kWh; $k_1 = 500$ US \$/kW; $\gamma = 0,1$; $z = 40$ years; $h = 5000$ hours of annual operation. Hence $K_T = 2$. Accounting for interest would yield a somewhat lower figure.

The example demonstrates, that the monetary equivalent of 1% loss may correspond to the initial cost of power transmission. Hence in the following, the design of any component of the power transmission line should be subjected to the direction, that the initial or first cost plus the monetary equivalent of the loss due to this element are made a minimum.

4.7.3. The optimization of the conductor

In the following the overall cost of the transmission line treated in the above sense is assumed to be proportional to that of the conductor by itself. The real conductor, usually a multitude of cables, each a bundle of distinct wires, having different functions e.g., as carriers or conductors, is assumed to be equivalent to one conductor of a certain material with a circular cross sectional area (see Fig. 4.7.1.3 a). Its conductivity may be distributed uniformly over the whole cross sectional area (no skin effect). Moreover DC is assumed to pass through the line. Hence only the ohmic resistance is accounted for, when losses are considered.
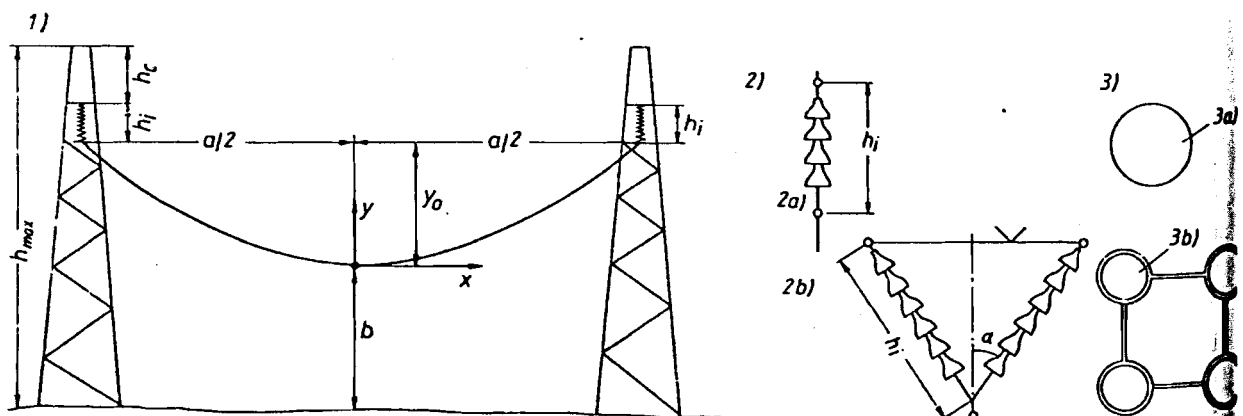
Fig. 4.7.1. Means of power transmission. 1 Schematic design of adjacent towers in plane terrain with conductor, 2 insulator: a, vertical; b, diagonal, 3 conductor: a, idealized; b, implemented.

164

The material cost of such a conductor with a length L, diameter d, consisting of a material with a density ϱ and a price k_1 per unit mass amounts to

$$K_1 = \varrho L\pi (d^2/4) k_1 . \qquad (4.7-1)$$

Assuming an admitted voltage drop ΔU, a current I, an electricity rate k_e, a load factor φ as the share of annual hours at rated load, a factor α from (4.2-3) due to interest rate and z years of depreciation, the cash value of loss at the instant the operation starts, is

$$K_2 = 8{,}76\, \Delta U\, I\, \alpha\, \varphi\, k_e . \qquad (4.7-2)$$

To account for the rise of power transmitted during the life of the plant, a mean power P transmitted is presumed the following consideration.

The power P kW transmitted by the line with its voltage available $U - \Delta U$, needs a current $I = 10^3 P/[U(1 - u)]$ to transmit the power P under an admitted relative voltage drop $u = \Delta U/U$, set preliminarily. According to Ohm's law for a conductor of length L in m, a diameter d in mm and a specific resistance ϱ^0 in $\Omega\,\text{mm}^2/\text{m}$, the drop in voltage becomes as function of the current I: $\Delta U = I \varrho^0 L/[(\pi/4)d^2]$.

Inserting $I = 10^3 P/[U(1 - u)]$ and then ΔU into (4.7-2) yields

$$K_2 = 8{,}76\,(4/\pi)\, 10^6\, P^2\, L\varrho^0\, \varphi\, \alpha\, k_e/[U^2(1 - u)^2\, d^2] . \qquad (4.7-3)$$

With the abbreviations $A = (\pi/4)\varrho L k_1$; $B = 8{,}76(4/\pi)\, 10^6\, P^2\, L\varrho^0\, \varphi\, \alpha\, k_e/[U^2(1 - u)^2]$ the resulting cost of cable from (4.7-1) and (4.7-3) takes the form $K = K_1 + K_2 = A d^2 + B d^{-2}$. Obviously the diameter minimizing the cost is obtained from $\partial K/\partial d = 0$, giving an optimum

$$d_{op} = (8{,}76 \cdot 10^6)^{1/4}\, (4/\pi)^{1/2}\, [\varrho^0\, \varphi\, \alpha\, k_e/(\varrho\, k_1)]^{1/4}\, \{P/[U(1 - u)]\}^{1/2} . \qquad (4.7-4)$$

Strictly speaking the relative voltage drop u in the above relation $\Delta U = uU = (4/\pi) \cdot 10^3 P\varrho^0 L/[U d^2(1 - u)]$ follows from the quadratic equation with the solution (d now d_{op})

$$u = (1/2)(1 - (1 - 4f)^{1/2}) \approx f, \qquad (4.7-5)$$

where $f = (4/\pi) \cdot 10^3 P \varrho^0 L/(U^2 d_{op}^2)$. Hence (4.7-4) and (4.7-5) have to be used for the determination of u and d_{op}. Example: $U = 10^6$ V; $P = 10^6$ kW; $u = 0{,}015$; $\varphi = 0{,}457$, $z = 25$ years, $p = 0$; $\alpha = 25$; material: Copper with $\varrho^0 = 0{,}016 \cdot 10^{-6}\,\Omega\text{m}$; $L = 1{,}5 \cdot 10^6$ m; $k_1 = 1{,}5$ US $/kg; $\varrho = 8300$ kg/m^3; electricity rate: $k_e = 0{,}025$ US $/kWh. From (4.7-4): $d_{op} = 0{,}048$ m $\hat{=}$ 48 mm. (For its rather large breaking length, the usual real cable has a core of steel wires and a conductor of aluminum wires.) From $u = 0{,}015$ the voltage drop $\Delta U = 15\,000$ V. With the resistance $R = 13{,}3\,\Omega$ the power loss becomes $\Delta P = (\Delta U^2/R)\, 10^{-3} = 17 \cdot 10^3$ kW. The cash value of loss is $K_2 = 34{,}2 \cdot 10^6$ US $. The initial cost is $K_1 = 33{,}8 \cdot 10^6$ US $. Note that K_2 and K_1 are of same order! Halving the cable diameter would reduce the initial cost to 25%. The cost of capitalized loss then would increase to $K_2 = 136{,}8 \cdot 10^6$ US $.

But in this case the current density would attain a value which would heat and lengthen the conductor in an inadmissible manner, since the cable then might lower its prescribed minimum distance from the ground to a dangerously small value. Therefore any layout has to be based on a maximum permissible electric current density, which is reached at the end of the depreciation period.

According to *Causse* the above optimization is also practised in the layout of underground cables [4.39]. Two types of economic current densities are to be considered, one with cables being continu-

ously loaded during the z years of depreciation, the other with cables with a linearly rising current density. In the first case 1,7 to 2,1 A/mm^2 are admitted, in the second case the final densities are 5,1 to 6,3 A/mm^2 depending on the extreme fluctuations of the price of copper.

Thus the economic use of underground concepts requires that, the maximum temperature of the conductor reaches the upper limit permissible from the thermal point of view at the end of the depreciation period.

4.7.4. The distance of adjacent towers and cable geometry

If the cable does not transmit any bending moment and if its centre line always makes a small angle with the horizontal (see Fig. 4.7.1.1), equilibrium in the vertical y-direction requires $d^2 y/dx^2 = q/H$, where q is the load per unit length of cable, H the horizontal pull in the cable.

With σ_{ad} denoting the permissible tensile stress in the latter, an admissible breaking length of cable may be defined by $A_{ad} = \sigma_{ad}/(\varrho\, g)$. Thereby the above simplified differential equation $(dy/dx \approx 0)$ reads

$$d^2 y/dx^2 = 1/A_{ad}.$$ (4.7-6)

Integration with respect to the coordinate system (Fig. 4.7.1) and the vertex of the cable curve in the mid point of adjacent towers, whose suspension points have the same altitude, yields the well known parabola as an approximation to the catenary [4.44]: $y = x^2/(2\,A_{ad})$. The sagging of the conductor with the chord between its suspension points (Fig. 4.7.1.1) due to the two following towers having a distance 'a' results as

$$y_0 = a^2/(8\,A_{ad}).$$ (4.7-7)

Assuming towers with a vertical distance h_c of the suspension points underneath the top (Fig. 4.7.1.1) and a vertical length h_i of insulators, the height h_{max} of the towers is obtained as a function of the minimum distance b of the conductor from the ground: $h_{max} = a^2/(8\,A_{ad}) + b + h_i + h_c$.

The distance b (Fig. 4.7.1) depends on vegetation, climate and the fact, that people may work for a longer period underneath a cable of a definite voltage. Hence b may be prescribed by legislation. In some regions it must be taken into account that the spark-over distance between conductor and ground may be diminished by fires, made regularily e.g., during the harvest, within fields of sugar cane to expel rats and snakes but also to facilitate the harvesting.

From the last mentioned relation, the distance between neighbouring towers 'a', when h_{max}, b, A_{ad}, h_c and h_i are given, follows as

$$a = [8\,(h_{max} - b - h_c - h_i)\,A_{ad}]^{1/2}.$$ (4.7-8)

Obviously 'a' increases with breaking length A_{ad}. This figure usually is enlarged by steel inlay (st) within the proper conductor from aluminum (al). The admissible breaking length of such a cable results from the admissible tensile strengthes $\sigma_{ad\,al}$ and $\sigma_{ad\,st}$ of aluminum and steel respectively with densities ϱ_{al} and ϱ_{st} respectively by means of relation

$$A_{ad} = 0,9\,(m\sigma_{ad\,al} + \sigma_{ad\,st})/[g\,(m\varrho_{al} + \varrho_{st})],$$ (4.7-8a)

where m is the ratio of cross sectional areas of the aluminum part A_{al} and the steel part A_{st}, 0,9 is a safety factor see [4.45]. For m = 6, $\sigma_{ad\,al} = 7 \cdot 10^7$ Pa, $\sigma_{ad\,st} = 45 \cdot 10^7$ Pa, $\varrho_{al} = 2,75 \cdot 10^3$ kg/m^3, $\varrho_{st} = 7,8 \cdot 10^3$ kg/m^3. Moreover $h_{max} - h_c - h_i = 40$ m and $b = 10$ m. Hence from (4.7-8a): $A_{ad} = 3285$ m, and from (4.7-8): $a = 888$ m.

The distance h_c is always positive and depends on the ground mainly as a lightning protection. The length h_i of the insulator depends mainly on the maximum voltage U_{max} between its ends, on climatic conditions (air moistness, rainfall, rime) and on the air pollution, and is much larger than the spark-over distance under the conditions above mentioned. The order of magnitude is very roughly given as (Fig. 4.7.1.2 a)

$$h_i(m) = 12 \cdot 10^{-6} U_{max}(V).$$ (4.7–9)

For DC transmission, U_{max} equals the nominal voltage of the insulator against earth. For 3-phase AC transmission, U_{max} equals the crest star voltage. Since the nominal voltage then is defined by the effective delta voltage U_{ef}, U_{max} becomes $U_{max} = \sqrt{2/3}\, U_{ef}$.

Example: 3-phase AC transmission by $U_{ef} = 735$ kV, e.g. Churchill Falls-Montreal. Then $h_i(m) = 7.2$ m! Naturally the latter is a very rough approximation.

Differentiating the relation (4.7–7) between sagging y_0 and admissible stress σ_{ad}, after substituting $A_{ad} = \sigma_{ad}/(g\varrho)$, and keeping ϱ and the distance 'a' of adjacent towers constant, gives the following relation between stress increment $d\sigma_{ad}$ and increment of sagging dy_0

$$d\sigma_{ad} = - [8\,\sigma_{ad}^2/(a^2\,\varrho\,g)]\,dy_0.$$

Hence a negative sagging of the cable, caused by its shrinkage under low temperatures in winter creates additional stress. Further loads in winter by snow, ice and rime also have to be accounted for, when deciding the distance and height of the towers. Moreover the fixing of the distance 'a' has to account for a given length of a cable in consequence of its manufacturing method. This finite length of any conductor requires "dead end towers" in certain distances from each other. Also additional stresses have to be accounted for in the case of a failure of the cable, or a sudden removal of its ice load, see [4.44] and [4.45].●

The cost of the towers follows from the voltage U_{ef} and the distance 'a' of adjacent towers:

For $U_{ef} =$ 20, 110, 220, 380 kV
cost   = 7,7; 32,5; 50; 60 10^3 US $/km
at a = 140; 300; 350; 400 m.

4.7.5. The optimum distance of adjacent towers

From (4.7–8) it is recognized for the general case of suspension by an inclinded insulator (Fig. 4.7.1.1)

$$h_{max} = a^2/(8\,A_{ad}) + b + h_i\cos\alpha + h_c,$$ (4.7–10)

where α is the angle the insulator makes with the vertical (Fig. 4.7.1.2 b). This angle shortens on the one hand the height of the tower, and on the other hand it prevents lateral motions of the line under wind force. Simplifying, a design parameter ζ given by $\zeta h_i = h_i\cos\alpha + h_c + b$ may be introduced, taking into account that b is porportional to the insulator length and so also generally h_c.

According to (4.7–9) terms may also be reduced to the voltage by $h_i\cos\alpha + h_c + b = k_4 U_{max}$, where k_4 is a design-linked parameter and U_{max} the crest voltage in V. The first cost of a tower may be expressed by the relation

$$K_{3P} = k_5\,h_{max}^n,$$ (4.7–11)

where k_5 and n are empirical parameters, n is in the range of $n = 2$ to 3. For a very long line of length L, the tower number i, now assumed as a continuously varying value follows

from $i = L/a$. The resulting cost of a line is $K_{3\,res} = i\,K_{3P}$. Inserting here $i = L/a$, K_{3P} from (4.7–11) and h_{max} from (4.7–10), the resulting cost as function of the distance 'a' becomes

$$K_{3\,res} = k_5\,L\,[k_4\,U_{max}\,a^{-1/n} + a^{2-1/n}/(8\,\Lambda_{ad})]^n.\qquad(4.7-12)$$

Under the assumption that the $(n - 1)$st power of the square bracket does not disappear and putting $dK_{3\,res}/da = 0$, a distance a_{op} is obtained, which minimizes the first cost of the transmission line as

$$a_{op} = \{8\,k_4\,U_{max}\,\Lambda_{ad}/[n(2 - 1/n)]\}^{1/2}.\qquad(4.7-13)$$

It is seen from this that the optimum distance between adjacent towers increases with the square root of $U_{max}\,\Lambda_{ad}$. This result does not consider separately the cost of the insulators. A somewhat more refined expression may be obtained with K_i as the first cost of insulators per tower for the resulting first cost of the line (always without cable) $K'_{3\,res} = K_i\,L/a + K_{3\,res}$. From this by putting $dK'_{3\,res}/da = 0$, an improved version for the optimum distance a_{op} is found

$$a_{op}^* = K_i^{1/2}/\{nk_5\,[k_4\,U_{max}\,a_{op}^{-1/n} + a_{op}^{2-1/n}/(8\,\Lambda_{ad})]^{n-1}\,M\}^{1/2},\qquad(4.7-14)$$

$$M = (2 - 1/n)\,a_{op}^{1-1/n}/(8\,\Lambda_{ad}) - k_4\,U_{max}\,a_{op}^{-1-1/n}/n.\qquad(4.7-15)$$

This relation can be solved by trial and error, starting from (4.7–13) Example: $U_{max} = 10^6$ V; $\Lambda_{ad} = 3320$ m (aluminum, steel), $k_4 = 36 \cdot 10^{-6}$ m/V; $n = 2,35$. Hence from (4.7–13): $a_{op} = 505$ m.

4.7.6. Future developments

There is an increasing tendency to use high voltage direct current (HVDC) transmission, in the case of distances of about 700 km and more, between power station and the next consumer centre [4.36 to 4.39].

Contrary to the common three phase AC transmission with its three cables, DC transmission needs only two cables. The cost of a high voltage transmission line depends first on the cost of the towers resulting from their area and height. Both factors are influenced favourably by shortening the number and length of insulators. Each additional 100 kV in effective 3-phase AC delta voltage U_{ef} needs roughly 1 m more in insulator length. Obviously the latter results from a crest voltage. Since this is $2^{1/2}$ times the effective voltage, 30% of the insulator length (usually corresponding to an additional height of tower) is saved by DC transmission of the same effective voltage of one pole to earth. Moreover in DC transmission, one conductor may be charged positively to earth and the other of the same voltage negatively to earth. Thus for a given insulator length, the effective voltage in DC transmission is $2 \cdot 2^{1/2}$ times that of a single phase AC transmission.

At an admissible relative power loss h'_1 along the line, the losses ΔP_{DC}, ΔP_{AC} of the DC and AC line, respectively, and the powers P_{DC}, P_{AC} transmitted along these lines, respectively, are related by

$$h'_1 = \Delta P_{AC}/P_{AC} = \Delta P_{DC}/P_{DC}.\qquad(4.7-16)$$

Expressing the loss in the AC System by $3\,I_{ef\,AC}^2\,R$, in the DC System by $2\,I_{DC}^2\,R$ (both systems having the same cross sectional areas of their cables and hence the same ohmic

resistance R of them), and introducing the power transmitted in the AC system as $3\, I_{ef\,AC}\, U_{ef\,AC}$ and in the DC System as $2\, I_{DC}\, U_{DC}$, the above relation is reduced to

$$I_{ef\,AC}/I_{DC} = U_{ef\,AC}/U_{DC}, \qquad (4.7-17)$$

where $I_{ef\,AC}$ is the effective current in each phase of the AC line, I_{DC} the current in the DC line, $U_{ef\,AC}$ the effective star voltage in each phase of the AC line and U_{DC} the voltage of each pole to the earth in the DC line. Applying the same length of insulators in both the systems, the voltages are related by

$$U_{DC} = 2^{1/2}\, U_{ef\,AC}. \qquad (4.7-18)$$

Putting this in (4.7-17) gives

$$I_{DC}/I_{ef\,AC} = 2^{1/2}. \qquad (4.7-19)$$

Hence the ratio of the power transmitted in both the lines

$$P_{DC}/P_{AC} = 4/3. \qquad (4.7-20)$$

Thus the DC line transmits 33 % more power than the AC line. If the conductors of both the lines have the same length and the cables of both the lines have the same cross sectional area (as expressed by $R = $ const), the required mass of material for conductors and insulators of the DC line is 66 % of that used for the AC line.

In favour of the AC line, the DC line requires the additional cost of the converter stations at the ends of the line, also the cost of the measures required to eliminate the higher harmonics in the DC line after conversion of the DC into AC. A further reduction of cost by DC results from the more uniform distribution of the current over the cross section of the conductor and from the absence of any loss due to skin effect.

The necessity to transport greater amounts of electric energy and simultaneously, the ever increasing difficulties of obtaining the rights-of-way for the transmission line, make it necessary, to investigate new possibilities of electric power transmission. In the following only methods are considered, which do not convert the electric energy into other forms of energy, e.g. chemical energy, especially hydrogen by electrolysis. As for the latter, see the respective chapter of Simeon's book on hydro power [1.55 a].

The change over to even higher rated voltages does not ideally solve this problem, as this requires larger cross sectional areas and land areas for the line (see Fig. 4.7.2). In the following the transmission by electric means only will be considered.

Transmission by compressed-gas-insulated cables would overcome these difficulties, since at a given voltage, 4 to 6 times more energy can be transported than with an overhead line and the corresponding land requirements are only one tenth [4.40].

Also the preservation of landscape is helped by underground cables. Single phase gas-insulated cables with a full sheath current have a surge impedance of approximately 69 Ω [4.40], from which e.g. 4500 MW surge impedance load can be obtained at 550 kV. The surge impedance load without sheath current would be 60 % and for 3 phases 80 % of the above mentioned values.

One possibility of technical realization is the so called "wellmantel" as a sheath for conventional cables. It combines stability with good bending characteristics. Cables with an outer diameter up to 250 mm can be wound on reels up to a length of 200 m, and they still can be transported by available carriers. The "wellmantel" has been proved as a construction element for thermally insulated tubes. Different expansions of the tubes need no balancing elements. Due to the corrugation there are only small longitudinal forces, which can be compensated easily.

Thus the thermal insulation of cryogenic and superconductive cables is possible. Such cables will be applied in future to eliminate the losses or to reduce the cross sectional area of a cable for a certain
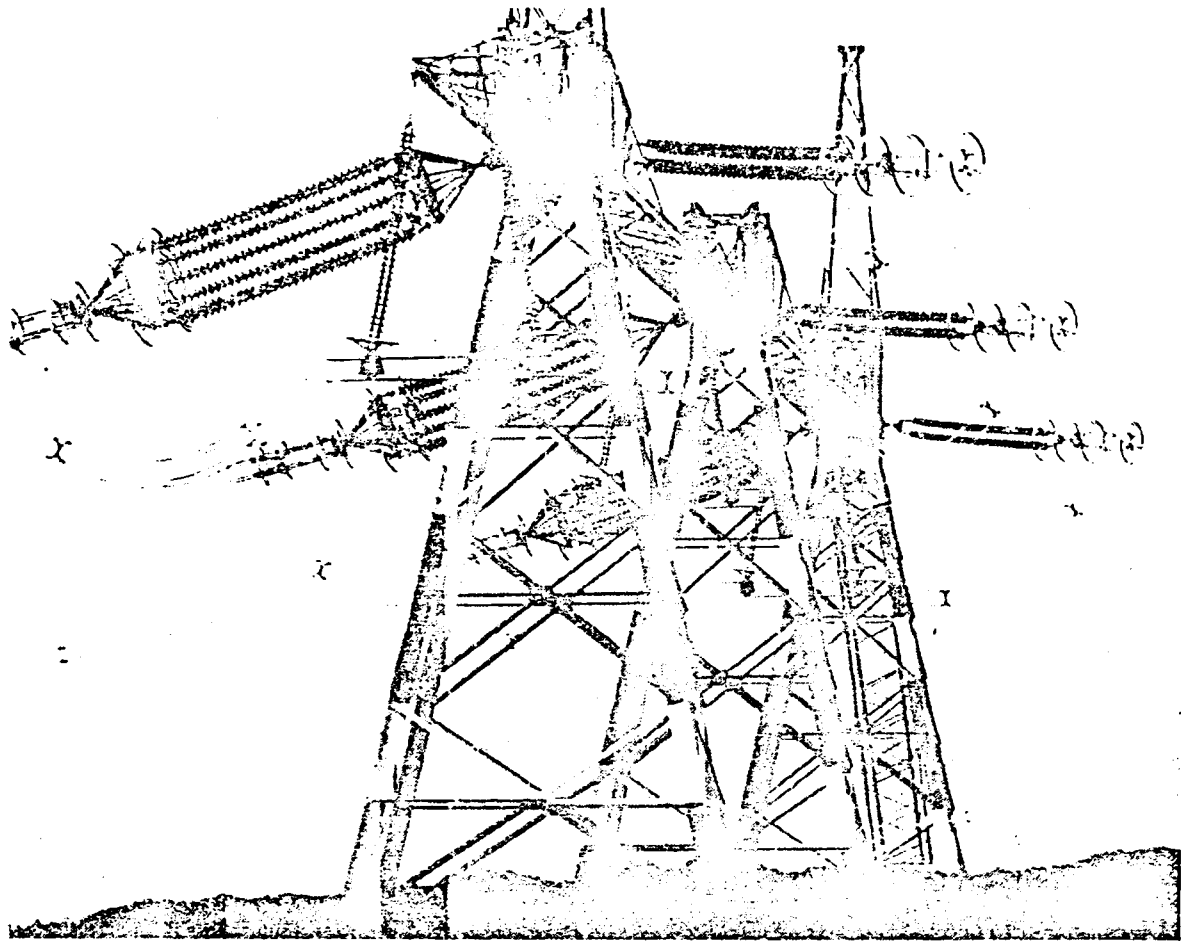
Fig. 4.7.2. Transmission tower near Quebec of high voltage 735 AC transmission line from Churchill Falls to Quebec (about 1200 km) for the continuous transmission of 10000 MW; insulator length about 7 m. Strong insulators, required, for the crossing of the St. Lawrence River. (Photograph courtesy professor Netsch, Laval University, Quebec).

load. The cooling may be effected by pressurized gas flow in the interspace between cable and sheath. The distance between the inner conductor and sheath is retained by adequate spacers [4.41].

Other available cable types for 3-phase high voltage transmission are low pressure oil-filled cables of the single conductor type, and oil pressure cables in steel pipes. Upper limits of the transmission voltage for cables with multilayer insulation are given by paper-impregnated or plastics-impregnated components, and for cables with homogeneous insulation are given by extruded plastics. Influencing variables are the cable type, cable design, layout arrangement, soil condition, and the load factor. Possibilities of increasing the current carrying capacity are, larger cross sections, laying in special back-filling materials, parallel systems, and forced cooling by oil or water. Future possible variants for underground bulk power transmission can be expected from SF_6-insulated pipe line cables, cryogenic, and super-conducting cables [4.42].

One of the most immediate economic objections to underground transmission is the obvious difficulty of inspection. Non-destructive test procedures for underground power cables were described and proven by Roemer et al [4.43].

170

5. Survey of basic hydrodynamics, with special reference to hydro power

5.1. Introduction

The project and design of hydro power has to be based on the principles of hydrodynamics. Starting from the early contributions of *D. Bernouilli* and *L. Euler* [5.1], this must include first the kinematics of ideal fluid flow due to mass conservation (continuity), rotation and irrotational flow in stationary or rotating frames of reference and the components of strain rate tensor. Velocity triangles and relative whirl must be considered.

The dynamics of fluids follows from these, when applying the equation of motion and the energy theorem derived from this for stationary and rotating frames of reference. The usual lack of detailed information about the flow field also requires the introduction of the momentum theorem. The meaning of unsteady flow in relation to energy conversion has to be discussed.

The dynamics of real fluids in turbo machinery has to start from liquid properties such as compressibility and viscosity together with turbulence-linked eddy viscosity. The relation between stress and strain rate yields the Navier-Stokes' equations.

Consideration of the boundary layer concept and fluid behaviour related to a flat plate and a pipe leads to the laminar and turbulent flow regimes. Turbulence and its connected apparent shear stresses have to be considered as the sources of dissipative energy loss. For ducts the influence of wall roughness and wall vibration on dissipation has to be accounted for.

The flow in stationary and rotating ducts requires a knowledge of stall and secondary flow as loss mechanisms. The significance of turbulence, wall curvature and duct rotation in the generation of secondary flow have to be understood. The rotor of reaction machines needs a consideration of leakage and disk friction losses as a function of the geometry of the component parts.

Windage loss and secondary flow in curved buckets are required for the understanding of the performance of impulse turbines.

A knowledge of different flow regimes in diffuser channel may show remedies for lowering loss in this element which is essential for the high efficiency of low head turbines and impeller pumps.

The concepts of circulation in connection with Joukovsky's theorem and simple aerofoil theory may increase the understanding of flow and loss mechanism in axial turbo-machines. The appreciation of relative whirl, the link between the velocity triangle and circulation and slip factor, may facilitate the understanding of effects in semi axial and radial machinery. A general survey and detailed treatment of certain problems is found in the references [5.2 to 5.8].

5.2. The kinematics of an ideal flow

5.2.1. Mass conservation (Continuity)

In steady flow the mass flow through an arbitrary cross sectional area A of a stream tube has to be constant. When A is very small, density ϱ and fluid velocity c, normal to A, can be assumed as constant over A. Hence (see Fig. 5.2.1a) $\dot{m} = \varrho c A = $ constant. For an incompressible ideal liquid this is simplified to a constant volume flow along the tube

$$Q \equiv \dot{V} = cA = \text{constant.} \tag{5.2-1}$$

For an unsteady flow the stream tube does not exist. Here mass conservation for the general case of a compressible fluid can be formulated at a certain instant and volume element assuming the fluid as a continuum.
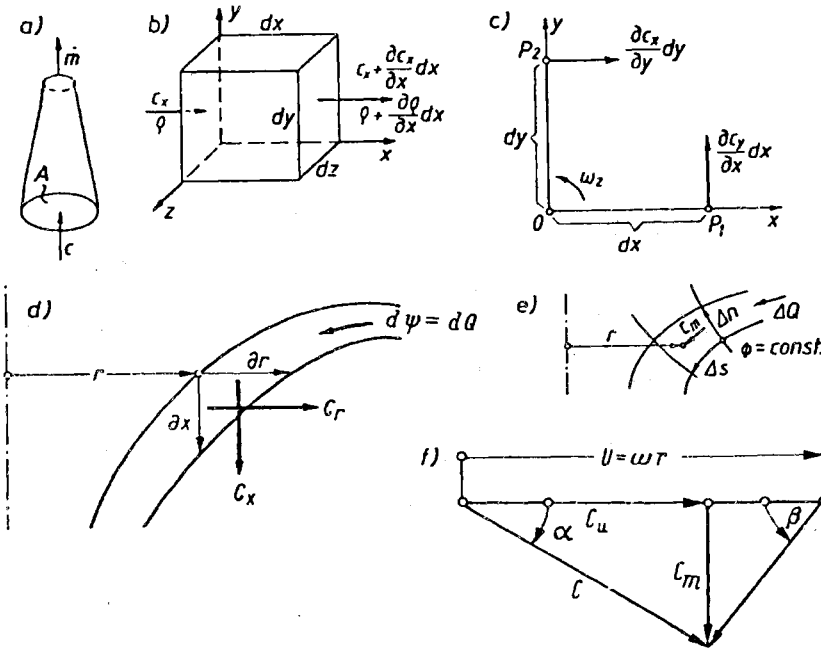
Fig. 5.2.1. Illustrations of kinematic facts: a) stream tube; b) continuity; c) velocities due to rotation (curl); d) stream function Ψ in axisymmetric flow; e) axisymmetric potential flow, and graphical method; f) velocity triangle of turbine.

The velocity components in the x, y and z-direction at a point with Cartesian coordinates x, y, z are c_x, c_y, c_z. An elementary parallel epiped with dx, dy, dz as its edge lengths is considered. The mass flow through the cross sectional area '$dydz$' at the point x is $c_x \varrho\, dydz$. At the point $x + dx$ it has increased by $[\partial(\varrho c_x)/\partial x]\, dxdydz$. Similar increments of mass flow occur in the other two directions (Fig. 5.2.1 b).

In the time interval dt during which the surplus of mass flow hence obtained $[\partial(c_x\varrho)/\partial x + \partial(c_y\varrho)/\partial y + \partial(c_z\varrho)/\partial z]\, dxdydz$ crosses the surface of the volume element, the rate of increase of density $\partial\varrho/\partial t$ causes an increment of mass within the volume $dxdydz$: $(\partial\varrho/\partial t)\, dt dxdydz$. Mass conservation requires a compensation of both the terms last mentioned. Thus

$$\text{div}(\varrho c) + \partial\varrho/\partial t = 0. \tag{5.2-2}$$

Hence the one dimensional flow in a pipe requires $\varrho(\partial c/\partial x) + c(\partial\varrho/\partial x) + \partial\varrho/\partial t = 0$. Obviously $\partial\varrho/\partial x = (\partial\varrho/\partial t)/(\partial x/\partial t)$. In the unsteady flow of a real compressible fluid the density rate $\partial\varrho/\partial t$

results mainly from a density wave with density gradient $\partial\varrho/\partial x$, which passes relative to the fluid in the x-direction with the speed of sound 'a' (also called celerity). Thus $\partial x/\partial t = -a$. Consequently continuity reads now $\varrho\,\partial c/\partial x + (\partial\varrho/\partial t)(1 - c/a) = 0$. In a hydraulic machine and its components, the ratio c/a is usually much less than unity.

Therefore in general the term c/a can be neglected. Thereby continuity becomes in the one dimensional case approximately, $\varrho(\partial c/\partial x) + \partial\varrho/\partial t = 0$, or in the general case

$$\operatorname{div} c = -(\partial\varrho/\varrho)/\partial t. \tag{5.2-3}$$

The relative increase in density $\partial\varrho/\varrho$ depends on the pressure increment ∂p and the bulk modulus E_L (which is assumed here to be constant property of the liquid) giving

$$\partial\varrho/\varrho = \partial p/E_L. \tag{5.2-4}$$

Hence the simplified continuity equation for a slightly compressible liquid reads

$$\operatorname{div} c = -(1/E_L)\,\partial p/\partial t. \tag{5.2-5}$$

5.2.2. Potential flow and the curl (vorticity)

In the case of a potential flow, the velocity vector c is a gradient of a scalar function Φ called the velocity potential or hence brief the potential, according to

$$c = \operatorname{grad}\Phi; \quad c_x = \partial\Phi/\partial x; \quad c_y = \partial\Phi/\partial y; \quad c_z = \partial\Phi/\partial z. \tag{5.2-6}$$

Inserting this into the continuity (5.2–5) of an ideal incompressible flow with $E_L \to \infty$ (from 5.2–4), the so called potential equation results

$$\operatorname{div}\operatorname{grad}\Phi \equiv \Delta\Phi = \partial^2\Phi/\partial x^2 + \partial^2\Phi/\partial y^2 + \partial^2\Phi/\partial z^2 = 0. \tag{5.2-7}$$

Since the sequence of partial derivatives of Φ can be changed, it results from (5.2–6) that

$$\partial c_y/\partial x - \partial c_x/\partial y = 0; \quad \partial c_x/\partial z - \partial c_z/\partial x = 0; \quad \partial c_z/\partial y - \partial c_y/\partial z = 0. \tag{5.2-8}$$

Obviously (Fig. 5.2.1 c) a mean angular velocity ω of the fluid about a certain axis is defined by the arithmetic mean value of angular velocities, that two adjacent liquid line elements have, both normal to each other and in a plane normal to the axis. Hence the components of ω are

$$\omega_x = (\partial c_z/\partial y - \partial c_y/\partial z)/2; \quad \omega_y = (\partial c_x/\partial z - \partial c_z/\partial x)/2 \quad \text{etc.} \tag{5.2-9}$$

The normal convention is, to omit the factor $\frac{1}{2}$ by introducing the rot c or from now on (after C. *Maxwell*) the curl c as twice the angular velocity as a scale of vorticity. Thus

$$\operatorname{curl} c \equiv \operatorname{rot} c = 2\omega, \tag{5.2-10}$$

For example a rotating solid body has a constant curl, as has a forced vortex. Comparing (5.2–8), (5.2–10), it is seen, that a flow with a velocity potential, a 'potential flow' has a vanishing curl c.

Nevertheless there exists also an example of a potential flow, where the flow circulates around an axis. This kind of circulating flow usually exists in the absence of viscous effects, where at a distance r from its axis the whirl velocity component c_u (here equal to the resultant velocity) follows the rule of constant moment of momentum along the circular streamlines about this axis

$$c_u r = \operatorname{const}. \tag{5.2-11}$$

According to (5.2-6), its potential obeys the law $c_u = (1/r)\,\partial\Phi/\partial\varphi$, with $\partial\varphi$ as the increment of the peripheral angle (azimuth). Integration yields the potential

$$\Phi = \text{const}\,\varphi + f(x, r),\qquad\qquad\qquad\qquad (5.2-12)$$

at which x and r are the coordinates normal to the peripheral velocity c_u. The last relation and the linearity of the potential equation (5.2–7) lead to the conclusion that any free vortex about an x-axis can be superimposed by a flow within the meridian of this axis and with potential $f(x, r)$.

In most of the hydro turbines, the moment of momentum of flow upstream of the runner is nearly constant. This follows from the intention, to extract from any stream tube the same available specific energy, namely head by means of the theorem of moment of momentum under the assumption of a whirl-free outlet ($c_{u1} = 0$) which usually occurs at least at the bep.

In such a turbomachine the rotary flow, given by the free vortex $c_u r = \text{const}$ can be superimposed on an axial symmetric potential flow represented by a potential flow in a meridian.

5.2.3. The potential flow in the meridian, stream function

In many cases of steady flow the flow energy per unit mass ($Y = p/\varrho + c^2/2 + gh$ (Cap. 5.3.1)) is constant and the same in the whole flow field (except the boundary layers). This case may be considered as natural, since no reason exists why the energies of adjacent streamtubes, usually originating from the same potential energy in a huge reservoir, differ from each other. The equation of motion (5.3–1) shows, that in this case of grad $Y = 0$ and $\partial c/\partial t = 0$ the flow is also a potential flow with curl $c = 0$.

Now such an axially symmetric potential flow, e.g., upstream of the rotor of a turbine is considered. It is represented by a potential flow in the meridian (Fig. 5.2.1 d). The velocity c has the components c_x and c_r in the axial and radial directions. A potential flow requires after (5.2–8)

$$\partial c_x/\partial r - \partial c_r/\partial x = 0.\qquad\qquad\qquad\qquad (5.2-13)$$

We assign to each streamline in the meridian a streamfunction Ψ, as a scalar due to a certain flow Q, that passes between this streamline and the axis. Hence and for formal convenience: $\Psi = Q/(2\pi)$. Any streamline in the meridian is described by $\Psi(r, x) = \text{const}$. Next two neighbouring streamlines Ψ and $\Psi + d\Psi$ are considered. The flow between these streamlines is $dQ = 2\pi d\Psi$.

Consider the flow past the area described by the rotation of the distance ∂r between these streamlines. Here this flow passes through an annular section of area $2\pi r\,\partial r$ with velocity c_x. Thus continuity gives (Fig. 5.2.1 d)

$$c_x = (1/r)\,\partial\Psi/\partial r.\qquad\qquad\qquad\qquad (5.2-14)$$

Next consider a movement ∂x to the adjacent streamline. Now the flow passes with c_r through the cylinder $2\pi r\,\partial x$. Hence

$$c_r = -(1/r)\,\partial\Psi/\partial x.\qquad\qquad\qquad\qquad (5.2-15)$$

Inserting (5.2–14) and (5.2–15) in (5.2–13) gives

$$\partial^2\Psi/\partial x^2 - (1/r)\,\partial\Psi/\partial r + \partial^2\Psi/\partial r^2 = 0.\qquad\qquad\qquad\qquad (5.2-16)$$

One solution, cited by *Lamb* [5.5] has the form

$$\Psi = r^2 \langle x^{n-1} - \{(n-1)(n-2)/[2(2n-1)]\}(r^2 + x^2)x^{n-3}$$
$$+ \{(n-1)(n-2)(n-3)(n-4)/[2 \cdot 4(2n-1)(2n-3)]\}$$
$$\cdot (r^2 + x^2)x^{n-5} + \ldots \rangle. \tag{5.2-17}$$

in which n is a positive integer. Another solution given by the products of harmonic functions in x with Bessel or Neumann functions in r was cited by *J. Raabe* [4.11].

Owing to the linearity of the differential equation (5.2–16) due to the streamfunction, these solutions can be superimposed after multiplication by constants, so as to be adaptable to the given boundary conditions $\Psi = \text{const}$. Graphical method: Let Δn be the normal distance between adjacent streamlines, between which a discharge ΔQ flows. At a selected point (Fig. 5.2.1 e), distance r from the axis, the flow through the truncated surface of area $2\pi r \Delta n$ normal to the velocity c becomes $\Delta Q = 2\pi r c \Delta n$. When the potential between adjacent equipotential lines normal to the streamlines, has the difference $\Delta \Phi$ along a distance Δs in the streamwise direction, the velocity is $c = \Delta \Phi / \Delta s$.

A combination of the last two relations gives, assuming $\Delta Q = \text{constant}$ and $\Delta \Phi = \text{constant}$, the following condition for the design of the grid formed by streamlines and equipotential lines

$$\Delta s / \Delta n = \text{const } r. \tag{5.2-18}$$

Within a cylindrical distributor of a fluid machine, the flow is nearly normal to the axis. Therefore along the equipotential lines in this component $r = \text{const}$. Thus $\Delta s = \text{const } \Delta n$. Δn is obtained by dividing the given span b_3 of the distributor vane into just as many equal sections as elementary turbines are required (usually 3 to 5).

At the draft tube inlet of the turbine the distance Δs of two adjacent equipotential lines can be assumed as nearly constant. Therefore now the relation $r \Delta n = \text{constant}$ holds good. An experimental method is shown in [5.9].

5.2.4. Velocity triangle and relative eddy

A stationary observer sees the absolute flow with its absolute velocity c from a stationary or absolute frame of reference. (Strictly speaking, according to the equation of absolute motion used, this frame should be an inertial frame with a rectilinear and uniform motion.)

In a rotor turning with local peripheral velocity 'u' about its axis, an observer at station r rotating with the rotor at angular velocity ω, observes the relative flow with its relative velocity w. From the theorem of the triangle of velocities (Fig. 5.2.1 f)

$$w + u \equiv w + \omega \times r = c. \tag{5.2-19}$$

Assume the absolute flow as a potential flow. Hence $\text{curl } c = 0$. Therefore from (5.2–20) $\text{curl } w = -\text{curl}(\omega \times r)$. From the well-known identity $\text{curl}(\omega \times r) = 2\omega$, it follows

$$\text{curl } w = -2\omega. \tag{5.2-20}$$

This curl is called the "relative whirl" or "relative eddy". That means in an absolute potential flow, an observer, rotating in the rotor at its angular velocity, sees always a rotational flow with a curl parallel to the axis of rotation, in the negative sense of the real rotation.

Assume the flow through the rotor is on axial symmetric stream surfaces (Fig. 5.2.2a). Obviously the governing vorticity due to the relative whirl in such a stream face is oriented normal to the latter and is given by the component $-2\omega\cos\mu$, μ being the angle, the streamsurface makes with a plane normal to the axis. Hence $(\text{curl}\,w)_n = -2\omega\cos\mu$ where n indicates a direction normal to the stream surface.

For the computation of the relative flow field in such an axial symmetric streamsurface the curl w may be expressed in terms of the velocity components w_m and w_u in the meridional and peripheral directions (Fig. 5.2.2a) by virtue of Stokes' theorem, after which $(\text{curl}\,w)_n = \lim_{A\to 0} \oint w\,ds/A$ [5.3]. Thus

$$(\text{curl}\,w)_n = \partial w_u/\partial s + \cos\mu\, w_u/r + \partial w_m/(r\,\partial\varphi), \qquad (5.2-21)$$

where s now is the meridional direction and φ the azimuth. Inserting here $(\text{curl}\,w)_n = -2\omega\cos\mu$ yields

$$\partial w_u/\partial s + \cos\mu\,w_u/r + \partial w_m/(r\,\partial\varphi) = -2\omega\cos\mu. \qquad (5.2-22)$$
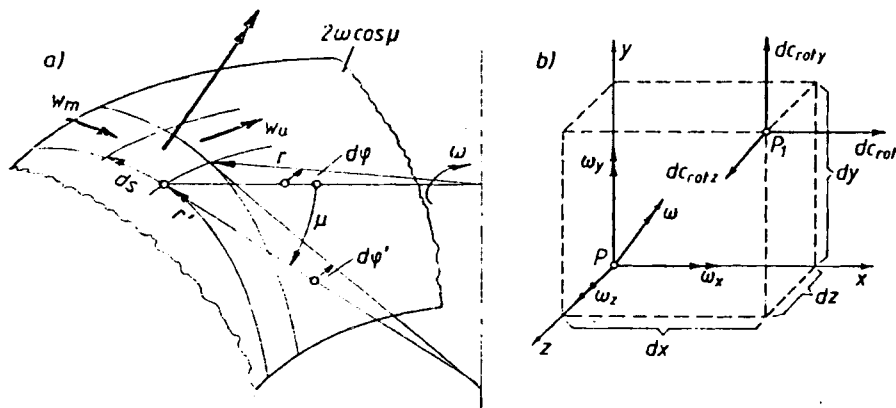
Fig. 5.2.2. Illustration of further kinematic facts. a) Relative eddy in axisymmetric relative flow. b) Velocity increments due to rotation.

Assuming axial symmetric flow laminae of varying thickness b and linking the relative streamline to a streamfunction $\Psi = \text{const}$ (along the streamline), continuity enables a reduction of the velocity components to Ψ analogous to (5.2-14) and (5.2-15)

$$w_m = (1/(br))\,\partial\Psi/\partial\varphi, \qquad (5.2-23)$$

$$w_u = (1/b)\,\partial\Psi/\partial s. \qquad (5.2-24)$$

Inserting these relations in (5.2-22) results in

$$\partial^2\Psi/\partial s^2 + (\cos\mu/r - (1/b)\,\partial b/\partial s)\,\partial\Psi/\partial s + (1/r^2)\,\partial^2\Psi/\partial\varphi^2 = -2\omega b\cos\mu. \qquad (5.2-25)$$

Any graphical or analytical solution has to start from preliminary given relations $\mu(s), r(s)$ and $b(s)$. Moreover it needs the vane traces of the suction and pressure faces given as $\Psi_S(s, \varphi) = 0$ and $\Psi_P(s, \varphi) = \Delta Q/z$, where ΔQ is the flow due to the flow lamina considered and z the vane number of the rotor.

The author has shown an analytical solution [5.10] and has presented the conversion of the differential equation into a difference equation and thus into a system of inhomogeneous linear equa-

176

tions, in which the Ψ value in the middle of a certain area element is expressed as a linear function of the Ψ values at points along the boundary of this area. .

Schilling [6.17] also presented some examples for the solution of this method. It must be kept in mind that the method gives information only about the flow within the mean stream surface of the flow lamina considered. The subdivision of the flow in a rotor of given geometry into flow laminae or elementary turbines is considered in Cap. 6.5.

The deviation of real flow from an axially symmetric one is considered in Cap. 10.6. The objection, that the method is wrong as it does not account for the vorticity in the absolute flow is weakened by the fact that the absolute vorticity in the free flow outside the boundary layer and the wakes from a cascade upstream in general is small and has a prevailing component in the streamwise direction. This only twists somewhat the streamface within the rotor channel, Cap. 10.6.

Problems due to unsteady flow, vortices passing a cascade, boundary layer, wakes, and flow about the inlet edge are dealt with in the chapters 6.4; 7.2; 7.3 respectively.

Naturally the method presumes an attached flow. Any stall, e.g. past the inlet edge, as reported by Betz [5.11], which may be attributed to a wrong estimate of the inflow controlled by the guide vane is predictable by continuity, momentum and energy theorem.

5.2.5. The rate of strain tensor

Consider a certain flow with velocity components c_x, c_y and c_z at a certain point P. These velocities vary at a distance $dn = dx + dy + dz$ from the first point by the following amount here given for the component c_x only

$$dc_x = (\partial c_x/\partial x)\, dx + (\partial c_x/\partial y)\, dy + (\partial c_x/\partial z)\, dz.$$

Due to the local curl and the resulting angular velocities ω_y, ω_x of the flow, the fluid gets an additional induced velocity in the x-direction, for example at the neighbouring point P_1 (Fig. 5.2.2 b) $dc_{\omega x} = \omega_y dz - \omega_z dy$. .

Substraction of $dc_{\omega x}$ from dc_x yields the velocity increment in the x-direction due to "deformation"

$$dc_{x\,def} = \frac{\partial c_x}{\partial x}\, dx + \frac{1}{2}\left(\frac{\partial c_y}{\partial x} + \frac{\partial c_x}{\partial y}\right) dy + \frac{1}{2}\left(\frac{\partial c_x}{\partial z} + \frac{\partial c_z}{\partial x}\right) dz. \qquad (5.2-26)$$

Obviously: $dx/dn = \cos(x, n)$; $dy/dn = \cos(y, n)$; $dz/dn = \cos(z, n)$. Dividing $dc_{x\,def}$ by dn and respecting the last relations yield the x-component of "strain rate" as a function of the direction the strain rate exists, at which the direction is given by its unit vector $n^0(\cos(x, n), \cos(y, n), \cos(z, n))$:

$$\frac{dc_{x\,def}}{dn} = \frac{\partial c_x}{\partial x}\cos(x, n) + \frac{1}{2}\left(\frac{\partial c_y}{\partial x} + \frac{\partial c_x}{\partial y}\right)\cos(y, n) + \frac{1}{2}\left(\frac{\partial c_x}{\partial z} + \frac{\partial c_z}{\partial x}\right)\cos(z, n).$$
$$(5.2-27)$$

This relation shows that the derivative of the "deformation velocity" in a certain direction depends linearly on the components of the directional vector n^0. Therefore the derivative of the deformation velocity is a tensor of the unit vector n^0 according to $dc_{def}/dn = T_c n^0$, with T_c as the following rate of strain tensor

$$T_c = \begin{pmatrix} \partial c_x/\partial x & (1/2)\,(\partial c_y/\partial x + \partial c_x/\partial y) & (1/2)\,(\partial c_x/\partial z + \partial c_z/\partial x) \\ (1/2)\,(\partial c_y/\partial x + \partial c_x/\partial y) & \partial c_y/\partial y & (1/2)\,(\partial c_z/\partial y + \partial c_y/\partial z) \\ (1/2)\,(\partial c_x/\partial z + \partial c_z/\partial x) & (1/2)\,(\partial c_z/\partial y + \partial c_y/\partial z) & \partial c_z/\partial z \end{pmatrix}.$$
$$(5.2-28)$$

The components of T_c are large in regions where the curl is also large, e.g. in boundary layers. On the other hand, a solid body vortex has a curl but no T_c, whereas the free vortex has.

5.2.6. The circulation and its relation to curl

The circulation Γ about the contour of a rotor vane in a turbo machine is an important feature, needed to obtain the forces acting on it. In general Γ is defined by a line integral along a line l, which usually is closed, by

$$\Gamma = \oint_l c\, ds. \tag{5.2-29}$$

In a plane and steady potential flow about an aerofoil but also about a cylindrical vane section of an axial turbo machine, Γ originates from a physical angle of attack δ_0, the undisturbed flow makes with the zero lift direction due to the profile.

More generally the curl from (5.2-8), (5.2-10) is defined by (A^0 being unit vector)

$$\operatorname{curl} c = \lim_{dA \to 0} (\oint c\, ds/dA)\, A^0. \tag{5.2-30}$$

Hence *Stokes'* theorem, which relates the circulation along an arbitrary spatial closed line to the flux of vorticity $\operatorname{curl} c$ through a surface, that ends on this line [4.26]:

$$\oint_l c\, ds = \iint_A \operatorname{curl} c\, dA. \tag{5.2-31}$$

In mixed flow turbo machines the circulation about a rotor vane, and the velocity difference $w_S - w_P$ between the suction and pressure faces of rotor vane hence derived, depends mainly on the relative eddy curl w. The link between curl w and $w_S - w_P$ in such a machine can be found as follows by (5.2-31).

Consider an elementary quasi-parallelogram (Fig. 5.2.3 a) on the axisymmetric streamface of a rotor vane channel, limited by a streamline element ds along the suction and pressure faces of the rotor vane and the unobstructed pitch arcs along two adjacent parallel circles with the radii r and $r + dr$ respectively.

For an irrotational absolute flow $\operatorname{curl} c = 0$, Cap. 5.2.4, the relevant component of relative eddy normal to the streamface, making an angle μ with a plane normal to the rotor axis, becomes $(\operatorname{curl} w)_n = -2\omega \cos \mu$. The unobstructed pitch between the z rotor vanes due to a contraction factor Φ in consequence of the boundary layer and vane thickness is $2\pi r \Phi/z$.

The relative flow is along the vane and has, according to the local velocity triangle, a pitch-averaged relative whirl component w_u (Fig. 5.2.3 a). With respect to the obvious relation $dr = ds \cos \mu \sin \beta$, β being the angle the vane makes with the circumference, *Stokes'* theorem (5.2-31), now applied to the quasi-parallelogram, gives the difference of relative velocities between suction (S) and pressure (P) face, at $\Phi = \text{const}$, as

$$w_S - w_P = 2\pi\Phi\cos\mu\sin\beta(2\omega r - d(w_u r)/dr)/z. \tag{5.2-32}$$

Here for pump turbines and pumps with backward curved rotor vanes, the following relation holds good: $w_u \approx \omega r_1 = \text{const}$. Hence $d(w_u r)/dr \approx \omega r_1$. For high head Francis turbines with pronounced foreward curved rotor vanes, $w_u r$ is approximately constant. Hence $d(w_u r)/dr \approx 0$.

178

Fig. 5.2.3. Circulation and its applications a) Stokes' theorem in an impeller channel for irrotational absolute flow T = velocity triangle. b) Circulation Γ_s around a rotor blade in an axisymmetric stream face, and whirl components c_{u1}, c_{u2}, for irrotational absolute flow and finite vane thickness, V vane trace in stream face. c) Lift on an aerofoil by a circulation Γ around it; b zero lift direction; sv starting vortex; --- control line at infinity, S suction face, P pressure face.
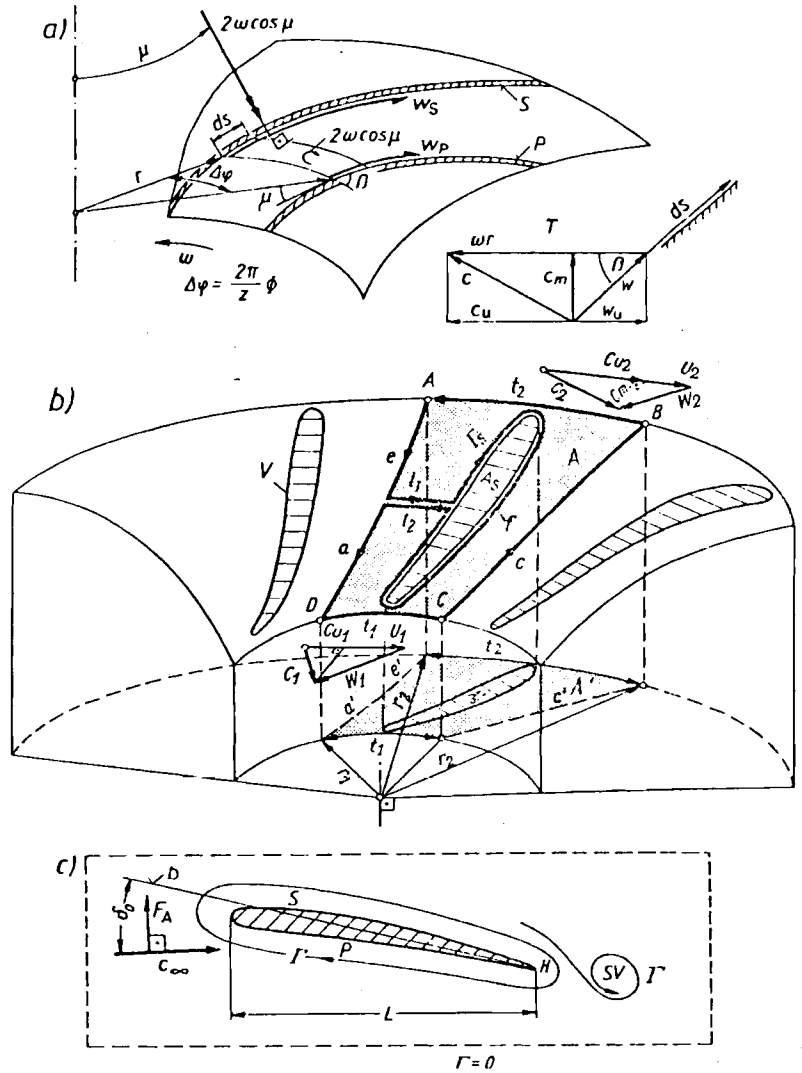
According to *Stanitz*, up to a certain radius within a rotor channel, the distribution of relative velocity in the tangential direction across the channel is linear [5.12]. Hence with $\Delta w = w_S - w_P$

$$w_S = w_M + \Delta w/2 \tag{5.2-33}$$

$$w_P = w_M - \Delta w/2 \tag{5.2-34}$$

in which $w_M = (w_S + w_P)/2$ is the mean relative speed at the channel centre line.

By means of $\Delta w = w_S - w_P$ from (5.2-32) and the energy theorem (5.2-3 or 7) for the rotating frame of reference, the pressure difference, $\Delta p = p_P - p_S$ between the pressure and suction faces of a rotor vane, results from

$$\Delta p = \varrho \, \Delta w \, w_M. \tag{5.2-35}$$

5.2.7. Vane circulation and lift

The vane circulation is desired for a rotor of known geometry and given velocity triangles (see Fig. 5.2.3 b). The Figure shows the runner vane traces in an axisymmetric streamface.

179

The absolute flow is irrotational. From (5.2–31), the circulation Γ around the area A within the streamface, that surrounds the vane trace A_s and extends peripherally over one pitch (Fig. 5.2.3 b), obeys the relation

$$\oint_{l_2} w\,ds + \oint_e w\,ds + \oint_{l_1} w\,ds + \oint_f w\,ds + \oint_{l_2} w\,ds + \oint_a w\,ds + \oint_{l_1} w\,ds + \oint_c w\,ds$$

$$= \iint_A \operatorname{curl} w\,dA.$$

As the axially oriented relative whirl is the only existing vortex, then $\iint_A \operatorname{curl} w\,dA = \iint_{A'} \operatorname{curl} w\,dA'$, with A' as the projection of A on a plane normal to the axis. With the relative eddy -2ω, and respecting the vanishing vortex through the vane's projection A_s' on a plane normal to the axis, then

$$\iint_{A'} \operatorname{curl} w\,dA' = 2\pi\omega(r_2^2 - r_1^2)/z - 2\omega A_s', \qquad (5.2–35)$$

with z as the number of blades. Obviously from the velocity triangles $\oint w\,ds = w_{ui}2\pi r/z$

$= 2\pi\,(\omega r_i^2 - c_{ui}r)/z$ (i being 1 or 2 at the rotor inlet or outlet) the circulation about A reads

$$\Gamma = \Gamma_s + (2\pi/z)\,[\omega(r_2^2 - r_1^2) - c_{u2}r_2 + c_{u1}r_1]. \qquad (5.2–36)$$

Equating Γ and $\iint_{A'} \operatorname{curl} w\,dA'$ according to *Stokes'* theorem, the circulation about the rotor vane reads

$$\Gamma_s = (2\pi/z)\,(c_{u2}r_2 - c_{u1}r_1) - 2\omega A_s'. \qquad (5.2–37)$$

The last term $2\omega A_s'$ appears only in mixed flow machines and increases with vane thickness compared with the radii r_1 or r_2, respectively. It results from the absence of flux of relative eddy within the contour of the rotor vane.

In axial turbomachines with coaxial cylindrical stream surfaces the area A_s' is zero. Hence

$$\Gamma_{sax} = (2\pi r/z)\,(c_{u2} - c_{u1}) = \Delta c_u t, \qquad (5.2–38)$$

in which t is the pitch, and $\Delta c_u = c_{u2} - c_{u1}$ is the so-called deflection [5.13].

The flow in such a cylindrical surface shall be a steady potential flow, of unit depth. Let $c_x = \text{const}$ be the undisturbed velocity. As is well-known [5.14], the lift on a vane with circulation Γ_s equals that on a bound vortex tube at its centre of pressure, strength $\operatorname{curl} c = \Omega$, cross section $ds\,dn$, ds being along c_∞, dn normal to it. Henceforth: $g = 0$.

The equation of motion (5.3–2) yields a pressure on this vortex in the n-direction $dp = \varrho |c_y \times \Omega|\,dn$. Hence according to *Kutta*, *Joukovsky* [5.15; 5.16], with the circulation Γ_s about the vane, being according to *Stokes'* theorem $\Gamma_s = \Omega\,ds\,dn$, and the unit vector on the flow plane $\Omega^0 = \Omega/\Omega$, the hydrodynamic lift on the vane becomes (see Fig. 5.2.3c)

$$F_A = \varrho(c_\infty \times \Omega^0)\,\Gamma_s. \qquad (5.2–39)$$

5.3. Dynamics of ideal flow

5.3.1. Equation of motion and energy for a stationary frame of reference

For the absolute flow, observed from a stationary frame of reference, the equation of motion of a unit mass reads

$$\operatorname{grad}(p/\varrho + c^2/2 + gh) = c \times \operatorname{curl} c - \partial c/\partial t, \qquad (5.3-1)$$

in which p is the pressure, ϱ the density, c the absolute velocity, h the elevation of the point considered. An element of an instantaneous streamline is parallel to the velocity vector c. An element of the instantaneous vortex line is parallel to the vector $\operatorname{curl} c$. At any instant the vector $c \times \operatorname{curl} c$ is normal to the surface element, formed by the instantaneous vortex and stream line element (see Fig. 5.3.1 a).

From this it can clearly be seen, that any change of the absolute flow energy $Y_a = p/\varrho + c^2/2 + gh$ in the direction of the streamline element can be caused only by an unsteady term $\partial c/\partial t$ of the flow. This unsteadiness occurs within a vaned rotor for a stationary observer since the velocity distribution relative to the rotor is pitch periodic (Fig. 5.3.1 b). For steady absolute flow (5.3–1) converts to

$$\operatorname{grad}(p/\varrho + c^2/2 + gh) = c \times \operatorname{curl} c. \qquad (5.3-2)$$
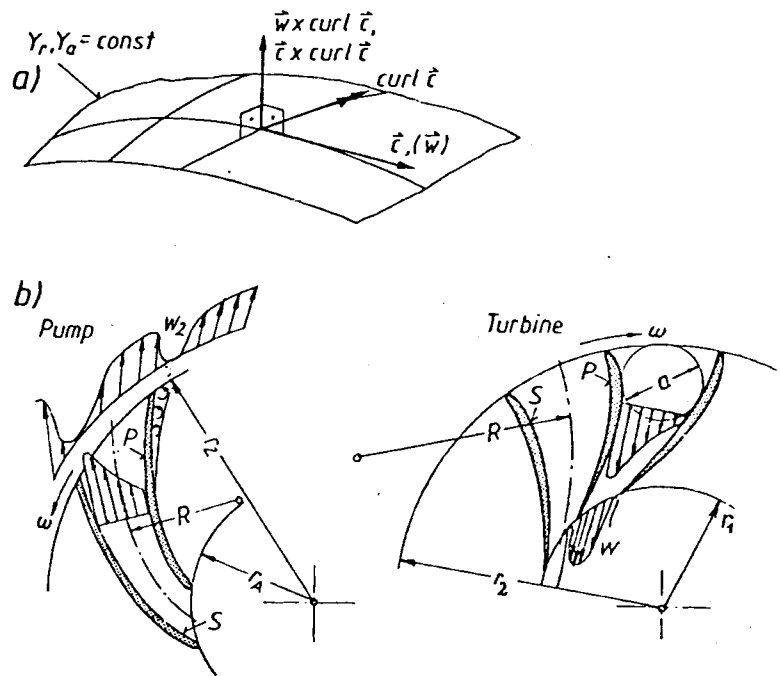
Fig. 5.3.1. Relative and absolute flow, their specific flow energies Y_r, Y_a: a) Surfaces of constant Y_r, Y_a in relation to vortex lines curl c and stream-line, parallel c, w. b) Distribution of relative velocity across the channel (left) of an impeller with backward curved vanes, and (right) of a runner with fore-ward curved vanes.

Obviously now any energy gradient is oriented normal to the surface, formed by the stream and vortex lines. Hence in a steady absolute flow any change of the specific flow energy (referred to the unit of mass) $Y_a = p/\varrho + c^2/2 + gh$ along a streamline vanishes, (*Bernouilli*'s theorem) namely

$$Y_a = p/\varrho + c^2/2 + gh = \text{constant}. \qquad (5.3-3)$$

In general the constant varies with the streamline. In the special case of a potential flow with curl $c = 0$, the right hand side in (5.3–2) vanishes. Here the relation (5.3–3) holds for the whole flow field with the same constant.

The same is also valid for a steady flow field, whose vortex and streamlines are parallel to each other (Beltrami flow). Since no energy is extracted from the fluid within the distributor of a turbine and the flow loss there is modest, it can be concluded, that within the space between the distributor and the runner any possible vortex line (mainly origi-

nating from a change of circulation over the span of a distributor vane) must be parallel to the streamlines [5.10].

5.3.2. Equation of motion and energy for a rotating frame of reference

Relation (5.1 - 1) can be adapted to a rotating frame of reference, when the absolute velocity c is replaced by the relative velocity w and the centrifugal force on unit mass due to rotation $- \text{grad}(r^2\omega^2/2)$ and the Coriolis force on unit mass $- 2w \times \omega$ are added to the left hand side of (5.3 - 1). Hence

$$\text{grad}(p/\varrho + w^2/2 - r^2\omega^2/2 + gh) - 2w \times \omega = w \times \text{curl}\, w - \partial w/\partial t. \quad (5.3-4)$$

With the transformations $\text{curl}\, u \equiv \text{curl}\, \omega \times r \equiv 2\omega$; $u + w = c$; and $\text{curl}(u + w) = \text{curl}\, c$, the equation of motion now reads

$$\text{grad}(p/\varrho + w^2/2 - r^2\omega^2/2 + gh) = w \times \text{curl}\, c - \partial w/\partial t. \quad (5.3-5)$$

Now instead of the absolute flow energy (5.3 - 3), a rothalpy appears without the term of internal energy, according to

$$Y_r \equiv p/\varrho + w^2/2 - r^2\omega^2/2 + gh. \quad (5.3-6)$$

On this occasion the individual terms of the energy Y_a and Y_r, all having the dimensions of energies per unit mass, will be comparatively interpreted. p/ϱ is a positive displacement work done by the unit mass of fluid, when shifted to a region under zero pressure. $c^2/2$ and $w^2/2$ are the kinetic energies due to the unit mass of fluid and gh the potential energy of it in the terrestrial gravity field. The term $- r^2\omega^2/2$ can be understood as the negative work done by the pressure, that balances the rotary system, to move a unit mass of fluid from the axis to a point on the radius r.

It may be mentioned that any real machine has to utilize the specific energy of a fluid within given surroundings (altitude, pressure, temperature and hence critical pressure) at inlet and outlet. Moreover a fluid flowing through a machine performs positive and negative displacement work on the system, when entering or leaving it.

Further a real slightly compressible liquid also performs expansion work within the machine. To this strictly speaking the change of internal energy of the fluid, neglected here has to be accounted for. At last for economical reasons the flow has to pass through finite cross sections, needing considerable speeds to pass, a source of losses or strictly speaking of converting orderly motion into heat.

The specific flow energy Y_a and the rothalpy (an expression used here against convention also without the internal energy term) are linked to each other by the triangular relation $c^2 = w^2 - r^2\omega^2 + 2c_u r\omega$. This gives in the case of steady flow and absolute irrotational flow (curl $c = 0$)

$$Y_a = Y_r + c_u r\omega. \quad (5.3-7)$$

On many occasions the same equations and statements may be used for either a turbine or an impeller pump. However the components in turbines and impeller pumps (from now on referred to as pumps) have different names. When this occurs, the name for the component in a turbine is followed by that for a pump in parenthesis or vice versa.

For the steady relative flow, which may be possible in a machine with sufficient distance between the runner (impeller) and distributor (diffuser) from (5.3 - 5):

$$\text{grad}(p/\varrho + w^2/2 - r^2\omega^2/2 + gh) = w \times \text{curl}\, c. \quad (5.3-8)$$

Hence the grad Y_r is normal to the relative streamline and vanishes along it. Thus $Y_r =$ constant along the relative streamline in steady relative flow (Fig. 10.3.20). This

182

constant is the same for any relative streamline if the absolute flow is irrotational (curl $c = 0$).

For the real flow with dissipation Φ_{21} along the relative stream tube of the rotor between the stations 2 and 1 due to the rotor's section of high and low pressure, the integrated relation (5.3-8) is converted into (Δ now difference)

$$\Delta_1^2(p/\varrho + w^2/2 - r^2\omega^2/2 + gh + e) = 0, \tag{5.3-9}$$

where e is the internal energy per unit mass of the fluid. According to energy theorem, and assuming the heat flow into the rotor to equal Φ_{21}, the difference of internal energy follows as $e_2 - e_1 = \Phi_{21} + \int\limits_2^1 p\,dv$.

The term $\Delta_1^2 p/\varrho$ corresponds to the surplus of displacement work, $\Delta_1^2 gh$ of gravity work, $\Delta_1^2 r^2\omega^2/2$ to that of centrifugal force due to rotation, $\Delta_1^2 w^2/2$ to that of kinetic energy, all referred to unit mass. The surplus is understood as the value at station 2 relative to 1. The measurements of Bär [5.17] and Schlemmer [5.18] have reconfirmed relation (5.3-9).

5.3.3. The role of unsteadiness for energy transmission

From the velocity triangle (Fig. 5.2.1) assuming the blade speed is constant: $dc/dt = dw/dt$. Furthermore the following relation holds between the peripheral angle φ_a of a point on the rotor, measured from a stationary radius and φ_r measured from a radius rotating with angular velocity ω, t as the time elapsed since the instant, when both radii coincided: $\varphi_a = \varphi_r + \omega t$. Since $d\varphi_a/dt = \omega$, $\partial\varphi_a/\partial\varphi_r = 1$, $w = w(\varphi_a, t)$ yields $dw/dt = (\partial w/\partial\varphi_r)(\partial\varphi_r/\partial\varphi_a)\,d\varphi_a/dt + \partial w/\partial t$. Hence

$$dc/dt = (\partial w/\partial\varphi_r)\,\omega + \partial w/\partial t. \tag{5.3-10}$$

From this it is seen, that even when the relative flow is steady $(\partial w/\partial t = 0)$, an unsteadiness of absolute flow is caused by the variation of relative velocity over the pitch of the rotor channel $(\partial w/\partial\varphi_r \neq 0)$, (see Fig. 5.3.1 b).

This variation of w gives from (5.3-6) for the case $Y_r = $ constant (i.e. absolute potential flow) the variation of pressure across the channel and with it the differential pressure on a blade element of the runner (impeller). This enables the conversion of shaft work into flow energy and vice versa.

5.3.4. The momentum theorems

I. General remarks: The application of the energy equation and the equation of motion requires a detailed knowledge of the flow field. In some cases, e.g., that of the jet onto the bucket of an impulse turbine, the flow field on a definite face is known, e.g. on the jet cross section upstream of the bucket. From this starting point, the force which is exerted by the fluid on a particular body is required, e.g. the force the jet exerts on the runner.

II. The momentum theorem: For the solution of this task, an inner control surface on a body (Fig. 5.3.2 a) with unknown force F is surrounded by the fluid, that is enclosed by an outer control surface A, on which the pressure and the momentum flow are known theoretically or by measurement.

Newton's equation of motion is applied to the fluid within this control space, see e.g. Truckenbrodt [5.3]. As this holds good for a certain fluid mass, special attention has to be
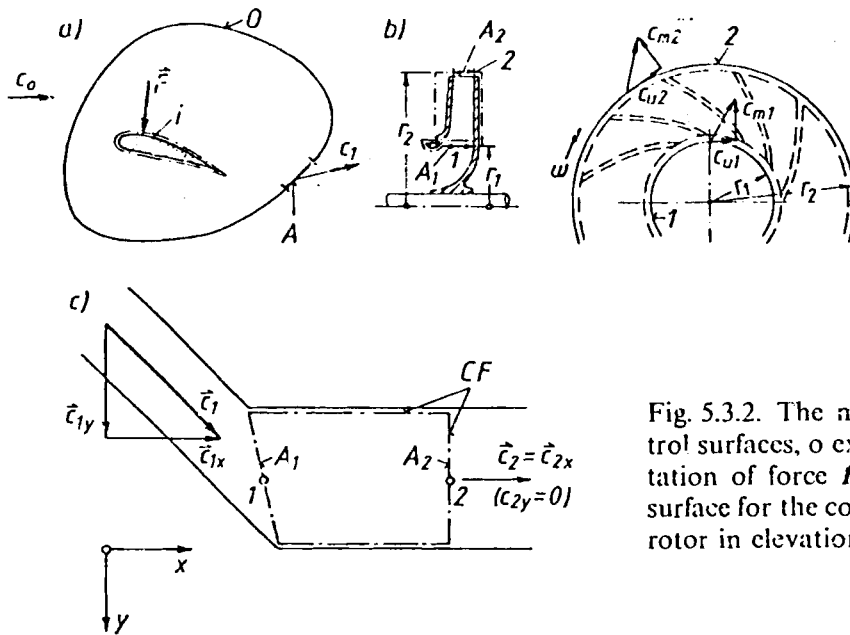
Fig. 5.3.2. The momentum theorem. a) Control surfaces, o external, i internal, for computation of force F on an aerofoil. b) Control surface for the computation of the torque on a rotor in elevation. c) Shock loss.

paid to the fact that this mass now passes through the outer control surface, acting on it by its momentum, when entering the control volume and reacting, when leaving it. Hence with k as a force per unit volume the momentum theorem for the control volume V and its outer control surface A, reads

$$F = \int_V k\,dV + \int_A p\,dA + \int_A \varrho c \cdot (c\,dA) + \frac{\partial}{\partial t} \int_V \varrho c\,dV. \qquad (5.3-11)$$

The first term on the right hand side is due to the volume force within V, the second due to pressure on the outer control surface A, the third due to the flow of momentum through A, and the fourth due to the rate of momentum within the volume V.

III. The Angular momentum theorem: This relates the unknown moment M on the submerged body (Fig. 5.3.2 b) to the known moments exerted on the control volume V and its outer control surface A by the force terms in (5.3–11). Hence the theorem

$$M = \int_V (r \times k)\,dV + \int_A p(r \times dA) + \int_A \varrho(r \times c)(c\,dA) + \frac{\partial}{\partial t} \int_V \varrho(r \times c)\,dV. \qquad (5.3-12)$$

5.3.5. Problems using the momentum and energy theorems

5.3.5.1. Euler's equation

For an ideal fluid ($e = 0$), and a steady absolute potential flow following from an infinitely high vane number in the rotor, the proof of *Euler*'s equation is easy. Then with $u = r\omega$, $gH = Y_{a2} - Y_{a1}$ from (5.3–7) and (5.3–9) it follows

$$gH = c_{u2}u_2 - c_{u1}u_1.$$

For the real unsteady absolute flow through a runner the angular momentum theorem (5.3–12) has to be applied. First, the runner is surrounded by a control surface A (Fig. 5.3.2 b). This follows the internal, wetted surfaces of hub, shroud and vanes and is closed before the rotor inlet 2 and behind the rotor exit 1 by axisymmetric faces A_2 and

184

A_1, with a distance from the inlet and outlet edges of blades such as to have whirl velocities c_{u2} and c_{u1} uniform along the periphery.

Leakage is neglected. Hence the mass flow $\dot{m}$ through the runner crosses only through the faces A_2 and A_1. The disk friction on the outer faces of hub and shroud is disregarded.

Because of the axisymmetrically assumed flow through the faces A_2 and A_1, the surface forces there due to p do not exert a torque about the axis, and those due to τ are negligible. The axisymmetric volume V excludes any torque by weight.

The torque on the runner M_a is transmitted by wall pressure and shear stress on the wetted surfaces of vanes, hub and shroud mentioned above.

Assuming either an elementary runner of small breadth b and axisymmetric streamfaces with the radii r_2, r_1 and the whirl components c_{u2}, c_{u1} at 2 and 1, or a real runner of finite breadth b, in which r_1, r_2, c_{u1}, c_{u2} are mean values over the spans [4] b_1 and b_2, the angular momentum theorem (5.3–12), considering the unsteady absolute flow in the runner channel (Cap. 5.3.3) gives the torque as

$$M_a = \dot{m}(c_{u2}r_2 - c_{u1}r_1) + \frac{\partial}{\partial t} \int_V \varrho(r \times c)\,dV. \tag{5.3–13}$$

The disappearance of the unsteady term in the final solution of the torque may be realized as follows.

Consider a volume strip dV of elementary breadth db and elementary meridional length ds_m along the unobstructed pitch $2\pi r\Phi/z$ (z being the vane number, Φ the contraction coefficient due to the thickness of vane, and wall-attached stall). The relevant component of $(r \times c)$ is rc_u.

The absolute whirl velocity c_u along the pitch can be split into a time-independent, pitch-averaged term c_{uM} and into a pitch-periodical term c_u', whose pitch-averaged value vanishes according to

$$0 = \int_0^{2\pi\Phi/z} c_u'\,d\varphi, \quad \varphi \text{ being the peripheral angle.}$$

Hence, the only unsteady contribution of dV to the unsteady torque term dM_a' in (5.3–13) reads as $\varrho r^2 ds_m db \int_0^{2\pi\Phi/z} (\partial c_u'/\partial t)\,d\varphi$, and this term vanishes according to the definition of c_u' and the obvious relation $\partial t = \partial\varphi/\omega$, in which ω is the angular velocity with which the increment of azimuth $d\varphi$ is covered in the time interval ∂t.

Hence the torque of the runner

$$M_a = \dot{m}(c_{u2}r_2 - c_{u1}r_1). \tag{5.3–14}$$

Note that the whirl c_{ui} here is in the sense of the runner's rotation with angular velocity ω. Hence the so-called peripheral output $P_u = \omega M_a$. In a real turbine with a peripheral efficiency η_u (due to loss in the distributor, the runner the draft tube and due to exchange of momentum between rotary and stationary parts), this output is also given as $P_u = \dot{m}gH\eta_u$. Eliminating P_u with $r\omega = u$ yields Euler's equation, originally cited without η_u, as [5.1]

$$gH\eta_u = c_{u2}u_2 - c_{u1}u_1. \tag{5.3–15}$$

5.3.5.2. The shock loss due to diffusion and deflection

At the inlet of vaned cascades, e.g. rotor, when a turbomachine operates away from the bep, its throughflow velocity is subjected to a sudden change in magnitude and direction.

---

[4] Span (here and elsewhere, sometimes also denoted by breadth) defines an extension of a rotor normal to its meridional streamlines.

The resulting shock-loss, especially in the case of deceleration, is studied on the model of ideal one-dimensional, steady pipe flow (Fig. 5.3.2c).

The shock loss ΔY_s appears as a change of specific flow energy Y_a, as in (5.3–3), between inlet and outlet of the hatched control face (Fig. 5.3.2c) due to the sudden change of channel geometry. Hence

$$\Delta Y_s = (p_1 - p_2)/\varrho + (c_1^2 - c_2^2)/2. \qquad (5.3-16)$$

To eliminate the pressure term, the momentum theorem in the horizontal direction is applied on the hatched control face with respect to the mass influx $\dot{m} = \varrho c_2 A_2$

$$(p_1 - p_2) A_2 = \varrho A_0 c_1 c_{1x} - \varrho c_2^2 A_2. \qquad (5.3-17)$$

By means of continuity, $c_2 A_2 = c_1 A_0$, the pressure term may be expressed by $(p_1 - p_2)/\varrho = c_2^2 - c_{1x} c_2$. This in (5.3–17)

$$\Delta Y_s = (c_1^2 - 2 c_{1x} c_2 + c_2^2)/2 = (c_1 - c_2)^2/2 = c_s^2/2. \qquad (5.3-18)$$

In practice, a correction factor $\varphi_s < 1$ is added to the right hand side. This is essential to distinguish between accelerating shock ($\varphi_s \to 0$) and decelerating shock ($\varphi_s \to 1$), see also *Petermann* [5.19]. $c_1 - c_2 = c_s$ is denoted as shock velocity.

5.3.5.3. The shock loss due to the action of turbo machines

The main aim of this section is to express the shock loss in terms of the discharge Q and Q_{op} of an arbitrary operating point and the bep. Hence the influence of this essential loss on the characteristic is obtained (bep = best efficiency point).

For this purpose the bep is assumed to be connected with

a) a whirl-free flow at runner exit 1. Hence $c_{u1} = 0$ and

$$\cot \beta_1 = u_1/c_{m1b}, \qquad (5.3-19)$$

where u_1 is the blade speed, c_{m1b} the meridional speed at the bep in 1, β_1 the angle the relative speed makes with the periphery, (β_1 nearly coincides with the vane angle β_1^* and is retained under any flow Q, being always assumed along the fixed runne vane),

b) a shockless flow at inlet 2 of the runner vane channel. Moreover the flow is assumed to behave like that in a pipe.

Hence the angle β_2^* the runner vane makes at 2 with the periphery, results from the inlet triangle of velocities and Euler's equation after a) as (Fig. 5.3.3)

$$\cot \beta_2^* = (u_2 - g \eta_{ub} H/u_2)/c_{m2b}, \qquad (5.3-20)$$

where c_{m2b} is the meridional speed at the bep at 2, η_{ub} the peripheral efficiency at the bep. Obviously (Fig. 5.3.3) the shock velocity vector (taken in the sense of (5.3–18)) at runner inlet reads

$$c_s = w_{u2} - w'_{u2}, \qquad (5.3-21)$$

where w'_{u2} is the relative whirl due to overload (here considered as that load which causes a decelerating shock at runner inlet, especially loss-linked) and w_{u2} the shockless relative whirl due to the meridional speed c_{m2} at 2 under overload (Q).

The velocity triangle demonstrates, that

$$w_{u2} = u_2 - c_{u2}, \qquad (5.3-22)$$

186
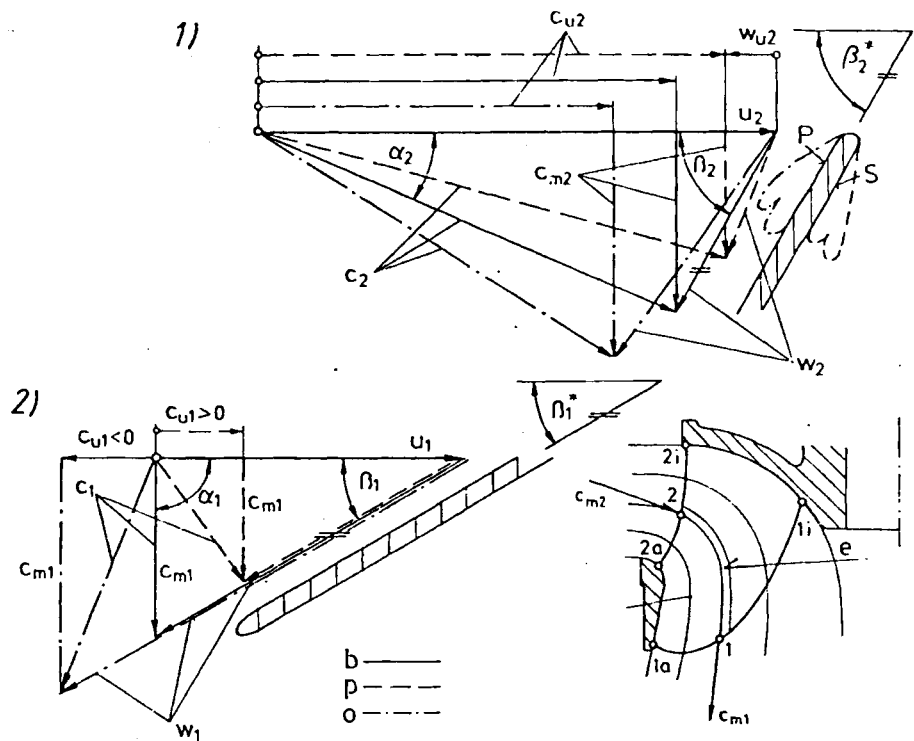
Fig. 5.3.3. Velocity triangles of a turbine runner at inlet 2, outlet 1; operating at: b bep; p part load; o overload. If the bep corresponds to $c_{u1} = 0$ and shockless inlet ($\beta_{2\,bep} = \beta_{2b} = \beta_2^x$), then the wake downstream of the inlet edge on the pressure face P is due to overload o, and that on the suction face S due to part load p.

$$w'_{u2} = c_{m2} \cot \beta_2^*, \tag{5.3-23}$$

where u_2 is the blade speed at 2. The absolute whirl c_{u2} at 2 under overload is obtained from *Euler*'s equation together with the reduction of the absolute exit whirl c_{u1} under overload due to c_{m1}, u_1 and β_1 by $c_{u1} = u_1 - c_{m1} \cot \beta_1$. Thus

$$c_{u2} = (gH\eta_u + u_1^2 - u_1 c_{m1} \cot \beta_1)/u_2, \tag{5.3-24}$$

where η_u is the peripheral efficiency under overload. Here c_{u1} turns against u_1, since $c_{m1} \cot \beta_1 > u_1$.

From now on the peripheral efficiency might be unvariable

$$\eta_u = \eta_{ub} = \text{const}, \tag{5.3-25}$$

which, in the usual working range, may include an error up to 10%. The continuity reads (henceforth subscript *op* instead of *b* at bep)

$$Q/Q_{op} = c_{m1}/c_{m1\,op} = c_{m2}/c_{m2\,op}. \tag{5.3-26}$$

Inserting (5.3–22) and (5.3–23) in (5.3–21) and respecting (5.3–19), (5.3–20) and (5.3–24) through (5.3–26), the shock velocity reads

$$c_s = [(Q_{op} - Q)/Q_{op}](u_2 - gH\eta_u/u_2 - u_1^2/u_2). \tag{5.3-27}$$

Hence and with respect to (5.3–18) the shock loss at rotor inlet in a certain turbo machine can be described by

$$\Delta Y_s = \text{const}(Q_{op} - Q)^2. \tag{5.3-28}$$

This holds especially for the decelerating shock. In a turbine this occurs under overload and in a pump under part load. Strictly speaking the description of the behaviour of a given hydro turbo-machine requires different values of the constant in (5.3-28) in the part and overload range. This is a consequence of the different dissipation by shock in acceleration and deceleration. The validity of the above shock loss relation also for a pump can be proved more easily than above by means of the velocity triangles at the leading edge of a pump rotor then valid for the different loads shown in Fig. 8.2.10.

5.4. Theory of real fluid flow

5.4.1. Properties of real liquids

I. Compressibility: Compressibility is defined by the relative change of density $d\varrho/\varrho$ under a pressure increment dp by (5.2–4) in which the bulk modulus E_L for water at 290 K: $E_L = 2,1 \cdot 10^9$ Pa. Hence ϱ varies even under the actual highest head (Reißeck, Austria with $H = 1760$ m) only by 0,83%.

Strictly speaking, the compressibility converts the pressure term of the specific energy from p/ϱ into $\int dp/\varrho$ and requires the introduction of a change of internal energy e into the head (1.6–1). Neglecting any heat transfer in the machine, then $e_{II} - e_I = -\int\limits_{I}^{II} p\,dv$, [4.26].

Once the admissible error of results is prescribed, compressibility has to be accounted for e.g., in efficiency calculation from a certain head on (about 200 m). It is always required for water hammer calculations, Cap. 8.3.

II. Surface tension: This is a force per unit length acting on the section of the interface of a liquid with gas e.g., water against air, $\sigma = 0,073$ N/m. It may be understood as the resistance of the adjacent fluids to increase the contact face in consequence of molecular attraction from the interior of the liquid [5.3].

σ influences the bubble growth rate at the onset of cavitation, if the bubble radius is below 0,1 mm. Capillarity effects influence the smallest diameter practicable of tappings and manometer tubes [5.3].

III. The viscosity and resulting classifications of liquids: Liquids are classified by their shear behaviour. A shear stress τ occurs between adjacent layers slipping against each other. τ depends as follows on the strain rate $\partial c/\partial y$:

a) Newtonian fluids: Here $\tau = \eta \, \partial c/\partial y$, in which c is the velocity, y the coordinate normal to it and η the dynamic viscosity. For the usual liquid the viscosity drops as temperature rises. This originates from the increasing distance between the molecules, since the viscous force is mostly caused by molecular attraction.

This "viscous shear stress" appears in a Newtonian fluid only, when the flow regime is laminar. This occurs below a definite strain rate and the related Reynolds number (see later). Above this threshold, the steady motion of the fluid has turbulent velocity fluctuations in and across the main flow direction superimposed.

Usually the kinematic viscosity is used, defined by $\nu = \eta/\varrho$. ν also drops with rising temperature, e.g., for water: at 0°C, $\nu = 1,8 \cdot 10^{-6}$ m²/s; at 20°C, $\nu = 10^{-6}$ m²/s; at 70°C $\nu = 0,4 \cdot 10^{-6}$ m²/s. It is therefore understandable, that as found by Riemerschmidt's [5.20] tests, the decisive wall shear stress losses of a hydro turbine drop by 25% with a temperature rise from 0° to 70°C.

This is also true for the turbulent flow regime, since the velocity fluctuations there dis-

appear in the laminar sublayer, next to the wall. The wall shear stress is the main source of loss.

b) Non-Newtonian fluids: Here $\tau = \tau_0 + k(\partial c/\partial y)^n$, in which τ_0 is the yield shear stress, e.g. tooth paste needs a definite pressure to overcome the yield stress before it pops out of the tube. k is the "stiffness number". It depends on the amount of suspended material in the liquid. Thus the above may also hold for "real water". Moreover these fluids have a "memory".

5.4.2. The stress tensor

For the following imagine a small parallelepiped with its edges dx, dy, dz in the directions of and its faces A_x, A_y, A_z normal to the directions of the x-, y-, z-axis respectively. On the face A_x normal to the x-axis, the following stress components exist (Fig. 5.4.1 a): σ_{xx} as a tensile stress, normal to the face A_x in the x-direction, σ_{xy} as a shear stress in the y-direction. (1st subscript: Direction of A, 2nd: Direction of σ_{ij}).
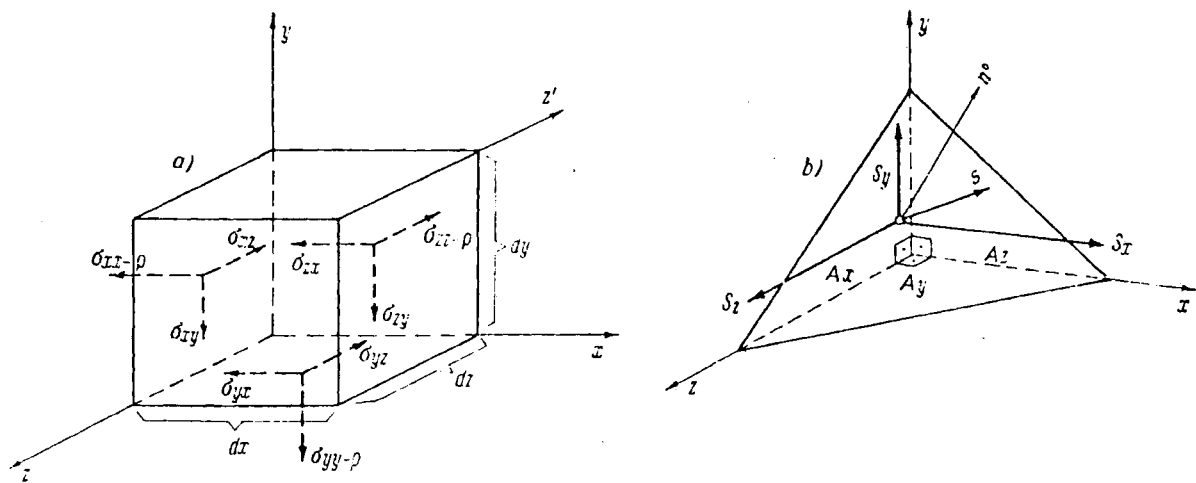
Fig. 5.4.1. Stresses. a) Parallel epiped with stresses on its surface. b) Tetrahedron with an arbitrarily orientated surface, area A, normal vector n^0, and stress s.

The balance of moments acting around the axes gives for the case of vanishing moments proportional to the element's volume: $\sigma_{yz} = \sigma_{zy}$; $\sigma_{yx} = \sigma_{xy}$; $\sigma_{xz} = \sigma_{zx}$. This holds good in the following.

Imagine now a tetrahedron (Fig. 5.4.1 b) formed by the coordinate planes and a plane face, whose orientation is given by its unit normal vector $n^0 = (\cos(n^0, x), \cos(n^0, y), \cos(n^0, z))$. On this face acts the stress $s = (s_x, s_y, s_z)$. The equilibrium of forces in the x-direction gives

$$s_x = \sigma_{xx} \cos(n^0, x) + \sigma_{xy} \cos(n^0, y) + \sigma_{xz} \cos(n^0, z). \tag{5.4-1}$$

That means, the x-component of stress s depends linearily on all the components of the normal vector n^0 of the face on which s acts. Hence s is a tensor T_s of n^0 or, $s = T_s n^0$. Because of the linearity of this relation a spherical tensor T_p due to the hydrostatic pressure $-p$ may be superimposed. Hence

$$s_{res} = (T_s + T_p) n^0, \tag{5.4-2}$$

189

where $s_{n,n}$ is the resulting pressure on the face, normal to n^0, T_s and T_p are defined by the following tensor matrix

$$T_s = \begin{pmatrix} \sigma_{xx} & \sigma_{xy} & \sigma_{xz} \\ \sigma_{xy} & \sigma_{yy} & \sigma_{yz} \\ \sigma_{xz} & \sigma_{yz} & \sigma_{zz} \end{pmatrix},$$ (5.4-3)

$$T_p = \begin{pmatrix} -p & 0 & 0 \\ 0 & -p & 0 \\ 0 & 0 & -p \end{pmatrix}.$$ (5.4-4)

In reality the stress components σ_{ij} are due to viscosity and hence appear only in a moving fluid, $-p$ acts also in a static fluid in consequence of weight and mainly of exchange of momentum due to the Brownian molecular motion. Hence in agreement with experience and after *Pascal's* theorem [5.3] at a certain point and on an arbitrarily oriented face large relative to the molecules, $-p$ is constant.

According to a rule for symmetrical tensors [4.26] like T_s and T_p the mean value of the sum of normal stresses due to the three coordinate planes, normal to each other, is independent of the orientation of these planes. Accordingly

$$\sigma_{res} = -p + (\sigma_{xx} + \sigma_{yy} + \sigma_{zz})/3 = \text{const.}$$ (5.4-5)

This includes also *Pascal's* theorem of an ideal fluid with $\sigma_{ij} = 0$ and hence $-p = \text{const.}$

5.4.3. The relation between stress and strain rate

From (5.4-3) and (5.4-28) it is seen that the tensors of stress and strain rate are symmetrical to their main diagonal. Under the assumption that the principal axes of both the tensor ellipsoids coincide, both the tensors are assumed to be proportional to each other according to $T_s = 2\eta T_c$, η being the dynamic viscosity.

With the relation $dc_{def}/dn = T_c n^0$ derived from (5.4-27) and (5.4-2) the above proportionality of T_s and T_c gives

$$s_{res} = 2\eta \, dc_{def}/dn.$$ (5.4-6)

In (5.4-27) any compressibility was neglected. In a real compressible fluid the rate of strain originating from pressure $-p$, being $-(1/3)\,\text{div}\,c$ is imagined to occur as an additional strain rate in the three coordinate directions due to the linear extension rates $\partial c_i/\partial i$. Incorporating this into dc_{def}/dn and using tensor notation gives the following relation between viscous stress σ_{ij} and the strain rate, when neglecting a special term due to bulk viscosity [5.3]. and employing "the *Kronecker* δ_{ij}", 0 for $j \neq i$ and 1 for $j = i$,

$$\sigma_{ij} = \eta(\partial c_i/\partial j + \partial c_j/\partial i - (2/3)\,\delta_{ij}\,\text{div}\,c).$$ (5.4-7)

A relation of this kind, without the δ_{ij} was first postulated by *Navier* [5.21] and *Stokes* [5.22]. The Newtonian relation between shear stress and strain rate, $\sigma_{xy} = \eta\,\partial c_x/\partial y$, may be considered as a forerunner.

5.4.4. The Navier Stokes equation

Constituting the equation of motion for unit mass of a real viscous fluid needs in addition to that of an ideal fluid, (5.3-1), the stress term $\partial p_x/\partial x + \partial p_y/\partial y + \partial p_z/\partial z$, where

190

$p_x = (\sigma_{xx}, \sigma_{xy}, \sigma_{xz})$, $p_y = (\sigma_{yx}, \sigma_{yy}, \sigma_{yz})$, $p_z = (\sigma_{zx}, \sigma_{zy}, \sigma_{zz})$ are the stress vectors in the three coordinate planes. Hence the equation of motion in tensorial manner is

$$\partial(p/\varrho + gh)/\partial j + c_j \partial c_i/\partial j + \partial c_i/\partial t - \frac{1}{\varrho}\partial\sigma_{ij}/\partial j = 0. \tag{5.4-8}$$

Introducing the stress σ_{ij} from (5.4–7) gives the *Navier Stokes'* equation for a slightly compressible fluid (div $c \neq 0$, from (5.2–5))

$$\text{grad } Y_a - c \times \text{curl } c + \partial c/\partial t - v(\Delta c + \tfrac{1}{3}\text{grad}(\text{div } c)) = 0. \tag{5.4-9}$$

5.4.5. Boundary layer theory

In a plane, incompressible, steady flow without gravity, the x-component of (5.4–9) reads

$$(1/\varrho)\,\partial p/\partial x + c_x \partial c_x/\partial x + c_y \partial c_x/\partial y - v(\partial^2 c_x/\partial x^2 + \partial^2 c_x/\partial y^2) = 0. \tag{5.4-10}$$

It is known by experience, that the plane flow around a smoothly curved body shows viscous effects only in the so-called "boundary layer" close to the wall (Fig. 5.4.2 a). According to *Prandtl* [5.23] a flow in the x-direction is assumed along the face of this body. The y-axis is normal to this face. On the surface of the body the fluid comes to rest. Within the very thin boundary layer of thickness δ the velocity reaches the constant value of the free flow C (U in Fig. 5.4.2 a).

The motion normal to the body nearly disappears. Therefore there is no pressure drop across the layer. The pressure from outside acts through the layer. Moreover the term with c_y vanishes. In the case of a flow along a plate, now considered, the pressure gradient of the free flow and hence the term $\partial p/\partial x$ vanishes. dx should be of the order of the distance x from the leading edge of the plate. c_x and dc_x should be of the order C. Hence $c_x \partial c_x/\partial x$ is of the order C^2/x.

The first viscous term in (5.4–10) being of the order of vC/x^2 can be neglected in comparison with the second term which is of the order vC/δ^2. Hence only the second and fifth term in (5.4–10) remain, being of the order C^2/x and vC/δ^2 respectively. Introducing a Reynolds number $Re = Cx/v$, the boundary layer thickness grows along the plate according to $\delta \sim x\,Re^{-1/2}$. Strictly speaking for laminar flow [5.24]

$$\delta = 1{,}75\,x\,Re^{-1/2}. \tag{5.4-11}$$

Example: Given $x = 1$ m, $C = 30$ m/s, $v = 10^{-6}$ m^2/s: $\delta = 0{,}32 \cdot 10^{-3}$ m. Hence the wall shear stress is of the order of $\tau \sim \eta C/\delta$. For water with $\eta = 10^{-3}$ Pas: $\tau \approx 100$ Pa.

5.4.6. Flow in straight pipes

5.4.6.1. General phenomena and laminar flow

In the case of an internal flow along a straight pipe, the boundary layer grows from the inlet up to the point, at which the boundary layers of oppositely located walls merge. Downstream of this station, the whole pipe is filled with boundary layer. For laminar flow this "inlet length" from the pipe inlet to this station depends on the Reynolds number and is of the order of 60 pipe diameters (see Fig. 5.4.2 b). For the turbulent flow regime, this length is shorter.
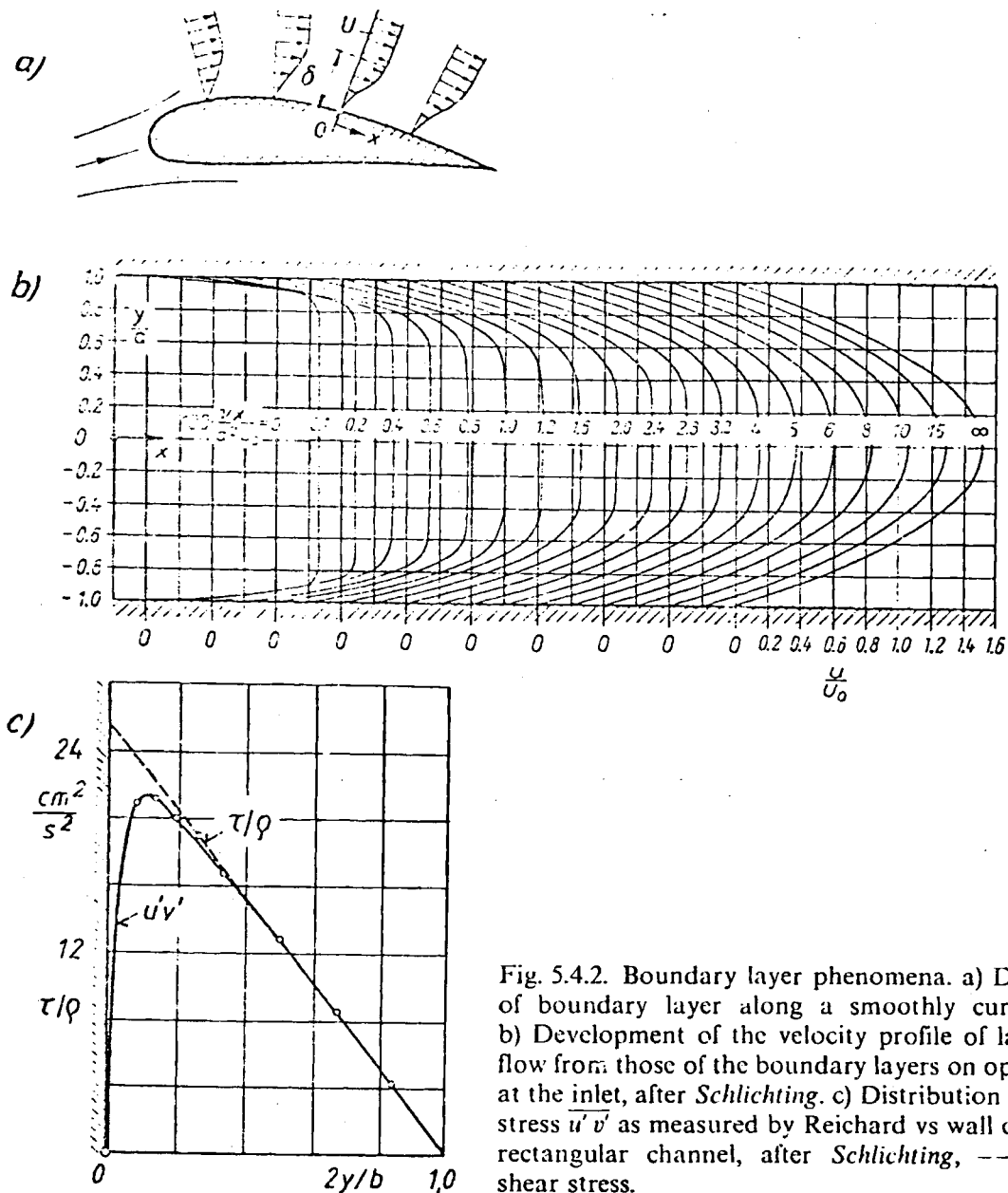
Fig. 5.4.2. Boundary layer phenomena. a) Development of boundary layer along a smoothly curved profile. b) Development of the velocity profile of laminar pipe flow from those of the boundary layers on opposite walls at the inlet, after *Schlichting*. c) Distribution of Reynolds stress $\overline{u'v'}$ as measured by Reichard vs wall distance in a rectangular channel, after *Schlichting*, – – – resulting shear stress.

Downstream of this station, the pipe flow is said to be fully developed. Hence only developed pipe flow is considered.

From theory the pressure gradient $\partial p/\partial x = \Delta p/L$ in the flow direction is constant across the pipe radius r. The pressure drop Δp along the pipe length depends on the mean velocity c_M. For an axial flow in a pipe of radius R this is defined by

$$c_M = (2/R^2) \int_0^R r\,c(r)\,dr.$$ (5.4–12)

Hence the pressure in a pipe of diameter $\bar{d} = 2R$

$$\Delta p = \lambda(L/d)\,\varrho\,c_M^2/2,$$ (5.4–13)

where the friction coefficient λ (Fig. 4.6.1) depends on the Reynolds number defined by

$$Re = d c_M / v. \qquad (5.4-14)$$

From the origin of (5.4-11) it is realized, that in a free laminar boundary layer with a certain ratio δ/x at a definite station x the Reynolds number may be understood as the ratio of momentum flux into the boundary layer, of thickness δ, to the force due to viscous shear stress, balancing it.

This may be extended to pipe flow, when $\delta = d/2$ and τ on the periphery of a fluid cylinder, coaxial to the pipe axis, of radius r and length L, is replaced by the pressure drop, balancing this in the x-direction of the pipe axis, according to

$$\tau = - \Delta p r /(2 L). \qquad (5.4-15)$$

In the case of laminar pipe flow with $Re < 2300$ and the shear stress σ_{rx} from (5.4-7), now $\tau = - \eta \partial c / \partial r$, (5.4-15) gives a parabolic velocity distribution $c = c_0 [1 - (r/R)^2]$ after Hagen and Poiseuille [5.25; 5.26], where c_0 is the velocity on the pipe centre line. Inserting this c in (5.4-12) yields $c_M = c_0/2$, which is now linked to Δp and η by

$$\Delta p = 8 \eta L c_M / R^2. \qquad (5.4-16)$$

Inserting this Δp in (5.4-13) gives for the laminar flow regime the pipe loss coefficient as a distinct function of Re, namely $\lambda = 64/Re$.

In the transition regime about $Re = 2300$, λ depends also on the relative wall roughness and its character, e.g. sand roughness according to Nikuradse [5.27] technical roughness as defined by Strscheletzky [5.28], but also, after tests of E. Burka, Gdansk (Poland) on such effects as the amplitude and frequency of wall vibrations. Such tests demonstrate that with Re increased the flow becomes increasingly unstable, especially through the layer close to the wall, where strain rate is highest and hence also the tendency to turbulence.

5.4.6.2. Turbulent flow and transition

Turbulent flow is defined by the fact, that on a time-averaged constant velocity component $\bar{c}_i$ and pressure $\bar{p}$ are superimposed corresponding fluctuations c_i' and p', the time-averaged value of each of which is zero. Thus: $c_i = \bar{c}_i + c_i'$ and $p = \bar{p} + p'$. The intensity of turbulence is defined by

$$Tu = [(\overline{c_x'^2} + \overline{c_y'^2} + \overline{c_z'^2})/3]^{1/2}/[\bar{c}_x^2 + \bar{c}_y^2 + \bar{c}_z^2]^{1/2}. \qquad (5.4-17)$$

Turbulence is created by the fact, that above a definite strain rate, i.e. $\partial c / \partial r$ in the case of pipe flow, which always occurs first close to the wall, the fluid elements there try to escape to flow regions with lower strain rate, away from the wall. Mass conservation requires, that fluid particles of high velocity more distant from the wall migrate into the wall zone [5.28].

Due to the cross fluctuations, adjacent flow laminae mix. Thus the flow is more uniform than a laminar one. This causes also an exchange of momentum, due to the main flow, between adjacent layers. Thus the so called "apparent shear stress" (after O. Reynolds [5.29]) act between them. With c_r' and c_x' as velocity fluctuations in the r-and x-directions, the shear stress τ_{Tu} due to turbulence on a coaxial fluid cylinder in a pipe reads

$$\tau_{Tu} = - \varrho \overline{c_x' c_r'}. \qquad (5.4-18)$$

Here the bar indicates a time-averaged value. Since both the velocity fluctuations are proportional to the mean pipe velocity c_M, the shear stress is given by $\tau_{Tu} = - \varrho k c_M^2$, in which the parameter k depends on Re and the relative roughness.

After (5.4 - 15) and according to tests of *Reichhardt* (Fig. 5.4.2c) [5.30], the resulting shear stress τ on a coaxial fluid cylinder in a pipe grows linearly with the radius r. τ must be split into τ_{r_u} and τ_{l_u} due to viscous effects. Reduction of τ_{l_u} to η and strain rate $\partial c/\partial r$ needs the velocity distribution $c(r)$. The latter, useful for calculation of wall shear stress in the so-called laminar sublayer, is not as simple as in the case of laminar flow. This holds true especially close to the wall, where the flow field is strongly influenced by the roughness structure of the latter.

Hence in practice the wall shear stress in the turbulent regime is expressed similar to τ_{r_u} and according to tests

$$\tau_{w} = k_0 \varrho c_M^2 Re^{-1/n}, \qquad (5.4-19)$$

where according to tests of *Blasius* [5.31] for Re about 10^5: $k_0 = 0,03955$; $n = 4$. Inserting τ_{w} into (5.4-15) with $r = R = d/2$ yields the pressure drop as $\Delta p = 8 k_0 Re^{-1/n} \varrho(L/d)$ $c_M^2/2$. This shows that the general relation for the pressure drop (5.4-13) agrees with the turbulence and equilibrium, when

$$\lambda = 8 k_0 Re^{-1/n}. \qquad (5.4-20)$$

This is proved by the λ vs Re plot in the turbulent regime for smooth-walled pipes (Fig. 4.6.1). The influence of wall roughness on λ due to magnitude and structure of obstructions, obviously predominating then, can be found only by careful investigations, as was done by *M. Strscheletzky* [5.28].

Many attempts have been made to describe the distribution of the time-averaged velocity $\bar{c}$ by one relation. A simple one reads

$$\bar{c} = c_0(1 - r/R)^{1/m}, \qquad (5.4-21)$$

with c_0 as the velocity along the pipe axis and m as a figure depending on Re. For $Re = 4 \cdot 10^3 \dots 3,24 \cdot 10^6$; $m = 6 \dots 10$. Inserting (5.4-21) in (5.4-12) relates c_0 to the mean pipe velocity

$$c_M = \{2m^2/[(1 + m)(1 + 2m)]\} c_0. \qquad (5.4-22)$$

The approximation (5.4-21) fails on the wall with $\partial c/\partial r = \infty$. A detailed investigation shows that a general law for the velocity distribution $c(r)$ over the whole range $0 < r < R$ is not practicable. At least three zones with transitions between them must be distinguished [5.4], [5.32; 5.33].

The most essential intermediate zone is characterized by the fact, that the turbulence-induced shear stress τ_{r_u} attains its maximum. Hence *Prandtl* has postulated $\tau_{r_u} = \text{const}$ [5.32]. Further he assumed the time-averaged amount $[c_i'^2]^{1/2}$ of both the fluctuation c_r' and c_x' in (5.4-18) to be proportional to a mixing length $l = \kappa y$, y being the wall distance, and proportional to the cross gradient of $\bar{c}$: $d\bar{c}/dy$. Inserting the above into (5.4-18) yields, in good agreement with tests, a logarithmic distribution of velocity vs wall distance y as

$$\bar{c}/c_0^x = A + B \ln(c_0^x y/v), \qquad (5.4-23)$$

with A, B and c_0^x as empirical parameters, which must be adapted to the neighbouring regions [5.3; 5.4].

O. Reynolds assumed initially, that turbulence is created by instability. For this purpose *H. A. Lorentz* developed the so-called energy method [5.34]. Since this did not agree with tests, the method of small perturbations was developed for two dimensional flow. On this base *W. Tollmien* [5.35 to 5.37] was the first to calculate the instability point of a flat plate [5.37].

This was experimentally proved later on by wind tunnel tests of *Schubauer* and *Skramstad* [5.38]. *Tollmien* found a streamfunction, which simultaneously satisfies the equation of motion and

194

continuity due to the fluctuations. Then he calculated the neutral line for retained fluctuation amplitude as a function of *Reynolds* number due to the boundary layer and wave length of distortion [5.3; 5.4; 5.35].

Recent findings on boundary layer prediction and an exhaustive survey on this subject came from *Truckenbrodt* [5.39]. An important perception is the increase or decrease of turbulence in the boundary layer by a streamwise deceleration or acceleration respectively of the adjacent main flow (see Cap. 9.7).

5.5. Loss mechanism due to real flow in hydro turbomachines

5.5.1. Some general remarks on loss in hydro turbo machinery

Since all the phenomena in nature are connected with an increase of entropy, each uniform motion has the tendency to convert itself by irreversible processes into irregular molecular motion and thereby into waste heat. Thus, e.g. in a turbine, a portion of energy first available in a form convertible into shaft work, is lost for this purpose.

This transformation occurs by dissipation mainly in boundary layers and wakes or zones of high vorticity. In certain sections of turbomachines the fluid possesses a larger portion of its specific energy as kinetic energy, when compared with positive displacement engines. A certain portion of this orderly planned motion is converted into disordered molecular motion of the fluid. Hence the loss of the fluid engine is relatively large.

This procedure increases the temperature of the fluid and hence its internal energy. It also increases somewhat the specific volume of the fluid and hence its expansion work $\int p \, dv$ in a turbine. In closed loops and high head machines the loss results in a measurable rise of fluid temperature.

5.5.2. Some loss mechanism of general character

The dissipation Φ as one of the essential loss mechanisms in real flow corresponds to the work done per unit time by the stresses σ_{ij} in connection with the rate of strain $\partial \bar{c}_i / \partial j$. Thus [5.3]

$$\Phi = \int_V \sigma_{ij} (\partial \bar{c}_i / \partial j) \, di \, dj \, dk. \tag{5.5-1}$$

τ_{ij} is composed of viscous and apparent (*Reynolds'*) stress as

$$\sigma_{ij} = \eta (\partial \bar{c}_i / \partial j + \partial \bar{c}_j / \partial i) - \varrho \overline{c_i' c_j'}, \tag{5.5-2}$$

where $\bar{c}_i$ = time-averaged velocity, c_i' = velocity fluctuation.

For convenience the non-linear fluctuating term, only known (if any at all) from measurements is replaced by $\eta_{ed} (\partial \bar{c}_i / \partial j + \partial \bar{c}_j / \partial i)$, in which η_{ed} is the eddy viscosity. There are several expressions for η_{ed}, e.g. that of *van Driest* [5.40].

The second term of (5.5-2) prevails in the practically important turbulent regime. Only in the laminar sublayer close to the wall is the viscous stress of the same order as the apparent stress [5.28].

195

5.5.3. Interaction of main flow and boundary layer, stall

Interaction between main flow and the boundary layer may cause a stall. This is a flow separation from the wall, and may occur for example in a diffuser (draft tube) (Fig. 5.5.1a). Here a "dead water region" or "wake" penetrates between the wall and the "main flow". The mechanism operates as follows:

It can be seen from Fig. 5.5.1a that an "inflection point" in the "boundary layer profile" may cause a "flow separation". This yields $\partial^2 c_x/\partial y^2 > 0$ as a prerequisite for "stall". For laminar flow the equilibrium without inertia terms close to the wall requires $\partial p/\partial x = \partial \tau/\partial y$, in which τ is the shear stress, x the streamwise coordinate and y the coordinate normal to the wall. Inserting $\tau = \eta\, \partial c_x/\partial y$ gives at constant η:

$$\partial p/\partial x = \eta\, \partial^2 c_x/\partial y^2. \tag{5.5-3}$$

Hence the above unequality reveals a streamwise pressure gradient

$$\partial p/\partial x > 0 \tag{5.5-4}$$

as the proper prerequisite for stall together with $\tau = 0$.
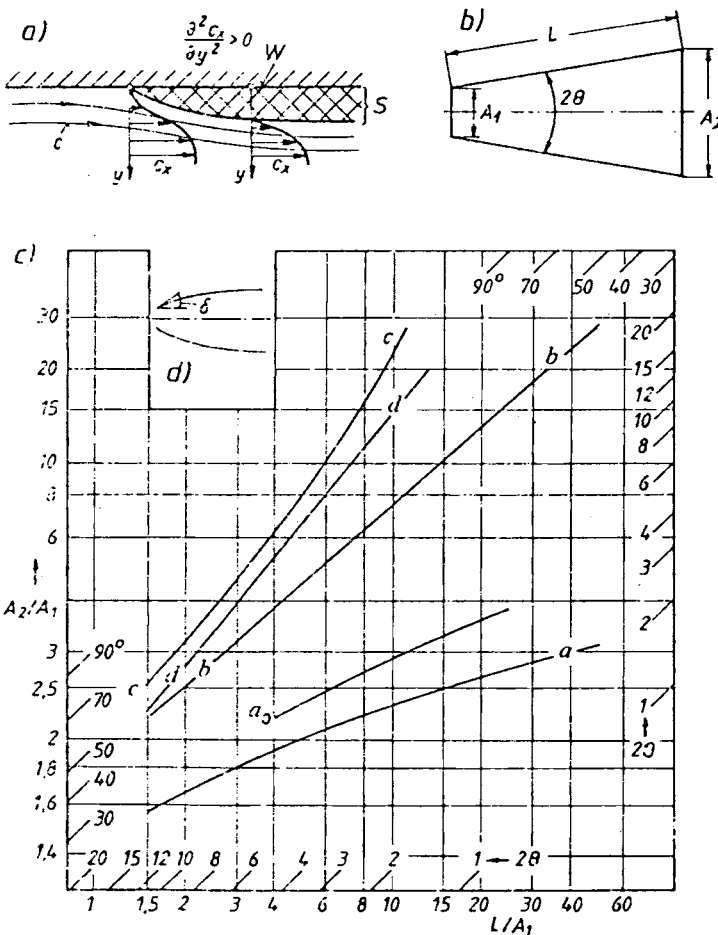
Fig. 5.5.1. Diffuser flow. a) $\partial^2 c_x/\partial y^2 > 0$ as a condition for stall. b) Model of 2-dimensional diffuser, investigated by Renau, Johnston, Kline [5.41]. c) Flow regimes in a 2-dimensional diffuser according to b): a limit of any stall; a_0 line of start of stall; b line for inception of one side stall; c upper limit of jet flow; d hysteresis zone; examples also valid for 3-dimensional diffuser flow without swirl. d) Bell-shaped diffuser.

5.5.4. Diffuser (draft tube) flow, rotating stall

A diffuser (draft tube) is a duct with a diverging cross section for the recuperation of the kinetic energy $c^2/2$ at its inlet. Here a streamwise pressure gradient occurs due to energy

196

and mass conservation. According to *Renau, Johnston* and *Kline* [5.41], the phenomena, which happen in a swirl-free, plane and straight diffuser, can be classified as follows guided by Fig. 5.5.1 b, c:

This figure shows a plot of lines with constant diverging angle 2Θ in a coordinate system with the length to inlet area ratio L/A_1 as abscissa and the area ratio A_2/A_1 as the ordinate. The types of flow regime are nearly independent of the *Reynolds* number and can be described as follows.

Close to the line $2\Theta = 0$ there is a "steady" and "smooth flow regime". At larger divergence angles, especially in long diffusers the flow becomes "unsteady without stall". Further increase in 2Θ brings in the regime of unsymmetrical stall (Fig. 5.5.1 b, c). The main flow here follows one wall and it may be either wall. For very large values of 2Θ there is a jet flow regime.

Between both of the last regimes a hysteresis may be observed. Thus the regime of a diffuser (draft tube) may depend also on the sequence of events.

As a remedy against stall due to the streamwise pressure gradient the cone angle of a conical draft tube should not exceed about 7°. This holds true for a long diffuser with a flow which is not swirling around the diffuser axis. Since the draft tube length strongly influences the excavation cost of a water turbine, remedies are required to increase the value of this threshold.

One such a remedy is the "bell-shaped" draft tube (Fig. 5.5.1 d). Here in a conical diffuser, the cone angle of 7° is exceeded in the inlet zone. This is possible, since the velocity profile there is not so susceptible to stall as it would be towards the outlet. Thereby diffuser length and hence excavation cost may be economized. Further studies on diffusers see [5.42 to 5.50].

A stall in the draft tube, even at higher diffuser angle can be avoided, when the flow rotates slightly around the diffuser axis. Here the centrifugal force on the particle in the flow outside the boundary layer causes it to replace a stalling fluid element on the wall. However a too strong rotation of the flow as it occurs under overload in reaction turbines with fixed runner vanes, leads to a stalled region along the centre line (Cap. 8.2) [5.51]. Here the tendency of the rotating fluid with nearly constant specific energy to form a free whirl with a high strain rate on the centre line favours the formation of a forced vortex there.

Moreover the low pressure in the vortex core leads to cavitation and may result in a back flow from the draft tube outlet towards the hub (Cap. 8.2), [5.2; 5.52].

Under part load the vortex core accepts a cork screw form (Cap. 8.2), [5.18; 5.53; 5.54] and precesses with a slip of about 70% against the speed of the runner. Stroboscopic observations by high speed camera demonstrate clearly that the origin of it may be within the runner channel on the hub. Hence the slip of this vortex relative to the runner against the sense of its rotational speed is an example of "rotating stall" [5.18; 5.55].

The latter originates from a decrease of meridional velocity by local blockage of the flow due to the vortex core. The absolute flow direction being retained from the gate yields via the velocity triangle an impact of the relative inflow onto the suction face of the vane. This causes stall on the pressure face, which sucks the vortex downstream by negative water hammer into the as yet unblocked channel against the sense of rotation.

5.5.5. Secondary flow in curved and rotating ducts

5.5.5.1. Due to turbulence, consequences on energy conversion

Consider a plane flow through a straight channel, which rotates around an axis perpendicular to the flow plane with angular velocity ω. In an ideal steady flow the relative

197

velocity w at a station a distance n from the pressure face would increase from the value w_0 on the pressure face by the relative whirl with $w = 2\omega n + w_0$. In a real flow with a boundary layer this increase of relative velocity towards the suction face of the channel would be enhanced across the boundary layer on the pressure face and then continued as before up to the outer edge of the boundary layer on the suction face of the channel.

Consider now an element within the boundary layer of the pressure face, on a streamline 1 with a time-averaged velocity w_1. The element of volume $dn\,dA$ (dn normal to the channel wall, dA face normal to dn) develops a Coriolis force in the $+n$ direction, pointing from the pressure face towards the suction face $dF_1 = -2\omega w_1 \varrho \, dn \, dA$, (Fig. 5.5.2 a).
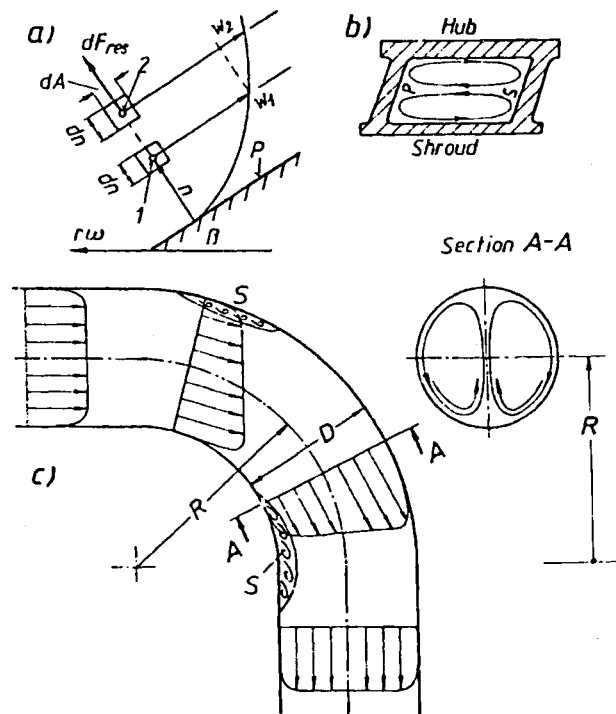
Fig. 5.5.2. Different types of secondary flow: a) Induced by turbulence and rotation of a channel, ω = angular velocity. Boundary layer adjacent to the pressure face P becomes destabilized. b) Induced by the interaction of the main flow and boundary layer flow in the cylindrical cross section of a semi-axial or radial rotor. Transportation of higher velocity fluid from the suction face to the pressure face along the channel centre line. c) Induced like b) in the cross section of a bend, when passing the bend, the streamwise velocity distribution of the main flow is changed by the secondary flow. S' = regions of stall.

Let this element be displaced by a turbulent fluctuation across the main flow with the same velocity w_1 to a station 2, farther than 1 from the pressure face, where the time-averaged velocity is $w_2 > w_1$. Thus its Coriolis force is retained. The pressure of the bulk of the fluid acting at 2 due to the time-averaged Coriolis force there leads to a force on the displaced fluid element in $+n$-direction

$$dF_2 = 2\omega \varrho w_2 \, dn \, dA.$$

Hence the resulting force on this element in its new position is given by $dF_{res} = 2\omega \varrho \, dn \, dA(w_2 - w_1)$. As far as $w_2 - w_1 > 0$ (and this holds good for all points within the boundary layer on the pressure face and the adjacent free flow) this force continues to move the displaced element in the same direction as it was displaced before. Thus the boundary layer on the pressure face under the turbulence described here is unstable and will be accumulated in the boundary layer on the suction face.

The same occurs also in a bend in consequence of the pressure drop across the main flow due to curvature. In both cases, the turbulence of the type described causes a secondary

198

flow by accumulating boundary layer material from the pressure face of the channel in the boundary layer on the suction face. For basic considerations on the generation of secondary flow, see also the report of *J. D. Johnston* [5].

In the channel of a rotor the effect due to Coriolis force usually predominates. Hence the boundary layer fluid from the pressure face is accumulated along the boundary layer of the suction face towards the outlet of this channel. This phenomenon was observed by colour injection, high speed camera, rotoscope and transparent shroud by *Fischer* and *Thoma* in 1930 [5.56] in a pump impeller.

It was reconfirmed by means of hot wire anemometry in a straight rotating channel with rectangular cross section by *Moon* at MIT in 1962 [5.57]. The measurements of *Moon* show also the retention of the logarithmic velocity distribution at the wall in the decisive loss-generating zones at pressure and suction face.

Although the energy relation for ideal flow postulates the velocity maximum shall be at the suction face of the channel, the secondary flow induced by turbulence and other effects from the pressure face towards the suction face shifts the velocity maximum in the main flow at the outlet of a rotor channel towards the pressure face. Simultaneously the accumulation of boundary layer material on the suction face towards the outlet of the channel tends to stall there at the rotor exit, rotating with blade speed.

With increasing streamwise channel length, this effect counteracts the energy conversion of a runner (impeller) channel. One remedy consists in the choice of a short channel together with an adequate number of rotor vanes. For the usual runner channel of turbines with forward curved vanes, the effects of curvature and Coriolis force are additive. For backward curved vanes, as are employed in pumps, pump-turbines and partially also in turbines, both effects act against each other. However, a balance is not possible, as it would annul the rotor's work.

As was demonstrated by *Strscheletzky*, also an ideal flow may have stalled zones in consequence of the principle of least action. In the rotor channel, the width of such a stalled zone could also be predicted by means of this principle [5.59]. A criterion for the minimum vane number, which prevent stall, could be derived from this by the author [5.59].

5.5.5.2. Interaction of the boundary layer and the main flow

Whereas the aforementioned secondary flow may be spread over the main and boundary layer flow, the following flow superimposed on the first, is usually due to the boundary layer. This follows from the interaction of a pressure gradient across the main flow and the boundary layers of the walls, covering the main flow in the direction, in which the retained pressure acts.

Owing to the relatively slow flow in the boundary layer, the pressure gradient from the main flow due to curvature and Coriolis force is not balanced by these velocity-linked forces within the layer. Therefore the fluid in the boundary layer is displaced from the pressure to the suction face of the duct.

Usually this shift is balanced by a motion of the main flow in the mean stream face of the duct. Thus the secondary flow due to this effect usually consists of two loops turning against each other. This may occur in a rotor channel (Fig. 5.5.2 b) or in a bend (Fig. 5.5.2 c).

The return flow in the mean stream face transports fluid of the main flow from the suction to the pressure face, thus distorting the original velocity distribution across the channel as the fluid flows downstream by shifting the velocity maximum from the pressure to the suction face. The consequence is essentially the same as that of turbulence-conditioned cross motion, described before.

---

[5]) The effects of rotation on boundary layer in a turbomachine rotor. Rep. MD-24, Mech. Engg. Dept. Stanford University 1970.

Additional attention must be paid to the flow in a bend. Besides this "secondary flow", a stalled region is observed in a bend on the inner wall, near the outlet (Fig. 5.5.2 c). This may considerably contract the main flow. This increases the velocity and consequently also the loss. A small but unimportant "stalled region" can be also observed past the inlet on the outer wall of the bend.

This effect can be explained as follows: Usually the specific energy of flow entering the bend is constant across the section (with the exception of the region next to the wall). When the main flow streamlines are forced into the curvature, a free vortex is produced (Cap. 5.2). Thus the pressure along the inner wall decreases with the increasing velocity there.

Near the outlet the flow again is straightened and hence the velocity distribution becomes more uniform over the cross section. The pressure on the inner wall then increases, in the flow direction causing a stall there past the bend's exit. In reality the aforementioned secondary flow changes the velocity distribution across the main flow from that of a "free vortex" at inlet to that of a forced one towards the outlet.

Since the kinetic energy at draft tube inlet for low head Kaplan turbines may be considerable (Kc_{m1}^2 up to 0,8) the draft tube bend has to be carefully designed. A remedy against stall is an acceleration of the main flow within the bend (see Fig. 5.5.3). Another remedy against the formation of secondary flow induced by the pressure drop across the width of bend is to "squeeze" this width by applying a laterally extended rectangular cross section in the bend (Fig. 5.5.3).

Shifting the bend's bottom from the runner throat (diameter D_1) at least by $2,5 D_1$ downstream lowers the kinetic energy in the bend and hence the loss. It also prevents the cork screw part load vortex core in FTs to distort or block the flow at bend inlet. Another remedy consists in smoothly lowering the curvature of the inner bend wall towards the
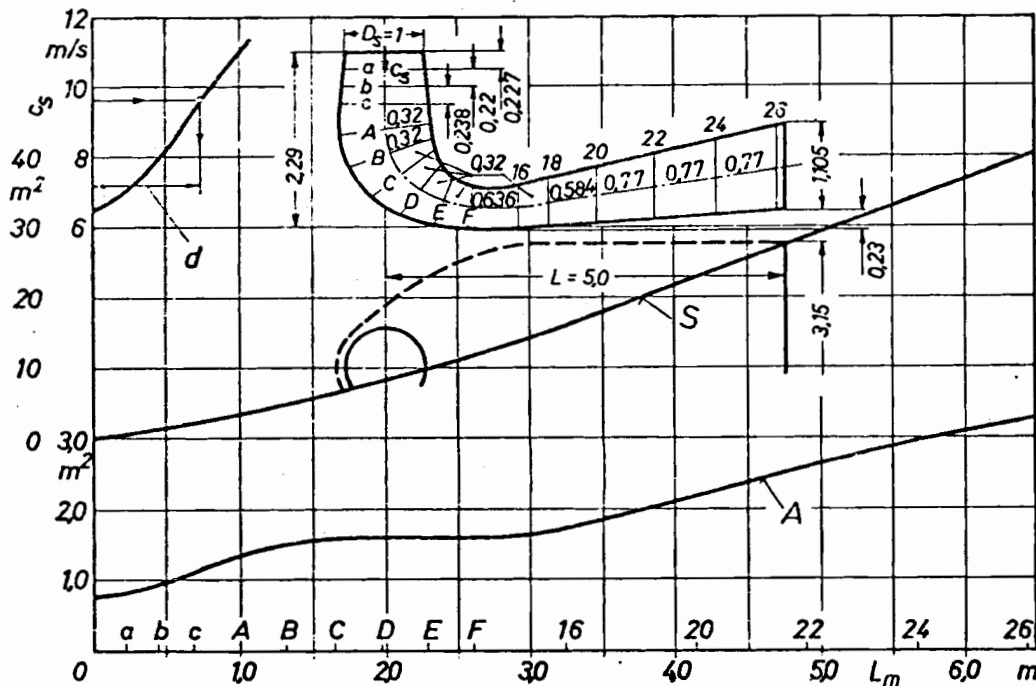
Fig. 5.5.3. Elevation and plan of an elbow draft tube with distribution of cross section-averaged velocity by cross sectional area A, surface S depth d of steel lining along the unrolled centre line. Inlet diameter $D_s = 1$ m. Volume $= 12,95$ m^3.

outlet (Fig. 5.5.3). Sometimes also laterally extended guide plates may help, when the main flow is not swirling, e.g. in runner blade adjusted KTs.

The kinetic energy of secondary flow is more or less lost. This is the reason, why although the loss in a bend depends mainly on its curvature, it depends also to a lesser extend on the deviation angle of the bend [5.60]. The generated secondary flow depends also on this angle and it produces the lion's share of the bend loss (Figs. 3.4.12; 3.4.14; 3.4.45).

5.5.5.3. Secondary flow in axial turbomachines

In axial machines the leakage flow, especially through the tip clearance, which is greatly increased in a pump by shear flow close to the throat ring, may be the origin of a special type of secondary flow, see [5.13]. Another type of secondary flow, first described in detail by W. Kühnel [9.60], (see Cap. 9.6), is limited to the boundary layer of rotor vane and is oriented either towards the hub or the tip and this, sometimes in one and the same boundary layer.

This depends on whether the whirl-induced radial pressure gradient $\varrho c_u^2/r$, acting towards the hub from the main flow on the boundary layer is larger or smaller than the centrifugal force due to the fluid particle in the boundary layer. Hence the secondary flow towards the hub occurs, when the whirl component c_u of the main flow close to the boundary layer is oriented against the blade speed, e.g. at suction face of runner adjusted KTs.

5.5.5.4. Secondary flow due to relative whirl in an axial turbine

In an axial machine with its usually irrotational absolute flow, the rotating observer sees the relative whirl -2ω (Cap. 5.2). Consider the secondary flow of an axial rotor in a plane normal to the axis between adjacent nearly radially oriented vane traces, which moves with constant meridional speed in the axial direction (Fig. 5.5.4). When the machine operates with a certain flow, the vorticity of a fluid sheet on this plane is described by [5.61; 5.62] as $-2\zeta\omega$ at which

$$\zeta = 2\Delta\beta/\sin 2\beta_a, \qquad (5.5-5)$$

where β_a is the angle the rotor vane makes at the tip with the periphery, $\Delta\beta$ the deviation of β from the amount, yielding a vanishing whirl c_u past the rotor.
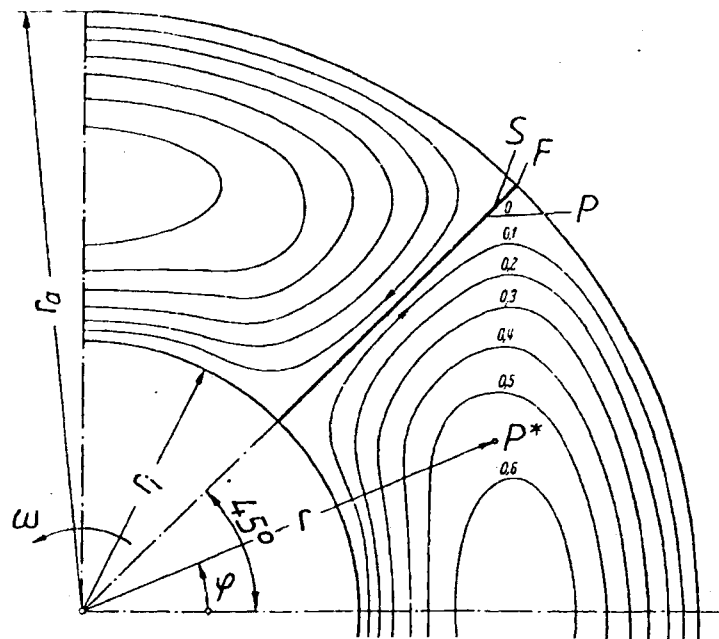
Fig. 5.5.4. Ring segment between radial traces of adjacent blade skeletons of an axial machine in a plane normal to the machine axis, moving with an axial velocity c_m. Secondary flow motion caused by the relative eddy. Streamline parameter: non dimensional stream function $2\Psi/(\omega r_i^2)$, r_i hub radius.

Introducing a stream function after Cap. 5.2, the plane and rotational flow in this circular ring sector can be reduced to a Poisson equation $\Delta\Psi = -2\omega\zeta$. Raabe has shown a solution of the type $\Psi = B\varrho^2 + B_1\,ln\varrho + B_2 + Re\sum_{n=1}^{\infty} A_n^* \sin[n\pi\,ln(z/r_i)/ln\varrho_a]$, at which $z = re^{i\varphi}$, $\varrho = r/r_i$, $\varrho_a = r_a/r_i$, r_a is the tip radius, r_i the hub radius, Re the real part, B, B_i, A_n^* are constants, [5.62].

The velocities v_r and v_u due to this secondary motion are linked to Ψ (see Cap. 5.2) by $v_u = \partial\Psi/\partial r$, $v_r = -\partial\Psi/(r\partial\varphi)$. These velocities are connected with the components of absolute velocity c_u and c_r by: $c_u = v_u + \zeta\omega r$, $c_r = v_r$. The kinetic energy of the secondary flow due to the effect described is assumed as loss $h'_{v\omega}$. With z as vane number, $Ku = r_a\omega/(2gH)^{1/2}$,

$$h'_{v\omega} = \{\zeta^2 Ku^2/[\varrho_a^2(\varrho_a^2 - 1)]\}$$
$$\cdot\left\{(\varrho_a^2 - 1)^2/(2\,ln\varrho_a) + (z/\pi^2)\sum_{n=1}^{\infty} nA_n^2\tanh[n\pi^2/(z\,ln\varrho_a)]\right\}, \qquad (5.5-6)$$

where

$$A_n = [(-1)^n\varrho_a^2 - 1](1/n)[(2/\pi)\,ln\varrho_a]^2/\{[(2/\pi)\,ln\varrho_a]^2 + n^2\}. \qquad (5.5-7)$$

An example with $\zeta = 0{,}1$; $Ku = 1{,}6$; $\varrho_a = 2$ gives for $z = 3, 4, 6, 12$ blades the loss $h'_{v\omega} = 0{,}0159$; $0{,}01604$; $0{,}01635$; $0{,}01702$. Since $h'_{v\omega}$ is nearly independent of the blade number, it can be approximated by

$$h'_{v\omega} = \zeta^2 Ku^2(\varrho_a^2 - 1)/(2\varrho_a^2\,ln\varrho_a). \qquad (5.5-8)$$

5.5.6. The prediction of component loss in fluid machines

5.5.6.1. The rotor vane loss by means of aerodynamics

Assume that the flow through an axial rotor occurs on coaxial cylinders. Hence imagine the unrolled cylindrical section of the runner (impeller) blade of an axial turbine (pump) to be an aerofoil in a plane potential flow within a straight cascade (Fig. 5.5.5). The undisturbed velocity w_∞ is given by $w_\infty = (w_1 + w_2)/2$ from the velocity triangles, (see Fig. 5.5.5) [5.2].

The forces, exerted on the blade are: a) The drag F_D in the direction of w_∞, b) the lift F_A normal to w_∞, see (5.2–29) and Fig. 5.5.5. The lost work by the drag is: $w_\infty F_D$. The
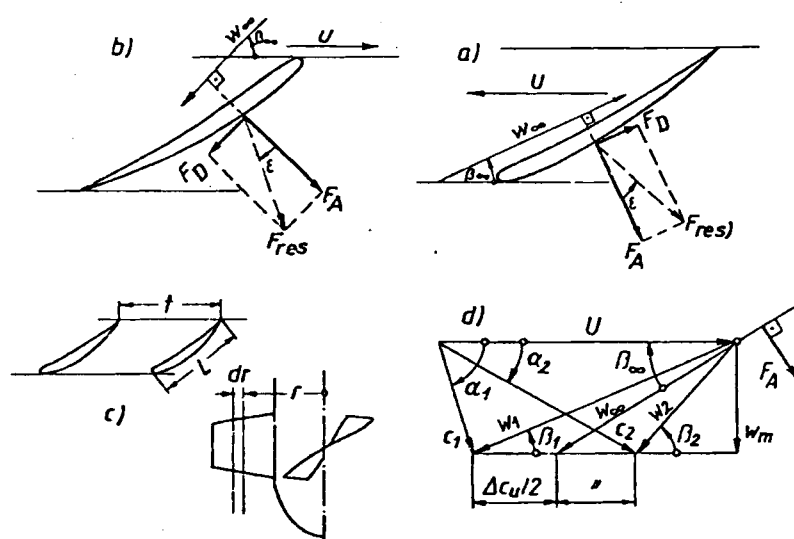
Fig. 5.5.5. Lift F_A, drag F_D on an axial rotor blade in plane flow, velocity w_∞ in the case of a) pump impeller, b) turbine runner, c) Cascade of the unrolled cylindrical section of a rotor vane. d) Velocity triangles at stations 1 and 2 and undisturbed velocity w_∞ derived therefrom.

202

effective work done by the resulting peripheral components of lift and drag with blade speed u is: $u(F_A \sin \beta_\infty \mp F_D \cos \beta_\infty)$ where β_∞ is the angle w_σ makes with the periphery; the positive sign holds true for an impeller, the negative for a runner.

The dimensionless loss is the ratio of the work done by drag to the energy transformed and this corresponds to the sum of the effective work done + the work done by drag. Hence

$$h'_{vR} = w_\infty F_D/[w_\infty F_D + u(F_A \sin \beta_\infty \mp F_D \cos \beta_\infty)]. \tag{5.5-9}$$

Usually the drag is very small compared with the lift. Therefore the terms containing F_D in the denominator may be omitted. Further the proportions of the usual velocity triangles of an axial machine (Fig. 5.5.5) are such that: $w_\infty \approx u$ [4.9]. Introducing the glide angle ε, $\tan \varepsilon = F_D/F_A \approx \varepsilon$ [4.9], from (5.5-9) approximately

$$h'_{vR} \approx \varepsilon/\sin \beta_\infty \approx \varepsilon u/c_m = \varepsilon/\varphi, \tag{5.5-10}$$

at which $\varphi = c_m/u$ is the "local throughflow coefficient".

The last relation, which gives the runner (impeller) loss due to the main flow, shows that the meridional velocity component must not be too small in relation to the blade speed. Owing to this loss and especially due to cavitation in a rotor with adjustable blades and hence a nonswirling flow on its suction side 1, the ratio c_m/u_a, the "throughflow coefficient", is linked to the angle β_1, the rotor vane makes with the periphery at tip and suction side, and must be in the range $\varphi = c_m/u_a = \tan \beta_{1a} = \tan (15^\circ \dots 25^\circ)$.

u_a being the blade tip speed. To save costs, u_a should be as high as possible. Usually u_a is related to the spouting velocity $(2gH)^{1/2}$ for the head H. Thus the blade speed coefficient is defined by $Ku = u_a/(2gH)^{1/2}$, ranging $Ku = 1,3 \dots 1,8 \dots 2,4$ for $H = 70 \dots 15 \dots 2$ m in the case of axial turbines.

5.5.6.2. The draft tube (diffuser) loss

In an axial machine φ and Ku, last mentioned, yield the meridional velocity c_m and hence by $c_m^2/(2gH)$ the kinetic energy referred to the head, e.g. at runner outlet. For a Kaplan turbine under rated flow $Kc_m^2 = c_m^2/(2gH) = 0,3 \dots 0,5 \dots 0,8$ for $H = 70 \dots 15 \dots 2$ m.

Thus without a draft tube as a decelerating device past the rotor the efficiency of a Kaplan turbine would not reach even 50% in the low head range. Therefore the draft tube has to transform this high kinetic energy into pressure with the lowest possible loss h'_{vD}.

In turbines with a whirl component c_{u1} at runner exit

$$h'_{vD} = \zeta_{Dm} c_{m1}^2/(2gH) + \zeta_{Du} c_{u1}^2/(2gH). \tag{5.5-11}$$

Here all the velocities and hence also the loss coefficients ζ_{Dm}, ζ_{Du} are flow-averaged quantities of the draft tube inlet section. ζ_{Dm} depends on the draft tube geometry. $\zeta_{Dm} = 0,09$ for the best straight draft tubes, as are used in tubular turbines (Fig. 3.4.25). For the best elbow draft tubes as usually installed in vertical turbines $\zeta_{Dm} = 0,12$ (Fig. 5.5.3).

The recovery of the whirl velocity c_{u1} is comparatively smaller with an upper limit of $\zeta_{Du} = 1$. This is one of the main reasons for the application of adjustable runner blades in machines which must often operate under off-design conditions. Owing to a streamwise increase of draft tube section (Fig. 5.5.3) and the nearly retained moment of momentum along any streamline, there is also a reduction of c_{u1} towards the draft tube exit. Therefore $\zeta_{Du} = 0,2 \dots 0,4$.

In an impeller pump the velocity triangle for a radial flow rotor (Fig. 10.4.14) has $c_{u2} = c_3$

203

approximately. Here c_3^2 must be best converted into pressure energy. Since the loss factor ζ_D in an impeller diffuser is given, the diffuser loss $h'_{v,Di} = \zeta_D c_3^2/(2gH)$ can be kept low only, when c_3 and hence c_{u2} are also low. For an impeller with vanishing swirl at its eye (at least at the bep), Euler's equation yields

$$c_{u2} = gH\eta_u^{-1}/u_2.$$

For a given peripheral efficiency η_u and head H, c_{u2}, the whirl at impeller exit, can be reduced only by increasing the blade tip speed $u_2 = \omega D/2$, thus increasing either the impeller tip diameter D or its angular velocity ω. Since the last measure would decrease, for reasons of optimum suction requirements, the diameter of the impeller eye by $D_1 \sim (Q/\omega)^{1/3}$, and hence increase the submergence and ground excavation, the only remedy for a reduction of diffuser loss in a pump is the increase of impeller tip diameter D_P compared with that of a turbine runner D_T.

This has to be done with due consideration of disk friction loss, which yields $D_P \approx 1.4\,D_T$ for machines with the same operating data H, Q, ω.

5.5.6.3. Disk friction loss

I. Simple treatment by disk model without leakage influence:

Consider a circular disk of external diameter D_a, that of the wheel, and a thickness Δb, which equals the axial thickness of hub and shroud at diameter D_a (Fig. 5.5.6a, b). A tangential shear stress τ between the fluid and the disk is exerted. It is due to turbulent motion in the boundary layer flow adjacent to the disk wall.

From (5.4–19) with $n = 4$ and when substituting for the pipe radius R the boundary layer thickness δ on the disk and for the pipe speed the peripheral speed $r\omega$, the shear stress at radius r becomes $\tau \sim \varrho r^2 \omega^2 (\delta r\omega/v)^{-1/4}$. A balance between the centrifugal force $\varrho \delta r \omega^2$ of a boundary layer element, base '1', at radius r, and its wall shear force τ gives, according to Schlichting [5.4] with k' as a constant

$$\tau(r) = k'\varrho r^2 \omega^2 (\omega r^2/v)^{-1/5}. \qquad (5.5-12)$$

Hence the power lost due to disk friction P_{df} with $R = D_a/2$, and $\tau(r) = \tau$

$$P_{df} = \omega \left[4\pi \int_0^R \tau r^2 dr + 2\pi R^2 \Delta b\tau(R) \right] = K_1 \varrho \omega^3 D_a^5 [1 + (23/5)\,\Delta b/D_a]. \qquad (5.5-13)$$
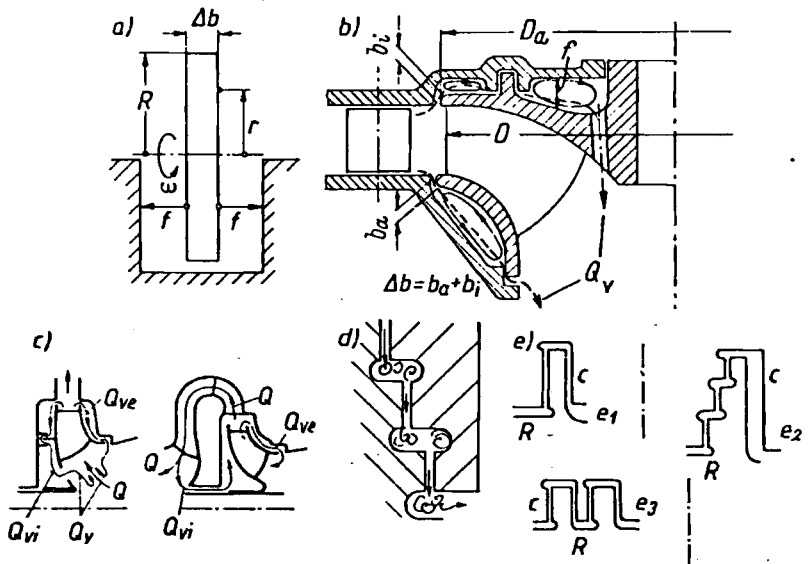
Fig. 5.5.6. Disc friction and leakage in the rotor of reaction machines. a) Rotating disc as a model for disc friction. b) Mixed flow rotor with leakage Q_v and secondary flow between rotor and the case. c) Leakage of the outer and inner rotor labyrinth Q_{ve}, Q_{vi} in a 1-stage and a multi-stage impeller. d) Successive gaps stepped off seal; e) Type labyrinth seals: e_1 cylindrical gap; e_2 stepped off seal; e_3 comb labyrinth. To dampen bending oscillation of the shaft, clearance of inner gap wider than that of outer gap.

According to tests of *Föttinger* [5.63], and from (5.5-12), K_1 depends also on the axial spacing f between the casing and disk as

$$K_1 = 0{,}256 \cdot 10^{-2}(D_a^2 \omega/v)^{-1/5}[1 + 1{,}4(f/D_a - 0{,}1)]. \tag{5.5-14}$$

II. Detailed treatment accounting for leakage: A more detailed investigation shows, that the torque due to disk friction M_{df} depends on the radial variation of mean angular velocity, the fluid between the casing and shroud has (Fig. 5.5.6 b). This local mean angular velocity $\omega(r)$ is also influenced by the leakage flow Q_V passing between the shrouds and the casing. This follows from the moment of momentum and direction of Q_V.

Assuming the torque on the "disk face", which rotates with angular velocity ω as

$$M_{df} = \int_{r_i}^{r_a} k(r) r^4 [\omega - \omega(r)]^2 \, dr,$$ knowledge of $\omega(r)$ is required for evaluation. From the moment balance on an elementary liquid ring between the casing and disk wall, due to the shear stress on the casing and disk wall, due to slippage of adjacent elementary fluid rings and due to the change of the moment of momentum by the leakage Q_V, crossing the elementary ring, a differential equation of second order for $\omega(r)$ was found by *Ruabe*, [6.8].

Neglecting the highest derivative gives a linear differential equation with the following solution for $\omega(r)$ under the assumption of a constant spacing f between disk and casing and with η^* as a constant assumed eddy viscosity between adjacent slipping fluid rings according to *Domm* [5.64] and $k = 1{,}238 \, \varrho \, (r_a^2 \, \omega/v)^{-1/5}$

$$\omega(r) = e^{-Z(r)}\left\{\omega_1 - [k\omega^2/(6\pi f\eta^* + \varrho Q_V)] \int_{r_i}^{r} e^{Z(x)} x^2 \, dx\right\}, \tag{5.5-15}$$

$$Z(r) = [2k\omega r^3/3 + 2(2\pi\eta^* f + \varrho Q_V) \ln(r/r_i)]/(6\pi\eta^* f + \varrho Q_V). \tag{5.5-16}$$

Here the leakage Q_1 is assumed in the usual direction towards the axis. The integration constant ω_1 can be determined from a given angular velocity of leakage at the entrance of the gap between the casing and the rotor $\omega(r_a) = \omega_a$ given by the whirl component of the flow entering the runner.

Starting from (5.5-12), substituting there ω by $\omega = \omega(r)$, on the model of (5.5-13), but without $[1 + 1{,}4(f/D_a - 0{,}1)]$ and substituting the factor 0,256 on the rough base $(r_i/r_a)^{23/5} \ll 1$ by $0{,}5 \cdot 0{,}256 \cdot 2^{23/5}/2\pi = 0{,}493$ the function $k(r)$ under the above integral of M_{df} (the disk friction torque of one shroud's face) becomes

$$k(r) = 0{,}493 \cdot 10^{-2} \varrho \{r^2 [\omega - \omega(r)]/v\}^{-1/5}. \tag{5.5-17}$$

Elimination of disk friction by aerating the inter space between casing and runner has been developed by *R. Sproule* on Canadian turbines [5.66]. The disk friction on a low specific speed Francis runner has been investigated by *J. Osterwalder* and *Geis* [5.67]. In the above, the loss due to disk friction and leakage are considered to be linked to each other. On the other hand, in a pump, the leakage may also be associated with the hydraulic loss, since it has to be delivered by the peripheral blade work. The analogue holds for a turbine. Both considerations are assessments and in usage (see Cap. 9.3.).

5.5.6.4. The leakage (volumetric) loss

Consider the runner of a Francis turbine (Fig. 5.5.6 b–c). The labyrinths there are located on hub and shroud at nearly the same radial distance from the axis. Thus the axial thrust

on the outer faces of hub and shroud is balanced. For a minimum leakage, the seals are nearly on the rotor throat diameter. With a figure R^* that accounts for the degree of reaction and the pressure drop between rotor tip diameter and labyrinth due to the rotation of fluid between the casing and rotor, the pressure drop within the seal is given by $\Delta p = R^*(p_2 - p_1)$. This pressure drop must overcome the following loss-conditioned pressure drops within the labyrinth:

a) Δp_{fr}, due to dissipation in the narrow gaps with small radial clearance s and a total meridional length L;

b) Δp_{in}, due to dissipation at the gap inlet;

c) Δp_{out}, due to dissipation at the gap outlet. Hence

$$\Delta p = \Delta p_{fr} + \Delta p_{in} + \Delta p_{out}. \qquad (5.5-18)$$

Since by continuity, the leakage Q_V, that passes the seal is linked to its mean meridional speed c_{sp}, the above loss terms are usually expressed in terms of c_{sp}. Strictly speaking, the mean resulting relative flow within the gap, considered now as the relevant one, makes a mean angle β_M with the circumference, approximated by $\tan \beta_M = c_{sp}/(\omega r/2)$ and hence found only by trial and error. However in the following, β_M is assumed as preliminarily given. Thus the resulting flow has the mean speed $c_{sp}/\sin \beta_M$ and the mean real flow path has the length $L/\sin \beta_M$.

Neglecting the inlet length of gap flow, Δp_{fr} can be expressed by the pipe loss formula (5.4–13), in which d is replaced by the hydraulic diameter $2s$ of a small gap.

With λ as a gap flow loss coefficient, depending after *Petermann* [5.19], *Wagner* [5.68], *Kosyna* [5.69], *Raabe* [5.70], *Stampa* [5.71], *Keller* [5.72], *Eichler* and *Wiedemann* [5.73] on the *Reynolds* numbers $Re_c = c_{sp}s/\nu$ due to gap flow, and $Re_\omega = sr\omega/\nu$ due to rotation

$$\Delta p_{fr} = \lambda \varrho(L/s) \, c_{sp}^2/(4 \sin^3 \beta_M). \qquad (5.5-19)$$

For an individual gap Δp_{in} and Δp_{out} can be reduced to c_{sp}^2 by

$$\Delta p_{in} = \zeta_{in} \varrho c_{sp}^2/2, \qquad (5.5-20)$$

$$\Delta p_{out} = \zeta_{out} \varrho c_{sp}^2/2. \qquad (5.5-21)$$

For a favourable gap inlet design (Fig. 5.5.6 d) the loss coefficient there can be assumed as $\zeta_{in} = 0{,}5$. This design has successive gaps radially displaced. Thus the leakage jet from an upstream gap is not in line with a downstream gap. Moreover a groove facilitates the formation of a ring vortex throttling the inlet, see Fig. 5.5.6 d.

The loss coefficient at gap outlet $\zeta_{out} = 1$, when successive gaps are radially displaced (Fig. 5.5.6 d, e_2) and when an axially extended expansion chamber provides for complete dissipation of kinetic energy $c_{sp}^2/2$ of the leakage jet. Recently Chaix informed on $\zeta_{out} + \zeta_{in}$.

For a rotor seal (labyrinth) with z equal gaps in series the last four relations yield the meridional gap velocity

$$c_{sp} = (2 \Delta p_\theta)^{1/2}/\{\varrho \langle z(\zeta_{in} + \zeta_{out}) + \lambda[L/(2s \sin^3 \beta_M)]\rangle\}^{1/2}. \qquad (5.5-22)$$

With a contraction coefficient Φ the leakage through this seal

$$Q_V = \Phi \pi D_{sp} s c_{sp}. \qquad (5.5-23)$$
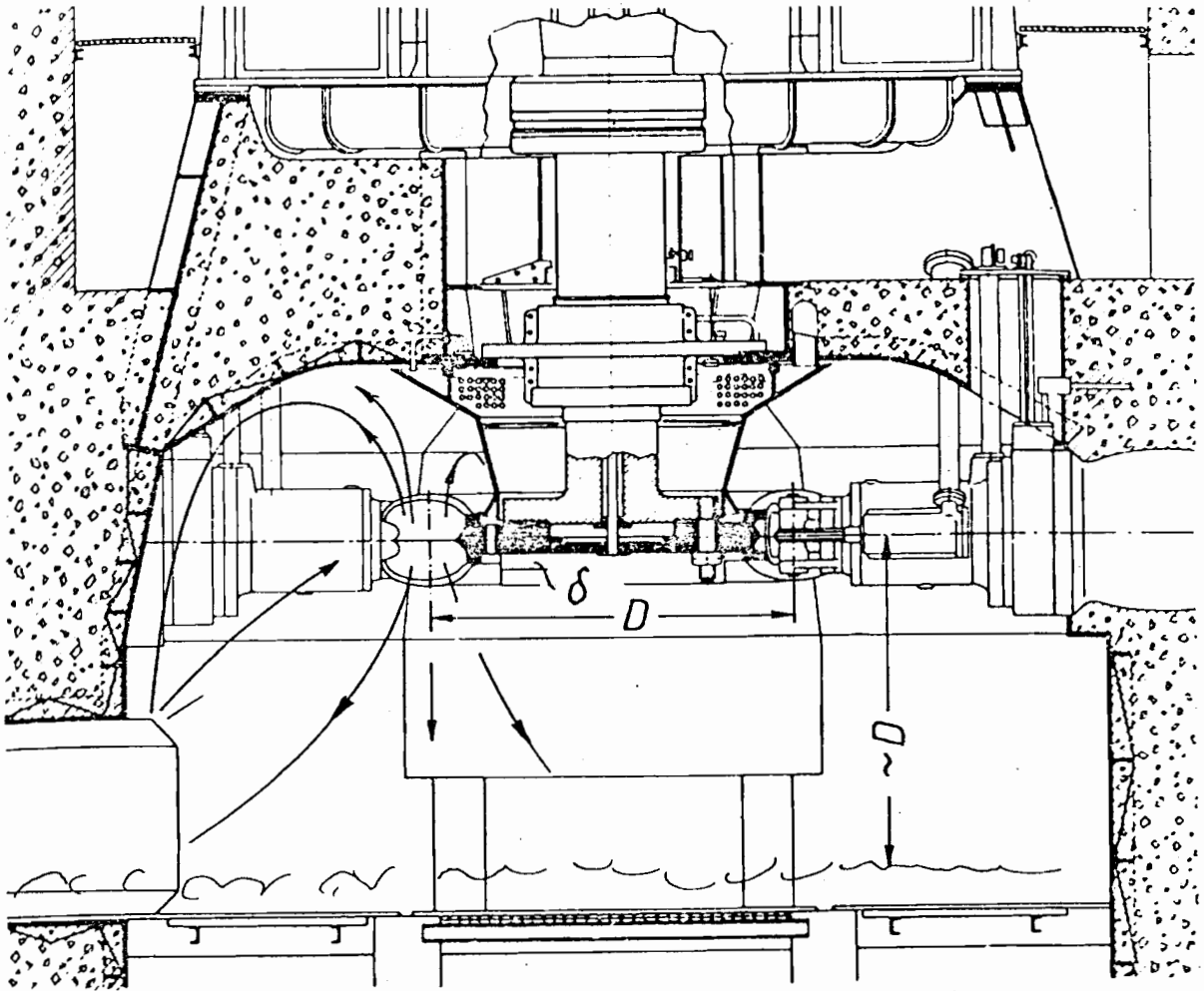
Fig. 5.5.7. Windage loss in the wheel chamber of a vertical Pelton turbine, PT Electra Masa S.A., Switzerland, $H = 733$ m; $n = 375$ rpm; $P = 146$ MW; 5 nozzles, built by Vevey Engineering Works. Ekman layer, depth δ, on the wheel disc. Windage due to sprinkling and droplets reflected from tailwater. (Drawing courtesy Vevey Engineering Works, Switzerland)

5.5.6.5. The windage loss of an impulse turbine

Imagine the case of an impulse turbine with vertical shaft (Fig. 5.5.7). Here obviously due to windage, droplets from the tailrace level are lifted towards the runner, which may have an elevation proportional to its diameter D above the tailrace level. Thus the specific head of the negative work done by droplet lift is $\sim gD$.

Imagine the front face of wheel to be covered with a fluid film with the thickness of an *Ekman* layer $\delta \sim D Re_\omega^{-1/5}$; where $Re_\omega = \omega D^2/\nu$ [5.65] and ω the angular velocity of the wheel. Therefore the liquid mass covering the wheel m: $m \sim \varrho \delta D^2 \sim \varrho D^3 Re_\omega^{-1/5}$. Since the time scale is ω^{-1}, the flow rate due to windage $\dot{m} \sim m\omega^{-1} \sim \varrho D^3 \omega Re_\omega^{-1/5}$. This gives the lost power due to windage, the "windage loss" as

$$P_{vw} \sim \dot{m}gD \sim \varrho g D^4 \omega Re_\omega^{-1/5}. \tag{5.5-24}$$

Hence with $Q/\omega \sim D^3$ the windage loss referred to $gH\varrho Q (Q = \text{flow})$

$$h'_{vw} = P_{vw}/(\varrho Q g H) \sim (D/H) Re_\omega^{-1/5}. \tag{5.5-25}$$

5.5.7. The loss due to cross flow on a bucket of a PT

The loss factor ζ of the individual specific losses may vary with the *Reynolds* or *Ekman* number *Re* or it may not, e.g. draft tube loss. The former, corresponding to an efficiency scale effect, usually rises with *Re*, e.g. loss due to pipe friction, disk friction, windage, but sometimes also decreases with rising *Re*.

The loss due to cross flow on the bucket of a PT is an example of the latter. Let this motion have velocity v. Hence the specific loss $h'_{v_{cr}} \sim v^2/(gH)$. This cross flow is caused by the pressure increase Δp across the jet normal to the bucket face. After *Pascal*'s theorem Δp acts also tangential to the bucket face. Thus $\Delta p/\varrho \sim v^2$. See also Fig. 5.5.8.
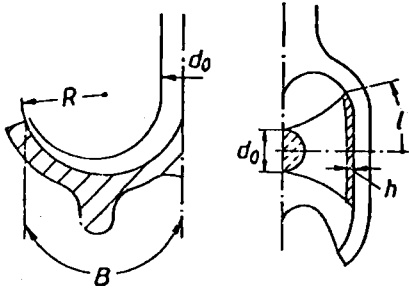
Fig. 5.5.8. Cross flow on the bucket of a Pelton turbine.

Δp is caused by the centrifugal force w^2/R of the relative flow with speed w in consequence of the curvature $1/R$ of the bucket face. Thus with d_0 as the jet diameter $\Delta p \sim \varrho w^2 d_0/R$. Hence the loss due to the bucket cross flow with $Kw = w/(2gH)^{1/2}$

$$h'_{v_{cr}} \sim K w^2 (d_0/R). \tag{5.5-26}$$

After *Raabe* [5.66] with $\lambda = Q/Q_{op}$ as load factor, continuity gives the following relation between the jet diameter d_0 under arbitrary flow Q, and this diameter $d_{0\,op}$ under Q_{op} at bep: $d_0 = \lambda^{1/2} d_{0op}$. An idealized velocity triangle formed by the velocity coefficient Kw due to the relative flow, Ku due to wheel speed and $Kc_0 = c_0/(2gH)^{1/2}$ due to the jet velocity at Q gives: $Kw = Kc_0 - Ku$. Assuming the loss within the nozzle pipe to follow that of a straight pipe in turbulent flow, then

$$Kc = (1 - kRe^{-1/m}Kc_p^2)^{1/2}, \tag{5.5-27}$$

in which k is the loss coefficient, $Kc_p = c_p/(2gH)^{1/2}$, c_p the speed within the nozzle pipe, diameter d_p. At bep: $Kc_p \to Kc_{pop}$ and $Re = c_p d_p/v \to Re_{op}$. With the above load degree λ, continuity gives $Re = \lambda Re_{op}$. Hence from the above, the approximated loss

$$h'_{v_{cr}} \sim \lambda^{1/2}(d_{0op}/R)\,[1 - (k/2)\,Re_{op}^{-1/m}Kc_{pop}^2\,\lambda^{1-1/m} - Ku^2]. \tag{5.5-28}$$

Obviously under overload ($\lambda > 1$) and corresponding to tests, $h'_{v_{cr}}$ increases with rising Re_{op}.

208

6. Prediction of internal flow in cascades and rotor

6.1. Introduction

The steady irrotational flow through a straight cascade of aerofoils can be considered as a simple model for the relative flow in axial turbomachines. It allows the prediction of the steady flow outside the boundary layers, which passes such a cascade of given geometry and given flow admission (indirect problem.) Its solution is based on the singularity method, where bound vortices are continuously distributed along the contour of the profiles.

The resulting linear integral equation for the contour velocity can be solved by dividing the contour into a finite number of elements, which gives a linear system for this velocity. The solution of the direct problem, as the task to design a certain cascade for given velocity triangles can be obtained from that of the indirect problem only by additional conditions.

Neglecting the finite thickness of profiles the singularity method can be simplified for the case of small angles of attack and profiles with small chamber by distributing the singularities on a straight line along the undisturbed velocity known from the velocity triangles.

The results of flow through straight cascades can be used also for the flow through mixed flow gates and rotors by means of conformal mapping, if the flow is assumed to be axisymmetric with respect to the stream faces. The varying thickness of flow laminae requires the introduction of a bound ring vortex.

The concept of axisymmetric elementary turbines requires information about the distribution of meridional velocity normal to them. A simplified estimate of the effects caused by finite vane number is given by introducing the slip factor.

A general survey of the flow in cascades is given by *Scholz* [5.13], *Traupel* [6.1], and *Raabe* [6.8].

6.2. The straight cascade as a model for axial fluid machines

6.2.1. Prediction of flow (indirect problem) by means of the method of singularities

6.2.1.1. Introduction, description and theory of problem

The steady ideal flow through an axial rotor is desired. This flow is assumed to be on coaxial cylindrical stream faces. As the predominating relative whirl (Cap. 5.2) here is parallel to the rotor axis, the plane relative flow within the cylindrical face, now unrolled in a plane, is a plane potential flow. The known cylindrical sections of the rotor vanes are

now arranged parallel to each other and at a distance from each other equal to the pitch t in the peripheral direction (Fig. 6.2.1 a).

This arrangement of aerofoils is known as a straight cascade. The desired knowledge of the distribution of contour velocity under a certain load and hence a certain flow enables the calculation of the pressure distribution along the vane surface. This is required for the stress calculation of the rotor vane and its neighbouring parts, e.g. the hub or the vane adjusting mechanism. Furthermore this enables a control of the susceptibility of the vane to cavitation under certain load conditions.

Imagine a straight cascade (Fig. 6.2.1 a) with chord L and pitch t. Its stagger angle may be expressed by the angle α_0 the zero lift direction makes with the circumference. A *Cartesian* coordinate system is introduced. Its y-axis points in the circumferential direction and its x-axis in the sense of the meridional speed, when pumping. Its origin is on the pointed trailing edge of an arbitrary profile, the so called zero profile.

Since all the profiles are congruent, and the assumed plane potential flow of an incompressible fluid is imagined to be steady, the streamline flow pattern is pitch-periodical. Therefore the boundary conditions need only be satisfied on this zero profile.

The indirect problem now considered asks for the contour velocity on this profile for a given cascade geometry and under a certain velocity c_1 at inflow.

An arbitrary point P on the contour of zero profile is determined by the arc 's', which is assumed to be oriented in the counter clockwise sense, along the contour of the profile, and to start from the origin 0. The complex coordinate of point P is $\zeta(s) = \xi(s) + i\eta(s)$
$\equiv \xi + i\eta$.

The core of the singularity method: The contour of the profiles is assumed to be a streamline. Along this the contour velocity $c(s)$, the unknown, exists. Usually in an ideal

flow highest speeds occur on the contour. The interior of the profiles is assumed to be filled with static fluid. Hence proceeding normal to the contour the velocity makes a step c on the contour.

From hydrodynamics it is known, that such a step is generated by means of a vortex layer, that is along the contour. Therefore so-called "bound vortices" with strength $\gamma(s)$, taken as circulation per unit length, and continuously varying are assumed to be continuously distributed along the contour. Applying *Stokes'* theorem along an infinitesimally small rectangle along the contour and surrounding it reveals the essential relation

$$\gamma(s) = c(s). \tag{6.2-1}$$

The vortex distribution might rotate in the counter clockwise sense. Hence the element ds of the contour has a circulation $\gamma(s)\,ds = \gamma\,ds$. A straight vortex row, consisting of elementary vortices, a distance t from each other, having a circulation $\gamma\,ds$ and situated on analogous stations to the point $\zeta(s)$ on the profiles (Fig. 6.2.1 a), induces, at a point with the complex coordinate z, the complex velocity $d\check{c}_\gamma$ (Fig. 6.2.1 b).

$$\zeta(s) = \xi(s) + i\eta(s), \qquad z = x + iy. \tag{6.2-2}$$

$$d\check{c}_\gamma = dc_{\gamma x} - i\,dc_{\gamma y} = i\,[\gamma(s)/2\,t]\,ds\,\coth\{(\pi/t)[z - \zeta(s)]\}, \tag{6.3-3}$$

where $dc_{\gamma x}$ and $dc_{\gamma y}$ are the components of the induced velocity in the x and y-directions, respectively. Splitting $d\check{c}_\gamma$ into real and imaginary part yields [6.5]

$$dc_{\gamma x} = (\gamma/2\,t)f_x\,ds, \tag{6.2-4}$$

$$dc_{\gamma y} = (\gamma/2\,t)f_y\,ds, \tag{6.2-5}$$

$$f_x = \sin[2\pi(y - \eta)/t]/D, \tag{6.2-6}$$

$$f_y = \sinh[2\pi(x - \xi)/t]/D, \tag{6.2-7}$$

$$D = \cos[2\pi(y - \eta)/t] - \cosh[2\pi(x - \xi)/t]. \tag{6.2-8}$$

Integrating around the contour of the zero profile gives

$$c_{\gamma x} = (1/2\,t)\oint\gamma(s)f_x[x, y, \xi(s), \eta(s)]\,ds, \tag{6.2-9}$$

$$c_{\gamma y} = (1/2\,t)\oint\gamma(s)f_y[x, y, \xi(s), \eta(s)]\,ds. \tag{6.2-10}$$

The components of the undisturbed throughflow velocity are

$$c_{\infty x} = c_m, \tag{6.2-11}$$

$$c_{\infty y} = c_m\cot\alpha_\infty, \tag{6.2-12}$$

where α_∞ is the angle between c_∞ and the y-axis (Fig. 6.2.1), c_m the meridional speed component. In a potential flow the velocities can be superimposed. This gives the resulting velocity

$$c_x = c_m + c_{\gamma x}, \qquad c_y = c_m\cot\alpha_\infty + c_{\gamma y}. \tag{6.2-13}$$

The boundary condition of a flow along the contour of the profile at an arbitrary point $A(z)$ on it requires

$$c_y(z)/c_x(z) = \cot\alpha(z), \tag{6.2-14}$$

where $\alpha(z)$ is the known angle between the contour element and the y-axis. Inserting the velocity components from (6.2-13) gives

211

$$2 t c_m [\cot \alpha(z) - \cot \alpha_\infty] = \oint \gamma(s) \{f_y[z, \zeta(s)] - \cot \alpha(z) f_x[z, \zeta(s)]\} ds.$$

$$(6.2-15)$$

From (5.2-38) *Stokes'* theorem yields the blade circulation

$$\Gamma \equiv \oint \gamma(s) \, ds = t(c_{y2} - c_{y1}) = t c_m (\cot \alpha_2 - \cot \alpha_1),$$

$$(6.2-16)$$

where α_2 and α_1 are the angles between the resulting velocities and the y-axis (circumference) on the points 2 and 1, strictly speaking at the infinities downstream and upstream of the cascade. In 1 and 2 the function f_x (6.2-6) tends to zero and the function f_y (6.2-7) tends to $f_{y2} = +1$, $f_{y1} = -1$. This put in (6.2-9), (6.2-10) with respect to $\Gamma = \oint \gamma(s) \, ds$ gives $c_{yx_2} = 0$, $c_{yy_2} = \mp \Gamma/(2t)$.

Hence the cascade acts at the infinities as a vortex layer with a linear vortex density Γ/t. Better: Seen from infinity the cascade with its profiles of circulation Γ, distant t to each other, shrinks to a vortex layer of vortex density Γ/t. Superimposing c_y and c_∞ at the points 1 and 2 changes only the peripheral component, namely $c_{y1} = c_{y\infty} - \Gamma/(2t)$, $c_{y2} = c_{y\infty} + \Gamma/(2t)$. Subtracting both yields the circulation and hence reconfirms (6.2-16) (Fig. 6.2.1 c).

Adding c_{y1} and c_{y2} gives $c_{y\infty}$. With respect to $c_{m1} = c_{m2} = c_m$ this proves the rule of $c_{x_\infty} = (c_2 + c_1)/2$. Introducing the angles α_2 and α_1 between c_2 and c_1 and the y-axis gives (Fig. 6.2.1 c)

$$\cot \alpha_\infty = (\cot \alpha_2 + \cot \alpha_1)/2.$$

$$(6.2-17)$$

Eliminating $\cot \alpha_2$ from this and (6.2-16) reduces $\cot \alpha_\infty$, usually not known, to $\Gamma = \oint \gamma(s) \, ds$ and the angle α_1 of the afflux, usually given, by

$$\cot \alpha_\infty = [1/(2 t c_m)] \oint \gamma(s) \, ds + \cot \alpha_1.$$

$$(6.2-18)$$

This in (6.2-15) yields the following linear integral equation for the distribution of vortex strength $\gamma(s)$ or respecting (6.2-1) also of contour velocity $c(s)$ due to a cascade of known geometry $x(z)$, t/L, under a given inflow angle α_1 and given meridional velocity c_m

$$2 t [\cot \alpha(z) - \cot \alpha_1] = \oint [c(s)/c_m] \{f_y[z, \zeta(s)] - \cot \alpha(z) f_x[z, \zeta(s)] + 1\} \, ds.$$

$$(6.2-19)$$

This integral equation is of the *Fredholm* type. Numerous procedures were introduced for its solution. In this connection the publications of *Martensen* [6.2], *Jacob* [6.3], *Isay* [6.4], *Traupel* [6.5] and *Birnbaum* [6.6] may be mentioned.

6.2.1.2. Practical solution of the indirect problem

For a practical solution the integral in (6.2-19) is converted into a sum. To this end the periphery of the profile has to be divided into a finite number of arc elements. For convenience the $n + 1$ elements might have the same length h. Thus the arc coordinate s for the mid points of these arc elements are $s_1 = h$, $s_2 = 2h \ldots s_\nu = \nu h \ldots s_n = nh$. At each of these points the contour velocity $c(s_\nu)$ is unknown.

Therefore the integral in (6.2-19) is converted into a sum with $c(s_\nu)$ as the unknown. The complex coordinate of the dummy variable $\zeta(s)$ is now denoted by z_ν. The complex coordinate of the point $P(z)$, on which the boundary condition (6.2-14) is satisfied, is denoted by z_i. Thus the equivalent of the integral equation (6.2-19) takes the form

$$(2 t/h)[\cot \alpha(z_i) - \cot \alpha_1] = \sum_{\nu=1}^{n} [c(s_\nu)/c_m][f_y(z_i, z_\nu) - \cot \alpha(z_i) f_x(z_i, z_\nu) + 1],$$

$$(6.2-20)$$

in which analoguous to (6.2–6) through (6.2–7),

$$f_x(z_i, z_v) = \sin[2\pi(y_i - y_v)/t]/D,$$ (6.2–21,1)

$$f_y(z_i, z_v) = \sinh[2\pi(x_i - x_v)/t]/D,$$ (6.2–21,2)

$$D = \cos[2\pi(y_i - y_v)/t] - \cosh[2\pi(x_i - x_v)/t].$$ (6.2–22)

The system of (6.2–20) is written down for n points z_i. Hence n inhomogeneous linear equations are obtained for the unknown contour velocities $c(s_v)$, enabling their solution. It must be mentioned, that the kinematic boundary condition (6.2–14) loses its sense on the pointed rearward edge of the profile. Therefore in good agreement with experience the *Kutta* condition [5.15; 5.16] is introduced as

$$c(s = 0) = 0.$$ (6.2–23)

6.2.1.3. Simplified method after Ackermann and Birnbaum

In this method [6.6; 6.7] the profile is simplified by·its skeleton. The bound vortices are located along a straight line, which coincides with the undisturbed throughflow velocity w_∞ being now the x-axis (Fig. 6.2.2 a). As the method is limited to small angles of attack between chord and w_∞, the bound vortices, now aside the skeleton, are on a stretch of about chord length L. The continuously distributed vortices with a strength $\gamma(x)$ induce at a point x' a velocity c_{Ey} with

$$c_{Eyy} = (1/2\pi) \int_{-L/2}^{L/2} \gamma(x)\,dx/(x' - x), \qquad c_{Eyx} = \pm\gamma(x')/2.$$ (6.2–24)

Analogous to (6.2–4), (6.2–5) for the components of induced speed of a row of elementary vortices of the circulation $\gamma(x)\,dx$, now located on analogous points of a lattice

$$dc_{yx}^* = [\gamma(x)/2\,t]f_x^*\,dx; \qquad dc_{yy}^* = [\gamma(x)/2\,t]f_y^*\,dx.$$ (6.2–25)

Obviously, in consequence of a transformation from the x, y-system, originally used, to the x^*, y^*-system, adopted now (Fig. 6.2.2 b), the following relations exist between the functions f_x, f_y from (6.2–9), (6.2–10) and the now valid general functions f_x^*, f_y^*:

$$f_x^* = f_x \sin\beta_\infty + f_y \cos\beta_\infty, \qquad f_y^* = f_x \cos\beta_\infty - f_y \sin\beta_\infty.$$ (6.2–26)

Further the coordinate differences $x - \xi$, $y - \eta$ in f_x, f_y, obviously are now transformed (Fig. 6.2.2 b) according to

$$x - \xi = (x^{*\prime} - x^*)\sin\beta_\infty, \qquad y - \eta = (x^{*\prime} - x^*)\cos\beta_\infty.$$ (6.2–27)
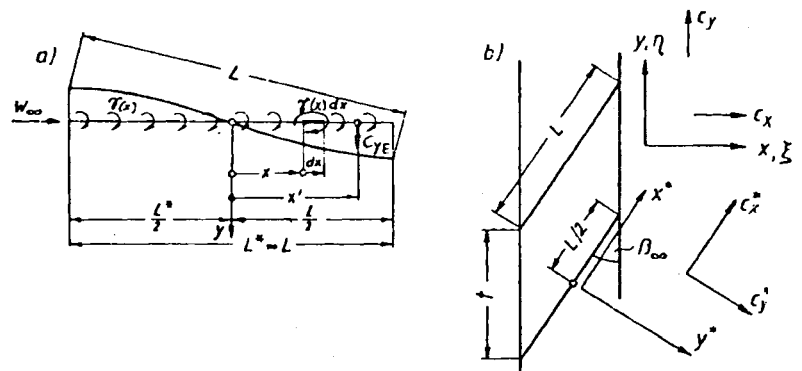
Fig. 6.2.2. Profiles substituted by skeletons, bound vortices on a line parallel to w_∞. a) Single skeleton. b) The coordinate transformation from the x, y- to the x^*, y^*-system.

213

Hence for convenience the star * is omitted. Further from now on the dummy variable is denoted by x' and the coordinate of the point considered by x. The relations (6.2-25) yield

$$c_{\gamma x} = \int_{-L/2}^{L/2} dc_{\gamma x}, \qquad c_{\gamma y} = \int_{-L/2}^{L/2} dc_{\gamma y}. \tag{6.2-28}$$

Station $x = x'$ makes it advisable to split c_γ into the following two terms 1) $c_{E\gamma}$ representing the "self induction" of the individual skeleton, see (6.2-24), 2) $c_{R\gamma}$ representing the velocity, induced by the residual cascade

$$c_{\gamma x} = c_{E\gamma x} + c_{R\gamma x}, \qquad c_{\gamma y} = c_{E\gamma y} + c_{R\gamma y}. \tag{6.2-29}$$

Once $c_{E\gamma x}$, $c_{E\gamma y}$ and $c_{\gamma x}$, $c_{\gamma y}$ are given with (6.2-24) and (6.2-28), (star hence omitted!) $c_{R\gamma x}$, $c_{R\gamma y}$ result from (6.2-29). For a strict solution of $c_{E\gamma}$: (6.2-24). Ackermann and Birnbaum [6.6] proposed the following distribution of the strength $\gamma(x)$ of bound vortices (Fig. 6.2.3)

$$\gamma(x) = 2 w_\infty [A \gamma_A(x) + B \gamma_B(x) + C \gamma_C(x)],$$
$$\gamma_A(x) = [(1 - 2x/L)/(1 + 2x/L)]^{1/2}, \qquad \gamma_B(x) = [1 - (2x/L)^2]^{1/2},$$
$$\gamma_C(x) = (2x/L)[1 - (2x/L)^2]^{1/2} - \gamma_A(x)/6. \tag{6.2-30}$$

In the above A, B, C are coefficients, which have to be adapted to the boundary conditions. All these elementary vortex distributions satisfy the Kutta condition (6.2-23), namely with respect to (6.2-24): $c_{E\gamma x}(x = L/2) = \gamma(x = L/2)/2 = 0$. Inserting (6.2-30) in (6.2-24) gives the self-induced velocities in the y-direction on the x-axis at the point x (Fig. 6.2.3)

$$c_{E\gamma y A} = w_\infty, \qquad c_{E\gamma y B} = w_\infty 2 x/L, \qquad c_{E\gamma y C} = w_\infty [(2 x/L)^2 - 1/3]. \tag{6.2-31}$$

The kinematic boundary condition of a single profile is now satisfied approximately on the x-axis. This is admissible for small angles of attack and on profiles with small camber. Hence (Fig. 6.2.3)

$$dy/dx = c_{E\gamma y}/w_\infty. \tag{6.2-32}$$

Assuming the skeleton to intersect the origin of the coordinate system, the following skeletons result from (6.2-31), (6.2-32)

$$y_A = x, \qquad y_B = x^2/L, \qquad y_C = (4/3)x^3/L^2 - x/3. \tag{6.2-33}$$

This corresponds to the elementary skeletons and operating conditions: A) Flat plate with angle of attack. B) Circular arc (approximated by a parabola) with zero angle of
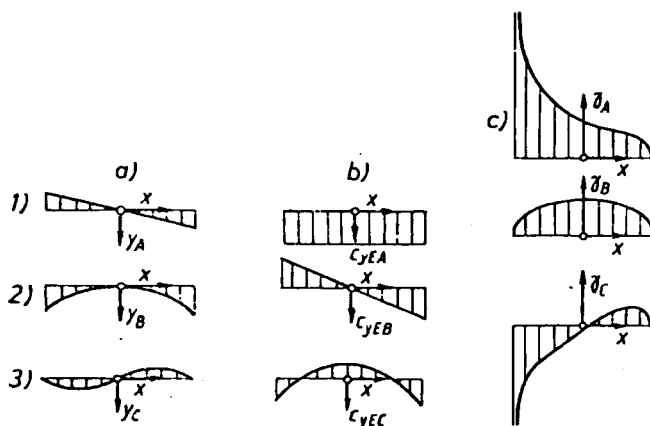
Fig. 6.2.3. Results of simplified singularity method. a) Form of skeleton due to the strength γ of bound vortex and w_∞ b) Velocity induced by γ on a single skeleton normal to it. c) Distribution of γ, with Kutta condition always satisfied. 1 plate; 2 single cambered skeleton; 3 double cambered skeleton.

attack against its chord. C) Double cambered skeleton with zero angle of attack against chord, (Fig. 6.2.3).

— Determination of the coefficients A, B, C after *Pantell* [4.10]:

a) Single aerofoil (E): Divide the small assumed inclination and angle dy/dx of the skeleton at an arbitrary point $x = x_i$, into 1) δ as the angle of attack, the chord makes with w_∞, 2) ϑ_i as the angle, the chord makes with the skeleton (Fig. 6.2.4), according to

$$dy/dx = \delta + \vartheta_i. \tag{6.2-34}$$

Inserting this and $c_{Eyy} = A\,c_{EyyA} + B\,c_{EyyB} + C\,c_{EyyC}$ from (6.2-31) into (6.2-32), gives with $A = A_E$, $B = B_E$, $C = C_E$,

$$\delta + \vartheta_i = A_E + B_E(2\,x_i/L) + C_E[(2\,x_i/L)^2 - 1/3]. \tag{6.2-35}$$
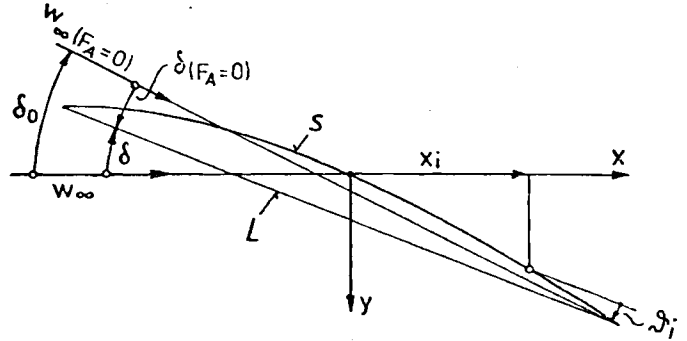
Fig. 6.2.4. Geometry of skeleton s and its chord L, angles ϑ_i and δ.

Writing down this relation for the three stations $x_1 = -L\sqrt{3}/4$, $x_2 = 0$, $x_3 = L\sqrt{3}/4$ (so-called *Birnbaum* stations), where the angle ϑ_i has the values $\vartheta_1, \vartheta_2, \vartheta_3$, this linear system gives

$$A_E = \delta + K_1; \qquad B_E = K_2; \qquad C_E = K_3, \tag{6.2-36}$$

$$K_1 = (2/9)\,\vartheta_1 + (5/9)\,\vartheta_2 + (2/9)\,\vartheta_3; \qquad K_2 = (\vartheta_3 - \vartheta_1)/\sqrt{3};$$

$$K_3 = (2/3)\,\vartheta_1 - (4/3)\,\vartheta_2 + (2/3)\,\vartheta_3. \tag{6.2-37}$$

After *Kutta* and *Joukovsky*, according to (5.2-29), the aerodynamic lift on an aerofoil, chord L, span 1, under the undisturbed velocity w_∞, depends on the circulation about the aerofoil Γ by: $F_A = \varrho\,w_\infty\,\Gamma$. Expressing F_A through the lift coefficient ζ_A as $F_A = (\zeta_A/2)\,\varrho\,w_\infty^2\,L$ and eliminating F_A gives the general relation between circulation and lift coefficient

$$\zeta_A = 2\,\Gamma/(w_\infty\,L). \tag{6.2-38}$$

With the circulation resulting from $\gamma(x)$ (6.2-30)

$$\Gamma = \int_{-L/2}^{L/2} \gamma(x)\,dx = \pi\,w_\infty\,L(A + B/2 + C/6), \tag{6.2-39}$$

the lift coefficient in general is obtained from

$$\zeta_A = 2\,\pi\,(A + B/2 + C/6). \tag{6.2-40}$$

For the single skeleton (E) with its coefficients from (6.2-36) and (6.2-37), the last relation is converted into

$$\zeta_{AE} = 2\,\pi\,(\delta + K_1 + K_2/2 + K_3/6). \tag{6.2-41}$$

The angle between zero lift direction ($\zeta_A = 0$) and chord, the so-called zero angle of attack follows from this as

$$\delta(F_A = 0)_E = -(K_1 + K_2/2 + K_3/6). \tag{6.2-42}$$

Obviously (Fig. 6.2.4) the so-called physical angle of attack δ_0, between zero lift direction (due to the aerofoil's geometry), and the undisturbed velocity w_∞ results from

$$\delta_{0E} = \delta - \delta(F_A = 0)_E = \delta + K_1 + K_2/2 + K_3/6. \tag{6.2-43}$$

Inserting this into (6.2–41) gives

$$\zeta_{AE} = 2\pi\delta_{0E}. \tag{6.2-44}$$

The exact theory would yield $2\pi\sin\delta_0$, which makes nearly no difference for the small angles of attack δ_0 ($< 15°$) considered here. In reality the constant is smaller than 2π namely 4,8 for slim profiles and up to 5,5 for thicker ones. The reason, discussed in [5.2] is given by the fact, that the real profile is accompanied by boundary layers and wakes, the displacement thickness of which has to be added to the solid aerofoil.

b) The aerofoil in cascade (G): Here an aerofoil with the geometry of the above single one is arranged in a cascade. The following three problems arise from this:

1) How does the lift coefficient (important for dimensioning a rotor vane) depend now on the physical angle of attack δ_0?
2) What is the ratio between lift coefficient of aerofoils in cascade to that of the single aerofoil, when the physical angle of attack is retained (so-called cascade factor)?
3) How does the zero angle of attack depend on the geometry of the aerofoil and the cascade?

Assuming relatively small induced velocities c_{Ry} of the residual cascade as compared with those c_{Ey} due to self induction and as compared with w_∞, compatible with the basic assumption of small angles of attack, the kinematic boundary condition corresponding to (6.2–32) may be approximated with the y-component of induced velocity c_y. According to (6.2–29) this is composed of c_{Eyy} and c_{Ryy}.

With $c_{Ryyi} = w_x(A_G c_{Ry\,Ai} + B_G c_{Ry\,Bi} + C_G c_{Ry\,Ci})$, i denoting the point considered, the kinematic boundary condition is now $dy/dx = (c_{Eyy} + c_{Ryy})/w_\infty$ and becomes with c_{Eyy} from (6.2–31) and dy/dx from (6.2–34) for the point $x = x_i$

$$\delta + \vartheta_i = A_G(1 + c_{Ry\,Ai}) + B_G(2x_i/L + c_{Ry\,Bi})$$
$$+ C_G[(2x_i/L)^2 - 1/3 + c_{Ry\,Ci}]. \tag{6.2-45}$$

If the profile with its angles ϑ_i in the cascade is the same as the single one and if also the angle of attack δ, the undisturbed speed w_∞ makes with the chord, is the same in both the cases, then the left hand sides of both the relations (6.2–35) and (6.2–45) are the same and hence can be eliminated.

Applying the remaining system at the three points $x_1 = -L\sqrt{3}/4$, $x_2 = 0$, $x_3 = L\sqrt{3}/4$, three linear equations are obtained for the coefficients A_G, B_G, C_G (due to the aerofoil in cascade) as a function of the coefficients A_E, B_E, C_E (due to the single aerofoil) according to (6.2–36), (6.2–37). Hence $A_G = f(A_E, B_E, C_E)$ etc.

Introducing now the coefficients A_G, B_G, C_G into (6.2–40) gives the lift coefficient in cascade of a certain aerofoil with the angles ϑ_i and hence certain figures K_i from (6.2–37) as

$$\zeta_{AG} = (C_1/C_4)\delta + (C_1 K_1 + C_2 K_2 + C_3 K_3)/C_4, \tag{6.2-46}$$

216

where C_1 through C_4 are functions of the parameters of the cascade, namely the pitch to chord ratio t/L and the angle β_∞ the straight carrier of bound vortices makes with the circumference. β_∞ stands for the undisturbed flow direction, the zero lift direction. Under the assumption of a small angle of attack δ_0, the angle β_0 the zero lift direction makes with the circumference can be substituted for β_∞. Table 6.2.1 contains the values C_1 through C_4 as functions of the so-called cascade parameters t/L and β_0.

Table 6.2.1. The cascade parameters C_1, C_2, C_3, C_4 as a function of β_0 and t/L.

β_0[°]	t/L	C_1	C_2	C_3	C_4	β_0[°]	t/L	C_1	C_2	C_3	C_4
15	0,25·	0,8169	0,7464	0,3709	0,2476	60	0,25	4,1990	3,5540	1.8620	3,4830
15	0,50	0,6904	0,3067	0,0691	0,0675	60	0,50	2,3350	1,7750	0,7794	0,9981
15	0,75	1,1610	0,5929	0,1108	0,1149	60	0,75	2,0490	1,3710	0.5346	0,6035
15	1,00	1,8460	0,6878	0,1482	0,1410	60	1,00	1,9970	1,2150	0,4450	0,4720
15	1,25	2,0120	0,7655	0,2128	0,1851	60	1,25	1,9900	1,1380	0,4036	0,4132
15	1,50	2,0150	0,8358	0,2510	0,2221	60	1,50	1,9920	1,0950	0,3814	0,3824
15	1,75	2,0090	0,8803	0,2735	0,2465	60	1,75	1,9940	1,0700	0,3683	0,3644
15	2,00	2,0060	0,9091	0,2879	0,2630	60	2,00	1,9960	1,0530	0,3599	0,3530
30	0,25	1,8810	1,6570	0,8413	0,9852	75	0,25	5,0170	4,2060	2.2140	4,5640
30	0,50	1,3330	0,9240	0,3389	0,3303	75	0,50	2,6370	2,0190	0,9098	1,2460
30	0,75	1,5220	0,8759	0,2638	0,2606	75	0,75	2,2070	1,5130	0,6128	0,7224
30	1,00	1,7820	0,8919	0,2629	0,2532	75	1,00	2,0820	1,3090	0,4977	0,5445
30	1,25	1,9150	0,9072	0,2787	0,2611	75	1,25	2,0380	1,2060	0,4411	0,4628
30	1,50	1,9640	0,9258	0,2925	0,2724	75	1,50	2,0190	1,1470	0,4093	0.4185
30	1,75	1,9830	0,9416	0,3022	0,2820	75	1,75	2,0110	1,1090	0,3897	0,3918
30	2,00	1,9910	0,9536	0,3090	0,2893	75	2,00	2,0070	1,0850	0,3768	0,3745
45	0,25	3,0810	2,6510	1,3760	2,1590	90	0,25	5,3020	4,3810	2,3450	4,9060
45	0,50	1,8870	1,4030	0,5783	0,6653	90	0,50	2,7320	2,0970	0,9486	1,3330
45	0,75	1,8130	1,1530	0,4130	0,4374	90	0,75	2,2580	1,5600	0,6358	0,7642
45	1,00	1,8810	1,0700	0,3636	0,3685	90	1,00	2,1110	1,3410	0,5133	0,5701
45	1,25	1,9350	1,0350	0,3465	0,3417	90	1,25	2,0550	1,2290	0,4525	0,4803
45	1,50	1,9650	1,0180	0,3399	0,3303	90	1,50	2,0300	1,1640	0.4178	0,4312
45	1,75	1,9800	1,0100	0,3369	0,3250	90	1,75	2,0170	1,1230	0,3964	0,4017
45	2,00	1,9880	1,0060	0,3354	0,3223	90	2,00	2,0110	1.0960	0,3821	0,3823

Analogous to (6.2–42) from ζ_{AG} the zero angle of attack is obtained for a certain skeleton having the parameters ϑ_i and hence K_i according to (6.2–37) and being within a cascade, having the parameters t/L and β_0 and consequently the coefficients C_1, C_2, C_3

$$\delta(F_A = 0)_G = -(C_1 K_1 + C_2 K_2 + C_3 K_3)/C_1. \qquad (6.2-47)$$

Similar to (6.2–43) the physical angle of attack δ_0 is introduced. This yields the lift coefficient of the profile in the cascade with the features C_1, C_4 as a function of the physical angle of attack as

$$\zeta_{AG} = (C_1/C_4)\delta_{0G}. \qquad (6.2-48)$$

A retrospective view of the achievements with respect to the problems of cascades (b) shows that problems 1) and 3) are solved by (6.2–48) and (6.2–47). Problem 2) is solved

217

by dividing (6.2–48) in ζ_{AE} from (6.2–44) with the assumption $\delta_{OE} = \delta_{OG}$. This results in the cascade factor

$$\varkappa = \zeta_{AG}/\zeta_{AE}(\delta_{OE} = \delta_{OG}) = (C_1/C_4)/(2\pi). \tag{6.2–49}$$

Hence

$$\zeta_{AG} = 2\pi\varkappa\delta_0. \tag{6.2–50}$$

It is seen from the $\varkappa(t/L, \beta_0)$-plot (Fig. 6.2.5), that the cascade factor $\varkappa$ deviates strongly from unity in the range of pitch chord ratios about 1. But this corresponds to the t/L range mostly used in axial machines [6.8].

The large $\varkappa$ at the rotor vane tip section (β_0 here about 18°) makes the lift coefficient and with it the susceptibility to cavitation there rather sensitive to small errors of vane position.
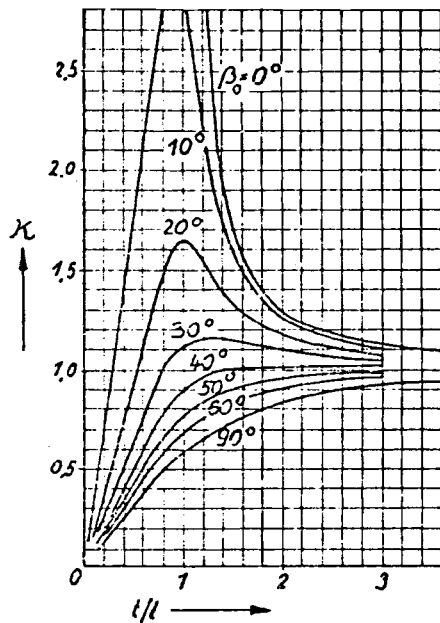
Fig. 6.2.5. Graph of the cascade factor $\varkappa$ of a straight cascade as a function of its pitch to chord ratio t/L and the angle β_0 of its zero lift direction.

The *Kutta* condition (6.2–23) at the rearward edge of a rotor vane requires a compensation of any flow induced by the residual cascade and tending to circulate about this edge by means of a change in circulation of the blade considered. This effect mainly dictates the lift coefficient and herewith $\varkappa$.

An approaching singularity method, similar to that of *Birnbaum*, but also valid for profiles of relatively small thickness, has been given by *Schlichting* [6.10]. *Raabe* [6.11] shows that the finite thickness of a profile mainly changes the zero lift direction of the cascade.

A rigorous method for an ideal flow through a cascade has been developed by *F. Weinig* [6.9]. This method uses conformal mapping to transform the contours of a straight cascade of straight skeletons into a circular contour. By means of conformal mapping, the domain, which corresponds to the flow about one skeleton, is expanded into a plane. Simultaneously the internal domain between the two stagnation points on the skeleton is transformed into a circular contour. Thus a treatment of the plane potential flow through the cascade is reduced to that around a circular cylinder. This is done by making the imaginary part of a regular function of a complex variable z a streamline and the real part of this function an equipotential line. Hence any conformal mapping must result in the same solution as the plane singularity method, since both methods assume a plane potential flow.

218

6.3. Some problems of steady flow through cascades

6.3.1. The circular cascade with axisymmetric stream surfaces

Imagine a stationary cascade (e.g., wicket gates) passed by a potential flow on axisymmetric and equidistant stream faces (Fig. 6.3.1 a). The solution of the indirect problem (Cap. 6.2) can be reduced to the above treated flow through a straight cascade by conformal transformation of the axisymmetric stream face onto a plane.

First the real stream face is conformally mapped on a coaxial circular cylinder (Fig. 6.3.1 b). The unrolling of the cylinder into a plane converts the circular cascade into a straight cascade.
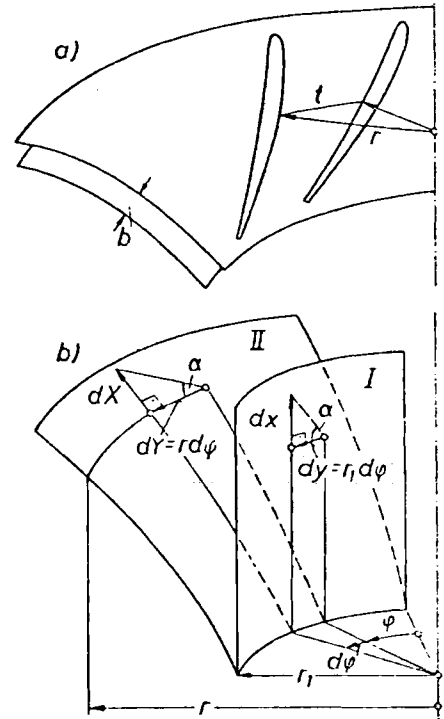
Fig. 6.3.1. Reduction of an axisymmetric cascade flow in a X, Y-surface to the flow around a straight cascade in the x, y-plane. a) Axisymmetric flow in a layer of constant depth b through a circular cascade in the X, Y-surface. b) Conformal mapping of an elementary triangle in the X, Y-surface to one in the cylindrical x, y-surface, developable onto a x, y-plane.

The conformal mapping is carried out such that the corresponding peripheral components of an elementary extension on the real face, having a variable radius r, and on the cylindrical image face, having a constant radius r_1, are enclosed between adjacent meridians, making an azimuth $d\varphi$ to each other. Hence the real peripheral component $r d\varphi$ is represented by an image $r_1 d\varphi$ and the azimuth of a real point equals that of its image.

Denoting the corresponding meridional components of this length by dx and dX on the image face and the real face, the similarity of elementary triangles on both the faces requires $dx/(r_1 d\varphi) = dX/(r d\varphi)$. Thus the meridional arc X of a point in the real face is represented by a length of $x = r_1 \int_0^x dX/r$. The above yields the local length scale of the mapping

$$M_l = dy/dY = dx/dX = r_1/r.\qquad(6.3-1)$$

Assume both the faces to be covered with a layer of the same depth passed by the same flow. Hence the local velocity scale

$$M_c = c/C = r\,d\varphi/(r_1\,d\varphi) = r/r_1\,,$$
(6.3-2)

where c and C are the velocities due to the image and real face. Obviously the scale of circulation being $M_t\,M_c$ is constant. See also [6.12; 6.13], [5.2].

6.3.2. The direct problem of a cascade in potential flow

This problem concerns the layout of a cascade including its profiles for given velocity triangles at its inlet and outlet. With respect to lift coefficient and cavitation sensitivity, the contour velocity of this cascade is usually somewhat restricted. The problem is considered in the simpler and better known case of a plane steady potential flow through a straight cascade.

Thereby full use can be made of the findings of Cap. 6.2 concerning the indirect problem due to the straight cascade. The governing integral equation (6.2–19), in its summed version (6.2–20) is the starting point, to solve the direct problem, which strictly speaking can be made only by means of relaxation methods and some additional conditions.

In the case of the direct problem the so-called deflection traingle is given (Fig. 6.2.1a). It consists of the velocities c_1 and c_2 upstream and downstream of the cascade and hence the so called deflection $\Delta c_u = c_{y2} - c_{y1}$ (in the case of a pump). Note that c in these considerations is always the velocity relative to the cascade.

For the design of an axial runner, gH, Q, and hence also the type number $n_q = \omega\,Q^{1/2}/(g\,H)^{3/4}$ are known. This gives the angular velocity ω. The vane number z follows from the head H. Expressing *Euler's* equation (see Cap. 5.3) for axial turbines in terms of runner vane circulation gives $\Gamma = 2\,\pi\,g\,H\,\eta_u/(z\,\omega)$. With Δc_u, Γ (6.2–15), also the pitch t is known and then by

$$\Gamma = \Delta c_u\,t = \oint c\,(s)\,ds = \sum_{v=1}^{n} c\,(s_v)\,h$$
(6.3-3)

also $\sum\limits_{v=1}^{n} c\,(s_v)\,h$ is given. Here the symbols are used in context with (6.2–20). There with $c_m = $ constant, the above sum appears in connection with the last term on the right hand side.

It appears that in an axial rotor of a hydro turbo machine the lift coefficient ζ_{AG} is prescribed. On its innermost cylindrical section close to the hub ζ_{AG} becomes highest. This is a consequence of the so-called "cascade dimensioning relation" of *Bauersfeld* [6.14] following from (6.3–3) in (6.2–38) as

$$\zeta_{AG} = (2\,t/L)\,\Delta c_u/w_\infty\,.$$
(6.3-4)

Hence in the innermost cylindrical section of a rotor vane, an upper limit of ζ_{AG} has to be set, to prevent stall. The outermost cylindrical section is most likely to cavitate. Because of a rise of the cavitation-linked factor λ (Cap. 8.2) with ζ_{AG}, formulated by *Raabe* [4.11] also a limit of ζ_{AG} must be fixed in this vane section.

Hence at Δc_u, w_x known from the deflection triangle (containing also w_∞ as the geometric mean value of w_1 and w_2), at ζ_{AG} prescribed, the pitch to chord ratio t/L yields from (6.3–4). From the velocity triangles also the angle α_1 of the influx is known.

Consider now again the governing equation (6.2–20). The direct problem consists in the determination of the angle $\alpha\,(z_i)$ of the vane contour at given α_1, c_m, $\Gamma = \sum\limits_{v=1}^{n} c\,(s_v)\,h$. With the contour unknown, also the points z_i and hence the functions f_x and f_y according to

(6.2-21) to (6.2-22) are not given. Obviously the problem must be solved by trial and error.

To introduce also the known t/L in the relation (6.2-20), the following ratio k is used

$$k = n\,h/(2\,L).$$
(6.3-5)

k corresponds to the ratio of contour length $n\,h$ to twice the chord L. Obviously this depends on the profile thickness and is about $k = 1{,}01$ for thin profiles at the outermost cylindrical vane section and about $k = 1{,}1$ for the thickest innermost cylindrical vane section (thick for reasons of solidity).

From this it is realized, that k may be fixed preliminarily. Introducing now from the last relation $h = 2\,k\,L/n$ into the basic equation (6.2-20) this then contains the known and essential pitch to chord ratio. Reducing this relation to the contour angle and accounting for (6.3-3) gives

$$\cot\alpha(z_i) = \left\{\Delta c_u/(2\,c_m) + \cot\alpha_1 + (L/t)(k/n)\sum_{v=1}^{n}[c\,(s_v)/c_m]\,f_y(z_i,z_v)\right\}/N,$$

$$N = 1 + (k/n)(L/t)\sum_{v=1}^{n}[c\,(s_v)/c_m]\,f_x(z_i,z_v).$$
(6.3 6)

The condition for the closure of the polygon formed by the elements of the contour reads

$$\sum_{v=1}^{n} h\cos\alpha(z_i) = 0.$$
(6.3-7)

To solve the direct problem, Inoue et al. use cascade data [6.15].

6.3.3. The indirect problem of the flow through a mixed flow rotor on axisymmetric stream faces of constant depth

Here again the solution may be facilitated by a conformal mapping of the circular cascade in the real axisymmetric flow plane into a straight cascade within the image plane. A rotor is considered (Fig. 6.3.2), which rotates with the angular velocity ω in the y-direction. Let μ be the angle, a normal to the flow plane makes with the rotor axis. The absolute flow shall be irrotational. Hence for an observer on the roating frame of reference, at a station of radius r, the fluid seems to move in the circumferential direction with a whirl velocity $-\,r\omega$. At a velocity scale from (6.3-2), this corresponds to a peripheral velocity $-\,\omega r^2/r_1$ in the image plane. Note in Fig. 6.3.2 ω is negative.

The absence of relative eddy $+\,2\,\omega\cos\mu$, within the vane contour of the flow plane and its image plane, induces the velocities $w_{hx}(z)$ and $w_{hy}(z)$ in the throughflow and peripheral direction respectively at a point $z(x,y)$ of the image plane.

They are function of $2\,\omega\cos\mu$ and the vane's cross sectional area A_s in the flow plane (Fig. 6.3.2). Accounting for this deficit of relative eddy $2\,\omega\cos\mu$, which is retained under conformal mapping, and recalling the circulation around a surface element dA_s to be $2\,\omega\cos\mu\,dA_s$, the velocities $w_{hx}(z)$ and $w_{hy}(z)$ can be approximately calculated by relations similar to (6.2-9), (6.2-10), where $\gamma(s)$ and s have to be changed a little. To this, imagine $dA_s = h\,ds$, where h is the local thickness of the profile in the flow plane, and ds its length along the vane skeleton, with the arc coordinate s. Now the line integrals in (6.2-9), (6.2-10) are transformed into integrals along the skeleton s, in which $\cos\mu$ and h are known functions of s.

221
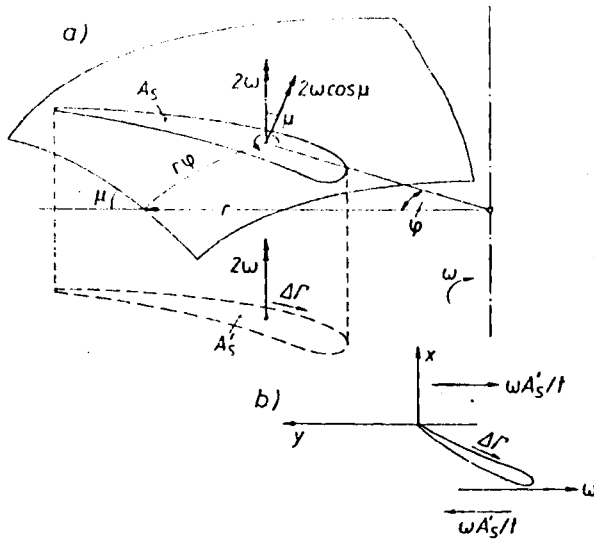
Fig. 6.3.2. Rotating circular cascade in an axisymmetric flow surface; *a* real flow plane; *b* flow plane in the image face after conformal mapping. Deficit of circulation $\Delta\Gamma = 2\omega A'_s$ due to the absence of flow within a profile is retained after conformal mapping. At infinity in the image plane, $\Delta\Gamma$ induces the peripheral velocities $\mp \omega A'_s/t$. *t* pitch. Note: $\Delta\Gamma$ appears in the text with the opposite sense of rotation. In this figure, the rotor turns in a sense opposite to that in the text.

The conservation of circulation in conformal mapping gives $\oint \gamma(S)\,dS = \oint \gamma(s)\,ds$, where S denotes the arc of the contour in the flow plane and s that in the image plane.

The velocities induced by the bound vortex element $\gamma(s)\,ds$ in the image plane result from (6.2–9) and (6.2–10). With respect to the velocity components $w_{h,x}(z)$, $w_{h,y}(z)$ due to the deficit of relative eddy within the contour, the whirl velocity $-\omega r^2/r_1$ due to rotation, and the undisturbed velocity components w_m and $w_m \cot \beta_\infty$ in the x and y-direction, the components of the relative velocity in the image plane become

$$w_x(z) = w_m + \frac{1}{2t}\oint \gamma(s) f_x[z, \zeta(s)]\,ds + w_{h,x}(z), \qquad (6.3-8)$$

$$w_y(z) = w_m \cot \beta_x + \frac{1}{2t}\oint \gamma(s) f_y[z, \zeta(s)]\,ds + w_{h,y}(z) - \frac{\omega r^2}{r_1}. \qquad (6.3-9)$$

The kinematic boundary condition at a station z_P on the contour, which makes there an angle β_P with the y-coordinate, reads

$$w_y(z_P) = w_x(z_P) \cot \beta(z_P). \qquad (6.3-10)$$

The angle β_x of the undisturbed relative flow with the circumference is rather impracticable and can be expressed by the more convenient known angle β_1 of relative influx with the negative y-axis, as follows

$$\cot \beta_x = \cot \beta_1 + \frac{1}{2t\,w_m}\oint \gamma(s)\,ds - \frac{\omega A'_s}{t\,w_m} + \frac{\omega r_1}{w_m}. \qquad (6.3-11)$$

This relation results from the known limit of the velocity components in the station 1 at rotor inlet, when this is imagined to be at infinity before the rotor cascade ($w_{x1} = w_m$),

$$w_{y1} = w_m \cot \beta_\infty - \frac{1}{2t}\oint \gamma(s)\,ds + \frac{\omega A'_s}{t} - \omega r_1,$$

and $w_{y1} = w_m \cot \beta_1$. With the abbreviation

$$w_h(z_P) = w_{hy}(z_P) - w_{hx}(z_P) \cot \beta(z_P), \qquad (6.3-12)$$

and with regard to (6.3–11), inserting the velocity components (6.3–8), (6.3–9) into the kinematic boundary condition (6.3–10), yields the following linear integral equation for the contour velocity $w(s)$ of the image plane

$$2t\left\{+\cot\beta(z_P)-\cot\beta_1+\frac{\omega r_1}{2w_m}\left[\left(\frac{r}{r_1}\right)^2-1\right]+\frac{\omega A'_s}{w_m t}-\frac{w_h(z_P)}{w_m}\right\}$$

$$=\oint\frac{w(s)}{w_m}\{1-\cot\beta(z_P)f_x[z_P,\zeta(s)]+f_y[z_P,\zeta(s)]\}\,ds.\tag{6.3-13}$$

The term $\omega A'_s$ contains in A'_s the projection of the vane trace in the real flow face onto a plane normal to the axis. See also (5.2-37). It follows from the absence of vortex flux due to the relative eddy in the interior of the vane and may be understood as the peripherally orientated velocity induced at infinity before and behind the cascade by a straight row of such "eddy-deficit-vortices" each having circulation $2\omega A'_s$ (Fig. 6.3.2).

After the solution of (6.3-13) e.g., by means of the conversion of the integral into a sum and hence a conversion into a system of linear equations for the determination of the contour velocity $w(s)$ (Cap. 6.2.1.2), the obtained velocities have to be divided by the velocity scale factor from (6.3-2) to obtain the real contour velocity.

6.3.4. Cascade in an axisymmetric flow lamina of variable depth

Consider an axisymmetric flow lamina of variable depth b (Fig. 6.3.3 a) passing a circular cascade. Here the mean streamface with its vane traces can be transformed into a straight cascade by conformal mapping (Cap. 6.3.1). The velocity scale after (6.3-2) postulates retaining the layer's depth due to corresponding points in the real and the image face. Hence the gradient of the depth b in the meridional direction appears as a new parameters of the image plane: $db/dx = b'$.

In such a wedged-formed flow lamina the individual bound vortex may be imagined to be normal to the mean stream face. On the faces, covering this lamina, the flow, due to a straight elementary vortex partly penetrates these faces and thus is no longer compatible with the kinematic boundary condition.

Therefore instead of straight elementary vortices the elementary bound vortex now has to be a ring vortex, that penetrates normal through the covering faces (Fig. 6.3.3 b).

Since the flow field induced by a ring vortex differs greatly from that of a straight one, the influence functions f_x, f_y (6.2-6), (6.2-7) due to the straight vortex row must be replaced by corresponding functions due to a row of ring vortices [5.5].
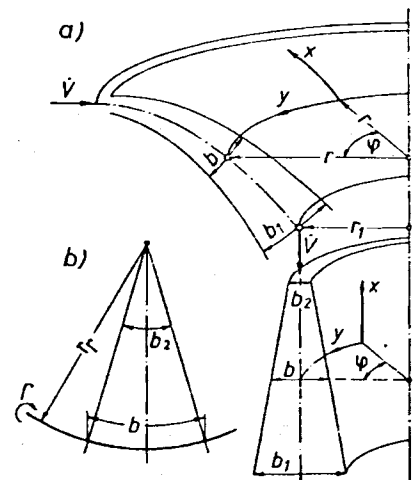
Fig. 6.3.3. Cascade flow in a layer of varying depth. a) Axisymmetric flow lamina of varying depth b in a real X, Y-flow plane and its image in a cylindrical x, y-plane, developable onto a plane. b) Substitution of a straight bound elementary vortex by an elementary ring vortex. $\dot V=$ flow within the layer.
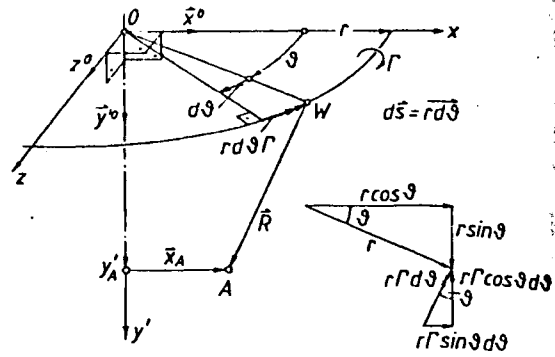
Fig. 6.3.4. Schematic perspective view of an elementary ring vortex with its element, length $rd\vartheta$, in W, inducing in A the velocity $dc_{\gamma b}$.

The flow induced by an individual ring vortex is composed of that induced by its vortex elements. The latter follows from the law of *Biot Savart* [5.5], (Fig. 6.3.4),

$$d^2 c_{\gamma b} = [d\,\Gamma/(4\,\pi\,R^3)]\,(ds \times R),\qquad(6.3-14)$$

where ds is the vector of a vortex element, $d\Gamma$ its circulation, R the distance of a point A from the vortex element.

For the computation of the induced velocity components in the axial and radial directions (both with respect to the axis of the ring vortex) $dc_{\gamma b y'}$ and $dc_{\gamma b x'}$ the ring vortex is located in the x', z-plane of a right hand *Cartesian* coordinate system (Fig. 6.3.4). The centre of the ring vortex is the origin of this system. An arbitrary point A has the coordinates y'_A and x'_A in the directions y' and x', thus $A\,(y'_A, x'_A, 0)$. An arbitrary vortex element of the ring of radius r, on the point of azimuth ϑ has the coordinates $W(0, + r\cos\vartheta, + r\sin\vartheta)$. Hence the vector R pointing from W to A: $R\,(y'_A, x'_A - r\cos\vartheta, - r\sin\vartheta)$. The vortex element ds has the components $(0, r\sin\vartheta\,d\vartheta, - r\cos\vartheta\,d\vartheta)$. Since the flow field induced by the ring vortex is axisymmetric, the components induced in the y', x'-plane are representative. With the above components and (6.3–14), (see Fig 6.3.4),

$$dc_{\gamma b y'} = - (d\Gamma\,r^2/2\,\pi) \int_0^\pi R^{-3}(1 - x_A \cos\vartheta/r)\,d\vartheta,\qquad(6.3-15)$$

$$dc_{\gamma b x'} = - (d\Gamma\,r\,y'_A/2\,\pi) \int_0^\pi R^{-3} \cos\vartheta\,d\vartheta.\qquad(6.3-16)$$

Next consider the ring vortex within the x, y-system of the image plane (Fig. 6.3.5). Here the field point A on the contour has the coordinates x, y and the singularity point W the coordinates ζ, η. The axis of the ring vortex is in x_0, η. The depth of lamina b varies, according to $db/dx = b'$. Hence obviously
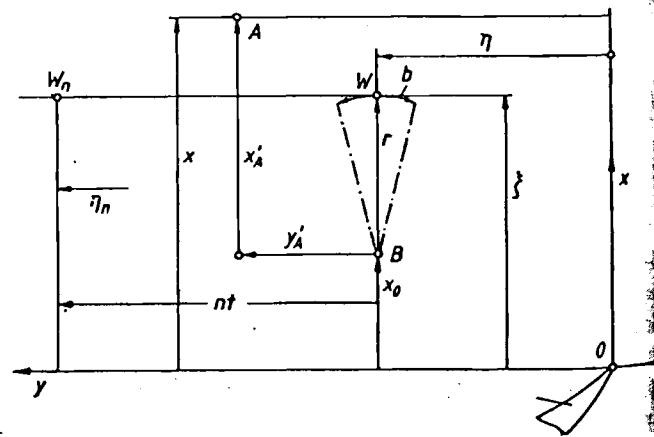
Fig. 6.3.5. Relations between the coordinates (ζ, η) or (ζ, η_n) of a ring vortex W, or W_n (of profile zero o, or n), those of its centre $B\,(x_0, \eta)$ and the point considered $A\,(x'_A, y'_A)$.

224

$$r = b/b', \tag{6.3-17}$$

$$x_0 = \xi - r = \xi - b/b'. \tag{6.3-18}$$

Obviously (Fig. 6.3.5) the coordinates x'_A, y'_A of the point A in the system with origin in the centre of the ring vortex can be related to the coordinates x, y of the point A in the image plane and to the corresponding coordinates ξ, η of the bound elementary vortex W by

$$x'_A = x - x_0 = x - \xi + b/b', \tag{6.3-19}$$

$$y'_A = y - \eta. \tag{6.3-20}$$

Placing the origin of the x, y-system at the sharp rearward edge of the zero profile, the coordinates ξ_n, η_n of a point W_n on the nth profile, which is shifted in y-direction by nt against the analogous point $W(\xi, \eta)$ on the zero profile are assigned to ξ, η by $\xi_n = \xi$ and $\eta_n = \eta + nt$. Hence for the nth profile

$$x'_{An} = x'_A, \tag{6.3-21}$$

$$y'_{An} = y - \eta - nt. \tag{6.3-22}$$

Like (6.2-4), (6.2-5) the components of the velocity induced by a straight row of elementary ring vortices with circulation $d\Gamma = \gamma(s)\,ds$ may be expressed by influence functions f_{bx}, f_{by} according to

$$dc_{ybx} = [\gamma(s)\,ds/(2\,t)]\,f_{bx}, \qquad dc_{yby} = [\gamma(s)\,ds/(2\,t)]\,f_{by}. \tag{6.3-23}$$

With the simplifications

$$- (y - \eta - nt)(b/b')^{-1} = h, \qquad - (\xi - x)(b/b')^{-1} + 1 = c,$$

$$h^2 + c^2 + 1 = a, \qquad 2c = f, \qquad 2/\{[h^2 + (1 + c)^2]^{1/2}\,[h^2 + (1 - c)^2]\} = s,$$

$$4/[(a + f)^{1/2}\,f] = l \tag{6.3-24}$$

by means of the complete elliptic integrals $E(\pi/2, k)$ and $F(\pi/2, k)$ of the first and second order [6.16], defined by

$$E(\pi/2, k) = \int_0^{\pi/2} (1 - k^2 \sin^2 \vartheta)^{1/2}\,d\vartheta, \qquad k = [2\,f/(a + f)]^{1/2},$$

$$F(\pi/2, k) = \int_0^{\pi/2} (1 - k^2 \sin^2 \vartheta)^{-1/2}\,d\vartheta \tag{6.3-25}$$

and using the elliptic integrals $I_1(\pi) = \int_0^{\pi} (a - f \cos \vartheta)^{-3/2}\,d\vartheta$,

$$I_3(\pi) = \int_0^{\pi} (1 - \cos \vartheta)(a - f \cos \vartheta)^{-3/2}\,d\vartheta,$$

depending on $E(\pi/2, k)$ and $F(\pi/2, k)$ by

$$I_1(\pi) = s\,E(\pi/2, k); \qquad I_3(\pi) = l\,[F(\pi/2, k) - E(\pi/2, k)], \tag{6.3-26}$$

the influence functions f_{bx}, f_{by} can be expressed by

$$f_{bx} = [t\,b/(\pi\,b')] \sum_{n=-\infty}^{+\infty} h\,[I_1(\pi) - I_3(\pi)], \tag{6.3-27}$$

$$f_{by} = - [t\,b/(\pi\,b')] \sum_{n=-\infty}^{+\infty} [(1 - c)\,I_1(\pi) - c\,I_3(\pi)]. \tag{6.3-28}$$

When calculating the sums, attention has to be paid to the fact, that the integer n exists in the term h, which then influences also the elliptic integrals. Usually $h' = db/dx < 0$.

Concluding remark about steady flow in cascades: In the foregoing sections the bound vortices have been assumed to be orientated normal to the stream face. When the bound vortex (and hence also the edge of a vane) makes an arbitrary angle with a yet axisymmetrically assumed streamface, the vortex can be split into a component normal to the stream face and another tangential to it.

The tangential component again can be split into a meridional and a peripheral one. The flow field due to the latter corresponds to that of vortex rings coaxial to the machine. The field of the meridional component twists the axisymmetric stream face within the vane channels, see also Cap. 10.6.

The axisymmetric flow through a rotor can be obtained also by other methods. *Schilling* uses a streamfunction for a layer of varying depth [6.17], similar Cap. 5.2. *Borel* [6.18] applies potential theory to calculate the flow through guide vanes and rotor in a mixed flow machine. *Hirsch* [6.19] uses the finite element method for axisymmetric flow in turbomachines. *Keck* [6.20], *Höller* [6.21], and *Pfoertner* [6.22], apply this method for a quasi 3 dimensional flow with the aid of measurements.

Martelli [6.23] uses the finite element method for the blade to blade flow calculation. *Murai* [6.24] limits his consideration on a mean flow plane. *Daiguji* [6.25] considers only upstream effects. *Adler* and *Ihlberg* present a simplified flow calculation for the entrance of radial and mixed flow impellers [6.26].

6.4. The unsteady flow through straight cascades in tandem arrangement, moving relative to each other[6])

6.4.1. Introduction

The flow past a cascade is pitch periodical and hence that through a cascade past another and moving relative to another is unsteady. This case exists usually in hydro turbomachines with a vaned stationary gate and the runner downstream. Hence vane oscillations, their fatigue problems, energy loss due to unsteady circulation and trailing vortex sheet due to it, falsified measurements of non-dynamical probes, are the consequences the engineer is confronted with.

6.4.2. Model of cascade and assumptions

The flow in hydraulic turbomachines with its cascades of blades in series moving relative to another (as represented by wicket gates and runner blades) is unsteady. This holds also for the plane potential flow of an ideal fluid. As a model consider the phenomena within two straight cascades moving relative to each other as shown in Fig. 6.4.1 a. As shown in Fig. 6.4.1 b assume the active cascade 'a' as located alternatively upstream or downstream of the passive cascade 'p'. The active cascade is the one which acts on the passive cascade 'p'. Following *M. Lotz* these assumptions are made (see also [6.27; 6.28]):

1. Steady flow through the active cascade.
2. Location of bound vortices for the profiles of the passive cascade along the sections $-1 < x_p < +1$ on a blade of length 2 according to Fig. 6.4.1 b. The direction of x_p coincides with the undisturbed throughflow velocity w_x. (Possible in consequence of the small angle of attack.)
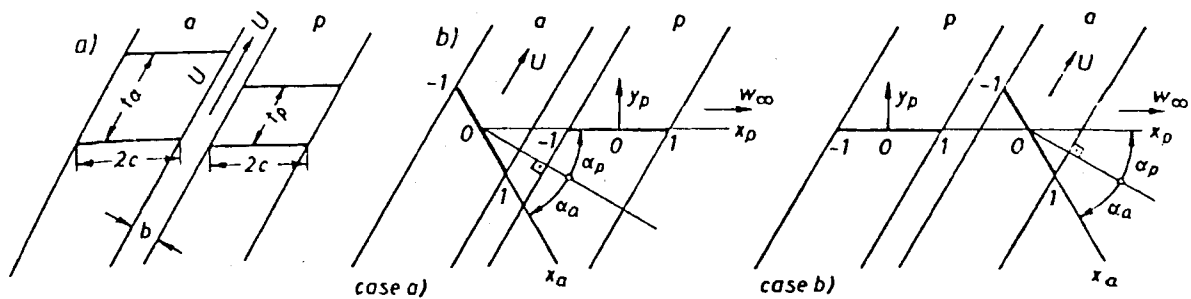
Fig. 6.4.1. Survey of cascades, investigated. a) Active cascade (a); passive cascade (p); their distance b and their pitches t_a, t_p. b) Cascade arrangements investigated; case (a), active cascade upstream, case (b), active cascade downstream.

3. Infinitely long vortex sheets, swimming in the x_p-direction from the trailing edge $(x_p = 1)$ of all the passive profiles with the undisturbed throughflow velocity w_∞ parallel to the line, charged with bound vortices. The variation with time of the vortex distribution of these vortex sheets obeys the theorem of Thomson with respect to the circulation around each blade of the passive cascade.

4. Plane potential flow of an incompressible nonviscous fluid, in which the vortex sheets. swimming from the trailing edge of the passive cascade, are located along a streamline.

5. The temporal arbitrary form of the flow is assumed as decomposable in its harmonic portions. One of these is considered here. This one has a basic frequency given by the geometry of the active cascade.

6. The cascades have blades of one and the same length $L_a = L_p$ (index 'a' means active, index 'p' means passive). Thickness of the profile, its camber and angle of attack are infinitesimally small.

6.4.3. Basic idea of the procedure

The vortex distribution of the passive cascade γ_p is assumed as a temporal harmonic function with unknown amplitude, which varies with the coordinate of the locus of the considered station of the passive "zero" profile. This is the profile, which carries in its mid chord the origin of the passive *Cartesian* coordinate system. The spatial vortex distribution along the chord of the passive zero profile results from the fact, that at any station of the passive profile the sum of all induced downwash velocities at any instant must be zero. This sum is composed of the following components:

a) Downwash velocity from the instantaneous vortex distribution of the passive profile considered.

b) Downwash velocity from all the neighbouring passive profiles, the vortex distribution of which oscillates between homologously located points of adjacent profiles with a definite phase shift.

c) Downwash velocity from all the free vortices of the vortex sheets, running from the trailing edge of the blades of the passive cascade, which also oscillates in homologously located points against the adjacent sheet with a definite phase shift, and the amplitudes of which vary due to Thomson's theorem with respect to the blade circulation of the passive blade, from which they start.

d) The downwash velocity of the active cascade. This moves against the passive cascade with a constant velocity U in the peripheral direction. Therefore also U must be added to this downwash velocity.

227

6.4.4. Realization of the procedure

The vortex distribution of the steadily operating active cascade is assumed to be composed by the first two terms of a *Glauert* series

$$\gamma_a = A_0(1 + \cos \vartheta)/\sin \vartheta - 2A_1 \sin 2\vartheta. \tag{6.4-1}$$

Herein ϑ depends on the coordinate ξ_a, which is numbered from the mid-chord of the active cascades' zero profile as follows

$$\xi_a = -\cos \vartheta, \quad 0 \le \vartheta \le \pi. \tag{6.4-2}$$

That means $\xi_a = 1$ coincides with the trailing edge of the blade. With the circulation around the active blade

$$\Gamma_a = \int_{-1}^{+1} \gamma_a(\xi_a)\, d\xi_a \tag{6.4-3}$$

follows the instantaneous downwash velocity of the active cascade at the locus x_p of the zero blade of the passive cascade as

$$v_i(x_p, t) = \sum_{h=1}^{\infty} Re\left[\frac{\Gamma_a}{t_a} G_h \exp(\lambda x_p) \exp(j h v_1 t)\right], \tag{6.4-4}$$

$$v_i(x_p, t)_a = \bar{v}_i(x_p)_a e^{j h v_1 t}. \tag{6.4-5}$$

The values herein have the following meaning

$$v_1 = 2\pi U/t_a, \tag{6.4-6}$$

$$\lambda = \mp h\pi \frac{L_p}{t_p} \frac{t_p}{t_a} e^{\pm i\alpha_p}, \tag{6.4-7}$$

$$G_h = \mp e^{\pm\alpha_p} \exp\left\{- h\pi \left(\frac{L}{t}\right)_p \frac{t_p}{t_a} e^{\pm i\alpha_p} \left[1 + \frac{\frac{2b}{L_p} + \frac{L_a}{L_p}\cos\alpha_a}{\cos\alpha_p}\right]\right\} H_h, \tag{6.4-8}$$

$$H_h = \varkappa H_h(\varkappa = 1) + (\varkappa - 1) H_h(\varkappa = 0), \tag{6.4-9}$$

$$\varkappa = A_0/(A_0 - A_1), \tag{6.4-10}$$

$$H_h(\varkappa = 1) = J_0\left[\pm i h\pi \left(\frac{L}{t}\right)_a e^{\mp i\alpha_a}\right] + J_1\left[\pm i h\pi \left(\frac{L}{t}\right)_a e^{\mp i\alpha_a}\right], \tag{6.4-11}$$

$$H_h(\varkappa = 0) = \mp \frac{2i}{h\pi}\left(\frac{t}{L}\right)_a e^{\mp i\alpha_a} J_1\left[\pm i h\pi \left(\frac{h}{t}\right)_a e^{\mp i\alpha_a}\right], \tag{6.4-12}$$

with J_0 and J_1 as *Bessel* functions of order zero and one. Generally the *Bessel* function of order p is defined by

$$J_p = \sum_{k=0}^{\infty} \frac{(-1)^k}{\Pi(k)\,\Pi(p+k)} \left(\frac{x}{2}\right)^{p+2k}, \tag{6.4-13}$$

with

$$\Pi(k) = k\,\Pi(k-1). \tag{6.4-14}$$

228

In the relations above, the upper sign is valid if the active cascade lies upstream from the passive cascade.

6.4.5. List of used symbols

U: velocity of the active cascade in the peripheral direction against the passive cascade.
Re: real part
t: pitch
x: stagger angle
L: length of profile chord
h: order of the harmonic
b: distance of the two cascades, normal to its axis
i, j: imaginary units
index a: active cascade
index p: passive cascade
index i: value, which depends only on the instantaneous motion, in contrary to the transient value, depending also on its history.

6.4.6. Derivation of governing linear integral equation

The velocity field of a row of homologously located passive vortex elements is defined by the fact, that two neighbouring vortices are oscillating with a phase shift of

$$
m \pi = 2 \pi h \left(1 - \frac{t_p}{t_a} \right), \quad 0 \leq m \leq 2 \pi. \tag{6.4-15}
$$

The induced downwash velocity of all the blades of the passive cascade and its vortex sheets is compensated by the downwash velocity $v_i(x_p)_a e^{i h v_i t}$ of the active cascade.

This passive downwash velocity of the whole passive cascade; with its blades of length $L_p = 2$ together with the infinitely long vortex sheets swimming from the trailing edge of each blade at its rear end becomes

$$
\bar{v}_i(x, t)_p = \int_{\xi = -1}^{\infty} \bar{\gamma}_i(\xi) e^{j v t} K(x, \xi) d\xi \tag{6.4-16}
$$

with

$$
\bar{\gamma}_i(\xi) = Re \, \bar{\gamma}_p(\xi) e^{j n m \pi}, \tag{6.4 17}
$$

$$
K(x, \xi) = \frac{P}{2 \pi} \sum_{n = -\infty}^{+\infty} \frac{e^{j n m \pi}}{\frac{P}{\pi}(x - \xi) - jn} + \frac{\hat{P}}{2 \pi} \sum_{n = -\infty}^{+\infty} \frac{e^{j n m \pi}}{\frac{\hat{P}}{\pi}(x - \xi) + jn}, \tag{6.4-18}
$$

n as integer number belonging to the individual passive blade, and

$$
P = \pi \frac{L_p}{2 t_p} e^{j a_p}, \tag{6.4-19}
$$

$$
\hat{P} = \pi \frac{L_p}{2 t_p} e^{-j a_p}. \tag{6.4-20}
$$

229

The equalization of $v_i(x_p)_a$ and $v_i(x_p)_p$ leads to the following integral equation for the vortex distribution $\bar{\gamma}_p(\xi)$

$$\frac{1}{2\pi} \int_{-1}^{+1} \bar{\gamma}_p(\xi) \left[K(x, \xi) - i k e^{ik} \int_{+1}^{\infty} e^{-ik\xi'} K(x, \xi') d\xi' \right] d\xi = \bar{v}_i(x_p)_a . \quad (6.4-21)$$

Herein $v_i(x_p)_a$ is defined by equation (6.4-5). Furtheron we have

$$k = v_1 L_p/(2 w_\infty) \quad (6.4-22)$$

as reduced frequency.

6.4.7. Solution of integral equation by polynomials following Lotz

Lotz has solved the basic linear integral equation (6.4-21) by introduction of a trigonometric auxiliary variable and a substitution proposed by *Schmeidler*. This procedure reduces the integral equation of our problem into a *Fredholm* integral equation of the first order. For a numerical computation the Kernel $K_R(x - \xi)$ for the neighbouring blades of the passive cascade is approximated by a polynomial

$$K_R(x - \xi) = j c_0 + c_1 r + j c_2 r^2 + c_3 r^3 + j c_4 r^4 , \quad (6.4-23)$$

with

$$r = x - \xi . \quad (6.4-24)$$

c_0 is chosen so, that $K_R(r)$ has its exact value in the considered point. The other constants will be computed so, that the integral of its squared error within $-2 \leq r \leq +2$ becomes a minimum. Thus it results

$$c_0 = \frac{\pi}{2} \left(\frac{L}{t}\right)_p (m - 1) \sin \alpha_p , \quad (6.4-25)$$

$$c_1 = \frac{75}{32} T_1 - \frac{105}{128} T_3 - \frac{5}{2} , \quad (6.4-26)$$

$$c_2 = \frac{245}{128} T_2 - \frac{315}{512} T_4 - \frac{7}{6} c_0 , \quad (6.4-27)$$

$$c_3 = -\frac{105}{128} T_1 + \frac{175}{512} T_3 + \frac{35}{48} , \quad (6.4-28)$$

$$c_4 = -\frac{315}{512} T_2 + \frac{441}{2048} T_4 + \frac{21}{80} c_0 , \quad (6.4-29)$$

with

$$T_1 = \int_0^2 Re(K_R) r \, dr , \quad (6.4-30)$$

$$T_2 = \int_0^2 Im(K_R) r^2 \, dr , \quad (6.4-31)$$

$$T_3 = \int_0^2 Re(K_R) r^3 \, dr , \quad (6.4-32)$$

230

$$T_4 = \int_0^2 Im(K_R) r^4 \, dr.$$

(6.4–33)

6.4.8. Lift and moment on the passive cascade

With $\gamma_p(\xi, t) = \gamma(\xi, t)$ and the circulation around the passive blade

$$\Gamma_p = \Gamma = \int_{-1}^{+1} \gamma(\xi, t) \, d\xi,$$

(6.4–34)

we get lift and moment related to the mid-chord of the considered profile as

$$F_A = \varrho \, w_\infty \Gamma + \frac{\varrho}{2} L \frac{d\Gamma}{dt} - \frac{\varrho L^2}{4} \int_{-1}^{+1} \frac{\partial \gamma(\xi, t)}{\partial t} \xi \, d\xi,$$

(6.4–35)

$$M_A = \frac{L^2}{8} \varrho \frac{d\Gamma}{dt} - \varrho \frac{L^2}{4} w_\infty \int_{-1}^{+1} \gamma(\xi, t) \xi \, d\xi + \varrho \frac{L^3}{16} \int_{-1}^{+1} \frac{\partial \gamma(\xi, t)}{\partial t} \xi^2 \, d\xi.$$

(6.4–36)

F_A and M_A are related to a blade of width "one". Obviously the lift as given by *Kutta* and *Joukovsky* holds only for steady flow.

6.4.9. Discussions of evaluated results

The aforementioned theory has been evaluated for the case $b = 0,1 \, L_p$, a relation, which may be realized at the outer parts of a tubular turbine with a fully opened runner. Furthermore it has been assumed that $t_p = t_a$, $\alpha_a = 45°$, $(t/L)_p = 1$. Computation has been carried out for case a) with the active cascade upstream of the passive one and case b) with the active cascade downstream of the passive one. Furthermore the computation has been made for the case $\varkappa = 1$ and $\varkappa = 0$. For $\varkappa = 0$ the angle of attack of the active cascade becomes zero. In this case the profile consists of a circular arc with the flow along its chord, due to $A_0 = 0$. For $\varkappa = 1$ the active cascade consists of plane plates with a finite angle of attack due to $A_1 = 0$.

A first computation shows that only the first harmonic need be considered. In Fig. 6.4.2 we see the relative lift amplitude of the first harmonic for the case a) and b) and $\varkappa = 1$, $\varkappa = 0$.

The result shows relative lift amplitudes up to 20% for stagger angles between 0° and 40° of the passive cascade, if the active cascade is arranged downstream and operates with an angle of attack against a plate as profile ($\varkappa = 1$). This case may be realized under fully opened runner blades in the cylindrical section of a tubular turbine near the throat ring. Even if the actual problem is not exactly a plane one, one can reduce it approximately by conformal mapping of the outer streamsurface into a plane.

The same can be done with a Kaplan turbine of cylindrical wicket gates. Here the distance is usually greater between wicket gates and runner blades.

Fig. 6.4.3 demonstrates for the case $\alpha_a = \alpha_p = 45°$, that the relative lift amplitude of the first harmonic increases with decreasing ratio t_p/t_a. That means: The higher the blade number of the stimulating active cascade the higher the lift amplitude. Similar results are obtained for the amplitudes of the moments about the mid-chord of the blade.

This holds more for an active cascade upstream. In the actual case of the downstream runner as the active cascade we have usually very low values of t_p/t_a as the runner has $z = 4$ to 5 blades and the distributor has 12 to 24 wicket gates. Therefore in this case the wicket gates are not seriously stimulated by vibrations.
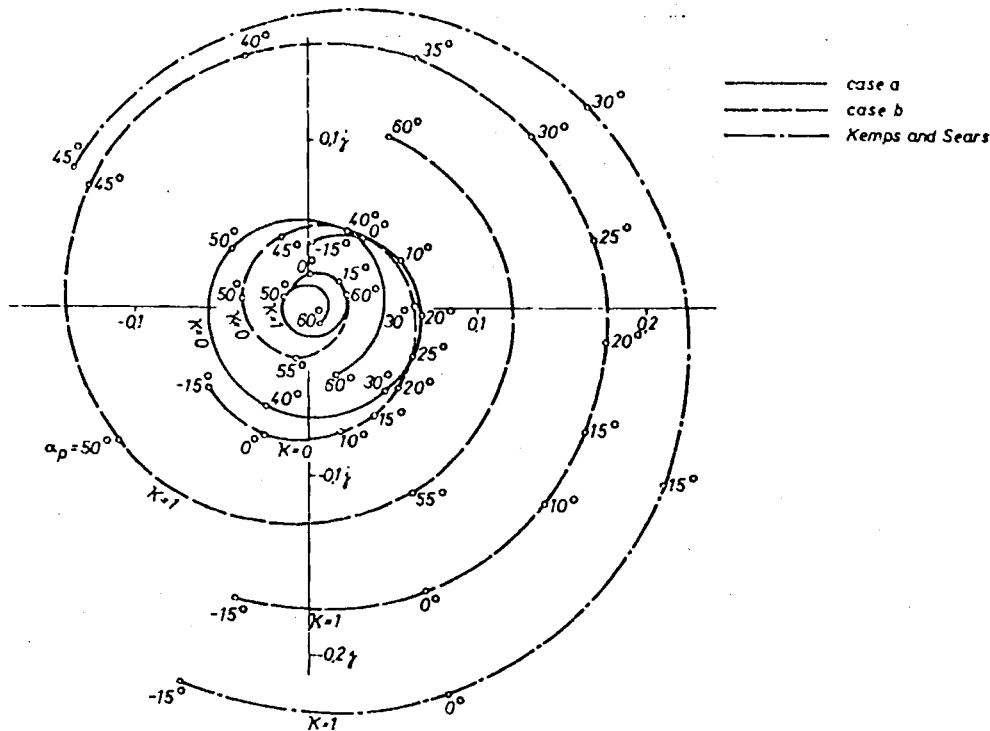
Fig. 6.4.2. Complex amplitudes of the unsteady lift as a function of the stagger angle α_p on the passive cascade, for the case $\alpha_a = 45°$, $t_p/t_a = 1$, and $L_p/t_p = 1$; order of harmonics $h = 1$.
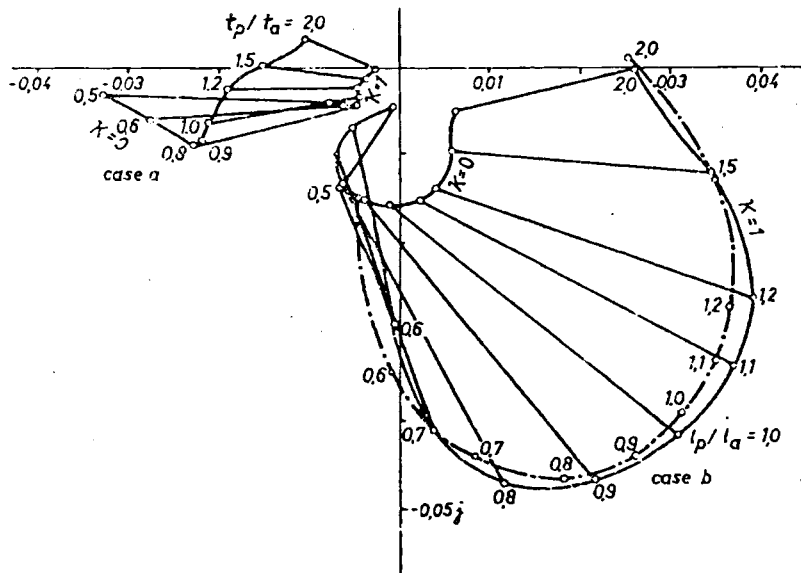
Fig. 6.4.3. Complex amplitudes of the unsteady lift moment as a function of the pitch/chord ratio t_p/L_p on the passive cascade, for the case $\alpha_p = \alpha_a = 45°$, $t_p/t_a = 1$, $h = 1$.

When the machine operates with a reversed flow as a pump or a tidal turbine, then the action of the fluctuations of downstream located wicket gates, now acting as diffusers, on the impeller or runner blades may be dangerous. This danger is enlarged by wakes.

6.4.10. Conclusion of practical results, effect of wakes

As measurements, carried out by *Castorph* [6.29], at Technical University, Munich, have shown, such wakes are relevant also in the case of a vertical Kaplan turbine, when they act from the upstream

232

located wicket gates on the outer section of the runner blade. Here indeed the streamwise distance between the exit of a cylindrical gate and the runner vane may be rather short.

The said measurements have been carried out with a special six port microsemiconductor vectorial probe of quick response which enables vibrations up to 5000 cycles to be indicated. Such a probe (Cap. 9.5) indicates behind the runner likewise the wakes produced by the runner blades, also, the wakes produced by the wicket gates, which have been cut into pieces by the runner blades. The magnitude of the measured unsteadiness caused by a wake can be predicted due to the measurements by the following method.

According to *Kemp* and *Sears* [6.30], the downwash velocity of an active cascade on a passive cascade downstream can be described by

$$v(x_p, t) = \sum_{h=1}^{\infty} Re\{u_m G \exp[-j(\varkappa x_p + h v_1 t)]\}. \tag{6.4-37}$$

Here u_m is the deviation of the velocity from the average of the adjacent velocities within the middle of the wake. G is given by

$$G = \frac{L_a Y}{t_a \cos \alpha_a} \sin(\alpha_a + \alpha_p) \exp\left\{-\left(\frac{\sqrt{\pi} h L_a Y}{2 \cos \alpha_a t_a}\right)^2\right.$$
$$\left. -j \pi h \left(\frac{L}{t}\right)_a \left[1 + \frac{2 b/L_p + \cos \alpha_p}{\cos \alpha_a}\left(\frac{L_p}{L_a}\right)\right] \cdot (\sin \alpha_a + \cos \alpha_a \tan \alpha_p)\right\}. \tag{6.4-38}$$

$2 Y$ is the measured breadth of the wake. For centrifugal impellers b/L_p can be very small. Therefore the action of the relatively large impeller wakes on a bladed diffuser must be taken into account. The aforementioned results strongly decrease with the distance b of the two cascades. This influences strongly the downwash velocity.

From Fig. 6.4.4 we recognize, that the amplitudes of unsteady lift drop strongly with the growing
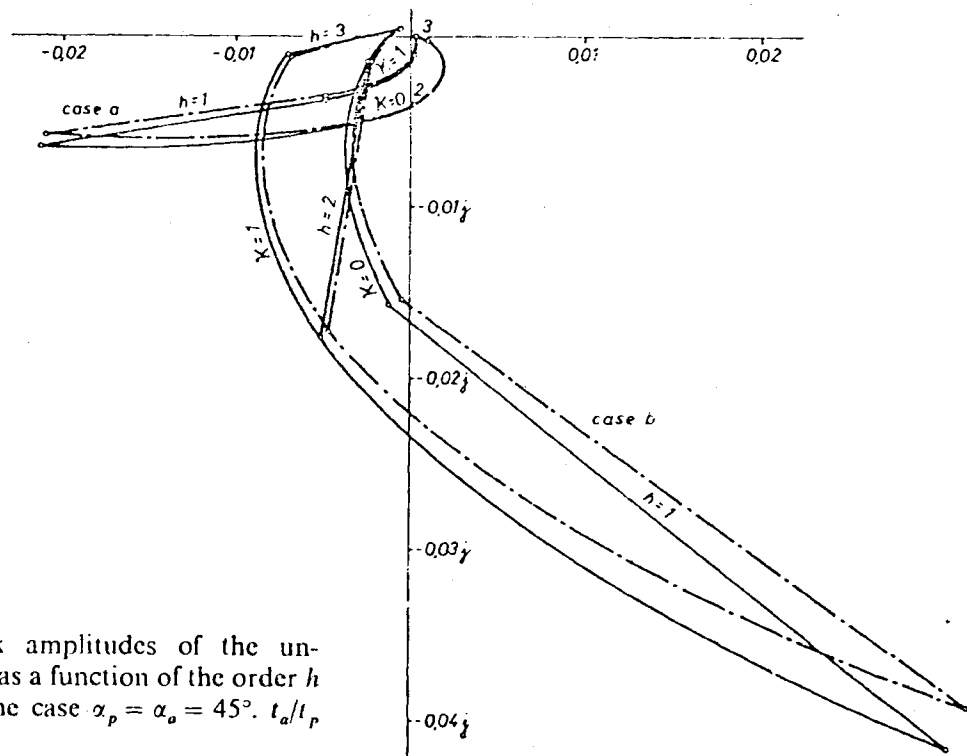
Fig. 6.4.4. Complex amplitudes of the unsteady lift moment as a function of the order h of harmonic, for the case $\alpha_p = \alpha_a = 45°$. $t_a/t_p = 1$, $L_p/t_p = 1$.

233

order of the harmonic 'h'. Therefore the first harmonic of any unsteadiness is usually sufficient with respect to the effect of unsteadiness.

An unsteadiness of the relative flow in the runner or impeller results also from non axisymmetry of the flow in the spiral casing. Especially the region near the tongue of the spiral casing may show 10 to 15% deviation from average flow along the periphery. Such a deviation may disappear at some working points.

Unfortunately it cannot disappear within the whole operational range of a turbine. This unsteadiness acts on the runner blade as a very big wake. It attacks one runner blade as a whole. Such a fluctuating force may cause strong overstress in the blade root section of a Kaplan runner near the hub especially in connection with fatigue effects of Chromium steel blades. According to the geometry of the bladeless space between the wicket gates and the runner and due to the usual distribution of the moment of momentum before the runner, any perturbation from the distributor in a Kaplan turbine acts much stronger at the outer parts of a blade.

Here these hydrodynamic forces have a large moment arm against the root section of the blade near the hub. A similar strong vibrating force acting on a long moment arm exists also in a Francis turbine when the shroud is omitted. Here the runner blades clamped on the one side may be badly overstressed at the inner blade cross section. The effect in a Kaplan turbine is more serious as it operates usually with a semi-spiral casing as distributor. This element produces more deviation from the axial symmetry of the inflow of the runner than the usual spiral casing would do.

The above procedure from M. Lotz is based on cascades of skeletons and the assumption of a steady flow through the active cascade. Lienhart [6.31; 6.32] has developed a rigorous method by a time step procedure, that accounts for arbitrarily shaped profiles with unsteady flow in both the cascades.

This method has been partly experimentally reconfirmed by tests of Lahm and Castorph [6.33; 6.34] with the aid of quickly responding semi-conductor probes. Tests of Castorph [6.35] reveal also the influence of shock waves on the unsteady behaviour.

The influence of wakes has been recently investigated by Lahm [6.33]. The effects resulting from cascades upstream and downstream of a considered cascade have been recently treated and measured by D. Castorph and Hubensteiner [6.36]. The influence of wakes on an unsteady flow through cascades in tandem arrangement moving relative to each other has been investigated by Krammer [6.37] on the base of Lienhart's rigorous theory. Fanelli and Siccardi [6.38] have treated the response of turbomachines with cascades to the oscillations in the penstock.

6.5. Distribution of meridional velocity normal to stream face

6.5.1. Introduction

In the foregoing section the flow within axisymmetric stream faces or flow laminae has been investigated under the assumption of a given flow-linked meridional velocity. For mixed flow rotors with a larger span in the vaned part the problem arises how the meridional component of velocity is distributed over the span b between the outer and inner shroud (hub).

For simplification of the problem a practical approach is made by assuming a uniform distribution of the meridional and whirl component c_m and c_u of the absolute flow in the peripheral direction. To obtain the influence of vane geometry, the angle β between the relative flow and periphery, is assumed to be given. This angle depends according to (6.5–13) on the given pattern sections and radial sections of the vane, and the geometry of an axisymmetric streamface, also determined by that of the inner and outer shroud

234

Assuming a flow along the vane, the influence of vane geometry is accounted for within the frame of simple assumptions. The following consideration deals only with velocities and pressure as they really occur within the fluid.

In an ideal fluid here assumed, according to *Pascal's* theorem, the pressure at a certain station is independent of the orientation of a face. The idea sometimes used of an imaginary force, normal to the vane, but uniformly distributed over the pitch [6.1; 6.39] is left aside.

6.5.2. Special assumptions

a) Infinite number of vanes reduced to their skeletons,

b) steady absolute flow on axisymmetric stream faces,

c) relative flow along the vane, vane angle β given,

d) gravity neglected as not contributing to the velocity distribution,

e) runner loss linked to individual flow lamina, like that of developed flow in a straight pipe,

f) vane skeleton given by its radial and pattern sections, hence the angles Θ between radial vane section and radius and β' between pattern vane section and periphery known (Fig. 6.5.1 a and b),

g) contours of hub and shroud with their angle μ with the radius given,

h) flow through a turbine runner,

i) constant specific flow energy on the runner exit,

j) hydraulic diameter of a flow lamina, spanwise depth Δn, equals that of a small rectangular cross section $2\Delta n$,

k) contraction factor Φ given.

Fig. 6.5.1. Determination of a spatial rotor vane surface. a) Elevation of the vane skeleton with a pattern section b'', and a radial section a'' (the latter is in circular projection). b) Plan of the vane skeleton with a pattern section b' and a radial section a'. c) Infinitesimal element of the vane surface and its traces $\overline{AB} = a''$ in meridian, $\overline{AD} = b'$ in a plane normal to the rotor axis, and $\overline{BD}$ (= relative streamline), in an axisymmetric stream surface.
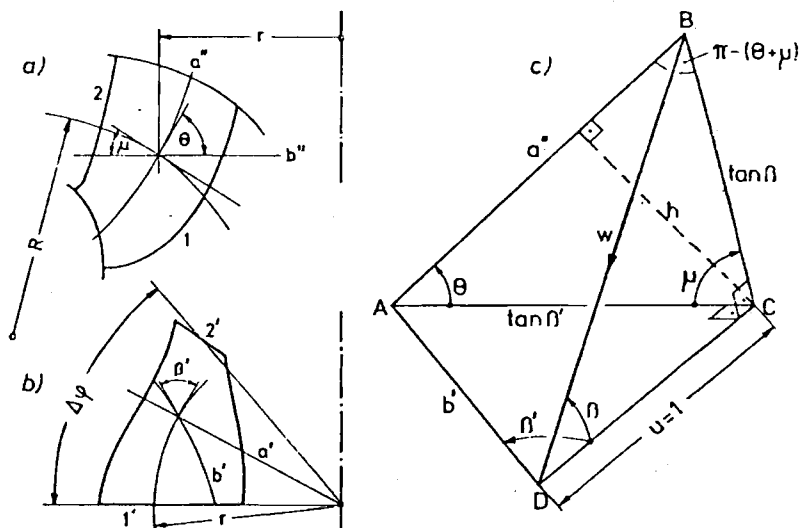
6.5.3. Equation of motion, Euler's relation, loss formulation

The equation of motion normal to the streamface in the direction of n (Fig. 6.5.2) reads

$$- (1/\varrho)\,dp/dn + c_m^2/R - c_u^2 \sin\mu/r = 0, \qquad (6.5-1)$$
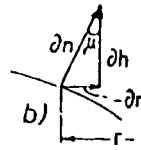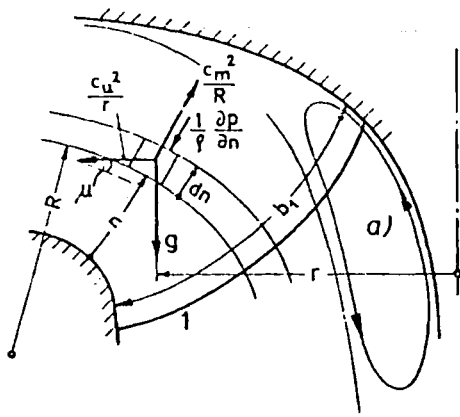
Fig. 6.5.2. Unit fluid mass between adjacent axisymmetric stream faces in a meridian. a) ring vortex, possible at part load. b) relation between ∂n, ∂r, $\partial \mu$. The location Δx_0 of the outer edge of the ring vortex a) results from (6.5–10) with $\Delta y = - y(x = 0) = -1: \Delta x_0 = 1/(f_{1M} - f_{2M})$, where f_{1M}, f_{2M} are mean values of f_1, f_2 within Δx_0.

where c_m is the meridional velocity, c_u the absolute whirl velocity, R the radius of streamline curvature in the meridian, μ the angle between the streamline and radius in the meridian, r the distance from the rotor axis.

The application of *Euler's* equation between the station under consideration and station 1 at runner outlet, with respect to a draft tube loss, expressed by $\zeta_s c_{m1}^2/2$ and a streamline-bound runner loss, between the point considered and the runner exit $\Delta p_i/\varrho$, gives

$$p/\varrho + c_m^2/2 + c_u^2/2 - p_A/\varrho - \zeta_s c_{m1}^2/2 - \Delta p_i/\varrho = \omega (c_u r - c_{u1} r_1), \qquad (6.5-2)$$

where p_A is the pressure on the tailwater level.

According to assumptions e) and j) and with respect to the relations from the velocity triangle $w = c_m/\sin \beta$ and the relative streamline element ds, $ds = dr/(\cos \mu \sin \beta)$, with a constant loss coefficient ζ, the runner loss is formulated by means of

$$\Delta p_i/\varrho = (1/4)\left\{ \int_{const}^{r} [\zeta c_m^2/(\Delta n \sin^3 \beta \cos \mu)] \, dr - \int_{const}^{r_1} [\zeta c_m^2/(\Delta n \sin^3 \beta \cos \mu)] \, dr \right\}.$$

$$(6.5-3)$$

6.5.4. c_m^2 as a function of moment of momentum $c_u r$

The pressure term $-(1/\varrho) dp/dn$ in (6.5–1) is eliminated by inserting it from the relation (6.5–2), differentiated with respect to n accounting for assumption i), and for (6.5–3). On this occasion, $\Delta p_i/\varrho$ has to be differentiated with respect to the upper boundary of the respective, definite integrals in (6.5–3).

For this reason also the obvious relations $dr/dn = - \sin \mu$, and continuity $c_m r \Delta n = c_{m1} r_1 \Delta n_1$ have to be taken into account. With the last but one relation the expression $d(c_u^2/2)/dn - c_u^2 \sin \mu/r$, can be reduced finally to $(c_u/r) d(c_u r)/dn$. Hence

$$dc_m^2/dn + \langle 2/R + [\zeta/(2\,\Delta n)]\{\tan \mu/\sin^3 \beta - [r\,\Delta n/(r_1\,\Delta n_1)]^2 \tan \mu_1/\sin^3 \beta_1\}\rangle c_m^2$$

$$= 2[(\omega r - c_u)/r]\, d(c_u r)/dn. \qquad (6.5-4)$$

This linear differential equation for c_m^2 is also valid for vanishing $c_m = 0$ (stalled region as shown in Fig. 6.5.2). It offers the opportunity to design a runner as a function of any desired distribution of the moment of momentum $c_u r$ by means of a step by step procedure. For the start ζ might be put to zero.

6.5.5. Linear differential equation for the c_m distribution

Initially (6.5–4) is reduced to c_m, ωr and β, by applying the relation

$$\omega r - c_u = c_m \cot \beta \qquad (6.5-5)$$

from the velocity triangle. In addition the identity $1 + \cot^2 \beta = 1/\sin^2 \beta$ is employed. Under the assumption of a non vanishing meridional velocity c_m, (6.5–4) is divided by $c_m/\sin^2 \beta$. Finally the variables are made dimensionless by

$$y = c_m/c_{me} \quad \text{(with } c_{me} = c_m(n = 0)\text{)}, \qquad x = n/b, \qquad (6.5-6)$$

b being the local span (breadth) of the runner in the n-direction. Hence the governing differential equation for the $y(x)$ distribution

$$dy/dx + f_1(x)\,y = -f_2(x), \qquad (6.5-7)$$

$$f_2(x) = (b\,\omega/c_{me}) \sin 2\beta \sin \mu, \qquad (6.5-8)$$

$$f_1(x) = (b/R) \sin^2 \beta - (b/r) \cos^2 \beta \sin \mu + (1/2) \sin 2\beta\, d(\cot \beta)/dx$$
$$+ [\zeta b/(4\,\Delta n)]\,\{\tan \mu/\sin \beta - \tan \mu_1\,(\sin^2 \beta/\sin^3 \beta_1)\,[r\,\Delta n_i/(r_1\,\Delta n_1)]^2\}. \qquad (6.5-9)$$

A related problem is the influence of a meridional profile of a mixed flow machine on its characteristics, see [6.40].

6.5.6. Step by step solution for the design task

Transforming (6.5–7) into a difference equation and putting $f_1(x) = f_1$ and $f_2(x) = f_2$ yields the increment Δy, y experiences, when a step Δx is made in the x-direction. by means of

$$\Delta y = -\Delta x(f_1 y + f_2). \qquad (6.5-10)$$

On the shroud, i.e., $y = 1$, due to $c_m(n = 0) = c_{me}$, the value c_{me} is set with respect to a limit of susceptibility to cavitation. This holds especially for points close to the exit 1.

In a design usually the flow rate Q is prescribed. Hence this procedure is finished, when according to continuity, with a mean contraction coefficient Φ

$$Q = 2\pi\,\Phi \int_{n=0}^{b} r\,c_m\,dn = 2\pi\,\Phi\,c_{me}\,b \int_{x=0}^{1} r\,y\,dx, \qquad (6.5-11)$$

at the station $x = 1$, with c_{me}, b preliminarily chosen, Q reaches the set value. Usually, because b is unknown in a design, the latter value of Q will be attained by an x differing from 1. This then gives the breadth b required for the flow Q.

6.5.7. Calculating c_m (n) or $y(x)$ for a runner of given geometry under a given flow rate Q

The originally posed task asks for the $c_m(n)$ or $y(x)$ distribution in a runner with known b and geometry (hence β, μ, are known as functions of x). For this purpose a preliminary plot of streamlines has to be made, with provisionally plotted x-lines normal to them. Thus μ, R, r, β are known preliminarily as function of x and then also f_1 and f_2 are provisionally known and then stepwisely improved.

Here also the procedure of Cap. 6.5.6 may be applied with the difference, that now by trial and error c_{mc} has to be set so as to satisfy continuity (6.5–11).

When the functions f_1 and f_2 are graphically given or expressed in terms of x, then graphical or numerical integration may facilitate obtaining y by means of the following strict solution of (6.5–7) given by the author [8.39]

$$y = \exp\left[-\int\limits_0^x f_1(u)\,du\right]\left\{1 - \int\limits_0^x f_2(u)\exp\left[\int\limits_0^u f_1(v)\,dv\right]du\right\}.$$ (6.5–12)

6.5.8. Computation of β as a function of vane geometry

The inclination β of relative flow with respect to the circumference follows from the angle β' between the pattern section of the vane and the periphery, the angle Θ of the radial vane section with the radius and the inclination μ of the meridional streamline with the radius as

$$\tan\beta = \tan\beta' \sin\Theta/\sin(\Theta + \mu).$$ (6.5–13)

This results from an infinitesimally small tetrahedron (Fig. 6.5.1 c). It is formed by two rectangular triangles, one parallel to the plan and another in the axisymmetric stream-face, and by two common triangles, one located in the vane face and the other in the meridian. The peripherally oriented leg, which is common to both rectangular triangles, might have unit length. From this the length of the meridional streamline element is obtained as $\tan\beta$ and that of the radial oriented edge as $\tan\beta'$. It is realized from the triangle within the meridian, that the angles $\pi - (\Theta + \mu)$ and Θ are opposite the legs having the length $\tan\beta'$ and $\tan\beta$. From this a basic trigonometric relation yields (6.5–13).

6.6. The slip effect in the flow past a rotor

6.6.1. Introduction

For the blading of a certain fluid machine, specific head gH, flow Q, speed ω and hence also size D being known, an estimate of efficiency η_u (resulting from internal flow) and the change of whirl c_{ui} by the rotor, between the stations 1 and 2 (see 5.3) from Euler's relation, are of importance.

As the whirl c_{ui} due to rotor's influx is either physically given e.g., $c_{u1} = 0$ in pumps, or adjustable e.g., by gates of turbines, special attention merits the whirl past the rotor exit. Hence the problem is limited to impellers. They have a low vane number z and thus a relative main flow, disordered by secondary flow (Cap. 5.5), and hence no longer following the vane. At exit 2 the latter makes an angle β_2^* with the periphery. Now the problem arises, to set β_2^* so as to generate the whirl, required for the head from $c_{u2} = gH/(\eta_u r_2 \omega)$ and thereby also needed for a desired flow Q (Fig. 6.6.1 a).

Obviously (Fig. 6.6.1 a) there is a discrepancy between the velocity triangles at station 2, one of which is due to the pitch-averaged flow and thus also due to Euler's relation and the other of which, denoted by a star *, is due to a relative flow along the impeller vane plotted for the same meridional velocity $c_{m2} = c_{m2}^*$.
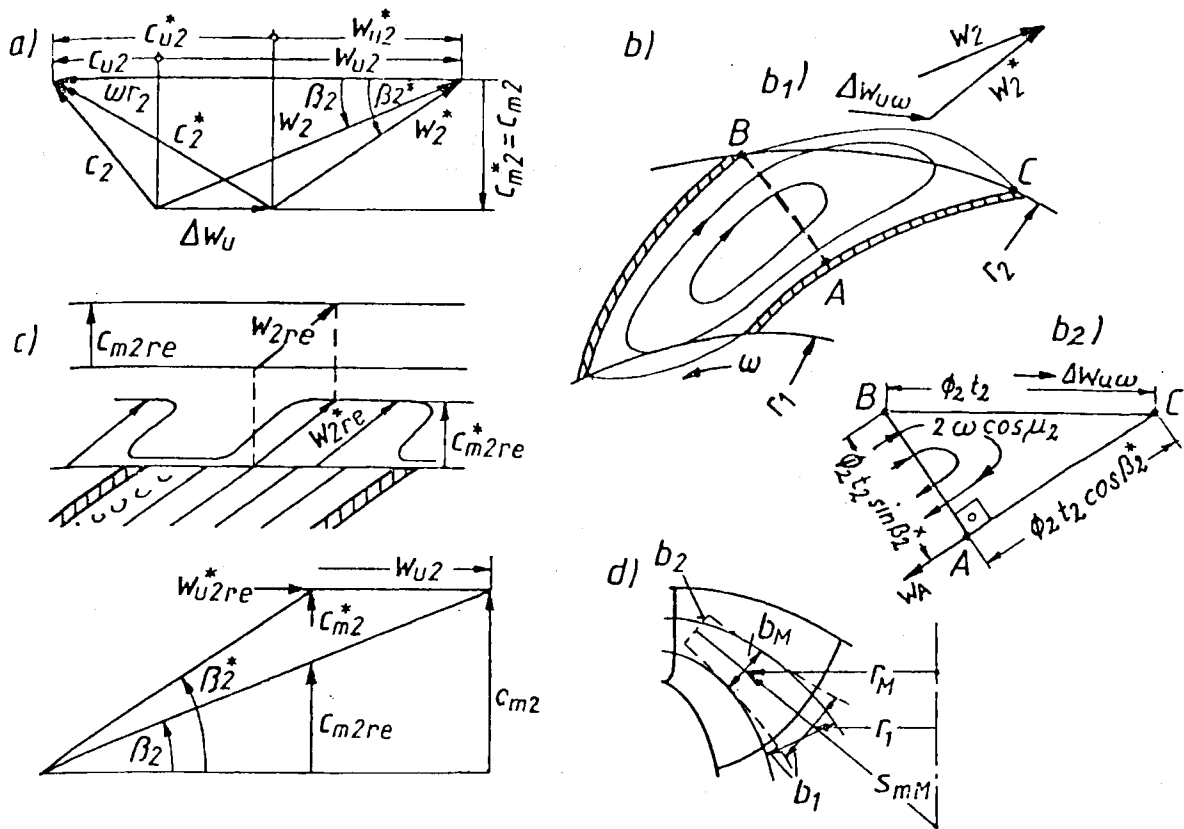
Fig. 6.6.1. Causes of slip at the impeller outlet. a) Definition of slip factor p^*, slip μ, deviation angle $\beta_2^* - \beta_2$. b) Slip due to the relative eddy b_1) streamlines due to relative eddy at zero flow b_2) triangle ABC to calculate $\Delta w_{u\omega}$. c) Slip due to the thickness of rotor vane and its wake. d) Slip due to the varying span of rotor. β_2^* is angle between rotor vane skeleton and the circumference.

Both the triangles differ from each other by their respective angles β_2, β_2^* the relative flow makes with the periphery, and by their respective whirl components c_{u2}, c_{u2}^*. Relating the difference $c_{u2}^* - c_{u2}$ to c_{u2}, by a so-called "reduced output factor", after Pfleiderer [6.41], hence denoted as "slip factor" and defined by

$$p^* = (c_{u2}^* - c_{u2})/c_{u2}, \qquad\qquad (6.6-1)$$

the whirl c_{u2}^*, needed to obtain β_2^* by the triangular relation $\cot \beta_2^* = (\omega r_2 - c_{u2}^*)/c_{m2}$ (Fig. 6.6.1 a), and at the rated point $(c_{u1} = 0)$ results from the following version of the Euler relation

$$c_{u2}^* = (1 + p^*)gH/(\eta_u r_2 \omega). \qquad\qquad (6.6-2)$$

Thus, once p^* is known, c_{u2}^* and hence the blading at least at the decisive impeller outlet 2 is obtained. Based on the model of a flow along the vane (a concept due to Euler) the slip factor p^* is a correction, that implies the discrepancy between such a flow and the pitch-averaged real flow past a rotor. Instead of p^*, also the value $\mu = 1 - p^*$ is used as slip.

In the sequel, the assumption is made that the individual effects influencing the slip factor p^* can be superimposed, even if strictly speaking the differential equation governing the real rotational flow is nonlinear [6.42]. Thus

$$p_{res}^* = \Sigma p_i^*. \qquad\qquad (6.6-3)$$

239

The following four effects are highlighted as the most influential ones on the slip factor: a) p_ω^* from rotation, b) p_h^* from wakes and finite vane thickness, c) p_{So}^* from cascade flow, d) p_b^* from varying breadth b of the rotor.

6.6.2. Slip p_ω^* in consequence of the relative eddy

After Cap. 5.2 the steady relative flow of an ideal fluid on axisymmetric stream faces under irrotational absolute flow, can be split into one due to throughflow (Q) and another due to the component $2\,\omega\cos\mu$ of the relative eddy normal to the stream face.

Obviously in Fig. 6.6.1 b$_1$, the relative eddy alone at zero flow $(Q = 0)$ reduces the whirl c_{u2}^* to c_{u2}. Hence the pitch-averaged differential whirl component $\Delta w_{u\omega} = c_{u2}^* - c_{u2}$ can be used to predict p_ω^*.

To obtain $\Delta w_{u\omega}$, by which then p_ω^* is gained from (6.6-1) and $c_{u2} = gH/(\eta_u r_2\,\omega)$, Stokes' theorem (Cap. 5.2) is applied to the triangular-like area ABC (Fig. 6.6.1 b$_2$). The circulation, then needed, along the unobstructed pitch arc $\Phi_2 t_2$ (Φ_2-contraction coefficient due to vane thickness and boundary layer in 2) reads: $\oint_{BC} w\,ds = \Gamma_{BC} = \Delta w_{u\omega} t_2 \Phi_2$. Obviously along the line BA the circulation vanishes. Hence $\Gamma_{BA} = 0$. With the hint (Cap. 5.2) applied to an impeller where approximately $w_u = \omega r_1$, the velocity at station A in consequence of the relative eddy alone becomes

$$w_A = t_2\,\Phi_2\,\omega\sin\beta_2^*\cos\mu_2[1 - r_1/(2r_2)]. \tag{6.6-4}$$

When the passage of the channel is assumed to be closed, for the case of vanishing flow Q, the flow then induced by the relative eddy on the outstanding corner C has to vanish. Assume that the relative flow drops from A to C, distance $t_2\,\Phi_2\cos\beta_2^*$, so as to make the circulation along CA: $\Gamma_{CA} = (w_A/2)\,t_2\,\Phi_2\cos\beta_2^*$.

The vortex flux due to the relative eddy, passing the triangular area, becomes $\iint \mathrm{rot}\,w\,dA = \omega\cos\mu_2\,\Phi_2^2 t_2^2\cos\beta_2^*\sin\beta_2^*$. Making this equal to the circulation about the triangle ABC: $\Gamma_{BC} + \Gamma_{AB} + \Gamma_{CA}$, Stokes' theorem (Cap. 5.2) thus yields [6.45]

$$\Delta w_{u\omega} = \pi\Phi_2\,\omega r_2\sin 2\beta_2^*\cos\mu_2[1 + r_1/(2r_2)]/(2z). \tag{6.6-5}$$

Hence from (6.6-1) with $c_{u2} = gH/(\eta_u r_2\omega)$ and applying the blade tip speed coefficient Ku (Cap. 9.2), p_ω^* reads

$$p_\omega^* = (\pi\,Ku^2/z)\eta_u\,\Phi_2\sin 2\beta_2^*\cos\mu_2[1 + r_1/(2r_2)]. \tag{6.6-6}$$

6.6.3. Slip p_h^* as a consequence of wakes

A wake usually exists past an impeller vane. This contracts the main relative flow by the contraction coefficient Φ_2. Assume that the wake is extinct at a station 2 (Fig. 6.6.1 c). downstream of the exit. Assuming straight and plane flow, continuity requires between the real meridional components $c_{m2\,re}$ at station 2 and $c_{m2\,re}^*$ at station 2* (exit)

$$c_{m2\,re}^* = c_{m2\,re}/\Phi_2. \tag{6.6-7}$$

Imagine between 2 and 2* vanishing peripheral forces on the flow, then the momentum theorem requires $w_{u2\,re} = w_{u2\,re}^*$ for the straight cascade now considered. The subscript re holds for the real flow at 2 and 2*. By definition (6.6.-1) the slip factor p^* results from

the comparison of the velocity triangles at 2 and 2*, having the same meridional component. This gives the slip (Fig. 6.6.1 c)

$$c_{u2}^* - c_{u2} = c_{m2}(1/\Phi_2 - 1) \cot \beta_2^*,$$ (6.6-8)

and by means of (6.6-1) the desired slip factor

$$p_h^* = 2\varphi_2 K u^2 \eta_u \cot \beta_2^* (1/\Phi_2 - 1),$$ (6.6-9)

where $\varphi_2 = c_{m2}/u_2$ is the flow coefficient (Cap. 9.2).

6.6.4. Slip $p_{\delta_0}^*$ as a consequence of cascade flow

The special influence the cascade of a mixed flow rotor has on the slip is that due to the relative eddy, as treated above. Under the assumption that the individual slip effects can be superimposed, the remaining effects due to a cascade will be studied at a stationary cascade with plane potential flow on axisymmetric stream faces. After Cap. 6.2.1 this can be transformed into a straight cascade at angles retained by conformal mapping.

Therefore imagine the cascade of the impeller considered to be thus transformed into a straight cascade. Retaining the angles β_2^*, β_2 under this procedure means also retaining the so-called "deviation angle" $\beta_2^* - \beta_2$ (Fig. 6.6.1 a) due to the slip $c_{u2}^* - c_{u2}$ and linked to it by the obvious relation

$$c_{u2}^* - c_{u2} = (\beta_2^* - \beta_2) c_{m2}/\sin^2 \beta_2^*.$$ (6.6-10)

Hence the slip factor from (6.6-1) is linked to the deviation angle (remember always in the case of pumps) by means of

$$p^* = 2(\beta_2^* - \beta_2) \eta_u K u^2 \varphi_2/\sin^2 \beta_2^*.$$ (6.6-11)

As will be seen in the following, the deviation angle $\beta_2^* - \beta_2$ can be easily obtained for a cascade of given geometry and within a certain undisturbed flow w_∞ (and the consequent physical angle of attack δ_0) by means of cascade theory according to Cap. 6.2.

The conformal mapping of a usual radial or mixed flow impeller with its small vane angles results in a straight cascade, having a pitch to chord ratio t/L smaller than "one" ($t/L < 1$).

- Consideration of the deviation angle $\beta_2^* - \beta_2$ at the outlet of a straight cascade with $t/L < 1$, vane angle β_2^* at exit 2 known: For this purpose some findings of the cascade flow in Cap. 6.2 and Cap. 6.3 must be reviewed.

First the lift coefficient ζ_{AG} of an aerofoil within a cascade is linked to its pitch to chord ratio t/L, the so-called "deflection" $\Delta c_u = c_{u2} - c_{u1}$, and the undisturbed throughflow velocity w_∞ by the relation (6.3-4)

$$\zeta_{AG} = (2t/L) \Delta c_u/w_\infty.$$ (6.6-12)

Obviously as in Fig. 5.5.5 d, the so-called "deflection triangle", extracted from both the velocity triangles, and consisting of $\Delta c_u, w_2, w_1$ and hence also $w_\infty = (w_1 + w_2)/2$, yields

$$\Delta c_u = c_m(\cot \beta_1 - \cot \beta_2).$$ (6.6-13)

On the other hand the same lift coefficient ζ_{AG} follows, according to cascade theory from (6.2-50). Substituting there for the physical angle of attack δ_0 the difference of the angle β_0, between zero lift direction and the circumference, and the angle β_∞, the undisturbed

velocity w_x makes with the circumference, according to $\delta_0 = \beta_0 - \beta_\infty$, and substituting for δ_0 the more exact expression $\sin \delta_0$, the relation (6.2–50) reads

$$\zeta_{A\,ii} = 2\pi\varkappa\sin(\beta_0 - \beta_\infty),$$ (6.6–14)

where $\varkappa$ the cascade factor, after (6.2–48), is a mere function of the cascade parameters t/L and β_0. Eliminating $\zeta_{A\,G}$ from (6.6–14) and (6.6–13), accounting for the relation $\sin \beta_\infty = c_m/w_\infty$ from the velocity triangle and together with the known theorem $\sin(\beta_0 - \beta_\infty) = \sin \beta_0 \cos \beta_\infty - \cos \beta_0 \sin \beta_\infty$, brings

$$2q(\cot \beta_\infty - \cot \beta_0) = (\cot \beta_1 - \cot \beta_2),$$ (6.6–15)

where q is the so-called "*Weinig* factor" [6.9], defined by the figure (Fig. 6.6.2)

$$q = (\pi/2)(L/t)\varkappa(L/t, \beta_0) \sin \beta_0.$$ (6.6–16)
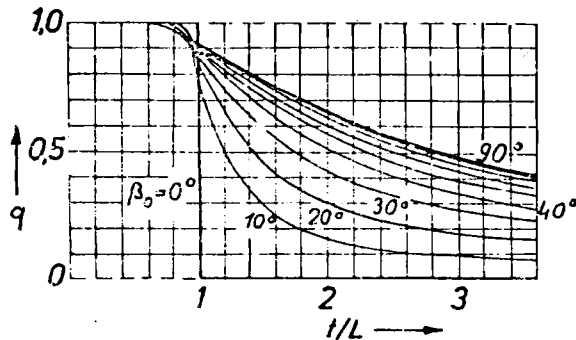
Fig. 6.6.2. Graph of Weinig's q-factor as a function of the pitch/chord ratio t/L, and the stagger angle (here β_0 is zero lift direction).

The angle β_x, the undisturbed velocity w_∞ makes with the periphery, can be reduced to the corresponding angles β_2, β_1 of the relative velocities w_2, w_1 at outlet 2 and inlet 1 of the rotor by the fact that $w_\infty = (w_1 + w_2)/2$. Hence

$$\cot \beta_\infty = (\cot \beta_1 + \cot \beta_2)/2.$$ (6.6–17)

Inserting $\cot \beta_\infty$ in (6.6–15) gives the angle β_2 due to the relative flow past the impeller, as a function of the corresponding angle β_1 upstream of the impeller, the angle β_0 of the zero lift direction and the figure q, depending on β_0 and t/L as

$$\beta_2 = \text{arccot}\{[(1 - q)/(1 + q)]\cot \beta_1 + [2q/(1 + q)]\cot \beta_0\}.$$ (6.5–18)

From the $q(t/L, \beta_0)$-plot (Fig. 6.6.2) it is seen that for the cascades considered here, with $t/L < 1$, independent of β_0, the value q tends to "1". Strictly speaking,

$$\lim_{t/L \to 0} \beta_2 = \beta_0.$$ (6.6–19)

That means, the flow past the cascade follows the direction of the zero lift direction, independent of the inclination of the inflow velocity. This reduces the task to that of calculating the angle β_0 of the zero lift direction β_0. For the given cascade with its known angle β_c, the chord of the skeleton makes with the periphery, and the known zero angle of attack between the chord and the zero lift direction, after (6.2–47) being a function of the cascade parameters C_i and the vane geometry (K_1, K_2, K_3 (6.2–37)), the desired deviation angle becomes $\beta_2^* - \beta_2 = \beta_2^* - \beta_c - \delta(F_A = 0)_G$. Hence from (6.6–11)

$$p_{\delta_0}^* = 2[\beta_2^* - \beta_c - \delta(F_A = 0)_G]\,\eta_u K u^2\, \varphi_2/\sin^2 \beta_2^*.$$ (6.6–20)

242

6.6.5. Slip p_b^* as a consequence of varying the breadth of the rotor

A conical streamface is considered (Fig. 6.6.1 d), touching the mean stream face of the flow lamina considered in the middle of the impeller. Imagine this conical face to be the mean face of a flow lamina with the same depth 'b' of the actual lamina at stations, whose distance from the point of contact x within the meridian (Fig. 6.6.1 d) is the same along the straight generatrix of the cone as along the curved line on the original mean stream face of the flow lamina considered.

The depth b is assumed as small compared with the distance r from the axis. Using the meridional coordinate s_m along the generatrix and the azimuth φ', normal to the meridian (Fig. 6.6.1 d), continuity due to an axisymmetrical flow within the flow lamina can be written down as (φ' being the angle between generatrices with in the cone plane)

$$\partial w_m/\partial s_m + w_m/s_m + (1/s_m)\, \partial w_u/\partial \varphi' = - (w_m/b)\, db/ds_m, \qquad (6.6-21)$$

where w_m is the meridional component, w_u the whirl component of flow. Hence the effect of varying depth $b = b(s_m)$ of the flow lamina can be interpreted as that of a source-distribution $- (w_m/b)(db/ds_m)$ due to a plane flow within the s_m, φ'-face.

Assuming for simplicity w_m on the right hand side to be constant over the pitch and to match the pitch-averaged meridional speed due to the given flow Q, an additional whirl component is generated at impeller exit 2 as compared with that, due to a rotor with constant breadth b (Fig. 6.6.1 d)

$$\Delta w_{ub} = w_{m2}(1 - b_2/b_1), \qquad (6.6-22)$$

b_1 and b_2 being the breadths at station 1 and 2 of the real elementary pump or whole pump (as the case may be). Making $\Delta w_{ub} = \Delta c_{ub} = c_{u2}^* - c_{u2}$, this implies a slip factor

$$p_b^* = 2\,\eta_u\,\varphi_2\,Ku^2(1 - b_2/b_1). \qquad (6.6-23)$$

The slip factor has been generally treated by *Adler* [6.4], and in connection with pump-turbines by *Anton* [6.43]. Recently 3-dimensional measurements of the relative flow field in the channels and past

Fig. 6.6.3. Values of slip factor $\mu = 1 - p^*$ obtained by several authors.
a) —— *Korcian* [6.44],
– – – *Raabe* [6.45],
――― *Siebrecht* [6.47],
//// *Pfleiderer* [6.41],
·—· *Stephanoff* [6.48],
―·― *Stodola* [6.49],
—···— *Pfoertner* [6.22],
···· *Busemann* [6.50], o *Eck* [6.51], × × *Noorbakhsh* [6.52], b) —— *Korcian* [6.44], – – – *Murakami* [6.53], ··· *Osterwalder, Ettig* [6.54].
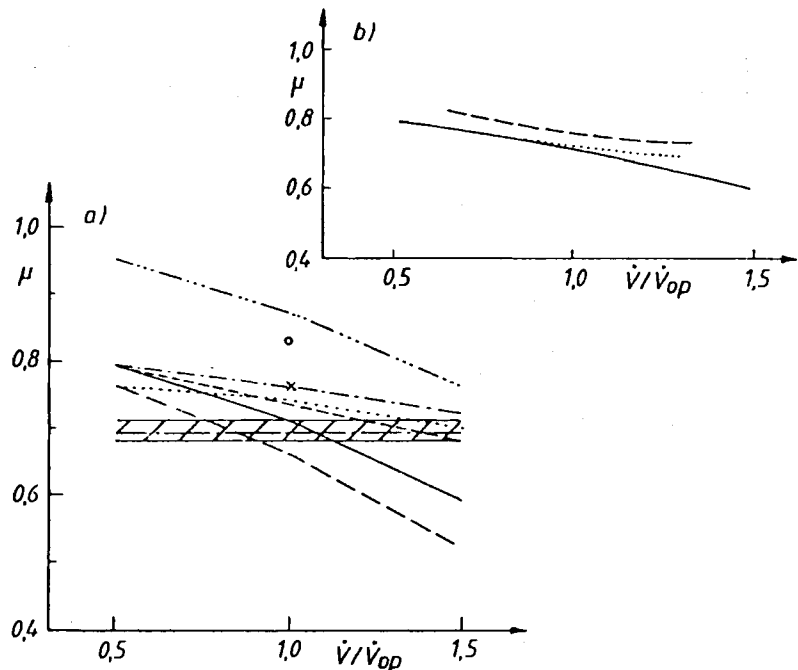
a radial pump impeller, carried out by *J. Korcian* at the Lehrstuhl und Labor für Hydraulische Maschinen und Anlagen der TUM [6.44] agree well with the slip factors predicted by *Raabe* [6.45]. These results were also compared with results obtained either from theoretical predictions or tests carried out or calculated by *Siebrecht* [6.47], *Stepanoff* [6.48], *Stodola* [6.49], *Busemann* [6.50], *Eck* [6.51], *Noorbaksh* [6.52], *Murakami, Kikuyama* and *Asakura* [6.53] and *Osterwalder* and *Ettig* [6.54]. In general, agreement was more or less good at the design point but failed in some cases at part load and overload, see Fig. 6.6.3.

Fig. 6.6.4 shows the rotor with the electrically adjusted 6-port probe used by *Korcian* by which pressure and the spatial relative velocity vector were measured simultaneously.

At the moment the pump works under developed cavitation, e.g. as an inducer, any prediction of the slip factor fails, since this is based on the assumption of a fully wall-attached and non cavitating flow.

The cavitating flow through a cascade has been treated by *Furuya* [6.46].
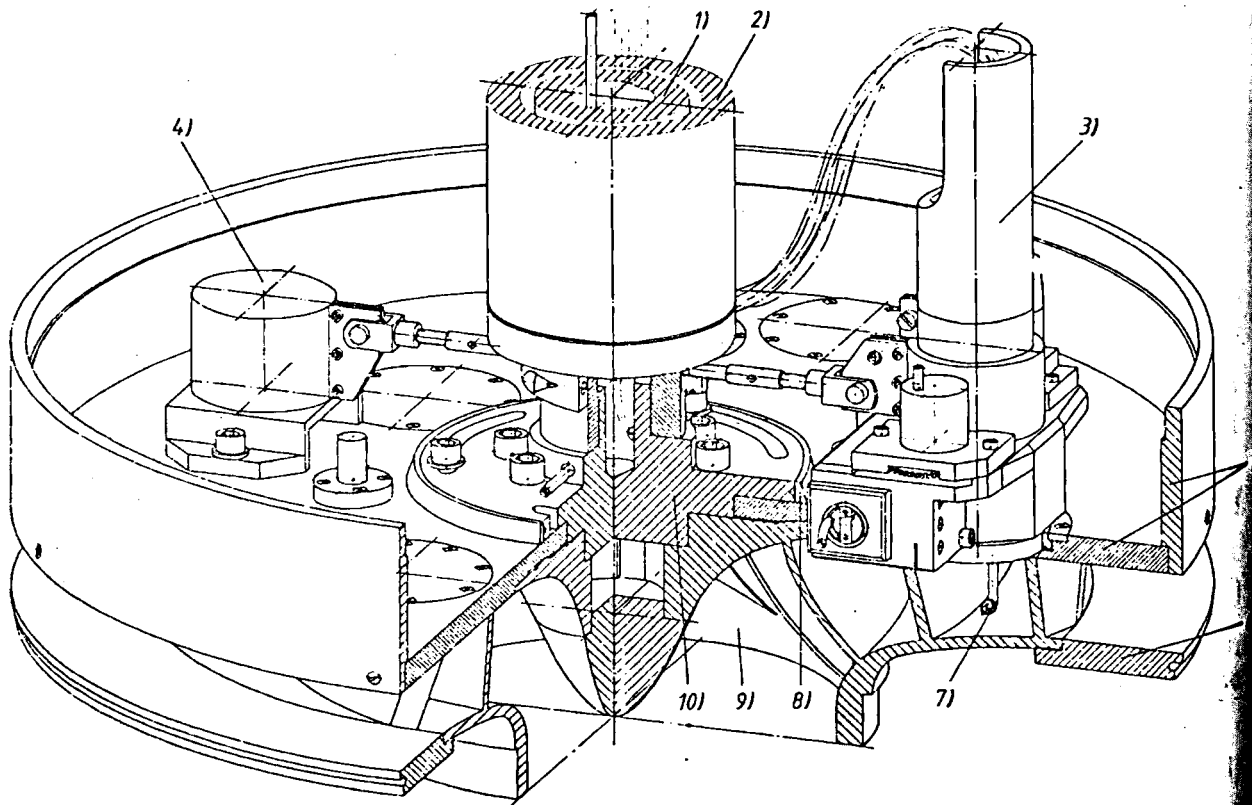
Fig. 6.6.4. Impeller and probe used for the measurement of the relative velocity vector and the slip factor in steady flow, carried out by *J. Korcian* [6.44] in the Laboratorium für Hydraulische Maschinen und Anlagen der TU München. 1) rotor shaft, 2) stationary tube, 3) device for electric probe adjustment by turning the probe about its shaft and by shifting its shaft in axial direction 4) mass for balancing the centrifugal force of the probe and its adjustment device, 5) covering plate for the slide ring of the seal, 6) radial extension of the shroud, 7) 6-hole probe, 8) scale ring for indication of the azimuth, 9) runner, 10) flange.

7. Losses due to vorticity and boundary layers

7.1. Introduction

Any real flow in fluid machinery is linked to the formation of vortices, boundary layers, and wakes as vortex sheets which are the origin of dissipation and energy waste.

Vortices normal to the main flow may contribute to the circulation about a vane, vortices in the main flow direction stimulate the generation of secondary flow. Hence understanding the production of streamwise vorticity at the outlet of structural members of fluid machines, like nozzles, bends, rotors, cascades may help to influence this loss mechanism.

Once the longitudinal vorticity in the main flow direction is known, the secondary flow and resulting loss can be predicted.

In mixed-flow fluid machines the rotor may be the main source of loss. Therefore an attempt is made to predict the dissipation in its vortex layers such as the boundary layer and wake.

The latter requires the knowledge both of boundary layer growth in the main flow direction along a double curved vane and also the secondary flow accompanying it. An estimation of this growth is obtained from the momentum equation, continuity and wall shear stress as functions of the flow regime of the boundary layer and its transition points. It includes the influence of *Coriolis* force and the body force due to the curvature of streamlines along the vane in the directions of the main and secondary flow in planes tangential and normal to the vane.

It needs the introduction of a reasonable velocity profile in the direction of the main and secondary flow. It also has to account for the flow about the leading edge of the rotor vane and the effects due to the formation of the wake.

7.2. Problems due to kinematics of vortices in fluid machines

7.2.1. Fundamentals of vortices

The forced vortices here considered may have their origin in the core of a free vortex generated by the curvature of guide walls. Vortices are mainly caused by means of viscosity in wall-attached boundary layers or wakes with a flow having a large strain rate across the main flow. According to the findings of *Oseen* [7.1] vortices fade by converting their rotational kinetic energy into waste heat.

In the following, idealized vortex tubes are imagined to be floating within the main flow neither subjected to heat transfer nor generating heat.
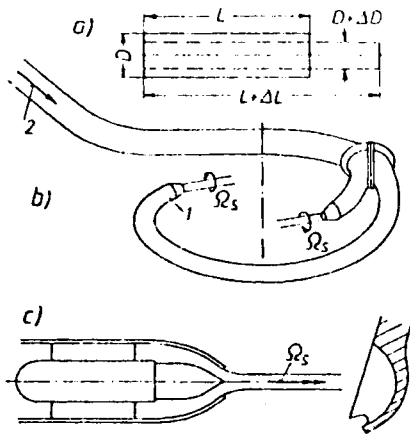
Consider a straight vortex tube of length l with the momentary constant circular cross section of diameter D. It rotates with constant angular velocity ω about its axis, corresponding to the vortex intensity $\operatorname{curl} c \equiv \Omega \equiv 2\omega$ (Fig. 7.2.1 a).

According to *Helmholtz* or *Kelvin* [7.2; 7.3], the vortex tube consists always of the same matter.

Assuming constant density of fluid ϱ, mass conservation requires

$$m = \varrho(\pi/4)\, D^2 l = \text{const}, \quad \text{or}\quad D^2 l = \text{const}. \tag{7.2-1}$$

According to *Stokes'* theorem (Cap. 5.2),

$$\Gamma = (\pi/4)\, D^2 \Omega = \text{const}, \quad \text{or}\quad D^2 \Omega = \text{const}. \tag{7.2-2}$$

In an ideal fluid the theorem of the moment of momentum requires

$$I = (\pi/32)\,\varrho D^4 l\omega = \text{const}, \quad \text{or}\quad D^4 l\omega = \text{const}. \tag{7.2-3}$$

Dividing (7.2-2) by (7.2-1) gives

$$\Omega/l = 2\omega/l = \varrho\Gamma/m = \text{const}. \tag{7.2-4}$$

With (7.2-2) the kinetic energy of the vortex tube results in

$$E = (1/2)\,\omega^2(\pi/32)\varrho D^4 l = \varrho\Gamma^2 l/(16\pi) = \text{const}. \tag{7.2-5}$$

Hence E increases by lengthening of a vortex tube.

7.2.2. Energy loss due to lengthening of a vortex tube

7.2.2.1. Lengthening of a vortex tube parallel to the main flow

This effect occurs, e.g., in the nozzle pipe of an impulse turbine (Fig. 7.2.1 a) when the main flow has a streamwise vorticity. This originates from a free vortex about the axis of the pipe in connection with the fluid viscosity and a large strain rate there.

Such a whirl usually is effected by two bends in series upstream of the nozzles, both being in planes that are inclined to each other.

For example a multi-nozzle impulse turbine with a vertical shaft (Fig. 7.2.1 b) has one of these bends in the elevation, which connects the penstock with the distributing pipe. The other bend is that of

246

the usual spiral-formed main and its nozzle pipes. Then a component of penstock velocity has a moment about the nozzle pipe axis and hence tends to generate a streamwise vorticity there.

Since in the nozzle the whole net head of the turbine is converted into kinetic energy, the largest strain rate of the main flow and hence also of vortices in the main flow direction occurs there. Thus according to (7.2–5) the kinetic energy of these vortices is increased and then lost to enable work to be done (Fig. 7.2.1 c). After Krause, streamwise vorticity may disappear by streamwise acceleration.

From this it can be seen that acceleration of main flow is not always a means of lowering losses.

7.2.2.2. Dislocation and lengthening of a vortex within a bend

Consider a plane potential flow in a channel of rectangular cross section (Fig. 7.2.2). It flows from a straight channel into a bend of curvature $1/R$, R being large compared with the width l_1. Imagine that a vortex, vorticity Ω_1, enters the bend, normal to the streamlines. Consisting always of the same fluid particles, it is surrounded by a free vortex where the mean angular velocity of fluid elements, normal to each other, vanishes.

Thus at the bend's inlet the vortex is along a fluid region, of length l_1 (Fig. 7.2.2), normal to a fluid element l_2 in the main flow direction. Within the bend, at a station where the streamwise oriented element l_2 makes now an angle $d\varepsilon$ with its initial direction, the element l_1 normal to it must turn by $-d\varepsilon$ from its initial position. Hence this element and consequently also the vortex tube make an angle $2d\varepsilon$ with the cross section, that is inclined by $d\varepsilon$ to the inlet of bend. This follows from the free vortex enclosing the vortex.
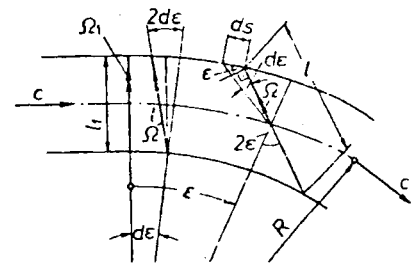
Fig. 7.2.2. Dislocation of a vortex tube, strength Ω_1, length l_1, at inlet of a bend while passing a bend and thus generating streamwise vorticity by bending the vortex tube towards the main flow.

Obviously a streamwise vorticity now appears (Fig. 7.2.2)

$$d\Omega_s = 2d\varepsilon \times \Omega_1 \approx 2d\varepsilon \times \Omega. \tag{7.2–6}$$

In steady flow the growth rate of streamwise vorticity follows from $d\Omega_s/dt = c\,\mathrm{grad}\,\Omega_s$. With the obvious relation $d\varepsilon/dt = c/R$, this growth rate yields (7.2–6),

$$c\,\mathrm{grad}\,\Omega_s = 2(c \times \Omega)/R. \tag{7.2–7}$$

According to Cap. 5.3, the equation of motion reads $\mathrm{grad}\,Y_a = c \times \Omega$. Inserting this in the last relation brings

$$\mathrm{grad}\,\Omega_s = [2/(cR)]\,\mathrm{grad}\,Y_a. \tag{7.2–8}$$

This is a general relation also valid for the case, when the vortex floats to a cross section of the bend, making an angle ε with its inlet. At this station the vortex also has been considerably lengthened from l_1 to l and changed its vorticity from Ω_1 to Ω, according to (7.2–4) (Fig. 7.2.2).

It is seen from (7.2–8) that the faces of constant absolute flow energy Y_a, the so called *Bernoulli* faces, coincide with those, in which the streamwise vorticity Ω_s does not change. The phenomenon is controlled by the figure $c/(R\Omega)$ which is comparable to the *Rossby* number. See also *Hawthorne* and others [7.4; 7.5].

7.2.2.3. The lengthening of a vortex tube within a rotor

Consider the steady plane relative flow of an ideal fluid in a straight rectangular channel, rotating with constant angular velocity ω (Fig. 7.2.3). The normal to the plane of the main flow makes an angle μ with the axis of rotation. Under an assumed irrotational absolute flow, the relative eddy has the relevant component $2\omega \cos \mu$ normal to the flow plane.

The meridional component of relative eddy $2\omega \sin \mu$ obviously has a component $2\omega \sin \mu \sin \beta$ in the direction of the main flow, which makes a constant angle β with the periphery. Consider a vortex tube of vorticity Ω_1 and length l_1, normal to the main flow at channel inlet (Fig. 7.2.3a). At an arbitrary instant later this vortex tube of length l makes an angle ε with the channel width and an angle $\pi/2 - \varepsilon$ with w, the relative velocity. Suppose it has a vorticity Ω in the stationary frame of reference.
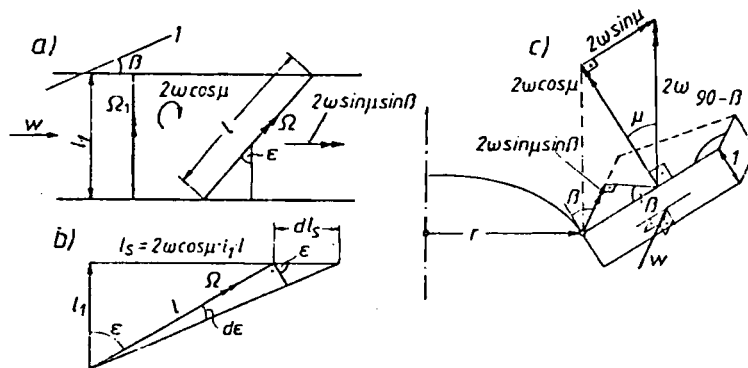
Fig. 7.2.3. Dislocation of a vortex tube passing a rectangular channel of a semi-axial rotor. a) Plan of channel, 1 tangential direction. b) Infinitesimal dislocation of the vortex tube. c) View of the spatial orientation of the vortex tube in the channel.

In the rotating frame of reference the vorticity then reads

$$\Omega_r = \Omega \mp 2\omega \sin \mu \cos(\beta + \varepsilon). \tag{7.2-9}$$

Now, relation (7.2-4) valid for the stationary frame of reference gives for the rotating one (note at inlet $\varepsilon = 0$),

$$\Omega_{r1} \pm 2\omega \sin \mu \cos \beta = (l_1/l)\,[\Omega_r \pm 2\omega \sin \mu \cos(\beta + \varepsilon)]. \tag{7.2-10}$$

The growth rate of relative streamwise vorticity reads formally

$$d\Omega_{rs}/dt = w\,|\mathrm{grad}\,\Omega_{rs}|. \tag{7.2-11}$$

The obvious relations $\Omega_{rs} = \Omega_r \sin \varepsilon$, $l_s = l \sin \varepsilon$ (7.2-10), and $\cos(\beta + \varepsilon)\cos\varepsilon - \sin(\beta + \varepsilon)\sin\varepsilon \equiv \cos(\beta + 2\varepsilon)$ give ($\dot\varepsilon = d\varepsilon/dt$, $\dot l_s = dl_s/dt$)

$$d\Omega_{rs}/dt = (l_s/l_1)\,(\Omega_{r1} \pm 2\omega \sin \mu \cos \beta) \mp 2\omega \sin \mu \cos(\beta + 2\varepsilon)\,\dot\varepsilon. \tag{7.2-12}$$

With the obvious relations (Fig. 7.2.3 b, c) $l_s = 2\omega \cos \mu l_1$, $l = l_1/\cos \varepsilon$, $\dot\varepsilon = \cos \varepsilon l_s/l = 2\omega \cos^2 \varepsilon \cos \mu$, usage of (7.2-11), (7.2-10) and (7.2-9), the relation (7.2-12) is reduced to

$$w\,|\mathrm{grad}\,\Omega_{rs}| = 2\omega\Omega \cos \mu \cos \varepsilon \mp 2\omega^2 \sin 2\mu \cos^2 \varepsilon \cos(\beta + 2\varepsilon). \tag{7.2-13}$$

By energy theorem for the rothalpy Y_r (Cap. 5.3), the relation $\cos \varepsilon = \sin(w, \Omega)$, (see Fig. 7.2.3), and hence $w\Omega \cos \varepsilon = |w \times \Omega|$, (7.2-13) can be converted into

$$|\mathrm{grad}\,\Omega_{rs}| = (2\omega \cos \mu/w^2)\,|\mathrm{grad}\,Y_r| \mp (2\omega^2/w) \sin 2\mu \cos^2 \varepsilon \cos(\beta + 2\varepsilon). \tag{7.2-14}$$

For the simple case $\mu = 0$ where the axis of rotation is normal to the channel's flow plane, the last relation is simplified to

248

$$\mathrm{grad}\,\Omega_{rs} = (2\omega/w^2)\,\mathrm{grad}\,Y_r.\qquad(7.2-15)$$

Now ω/Ω appears as the decisive number. From this it is seen, that now the streamwise relative vorticity remains constant on faces of constant "rothalpy" $Y_r = p/\varrho + gh + w^2/2 - r^2\omega^2/2$ [7.6; 7.7]. The latter taken without internal energy term.

7.2.2.4. Generation of secondary flow past a cascade

Consider a straight cascade (Fig. 7.2.4) passed by a plane potential flow. At station 1, upstream of the cascade, at a certain instant, a vortex line, length l_1 is normal to the main flow and between two streamlines, which pass the stagnation points of two neighbouring profiles. At station 1 this vortex has intensity Ω_1, downstream of the cascade, at station 2 it has length l_2 and intensity Ω_2, with a streamwise component Ω_{2s}. The latter is a source of secondary flow generated by the main flow, when passing through the cascade.
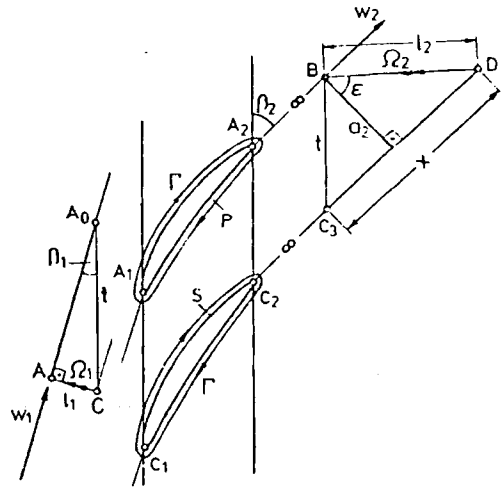
Fig. 7.2.4. Dislocation of a vortex tube and the generation of streamwise vorticity if passing through a straight cascade. $\overline{CC_1}$ and $\overline{A_0A_1}$ are straight lines infinitesimally long.

The velocities w_1, w_2 with their angles β_1, β_2 with the circumference at stations 1 and 2 are known from the velocity triangles. Consider a strip enclosed in the stream lines, touching the suction and pressure faces of two neighbouring profiles of the cascade. The one streamline $A\,A_0A_1\,A_2B$ along the pressure face (P) of the upper profile, and the other streamline $C\,C_1C_2C_3D$ along the suction face (S) of the lower profile.

The points A, C in front of the cascade and B, D past the cascade mark the positions of the vortex line's ends when it passes through stations 1 and 2, in front of and downstream of the cascade. The sections A_0A_1 and CC_1 as also A_2B and C_2C_3 for congruity are covered in the same time intervals. Furthermore the fluid covers the stretch $AA_0 = t\cos\beta_1$ (Fig. 7.2.4) with the velocity w_1 and the distance $C_3D = x$ with the velocity w_2.

The time intervals, the fluid needs to cover the suction face (S) and pressure face (P), result from the respective contour velocities (known for example from cascade theory) by

$$\tau_P = \int_P ds_P/w_P, \qquad \tau_s = \int_S ds_S/w_S.\qquad(7.2-16)$$

The time intervals, to cover the distances $A\,A_0$ and C_3D, are

$$\tau_{A-A_0} = t\cos\beta_1/w_1,\qquad(7.2-17)$$

$$\tau_{C_3-D} = x/w_2.\qquad(7.2-18)$$

249

The obvious equality $\tau_{A-B} = \tau_{C-D}$ gives

$$x = w_2(\tau_P - \tau_S) + t \cos\beta_1 (w_2/w_1).$$

(7.2-19)

Obviously the angle ε the vortex makes with a normal to the streamline past the cascade follows from

$$\sin \varepsilon = (x - t \cos\beta_2)/l_2.$$

(7.2-20)

With the relation $l_1 = t \sin\beta_1$, the relation $\Omega_2 = \Omega_1 l_2/l_1$ from (7.2-4), the desired streamwise vorticity past the cascade $\Omega_{2s} = \Omega_2 \sin\varepsilon$ follows from (7.2-20) as

$$\Omega_{2s} = (x - t \cos\beta_2)\,\Omega_1/(t \sin\beta_1).$$

(7.2-21)

Introducing $a_1 = t_1 \sin\beta_1$, assuming the depth of flow layer to be '1', Stokes' theorem (Cap. 5.2) gives the circulation due to secondary flow about the cross section of the strip considered past the cascade as

$$\Gamma_{2s} = \Omega_1(\sin\beta_2/\sin\beta_1)\,[w_2(\tau_P - \tau_S) + t(w_2 \cos\beta_1/w_1 - \cos\beta_2)].$$

(7.2-22)

See also Hawthorne [7.4], and Squire [7.5].

7.2.2.5. The streamwise vorticity past a radial flow impeller

Many reasons may exist for the streamwise vorticity past a radial flow impeller. The one considered here is the peripheral oriented vorticity entering the impeller eye from the boundary layer of the suction line, denoted by Ω_1.

Consider a vortex line covering the pitch at impeller inlet, length l_1, vorticity Ω_1 (Fig. 7.2.5). Downstream of the impeller it has length l_2 and absolute vorticity Ω_2 and makes an angle ε with the width a_2 of a strip that extends over one pitch. In the following the absolute velocity downstream of the impeller is assumed to be steady.

The absolute flow there makes an angle α_2 with the periphery known from the velocity triangles. Hence the streamwise vorticity of the absolute flow there as a function of the streamwise vorticity Ω_{2s} and that normal to it Ω_{2n} due to relative flow (Fig. 7.2.5) is given by

$$\Omega_{2as} = \Omega_{2n} \sin(\alpha_2 + \beta_2) - \Omega_{2s} \cos(\alpha_2 + \beta_2).$$

(7.2-23)
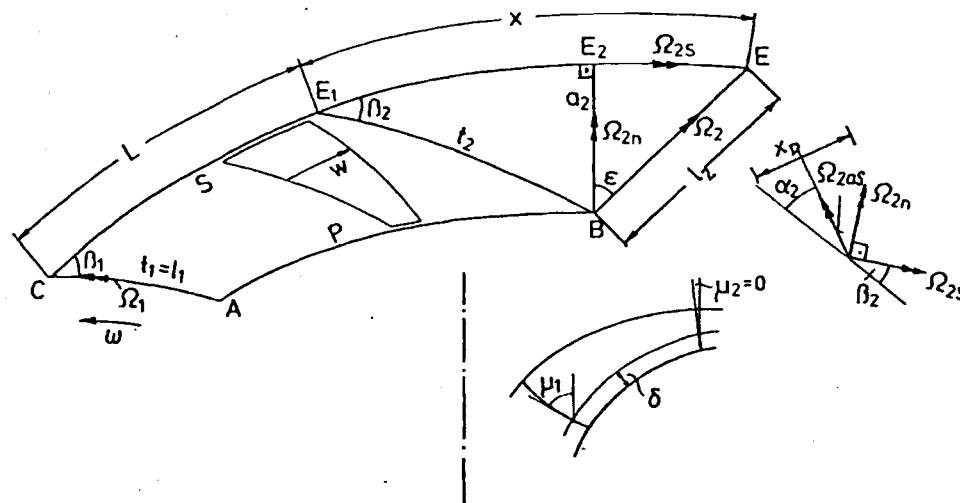
Fig. 7.2.5. Generation of a streamwise vorticity Ω_{2as} in an absolute flow of the diffuser inlet by the tangential vorticity of the boundary layer in the suction pipe of a radial impeller.

To calculate Ω_{2n} and Ω_{2s}, the relation (7.2–4) in the form $\Omega_2 = \Omega_1 l_2/l_1$, and the following approximative geometrical relations (Fig. 7.2.5) are used:

$$\Omega_{2s} = \Omega_2 \sin \varepsilon, \qquad \Omega_{2n} = \Omega_2 \cos \varepsilon, \qquad \sin \varepsilon = (x - t_2 \cos \beta_2)/l_2,$$

$$\cos \varepsilon = [l_2^2 - (x - t_2 \cos \beta_2)^2]^{1/2}/l_2, \qquad l_2^2 = t_2^2 + x^2 - 2t_2 x \cos \beta_2,$$

$$x = w_2 \tau_{E_1-E}. \tag{7.2-24}$$

The time intervals τ_S and τ_P from (7.2–16), needed to cover the suction and the pressure face of the impeller vane (known from cascade theory or measurement) yield the time interval τ_{E_1-E}, to cover the length x by means of

$$\tau_{E_1-E} = \tau_P - \tau_S. \tag{7.2-25}$$

Hence from the above the streamwise vorticity at diffuser inlet is

$$\Omega_{2as} = (\Omega_1/l_1)\,[\sin(\alpha_2 + \beta_2)\,t_2 \sin \beta_2 - \cos(\alpha_2 + \beta_2)(x - t_2 \cos \beta_2)]. \tag{7.2-26}$$

7.3. The boundary layer and its dissipation at the rotor walls

7.3.1. Introduction

As the real fluid adheres to a solid, the velocity close to such a face drops from a nearly frictionless value in the external flow across the thin boundary layer to zero at the wall. Hence the strain rate and consequently also the dissipation as the power lost due to strain rate and stress induced by turbulence and viscosity is greatest there. To calculate the loss in a machine, the thickness of the boundary layer and its velocity distribution must be known. Therefore it is shown in the following, how the boundary layer thickness can be computed for the general case of a relative flow along a double curved rotor vane, if the main flow outside the boundary layer is known. Hence by means of the energy theorem of the boundary layer the essential loss due to dissipation can be predicted also with respect to secondary flow and the flow regime within the boundary layer. Since a wake originating mainly from the boundary layer of a vane has also a high dissipation, this also will be considered.

7.3.2. Assumptions

a) Steady, unstalled, wall-attached flow of an incompressible Newtonian fluid along a double curved inelastic wall face rotating with constant speed.
b) According to *Prandtl* [7.23] the pressure at the outer edge of the boundary layer from the adjacent external flow remains constant across this layer. This external flow is known.
c) Vanishing velocity normal to the wall surface.
d) The following body forces are accounted for within the boundary layer: 1) *Coriolis* force, 2) Centrifugal force due to the curvature of streamlines, 2a) $1/R_x$ in a face normal to the wall in the main flow direction and $1/R_z$ in the direction of the secondary flow, 2b) $1/R_1$ in a face tangential to the wall in the main flow direction and $1/R_2$ in the direction of the secondary flow (see Fig. 7.3.1).

251
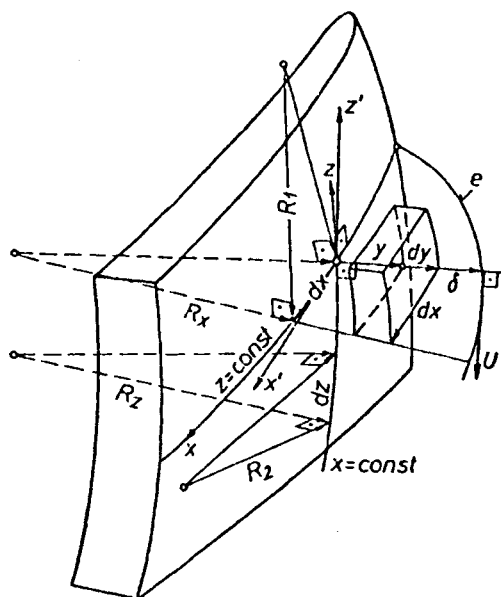
Fig. 7.3.1. Perspective view of the boundary layer thickness δ, along a double curved rotor vane. Curvilinear coordinates: x main flow direction, y normal to wall, z secondary flow direction, e outer edge of the boundary layer, R_1, R_2 radii of streamline's curvature in x, z-direction, in a plane tangential to vane surface. R_x, R_z radii of streamline's curvature in x, z-direction, in a plane normal to vane surface. x', z': axes of a *Cartesian* coordinate system in the point considered.

e) Small thickness of the boundary layer relative to the radius of curvature of the streamline.

f) Vanishing secondary flow outside the boundary layer with its thickness δ, whose amount has to be computed.

g) The angle ε, the velocity close to the wall makes with the main flow direction (x) (see Fig. 7.3.2) is known from observation (e.g. small grooves in a tinge) or by estimate.

h) The specific energy of relative flow ("rothalpy") contains a term e due to a loss linked to the streamline, that depends only on the coordinate z normal to the main flow direction. This "rothalpy" is taken without the term of internal energy.

i) Only wall shear stresses are accounted for.

j) Smooth wall.

k) Weight (g) and centrifugal force due to the rotating frame of reference ($r\omega^2$) both acting on unit mass are omitted, since both are balanced by an increment of pressure dp.

l) Because of the smallness of the boundary layer thickness δ in relation to the radius of the point considered $\partial[\cos(i, Z)]/\partial y = 0$, where i is either the x or the z axis, and Z the rotor axis.
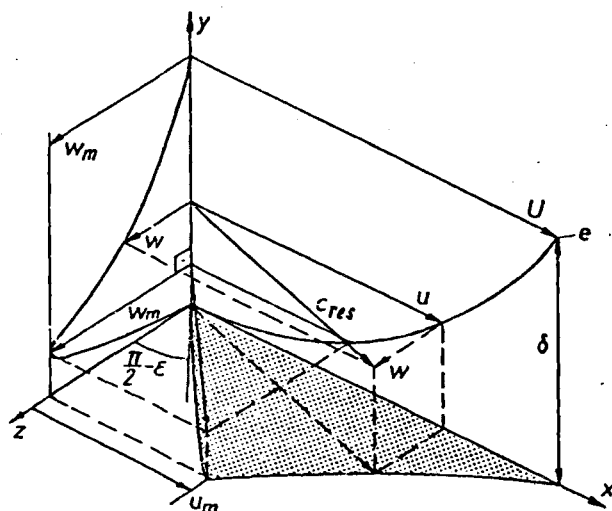
Fig. 7.3.2. Triangular diagram assume the flow in the boundary layer, in x, z-plane, and its features. e outer edge the boundary layer; c_{res} resulting velo

252

.. Velocity:

Strictly speaking, the velocity within the boundary layer as a function of distance y from the wall obeys different laws due to 3 zones. Close to the wall in a so-called laminar sublayer, a laminar shear flow exists, that adheres to the wall. Then a velocity distribution follows, which obeys a logarithmic law according to $u/u_0 = A + B \ln(yu/v)$, where u_0 is the velocity at the boundary of this zone, v the kinematic viscosity and A and B constants, y the wall distance (see Cap. 5.4).

In the following third zone adjacent to the external flow close to the boundary layer a so-called external law prevails. This depends in a manner, not completely clarified todate, on the pressure gradient of the adjacent flow outside the boundary layer. Using these three laws reveals also the problem of the location of its transition zone, thus aggravating the prediction of the boundary layer.

Limiting the considerations to the rotor vane also requires accounting for the role of hub and shroud. Within the boundary layer of a rotor vane, the secondary flow mainly originates from the boundary layer flow on hub and shroud (so-called interference of the boundary layer with those of its end wall faces). Strictly speaking, along the corners formed by these end walls and the rotor vane face, continuity, momentum and energy equation have to be satisfied by the flow passing from one boundary layer to the adjacent layer.

For the sake of simplicity and in tolerable agreement with experience of turbulent pipe flow and secondary flow [7.8; 7.9] the velocity distribution within the boundary layer of thickness δ is described as follows (Fig. 7.3.2).

- in the main flow direction:

$$u = U(y/\delta)^n \qquad (7.3-1)$$

- in the secondary flow direction:

$$w = \tan \varepsilon \, U(y/\delta)^n[1 - (y/\delta)^n]^l, \qquad (7.3-2)$$

where y is the coordinate normal to the wall, n an exponent, which lies within the turbulent flow regime of the order of $1/6$ to $1/10$ according to the *Reynolds* number of the boundary layer of $Re = 2 \cdot 10^3$ to $1,6 \cdot 10^6$, Re being $U\delta/v$ with U the velocity at the outer edge of the boundary layer ($y = \delta$) in the main flow (x) direction. In the laminar flow regime (7.3-1) has to be replaced by $u = U(2y/\delta)[1 - y/(2\delta)]$ or approximated by $u = 2Uy/\delta$. In the above, ε is the angle, the velocity close to the wall ($y = 0$) makes with the main flow direction (x-axis). The exponent l in (7.3-2) can be assumed as 'one' in a first order approximation. To adapt (7.3-2) to a known triangular diagram [7.8] (see Fig. 7.3.2) with its ratio,

$$\alpha = u_m/U \qquad (7.3-3)$$

due to the top of triangle, l must be chosen

$$l = (1 - \alpha)/\alpha. \qquad (7.3-4)$$

This arives from $\partial w/\partial u = 0$ at the top of triangle with the aid of (7.3-1) and (7.3-2). According to experience (7.3-1) and (7.3-2) show, that: $u(y = 0) = 0$; $u(y = \delta) = U$; $w(y = 0) = 0$; $w(y = \delta) = 0$ and

$$\lim_{y \to 0} (w/u) = \tan \varepsilon. \qquad (7.3-5)$$

- Coordinates: Curvilinear orthogonal coordinates are used. Their origin is at an arbitrary point of the wall. In the case of a vane face it is at the stagnation point near the leading inlet edge. The x-axis points in the direction of the main flow, y normal to the wall, z in the direction of secondary flow. The x- and the z-axis are always in a plane tangential to the wall surface.

– Wall shear stress: Since the direction of the shear stress and velocity coincide close to the wall, the following relation holds between the components of wall shear stress τ_{wx} and τ_{wz} respectively due to the directions of the main and secondary flows respectively

$$\tau_{wz}/\tau_{wx} = \tan\varepsilon. \tag{7.3-6}$$

In general the wall shear stress in the main flow direction follows

$$\tau_{wx} = c_\tau \varrho\, U^2/2, \tag{7.3-7}$$

where c_τ is a coefficient. For laminar flow within the boundary layer c_τ results, after *H. Schlichting* [5.4], from the *Reynolds* number $Re = U\delta/\nu$ and the pressure gradient of the main flow $\partial P/\partial x$ as

$$c_{\tau L} = 2\,Re^{-1}[2 - (\partial P/\partial x)\,(\delta/U^2)\,Re/6\varrho]. \tag{7.3-8}$$

In the turbulent flow regime c_τ depends on the momentum thickness

$$\vartheta_{11} = \int_0^\delta (u/U)\,(1 - u/U)\,dy \tag{7.3-9}$$

as follows

$$c_{\tau T} = \alpha(\vartheta_{11}\,U/\nu)^{-1/n_1}, \tag{7.3-10}$$

where after *L. Prandtl* [5.3]: $n_1 = 4$; $\alpha = 0,0064$ or after *Falkner* [7.10]: $n_1 = 6$; $\alpha = 0,00325$.

Strictly speaking $c_{\tau T}$ follows from

$$1/\sqrt{c_{\tau T}} = (1/\varkappa)\,ln(U\delta\,\sqrt{c_{\tau T}}/\nu) + B + 2\Pi/\varkappa, \tag{7.3-11}$$

where $\varkappa = 0,4$, B a constant parameter and Π a parameter that depends mainly according to *Coles* [7.11] on the pressure gradient of the external flow, namely: For $\partial P/\partial x < 0$: $0 < \Pi < 0,5$; for $\partial P/\partial x = 0$: $\Pi = 0,5$; for $\partial P/\partial x > 0$: $\Pi > 0,5$.

As the wall shear stress influences the growth of the boundary layer thickness δ as a kind of foreign excitation, it is important to know whether the boundary layer flow is laminar or turbulent. In general the boundary layer starts at the stagnation point heading the profile contour (in the case of a rotor vane) in the laminar regime. The transition point *Tr* lies, according to tests on turbine cascades carried out by *Faulders* [7.12], approximately at a distance Δx_{Tr} downstream of the minimum pressure point, usually located on the suction face. Δx_{Tr} depends as follows on the velocity U_{Tr} at the outer edge of the boundary layer due to the point *Tr* and the corresponding displacement thickness $\delta_{1\,Tr}$ of the boundary layer

$$\delta_{1\,Tr}/\Delta x_{Tr} = 90(\Delta x_{Tr}\,U_{Tr}/\nu)^{-0,758}, \tag{7.3-12}$$

where δ_1 is defined by

$$\delta_1 = \int_0^\delta (1 - u/U)\,dy. \tag{7.3-13}$$

According to *Schlichting* [5.4] for a rough calculation the transition point can be located at the minimum pressure point.

Strictly speaking the point of instability has to be distinguished from that of transition. The first is a prerequisite for the transition and is always upstream of the latter. And it is the point of instability which can be predicted by the method of small disturbances it

254

two dimensional flow, introduced by *Tollmien* and others [5.36] and confirmed by the tests of *Schubauer* and *Skramstad* [5.38] which were related to the simple case of a flat plate.

The objection that the model of two dimensional disturbances in two dimensional flow would not correspond to the real flow was invalidated by *Squire* [7.13] who proved that two dimensional disturbances have a lower stability limit than three dimensional ones and are more dangerous.

In general the instability point depends on the *Reynolds* number, the angle of attack, the geometry and the thickness distribution of a profile, see *Schlichting* [5.4].

7.3.3. The momentum theorem of a boundary layer on a curved rotor vane

Accounting for continuity, the momentum theorem in the main flow direction, applied to a boundary layer element of depth δ and cross section $dx\,dz$ (Fig. 7.3.3) results in

$$\int_0^\delta u^2\,dy\,dz - \left\{ \int_0^{\delta+(\partial\delta/\partial x)\,dx} [u^2 + (\partial u^2/\partial x)\,dx]\,dy \right\} dz$$
$$+ \int_0^\delta wu\,dy\,dx - \int_0^{\delta+(\partial\delta/\partial z)\,dz} \{wu + [\partial(wu)/\partial z]\,dz\}\,dy\,dx$$
$$+ U \left\{ \left\langle \int_0^{\delta+(\partial\delta/\partial x)\,dx} [u + (\partial u/\partial x)\,dx]\,dy - \int_0^\delta u\,dy \right\rangle dz \right.$$
$$\left. + \left\langle \int_0^{\delta+(\partial\delta/\partial z)\,dz} [w + (\partial w/\partial z)\,dz]\,dy - \int_0^\delta w\,dy \right\rangle dx \right\}$$
$$+ [F_{Cor\,x} + F_{Cx} - (\delta/\varrho)\,\partial P/\partial x - \tau_{w\,x}/\varrho]\,dx\,dz = 0 \qquad (7.3-14)$$

where $F_{Cor\,x}$ is the *Coriolis* force, and F_{Cx} the body force due to streamline curvature both in the x-direction acting on a boundary layer element of cross sectional area $dx\,dz = 1$ and density $\varrho = 1$.

The rothalpy (without the internal energy) of the external flow reads with respect to assumption h)

$$P/\varrho + U^2/2 - r^2\omega^2/2 + gh = e(z). \qquad (7.3-15)$$
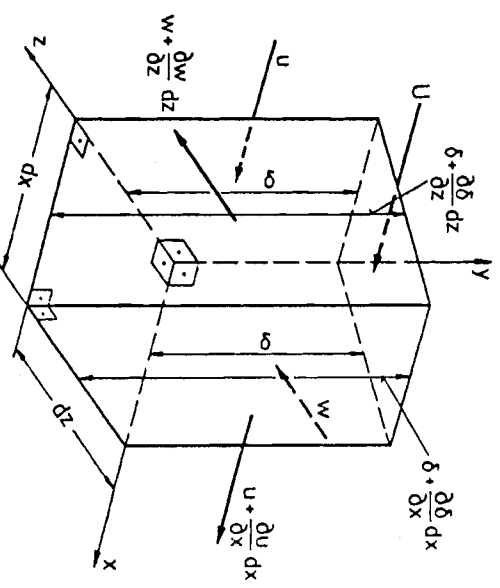
Fig. 7.3.3. Boundary layer element for application of the momentum and the energy theorem.

255

Hence according to assumption k)

$$\partial P/\partial x = - U\,\partial U/\partial x. \tag{7.3-16}$$

Inserting this in (7.3-14) and integrating stepwise, first from $y = 0$ to δ and then from $y = \delta$ to $\delta + (\partial\delta/\partial x)\,dx$ or $\delta + (\partial\delta/\partial z)\,dz$ respectively, gives with respect to $u(\delta) = U$ and $w(\delta) = 0$ after dividing by $dx\,dz$

$$\int_0^{\delta}[- \partial u^2/\partial x - \partial(wu)/\partial z + U\,\partial u/\partial x + U\,\partial w/\partial z + U\,\partial U/\partial x]\,dy$$

$$+ F_{Cor\,x} + F_{Cx} - \tau_{wx}/\varrho = 0. \tag{7.3-17}$$

Adding and substracting $u\,\partial U/\partial x$ and $w\,\partial U/\partial z$ respectively, taking into account Leibnitz's rule $\partial(uU)/\partial x = U\,\partial u/\partial x + u\,\partial U/\partial x$ etc., and the following identities [as a consequence of $u(\delta) = U$ and $w(\delta) = 0$]

$$\frac{\partial}{\partial x}\int_0^{\delta} u(U - u)\,dy = \int_0^{\delta}\frac{\partial}{\partial x}[u(U - u)]\,dy \tag{7.3-18}$$

$$\frac{\partial}{\partial z}\int_0^{\delta} w(U - u)\,dy = \int_0^{\delta}\frac{\partial}{\partial z}[w(U - u)]\,dy \tag{7.3-19}$$

and introducing the boundary layer parameters ϑ_{11} from (7.3-9), δ_1 from (7.3-13) and

$$\delta_3 = \int_0^{\delta}(w/U)^2\,dy, \tag{7.3-20}$$

$$\delta_2 = \int_0^{\delta}(w/U)\,dy, \tag{7.3-21}$$

equation (7.3-17) yields the following form of the momentum equation in the main flow direction

$$\frac{\partial}{\partial x}(U^2\vartheta_{11}) + U\frac{\partial U}{\partial x}\delta_1 - \frac{\partial}{\partial z}(U^2\delta_3) + \frac{\partial U}{\partial z}U\delta_2 + F_{Cor\,x} + F_{Cx} - \frac{\tau_{wx}}{\varrho} = 0. \tag{7.3-22}$$

Using the further boundary layer parameter

$$\delta_4 = \int_0^{\delta}(w/U)(u/U)\,dy \tag{7.3-23}$$

and employing a procedure similiar to that for the main flow, results in the following momentum equation in the direction of the secondary flow

$$-\frac{\partial}{\partial z}(U^2\delta_3) - \frac{\partial}{\partial x}(U^2\delta_4) + U\frac{\partial U}{\partial z}\delta - \frac{\partial e}{\partial z}\delta + F_{Cor\,z} + F_{Cz} - \frac{\tau_{wz}}{\varrho} = 0 \tag{7.3-24}$$

in which e is defined by (7.3-15) as a streamline-linked loss. $F_{Cor\,z}$ is the Coriolis force, F_{Cz} the body force due to the curvature of the streamline both acting on a boundary layer element of cross sectional area $dx\,dz = 1$ and density $\varrho = 1$.

Under assumptions b), e), and l), the body forces $F_{Cor\,i}$, F_{Ci} read:

a) The Coriolis forces in the x and z-direction respectively are

256

$$F_{Cor\,x} = -2\omega\left\langle U\,\delta_2\cos(y, Z) + \delta\frac{\partial}{\partial x}\{U[\delta_2\cos(x, Z)\right.$$

$$\left. - \delta\cos(z, Z) + \delta_1\cos(z, Z)]\}\right\rangle, \tag{7.3-25}$$

$$F_{Cor\,z} = 2\omega\left\langle U[\delta\cos(y, Z) - \delta_1\cos(y, Z)] - \delta\frac{\partial}{\partial z}\{U[\delta_2\cos(x, Z)\right.$$

$$\left. - \delta\cos(z, Z) + \delta_1\cos(z, Z)]\}\right\rangle, \tag{7.3-26}$$

where ω is the angular velocity, and Z the axis of the rotor. [The derivatives in (7.3–25), (7.3–26) follow from the increment of pressure P in the external flow adjacent to the boundary layer as a consequence of the Coriolis force of the boundary layer.]

b) The body forces due to the curvature of the streamline in the x and z-direction respectively are

$$F_{C\,x} = (U^2/R_1)\,\delta_4 - (U^2/R_2)\,\delta_3 - \delta\frac{\partial}{\partial x}[U^2(\delta_5/R_x + \delta_3/R_z)], \tag{7.3-27}$$

$$F_{C\,z} = (U^2/R_1)\,\delta - (U^2/R_1)\,\delta_5 + (U^2/R_2)\,\delta_4 - \delta\frac{\partial}{\partial z}[U^2(\delta_5/R_x + \delta_3/R_z)], \tag{7.3-28}$$

where

$$\delta_5 = \int_0^\delta (u/U)^2\,dy. \tag{7.3-29}$$

7.3.4. Differential equation for the growth of the boundary layer

Inserting (7.3–1), (7.3–2) and $y/\delta = s$ in (7.3–9), (7.3–13), (7.3–20), (7.3–21), (7.3–23), (7.3–29), the boundary layer parameter ϑ_{11} and δ_i read

$$\vartheta_{11} = \delta\int_0^1 s^n(1 - s^n)\,ds = A\,\delta, \tag{7.3-30}$$

$$\delta_1 = \delta\int_0^1 (1 - s^n)\,ds = B\,\delta, \tag{7.3-31}$$

$$\delta_2 = \delta\tan\varepsilon\int_0^1 s^n(1 - s^n)^l\,ds = \tan\varepsilon\,D\,\delta, \tag{7.3-32}$$

$$\delta_3 = \delta\tan^2\varepsilon\int_0^1 s^{2n}(1 - s^n)^{2l}\,ds = \tan^2\varepsilon\,E\,\delta, \tag{7.3-33}$$

$$\delta_4 = \delta\tan\varepsilon\int_0^1 s^{2n}(1 - s^n)^l\,ds = \tan\varepsilon\,F\,\delta, \tag{7.3-34}$$

$$\delta_5 = \delta\int_0^1 s^{2n}ds = H\,\delta. \tag{7.3-35}$$

The above integrals without the exponent l in their integrand can be solved easily, those with this exponent only, if l is an integer. Otherwise the respective terms in the integrands must be converted into binomial series, usually converging, which can be integrated term by term. The parameters A through H depend only on l and n and are therefore assumed to be constant within a certain section of the boundary layer considered.

When the velocity distribution within the boundary layer is known from measurements, such as have been carried by *Furtner* [9.7] on the runner vanes of Kaplan and Francis turbines, the above boundary layer parameters can also be computed on the base of integrals defining them after (7.3–9), (7.3–13), (7.3–20), (7.3–21), (7.3–24), (7.3–29). This can be done numerically and would lead to continuously varying figures A to H. In the following these figures are assumed to vary to such a low degree, that their derivatives are vanishing small. (According to Mosonyi, the most questionable parameter is a constant.)

Inserting the boundary layer parameters ϑ_{11} and δ_i, now expressed after (7.3–30) through (7.3–35) by the boundary layer thickness δ and the values A through H, into (7.3–22), into $F_{Cor\,x}$ after (7.3–25) and $F_{C\,x}$ after (7.3–27), and putting both the latter in (7.3–22), then the momentum theorem of the boundary layer in the main flow direction (7.3–22) reads

$$(a_0 - a_1\delta)\,\partial\delta/\partial x + a_2\delta + a_3\delta^2 + a_4\,\partial\delta/\partial z - \tau_{wx}/\varrho = 0, \qquad (7.3–36)$$

where

$$a_0 = U^2 A, \qquad\qquad (7.3–37)$$

$$a_4 = U^2 E \tan^3 \varepsilon, \qquad\qquad (7.3–38)$$

$$a_1 = -2\omega U[(1-B)\cos(z, Z) + D \tan\varepsilon \cos(x, Z)] + U^2\left(\frac{H}{R_x} + \frac{E \tan^2\varepsilon}{R_z}\right), \qquad (7.3–39)$$

$$a_2 = U\frac{\partial U}{\partial x}(2A + B) + U\frac{\partial U}{\partial z}(D - 2E \tan\varepsilon)\tan\varepsilon$$
$$- 2\omega U D \cos(y, Z)\tan\varepsilon + U^2\left[\frac{F\tan\varepsilon}{R_1} - \frac{E \tan^2\varepsilon}{R_2} - \frac{2E\tan\varepsilon}{\cos^2\varepsilon}\frac{\partial\varepsilon}{\partial z}\right], \qquad (7.3–40)$$

$$a_3 = 2\frac{\partial U}{\partial x}\left\{\omega[(1-B)\cos(z, Z) - D\tan\varepsilon\cos(x, Z)] + U\left(\frac{H}{R_x} + \frac{E\tan^2\varepsilon}{R_z}\right)\right\}$$
$$+ 2\omega U\left[(1-B)\frac{\partial\cos(z, Z)}{\partial x} - D\tan\varepsilon\frac{\partial\cos(x, Z)}{\partial x}\right]$$
$$+ U^2\left[\frac{2E}{R_z}\frac{\tan\varepsilon}{\cos^2\varepsilon}\frac{\partial\varepsilon}{\partial z} - \frac{E}{R_z^2}\frac{\partial R_z}{\partial x}\tan^2\varepsilon - \frac{H}{R_x^2}\frac{\partial R_x}{\partial x}\right]. \qquad (7.3–41)$$

In a similar manner the momentum theorem in the secondary flow direction is obtained as

$$(b_0 + b_1\delta)\,\partial\delta/\partial z + b_2\delta + b_3\delta^2 - b_4\,\partial\delta/\partial x - \tau_{wx}/\varrho\tan\varepsilon = 0, \qquad (7.3–42)$$

where

$$b_0 = -U^2 \tan^2\varepsilon, \qquad\qquad (7.3–43)$$

$$b_4 = U^2 F \tan\varepsilon, \qquad\qquad (7.3–44)$$

$$b_1 = -2\omega U\left[D\tan\varepsilon\cos(x, Z) - (1-B)\frac{\partial\cos(z, Z)}{\partial z}\right]$$
$$- U^2\left(\frac{H}{R_x} + \frac{E\tan^2\varepsilon}{R_z}\right), \qquad (7.3–45)$$

$$b_2 = U \frac{\partial U}{\partial z}(1 - 2E\tan^2\varepsilon) - 2U\frac{\partial U}{\partial x}F\tan\varepsilon$$

$$- U^2\left(\frac{2E\tan\varepsilon}{\cos^2\varepsilon}\frac{\partial\varepsilon}{\partial z} + \frac{F}{\cos^2\varepsilon}\frac{\partial\varepsilon}{\partial x}\right) - \frac{\partial e}{\partial z} + 2\omega U(1 - B)\cos(y, Z)$$

$$+ U^2\left(\frac{1 - H}{R_1} + \frac{F\tan\varepsilon}{R_2}\right), \tag{7.3-46}$$

$$b_3 = -2\frac{\partial U}{\partial z}\left\{\omega[D\tan\varepsilon\cos(x, Z) - (1 - B)\cos(z, Z)] - U\left(\frac{H}{R_x} + \frac{E\tan^2\varepsilon}{R_z}\right)\right\}$$

$$- 2\omega U\left[\frac{D}{\cos^2\varepsilon}\frac{\partial\varepsilon}{\partial z}\cos(x, Z) - D\tan\varepsilon\frac{\partial\cos(x, Z)}{\partial z} - (1 - B)\frac{\partial\cos(z, Z)}{\partial z}\right]$$

$$+ U^2\left(\frac{H}{R_x^2}\frac{\partial R_x}{\partial z} - \frac{2E\tan\varepsilon}{R_z\cos^2\varepsilon}\frac{\partial\varepsilon}{\partial z} - \frac{E\tan^2\varepsilon}{R_z^2}\frac{\partial R_z}{\partial z}\right). \tag{7.3-47}$$

Assuming $b_1\delta \ll b_0$, which is usually satisfied, the relation (7.3-42) can be transformed into

$$\partial\delta/\partial z = -(1 - b_1\delta/b_0)(b_2\delta + b_3\delta^2 - b_4\partial\delta/\partial x - \tau_{wx}\tan\varepsilon/\varrho)/b_0. \tag{7.3-48}$$

Putting this in equation (7.3-36) gives the following partial differential equation for the growth of the boundary layer thickness δ in the main flow ($= x$) direction

$$(c_0 - c_1\delta)\,\partial\delta/\partial x + c_2\delta + c_3\delta^2 + c_4\delta^3 = [1 - c_5(1 - c_6\delta)\tan\varepsilon]\,\tau_{wx}/\varrho, \tag{7.3-49}$$

where

$$c_0 = a_0 + a_4b_4/b_0, \tag{7.3-50}$$

$$c_1 = a_1 + a_4b_4b_1/b_0^2, \tag{7.3-51}$$

$$c_2 = a_2 - a_4b_2/b_0, \tag{7.3-52}$$

$$c_3 = a_3 - (b_3 - b_1b_2/b_0)(a_4/b_0), \tag{7.3-53}$$

$$c_4 = a_4b_1b_3/b_0^2, \tag{7.3-54}$$

$$c_5 = a_4/b_0, \tag{7.3-55}$$

$$c_6 = b_1/b_0. \tag{7.3-56}$$

After converting equation (7.3-49) into a difference equation and then dividing the known streampath of the external flow adjacent to the boundary layer into finite sections of finite length Δx, the increment of boundary layer thickness $\Delta\delta_{i+1}$, at the end of $i + 1$ st stretch Δx_{i+1}, can be computed to a first approximation stepwise from the boundary layer thickness δ_i of the preceding stretch by

$$\Delta\delta_{i+1} = \Delta x_{i+1}\{[1 - c_{5,i+1}(1 - c_{6,i+1}\delta_i)\tan\varepsilon_{i+1}]\tau_{wx,i+1}/\varrho - c_{2,i+1}\delta_i$$

$$- c_{3,i+1}\delta_i^2 + c_{4,i+1}\delta_i^3\}/\{c_{0,i+1} - c_{1,i+1}\delta_i$$

$$+ \Delta x_{i+1}[c_{2,i+1}/2 + c_{3,i+1}\delta_i + 3c_{4,i+1}\delta_i^2/2$$

$$- c_{5,i+1}c_{6,i+1}\tan\varepsilon_{i+1}\tau_{wx,i+1}/(2\varrho)]\}. \tag{7.3-57}$$

For this calculation the parameters c_0 through c_6, ε and τ_{wx} for the $i + 1$ st section Δx_{i+1} have to be known as mean values, from estimates of the angle ε (e.g. indicated by paint), the given vane geometry, and the known flow along the outer edge of the boundary layer according to assumption b). Strictly speaking (7.3-49) would be converted into an equation of the 3rd degree, somewhat more

complicated to solve than (7.3 – 57). However, in general (7.3 – 57) may be sufficiently accurate, except for the first steps past the stagnation point, where the calculation starts in the case of a vane.

Close to the stagnation point the boundary layer flow is laminar. Hence τ_{wx} after (7.3 – 7) and (7.3 – 8) is proportional to $Re^{-1} U^2$ and therefore also to $U \delta^{-1}$. Thus the wall shear stress tends to become indefinite at the stagnation point, since δ and U vanish there. This requires a more exact treatment of the stress term at the first step downstream of the stagnation point. This yields

$$\Delta \delta_1 = 2[U_1 \Delta x_1 \, v/c_{0,1}]^{1/2} \tag{7.3 – 58}$$

where the subscript 1 indicates the first step.

From the growth of the boundary layer thickness along several main streamlines, also the course of δ in the secondary flow direction is obtained.

For a given initial value of δ, the above calculation can also be made for the boundary layer on shroud and hub. Strictly speaking the secondary flow causes also an interference of the boundary layers along a corner formed e.g., by shroud and rotor vane. This is neglected here.

An analysis of the 3-dimensional boundary layer in fluid machinery was made by *Arakawa, Tagori* and *Shirakura* [7.14].

7.3.5. Computation of the wake past a rotor vane

According to the introductory remark also the wake past a rotor vane is a zone of high energy dissipation. Hence any loss prediction requires also the velocity distribution of a wake and its width b as a function of the distance from its origin.

In the following the observations on a wake past a single profile in plane flow are used as a model. They may be extended also to wakes past an airfoil in a straight cascade.

In this case, as is well known, the drag F_D, its corresponding drag coefficient ζ_D, the undisturbed velocity U_0, the streamwise length L and the depth t_m of the body submerged are related to each other by [7.3]

$$F_D = (\varrho/2) \, \zeta_D \, U_0^2 \, L \, t_m. \tag{7.3 – 59}$$

As is well-known the momentum theorem together with continuity yield the following relation between drag and velocity deficit $U_0 - u$ in a wake of width $2b$, normal to U_0 [5.4]

$$F_D = \varrho \, U_0 \int_{-b}^{+b} (U_0 - u) \, dy, \tag{7.3 – 60}$$

where y is the coordinate normal to the velocity u in the main flow direction. This relation holds also for a profile in a straight cascade in plane flow.

By means of similarity considerations and the equations (7.3 – 59), (7.3 – 60), *H. Schlichting* [5.4] has derived the following relation between b, L, ζ_D and the length of the wake x,

$$b = \sqrt{10} \, \beta (x \zeta_D L)^{1/2}, \tag{7.3 – 61}$$

in which β is the ratio: mixing length to half the breadth b of the wake. By tests on cylinders *Reichard* [7.15] found

$$\beta = 0{,}18. \tag{7.3 – 62}$$

Assuming constant pressure across the wake and only *Reynolds* shear stress in the flow direction, expressed by the mixing length after *L. Prandtl* [5.32]. *H. Schlichting* has derived from the equation of motion the following distribution of velocity in the symmetrical wake within plane flow [5.4]

$$u = U_0 \{1 - (\zeta_D L/x)^{1/2}(0,176/\beta) [1 - \langle y/[\sqrt{10}\beta(\zeta_D L x)^{1/2}]\rangle^{3/2}]^2\}, \qquad (7.3-63)$$

where x is the distance of the cross section of the wake considered from the origin of the wake taken in the flow direction of u and U_0.

Contrary to this model the wake past a rotor vane may show also a secondary flow. This will be neglected in the following. An adoption of the above wake model instead of the real one at a rotor vane requires the clarification of the following five problems:

I) How does the width 2b of the wake depend on the thickness of the vane's trailing edge and on its boundary layer thicknesses on the suction and pressure faces, respectively?

II) What is the distance x_1 in the streamwise direction of the trailing edge of the vane from the imaginary origin of the wake?

III) How does the undisturbed velocity U_0 of the model depend on the velocities U_{P1} and U_{S1} respectively at the outer edges of the boundary layer on the suction and pressure faces respectively at the trailing edge of the rotor vane?

IV) How does the drag coefficient of the model ζ_D or its corresponding drag (7.3-59) depend on the drag of the rotor vane?

V) What happens to the flow field, when the wake lies within a layer, the thickness t of which varies in the streamwise direction?

Before entering in detail the following assumptions are made: The flow around the rotor vane is axisymmetric. Secondary flow in the wake is neglected. The normal of the vane surface makes an angle γ with a plane tangential to the stream surface. Then obviously any length n normal to the vane (i.e., its thickness h or the thickness of its boundary layer δ) appears as a thickness $n/\cos\gamma$ within the stream surface.

The angle γ can be found by the relation

$$\cos\gamma = 1/[\sin\beta(1 + \cot^2\beta'/\sin^2\theta)^{1/2}]$$

where β' is the angle the pattern making section of the vane makes with the circumference, β the angle the relative flow along the vane makes with the circumference, θ the angle the radial vane section makes with the radius (Fig. 6.5.1).

To I) and II): Both the problems belong to each other as the half width of wake b and its length x are linked to each other by relation (7.3-61). At a trailing edge the vane thickness is h_1 and the thickness of its boundary layers on the suction and pressure faces δ_{S1} and δ_{P1} respectively. Since the wake originates from the boundary layers at the trailing edge

$$2b_1 \equiv 2b(x_1) = (\delta_{S1} + h_1 + \delta_{P1})/\cos\gamma. \qquad (7.3-64)$$

Hence from (7.3-61) the desired distance x_1 of the wake's origin from the trailing edge

$$x_1 = \{[(\delta_{S1} + h_1 + \delta_{P1})/\cos\gamma]/(2\sqrt{10}\beta)\}^2/(\zeta_D L). \qquad (7.3-65)$$

To III): Inserting $x = x_1$ into (7.3-71), then the velocity $u_1 = U_0 - u$ at station x_1, y of the wake model depends on the undisturbed velocity U_0. To express this figure as a function of the known velocities u_{S1} and u_{P1} on the suction and pressure face respectively at the vane's trailing edge, it is assumed that the flow of kinetic energy through this section of the wake model equals the flow of kinetic energy through both the real boundary layers at station 1 of the trailing edge for a flow layer of unit thickness. Accordingly

$$\int_{-b_1}^{b_1} u_1^3 \, dy = \int_0^{\delta_{S1}} u_{S1}^3 \, dy + \int_0^{\delta_{P1}} u_{P1}^3 \, dy. \qquad (7.3-66)$$

$$u_{S1} = U_{S1}(y/\delta_{S1})^n, \qquad\qquad (7.3-67)$$

$$u_{P1} = U_{P1}(y/\delta_{P1})^n, \qquad\qquad (7.3-68)$$

where U_{S1} and U_{P1} are the known velocities at the outer edge of the boundary layer of the vane's suction and pressure faces at station 1 respectively and δ_{S1} and δ_{P1} are the known boundary layer thicknesses on the suction and pressure faces also at station 1 [7]).

Putting (7.3-67, 68) in (7.3-66) yields the undisturbed velocity U_0 of the wake model as a function of the known figures U_{S1}, U_{P1}, δ_{S1}, δ_{P1}, L (chord of the vane), x_1, β (see (7.3-62)) and ζ_D

$$U_0 = \{(\delta_{S1} U_{S1}^3 + \delta_{P1} U_{P1}^3)/[(3n + 1) N]\}^{1/3}, \qquad\qquad (7.3-69)$$

where

$$N = 2b_1\{1 - (0.075 \sqrt{10}/\beta)(\zeta_D L/x_1)^{1/2} + (0.0825/\beta^2)(\zeta_D L/x_1)$$
$$+ (0.039/\beta^3)(\zeta_D L/x_1)^{3/2}\}. \qquad\qquad (7.3-70)$$

IV): To express the drag coefficient or the corresponding drag F_D of the real vane part considered, the axisymmetrically assumed flow layer around the vane part considered with its thickness $t(x)$ varying as a function of the relative streampath coordinate x is reduced to an imaginary layer of constant mean thickness by

$$t_m = \int_0^L t(x)\, dx/L. \qquad\qquad (7.3-71)$$

In the following the vane within the flow layer considered is assumed to be straight. From the computation of the boundary layer thickness, the wall shear stresses in the laminar and tubulent flow regime τ_{wxL} and τ_{wxT} respectively are known along the pressure and suction face. They are assumed to yield the main part of the drag. Since the drag is now oriented in the same direction as the wall shear stresses, it is approximated by integrating the tangential wall forces due to the wall shear stresses in a flow layer of varying thickness $t(x)$. This drag is equal to that in a plane flow layer of thickness t_m from (7.3-59). Hence the desired drag coefficient of the plane wake model is obtained by integrating along the suction and pressure faces from the stagnation point $x = 0$ via the transition point laminar turbulent $(x = x_{Tr})$ to the trailing edge $(x = L)$.

$$\zeta_D = 2\left(\int_0^{x_{Tr}P} \tau_{wxL} t\, dx + \int_{x_{Tr}P}^L \tau_{wxT} t\, dx + \int_0^{x_{Tr}S} \tau_{wxL} t\, dx + \int_{x_{Tr}S}^L \tau_{wxT} t\, dx\right)/(U_0^2 t_m \varrho L).$$
$$(7.3-72)$$

Using b_1 from (7.3-64) and x_1 from (7.3-65), U_0 follows from (7.3-69).

V): For a flow layer limited by axisymmetric stream surfaces, continuity requires that the local thickness t of this flow lamina at a station with radius r depends on r according to a previous function $t(r)$. Moreover it requires, that the real velocity at this station u_{re} follows from the velocity u from (7.3-63) due to the plane wake model with a layer of constant depth t_m by means of

$$u_{re} = u t_m r_0/[t(r) r], \qquad\qquad (7.3-73)$$

where r_0 is the radius of the station at the wake's origin $(x = 0)$.

Once the mean angle β the velocity makes with the circumference and the mean angle μ the stream surface makes with a plane normal to the axis are known, r depends approximately on the distance y the point considered has from the wake's centre line with its length x

$$r = r_0 - (x \sin\beta - y \cos\beta)\cos\mu. \qquad\qquad (7.3-74)$$

7.3.6. The energy theorem of the boundary layer and loss prediction

Once the size and form of the velocity field of the boundary layer or wake are known, the energy theorem gives the loss in the layer in consequence of dissipation. In the following the energy theorem is derived for a boundary layer element of thickness δ on the area $dx\,dz$ and its secondary flow characterized by the angle ε the velocity close to the wall makes with main flow direction. The procedure can be adopted also to half a wake of width b instead of δ, when the loss thus obtained is doubled and the terms due to secondary flow containing $\tan \varepsilon$ are cancelled.

An element of boundary layer shown in Fig. 7.3.3 of cross sectional area $dx\,dz$ is considered. Here the following inflow of kinetic energy $\dot{E}_i$ can be distinguished:

$$\text{Through the area } \delta dz: \quad d\dot{E}_{ix} = (\varrho/2) \int\limits_{y=0}^{\delta} (u^3 + uw^2)\, dy\, dz.$$

$$\text{Through the area } \delta dx: \quad d\dot{E}_{iz} = (\varrho/2) \int\limits_{y=0}^{\delta} (w^3 + wu^2)\, dy\, dx.$$

Through the outer limiting area of the element $dx\,dz$ flows with respect to continuity:

$$d\dot{E}_{iy} = (\varrho/2)\, U^2 \left\{ \left\langle \int\limits_{y=0}^{\delta + (\partial \delta/\partial x)\,dx} [u + (\partial u/\partial x)\, dx]\, dy - \int\limits_{y=0}^{\delta} u\, dy \right\rangle dz \right.$$
$$\left. + \left\langle \int\limits_{y=0}^{\delta + (\partial \delta/\partial z)\,dz} [w + (\partial w/\partial z)\, dz]\, dy - \int\limits_{y=0}^{\delta} w\, dy \right\rangle \right\}.$$

The outflow of kinetic energy $\dot{E}_0$ leaving this boundary layer element reads:

Through the area $[\delta + (\partial \delta/\partial x)\, dx]\, dz$:

$$d\dot{E}_{0x} = (\varrho/2) \left\{ \int\limits_{y=0}^{\delta + (\partial \delta/\partial x)\,dx} \langle u^3 + (\partial u^3/\partial x)\, dx + uw^2 + [\partial(uw^2)/\partial x]\, dx \rangle\, dy\, dz \right\}.$$

Through the area $[\delta + (\partial \delta/\partial z)\, dz]\, dx$:

$$d\dot{E}_{0z} = (\varrho/2) \left\{ \int\limits_{y=0}^{\delta + (\partial \delta/\partial z)\,dz} \langle w^3 + (\partial w^3/\partial z)\, dz + wu^2 + [\partial(wu^2)/\partial z]\, dz \rangle\, dy\, dx \right\}.$$

The above yields the following resulting inflow of kinetic energy into the boundary layer element:

$$d\dot{E} = d\dot{E}_{ix} + d\dot{E}_{iz} + d\dot{E}_{iy} - d\dot{E}_{0x} - d\dot{E}_{0z}. \tag{7.3-75}$$

The work done by the increment of the pressure P from the adjacent external flow per unit time becomes with assumption k)

$$d\dot{W}_P = - \left[(\partial P/\partial x)\, dx \int\limits_{y=0}^{\delta} u\, dy + (\partial P/\partial z)\, dz \int\limits_{y=0}^{\delta} w\, dy \right] dx\, dz. \tag{7.3-76}$$

Assuming the absence of any heat transfer on this element, and neglecting the expansion work $\int p\, dv$ of the fluid within the element, the dissipation $d\Phi$ as the negative work done per time unit of the internal stresses in connection with strain rate, follows from the energy theorem due to the element as

$$d\Phi = d\dot{E} + d\dot{W}_P. \tag{7.3-77}$$

Finally the dissipation, as a heat transfer on the fluid, increases the internal energy of the fluid by increasing its temperature and hence usually also the volume of the fluid. This also influences the expansion work $\int p\,dv$ of the fluid, neglected here. .

The pressure gradients in (7.3–76) can be eliminated by differentiating the rothalpy, using (7.3–15) and accounting for the assumption I).

Inserting (7.3–75) in (7.3–76) and (7.3–77), integrating from $y = 0$ to δ and then over $d\delta$ in the x and z-directions respectively, accounting for Leibnitz's rule and the following identities [as a consequence of $u(\delta) = U$ and $w(\delta) = 0$]

$$\frac{\partial}{\partial x} \int_0^\delta u^3\,dy = \int_0^\delta \frac{\partial u^3}{\partial x}\,dy, \qquad (7.3-78)$$

$$\frac{\partial}{\partial x} \int_0^\delta u w^2\,dy = \int_0^\delta \frac{\partial(u w^2)}{\partial x}\,dy, \qquad (7.3-79)$$

$$\frac{\partial}{\partial z} \int_0^\delta w^3\,dy = \int_0^\delta \frac{\partial w^3}{\partial z}\,dy, \qquad (7.3-80)$$

$$\frac{\partial}{\partial z} \int_0^\delta w u^2\,dy = \int_0^\delta \frac{\partial(w u^2)}{\partial z}\,dy, \qquad (7.3-81)$$

convert the energy theorem (7.3–77) into the form

$$d\Phi = \frac{\varrho}{2}\left[\frac{\partial(\vartheta_2 U^3)}{\partial x} - \frac{\partial(\vartheta_3 U^3)}{\partial z} - 2\frac{\partial e}{\partial z} U\delta_2\right], \qquad (7.3-82)$$

where δ_2 is defined by (7.3–21) and ϑ_2 and ϑ_3, by

$$\vartheta_2 = \int_0^\delta (u/U)\,[1 - (u/U)^2 - (w/U)^2]\,dy, \qquad (7.3-83)$$

$$\vartheta_3 = \int_0^\delta (w/U)\,[(u/U)^2 + (w/U)^2]\,dy. \qquad (7.3-84)$$

The parameters ϑ_2, ϑ_3 are so-called energy thicknesses of the boundary layer. They can be determined by boundary layer measurements, such as have been carried out by Furfner [9.6].

Using (7.3–1) and (7.3–2) with the substitution $y/\delta = s$ gives the boundary layer parameters as

$$\vartheta_2 = \delta \int_0^1 s^n[1 - s^{2n} - \tan^2\varepsilon s^{2n}(1 - s^n)^{2l}]\,ds = \delta(M - O\tan^2\varepsilon), \qquad (7.3-85)$$

$$\vartheta_3 = \delta \int_0^1 s^n \tan\varepsilon(1 - s^n)^l\,[s^{2n} + s^{2n}\tan^2\varepsilon(1 - s^n)^{2l}]\,ds$$

$$= \delta(T\tan\varepsilon + V\tan^3\varepsilon). \qquad (7.3-86)$$

To evaluate these integrals and thus to obtain M, O, T and V, see remarks on the boundary layer parameters (7.3–30) to (7.3–35). Putting these relations in (7.3–85) results in the dissipation Φ as the power lost in the boundary layer by generation of heat

$$\Phi = \frac{\varrho}{2} \int_x \int_z \left[(M - O \tan^2 \varepsilon) \frac{\partial \delta U^3}{\partial x} - \frac{2 O \delta U^3 \tan \varepsilon}{\cos^2 \varepsilon} \frac{\partial \varepsilon}{\partial x} \right.$$

$$- (T \tan \varepsilon + V \tan^3 \varepsilon) \frac{\partial \delta U^3}{\partial z} - \frac{\delta U^3 (T + 3 V \tan^2 \varepsilon)}{\cos^2 \varepsilon} \frac{\partial \varepsilon}{\partial z}$$

$$\left. - 2 \delta U \tan \varepsilon \frac{\partial e}{\partial z} \right] dx \, dz. \tag{7.3--87}$$

In practice the integrals over the rotor surface (xz) are converted into sums. In a rotor for example, this double integral implies the faces of the rotor vanes and the faces of hub and shroud. Both the latter require an initial value for the boundary layer thickness at the entrance. Strictly speaking also the wakes should be included in the loss calculation.

Neglecting heat expansion, the nondimensional loss in a hydro turbo machine, specific head gH, discharge Q, becomes

$$h'_l = \Phi/(g H \varrho Q).$$

In exact terms, Φ as heat also expands the specific volume of the fluid by Δv. In a high head turbine with a pressure head roughly p_{II}, this gives a surplus of expansion work $p_{\mathrm{II}} \Delta v/2$.

Δv results from the temperature rise ΔT by heat transfer and the coefficient of cubical expansion β (note that β for water is always positiv, when the temperature is above 4 °C) by

$$\Delta v = \beta v \Delta T.$$

Since the dissipation Φ heats the discharge Q, of a fluid with specific heat c, the temperature increase becomes

$$\Delta T = \Phi/(\varrho Q c).$$

Hence the specific head Y experiences a relative increase by expansion work of approximately $(\Delta Y \approx g H \Delta v/2)$

$$\Delta Y/Y = \beta g H h'_l/(2 c).$$

For water of 20 °C, specific heat $c = 4200$ J/(kg K), a head of 1800 m, a nondimensional loss $h'_l = 0.1$ and a coefficient of cubical expansion $\beta = 1{,}8 \cdot 10^{-4}$ K^{-1}, the relative head gain becomes negligibly small, namely

$$\Delta Y/Y \approx 3{,}8 \cdot 10^{-4}.$$

Since this holds good for the largest head implemented in turbines of $H = 1800$ m, it can be concluded that according to the assumption of the preceding calculation, any expansion by heating the water through the losses in a turbine can be practically neglected.

Loss prediction was also given by *Ueda* et al. [7.16] and *Raabe* [7.17; 7.18]. *Keller* [7.19] calculates the loss due to fluctuating circulation about the rotor vane. As a requirement for loss prediction *Nakkasyan* [7.20] calculates the 3-dimensional boundary layer using isotropic and anisotropic turbulent viscosities.

Strictly speaking the energy theorem has to start from turbulent flow [5.7]. In tensorial nomenclature used by *Hartner* [8.136], the energy theorem of turbulent flow reads

$$\underset{\text{I}}{\frac{d\overline{q^2}/2}{dt}} = - \underset{\text{II}}{\overline{u'_i u'_j} \frac{\partial U_j}{\partial x_i}} - \underset{\text{III}}{\frac{\partial}{\partial x_i} \left[\overline{u'_i \left(\frac{q^2}{2} + \frac{p'}{\varrho} \right)} \right]} + \underset{\text{IV}}{v \frac{\partial^2 \overline{q^2}/2}{\partial x_j^2}} - \underset{\text{V}}{v \overline{\left(\frac{\partial u'_i}{\partial x_j} \right)^2}}, \tag{7.3--88}$$

where u'_i is the turbulent fluctuation in the x_i direction, p' the fluctuating pressure, $q^2 = \overline{u'^2_i}$ the kinetic energy due to turbulent velocity fluctuation, and U_j the time-averaged velocity in the x_j-direction. In the above, I is the substantial rate of kinetic turbulence energy. II is the energy production term and corresponds to the power produced by the gradient of time-averaged flow and the apparent shear stress $\overline{u'_i u'_j}$. III is a diffusion term, that corresponds to the diffusion of total turbulent energy

as a consequence of turbulence. IV is the diffusion of kinetic turbulence energy by means of viscosity. V is the dissipation, as the power lost due to turbulence-induced viscous stress, and strain rate due to turbulent fluctuations.

To simplify the problem, in the case of straight pipe flow, the apparent shear stress, according to a proposal of *Boussinesq* [5.4], is reduced to an eddy viscosity ε by

$$\overline{u_i' u_j'} = \varepsilon \, \partial U_i / \partial x_j. \tag{7.3-89}$$

The mixing length L, introduced by *Prandtl*, is expressed, according to *Nikuradse* [7.21], in terms of the distance from the pipe axis, in a pipe of radius R by

$$L/R = k_6 + k_7(r/R)^2 + k_8(r/R)^4. \tag{7.3-90}$$

Prandtl introduced a *Reynolds* number due to turbulence as

$$Re_t = (\overline{q^2})^{1/2} L/v. \tag{7.3-91}$$

To predict the loss coefficient of a channel in unsteady flow, *Vasiliev* and *Kvon* [7.22] postulated the eddy viscosity to be the following function of Re_t, and the empirical constants k_i,

$$\varepsilon/v = k_2 Re_t (1 - e^{-k_3 Re_t^2} + k_4 Re_t^{1/2} e^{-k_5 Re_t^2}). \tag{7.3-92}$$

According to a proposal of *Prandtl* [7.23] and *Kolmogoroff* [7.24] the relevant diffusion term with the radial fluctuation v' can be simplified as follows:

$$- v'(\overline{q^2}/2 + p'/\varrho) = k_9 \varepsilon \partial(\overline{q^2}/2)/\partial r, \tag{7.3-93}$$

where k_9 is an empirical constant. For the dissipation term, *Vasiliev* and *Kvon* used the expression [7.22]

$$\Phi = - k_1 (v + k_9 \varepsilon) L \overline{q^2}/2. \tag{7.3-94}$$

A comparison of this theory with real effects can be made only, if the apparent shear stresses $\overline{u_i' u_j'}$ are measured. In a general unsteady flow this is rather troublesome. On the basis of experiments in a turbulent pulsating pipe flow carried out by *Kirmse* [8.135], *Hartner* recently succeeded in comparing the eddy viscosity, measured by using a laser system with two beams at 90° inclined planes, with the eddy viscosity from *Vasiliev*'s and *Kvon*'s theory [8.136].

As a result, he states that agreement exists only at weak pulsation amplitudes (compared with the time-averaged flow), and at *Reynolds* numbers larger than 10^5 (better 10^6). In an example calculated by *Hartner* for the radius range $r/R = 0.6$ to 0.87, the calculated value of ε is about 25% below the measured one. Towards the axis this increases up to 30%. Towards the pipe wall the deviation becomes yet larger.

Fig. 7.3.4 shows the instantaneous distribution of the apparent shear stress $\overline{u'v'}$ in a pulsating pipe flow measured by *E. Hartner* [8.136].
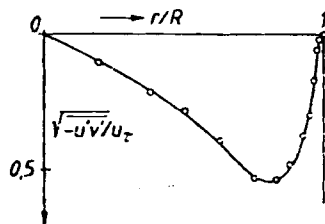
Fig. 7.3.4. Reynolds shear stress $- \overline{u'v'}$ vs pipe radius in a pulsating turbulent pipe flow. Reynolds number of time-averaged through flow about 10^5. Pulsation period 1 s. Measured by means of 2 Laser beams. From *Hartner* [8.136]. Deviation from the non inflected curvature of the corresponding graph in steady flow, see Fig. 5.4.2c

7.3.7. The flow about the inlet edge

Usually a stall or cavitation at or near the inlet edge of a vane occurs, if the flow shows an angle of attack or incidence on the vane, whence it streams about the usually rounded nose of the inlet. As stall results from the velocity distribution in the boundary layer, a study of such a flow requires knowledge of undisturbed potential flow about such a round contour. In the following a practical approach is tried on the base of a plane potential flow through a straight cascade with a nose having the form of a parabola of the second degree.

The problem is treated approximately by considering separately the flow in the region st close to the stagnation point St (Fig. 7.3.5a) and the section c around the point of largest curvature C (see Fig. 7.3.5b) which coincides with the vertex of the parabola, and then combining both the types of flow by a simple function.
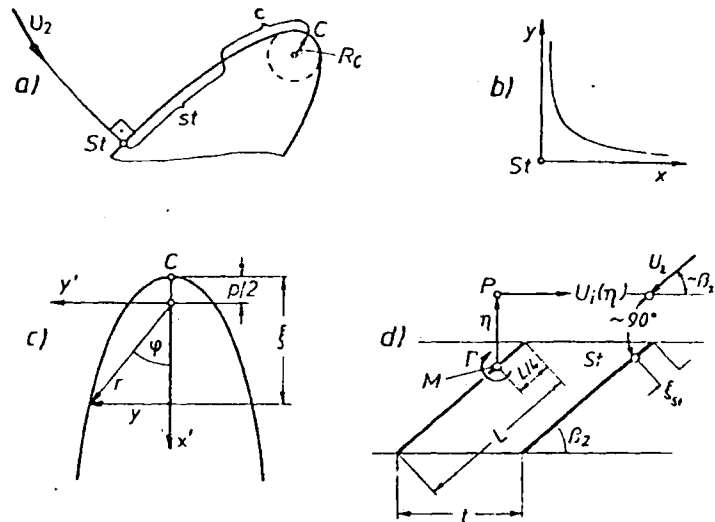
Fig. 7.3.5. Flow around the leading inlet edge of a vane. a) Stagnation point St distant from the vane's inlet C. b) Equilateral hyperbola as a streamline close to St. c) Approximation of the profile's head by a parabola of the 2nd degree. d) Point P, by η level with the centre of pressure M, where the velocity, induced by circulation Γ, approximately equals the value $\Gamma/2t$.

- The flow in st close to the stagnation point: This flow can be described by the complex potential $\boxed{\coprod}_{st} = a_{st}z^2/2$ [5.3], $z = x + iy$ being the complex coordinate in a Gaussian plane. Splitting this into real and imaginary parts yields the streamlines $\Psi = xy = const$ as the imaginary part. For vanishing Ψ this degenerates to the axes of coordinates.

The complex velocity $\bar{w} = d\boxed{\coprod}_{st}/dz = a_{st}z$ yields the velocity components on the streamline to the stagnation point and then from it along the contour by $w_y = -a_{st}y$ and $w_x = a_{st}x$.

Assuming now the vane contour past the stagnation point St as the x-axis, the relative velocity along the contour past the stagnation point reads approximately as function of the distance x from the stagnation point

$$U = U_{st} = a_{st}x.$$

- The flow in the section around the vertex C of a parabola: Now the complex potential reads $\boxed{\coprod}_c = 2a_cz^{1/2}$. In polar coordinates (Fig. 7.3.5c) the contour streamline as the imaginary part, squared, reads $\Psi^2 = 2a_c^2 r(1 - \cos\varphi) = const$, where r is the radius from the focus (Fig. 7.3.5c) to a point on the contour, φ the angle r makes with the x'-axis.

Putting $r\cos\varphi = x', r = (x'^2 + y'^2)^{1/2}$ and introducing the parameter $p = \Psi^2/(2a_c^2)$, yields the well-known equation of a parabola, $y'^2 = 2p(x' + p/2)$, whose vertex is shifted from the origin of the coordinate system by $p/2$. Now the complex velocity is $\bar{w} = a_c/z^{1/2}$, whence the velocity components: $w_x = a_c\cos\varphi/r^{1/2}$, $w_y = a_c\sin\varphi/r^{1/2}$ and

$$U = U_c = a_c/r^{1/2}.$$

267

– Combining the velocities U_{st} and U_c of both the sections st and c: The contour velocity between st and c is

$$U = f_1 U_{st} + f_2 U_c = f_1 a_{st} x + f_2 a_c/r^{1/2} \qquad (7.3\text{-}95)$$

where f_1 and f_2 are arbitrary steady functions along the contour with the property of converging to $f_1 = 1$ and $f_2 = 0$ at the point St and converging to $f_1 = 0$ and $f_2 = 1$ at the point C. Hence U represents an exact solution only at the points St and C. The following functions satisfy these conditions.

$$f_1 = \sin\frac{\pi}{2}\frac{r - r_c}{r_{st} - r_c}, \qquad f_2 = \sin\frac{\pi}{2}\frac{r_{st} - r}{r_{st} - r_c}.$$

To express r in (7.3-95) in terms of the contour coordinate x (taken from the stagnation point St), $r(x)$ has to be known. Assuming a point on the contour, distance ξ from the vertex (Fig. 7.3.5), then by Pythagoras's theorem, $r(y)$ follows from the local thickness $2y$ of the profile. Hence $r(x)$ can be reduced to $y(x)$.

Approximating the vane between the points C (leading inlet edge) and St (stagnation point) by a parabola, the inversion $x(y)$ can be expressed as an arc length of a parabola between an arbitrary point with profile thickness $2y$ and the stagnation point with profile thickness $2y_{st}$. For a parabola of equation $y^2 = 2p\xi$, $x(y)$ follows by

$$x = (p/2)\,\{ ln\langle[y_{st}/p + \sqrt{1 + (y_{st}/p)^2}]/[y/p + \sqrt{1 + (y/p)^2}]\rangle$$

$$+ (y_{st}/p)\sqrt{1 + (y_{st}/p)^2} - (y/p)\sqrt{1 + (y/p)^2}\}. \qquad (7.3\text{-}96)$$

Hence also $y(x)$ and $r(x) = \sqrt{\xi^2 + y^2} = \sqrt{\xi^2 + y(x)^2}$ for an arbitrary point a distance ξ from the leading edge, taken in the direction of the vane skeleton.

– Determination of the parameter p: Since the profile has at the stagnation point at ξ_{st} the local thickness $t_{st} = 2y_{st}$, the parameter p of the parabola becomes

$$p = t_{st}^2/(8\,\xi_{st}). \qquad (7.3\text{-}97)$$

– Determination of the parameters a_{st} and a_c in (7.3-95): The flow in the section st with the approximated velocity U_{st} has also a velocity that rises linearly with the distance from the stagnation point along that stagnation streamline which is orientated upstream of St. This feature is now extended also to the curved part of this streamline. At a known distance y_0 from St, the velocity along the stagnation streamline is assumed to have attained the relative velocity U_2 before the entrance into the rotor. Hence

$$a_{st} = U_2/y_0. \qquad (7.3\text{-}98)$$

To obtain an idea how large a y_0 to choose, the rotor cascade is approximated by a lattice (Fig. 7.3.5 d) whose plates are inclined by an angle β_2 to the circumference and have a chord L. As is well known, such a lattice can be approximated by a row of straight vortices each located on the chord of a plate at a distance $L/4$ from the inlet edge [5.3].

The velocity field of such a vortex row is known: Hence the ratio of the velocity $U_i(\eta)$ induced at distance η from the circumference of the vortex row, level with a vortex, to the velocity $U_{i\,\infty}$ at infinity before the cascade,

$$U_i(\eta)/U_{i\,\infty} = \coth(\pi\eta/t).$$

Approximating now $\coth(\pi\eta/t) \approx t/(\pi\eta)$, the quotient $U_i/U_{i\,\infty}$ tends to unity, if η tends to η_∞ given by

$$\eta_\infty = t/\pi. \qquad (7.3\text{-}99)$$

That means: In a lateral distance t/π from the vortex row, which represents the cascade, and level with vortex, the relative velocity attains nearly the value uniformly distributed along the circumference.

As will be shown below, the distance of the stagnation point ξ_{st} from the profile's head (vertex of the parabola) depends as follows on the physical angle of attack δ_0, the undisturbed flow velocity U_∞ makes with the plate of the lattice

$$\xi_{st} = \delta_0^2 L/(1 + \delta_0^2).$$

Assume that the streamline towards the stagnation point starts tangential to U_2 (inclined at β_2 to the circumference) at a distance η_s from the vortex row, which models the cascade, then makes a quarter of a circle (on behalf of the smallness of δ_0 relative to β_2) and ends normal to the plate at St, the arc length of this circle yields

$$y_0 = (t/2)[\tan \beta_2/(1 + \tan \beta_2)][1/\cos \beta_2 - (\pi/4)(L/t) + \pi(\xi_{st}/t)].$$

Inserting this with respect to (7.3–99) and (7.3–100) in (7.3–98) gives the desired parameter

$$a_{st} = \frac{(2U_2/L)(1 + \tan \beta_2)/\tan \beta_2}{1/\sin \beta_2 - (L/t)[(\pi/4) - \pi\delta_0^2/(1 + \delta_0^2)]}.$$

(7.3–101)

The parameter a_c in (7.3–95) results from the known velocity U_c (in relation to the undisturbed velocity) at the leading inlet edge as

$$a_c = U_c r_c^{1/2}.$$

(7.3–102)

Here r_c is the distance of the focus of the parabola from its vertex. Usually the radius of curvature R_c is known for the leading edge of the vane. According to a theorem of geometry for a parabola-like profile

$$r_c = R_c/2.$$

In Cap. 8.2.3, the velocity U_c (there denoted by w_{max}) is reduced to the blade velocity u (Kaplan turbine) by means of $k = U_c/u$ (8.2.3–19). (8.2.3–21) shows k as a function of the cascade parameters t/L, $\varkappa$ and the curvature $1/R$ the vane contour has at its leading edge.

The distance ξ_{st} of the stagnation point from the inlet: As a simple approach to the effects under a strong angle of attack, the profile is modelled by a plate of chord L. After Birnbaum [6.6] the density $\gamma(\xi)$ of bound vortices under an angle of attack δ_0 between undisturbed velocity U_σ and the plate reads at stations close to the leading edge (see (6.2–30))

$$\gamma(\xi) = 2\delta_0 U_\infty [(L - \xi)/\xi]^{1/2}.$$

(7.3–103)

As the contour velocity given by $U = U_\infty - \gamma(\xi)/2$ vanishes at the stagnation point $st(\xi = \xi_{st})$ according to

$$0 = U_\infty\{1 - \delta_0[(L - \xi_{st})/\xi_{st}]^{1/2}\},$$

(7.3–104)

this gives the distance ξ_{st} of the stagnation point from the leading edge of the vane according to (7.3–100).

Effects of elastic walls: Hitherto the wall has been assumed to be inelastic. With machine size increased, any wall becomes elastic. Then the flow along the wall depends mainly on its lateral vibrations, and not so much on the boundary layer development. These vibrations are either excited by unsteady flow or by flutter. E.g., at a trailing edge, the latter may originate from the formation of a *Karman* vortex street.

8. Cavitation and water hammer as detrimental effects

8.1. Introduction

For given site conditions, cavitation and water hammer influence the design and operation of a hydro power plant. They also affect the economy and reliability, because wear, efficiency drop, possible loss of control, and wall thicknesses are to be kept within reasonable limits. Both are unsteady flow phenomena.

Generally both effects are related to each other, since water hammer may cause water column separation, the worst form of cavitation, which in turn may lead to reversed water hammer as its worst consequence, whilst any cavitation also causes water hammer.

Cavitation results from the fact that real water with its impurities evaporates, when the pressure falls short of a critical value. Since the density of cold water is 10^5 times that of steam at the same pressure and temperature, the sudden condensation of a vapour cavity on a solid wall causes a severe droplet impact there with the consequence of pitting and material destruction.

Therefore the fundamentals for the onset of cavity formation and collapse and its final impact on material, have to be studied with respect to different effects on various materials.

Cavity formation and pittings, their influence on characteristics in reaction machines, as well as remedies to encounter them, have to be considered with respect to operational limits.

Water hammer results from the elasticity of pipe walls and the compressibility of real water as a consequence of speed control at load regulation, under transients like starting or sudden load rejection of a set. The real phenomena with sets on different pipe systems, their prediction by the method of characteristics and remedies are given in this chapter.

The various aspects of cavitation and water hammer are reflected by numerous references. Concerning cavitation, general surveys are given in [8.1 to 8.7], from which the first four references deal with turbomachines. The following references treat special problems in machinery, and [8.8 to 8.12] namely in pumps, [8.13; 8.14] in Francis turbines, [8.15] in pump-turbines, [8.16; 8.17] in Kaplan turbines, and [8.18] in Pelton turbines. In the latter it is mainly a kind of droplet erosion. The publications [8.19; 8.20] deal with the problem of the existence of nuclei, [8.21 to 8.30] treat the problems of their measurements and their influence, e.g., by additives. The contributions [8.31 to 8.46] deal with growth and collapse of bubbles. The following references treat scale effects: [8.47] influence of turbulence. [8.48 to 8.50] roughness effects, [8.23] influence of bubble history, [8.31] added mass, [8.35; 8.36] gas diffusion, [8.51] pressure pulsation, [8.52] cavitation type, [8.53] secondary vorticity, [8.45; 8.54] tensile stress, [8.55] boundary layer turbulence, [8.44; 8.56] viscosity, [8.34; 8.36; 8.57; 8.58] heat transfer [8.59] other effects observed, [8.60] hysteresis, [8.13] head, [8.40] bubble coalescence, [8.61] cavity size proportional to that of apparatus.

270

Further publications are dedicated to cavitation erosion and cavity collapse. namely a) prediction [8.62 to 8.64], b) cavitation resistance [8.65]; c) testing of the latter [8.66 to 8.69]; d) jet formation [8.70]; e) remedies against erosion [8.25; 8.71; 8.72]; f) scale effects due to erosion [8.73; 8.74]; g) mechanism of erosion [8.75]; h) its connection with hydrodynamic cavitation [8.76]; i) detection of critical point by isotopes [8.77]; j) prediction of celerity with respect to partial condensation under pressure pulses [8.64] (Note that the speed of sound in a fluid, which surrounds a collapsing bubble, is needed for the prediction of the pressure pulse due to implosion using Joukovsky's water hammer formula); k) cavitation in spool valves [8.78]; l) collective bubble collapse [8.79].

Finally some authors have considered the phenomena on large, quasi fixed, partly vented cavities [8.80 to 8.83].

Concerning transients and water hammer, a survey is given in the books of C. Jaeger [8.84; 8.85]. The various characteristics of controlled and cavitating fluid machines with their surging draft tube vortex and the different modes as the origin of transients or pulsations are treated in [8.86 to 8.92]. remedies for preventing or optimizing certain sources of excitation in [8.93 to 8.96], the prediction and measurement of speed of sound in different types of flow in [8.64; 8.97; 8.98], prediction and measurements of penstock responses in [8.99 to 8.105]. The influence of air is given in [8.106], damping mechanism in [8.107], water column separation in [8.108 to 8.110], accidents by reversed water hammer in [8.109], and needs for improvements in [8.111].

8.2. Cavitation

8.2.1. Survey of the fundamentals of cavitation and resulting erosion

8.2.1.1. Introduction to the various phenomena and aspects

Cavitation is evaporation of a liquid, caused by lowering its pressure. It occurs in liquids with free and dissolved gas at stations, where the pressure falls short of a certain critical value, roughly corresponding to the vapour pressure. Before the proper cavitation, the liquid diffuses dissolved gas in the gaseous nuclei, when under lowered pressure, e.g. when passing the critical zone.

The following phenomena can be divided into two parts:

a) Formation of bubble-, patch-, hose-, bubble ring- or sheet-like mainly vapourous cavities, that rest on walls or float within the liquid, in areas of lowest pressure. These are located on high points of closed ducts, on the centre of streamline curvature, on low pressure (suction) faces, on convex or vibrating wetted walls, and slightly downstream of peaks of wall roughnesses.

b) Implosive, irreversible collapse of the vapourous part of the cavity in areas of rising pressure by sudden condensation, which is favoured in the case of "cold water" by a liquid to steam density ratio of 10^5. Simultaneously, this leaves the residual gas in smaller cavities, slowly reabsorbed afterwards.

- Detrimental effects: Change of machine characteristics, efficiency drop, water column separation, generation of sonic and ultrasonic noise, water hammer, flow dissipation, quick sponge-like erosion of walls by pitting. For the engineer the most essential effects of cavitation, which he has to control are, material erosion, efficiency and head drop, and loss of control over the machine or device.

- Appearance in practice and consequences: Excepting highest heads, any hydraulic apparatus or machine, which has a longer useful life, especially when it works away from its bep, due to economic compulsions, usually operates under limited cavitation. As extreme examples are mentioned: Super-

cavitating ship propellers and inducer pumps, cavitating valves or *Venturi* nozzles. Due to this the liquid is converted locally into a two-phase mixture with predominant vapourous cavities.

In serious cases the loss of control in a hydraulic plant may cause water column separation and the subsequent "reversed water hammer". Thus the water column in a condenser loop, e.g. may be separated under shutdown of pump drive. Quickly closing gates may cause water column separation past them, followed by dangerous collapse of this cavity under reversed water hammer. Destroyed head covers, broken runners, power drop, power swing, loss of control or at least noise, vibration and material erosion on cavitating hydro turbines make evident the effect of cavitation.

– Cavitation a high speed phenomenon: Cavitation is always combined with pressure and velocity fluctuations of high and highest frequency. Any observation of elementary effects like bubble collapse requires light exposure time intervals down to 10^{-6} s. Cavitation in the words of *Hermann Föttinger* is a phenomenon, which limits the transmission of any observation made on gaseous fluids to liquid fluids [8.114].

8.2.1.2. Nuclei as origin

I. General remarks: Cavitation has its origin in the existence of gaseous nuclei, especially in cold water. Such nuclei may be also within crevices of floating particles or stationary walls (Fig. 8.2.1 a). They constitute the so-called "free gas content", decisively responsible for the onset of cavitation. In cold water (290 K) this amounts to only about 10^{-3} void fraction of the total gas content.
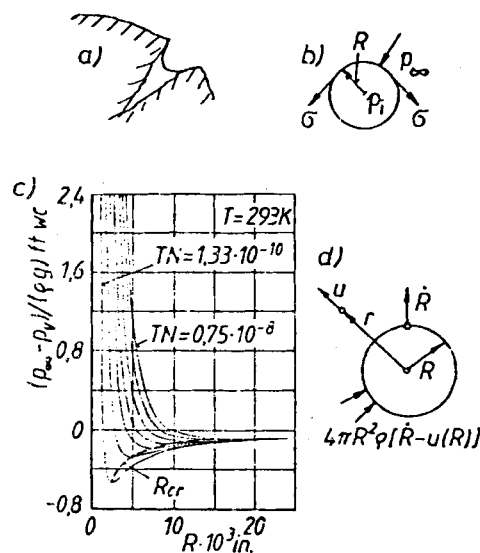
Fig. 8.2.1. Nuclei. a) Harvey's model of the gas remaining in a liquido-phobe crevice of a suspended solid body. b) Forces on a bubble wall. c) External excess pressure $p_\infty - p_v$ vs bubble radius R. The line of the critical bubble radius R_{cr} (———) divides the stable range (left) from the unstable range (right). d) Mass conservation for the motion of a spherical bubble in an incompressible fluid, if accounting for evaporation ($\dot{R} > u(R)$).

As a model consider a stationary spherical bubble, radius R, resting within the surrounding liquid, uniformly and rectilinearily moved, (Fig. 8.2.1 b). The equilibrium between surface tension σ, internal pressure p_i and external pressure p_∞ requires: $p_\infty = p_i + 2\sigma/R$.

II. Vapour bubbles: In a vapour bubble, the pressure p_i equals the constant steam pressure p_v of the liquid. An accidental growth of bubble radius R diminishes the term $2\sigma/R$.

Equilibrium now needs a smaller pressure p_i than the retained steam pressure. Hence an unlimited growth of bubble. Similarily an accidental decrease of bubble radius R leads to a bubble collapse. Thus a vapour bubble is unstable.

III. Gaseous bubble within a gas-permeable bubble wall: Here the pressure p_i of gas within the bubble increases with accidental decrease of bubble radius R. Consequently all the gas diffuses into the liquid. Any accidental increase of radius R would be continued by diffusion of gas into the bubble.

272

In this context a bubble model after *Harvey* may be mentioned [8.20]. Here the gas is assumed to be included in crevices of suspended bodies with liquido-phobc walls (Fig. 8.2.1 a). Now the term due to surface tension reverses its sign. Hence $p_{\omega} = p_i - 2\sigma/R$. Now gas diffuses from the liquid into the cavity until the crevice is filled with gas. Then such a cavity may supply free gas, when the pressure p_x in the liquid is lowered at the entrance into the cavitation zone.

IV. Gaseous and vaporous nuclei with walls impermeable for gas: Now if the gas follows perfect gas law: $p_i = NT/R^3 + p_v$. Hence

$$NT/R^3 - 2\sigma/R + p_v - p_\infty = 0. \tag{8.2-1}$$

When the bubble radius R grows accidentally within the branch, falling vs R (Fig. 8.2.1 c), the external pressure required p_∞ for a vapour pressure p_v, to be retained, falls short of the actually existing pressure p_∞. This shrinks the bubble into its original size. When the bubble accidentally shrinks under retained vapour pressure, the external pressure required grows above the actually existing p_∞. Thus the bubble expands at last to its initial radius R. Hence this falling branch of the $p_\infty(R)$ graph is stable.

On the branch (Fig. 8.2.1 c) of the $p_\infty(R)$ graph, that rises vs R, the bubble, accidentally disturbed, grows either to infinity or shrinks to the radius R^*, at the minimum of the graph. Hence the largest stable bubble radius, possible, the so-called "critical bubble radius" follows from $d(p_\infty - p_v)/dR = 0$ as

$$R^* = (3/2)(NT/\sigma)^{1/2}. \tag{8.2-2}$$

Thus the critical pressure due to R^* [8.6]

$$p_{cr} = p_{\infty\,cr} = p_v - (4/3)\sigma/R^*. \tag{8.2-3}$$

V. The critical pressure as a function of flow velocity: After tests of *Parkin et al* [8.112], the critical pressure for the onset of cavitation past the station of minimum pressure in water depends strongly on the flow velocity w_∞ (Fig. 8.2.2). The following relation can be extracted from these tests

$$p_{cr} = p_v - C_2 w_\infty^\mu, \tag{8.2-4}$$

where $\mu = 3,3$ and $C_2 = 0,0137 \text{ kg m}^{-\mu-1} s^{\mu-2}$.

Negative values of p_{cr} hint at tensile stress in the water between the nuclei such as was found by tests of *Knapp* in real water, when this has been pressurized before, or also in pure water [8.6].
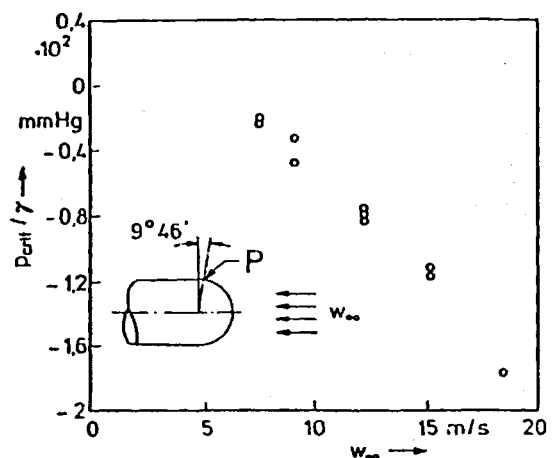
Fig. 8.2.2. *Parkin's* test [8.112] showing the critical pressure on a hemispherical body vs velocity. P probe station.

8.2.1.3. Equation of motion of a bubble resting in the fluid

The dynamics of a spherical bubble, radius R, resting within an infinitesimally extended incompressible liquid is based on the model of *Rayleigh* [8.46], supplemented later on by *Scriven* [8.43], and *Poritzky* [8.44]. Continuity requires, that the velocity u of the liquid due to spherosymmetric wall motion of a bubble, radius R, depends as follows on the velocity $u(R)$, the liquid has at the bubble wall (Fig. 8.2.1 d)

$$u = u(R)\,R^2/r^2\,.$$

(8.2-5)

– Relation between the velocity $u(R)$ and growth rate $\dot{R}$ of bubble due to its evaporation. The mass growth rate of the vapour bubble, density ϱ_v, $\dot{m}_v = 4\pi\varrho_v R^2 \dot{R}$ must coincide with the mass flow of liquid, density ϱ_L, passing the bubble wall $\dot{m}_L = 4\pi R^2 \varrho_L [\dot{R} - u(R)]$. (By evaporation, the bubble is "eating through" the liquid.) Introducing the figure

$$\varepsilon = 1 - \varrho_v/\varrho_L$$

(8.2-6)

(being nearly "one" for cold water with $\varrho_v/\varrho_L = 10^{-5}$, and being "zero" at the critical point), the above mass flow balance gives

$$u(R) = \varepsilon R\,.$$

(8.2-7)

Inserting this in (8.2–5) results in the velocity of the liquid due to bubble growth at an arbitrary station r as $u = R^2 \dot{R}\varepsilon/r^2$. For $\varepsilon = $ constant, the flow is irrotational. Hence the equation of motion of the spherosymmetric field

$$\partial u/\partial t + u\,\partial u/\partial r = -(1/\varrho_L)\,\partial p/\partial r\,.$$

(8.2-8)

Inserting $u = R^2 \dot{R}\varepsilon/r^2$ and integrating this from $r = R$ (bubble wall) to infinity $r = \infty$ (where u vanishes) at $\varepsilon = $ constant yields

$$[1/(\varepsilon\varrho_L)](p_{bw} - p_\infty^*) = \ddot{R}R + \dot{R}^2(2 - \varepsilon/2)\,,$$

(8.2-9)

at which p_∞^* is the pressure at infinity of the bubble, $p_{bw} = p(R)$ the pressure in the liquid at station $r = R$. For a real Newtonian liquid, now assumed, with kinematic viscosity v, by means of the equilibrium normal to the bubble surface, the pressure p_{bw} can be deduced from the surface tension σ, the vapour pressure p_v, the pressure p_i of a permanent gas within the bubble and the radial viscous tensile stress, induced by the radial strain rate close to the bubble wall, being according to *Navier* and *Stokes* (Eq. (5.4–6)) [5.21, 5.22], [8.44], and with respect to (8.2–5) $2\eta\,\partial u/\partial r_{r=R} = -4v\varrho_L\varepsilon\dot{R}/R$:

$$p_{bw} = p_i + p_v - 2\sigma/R - 4\varepsilon v\varrho_L\dot{R}/R\,.$$

(8.2-10)

Putting this in (8.2–9) results in

$$[1/(\varrho_L\varepsilon)](p_v + p_i - p_\infty^* - 2\sigma/R) = \ddot{R}R + \dot{R}^2(2 - \varepsilon/2) + 4v\dot{R}/R\,.$$

(8.2-11)

For cold water the surface tension term $2\sigma/R$ is relevant only in the mm range of R. For radii greater than 1 mm also the viscous term $4v\dot{R}/R$ vanishes. Moreover in consequence of $\varrho_v/\varrho_L = 10^{-5}$, $\varepsilon = 1$. Also p_i can be neglected for larger radii R. Hence, after *Plesset* [8.42], the last relation may be written

$$(1/\varrho_L)(p_v - p_\infty^*) = \ddot{R}R + 3\dot{R}^2/2 = d(R^3 \dot{R}^2)/(2R^2 \dot{R}\,dt)\,.$$

(8.2-12)

The upper limit of growth rate $\dot{R}$ yields from $\ddot{R} = 0$ as

$$\dot{R}_m = [(2/3\varrho_L)(p_v - p_\infty^*)]^{1/2}\,.$$

(8.2-13)

274

From this it is seen, that the growth of a bubble is mainly induced by tensile stress, namely negative values of p_x^*. This acts in the pure liquid, between the bubbles.

8.2.1.4. Some estimates on cavitation scale effects at onset

The onset of cavitation requires $p_\infty^* = p_{cr}$. Inserting p_{cr} from (8.2–4) in (8.2–13) brings

$$\dot{R}_m = [(2/3\,\varrho_L)\,C_2\,w''_\infty]^{1/2}. \tag{8.2–14}$$

Imagine the critical zone to have a length $y_0 l$, with l as a typical dimension of the body considered and y_0 as a figure due to a certain geometry of the body and its streamline pattern. The bubble passes this zone with velocity $w_{max} = k_1 w_\infty$, in which w_∞ denotes the undisturbed flow velocity in front of the body. As shown in Cap. 8.2.2.3, $k_1 = w_{max}/w_\infty$ depends on the cavitation index σ_{ith} due to the critical zone considered (ith omitted) by

$$k_1 = (1 + \sigma)^{1/2}. \tag{8.2–15}$$

During the time period $t = l\,y_0/(k_1 w_\infty)$, in which the bubble covers the critical zone, the bubble radius increases from its initial value R_0 to its final value $R_f = R_0 + t\,\dot{R}_m$. Hence

$$R_f = R_0 + (2\,C_2/3\,\varrho_L)^{1/2}\,y_0 l\,w_\infty^{\mu/2\,-\,1}/k_1. \tag{8.2–16}$$

For comparing similar phenomena at cavitation inception on similar bodies and under similar flow (same y_0) the increase of the bubble $R_f - R_0$ in the critical zone is assumed to be proportional to the length $y_0 l$ of this zone. Accordingly

$$(R_f - R_0)/(y_0 l) = \chi = \text{constant}.$$

Putting this into (8.2–16) and squaring the result brings $\chi^2 = (2\,C_2/3\,\varrho_L)\,w_\infty^{\mu-2}/k_1^2$. Inserting k_1 from (8.2–15) and making $\mu = 3,3$ after Parkin [8.112], gives the real cavitation index for the onset of cavitation due to a certain body

$$\sigma = (2\,C_2/3\,\varrho_L)\,w_\infty^{1,3}/\chi^2 - 1. \tag{8.2–17}$$

From this it is seen, that at a certain proportional bubble growth χ, the cavitation index σ increases with the velocity w_σ the fluid flows against the cavitating body. This tendency is reconfirmed by tests (Fig. 8.2.3 a). Also the increase of σ with lowered density ϱ_L of the fluid around the bubble is reflected by the increasing of σ with rising free air contents, also found in tests of incipient cavitation (Fig. 8.2.8).
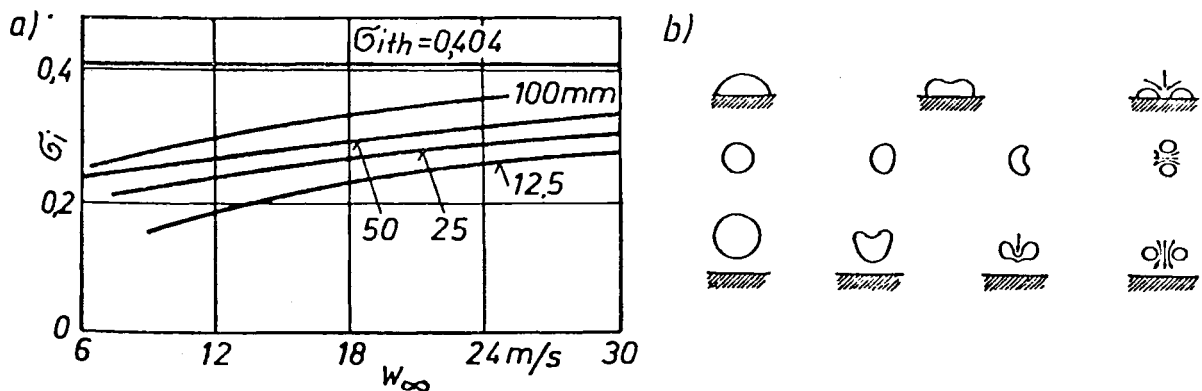
Fig. 8.2.3. a) Scale effects at incipient cavitation. Cavitation index σ_i vs free stream velocity at different diameters d of an ogival body after J. F. Rippken and J. M. Killen: Gas bubbles, their measurement and influence in cavitation testing. Proc. IAHR Symp. Sendai 1962 p. 37. b) Forms of collapsing bubbles.

To understand the latter effect, imagine that the volume of the free air content expands considerably within the critical zone of low pressure. The greater indifference of σ vs rising total air content shows a certain independence of the relevant free air content from the total air content. Note that the mass of the free air content usually is only about one thousandth of the total. Any exchange of reabsorbed and free air by mass diffusion in the critical zone needs time, usually not available during the quick passage of nuclei across the critical zone.

8.2.1.5. Transfer of energy under cavitation

The kinetic energy communicated to the ambient liquid by a sudden expanding bubble, radius R, growth rate $\dot{R}$, amounts from (8.2-5) with $u(R) = \dot{R}$ according to Rayleigh [8.46]

$$E = (1/2) \int_{r=R}^{\infty} u^2 \, dm = 2\pi \varrho_L \dot{R}^2 R^3. \tag{8.2-18}$$

It originates partly from positive displacement work $\int p\,dv$ of the differential pressure between the ambient fluid and the bubble but is partly due to the heat transfer from the liquid into the bubble. This accompanies the evaporation of the liquid into the bubble. The latter originates from the superheating of the liquid, when crossing the critical zone, whose pressure falls short of the steam pressure due to the liquid's temperature T_L.

Moreover an additional temperature drop of the gaseous content in the bubble, that favours heat transfer, may be caused by the sudden expansion, when the bubble penetrates quickly into the low pressure zone. Limiting the heat transfer to heat conduction, the governing differential equation for a spherosymmetrical temperature field with 'a' as thermal diffusivity reads

$$\partial T/\partial t + u\,\partial T/\partial r = a[\partial^2 T/\partial r^2 + (2/r)\,\partial T/\partial r], \tag{8.2-19}$$

u being the radial velocity according to (8.2-5).

For larger bubbles the surface available usually limits the bubble growth by heat transfer. In this case the bubble growth is described by the simple relation $R = 2\beta(at)^{1/2}$, in which β depends, after Scriven [8.43], on the density ratio of vapour to liquid ϱ_v/ϱ_L, on the latent heat Λ, the specific heats of vapour and liquid c_v, c_L and the superheating $T_0 - T_s$.

8.2.1.6. Gas diffusion under cavitation

A strict computation of cavity growth must also account for gas diffusion from the liquid into the cavity. Even if diffusion in general needs much more time than evaporation, it may become important in the case, when the liquid entering the critical zone has passed before a longer low pressure zone, e.g. a suction line in case of an impeller.

The bubble growth by diffusion is controlled by Fick's law. Hence the governing differential equation is of the type (8.2-19). But now the concentration of dissolved gas $C\,(kg/m^3)$ appears instead of the temperature T, and the mass diffusivity $D\,(m^2/s)$ instead of the thermal diffusivity $a\,(m^2/s)$. For a relatively large bubble this converts to $R \sim (Dt)^{1/2}$.

A special case of diffusion is the rectified diffusion of an oscillating bubble within a surging pressure field. During one oscillation the gas content of the bubble is alternatingly compressed and expanded. In the compressed phase gas diffuses from the bubble into the liquid. In the expanded phase from the liquid into the bubble. Since the area for diffusing is larger in the expanded bubble than in the compressed bubble, the gas content grows by this so-called "rectified diffusion".

Any diffusion is favoured, when the pressure falls short of the saturation pressure, which is required to prevent a certain air quantity absorbed to diffuse. According to Henry's law this saturation quantity grows with the pressure.

_ Slipping bubble: Any real bubble slips, when it passes a zone with a pressure gradient. A slipping bubble has an added liquid mass proportional to its volume. This may increase considerably its momentum-induced impact on a wall by the so-called "rocket effect" after *Chincholle* [8.113].

8.2.1.7. Bubble collapse, impact pressure and related effects

When a vapour bubble, radius R_i, growth rate $\dot{R}_i = 0$, enters a zone where the pressure rises suddenly by Δp against the critical one, it suddenly collapses by condensation to a cavity with the vanishingly small radius R_f of the remaining gas. Then according to *Rayleigh* [8.46], the positive displacement work done by Δp: $(4/3)\pi(R_i^3 - R_f^3)\Delta p$ can be found in the kinetic energy $2\pi\varrho_L\dot{R}_f^2 R_f^3$ (see 8.2-18) of the collapsing bulk of liquid. Equating both yields the bubble implosion rate

$$\dot{R}_f = \{[2\,\Delta p/(3\,\varrho_L)][(R_i/R_f)^3 - 1]\}^{1/2}. \tag{8.2--20}$$

Treating the bubble impact pressure p_i due to the sudden destruction of $\dot{R}_f$ as water hammer (8.3-54), and imagine 'a' to be the velocity of sound (celerity) of the liquid, then

$$p_i = \varrho a \dot{R}_f. \tag{8.2-21}$$

Contrary to a growing bubble a collapsing bubble usually buckles [8.6], (Fig. 8.2.3 b). A spherical bubble, collapsing near a wall, is transformed into a toroidal surface. Then a liquid jet penetrates through its inner orifice. When a bubble collapses close to a solid wall, its surface may buckle so as to focus a multiplicity of liquid jets on it, where they impinge like droplets. This may be the reason why cavitation erosion looks as though caused by droplet impact.

Because of the sudden collapse of a vapourous bubble its gaseous remnant is strongly compressed and heated. This creates pressures up to some 10^4 bar lasting only for micro seconds. The temperature rise is indicated by luminescence of the imploding bubble [8.6].

8.2.1.8. Cavitation erosion, cause, test devices, results

The causes of cavitational erosion at cavity collapse are of different nature.

a) Chemical causes: Chemical reactions result as a consequence of high local and sudden pressure and temperature rise in connection with the larger oxygen content of the cavities than that of air. They may be accelerated by corrosive qualities of the liquid. A temporary corrosion also originates from turbulence and hence a high exchange of matter within the cavitating boundary layer. The very brief collapse damps the relatively small overall influence of chemical phenomena, which generally require some time to react.

b) Electrolytic causes: Galvanic elements are formed in the acid, base, or salt liquid in connection with inhomogeneities in the structure of the wall surface and in connection with local temperature rise due to bubble collapse [8.114].

c) Mechanical causes: With notch-tough material having sufficient glide directions and planes, the impact of a bubble collapsing on a wall is absorbed easier than by a material with glide capacity reduced (brittle material). By hard second phases and reduced glide planes and directions, the plasticity of the material is diminished.

If the plasticity is exhausted, micro cracks are generated and material particles are separated from the surface which is aided by flushing of the turbulent flow. Hence cavitation pitting is influenced mainly by the structure and the mechanical and chemical properties of the material [8.65].

d) Other causes: The sudden growth of liquid-gas interfaces and the shear stress on them induced by slip between the phases, may release there electric charges of high potential. (Remember, that a

steam boiler supported on insulators, is strongly electrically charged under blow down of its safety valve, an effect which, by the way, was used in Armstrong's electrostatic high voltage generator.)

c) Further consequences of mechanical destruction:

Vapour cavities in the bottom of the eroded crater then collapse under pressure fluctuations. This causes water hammer blow focussed on the crater bottom. Fatigue cracks and ruptures due to the notch effect may originate from this sharp-edged part. After flushing of loosened particles, the pittings and cracks due to further fatigue cracks may penetrate deeper into the wall material, leading finally to a sponge-like erosion as one of the typical features of cavitation erosion.

Destruction of chemically neutral material, e.g. glass may be considered as a decisive proof of primarily mechanical causes for material erosion.

In this context it may be mentioned, that only cavities collapsing on or near to the walls may cause pittings and this is deemed to be above 10^{-5} the part of all the cavities collapsing in a cavitating liquid [8.3; 8.6].

The impact of the impinging droplets due to a collapsing cavity on a wall surface fatigues the material so as to show the first pittings after a certain incubation time t_i. This may result from the time needed for the destruction of a protective layer, due to oxidizing, rolling, forging, or welding.

After the incubation time the material erosion proceeds faster, following the law of Knapp [8.6] which combines the material loss Δm, the exposure time t and the velocity w relative to the wall by

$$\Delta m = \text{const } t w^n, \tag{8.2-22}$$

with n ranging from 0 to 6. Since, e.g. the relative velocity on the hub section of a Kaplan turbine is roughly one half that on the runner tip section, during a certain time t, the pitting by fillet cavitation at the hub groove is, at $n = 6$, only 1/64th of pitting due to tip clearance cavitation and hence usually negligible.

Note that any relevant pitting of a wall-attached cavity is past the cavity and hence exists only if the rear of the cavity is yet on the wall. Otherwise so-called "super cavitation", which encloses the face of a body into a cavity, does not harm the body [8.115].

The erosion past such a wall-attached cavity reaches its maximum for a certain back pressure or cavitation index σ (Cap. 8.2.3). If both tend to zero, the erosion rate disappears in consequence of too strong a ventilation of the cavity by diffusion. The same occurs also by the absence of cavity formation if the back pressure and cavitation index σ tend to large values. Thus the erosion rate attains a maximum at a certain cavitation index or back pressure. Naturally this σ-value must not be combined with the best performance of the machine.

In the case of material with low cavitational resistance, the erosion rate also somewhat depends on the chemical composition of the liquid (Fig. 8.2.4 a). Hence salty ocean water erodes a runner of low cavitational resistance somewhat more than fresh water. This difference vanishes nearly for stainless steel and completely for alloys with the highest cavitational resistance (Fig. 8.2,4 b) [8.116].

– Material properties due to cavitation resistance: The erosion rate decreases with the following qualities: Homogeneous structure, high resistance against corrosion, high resilience, high notch impact strength, ductility, internal pressure (due to prestress or thermal treatment), large deformation potential, e.g. breaking elongation, high tensile strength, flat surface, fine granular structure, large surface hardness, great portion of hard components, rolled structure [8.3; 8.115].

Thus the cavitation resistance rises in the order of: cast iron, cast steel, forged steel, bronze, aluminum bronze, chromium nickel steel. Note: non-metallic coats fail due to their bad conduction of the heat from cavity collapse.
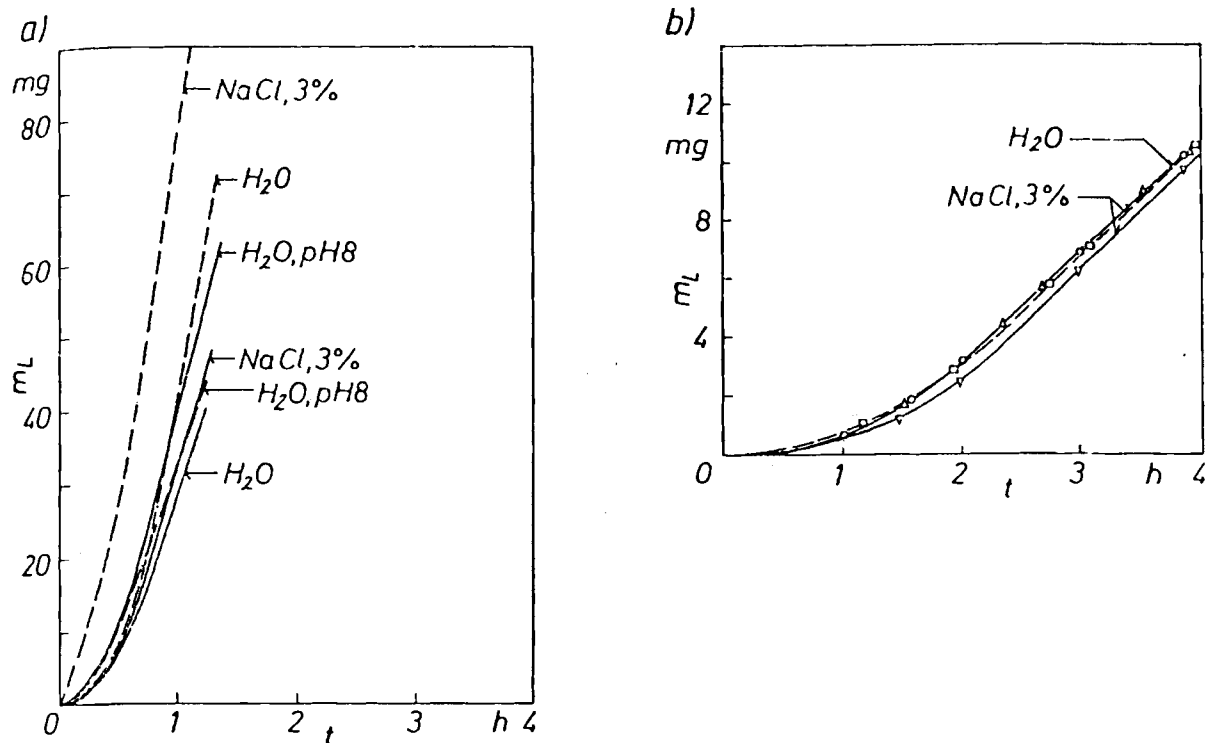
Fig. 8.2.4. Cavitation erosion as a function of material and liquid under steady ——— and intermittent ——— cavitation. a) Material loss m_l vs time elapsed t of mild steel in 3% NaCl solution, distilled water with pH 8 value. b) Ditto of Inconel 718. o steady cavitation; △ intermittent cavitation, both in distilled water; ∇ steady cavitation, □ intermittent cavitation both in 3% NaCl solution [8.116].

– Cavitation intensity: After *Thiruvengadam* [8.117], the cavitation intensity can be defined by the relation

$$I = K h S_e/t,$$
(8.2–23)

where I is the cavitation intensity in W/m^2, h the mean depth of eroded area, S_e the deformation energy of the material linearly extrapolated up to the tensile strength in bar, t the exposure time. K depends on the material and has the following value in brackets: Stellite ($65 \cdot 10^3$), alloyed steel ($35 \cdot 10^3$), bronze ($18 \cdot 10^3$), aluminum ($12 \cdot 10^3$), cast iron ($9,5 \cdot 10^3$), copper ($7,5 \cdot 10^3$).

Test devices for cavitation erosion:

a) Droplet impact apparatus (Fig. 8.2.5 a), based on true destruction mechanism and time-saving,

b) Magneto-strictive apparatus (Fig. 8.2.5 b), very time saving, fast, but with unrealistic vibratory cavitation.

c) Cavitation with adjustable nozzles after *Erdmann Jessnitzer* [8.118] and others, very flexible but not rotating and time consuming (Fig. 8.2.5 c),

d) Rotating disk (Fig. 8.2.5 d), time saving and realistic for rotor cavitation.
To reduce exposure time in real fluid machines, radioactive coats have been tried by *Floriancic* [8.119].
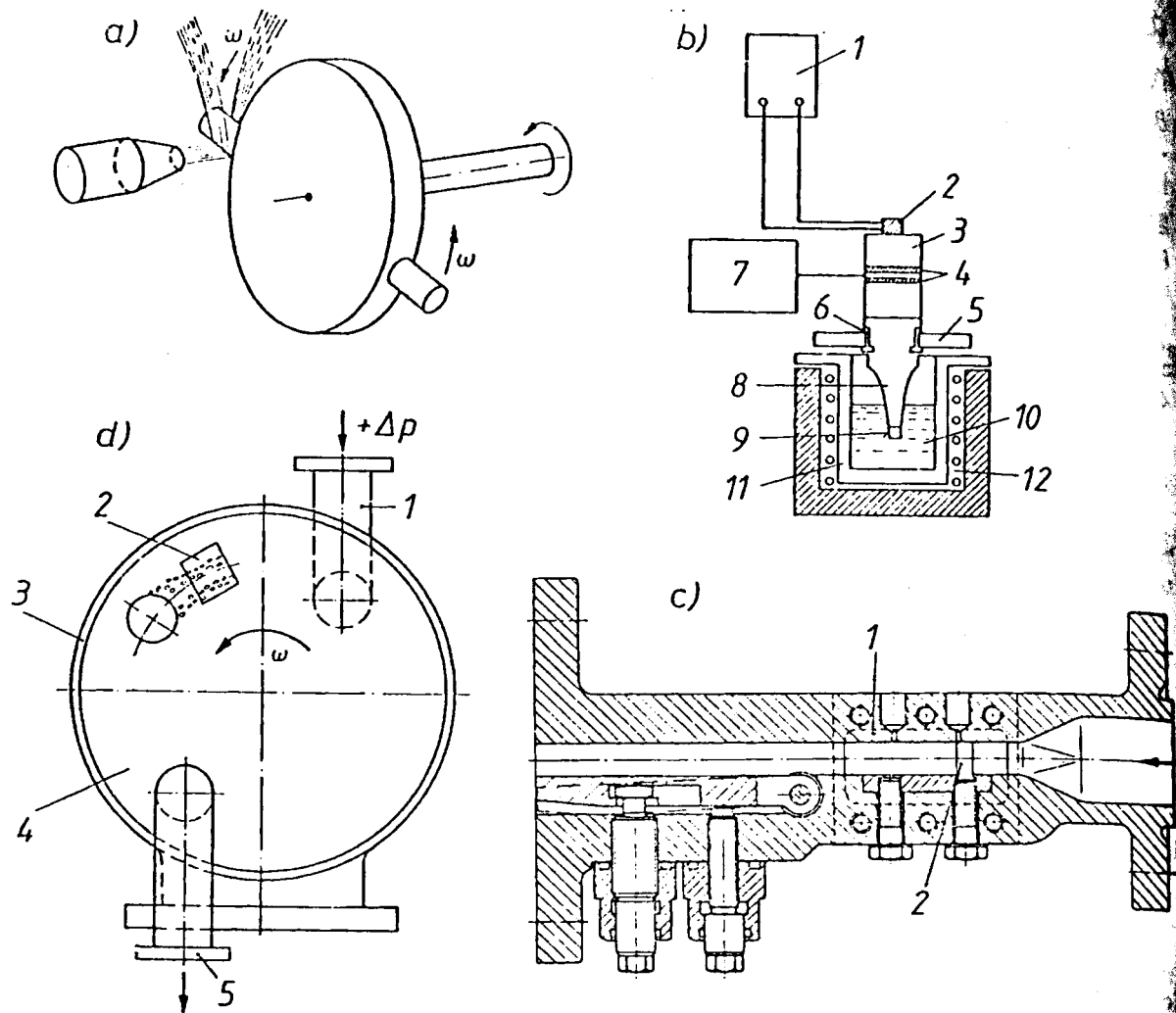
Fig. 8.2.5. Cavitation erosion devices. a) Dropiet impact disk. b) Magnetostrictive device, 1 oscilloscope and frequency counter; 2 accelerometer; 3 transducer; 4 piezoelectric crystal; 5 vessel top plate; 6 snap ring; 7 oscillator, power amplifier; 8 exponential horn; 9 probe; 10 test fluid; 11 electric furnace element; 12 high temperature cavitation vessel (after *Knapp*, *Daily*, and *Hammitt* [8.6]. c) Cavitation nozzle adjustable; 1 observation window; 2 probe. d) Rotating disk in casing; 1 inlet, 2 probe, 3 clearance, 4 rotating disk, 5 outlet.

8.2.2. Cavitation with respect to hydro turbomachinery

8.2.2.1. Suction head required, cavitation indices used

Consider a hydro turbomachine of the reaction type (Fig. 8.2.6 a) in service. In its draft tube (suction pipe), loss coefficient ζ_D, absolute velocity at the outermost point 1 of the rotor exit, c_1, a pressure drop, $\pm \zeta_D \varrho c_1^2/2$ (+ in pumps), occurs in the flow direction. A further pressure drop in the rotor, $\lambda \varrho w_1^2/2$, exists from this exit 1, to the critical point, cr, having the pressure number λ, where w_1 is the relative velocity in the outermost point 1 of the rotor exit. (In pumps, ζ_D shall also include the loss in a longer suction line.)

With the suction head h_s, as elevation of the critical point, pressure p_{min}, above the tail water level, on which the pressure p_A acts, the pressure p_{min} follows from
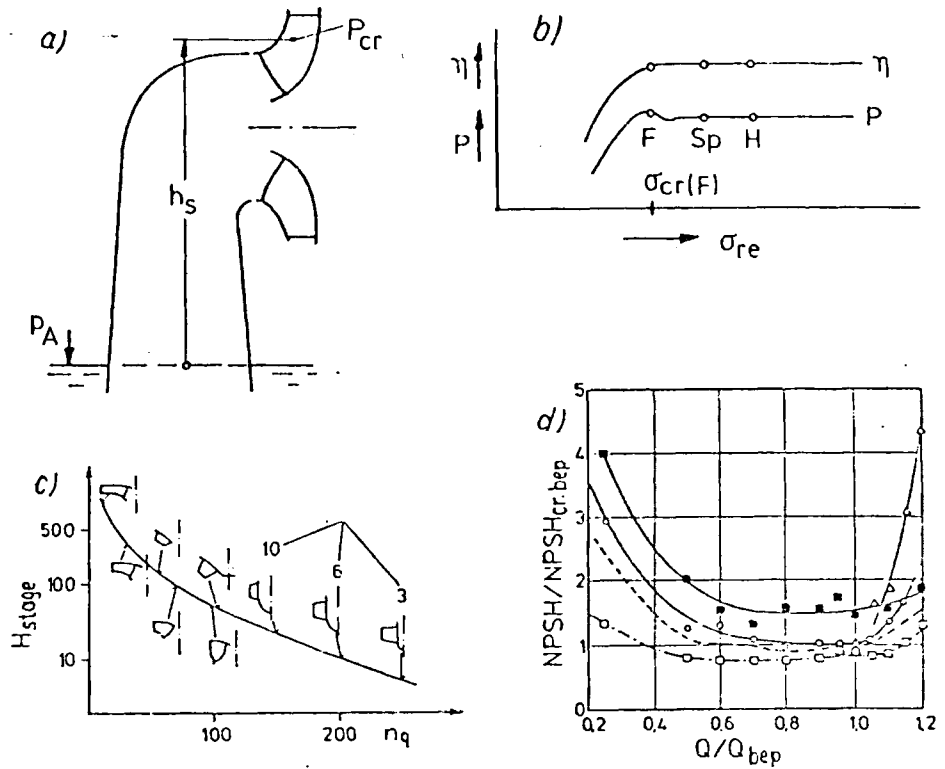
Fig. 8.2.6. Cavitation index σ_{av}, or $NPSH_{av}$, available, and cavitation index σ_{re}, or $NPSH_{re}$, required: a) Definition of suction head h_s, pressure head on suction level $p_A/(\varrho g)$. Hence cavitation index available $\sigma_{av} = [(p_A - p_{cr})/(\varrho g) - h_s]/H$, H being the head, and p_{cr} being the critical pressure of the plant. b) efficiency η and power P of an axial turbine as a function of σ. H fillet cavitation: Sp tip clearance cavitation, F surface cavitation on the suction face. If a certain type of cavitation should be avoided, then $\sigma_{re} > \sigma_{av}$, where σ_{re} is due to this type of cavitation. c) Net head H per stage for reaction turbomachines as a function of the specific speed n_q as a consequence of a) and a limited value of submergence $- h_s$, due to economic limitations. d) $NPSH_{re} = \sigma_{re}H$ vs flow Q/Q_{bep} as a function of cavitation degree of impeller in terms of efficiency drop $\Delta\eta$, or due to cavitation on the suction face S, or the pressure face P. —o— $\Delta\eta = 1\%$; --- $\Delta\eta = 5\%$; --o-- $\Delta\eta = 100\%$; —△— cavitation on P; —•— cavitation on S.

$$p_{min} = p_A - \varrho g h_s - \varrho[(1 \pm \zeta_D)c_1^2 + \lambda w_1^2]/2. \tag{8.2-24}$$

When p_A is the atmospheric pressure, under an isothermal change of state through the atmosphere, p_A depends on the data of the normal atmosphere [5.3] $p_{A0} = 1,013 \cdot 10^5\ Pa$, $T_0 = 288,15\ K$, and the altitude above sea level 'h' by the law $p_A = p_{A0}\exp(- h/H_0)$, where $H_0 = 8435$ m. This reads approximately

$$p_A = p_{A0}(1 - 0,0001186\,h). \tag{8.2-25}$$

With the coefficients of relative and absolute velocity at station 1, $Kw_1 = w_1/(2gH)^{1/2}$ and $Kc_1 = c_1/(2gH)^{1/2}$ and the cavitation index due to *Thoma* [8.120], hence derived

$$\sigma = \lambda Kw_1^2 + (1 \pm \zeta_D)K c_1^2, \tag{8.2-26}$$

the condition for a cavitation-safe operation $p_{min} \geq p_{cr}$ and (8.2-24) yield the suction head required for the set as

$$h_s \leq (p_A - p_{cr})/(\varrho g) - \sigma H, \tag{8.2-27}$$

281

where H is the head. In the above h_s and σ are, at certain operating point and station, critical with respect to cavitation. According to the *HEC* code, and with a safety margin, there defined, the critical pressure p_{cr} and the corresponding cavitation number are defined so as to operate the set above a critical cavitation index σ_{cr}, causing undesirable effects, like drop of head or efficiency (Fig. 8.2.6 b). By (8.2–26) such a 'σ' is linked to certain operating data Kw_1, Kc_1, λ and ζ_D of a certain machine and hence denoted by σ_{re}, meaning "σ required" for this and a certain H, Q and ω:

$$\sigma_{re} = \lambda K w_1^2 + (1 \pm \zeta_D) K c_1^2 . \tag{8.2–28}$$

On the other hand, the cavitation index follows also from the data of the plant's surroundings by (8.2–27), (taken with = sign) as

$$\sigma = (p_A - p_{cr})/(\varrho g H) - h_s/H . \tag{8.2–29}$$

Leaving aside the dependence of p_{cr} on the flow, as expressed by (8.2–4) or on the critical size of the nuclei, as expressed by (8.2–3), and replacing p_{cr} in (8.2–28) by the ambient-related vapour pressure p_v, so as to have now σ as a function of the ambient-related values h_s, H, ϱ, p_v, p_A (directions for the planner), hence denoted by σ_{av}, meaning σ-available, the last relation reads

$$\sigma_{av} = (p_A - p_v)/(\varrho g H) - h_s/H . \tag{8.2–30}$$

A cavitation-safe operation of a set requires that (Fig. 8.2.6 b): $\sigma_{re} < \sigma_{av}$. The problem arising is that strictly speaking h_s and H, e.g. in a run-of river plant may depend on the hydrograph and on the backwater effect. The latter depends first on the topography of the valley, the flow-off of the river, the storing capacity of the plant, and the hence derived necessity of spillage operation but to a smaller extent also on the working programme of the plant. Hence σ_{av} is also defined as σ_{Plant}.

It may be realized from this, that the proper setting of a plant's suction head by means of (8.2–27) has to be handled very carefully with due consideration of the condition $\sigma_{re} < \sigma_{av}$ and with respect to the plant-conditioned and river-conditioned oscillations of head-and tail-water level and the hence following variations of the suction head h_s. Note that any cavitation area has its own suction head!

− The dependence of σ_{re} (denoted here by σ) on the specific speed, used as type number n_q: For simplicity this relation is established now for the bep with vanishing whirl at the rotor's throat, $c_{u1} = 0$. But, on the base of a remark in Cap. 4.2.2.1., it can be expanded also to a rated point with an arbitrary gate opening and $c_{u1} \neq 0$. For the bep $Kw_1^2 = Ku_1^2 + Kc_{m1}^2$. Hence

$$\sigma = K u_1^2 [\lambda + (\lambda + 1 \pm \zeta_D) \varphi_1^2], \tag{8.2–31}$$

where $\varphi_1 = K c_{m1}/K u_1 = \tan \beta_1$ is a design parameter, usually resulting from the opti-mizing of the rotor's cavitational susceptibility. Hence: Setting φ_1, ζ_D, λ gives $\sigma \sim K u_1^2$.

The similarity laws (Cap. 9.2) indicate that the specific speed n_q in terms of Ku_1 proportional to $Ku_1^{3/2}$ or then $Ku_1 \sim n_q^{2/3}$ and $Ku_1^2 \sim n_q^{4/3}$. Thus $\sigma \sim n_q^{4/3}$ or $\sigma = \text{const } n_q^{4/3}$. With the latter relation and = sign, (8.2–27) reads: $h_s = (p_A - p_{cr})/(\varrho g)$ − const $H n_q^{4/3}$. With the tendency of increasing n_q, especially under higher head H, becomes negative (so-called submergence). Then the excavation cost rises with − h_s, the submergence.

From the last relation follows: const $H n_q^{4/3} = (p_A - p_{cr})/(g \varrho) - h_s$. The value $p_A - p_{cr}$ together with $p_{cr} = p_v$ and p_A from (8.2–25) varies only slightly. There may be a tendency

to admit higher submergence $-h_s$ when the head H increases. Putting this aside, assuming $p_A - p_{cr}$ = constant, and also $-h_s$ = constant for reasons of economy, and introducing $NPSH$ (net positive suction head)

$$NPSH = \sigma H,\qquad\qquad (8.2-32)$$

then the above and (8.2-27) result in $NPSH$ = const and

$$n_q^{4/3} H = \text{const}.\qquad\qquad (8.2-33)$$

Fig. 8.2.6c demonstrates such a linkage between the head H and the specific speed n_q for the case of reaction turbines.

_ Other cavitation indices used: Preferably in pumps instead of σ, the parameter $NPSH = \sigma H$ is used. Anglo Saxon countries also use the suction specific speed S, a non dimensional specific speed formed with $NPSH$ instead of $H: S = n' Q^{1,2}/(g\, NPSH)^{3/4}$.

_ Dependence of cavitation parameters on working data: After Pfleiderer [6.41] at bep, λ, ζ_D and operating data of the set given, σ_{re} (8.2-28), then expressed in terms of known data like n_{qop} (at bep) can be made a minimum:

$$\sigma_{min} = (3/2)\{[2\pi\lambda/(1 - N^2)]^2(1 \pm \zeta_D + \lambda)\}^{1/3} n_{qop}^{4/3}.\qquad\qquad (8.2-34)$$

Hence the minimum $NPSH$:

$$NPSH_{min} = \sigma_{min} H,\qquad\qquad (8.2-35)$$

and the optimum suction specific speed S:

$$S_{op} = (2/3)^{3/4}\{[2\pi\lambda/(1 - N^2)]^2(1 \pm \zeta_D + \lambda)\}^{-1/4},\qquad\qquad (8.2-36)$$

where N is the hub to tip ratio in the rotor throat.

Whereas σ_{min} varies greatly with the type number n_{qop}, the economic reasons, which yield (8.2-33), make $NPSH_{min}$ more or less independent of the type number. The same holds also for S_{op}, but for physical reasons. (Small variation of λ, ζ_D at bep.)

At the moment, the machine operates away from the bep, the pressure number λ of its critical point, due to the then growing angle of incidence and the corresponding σ and $NPSH$ increases rapidly with the distance of the operating point from the bep (Fig. 8.2.6 d). (σ_{min} follows from inserting $Ku_1 \sim n_q/\sqrt{Kc_{m1}}$ (see Cap. 9.2) in (8.2-26).)

8.2.2.2. The meaning of cavitation index

With (18.2-29) and (18.2-32):

$$\sigma = NPSH/H = (p_A - \varrho g h_s - p_{cr})/\varrho g H.\qquad\qquad (8.2-37)$$

Imagine the fluid to pass, instead of the rotor, a horizontal test tunnel around the critical point. Downstream of the critical point the pressure may recover to $p_A - \varrho g h_s$. Since the cavity has the pressure p_{cr}, it collapses under the differential pressure $p_A - \varrho g h_s - p_{cr}$, corresponding essentially to $NPSH$ and found in the numerator of σ in (8.2-37). The denominator of $\sigma, \varrho g H$ consists of the pressure, which induces the cavity by the high velocity in the critical section.

In the usual horizontal cavitation tunnel the head produces the velocity head $\varrho w_0^2/2$ and a pressure head p_0 before the test section. Here the numerator of σ contains $p_0 - p_{cr}$. For convenience the total head in the denominator is replaced by the velocity head, see also R. Knapp, J. Daily and

F. G. Hammitt [8.6]. The pressure p_{cr} at the critical point can be defined by a pressure number

$$K_{p_{cr}} = 2(p_{cr} - p_v)/(\varrho w_0^2).$$

(8.2–38)

With the above the conventional cavitation index reads

$$\sigma_i = - K_{p_{cr}} = 2(p_0 - p_{cr})/(\varrho w_0^2).$$

(8.2–39)

8.2.2.3. Theoretical cavitation index, scale effects

Accounting for the energy theorem of ideal flow, the last relation reads as $\sigma_{i,th} = (w_{max}/w_0)^2 - 1$, with w_{max} the velocity at the minimum pressure point. Obviously for a certain steady potential flow around a body, the ratio w_{max}/w_0 depends only on the geometry of the body and neither on its flow velocity nor its size, so-called scale effects.

Because of the scale effects the real cavitation index σ_i at onset is smaller than $\sigma_{i,th}$ (Fig. 8.2.3 a). One reason for this seems to be the boundary layer. It diminishes w_{max} by viscosity and by the then diminished curvature of the main flow.

Arakeri and *Acosta* [8.56] found the re-attachment of laminar separation region and – in case of desinent cavitation – the transition into turbulent boundary layer to influence σ_{cr} when they occur in the critical region. Surely the then longer period of dwell of nuclei, the high turbulence there, and strong pressure pulsations which facilitate the pressure to fall short of its critical value, may favour the sudden growth of nuclei especially by rectified diffusion [8.121].

Other reasons as structure and level of turbulence, and surface roughness were mentioned by *Arndt* [8.51] and *Billet* [8.48]. In the case of developed cavitation, the '*B* factor' after *Stepanoff* [8.122] or thermodynamic effects mentioned by *Bonnin* [8.58] and *Raabe* [8.36; 8.61] may influence the scale effect. An attempt was also made by (8.2–17) to explain scale effects.

8.2.2.4. Influence of air content and its control

On the one hand the free air content is a prerequisite for the onset of cavitation. On the other hand the air content influences the cavitation index σ as a function of flow.

Therefore any cavitation test stand (Fig. 8.2.7) requires the control of air content. Usually the total air content is controlled by means of a *van Slyke* apparatus [8.123]. Fig. 8.2.8 b reveals that this parameter is not as significant for the onset of cavitation as the free air content (Fig. 8.2.8 a).

The usual closed test rig (Fig. 8.2.7) has a device, which deflects the undissolved free air into a dome before the fluid enters the test section. Otherwise the preparedness of liquid there to cavitate would increase by too large nuclei entrained. On the other hand by the deaeration the natural air content of the liquid is lowered and hence also σ measured at the critical point.

The best guarantee for a natural air content may be an open test rig. For a turbine stand the upper reservoir must have a free level. This limits the erection of such a stand by the topography of its surroundings. Some laboratories in the USA and Canada [8.124] with closed test rigs use big resorber vessels for recuperation of the natural free air content (Fig. 8.2.9).

A stand should have a device for the control of the free air content with respect to spectrum and density of nuclei entrained in the test section. This may operate on acoustic basis after *Meyer* and *Skudozyc* [8.125], by means of Laser after *Keller* [8.28], by visualization of the cavitation susceptibility through a transparent Venturi tube by-passing the test section after *Oldenziel* [8.27].

284
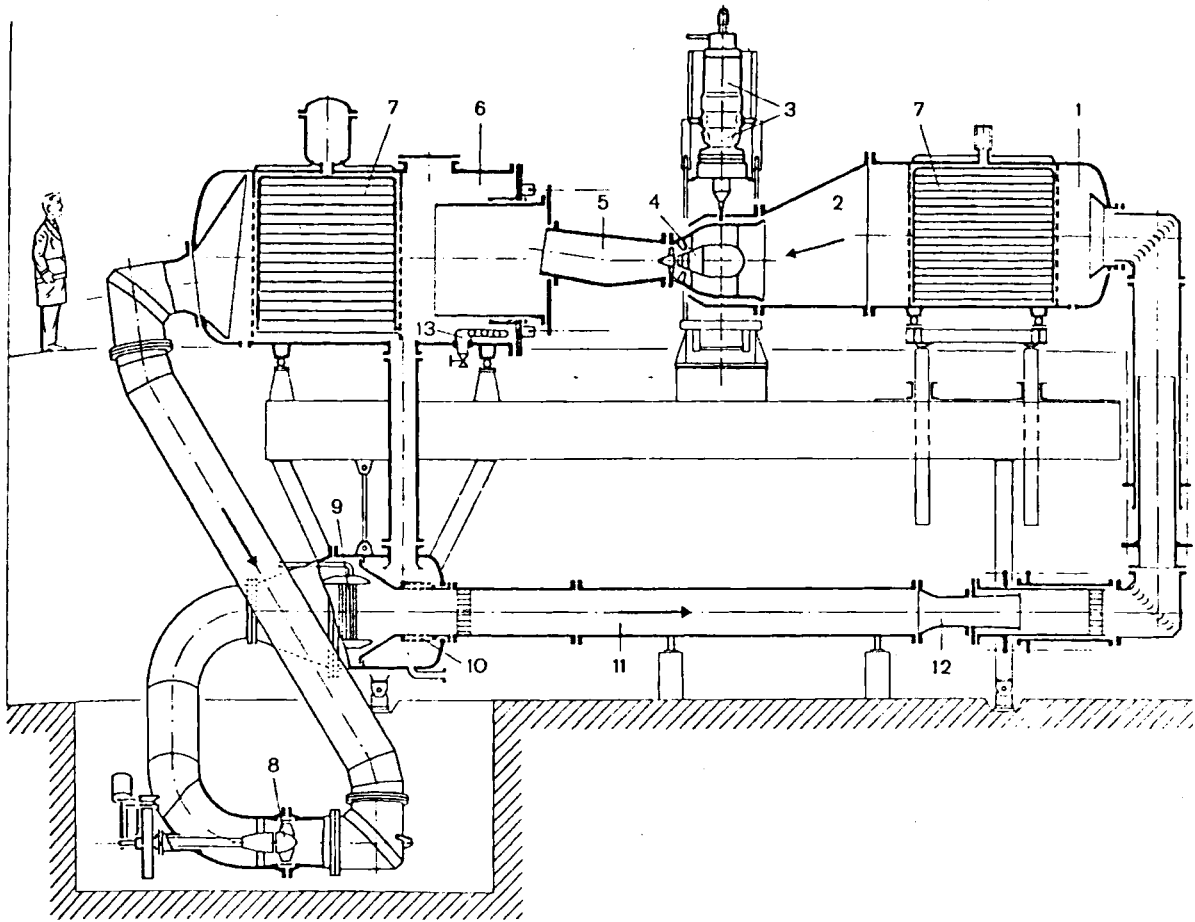
Fig. 8.2.7. Section of universal closed test rig for air and water, for efficiency and cavitation tests on low head reaction turbines (here bulb turbines). With minor changes, the test section can be adapted also to a vertical set with spiral casing. 1 head water tank; 2 intake; 3 turbine block with bulb turbine 4, power take-off via bevel gear. To eliminate bearing friction, the bearing box is connected to the swinging stator of an air-cushioned electric torque reaction dynamometer; 6 tailwater tank; 7 air separator; 8 circulation pump; 9 cooling circuit; 10 bypass; 11 flow measuring section; 12 Venturi nozzle; 13 cooler, heater respectively for change of viscosity also changing Reynolds-number. A similar stand with a vertical Francis turbine in the test section is in the author's laboratory at the Technical University Munich. (Drawing courtesy Sulzer Escher Wyss)

Before a flow lamina enters the critical zone a portion of its nuclei is screened away from the body's face. This originates from the concave curvature of the flow around the stagnation point. The convex curvature of the body's face near the critical point has the opposite effect. This raises the question, whether the nuclei measured upstream of the critical point are representative for those entrained into the area of cavitation [8.6; 8.75].

8.2.2.5. The influence of roughness on cavitation

Obviously a wall roughness causes an increase of velocity along a convex curved wall. This enlarges the cavitation index. As a model *Holl* [8.49] has assumed a roughness formed by a rectangular equilateral triangle facing the flow with its small side and located on the point of minimum pressure of a profile with its pressure number $K_{p\,min} = 2(p_\infty - p_{min})/(\varrho\,w_\infty^2)$. For incipient cavitation the cavitation index of this roughness on a flat plate reads $\sigma_{i\,rpl} = 2(p_{min} - p_{cr})/(\varrho\,w_{min}^2)$, where w_{min} is the local velocity at

a)

c)

$W_\infty = 7.6$ m/s

$\alpha = 11\text{-}12$ g/m³

b)
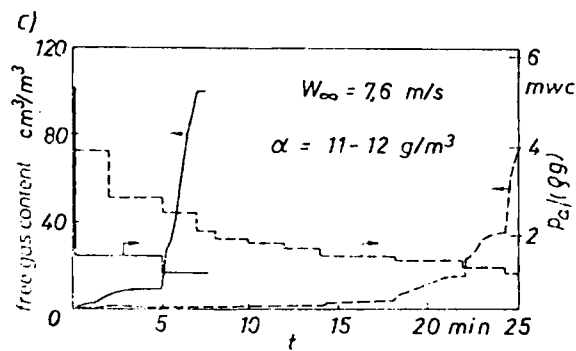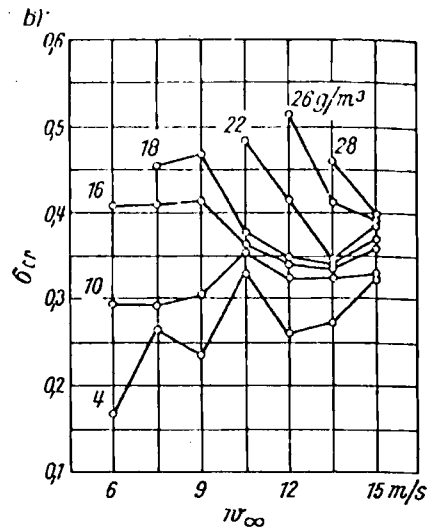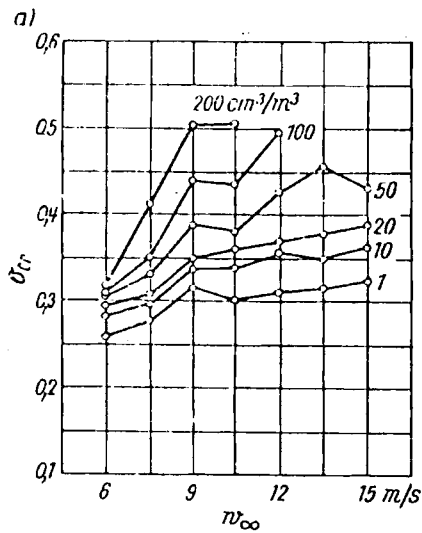
Fig. 8.2.8. Cavitation phenomena as a function of gas content. a) Cavitation inception index vs velocity w_∞ as a function of free air content. Tests on ogival body 1,5/15,9 mm. b) Ditto with respect to varying total air content. c) Free air content of a closed test rig as a function of pressure and time. After *J. Rippken, J. M. Killen*: Gas bubbles, their measurement and influence in cavitation testing. Proc. IAHR Symp. Sendai 1962, p. 37.
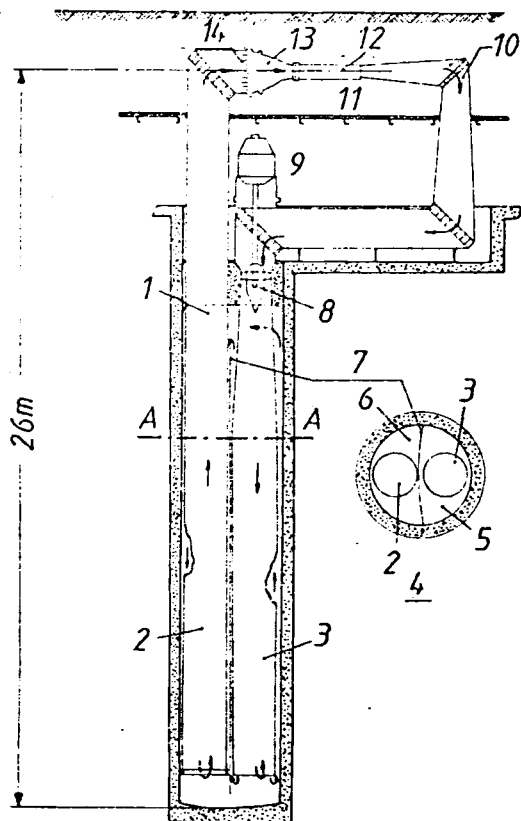
Fig. 8.2.9. Closed test rig with cavitation nozzle and resorber of Californian Institute of Technology, Pasadena. 1 resorber; 2 upward flow pipe; 3 downward flow pipe; 4 section $A - A$; 5 upwards flow chamber; 6 downwards flow chamber; 7 separation wall of resorber; 8 circulation pump; 9 260 kW motor; 10 diffuser; 11 working flow; 12 probe; 13 nozzle; 14 rectifier. After *Knapp, Daily, Hammit* [8.6].

the point of minimum pressure, in the same distance from the wall as the top of the roughness. Hence the cavitation index due to the roughness

$$\sigma_{ir} = - K_{p\,min} + (1 - K_{p\,min})\sigma_{ir\,pl}.$$ (8.2-40)

According to this relation, the following relative increase $\Delta \sigma_i/\sigma_i$ as a consequence of roughness is seen as a function of the roughness elevation h referred to the boundary layer thickness δ: $h/\delta\,(\Delta\sigma_i/\sigma_i)$: 0,01 (0,81); 0,02 (1,05); 0,04 (1.41): 0.08 (1,89); 0,16(2,49). An individual roughness is not dangerous, when the zone of its pressure through is covered in a short time interval.

The influence of a roughness zone, e.g. due to machining, on cavitation depends on the location of this zone, whether it is on the suction face, and then on the profile's head (very unfavourable), or on the pressure face (usually harmless), or whether the roughness grooves are normal to the flow (unfavourable) or along the flow (harmless) [8.50].

Low head Kaplan turbines with carbon steel runner blades in run-of-the river plants with nonsubmergence, having long periods of standstill as a consequence of varying flow-off, tend to rust and hence encrease their susceptibility to cavitation. This may be avoided by employing stainless steel blades.

Sand erosion does the same, but in a smaller degree, since then the grooves are along the flow close to the surface.

8.2.2.6. Differences in cavitation in turbines and pumps

The differences now listed between turbines and pumps. obviously occur also between the turbine and pump regimes of a pump-turbine. The following holds true only for machines with fixed runner vanes.

In a pump, the fluid passes the low pressure zone of the suction line with low velocity before it enters the impeller. This and eventual straightening baffles on the wall of a pump's suction pipe may favour the growth of nuclei by diffusion and enhance the readiness of fluid to cavitate before it enters the proper cavitation zone of the impeller.

In a turbine within the distributor the fluid passes a zone of high pressure with highest velocity before it enters the runner as the origin of cavitation. However, the boundary layers of stay and gate vanes enlarge the turbulence as a prerequisite of growth of nuclei. Moreover the latter may grow by rectified diffusion induced by the pressure pulsations from the motion of gates and runner vanes to each other.

The latter may also lead to coalescence of pulsating nuclei [8.40]. In turbines, before the rotor, the growth of nuclei is also stimulated by diffusion in consequence of the very strong pressure release within the gates (about 50% of the head in Francis turbines) due to Henry's law. However due to the very high absolute velocity there, this all occurs in a very short time interval. And diffusion needs time.

The considerations of inlet shock of the runner vane, as expounded in Cap. 5.3.5.3 show, that the so-called inlet shock appears at over load and part load. This consideration was made under the assumption that the points of whirl-free outflow and shockless inflow of the runner coincide. When the two points differ from each other, and when the consideration is extended on pump-impellers, part load operation shall be defined as one with the rotor inflow against the rotor vane pressure face and overload operation as one with an inflow against the rotor vane suction face. Hence under over (part) load, in a machine with fixed rotor blades, the relative flow at the leading inlet edge makes a pronounced angle of incidence (Fig. 8.2.10) with the suction (pressure) face of a rotor vane. This causes

287
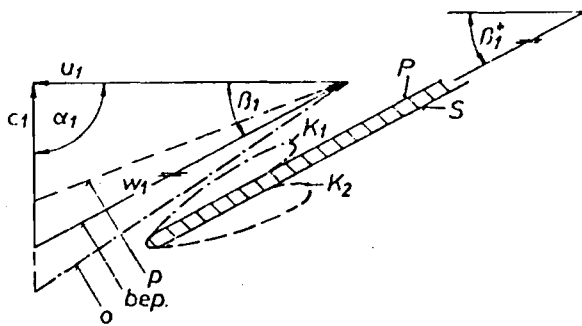
Fig. 8.2.10. Cavitation phenomena at the impeller inlet as a function of flow $Q \sim c_1$. p part load; bep best efficiency point; o overload; P pressure face; S suction face (both of the rotor vane), K_1 cavity on P under o; K_2 cavity on S under p. Phenomena similar to those in turbines, see Fig. 5.5.3.

a flow with overspeed about the sharply curved leading inlet edge and hence a cavity past it on the pressure(suction) face under over(part)load [8.14; 8.16]. See also Fig. 5.3.3.

At larger deviations of the flow Q from the bep flow Q_{op} the initially wall-attached cavity stalls and may lead to a cavitating vortex street along the channel centre line [8.14].

Obviously (Fig. 8.2.10) in an impeller (pump rotor) of a pump analogous phenomena appear, with the difference that the angle of incidence at over(part)load on the suction (pressure) face is now combined with an accelerating(decelerating) inlet shock. Since cavities and pitting under overload operation in pumps are difficult to observe, these consequences of overload in pumps require special attention [2.27], [8.14; 8.127].

In consequence of the above, cavitation in a pump impeller starts usually at the leading inlet edge close to the shroud whereas in a turbine runner it starts more in the middle of the rotor and extends towards the draft tube [8.127].

In a pump impeller, a relatively thick, usually quasi wall-attached cavity past the leading inlet edge chokes the intended flow. This follows also from the now rather small angle the rotor vane makes with the circumference. Downstream of this cavity, the relative flow, which especially under part load is already decelerated, is additionally decelerated by diffusion.

On the contrary in a turbine's runner vane channel, with its relative flow, strongly accelerated, especially under part load and then together with the accelerating "inlet shock", and the vanes. more inclined against the circumference than in a pump impeller such a diffusion past a wall-attached cavity does not harm the efficiency and the machine's behaviour as it does in a pump rotor.

Moreover pitting by cavities in the impeller damages the strength of this vital part in the case of a pump more severely than it does in a turbine, where the majority of cavities collapse in the stationary draft tube. Hence the cavitation index σ required for a pump with a certain specific speed n_q must be larger than that due to a turbine with the same specific speed.

8.2.2.7. Cavitation in pumps or pump-turbines when pumping

Cavitation of radial impellers occurs in 5 zones (Fig. 8.2.11 a). They usually appear under flow away from the bep and may be visualized, e.g. stroboscopically by a window in the suction pipe. The zones K_1, K_2, K_3 and K_4 [8.122] are usually stationary wall-attached sheet-like cavities. The zone K_5 consists of smaller bubbles floating relative to the impeller. Especially under part load, vortex-like cavities from the outer gap enter into the impeller eye. This originates from superheating the leakage by disk friction and dissipation within the labyrinth [8.128]. To understand K_1 and K_2, see also Fig. 8.2.10.
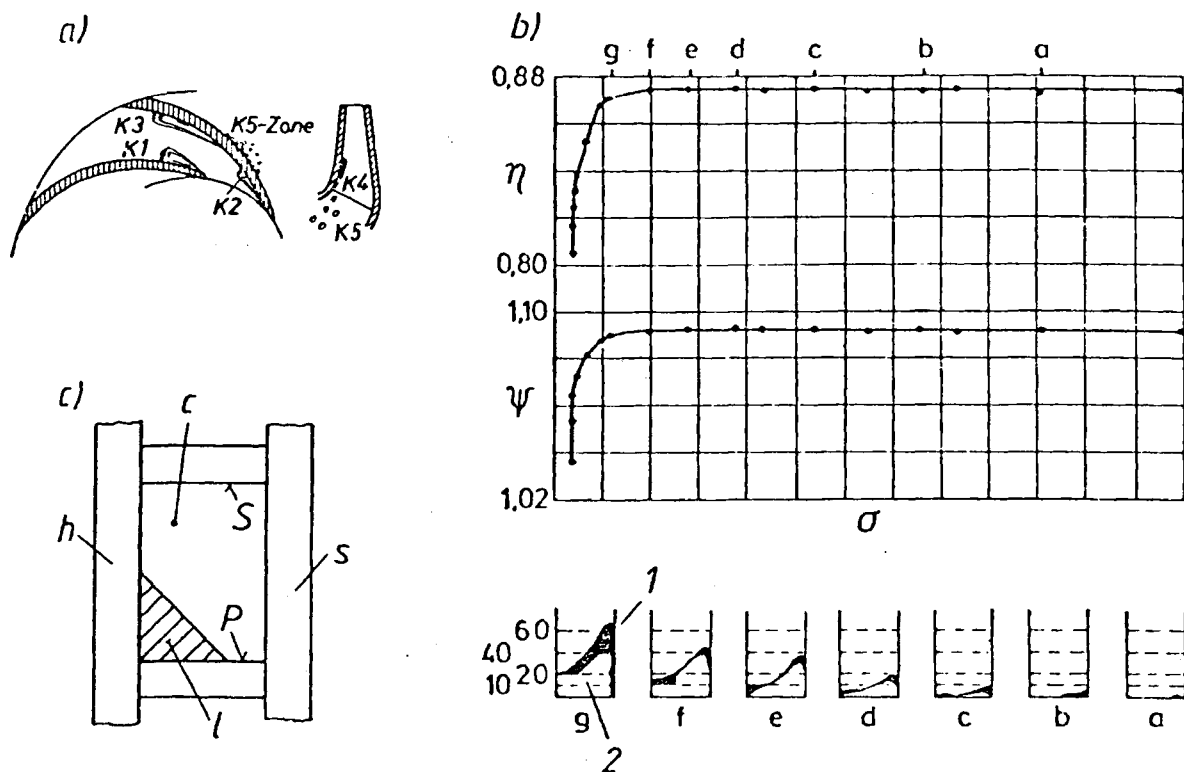
Fig. 8.2.11. Cavity formation in pump impeller. a) Areas of cavities. Close to and past the inlet edge: K_1 on the pressure face P; K_2 on the suction face S. K_3 on S past midchord. K_4 on the shroud. K_5 close to the shroud. b) Development of K_2 with lowered back pressure flow retained, as a function of cavitation index σ, shroud right; 1 bubbling end of cavity; 2 glassy quasi resting cavity from inlet edge. Distance of incipient cavitation at 'a' from critical cavitation, at which η or Ψ begin to drop. c) Cross section of an impeller after the inlet shortly before water column separation. h hub; s shroud; l liquid; c cavity. a) From *Kasai* et al., b) from *Floriančič* et al.

Usually the zones K_1 and K_2 cover a triangular area on the vane face (Fig. 8.2.11 b) that starts from the outer part of the inlet edge (highest w_1 and hence highest σ there) with its longest streamwise extension along the shroud. Lowering the back pressure and hence also σ causes an expansion of this area along the shroud and towards the hub (Fig. 8.2.11 b).

The zone K_1 on the pressure face can be observed either by a partly transparent vane or by its mirror image on the polished suction face. Cavitation inception usually occurs at the tip of the inlet edge with a cavitation index σ up to 6 times larger than the critical σ value, that influences the characteristic by a drop of head and efficiency [8.129].

The zone K_2 on the suction face is due to part load, K_1 on the pressure face due to overload. Both originate from an angle of incidence after Cap. 8.2.2.6. The zone K_4 originates from the curvature of the shroud and increases with the flow. The zone K_3 on the middle of the suction face appears only under overload together with K_1 on the pressure face past the inlet. Here the impeller operates partly near the inlet as a turbine, which then has to be compensated by an extra strong pressure trough on the suction face.

The zone K_5 appears at very low discharge. It originates from a ring vortex close to the shroud, that causes cavitation by a high angle of incidence when entering the impeller. Its backflow close to the shroud sweeps these cavities into the impeller eye.

289

With back pressure decreased. the cavities K_1, K_4 or K_2, K_3 coalesce. leaving finally a small triangular cross section for the flow (Fig. 8.2.11 c) before the latter is cut off by cavitation. At any rate, pitting occurs only on the rear of the wall-attached cavities, looking somehow "foamy" in contrast to the more "glassy" appearance of the cavity part ahead.

Diagonal and axial impeller pumps have only· the three areas K_1, K_2, K_3 from the aforementioned cavitation zones (Fig. 8.2.11 a). Moreover these impellers have gap cavitation in the tip clearance and in the case of adjustable vanes also in the hub clearance. Then, to avoid fatigue effects at the transition between blade and pivot. the innermost vane profile must be thickened at the groove between blade and disk of the pivot. This causes fillet cavitation there (Fig. 8.2.11 a) [8.126].

Fluctuating cavities, which may occur away from the bep, may temporarily choke the flow. This causes water hammer, which in return influences the cavities [8.11].

8.2.2.8. Cavitation in turbines

In a turbine the cavitating zones are similarly located as corresponding in pumps. Also here the wall-attached cavity past the leading inlet edge of the runner vane in a rotor with fixed vanes due to part load appears on the suction face and the corresponding cavity due to overload on the pressure face. That means in the partload regime the additional pressure trough due to an angle of incidence supports the intended flow and hence improves the efficiency. However, in the over load regime of a turbine this pressure trough on the pressure face counteracts the pressure distribution of a turbine runner intended and hence worsens the efficiency.

In addition turbines with fixed runner vanes have also wall-attached cavities past the leading inlet edge of runner under varying head (Fig. 5.3.3). When the head falls short of its rated value such a cavity appears on the pressure face. This may occur when a turbine is supplied by a reservoir during its filling. If thereby the angle of incidence exceeds a certain value, the flow stalls at the leading edge, then shedding a cavitating vortex sheet along the interior of the channel, causing noise and vibrations [8.130].

The problems due to wall-attached or stalling cavities as a consequence of flow and head variation are somewhat facilitated, but not completely eliminated by means of adjustable runner vanes; described by Eichler and Jaeger [8.16].

In these machines, at retained head, the inlet shock at over (part) load results in a cavity on the suction (pressure) face of the runner blade. The contrary happens in machines with fixed runner blades. Usually in run-of-river plants, according to the flow and head duration line, KTs with adjustable runner blades operate under part load with a head larger and under overload with a head smaller than the rated one. Thus the overload cavity usually shifts again towards the pressure face and the part load cavity towards the suction face. (Load is used here in the sense of discharge expounded in Cap. 5.3.5.3.)

In reaction turbines with fixed runner vanes the precessing cork screw vortex past the runner usually cavitates in its core (Fig. 8.2.12 a) (details Cap. 5.5). Also the core of the straight vortex in the draft tube due to overload cavitates. See Fig. 8.2.12 b.

By the radial pressure gradient, air diffuses also into the vortex core. This makes the vortex core elastic and capable of oscillating in connection with the surrounding mass water. Such oscillations may be excited by water hammer-induced pressure surges of the system penstock turbine draft tube tailrace gallery, stimulated by changes in gate position due to varying load demand, but also excited by the precessing excentric velocity field to the cork screw vortex [5.51 to 5.55], [8.95], [9.45 to 9.51].

290

Fig. 8.2.12. Cavitating draft tube vortices in reaction turbines with non-adjustable runner vanes away from the bep. a) Precessing cork screw vortex under part load. Origin here on the hub cone. In general, origin depends strongly on the operating point and design of the runner; also possible are e.g. twin vortices opposite to each other. b) Coaxial vortex under overload. Here origin usually on the hub cone. Downstream end sometimes also with cork screw form, but then contrary to a) always unstable and irregularly precessing. (Photograph a) from G. Schlemmer [5.18] photograph b) Courtesy Voith)
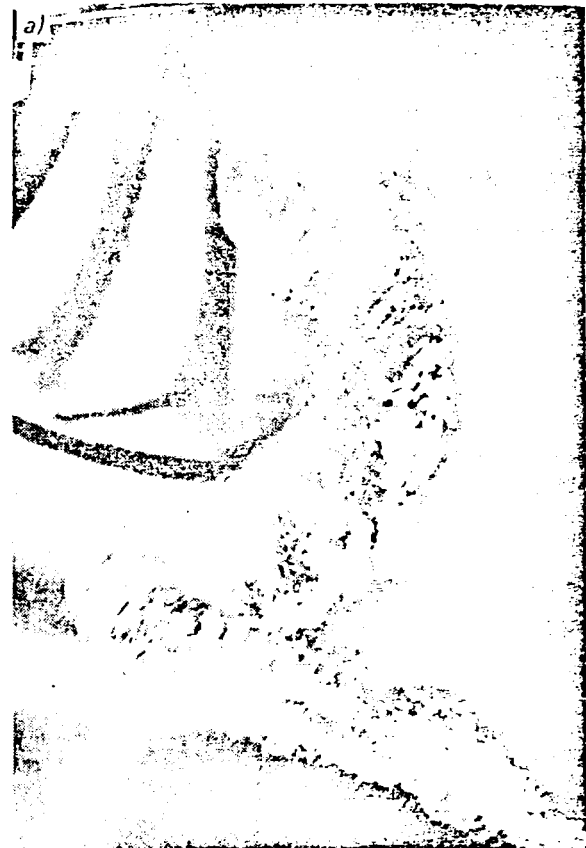
When the turbine works at a larger distance from the range of vortex free operation (nearly coinciding with zero whirl past the runner) then the initially straight vortex due to overload may be split into fluctuating and irregularily precessing branches, causing bad vibration.

The great resistance of quasi two dimensional motion of the vortex against deformation in the draft tube bend together with a growth of its core by convective diffusion in connection with radial oscillation may block the outer flow. The pressure rise hence induced, may stimulate a break down

291

of the vortex by sweeping it downstream. Such accidental effects may be accompanied by hammering load changes on the head cover and the shaft [8.131; 8.132]. This occurs at overload. After *Krause* an occasional break down of the vortex might also originate from the acceleration of main flow in the diffuser bend.

Turbines of higher specific speed especially KTs cavitate severely under runaway. *Ishii* [8.17] has hinted at a non pitch periodical cavity formation of KTs under runaway, linked to an extra high runaway speed.

A special cavitation-like erosion occasionally is observed on the back side of the bucket of impulse turbines (PTs) near the jet cut out [8.18]. This can be attributed to the impact of droplets, that are overtaken by the bucket.

Some of the cavitational phenomena originating from a varying angle of incidence of the flow (and then also the losses due to it) could be eliminated by operating the set with a variable speed. This could be done more easily in plants using DC high voltage power transmission. On the other hand this would bring in a lot of rather expensive problems on the side of stable regulation and electric power transmission. That is to say it would shift the problems from the turbine side to the electrical side.

Contrary to small pumps with permissible head drop of up to 3% due to cavitation, for the loss of revenue, an efficiency drop due to cavitation is not admitted in turbines. For *Knapp's* erosion law (8.2-22) in high head turbo machines the slightest cavitation erosion should be avoided.

Therefore the suction head and the cavitation index required have to be determined carefully beforehand with respect to the corresponding critical cavitation index (either due to efficiency or due to erosion). This is done on the basis of model tests, preferably on one and the same stand for efficiency and cavitation tests [8.10].

The hydrodynamic effects of cavitation are usually stroboscopically observed through a window in the draft tube of a model.

As an example consider a Kaplan turbine, (Fig. 8.2.13 a), [8.132]. Under $\sigma = 0,7$ it operates without any effect on η, H or Q. At lowered back pressure with $\sigma = 0,67$ fillet cavitation at the hub groove occurs (Fig. 8.2.13 b). Owing to the erosion law (8.2-22) and the relatively small relative velocity there, this does not cause any harm. A further drop in σ leads to tip clearance cavitation (Fig. 8.2.13 b). Because of the relatively high relative velocity there and *Knapp's* erosion law (8.2-22), this kind of cavitation has to be limited.
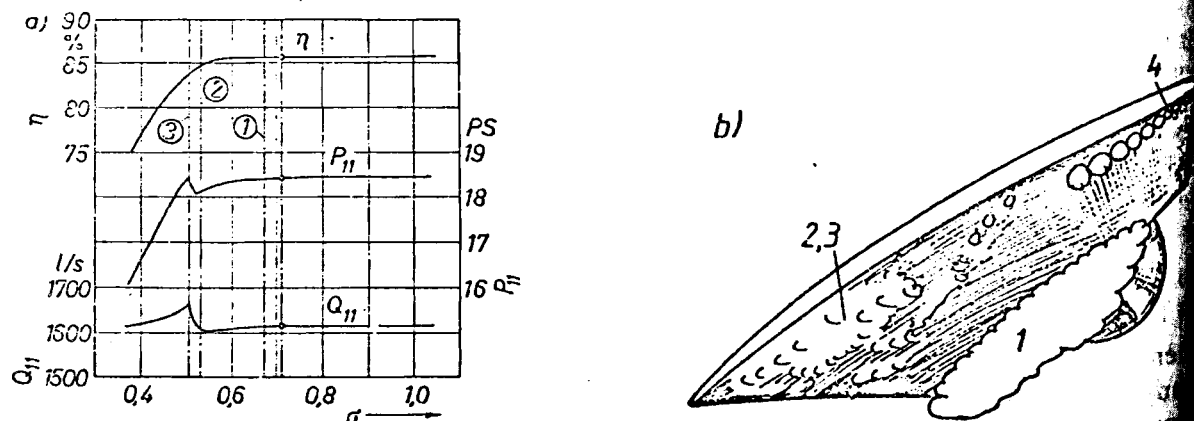
Fig. 8.2.13. Cavitation phenomena in axial turbines, e.g., KTs, or BTs. a) Influence of the cavitation index σ of a KT on efficiency, output, and discharge. 1 onset of fillet cavitation (see also Fig. 2 beginning of surface cavitation and stall on suction face (see also b)); 3 amplified stall on suction face (see also b)). b) Cavitation phenomena mentioned in a) on runner vane of KT, 1 developed cavitation. 4 tip clearance cavitation. From *Gerber*.

292

This is done either by cavitation fins (Fig. 10.2.25) or by material, resistant to cavitation erosion at least in the form of building up welding or that of lining on the vane and the throat ring.

Usually the suction head is defined up to the runner exit. However in a large KT (D up to 11,3 m) the critical point due to tip clearance cavitation on the prototype may be about 3 m above the runner vane's rearward edge. Therefore the prediction of h_s for this case by means of (8.2–27) has to be based not on the small model ($D = 0,3$ to $0,6$ m) but on the elevation the real critical point of the prototype has above tailwater.

When σ of the turbine considered falls short of 0,5, flow separation starts due to cavitation on the suction face of runner vane. Hence a drop in output and efficiency appears. This point has to be avoided in the prototype with due consideration to cavitation scale effects. For the latter the head might be $H = 30$ m and the safety margin at this point with respect to scale effects $\Delta\sigma = 0,04$. Then $\Delta h_s = 0,04 \cdot 30 = 1,2$ m must be subtracted from the h_s obtained from the measured σ of this critical point by formula (8.2–27).

Only for information but without consequence to application it may be stated (Fig. 8.2.13) that, when σ on the machine is lowered below 0,5, the efficiency continues decreasing but flow and output show a slight peak, probably from a lowered drag. A further drop of σ chokes and finally blocks the flow.

In the following some practical hints may be given after *Jaeger* and *Eichler* [8.16] concerning observations on cavitating machines and keeping cavitation under control. The following items should be observed in model and prototype if possible:

a) Extent of cavitation in area (cavity or pitting)
b) Characteristic cavitation pattern (cloudy, compact, vortical)
c) Effect of cavitation on performance.

Plant should be reviewed over a certain working period. The following items should be noted during operation, to obtain the linkage between flow field and pitting rate at a certain prototype:

d) Flow range
e) head range
f) altitude range of tail water,
g) hours of operation due to conditions d) through f), the items d) and e) should be referred to rated figures.

At a runner inspection, location, extent and depth of pitting or pitting area should be noted.

8.2.2.9. Protective measures against cavitation

1) Correct fixing of suction head: (Fig. 8.2.6 a) h_s follows from (8.2–27). To limit a certain undesirable cavitation, h_s as the elevation of this special critical zone above the tail-water in the prototype must be accounted for. Fixing of σ with sufficient distance from σ_{cr}, defined by *IEC* code. When σ_{cr} is from a model test, then adding to this $\Delta\sigma_{sc}$ due to scale effect.

The latter may be divided into predictable physical scale effects (due to length scale, due to *Reynolds* number etc.) and accidental scale effects, e.g. due to non retained geometry of the prototype with respect to the draft in consequence of errors of foundary, of machining, failures due to transport (roughnesses due to crane cable, road accidents), failures during assembly on site, e.g. by wrong adapted civil engineering work e.g., from the lining of the throat ring to the concreted draft tube wall.

Fixing h_s requires complete knowledge of the hydrograph, back water effect, working programme of the plant, the altitude of the site and its lowest possible barometric pressure, the highest possible water temperature and corresponding vapour pressure. It must be mentioned that setting h_s must be done also with a side glance on the excavation

cost implied. Unusual operation, e.g. with a strong angle of incidence during filling of a huge reservoir cannot be taken into account. The duration of such "eccentric operation" must be noticed.

In general the σ value due to the pressure trough caused by an angle of incidence at the leading inlet edge of the runner would result in an uneconomically deep submergence of the set.

Such an operation should be avoided or limited in time. Its consequences should be included into a revision and repair program. The operator of a plant must be conscious that the momentary lucrative operation below the critical σ value, ruins the overall economy and availability of a plant. In general a turbine could escape such operating conditions by adequate position of gates.

In pump-turbines during pumping this flexibility is lost by the then necessary blockage of gates in the optimum position, situation which also exists in storage pumps. To avoid pitting in high head pump-turbines, *Knapp*'s erosion law may require submergences up to 60 m. The working cycle of a pumped storage plant with its strong fluctuations of tail and headwater level and the consequent variations of head and suction head require adhering as strictly as possible to the direction that σ_{av} (available due to the momentary head and tail water level) is always above the σ_{re} (required for operating the machine according to its characteristics and with respect to penstock loss).

The typical values of σ_{av} due to characteristic positions of head and tailwater level are located on the so-called operating trapezium, introduced by E. Meier et al. [1.68] shown in (Fig. 8.2.14), within a σ, Q plot. This also contains the machine (here pump) charac-
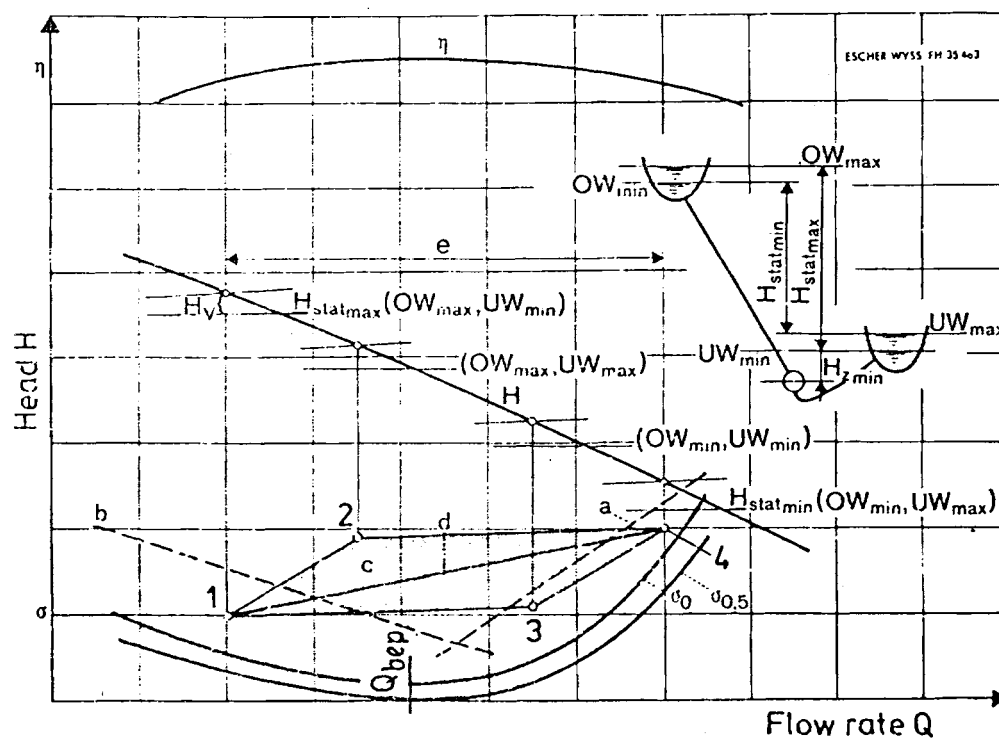
Fig. 8.2.14. Operating trapezium of an impeller pump with strongly fluctuating levels OW of head water, and UW of tail water, and values of σ_{av} resulting from this and the pump characte r 1, 2, 3, 4 corner points of trapezium; b cavitation inception on the suction face of impeller vane; a cavitation inception on the pressure face of impeller vane; σ_0 line of zero efficiency drop; $\sigma_{0.5}$ of 0,5% efficiency drop. From *W. Meier, J. Müller* a. *M. Jaquet* [1.68].

teristic for constant speed and gate position. The graph of σ_{re} (of the pump) vs Q shows a minimum at bep, since there usually the angle of incidence is zero and hence also λ, see (8.2-28), and therefore σ_{re} is smallest.

From this diagram it is seen, that the pump considered, always satisfies the condition $\sigma_{av} > \sigma_{re}$ with respect to the σ_{re} graph due to zero efficiency drop. However it shows, e.g. that the operating point 1 of the operating trapezium has a σ_{av} that falls short of σ_{re} due to a certain cavitation on the suction face, that causes no efficiency drop.

It is then up to the maker and the operator of the plant to decide if the duration of the operation at point 1 would cause pitting damage or not.

According to the author's observations in some of the world's modern units a departure from this procedure causes months of repair during which the set is not available. This may cost more than an additional excavation in consequence of a correctly set suction head.

In some planners' head often prevails the wrong hope that measures against cavitation pitting, e.g. the building up welding of a highly cavitation-resistant material could bring great relief when the machine cavitates against expectation.

2) Correct profiling of the cavitating surface: The form of a profile unsusceptible to cavitation intentionally must be calculated so as to make σ a minimum, at least at the bep (Fig. 8.2.3). The drawing of a draft tube, e.g. should be such as to facilitate correct fabrication. Then the truth to size must be controlled e.g., by a pattern. Any later roughening of a profile by corrosion, erosion or accidental scratch must be avoided.

3) Adequate material for parts subjected to cavitation pitting. This includes also welding programs, for the periodic repair of parts, extremely exposed to cavitation (see Cap. 8.2.1), and shape control by pattern afterwards. Clads or building up welding of resistant material are used in areas where pitting is expected. They are on the rear of wall-attached cavities in zones of high relative velocity. Fins may deflect cavities from certain areas. Guide ribs may lessen erosion by impeding focussed impact of the cavity's implosion. Note, anticavitation fins at the runner blade tip diameter of KTs are tending to fade away, and their replacement is difficult. To increase a plant's availability, the time- and wage-consuming weld repairs will be made unnecessary by applying stainless steel.

4) Aeration upstream of the critical zone by means of a snifting valve or a compressor. A dosage of more than 1% of the rated flow under atmospheric pressure may worsen the efficiency.

8.2.3. An approach for the prediction of pressure number at the critical point in the rotor

8.2.3.1. Introduction

The prediction of submergence of a turbo machine requires the knowledge of $NPSH$ or the cavitation index $\sigma = NPSH/H$. This depends, see (8.2-31), at the bep of a machine, according to the relation (+ pump, − turbine)

$$\sigma = Ku_1^2 + (\lambda + 1 \pm \zeta_D) Kc_{m1}^2$$

on the velocity coefficients Ku_1 and Kc_{m1} at the runner exit, the draft tube loss coefficient ζ_D, and the pressure number λ of the critical point with respect to cavitation. Whereas Ku_1 and Kc_{m1} are known by the working point of the machine and ζ_D varies only slightly with the latter, the value λ depends on the pressure distribution along the contour of the rotor vane for the working point considered. Should this be away from the bep a similar relation is valid for λ [see the comment on (4.2-11)].

Strictly speaking λ can be computed assuming a non cavitating, steady, and ideal flow by means of the method of singularities. The following approach is based on values and features easily available for a certain rotor design, such as: elevation of the rotor, the meridional streamline pattern, the angle β the skeleton of the rotor vane makes with the circumference, the angle μ the meridional streamline makes with the radius, the profile of the rotor vane, the velocity triangles at the pressure edge 2 and suction edge 1 respectively of the rotor vane for the working point considered, the contraction coefficient Φ hence derived and the location of the critical point cr.

The pressure number λ of the critical point is defined by

$$\lambda = 2(p_1 - p_{cr})/(\varrho \, w_1^2), \tag{8.2.3-1}$$

where p_1 and w_1 are pressure and relative velocity respectively at the suction edge of the rotor vane for the working point considered, p_{cr} the critical pressure with respect to cavitation.

8.2.3.2. Assumptions

a) Steady relative flow along the rotor vane.
b) Irrotational absolute flow (curl $w = -2\omega$), axisymmetric flow, divided into elementary turbines.
c) The contraction coefficient Φ of the relative flow within the rotor channel due to the thickness of the rotor vane and its boundary layer or wake is known at the stations 1,2 and cr.
d) The machine operates with zero whirl at station 1 ($c_{u1} = 0$).
e) The machine has a vertical shaft.
f) The rotor loss of the pump or turbine respectively increases linearly with the meridional streampath s_m from point 1 at the suction edge of the rotor vane to the critical point cr when the machine operates as a pump and decreases linearly with s_m over this section for the case of a turbine.
g) The cavitation originates in the flow sheet close to the shroud or tip of the rotor vane at the critical point cr usually located at the suction face of the rotor vane or its leading inlet edge.

8.2.3.3. Mixed flow machines

Here the critical point cr with respect to cavitation lies on the suction face of the rotor vane in the elementary turbine close to the shroud with local breadth (span) b (Fig. 8.2.15 a and b).

In addition to the assumptions made above, it is assumed:

h) The contraction coefficient Φ, the rotor vane angle β, and the meridional velocity w vary linearly within the rotor in flow direction.
i) Pressure and relative velocity vary linearly in the circumferential direction over the unobstructed width of the rotor channel.

According to the identity

$$p_1 - p_{cr} = p_1 - p_M + p_M - p_{cr}, \tag{8.2.3}$$

the pressure difference in the numerator of (8.2.3-1) is split into the following term

a) $p_1 - p_M$. This is a pressure difference along the channel centre line between the stat 1 located on a circle with the radius r_1 between the suction edges of neighbouring va
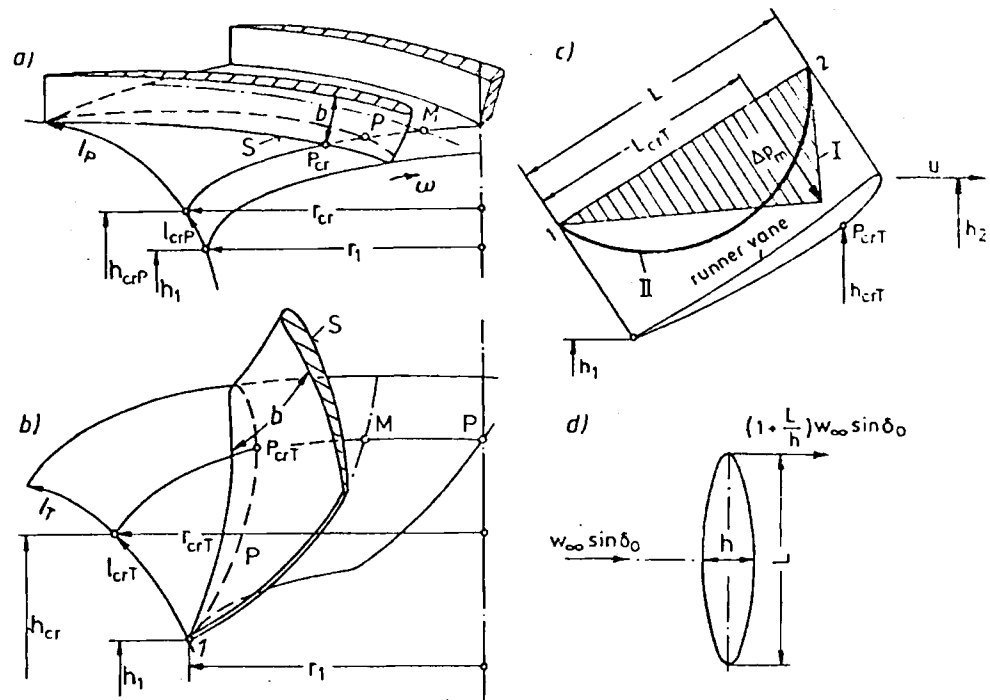
Fig. 8.2.15. The calculation of pressure number λ at critical point. a) perspective view of a mixed flow pump rotor with the critical point P_{cr} on an axisymmetric stream surface and on the vane's suction face. b) Ditto for mixed flow turbine rotor. c) Unrolled cylindrical section of an axial turbine with various distributions of the differential pressure $\Delta p = p_P - p_S$ along the chord. I, triangular, II. elliptic. d) Theoretical velocity at vertex of ellipse.

and the station M, located in a similar extended section, in which the critical point lies on the suction face with a radius r_{cr}.

b) $p_1 - p_{cr}$. This is the pressure difference between the station M at channel centre line and the critical point on the suction face of the rotor vane, both lying on a circle of the radius r_{cr} (see Fig. 8.2.15 b).

The energy theorem for the rotating frame of reference and both the points 1 and M reads with respect to $r_M = r_{cr}$, $h_M = h_{cr}$:

$$(p_1 - p_M)/\varrho = (w_M^2 - w_1^2)/2 - \omega^2 (r_{cr}^2 - r_1^2)/2$$
$$+ g(h_{cr} - h_1) \pm h'_R g H s_m/L_m, \qquad (8.2.3-3)$$

where h'_R is the nondimensional loss of the rotor, (positive sign for a pump and the negative sign for a turbine), L_m the meridional length of the rotor vane, s_m the distance between the critical point cr from the edge 1 of the rotor vane in the direction of the meridional streamline [the last term implies according to the assumption f) a linear change of rotor loss along such a line], H the net head, h the altitude of a point, ω the angular velocity of the rotor. Obviously h'_R is based on an estimate.

Similarly the energy theorem for the rotating frame of reference gives the pressure difference between the points cr and M with respect to $r_{cr} = r_M$, $h_{cr} = h_M$ and the assumption i)

$$(p_M - p_{cr})/\varrho = (w_S^2 - w_P^2)/4 = (w_S - w_P) w_M/2, \qquad (8.2.3-4)$$

where w_S, w_P, w_M are the relative velocities at the suction face (S), the pressure face (P) and the channel centre line (M) respectively. w_M in (8.2.3-4) results from continuity,

297

applied to an elementary turbine with local breadth (span) b, local contraction coefficient Φ, and the relation from the velocity triangle, $w_m = w \sin \beta$, by

$$w_M = w_1 (\Phi_1/\Phi_{cr})(\sin \beta_1/\sin \beta_{cr})(r_1/r_{cr})(b_1/b_{cr}), \qquad (8.2.3-5)$$

where the values with the subscript cr are due to the critical point.

The velocity difference $w_S - w_P$ in (8.2.3-4) follows from the application of Stokes' theorem to the elementary parallelogram-like boundary (see Fig. 5.2.2 a) in the stream surface of the rotor. It is formed by arcs of adjacent parallel circles, that extend from a streamline element close to the suction face of the rotor vane to an element close to the pressure face. These streamline elements are at the displacement thickness of the boundary layer from the vane face. Thus the arc of the parallel circle is a pitch multiplied with a contraction factor Φ that accounts for the obstruction of the flow by the boundary layers and by the vane. Stokes' theorem (Cap. 5.2.2) gives with respect to the assumptions a) to c)

$$w_S - w_P = \frac{2\pi}{z} \sin \beta \cos \mu \left[2\omega \Phi r \pm \frac{\partial (w_u r \Phi)}{\partial r} \right], \qquad (8.2.3-6)$$

where z is the rotor vane number, w_u the pitch-averaged whirl component of the relative velocity, and the +-sign and --sign for turbine and pump respectively.

The following relation holds true between w_u and the pitch-averaged meridional component of the relative velocity w_m: $w_u = w_m \cot \beta$. Hence

$$\frac{\partial (w_u r \Phi)}{\partial r} = \frac{\partial (w_m \cot \beta r \Phi)}{\partial r} = r\Phi \cot \beta \frac{\partial w_m}{\partial r} - \frac{w_m r \Phi}{\sin^2 \beta} \frac{\partial \beta}{\partial r}$$

$$+ w_m \cot \beta \Phi + w_m \cot \beta r \frac{\partial \Phi}{\partial r}. \qquad (8.2.3-7)$$

Inserting this in (8.2.3-6) yields

$$w_S - w_P = \frac{2\pi}{z} \Phi 2\omega r \sin \beta \cos \mu \pm \frac{2\pi}{z} \sin \beta \cos \mu \left[w_m \Phi \cot \beta - \frac{w_m r \Phi}{\sin^2 \beta} \frac{\partial \beta}{\partial r} \right.$$

$$\left. + r\Phi \cot \beta \frac{\partial w_m}{\partial r} + w_m r \cot \beta \frac{\partial \Phi}{\partial r} \right]. \qquad (8.2.3-8)$$

According to assumption h) these partial derivatives in a first order approximation can be obtained from the values $\beta_2, \beta_1, w_{m2}, w_{m1}$ at stations with radius r_2 and r_1 respectively, which are known from the velocity triangles of the elementary turbines considered, and from the contraction coefficients Φ_2 and Φ_1, which have to be estimated for these stations. Thus

$$a) \quad \frac{\partial \beta}{\partial r} = \frac{\beta_2 - \beta_1}{r_2 - r_1}, \quad b) \quad \frac{\partial w_m}{\partial r} = \frac{w_{m2} - w_{m1}}{r_2 - r_1}, \quad c) \quad \frac{\partial \Phi}{\partial r} = \frac{\Phi_2 - \Phi_1}{r_2 - r_1}. \qquad (8.2.3-9)$$

Inserting (8.2.3-9) in (8.2.3-8), this and w_M from (8.2.3-5) in (8.2.3-4), and then (8.2.3-5) and (8.2.3-4) in (8.2.3-2), and this in (8.2.3-1) yields λ with respect to the assumption d) by which $w_1 = u_1 \cos \beta_1$ and $c_{u1} = 0$,

298

$$\lambda = \left(\frac{\Phi_1 \sin \beta_1 \, r_1 \, b_1}{\Phi_{cr} \sin \beta_{cr} \, r_{cr} \, b_{cr}}\right)^2 - 1 - \left[\left(\frac{r_{cr}}{r_1}\right)^2 - 1\right] \cos^2 \beta_1$$

$$+ \left(\frac{h_{cr}}{H} \pm \frac{h'_R \, S_{m\,cr}}{L_m}\right)\left(\frac{r_2 \cos \beta_2}{r_1 \, Ku_2}\right)^2$$

$$\pm \frac{2\pi}{z} \frac{\Phi_1}{\Phi_{cr}} \frac{r_1}{r_{cr}} \frac{b_1}{b_{cr}} \sin \beta_1 \cos \mu_{cr} \left\{ 2 \cos \beta_1 \, \Phi_{cr} \frac{r_{cr}}{r_1} \right.$$

$$- \left\langle \frac{r_{cr} \, \Phi_{cr}}{r_2 - r_1} \left[\frac{w_{m2} - w_{m1}}{w_1} \cot \beta_{cr} - \frac{w_{m\,cr}}{w_1} \frac{\beta_2 - \beta_1}{\sin^2 \beta_{cr}}\right] \right.$$

$$\left. \left. + \frac{w_{m\,cr}}{w_1} \cot \beta_{cr} \left[\Phi_{cr} + \frac{\Phi_2 - \Phi_1}{r_2 - r_1} r_{cr}\right] \right\rangle \right\}. \qquad (8.2.3-10)$$

with the positive sign for a pump, the negative sign for a turbine.

Example: Pump: $\Phi_1 \sin \beta_1 \, r_1 \, b_1/(\Phi_{cr} \sin \beta_{cr} \, r_{cr} \, b_{cr}) = 1,1$; $r_{cr}/r_1 = 1,1$; $\beta_1 = \beta_{cr} = 20°$; $h'_R = 0,1$; $s_{m\,cr}/L_m = 0,1$; $h_{cr}/H = 0,01$; $\Phi_1/\Phi_{cr} = 1,2$; $z = 6$; $\Phi_{cr} = 0,833$; $r_2/r_1 = 2$; $Ku_2 = 1$; $\mu_{cr} = 20°$; $\beta_2 - \beta_1 = 0,087$; $\Phi_2 - \Phi_1 = -0,3$; $w_{m2}/w_{m1} = 1,1$. This gives $\lambda = 0,429$. Strictly speaking, the critical point makes λ a minimum as a function of r_{cr} and hence β_{cr}, $s_{m\,cr}$, μ_{cr}, b_{cr}.

8.2.3.4. Axial machines

1. Critical point on the suction face. In general $r_{cr} = r_1$. Hence (8.2.3-3)

$$(p_1 - p_M)/\varrho = (w_M^2 - w_1^2)/2 + g(h_{cr} - h_1) \pm h'_R \, g \, H \, s_m/L_m. \qquad (8.2.3-11)$$

With $b_1 = b_{cr}$, $r_{cr} = r_1$ Eq. (8.2.3-5) is simplified to

$$w_M = w_1 (\Phi_1/\Phi_{cr})(\sin \beta_1/\sin \beta_{cr}). \qquad (8.2.3-12)$$

An application of Stokes' theorem to obtain $p_S - p_{cr}$ in (8.2.3-4) according to (8.2.3-6) does not work since $\mu = 90°$. Assuming a linear variation of pressure along the circumference according to assumption i), the differential pressure Δp between pressure and suction face at the critical point depends as follows on $p_M - p_{cr}$

$$\Delta p = 2(p_M - p_{cr}). \qquad (8.2.3-13)$$

To simplify the task, the following two cases are distinguished:

Case a): Triangular distribution of the differential pressure along the blade due to an angle of attack (see Fig. 8.2.15 c). Hence

$$\Delta p = \varrho \zeta_{AG} w_\infty^2, \qquad (8.2.3-14)$$

where ζ_{AG} is the lift coefficient of the blade in cascade, w_∞ the undisturbed velocity (obtained from the velocity triangles as $w_\infty = (w_1 + w_2)/2$). With the relations of Bauersfeld $\zeta_{AG} = (2\,t/L)\Delta c_u/w_\infty$, of Euler $\Delta c_u = g\,H\,\eta_u^{\pm 1}/u$, the blade tip velocity $u \approx w_u$, $h_1 = 0$, the blade tip velocity coefficient $Ku = u/\sqrt{2gH}$ and (8.2.3-2), the relations (8.2.3-11) through (8.2.3-14) yield

$$\lambda_a = \left(\frac{\Phi_1 \sin \beta_1}{\Phi_{cr} \sin \beta_{cr}}\right)^2 - 1 + \left(\frac{h_{cr}}{H} \mp \frac{h'_R \, S_m}{L_m} + \frac{t \, \eta_u^{\mp 1}}{L}\right)\left(\frac{\cos \beta_1}{Ku}\right)^2. \qquad (8.2.3-15)$$

299

Case b): Elliptic distribution of the differential pressure along the blade due to a vanishing angle of incidence on a blade section with circular skeleton. Hence (Fig. 8.2.15 c)

$$\Delta p = (2/\pi)\,\varrho\,\zeta_{AG}\,w_\infty^2\,.$$

(8.2.3-16)

In this case

$$\lambda_b = \left(\frac{\Phi_1 \sin\beta_1}{\Phi_{cr}\sin\beta_{cr}}\right)^2 - 1 + \left(\frac{h_{cr}}{H} \mp \frac{h'_R\,s_m}{L_m} + \frac{2\,t\,\eta_u^{\mp 1}}{\pi L}\right)\left(\frac{\cos\beta_1}{Ku}\right)^2\,.$$

(8.2.3-17)

The $--$sign before h'_R and the exponent of η_u holds true for a pump, and the $+$-sign for a turbine.

Example: Kaplan turbine, case a: $Ku = 1,53$; $\beta_1 = 20,5°$; $h'_R = 0,03$; $s_m/L = 0,2$; $\beta_{cr} = 22°$; $\Phi_1 = 0,85$; $\Phi_2 = 0,9$; $t/L = 1$; $h_{cr} = 1,5$ m; $Kc_m = 0,572$; $\eta_u = 0,95$. This results in

$$\lambda_a = 0,156\,.$$

In an example for case b): $h_{cr} = 0,85$; $s_m/L_m = 0,5$. This lessens the term $(h_{cr}/H + h'_R s_m/L_m)(\cos\beta_1/Ku)^2$ from 0,023 to 0,0174. Also the last term $(2\,t/\pi\,L)(\cos\beta_1/Ku)^2\,\eta_u^{\pm 1}$ is reduced from 0,354 to 0,226. Thus

$$\lambda_b = 0,023\,.$$

At a value $\lambda_a = 0,156$, a draft tube efficiency of $\eta_s = 1 - \zeta_D = 0,85$ gives a cavitation index σ

$$\sigma = \lambda\,Ku^2 + (\lambda + \eta_s)\,Kc_m^2 = 0,7\,.$$

The plant, having barometric pressure head of $B' = 9,5$ m, a critical pressure head $h_{cr} = 0,25$ m and a head of $H = 27$ m, requires a suction head

$$h_s = B' - h_{cr} - \sigma H = - 10,52 \text{ m}\,.$$

Usually the essential pitting by cavitation in the outermost part of a runner vane results from the two modes of operation a and b, described above. Since the outermost elementary turbine of a high specific speed Francis turbine runner ($n_s > 200$) is nearly on a coaxial cylinder, the preceding considerations and hence the validity of equation (8.2.3-17) can also be extended into this type.

II. Critical point at the inlet edge of rotor: The solution of this case can be used also approximately for semiaxial machines, when operating with a critical point on the rotor inlet edge. In this case the distribution of the differential pressure along the blade is triangular like. Hence the solution for λ_a (8.2.3-15) can be applied. Since this result was based more on an estimate, a more exact approach is presented, which contains also the cascade factor and the curvature of the inlet edge.

Denoting the velocity peak at the critical point by w_{max}, λ follows from the energy theorem between the points 1 and cr lying now on a streamline along the contour of the blade by

$$\lambda = (w_{max}/w_1)^2 - 1 = k^2\,(Ku/Kw_1)^2 - 1\,,$$

(8.2.3-18)

where $Kw_1 = w_1/(2\,gH)^{1/2}$, $Ku = u/(2\,gH)^{1/2}$ follow from the velocity triangles and

$$k = w_{max}/u\,,$$

(8.2.3-19)

may be approximated by the following simple hydrodynamic model for the blade in straight cascade.

300

As is well-known, the critical point with its velocity peak at the inlet edge of a blade results from the angle of attack δ_0, the zero lift direction of the blade makes with the undisturbed velocity w_x, due to the velocity triangles. Hence the plane potential flow around the vane has a circulation, see (5.2–38)

$$\Gamma = \Delta c_u t, \qquad (8.2.3-20)$$

where Δc_u is the difference of the whirl components of the absolute velocity at the stations 1 and 2 due to the velocity triangles, t the pitch of the straight cascade formed by the rotor vanes by unrolling its cylindrical section into a plane.

Consider a model of a single plate, chord length L, for the vane. As is well-known, its pressure centre is a distance $L/4$ from the leading edge. Moreover, a straight vortex filament with the circulation Γ at this point of lift attack is a hydrodynamic equivalent of the plate [5.14]. Γ induces at the inlet edge the velocity

$$w_\Gamma = (\Gamma/2\,\pi)(4/L) = (2/\pi)\,\Delta c_u\,(t/L). \qquad (8.2.3-21)$$

To this must be added the velocity originating from the sharp curvature $1/R$ at the profile's head.

For this purpose, an ellipse of chord L as its major axis, and the maximum profile thickness h as the minor axis, in a flow with undisturbed velocity w_x sin δ_0, normal to the chord, is chosen as a model. Accordingly the velocity at the vertex of the major axis [5.3] (Fig. 8.2.15 d)

$$w_R = w_x \sin \delta_0 (1 + L/h), \qquad (8.2.3-22)$$

where δ_0 is the angle of attack, w_∞ the undisturbed velocity.

Since the velocity peak w_R is more induced by the curvature $1/R$ of the inlet edge at the vertex of the ellipse than by the thickness ratio h/L, the known curvature $1/R$ at the vertex of an ellipse is remembered as $1/R = 2\,L/h^2$. (See Hütte I. des Ingenieurs Taschenbuch. Mathematik p. 139. Berlin: Ernst 1955). Hence $h = (2\,RL)^{1/2}$. Thus w_R reads in terms of the vane's inlet curvature

$$w_R = w_\infty \sin \delta_0 [1 + (L/2\,R)^{1/2}]. \qquad (8.2.3-23)$$

As is well-known [6.3], the physical angle of attack δ_0 follows from the lift coefficient in the cascade ζ_{AG} and the cascade factor $\varkappa$ (see 6.2–50) by

$$\sin \delta_0 = \zeta_{AG}/(2\,\pi\,\varkappa). \qquad (8.2.3-24)$$

Introducing the relation of *Bauersfeld* (6.3–4) for ζ_{AG}, *Euler*'s equation $\Delta c_u = g\,H\,\eta_u^{\mp 1}$ and the coefficient of the blade speed $Ku = u/(2\,g\,H)^{1/2}$ yield

$$w_\infty \sin \delta_0 = (\eta_u^{\mp 1}/2\,\pi\,\varkappa)(t/L)u/Ku^2, \qquad (8.2.3-25)$$

where u is the peripheral blade tip velocity, t/L the pitch to chord ratio, η_u the peripheral efficiency of the machine, with the negative exponent for a pump and the positive for a turbine.

Substituting also for Δc_u in (8.2.3–21), *Euler*'s equation and employing the blade tip speed coefficient Ku result in

$$w_\Gamma = (1/\pi)(t/L)\eta_u^{\mp 1}u/Ku. \qquad (8.2.3-26)$$

Summing up w_Γ and w_R gives the desired maximum velocity

$$W_{max} = W_I + W_R.$$

$$(8.2.3-27)$$

Hence the desired coefficient k (8.2.3-19), also needed for λ

$$k = (1/\pi)(t/L)(\eta_u^{\mp 1}/K u^2)\{1 + (1/2\varkappa)[1 + (L/2R)^{1/2}]\}.$$

$$(8.2.3-28)$$

Example: Kaplan turbine: $t/L = 1,2$; $Ku = 1,4$; $L/R = 200$; $\varkappa = 1$; $\beta = 20°$; $\eta_u = 0,95$; $Kc_m = 0.5$; $Kw_1 = 1,15$ yield; $k = 1,2$; $\lambda = 0,24$. Hence a machine with the draft tube efficiency $\eta_s = 0,88$ has $\sigma = 0,75$.

8.2.4. Fundamentals of pitting rate as function of velocity

8.2.4.1. Introduction

Erosion (pitting) by cavitation occurs usually downstream of the rear of a static wall attached sheet-like cavity (Fig. 8.2.16). According to tests of *Knapp* [8.6], the pitting rate for soft aluminum may vary, (8.2–22), under a definite modest cavitation degree (in the neighbourhood of the critical cavitation index σ) with up to the sixth power of the velocity, hence $n \geq 6$ in (8.2–22).

With a rising degree of cavitation (falling σ) this power may drop to zero. The same also occurs when σ increases above its critical value.

Allowing cavitation erosion and its regular repair is common practice to save excavation cost due to excessive submergence. Modern sets especially in developing countries are often planned for larger output than necessary in the first period of the plant's operation. Usually under this the needed service away from the bep, the machine cavitates.

In a second stage sometimes the unit power is enlarged by lifting the head of the plant by means of lifting the crest height of its dam [2.34]. At the same speed, this increases as well the relative velocity and also the angle of incidence and hence the susceptibility to pitting. Here again the problem of sequence of repairs arises.
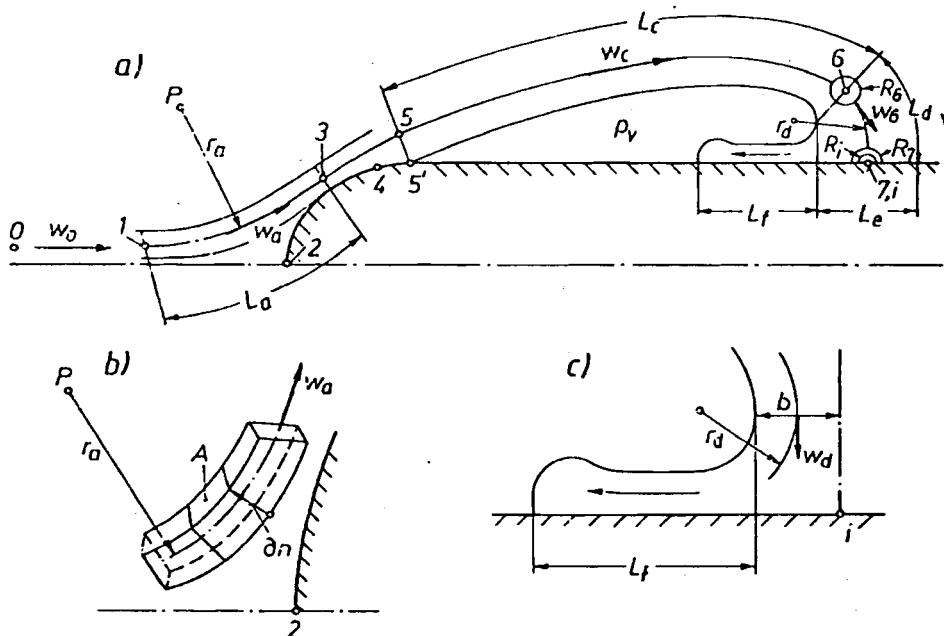
Fig. 8.2.16. Erosion due to a bubble moving around a quasi resting wall-attached cavity a) Schematic view with re-entrant jet and important stations the bubble passes. b) Stream tube element the screening section ahead of the profile. c) Detail of re-entrant jet of local depth b.

302

Therefore in the following a theoretical approach is made to help understand the linkage between pitting rate and relative velocity.

8.2.4.2. Assumptions about wall-attached cavity and its erosion

Consider a wall-attached static cavity with a re-entrant jet (Fig. 8.2.16a). A stream tube of cross sectional area A_0 before the body at station 1 in part encloses the cavity along the path marked by the stations 1, 3, 5, 7. This stream tube is arranged around and along a streamline that intersects the stagnation point 7 downstream of the rear of the cavity.

This stagnation point results from a splitting of the flow in this stream tube at the point 7 into the re-entrant jet and a branch oriented downstream following its original direction. A vapour bubble moves along this stream-tube slipping against the liquid and hence with an added mass especially near the stagnation point with its streamwise pressure gradient. One consequence of this pressure gradient is the propulsion of the re-entrant jet against the wall shear force acting on it.

Thus the sudden deceleration of this bubble together with its added mass before the stagnation point 7 results in a strong pressure rise along the streamline towards this point.

In consequence of the momentum theorem (here the so-called "Rocket effect" after Chincholle [8.113]), the pressure increase is amplified by the sudden shrinkage of the bubble volume, when approximating to the stagnation point 7.

This shrinkage results from the compression of the bubble by the rising pressure around it but mainly by the sudden condensation of its dominating vapour content, when the pressure rises above the steam pressure of the liquid. This pulsating pressure due to the implosion of the bubble in 7, causes pitting. According to experience pitting rate is greatest around the stagnation point 7, past the rear of the static cavity.

The pitting might occur exclusively in the above cited stream tube that crosses the stagnation point 7.

8.2.4.3. Realization of the approach

The unit volume entering the above stream tube of cross section A_0 at station 0 before the body (Fig. 8.2.16a), velocity w_0, may have z_0 spherical nuclei, radius R_0. Hence the time, the unit volume needs, to pass the section

$$t = 1/(w_0 A_0). \tag{8.2.4-1}$$

Assume that all the nuclei passing A_0 also collapse at station 7. Thus the collapse rate of bubbles there

$$i = z_0/t = z_0 A_0 w_0. \tag{8.2.4-2}$$

The erosion rate (pitting rate) is assumed proportional to i and the pressure p_i, induced by the bubble collapse. Hence

$$\dot{m}_{er} = C_0 i p_i = C_0 z_0 A_0 w_0 p_i, \tag{8.2.4-3}$$

where C_0 is a parameter due to the wall material and cavitation degree, e.g. expressed in terms of $|\sigma - \sigma_{cr}|$. Knowing how p_i depends on w_0 will answer the problem of erosion rate $\dot{m}_{er}$ as a function of the flow w_0. For this purpose the following considerations are made.

The bubble imploding at 7, under the external pressure p_7 from its initial radius R_7 = 0, to its final radius has the implosion rate $\dot{R}_i$. Since the volume ratio due to bubble shrinkage by condensation, is proportional to $(R_7/R_i)^3$ and of the order of 10^5, unity can be neglected in proportion to it. Hence *Rayleigh's* formula (8.2–20) brings

$$\dot{R}_i = [(2/3)(p_7/\varrho_L)(R_7/R_i)^3]^{1/2}.$$

(8.2.4–4)

Imagine that $\dot{R}_i$ is suddenly stopped, then the water hammer-induced pressure p_i (8.2–21) becomes

$$p_i = \varrho_L a_L \dot{R}_i,$$

(8.2.4–5)

where $a_L = (\varrho_L/E_L)^{1/2}$, E_L the bulk modulus of liquid, a_L the speed of sound of the pure liquid, surrounding the bubble.

Assume that the gas remaining within the bubble of radius R_7 behaves isentropically between 7 and station 3 at the entrance of the critical zone (Fig. 8.2.16 a), radius R_3, under vapour pressure p_v, and expressing an eventual gas diffusion into the bubble between 7 and 3 by a factor χ (> 1), R_i reads

$$R_i = \chi R_3 (p_v/p_i)^{1/(3\,x)},$$

(8.2.4–6)

where x is the adiabatic exponent.

The pressure p_7 at 7 under which the bubble, radius R_7, implodes is assumed to originate from the sudden cessation of the velocity w_7, due to the bubble's added liquid mass being proportional to R_7^3. Hence *Joukovsky's* water hammer shock (8.3–54), now applied to a mass large compared with that of the gas remaining (being proportional to R_i^3) and consequently in a two phase mixture environment, having the velocity of sound, a, differing from that of the liquid, a_L, results in

$$p_7 = \varrho a w_7,$$

(8.2.4–7)

where ϱ is the density of the two phase mixture.

Now the momentum theorem is applied to the bubble between the stations 6 and 7, at which the bubble has the velocities w_6 and w_7 (Fig. 8.2.16 a). Its added liquid masses being proportional to R_6^3 and R_7^3, now only relevant (as the mass of the bubble content is negligible compared with them). Hence with $w_6 = k_6 w_0$

$$w_7 = k_6 w_0 (R_6/R_7)^3.$$

(8.2.4–8)

Assuming the bubble to cover the cavity section from 5 to 6 (Fig. 8.2.16 a), length L_c, with the mean velocity $k_c w_0$, its travelling time interval needed is $t_c = L_c/(k_c w_0)$. Assuming further the bubble to have there the maximum growth rate from (8.2–13) under a critical pressure, which depends on w_0 after *Parkin* [8.112] yielding the bubble growth rate from (8.2–14) and neglecting the initial bubble radius R_5 at 5 against R_6, then with $t_c = L_c/(k_c w_0)$

$$R_6 = \dot{R}_m t_c = [(2/3) C_2 w_0^\mu/\varrho]^{1/2} [L_c/(k_c w_0)].$$

(8.2.4–9)

Imagine that in the so-called screening section (Fig. 8.2.16 b) from station 1 to 3, length L_a, the radius of the nucleus considered decreases in consequence of screening from $R_1 = R_0$ at the inlet 1 to R_3 at the exit 3. By a simple consideration after *Raabe* [8.75]

$$R_3 = C_3/w_0,$$

(8.2.4–10)

where

$$C_3 = (3/2)^{1/2} \pi z_0 R_1^3 v r_a/(k_a \varphi L_a \partial R/\partial n),$$

304

where z_0 is the number of nuclei per unit volume along L_a, R_1 the radius of nucleus entering the section L_a, v the kinematic viscosity of the liquid. r_a the mean radius of streamline curvature in L_a (Fig. 8.2.16 a). k_a (< 1) the factor, that relates the bubble velocity w_a in the screening section to w_0 by $w_a = k_a w_0$. φ the portion of surface A in the liquid phase along a main stream line in the screening section and perpendicular to the element ∂n (Fig. 8.2.16 b).

Through the latter surface passes the cross flow of nuclei, which are screened towards the centre of curvature P in the screening section (Fig. 8.2.16 b). $\partial R/\partial n$ is the gradient of the bubble radius, the nuclei have towards the point P.

Inserting R_6 from (8.2.4 – 9) into (8.2.4 – 8), then w_7 for p_7 into (8.2.4 – 7), then p_7 for $\dot{R}_i$ into (8.2.4 – 4), then R_3 from (8.2.4 – 10) into (8.2.4 – 6), then R_i into (8.2.4 – 4) and finally $\dot{R}_i$ from (8.2.4 – 4) into (8.2.4 – 5) gives an implicit relation for the pressure p_i due to bubble implosion in 7. Explicitly written down, the latter gives

$$p_i = C_4 \, w_0^{[x/(2\,x-1)](3\,\mu/2\,+\,1)},$$

(8.2.4 – 11)

where

$$C_4 = \left[\varrho_L a_L \left(\frac{2}{3} a\,k_6\right)^{\frac{1}{2}} \left(\frac{2}{3\varrho} C_2\right)^{\frac{3}{4}} \left(\frac{L_c}{k_c \chi C_3}\right)^{\frac{3}{2}} p_c^{-\frac{1}{2x}}\right]^{\frac{2x}{2x-1}}.$$

(8.2.4 – 12)

8.2.4.4. Erosion rate as a function of the velocity w_0

Inserting (8.2.4 – 11) into (8.2.4 – 3) gives the erosion rate as a function of the velocity w_0

$$\dot{m}_{er} = C_1 C_4 \, w_0^{1\,+\,[x/(2\,x-1)](3\,\mu/2\,+\,1)} = K \, w_0^n.$$

(8.2.4 – 13)

For an interpretation of the last relation the celerity (= velocity of sound) of the two phase mixture 'a' in the retarding section L_d (Fig. 8.2.16 a) has to be presented in terms of the velocity w_0.

For this purpose the following approximate relation was derived by Raabe [8.75]

$$a = k_d w_0 \left\{ [(2\,r_d)/b] \left\langle \alpha/[n(\alpha + 1)] \right\rangle + 1 \right\}^{-1/2},$$

(8.2.4 – 14)

where (Fig. 8.2.16 b) k_d determines the mean velocity w_d of the re-entrant jet by $w_d = k_d w_0$, b is the mean depth of this flow branch, r_d the mean radius of curvature this flow branch has, α the void fraction of the mixture there, n the polytropic exponent the gaseous phase has according to its equation of state $p v^n = $ const.

Assuming $\mu = 3,3$ after the test of Parkin [8.112], $x = 1,4$ for air, the exponent of the velocity w_0 in (8.2.4 – 13) becomes $n = 5,63$. This corresponds nearly to the largest value of this exponent according to the tests of Knapp [8.6].

For a growing degree of cavitation (i.e. with decreasing σ) in consequence of the then rising turbidity of the mixture, having a void fraction rising proportional to w_0 within the zone of pitting, many of the bubbles entrained may be repelled from the wall. Thus contrary to the assumption above the number of collapsing bubble may be constant. Thereby the exponent drops by 1 to 4,63.

It may be supposed also that the turbidity around the cavity increases with the velocity, and hence stimulates gas diffusion into the bubble, for which χ is proportional to w_0. This drops the exponent by the term $(3/2)[2\,x/(2\,x-1)] = 2,33$, so that then n becomes 2,1.

Assuming the celerity 'a' of the mixture to be inversely proportional to the void fraction α and this to be proportional to the velocity w_0 (by stimulating the convective diffusion). the exponent n may drop again by the term $(1/2)[2\,x/(2\,x-1)] = 0,78$ resulting in $n = 1,32$. For a very large degree of

cavitation (due to a cavitation index far below the critical), the distance between adjacent imploding bubbles becomes so small, that the celerity of the liquid $a_L = \sqrt{\varrho_L/E_L}$ responsible for the impac pressure of the imploding bubble has to be substituted by that of the mixture 'a' (8.2.4-14).

Assuming then 'a', as previously, to be inversely proportional to w_0, the exponent n drops again the term $2z/(2z - 1) = 1,5$, which leads finally to n about zero. Thereby the decrease of the expon n, according to the tests of Knapp [8.6] can be realized on the basis of reasonable physical princi shown above. Usually a wall-attached cavity with re-entrant jet consists of a sequence of alternat cavities originating from the wall and then detaching themselves and then collapsing. Here the nak eye may only observe the maximum cavity length. The cavity starts from its fixed head and its leng grows with time elapsed t by $\sqrt{at}$ (a = thermal diffusivity). Its growth ends when the jet cuts off t cavity head from the wall. As the velocity of the re-entrant jet increases with $NPSH$, the maximu cavity length L observable is decreasing with $NPSH$ increasing. The frequency of this cavi alternation is controlled by a certain Strouhal number formed by L and the undisturbed veloci

8.3. Water hammer

8.3.1. Celerity, fundamentals of method of characteristics in c, p-plane

Consider a real compressible liquid, density ϱ, bulk modulus E_L, within a straight pip having a constant cross sectional area A, diameter D, with a thin wall, thickness s smal compared with D, of elastic material, modulus of elasticity E (Fig. 8.3.1 a). A pressur pulse with cross sectional-averaged value dp propagates along the pipe axis in th x-direction relative to the liquid with celerity a.
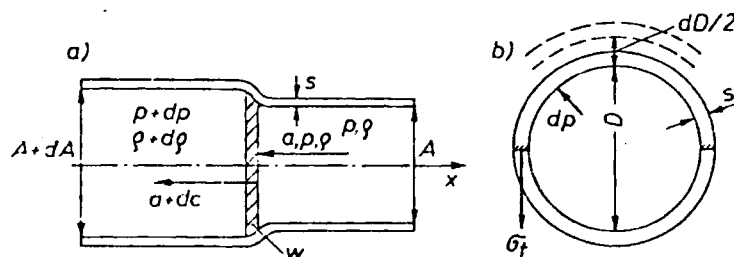
Fig. 8.3.1. Phenomena in a wav front, moving with celerity (veloci of sound) a: a) Increments of valu along the pipe axis seen by a observer in the wave front. b) Pip dilatation due to pressure incr ment.

Simultaneously disturbances of fluid density and velocity with the cross section averaged values $d\varrho$ and dc also propagate themselves in the x-direction with celerity All disturbances are assumed as time-independent.

Moreover an increment of the pipe's cross section dA propagates together with th pressure pulse dp with celerity a in the x-direction. First the problem rises to obtain th celerity as a function of the known properties of the liquid and pipe.

Obviously an observer moving relative to the fluid with celerity sees a steady motion. According Galilei's principle of relativity such a coordinate system is equivalent to a stationary one, when latter is an inertial frame of reference uniformly and rectilinearily moved. Hence assuming all th the theorems of mechanics (mass conservation, momentum theorem) can be applied to the frame reference, that moves with celerity a.

Obviously the above consideration about the equivalence of both the systems of reference hol good, if the fluid moves with constant velocity or is at rest. The latter is assumed since a consta motion of the fluid, according to Galilei's principle, cannot contribute anything to a phenomen of mechanics like celerity.

Locating now the observer in the wave front of the pressure pulse, in which all the valu p, ϱ, c, A experience a steplike increment by $dp, d\varrho, dc, dA$ (Fig. 8.3.1 a) that lasts u attenuatedly, the following is observed.

306

In front of the observer the fluid enters the wave front with celerity a. Hence the influx of mass into the shock plane is: $\dot{m} = \varrho\, A a$. To employ mass conservation imagine the wave front to be a fluid lamina with infinitesimally small thickness in the direction of the pipe axis. The mass flow leaving this lamina is: $\dot{m} + d\dot{m} = \varrho A a + d(\varrho A a)$. Mass conservation requires $d\dot{m} = 0$ or $d(\varrho A a) = A a\, d\varrho + \varrho\, a\, dA + \varrho\, A\, da = 0$.

Since the celerity a is a constant figure, the problem rises if 'da' must be cancelled or not. Here the following consideration helps. As above mentioned, also the velocity of the fluid c (now assumed as zero) is subjected to a stepwise increment dc within the wave front. As the celerity of a fluid is relative to the fluid, now the celerity within the wave front experiences a stepwise change that equals dc. Hence $da = dc$.

Keeping this in mind the mass conservation and the momentum equation for the moving observer read:

$$d(\varrho\, a\, A) = 0 \quad \text{or} \quad \varrho\, A\, dc + a\, A\, d\varrho + \varrho\, a\, dA = 0, \tag{8.3-1}$$

$$dp\, A + d(\varrho\, A\, a^2) = 0 \quad \text{or} \quad dp\, A + a^2 A\, d\varrho + 2\varrho\, a\, A\, dc + \varrho\, a^2\, dA = 0. \tag{8.3-2}$$

Elimination of dc gives the celerity as

$$a = [d\varrho/dp + (\varrho/A)\, dA/dp]^{-1/2}. \tag{8.3-3}$$

Obviously this relation holds good for a pipe with arbitrary cross sectional area A, constant along the pipe axis.

Application of (8.3-3) to a cylindrical pipe: Now $A = (\pi/4)\, D^2$, $dA = 2(\pi/4)\, D\, dD$. Obviously the increment of tangential strain $d\varepsilon_t = dD/D$. Hooke's law for a one-dimensional state of stress in the pipe wall, modulus of elasticity E', reads

$$\varepsilon_t = \sigma_t/E', \tag{8.3-4}$$

where ε_t is the tangential strain, σ_t the tangential tensile stress. Obviously $dD = D\, d\varepsilon_t$ and with (8.3-4) and the equilibrium on the thin-walled pipe, $\sigma_t = pD/(2\,s)$ (Fig. 8.3.1 b), $dD = D^2\, dp/(2\,s\,E')$ and $dA = A\,(D/s)\, dp/E'$. This reduces the second term in (8.3-3) to $(\varrho/A)\, dA/dp = (\varrho/E')(D/s)$.

The first term in (8.3-3) follows from the equation of state

$$d\varrho/dp = \varrho/E_L. \tag{8.3-5}$$

With the above, the celerity of (8.3-3) is converted into

$$a = \{\varrho\,[1/E_L + (1/E')(D/s)]\}^{-1/2}. \tag{8.3-6}$$

The one-dimensional state of stress according to (8.3-4), in which E' corresponds to the real modulus of elasticity of wall material, exists in a pipe, that is supported at both its ends by a frictionless stuffing box. When the pipe is closed at one of its ends, but can freely expand there, then E' is related to the real value E by: $E' = E/(1 - m/2)$ with $m = 0,3$ as Poisson's ratio. In the case, the pipe is axially fixed at both its ends: $E' = E/(1 - m^2)$, (see also [8.84; 8.85]). In general E' depends on the support of the pipe.

- Provisional measurement of the celerity: Imagine a penstock, whose length is L between its shut off valve at the lower end and its upper end, usually open into a head reservoir or surge tank. Any instantaneous reduction of the valve's cross sectional area by a corresponding adjustment induces a pressure wave, which propagates with celerity 'a' towards the upper end (Fig. 8.3.2 a and b). There it is reflected as a negative pressure wave. With the so-called reflection time T_r measured by the indication of a manometer, elapsed since the intentional sudden throttling of valve, the celerity yields

$$a = 2L/T_r. \tag{8.3-7}$$
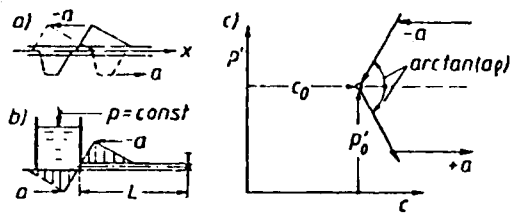
– The pulses of density $d\varrho$, pipe expansion dA and velocity dc, due to the pressure pulse. The density wave $d\varrho$, relatively small in the case of water follows from (8.3–5). The "breathing" of the cross sectional area results from the above as (Fig. 8.3.1 b) $dA = A (D/s) dp/E'$ and that of diameter as $dD = D^2 dp/(2 s E')$.

The important velocity pulse due to dp results from (8.3–1) after multiplying through with dp on the right hand side as $dc = - (a dp/\varrho)[d\varrho/dp + (\varrho/A) dA/dp]$. This gives with respect to (8.3–3)

$$dc = - (1/(a \varrho)) dp. \tag{8.3–8}$$

This last relation may be obtained more easily from the one-dimensional equation of motion of the fluid in the direction of pipe axis: $(1/\varrho) \partial p/\partial x + \partial c/\partial t = 0$, when, after Galilei's principle, this is described from an inertia frame of reference moving with celerity a in the x-direction and hence $\partial x = a \partial t$.

(8.3–8) holds for a pressure pulse, travelling with the celerity a in the direction of c and hence also of x. Consequently for a pressure pulse moving with a in the $- x$-direction

$$dc = (1/(a \varrho)) dp. \tag{8.3–9}$$

After Schnyder [8.133] and Bergeron [8.134] the integration of both the last relations under the assumption of a constant celerity 'a' for an observer moving relative to the fluid with the celerity $\pm a$ in the $+ x$-direction (positive in the flow-direction), yields straight lines (characteristics) in a p, c-graph (Fig. 8.3.2 c) as the possible values p and c assigned to each other, seen by such an observer. This feature is used by the method of characteristics of Schnyder and Bergeron in the p, c-plane, discussed later on in more detail.

8.3.2. Fundamentals of method of characteristics in the x, t-plane

For a stationary observer the mass conservation due to a fluid-filled pipe element, volume $A\,dx$, reads

$$\varrho A \partial c/\partial x + c A \partial \varrho/\partial x + c \varrho \partial A/\partial x + A \partial \varrho/\partial t + \varrho \partial A/\partial t = 0. \tag{8.3–10}$$

Assuming barotropic relations, some derivatives may be reduced to p:

$$\partial \varrho/\partial x = (\partial \varrho/\partial p) \partial p/\partial x, \quad \partial \varrho/\partial t = (\partial \varrho/\partial p) \partial p/\partial t, \quad \partial A/\partial t = (\partial A/\partial p) \partial p/\partial t,$$
$$\partial A/\partial x = (\partial A/\partial p) \partial p/\partial x.$$

Putting this in (8.3–10), respecting a and dividing by a gives

$$\varrho a \partial c/\partial x + (c/a) \partial p/\partial x + (1/a) \partial p/\partial t = 0. \tag{8.3–11}$$

Neglecting the gravity term, which may be superimposed later, the one-dimensional equation of motion in the x-direction (pipe axis) for a fluid element in a pipe reads

308

$$\varrho c\, \partial c/\partial x + \varrho\, \partial c/\partial t + \partial p/\partial x = -\,4\tau_0/D,\qquad\qquad (8.3-12)$$

where τ_0 is the wall shear, standing for the internal loss.

Adding both the last relations and then multiplying by '$a\,dt$' gives

$$a\varrho(a + c)\,dt\,\partial c/\partial x + a\varrho\,dt\,\partial c/\partial t + (a + c)\,dt\,\partial p/\partial x + dt\,\partial p/\partial t$$
$$= -\,4a(a + c)\,dt\,\tau_0/[(a + c)\,D].\qquad\qquad (8.3-13)$$

The flow now is referred to a x_+-coordinate system, moving relative to the flow with the celerity 'a' in the flow direction ($+ x$-direction). This system has the velocity $(a + c)$ relative to a stationary frame of reference with coordinate x. Hence (Fig. 8.3.3 a)

$$x_+ = x + (a + c)\,t.\qquad\qquad (8.3-14)$$

The time elapsed t is counted from the instant, when x and x_+ coincide. The line

$$x_+ = x_+ (t)\qquad\qquad (8.3-15)$$

is defined as the positive characteristic within the x_+, t-system. The celerity 'a' may vary along the pipe axis, when E' or D/s changes. Hence, strictly speaking, the relation (8.3-14) holds only for the time interval dt in the form

$$dx_+ = (c + a)\,dt.\qquad\qquad (8.3-16)$$

Substituting this in (8.3-13) brings with $\partial x = \partial x_+$, and then accounting for $dc_+ = (\partial c/\partial x_+)\,dx_+ + (\partial c/\partial t)\,dt$ and $dp_+ = (\partial p/\partial x_+)\,dx_+ + (\partial p/\partial t)\,dt$, the p, c-characteristic in the x_+-system, now with the pipe loss, reads

$$dp_+ + a\varrho\,dc_+ = -\,[a/(c + a)]\,4\tau_0\,dx_+/D.\qquad\qquad (8.3-17)$$

As (8.3-8), but now referred to a real fluid with internal friction and moving in the $+ x$-direction with velocity c, the last relation combines the pressure increment dp_+ and the corresponding velocity increment dc_+ for an observer, moving with celerity 'a' in the $+ x$-direction relative to the fluid. Similarily for an observer, moving with celerity 'a' relative to the fluid in the $- x$-direction along the so-called negative characteristic (see Fig. 8.3.3 a), infinitesimally defined by

$$dx_- = (c - a)\,dt,\qquad\qquad (8.3-18)$$

the relation that now corresponds to (8.3-17) is taking the form

$$dp_- - a\varrho\,dc_- = [a/(c - a)]\,4\tau_0\,dx_-/D.\qquad\qquad (8.3-19)$$

Assuming quasi steady flow, the wall shear stress can be reduced to the pipe loss coefficient λ (see (5.4-14)) by

$$\tau_0 = (\lambda/8)\varrho|c|c.\qquad\qquad (8.3-20)$$

Fig. 8.3.3. Characteristics in the x, t-plane. a) Characteristics ζ_+, ζ_- in the x, t-system of an observer moving relative to the fluid, velocity c, with celerity $+ a$, $- a$ in the x-direction. b) Application of the characteristics-method by means of a prescribed grid of points, whose state (p, c) is known, or to be determined. Δt: $t_C - t_A$, $t_B - t_C$.

309
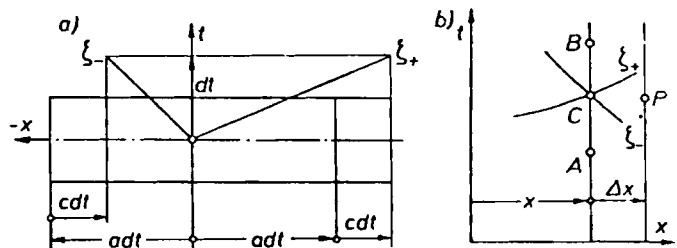
Thus (8.3-17), (8.3-19) are converted into

$$dp_+ + a\varrho\,dc_+ = -\varrho\,[a/(c+a)]\,dx_+\,[\lambda/(2\,D)]|c_+|c_+,$$ (8.3-2

$$dp_- - a\varrho\,dc_- = \varrho\,[a/(c-a)]\,dx_-\,[\lambda/(2\,D)]|c_-|c_-.$$ (8.3-2

8.3.3. Application of method of characteristics in x, t-plane

Assume, that x and t for the different stations A, B, C of a pipe are known along the lin x, but unknown and required along the line $x + \Delta x$ (Fig. 8.3.3 b) in the characteristi x, t-plane. The characteristics ζ_+, ζ_-, as defined by

$$dx_+ = (c+a)\,dt = \zeta_+\,dt, \qquad dx_- = (c-a)\,dt = \zeta_-\,dt,$$ (8.3-2

are known at the station C, but unknown at the stations on the line $x + \Delta x$. The ma aim of the following computation is the determination of pressure p and correspondin velocity c at the station P, when p and c are known at the stations A, B, C and when t coordinates of P in the x, t-plane are fixed. It follows *de Bernardinis* et al. [8.99].

On the stations, A, B, C as subscripts are added to the variables. The characteristi ζ_-, ζ_+ through the point P intersect the line x at the stations R and S. From this t periods t_R and t_S follow by an extrapolation as (Fig. 8.3.3 b)

$$t_R = -(x_P - x_R)/\zeta_{+c} + t_P, \qquad t_S = -(x_P - x_S)/\zeta_{-c} + t_P.$$ (8.3-2

With

$$\Delta x/\Delta t = \vartheta, \qquad \zeta_{+c} = \Delta x/(t_C - t_R), \qquad \zeta_{-c} = \Delta x/(t_S - t_C),$$ (8.3-2

the values p_R, p_S, c_R, c_S result from 4 linear equations, written as follows in matr notation

$$\begin{Bmatrix} p \\ c \end{Bmatrix}_R = \begin{Bmatrix} p \\ c \end{Bmatrix}_C [1 - \vartheta\zeta_{+c}^{-1}] + \begin{Bmatrix} p \\ c \end{Bmatrix}_A \vartheta\zeta_{+c}^{-1},$$ (8.3-2

$$\begin{Bmatrix} p \\ c \end{Bmatrix}_S = \begin{Bmatrix} p \\ c \end{Bmatrix}_C [1 - \vartheta\zeta_{-c}^{-1}] + \begin{Bmatrix} p \\ c \end{Bmatrix}_B \vartheta\zeta_{-c}^{-1},$$ (8.3-2

in which p_A, c_A, p_C, c_C, p_B, c_B are known. With p_R, p_S, c_R, c_S, the pressure p_P and velocity c_P follow by (8.3-21), (8.3-22) as

$$p_P - p_R + a\varrho(c_P - c_R) = -\{\varrho\,a\,\lambda/[(c_R + a)2\,D]\}\,|c_R|c_R(x_P - x_R),$$ (8.3-2

$$p_P - p_S + a\varrho(c_P - c_S) = -\{\varrho\,a\,\lambda/[(c_S + a)2\,D]\}\,|c_S|c_S(x_P - x_S).$$ (8.3-2

Herein x_P, x_R, x_S, a, p_R, c_R, c_S and $\lambda/(2\,D)$ are known. Thus p_P and c_P can be determin from the last two relations.

8.3.4. The celerity in a two phase mixture

When the pressure falls short of its critical value, evaporation creates two phase flow. T same may also occur when the liquid, saturated with dissolved gas, passes a low press zone. Here the gas may be released so as to have a two phase mixture.

In the following the prediction of the celerity in two phase flow is introduced accord to a method proposed by *Reali* and *Fanelli* [8.97].

Assumptions: A liquid split into two phases, the one of which is both gaseous an vapour in its state, the other is liquid. The liquid is mixed with gas- and vapour-fi bubbles, having the same effective radius R. The following nomenclature is used: p is

310

pressure in the liquid phase, p_g that in the gas, p_v that in the vapour phase, p_m that of the mixture, v_m is the specific volume of the mixture, v_g and v are "specific volumes" of likewise gaseous and vapour phase (v_g) and the liquid phase (v) each referred to the unit of mass of the mixture. Hence the pressure of the mixture

$$p_m = p\,v/v_m + (p_g + p_v)\,v_g/v_m .\tag{8.3-30}$$

For stiffly assumed walls the celerity a_m of the mixture

$$a_m = (\partial\varrho_m/\partial p_m)^{-1/2} = (\varrho_m\,\Gamma_m)^{-1/2} ,\tag{8.3-31}$$

$$\Gamma_m = -(1/v_m)\,|\partial v_m/\partial p_m|_T .\tag{8.3-32}$$

Contrary to the usual thermodynamic procedure, the absolute temperature T is assumed as constant for $\partial v_m/\partial p_m$. This is in accordance with observations [8.97].

Additional assumptions:
a) Gravity negligible, gas and vapour phase are uniformly distributed over N spherical bubbles in the unit of mass of mixture, radius R. Hence the "specific volume" of the gas phase $v_g = (4/3)\,\pi\,NR^3$. Thus

$$dv_g = 4\pi N R^2\,dR .\tag{8.3-33}$$

b) The interface between gas and liquid has a surface tension σ. This requires $p = p_v + p_g - 2\sigma/R$. Hence at $\sigma = $ constant

$$dp = dp_v + dp_g + (2\sigma/R^2)dR .\tag{8.3-34}$$

c) Gas and vapour follow the perfect gas law. Thus with k as gas constant and M_g and M the molecular masses of gas and vapour: $p_g = k\varrho_g T/M_g$, $p_v = k\varrho_v T/M$. Hence

$$dp_g = (kT/M_g)\,d\varrho_g,\tag{8.3-35}$$

$$dp_v = (kT/M)\,d\varrho_v .\tag{8.3-36}$$

d) The mass in each bubble is conserved. Thus $\varrho_g R^3 = $ const or

$$R\,d\varrho_g + 3\varrho_g\,dR = 0.\tag{8.3-37}$$

e) The masses of liquid and vapour plus gas within the unit mass of mixture are conserved. Hence $\varrho v + \varrho_v v_g = $ const or

$$\varrho\,dv + v\,d\varrho + v_g\,d\varrho_v + \varrho_v\,dv_g = 0.\tag{8.3-38}$$

Note that here ϱv is not "one" but kg liquid/kg mixture.
f) Pressure and density of the liquid obey an empirical equation of state. With bulk modulus E_L,

$$d\varrho = (\varrho/E_L)\,dp .\tag{8.3-39}$$

g) Liquid and vapour are in thermodynamic equilibrium. Therefore the chemical potentials are the same. Hence for $T = $ const:

$$\varrho_v\,dp = \varrho\,dp_v .\tag{8.3-40}$$

The following unknown X_i appear in the linear inhomogeneous system, represented by (8.3-33) through (8.3-40):

$$X_1 = d\varrho/dp, \quad X_2 = d\varrho_v/dp, \quad X_3 = d\varrho_g/dp, \quad X_4 = dp_v/dp, \quad X_5 = dp_g/dp,$$
$$X_6 = dv/dp, \quad X_7 = dv_g/dp, \quad X_8 = dR/dp .$$

Once this system has been solved, the celerity follows as

$$a_m = \sqrt{\frac{(v+v_g)\left\{v+\left[p-\dfrac{p_v+(p_g+p_v)v_g}{v+v_g}\right]X_6-\left[\dfrac{pv-(p_g+p_v)v}{v+v_g}\right]X_7+v_g(X_4+X_5)\right\}}{-(X_6+X_7)}}$$

(8.3-4)

Typical examples of a_m can be seen in the a_m graph vs x at constant bubble radius R. Here x depends on the void fraction $\alpha = v_g/v$ by $x = \log_{10} v/v_g$. Note the sharp drop of a_m in a very small range of very small values v_g/v (Fig. 8.3.4), which is a typical feature of any two-phase-flow even if this gradient depends on the flow type, e.g., dispersed flow, plug flow, slug flow, stratified flow. See also [8.64; 8.98].
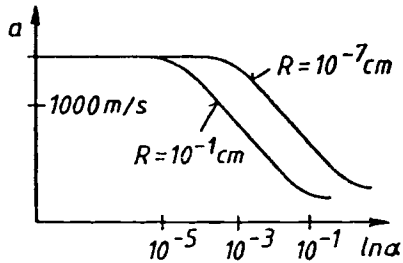
Fig. 8.3.4. Celerity of gas water mixture vs ln α (where α is the void fraction: $\alpha = v_v/(v_v + v_L)$) at different radii R of spherical gaseous and vaporous nuclei. From *Fanelli* and *Reali*, [8.97]

8.3.5. Influence of evaporation and diffusion

According to the last relation, the celerity of a mixture depends strongly on the void fraction, which contrary to the above section is now written in more detail as $(V_g + V_v)/V_m$ where V_g is the gas part and V_v the vapour part of the void volume, and V_m the volume of the mixture due to the void.

For a void with impermeable walls, not subjected to gas diffusion and evaporation, the void's volume and hence the void fraction depends on the pressure by an equation of state. This may have the form $p(V_g + V_v)^n = const$.

For a void, partly subjected to evaporation, or condensation, but not to diffusion, the exponent n can be approximated after *Raabe* [8.30] by the molecular masses M_g, M_v of gas and vapour and the real masses of gas and vapour m_g and m_v, contained within the average void considered by means of

$$n = 1 + m_v M_g/(m_{g0} M_v).$$

(8.3-5)

In the case of evaporation, the growth of the void is governed by the differential equation of heat transfer (8.2-19).

The volume of a spherical void, radius R, that contains a gas mass m_g and a vapour mass m_v, at an absolute temperature T and the total pressure p, can be determined, if gas and vapour follow the behaviour of an ideal gas, and have the corresponding gas constants k_g and k_v. Thus

$$V = V_g + V_v = (4/3)\pi R^3 = (k_g m_g + k_v m_v) T/p.$$

(8.3-6)

The increment Δm_v of the vapour mass m_v during a certain time t elapsed and due to evaporation of the liquid, that surrounds the bubble, having a latent heat Λ, a specific heat c_L, a density ϱ and a superheat $T_L - T$, can be achieved by balancing the heat content within the thermal boundary layer of the bubble, thermal diffusivity a, with the

required for evaporation. Hence, with a thickness $4\sqrt{at}$ of thermal boundary layer

$$\Delta m_v = 8\pi R^2 c_L \varrho (at)^{1/2} (T_L - T)/\Lambda.$$ (8.3-44)

The increment Δm_g of gas mass by diffusion during a certain time elapsed t can be obtained from the supersaturation $C - C_0$ of the diffusion boundary layer, thickness $4\sqrt{Dt}$, mass diffusivity D, adjacent to the bubble wall, with dissolved gas. Hence

$$\Delta m_g = 8\pi R^2 (C - C_0)(Dt)^{1/2},$$ (8.3-45)

where C is the gas mass dissolved per unit volume, existing in the instant t, and C_0 the value C due to saturation, that follows from *Henry'* law $C_0 = \text{const } p$, [8.6].

The role of diffusion during water hammer was highlighted by *Oldenziel* [8.35].

8.3.6. Boundary conditions in the p, c-plane, loss influence

At the end of a pipe attached to a larger reservoir (surge tank), the pressure is given by the elevation of the free water level above the pipe connection and hence is more or less constant. Here, a positive pressure wave, that arrives at this station is reflected as a negative pressure wave.

When the pipe diameter changes in stepwise manner, the pressure is the same for both the adjacent parts of the pipe. In bifurcations, the pressure, which acts in each branch, is the same. In bifurcations and at a station, with a change of the cross section of the passage, the velocity must obey mass conservation with due respect to eventual contraction or limited diffusion. In the latter case the pressure acting on the adjacent branch must be diminished by the corresponding shock loss.

When the flow passes a special device or machine, pressure drop between inlet and outlet of the device, and the mean velocity of the through flow, have to be related to each other by the characteristic of this device with a certain sense of throughflow.

In the case of a valve or the nozzle of a Pelton turbine this relation reads

$$\Delta p = k_1 c^2,$$ (8.3-46)

where k_1 depends on the position of a regulating device (provided the apparatus has one). In a PT the pressure past the nozzle is constant. Hence the above relation yields the pressure upstream of the nozzle or at the lower end of the penstock.

In reaction fluid machines the above pressure drop depends also on the speed n of the machine. Thus the characteristics of the machine with a certain flow c_{op} at its bep, under a gate opening α_3, in the case of a turbine is given by the following parabola-like function

$$\Delta p = -k_0 n^2 + (k_1 + k_2 \cot\alpha_3)nc + k_3 n(c - c_{op})^2 + k_4 c^2$$
$$+ k_5 n^3 + k_6 c^{-1}.$$ (8.3-47)

With the k_i as design parameters, both the first terms are due to the change of whirl velocity component in the rotor at a certain gate opening angle α_3, the third term is due to the shock loss at rotor inlet, the fourth term due to the loss in the flow passages, the fifth term due to disk friction loss and the last term due to leakage loss.

Once the pressure at the exit of the turbine is known from the elevation of tailwater above the exit, then the pressure at the inlet of the turbine follows from the latter and Δp.

If the machine has speed regulation. and supplies an electric grid. 'n' is retained. On
during start up or after disconnecting the set from the electric grid. the speed n varies. I
this case the angular acceleration $d\omega/dt$ as a scale for the speed rate n results from t
equation of motion of the set with its moment of inertia Θ and its eventual excess torq
M by means of

$$M = \Theta \, d\omega/dt.$$ (8.3–4

In the case of load rejection the excess torque corresponds to that of the machine an
follows from flow, head, efficiency of its instantaneous working point (gH, Q) by ·

$$M = \varrho \, Q \, gH \, \eta/\omega.$$ (8.3–4

The pressure drop Δp within machines or devices (especially valves) depends also on th
internal loss. The latter, as empirical datum, is only known from stationary tests. Th
same holds also for the pipe loss coefficient λ. This influences the pressure p_+ accordin
(8.3–21) on the wave front as a function of the velocity c_+ there. Assuming consta
celerity 'a' along a pipe section, length x_+, the pressure p_+ and the velocity c_+ on th
wave front. moving with 'a' in x_+-direction depend after (8.3–21) on the pipe loss alo
a certain stretch. covered in the time interval $t = x_+/(c + a)$. x_+ begins at a station, whe
the pressure p_0 and the velocity c_0 on the wave front are known. Hence at $c = $ consta

$$p_+ = p_0 - \varrho a(c_+ - c_0) - [1/(2D)]\varrho \int_{x_- = 0}^{x_-} [a_i(a + c)]\lambda |c_+| c_+ \, dx_+ .$$ (8.3–5

Here any evaluation of the loss influence needs knowledge of the loss coefficient λ due
unsteady flow. Usually the pipe velocity c can be neglected in comparison with th
celerity a. Since the pipe loss is small as compared with the head, c_+ and λ are prelim
narily assumed as constant along x_+, which may be corrected later on by trial and erro
Hence

$$p_+ = p_0 - \varrho a(c_+ - c_0) - [\lambda \varrho/(2D)]x_+ |c_+| c_+ .$$ (8.3–5

Usually x_+ is extended over the whole pipe length from the machine to the reservoir
surge tank heading the pipe.

Again here the question arises if the loss coefficient λ can be taken from steady flow test results. T
decision must be based on pulsating and unsteady pipe flow. Many investigations by means o
Laser velocimeter have been carried out in such a flow during the last 13 years in the lab of the ch
für Hydraulische Maschinen und Anlagen TU Munich, Federal Republic of Germany by Kin
[8.135]. and Hartmer [8.136]. In the latter case also the Reynolds stresses due to $u_i' v_j'$ have be
measured by two Laser beams simultaneously. Moreover wall influence has been eliminated by us
a fluid with the same refractive index as the block of plane-faced plexi glass around the measur
section.

Special theoretical investigations on this subject have been carried out also by H. Brekke, Kvaer
Brugg [8.89; 8.107]. The flow concentration on a small annular section close to the pipe wall,
so-called Richardson effect [8.137] is a typical feature of real unsteady and pulsating flow as it m
occur under the influence of water hammer especially under very low flow rate. This effect accum
lates and concentrates the loss close to the wall and increases also the loss coefficient by the t
large strain rates of flow. By internal friction all disturbances are fading.

The largest pressure surge due to water hammer appears shortly before cutting-off the flow. Th
due to the steep slope the characteristic of the machine has in the p, c-plane shortly before shut do
There the resulting highest pressure induced by water hammer may be increased by an additio
sloping of the machine's characteristic caused by enlarged loss due to unsteady flow.

One special feature of pulsating unsteady flow is the fact, that the velocity may change its direc
within a certain flow passage. On the one hand this results from a coincidence of the p

314

relationship between pressure and velocity close to the wall. On the other hand this follows from a 90° phase shift between velocity and pressure vs time at the pipe axis, provided the phase relationship of the pressure is the same over the whole cross section (a known consequence of the equation of motion).

The first results from the proportionality of pressure and velocity close to the wall in the absence of inertia terms yielding $\partial p/\partial x = \eta \partial^2 c/\partial x^2$. The second follows from the exclusive balance between pressure drop and inertia force on the pipe's centre line yielding $(1/\varrho)\partial p/\partial x = -\partial c/\partial t$.

8.3.7. Examples of the method of characteristics in the c, p-plane [8])

Consider a pipe flow of constant celerity a and vanishing wall shear stress τ_0. After (8.3-21), (8.3-22) the so-called positive (+) and negative (−) characteristics in a p, c-plane due to pressure waves, moving with $+ a$ and $- a$ in x-(pipe axis) direction read as follows

$$p_+ = - a\varrho(c_+ - c_{0+}) + p_{0+},$$ (8.3-52)

$$p_- = a\varrho(c_- - c_{0-}) + p_{0-}.$$ (8.3-53)

For the interpretation see the remarks due to (8.3-9). Hence the possible state p, c for an observer, moving on the wave front with $\pm a$ in the x-direction (flow direction) is on a straight line in a p, c-plane, that has a slope $\mp a\varrho$ with the c-axis. The definite position of this straight line (the so-called characteristic) is known only, when pressures p_{0+}, p_{0-} and corresponding velocities c_{0+}, c_{0-} are known (Fig. 8.3.2 c).

An application of the above is illustrated by an example. In an impulse turbine (Fig. 8.3.5) the state on the lower end U_i of the penstock (horizontal since gravity effects may be superimposed later on) is given by a parabola $p = k_1 c^2$. This follows from the law of the spouting velocity on the section of nozzle and the linkage of this velocity to that on the lower pipe section by continuity. Gauge pressure is applied for convenience.

The state at the upper end O_i of the penstock is dictated by the assumed constant elevation of the nonpressurized level above the pipe connection and hence is a constant pressure p_0'. Accounting for the friction loss of the pipe on the basis of (8.3-51) the latter may be imagined to be concentrated in a throttle upstream of the upper end of the penstock between the station O_i' with $p_{O_i}' = $ constant and the station O_i with a flow-dependent pressure drop Δp against O_i' being $\Delta p_l = \zeta c_i^2$, where ζ is the loss coefficient $\varrho \lambda L/(2 D)$ of the whole pipe.

The graphical procedure is pursued in adequate time intervals. As such the time of travel of a wave $T_L = L/a$, to cover the penstock length L with a mean celerity, 'a' fits mostly. Hence let the subscript at the station O_i and U_i indicate the multiple of T_L after starting the closing of the needle. Then obviously the station O_1' on the upper end of the penstock coincides with U_0' on the lower end at the instant, the needle starts closing. Hence the state U_2' on the lower end, at the instant $t_2 = 2 T_L$ results from the intersection of the negatively inclined positive characteristic, due to a wave moving in flow direction, across the point O_1' with the parabola of the needle due to $t_2 = 2 T_L$.

In the so-called "linear closure" the velocity due to the intersection point of the parabola with the constant pressure line p_0 decreases linearly vs time down to zero. Performing such a linear closure between subsequent needle positions and beginning with the largest openings and then continuing to the smaller ones, the pressure surge due to U_2' at the lower end obviously increases as the opening decreases.

---

[8]) In this subchapter, the method of characteristics in the p, c-plane is applied on the admissible assumption that pipe velocity c is negligible compared with celerity a.

Hence the largest pressure surge on the lower end of the penstock results (provided linear closure with the same closing rate) when the turbine is closed completely within $2\,T_L = 2\,L/a$, the so-called reflection time T_r (see (8.3–7)). This gives the highest water hammer blow, the so-called *Joukovsky* shock, described 1898 [8.138] but sometimes also ascribed to *Allievi*, who published this later in 1903 [8.139]

$$\Delta p = \varrho\, a\, c .$$ (8.3–54)

Usually this pressure rise is only attained, when the turbine is shut down from smaller opening. When the shut down period lasts longer than the reflection time, a further pressure rise on the turbine is suppressed by the negative pressure wave, caused by the reflection of the originally positive wave on the upper open end of the penstock.

Usually the shutoff rate of a valve or gate before a turbine is lowered in steps (at least in two steps) when approximating to its closing position. A reasonable timing of the shut down would be such as to cause a constant pressure surge from any position of gate or valve.

To date the following upper limits of water hammer-induced pressure surge Δp in relation to static pressure p_0 are accepted to depend on the plant's head: $\Delta p/p_0 = 0{,}2$ to 2 for $H = 100$ m to 5 m

Where the pressure falls short of its critical value by a pressure wave, that is reflected as an underpressure wave, the penstock wall has to withstand buckling. Such stations on the penstock are usually located at the upper end near the surge tank. Also an emergency device for sudden aeration may prevent a water column separation and its subsequent dangerous collapse due to reversed water hammer. Such a snifting valve, operated by the gate ring in the case of a rapid shut down, is usually applied on the head cover of Kaplan turbines.

→ The time step procedure for an impeller pump during valve closure (Fig. 8.3.6): Here again the state on the lower end of the penstock U follows from the state at the upper end O at an instant earlier by the wave travel time L/a (required to cover the penstock length L with celerity a).

Fig. 8.3.6. Scheme of comput-
ing transients in case of failure
of impeller pump drive (e.g.,
(pump-turbine at pumping). a)
Procedure by characteristics-
method in the p, c-plane with
and without closure of the main
valve on the pressure side of the
pump (between U and P, see b))
in the pump range ($c > 0$) and
brake range Br ($c < 0$). g_2, g_1
characteristics for states p, c
moving with celerity $+ a$, $- a$
in x (c)-direction. Subscripts see
Fig. 8.3.5. b) Scheme of pump,
penstock, valve; penstock loss
concentrated between O' and O.
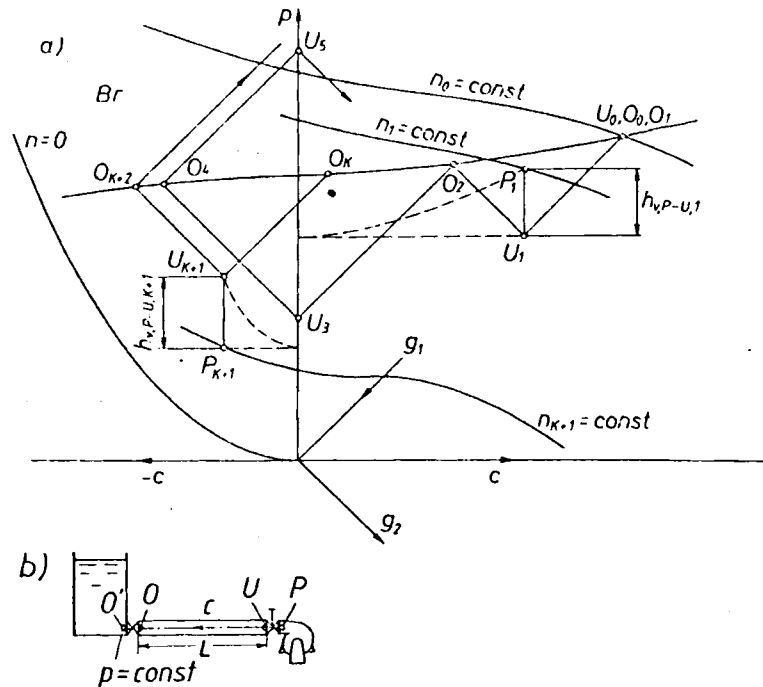
Hence for an impeller pump, with its positive flow from the lower end to the upper end,
the state on the lower end U_{k+1} at the instant t_{k+1} ($(k + 1) T_L$ after cutting out pump
drive) follows from the "state" O_k at the time t_k on the upper end of the penstock.

In this case the straight characteristic according to (8.3–53), which crosses O_k, intersects
the characteristic of the pump with its speed n_{k+1} (now variable in consequence of the
assumed cut out of the drive) at the instant t_{k+1} (Fig. 8.3.6). When the throttle valve is
located upstream of the impeller, the intersection of the straight characteristic (8.3–53)
coming from O_k occurs at a point U_{k+1} (Fig. 8.3.6 shows this for $k = 0$) with a pressure
drop due to the instantaneous loss in the valve $\Delta p_{k+1} = K_{k+1} c_{k+1}^2$ against the point P_{k+1}
on the characteristic of the pump at the instant t_{k+1} with the speed n_{k+1}. Continuity
requires that P_{k+1} and U_{k+1} have the same velocity c_{k+1}. The parameter K_{l+1} of the
instantaneous valve characteristic depends on its instantaneous position (opening) and
the sense of throughflow.

The instantaneous speed n_{k+1} of the pump results from the speed n_k, a period T_L earlier,
from the braking torque on the impeller (taken from the characteristic or calculated from
qH, Q, η, if available) M_{k+1} and M_k due to the instants t_{k+1}, t_k and the moment of inertia
of the set θ, by means of the set's equation of motion, which reads in terms of angular
velocity $\omega = \pi n/30$ (instead of n rpm)

$$\omega_{k+1} = \omega_k - (T_L/2\theta)(M_k + M_{k+1}). \tag{8.3–55}$$

Other examples: Fig. 8.3.7a shows a failure of pump drive together with a throttling of the main
valve during pump operation. The following is seen. Owing to the inertia of the rotating set, the
pressure at the lower pipe end preliminarily falls short of its original value. This is later on followed
by pressure rises above the original pressure. By the actuation of the valve yet during the normal
pump regime, the pressure drop on the lower end U of the pipe is enlarged compared with an
operation without actuating the valve. The diagram contains also the lines of constant torque.

Fig. 8.3.7b shows the consequences of a pump drive failure in the brake field of the pump under
reversed flow. Contrary to the previous example, here the pressure drop at the lower pipe end is
somewhat smoothed. Fig. 8.3.7c shows the shut down of a turbine supplying a grid by itself to zero
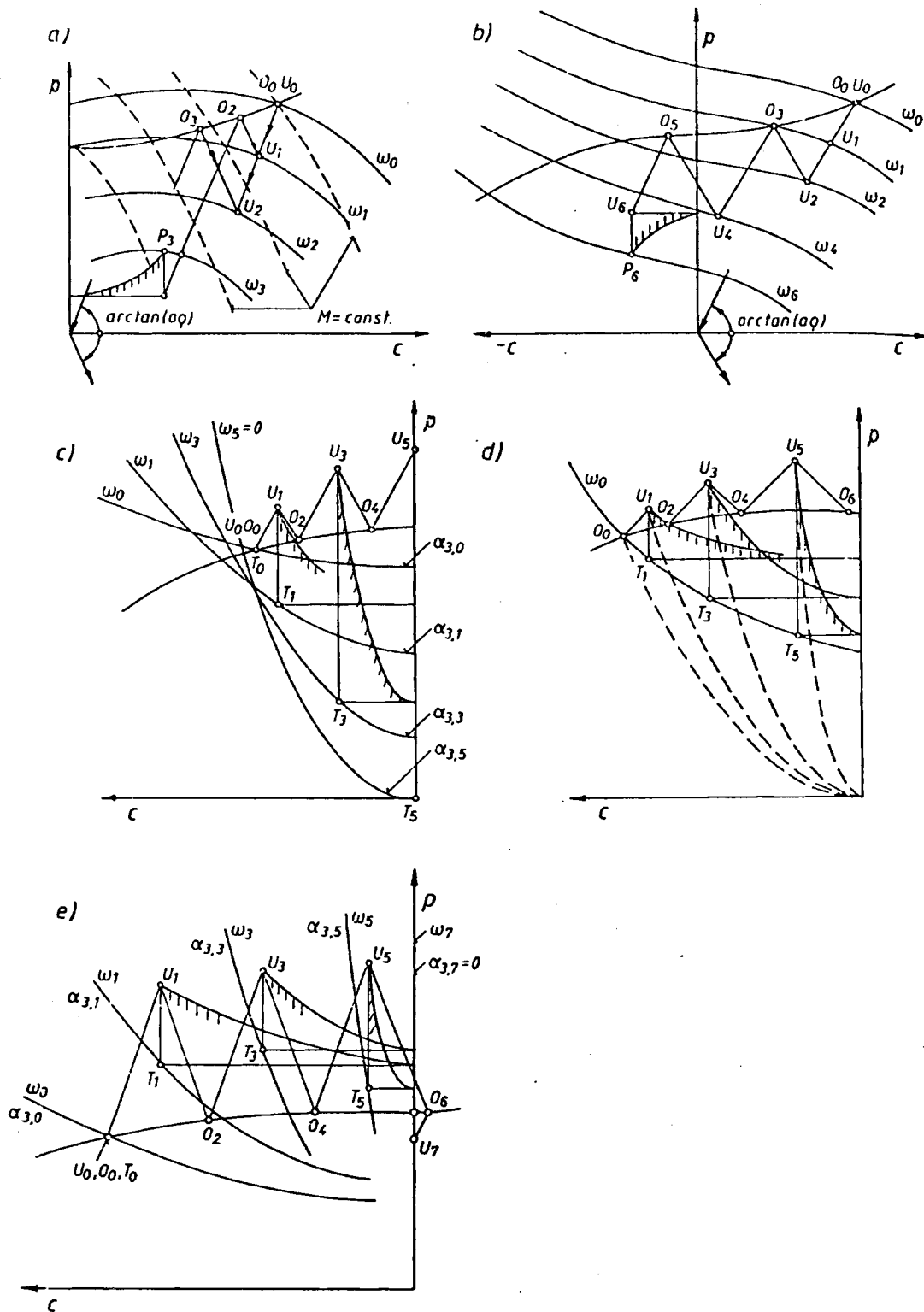
Fig. 8.3.7. Various examples of prediction of transients in reaction machines by means of the me
of characteristics in the p, c-plane. a) Drive failure on pump. Speed drop with respect to fly ν
moment and braking torque, shut down of main valve whilst working as a pump. b) The same
shut down of main valve somewhat retarded whilst working as a brake. c) Shut down of tu
without disconnection from the grid, when this is supplied by the set itself (insular operation)
hence with speed slowing down. d) The same but with a large grid and retaining the grid conne
and hence the speed. (changing from turbine to pump operation of a ternary set). e) Shut do
turbine but disconnecting the set from the grid and hence raising the speed.

318

speed by means of a synchronous closing of gate and main valve (indicated by the hatched parabola $p_i = k c_{ii}^2$ where k depends on the timing of shut down) without disconnecting the set from the grid. Generally pressure rise at the lower pipe end, speed dropping.

Fig. 8.3.7d shows a closure of gates under constant speed. This case may happen in a ternary set, when changing quickly from turbining to pumping. Also here generally pressure rises at the lower penstock end.

Fig. 8.3.7e shows the same as in Fig. 8.3.7c but with disconnection of the set from the electric grid. Now speed rising.

8.3.8. Characteristic method in the c, ω-plane

The disadvantage of a water hammer computation in the p, c- or the related Ψ, φ- or H, Q-plane exists for pumps in the fact, that the brake and turbine zone overlap each other.

Therefore a point of the H, Q-plane is not always assigned unequivocally to a definite operating point of a machine. This trouble can be avoided by the application of the ω, c- (or n, Q-)graph (Fig. 8.3.8). This is especially advisable, when the machine operates at quickly varying speed at start up or run down. In this graph any point of the plane is definitely assigned to a special operation of the machine.

The question arises: How the straight characteristics of the p, c-plane should be replaced? For this purpose consider again the positive characteristic in the c, p-plane in its differential form without losses (8.3 - 21):

$$dp_+ + \varrho a\, dc_+ = 0. \tag{8.3-56}$$

The increments dp_+ and dc_+ due to $dx_+ = (a + c)\, dt$ can be written down in a more expanded manner

$$dp_+ = (\partial p/\partial x)(a + c)\, dt + (\partial p/\partial t)\, dt,$$
$$dc_+ = (\partial c/\partial x)(a + c)\, dt + (\partial c/\partial t)\, dt. \tag{8.3-57}$$

As p is a function of c and ω

$$\partial p/\partial x = (\partial p/\partial \omega)(\partial \omega/\partial x) + (\partial p/\partial c)(\partial c/\partial x),$$
$$\partial p/\partial t = (\partial p/\partial \omega)(\partial \omega/\partial t) + (\partial p/\partial c)(\partial c/\partial t).$$

Inserting this in (8.3 - 57) the relation (8.3 - 56) can be written as

$$\left(\frac{\partial p}{\partial \omega}\right)\left[\frac{\partial \omega}{\partial x}(a + c)\, dt + \frac{\partial \omega}{\partial t}\, dt\right] + \left[\frac{\partial p}{\partial c} + \varrho a\right]\left[\frac{\partial c}{\partial x}(a + c)\, dt + \frac{\partial c}{\partial t}\, dt\right] = 0. \tag{8.3-58}$$

Fig. 8.3.8. Characteristics-method in the velocity (c) speed (ω) plane. Curved characteristics ζ_-, ζ_+ for states moving with celerity $- a$, $+ a$ along a pipe (x)-axis. Lines of constant pressure. Preferably used, if transients cross the 1st brake regime of pump and the following regime of a centripetal turbine (= Francis turbine) since there is no overlapping of machine characteristics as existing in the p, c-system.

319
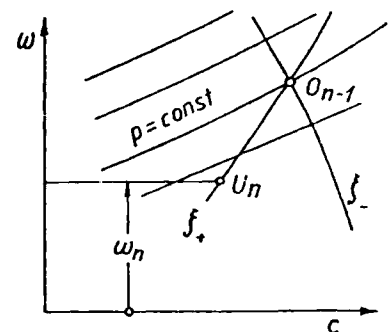
Obviously, for a substantial increment of a variable within the system of characteris...
due to $dx_+ = (a + c)dt$ and with respect to $\partial x = \partial x_+$, $dx = dx_+$ the last equation can...
converted into

$$d\omega_+ + \{[(\partial p/\partial c)_\omega + \varrho a]/(\partial p/\partial \omega)_c\} dc_+ = 0.$$
(8.3-...

In this relation $d\omega_+$ and dc_+ are substantial increments of ω and c in the characteris...
system, which moves with celerity a relative to the fluid in $+ x$-direction. It is seen, th...
also in the simple case of constant celerity a, the inclination $(d\omega/dc)$ of the water hamm...
line in the ω, c-plane depends on machine-conditioned values such as $(\partial p/\partial c)_\omega$ an...
$(\partial p/\partial \omega)_c$, from which the first usually can be neglected compared with ϱa.

For calculating water hammer and resonance due to it in pipe systems, see Cap. 11.3...

8.3.9. Remedies against water hammer

-- By-pass outlet on FTs with long penstock: Here the water hammer is limited...
eliminated by a valve through which the flow can be by-passed in the case of a sudd...
shut down. This is done by a valve, operated, in the case of a rapid shut down by the g...
ring (provided the machine has one). The valve is designed so as to function as an ener...
dissipator in its downstream area (Fig. 8.39 a). (Usually two halves of a pump spiral casi...
wound against each other with a diffuser joined to it, sometimes also a conical jet val...
known as a Howell Bunger valve in North America).

Afterwards this valve is smoothly shut off by a spring or oil pressure-induced force so...
to limit pressure surge in the penstock's lower end.

The control scheme and valve design (Fig. 8.3.9) show a valve, that is operated by an...
pressure loaded piston 19, actuated from the speed governor through the gate serv...
motor. It operates as follows.

A quick shut down raises the pressure by a dash pot 4 linked to the gate servomotor piston. T...
relieves the closing piston 19 of the by-pass valve and loads an auxiliary opening piston 20 on...
valve rod. When the rapid shut down of the distributor is completed, the by-pass closes smooth...
by the action of a throttle 17 and the spring 5 in the dash pot.

Due to the flow passing the throttle 34, the opening piston 20 is relieved of its oil load. Simul...
neously the relief valve 8 of the dash pot piston 5 closes the by-pass outlet 19.

The design has a safety device. When the motion of the by-pass valve 19 is blocked, e.g. by jammi...
a further quick shut down of the gate is also blocked. This follows from the oil now displaced...
the dash pot 7 and its valve piston 6. This closes the oil outflow from the closing side of the gate se...
motor by closing the spring-loaded needle valve 16 in the duct of this outflow.

In Pelton turbines water hammer is limited by a jet deflector (jet presser, jet cutt...
(Fig. 11.2.9), which in the case of a quick shut down, deflects at least a part of the jet fro...
the bucket. Simultaneously the needle closes slowly by means of a throttle in the...
admission line of the needle servo motor. Then under steady state condition, the deflec...
is brought to the ready position. Usually this position is next to the jet edge. This requi...
a cam or a corresponding device to assign a certain opening (needle position) to a posit...
of the jet deflector.

Therefore two control loops are required for needle and jet deflector. They may be connecte...
parallel or in series, the first being preferred nowadays. The control of the recently inaugur...
260 MW, 6-nozzle PTs Silz (Austria) does not use the cam device. Here under steady state condit...
the ready position of the jet deflector is always the same and given by a stop collar. The q...

Fig. 8.3.9. Oil- and dash-pot-operated by-pass outlet of Francis turbine. Against excessive pressure rise during the shut down with long penstocks or an expected fast regulation. Safety needle valve 16 closes if valve 19 of the by-pass outlet jams.
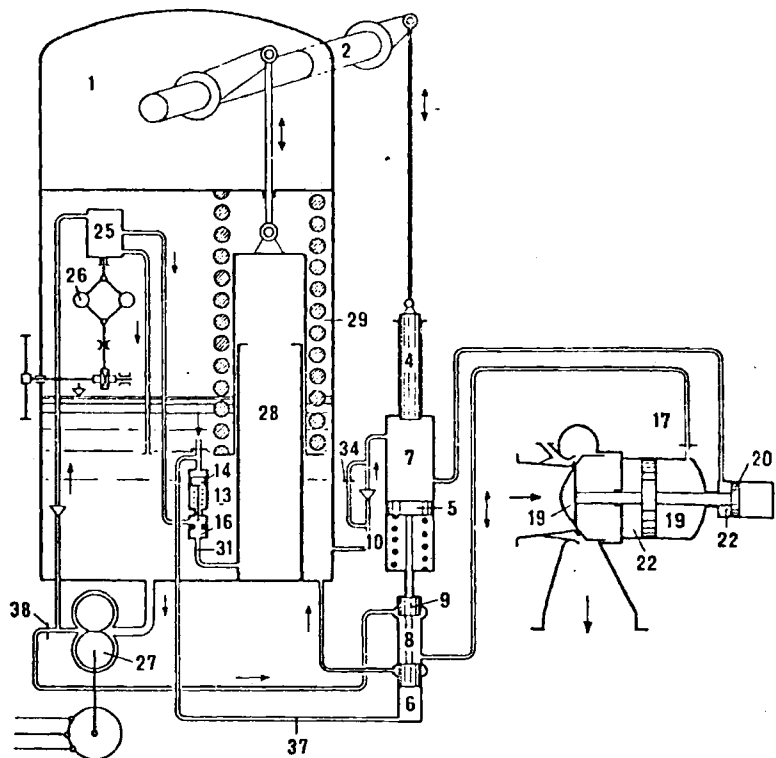
response required now results from the very short time needed to move the deflector to the edge of the jet.

Water hammer and cavitation: As shown with (8.2–21) and expounded in Cap. 8.2.4, the collapse of a vaporous cavity causes water hammer. And water hammer waves may propagate the pressure pulse from a bubble collapsing within the liquid to a distant wall. Hence water hammer connects the hydrodynamic cavitation with its erosion. However, the linkage of a distinct hydrodynamic cavitation of known duration, e.g. on the runner vane surface of a Kaplan turbine to the resulting pitting, is one of the major unsolved problems the operator of hydro turbines is confronted with. This has several reasons. Firstly, at a full-size machine hydrodynamic cavitation cannot be visualized. Only an ultrasonic noise due to cavitation could be recorded. Secondly, for economic reasons any observation of eventual pittings can only be made after a longer period with an usually strongly varying mode of operation and hence also of cavitation. Hence the pitting then observed is a time-averaged value Δm_{er}. Provided the gate and runner vane position relative to each other and according to the draft are also occurring in the real turbine, a record of discharge and net head vs time elapsed t, in connection with known cylindrical runner vane section, may help to recalculate also σ or w_{max} (along the critical vane section) vs time elapsed. Thus according to Knapp's law.

$$\Delta m_{er} = \int_{t=0}^{T} K_1 \, w_{max}^n (t) \, dt \, ,$$

where T is the observation period, K_1 a parameter for the given material but usually due to a certain tests device (e.g., magneto strictive apparatus), whose pitting generation mechanism differs greatly from that in the turbine and probably is a function of w_{max}. According to Knapp's test also n depends on the type and degree of cavitation and hence probably also on w_{max}. Hence any prediction of pitting on the basis of the usual test results from the lab and over a longer period of continuously varying operation at a real turbine, is rather unsafe.

9. Similarity laws, characteristics, research

9.1. Introduction

In hydro power machines, model tests are needed to predict the behaviour of prototype by means of similarity laws either known or yet to be found. The strict application model tests to a prototype requires also knowledge of efficiency scale effects due to Reynolds number, roughness and probably other effects such as structure and level of turbulence.

A survey of a fluid machine's behaviour may be obtained by the so-called hill diagram. Here the limits of operation in consequence of surging, due to working away from the best of cavitation index required, gate limit, runaway and generator capacity are of interest. Scaling of efficiency also needs knowledge of loss in the different elements of a fluid machine.

The measurement of loss and its components can be made on the model or the prototype by conventional methods using flow meters, strain gauge and dynamometers. The thermodynamic method limited to higher heads and prototypes saves test time.

The unsteady behaviour of machines especially under off-bep conditions may be investigated by model tests carried out by instrumentation with a quick response. This requires a knowledge of probes and manometers for measurement of pressure and velocity magnitude and direction and also very close to the wall. This includes also information about sources and magnitude of measuring errors.

Tests may be carried out in water or in air. The measurement on rotary devices requires special signal transmission devices. The visualization of flow phenomena merits special attention. Actual test results of quasi-steady and dynamic measurements in air and water on stationary and rotary elements of hydro turbomachines by means of air injection multi port vectorial probes of quick response and laser anemometer are shown to solve the problems.

The references on this topic span a wide range. [9.1; 9.2] deal with similarity laws, [9.3 to 9.5] with the related problem of technical roughness on the wetted surface of hydraulic machines, [9.6] the uncertainty of their characteristics. Comparative measurements of characteristics between model and prototype are reported on pumps and turbines [9.7], on Francis turbines [9.8], on pump-turbine [9.9]. The thermodynamic method for efficiency is treated in [9.10 to 9.12], tests on prototype high-head pump-turbines in [9.13; 9.14], on large pump-turbines in [9.15; 9.16], general prototype tests in [9.17], and flow measurement on prototype in [9.18]. Experiences on large Pelton turbine are given in [9.19].

Acceptance tests on large pump-turbines [9.20] were compared with model tests instead of prototype tests [9.21 to 9.23]. Test rigs were described for high head [9.24; 9.25], for 1,5 MW output [9.26] impulse turbines [9.27], for different reaction machines [9.28 to 9.31], and for the purpose hydraulic engineering [9.32].

322

Tests have been carried out in water and air [9.33; 9.34], in different air test rigs [9.35], by air tests under variable density [9.36], and thus for scaling efficiency.

Investigations have been made on 2-stage pump-turbines with adjustable gates [9.37], research was carried out on components of pump-turbines, such as the components of their stages [9.38], the intake [9.39], the gates [9.40], the turning passages [9.41].

Measurements are discussed, besides the bep on radial impeller pumps [9.42] and on Kaplan turbines [9.43], on the pump torque under zero flow [9.44], and on Francis turbines during unstable operations (draft tube vortex) [9.45 to 9.51].

System oscillations were investigated in [9.52 to 9.54], the noise in power stations [9.55], the radial forces on the rotor [9.56]. The instrumentation of test rigs is described in [9.57], their automation in [9.58], speed measurement in [9.59], acoustic velocity measurement in [9.60], the use of strain gauges on Kaplan runner vanes in [9.61], flow control in [9.62], the utilization of lasers in the laboratory in [9.63 to 9.67].

Scaling in general is discussed in [9.68], the scaling down of efficiency in [9.69], the scaling up of efficiency in connection with roughness in [9.70], the scaling of performance data in [9.71]. Influences of wall nearness and orientation of the head of a directional probe have been measured by *Kühnel* through the pressure distribution on the amplified probe head [9.72]. Measurements of the 3-dimensional flow in a diagonal pump are described in [9.73], those of the 3-dimensional absolute and relative flow in axial machines with variable runner vane numbers by *Kühnel* in [9.74].

The relative flow field on the runner vane of a Francis turbine has been measured by *Bär* [9.75]. The measured and predicted flow in such a turbine is compared in [9.76] and by *Pfoertner* in [6.22].

Other effects like the influence of a variable geometry of runner outlet [9.77], the *von Karman* vortex street [9.78], the runner inlet geometry [9.79], the geometry of the draft tube inlet [9.8] on the characteristics of Francis turbines, have been measured. Dynamic measurements of the absolute and relative flow field in Kaplan turbines were carried out by *Castorph* [9.81] and on Kaplan and Francis turbines close to the wall of runner vanes were reported by *Furtner* [9.82]. The relative and absolute flow field of a Francis turbine under several modes was observed dynamically by *Schlemmer* and *Gerich* [9.83].

9.2. Similarity laws and characteristics of machines

9.2.1. Criteria of similarity, numbers of *Froude*, *Euler*, *Reynolds*

In hydraulic fluid machines, similarity laws are required for the interpretation of model tests and hence predicted behaviour of full sized prototypes [9.84].

The first supposition for any prediction of this kind is the geometric similarity of the flow passages. Strictly speaking this includes also the technical roughness of the wetted surfaces. According to experience the latter influences the loss only, when the Reynolds number due to this roughness elevation k, defined by kc/v does not exceed 50 to 80, c being the mean velocity and v the kinematic viscosity [9.3].

Time-averaged steady flow is considered. The observations on the model then transferred to the prototype have to be referred to a certain load factor with respect to the bep. Here a great problem exists, since the bep itself is subjected to scale effects usually not clearly-known. This difficulty in the case of water turbines usually is lessened as the Reynolds number of real water-operated prototypes is in the range, where the change of efficiency with the Reynolds number becomes a problem of the second order. Therefore to a first order approximation the load factor referred to the bep might be used as a criterion for similar or homologous operation of model and prototype.

323

For the above reasons. in the following consideration of first order effects, the scale effect of the internal loss and efficiency due to size and head is neglected.

All the similarity laws are related to non-cavitating flow, since wall-attached cavities disturb similarity of profiles considered. Strictly speaking, they would also induce an unsteady flow, not considered here.

Any similarity is related to homologous stations in model and prototype, e.g., on the nominal rotor diameter D (Fig. 9.2.1). Neglecting the boundary layers as second order effects, steady flow in geometrically similar ducts implies also a similar flow pattern at homologous stations and similar velocity triangles there on model and prototype. The all the velocity terms in the triangle at a given station under given load factors are proportional to each other, namely $c_m \sim u \sim c \sim w$.

- *Froude*'s law: Here only the kinetic energy $c^2/2$ and the potential energy gh at a definite station under definite load factor in the model and prototype are proportional to each other. Hence

$$Fr = \sqrt{c^2/(gh)} = \text{const}.$$ (9.2-)

In geometrically similar plants without losses, the net head H and the elevation h are proportional to each other. Thus the last relation leads to a *Froude* number in a widened meaning: $c^2/(gH) = \text{const}$. This brings the important relation

$$c = \text{const}\,(gH)^{1/2}.$$ (9.2-)

- *Euler*'s law: Here only the pressure energy p/ϱ and the kinetic energy $c^2/2$ at a certain station under a definite load factor are proportional to each other. Hence

$$Eu = p/(\varrho c^2) = \text{const}.$$ (9.2-)

This type of number is also used as cavitation index, (see 8.2).
- *Strouhal* number: This number appears in unsteady flow, put aside in this section. is proportional to a time interval t' required, to cover a certain distance L, e.g. the distance of neighbouring vortices in a v. *Karman* vortex street, with a certain velocity c. Here

$$Sr = L/(ct) = \text{const}.$$ (9.2-)

- *Reynolds* number: This determines the portion of viscosity – conditioned loss, an effect of the second order, put aside in this section. For its strict definition Cap. 5.4. In general it is defined as the ratio of inertia force to viscous force

$$Re = L\,c/v = \text{const},$$ (9.2-)

where L is a length mostly responsible for energy dissipation, e.g. chord of axial rotor vanes, and c the velocity due to it.

9.2.2. The unit values of speed, flow, power

- The unit speed: The angular velocity (in rad/s) of a rotor with a reference diameter (Fig. 9.2.1) and a blade speed u at D is given by $\omega = 2u/D$. With respect to (9.2-2), the similarity of all the velocity components of a velocity triangle, including the blade speed u and the meridional velocity c_m, the following holds true

$$u \sim c_m \sim c \sim (gH)^{1/2}.$$ (9.2-)

Hence: $\omega \sim (gH)^{1/2}/D$ or with n'_{11}, the unit speed,

$$\omega = n'_{11}(gH)^{1/2}/D.$$ (9.2-)
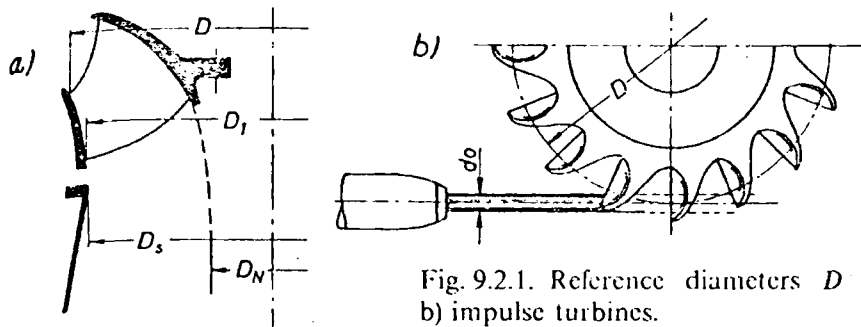
Fig. 9.2.1. Reference diameters D of a) reaction machines b) impulse turbines.

Strictly speaking, the unit speed is an angular velocity of a similar machine, operating at bep with $gH = 1$ m²/s², having the nominal rotor diameter $D = 1$ m. For practical purposes g is omitted and the rotational speed is expressed in n rpm. Hence

$$n = n_{11} H^{1/2}/D. \tag{9.2-8}$$

Contrary to n'_{11} the unit speed n_{11} depends upon the system of units used. Its meaning is the speed in rpm for a machine with $H = 1$ m and $D = 1$ m under a definite load, usually the rated one.

- The unit discharge: The discharge (flow) Q, for a certain load can be determined from a certain area A of a flow passage with the mean meridional velocity c_{mM} by $Q = c_{mM} A$. Assuming $A \sim D^2$ and from (9.2-6) $c_{mM} \sim (gH)^{1/2}$, then at bep

$$Q_{op} = Q'_{11op} D^2 (gH)^{1/2}, \tag{9.2-9}$$

where Q'_{11op} is the unit flow at the bep, a non-dimensional figure, valid for a similar machine with $D = 1$ m, when $gH = 1$ m²/s². For practical purposes sometimes the rated discharge Q (usually above Q_{op}) is taken at a point in the overload range, which has a definite efficiency drop compared with the bep (usually about 2%). Moreover g is omitted. Hence

$$Q = Q_{11} D^2 H^{1/2}. \tag{9.2-10}$$

Q_{11} being the unit flow of a geometrical similar machine of $D = 1$ m operating under $H = 1$ m at rated load. Contrary to Q'_{11op} and n'_{11}, dimensionless numbers of a certain machine type, the values Q_{11} and n_{11}, both dimension-linked, depend on the system of units for the same machine.

- Unit power: The power follows from the relation $P = \varrho Q g H \eta^{\pm 1}$, where η is the efficiency at reference load, the positive sign for a turbine, the negative for a pump. Thus

$$P = 10^{-3} P'_{11} \varrho D^2 (gH)^{3/2} \eta^{\pm 1} \text{ kW}. \tag{9.2-11}$$

P'_{11} being the non-dimensional unit output (input) for a geometrically similar machine of $D = 1$ m, operating under $gH = 1$ m²/s² at the reference load point with a fluid of density ϱ and the imaginary efficiency $\eta = 1$. Eliminating gH in (9.2-8), (9.2-9), (9.2-11) yields the relations $n \sim Q$, $P \sim n^3 D^5$, also used.

9.2.3. The type number (specific speed)

1. As a function of the working data gH, Q, ω or n: The type number (specific speed) n'_q as a non-dimensional figure is the angular velocity (rad/s) of a similar machine, whose

325

flow $Q_{np} = 1$ m³/s at bep. when $gH = 1$ m²/s². From (9.2-7) $n'_q = n'_{11}/D_1$, where the diameter D_1 follows from (9.2-9) as $D_1 = 1/Q'^{1/2}_{11op}$. Inserting this in the foregoing relation yields the type number in terms of the unit values n'_{11}, Q'_{11op}

$$n'_q = n'_{11} Q'^{1/2}_{11op}.$$ (9.2-12)

With the similarity laws (9.2-7), (9.2-9), from which

$$n'_{11} = \omega D/(gH)^{1/2}; \qquad Q'_{11op} = Q_{op}/[D^2(gH)^{1/2}],$$ (9.2-13)

the relation (9.2-12) gives the type number as a function of the working data of set gH, Q_{op}, ω as

$$n'_q = \omega Q^{1/2}_{op}/(gH)^{3/4}.$$ (9.2-14)

n'_q is a dimensionless figure for a certain machine type, and hence independent of the system of units, when Q_{op}, gH and ω are measured in corresponding units. For practical purposes in Europe, the following unit-linked parameter n_q is still used. It is defined as the speed in rpm of a similar machine under a head $H = 1$ m with the flow $Q = 1$ m³/s at the reference point (bep or overload)

$$n_q = n Q^{1/2}/H^{3/4} = n_{11} Q^{1/2}_{11}.$$ (9.2-15)

The values n'_q and n_q are related to each other by $n_q = (333/2\pi) n'_q$. For a n_q, related to an overload point of $Q = 1,17 Q_{op}$ (indicated by the subscript 1/1): $n_{q\,1/1} = 57,3 n'_q$. In the above the values n_q and n'_q are linked to a particular turbomachine with definite features of design either for a pump or a tubine (see also below).

In the design of water turbines also the specific speed introduced in 1905 by *Camerer* is used [9.85]. This is defined as the speed in rpm of a similar turbine, which develops a full load output $P_{1/1} = 1$ hp under a head of $H = 1$ m. The full load output usually corresponds to a point with a certain efficiency drop of about 2% compared with the bep. Thus

$$n_s = n_{11} P^{1/2}_{11\,1/1} = n P^{1/2}_{1/1}/H^{5/4} = n_q(g \varrho \eta_{1/1}/736)^{1/2}.$$ (9.2-16)

With a full load efficiency $\eta_{1/1} = 0,9$; a density $\varrho = 10^3$ kg/m³: $n_s = 3,5 n_q = 180 n'_q$. Actually P, measured in kW. is used. The following relation exists between $n_s(hp)$ and $n_s(kW)$: $n_s(hp) = 1,17 n_s(kW)$. The formulas (9.2-14) to (9.2-16) yield the type number as a function of the working data ω (or n), Q_{op} (or $Q_{1/1}$) and hence P_{op} (or $P_{1/1}$).

II. The type number as a function of design features: Next the type number is expressed by the geometry of a certain turbomachine design and its velocity coefficients Ku, Kc_{m1op}

$$Ku = u/(2gH)^{1/2} = \omega D/[2(2gH)^{1/2}],$$ (9.2-17)

$$Kc_{m1op} = c_{m1op}/(2gH)^{1/2} = Q_{op}/[(\pi/4) D^2_1(1 - N^2_1)(2gH)^{1/2}],$$ (9.2-18)

where D_1 is about the runner throat diameter (strictly speaking the outermost runner exit diameter), N_1 the hub/tip diameter ratio there. Comparison of (9.2-17), (9.2-18) and (9.2-7), (9.2-9) brings

$$n'_{11} = 2^{3/2} Ku,$$ (9.2-19)

$$Q'_{11op} = \pi 2^{-3/2}(1 - N^2_1)\left(\frac{D_1}{D}\right)^2 Kc_{m1op}.$$ (9.2-20)

Using the unit speed n_{11} and unit flow Q_{11} from (9.2-8) and (9.2-10) gives

$$n_{11} = (60/\pi)(2g)^{1/2} Ku,$$ (9.2-21)

326

$$Q_{11} = (\pi/4)(2g)^{1/2}(1 - N_1^2) K c_{m1}(D_1/D)^2 \qquad (9.2-22)$$

where $K c_{m1}$ follows from a relation similar to (9.2–18), in which Q_{op} is substituted by a rated flow Q. Inserting (9.2–19), (9.2–20) in (9.2–12) and (9.2–21), (9.2–22) in (9.2–15) and then (9.2–16), gives the different type numbers as functions of the velocity coefficients $K u$ and $K c_{m1}$ and the design features N_1 and D_1/D

$$n_q' = 2^{3/4} \pi^{1/2}(1 - N_1^2)^{1/2}(D_1/D) K u K c_{m1 op}^{1/2}, \qquad (9.2-23)$$

$$n_q = 158(1 - N_1^2)^{1/2}(D_1/D) K u K c_{m1}^{1/2}, \qquad (9.2-24)$$

$$n_s = 578(1 - N_1^2)^{1/2} \eta_{1/1}^{1/2}(D_1/D) K u K c_{m1}^{1/2}. \qquad (9.2-25)$$

With the obvious relation $K u_1 = (D_1/D) K u$, (9.2–23) reads

$$n_q' = 2^{3/4} \pi^{1/2}(1 - N_1^2)^{1/2} K u_1 K c_{m1 op}^{1/2}. \qquad (9.2-26)$$

For the bep, characterized by $c_{u1} = 0$, the flow coefficient is

$$\varphi_{1 op} = c_{m1 op}/u_1 = K c_{m1 op}/K u_1 = \tan \beta_1, \qquad (9.2-27)$$

in which β_1, the angle between rotor vane and periphery, usually is optimized for $NPSH$ or η, see Cap. 4.11. Hence

$$n_q' = 2^{3/4} \pi^{1/2}(1 - N_1^2)^{1/2} \varphi_{1 op}^{1/2} K u_1^{3/2}; \qquad (9.2-28)$$

$$n_q' = 2^{3/4} \pi^{1/2}(1 - N_1^2)^{1/2} \varphi_{1 op}^{1/2}(D_1/D)^{3/2} K u^{3/2}. \qquad (9.2-29)$$

Again both the last relations show the type number as functions of the blade speed coefficient $K u_1$ at throat diameter and $K u$ at rotor tip diameter, the hub to tip diameter ratio N_1, the throat to tip diameter ratio D_1/D^9), and the flow coefficient.

III. How to increase the type number and its limits: According to (9.2–14) the type number n_q' is an expression proportional to the rotational speed (ω or n) and hence inversely proportional to the size of a machine. But n_q' increases also with Q or P and hence with the "power density" under a certain head. n and P are often desired to be as high as possible.

This raises the question about measures to increase n_q'. As the figures $\varphi_{1 op}$ and N_1 are usually given, it is seen from both the last relations that n_q' rises with $K u$, $K u_1$ and D_1/D. Thus a machine of higher n_q' operates with a larger blade speed coefficient $K u$. Moreover it has a larger draft tube inlet to tip diameter ratio. In Kaplan turbines, having $D_1 = D$, only an increase of $K u$ helps to increase the type number. Table 9.2.1 and 10.3.1 reflect these tendencies.
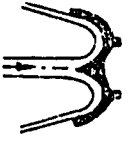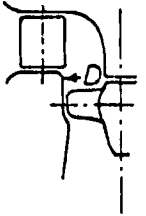
Usually n_q' is given by the working data gH and Q of the set, since they, at least in the case of a reaction machine, limit n_q' in consequence of suction requirements. This raises the problem of the lowest limits of n_q' for a reaction machine (FT). In high head FTs, with lowest n_q' the angle β_2, the runner vane makes with the periphery at the inlet, should not exceed 90°, to limit the curvature of the rotor vane. Hence $c_{u2} = u$. Thus in this case the lowest $K u$ value is obtained from Euler's relation as

$$K u_{min} = (\eta_u/2)^{1/2}, \qquad (9.2-30)$$

where η_u is the peripheral efficiency. Usually the breadth of the rotor b follows the rule $D b = D_1 b_1$, where b holds for the runner inlet and b_1 for the runner exit. Since too small a value of b/b_1 deforms the cross sectional area of runner channel into a flat rectangle with its uneconomical small hydraulic radius $2b$, also too small a value of the diameter ratio D_1/D is bad. Hence $D_1/D \geqslant 0.5$. In an example:

---

[9] Strictly speaking, throat diameter D_1, at a turbine, defines the outmost diameter of the runner vane's exit edge, and, at a pump, the same diameter of the impeller vane's inlet edge.

Table 9.2.1. Characteristic features of turbine vs specific speed $n_S = \dfrac{n\,(\text{rpm})\sqrt{P\,(\text{kW})}}{H\,(\text{m})^{5/4}}$

	Type		Type	n_s*) rpm	Q_{11} m³/s	n_{11} rpm	H_{max} m	$n_{11\,ra}$ rpm	$n_{11\,ra\,max}$ rpm	σ
Impulse Turbines	Pelton T.		1 nozzle, 1 wheel	(7)9–11 11–17 17–(26)	0,007–0,011 0,011–0,024 0,024–0,055	39,8–39,4 39,4–38,9 38,9–37,6	1800–1650 1650– 700 700– 350	71,6–70,9 70,9–70,0 70,0–67,7	– – –	– – –
Reaction Turbines	Francis T.		slow	51–107	0,1 –0,35	60,8–63,6	700– 410	102 –112	–	0,04 –0,06
			medium	107–150 150–190	0,35 –0,59 0,59 –0,83	63,6–67,5 67,5–72,6	410– 240 240– 150	112 –124 124 –138	– –	0,06 –0,085 0,085–0,12
			fast	190–250 250–300	0,83 –1,13 1,13 –1,28	72,6–81 81 –92,2	150– 90 90– 64	138 –158 158 –180	– –	0,12 –0,185 0,185–0,27
	Kaplan T.		8 vanes 6 vanes 5 vanes 4 vanes 3 vanes	240 340 450 330 450 560 390 540 690 490 610 750 570 630 920	0,930–1,220 1,290–1,600 1,600–2,000 2,000–2,350 2,350–2,450	85–145 100–155 110–170 120–180 135–200	50 35 20 15 6	205–250 260–280 245–300 300–355 355–400	300 330 330–360 400 430	0,3 –0,55 0,65–0,85 0,8 –1,2 1,2 –1,6 1,8 –3,5

*) referred to $\eta_i = 0,88$

$\varphi_{1\,op} = \tan\beta_1 = \tan 18 = 0.327$, $\eta_{1/1} = 0.88$, $\eta_u = 0.92$, $Ku = 0.677$, $D_1/D = 0.5$: $n'_q = 0.318$ or $n_s = 57$. In general n_s in FTs should not fall short of $n_s = 60$ corresponding to $n'_q = 0.33$. Example: FT Rosshaag, Zemmgrund, Austria, with $H = 672$ m, $n = 750$ rpm, $P_{1/1} = 79\,500$ hp, yields $n_s(hp) = 62.3$.

Instead of the consideration in Cap. 8.2.2 concerning the limit of n_q due to ground excavation by submergence required, the following consideration on the $n_q(H)$ relation is based on an estimate of rotor strength and optimum value for the flow number at runner exit $\varphi_{1\,op}$.

Introducing $D_1/D = b/b_1$ (often realized) and Ku from (9.2–17) into (9.2–29) results in

$$n'_q = \pi^{1/2}(1 - N_1^2)^{1/2}\,\varphi_{1\,op}^{1/2}(b/b_1)^{3/2}\,u^{3/2}/(g\,H)^{3/4}.\tag{9.2–31}$$

Usually N_1 is negligibly small. In general $\varphi_{1\,op} = \tan\beta_{1\,op}$ is prescribed either by suction requirement (minimizing $NPSH$) or by efficiency requirement (optimizing η). The peripheral blade velocity u at rotor tip diameter is limited by the strength of the rotor (especially with respect to runaway). For a certain type b/b_1 is also limited by the rotor strength. Hence for reaction machines the n'_q limit depends on H by

$$n'_q(g\,H)^{3/4} \approx \text{const}.\tag{9.2–32}$$

This dependence of H on n'_q is reflected by existing designs of reaction machines (Fig. 8.2.6 c) in the form of a strip approximating a function of this type.

For an impulse turbine the throat diameter, introduced in (9.2–18) must be replaced by the jet diameter d_0. Obviously $N_1 = 0$. Since then c_{m1} corresponds to the spouting velocity $Kc_{m1} = Kc_{m3} = 1$ (when loss in the nozzle is neglected), hence

$$n'_{q\,wheel} = 2^{3/4}\,\pi^{1/2}(d_0/D)\,Ku, \qquad n_q = 158(d_0/D)\,Ku;$$
$$n_s = 578\,\eta_{1/1}^{1/2}(d_0/D)\,Ku,\tag{9.2–33}$$

where D is now the jet circle diameter (Fig. 9.2.1) as the reference diameter in an impulse turbine. From this it is seen, that the type number (specific speed) of a single impulse wheel with one nozzle increases by the jet diameter ratio d_0/D. Usual values of D/d_0 are (6) 8 to 15(17) at H of (200) 300 m to 1200(1800) m, where high D/d_0 values are related to multi nozzle wheels.

For an impulse turbine with i_w being the number of wheels and i_n the number of nozzles per wheel, the resulting type number follows from the fact that $Q_{nozzle} = i_w\,i_n\,Q_{wheel}$ as

$$n'_{q\,res} = n'_{q\,wheel}(i_w\,i_n)^{1/2}.\tag{9.2–34}$$

In the case of PT with a vertical shaft there is a maximum $i_w = 1$ and $i_n = 6$. In the case of a PT with a horizontal shaft $i_w = 2$ (in single case 3), $i_n = 2$. Both the last formulas can be applied also to reaction machines. In rare cases there are more stages in series (for pump-turbines up to 5 stages) in impeller pumps the number of stages can be even more. Here with i_{st} as the number of stages

$$n'_{q\,res} = n'_{q\,wheel}/i_{st}^{3/4}.\tag{9.2–35}$$

Besides the characteristic factors $n'_{11}, n_{11}, Ku, Q'_{11}, Q_{11}, P'_{11}, Kc_m, \varphi = Kc_m/Ku$, also the pressure coefficient Ψ is used

$$\Psi = 2gH/(\omega D/2)^2 = 1/Ku^2.\tag{9.2–36}$$

The following similarity relations are needed for a force F and its moment M: $F \sim pA \sim \varrho\,gH\,D^2 \sim \varrho\,n^2\,D^4$, $M \sim FD$.

9.2.4. The efficiency hill diagram

In the usual $\Psi(\varphi)$ plane the characteristic of a reaction type fluid machine may be approximated by

$$\Psi = \pm a_0 n^2 \mp a_1 \varphi n \mp a_2 n(\varphi - \varphi_{op})^2 \mp a_3 \varphi^2 \mp a_4 n^3 \mp a_5 \varphi^{-1}, \qquad (9.2-37)$$

where n is a dimensionless speed. The upper sign holds for a pump, the lower for a turbine. Both the first terms are due to the change of whirl within the rotor in consequence of Euler's relation. a_0 and a_1 being design-linked parameters, from which a_1 in a turbine depends also on the gate position. The third term is due to the angle of incidence at the rotor's inlet edge when the machine operates away from its bep due to φ_{op}. Here the coefficient a_2 varies strongly when passing the bep so as to be smallest either in the overload range of a pump or in the part load range of a turbine. The fourth term is due to the loss in the flow passages of the admission duct (guide apparatus, suction line), rotor and diffuser. The fifth term is due to disk friction loss of the rotor and the last term due to leakage flow loss there. In an impulse turbine, both the last losses and the third term due to shock loss at rotor inlet, are vanishing.

Adding these losses, the non-dimensional loss h'_r of a hydro turbomachine becomes

$$h'_r = [a_2 n(\varphi - \varphi_{op})^2 + a_3 \varphi^2 + a_4 n^3 + a_5 \varphi^{-1}]/\psi. \qquad (9.2-38)$$

Hence lines of constant loss h'_r or constant efficiency $\eta = 1 - h'_v$ are represented by the graph

$$\Psi = [a_2 n(\varphi - \varphi_{op})^2 + a_3 \varphi^2 + a_3 n^3 + a_5 \varphi^{-1}]/h'_v. \qquad (9.2-39)$$

Naturally such a simple approximation describes only the range of constant efficiency for Ψ values not too far away from the bep. The real lines of constant efficiency are closed (Fig. 9.2.2), hence the name hill diagram.

To demonstrate the machine's behaviour, also the $Q_{11}(n_{11})$ plane is used instead of the $\Psi(\varphi)$ plane (Fig. 9.2.3). This is also called a hill diagramm because of the similarity of its curves of constant efficiency to the contour lines of a hill.

If the loss within a machine is of the simple form $h'_r \sim c_m^2/(gH) \sim Q^2/(gH)$, then the graphs of constant efficiency must be parabolas $\psi = k\varphi^2$ in the $\Psi(\varphi)$ plane and lines $Q_{11} = $ const in the $Q_{11}(n_{11})$ plane. The deviation of the real lines due to $\eta = $ const from these parabolas may hint at shock loss, leakage, disk friction and scale effects, due to a partial linkage of the a_i to Re.
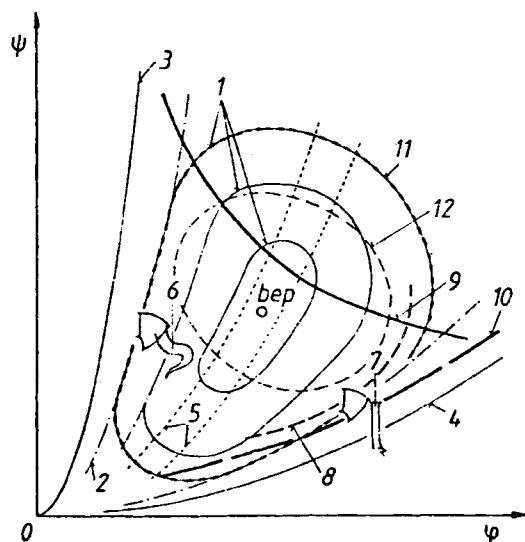
Fig. 9.2.2. Hill (shell) diagram of a reaction turbine with fixed runner blades in Ψ, φ-plane. 1 lines of constant efficiency η; 2 idealized continuation of η const lines as parabolas; 3 runaway-line (approximately parabola); 4 zero speed line (approximately parabola); 5 ::: band of whirl-free and surge-free operation in draft tube; 6 part load range with precessing corkscrew vortex; 7 overload range with more central axial vortex in the draft tube; 8 — — line of admissible pressure surge; 9 limit by maximum output of generator; 10 limit due to opening of wicket gates; 11 lower limit of efficiency η; 12 upper limit of cavitation index σ_{re} given by plant.

Fig. 9.2.3. Efficiency hill diagram of a Francis turbine $n_q = 60$ in the Q_{11}, n_{11}-plane. F operating range free of surge and whirl in draft tube. T part load range with cork screw vortex in the draft tube, Ü overload range with straight vortex in the draft tube.

___ lines of constant gate opening; —·— lines of constant cavitation index σ.
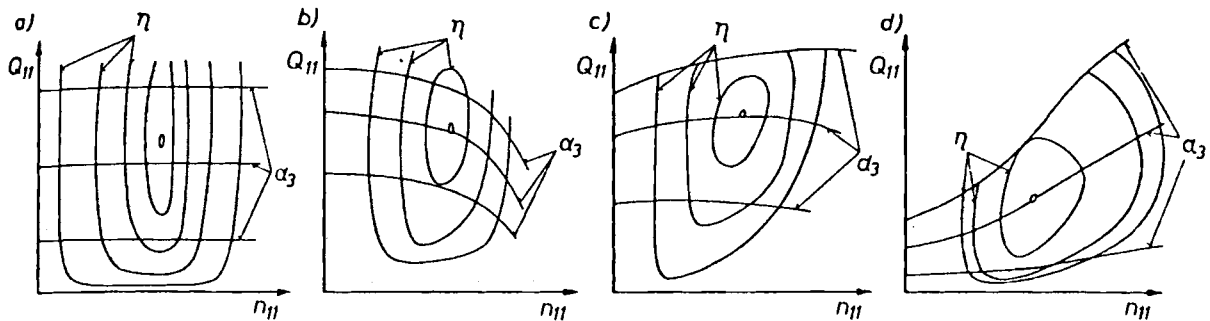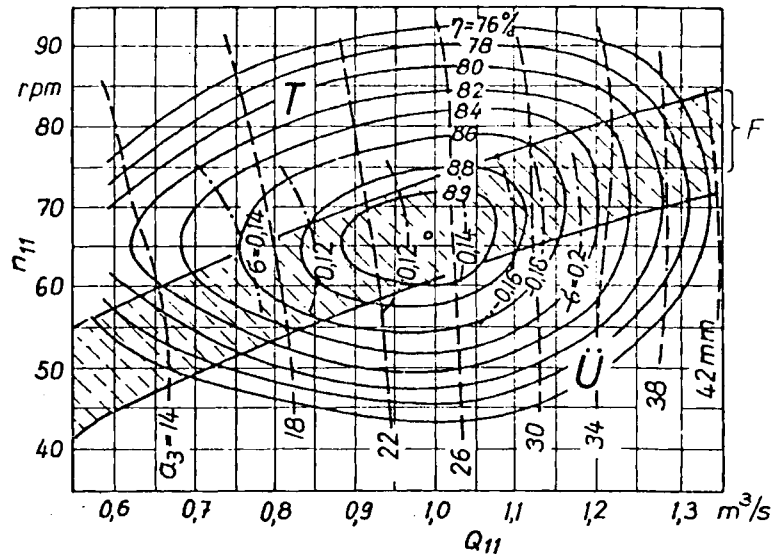
Fig. 9.2.4. Efficiency hill diagram with lines of constant opening a_3. a) Impulse turbine, $n_q = 15$. b) Francis turbine, $n_q = 26$. c) Francis turbine, $n_q = 90$. d) Kaplan turbine, $n_q = 160$ double regulated with cam-on operation.

However, in two cases the simple similarity law fits also to loss-linked real flow. The first case is runaway. Here the conversion of the specific head gH into heat through dissipation results in a runaway parabola $\Psi \sim \varphi^2$. A similar relation holds also for a set at rest, which functions as a throttle. This indeed results also from tests (Fig. 9.2.2).

- Different flow vs speed behaviour of individual turbines: For impulse turbines at constant needle position, the flow Q_{11} is independent of the speed n_{11} (Fig. 9.2.4 a). For Francis turbines of low specific speed at constant gate position, the flow Q_{11} drops vs speed n_{11}, whereas for Kaplan turbines and Francis turbines of high specific speed it increases (see Fig. 9.2.4 b to d).

The first mentioned is a consequence of the large radial extension of such a Francis runner. It originates from centrifugal forces acting opposite to the flow direction. The effect secondly mentioned follows from the approximate proportionality of the flow-linked meridional velocity and the speed-linked peripheral blade velocity for the case that the difference of absolute whirl velocities at the runner's inlet and outlet becomes negligibly small compared with the blade velocity.

- The limits for operation: The operation of a turbine is first limited by the maximum gate (needle) opening. The next limit follows from the maximum power capacity of the electric machine. In a hill diagram of the φ, ψ-plane this limit is described by a line $\varphi \Psi \eta^{\pm 1} = $ const where η is the shaft efficiency of the machine (+ for turbine). In the Q_{11}, n_{11}-plane this line is described by $Q_{11}\eta^{\pm 1} n_{11}^{-3} = $ const.

A third limit on the hill diagram is due to the cavitation index required rising with the distance of the operating point from the bep, where σ_{op} is lowest by the then vanishing angle of incidence. Hence σ required may be described approximately by (Fig. 9.2.2)

$$\sigma = \sigma_{op} + K_1(n_{11} - n_{11op})^{m_1} + K_2(Q_{11} - Q_{11op})^{m_2}. \tag{9.2-40}$$

Moreover the hill diagram of a reaction turbine with fixed runner vanes shows only a small hatched strip of quiet operation crossing the bep and usually connected with a nearly vanishing whirl component in the draft tube.

Outside this zone there are areas of draft tube surge. The one with a flow larger than in the quiet zone corresponds to a straight vortex only surging at larger distance from the quiet zone. The other area has a flow below the quiet one. It is surging in consequence of a precessing cork screw formed vortex in the draft tube [9.45; 9.46].

To calculate transients, the characteristic (9.2−36) must be plotted for different speeds n, but also (in the case of turbines) for different opening angles of the gates α_3 and (in the case of adjustable runner vanes) for different position angles β_1 of the runner vanes. Both the angles appear with the parameter a_1 in the form of a factor $\cot\alpha_3 + (b_3/b_1)\cot\beta_1$.

Hence for small angles α_3 and β_1, the gate vane and the runner vane make with the periphery, the term a_1 in (9.2−37) becomes inversely proportional to each of the angles by $a_1 \sim 1/\alpha_3 + (b_3/b_1)/\beta_1$, where b_3/b_1 is the gate/rotor outlet breadth ratio. Transients also have to account for the constant torque lines. In the ψ, φ-system they read const $= \varphi\Psi(1 - h'_v)^{\pm 1}$, $-(+)$ sign for pump (turbine).

As an interesting feature in case of high head impeller pumps, the torque at zero flow (against closed valve) may reach up to 50% the rated value. In any turbine the torque drops vs speed. Hence any machine must resist the starting torque. This attains 1,4 of the rated one in KTs and up to twice the rated one in PTs.

Vanishing torque appears under runaway speed. This attains in FTs of low specific speed 1,5 times the rated speed and in KTs under off-cam operation (when the usual linkage between gate and runner vane position is interrupted by failure), as the other extreme, up to 3 times the rated speed, values, for which the set must be eventually mechanically suitable.

To study the behaviour of reaction turbomachines under various modes of operation, e.g. as a pump-turbine or under transients (occurring at start up and slowing down the set), the 4-quadrant characteristic in the n, Q-plane is used. See Fig. 9.2.5. Here lines either of constant gate position or constant torque or head, unequivocally assign a certain operating point, with a certain speed and discharge, to a certain mode of operation of the
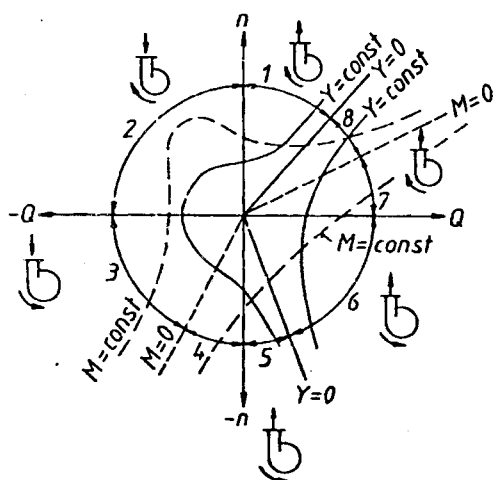
Fig. 9.2.5. Four quaduadrant characteristics of a radial reaction turbomachine in speed (n), flow (Q)-plane. 1 pump regime with normal sense of operation given by its volute; 2 dissipating (brake) regime; 3 centripetal (Francis) turbine regime; 4 dissipating (brake) regime; 5 reversed pumping regime; 6 dissipating (brake) regime; 7 centrifugal (Fourneyron) turbine regime; 8 dissipating (brake) regime. M constant torque line ———. Y const specific head line ———. Lines of constant gate opening have a hump in 2 similar that of constant torque lines. Hence a possible lack of coordinating flow to speed with troubles in operating the machine.

machine such as normal pumping, reversed pumping. centripetal turbining (Francis turbine), centrifugal turbining (Fourneyron turbine) and the four braking ranges inserted in between the aforementioned modes of proper machine operation with their boundary conditions, as runaway-(zero torque) or zero-head-lines.

Naturally these different modes of operation may also be represented in a H, Q-plane. However, here the different modes of operation with their lines of constant speed or constant gate opening may overlap each other in certain regions. Then the unequivocal assignment of a certain point (H, Q) to a certain mode of operation of the machine does not exist any more.

At certain modes of operation, loops in the curves of constant speed or gate position which may assign two different flows to a given head or a given gate opening, are supposed to cause a dynamically unstable behaviour of the set. Such a conclusion has to be based on the set's working together with its piping, its grid, its governor in connection with the inertia of the set and the water hammer of the piping.

9.2.5. The cam curves of double regulated turbines

Fig. 9.2.6 shows a set of so-called "cam curves" as a plot of efficiency vs flow under constant runner vane position φ (proportional to β_1), the whole at constant head. Simultaneously the diagram contains also lines of gate opening a_3 (or z_3) vs flow under constant runner vane position, all at constant head.
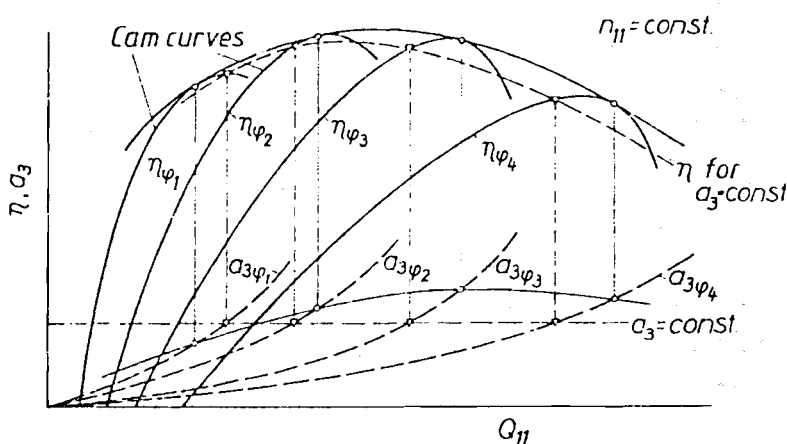
Fig. 9.2.6. Cam curves $(\eta(Q_{11})$-curves, and gate a_3 vs flow (Q_{11})-curves), both at constant position φ_i of runner blade for double regulated turbines (Kaplan turbines, tubular turbines, bulb turbines, Straflo turbines, diagonal (Deriaz) turbines).

The maximum of the efficiency, is located on the envelope curve for the individual cam curves. A perpendicular from the point of contact of the envelope curve with a definite cam curve intersects the line of the gate opening belonging to the same φ at a point which determines the most effective gate opening for a given runner vane angle (Fig. 9.2.6).

It is recognized that a double regulated turbine (of the *Kaplan* or *Deriaz* type) has in the whole range, between $0.2\ Q_{op}$ and $1.4\ Q_{op}$ a superior efficiency than a single regulated turbine with adjustable runner vanes. Otherwise such a single regulated turbine has also a superior efficiency over the whole operating range than a turbine regulated only by wicket gates.

The assignment of gate and runner vane position is by a cam connecting (Fig. 11.2.8) the control loops of gate and runner vane servomotors in parallel or in series.

9.3. Head and efficiency measurement by the thermodynamic method and the usual method

9.3.1. Specific head, enthalpy, component measurement

Strictly speaking the specific head of a fluid machine, the work per unit mass of the fluid, converted within the machine from fluid energy into shaft work and loss implied, or vice versa, is given by the difference of total enthalpy i_t between the pressure (II) and suction (I) flange of the machine (Fig. 9.3.1 a)

$$Y = \Delta i_t = \Delta(p/\varrho + e + c^2/2 + gh)_I^{II} \tag{9.3-1}$$

where the terms are defined in Cap. 1.6.1. A strict treatment of the last relation should also account for the change of density ϱ within the machine. Under atmospheric pressure ϱ of water is 10^3 kg/m^3. This value can be used approximately for the suction flange I. To obtain the density ϱ_{II} in the pressure connection, the simple equation of state (8.3–5) is used. In Cap. 5.4.1 it was shown that the actual highest head of $H = 1760$ m would result in a compression of $\Delta\varrho/\varrho = 0.86 \cdot 10^{-2}$.

However, accounting also for the change of internal energy Δe_I^{II}, with its sign, adverse to that due to the error of the $\Delta(p/\varrho)_I^{II}$-term, then the error due to neglecting the compressibility of water under the actual highest head approximately amounts to one half of the above figure.

Thus a short recapitulation of basic thermodynamic principles necessary for fluid machines is now made. Neglecting heat flow ($dq = 0$) into the machine, the first law of thermodynamics $dq = de + pdv$, v specific volume, gives the change of internal energy as

$$\Delta e_I^{II} = - \int_I^{II} p\,dv \approx (p_I + p_{II})/2 \cdot (v_I - v_{II}).$$

The efficiency η_i of a high head machine is proportional to

$$\eta_i \sim 1/(p_{II}/\varrho_{II} + \Delta e_I^{II}) \sim (\varrho_{II}/p_{II})\,[1 - (1/2)\,\Delta\varrho/\varrho].$$

More concisely the influence of compressibility results from the so-called control surface work $\int_I^{II} v\,dp$ as the surplus of displacement work per unit fluid mass due to admission, expansion and exhaust of fluid and is represented by the term $\Delta(p/\varrho + e)_I^{II}$ in (9.3–1), which at vanishing heat input and small compressibility of the fluid is converted into

$$\Delta(p/\varrho + e)_I^{II} = \int_I^{II} v\,dp \approx (p_{II} - p_I)\,[v_{II} + (1/2)\,(v_I - v_{II})],$$

$$\Delta(p/\varrho + e)_I^{II} \approx [(p_{II} - p_I)/\varrho_{II}]\,[1 + (p_{II} - p_I)/(2\,E_L)]. \tag{9.3-2}$$

Now neglecting compressibility in the example of Reisseck, $H = 1760$ m, would yield only an error of $+ 0.425\%$ in the calculation of efficiency. In practice the error made by neglecting the expansion work due to compressibility of the fluid is superimposed by other effects. When the dissipation Φ in the machine heats the fluid, the change of its internal energy becomes $e_{II} - e_I = \Phi + \int_{II}^I p\,dv$.

The non-dimensional loss h_i' of a machine heats its fluid of specific heat c. The coefficient of cubical expansion of the fluid β results in an additional expansion work $\beta h_i'(gH)^2/(2c)$ (Cap. 7.3). In relation to the expansion work due to compressibility, the latter becomes $f = 2\beta h_i' E_L/(\varrho c)$. For water at 20 °C with $c = 4187$ m^2/(s^2 K), $E_L = 2.06 \cdot 10^9$ Pa, $\beta = 1.8 \cdot 10^{-4}$ K^{-1}, the usual loss of $h_i' = 0.1$ results in $f = 1.765 \cdot 10^{-2}$. Below 4 °C f becomes negative.

The elasticity of the wetted ducts exposed to the pressure causes another error in the expansion work. Assuming water hammer in a penstock as a model (Cap. 8.3), the bulk modulus E_L has to be substituted by the value $E_L/[1 + E_L d/(a E h)]$, where d is a mean "diameter" of the duct, h the thickness of its wall, E the Young modulus of the wall material and a a design-linked parameter. In large machines, the second term in the square bracket is always larger than 1. Hence the influence of the error due to expansion with E_L in the denominator becomes larger than shown by (9.3–2).

The measurement of the static pressure (simply pressure) can be made only by tappings, distributed uniformly over the periphery of the flow passage of interest, thus resulting in a cross sectional-averaged value. The method is only applicable, when the streamline curvature in this cross section is negligibly small so as to make any increase of the pressure across the passage due to centrifugal force irrelevant.

The flow-averaged square of the velocity at section II and I of arbitrary cross section A can be found by measurement of the local velocity c under the assumption of steady flow as

$$c^2 = (1/Q) \int_A c'^2 c' \cdot dA \tag{9.3–3}$$

with Q as the flow $Q = \int_A c \cdot dA$.

In the simple case of an axial velocity profile, e.g. of the type $c_0(1 - r/R)^{1/m}$, r distance from pipe axis, R pipe radius, c_0 velocity on pipe axis (for m, Cap. 5.4), the time consuming measurement of the velocity within the passage is reduced to that of the velocity on the pipe axis c_0. Hence from (9.3–3)

$$c^2 = (1 + m)(1 + 2m) c_0^2/[(3 + m)(3 + 2m)]. \tag{9.3–4}$$

Thus for $m = 7$, $c^2 = 0{,}7058 \, c_0^2$. The measurement of c_0 can be made with a flow meter. An exact measurement of the velocity e.g., by means of a *Prandtl* tube can be made only under a steady flow regime.

Owing to turbulence, the real flow is unsteady. The temporal distribution of the velocity is assumed to be

$$c = c_1 + c_2 \sin \omega t, \tag{9.3–5}$$

with c_1 and c_2 as constants. Since the *Prandtl* probe measures the time-averaged dynamic pressure as a basis for the measurement of velocity $\overline{c^2} = c_1^2[1 + (c_2/c_1)^2/2]$, an error of $(c_2/c_1)^2/2$ is made. This error may be negligible if the level of turbulence is small and if the kinetic energy term is small as compared with $gh + p/\varrho$.

For high head machines the term c_1^2 usually is not negligible as compared with the head $gH \sim p_{II}/\varrho$, on the other hand in such a machine the level of turbulence at the inlet (II) given by $(c_2/c_1)^2$ falls short of 10^{-4}. This does not hold true for the outlet of the machine (I) especially when it operates under off-design load. Here the degree of turbulence can easily reach 20%, which includes an error of 2%. However, this is also negligible, if we consider a high head machine, where the kinetic energy at II or I falls short of 6% of the specific head. Moreover the cross sectional areas A_{II} and A_I are usually of the same order so as to cancel the difference $c_{II}^2 - c_I^2$ in (9.3–1).

However, for part load operation of the machine, account must be taken of the fact, that by stall the main flow occupies only a portion of the available cross section of the draft tube outlet. Once the sections A_{II} and A_I are equal and the stall blocks 50% of the section A_I, in a machine, where the kinetic energy at A_I under regular flow is only 1% of the head, now the kinetic energy becomes 4% of the head. And this would yield a surplus of 3% of kinetic energy at the exit, which is not used.

The latter is a considerable amount, since at continental price level the revenues due to 1% loss at rated load may be of the order of the cost of one set[10]).

---

[10]) This statement for 1% loss at rated load is equivalent to 3% loss at 30% of rated load.

To avoid unnecessary troubles and misunderstandings during the evaluation of head and efficiency measurements, the committees of IEC have agreed standard procedures of measurements. At this international level there exist also standards with respect to the selection of the location of the section *I* and *II* for the individual types of turbines (see Table 1.6.1).

The IEC code also provides rules where to install flow meters for efficiency tests. For example, in a run-of-river plant with its slow current in the head pond and through the thrash-rack (to reduce loss there) the flow meter is to be mounted in the exit section I, where the velocity c_I should not be below that of the tail water. In pump-turbines, where a low thrash-rack loss during pumping requires a low velocity c_I, only the velocity c_{II} is necessary. Hence the flow meter (also used for Q) is to be mounted in cross section II.

It must be clarified to the manufacturer, in what way one intends to control the guarantees of the maker. On the one hand the customer must follow the advice, that "trust is good, but control is better". On the other hand, he must be aware of the fact, that any kind of guarantee given by the model test, cannot be obtained exactly on the prototype. This is due to the fact that machining, transportation and assembly of the prototype is subject to imponderabilities and unforeseeable events, which cannot be included in exact formulas. Moreover full scale measurements on the prototype are time-consuming, expensive and less exact than model tests.

9.3.2. Fundamentals of thermodynamic head measurement

With the enthalpy $i = p/\varrho + e$ and its increment [9.86]

$$di = (\partial i/\partial T)_p \, dT + (\partial i/\partial p)_T \, dp = c_p \, dT + [v - T(\partial v/\partial T)_p] \, dp, \tag{9.3-6}$$

the enthalpy change in the machine can be written as

$$\Delta i = (1/C) \, c_{pII} \Delta T + A_{TII} v_0 \Delta p, \tag{9.3-7}$$

where $C = 4187$ kcal/Nm, T is the absolute temperature in K, v_0 the specific volume related to 177 K and 1 bar pressure, c_p the specific heat under constant pressure, related to the state II, A_{TII} the so-called isothermal coefficient related to the state II and defined by

$$A_T = [v - T(\partial v/\partial T)_p]/v_0. \tag{9.3-8}$$

The coefficient A_T varies for water as shown in Table 9.3.1.1. The specific heat c_p for water can be obtained from the same table. These values were taken from A. S. Thom (see Water Power vol. 7, no 3 (1965)). Alming and Overli [9.90] have found the coefficient A_{TII} to depend slightly on additives of the water.

It should be remembered, that the specific heat contrary to A_T is known in the low temperature range with an accuracy of only four decimals. This point may cause some trouble in the application of the thermometric efficiency measurement after Willm and Campmas [9.86]; see also [9.10; 9.12], and [9.87 to 9.90].

Here the temperature difference ΔT between the stations II and I is measured. From this is obtained the first term in (9.3-7) with c_p as the specific heat. Since the temperature difference is crucial for the losses and the efficiency, this term becomes meaningful.

On the other hand, the exact measurement of the mass flow-averaged representative water temperature has its limitations shown by the following example:

Let us assume a plant with a head of 427 m water column, corresponding to a specific head of 4187 m²/s². When the water under this head expands in a device (throttle) without doing work, the flow energy is converted into heat. Thus the temperature rises say by 1 K (or 1 °C). Imagine instead of this device a water turbine with 10% internal loss, then the temperature rises in this machine only by 10^{-1} K.

Table 9.3.1. Parameters for thermodynamic efficiency measurements.

1) Values for A_{TII} averaged between p and 1 bar

p bar	T °C					
	0	5	10	20	30	50
1	1,01822	0,99599	0,97591	0,94137	0,86295	0,86295
25	1,01666	0,99421	0,97478	0,94064	0,91321	0.86273
50	1,01503	0,99246	0,97358	0,93991	0,91221	0,86241
100	1,01154	0,98906	0,97096	0,93844	0,91045	0,86146
200	1,00466	0,98242	0,96530	0,93537	0,90741	0,85965

2) Specific heat c_p under constant pressure as a function of temperature and pressure

p bar	T °C					
	0	10	15	20	30	50
1	1,0078	1,0015	1,0000	0,9990	0,9982	0,9988
25	1,0057	1,0006	0,9987	0,9973	0,9957	0,9962
100	1,0021	0,9972	0,9954	0,9939	0,9922	0,9918
200	0,9981	0,9927	0,9906	0,9889	0.9867	0,9856

3) Isentropic coefficient $A_{s,II}$

p bar	T °C					
	0	5	10	20	30	50
1	1,00013	1,00001	1,00027	1,00177	1,00434	1,01195
25	0,99950	0,99940	0,99967	1,00118	1,00376	1,01138
50	0,99886	0,99878	0,99906	1,000062	1,00319	1,01082
100	0,99759	0,99756	0,99786	0,99946	1,00204	1,00969
200	0,99511	0,99516	0,99552	0,99717	0,99981	1,00749

If by standards the efficiency has to be measured with 1 % accuracy, there must be at least an error of less than 1 % for any value implied in the formula for the efficiency. Since the temperature is one of these parameters, it has to be measured with an accuracy of 10^{-3} K at least.

Employing this method for a head of roughly 50 m (which corresponds to the lowest limit of the method actually recommended) the temperature must be measured with an accuracy up to 10^{-4} K. These considerations have any value only, if the specific heat c_p as a multiplier of the temperature difference, is known with the greatest accuracy. Unfortunately this is not the case, as can be seen from Table 9.3.1.2).

Therefore in water turbines a zero method has been developed by which $c_p \Delta T$ is eliminated. This method is based on the thermodynamic law, that the enthalpy of a fluid is kept constant, when the flow is throttled isenthalpically. In the thermodynamic zero method for a turbine, the fluid to be throttled is tapped from the main flow past station II, then passes a throttle, insulated against heat transfer, and then is converted into the state 4. Hence with respect to (9.3–7)

$$A_{TII} v_0 (p_{II} - p_I) + \frac{1}{C} c_{pII}(T_{II} - T_I) = A_{TII} v_0 (p_4 - p_I) + \frac{1}{C} c_{pII}(T_4 - T_I).$$

(9.3–9)

337

The trick of the zero method consists in throttling so that the temperature T_4 (past the throttle) and T_1 in the exhaust connection become equal by adequate adjustment of the throttle. Thus the enthalpy difference between the pressure and the exhaust connection of the machine becomes

$$\Delta i = A_{TII} v_0 (p_4 - p_i). \qquad (9.3-10)$$

By this the net head as the total enthalpy difference gives

$$\Delta i_t = A_{TII} v_0 (p_4 - p_i) + (1/2)(c_4^2 - c_i^2) + g(h_4 - h_i). \qquad (9.3-11)$$

It should be mentioned that in an exact test, the very slight variation of gravity acceleration g vs altitude and latitude should be considered [8.123].

By making equal the cross section A_I and A_4 and arranging the same velocity distributions in them, continuity eliminates the term due to c_4 and c_I in (9.3-11). Thus the measurement of the enthalpy as the work done per unit mass of the real machine is reduced to the measurement of a pressure difference $p_4 - p_I$.

The problem arises, from what point of the cross section II the flow should be taken. With the fluid temperature of what point in section I it should be compared? It should be a point with the same mass-averaged values of c^2 and T in both the cross sections. Such a point can be obtained only from tests over the cross section for each flow regime. Obviously the station for the mass-averaged temperature differs from that due to the mass-averaged kinetic energy. Since the temperature term is decisive this must be preferred.

To avoid disturbances of measurement by oscillations of the intake tapping, the support of this streamlined body should be sufficiently stiff. Positioning too near to the wall is not advisable for the following reasons. As previously shown, this method is restricted to heads above 50 m. Since the mixed flow machine predominates in this range, attention should be directed to the fact, that most of the losses here are caused by leakage and disk friction and then transmitted to the relatively small leakage flow, thus being excessively heated compared with the bulk of the main flow passing the runner.

Because of the low thermal diffusivity of water, this heated liquid layer close to the draft tube wall cannot be expected to mix with the adjacent main flow down to station I. Fortunately many draft tubes, especially those for vertical sets have a bend. Owing to the secondary flow in this bend (now for once useful), the warmer outer layers are mixed with the main flow.

If the head gH falls short of 50 m, the internal energy term of (9.3-1) cannot be measured accurately enough. Thus the conventional method must be applied according to which the specific head (now restricted to the mechanical energy terms)

$$Y = gH = \Delta(p/\varrho + c^2/2 + gh)_I^{II} \qquad (9.3-12)$$

requires the measurements of the flow-averaged values p/ϱ, $c^2/2$ and gh in the cross sections II and I.

9.3.3. Thermodynamic measurement of internal efficiency

In the case of a turbine, the internal efficiency represents the energy converted into blade work in relation to the energy offered by the fluid, both referred to unit mass of the fluid. The difference of both the energies implies the losses, converted into heat and transferred to the fluid.

These are: The hydraulic flow losses in the admission part (distributor, suction pipe) the rotor and the diffuser, including also the so-called exchange losses between rotor and stationary part (diffuser distributor, suction pipe) in consequence of the closed flow loops at the ends of the rotor vane

338

shroud and hub especially when working under off-design conditions. Lastly it comprises the losses of disk friction and leakage (volumetric loss) in the rotor.

The energy offered by the head in the case of a turbine corresponds to the difference of enthalpy in an ideal machine without these losses and without the heat flow connected herewith.

Any entropy increment 'ds' is combined with a heat dq transferred irreversibly into the fluid from outside according to

$$ds > dq/T. \qquad (9.3-13)$$

Strictly speaking, this relation is valid first for a heat flow crossing the system boundary of the machine. Now, we know, that the heat transfer through the walls of a hydraulic machine is negligibly small. The heat, flowing into the fluid of a real machine, as a black box, from outside can be interpreted as follows: First the internal loss as an irreversible work is done by virtue of viscous and turbulence-conditioned stress under the strain rate of the fluid. This dissipation generates heat, which can be considered as being afterwards transferred from outside into the system (machine). Contrary to multistage thermal turbo engines, this heat revovery cannot be used in the following stages, as they usually don't exist in a water turbine.

Thus the real machine can be understood as a machine with heat flow from outside the system into it. Then the entropy varies in the case of a real machine. The thermodynamic relation for the increment of the enthalpy as a function of that of the entropy ds is given by [9.86]

$$di = (\partial i/\partial s)_p ds + (\partial i/\partial p)_s dp. \qquad (9.3-14)$$

For an ideal machine, the increment of entropy vanishes. Consequently

$$ds = 0; \qquad di_s = (\partial i/\partial p)_s dp. \qquad (9.3-15)$$

Hence the finite difference of total enthalpy of an ideal machine

$$\Delta i_{I_s} = A_{sII} v_0 (p_{II} - p_I) + (c_{II}^2 - c_I^2)/2 + g(h_{II} - h_I) \qquad (9.3-16)$$

with the so-called isentropic coefficient (Table 9.3.1.3)

$$A_{sII} = (1/v_0)(\partial i/\partial p)_s. \qquad (9.3-17)$$

Together with Δi_t from (9.3–11) the internal efficiency reads for a turbine (T) and a pump (P) (Table 9.9.3),

$$\eta_{iT} = \Delta i_t/\Delta i_{ts}; \qquad \eta_{iP} = \Delta i_{ts}/\Delta i_t. \qquad (9.3-18)$$

The divergence of isobars in Fig. 9.3.1 a reveals that for a certain increment of entropy, the internal efficiency of a pump is lower than that of a turbine operating with the same pressure difference $p_{II} - p_I$.

From (9.3–18), (9.3–16), (9.3–11) it is seen, that the efficiency is only given by the measurement of the differential pressures $p_4 - p_I$, $p_{II} - p_I$, when the energy differences $c_4^2 - c_I^2$, $c_{II}^2 - c_I^2$ are imagined as small or compensated by adequately setting A_{II}, A_I, A_4. Thus any flow measurement is eliminated.

9.3.4. Conventional measurement of internal efficiency

This so-called conventional measurement of the internal efficiency has to be applied, when the head falls short of 50 m. Here the measurement of flow Q, especially on the prototype is a rather time-consuming and error-charged procedure, which makes this
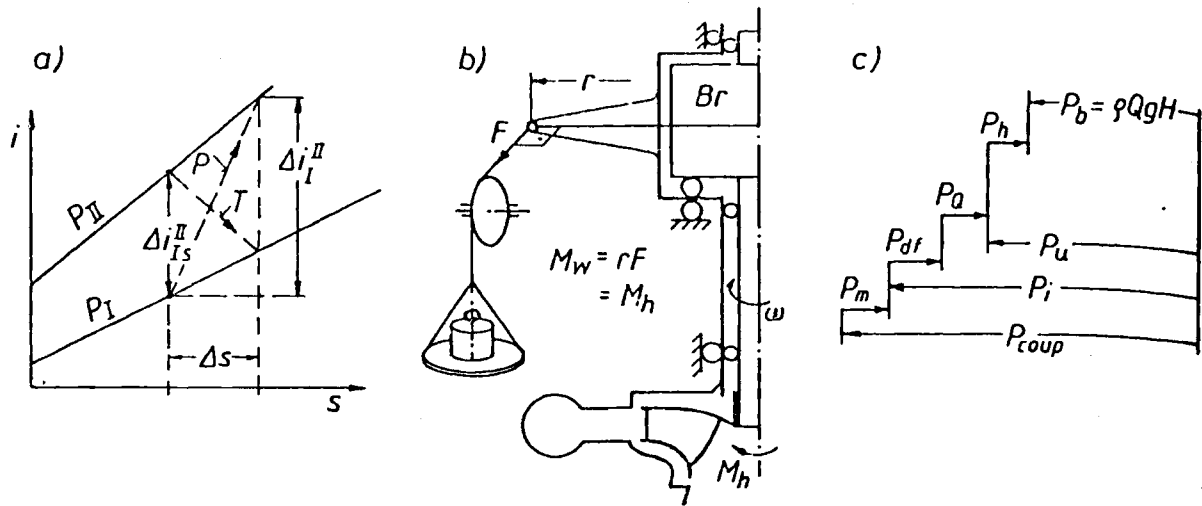
Fig. 9.3.1. Working process of real machine with losses. a) Real process (– – –), and ideal process ds = 0 of fluid machine on the enthalpy (i), entropy (s)-diagram between isobars p_{II}, p_I. T turbine, P pump. Divergence of isobars causes a better efficiency in turbine process than in pump process for a given increase in entropy. b) Torque reaction dynamometer with elimination of shaft friction when measuring the internal torque $M_h = M_i$ by weight-induced load F. c) Scheme of power loss components in an impeller pump from the shaft power P_{coup} to the net hydraulic power input P_b. P_m mechanical power loss, P_{df} power loss by disk friction, P_Q power loss by leakage flow, P_h hydraulic loss in suction line, impeller, diffuser and by exchange losses between stationary part and impeller, P_i internal input, P_u peripheral input. In a turbine transformation of power is reversed.

method inferior to the thermodynamic method, (provided the head allows its application).

As methods for flow measurement may be mentioned:

a) In the prototype: Measurement of the velocity profile by flow metering, salt solution method, in closed ducts also by salt velocity method, Gibson water hammer method [9.91 to 9.94], ultrasonic method by Knapp, Boettcher [9.95].

b) In the model test: Venturi meter, weighing machine, measuring tank, calibrated weir, flow metering, Prandtl probe or similar probe, inductive method, Laser velocimeter, hot film probe, hot wire probe, semiconductor probe. Hence the gross(in)output

$$P_b = \varrho Q\, Y = \varrho Q g H. \tag{9.3-19}$$

The internal out(in)put results from the speed ω, usually measured by induction, and the torque M, measured either on the prototype by means of strain gauges or on the model by means of a torque reaction dynamometer (of the hydraulic, electrodynamic or frictional type). The needed internal torque M_i can be obtained by strain gauges when the spring-suspended, oil- or air-cushioned stator of the reaction torque meter also contains the shaft bearings (Fig. 9.3.1 b). Hence the internal out(in)put

$$P_i = \omega M_i. \tag{9.3-20}$$

Thus the internal efficiency (negative sign pump, positive turbine)

$$\eta_i = (P_i/P_b)^{\mp 1}. \tag{9.3-21}$$

Even if the conventional method is more time consuming, it may be more exact than any measurement on the prototype, when the measurement is carried out on accurately

340

machined models of 300 to 500 mm nominal diameter D, by means of a hydrostatic, air-, or oil-bearing-mounted torque reaction dynamometer for torque measurement and a weighing machine or a tank for measurement of the flow. Hence accuracy of η on model tests is $\mp$ 0,5 %, including, e.g. maximum relative errors of flow and head up to $2 \cdot 10^{-3}$.

Therefore in future the model test will be preferred more and more as the decisive and selective procedure for getting an adequate design of a certain turbine. The prototype test will be degraded to a control for the results predicted by the model test. Because of efficiency scale effects the efficiency of the smaller model, operating under a smaller Reynolds number than the prototype becomes smaller than the efficiency of the latter.

Hence to predict the efficiency of a prototype on the basis of model tests, efficiency scaling formulas are required. Such formulas have been either found by experience on models and prototypes by means of rather simple rules postulated and improved since the eve of this century, or on the basis of pipe loss formulas by *Camerer* [9.85], *Moody* [9.96], *Pfleiderer* [4.12], *Ackeret* [9.97], *Hutton* [9.98; 9.99], *Osterwalder* [9.70; 9.100; 9.101], *Rütschi* [9.102], *Mühlemann* [9.103], and *Fay* [9.99; 9.104]. A special working group of the IAHR headed by professor *Osterwalder* [9.70] in the past 17 years has collected much test material from industry. A compilation of all the findings was published by *Osterwalder* [9.70; 9.105]. An essential contribution was also made by *Strscheletzky* [9.106] who assigned the losses to an equivalent technical roughness typical for the machined surfaces of elements found in hydro turbomachines.

9.3.5. The scale effect of internal efficiency

According to experience, the hydraulic loss depends on the Reynolds number and the relative roughness of the duct walls.

- Roughness: From pipe test we know, that the friction coefficient in the turbulent range depends decisively on the relative sand roughness of the pipe wall [5.27]. An application of these test results to the ducts of hydraulic machines requires at first a substitution for the pipe diameter of the hydraulic diameter of the duct's passage defined by $d_h = 4 \times$ cross sectional area/periphery. Then it must be remembered, that the pipe test is related to developed pipe flow, whereas the boundary layer, as the decisive carrier of loss in a structural member of a fluid machine, e.g. the rotor, is one, developing along a starting length. Thus at an arbitrary station within the duct considered, the boundary layer thickness is surely below the hydraulic diameter d_h. The latter is the value to which the roughness elevation is related in pipe tests.

Moreover application of sand roughness test results is not correct, since the structure of wall roughness there differs from that of sand roughness. In general the technical roughness is more pointed than the sand roughness and depends on the kind and the orientation of surface finish. Hence relying further on the test results of sand roughness, requires the definition of an equivalent sand roughness due to a certain measured technical roughness. *Strscheletzky* made some efforts to do this [9.106] by means of penetrating deeper into the structure of a roughness and the flow about it. Hints at roughness on hydro turbomachines are given by *Grein* [9.3].

An older roughness model assumed, that any roughness has no influence on the loss, if the highest roughness elevation on a surface is submerged in the so-called laminar sublayer. The thickness of this layer, having no turbulence-conditioned cross fluctuations of velocity, obviously was overestimated.

Recent measurements in the flow laminae close to the pipe wall by *Hartner* [8.136] by means of a Laser anemometer within a liquid having the same refraction index as the adjacent planely ground plexiglass block, forming the pipe wall, have indicated, that these cross fluctuations of velocity have unexpectedly high amplitudes at a very small distance from the wall.

341

The reason for this phenomenon is given by the mechanism of turbulent flow, which operates that way according to Strscheletzky [9.106]. Particles in the neighbourhood of the wall with its high strain rate try to escape into regions with lower strain rate. This leads owing to conservation of mass to a movement towards the wall of other fluid elements with higher velocity. Thus the fluid between roughness elevation is always stimulated by fluctuations.

The influence of roughness is of highest interest for the manufacturer, who wants to know, to what degree any particular surface finish of the ducts, e.g. grinding, has effects on the efficiency.

– Reynolds number. Here the influence might be limited to that on ducts with hydraulically smooth walls. Now follows a review of the elementary effect on the basis of loss in a straight pipe. An elimination of the pressure drop in a pipe from relations (5.4–13) and (5.4–15) gives with $r = R = d/2$ the loss coefficient of the pipe as a function of the wall shear stress $\tau = \tau_w$

$$\lambda = 8\tau_w/(\varrho c_M^2),$$ (9.3–22)

where c_M is the mean velocity of the cross section. Since the flow close to the wall is always laminar $\tau_w = \varrho v(\partial c/\partial y)_{y=0}$, where y is normal to the wall.

In the relevant turbulent regime now considered the velocity distribution across the boundary layer, thickness δ, may be approximated by $c = c_0(y/\delta)^{1/m}$, where c_0 is the velocity at the outer edge of the boundary layer. Hence $\partial c/\partial y = [c_0/(m\delta)] (y/\delta)^{1/m-1}$. In consequence of the approximative velocity distribution, this derivative tends to infinity at the wall ($y = 0$). Assuming a laminar sublayer with constant strain rate $\partial c/\partial y$ and depth y_0 ($y_0 \ll \delta$), the wall shear stress may be expressed by

$$\tau_w = [\varrho v c_0/(m\delta)] (\delta/y_0)^{1-1/m}.$$ (9.3–23)

For simplicity the transition laminar turbulent is put aside. In a first order approximation the boundary layer thickness δ of the face considered, is assumed to be proportional to the nominal diameter of the machine D. But this is done only in context with $m\delta$, since the ratio y_0/δ may be assumed to vary only very little as a function of D. Doing so in (9.3–23) and then inserting this in (9.3–22) yields

$$\lambda = \text{const}(1/m) (c_0/c_M) [v/(c_M D)] (\delta/y_0)^{1-1/m}.$$ (9.3–24)

According to experience the velocity distribution across the boundary layer becomes more "full" with increasing Reynolds number now defined by

$$Re = c_M D/v.$$ (9.3–25)

Hence the ratio c_0/c_M decreases slightly vs Re. Due to this also m rises vs Re. After Schlichting [5.4] for a pipe whose Reynolds number Re' is defined by the pipe diameter, m grows from $m = 6$ to $m = 10$, when Re' increases from $Re' = 4 \cdot 10^3$ to $Re' = 3240 \cdot 10^3$. Then the exponent $1 - 1/m$ changes from 0,832 to 0,9. Also δ/y_0 may increase slightly vs Re. However, this is strongly compensated by the decrease of $1/m$ vs Re, ranging from 0.166 to 0,1. For $\delta/y_0 = 10$, the product $(1/m)(\delta/y_0)^{1-1/m}$ decreases from 1,29 at $Re' = 4 \cdot 10^3$ to 0,79 at $Re' = 3240 \cdot 10^3$. From this it is seen that the pipe loss coefficient decreases vs the Reynolds number. Substituting the machine duct considered by a straight pipe and remembering $c_M^2/(2gH) = (c_M/c_{Mop})^2 c_{Mop}^2/(2gH) = \Lambda^2 Kc_{Mop}^2$ to depend on the design (Kc_{Mop}) and on the load factor $\Lambda = c_M/c_{Mop}$, the loss ratio of the particular element considered (may be the whole machine) can be expressed as

$$h_v' = \lambda(L/d_h) \Lambda^2 Kc_{Mop}^2.$$ (9.3–26)

342

For a certain machine or part of a machine the ratio L/d_h of duct length to hydraulic diameter is given, also $Kc_{M\,op}$ is given and constant (if scale effects of the bep are put aside). Hence the loss ratio depends only on the load factor $A = Q/Q_{op}$ and λ according to (9.3–24). From this it is seen that at a certain load factor the loss h'_v decreases vs Re. Some problems arise when the above is applied to a real machine. The latter has some sections such as the draft tube, that do not have remarkable scale effect. Hence only a portion 'a' of the internal loss of the machine is subjected to scale effects. The portion 'a' of scale-subjected loss depends on the design. A high head Francis turbine with its relatively small throat velocity coefficient Kc_{m1} has at least at bep a rather large 'a'.

The generally adopted insensibility of the diffuser loss coefficient against scale effects might result, from a growth of the dissipation-linked turbulence level in the draft tube proportional to its size, and from its rather invariable inlet velocity c_{m1} in consequence of the economicly restricted submergence of any limiting reaction turbine design.

On the other hand 'a' depends also on the load factor. A low head Kaplan turbine may have a small value of 'a' since the draft tube loss $\zeta_s Kc_m^2$ may amount to 0,07 at full load. However, at 20% of this load, this loss is reduced to 1,4%, whereas the runner loss, before say 2% beomes now 10%, so that 'a' being 0,22 under full load is now increased to 0,88.

Moreover also the bep and its velocity coefficients may depend on the Reynolds number. Furthermore the neglect of Reynolds – dependent transition points and superimposed roughness effects may complicate the whole. Contrary to pipe flow, the boundary at the essential elements of hydro turbomachines is subjected to scale-conditioned pressure gradients of the main flow. Finally, rotation, wall curvature and secondary flow in fluid machines, makes the loss generation there different from that in a straight pipe.

– Practice oriented scaling due to Reynolds number without roughness effects: the following relation holds between the internal loss h'_{vi} on the Model (M) and the prototype (P) with a fluid of kinematic viscosity v

$$h'_{viP}/h'_{viM} = a[(H_M/H_P)^{1/2}(D_M/D_P)(v_P/v_M)]^{1/n} + 1 - a. \qquad (9.3-27)$$

The value

$$\Delta\eta_i = \eta_{iP} - \eta_{iM} \qquad (9.3-28)$$

is called efficiency scaling or efficiency valorization.

The number 'a' depends on the type of machine and its load factor. For Kaplan turbines within $0,4 < Q/Q_{op} < 2,2$, Osterwalder assumed [9.100]

$$a = 0,9 - 0,273\,(Q/Q_{op})_M. \qquad (9.3-29)$$

The same author proposed the exponent 'n' to be in the case of a Kaplan turbine

$$n = 0,893\,log_{10}Re \qquad (9.3-30)$$

with a Reynolds number for Kaplan turbines defined by

$$Re = w_\infty L/v \qquad (9.3-31)$$

where L is the chord of a mean cylindrical section, w_∞ the undisturbed throughflow velocity given by $w_\alpha = (w_1 + w_2)/2$, where w_2 and w_1 are the relative velocities at inlet edge 2 and outlet edge 1 of the runner vane.

According to an older proposal of Ackeret [9.97], $a = 0,5$, $n = 5$. This was occasionally improved by Hutton [9.98; 9.99]. For Francis turbines Osterwalder has found by tests [9.107]

$$a = 1 - 0,082\,Q'_{11\,op}/(1 - \eta_D) \qquad (9.3-32)$$

in which $Q'_{11\,op}$ is the unit flow at bep, η_D the draft tube efficiency.

9.3.6. Several efficiences and their measurement

In general the measurement of the internal input (output) P_i of a prototype (full size machine) has to start from the measurement of the indicated electric output (input) of the generator (motor) P_{el} as from

$$P_{el} = U_{eff}\, i_{eff}\, \cos\varphi, \tag{9.3-33}$$

in which U_{eff} is the effective voltage, i_{eff} the effective current, $\cos\varphi$ the power factor.

The following losses have to be added (subtracted) to (from) P_{el} to obtain P_i:

1) The electric alternator (motor) loss under load $P_{alt\,loss\,el}$ containing a resistance and reactance term.

2) The mechanical loss of the alternator (motor) $P_{alt\,m}$ due to ventilation, disk friction and due to its share of bearing loss (if separable).

3) The mechanical loss of the hydraulic machine P_m, due to its shaft seal $P_{loss\,seal}$ and its share of bearing loss $P_{loss\,brg}$.

Both the machines may have different manufacturers, but the bearing losses $P_{loss\,brg\,el}$ and $P_{loss\,brg}$ can be measured only simultaneously. Therefore a separation of these loss components on the basis of tests needs an argreement such as a) the only relevant mechanical losses are due to the thrust bearing load and due to the ventilation of the generator rotor. b) The loss in the thrust bearing is proportional to the load on it and the latter proportional to the deflection of its support. For example, in a machine with vertical shaft, the thrust bearing load due to the turbine consists on the one hand of the weight of its runner and its shaft portion, and on the other hand of the hydraulic axial thrust. c) The ventilation loss of the generator rotor can be obtained by scaling up model tests.

Thus with the lower sign valid for the pump, the internal output (input) P_i becomes

$$P_i = P_{el} \pm P_{alt\,loss\,el} \pm P_{alt\,m} \pm P_m. \tag{9.3-34}$$

With the gross (net) input (output) $P_b = \varrho Q g H$, the internal efficiency for the prototype is given as (Fig. 9.3.1 c)

$$\eta_i = (P_i/P_b)^{\pm 1}. \tag{9.3-35}$$

The coupling (out)input P_{coup} is defined by

$$P_{coup} = P_i \mp P_m. \tag{9.3-36}$$

The loss by disk friction P_{df} and leakage flow P_Q may be obtained from a model test on a rotor, whose inlet and outlet cross section have been blanked off, where the friction on both the blanking sheets and bearings has been eliminated by separate tests. Hence after an adequate scaling according to $P_{df} = \text{const}\,\omega^3 D^5 (\omega D^2/v)^{-1/5}$, the hydraulic or peripheral (out)input of the prototype

$$P_u = P_i \pm P_{df} \pm P_Q. \tag{9.3-37}$$

P_u differs from P_b by the hydraulic losses P_h occuring in the wetted passages of the machine such as distributor (diffuser), rotor, draft tube (suction pipe), and exchange of angular momentum between rotor and adjacent stationary parts of the machine.

$$P_u = P_b \mp P_h. \tag{9.3-38}$$

P_b, P_i, P_{df} and P_Q can be obtained by reliable and rather simple, but sometimes time consuming (Q) measurements. Since the measurement of the loss P_h in wetted duct especially within the rotor and between the latter and the adjacent stationary part

344

troublesome, the last two relations can be used for the computation of the hydraulic loss P_i. Hence the so-called peripheral or hydraulic efficiency (Fig. 9.3.1 c)

$$\eta_u = (P_u/P_b)^{\pm 1}. \tag{9.3-39}$$

The latter is required for the Eulerian equation, (Cap. 5.3). The mechanical efficiency for the imaginary case of a separate electric machine is defined by

$$\eta_m = (P_{coup}/P_i)^{\pm 1}. \tag{9.3-40}$$

This value describes the quality of the bearings and the shaft seal. The disk friction loss and its efficiency results from

$$h'_{df} = P_{df}/P_i, \qquad \eta_{df} = 1 - h'_{df}. \tag{9.3-41}$$

Similarly the loss and efficiency due to leakage flow Q_V

$$h'_Q = Q_V/Q, \qquad \eta_Q = 1 - h'_Q. \tag{9.3-42}$$

The value η_m can be estimated or obtained from bearing and shaft seal tests. It ranges between 0.995 to 0.98. The internal efficiency can be measured by the conventional or the thermometric method (see above), the disk friction efficiency and the volumetric efficiency can be measured as described above or calculated according to Cap. 5.5. For the linkage of P_{df} and P_Q used here. see Cap. 5.5.

For the design of a machine by Euler's equation the peripheral efficiency η_u is required. Since model tests on hydraulic loss are rarely found and complicated, η_u can be calculated from η_i, h'_Q and h'_{df} as follows

$$\eta_u = \eta_i/(\eta_{df}\eta_Q) \approx \eta_i(1 + h'_Q)(1 + h'_{df}) \approx \eta_i + h'_Q + h'_{df}. \tag{9.3-43}$$

9.4. Experimental techniques

9.4.1. Instrumentation for steady flow

9.4.1.1. Manometers: Fundamentals:
Manometers are used for the measurement of the static pressure, which is strictly speaking a pressure at the wall which guides a fluid. It is measured by a pressure difference between the desired and a known pressure. Usually the latter is that of the surrounding atmosphere. Therefore each measurement of a pressure needs a simultaneous reading of the reference pressure.

- Liquids mostly used in manometers: Usually the measured pressure is in equilibrium with the height difference of a liquid column. Mercury, water and carbontetrachloride are used, the latter especially for accurate measurements in air tests. Air tests are more easily carried out and therefore often used at least as preliminary tests.
- Types of manometers:
a) U type manometer. The two branches should be of equal, constant and not too small diameter. Thus eliminating errors due to surface tension.
b) Inclined tube manometer. A very sensitive instrument.
c) Betz manometer. The vertical branch with a very small tube is located coaxially in the interior of a much larger vessel, closed at its top, on the level of which acts the unknown pressure. The narrow branch contains a float which moves with its vertical scale along an optical projection device.
d) Weight manometer. For high pressure. The pressure acts on a floating piston, which

345

is nearly frictionless. Its force is balanced by calibrated weights on the piston. Elimination of friction by vibratory motion or rotation of piston.

c) Manometer for simultaneous measurement at many stations. Here each station is connected by a measuring tube with a large vessel on the level of which acts the reference pressure.

- Conversion of pressure into an electric signal: In general this avoids time loss and eliminates human observation errors. It also facilitates the use of such an electric output as the input of a computer.

- Type of conversion:

a) Photo cell: The cell is fixed on a carrier, which moves with constant velocity from a point of certain elevation down along the manometer tube. When the meniscus of the liquid column is reached, the light beam crossing the tube is weakened by absorption before reaching the photo cell. Then counting starts. It ends when the carrier passes a zero mark of height level.

b) Capacitor: This is fixed on a moving carrier similar to a). At the moment, the cylindrical capacitor moves along the liquid column, amplitude or frequency of a given electrical oscillation undergo a change.

c) Resistor: If the manometer liquid is an electric conductor, it can be connected to one pole of a battery. The other pole is connected via a straight stiff thin wire attached to the tube and dipping in the manometer liquid at its opposite end. The electrical resistance of the non submerged part of this wire and the current resulting hereof indicates the length of the manometer column.

d) Deformation by pressure: This can be used by piezo quartz crystal or by a disk with a micro strain gauge.

- Problems involved in measurement of pressure:

a) Damping of oscillations. A narrow throat at the inlet of the manometer tube may be useful.

b) Guiding walls with non-stalled flow as a prerequisite for any pressure measurement: Measurement of pressure within a flow field requires the use of a measuring probe so that flow separation is not caused and generally so that the main flow is disturbed as little as possible. This is attained by making the streamlined carrier of the pressure tappings small in comparison with the size of the duct where the measurement is made. Furthermore the surface of this probe near the tappings has to be as far as possible in the tangential direction of the flow to be measured.

Such a streamlined body contains usually four tappings in its cylindrical part, distributed uniformly around the circumference of the probe. These four tappings are interconnected. This gives a cross section-averaged pressure along the periphery, used for pressure measurement. To minimize the size of the probe, these static pressure tappings are located as near as possible to the curved axial symmetric head of the probe.

Due to curvature of the streamlines in this region the static pressure at the surface falls somewhat short of its desired magnitude in the undisturbed flow. This can be compensated either by a sufficient distance of the tappings from probe head or by the artificial impact pressure on the front face of an axially movable ring (see Fig. 9.4.1 c). The correct position of the ring depends on the Reynolds number of the flow [9.72; 9.74].

- Limits for the size of the probe and its tappings: The diameter of the probe can be reduced down to 3 mm. This takes account of the capillarity effects of too small holes, the limitation of measuring time and the limits of resistance in the tubes connecting the tappings with the manometer. A pressure port or tapping should be as small as possible. However with respect to surface tension and pipe friction it should not be less then 0.3 mm in diameter. When the ports are connected with micro semiconductor probes the diameter of the probe's head is limited by the actual smallest diameter of 2 mm of such

346
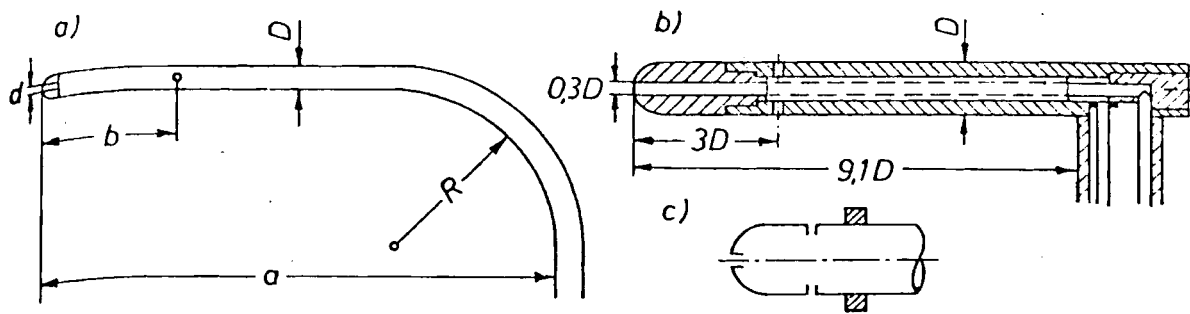
Fig. 9.4.1. Probes for simultaneous measurement of static pressure and impact pressure, facilitating the measurement of the velocity magnitude in steady flow. a) AVA, ASME probe. For the separate measurement of static and total pressure tappings not in use blanked off. Dimensions AVA/ASME probe a: 20 D/25 D; b: 5 D/8 D; d: 0,3 D/0,5 D; r: 5 D/3 D; number of tappings: 4/8. b) Prandtl probe. c) Ditto with axially adjustable ring to adjust static pressure.

devices and by the desire to place them as near as possible to the probe's head. In general a larger tapping within the wall will also be subjected to disturbing turbulent pressure fluctuations.

- Finish: The edges of the tappings must be smoothed without any burrs. Otherwise additional impact pressure may be caused.

- Reasons for falsification of pressure measurement by means of drilled holes (tappings):

a) Any hole curves the adjacent flow. This enlarges the pressure by centrifugal force.

b) Diffusion of the flow into the hole in the streamwise direction causes stagnation in the rear.

c) The strain rate $\partial c_y / \partial y$ normal to the wall is connected with an additional viscous normal stress $2\eta \partial c_y / \partial_y$ with η as the viscosity of the fluid.

d) The turbulent fluctuation c'_y normal to the wall causes apparent stresses according to Reynolds of the magnitude $- \varrho \overline{c'_y{}^2}$.

9.4.1.2. The measurement of velocity by piezometry: Fundamentals: This kind of velocity measurement is based on the measurement of pressure in different tappings on the wall of a probe. Strictly speaking it therefore can be applied only to a flow which is uniform within the space occupied by the probe.

- Magnitude of the velocity: The total pressure, stagnation pressure or impact pressure is measured by a Pitot tube, a hook-formed probe with a tapping at its front. The dynamic pressure linked to the kinetic energy of the flow may be obtained, if the static pressure measured at a station as near as possible to the impact pressure tapping is subtracted from the impact pressure.

- Design of probes for one dimensional flow:

a) ASME/AVA probe, Fig. 9.4.1 a.

b) Prandtl probe, Fig. 9.4.1 b.

c) Probe with conical head (Brabeé, NPL, England).

d) Probe with ellipsoidal head (NPL).

e) Streamlined probe (Numachi, Murai, Abe, Tohoku Univ. Japan).

The shaft of the probe must be reasonably stiff to avoid any deformations caused by bending moment due to the drag of the probe. The main advantage of the Prandtl tube consists in its stiff structure. Moreover the directional influence here is very low.

347

A Reynolds number influence is given by its stem. For the ASME probe any interference between probe head and stem becomes smallest. Also the Reynolds number influence is negligible for higher numbers [9.108]. The probe with ellipsoidal head behaves similarly to the *Prandtl* tube although its boundary layer may be smaller [9.108]. The conical probe c) gives a predictable stall at the corner between cone and cylinder. Due to this the static pressure measured on the cylindrical part, becomes more independent of the Reynolds number than in the case of a probe with a smooth transient curvature from the head to its cylindrical part.

-- Directional sensitivity: The sensitivity of the *Pitot* tube or the tapping at the front of the tube is very small. For a flow deviating by 20° from the axis of the tube, the impact pressure deviates only by 1%.

-- Influence of shear flow: In the neighbourhood of walls or within a rotating channel an influence of shear flow exists. Such that the station of indicated velocity deviates from the tube axis.

-- Design of flow directional probes:

a) Two-(Three)-finger probe. Fig. 9.4.2 a shows a characteristic of a two-finger probe after *W. Kühnel* [9.74]. The differential pressure $p_{\alpha'}$ between both the tubes, related to the dynamic pressure $q = \varrho c^2/2$, grows linearly with the angle α', the velocity c makes with
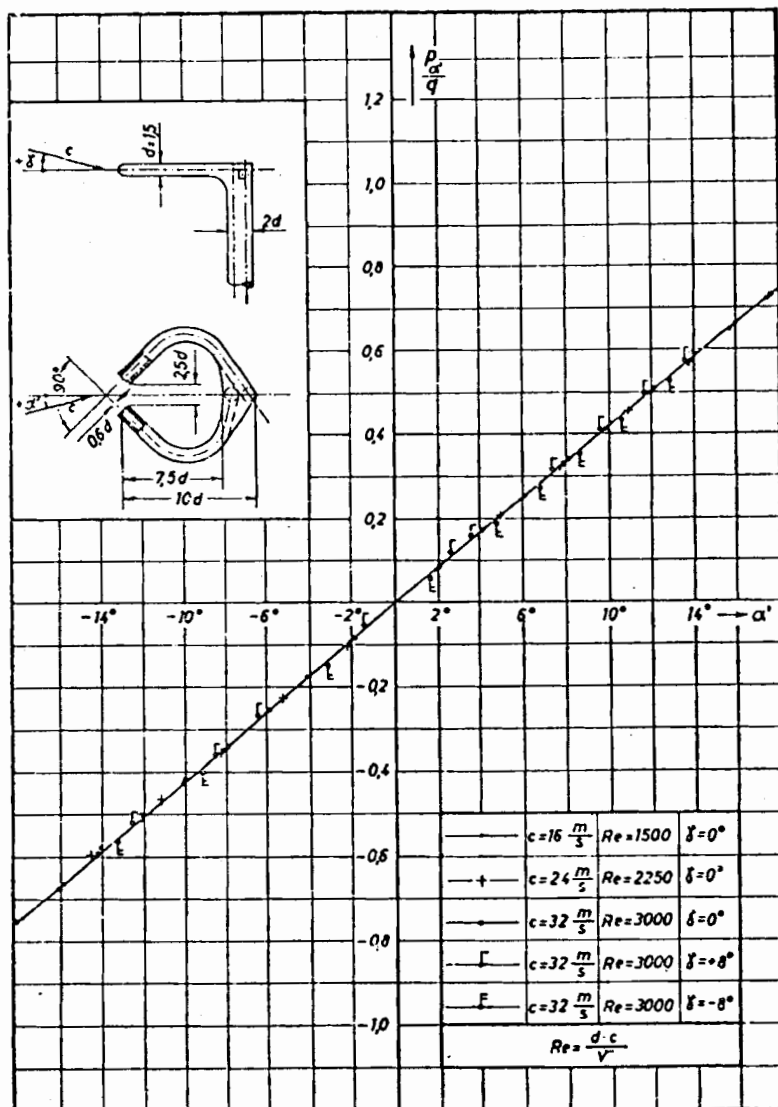
Fig. 9.4.2. Characteristic of finger probe in air as a function of Reynolds number $Re = $ from *Kühnel* [9.127].

348

the probe's axis. It is independent of the Reynolds number, when the front face of each tube is planely ground and perpendicular to the axis of the tube. The measurement is also independent of the pitch angle γ in a range of $\gamma = \pm 10°$. Here the magnitude of the velocity c can be found by the dynamic pressure, when one of the tubes is turned in the direction of c. In the three-finger probe, this is effected by the mean tube.

b) Cylindrical probe (see Fig. 9.4.3 b). Here the directional sensitivity is greatest, if the 3 tappings are 24° apart.

c) Spherical probes. c1) Probe after *van der Hegge Zijnen*, Fig. 9.4.3 c, with a hook-shaped stem. Such a stem facilitates the determination of flow direction by rotating the probe about its stem axis until the pressures in the two directional tappings in a plane normal to this axis are equal. The inclination of the velocity vector c against the axis of the probe's head is determined by the difference of pressures on the two tappings located then in the plane of c. This procedure can be used for all the probes with four directional tappings on their head. c2) Hemispherical probe, Fig. 9.4.3 d, with advantageous small size. Diameter 3 mm in water, 2 mm in air. As with the previous probes it can be equipped with static pressure tappings behind the head.
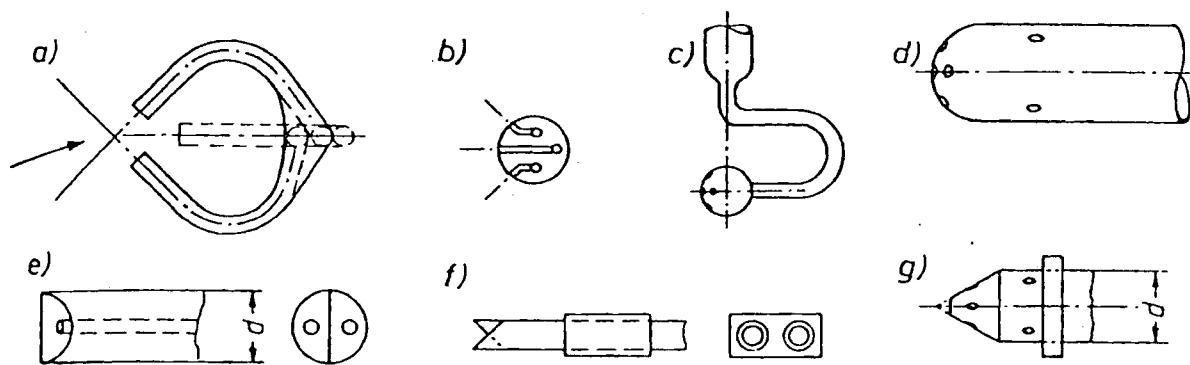
Fig. 9.4.3. Probes for the measurement of the velocity magnitude and direction in a steady flow. a) 2(3)-finger probe for plane flow. Because of low directional sensitivity of tappings, also the impact pressure can be measured by one of the fingers. With 3 fingers the central finger for impact pressure, then more exactly measured than by 2 fingers. Turning of the probe by 90° facilitates also a measurement of the static pressure. b) Cylindrical probe for plane flow. c) Spherical probe by van der Hegge Zijnen for spatial flow. d) Hemispherical probe for spatial flow, diameter down to 3 mm. e) Chisel shape probe with small diameter $d = 1,5$ mm; surface angle $\mp 45°$, for plane flow. f) Boundary layer probe for plane flow after Reichardt, surface angle $\mp 45°$. g) Conical probe with adjustable ring (see also Fig. 9.4.1.c) for spatial flow after *Conrad*, vertex angle 30°, $d = 4$ to 7 mm [9.127].

d) Wedge shaped or conical probes: d1) Double hole chisel probe, Fig. 9.4.3 e, advantageous small diameter down to 1,5 mm. d2) Double hole boundary layer probe after *Reichhardt*, Fig. 9.4.3 f, for the finding of the velocity direction in thin boundary layers with plane flow. d3) 6-hole conical probe after *Conrad* [9.109] Fig. 9.4.3 g, with an axially movable ring behind the static pressure tappings for eliminating the Reynolds number influence on the indication of static pressure. Fig. 9.4.4 shows the characteristics of such a probe after *W. Kühnel* [9.74] for a flow in the plane of the probe's stem and the axis of the probe's head ($\alpha = 0$). The differential pressure $p_{y'}$ between the tappings due to the pitch angle γ' grows nearly linearly with γ' when it is related to the uncorrected dynamic pressure q'. The deviation of q' from the correct dynamic pressure $q = \varrho c^2/2$, the deviations of static pressure Δp and total pressure Δg are shown also as function of the
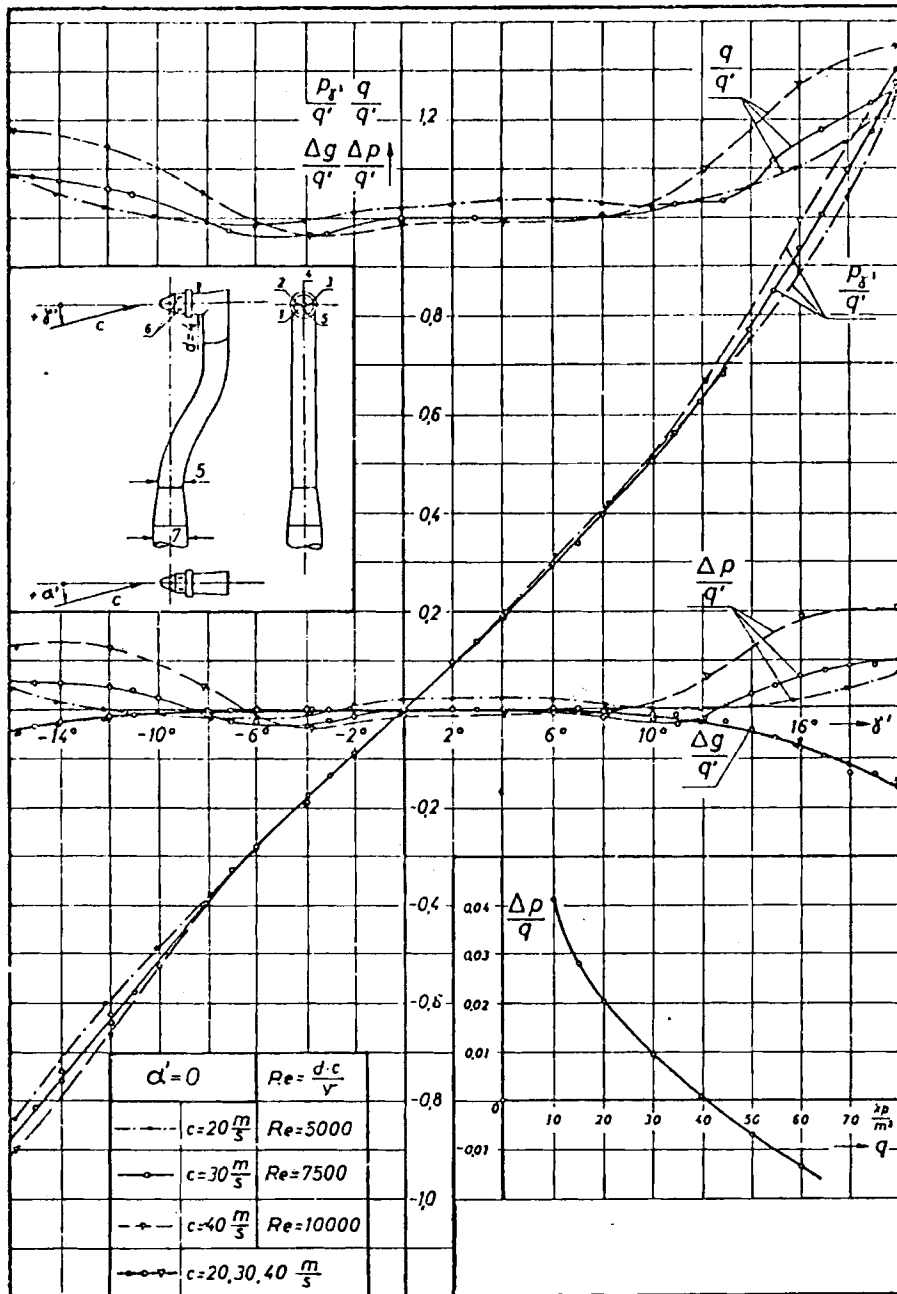
Fig. 9.4.4. Character-istic of a 6-hole Con-rad probe in air as function of Reynolds number for $\alpha' = 0$. p_γ differential pressure due to pitch angle γ', p static pressure, g total pressure, Δ de-viation, $\Delta p/q$ cor-rection of p. After Kühnel [9.127].

Reynolds number. d 4) 6-hole conical probe with wide U-turn of its stem for measuremen of relative flow especially close to the vane surface, with minimum influence of the ste on the probe's head, after W. Kühnel [9.72] (Fig. 9.4.5).

- Disturbing influences:

a) Influence of velocity gradient on directional probes. For a given gradient the influen on measurement of direction diminishes with reduced probe diameter. A probe of m imum gradient sensitivity has been developed by Reichardt, Fig. 9.4.3 f, with a directio error of less than 0,1°. For wedge probes with three holes a directional error of 2 known [9.108].

b) Influence of vibration: The vibration of the probe also produces oscillations of liquid columns from the probe to the manometer. A lateral oscillation of the probe sur

350

Fig. 9.4.5. Conical 6-hole probe with wide U-turn, to reduce stem influence on the head of rotating probe, after *Kühnel* [9.127].
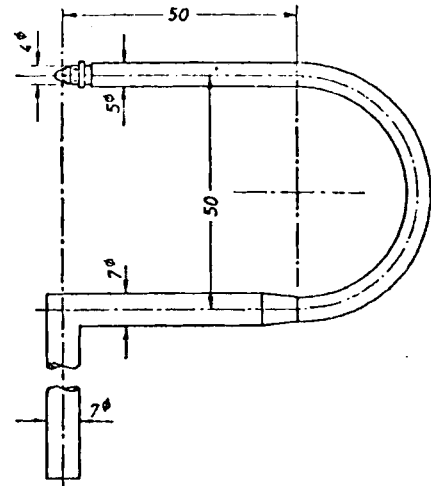
near the tappings may falsify the pressure indication as it results in an additional apparent impact pressure.

c) Errors due to time-averaging procedure of non dynamic measurement: A sinusoidal pulsation of the flow with amplitude c_1 creates a time-averaged error of the indicated mean dynamic pressure of about $\varrho c_1^2/4$. For a stationary probe such pulsations exist near to a rotor for the periodicity of the relative flow field through a vaned cascade especially past the rotor due to the wakes.

9.4.1.3. Pressure measurement by air injection: Fundamentals: Air is injected into the flowing liquid, passing the model measured through tappings at guiding walls or probes by a very small bubbling air flow from the tapping into the liquid. The air may be preferably also used for the transmission of the pressure, to be measured from the tapping to the manometer. As the density of air is small in comparison to that of water, errors due to surface tension may be neglected in the case of not too small a pressure. The relatively small density of air especially in the case of not too thigh pressures results also in negligibly small body forces in the air transmission pipe due to gravity and centrifugal action, when the pressure is transmitted from a rotary tapping to a stationary manometer.

Experiences: This method was used for the measurement of the relative flow field along the vane of a Francis turbine runner by *E. Bär* [5.17] and *G. Schlemmer* [5.18]. *R. Jahn* did the same with a Kaplan turbine [9.110]. *J. Korcian* applied this method to the measurement of the relative flow field in a semi axial pump impeller [6.44].

- Error: A comparison of the torque measured by means of a spring-suspended torque reaction dynamometer with the torque calculated from the measurement of pressure gained by this method, shows a maximum error of 7% [5.17].

- Practical advice. Care has to be taken, that the pipe from the tapping to the manometer is completely filled with air. This may be controlled by an artificially high air flow by operating a valve between a pressurized air vessel and the piping. The desired state of a slightly bubbling air flow out of the tapping may be observed either by a manometer column coming to rest or (if possible) through a partly transparent casing and rotor by means of a stroboscope.

Example: Fig. 9.4.6 shows a test turbine [5.17] equipped with such a device. Here the runner vanes for measurements were made of Acryl glass. The tapping is a bore in the centre of a small disk. This covers a larger bore of 5 mm drilled in the vane. In this hole the transmission pipe ends. This is fixed in a slot of the vane. The vane surface is finished in such a way, that no projection disturbs its smoothness.
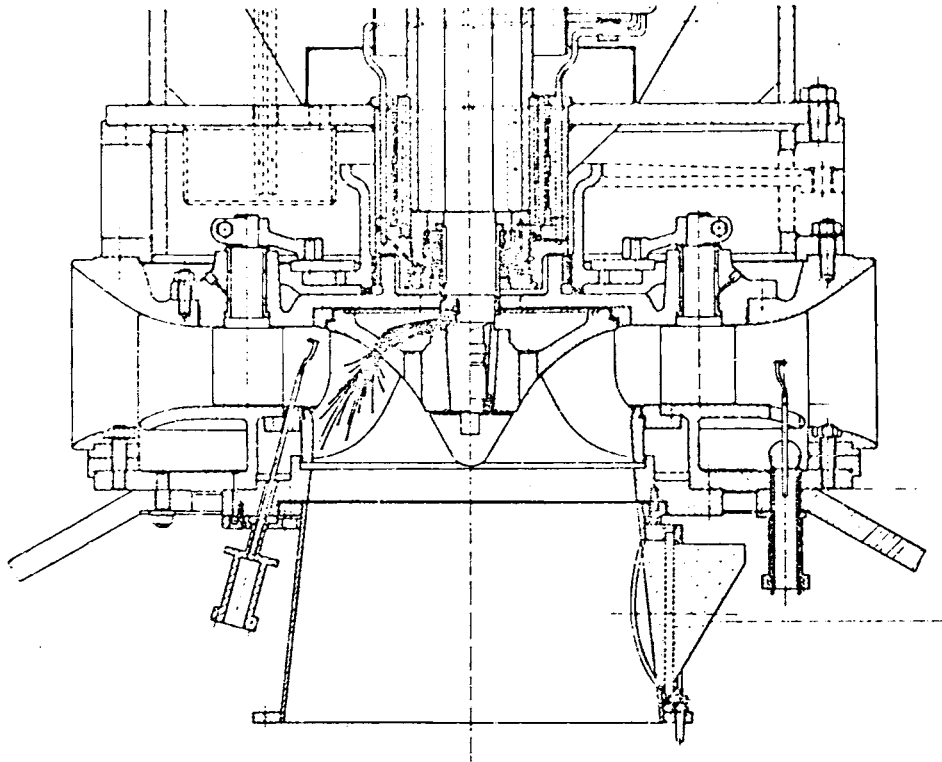
Fig. 9.4.6. Water-operated model Francis turbine. Measuring vanes of acryl glass integrally cast with inlaid pipes, each leading from tapping on the vane surface via a scanning valve (Fig. 9.4.9) to a stationary manometer, after Bär [5.17]. Inflow from an open tank via stay and guide vanes. Guide and thrust bearing in a tube screwed to the swinging stator of the torque reaction dynamometer. Tube guided by hydrostatic bearings and suspended on a torsion rod (Fig. 9.4.10). $D = 0{,}455$ m.

9.4.2. Calibration of probes for arbitrary flow

The calibration of a probe needs a water or air tunnel. For the elimination of wall influence, which is a considerable handicap for any probe [9.72], this tunnel should have a similar size possibly with a similar form as the duct in which the probe is used afterwards. Probes for steady flow are calibrated in steady flow. Probes for unsteady flow are usually also calibrated in steady flow. Strictly speaking they should be calibrated in an unsteady flow of exactly the same type, as occurs in the test. Since this is impossible an approximation is made by a special and typical unsteady flow, e.g. a sinusoidal one, generated by a correspondingly moved piston.

9.4.3. Methods for dynamical measurement of unsteady flow

9.4.3.1. General remarks on unsteady flow: The real temporal course of unsteady flow is of growing interest as it causes losses (by vortex generation) and vibration in the guiding structure. These vibrations may be self excited or excited from external sources. They also include the danger of resonance and fatigue cracks in the construction. This becomes more important as the recent trend in modern design tends towards a larger size of units. This entails a greater structural elasticity of the machine. Also the trend towards welded and thereby more elastic structures favours hydroelastic response and thereby unsteadiness of the flow.

352

9.4.3.2. Velocity measurement: Fundamentals: Contrary to the measurement of steady flow, in an unsteady flow only the magnitude or one component of the velocity can be obtained through direct measurement of one device, which uses thermal, optical or elastic effects of the flow with quick response. Moreover a simultaneous measurement of instantaneous pressure and velocity is not possible by these direct velocity measurements. The measurement of the velocity vector needs a method such as the Laser anemometry, which does not disturb the flow. Moreover it requires as many devices as velocity components exist. Principally the velocity vector now also can be measured by the simultaneous measurement of instantaneous pressure at different ports of one probe similar to the corresponding vectorial probes for steady flow. Such probes are described under the section 'pressure measurements'. They have a practical value only, if the gradient and the growth rate of the velocity is small in the space, occupied by the probe. Further, the interference of water hammer waves which are generated or reflected by the probe's stem, with the probe itself does not allow an elimination of the influence of the stem. At last the strictly needed calibration of such a probe in real unsteady flow is rather troublesome.

– Designs of different probes:

a) Probes using thermal effects:

aa) Hot wire probe: It uses the cooling effect of an electrically heated very thin wire which is exposed to the flow. Unfortunately this very sensitive device cannot be used in liquids with their strong impact stress and erosion.

ab) Hot film probe: The probe, Fig. 9.4.7, has a front of a wedge formed glass body covered with a thin platinum layer (film). This is electrically heated to a constant temperature somewhat above that of the surrounding streaming fluid. This enables a heat flow from the film into the fluid. Therefore the heating current through the film depends on the heat flow into the fluid and its velocity. As the film has a constant electrical resistance and as its temperature is kept constant, the voltage between its ends depends on the electric current passing the film and on the flow velocity. This voltage is measured and amplified. The probe is very sensitive. It needs a clean liquid without too many gas bubbles and without vapour cavities. The working life increases as the velocity is reduced. At about 2 m/s the durability within water of greater hardness ranges up to 50 hours [9.46].

b) Probes using elastic effects: Any obstruction in a flow in a certain direction, which is fixed by a laminated spring on the wall, deviates with the velocity from its zero position by virtue of balance
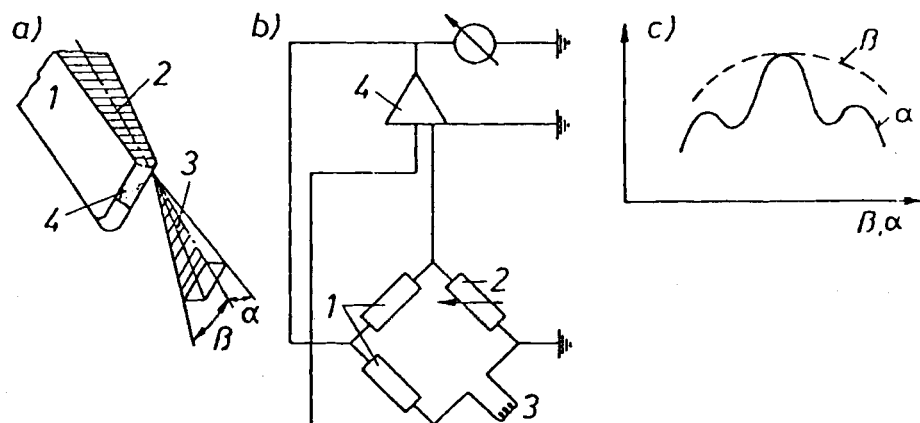
Fig. 9.4.7. Hot film probe for dynamic measurement of the velocity magnitude a) Probe, 1 glass, 2 probe axis, 3 mean plane, 4 film of platinum. b) Circuit diagram of probe: 1 constant resistor; 2 variable resistor; 3 film of probe; 4 DC amplifier. c) Angular sensitivity of probe. After *Mollenkopf* [9.46].

between the drag and spring-born force on this obstruction. This deviation can be converted into an electric signal. Such an instrument can also indicate a reversing oscillating flow. The so-called "flow pendulum" consists of a disk of 1 mm diameter, suspended on a laminated spring. This passes through a slot in the streamlined transducer, which is attached to the wall by a hollow shaft. The end of the spring is clamped in the interior of this shaft. The mean part of the spring carries an iron core. At rest in the zero position this core is located symmetrically between two coils. One of them is the primary the other the secondary winding of a transformer. Both the coils are connected to each other, so that in the zero position the voltage between the ends of one of these coils is compensated by that of the other coil. If the disk is shifted by the flow, the resulting voltage then induced is used as signal for the velocity, provided the probe's exciting frequency differs from its natural one.

c) Probes using optical effects: Here only Laser anemometers are mentioned:
ca) Focus method: Laser beams are focussed on 2 stations a known distance from each other. The velocity is measured by the time interval a suspended particle needs to cover this distance. A 2-focus Laser was developed by *Eckardt* for an air compressor in 1976 and recently has been applied on a model Kaplan turbine in water by *Brand* and *Selbach* [9.63].

cb) Interference pattern method. Here a pattern of streaks parallel to each other and with known distance from each other is generated by the interference of a Laser beam with itself after its reflection and corresponding phase shift. The velocity component normal to these fringes is measured by the time interval a particle needs to cover this known distance [9.66], [8.136].

– Problems arising with the Laser: An observation window is required with an outer surface normal to the beam. For internal flow in fluid machines a back-scatter arrangement is needed with its weakened light radiated back, whose signal strength is reduced by wall and window flare as reported by *Brand* and *Selbach* [9.63]. Generally see [9.64; 9.65; 9.67].

9.4.3.3. Measurement of pressure: Fundamentals: Similar to the measurement of pressure in steady flow the dynamic measurement of pressure in unsteady flow is restricted only to that on walls. A streamlined carrier of the proper probe, as used in steady flow, experiences in unsteady flow a greatly varying angle of incidence.

This induces an additional unsteadiness by starting vortices originating from the rear of the body and possibly also by stall. Mainly the piezo electric effect or the elastic deformation of a pressure loaded membrane of low inertia are used for conversion of unsteady instantaneous pressure into an electric signal. Here the elastic deformation induces an unsteady displacement of the flow which does not exist originally.

– Piezo quartz indicator: Such probes operate by the principle, that the surface of a quartz crystal is electrostatically charged if a pressure acts on it. Unfortunately the probe is rather large. It has a favorably high resistance against erosion.
– Membrane with strain gauge: By application of adequate material and not too small a size also such probes may be very highly resistant against corrosion and erosion. For the usual small models the "Kulite type micro semi conductor probe" was developed [9.81]. It consists of a disk, which is 2,3 mm in diameter and which is soldered to a small cylindrical box so as to be watertight. The interior of this box is exposed to a constant reference pressure. The strain of the disk due to its pressure-induced bending is measured by a semi conductor fixed on the surface of the disk in the region of its largest strain under external pressure. This generates a voltage by change of resistance.

Unfortunately the probe often shows a drift of its zero point, which has to be countered by repeated calibration. Moreover the probe is not very resistant against a cavitating flow.

354

9.4.4. Problems arising with rotating probes

9.4.4.1. General remarks about rotating probes: Calibration: For the calibration of a rotating probe it seems the best thing is, to locate it at the same station as it will be used later on for taking measurements. In an air test this procedure may be done at zero discharge without the rotor. Secondary flow, caused by the stem of the probe as well as the wakes of the stem must be kept off the head of the rotating probe, usually oriented peripherally.

Rotating Kulite probes may be calibrated by known air pressure conducted by a piping within the rotor vane from a pressure vessel at rest.

_ Turning the probe about its stem: Here an adjustable stationary cam, Fig. 9.4.8 a, shifts axially a rack, located on the axis of the rotor. This rack turns the radially directed rotating shaft of the probe by means of a cog wheel. A source of trouble in such a device may be backlash and additional uncontrolled deformation. Furthermore the space required is usually limited by that available.
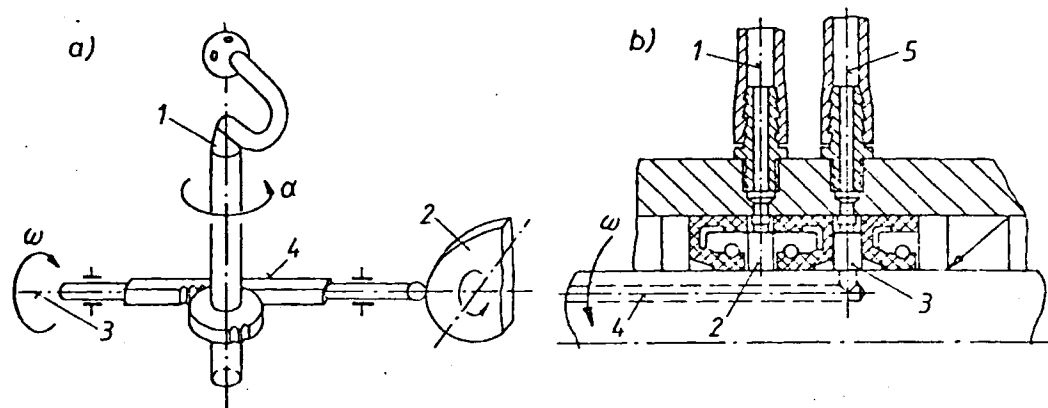
Fig. 9.4.8. Devices used for rotating probes. a) Device for turning the radially oriented and rotating stem of a vectorial probe (here spherical probe) about its axis. Probe is turned until velocity vector (of the assumed steady relative flow) coincides with the plane formed by the axis of stem and the axis of the probe's head; then the pressure in the tappings due to the yaw angle is equal. 1 radial stem of probe; 2 cam for axially shifting adjustment rod 4; 3 axis of machine and of rotation; 4 probe adjusting rod with drive of probe stem by rack-and-pinion gear. b) Transmission chamber for pressure from tapping on rotating probe to stationary manometer. 1 oil from high level tank; 2 seal chamber to both sides of pressure transmission chamber 3; 4 boring to tapping; 5 hose to stationary manometer.

Therefore fixed probes or probes, which are turned by electromotor fixed at the rotor are preferred [6.44], see Fig. 6.4.4.

- Strength problems: When the prove stem is hook-shaped or has a wide U-turn, Fig. 9.4.5, centrifugal forces may bend and twist it. Therefore a rotating probe should be very stiff in its stem. The unbalance caused by the probe must be balanced by countermasses as a function of the radial position of the probe. To measure the flow between the rotor vanes over one pitch, a peripheral slot in the hub is needed. This weakens the hub wall, which has to be taken care of. For a definite position of the probe the slot must be closed. Otherwise a secondary flow along the shaft is generated. Such a flow exists also without the slot but on a smaller scale. Care must be taken that this flow does not meet any tapping at the probe's head.

355

9.4.4.2. Transmission of values measured from rotor to stationary indicator

- Rotating indicator: Here the indicator, e.g. manometer, is fixed on the shaft, which therefore has to be vertical. The indicated value may be received either by a rotating camera or by a stationary camera with the aid of a rotoscope or a stroboscope, in which case the flow has to be steady. Disadvantage: Rotating masses, which must be balanced. Advantage: No additional torque of the transmission device. No transmission error.

- Rotating transmitter: Electric signals or other signals transformed into such signals are transmitted to a stationary receiver. Advantage: No frictional torque by transmitting device, no transmission error. Disadvantage: Expensive, measured value must be transformed into electric signal.

- Stationary indicator for electrically transmitted signals: Here the electrical measuring signals can be transmitted by mercury chambers, serving as sliding rings. Advantage: Small friction. Disadvantage: Transmission error, as transmitted currents are rather small [9.81].

- Optical transmission: Indirect by stationary camera and stroboscope or rotoscope as above or direct by Laser anemometry. Advantage: No transmission error, no friction. Disadvantage: Very expensive.

- Stationary indicator with mechanical transmission: For the transmission of pressure from a tapping on the rotor to a stationary manometer (used as an indicator) a carefully sealed ring chamber, Fig. 9.4.8 b, is required. This may be tightened on both sides by radially elastic ring elements gliding on a polished and chromed sleeve around the shaft. Moreover this may be tightened by ring chambers, filled with pressurized oil on both sides. The oil pressure hitherto has to be above the pressure transmitted and is produced by an oil vessel located above the oil chamber. It must operate before the shaft starts rotating [9.127]. Advantage: No transmission error. Disadvantage: Frictional torque.

9.4.4.3. Scanning valve for connection of rotating tappings with stationary manometers.

Fundamentals: Usually many rotating measuring tappings have to be connected to several available stationary manometers. In the case considered of a steadily operating
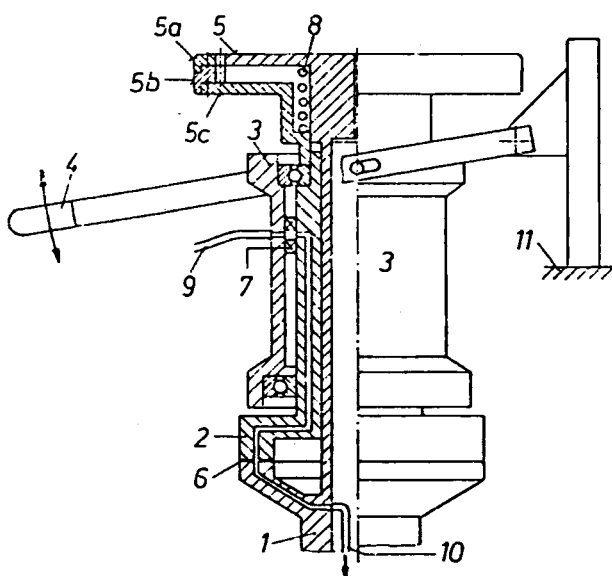
Fig. 9.4.9. Scanning valve, connecting the tappings on the runner vane face to a stationary manometer. 1 shaft with borings from tappings 10 on vane face, 2 inner sleeve connected to a stationary manometer 9 stepwise turnable relative to 1; 3 outer sleeve connected to the swinging stator frame of brake 11 by means of lever 4, at up and down motion of the friction of slipping parts turns the sleeve relative to 1 by one pitch; 5 inmost part connected to shaft 1 having external teeth. 5 a upper internal gear rim, at which each 2nd tooth is omitted, is fastened on similarly toothed internal gear rim 5 b, tangentially turned against 5 a by 1/2 pitch; 5 c fixed on 5 b; 6 disk seal 7 oil seal (Fig. 9.4.8. b); 8 spring pressing down 5 c and 2 against 1; 9 hose to stationary manometer 10 hose from shaft to tappings on runner vane; 11 swinging frame of stator.

machine, the rotating tappings can be connected one after another by a scanning valve to the stationary manometer. For the abbreviation of this procedure two things have to be provided. Firstly: The switching operation must be possible under full speed. Secondly: With any switching several tappings are connected with the corresponding number of stationary manometers.

Mechanical design of a scanning valve: Fig. 9.4.9 shows a mechanical switching device, developed by *E. Bär* [5.17]. It operates as follows: By the reciprocating motion of lever 4, parts 3 and 2 move up and down, guided peripherally in the teeth 5_a, 5_b. The friction of the seal decelerates the rotating part 2 against part 5 and 1. By this both parts are moved tangentially by one tooth pitch against each other. This is possible in the lifted position of the lever 4 due to the clearance of one pitch in the tangential direction (effected by the omission of each second tooth) and also in the lowered position of the lever due to similar tangential clearance (see Fig. 9.4.9).

This switching by moving the lever 4 up and down turns part 2 about the axis against part 1 in the desired manner, so that the pick up bore in 2 advances along the seal 6 from one measuring port to the next. The up and down motion of part 2 against shaft 1 is also needed to avoid any wear and friction during the switching and to provide tightness of the joint flange between part 1 and 2 after any switching by means of the seal 6.

Since the scanning valve is fixed on the frame of the stator of the torque reaction dynamometer (here two oil-operated radial 12 cylinder positive displacement pumps are used to obtain a strong and steady braking torque down to zero speed), the frictional torque of its seal 7 is eliminated as an internal force.

Fig. 9.4.10 shows the arrangement on a model Francis turbine with its pipes connecting the tappings or ports on the vane to the stationary manometer via the scanning valve shown in Fig. 9.4.9.

9.4.5. Measurement of the torque

– Fundamentals: The hydrodynamic torque exerted by the flowing fluid on the rotor may be measured by the twist of the shaft between the runner and the adjacent journal bearing with the aid of strain gauges. As the shaft is rather stiff, very sensitive strain gauges must be applied or their output is very small and therefore liable to errors. Moreover this doubtful small electric value must be transmitted to a stationary indicator. Therefore on models, torque measurement by reaction torque dynamometers is preferred.

Here the reaction torque, which is nearly equal to the hydrodynamic torque of the runner, is measured at the quasi-stationary, slightly swinging stator of the brake. This can be done mechanically by weight or electrically via bending of a beam by means of strain gauges, as used e.g. in the lab of Hidroart, Milan [11]). To approximate the measured reaction torque as far as possible to the desired hydrodynamic torque on the runner, the friction of the support of the brake's stator must be made as small as possible. This can be done by incorporating the shaft bearings in a tube which is attached to the stator of the brake, see Fig. 9.4.6 and 10. This eliminates the bearing friction as an internal force of the system motor brake. The swinging quasi-stationary brake stator of this system should be supported at least by means of roller bearings. A more favorable solution is to support it by oil- or air-lubricated hydrostatic bearings. This is done in Fig. 9.4.6 and 10 with radial bearings. Another solution is a spring suspension of the brake stator in such a way, that either no spring force is exerted on the system, when it is in its measuring

---

[11]) According to information given to the author by Mr. *Ucelli*, the lab of Hydroart, Milan, applies this kind of strain gauges to a small loaded beam for all kinds of load and torque measurements. In recent research work, the author's lab at TUM has also used this very sensitive device successfully.

357
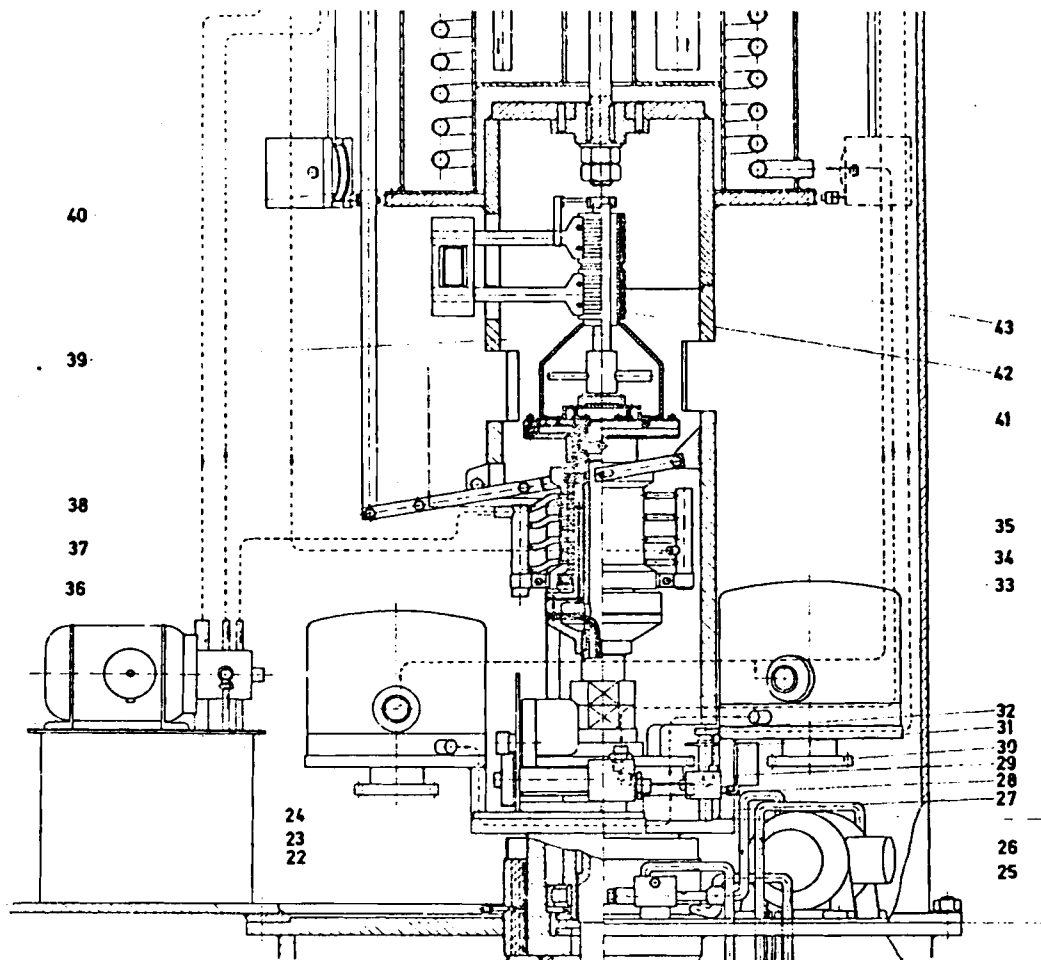
Fig. 9.4.10. Torque reaction dynamometer with scanning valve. Brake: two multipiston radial positive displacement pumps with stator on swinging frame suspended on torsion rod. Upper end of latter fixed on stationary part. Zero output by throttling oil flow. Reaction torque on the pump casing twists the torsion rod, the twist of which is measured by the deflection of a light beam. From *Bär* [5.17].

position, or that the tangential deformation of its suspension is used for the measurement of the torque and the deformation due to the axial suspension is used for the measurement of an additional axial thrust during operating of the machine, see Cap. 9.6.

– Special brake design: Fig. 9.4.10 shows a special brake design in which the last mentioned principles are realised. At first the shaft of the turbine is radially and axially supported in a tube attached to the brake stator, which eliminates the shaft friction as an internal torque.

This tube of the brake stator is radially supported by oil-lubricated hydrostatic bearings. The tube-like system is axially supported by means of the twisted rod. This rod is tangentially clamped at its upper end by means of roller bearings, enabling only an axial motion of this rod end. At this end the rod is fixed in the axial direction to a short axially elastic rod, fixed at its upper end to a rigid frame. This short rod is covered with strain gauges, to measure the variable axial thrust under operation of the turbine.

The reaction torque on the lower end of the elastic rod twists the latter. This twist is optically indicated by a light beam, which is emitted from a stationary lamp and then

reflected by a mirror attached to the twisted rod. This device developed at Lehrstuhl und Labor für hydraulische Maschinen und Anlagen der TU München is calibrated by a weight-induced torque.

The internal torque can also be measured by a simpler brake if the bearing torque is eliminated by measurement, see Fig. 9.4.11.

Fig. 9.4.11. Scheme of torque metering on a high pressure test rig in the Brunnenmühle research station of J. M. Voith, Heidenheim, used for models of turbines and pumps. 1 generator motor; 2 cradled electric dynamometer; 3 load cell for coarse measurements; 4 coarse weight balancing unit, 20×10 kg weights; 5 load cell for friction torque W_R of turbine bearing; 6 load cell 200 N for precision measurement of F_F; 7 constant preload $m_v = 2000$ kN at reversed direction of rotation; 8 normal direction of rotation and torque; 9 model machine. See O. Eichler, G. Heimann, L. Brandt [9.58]. Similar load cells in the form of bending cantilevers pasted with strain gauges are used by Hydroart, Milano. An elimination of the friction torque of the guide bearing requires annulled radial bearing load. This can be reached by putting on the torque in form of a couple without radial load on the bearing.
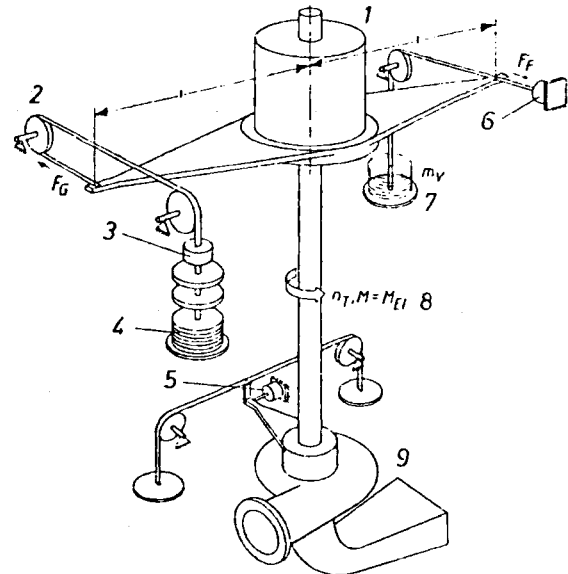
9.4.6. The visualization of flow

- General remark: No measurement at a series of individual points can replace the visualization of the whole flow field. This holds true especially under off-design point operation and moreover in the cavitating regime. Up to the present there is no device, which enables the measurement of pressure and velocity in a cavitating flow.

- Absolute flow: A simple method of visualization consists in fixing light threads on the boundary walls of the flow field. For an air flow, eiderdown enables good observation of wakes and the boundary layer adjacent to the wall under stalled conditions. The injection of smoke in air, of coloured dyes or gas bubbles in water, or the electrolytic generation of bubbles there also enables an observation of flow effects especially close to the wall.

At any rate the size of bubbles should be small to limit slip by pressure gradient. In this respect the use of polymeric suspension instead of water according to Fleischner [9.111] facilitates an approximate measurement of flow velocity. The spark method, introduced by Weske, and later on developed by Fister [9.113] and Gallus [9.114], shows the strain rate of a spark-ionized fluid path e.g., in rotor channels and hence the temporal change of velocity profiles in badly accessible ducts.

All these methods need at least one observation window and one illumination window, the first with a plane external surface. For the observation of the flow in a rotor channel they require at least a partly transparent shroud, hub or, in case of need, also vane. Moreover any observation requires a high speed camera with a steady or speed-triggered (stroboscopic) light source.

359

- Relative flow: A perfect observation of the flow in a radial rotor is obtained by a transparent hub and adjacent transparent casing. This needs a drive from the side of the shroud. A convenient method is offered by the rotoscope. Here the camera rests.

A light beam from the observed rotor passes a prism which rotates with 50% of the angular velocity of the rotor (Dove prism). Thus the reflected beam of the prism remains stationary. Therefore the receiving camera or human eye of a resting observer can also be stationary.

- Visualization of relative flow direction close to the vane: This method has been developed by G. Schlemmer [9.83] for a Francis runner. The mean flow direction a certain distance from the runner vane face can be indicated by micro flags. These light metallic flags of triangular form are arranged so as to rotate easily about their shafts. At the end of each shaft a piston-like disk is fixed. This lies with a very small axial clearance in a specially adapted cylindrical chamber within the runner vane surface. This piston can be blocked by friction, when it is loaded by compressed air. This pressure lasts also during the rundown of the turbine and the following dismantling of the individual rotor vanes. With the aid of pattern making sections and radial sections, scratched on the runner blade, the "frozen" quasisteady direction of the time-averaged relative flow can be obtained easily from this flag position [9.83], [5.18].

9.4.7. Fluids to be used in tests

In practice water and air dominate as test fluids. The advantage of air consists in the easy handling of the light test equipment. This facilitates especially preliminary selective tests. Gas in a closed test rig may also allow the Reynolds number to be varied in a wide range for efficiency scale effects. This can be attained, e.g. by changing the kinematic viscosity by means of heating or pressurizing the fluid.

Measurements carried out by Klein at Lehrstuhl und Labor für hydraulische Maschinen und Anlagen at Technical University Munich with air, Argon, CO_2 operating a FT have revealed that the efficiency characteristic, e.g. the hill diagram, of a hydraulic machine does not only vary (as always suspected) with the Reynolds number but in a much stronger degree with some molecular properties of a fluid.

These are e.g. the number of atoms in a molecule and hence the adiabatic exponent. These changes concern as well the level as also the form of the characteristic.

These investigations may be considered as a proof, that a reliable prediction of the characteristic of a hydraulic machine can be made only by tests in water and these under a Reynolds number as close as possible to that of the prototype [9.115]. Changing the fluid results also in a change of the calibration curves for the instruments use, e.g. Venturi nozzle etc.

9.5. Measurement of unsteady relative and absolute flow in a Kaplan Turbine by a vectorial probe of quick response from D. Castorph

9.5.1. Introduction

For stress calculations in the runner vanes of a Kaplan turbine, the dynamic measurement of the real unsteady flow field, around the runner vane with periodically and randomly varying fluctuations of pressure and velocity, is of special interest. A great number of references described by Lotz [6.27; 6.28] and Lienhart [6.32] show that, in many theoretical investigations, approximate computations of the fluctuations in the velocity field of two cascades in series moving relative to each other, have been made, whereas

because of the extensive work involved, experimental investigations of the unsteady flow-induced forces especially acting on Kaplan runner vanes are rare.

Measurements of the stresses in the vane surface by strain gauges are given by *Grein* and *Barp* [10.37]. Since fluctuations of hydrodynamic forces are caused by fluctuations of pressure and velocity, the knowledge of the real unsteady flow field as the source of unsteady load is of importance.

The usual method of dynamic measurement in water are based either on the measurement of unsteady flow velocity by means of hot film probes, as has been carried out by *Mollenkopf* [9.46], or on the measurement of unsteady total pressure by means of a *Pitot* probe with built-in transducer, as used by *Gerich* [9.45]. Both methods suffer from the fact, that the simultaneous measurement of pressure and velocity at a definite station is impossible and that the velocity direction can be measured only in a limited range.

9.5.2. Measurement of the absolute velocity field of the runner

9.5.2.1. Instrumentation

In order to avoid the above-mentioned disadvantages, a new conical vector probe, similar to that of *Conrad* (Fig. 9.5.1) but of quick response has been developed by *Castorph* at Lehrstuhl und Labor für hydraulische Maschinen und Anlagen at Technical University Munich, West Germany. This was for the measurement of the unsteady flow field within a KT operating in water [9.116; 6.29]. Six micro pressure-transducers of the type Kulite MQL 080-25 (frequency 70 kilo cps) enable the simultaneous indication of six fluctuating pressures in the six ports in the head of the probe. This is done by application of DC amplifiers and a light beam oscillograph with moving coil galvanometer of 4 kilo cps.
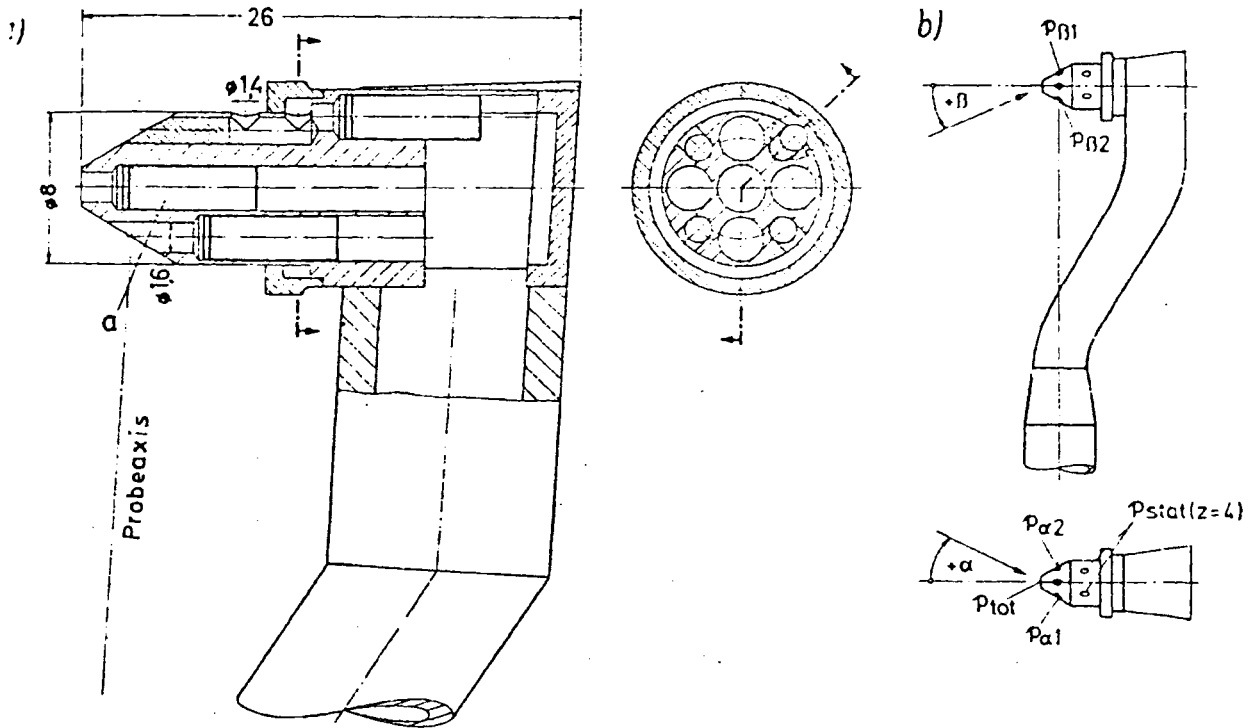
Fig. 9.5.1. Vectorial probe of quick response for simultaneous measurement of instantaneous pressure and velocity vector in water operated turbines, developed by *Castorph* [6.29]. a) Sectional view of 6-hole probe. b) Pressure transducer, stations of pressures $p_{\beta 1}$, $p_{\beta 2}$ due to pitch angle β, $p_{\alpha 1}$, $p_{\alpha 2}$ due to yaw angle α.

Four of the pressure transducers are used for the indication of the spatial local velocity direction, one at the apex of the cone indicates the total pressure, and the last one averaging the values of four ports uniformly distributed along the periphery of the cylindrical part, indicates the peripherally averaged static pressure. The difference of these last two figures gives the local dynamic pressure and hence the velocity.

Because of its compact construction, the head of the probe has a diameter of only 8 mm, which is fairly small compared with the runner diameter used of 612 mm. Because of the measurement in cold water and the frequently made control of zero load point under atmospheric pressure used as a reference figure, the influence of temperature and time elapsed on the calibration characteristic could be practically eliminated.

The pressure transducer MQL has a diaphragm of stainless steel and a full Wheatstone bridge on its back. The rearside moreover is connected with the atmosphere. Thus the pressure indicated coincides always with the gauge pressure. The simultaneous indication of this figure by all the six transducers in the head of the probe has been tested under unsteady conditions. The whole probe has been calibrated dynamically in the pressure conditions of the prototype turbine, e.g. in a pulsating pipe flow.

Since in unsteady flow the probe cannot be turned for a permanent compensation of its angle of yaw α (between the velocity vector and the probe head axis in a plane normal to the probe shaft), the calibration curves depend on the yaw angle α and the pitch angle β (between velocity vector and probe head axis in a plane containing both).

9.5.2.2. Measuring planes, results upstream and downstream of the rotor

The turbine, with a vertical shaft fed by a semi-spiral casing and equipped with a straight conical draft tube, was operated in an open test circuit under the two heads of $H = 1.8$ m and 2.8 m. The location of the measuring planes and the positions of the probe relative to the runner are shown in Fig. 9.5.2. The following measurements were carried out at the bep with $n_{11} = 127.5$ rpm, $Q_{11} = 1.39$ m^3/s.

- Measurements between the gate and runner: Fig. 9.5.3a shows the pressure fluctuations indicated by the six ports of the probe for a typical position. The components of the
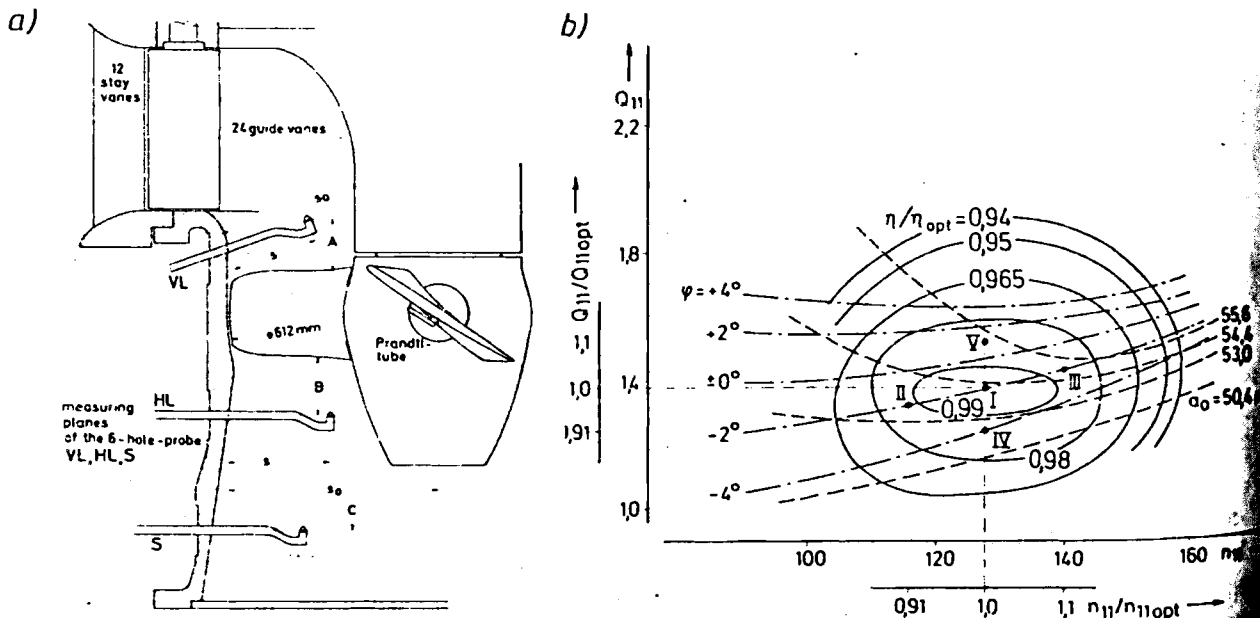
Fig. 9.5.2. Dynamic measurements of a vectorial probe on a Kaplan turbine. a) Sectional drawing of model KT, position of measuring planes. b) Efficiency hill diagram of KT with its test points. After Castorph [6.29].

Fig. 9.5.3. Measurements. a) test head $H = 2,8$ m, point 1, measuring plane (VL) between guide vanes and runner, position of probe s/$s_0 = 0,17$. a) Pressure records of the six pressure transducers vs time elapsed. b) Absolute meridional velocity component c_m, and whirl velocity component c_u vs time elapsed, after elimination of minor disturbances. After *Castorph* [6.29].
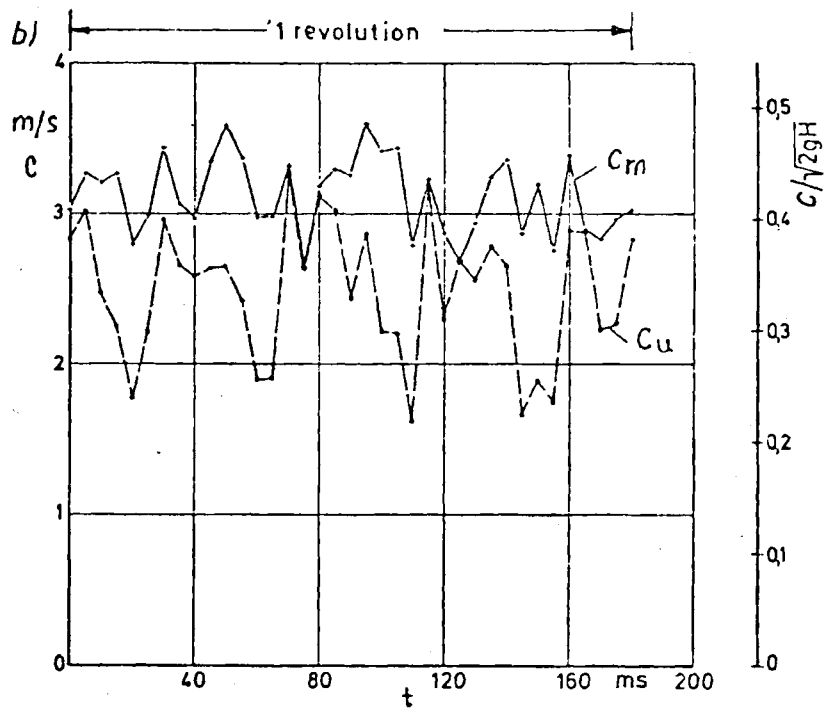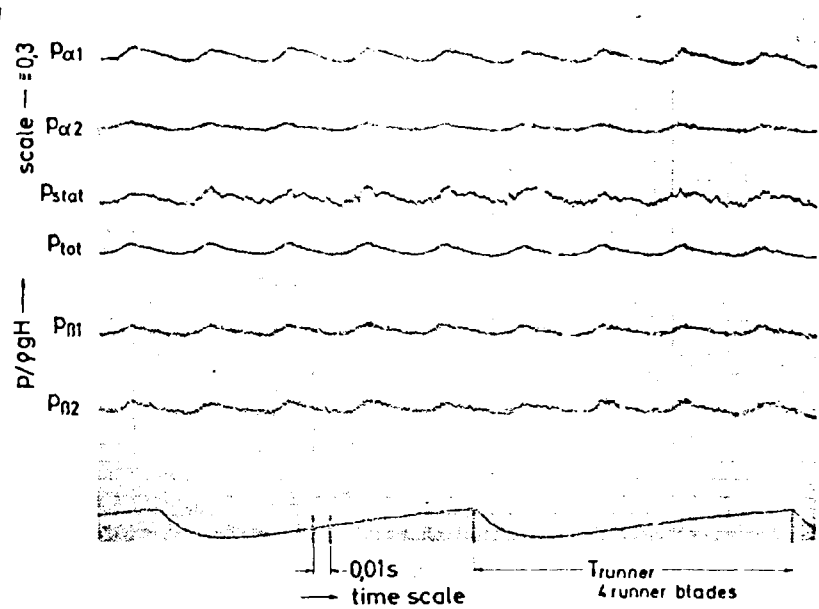
velocity resulting from this and the calibration chart are presented in Fig. 9.5.3 b. From the curves for the probe position $s/s_0 = 0,17$ the upstream influence of the four runner vanes on the absolute flow can be recognized (Fig. 9.5.3 b).

For the cylindrical section near to the hub the influence of the runner and the gates is reduced to almost nil. This may be due to the large distance of the measuring station in the streamwise direction either from the runner or the gates. All the measurements have been repeated by a conventional *Conrad* probe with its time-averaged indications. See [9.109].

- Measurements past the runner: The Fig. 9.5.4 a shows the pressure fluctuations of the vectorial probe for a typical position. The evaluated components of the velocity are

363

a)

p_{a1}

p_{a2}

p_{stot}

p_{tot}

$p_{\beta1}$

$p_{\beta2}$

scale — ±0,12

$p/\rho gH$ —

- - 0,01s -
—• time scale

T_{runner}
4 runner blades

b)

shown in Fig. 9.5.4b. Note the wakes of the four runner vanes. The presence of tip clearance vortices could be recognized by the large fluctuations in a measuring station close to the runner tip.

At the outer cylindrical section $s/s_0 = 0,32$ the pressure fluctuations were found to have a frequency equal to that created by the gates. This means that the viscous wakes due to the gates extend even past the runner, naturally then sliced into pieces.

Fig. 9.5.5 shows the comparison of the time-averaged (for one runner revolution) results of the dynamically measuring probe with those of the *Conrad* probe for measuring plane VL.

Fig. 9.5.5. Comparison of time-averaged velocity components at the draft tube inlet (S), head $H = 2.8$ m, point I, in plane S. —— time-averaged values of dynamic measurement with the probe developed by Castorph [6.29]. --- time-averaged quasi-stationary measurement with usual 6-whole conical probe and records by mercury manometers. After Castorph [6.29].
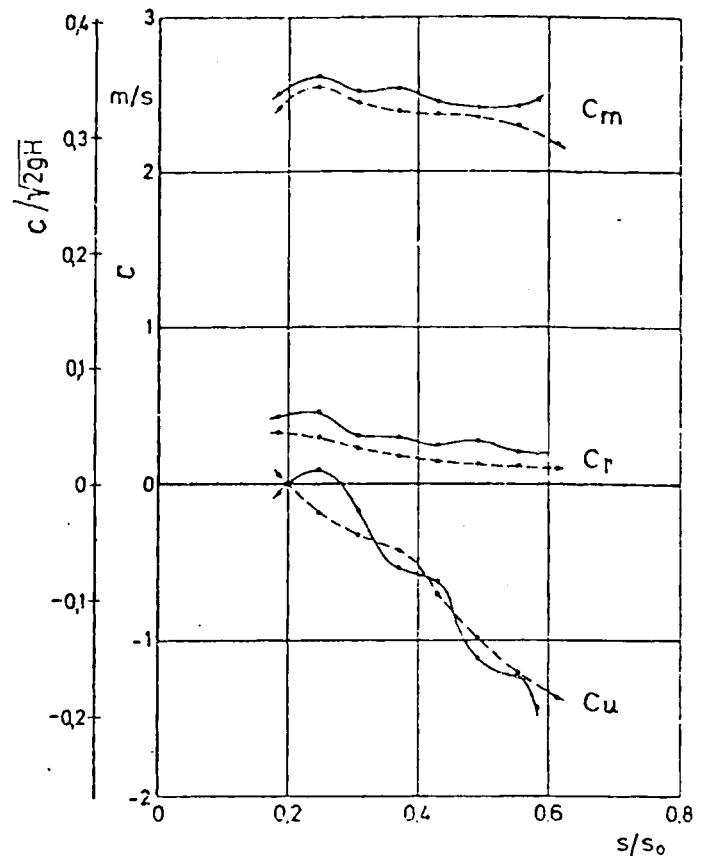
9.5.3. Measurement of unsteady relative flow

9.5.3.1. Instrumentation

For the determination of the influence of the gates' pitch and the non-uniform inflow from the semi-spiral casing on the relative velocity field, a *Prandtl* tube. Fig. 9.5.6 a, also equipped with two Kulite pressure transducers, has been fixed on the runner face. The supply voltage as well as the signals of the transducers have been transmitted from the rotating system through an eight channel mercury-operated ring chamber.

For calibration the time-averaged values of the ports within the relative flow field have been compared with the values indicated by respective ports under air injection.

9.5.3.2. Experimental results from the rotating probe

Fig. 9.5.6 b shows the pressure distribution for two different positions given by the transducers of the *Prandtl* probe. At the outer section $s/s_0 = 0.25$ it can be recognized, that the frequency of the fluctuations of total pressure equals that of the gate number. Additionally the lack of axisymmetry in the flow due to the semi-spiral casing may be noted.

The pressure fluctuations due to the gate pitch, have been found at the outer section to be equal to velocity fluctuations of ∓ 1 to 3% of the average value. The computation of

a)

b)
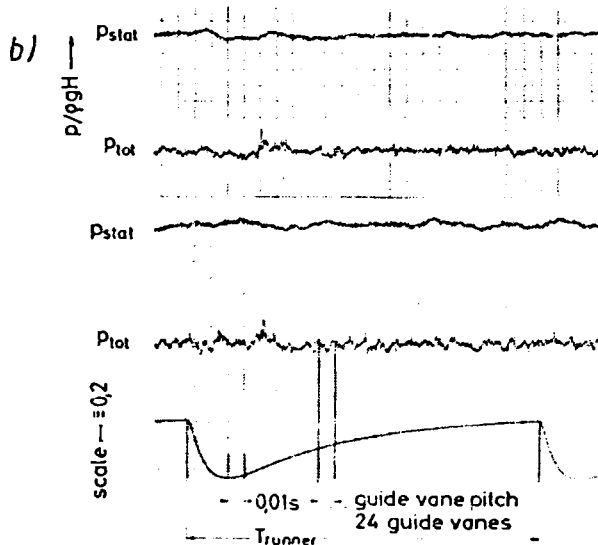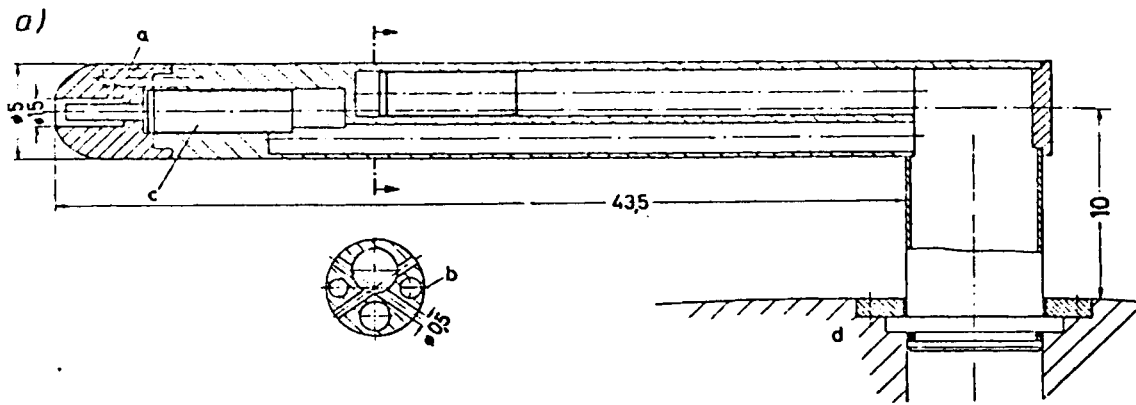
Fig. 9.5.6. Measurement with a quick response probe on the runner blade of a KT. a) Prandtl tube on the runner vane face in the longitudinal section and cross section, a air ejection for calibration of p_{tot} on site, b air ejection for calibration of p_{stat} on site; c Kulite transducer; d runner vane face. b) Pressure records of the two transducers of Prandtl tube. Test point I, head $H = 2,8$ m; $s/s_0 = 0,25$; above pressure face; below suction face. After *Castorph* [6.29].

wakes according to *Kemps* and *Sears* [6.30] leads to velocity fluctuations depending on the gate pitch, which agree approximately with the values measured [12].

9.6. Influence of runner vane number on relative and absolute flow in axial turbines according to air tests and comparative-predictions carried out by *W. Kühnel*

9.6.1. Formulation of the problem

The main aim of the following treatise on the one hand is to obtain an experimental proof of the real relative and absolute flow field in an axial reaction wheel with the typical design features of an hydraulic axial turbine.

---

[12]) This seems to be small. But in addition to this, there also exist velocity fluctuations up to 4% which are independent of the guide vane pitch. This results in velocity fluctuations of up to ± 7% on the pressure and suction face of the blade. Thereby the fluctuation of the differential pressure may reach up to 14% of the average value.

On the other hand an attempt is made here to find which calculation predicted these test results most accurately with respect to the solutions available from Schlichting [9.117], Raabe [4.11], Finke [9.118], Touchy [9.119], Jochem [9.120], Rahmo [9.121], Strscheletzky [9.122], Glanert [9.123], Birnbaum [6.6], Schilhansl [6.7], Pantell [4.10; 9.124], Betz [9.125], Imbach [9.126], Kühnel [9.127].

To the present such tests have been carried out only with varying pitch to chord ratio t/L by Hahn [9.128] at corresponding cylindrical sections of the rotor.

The tests described here were made on different turbine runners with the same hub to tip diameter ratio 0,5 and three, four, six and twelve runner vanes as for example on a Kaplan turbine. As shown (Fig. 9.6.1 a) the vanes are thin, have a small camber and are geometrically similar to each other in a certain cylindrical section.

The parameters of the straight cascades, originated from unrolling the cylindrical sections into a plane, were retained for sections on a distinct radius. Thus the pitch to chord ratio and angle β_0, the zero lift direction makes with the circumference, are retained whereas the vane number varies. For simplified test conditions the runner operates with a whirl-free absolute flow at inlet. This was obtained by a flow straightener upstream of the runner. For the same reason air has been used for the tests.

A whirl-free admission facilitates also a good examination of the secondary flow resulting from the relative whirl (Cap. 5.5.5.4). Downstream of the runner considered, there is an absolute whirl opposite in sense to the speed of the runner (Cap. 9.6.3.3). Therefore the runner vane needs a smaller twist than that due to a runner with inlet whirl. Hence the face of vane skeletons can be approximated fairly well by spatially arranged bound vortex stars on a conical face, see Cap. 9.6.4.2.

An essential difference exists between runners with no prewhirl and those with whirling inlet flow. Contrary to the first case in the second case the whirl and hence the radial pressure gradient decrease with increasing boundary layer thickness in the streamwise direction. Now from this, two flow laminae within the boundary layer originate with oppositely oriented secondary flow (Cap. 5.5.5.3).

9.6.2. Test devices and instrumentation used

9.6.2.1. Air test rig

The measurements were carried out in an open air test rig (Fig. 9.6.1 b). Downstream of the diffuser 7 the flow passes an axial flow straightener with four screens in series distributing the flow uniformly over the inlet cross section of the turbine. The transition to the test section is formed by a nozzle with a contraction of 5 to 1.

An electric torque reaction dynamometer was used to load the turbine (Fig. 9.6.2 a). By extension of the runner shaft supported at the stations A and B, the dimensions of the dynamometer could be adapted to the form of the hub. Moreover this allowed for an overhung design, facilitating dismantling. Besides this the extension of the runner hub facilitates the inserting of the rotating probe without the hindrance of bearings. The wakes from the stay vanes generated in the generator region have nearly faded out in the test section. Negligibly small stall effects occurring in the zone of intersection of stay vanes and the casing were eliminated by a trip wire.

The following investigations have been carried out at Lehrstuhl und Laboratorium für Hydraulische Maschinen und Anlagen of The Technical University Munich, West Germany.
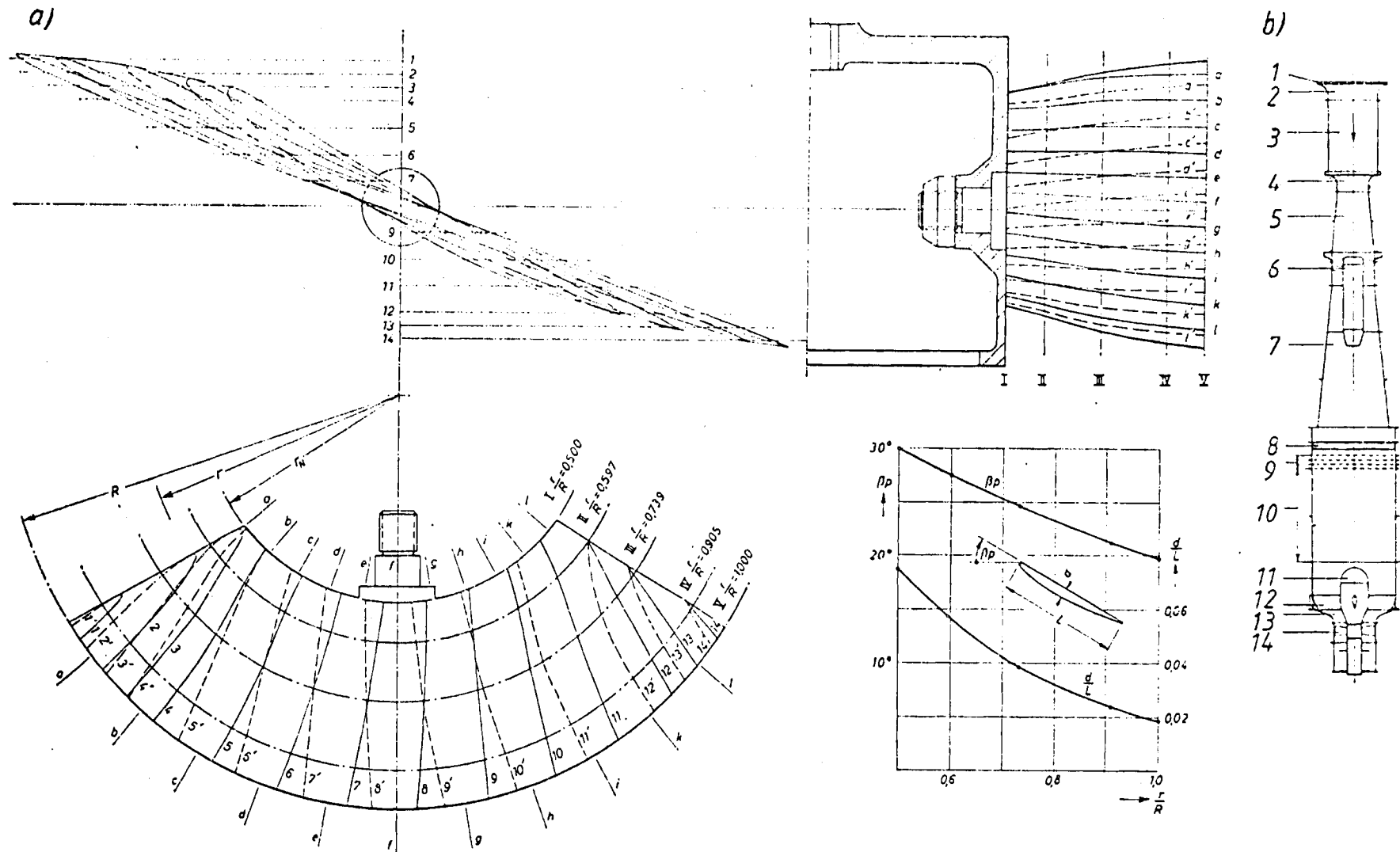
Fig. 9.6.1. Runner and test rig for investigations. a) Blade design of the 3 vaned runner in elevation (above) and plan (below). —— pressure face of the vane — — — suction face of the vane. b) Schematic representation of the horizontal air test rig. 1 gauze; 2 intake nozzle; 3 settling chamber; 4 Venturi meter; 5 diffuser; 6 blower; 7 diffuser; 8 rectifier; 9 gauze section; 10 settling section; 11 casing for brake generator; 12 stay ribs; 13 nozzle; 14 turbine runner. After Kühnel [9.127].
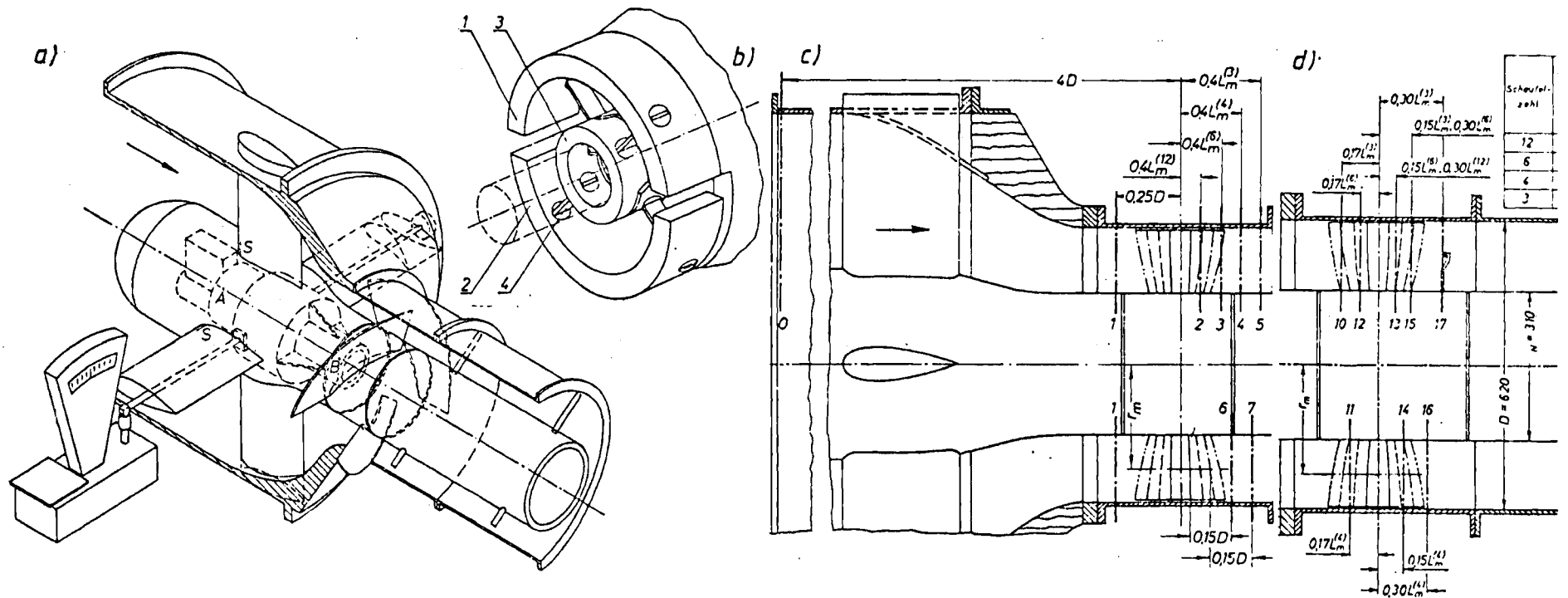
Fig. 9.6.2. Details of the test section. a) Perspective sectional drawing of the turbine with an electric reaction torque dynamometer and a weighing machine. S trip wire; A, B stations of support for generator rotor. b) Detail of the leaf spring suspension of the generator stator; 1 upper half ring; 2 lower half ring; 3 bridging ring; 4 leaf springs. c) Location of the measuring cross sections for measurement of the absolute flow. Circular projection of runner vane: $-\cdots-z\ 3$; $-\cdot-z\ 4$; $---z\ 6$; $\text{------}z\ 12$. Chord length L_m of a mean cylindrical section, radius r_m; $L_m^{(z)}$ = chord length of z-vaned runner. Blade number 12, 6, 4, 3 in respective measuring sections 2/1, 3/1, 4/1, 5/1. d) Location of the measuring sections for the measurement of relative flow within a runner. Circular projection of runner vane: $-\cdots-z\ 3$; $-\cdot-z\ 4$; $---z\ 6$; $\text{------}z\ 12$. Chord length in a mean cylindrical section for z-vaned runner: $L_m^{(z)}$. Blade number 12/6/4/3 in the measuring sections in the runner 12/13, 11/14, 10/15, and past the runner 13, 15, 16, 17. After Kühnel [9.127].

9.6.2.2. Layout of the runner

At test section the runner has a tip diameter of 620 mm. Profiles of the series Gö 9 K, Gö 10 K and Gö 11 K were used. They can be converted into each other by increasing their thickness coordinates y_{oh} and y_{uh}.

The greatest profile thickness decreases linearly along the radius, being 24 mm at hub and 12 mm at tip. The pitch to chord ratio t/L was assumed constant and equals to one for all the radii and blading.

For the design the flow was assumed to be of constant angular momentum and hence of constant energy with a constant axial velocity along each radius upstream the rotor. The performance data are as follows: Specific head $Y = 900 \ m^2/s^2$, flow $Q = 5 \ m^3/s$, speed $n = 1700$ rpm. The design was made under the assumption of a plane, incompressible flow without internal friction [9.124; 9.129; 4.10].

9.6.2.3. Instruments and probes used

I. Probes for the measurement of absolute velocity:

-- Six-hole probe: The velocity vector, the total and the static pressure of the assumed steady absolute flow were measured upstream and downstream of the rotor. To do this, a six-hole Conrad probe [9.109] was used (Fig. 9.4.3 g). To minimize the error, measurements have been repeated by means of a two finger probe (Fig. 9.4.3 a). The head of the probe has a diameter of 4 mm.

II. Rotating probes for relative flow: The measurement of relative flow between and past the rotor has been carried out by means of a probe rotating together with the runner. The probe stem reaches into the flow passing a slot within the hub wall.

-- Adjustment devices for rotating probes: The design of the adjustment device for a rotating probe is shown in principle in Fig. 9.4.8 a.

-- Each of the tappings of the probe is connected by hose and brass pipes within the hollow shaft with one of the chambers of the pressure transmitter (Fig. 9.4.8 b). The probe stem could also be ajusted during rotation to cancel the yaw angle. This was effected by axial displacement of an adjustment rod similar to Fig. 9.4.8 a. coaxially located within the shaft. This rod has on one of its ends a slotted link-like lever for turning the probe about its radially oriented stem by means of a block-link mechanism.

-- Designs of rotating probes: Two designs of rotating probes were used. In the usual one (Fig. 9.4.4) the stem is turned through a short U-shape and in the other (Fig. 9.4.5) through a wide U-turn. This was made to obviate any influence of the total pressure caused by the radial stem on the head of probe.

-- Calibration: The calibration of the indication of the relative flow angle β' was made within the measuring section with the rotating probe, but with the runner removed.

III. Measurement of flow: To measure the flow, a standardized Venturi meter with an area ratio $m = 0,34$ (Fig. 9.6.1 b) was used. The throughflow coefficient was evaluated by calibration test.

The velocity profile was measured by a Prandtl probe in the narrow cross section. Hence the flow was obtained by integration. The deviation of the results given by the Venturi meter was in the range of $\pm 0.2\%$. Angular deviations from the axial flow direction amounted about $\pm 0.4°$.

IV. Measurement of torque and speed: The torque was measured by means of an electric reaction torque dynamometer (Fig. 9.6.2 a). The fulcra of its stator consist of two semi-circular rings connected with each other by a pair of leaf springs normal to each other (Fig. 9.6.2 b). [9.131]. The upper half ring is connected with the stator. The lower is fixed

by the stationary and solid support. With the aid of a calibration it is ensured that the leaf springs do not exert any torque about the turbine axis in the zero position of the weighing machine.

The shaft of the generator rotor is supported so as to make the frictional torque in these bearings an internal load on the rotor (see Fig. 9.3.1 b). The sensitivity of the measuring device amounts to 0,05% of the smallest torque.

v. Measurements of the pressure: For the measurement of the pressure, an inclined tube manometer and a projection manometer of the *Betz* type were used (Cap. 9.4.1.1).

9.6.3. Measurement of flow, discussion of results

9.6.3.1. Investigations of the absolute flow

I. Measuring programme: Distribution of absolute velocity c, static pressure p and total pressure g was measured upstream and past the runner. Tests carried out at 15 stations along the radius by 6-hole and two-finger probes (Fig. 9.4.2) after axisymmetry of flow was tested. Each blading was assigned to a measuring section, at a distance of 0,4 times the chord length of the mean cylindrical vane section from the plane of runner vane axes (Fig. 9.6.2 c).

The vanes were fixed on the hub. Therefore a varying angle of attack of the relative flow with respect to the cylindrical section of vane was obtained by the variation of speed. The range of the Reynolds number varied between $Re = 2 \cdot 10^5$ and $3 \cdot 10^6$ in which $Re = w_x L/v$, with w_x as the undisturbed velocity, defined by $w_x = (w_1 + w_2)/2$, w_1 and w_2 being the relative velocities at runner inlet and outlet, and with L as the chord. Hence any disturbance by hub clearance flow was removed.

II. Evaluation of measurements:
- Computation of the velocity components: The absolute velocity c is obtained as in Cap. 9.4.1.2 from the dynamic pressure, sensed by the six-port probe as the differential pressure between the total pressure g and the static pressure p, and in the case of the two-finger probe as the differential pressure p'_a between the two ports of the probe.

In the case of a six-hole probe, the spatial flow direction is fixed by the two angles α' and $\gamma = \gamma'$ (Fig. 9.4.4). Thus the three components of velocity are obtained from

$$c_u = -c \sin \alpha' \cos \gamma = c \cos \alpha \cos \gamma, \qquad (9.6-1)$$

$$c_a = c \cos \alpha' \cos \gamma = c \sin \alpha \cos \gamma, \qquad (9.6-2)$$

$$c_r = c \sin \gamma, \qquad (9.6-3)$$

α' being defined by $\alpha' = \alpha - \pi/2$. The time-averaged measurements past the rotor show that γ is small, hence $\cos \gamma = 1$.

In the following text the subscript 1 is used for the section upstream of the runner and 2 for the section 2, 3, 4, 5 past the rotor. The bar over any value characterizes the mean value of a certain cross section. Hence

$$\bar{g}_0 = \varrho \bar{Y}_0 = (\varrho/2) \bar{c}_0^2 + \bar{p}_0, \qquad (9.6-4)$$

which was kept constant as a reference value during the measurement by speed control of the blower.

III. Analysis of measured results:
- The volume flow: From the distribution of the axial velocity obtained by (9.6–1 to 4) the flow can be calculated as

$$Q = 2\pi \int_{r=r_N}^{R} c_a r\, dr = 2\pi R^2 (2\bar{Y}_0)^{1/2} \int_{r/R=0,5}^{1} K c_a(r/R)\, d(r/R). \qquad (9.6-5)$$

The solution of this relation agrees with the flow measured simultaneously by the Venturi meter with an error below 1%.

-- Torque: Application of the theorem of moment of momentum gives the torque for the existing case of vanishing inlet whirl as

$$M = -2\pi\varrho \int_{r=r_N}^{R} c_{u2} c_{a2} r^2\, dr = -4\pi\varrho R^3 \bar{Y}_0 \int_{r/R=0,5}^{1} K c_{u2} K c_{a2}(r/R)^2\, d(r/R). \qquad (9.6-6)$$

The torque from the weighing machine equalled that from the velocities Kc_{u2}, Kc_{a2} measured with an error up to 3,5%.

-- Critical analysis of results measured: The values obtained by both the probes aforementioned, for speeds of 1400, 1700, 2000 rpm showed good agreement. Considerable differences exist between the results of the six-hole probe and two-finger probe for working points with large deflection of the absolute flow, e.g. in the cases of 800 and 1100 rpm, especially in the hub region and for the smallest vane number $z = 3$. The two-finger probe was preferred as the more accurate one.

9.6.3.2. Investigation of the relative flow

I. Measuring program: The measurement of the relative flow was carried out at speeds of 800 and 1400 rpm since the bep was in this range. The measuring stations were distributed for the runners with 3, 4, 6 vanes in three planes normal to the machine axis (Fig. 9.6.2 d), the first sections 10, 11, 12 being close behind the rotor's inlet edge, the second stations 13, 14, 15 upstream of the runner exit and the third past the latter. Due to a lack of space, the measurements of the runner with 12 vanes were limited to the flow past the rotor, section 13. The location of the measuring stations relative to the cascades of the unrolled cylindrical sections considered can be seen in Fig. 9.6.2 d and the following corresponding figures.

II. Evaluation of measurements:

-- Corrections due to centrifugal force: The effect of centrifugal load on the air columns enclosed between the probe head and manometer as well as the Mach number effect under isothermal behaviour of the gas were accounted for.

-- Critical examination of the measured results: For an estimation of the disturbances by the stem of the rotating probe on the relative flow, the measurements at 800 rpm have been compared with a specially shaped six-hole probe (with wide U-turn in the stem, Fig. 9.4.5). The results with both probes coincide also in the wakes. Only at very small distances between the probe tapping and the runner vane face, the usual form of the six-hole probe indicates up to two degree larger or smaller flow angle than that indicated by the probe with an U-shaped stem.

This is due to the fact that the stem of the usual probe displaces the flow from the vane.

III. Photographic observations of the boundary layer flow: The flow direction within the boundary layer adjacent to the rotating wall has been visualized under stroboscopic illumination using eiderdowns (small feathers) fixed at one end to the vane face. Due to its small mass in relation to its large flow resistance the ratio of centrifugal force to resistance force under 1400 rpm, for instance is only 1 in 20.

Therefore a photograph of a rotating vane carrying eiderdowns illuminated stroboscopically facilitates qualitative analysis of the flow field close to and within the boundary layer of the rotating vane (Fig. 9.6.3 a) relative flow is from left to right.

372
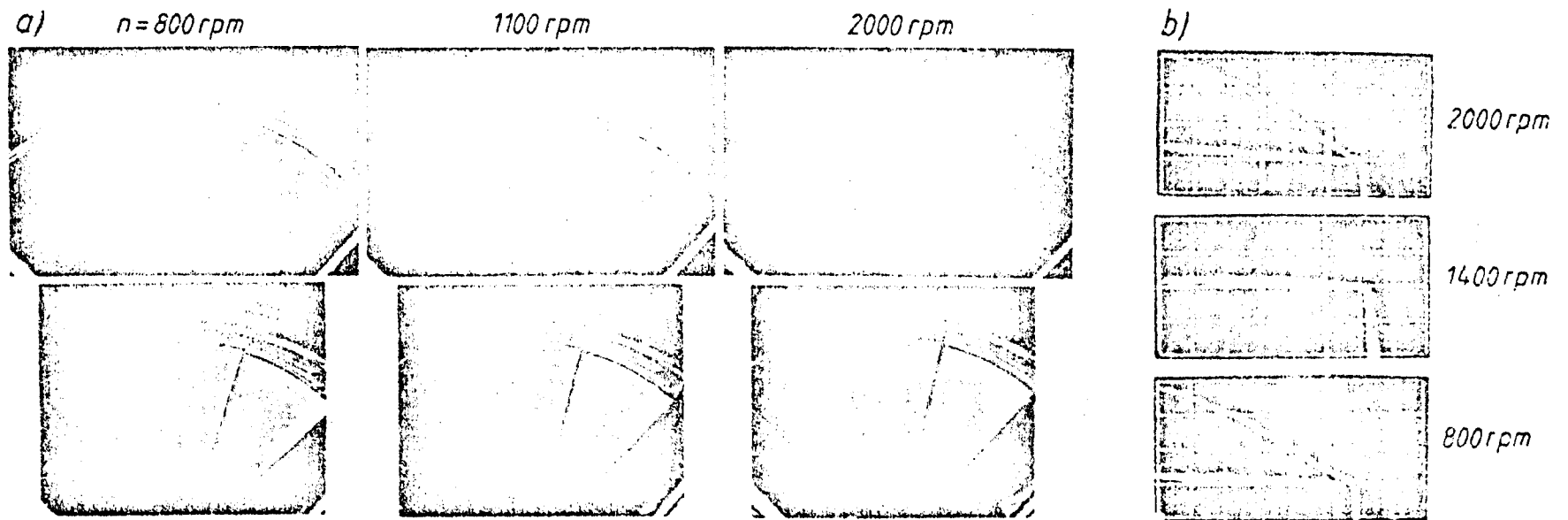
Fig. 9.6.3. Visualized flow close to the runner vane face. a) Flow direction in the boundary layer on the suction face of the runner with 3 blades (above) and 12 blades (below) at speeds of 800, 1100, and 2000 rpm visualized by Eider down tufts pasted at one of their ends on the rotating runner vane face. b) Comparative centrifugal tests with a woolen thread and Eider down fixed on a rotating rod. Above: down and woolen thread at 2000 rpm, down nearly tangential in flow direction; middle: down at 1400 rpm again nearly tangential; below: Down and woolen thread at 800 rpm, down again nearly tangential in flow direction. After *Kühnel* [9.127].

9.6.3.3. Discussions of the measuring results

I. Absolute flow upstream of the runner inlet edge: Upstream of the runner inlet edge the absolute flow posseses its expected uniform distribution of total pressure and static pressure and hence also of velocity.

II. Relative flow:

– Relative flow past the inlet edge of a rotor vane: In the measuring sections 10, 11, 12 on the pressure face of the vane the whirl component of relative flow comes close to the
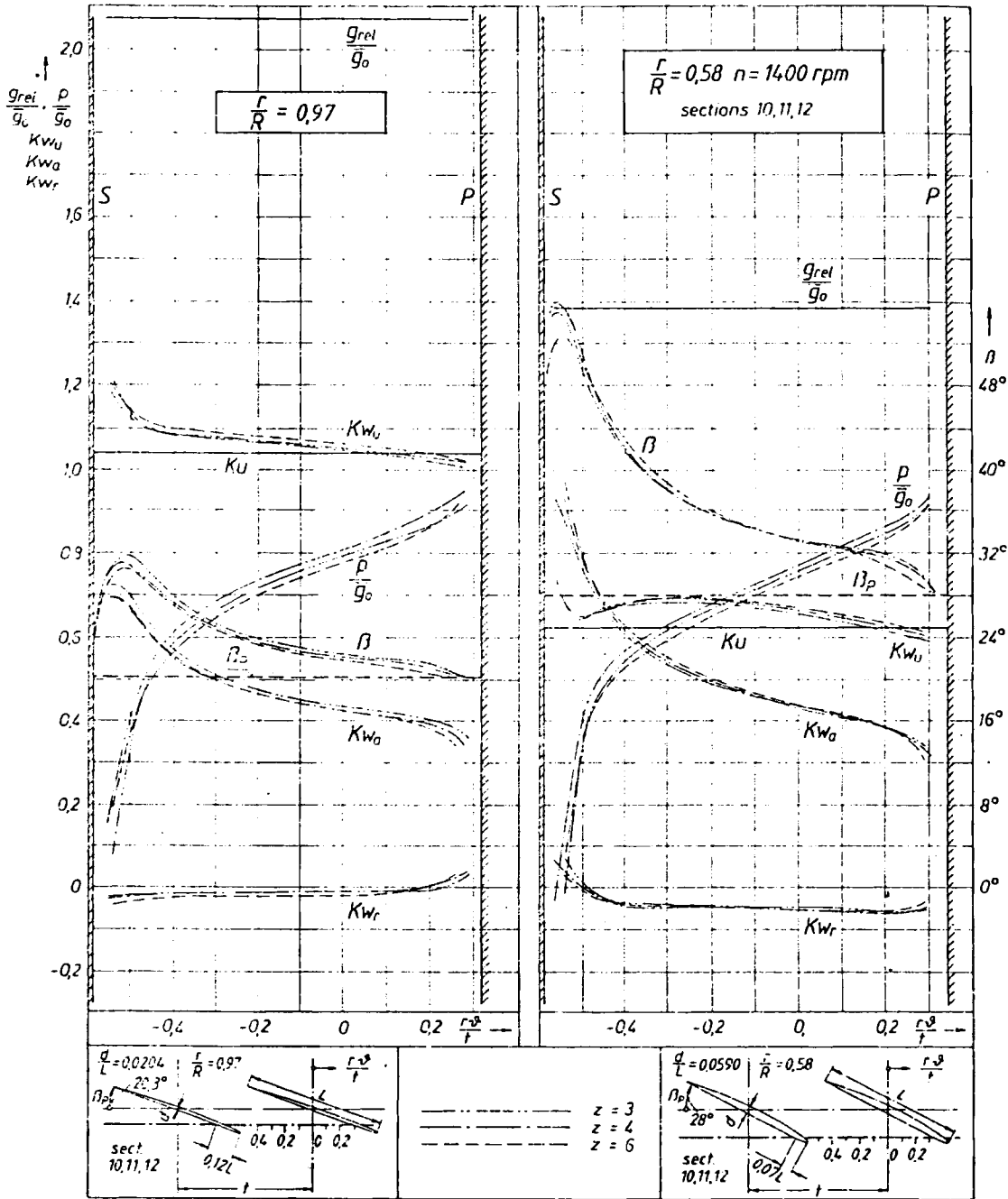
Fig. 9.6.4. Relative flow past the runner's leading edge at a speed of 1400 rpm. Plot of the rothalpy $g_{rel} \bar{g}_0$ (g_{rel} without internal energy), static pressure $p/\bar{g}_0$, components of the relative velocity (coefficient) Kw_u, Kw_a, Kw_r, and flow angle β vs circumference. Furthermore also the blade velocity (coefficient) Ku and the vane angle β_r. S suction face; P pressure face. After Kühnel [9.127].

374

blade speed Ku. This means the flow was nearly undeflected (Fig. 9.6.4). Under a speed of 1400 rpm even a positive absolute whirl of 2 to 4 % of Ku occurs. An increment of Kw_u (the relative whirl) towards the suction face indicates the beginning of flow deflection within the cascade.

The curves of the static pressure, only depending on radius and speed, show a pronounced trough of low pressure caused by the flow around the head of the profiles in the neighbourhood of the suction face. In connection with this, steep gradients of the flow angle β and the axial velocity Kw_a are observed.

The pressure rise following the reduced pressure causes a stall in the speed range between 800 and 1100 rpm on the suction face past the inlet edge of runner vane. This can easily be recognized from the orientation of the eiderdowns pasted to the suction face (Fig. 9.6.3). The rotation of the stalling region is seen to be opposed to the sense of the runner rotation for the case of the 3-vane runner at speeds of 800 rpm (Fig. 9.6.3). The stalled region is subjected to the influence of centrifugal force and grows therefore from the hub towards the casing wall. The length and thickness of the stalled zone grows with decreasing vane number.

– Flow effects within the boundary layer: The course of the flow between the vanes and past them is essentially influenced by secondary flow in the boundary layer region (Cap. 5.5.5.4). Because of the pressure trough immediately past the leading edge a turbulent boundary layer on the whole suction face may be expected.

As it has been found that the whirl Kc_u increases along the runner vane in the streamwise direction, the radial pressure gradient of the main flow also increases towards the casing. Very roughly

$$(1/\varrho)\, \partial p/\partial r = c_u^2/r. \tag{9.6-7}$$

Since in an axial runner the *Coriolis* force and centrifugal force due to rotation are nearly radial in direction, the pressure gradient $\partial p/\partial r$ outside the boundary layer acts through it.

A decrease of the relative velocity within the boundary layer from w to w' (Fig. 9.6.5a) causes a decrease of the whirl from c_u to c_u' with angle β retained. This leads by relation (9.6–7) to a disturbance of the radial equilibrium, which exists in the main flow at the outer edge of the boundary
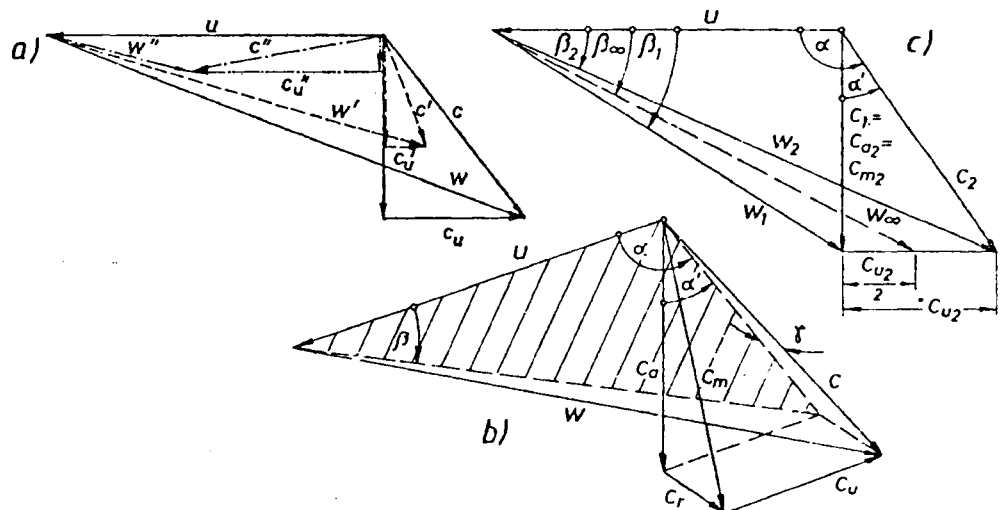
Fig. 9.6.5. Velocity triangles of a runner with zero prewhirl. a) Velocity triangles for an axial runner with zero prewhirl in the region of boundary layer under the assumption of a plane flow parallel to the vane face. b) Velocity triangles in three dimensional flow (flow in between and downstream of the runner vanes). c) Inlet and outlet triangles (assuming a flow on coaxial cylindrial stream faces, $r_r = 0$). After *Kühnel* [9.127].

375

layer. The fluid elements in the outer region of the boundary layer move towards the axis. This is a consequence of the whirl $K c_u$ increasing in the streamwise direction and thus causing an increase of static pressure towards the tip (Fig. 9.6.5 a). Radial pressure gradient and boundary layer thickness increase in the streamwise direction.

Very close to the vane face the fluid elements in the boundary layer are flung towards the casing wall. In this region the relative velocity w decreases towards the value w''. Thus with $c_u'' > c_u$ the centrifugal force $c_u''^2/r$ dominates over the pressure gradient $\partial p/\partial r$ from outside the boundary layer, resulting from c_u^2/r as in (9.6-7).

If the blade speed u on the innermost radius equals the whirl velocity c_u as may happen with speeds of 800 and 1100 rpm, then the layer with the dominating centrifugal force completely disappears and the boundary layer material is accumulated at the hub. In other parts of the runner the boundary layer next to the wall is centrifuged and the external boundary layer is shifted towards the hub.

The tip clearance vortex: Between the tip of the vane and the casing a gap exists with a clearance of 0.8 mm. The leakage through this gap is wound up together with the centrifuged boundary layer fluid on the suction face into a vortex, transported streamwise by the surrounding flow and rotating in the sense of the runner.

The hydrodynamic parameters influenced by this tip clearance vortex are shown in Fig. 9.6.6. Its centre line coincides with a minimum of total pressure. The static pressure reaching its minimum at the same station increases parabolically on both the sides of the vortex axis. The vortex causes also [5.3] an additional radial flow component $K w_r$ with reversed sign on both the sides from the vortex axis along a normal to the blade.

A convex plot of flow angle vs circumference hints at a vortex axis within the measuring section (Fig. 9.6.6 for 3 vanes). A concave shape (Fig. 9.6.6 for 4 and 6 vanes) indicates a vortex centre line outside this section. Because of the large loss of total pressure due to the tip vortex the relative velocity also decreases in the neighbourhood of this vortex.

– Relative flow before the outlet edge of runner vane: Outside the boundary layer and outside the tip clearance vortex the total pressure g_{rel}/g_0 within the relative flow remains constant past the inlet edge of the rotor. Since at 1400 rpm the static pressure p/g_0 grows approximately parabolically vs the circumference from the suction to the pressure face, the relative velocity drops linearly along the unobstructed pitch. The curves of the axial component $K w_a$ are nearly constant, with a slight growth towards the pressure face.

Therefore the variation of the relative velocity is caused mainly by the whirl component $K w_u$ whose linear variation along the circumference is significant over the whole measuring range. Hence the relative flow does not follow the direction of the vane. At 800 rpm the growth of the static pressure is restricted (more than that at 1400 rpm) to the region close to the pressure face with a smaller differential pressure between adjacent vane faces.

The large difference the component $K w_a$ has past the inlet edge between suction and pressure face, is nearly compensated. The fluid elements within a plane perpendicular to the turbine axis and moving with a nearly constant axial velocity remain in this plane. Relative to the annular sector formed by two adjacent vanes, the casing and hub, fluid rotates with an angular velocity increasing together with deflection from zero at inlet to a maximum at the outlet in the same sense as the runner [5.62]. As a consequence of this a secondary flow due to the relative eddy is generated. This causes a positive radial velocity at the outer edge of the boundary layer on the suction face and on the pressure face a radial negative velocity (Fig. 9.6.6). This flow can be predicted according to Cap. 5.5.5 but with a ζ, now negative because of the negative whirl c_u, oriented against the speed u.

376
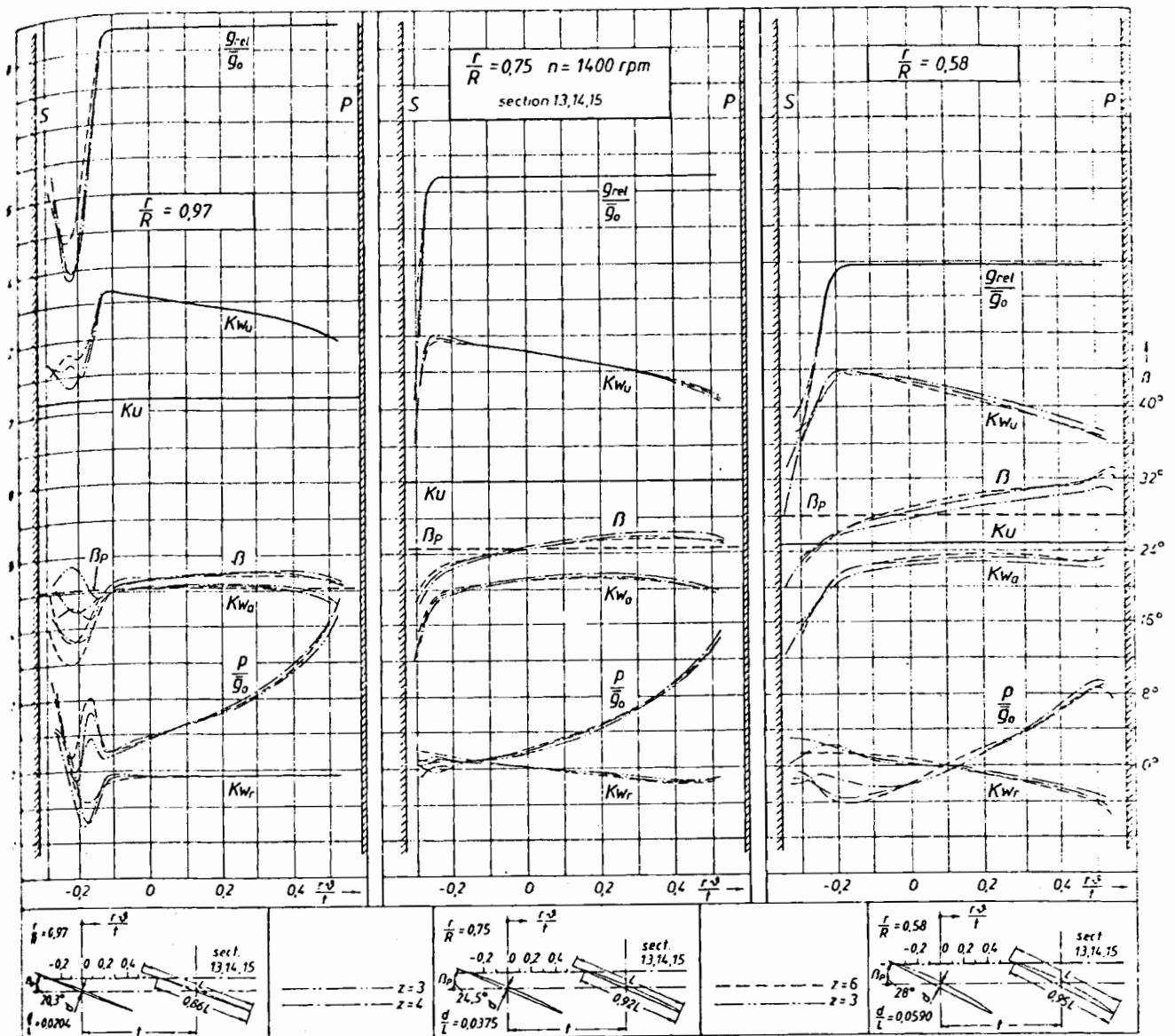
Fig. 9.6.6. Relative flow upstream of the trailing edge of the runner vane at a speed of 1400 rpm. Plot of rothalpy $g_{rel}/\bar{g}_0$, static pressure $p/\bar{g}_0$, components of relative velocity (coefficient) Kw_u, Kw_a, Kw_r, and flow angle β vs circumference. Furthermore also blade velocity (coefficient) Ku and vane angle β_r. S suction face, P pressure face. After *Kühnel* [9.127].

The components Kw_r show this effect for $r/R = 0.75$, Fig. 9.6.6. It appears pronounced at the speed of 800 rpm, see Fig. 43 in [9.74]. Next to the boundary layer the radial velocities reverse their direction. The boundary layer fluid, accumulated by the disturbed equilibrium at the root of the suction face next to the hub, rotates about the streamlines.

This streamwise vorticity can be recognized from the graphs of Kw_u vs r/R in the circumferential range $-0.3 < r\vartheta/t < 0.5$.

The boundary layer of the runners with 4 and 6 blades are relatively thin because of their short chords. Therefore the relative flow leaves the blade smoothly and without stall. This contrasts to the boundary layers of the runner with 3 vanes in the regions of hub and tip. They are the thickest because of the longer chord.

However, in the mean cylindrical section ($r/R = 0,5$) the 3-vane runner with its longest chord possesses at the lowest speed of 800 rpm the thinnest boundary layer on the suction face, where in general the boundary layer should be thickest. A loss analysis shows that the local efficiency in the mean cylindrical section of the 3 blade runner becomes the highest [9.127].

This follows from the above-mentioned interaction of centrifugal force of an element within the boundary layer and the whirl (c_u)-induced radial pressure gradient of the main flow, acting across the layer. The corresponding secondary flow shifts the boundary layer material close to the wall towards the tip and that close to the outer edge of the boundary layer towards the hub, so as to denude the mean cylindrical vane section of the boundary layer.

Since the boundary layer under the influence of the radial pressure gradient is thickened along the inner cylindrical vane section, the vane deflects the flow additionally in the circumferential direction in the neighbourhood of the hub, ($r/R = 0,58$) at 1400 rpm and especially at 800 rpm. This deflection by the vanes in the circumferential direction increases with vane length directly and inversely with the vane number. This is reconfirmed by measurements.

Adjacent to the casing ($r/R = 0,97$) on the suction face of the vane the plot of the hydrodynamic values is governed by the tip clearance vortex. The region in which the vortex leaves the clearance of the gap is shifted to the profile's head with increasing angle of attack so that the range influenced by this vortex has been doubled at 800 rpm compared with 1400 rpm, see Fig. 43 in [9.74] at $r/R = 0,97$. The diameter of the tip clearance vortex core grows nearly proportional to the vane length and hence inversely with the vane number.

- Wakes downstream of the runner exit: Past the exit of the runner the boundary layers of the suction and pressure faces touch each other. Thus they form wakes in the graph of the velocity w and p (Fig. 9.6.7). In the neighbourhood of the casing ($r/R = 0,97$) and the hub ($r/R = 0,58$) the vortices flowing off the suction face of vane are included in the wakes.

Thus the total pressure curve contains two characteristic minimums. The left sink is caused by the vane's wake, the right by the vortex. As well as the boundary layers, the wakes are also subjected to a radial pressure gradient.

Since the static pressure of the flow outside the wake also acts across the wakes, the disturbance of radial equilibrium caused by the velocity drop within the wake leads to negative radial velocities (Fig. 9.6.7) ($r/R = 0,75$ and 0.58). In the wakes past the outer cylindrical section ($r/R = 0,97$), the tip clearance vortex essentially determines the graph of the radial components and the other values. This appears pronouncedly in the graph of the 12-vane runner at radius $r/R = 0,97$.

The compensation of the velocity differences between the wake and outer flow by turbulent mixing leads to a decrease of axial velocity and the flow angle β which is confirmed by the measurements (Fig. 9.6.7). For the runner with 12 vanes β is reduced mostly in the hub region, leading to a displacement of the wake more to the tip region (Fig. 9.6.7).

The wakes of long vanes dissipate more slowly than those of short vanes. This follows from the negative radial velocities and the rotating fluid of the wake. The breadth and depth of wakes in the graphs of total pressure reflect the amount of flow loss. A more detailed analysis of the loss can be found in Kühnel's dissertation [9.127].

378
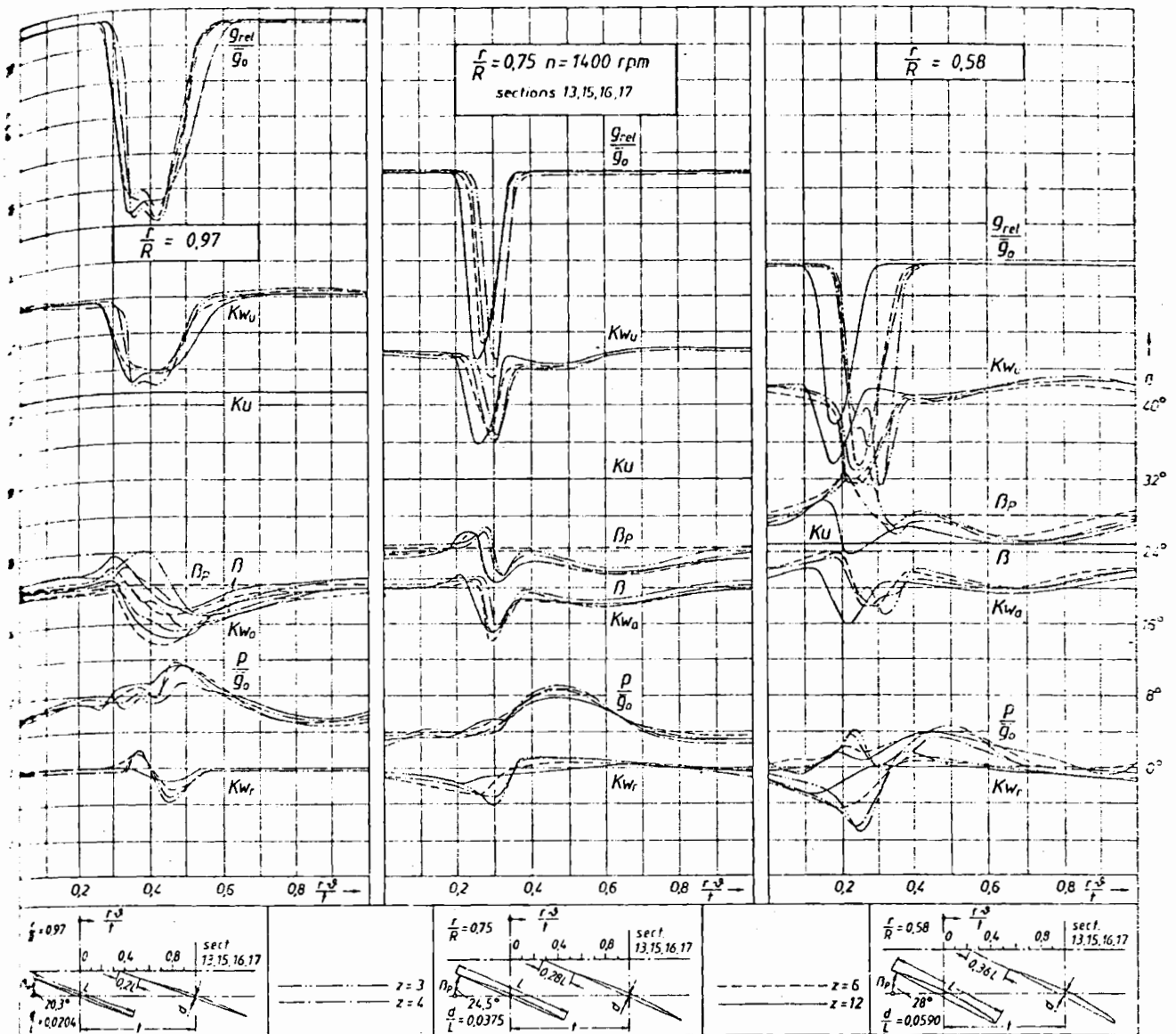
Fig. 9.6.7. Relative flow downstream of the trailing edge of a runner vane (wake region) at a speed of 1400 rpm, plot of rothalpy $g_{rel}/\bar{g}_0$, static pressure $p/\bar{g}_0$, components of the relative velocity (coefficient) Kw_u, Kw_a, Kw_r, and the flow angle β vs circumference. Furthermore blade velocity (coefficient) Ku and vane angle β_p. S suction face (left); P pressure face (right), analogous to Fig. 9.6.6. After Kühnel [9.127].

III. The absolute flow downstream of the runner: In the test sections past the runner the radial distribution of the whirl Kc_{u2} at speeds of 1400 and 1700 rpm fairly reflects the free vortex law. Therefore no remarkable influence of the vane number exists in this respect. Only near the hub and the casing smaller values occur. In the region of the tip, the deviations from the free vortex distribution appear as indentations in the curves. They shift towards the casing with rising vane number.

The cause of these rather striking depressions, which appear in the graphs of the axial and radial velocity vs radius (see [9.74], Fig. 25 and 26) and which are especially pronounced in the graph of the total pressure $g/\bar{g}_0$, is probably the tip clearance vortex.

379

For the 3- and 4-vane runner the zone, in which the whirl Kc_{u2} falls short of the value for a potential vortex, extends at 2000 rpm more over a mean part of the cross section than it does at 1400 rpm to 1700 rpm, thus having then a nearly linear drop of the whirl Kc_{u2} versus r over a wide range of radius.

The reason for these unexpected irregularities and also for the deviation near the hub is the growth of the boundary layer under the influence of centrifugal force and radial pressure gradient. For the speed 1100 rpm and especially for 800 rpm only the 12-vaned runner approximately achieves the free vortex relationship. The smaller the vane number the more the values of the whirl decrease near the casing and hub, whereas they grow in the mean vane section.

The rise of the axial velocity from the casing towards the hub, enlarged by decrease of speed (see [9.74], Fig. 25) can be explained also by the resulting drift of fluid within the boundary layer towards the axis when passing the runner.

9.6.4. Theoretical computation of relative flow field and comparison between this and experiments

9.6.4.1. Introduction

The problem considered consists in the computation of the relative flow through a known cascade (indirect problem).

A spatial singularity method was developed. This indeed allows in a simple manner the fulfilment of the kinematic boundary conditions on the faces of vanes, casing or hub but not for the secondary flow produced by the relative eddy in a plane normal to the axis between the runner vanes.

Therefore the flow generated by the singularities has to be superimposed on the flow pertinent to the relative eddy following a proposal of *Raabe* [4.11], [5.62], [8.6], explained in Cap. 5.5.

In accordance with the assumptions made with respect to the singularity method the comparison of values computed and measured was limited to a speed $n = 1400$ rpm in the neighbourhood of the bep.

9.6.4.2. The spatial singularity method

I. The model used for the bound vortices: In the following computation method the blading is replaced with respect to its effects on the flow by spatially arranged bound vortices (Fig. 9.6.8 a). The application of the procedure is limited to a) small-cambered ($f/L < 0,1$), and thin-vaned profiles ($d/L < 0,1$), b) approximate constant runner vane circulation along the radius, c) approximate location of the leading inlet edge and the trailing edge of runner vane within meridional planes.

The vortex filaments are all formed by continuously distributed elements of vortex stars. Each vortex star consists of z straight-lines vortex filaments, extending from the runner axis towards infinity (Fig. 9.6.8 a). Since the vortex filaments make an angle $\pi/2 - v$ with the runner axis, the elementary vortices of an elementary star are located on the surface of a circular cone, whose apex on the axis forms the common origin of the straight-lined bound vortices.

To satisfy *Helmholtz*'s theorem, any straight vortex line of an umbrella-like vortex star is split on the apex into two oppositely rotating axial vortices of the same magnitude reaching from the apex to both the ends of the turbine axis at infinity (Fig. 9.6.8).

Passing over the apex of the cone of such an elementary umbrella-like vortex star from one of its axial ends to the other, the circulation around the axis experiences a step equal to the sum of the circulations of all the z vane-linked elementary vortices for a definite radial section.

380

Fig. 9.6.8. Scheme of the spatial
singularity method. a) Vortex
model of a 3-blade runner with
inlet triangle. Replacement of
the blade by a vortex sheet
formed by continuously dis-
tributed elementary vortex stars
in the inlet triangle, the very
small radial component has
been neglected)). b) Induced
velocities of an elementary
vortex star at a point of
reference. After *Kühnel* [9.127].
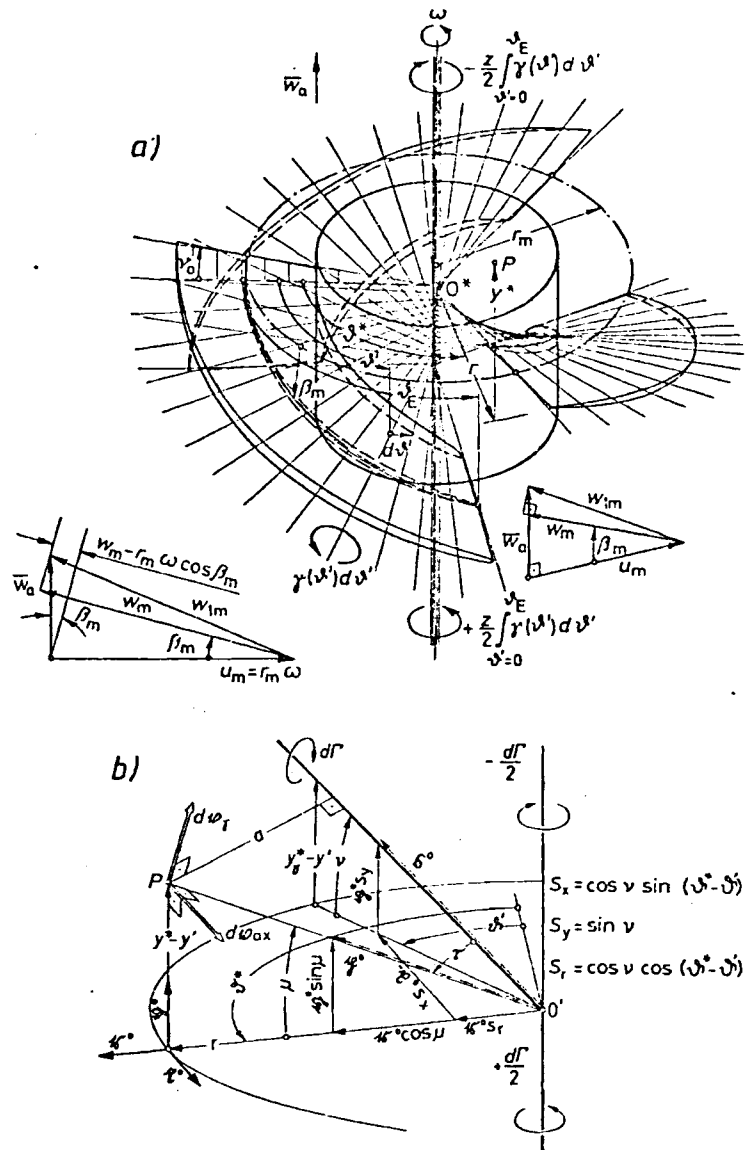
A cylindrical coordinate system was used, whose origin coincides with the apex of an elementary vor-
ex star. The elementary vortex stars are peripherally turned and axially shifted against each other
o that the elementary straight vortex line belonging to one vane intersects a cylinder of mean radius
r_m along a helix. Such a helix with constant angle with the periphery β_m is identical to the chord of
a profile's skeleton in a mean cylindrical section of the vane.

Linearizing the inclination $\tan v$ of an elementary bound vortex to the radius vs the
azimuth ϑ' by

$$\tan v = b\,\vartheta' + \tan v_0 \qquad (9.6-8)$$

with the present twist of the vane (Fig. 9.6.1 a) and the small camber of its profile skeleton
$f/L < 0.028$, a fair approximation of the skeleton vane face is obtained by the vortex face.
The gradient

$$b = d(\tan v)/d\vartheta' = \text{const}, \qquad (9.6-9)$$

and the inclination angle v_0 of the vortex filament of the elementary vortex star located
at the origin are taken from the plan and elevation of the vane (Fig. 9.6.1 a). The largest

381

distance between skeleton face and vortex face amounts in the present case to $0,023 \, L$. Hence the equation of the vortex surface reads

$$y^* = -r_m(\vartheta' \tan \beta_m - \tan v_0) + (r - r_m) \tan v. \qquad (9.6-10)$$

Denoting $\sin \beta_m + b \cos \beta_m = B$, the last relation reads

$$y^* = \tan v_0 r + b r \vartheta' - (r_m B/\cos \beta_m) \vartheta'. \qquad (9.6-11)$$

The magnitude of the elementary vortex filament in the elementary vortex star, $\gamma(\vartheta') \, d\vartheta'$, as well as the inclination angle v are functions of the azimuth ϑ', where $\gamma(\vartheta')$ indicates the circulation per unit azimuth, the so-called vortex density. According to the assumptions, the circulation round a vane

$$\Gamma_s = \int_{\vartheta'=0}^{\vartheta_E} \gamma(\vartheta') \, d\vartheta' = \text{const} \qquad (9.6-12)$$

This, with constant specific flow energy $\bar{Y}_0$, gives, according to Euler's relation and Stokes' theorem for infinitely thin runner vanes, at $\eta_u = \text{const}$,

$$\eta_u \bar{Y}_0 = -\omega r_2 c_{u2} = [z\omega/(2\pi)] \, \Gamma_s, \qquad (9.6-13)$$

which requires a free whirl past the runner $(c_{u2} r_2 = \text{const})$.

The last requirement is satisfied fairly well at speeds of 1400 rpm and 1700 rpm (see [9.74] Fig. 24, 28). To obtain the existing zero whirl at the inlet, a straight vortex of the circulation Γ_s along the runner axis is superimposed.

II. Induced velocities: According to the law of Biot and Savart an individual straight semi-infinitely extended elementary vortex filament induces at the point of reference P (Fig. 9 6.8 b),

$$dv_\gamma = [d\Gamma/(4\pi a)] \, [(1 + \cos \tau)/\sin \tau] \, (s^0 \times p^0), \qquad (9.6-14)$$

s^0 being the unit vector of the elementary vortex with circulation $d\Gamma$, and p^0 the unit vector in direction $0'$ (Fig. 9.6.8). Since $a = r \{1 + [(y^* - y')/r]^2\}^{1/2} \sin \tau$ and $\cos \tau = s^0 \cdot p^0$, the last equation can be converted into

$$dv_\gamma = [d\Gamma/(4\pi r)] \, (s^0 \times p^0)/\{\langle 1 + [(y^* - y')/r]^2 \rangle^{1/2} (1 - s^0 \cdot p^0)\}. \qquad (9.6-15)$$

In the following the substitutions introduced by Finke [9.118] are adopted

$$(y^* - y')/r = \tan \mu = \sinh \lambda, \qquad (y_\gamma^* - y')/r = \tan v = \sinh \lambda_y. \qquad (9.6-16)$$

Obviously the unit vectors can be reduced to their components in a x, y, r-system as follows:

$$s^0 = -[\sin(\vartheta^* - \vartheta')/\cosh \lambda_y] \, x^0 + \tanh \lambda_y y^0 + [\cos(\vartheta^* - \vartheta')/\cosh \lambda_y] \, r^0,$$

$$p^0 = \tanh \lambda \, y^0 + \cosh^{-1}\lambda \, r^0. \qquad (9.6-17)$$

Computing from this the products $s^0 \times p^0$ and $s^0 \cdot p^0$ and inserting these in (9.6-15) gives

$$dv_\gamma = \frac{d\Gamma}{4\pi r} \, \frac{[\sinh \lambda_y - \sinh \lambda \cos(\vartheta^* - \vartheta')] \, x^0 + \sin(\vartheta^* - \vartheta') \, y^0 - \sinh \lambda \sin(\vartheta^* - \vartheta') \, r^0}{\cosh \lambda [\cosh(\lambda - \lambda_y) - \cos(\vartheta^* - \vartheta')]}. \qquad (9.6-18)$$

Both the semi-infinite vortices along the machine axis with their circulation induce in the peripheral direction at the point P

$$dv_{ax} = -[d\Gamma/(4\pi r)] \tanh \lambda x^0. \qquad (9.6-19)$$

382

The velocity dv induced by all the vortex filaments of an elementary vortex star at the station P results from the addition of dv_i and dv_{ax} over the vane number z, where the azimuth of the nth vane must be expressed by $\vartheta'_n = \vartheta' + 2\pi n/z$ and the summation has to be made from $n = 0$ to $n = z - 1$. Applying the sum formula of *Finke* [9.118], the individual components of $dv = \sum\limits_{n=0}^{z-1} dv_y + dv_{ax}$ take the form

$$dv_u = -\frac{z\,d\Gamma}{4\pi r}\frac{\sinh z(\lambda - \lambda_y)}{\cosh z(\lambda - \lambda_y) - \cos z(\vartheta^* - \vartheta')}, \qquad (9.6-20)$$

$$dv_a = \frac{z\,d\Gamma}{4\pi r}\frac{1}{\cosh \lambda}\frac{\sin z(\vartheta^* - \vartheta')}{\cosh z(\lambda - \lambda_y) - \cos z(\vartheta^* - \vartheta')}, \qquad (9.6-21)$$

$$dv_r = -\frac{z\,d\Gamma}{4\pi r}\tanh \lambda\,\frac{\sin z(\vartheta^* - \vartheta')}{\cosh z(\lambda - \lambda_y) - \cos z(\vartheta^* - \vartheta')}. \qquad (9.6-22)$$

From (9.6-8) and $\sin\beta_m + b\cos\beta_m = B$ it follows

$$y' = - r_m B\,\vartheta'/\cos\beta_m. \qquad (9.6-23)$$

The arguments λ and λ_y defined by (9.6-16) can be expressed with (9.6-23) and a known identity [9.132] as

$$\lambda = \ln\langle y^*/r + [r_m B\vartheta'/r\cos\beta_m] + \{[y^*/r + r_m B\vartheta'/(r\cos\beta_m)]^2 + 1\}^{1/2}\rangle,$$
$$\lambda_y = \ln\langle\tan v_0 + b\vartheta' + [(\tan v_0 + b\vartheta')^2 + 1]^{1/2}\rangle. \qquad (9.6-24)$$

For convenience the last two relations are reduced to

$$\lambda = \ln[f(\vartheta', y^*, r)], \qquad \lambda_y = \ln[g(\vartheta')]. \qquad (9.6-25)$$

The circulation $d\Gamma$ is expressed by the strength $\gamma(\vartheta')$ of the bound vortex element between adjacent meridians, angular distance $d\vartheta$, as

$$d\Gamma = \gamma(\vartheta')\,d\vartheta'. \qquad (9.6-26)$$

Using the pitch $t = 2\pi r/z$, inserting λ, λ_y in (9.6-20) through (9.6-22), integrating along the peripheral length of the vane from $\vartheta' = 0$ to ϑ_E, adding to these induced velocities in the axial direction the throughflow velocity w_a and in the peripheral direction the term $-r\omega$ due to the relative eddy, then after *Kühnel* the following velocity components appear at a certain point $P(y^*, \vartheta^*, r)$ [9.74]

$$w_u = -\frac{1}{t}\int\limits_{\vartheta'=0}^{\vartheta_E}\gamma(\vartheta')\frac{\left[\dfrac{f(\vartheta', y^*, r)}{g(\vartheta')}\right]^z - \cos z(\vartheta^* - \vartheta')}{\left[\dfrac{f(\vartheta', y^*, r)}{g(\vartheta')}\right]^z + \left[\dfrac{g(\vartheta')}{f(\vartheta', y^*, r)}\right]^z - 2\cos z(\vartheta^* - \vartheta')}\,d\vartheta' - r\omega, \qquad (9.6-27)$$

$$w_a = \frac{1}{t}\int\limits_{\vartheta'=0}^{\vartheta_E}\gamma(\vartheta')\frac{2f(\vartheta', y^*, r)}{[f(\vartheta', y^*, r)]^2 + 1}$$
$$\cdot\frac{\sin z(\vartheta^* - \vartheta)}{\left[\dfrac{f(\vartheta', y^*, r)}{g(\vartheta')}\right]^z + \left[\dfrac{g(\vartheta')}{f(\vartheta', y^*, r)}\right]^z - 2\cos z(\vartheta^* - \vartheta')}\,d\vartheta' + \bar{w}_a. \qquad (9.6-28)$$

383

$$w_r = -\frac{1}{4}\int_{x'=0}^{x_F} \gamma(\vartheta') \frac{[f(\vartheta', y^*, r)]^2 - 1}{[f(\vartheta', y^*, r)]^2 + 1}$$

$$\cdot \frac{\sin z(\vartheta^* - \vartheta')}{\left[\frac{f(\vartheta', y^*, r)}{g(\vartheta')}\right]^2 + \left[\frac{g(\vartheta')}{f(\vartheta', y^*, r)}\right]^2 - 2\cos z(\vartheta^* - \vartheta')} \, d\vartheta'. \qquad (9.6-29)$$

III. Distribution of the bound vortices: As a distributive function for the vortex density $\gamma(\vartheta')$ in the azimuthal direction a *Glauert* series is used. Hence with $\Theta' =$ arccos $(1 - 2\vartheta'/\vartheta_E)$:

$$\gamma(\vartheta') = \gamma(\Theta') = (2w_m r_m/\cos\beta_m)(A_0 \tan\Theta'/2 + \sum_{k=1}^{i-1} A_k \sin k\Theta'). \qquad (9.6-30)$$

The coefficients A_k are obtained from the kinematic boundary condition according to which the vector w must be normal to the face of the vane skeleton.

9.6.4.3. Comparison of computed results with measured

Three kinds of distributions for the points of reference have been applied for the situation that the points of reference are located on the face of the skeleton as well as on the face of the vortex sheet. They were:

a) Three points on the mean cylindrical section in a circumferential sequence following the $\frac{3}{4}$th chord theorem: $\frac{3}{12}\vartheta_E, \frac{7}{12}\vartheta_E, \frac{11}{12}\vartheta_E$; .
b) 3 points on the above section in the sequence $\frac{1}{12}\vartheta_E, \frac{6}{12}\vartheta_E, \frac{11}{12}\vartheta_E$ (approximated distribution after *Birnbaum*);
c) 9 points, three of which have been located on the outermost, the middle and the innermost cylindrical section in the sequence of the $\frac{3}{4}$th chord theorem [9.117].

The best agreement between measured and computed velocities has been achieved with method b).

Apart from the boundary layer and the field of the tip clearance vortex the measured results do not show any relevant influence of the vane number (Fig. 9.6.9 a). The same can also be proved for the theoretical prediction of the relative flow field.

It is of interest to see, that the influence of the relative eddy, when added to the flow of the singularities improves agreement between measurements and the method sketched in Cap. 5.5.5 (Fig. 9.6.9 b).

Also the two dimensional method of *Schlichting* has been used for the comparison between experiment and theory.

The results show that the velocity distribution along a mean cylindrical vane section is nearly identical with the spatial singularity method. This reveals the fact that the vane number has almost no influence on the flow field from the theoretical point of view when using a potential flow. The differences due to the vane number result more or less all from the boundary layer and the tip clearance.

384
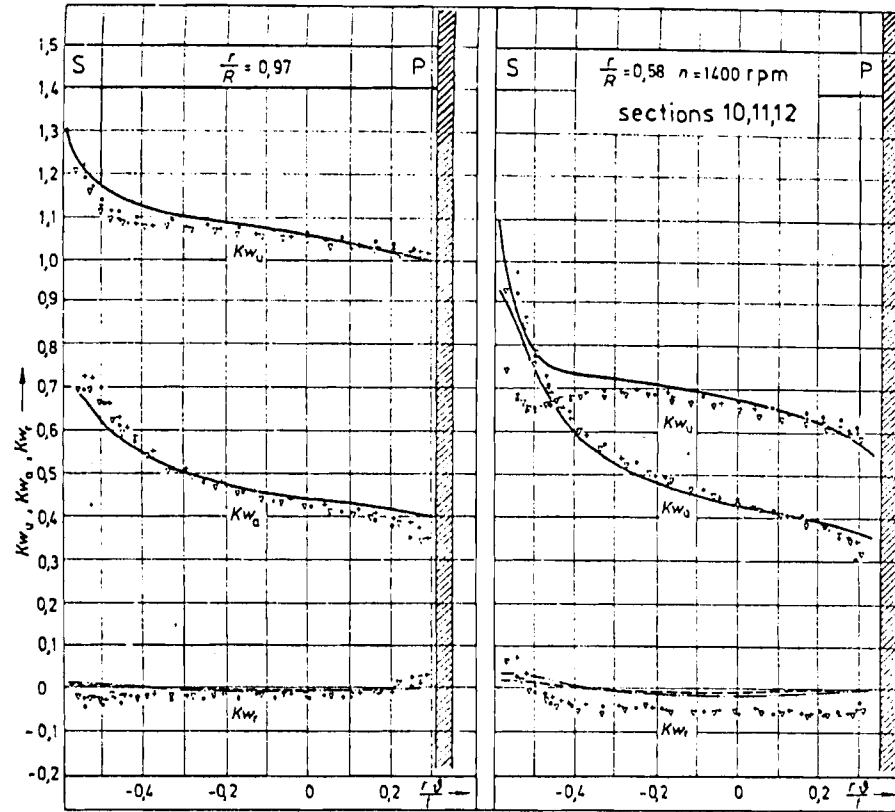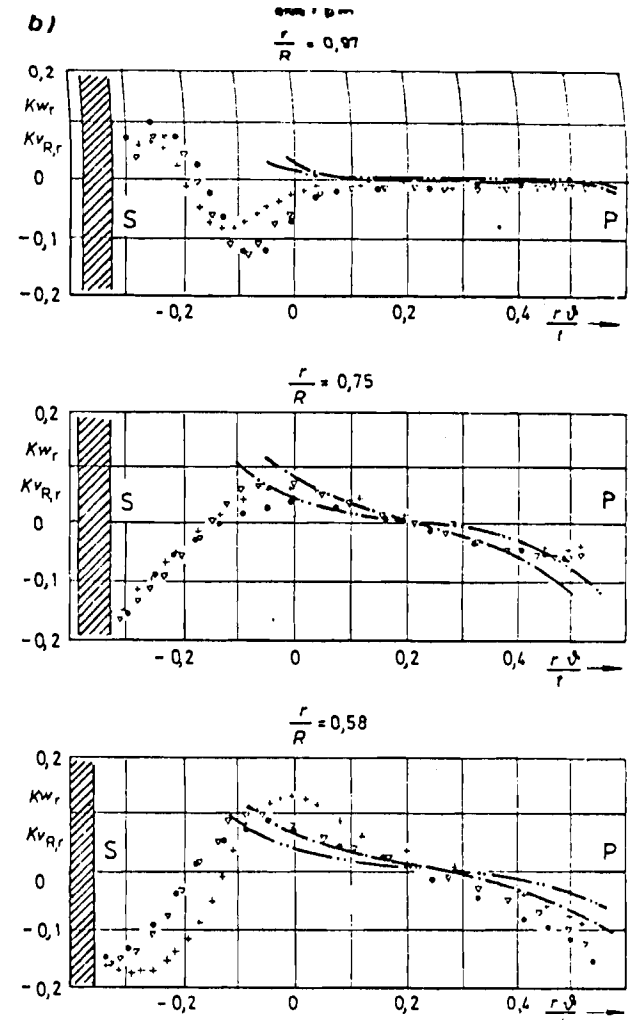
Fig. 9.6.9. Comparison between measured and calculated velocities.
a) Comparison of calculated and measured components of the relative
velocity (coefficient) downstream of the runner blade's leading edge at a
speed of 1400 rpm: Kw_u: whirl component of the relative velocity (coefficient), Kw_a: axial component of the relative velocity (coefficient), Kw_r: radial component of the relative velocity (coefficient). Measured velocities for z 3 blades: (+ + +), z 4 blades: ($\nabla \nabla \nabla$), z 6 blades: ($\cdots$). Velocity components computed by the method of singularities alone at z 3, 4. 6, 12: ———, at z 3: —·—; at z 6: ———. Only the relatively very small radial components show small dependence on vane number. b) Comparison of computed and measured radial components of the velocity before the trailing edge of a runner blade at 800 rpm (z 3: + + + ; z 4: $\nabla \nabla \nabla$; z 6: ····) (Calculation after Raabe [5.6.2], z 3: —··—, z 4: —···—). After Kühnel [9.127].

9.7. Dynamic measurements of unsteady flow near and within the boundary layer of runner vanes by N. Furtner

9.7.1. Introduction

A non axisymmetric and pulsating absolute flow is produced past the guide apparatus of a water turbine by the wakes of its whirl generating elements (spiral casing, stay and guide vanes). Thus a periodically or randomly pulsating relative flow appears in the runner vane channels and as a consequence unsteady vane loading which frequently leads to vane or machine vibration, causing fatigue cracks or in the worst case a rupture of runner vanes, then found in the draft tube.

Several authors, e.g. *Mollenkopf* [9.46], *Gerich* [9.133], *Schlemmer* [5.18], and *Castorph* [9.81; 9.116] have proved by measurements and observations on Kaplan and Francis-turbines the existence of fluctuating wake or stall areas in the absolute flow pattern and also in the relative flow pattern. *Kemp* and *Sears* [6.30], *Kazacov* [9.134], and *Lotz* [6.28] have carried out fundamental research on the determination of the mutual influence of adjacent blade rows when they move relative to each other also in the case of spatial flow.

According to the simplified statements of the research work carried out, the influences of unsteady flow in boundary layers produced by the events in the main flow must be left out of consideration.

An exact determination of unsteady vane forces requires knowledge of the unsteady dynamic pressure acting on the vane faces within the boundary layer. The principal subject of the following section is the dynamic measurement of the unsteady flow near to the runner vanes and within their boundary layers in the case of axial and mixed flow (Francis) turbines.

9.7.2. Experiments on a Kaplan water turbine model

I. Four port probe with quick response: For the analysis of this unsteady boundary layer flow a suitable instrument has been developed by *Furtner* at Lehrstuhl und Labor für hydraulische Maschinen und Anlagen. TU München. West Germany. (Fig. 9.7.1 a) [9.135]. As it is near to the wall, the flow was assumed to be parallel to the known wall face. Hence only four ports were needed for the simultaneous measurement of the spatial velocity vector and the static pressure. The port B was used for the total pressure, ports A and C for the yaw angle the velocity makes with the axis of the probe's head and the port D for the static pressure, (Fig. 9.7.1 a).

Each port was connected with a Kulite transducer, described in 9.5. The probe could be shifted in steps of 0.05 mm by hand. In a later version, used on the FT, this probe could be adjusted 'on site' by a lock at draft tube exit. Then Mr. *Kriegl* from the above institution developed a hydrostatic actuator 15 mm high and of 20 mm diameter, on the vane face opposite to that needed for measurement and supplied by pipes laid in smoothly covered grooves in the vane, coming from a stationary vessel via a transmitting chamber around the shaft. A worm and locking gear in the actuator enabled a stepwise shift of the probe by remote control [9.82; 9.13], Fig. 9.7.1 b.

II. Measuring points: Measurements were made on a runner with 4 vanes, diameter $D = 612$ mm. at bep with $n_{11} = 127,5$ rpm and $Q_{11} = 1.39$ m^3/s. On each side of the vane 9 measuring points were provided, 3 each at intersections with three different coaxial cyl-
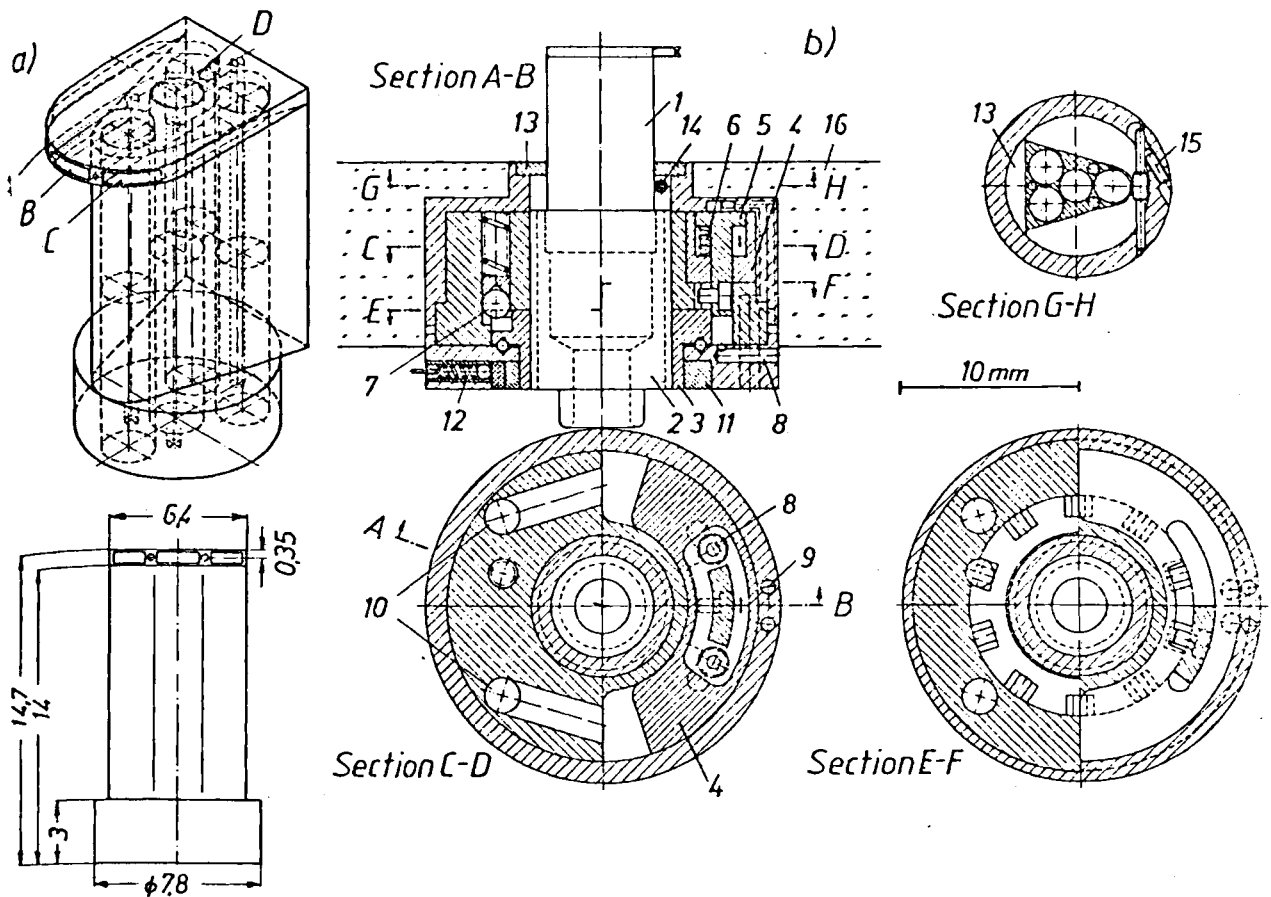
Fig. 9.7.1. 4-hole quick response boundary layer probe on runner vane after *Furtner* [9.135] with micro transducers, 2 mm in diameter. a) Perspective view and frontal view of the probe. A. C ports for directional measurement; B port for total pressure; D port for static pressure. b) Hydraulic device facilitating a stepwise axial adjustment of rotating probe by means of gasoline fed annular servomotor, supplied by pipes from a stationary head via shaft and vane, 1 probe; 2 threaded bush; 3 screw for adjustment with grooved ball bearings; 4 annular piston; 5 axial piston; 6 restoring spring; 7 free wheel device; 8 relieving boring; 9 pressure bore for axial piston; 10 pressure bore for annular piston; 11 toothed ring for feedback; 12 contact for feedback; 13 head cover and guide of probe; 14 probe's guide bearing; 15 adjustment screw for prestressing the bearing; 16 runner blade. Note the annular piston in Section C–D. After *Furtner* [9.135].

inders (Fig. 9.7.2 a). The positioning device, incorporated into the vane permits displacement of the probe head up to 9 mm normal to the vane surface.

III. Time-averaged measurements: Quasi steady investigation of the relative flow in the proximity of the vane face was made possible by averaging the synchronous records of pressure fluctuations from the 4 ports vs elapsed time obtained by a light beam oscillograph over a certain period, say one runner revolution (Fig. 9.7.2 b). Hence the variations of the velocity components in the radial and circumferential directions on both sides of the vane can be obtained. An essential characteristic of this flow pattern is the secondary flow, directed towards the outside wall on the pressure face and towards the hub on the suction face of the vane (Fig. 9.7.2 b). This follows from the relative eddy (Cap. 5.5.5.4).

IV. Comparison between time-averaged results with predictions by the method of singularities and boundary layer theory: Velocities parallel to the surface as functions of the

387
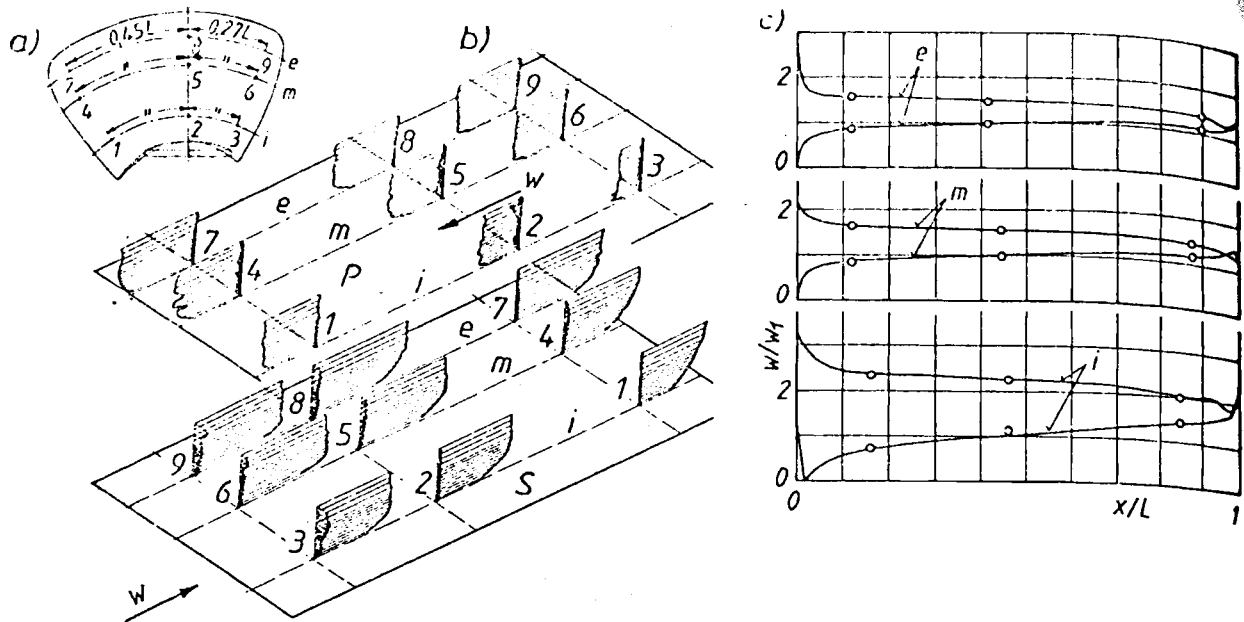
Fig. 9.7.2. Time-averaged velocities from dynamic measurements after N. Furtner. a) Scheme of measuring stations. L chord; e external cylindrical section, radius $r = 0.9\,r_0$; m mean cylindrical section, radius $r = 0.77\,r_0$; i internal cylindrical section, radius $r = 0.56\,r_0$, r_0 runner tip radius. b) Schematic view of profiles of the relative velocity on a Kaplan turbine runner vane close to the wall. P pressure face; S suction face. Outwards oriented radial velocities on the pressure face, inwards oriented on the suction face. $D = 0.615$ m; bcp. c) Comparison of the calculated and measured velocities in the cylindrical sections, calculation by the singularity method after Martensen and Jacob [6.2; 6.3]. o point measured, ——— line calculated. After Furtner [9.135].

actual vane geometry and the inflow and outflow angles measured by Castorph [9.116] were computed by means of the method of singularities of Martensen and Jacob [6.2; 6.3]. Results show a very good agreement with the time-averaged velocities measured at the outer edge of the boundary layer, Fig. 9.7.2c.

Characteristics of the boundary layers at the three cylindrical vane sections have been computed, using an integration method described by Rotta [9.136]. Approximation of the time-averaged boundary layer profiles by means of exponential functions and their integrations, yielded the values determined experimentally. Only the results obtained for the outer cylindrical section were very satisfactory [9.82].

V. Unsteady measurements: Essentially the wake areas of the 24 guide vanes in the relative flow can only be found by pressure measurements in the unsteady state. The resulting modifications of relative velocity in magnitude and direction were of the order of 20% of the mean relative velocity and 6 degrees. This gives, by the way, an amplitude of the hydrodynamic lift, at least in the outer cylindrical section of the order of 40% of the time-averaged lift.

Imagine that this fluctuating force attacks the vane with a long moment arm with respect to the vane's root at the hub, creating there an oscillating bending stress of the same order, and in connection with fatigue effects a possible rupture of the vane from the disk.

The usual cause for such wake-induced stress fluctuations is on the one hand the endeavour to run with overgate and then to shift the gate's stem towards the shaft so as to have

388

at overgate, guide vanes that extend deeply into the flow with their rearward edges and the adjacent blunt lower front faces ("lower" at a turbine with vertical shaft).

Because of the excessive thickness of the gates (vane thickness to chord ratios of 1 : 5 are found), the gate structure from welded plates also on the rear, and the impossibility of sharpening such a welded guide vane at its lower front surface in the streamwise direction, the opened guide vane leaves a big wake in this direction.

It follows from theoretical considerations that fluctuations of direction and magnitude of velocity and hence also pressure will increase on approaching the vane surface. This is confirmed by measurements (Fig. 9.7.2). According to the findings of *Sexl* [9.137] with respect to an oscillating laminar flow (not a bad model since any flow has a laminar sublayer), the maximum of the oscillations induced by the gates with 112 cycles must be located at a wall distance δ^* of

$$\delta^* = 2.28\, n^{-1/2}/(\pi/\nu)^{1/2} = 1.3 \cdot 10^{-3}\ \text{mm}.$$

Obviously this range cannot be covered by the probe.

Even if fluctuations of the velocity in magnitude and direction along the leading edge of the vane are of the same nature both on the pressure and suction faces of the vane, their further development in the streamwise direction differs strongly along both the faces.
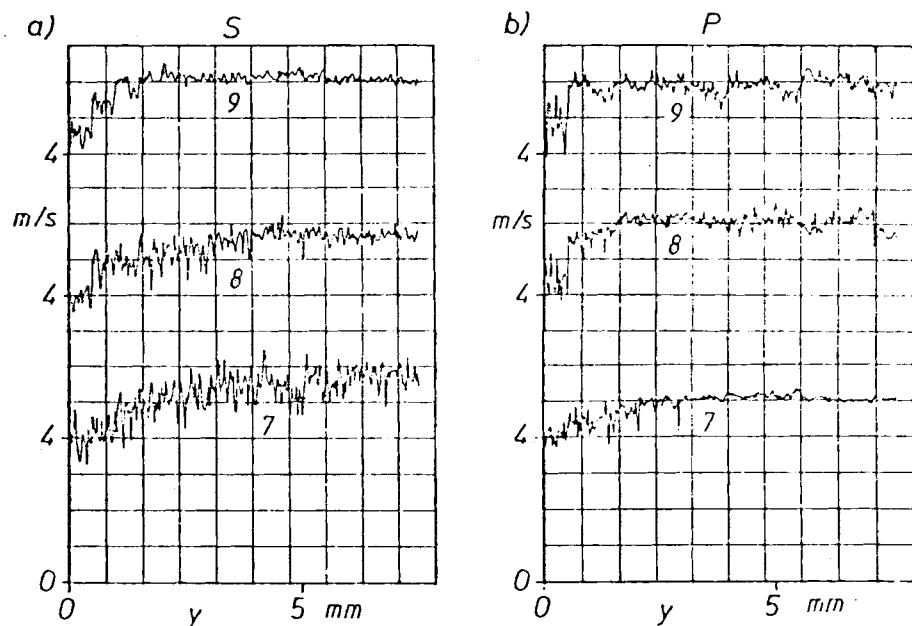
Fig. 9.7.3. Velocity fluctuations along the runner vane. a) Fluctuations of the relative velocity at 0.9 D against wall distance in the streamwise direction on the suction face, stations 9, 8, 7 of Fig. 9.7.2. Increase of the fluctuation in the streamwise direction and also towards the wall. b) Ditto on the pressure face. Here also an increase of fluctuations towards the wall, but a decrease stream-wise. In general a streamwise decrease, or increase of fluctuations with streamwise decrease, or increase of pressure in the main flow, in accordance with turbulence theory. After *Furtner* [9.135].

Measurements made on the outmost cylindrical vane section (Fig. 9.7.3) show a pronounced streamwise increase of fluctuations on the suction face, whereas fluctuations tend to decrease on the pressure face. This is in agreement with the damping or exciting effect of turbulent disturbances under a main flow having a pressure drop or a pressure rise in the streamwise direction [5.4].

I. Arrangement of measuring points: Investigations were made on a high specific speed Francis runner of $D = 455$ mm at the bep with $n_{11} = 72$ rpm and $Q_{11} = 0.836$ m³/s. The measuring stations were uniformly distributed on the pressure and suction faces, 6 along a streamface near the hub, 6 along a mean stream face and 4 along a stream face near the shroud (Fig. 9.7.4 a).

II. Test results of time-averaged measurements: The time-averaged relative flow in the proximity of the vane surface shows acceleration in the flow direction and from the hub towards the shroud on the pressure face of the vane.
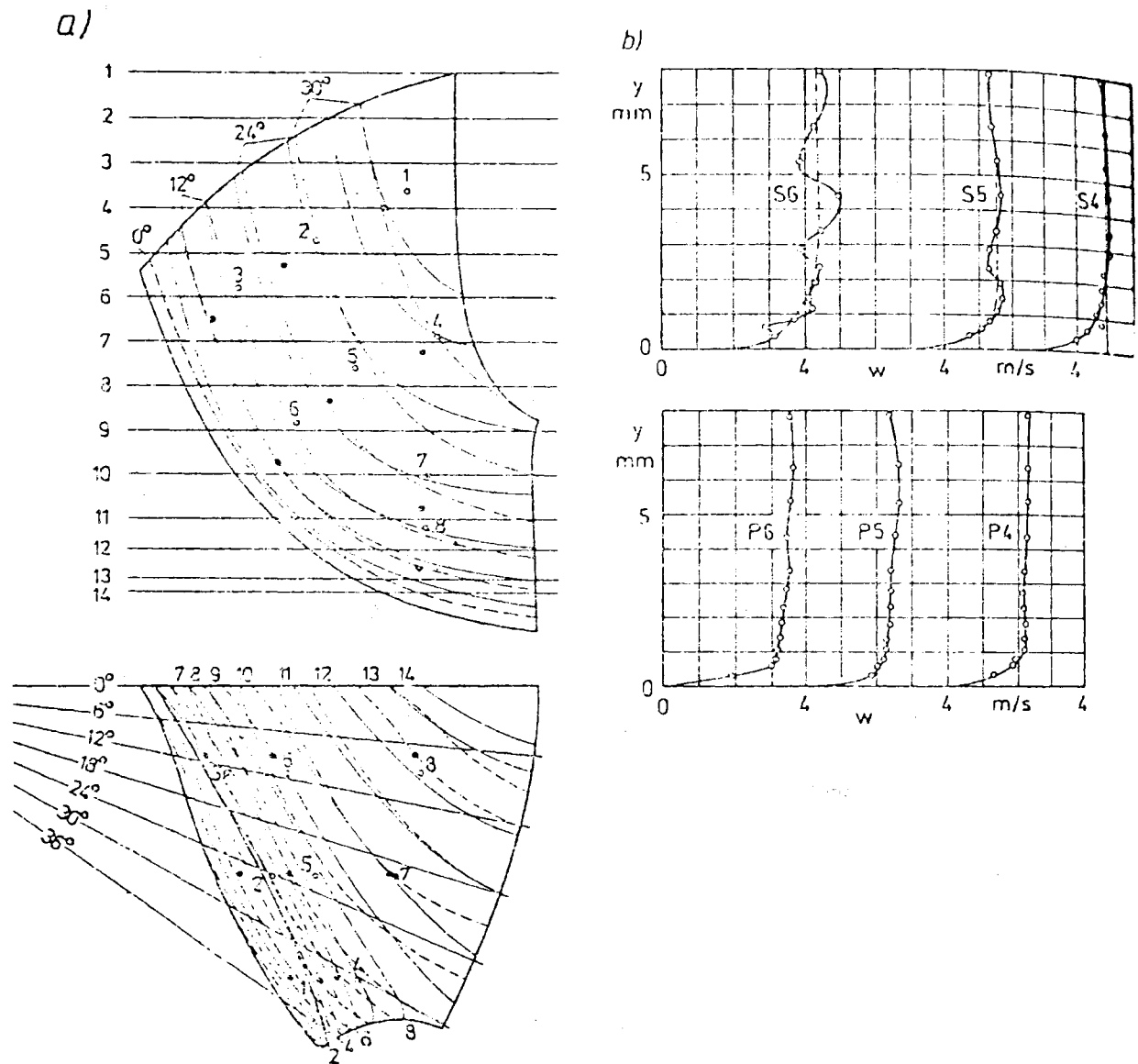
Fig. 9.7.4. Dynamic measurement of the relative flow close to a runner vane of a Francis turbine a) Radial and pattern section in elevation (above) and plan (below) with stations of measuring point on the suction face S (●), and pressure face P (o). b) Time-averaged profiles of the relative velocity obtained from dynamic measurements, arranged in the streamwise direction from the right to the left hand side on a mean stream surface, on the suction face S (above), and on the pressure face P (below), at station 6, 5, 4 according to a). After Furtner [9.135].

The very thin boundary layer suggests the presence of a laminar boundary layer as a basis of a comparison with that on a plate. Quite contrary, on the suction face of the vane a strong increase in thickness of the boundary layer in the direction of flow and also from hub towards the shroud is found. Increasing distortions of the velocity profiles in the flow direction (Fig. 9.7.4 b) is a reason for assuming the formation of vortex layers in the boundary layer.

Characteristics for this configurations are the drop of total and static pressure in the area of vortex axes, as determined in the course of investigating pressure variations on the suction face [9.135]. The steady pressure variations on the pressure face are quite contrary. From the measurements it is seen how in the region of maximum vane curvature (point 8) the static pressure increases on approaching the vane surface.

Evidently these modifications here are attributed to centrifugal forces acting on the particles, linked to the sharp vane curvature.

III. Unsteady measurements: Unsteady measurements permit the demonstration of the presence of the wakes of 28 stay vanes and 12 guide vanes at 141 rpm which corresponds to 60,4 Hz in the relative flow. Unequal spacing of the guide elements is responsible for interference frequencies up to 980 Hz. This leads at this measuring point to average velocity fluctuations of 18 % of the mean velocity with directional fluctuations of approximately 12°.

In analogy with measurements carried out on the axial turbine, velocity fluctuations in the mixed flow runner show a reduction of velocity fluctuations on the pressure face for accelerated general flow. On the suction face the fluctuations are increased as the general flow is decelerated.

9.8. Investigation on unsteady flow in a Francis turbine
by R. Gerich and G. Mollenkopf

9.8.1. Introduction

The bulk of hydroelectric energy demand now is covered with Francis turbines. By virtue of their adjustable gates they are also predestined for the supply of peak load. Unfortunately this is usually connected with working away from the bep with a resulting unsteady flow, as was mentioned in Cap. 9.2 and 5.5.5. This can be predicted only on the basis of model tests.

The following research has been carried out in a closed test rig by Mollenkopf [9.46] and Gerich [9.45] in the Lab. f. hydraulische Maschinen und Anlagen, TU München, West Germany. The shell diagram of the turbine with its individual operating points is shown in Fig. 9.8.1. For the protection of the hot film probe used the research work has been carried out under cavitation free operation and with a head of $H = 2$ m. The tests were made on a model with $D = 272$ mm and a bep at $n_{11} = 76,8$ rpm, $Q_{11} = 1,275$ m^3/s [9.45].

9.8.2. Unsteady flow and turbulence level at runner exit

These investigations were carried out by means of a measuring device shown in Fig. 9.8.3 a, in which the semi-conductor probe shown in the drawing was substituted by a hot film anemometer. The method of holding the instrument enabled the probe to be
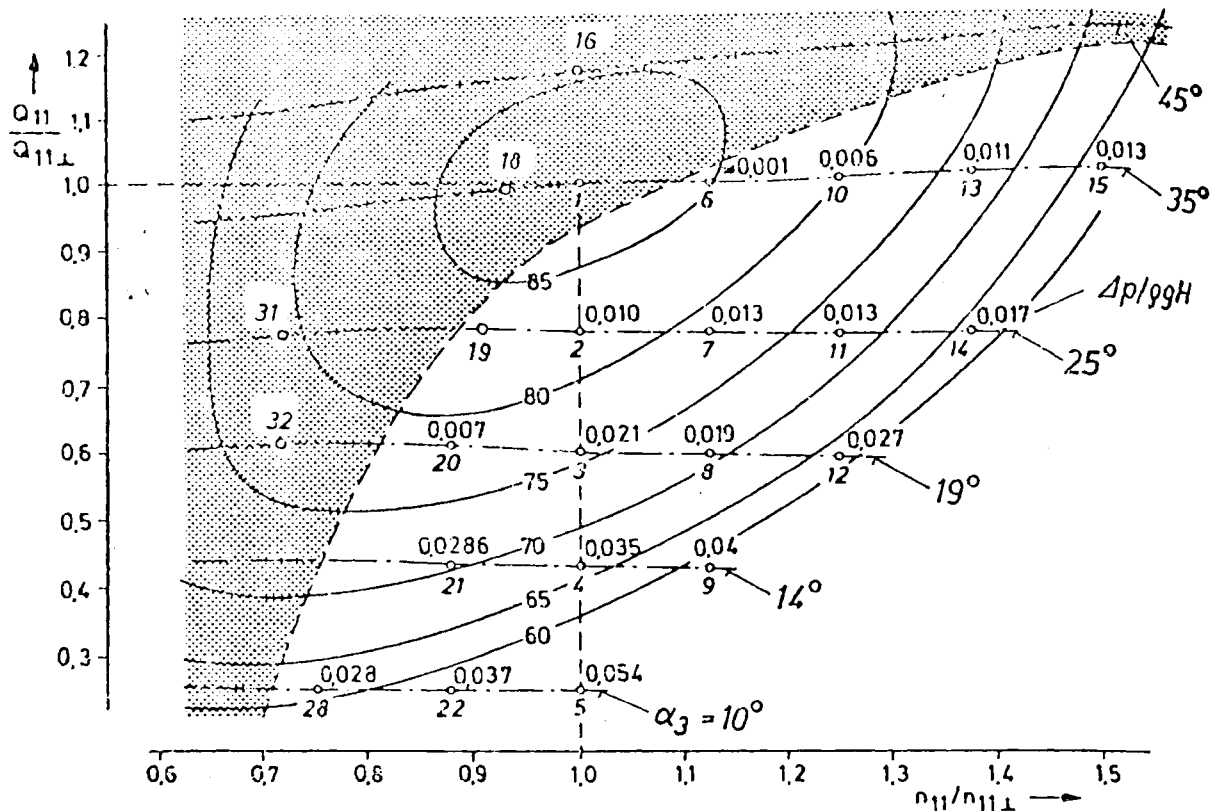
Fig. 9.8.1. Efficiency hill diagram of Francis turbine investigated with periodical fluctuations of total pressure $\Delta Y/Y$ at the bottom ring before the runner, plane V 2 (see Fig. 9.8.3), from the cork screw draft tube vortex. (White area.) In the hatched area non periodical fluctuations from the draft tube vortex. — — — right limit of a band with whirl-free and surge-free operation of an approximate width Δn in the speed axis direction: Δn $n \sim 0.2$. Data of the FT at bep: $Q_{11} = 1.275$ m^3/s, $n_{11} = 76.8$ rpm, $n_q = 86.7$ rpm; test head $H = 2$ m. See Gerich [9.133]. Stronger pressure fluctuations appear under overgate (hatched area). At point 32, and on the wall of the draft tube inlet, they can attain see [9.133] 10% of the head, and even 20% of head in the mixing layer of the draft tube vortex core.

turned about its stem during its rotation with the runner. The electrical signal was transmitted by means of mercury chambers.

Fig. 9.8.2 a shows the distribution of the time-averaged relative velocity at the individual points of operation. From this it is recognized that the wakes are not symmetric to the runner vane. They show a nearly constant thickness past the boundary layer on the pressure face. The velocity distribution towards the suction face and especially the wake past it varies strongly with the point of operation and is usually thicker than that from the pressure face. Because of the extreme large angle of incidence especially the operational points 4 and 31 show periodical stall of the flow past the runner[13].

This is reconfirmed by the level of turbulence (Fig. 9.8.2 b). In general this level increases within the wake towards its centreline except point 4. As an average magnitude of these fluctuations 11% of the mean relative velocity were measured. Periodic fluctuations of relative velocity due to the pitch of the gates could be recognized clearly at points of large gate opening, e.g. point 16 with 6,5% of w.

[13]) See also footnote [7]).

392
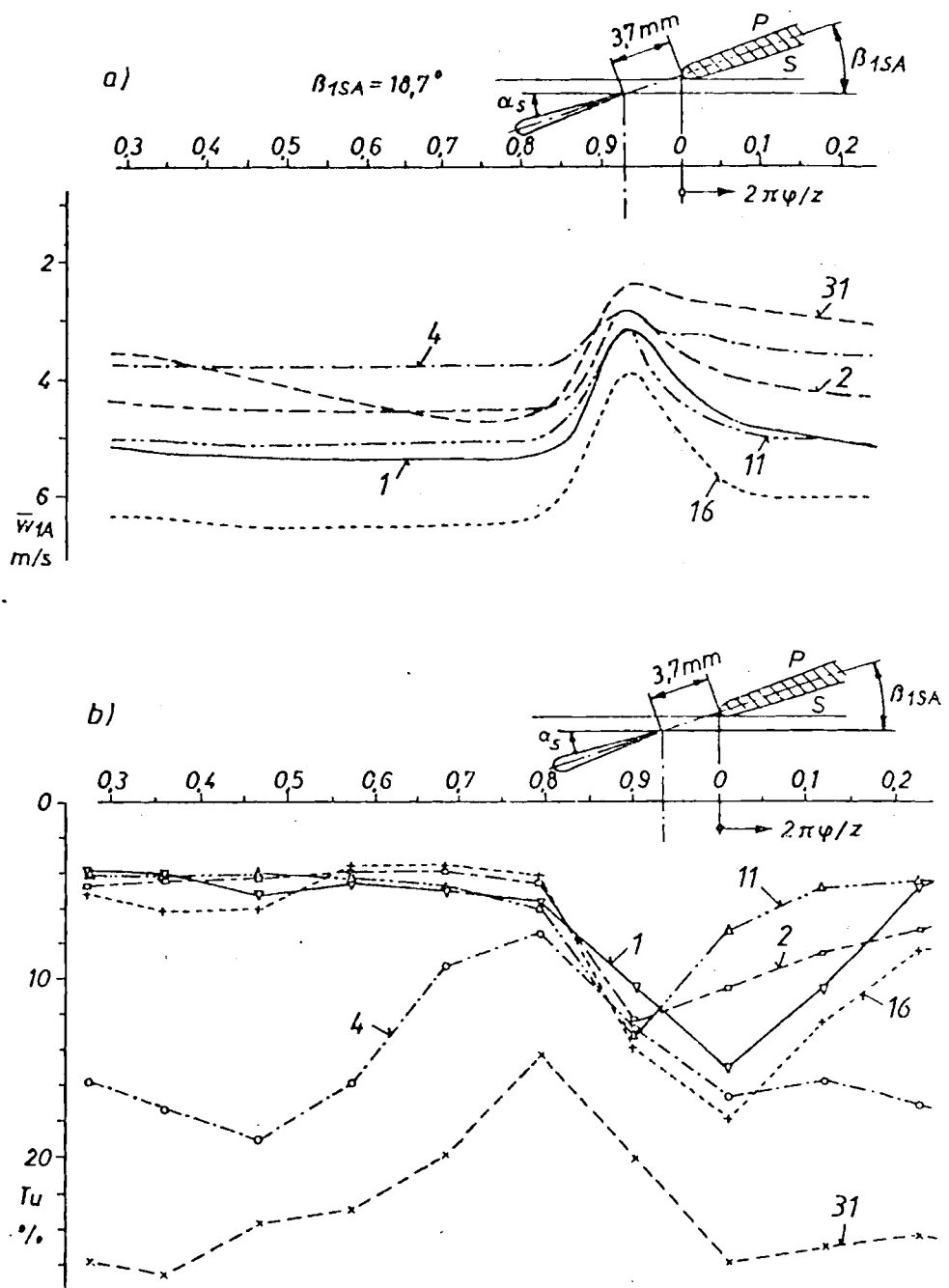
Fig. 9.8.2. Relative velocity and level of turbulence past the runner vane close to the shroud at $H = 2$ m measured by a hot film probe from *Gerich* [9.133] and *Mollenkopf* [9.46]. Numbers mark the test point on the hill diagram of Fig. 9.8.1. a) Relative velocity vs circumference across the pitch. b) Level of isotropic (assumed) turbulence. Note probe position relative to runner vane exit edge.

Fluctuations of the relative velocity due to the precession and frequency of the unstable cork screw part load vortex past the runner could be observed in the neighbourhood of the shroud only in the extreme part load points 4 and 11, with small and irregular amplitudes. Near to the hub these fluctuations have been registrated, as expected, with greater amplitude.
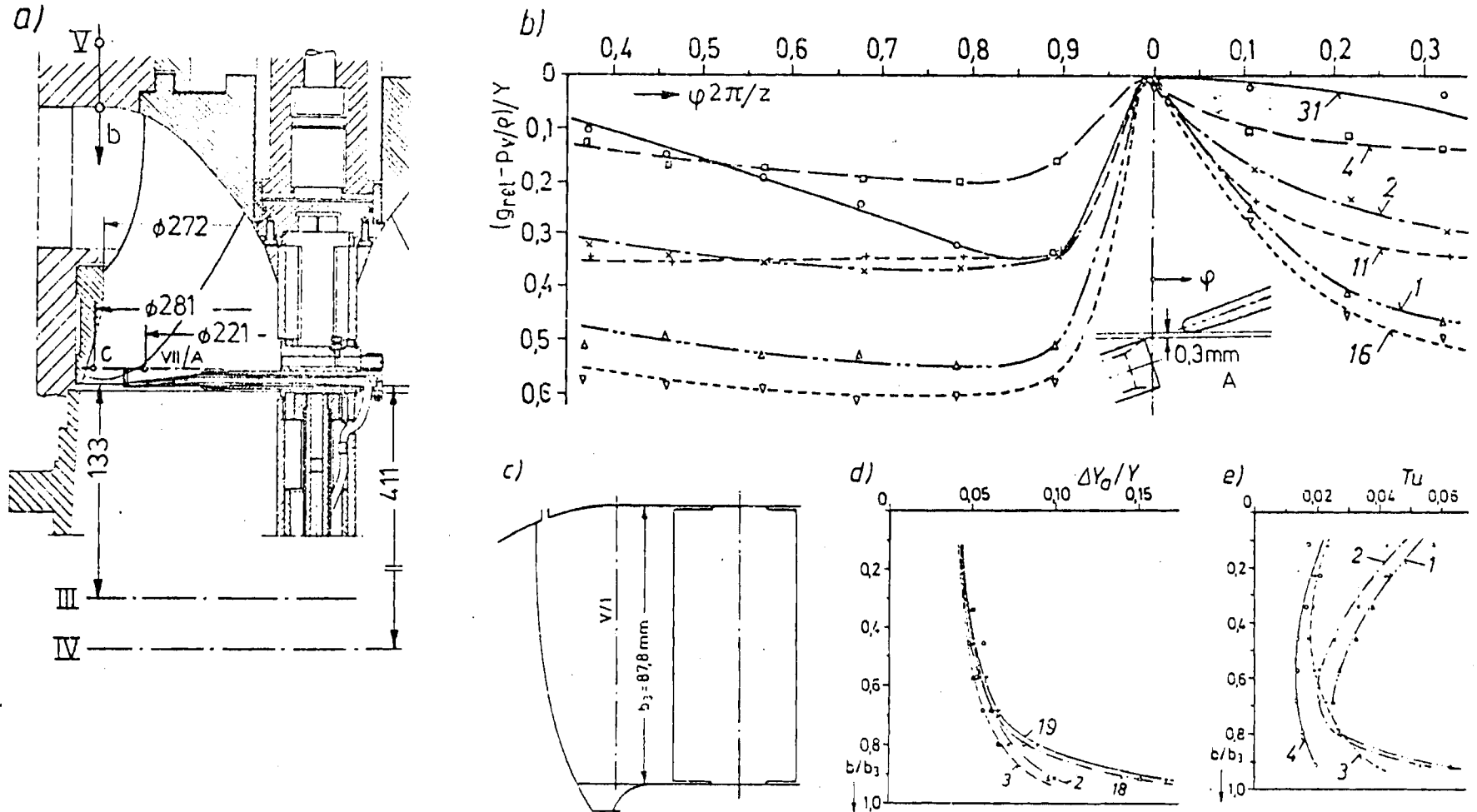
Fig. 9.8.3. Dynamic measurement of total pressure in a rotating and stationary frame of reference. a) Elevation of turbine test section with a rotating Kulite semi-conductor probe of quick response for dynamic measurement of total pressure in the relative, or absolute system. b) Distribution of the referred time-averaged total pressure minus the vapour pressure in the relative flow at runner outlet, close to shroud vs circumference, in measuring plane VII/A, see a) number indicating test points according to Fig. 9.8.1. z 13 vanes. b) Distribution of the surplus of the total pressure g_{rel} in the relative system over the vapour pressure, referred to head Y, at runner outlet near the shroud measuring plane VII/A (see a). Vane number z 1⌐. Detail A: probe orientation against outlet edge of runner vane. c) Measuring plane V/1 between gate and runner. d) Fluctuations of total pressure in relation to head $\Delta Y_a/Y$ across the runner inlet, plane V/1. e) Turbulence level Tu across runner inlet, plane V/1. After Gerich [9.133].

9.8.3. Fluctuations of total pressure at runner exit

These fluctuations were measured in plane VII/A. For the measurement the arrangement in Fig. 9.8.3a was employed with a transducer of 2 mm diameter for the dynamic measurement of total head. The curves in Fig. 9.8.3b show the distribution of time-averaged available.

Analogous to the distribution of the relative velocity a rather steep change of total pressure in the wake past the pressure face is seen here, whereas in the wake due to the suction face the range of total pressure drop vs circumference becomes more broad and depends more on the individual point of operation. Only at operating point 31 a rather large trough of total pressure extends across the wake, probably due to a vortex there.

The fluctuation of total pressure reaches a maximum within the transient region between the boundary layer or wake and the main flow. The maximum of total pressure fluctuations due to gate position 16 occurs there at overgate.

9.8.4. Unsteady absolute flow between gate and runner

This unsteady flow is generated mainly by the two bladed cascades of runner and gate moving against each other. Besides them fluctuations of lower frequency are expected due to the action of the asymmetric and precessing flow field within the draft tube at part load also propagating into the runner. In Fig. 9.8.3d the fluctuations of total pressure during the period of a runner vane and the resulting turbulence level, are plotted versus the span of the gates. They are generated by displacement of the runner blade. The strong increase of these fluctuations towards the shroud and with increased gate opening is caused by the decreasing distance between gate exit and runner. Hence the pulsations originating from cutting of the wakes from the gates by the runner vanes become enhanced. (Note that the turbulence level increases towards both the walls, Fig. 9.8.3e.)

The precessing cork screw vortex under part load within the draft tube, produces also periodical variations of flow both before and past the runner. The consequences are more or less strong fluctuations of pressure and velocity propagating also into the spiral casing and the penstock. A growth of the wake region past the hub and an increase of the vortex core diameter with decreasing flow and increasing moment of momentum past the runner causes an increase of pressure fluctuations due to the draft tube vortex with increasing distance from the bep.

At a certain gate opening, they belong to a draft tube vortex of a certain form and origin, which depends as well on the runner design. So, e.g. at part load with its cork screw vortex, the origin may be on the hub, sometimes deep in the vaned zone of the runner as was described by *Schlemmer, Gerich* and *Raabe* [9.83], or it may be on the top of the hub cone as was described by *Henry* [10.49]. The great diversity of torch-like, rope-like, twin, axial, helicoidal, steadily precessing and unsteadily precessing draft tube vortices as a function of speed and discharge of the working point at a certain turbine has been shown by *Schlemmer* [5.18] for a given Francis turbine.

Usually only the fluctuations due to the draft tube vortex could be recognized from the measuring signals of the static or the total pressure or the velocity. The broad spectrum of all the disturbances appearing could not be determined from the apparently stochastical measuring signals. As all the signals have been combined with considerable noise, an analysis of frequencies has been carried out for the most important signals.

Gerich [9.133] has registered several power spectra of pressure fluctuations at the head cover and within the interspace between runner and gate by means of a correlator and Fourier transformer. Besides the expected resonance frequencies f_i of pressure surges
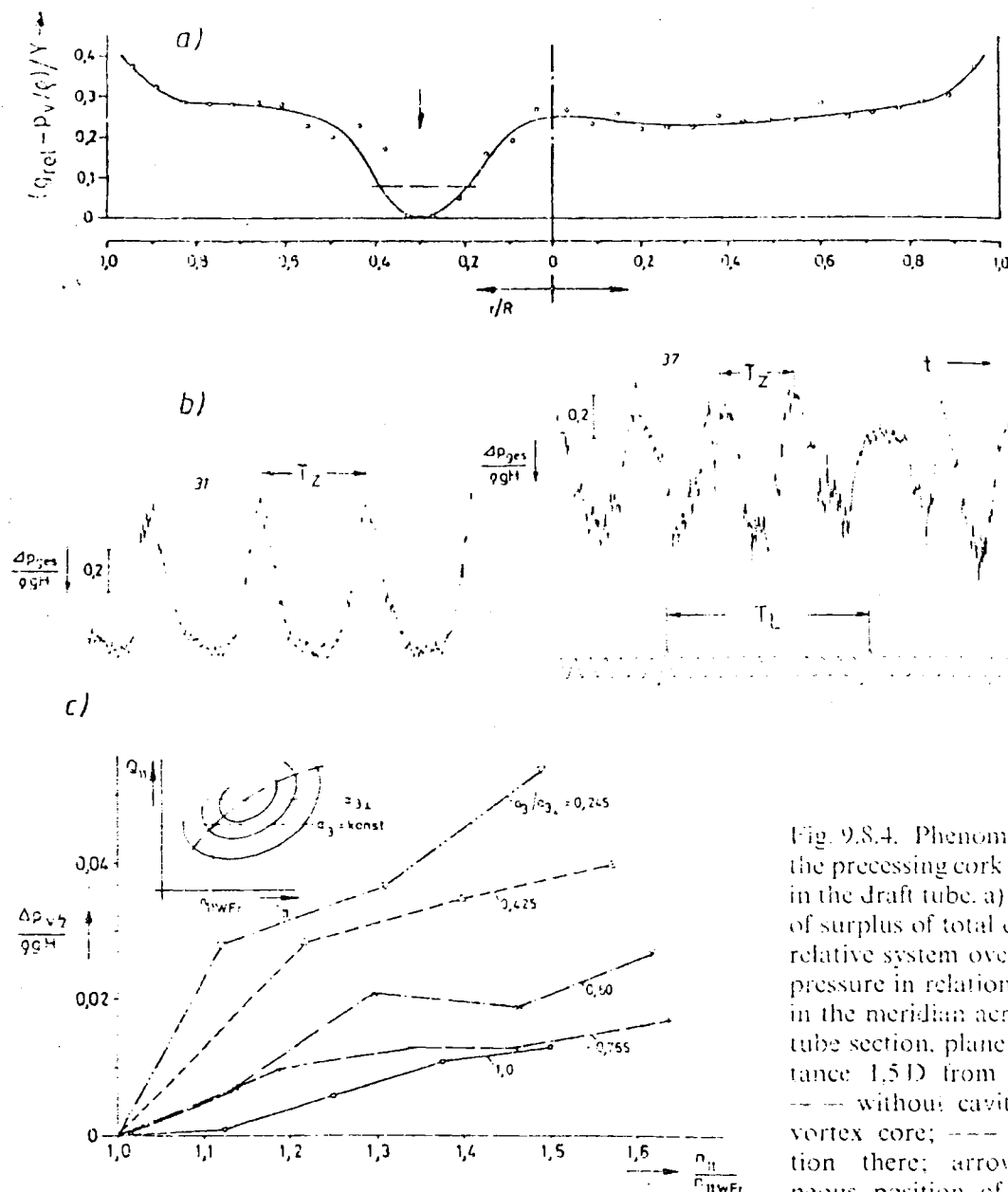
Fig. 9.8.4. Phenomena due to the precessing cork screw vortex in the draft tube. a) Distribution of surplus of total energy in the relative system over the vapour pressure in relation to the head in the meridian across the draft tube section, plane IV, in a distance 1.5 D from runner exit. — — without cavitation in the vortex core; — — — with cavitation there; arrow: instantaneous position of vortex axis.

b) Recorded dimensionless total pressure vs time along circumference for a stationary probe, at test point 31 (left) and 37 (right). (Test point see Fig. 9.8.1.). T precession period of the vortex core, T_L period of a runner revolution. $H = 2$ m, measuring plane III (Fig. 9.8.3). c) Distribution of the pressure fluctuations of the total pressure referred to the head, synchronous with a precessing draft tube vortex near the draft tube wall in relation to the different values of the ratio of unit speed (n_{11}) to the unit speed with zero whirl ($n_{11\,w.fr}$), according to the sketch, at different ratios of the gate angle x_3 to the gate angle of the — — — line crossing the bep. (See sketch.) After *Gerich* [9.133].

with f_1 (runner), f_2 (runner blade), f_4 (draft tube vortex) and f_7 (vibration of casing) a multitude of other resonance frequencies exists.

From the spectra of the total pressure within the penstock and in the neighbourhood of the draft tube wall, a statement could be made about the reaction of the penstock on the pressure fluctuations of the draft tube comparing the "power" of the signals measured on

396

penstock and draft tube. The ratio of both the last figures was recognized to increase with increasing distance of the operating point from the stripe of zero whirl past the runner and hence quiet operation.

9.8.5. Unsteady flow in the draft tube of the turbine

This investigation is limited to part load operation. In a system rotating with the vortex core, the time-averaged distribution of total pressure across the draft tube section shows generally a parabolic drop of the pressure towards the eccentric axis of the vortex core at a certain instant, (Fig. 9.8.4 a). At a certain load this distribution is independent of the head provided the core does not cavitate (as usually happens). Then the vortex core is characterized by constant critical pressure (Fig. 9.8.4 a).

The origin of the vortex core is usually in the runner and due to a rotating stall by flow asymmetry. Greater stall in the runner happens with growing distance from the line of quiet operation without whirl. Hence the periodicity and the form of the draft tube vortex are subjected to stronger changes.

The variation of moment of momentum past the runner and the throughflow distribution and the variation of the vortex core combined herewith cause pressure fluctuations on the draft tube wall with varying amplitudes.

Approximately it can be said, that the amplitudes increase with growing moment of momentum at runner exit and with increasing distance from the bep, Fig. 9.8.4 c. (Note that also the frequency of the surge increases with its amplitude.)

9.8.6. Remedies against draft tube surge and power swing

I. Guide ribs at the hub: The hydraulic fundamentals for this remedy consists in the following. Any flow guided by vanes or baffles arranged in a pitch to chord ratio below 'one' follows more or less the direction of these devices. But this is at the expense of so-called inlet shock loss under a flow not along this device at its inlet, Cap. 5.3 [8.95].

Hence the whirl c_{u1} in the draft tube as the origin of the vortex formation may be suppressed by such guide ribs attached to the hub as the local origin of the effect. But this functions only at a certain desired gate position and shifts the bep into this position. This occurs in connection with eventual shock loss at the inlet of the guide ribs and hence at the expense of optimum efficiency.

Moreover the loss due to inlet shock in connection with possible stall there may worsen the efficiency over a larger operating range. In an imaginary design the lowest part of the hub's end may be arranged axially adjustable by means of a servomotor which comes into action only at the desired point.

On the basis of his thesis work also dealing with this phenomenon, Mr. *Schlemmer* at Lehrstuhl und Labor für hydraulische Maschinen und Anlagen der TU München, made such a proposal about 1972, but in vain since the author, heading the lab did not believe in it. Afterwards the author learned also from other investigators, Mr. *Grein* from Sulzer Escher Wyss, and Mr. *Alestig* from KaMeWa, that such a remedy would help in the case of emergency (by the way the adjustable hub was never made) [8.95].

II. Guide ribs at draft tube wall: Here the ribs may have the same effect. But they are not so effective, since they are now more distant from the hub region as the origin of the

vortex. Moreover any guide rib or baffle wherever it may be stalls and is subjected to wear, tear and vibration and may be washed away in the course of time [8.95].

III. Guide tube in the interior of the draft tube: This is a remedy often practiced in cases where the draft tube surge has been later detected as being the cause of the trouble. Here the vortex core is more or less caught in the interior of a tube coaxial to the draft tube or its bend [9.138]. The appealing aspect of this device is its quietening effect. But nevertheless the device itself and its carrying radial ribs attached to the draft tube wall, are the cause of additional loss, wear, tear and vibrations and the whole again may be washed away in the course of time.

IV. Air injection: This can be effected by snifting valves connecting the vortex core (provided they found it) with the atmosphere. But it can be done also by pressurized air (consumption 1% of rated flow measured at normal m³/s) to different stations. They may be before the runner, on the wall of the throat ring, at the hub (through the hollow shaft) and in the centre of draft tube inlet [9.138; 9.139].

In the latter case the air injection may be through a perforated pin carried by a tripod on the draft tube wall or through such a pin, penetrating the bend of the draft tube. The latter results in a rather stiff design. All these devices may suffer from wear, tear and vibration. Air injection along the runner vane face may occasionally reduce somewhat the drag and hence increase the efficiency. A possible efficiency drop by such devices increases with the specific speed of the turbine, whereas the wear decreases.

V. The real remedy: A properly planned plant, especially in developing countries should have a first set dimensioned as to meet the first power demand by operating around its bep. If a set is forced to work far away from its bep during longer periods then a turbine with adjustable runner vane (Kaplan T, Deriaz T) should be preferred, if the head range allows this. They alone facilitate a whirl-free operation past the runner at any load and hence abolish the main source of pressure surge in the draft tube.

9.9. Laser Doppler Anemometry for *Reynold* stress measurements
by *E. Hartner*

9.9.1. Introduction

From today's point of view, Laser Doppler Anemometry (LDA) surely is the most modern and as we think best way of measuring velocities in turbulent flows. Especially in the vicinity of walls, LDA-technique is superior to all other anemometers, because no probe is placed in the flow passage. The only disadvantages of LDA's are the rather high price and the complicated handling.

At the Lehrstuhl für hydraulische Maschinen und Anlagen of the Technical University Munich, LDA's have been used in flow measurement for ten years (1983). Before describing assignments, operational modes, signal processing units, let us have a short view of the physical principles of Laser Doppler Anemometry. [8.136], [9.66].

As expressed by its name, the basic principle of LDA measurement is the optical *Doppler*-effect [9.140]. Although it is not precise in all cases, the basic theory is more easily described by the so-called interference model. Two focussed laser beams produce in the

398

crossing-section a stationary fringe pattern. The distance Δx of the fringes is given by the relation:

$$\Delta x = \frac{\lambda_L}{2 \sin \Theta/2},$$

where λ_L = wavelength of laser beam
Θ = cross-angle between the two beams.
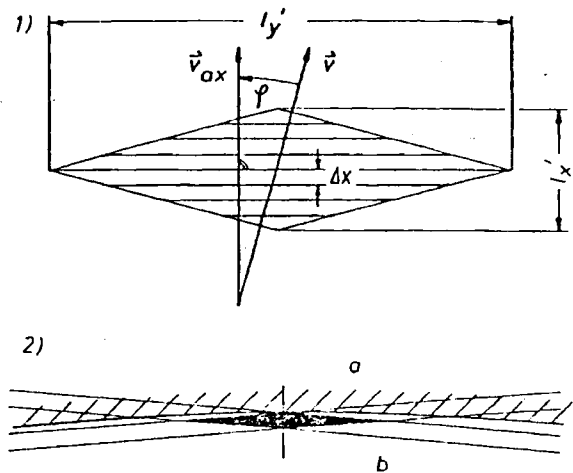
Fig. 9.9.1. Illustrating the measuring principles in Laser ancmometry. 1) Interference model with stationary fringe pattern, velocity component v_{ax} measured by the Laser, major axis l'_y, minor axis l'_x of the probe. 2) The probe's volume close to the wall, a glass wall. b liquid with the same refractive index as glass.

Nearly every kind of flow, carries microscopically small particles with it. These scattering particles, cause a portion of scattered light, passing through the probe volume (= cross-section of the laser beams). If the flow does not carry enough scattering particles, one must inject synthetic ones. The size of scattering particles has to be smaller than $\Delta x/2$. The frequency Δv of the scattered light is directly proportional to the particle-velocity, according to the equation:

$$\Delta v = \frac{1}{\Delta x} \ |v_{ax}|.$$

In a way, we do not measure flow velocity, but particle velocity. But if the scattering particles satisfy certain conditions, they represent the flow velocity, because they are carried by the flow nearly without inertia. For more information about this see: *Durst, Melling, Whitelaw* [9.140].

Difficulties in applying LDA-technique often appear by diffraction of light beams at optical contact surfaces, complicating the determination of the probe volume. Redress can be made by tuning the refractive index.

In doing so, a fluid is used, having at a certain temperature the same refractive index as the observation window of the test section. At our laboratory decisive successes were made with this technique by measuring *Reynolds* stresses in an unsteady turbulent pipe flow. One of the main advantages by tuning the refractive index is beside the simple determination of the probe volume's coordinates, that we are able to approach to the wall with the narrow edge of the probe volume. Probe volumes usually are ten times larger along the major axis than along the minor axis. This means that we may approach the wall with the narrow edge ten times closer without touching the wall (Fig. 9.9.1.2). Probe volumes hitting the wall, are a critical point in LDA measurement, as they produce "wall signals", caused by particles adhering to the wall.

Reference beam system for 1-dimensional measurement.

Double reference beam system (2-dim. measurement).

Forward and back scattering fringe system for 1, 2, and 3 velocity components.

Some assignments

Measurement of flow velocities in all kind of transparent media at different temperatures.

Measurements in the vicinity of walls without any disturbance of the flow.

Using frequency shifting, forward and backward turbulent velocities of high frequency are discriminated between.

Signal processing

Frequency tracking processors.

Counting processors.

Transient recorders.

9.9.2. Example of a flow measurement, carried out by means of a two dimensional LDA with tracking processors

In the lab of Lehrstuhl für hydraulische Maschinen und Anlagen of TUM, Munich in a periodically unsteady, fully developed turbulent pipe flow, the turbulent kinetic energy $\overline{q^2}/2$ and the *Reynolds* stress $-\varrho \overline{u'v'}$ were measured. Because all velocities and even the mean ones were time-dependent, an electronic data handling system was indispensable. A period of this flow may look as shown in Fig. 9.9.2. The ensemble mean values of the velocities were calculated within a small time-space Δt, in which the flow was considered to be steady. The flow period T was divided into up to 100 time-spaces according to Fig. 9.9.2. In each mean values and *Reynolds* stresses were computed and stored. This was done by repeating N times the same mean flow condition. The pulsation period also was measured and controlled by the computer. Fig. 9.9.3 is a scheme of the electronic equipment, used for the measurements. The oncoming analogue data from the tracking processors were digitalized by a fast 12-bit AD-unit and transmitted to the computer, doing the calculations and storings of the mean values for every time-space. So in two series of measurements the radial and temporal distributions of U, u', v', w' and thereby the
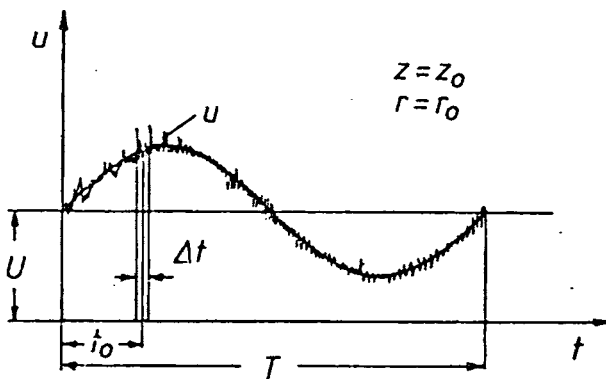
Fig. 9.9.2. Graph of an axisymmetric pulsating flow in a straight circular pipe, showing the velocity u in the direction of pipe axis z versus time elapsed t, a certain cross section given by z_0 and at a radius r_0. Δt time increment at the instant t_0. T period. After *Hartner*.
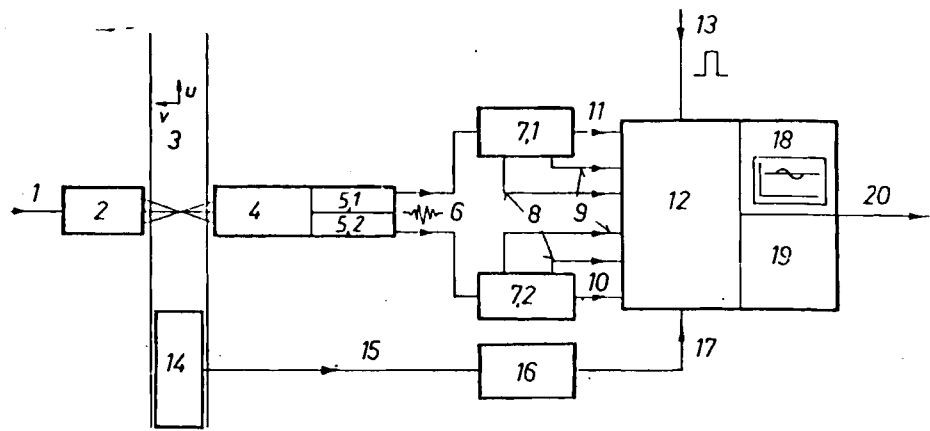
Fig. 9.9.3. Scheme of electronic equipment used for measurement and data acquisition. 1 Laser-beam, 2 optical head, 3 measuring section (pipe), measurement of the instantaneous velocity components in the 3 coordinate directions u, v, w. 4 detecting unit; 5.1 photo multiplier for $+ VV$, u; 5.2 ditto for $+ VV$, v, w; 6 Doppler signal; 7.1 Doppler signal processor type Brown Boveri and Cie for w; 7.2 ditto for v and w; 8 loop closed signal; 9 signal noise ratio ok; 10 v, w; 11 u; 12 computer PSI 80 type Kontron, analog digital conversion of U, V, W, ΔP, T, $\sqrt{u'^2}$, $\sqrt{v'^2}$, $\sqrt{w'^2}$, $\overline{u'v'}$, $\overline{u'w'}$, $\overline{v'w'}$; 13 trigger signal; 14 inductive pressure transducers to measure the instantaneous pressures p_1 and p_2 simultaneously at stations 1 and 2 a distance apart Δz in the streamwise direction; 15 p_1, p_2; 16 carrier frequency amplifier KWSI 3S-5 type Hottinger Baldwin; 17 pressure gradient $\Delta P/\Delta z$; 18 terminal; 19 data logger, discs; 20 to subsequent treatment in the computer centre. After *Hartner* [9.133].

dynamic pressure $q^2/2$ and the most interesting value $\overline{u'v'}$ were obtained. Logical signals from the *Doppler* processor told the computer whether the oncoming velocity signals were good or not. These signals were "SNR-ok" (= signal noise ratio ok) and "loop closed" (= signal processor has found a *Doppler* signal). In this way only good *Doppler* signals were taken by the computer.

An example of the measurement results is given below in the Fig. 9.9.4. At a constant point of time, radial distributions of u'^*, v'^*, w'^*, $q^2/2$, and $\overline{u'v'}$ were plotted.

Nomenclature

N	= counting variable
T	= period of pulsation
Δt	= time-space
U, V	= mean velocity component in the direction of the pipe axis, normal to it
u', v', w'	= fluctuating velocity components in the z, r, φ-directions
u'^*, v'^*, w'^*	= root-mean-square values of u', v', w'
$\overline{u'v'}$	= Reynolds-shear-stress per unit mass
Δx	= fringe distance
$\tilde{u}_m$	= measured velocity component by LDA
z, r, φ	= cylindrical coordinates in axial, radial and azimuthal direction, respectively
λ	= wavelength of light
θ	= cross-angle between illumination beams
Δ_ν	= Doppler frequency
ρ	= density
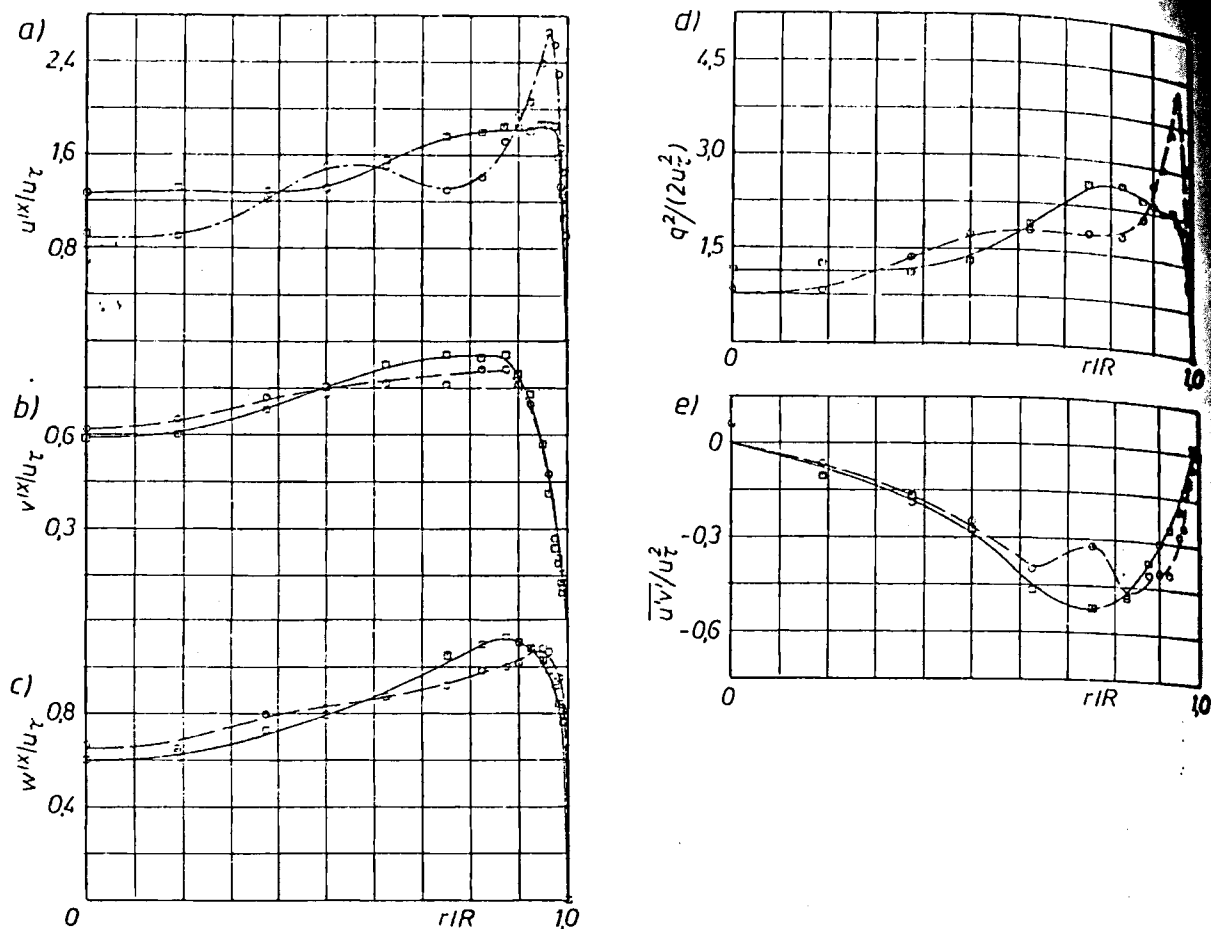
Fig. 9.9.4. Examples for measurement of a pulsating pipe flow at a certain cross section versus dimensionless pipe radius: Reynolds number of the time-averaged flow $Re = 20,1 \cdot 10^3$; period $T = 1$ s; ratio of stroke of pulsation generator to pipe radius $OS = 2,03$; ratio of amplitude of the sinusoidally oscillating part of the flow to the time-averaged flow rate $P = Q_1/Q = 0,197$; Womersley Parameter $\Omega = R\sqrt{\omega/\nu} = 53,5$. The root-mean-square values of the fluctuating velocity components u'^x, v'^x, w'^x are made dimensionless by dividing by the wall shear velocity u_τ; the kinetic energy of the turbulent motion is made dimensionless by dividing by the squared wall shear velocity u_τ^2; phase relationship: full line: 0,075 T; hatched line; 0,563 T. a) Root-mean-sqaure values u'^x of velocity fluctuation in the pipe axis direction; b) ditto v'^x in the radial direction; c) ditto w'^x in the tangential direction; d) kinetic energy of turbulent motion; e) correlation $\overline{u'v'}$ corresponding to apparent (Reynolds) shear stress on a coaxial cylinder and in direction of the pipe axis. After *Hartner* [8.136].

Concluding remarks on measuring techniques:

The conversion of any measurement into a signal as a computer input by analogue or digital technique and its computerized evaluation for the desired output as described above, may be considered to be the present trend in any up to-date experimental techniques. The computerized processing of measuring signals is of special value for dynamic measurements of unsteady phenomena. Quickly repeated measurements at a certain measuring point in connection with the high processing speed of a computer also yields the time-averaged mean value of any measurement and its time-averaged errors during a certain observation period. Hence human errors in observation will be excluded more and more.

10. The turbomachine, its design and construction

10.1. Introduction

Many types of hydro turbo machines exist. This is a consequence of their different duties such as

a) turbining alone,
b) pumping and turbining in a pump-turbine,
c) direct and reversed turbining and pumping in tidal power plants, and
d) pumping in a pumped storage plant with a ternary (tandem) set.

But it is also a consequence of the varying water requirements and topography, the hydro turbo machine has to be adapted to.

Harnessing of low head requires axial turbines (AT) with high percentage reaction and susceptibility to cavitation. Their appearance is characterized on the one hand by the classical design of V. Kaplan, namely the Kaplan turbine (KT) with vertical shaft and a spiral or semispiral casing as the generator of angular momentum required, an elbow draft tube and a runner usually with adjustable vanes. The version with full spiral casing overlaps the range dominated earlier by the Francis turbine (FT).

In the lower head range the AT has the variant of the tubular turbine (TT). This is characterized by a straighter water duct than the original KT. Here the generation of whirl is left to the stay and gate vanes. The variants of the TT are manifold. With the generator in a submersible bulb, they appear as bulb turbines (BT).

They have also the generator outside the water duct directly coupled or connected by a bevel gear. Then they may have the straightest possible water duct in the form of a rim generator type (RGT) or Straflo type (ST).

In the lowest head range, the TT may enable the harnessing of the kinetic energy in river rapids. To date, the TT, especially in its straflo version, seems to be the effective tool for harnessing tidal power. But there, in the usual case of a one basin plant, the function of a reversible turbine and pump requires special consideration and compromises of the blading, when the runner vane position is nearly retained.

The conical and axial distributor of a TT is a rather poor generator of whirl and needs careful consideration of the flow in the gates both with respect to geometry and loss.

The design of a KT has to start from the runner tip diameter either with respect to internal loss or suction requirements. Emphasis has to be given also to the proper draft tube design, since the kinetic energy at runner exit may amount to 80% at overgate. Therefore TTs, with two bends in the draft tube to allow the shaft passing through the latter, may have additional losses.

The layout of a turbine has to account for the stresses in the rotor vanes, the hub and the

shroud under the emergency case of runaway. The shaft design should shift the lowest critical speed above this threshold.

The design of accessories like bearings, shaft seals etc., should follow the direction of stiffening the shaft with respect to lift critical speed. Moreover these elements must have easy accessibility for assembly and dismantling.

The circulation of the lubricant should be effected by the shaft itself. Head cover, gates, stay vanes and their rings and the spiral casing have to be designed for low values of loss, deformation, and admissible stress even under emergency loads, like water hammer, and runaway, and for a limited radial extension, particularly of the outmost parts like the spiral casing, stay vane and gate ring.

In vertical sets, the accessibility of the lower parts such as the runner and the bottom cover of gates should be facilitated by auxiliary cranes, inspection doors in the draft tube or intermediate shaft pieces to be removed for dismantling of the runner.

Harnessing higher heads requires Francis turbines (FT) with medium percentage reaction. For highest heads, smallest discharges, and mean heads, impulse turbines of the Pelton type (PT) without any reaction are applied. Wide zones of overlapping exist between FT and KT on the one hand and FT and PT on the other.

The cross flow turbine, a cross-breed between reaction and action turbines, but more an action turbine, originally designed by Michell and Banki, and now built by Ossberger, appears mostly in micro power plants. It may be interposed between FT and KT especially in cases of highly varying discharge, head, and tail water level.

The flatness of the efficiency vs flow and the bep efficiency characteristics of a FT depend mainly on the head and hence on the given specific speed. This figure determines decisively the geometry in the sectional view of a FT.

Transportation, fabrication on site, submergence of the set, mode of working and overall economy, sand erosion and simplicity of dismantling, and maintenance may further decide the final type of a turbine.

Flow field and strength of a FT runner are related to geometry of the runner vane and shrouds. The limitation of output for a given runner diameter results mainly from its relative span of vanes, and the permissible stress of runner vane material under emergency conditions such as runaway.

The design of a pump-turbine has to start from that of a mere pump. It is based on suction requirements, optimum efficiency, different hill diagrams during pumping and turbining and speed change.

The broad field of hydroturbomachinery is reflected in a long reference list. [10.1 to 10.5], [1.50], [6.8], [6.45], [8.132] give a survey on machinery. Kaplan turbines are treated in general in [10.6], special constructions of them, with emphasis on high-head design, in [10.7 to 10.10], their layout, based on modern tendencies in [10.11], special design problems, like geometry of the runner chamber, in [10.12], the torque on the runner vane spindle in [10.13], predicted and calculated flow in [10.14], its losses, generally in [10.15], and on the runner blades in [10.16; 10.17]. The tubular turbine, as the other important variant of the axial turbine, is presented in a survey of bulb turbines [10.18], in general treatises [10.19 to 10.21] by studies of individual constructions [10.22; 10.23], with its problems at the intake [10.24], with experiences on its operation [10.25; 10.26], by a comparison of predicted and measured stresses [10.27].

A special diagonal turbine emerged from the bulb turbine [10.28], then the Straflo design [10.29; 10.30], also used to exploit tidal power [10.31; 10.32].

404

Modern trends in Francis turbine design are given in [10.33], somewhat older in [10.34], the constructional limits of Francis turbines in [10.35], its computer-aided design in some actual constructions in [10.37 to 10.41], its high head designs in [10.42 to 10.44], its relative flow in [10.45 to 10.47], its draft tube surges in [10.48 to 10.50], the welding of one of its largest runners in [10.51], the stresses in runners in [10.52]. Operating experience on Francis turbines and problems due to the design of large units are reported in [10.53 to 10.58], the features of its single gate servomotors in [10.59], its start up in [10.60], and the design of blading in [10.61].

Modern trends of Pelton turbine design are found in [10.62], the alternative of Francis or Pelton turbine is discussed in [10.63], details of actual Pelton turbines are found in [10.64; 10.65], the stresses in their important parts in [10.66; 10.67], and the questionable potential reduction of their runaway speed ratio in [10.68].

Storage pumps of ternary sets (tandem sets) for pumped storage are treated in [10.69 to 10.72], problems of pumped storage plants in [10.73]. The pump-turbine in general is described in [10.7], [10.75 to 10.79], modern design trends in [10.80; 10.81], some actual constructions in [10.82 to 10.89], operating experiences in [10.90 to 10.92], its optimization, with respect to loss and cavitation features, in [10.93].

The following other topics, related to pump-turbines, are treated: limit of head per stage [10.94], start up into pumping mode [10.95], dynamic load [10.96], transients [10.97], axial thrust [10.98], runaway [10.99], part load operation [10.100], the stresses on its components [10.101], a possible hysteresis of its characteristics [10.102], gate vibrations [10.103 to 10.105], gate spindle torque under misaligned gates [10.106], start up through a booster Francis turbine [10.107], the stochastic radial forces on its rotor [10.108 to 10.110].

A novelty is the gate-regulated two-stage pump turbine [10.111]. Unregulated multistage pump turbines [10.112 to 10.114] and the Isogyre design [10.115] are sporadically used.

With rising size and speed of the set, its critical shaft vibration, its response to radial forces and the added mass due to flexural vibrations become interesting [10.117 to 10.121], also the behaviour of elastic adjustable gates [10.122].

Losses in the spiral casing [10.123], its stress calculation [10.124; 10.125], reduced to a conical shell [10.126], its useful life under cycles of pumped storage [10.127], its design with a stay ring of parallel plates [10.128], the distribution of the dynamic pressure on it [10.129] are treated; further the fatigue problems of stay vanes [10.130] and their dynamic behaviour [10.131].

The thrust bearing of the tilted pad type [10.132 to 10.134], and of the newly introduced hydrostatic type [10.135] were described, also self lubrication of trunnions without any lubricant [10.136], shaft seals [10.137], the condenser operation of pumped storage sets [10.138], and computer aided design [10.36], [10.122], [10.139], supported by the finite element method [10.140; 10.141]. The standardization of small turbines makes progress [10.142]. Special features of small turbine types have been investigated, e.g. the influence of the jet and wheel size on the performance of inclined jet impulse turbines [10.143].

10.2. Project and construction of axial turbines

10.2.1. General survey of types

Axial turbines exist actually in two variants. One usually with a vertical shaft, radial distributor, adjustable runner blades with fulcrum in the hub is an invention of V. Kaplan and hence called KT. This is also valid for the KT with fixed runner blades the so-called propeller turbine.

The second axial turbine type used, has a more or less horizontal shaft, an axial or conical distributor as the generator of the whirl component c_u before the runner, and an axial

405

runner of the KT type with usually adjustable runner vanes. It is defined here as a tubular turbine (TT). The axial turbine with horizontal shaft and its generator shrunk on its shroud, according to an US patent of *Harza* from 1919, realized at first by *A. Fischer* and Escher Wyss, belongs also to this type of KT. It will be considered more in detail.

Adjustability of runner vanes originally was rare in this design. With a hydrostatic water-lubricated, self-adjusting radial and axial bearing for the axial thrust arranged on the shroud, to facilitate runner vane adjustment, this type now has been revived under the name of Straflo turbine. This was a special development of the Swiss firm Escher Wyss, a joint venture of the Sulzer Concern, hence named Sulzer Escher Wyss.

10.2.2. The true Kaplan turbine

This has usually (Figs. 10.2.1 to 7) a vertical axis and a generator outside the water duct. The flow admission is usually by a radial gate preceded by a spiral casing when the turbine has a larger size. This tends to be a semi-spiral casing (Fig. 3.4.12; 14) with a trapezoidal cross section of concrete in the lower head range. For higher heads, the full spiral casing is used of circular cross section, either lined with steel, or welded from steel (Figs. 3.4.15 and 10.2.8). In conjunction with radial gates, the generation of a constant angular momentum before the runner is achieved easily.

In a few cases, small high head KTs have also a horizontal shaft and a metal spiral casing (Fig. 3.4.17). In the usual design with a vertical axis, the machine is equipped with an elbow draft tube. Its bend increases the diffuser loss which becomes important for the low head KT with its relative high kinetic energy (up to 80%) at the runner exit. Therefore this element (Figs. 3.4.12, 13, 14) has to be carefully dimensioned.

The large cavitation coefficient σ of a KT may require submergence even at modest heads. Thereby the head of KTs is limited [10.7] up to 70 (80) m.

Because of its high degree of reaction up to 90% and the impossibility of an axial double flow design, the KT has a high axial thrust. This may lead with high heads to a diameter of thrust bearing even larger than that of the runner. Hence the axial thrust also limits the head of KTs.

The width of a power house with vertical sets results from the lateral distance of 3 or 4 runner diameters for semi or full spiral casings (Fig. 3.4.45).

10.2.3. The tubular turbine (TT)

The previously mentioned features of performance of design also occur in TT with the difference that the straight draft tube used here has a low diffuser loss and requires a smaller excavation. Further the distance between sets can be reduced to 2 runner diameters. Moreover the TT saves the flow deflection between gate and runner (see Fig. 10.2.9).

For its smaller draft tube loss the TT is more susceptible to cavitation than a usual KT. Therefore its head is limited to about 20 m. A weak point of the TT is its nearly horizontal shaft in the case of the bulb turbine (Figs. 10.2.10 to 16).

Here the assembly is complicated by the shaft's bending line in order to retain the small gaps of both the rotors within their stationary part (throat ring, generator stator). In the usual case of a directly coupled alternator and small admission hatch to the bulb through a vertical hollow rib, the assembly and dismantling of the generator through a hatch at the downstream end of the bulb becomes difficult.

406
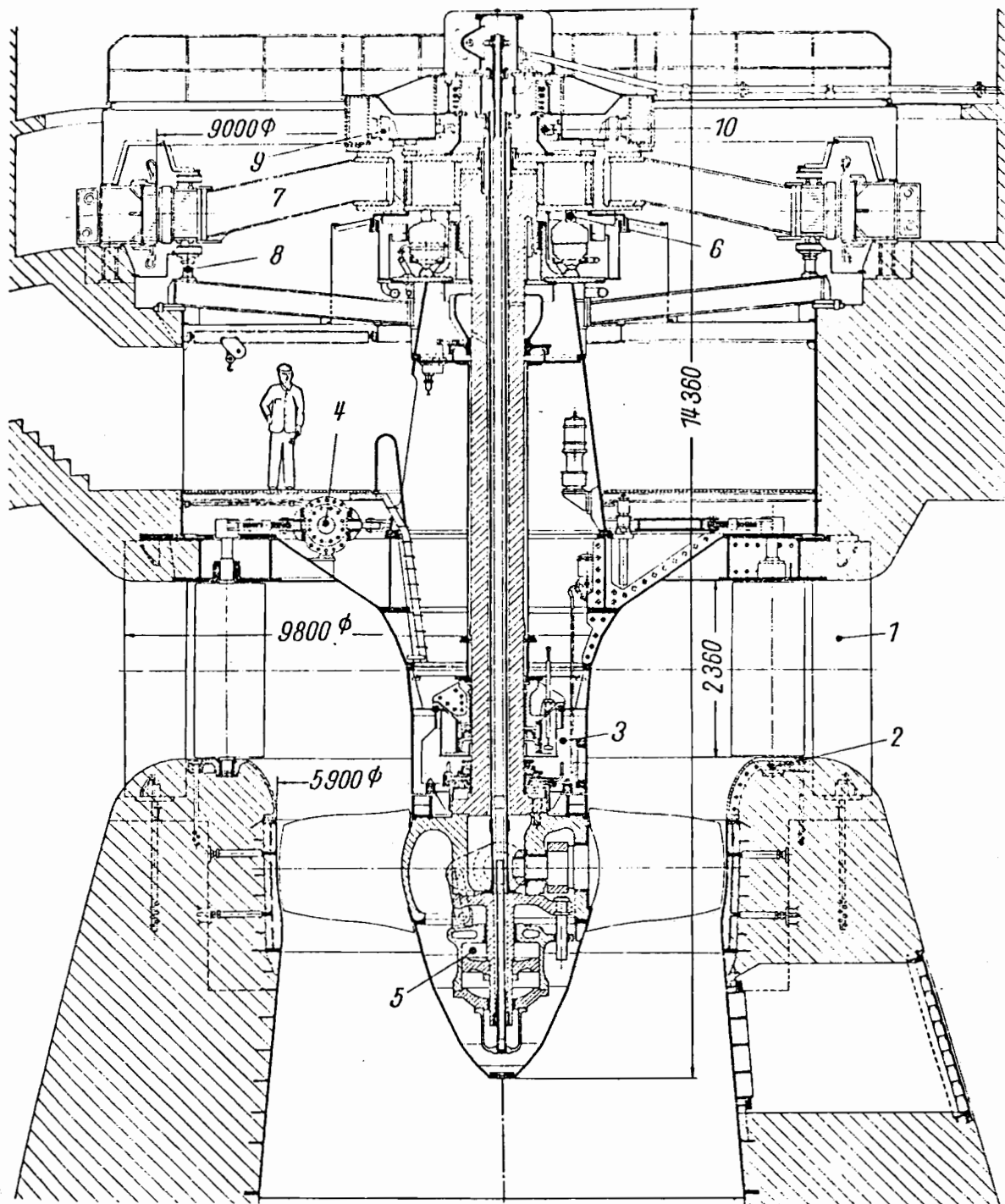
Fig. 10.2.1. Elevation of the KT at Schaffhausen, Rhine, Switzerland (owner: EW Schaffhausen, Switzerland), design Sulzer Escher Wyss $H = 9,3$ m; $n = 71,4$ rpm; $P = 14,5$ MW. Widely welded design, thrust bearing easily accessible after dismantling and lifting the connecting ring between the shaft and the generator rotor. Facilitated by leading off the thrust via a tall truncated cone and head cover into the stay vanes without stressing the concrete of the pit. This principle of shortest flux of force is also implemented by propping 2 pairs of oppositely located gate servomotors (only a couple on the gate operating ring) on the head cover. Only 2 guide bearings thus loads statically determined. Small high pressure runner servomotor underneath the blades shifts the runner's centre of gravity towards that of the adjacent bearing. Servomotor piston bolted on the hub facilitates oil admission from an oilhead above the rotor. Generator rotor of umbrella design, with a centre of gravity in the plane of upper guide bearing. 1 stay vane; 2 guide vane bottom ring elliptically curved (otherwise stall and increased sensitivity to cavitation of the outer part of the runner blade); 3 guide shield with inspection window for the runner shaft seal and "stand still" seal to remove or inspect the shaft seal; 4 gate servomotors; 5 runner servomotor; 6 thrust bearing; 7 alternator rotor; 8 jacking and brake device for the rotating parts; 9 exciter; 10 seal. (Drawing courtesy Sulzer Escher Wyss)
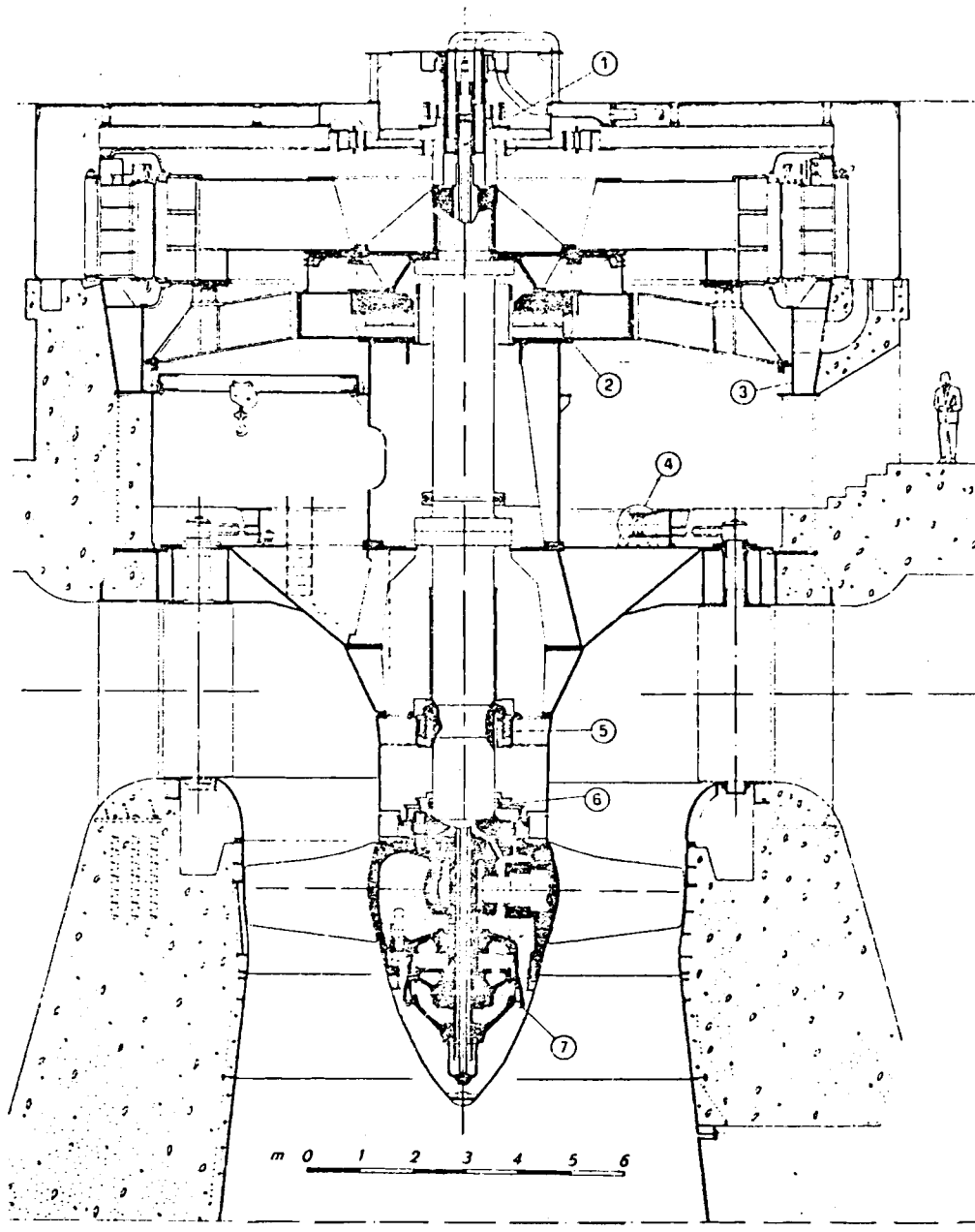
Fig. 10.2.2. Elevation of the KT, at Jupia, Rio Paraná, Brazil (owner Centrais Electricas de São Paulo CESP). 14 KTs built by Sulzer Escher Wyss, Switzerland and Hydroart, Milan, Italy under CIE as main contractor. $H = 24,4$ m; $n = 78,3$ rpm; $P = 103$ MW. To date the largest block of KT power built in the West. Runner: 13/1 Chromium/Nickel stainless steel blades; $D = 8,4$ m; axial thrust 2300 tons. Thrust bearing with balancing hydraulic chamber (Hydroart) well accessible below electric rotor like that in Fig. 10.2.1. 1 oil head, oil admission to the runner servomotor by telescopic tubes; 2 thrust bearing; 3 alternator stator support via stiff armour plate on the stay vanes; 4 pairs of gate ring servomotors on the head cover; 5 bell-shaped permanently lubricated lower guide bearing; 6 shaft seal; 7 runner servomotor with piston screwed on the hub. (Drawing courtesy Hydroart, Milan, Italy)

408
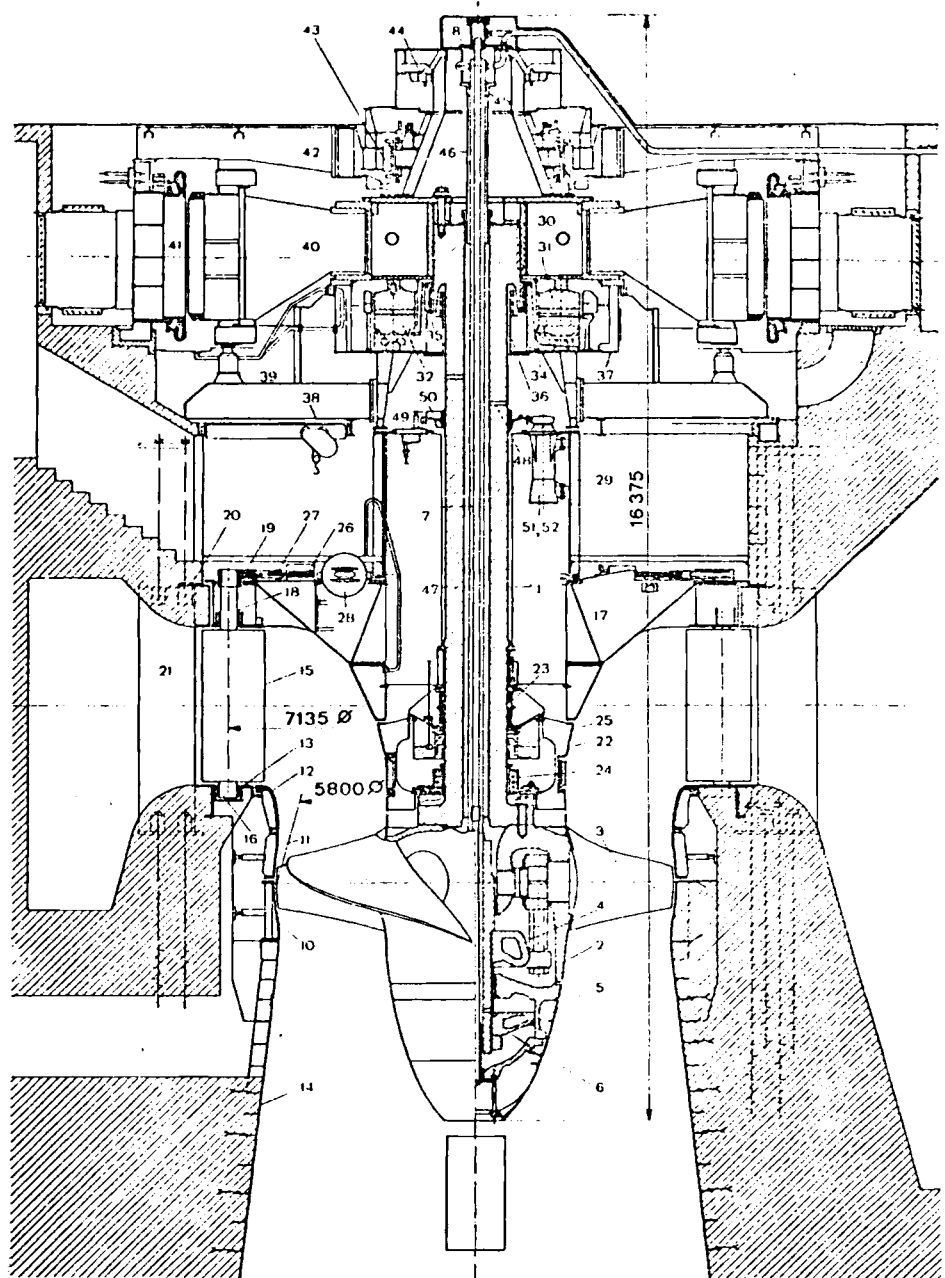
Fig. 10.2.3. Elevation of high head KT Pirttikoski, Finland. 2 sets built by Sulzer Escher Wyss. $H = 27$ m; $n = 115.4$ rpm; $P = 66.3$ MW. Runner $D = 5.8$ m; 6 blades. Good accessibility of the important parts such as the pivot of the gates and thrust bearing. 1 shaft; 2 hub; 3 runner blade; 4 blade drive; 5 servomotor cylinder as part of hub; 6 piston; 7 oil supply by telescopic tubes; 8 oil head and runner blade feed back; 10 lower throat ring; 11 upper throat ring removable to dismantle the runner; 12 insert ring dismantable with 11; 13 bottom gate ring; 14 draft tube steel lining; 15 gates; 17 head cover; 18 bushing of gate stem; 19 guide vane lever; 20 stay vane ring; 21 stay vane with long tie rods to transmit its tension into the concrete; 22 water guide shield with a man hole for the seal; 23 lower guide bearing; 24 shaft seal; 25 leakage pump; 26 gate operating ring; 27 link; 28 4 pairs of gate servomotors; 29 supporting tube; 30 connecting ring between shaft and generator rotor to facilitate easy revision of the thrust bearing; 31 support ring; 32 pads; 34 support of the guide bearing 35; 36 oil pan; 37 thrust bearing case; 38 spider for guide bearing; 39 brake and jacking device for the alternator rotor; 40 alternator rotor; 41 alternator stator; 42 spider of exciter; 43 exciter; 44 pendulum generator; 45 throttle bush; 46 outlet pipe; 47 leak oil chamber; 48 pressure relieving bore; 49 leak oil chamber; 50 emergency shut down pendulum; 51 oil circulation pump for the thrust bearing; 52 ditto for the governor. (Drawing courtesy Sulzer Escher Wyss)
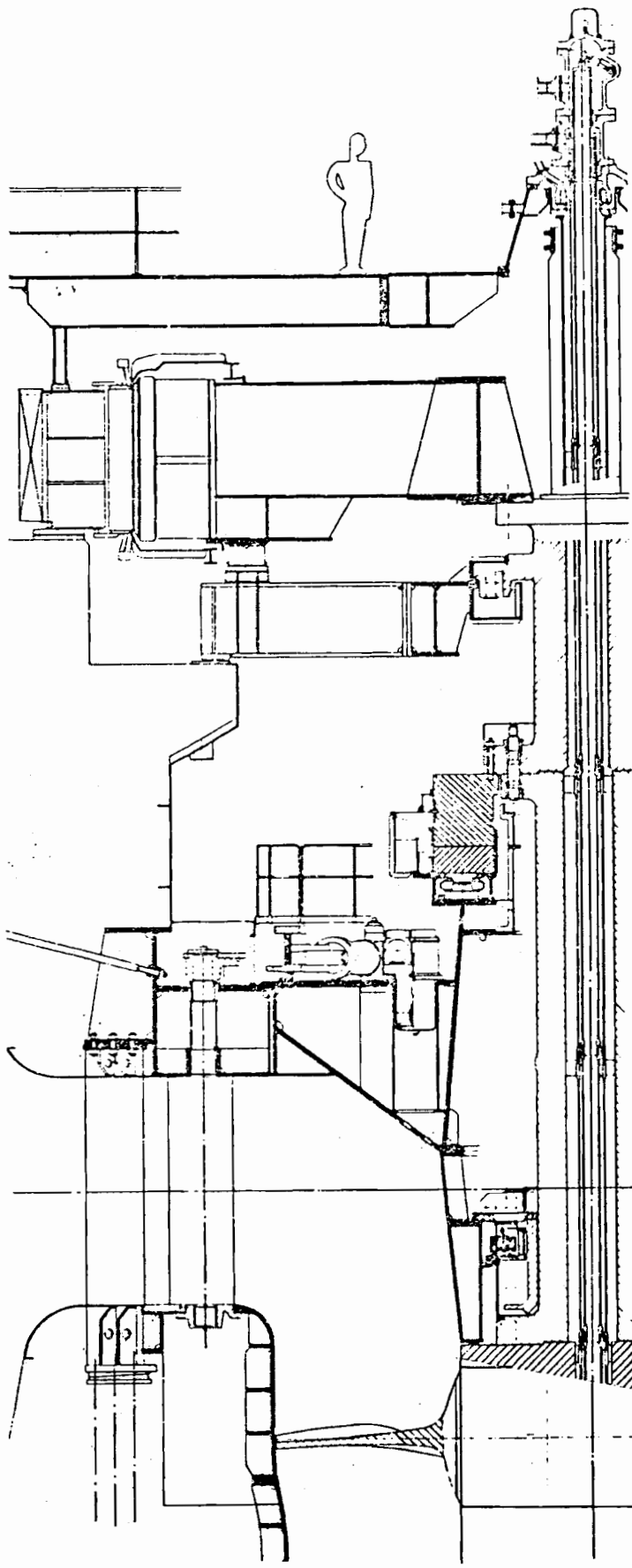
Fig. 10.2.4. Elevation of KT Palmar, Brazil (owner: Mendes Junior) (Design Neyrpic). $H = 32$ m; $n = 88.2$ rpm; $P = 113.4$ MW. Most powerful Western KT. Simplified welded design. Thrust bearing close to the head cover; lower guide bearing close to the runner; single servomotors for gates. (Drawing courtesy Neyrpic, Grenoble, France)
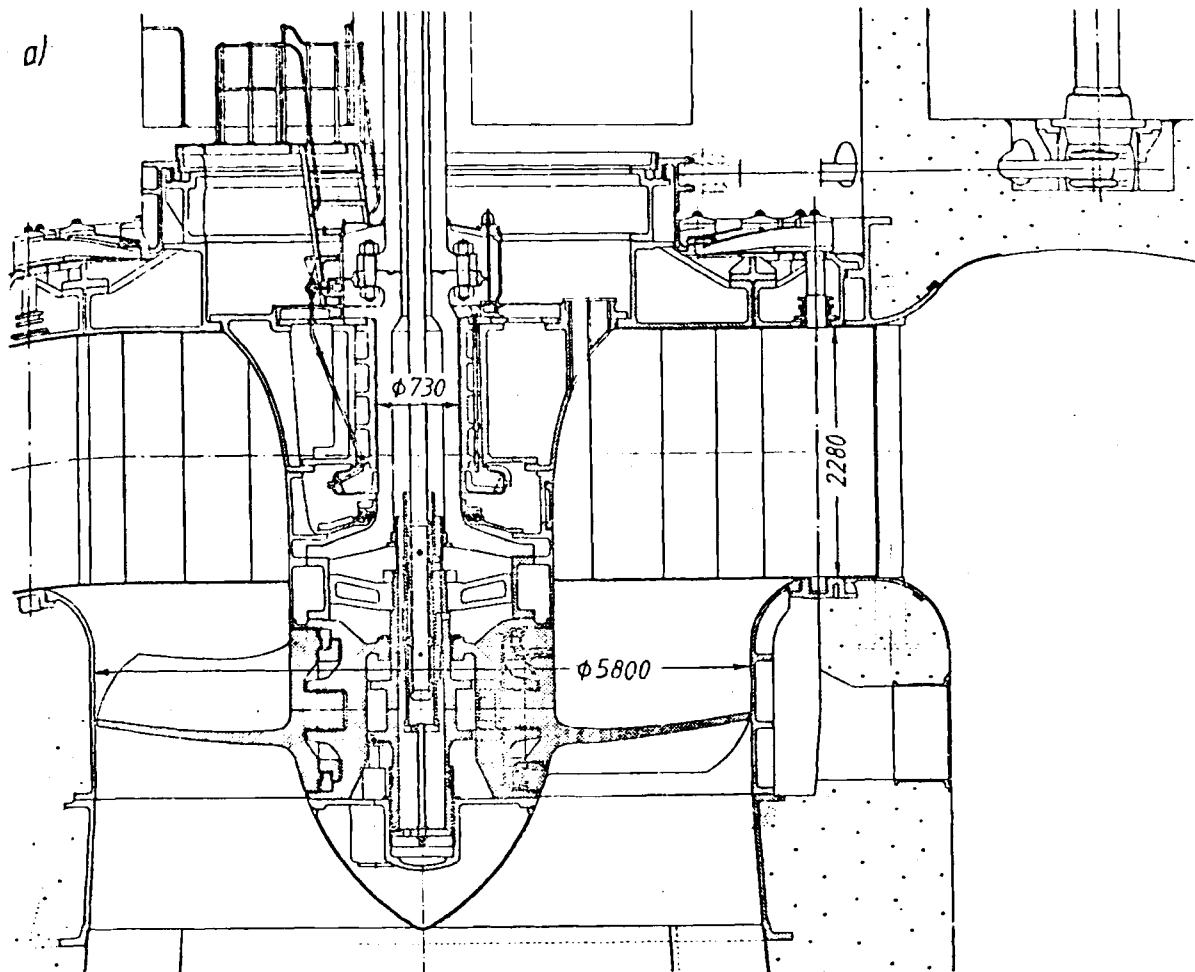
Fig. 10.2.5. a) Sectional drawing of KT Lilla Edet, Göta Älv, Sweden (owner, Swedish state power board), ordered 1922 and built by KaMeWa AB, Kristineham, Sweden, data: $H = 6,5$ m, $n = 66,7$ rpm. $P_m = 14$ MW, runner diameter $D = 5,8$ m. The first Kaplan turbine in the world of large dimensions, designed by *Olov Englesson*, chief engineer of KaMeWa and active there between 1906 and 1953. Contrary to V. Kaplan's patent with a stationary runner servomotor operating the runner blades via a stationary rocking lever with blocks which axially moved a grooved ring around the shaft, the runner servomotor was arranged in the hub. Well informed about previous failures on the European continent, the Swedish engineers paid the greatest attention to the cavitation problem. A special test tunnel was built and put to work in 1924. This was, according to Hansson probably the first cavitation test stand in the world for cavitation research at a turbine manufacturer's shop. Efficiency tests, carried out in 1926 by *H. Dahl*, showed a bep efficiency of 92,5%, an efficiency above 90% between 3,5 and 10,5 MW and above 82,7% between 2,5 and 14,3 MW. Flow admission by a semi-spiral casing of reinforced concrete with a cylinder as core, 12 stay vanes, 24 gates with shear pins against overstressing, runner chamber cast iron, hub of cast steel and of cylindrical shape, 4 blades of cast steel attached by a bronze coated bearing, screwed on the hub body. Inside the bearing ring are crank pins bolted to the blade with a block, sliding in a groove of the cross head underneath the piston. The oil pressure of 20 bar is supplied through a steel pipe in the central bore of the shaft. The control valve is located inside the piston and actuated from the combinator cam on the top of the generator by means of the oil pipe. The lower part of the hub is filled with low pressure oil, which is brought to cirulate through all bearings including the blade pivoting bearings by means of a piston pump and by the movement of the blade mechanism. At the blade flanges there are double acting seals of leather which effectively prevent oil from leaking out and water from entering the hub. The relatively long lower guide bearing is lubricated with self circulating oil. The shaft seal of the labyrinth type. The thrust bearing is placed on a spider above the alternator stator. Its load is carried by 16 segment pads supported on a great number of coil springs. The average oil pressure on the bearing surface corresponding to the maximum axial thrust, is 25 bar. There is an external pump circulating the lubricating oil. The draft tube is of the elbow type with oval sections in the outlet of the bend. It is made of reinforced concrete with a plate lining in its upper conical part. (Drawing courtesy KaMeWa AB, Kristineham, Sweden)
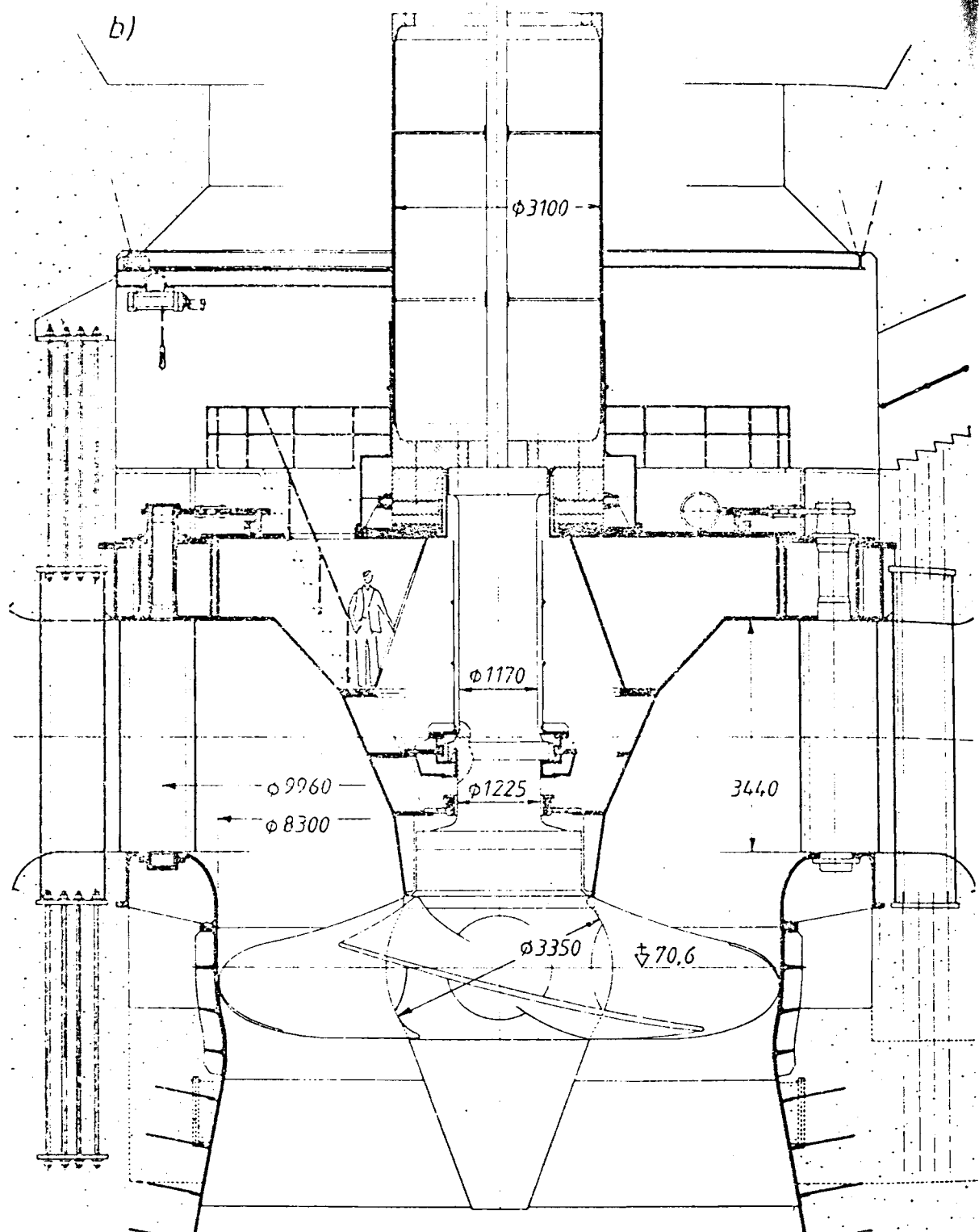
Fig. 10.2.5. b) Sectional drawing of a KT at Solbergfoss, Norway (owner Oslo Lyswerker), commissioned in 1981. Data $H = 20$ m, $n = 78.9$ rpm, $P = 106.7$ MW. Runner $D = 8,3$ m. Hollow thin walled welded shaft with an outermost diameter equal to that of the thrust bearing collar on its lower end. hence a favourable low ratio of weight to torsional stiffness. Thrust bearing directly supported on welded head cover. Adequate curvature of the water deflecting shield creates a spacious head cover with good access to the lower guide bearing. The latter is bell shaped and submersed in the oil pan, facilitating start up with liquid friction. Stay vane tie rods to transmit its tension into the concrete surrounding the spiral casing. Runner servomotor in the hub above the blades with movable piston after Englesson. (Drawing courtesy KaMeWa AB, Kristineham, Sweden)

412

Fig. 10.2.6. Elevation of KT Porto Primavera, Brazil (Design Neyrpic). $H = 18,3$ m; $n = 69.3$ rpm; $P = 103$ MW. Runner servomotor piston screwed on the hub. Runner blade with detachable pivot. (Drawing courtesy Neyrpic, Grenoble, France)
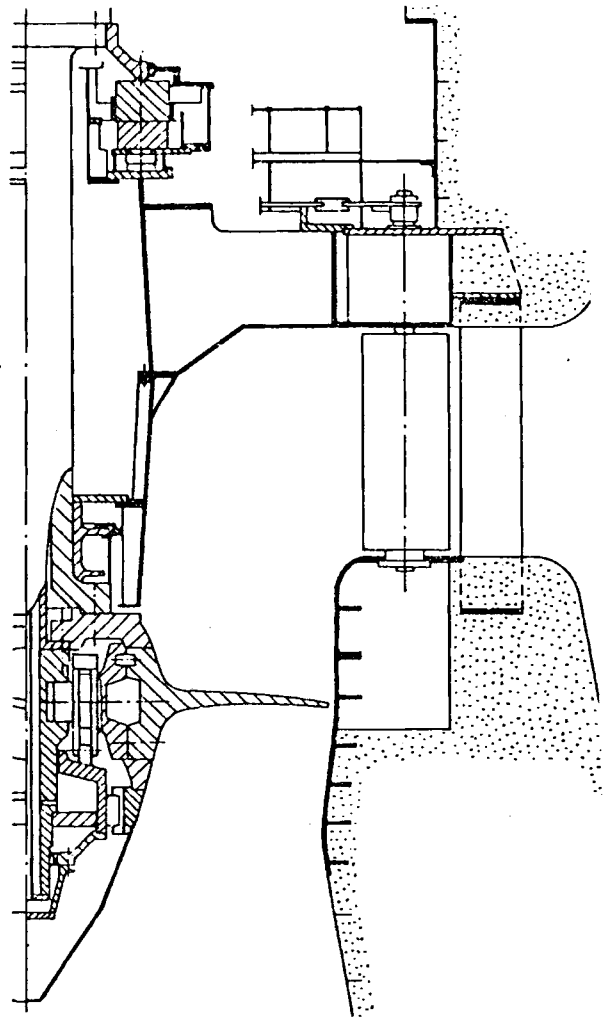
The latter is facilitated by wide vertical and streamlined admission shaft and a highly geared and thus small generator (Figs. 10.2.16 and 13 b) usually equipped with a planetary gear. This design is limited in output because of the gear (about 15 MW).

Because of the flow-conditioned limited external diameter of the bulb in relation to the turbine runner and the increasing diameter of the generator with decreasing head, a direct coupling is preferred at heads above 10 m. In West Germany at present, because of some troubles with planetary gears, there is partially a tendency to restrict use of this gear in favour of direct coupling even in plants with heads below 10 m.

Because of its radially limited bulb, the bulb turbine, with the generator inside the bulb, has a rather small fly-wheel mass. This is contrary to the requirements of stable regulation. In this respect all designs of TTs with the generator outside the water duct are superior. These are, e.g. the bulb turbine with bevel gear, the so-called S-turbine (see below), and above all, the Straflo turbine.

A special feature of adjustable conical or axial gates (usually found in TTs) is the fact that the tight closure usually required, restricts a vane design with twist, needed for the generation of a constant moment of momentum vs radius before the runner.

Since the gate operating ring turns about the shaft and the gates about a stem on a cone, the links between gate lever and gate operating ring require spherical joints.

413
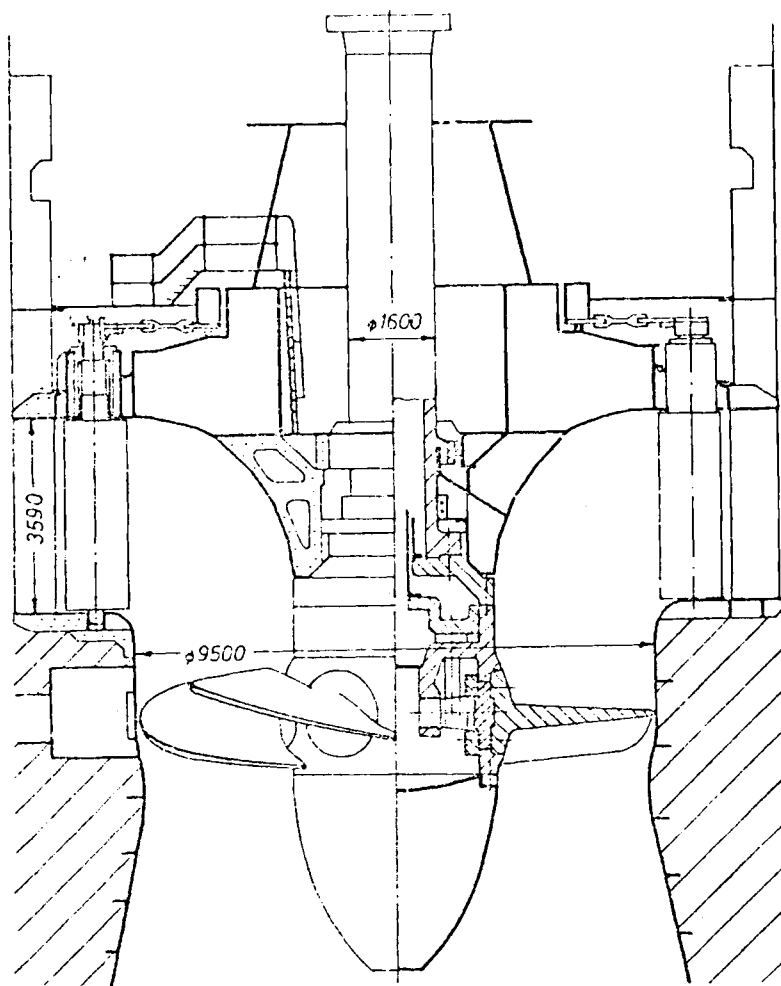
Fig. 10.2.7. Elevation of KT Iron Gate, Danube, Rumania, Yugoslavia (owner 6 sets Rumanian, 6 sets Yugoslavian state power board). (Design Leningrad Metal Works LMZ, USSR) 3 sets built by Resita Works, Rumania. $H_m = 35.46$ m; $n = 180$ rpm; $P_m = 178$ MW. Now largest output for a KT in the world. Rotor: 6 blades; $D = 9.5$ m. Servo-motor housed in the hub above the blade, drive with plungers passing through the cylinder cover. Thrust bearing supported by a truncated cone on the head cover; 2 rows of tilted pads in parallel. Start up with the pads retained by slide dogs and the rotor slightly hydraulically lifted by the generator brake then used as a jack. Smooth operation, but serious cavitation pitting on blade tip after overload. (Drawing courtesy Resita Works, Rumania)

The generator can be outside the main flow, either driven by a bevel gear (Fig. 3.4.30) or by a shaft passing the draft tube double curved (Fig. 3.4.27), (S-turbines).

These variants are limited to small turbines. The type with a shaft passing through the draft tube also facilitates the syphon design (Fig. 3.4.29) favourable for quick and simple shut down of the set by aeration.

Although the S-turbine design has an additional loss due to its extra bend and the disturbance of the flow by the rotating shaft, its generator is more easily accessible. In areas with low rainfall, not requiring a power house, with its protective roof for the generator, it enables the lowest specific investment cost of a plant (see Fig. 3.4.28).

Another variant is the rim generator turbine (Figs. 10.2.17 and 3.4.20). This was designed between 1936 and 1953 in about 70 nearly equal turbines of about $D = 1.8$ m by the firm Escher Wyss (now Sulzer Escher Wyss), after an initiative of A. Fischer, on the West German rivers Iller, Lech, Saalach.

Here the rotor of the alternator shrunk on the rim of the runner is effectively water-cooled and possesses the desired high fly-wheel mass. Fig. 10.2.17 shows the decisive seal on the front faces of the shroud (rim), that reduces the leakage to some l/s (in case of about 2 m runner diameter), but only proof against water with no sand suspension. Zintner [10.25] reported good operating experiences but also initial troubles with these machines during service.

414
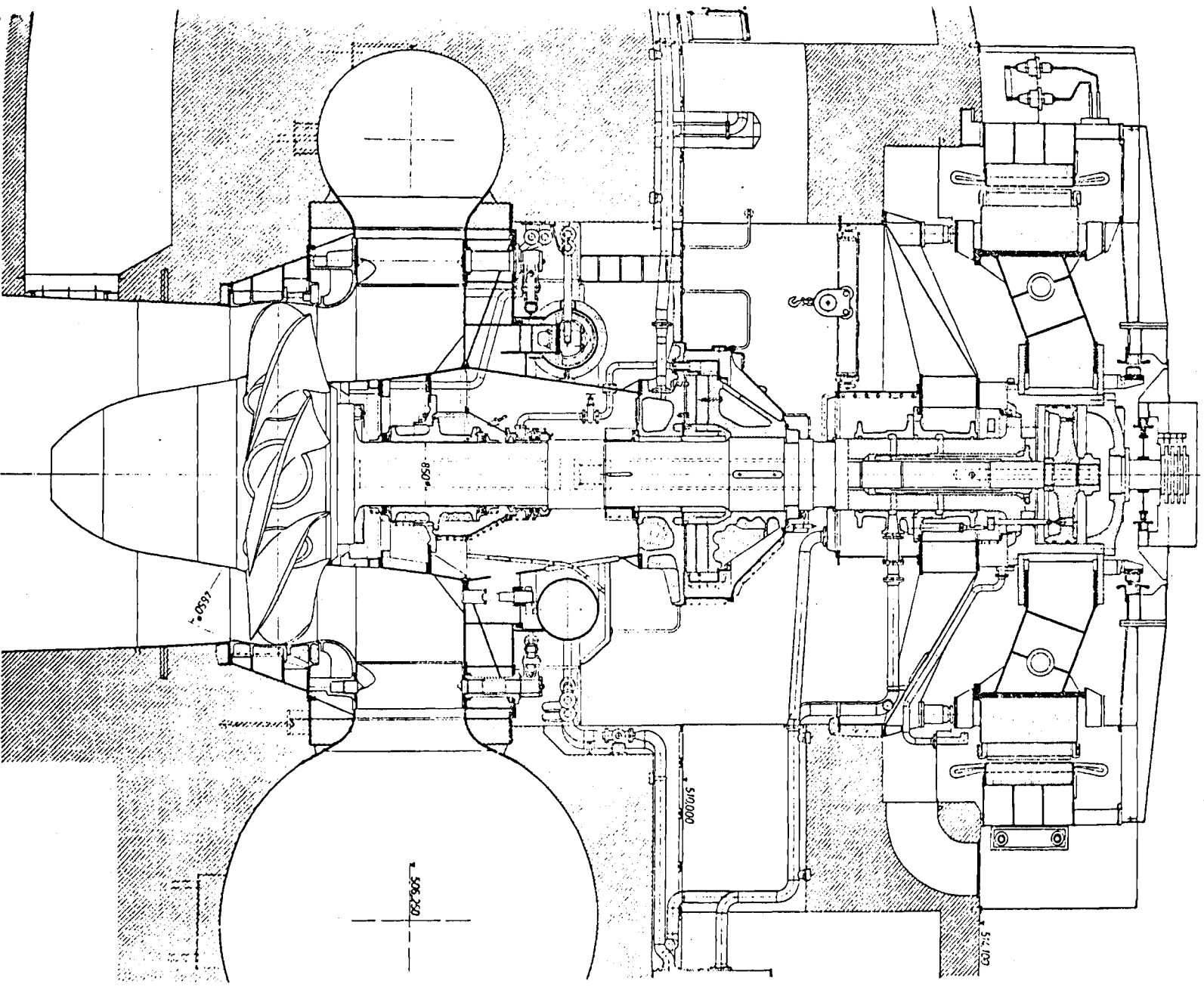
Fig. 10.2.8. Elevation of a high head KT with spiral casing Tres Marias, Rio São Francisco, Brazil. (Voith design) $H = 50$ m; $n = 163.6$ rpm; $P = 4 \cdot 67$ MW. Runner 8 blades; $D = 4.65$ m, servomotor in the hub of the alternator rotor; oil head in the upper guide bearing; double spherical throat ring. Lower guide bearing grease-lubricated. Gate ring operated by 2 pairs of toroidal servomotors on head cover. (Drawing courtesy Voith).

415
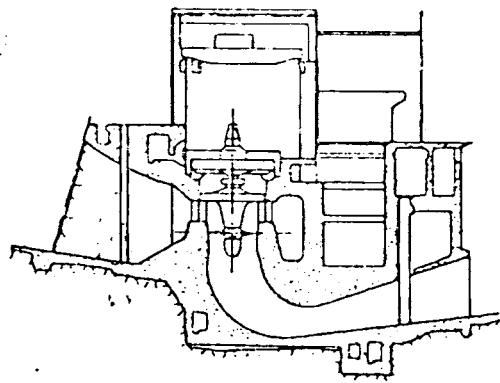
vertical shaft Kaplan turbine
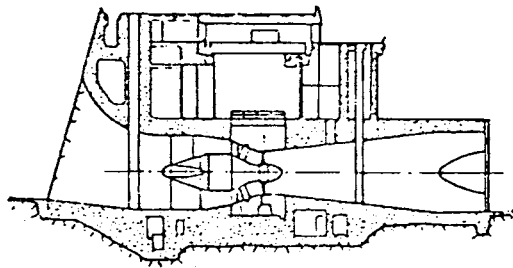
bulb unit

Except for one double regulated turbine shown in Fig. 10.2.17, this design was made with fixed runner vanes. Since the runner blade adjustment needs a radial clearance of the outer pivot of the vane, which must transmit the torque, a quiet running rim needs at least a radial support by a guide bearing. This is found in the Straflo turbine [10.22; 10.29 to 10.32].

In any TT the axial thrust of the runner has to be transmitted from the thrust bearing support in the bulb via stay vanes into the surrounding concrete by long anchors (because the admissible shear stress between iron and concrete is only 2 bar). If an outer radial support of the rim generator is required for runner vane adjustment, it is also possible to transmit the axial thrust originating from the runner vane (at least partially) through the latter to an axial thrust bearing on the rim. Hence the hub and its stay vanes, now disloaded from the torque and possibly partially from the axial thrust may be designed slim and usefully streamlined to the flow.

This was also the main idea of the "Straflo" design of Sulzer Escher Wyss. Here the radial and eventually also the axial bearing of the rim consists of a number of water-lubricated, self-adjusting hydrostatic water heads (supporting sources), uniformly distributed over the circumference. These water heads serve simultaneously also, in connection with labyrinths and rubber hoses, to repulse sand from the working water (if existing). See Figs. 10.2.18 and 19 [10.29 to 10.31].

Fig. 10.2.20 shows the self adjustment of such a supporting water head in the case of any disturbance by tilting. To obtain the same tangential force from all the outer blade trunnions, these are linked to the alternator rotor by nearly tangential oriented plungers. The load on the latter is equalized by interconnecting their oil cylinders, which are attached to the alternator rotor.

416
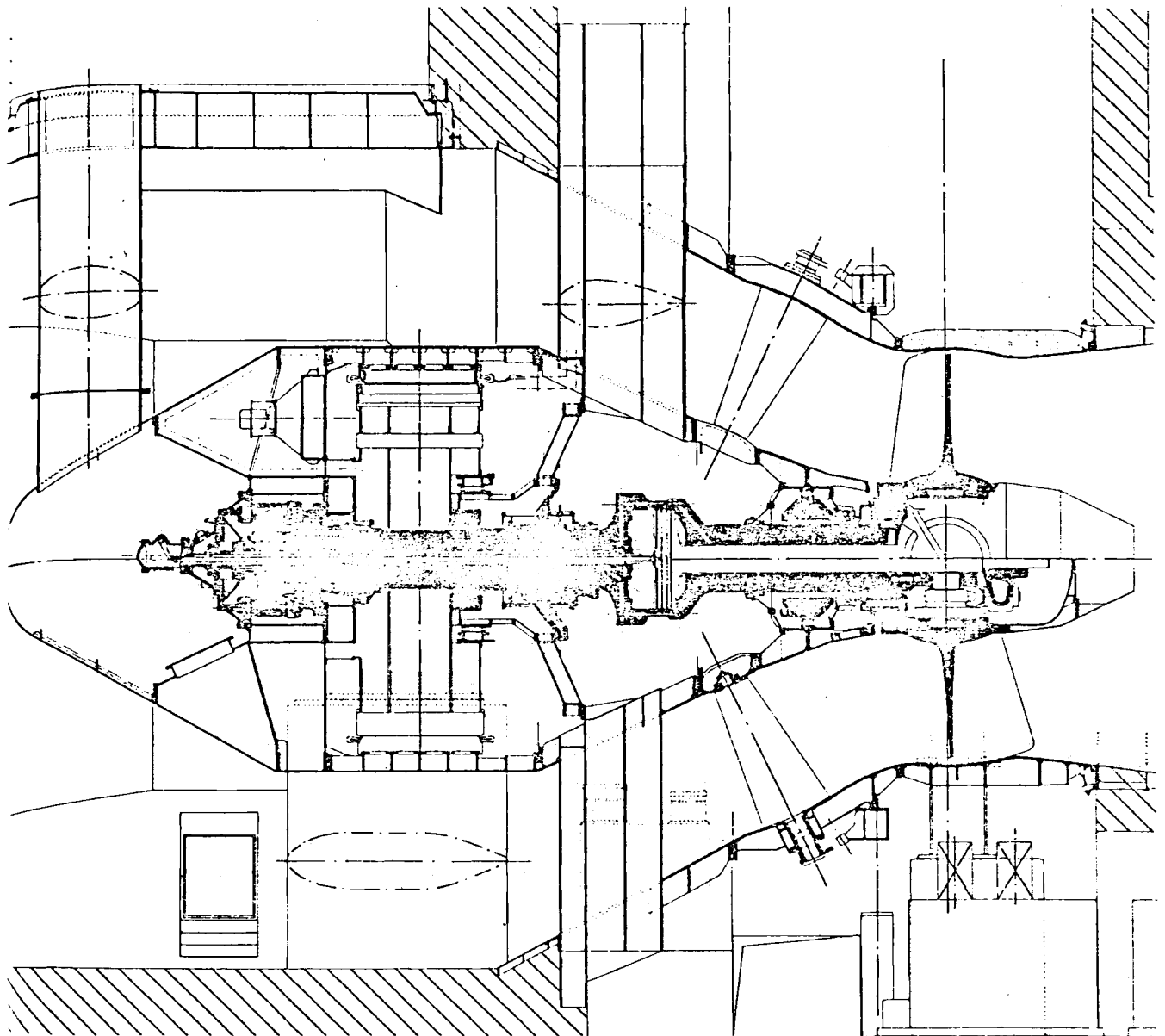
Fig. 10.2.10. Elevation of BT Rock Island, Columbia, Washington, USA (owner public utility no 1 Chelan County Washington). (Neyrpic design). $H_m = 12,1$ m; $n = 85,7$ rpm; $P = 53$ MW. To date the largest bulb turbine with respect to output. 3 guide bearings. Runner $D = 7,4$ m; servomotor in the shaft. (Drawing courtesy Neyrpic).

Spherical articulations at the ends of the connecting rods also facilitate a tangential load compensation when the alternator rotor is not coaxial to the runner.

The space requirements of different types of axial turbines can be seen from Fig. 10.2.21. This shows that at a given runner diameter, the Straflo turbine requires only 70% of the space a bulb turbine needs. Therefore the Straflo turbine design seems to be predestined for the harnessing of tidal power in its largest style.

To prove this, a prototype with 7,6 m runner diameter and $P = 20$ MW maximum output is now installed in the Canadian tidal power plant Annapolis, which has a single pool scheme with single effect (Figs. 10.2.22 and 23) [10.32].

417
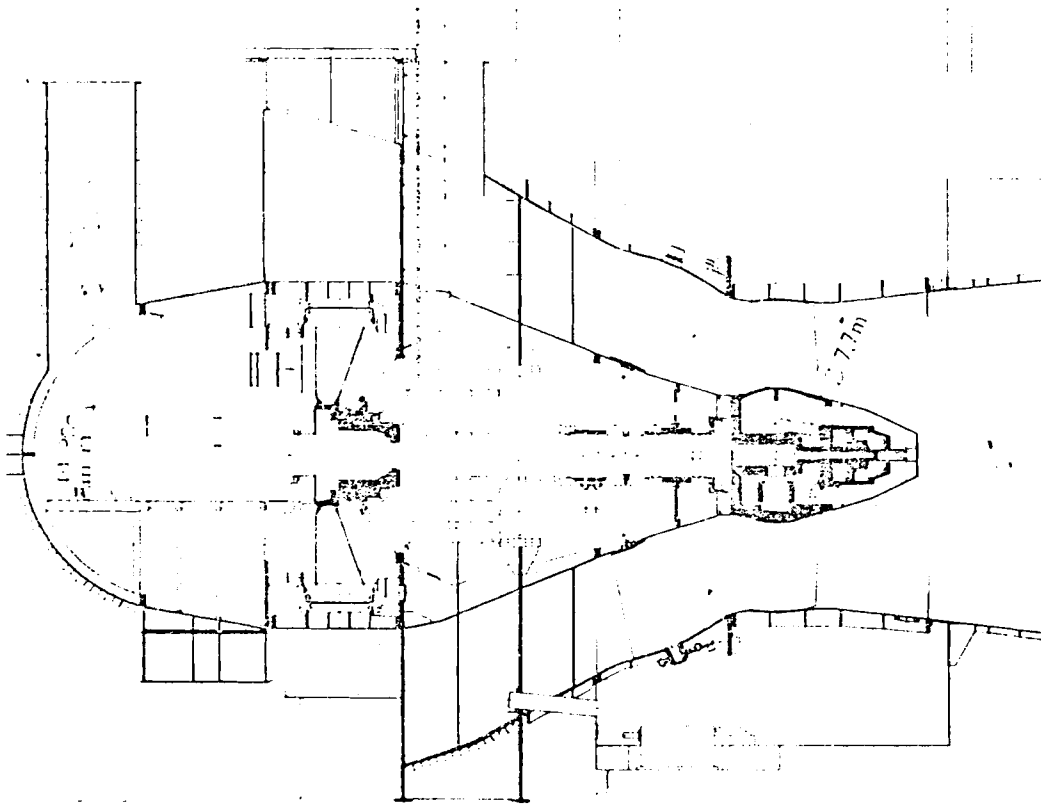
Fig. 10.2.11. Elevation of BT Racine. Ohio. USA. (Design Sulzer Escher Wyss) 2 sets. $H_m = 7$ m; $n = 62,1$ rpm; $P = 24,6$ MW. To date the largest BT with respect to runner diameter: $D = 7,7$ m. Alternator overhung. semi-umbrella design, 2 guide bearings. Piston of the runner servomotor screwed on the hub. Bulb embedded in concrete of the intake pillar. From *M. Hollenstein, W. Soland*: Die Rohrturbinen für das Kraftwerk Racine. EW Mitt. 1981/82 no 1 p. 13/16. (Drawing courtesy Sulzer Escher Wyss).

To date tidal power has been harnessed in a larger scale in the French station Rance. This is a single pool and double effect scheme equipped with reversible axial pump turbines of the bulb type. the prototype of which is seen in Fig. 10.2.15 [10.145; 10.146].

With respect to their adjustable runner vanes, all turbines with this device are basing on Kaplan's patent. This includes also diagonal turbines of the Deriaz type (Fig. 3.4.32). This turbine may also appear with a horizontal shaft then being a cross breeding between diagonal and bulb turbines. as has been implemented in the machines of the plant Guijo de Granadilla, Spain, built by Sulzer Escher Wyss (Fig. 10.2.24) [10.28].

10.2.4. General limitations and reasons for Kaplan turbines

a) In the field of plants with small and strongly varying head, greatly varying discharge consumed by a few sets only, KTs with runner vane adjustment at least, are the more economical solution. provided the head is below about 30 m. This follows mainly from the higher speed of a KT (Ku between 1,2 and 2,4) compared with a FT (Ku between 0,65 and 1,1) at the same head and output.

418
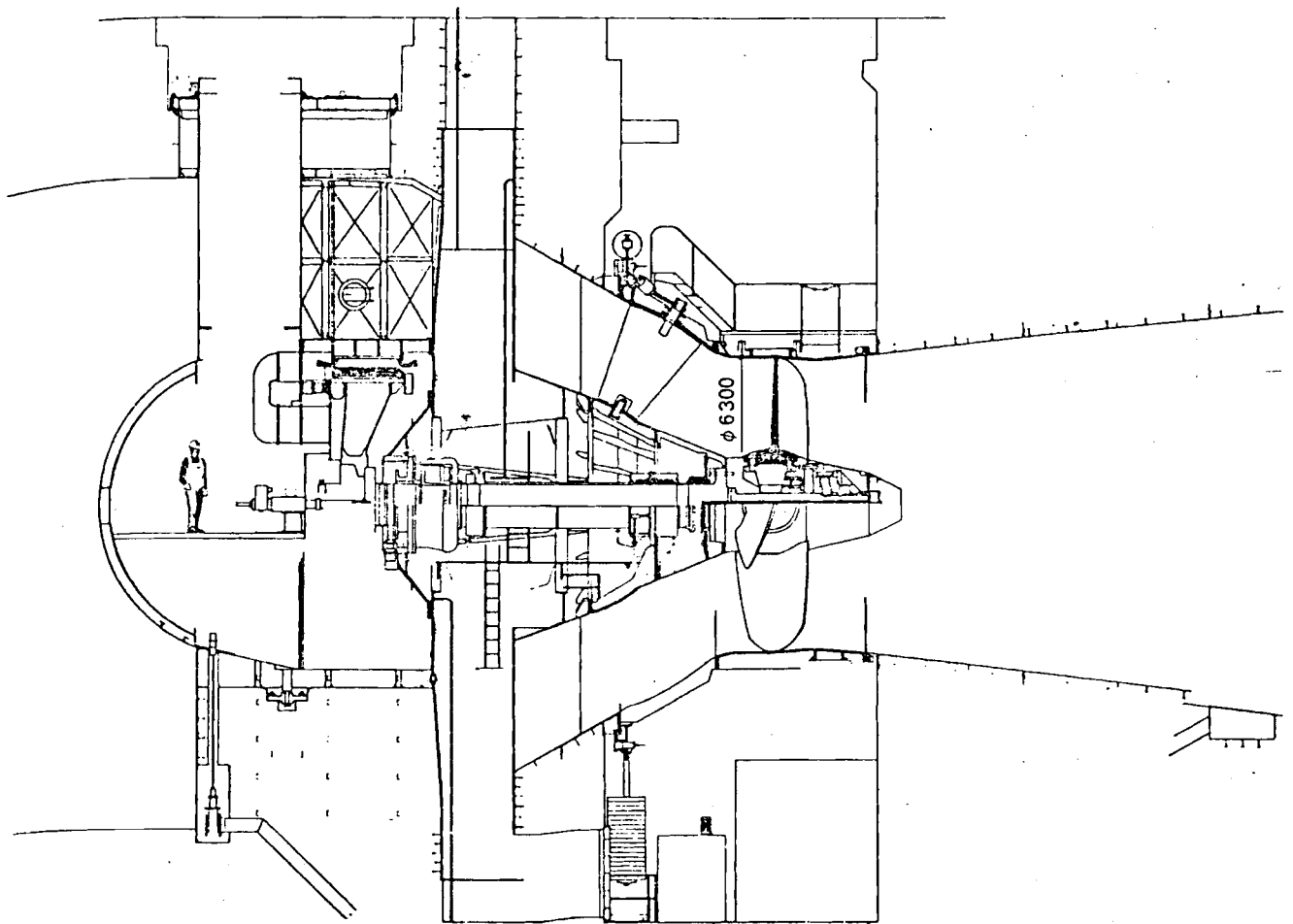
Fig. 10.2.12. Elevation of BT Melk, Danube, Austria (owner Österreichische Donaukraftwerke AG). 9 sets, 3 built by Voest Alpine, Linz, Austria. $H = 8,2$ m; $n = 85,7$ rpm; $P = 22,3$ MW. Preliminary model tests by Voest, final tests at Anströ, Graz. Runner: $D = 6,3$ m; 4 blades cast in stainless steel Cr/Ni 13/6; hub cast in stainless steel Cr/Ni 13/4. Throat ring with lining of stainless steel. 2 guide bearings; all bearings oil pressure lubricated from overhead tank. For start up and shut down special pumps. Special alternator hatch. Welded guide vanes with self-lubricated bearings for the trunnions, links and regulating ring, operated by 2 servomotors with closing weights. Links with safety devices (telescope springs), gate ring locked in the end positions. (Drawing courtesy Voest Alpine, Linz, Austria).

b) For heads larger than 30 m, a KT has always a larger runner diameter D than a FT. This results mainly from about 25% blockage the throat section of a KT experiences from its hub. Hence above 30 m head (Fig. 10.2.25), a KT is installed only if large variation in head and discharge justify this design for its flatter efficiency vs discharge curve and hence for its superior efficiency, when operating away from the bep. This advantage must be more weighty than the additional cost of a KT which is radially and axially more extensive than a FT.

c) If the higher submergence of a KT does not result in large additional excavation cost, e.g. if the KT is located at the base of a dam whose reservoir serves as tailwater.

d) If the customer insists on the runner being fabricated in the workshop and if the loading gauge of the admission roads or railroads is limited, then by separating the hub during transport a KT allows for the installation of a more powerful set than a FT design.

419
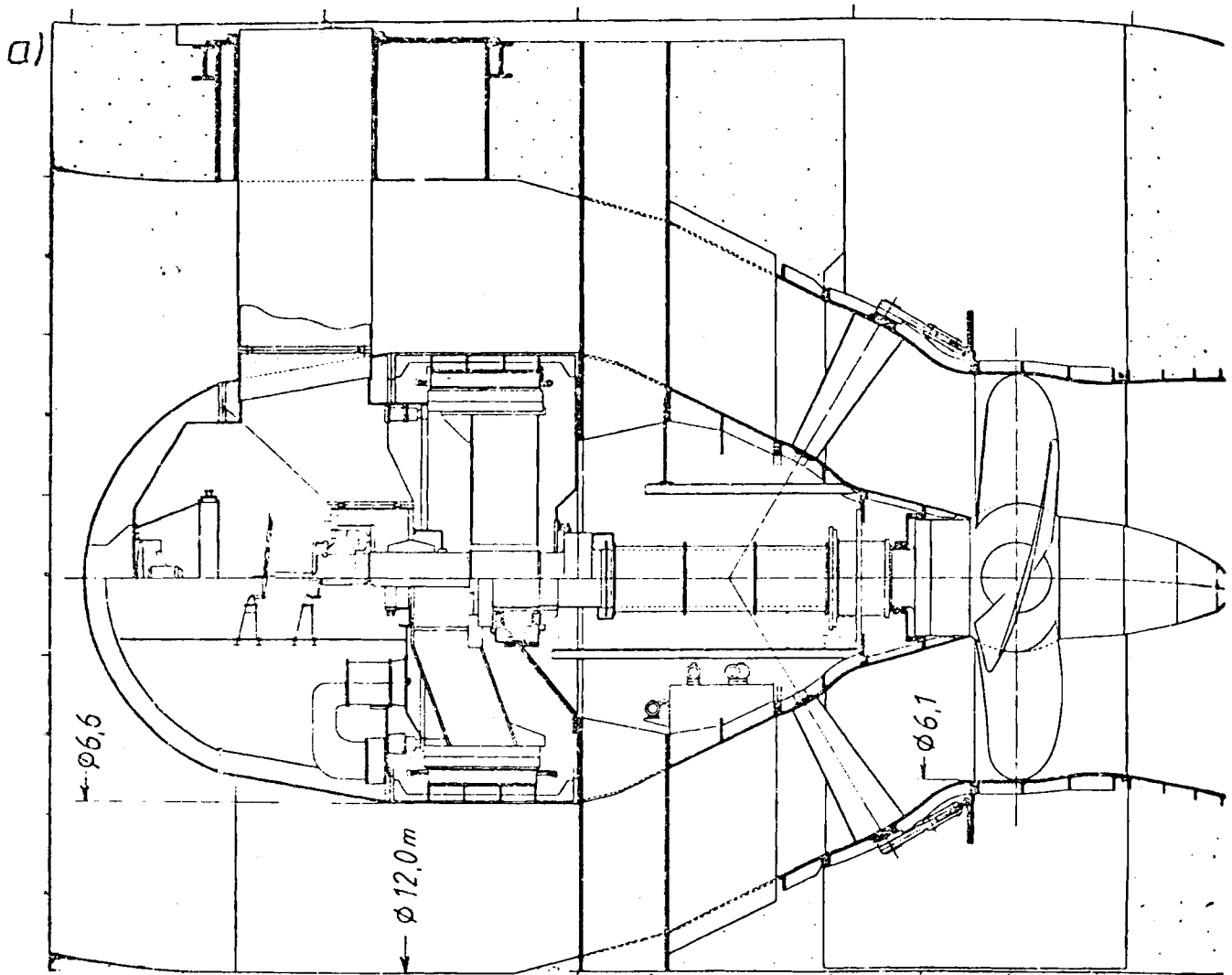
Fig. 10.2.13. a) Sectional drawing of BT Asele, Sweden (owner Swedish state power board built by KaMeWa AB, Sweden). $H = 10,1$ m, $P = 28,3$ MW, $n = 93,8$ rpm, runner $D = 6,1$ m. Alternative design with overhung alternator rotor and thrust bearing between the guide bearings (below) (drawing courtesy KaMeWa, Kristincham, Sweden).

Since the runner vanes of a KT can be transported separately, the upper limit of size, the requirement of transport usually imposes on the hub, is actually conceived to be 4,4 m (Fig. 10.2.7).

e) Provided the suppositions under b) to d) are accomplished, no difficulty exists nowadays for the installation of KTs up to a head of about 90 m and outputs up to 200 MW.

f) The upper head limit actually reached by KTs is now $H = 73$ m at Orlik, Vultava, Czechoslovakia with 2 sets of 80 MW output.

In the head range up to 25 to 30 m the KT is installed in semi-spiral casings of concrete reinforced as the head rises. Above 30 m full spiral casings of reinforced concrete, lined with steel are used.

420
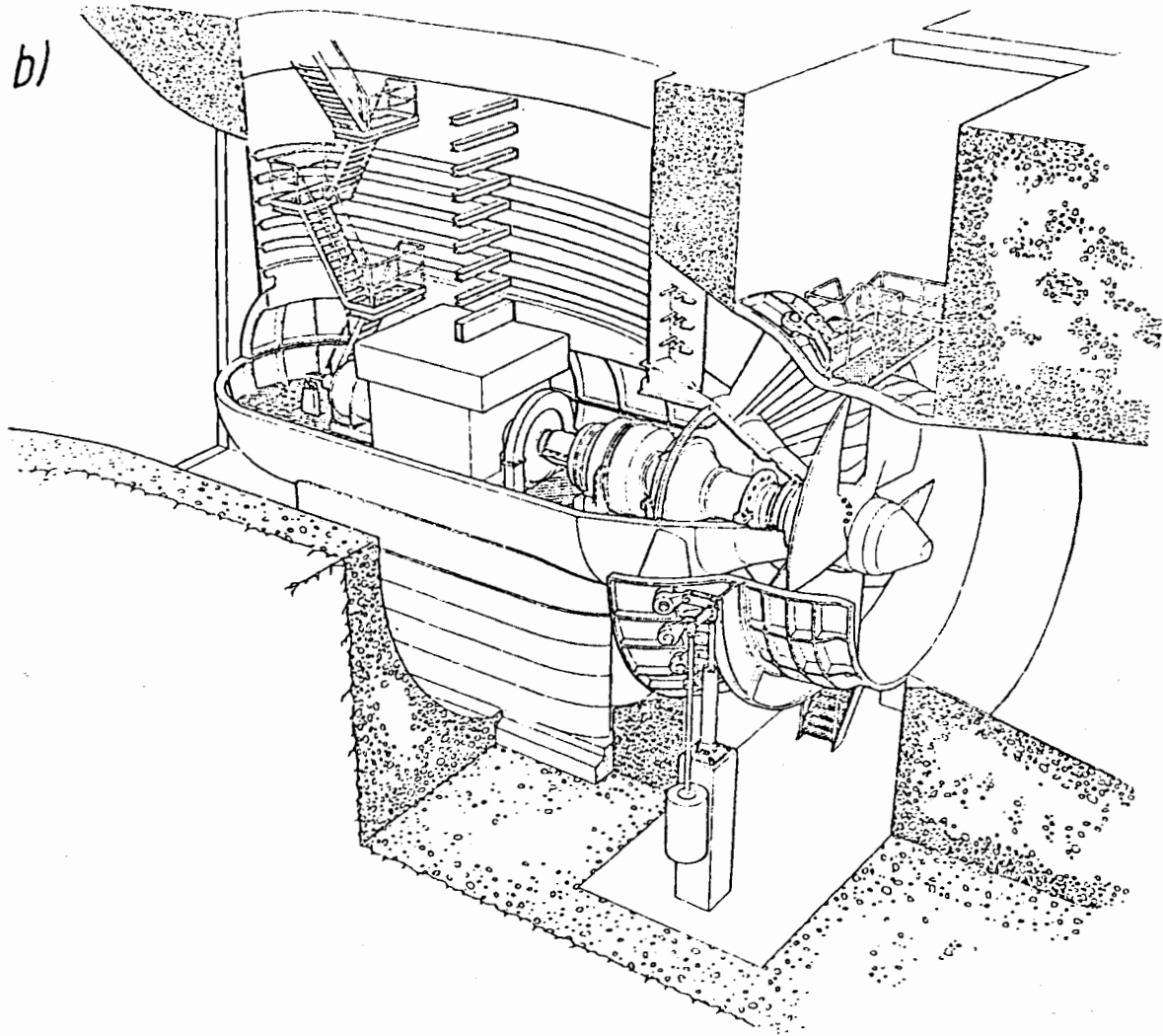
Fig. 10.2.13. b) Perspective sectional view of BT at Avesta-Lillfors (owner Avesta Jernverks AB). 2
BTs built by KaMeWa AB, Sweden, commissioned 1981, 1982, generator with planetary step up gear
of 2 stages. $H_r = 5,3$ m, $H_m = 6,25$ m, $P_m = 14,3$ MW, $n_T = 68,2$ rpm, $n_G = 750$ rpm. Runner
$D = 6,1$ m. Most powerful geared BT. Gear efficiency 99,2%, gear weight 18 tons manufactured by
Stal Laval. Generator 10 kV, efficiency 98%, weight 33 tons. Total weight of unit 461 tons. Standar-
dized high speed synchronous generator. Reduced bulb diameter and hence narrower water pass-
ages. All internal parts can be dismantled through a large access hatchway without dewatering the
unit. Erection time only 16 months for the sets. The rated voltage can be adapted to the voltage of
the grid up to 13,8 kV. The unit transformer is thus eliminated. A fly-wheel can be attached to the
high speed shaft to improve governing properties. The design opens possibilities for standardization
of the complete plant. The final result will lower the investment cost and improve the overall
economy. (Drawing courtesy KaMeWa, Kristineham, Sweden).

Against pitting by cavitation, runner vanes of stainless steel are used for heads above
10 m. For heads lower than 10 m, at least the outermost part of the runner blade must
be lined with stainless steel. In any case the throat ring should be lined with stainless steel.
This holds good especially for throat rings embedded in concrete. The draft tube inlet
region is lined with steel in stations, where the velocity is larger than 6 m/s.

421
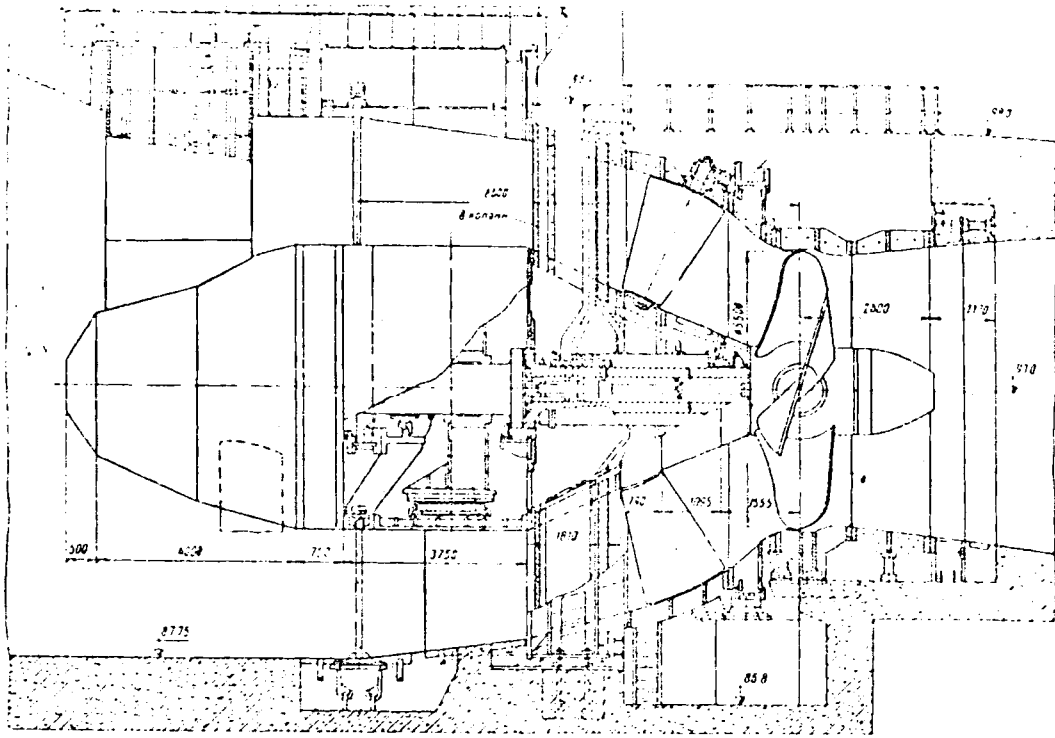
Fig. 10.2.14. Elevation of the BT Kiew, Dnjepr, USSR (owner State Power Board of USSR), 20 sets (design LMZ). $H = 7.7$ m; $n = 166.6$ rpm; $P = 16$ MW. (Drawing courtesy LMZ, Leningrad, USSR).
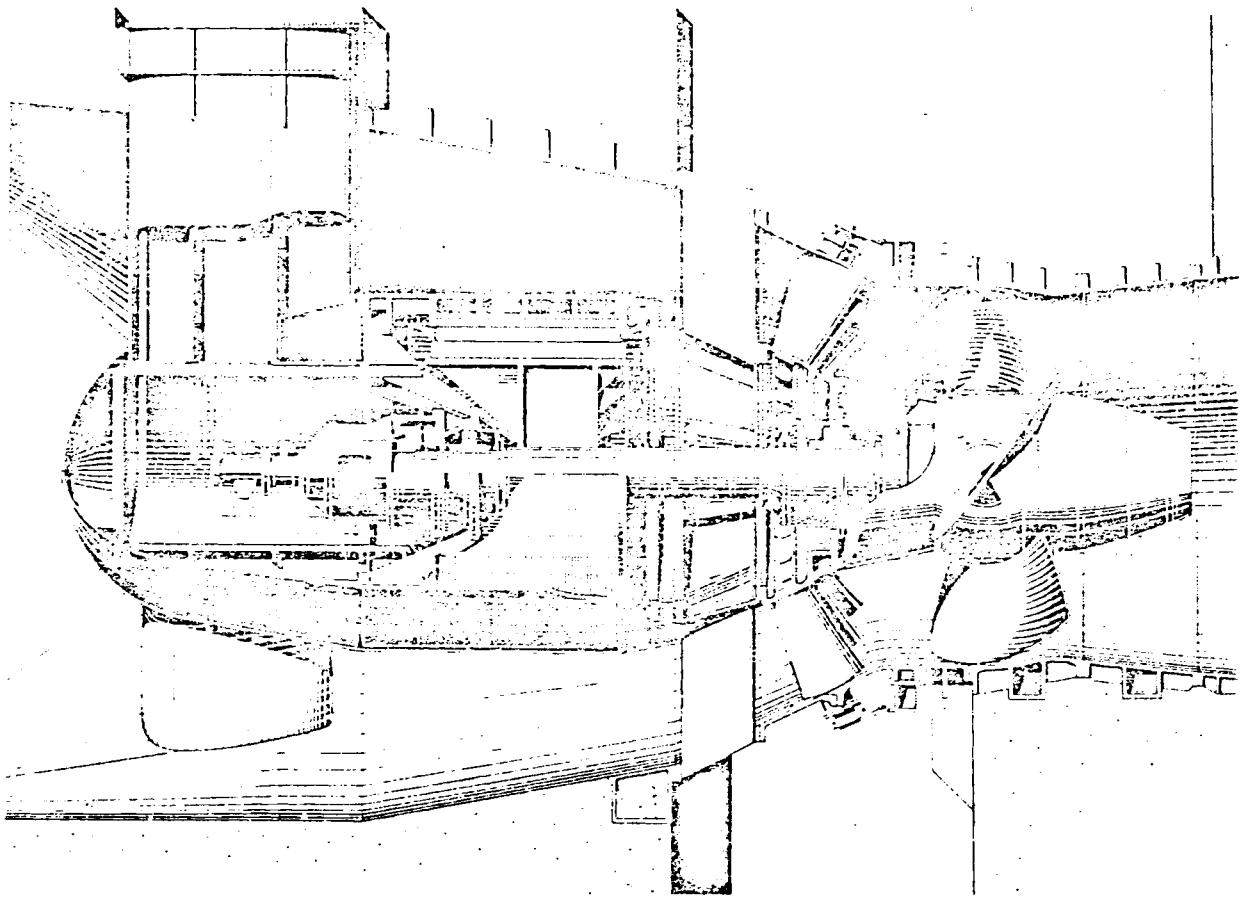
Fig. 10.2.15. Elevation of BT Beaumont-Monteux, France (owner EdF) (Design Alsthom Neyrpic, $H = 11.3$ m; $n = 150$ rpm; $P = 9$ MW. Prototype for tidal power machines of the "Rance". (Drawing courtesy Neyrpic Grenoble, France).
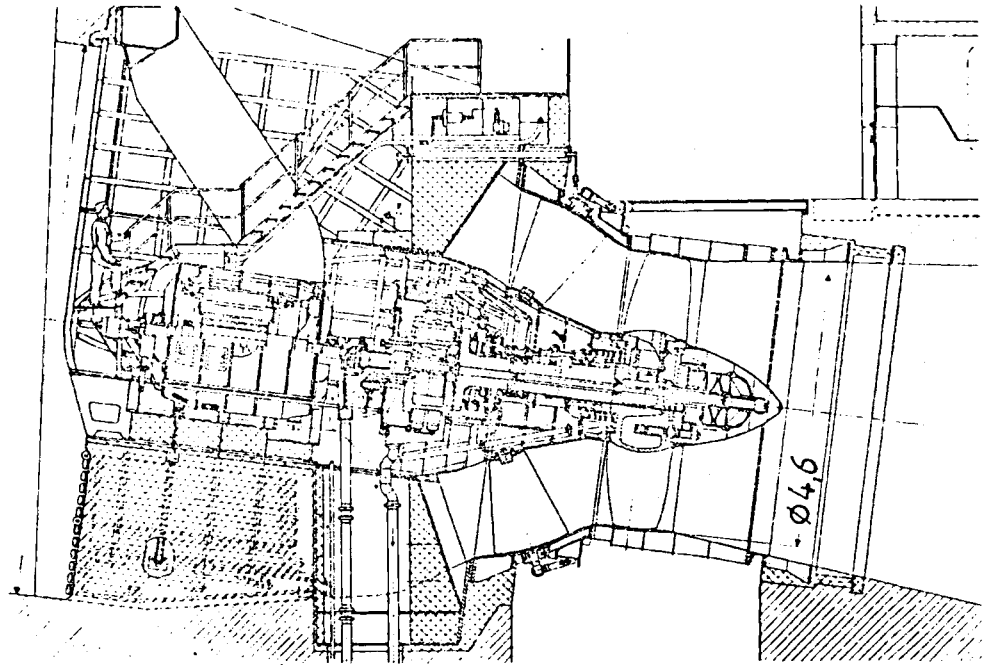
Fig. 10.2.16. Elevation of a BT with inclined shaft at Trier, Mosel, West Germany (owner Rheinisch Westfälische Elektrizitätswerke AG, Essen) 4 sets (Design Sulzer Escher Wyss) with planetary gears Krupp Stöckicht. $H = 7,7$ m; $n = 78/750$ rpm; $P = 4,4$ MW. Runner $D = 4,6$ m, 4 blades; servo-motor welded with piston bolted on the hub. Generator mounted through streamlined access pit to the bulb. Drive of the conical guide apparatus with spherical articulations. Safety device: buckling links. A flexible external gear and gear coupling between the sunwheel and the alternator rotor facilitate uniform load distribution of the 3 planet pinions for outputs up to 10 MW. All Mosel BTs were equipped with such gears. Minor failures of these gears and thus lost working time have induced the owner to limit their use in future designs. (Drawing courtesy Sulzer Escher Wyss).

10.2.5. The design of an axial turbine

10.2.5.1. The optimization of runner diameter D

1. With respect to efficiency: As known from Cap. 5.5, the runner loss of an axial machine can be approximated by $h'_{vL} = \varepsilon K_0 Ku/Kc_m$, where ε is the glide angle of the average cylindrical vane section, $Kc_m = c_m/(2\,gH)^{1/2}$ the coefficient of a mean meridional velocity, $Ku = u/(2\,gH)^{1/2}$ the coefficient of the blade tip speed, K_0 the following function of the hub to tip diameter ratio N: $K_0 = (2/3)(1 - N^2)/(1 - N^3)$. N follows from Table 10.2.1.

For the case of whirl-free flow downstream of the runner, the draft tube loss as the other relevant loss in the turbine reads after Cap. 5.5: $h'_{vD} = \zeta_D K c_m^2$, where ζ_D is the diffuser loss coefficient. Hence the loss ratio of a KT is approximately

$$h'_{vT} = \varepsilon K_0 Ku/Kc_m + \zeta_D Kc_m^2. \qquad (10.2-1)$$

Assume a certain design, for which the operating data, namely head H, flow Q and the angular velocity ω are known. Then continuity and the relation $u = \omega D/2$ give the velocity coefficients as functions of the runner tip diameter D as follows

$$Kc_m = (4/\pi)\,Q/[(2\,gH)^{1/2}(1 - N^2)]\,D^{-2}; \quad Ku = \omega D/[2(2\,gH)^{1/2}]. \qquad (10.2-2)$$

423

Table 10.2.1. Design features of axial turbines.

n_s	n_q	n_q'	H_{max} (m)	z	$N = D_{ll}/D$	L/t_e	L/t_i	σ	Ku	Kc_m	b_3/D*)	H/H_2*)
300	87	1,64	90	10(12)	0,65(0,7)	1,1	1,9	0,25	1,0	0,31	0,35	0,45
400	116	2,19	50	8	0,6	1,08	1,8	0,35	1,2	0,38	0,37	0,41
500	145	2,7	30	6	0,5(0,45)	1,0	1,7	0,52	1,4	0,44	0,39	0,37
600	174	3,28	15	5	0,44	0,9	1,6	0,70	1,6	0,50	0,40	0,33
700	203	3,84	8	4	0,44	0,8	1,4	0,95	1,7	0,54	0,42	0,28
1100	318	6,0	4	3	0,39	0,7	1,1	2,1	2,3	0,70	0,45	0,23

*) b_3 gate span, H_2 distance runner vane axis from bottom of guide vane channel
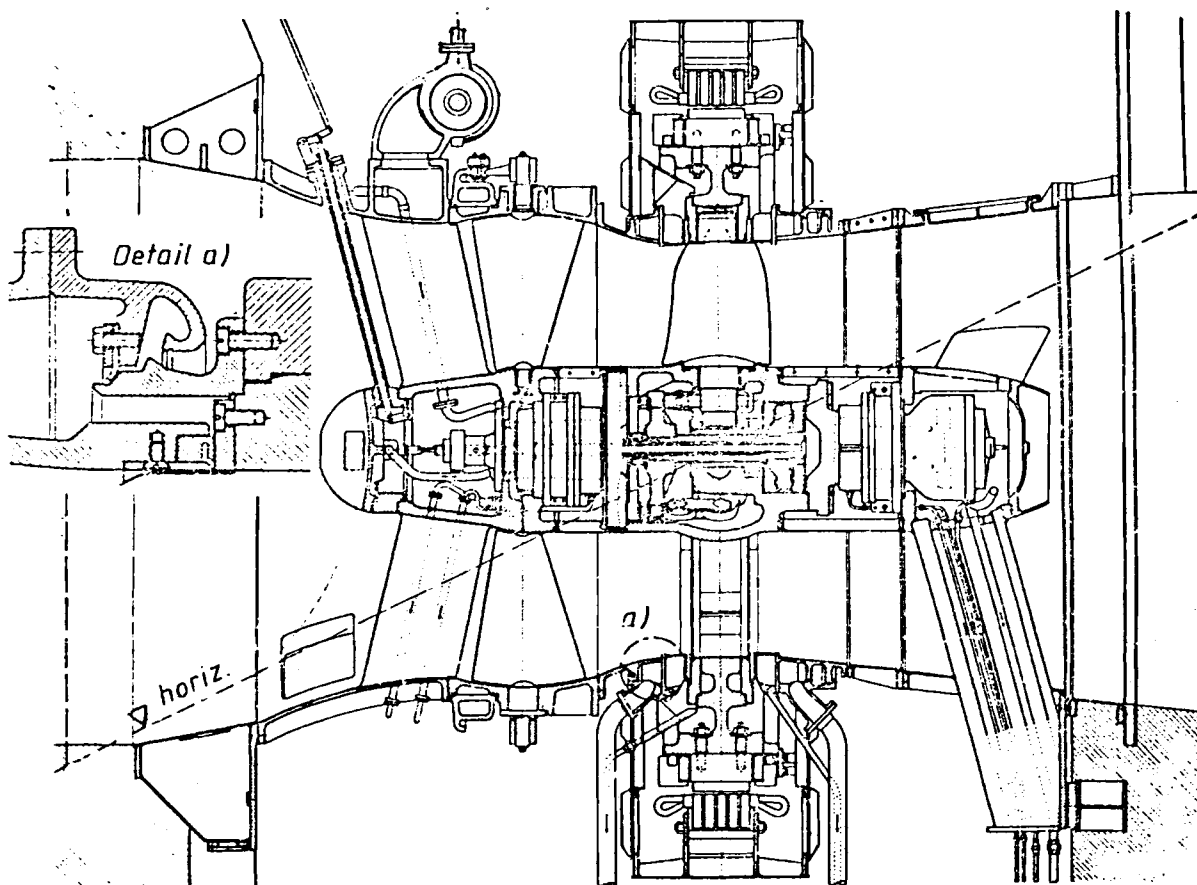
Fig. 10.2.17. Elevation of a tubular turbine with rim generator, alternator rotor shrunk on the shroud, according to Harza's patent. Implemented by A. Fischer and Escher Wyss on 73 plants on Iller, Lech, Saalach (Germany) during 1936 and 1953. Adjustable axial guide vanes. Smallest flow deflection in connection with most effective cooling, best accessibility, largest flywheel moment and hence most stable regulating action of alternator. Shaft inclined. The shroud seal, shown in detail a), only useful for sand free water. One sample equipped with adjustable runner blades as in the figure. Contrary to the straflo design no radial shroud guidance. Radial clearance needed for the adjustable runner blades caused shroud to be out of round. Displacement of the trunnion in the shroud thus produced was used for lubrication. Efficiency reduced by the wake of a butterfly valve close upstream. Typical dimensions: $D = 1,95$ to $2,05$ m. $H = 7,5$ to 9 m; $P = 1,5$ to $1,9$ MW. (Drawing courtesy Sulzer Escher Wyss).
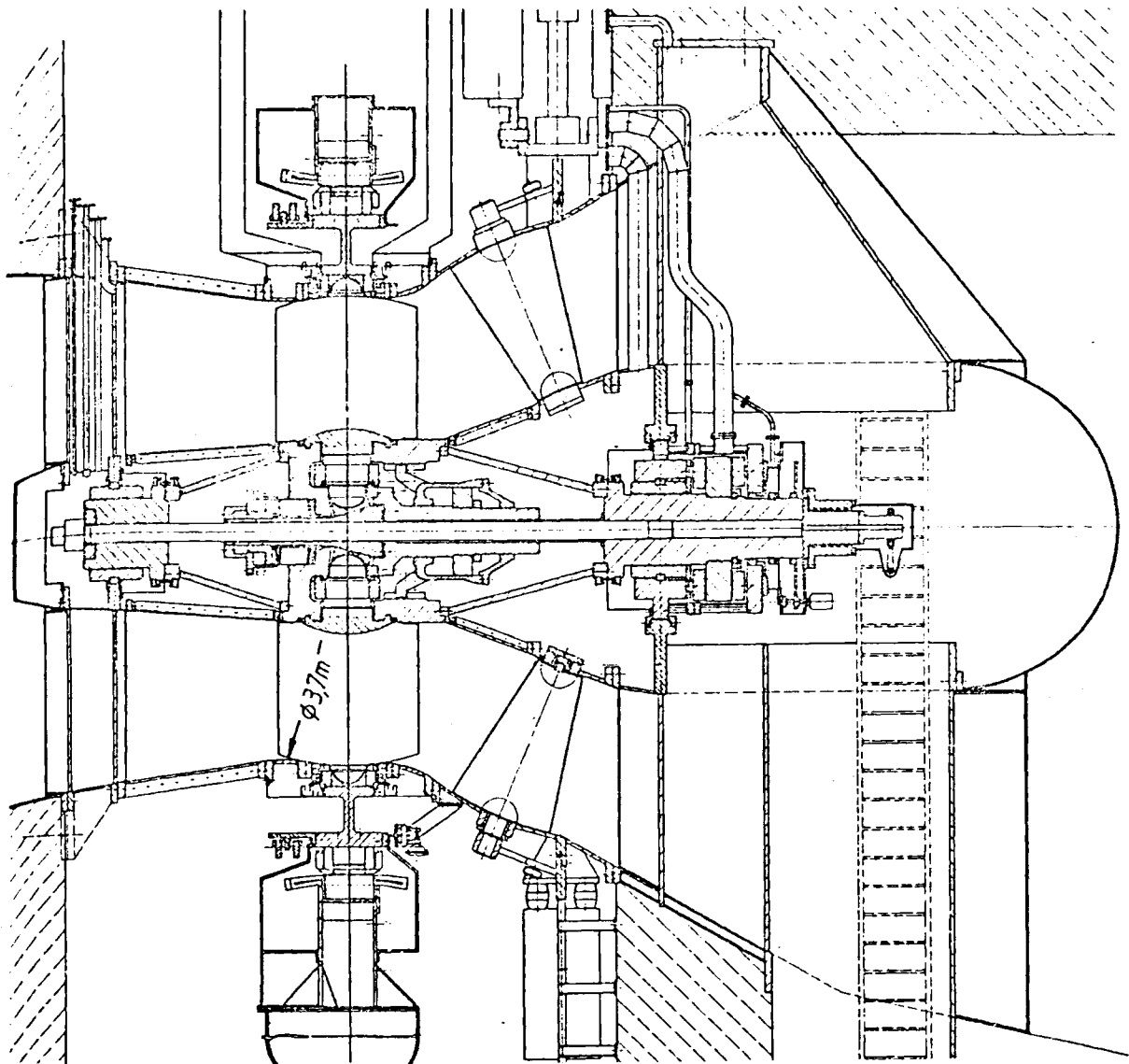
Fig. 10.2.18. Elevation of a double regulated straflo turbine Weinzödl, Austria, 1982. 2 sets built by Sulzer Escher Wyss (patentee). $H = 10,3$ m; $P = 8,35$ MW. Shroud axially and radially supported by self adjusting water heads according to Fig. 10.2.20. Therefore the thrust led off into the hub is relatively small. Contrary to the design in Fig. 10.2.17 the runner blade adjustment is trouble free. Also for sandy water. (Drawing courtesy Sulzer Escher Wyss).

Inserting this in (10.2−1) the loss reads

$$h'_{vT} = K_1 \omega D^3 + K_2 D^{-4}, \qquad (10.2-3)$$

where K_1 and K_2 are parameters, depending on the design (ε, ζ_D, N and K_0) and the working data (ω, Q, gH). Making the loss a minimum by $dh'_{vT}/dD = 0$, gives an optimum diameter with respect to efficiency (η) according to Keller [4.9]

$$D_{op\,\eta} = 1,155\,[\zeta_D/(K_0\,\omega\,\varepsilon\,gH)]^{1/7}\,[Q/(1 - N^2)]^{3/7}. \qquad (10.2-4)$$

L With respect to suction requirement: According to Cap. 8.2 the suction head reads $_{\eta} = H_A - h_{cr} - \sigma H$, where the barometric pressure head H_A, the head of critical pressure
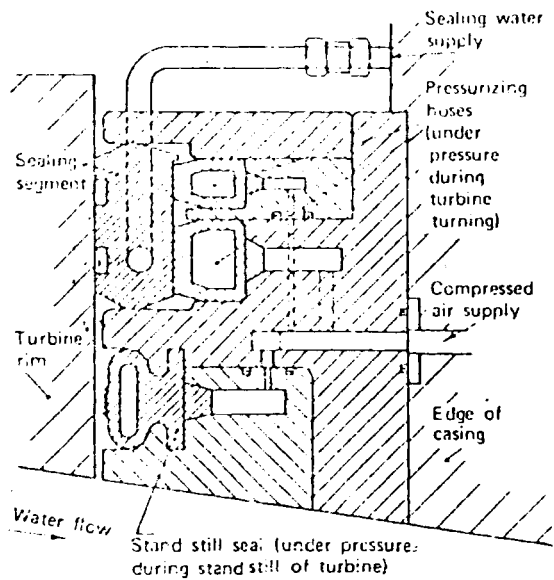
Fig. 10.2.19. Axial shroud seal of a straflo turbine runner. May be also applied to sandy water by means of clean pressurized blocking water. Air-operated "standstill seal" (below). (Drawing courtesy Sulzer Escher Wyss).

Fig. 10.2.20. Left: Schematic plan and elevation of the water head, a hydrostatic supporting component of a straflo turbine's shroud. Right: Tilting of the water head automatically creates a restoring force acting against the tilt. Hence there is stable axial and radial support of the shroud in a straflo turbine. From W. Meier a. H. Miller [10.30].
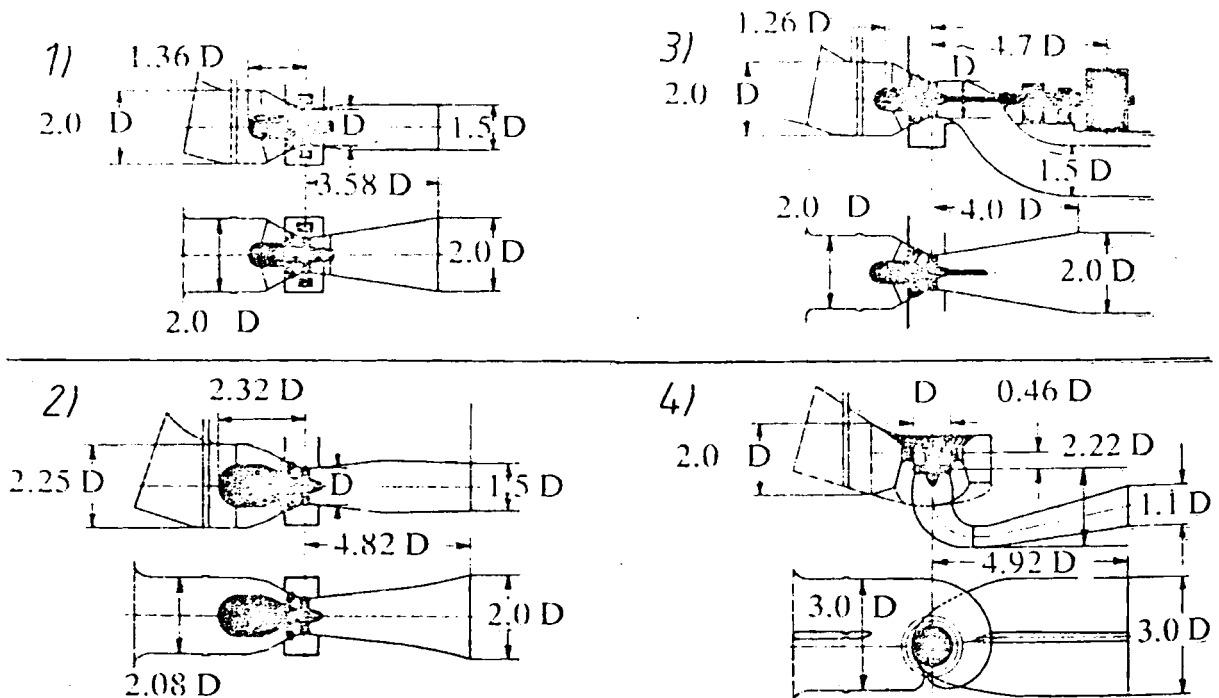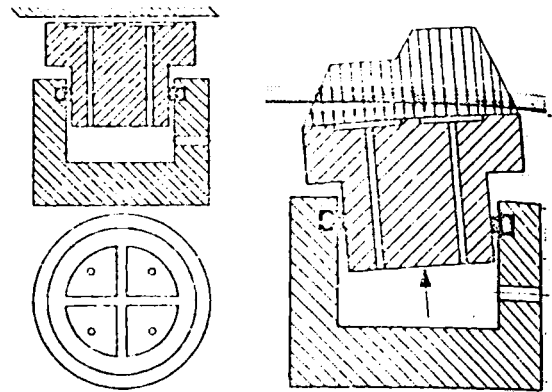
Fig. 10.2.21. Schemes of different axial turbine designs and their space requirements for civil engineering work in elevation and plan. 1 straflo turbine, 2 bulb turbine, 3 tubular S turbine, 4 vertical Kaplan turbine. From Miller, H.: Choice of hydro electric equipment for tidal energy. Paper, Symposium tidal power, Seoul, Korea 1978, special issue Sulzer Escher Wyss.

426

Fig. 10.2.22. Longitudinal section of power house and straflo turbine Annapolis, Fundy Bay, Canada (Atlantic Coast). Prototype of single effect tidal power plant. Annual production 50 GWh. From *A. Douma, G. D. Stewart* and *W. Meier* [1.59].
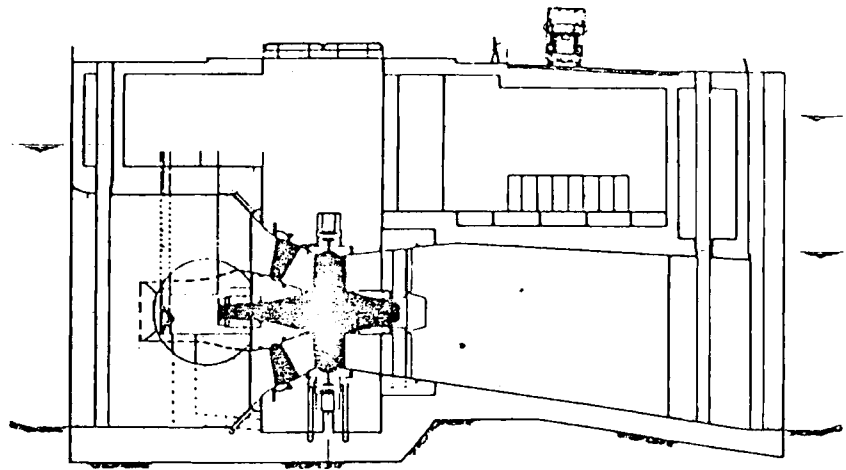
h_σ and the head H are given. According to Cap. 8.2, $NPSH$ can be expressed by the pressure number of the critical point on the runner vane face λ and the draft tube efficiency $\eta_D = 1 - \zeta_D$ as $NPSH = H[\lambda K u^2 + (\eta_D + \lambda) K c_m^2]$. Inserting here $K c_m$ and $K u$ from (10.2-2) gives

$$NPSH = K_3 \omega^2 D^2 + K_4 D^{-4}.$$ (10.2-5)

Making σ a minimum and hence also h_s by $dNPSH/dD = 0$ gives the runner diameter with respect to suction requirements

$$D_{op\,NPSH} = 2[2(\eta_D + \lambda)/\lambda]^{1/6} \{Q/[\pi\omega(1 - N^2)]\}^{1/3}.$$ (10.2-6)

III. Critical comparison of both the optimum diameters on the base of cost: Both the optimum diameters after (10.2-4) and (10.2-6) optimize the turbine under certain aspects. Experience shows that $D_{op\,\eta} < D_{op\,NPSH}$. Usually the suction head h_s is small compared with D. In case of a KT with a vertical shaft the bottom of the draft tube bend is more than 2,5 D below the runner exit. This gives additional excavation cost proportional to D^3. Thus $D_{op\,NPSH} > D_{op\,\eta}$ is not always the cheapest solution.

This reveals that only in the case of a KT with a horizontal shaft does $D_{op\,NPSH}$ result in a more economical solution with respect to excavation cost.

If the diameter is small as compared with the suction head (high head) then also $D_{op\,NPSH}$ gives the more economical solution concerning excavation cost. However the excavation cost depends also on the structure of the ground. Moreover it is only a portion of the cost due to fabricating, erecting and operating a set. This last item merits a more detailed consideration.

The cost of making a set, including erection but without ground excavation is assumed to be $K_s = k_s D^m$, where $m = 2,3$ to 2,5 and k_s an empirical cost factor for a similar turbine with $D = 1$ m diameter. The excavation cost is approximately described by $K_{ex} = k_{ex} D^3$ where k_{ex} is an empirical cost factor depending on the quality of the ground.

To this might be added the following operation-linked cost of the set during its z years of useful life:

The set has a unit power P_{11}. Then by the similarity laws the output of a set, head gH, diameter D, is $P = P_{11} D^2 (gH)^{3/2}$. During the z years of its useful life it might work annually for h hours under rated load P and might supply its energy at a constant

427
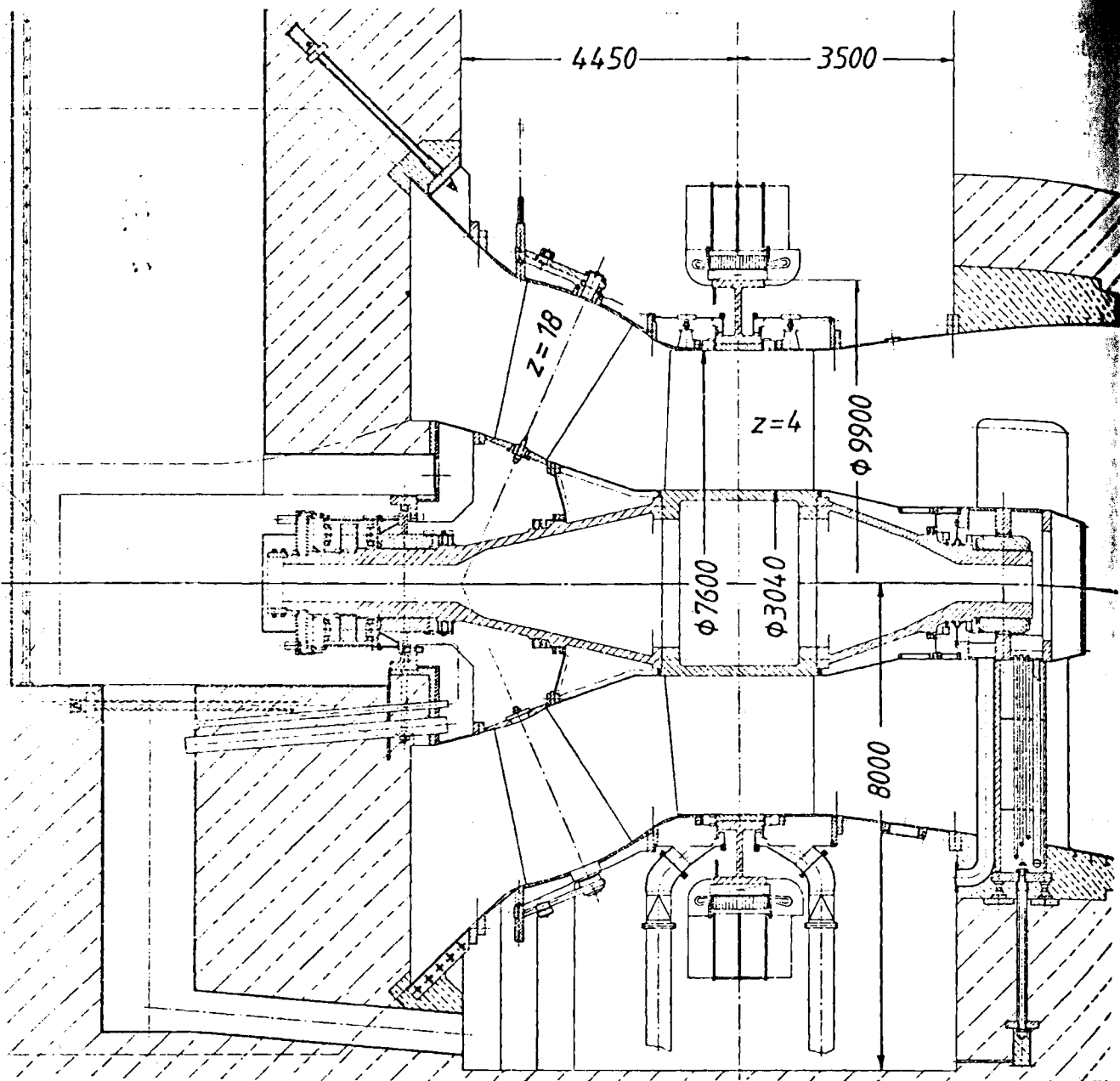
Fig. 10.2.23. Elevation of a gate regulated straflo turbine of the single effect tidal power plant Annapolis. Fundy Bay, Canada. $H = 1,4$ to $7,1$ m; $H_r = 5,5$ m; $n = 50$ rpm; $n_{r_a} = 98$ rpm; $P_r = 18$ MW; $P_m = 20$ MW. Runner: $D = 7,6$ m; 4 blades. 18 adjustable conical guide vanes. To date the largest tidal power and straflo turbine. Flywheel moment $GD^2 = 12800$ t m^2. Rated voltage at alternator terminals $4,16$ kV. Governor pressure 100 bar. Guaranteed bep efficiency $0,89$. From *A. Douma* a. *G. D. Stewart*: Annapolis Straflo. Special issue Sulzer Escher Wyss.

electricity rate k_e, which also comprises the operation, maintenance and replacement cost. With the interest factor α (Cap. 4.2), the present value of the loss (10.2–3) during z years at the beginning of power generation reads

$$K_e = k_e \, \alpha \, h \, P_{11} \, (gH)^{3/2} (K_1 \, \omega \, D^5 + K_2 \, D^{-2}).$$
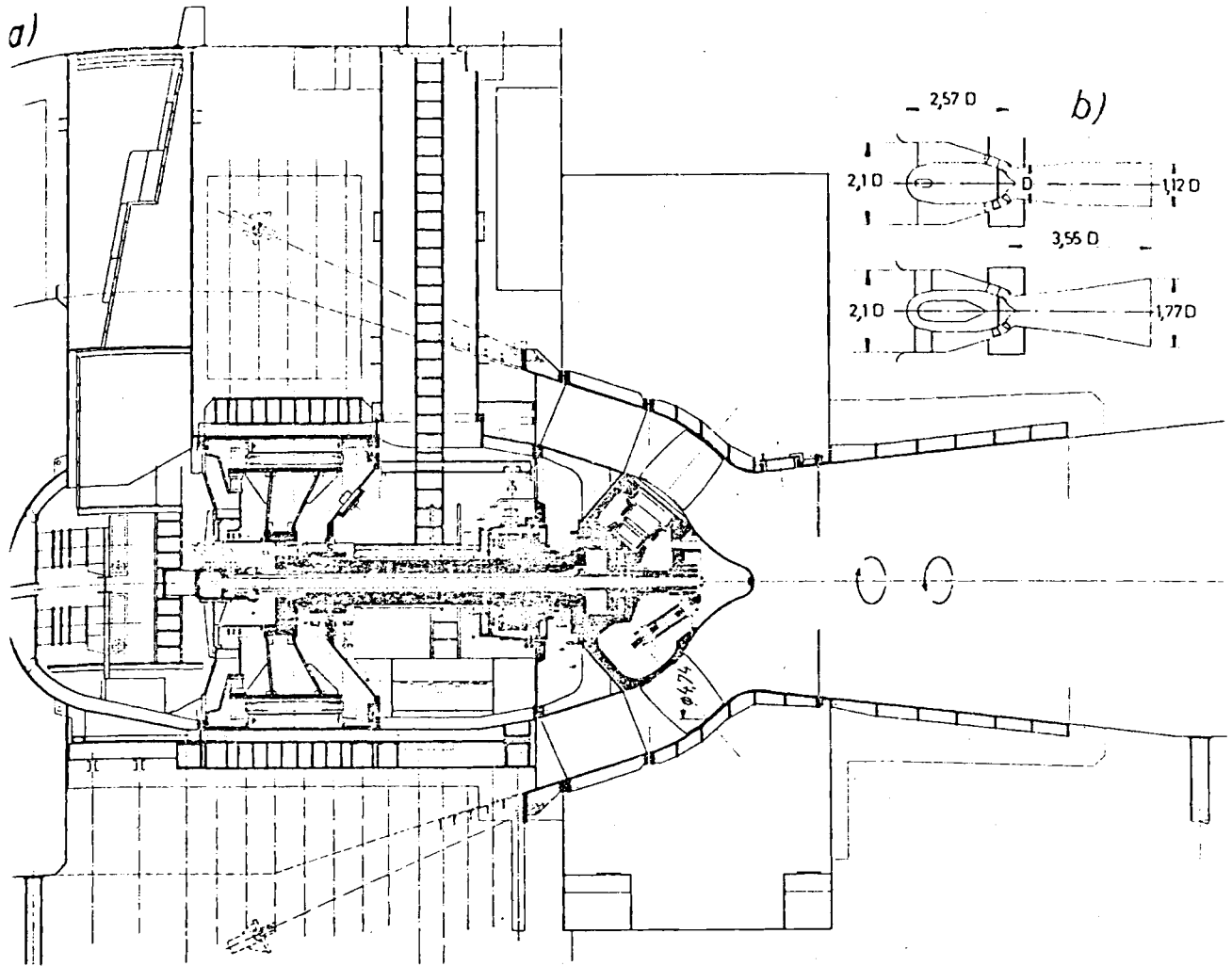
Fig. 10.2.24. a) Elevation of a newly developed high head diagonal bulb PuT also applicable to tidal power. Plant Guijo de Granadilla, Spain (owner: HEE, Madrid); design Sulzer Escher Wyss. $H = 24$ to 25 m; $n = 130,4$ rpm; $P = 27$ to 26,3 MW. 2 sets, rotor tip diameter at outermost point of blade axis $D = 4,74$ m. 2 guide bearings, both rotors of overhung design. To transmit the axial thrust into the concrete, the flange of the stay ring is fixed by long tie rods. Special hatch for the generator. b) Schematic view in elevation and plan with space requirements in terms of the above rotor diameter. (Drawing courtesy Sulzer Escher Wyss.)

Hence the resulting cost of the machine during its z years of operation are

$$K_{res} = k_s D^m + k_{ex} D^3 + k_e \alpha h P_{11} (gH)^{3/2} (K_1 \omega D^5 + K_2 D^{-2}). \qquad (10.2-7)$$

When the diameter varies by ΔD the resulting cost varies by

$$\Delta K_{res} = [m k_s D^{m-1} + 3 k_{ex} D^2$$
$$+ k_e \alpha h P_{11} (gH)^{3/2} (5 K_1 \omega D^4 - 2 K_2 D^{-3})] \Delta D. \qquad (10.2-8)$$

Assume that the variation of diameter corresponds to the difference $\Delta D = D_{op\,NPSH} - D_{op\,\eta}$ according to (10.2-4), (10.2-6). If ΔD introduced in (10.2-8) yields a positive value of ΔK_{res}, then the optimum diameter $D_{op\,\eta}$ has to be preferred. This depends decisively on the difference $(5 K_1 \omega D^4 - 2 K_2 D^{-3})$, where

$$K_1 = (\pi/8) \varepsilon K_0 (1 - N^2)/Q; \qquad K_2 = (16/\pi^2) \zeta_D Q^2/[2 gH (1 - N^2)^2]. \qquad (10.2-9)$$

429
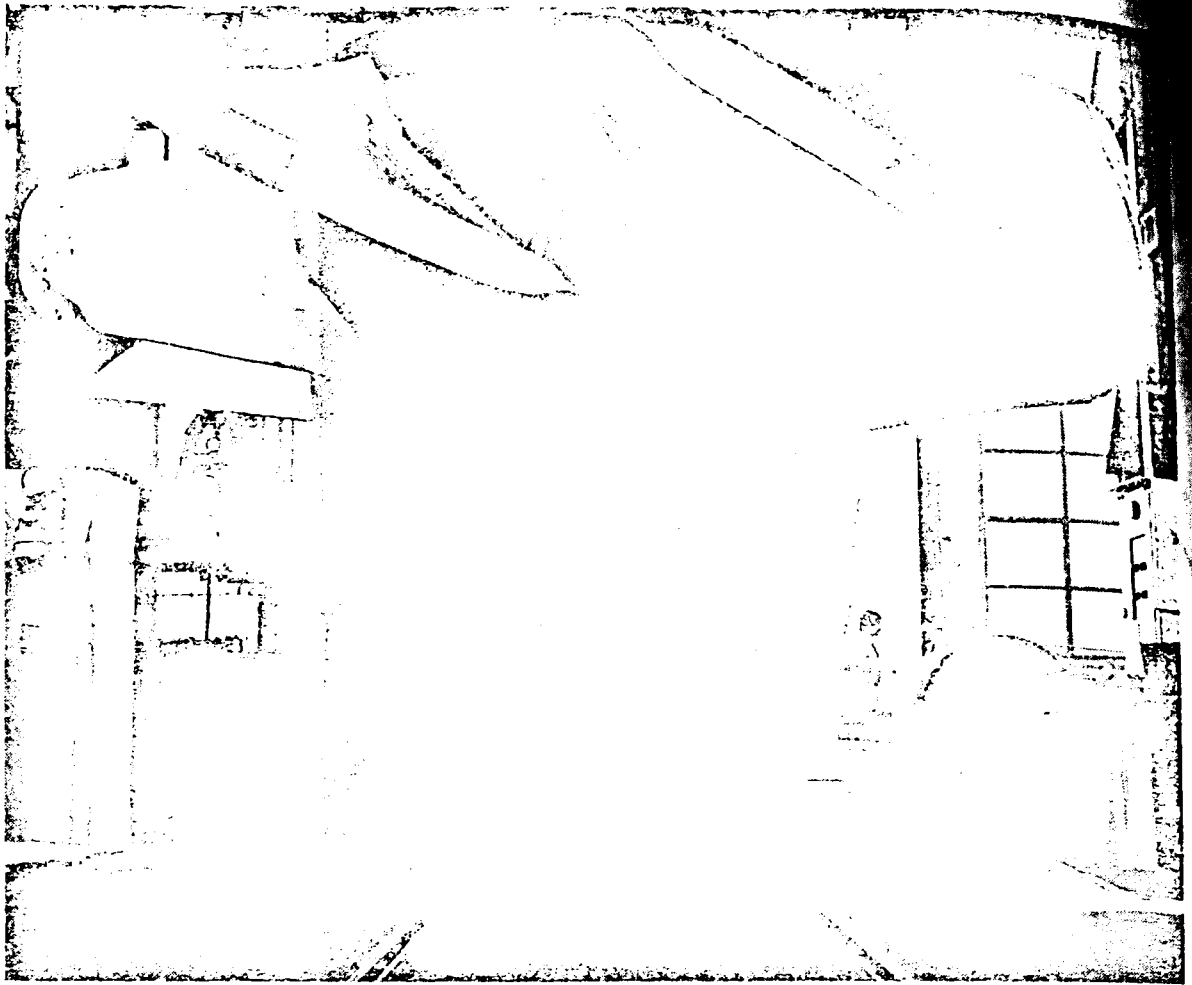
Fig. 10.2.25. Anticavitation fin on a KT runner blade. KT runner of Vangen Norway (owner Oslo Lysverker) in the Vevey Engineering Works, Switzerland. $H = 50$ m; $n = 250$ rpm; $P = 35$ MW; 8 runner blades. (Photograph courtesy Vevey Engineering Works, Switzerland).

10.2.5.2. The "best possible" type number (specific speed)

$\Delta K_{res} = 0$ yields an optimum of (10.2–8). Ignoring a vanishing square bracket value of (10.2–8), this needs $\Delta D = 0$ or

$$D_{op\,NPSH} = D_{op\,\eta}. \tag{10.2–10}$$

Obviously such a turbine combines the lowest possible internal loss with the cheapest suction requirements, provided the operating data gH, Q and ω are given, and the parameters ε, ζ_D, N, λ, $\eta_D = 1 - \zeta_D$ are known. The last relation yields a nondimensional specific speed (type number), according to Cap. 9.2. $n'_q = \omega\,Q^{1/2}/(gH)^{3/4}$, depending only on the above mentioned parameters due to the suction qualities and efficiency

$$n'_{qop\,\eta\,NPSH} = \pi^{1/2}\,(1 - N^2)^{-1/4}\,(1 - N^3)^{3/4}\,[\varepsilon/(1 - \eta_D)]^{3/4}\,[2(1 + \eta_D/\lambda)]^{7/8}. \tag{10.2–11}$$

Once H and Q are known the last relation determines the optimum angular velocity of the set by

$$\omega_{op\,\eta\,NPSH} = n'_{q\,op\,\eta\,NPSH}\,(gH)^{3/4}/Q^{1/2}. \tag{10.2–12}$$

430

Obviously in relation (10.2–11), in connection with (10.2–12), if $n'_{q\,op\,\eta\,NPSH}$ is in the range of an axial turbine, which needs $n'_q > 1$, $n'_{q\,op\,\eta\,NPSH}$ might be called "the best possible type number" (specific speed) of an axial turbine.

10.2.5.3. The velocity triangles

The known diameter gives by means of Q, gH and (10.2–2) the velocity coefficients Ku and Kc_m. The velocity coefficient due to the so-called deflection $\Delta c_u = c_{u2} - c_{u1}$ is obtained from Euler's relation by $K\Delta c_u = \eta_u/(2\,Ku)$, where η_u is the peripheral efficiency. For the bep the whirl at the runner exit approximately vanishes. Hence $Kc_{u1} = 0$.

For simplicity the meridional velocity c_m is assumed constant over the radius. Hence also $Kc_m = \mathrm{const}$. With Ku, Kc_m, $K\Delta c_u$, Kc_{u1}, the velocity triangles may be plotted for an arbitrary cylindrical section. Hence also the so-called undisturbed throughflow velocity $Kw_\infty = (Kw_1 + Kw_2)/2$ (Cap. 6.2). For c_m variable, see 10.2.8.

10.2.5.4. Design features of axial turbines

Table 10.2.1 shows some important design parameters of axial turbines as functions of the specific speeds n_q, n_s, n'_q. From this it is seen, that the hub diameter D_N increases in relation to the tip diameter D with the head H. This follows from the fact, that an axial turbine has a large reaction degree (0,6 to 0,9), hence the specific axial thrust nearly equals $\varrho\,gH$. This loads the ring-formed cross sectional area of the rotor's flow passage. The strength requires retaining the axial thrust per runner blade and hence an increase of vane number with head. This also implies an increase of the hub diameter, since the hub has to house the vane drive linkage due to a rising vane number.

To reduce the cost of excavation, $NPSH = \sigma H$ increases less than proportionally to the head H. Hence the cavitation index σ varies more than inverse to the head. To retain the cavitation susceptibility the chord to pitch ratio L/t of the outmost cylindrical section varies with H_{max}. The ratio L/t of the inmost cylindrical section can be understood, if the Bauersfeld equation (Cap. 6.3) is accounted for

$$\zeta_{AG} = (2\,t/L)(K\,\Delta c_u/Kw_\infty),\qquad\qquad (10.2-13)$$

where ζ_{AG} is the lift coefficient in the cascade, roughly $Kw_x = Ku$. From Euler's relation $K\Delta c_u = \eta_u/(2\,Ku)$. This in the last relation gives $\zeta_{AG} \approx (t/L)\,\eta_u/Ku^2$. Since t/L vs r varies between $1/r$ and constant and since $Ku \sim r$, the lift coefficient after the last relation becomes largest at the hub. Hence $\zeta_{AG\,max} = \zeta_{AG\,i}$.

To avoid stall $\zeta_{AG\,i} \leq 1{,}4$. Hence with $Ku_i = N\,Ku$

$$(L/t)_i \approx \mathrm{const}/(Ku\,N)^2.\qquad\qquad (10.2-14)$$

With the above, the pitch to chord ratio at the hub follows from (10.2–13) with $\zeta_{AG\,i} = 1{,}4$ (or so). Usually L/t drops somewhat with the radius. This may raise the susceptibility of the outmost cylindrical section to cavitation in favour of a lower mass of blade and hence of torque about the pivot in consequence of centrifugal load. Further procedure for vane design, Cap. 10.2.10 and [10.11].

10.2.6. Rapids turbines for using kinetic energy only

10.2.6.1. Fundamentals, design, head, discharge

In its lowest head range, namely 1,5 to 2,5 m, and in its variant as tubular turbine, the KT can be employed to use only the kinetic energy of river rapids. The problem concerns

rapids with velocities of 5,5 m/s and more as they may occur, e.g., in the Amazon, values correspond to a head about 1,5 m. Such a turbine (Fig. 10.2.26) is kept i stream of a river, possibly by means of a float, anchored to the ground (Fig. 10.2

In these turbines the kinetic energy of the flow is exclusively used by diffusion in the tube. In the intake of this design the kinetic energy amounts to about 100% of the now-defined as $gH = (c_{II}^2 - c_I^2)/2$. Hence this part has to be made as short as possible minimize losses.

In a set without guide vanes before the runner and hence a whirl velocity c_{u1} past runner, the stay vanes, which support the bulb of the draft tube, may be used to null this whirl velocity up to the draft tube exit (Fig. 10.2.26).

Because of the low speed due to the small head, the application of a step up gear betwe turbine and generator seems to be advisable to reduce the cost of the generator.

This can be effected by a spur gear (Fig. 10.2.26) with a generator laterally displace within the hub. With such a simple gear, which any turbine maker is capable of machinin
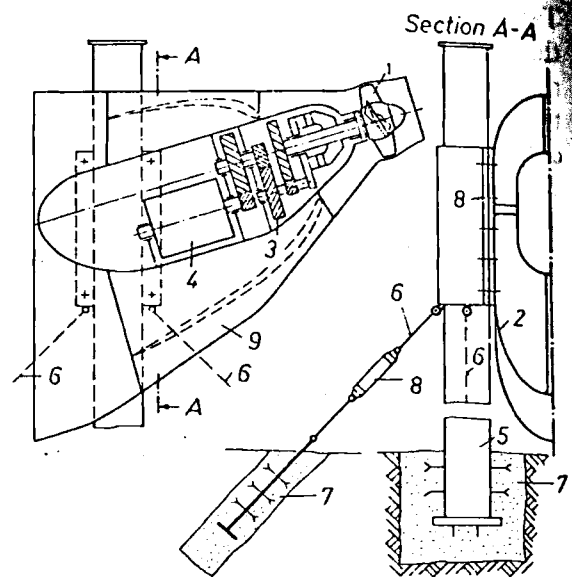
Section A-A

Fig. 10.2.26. Longitudinal section and cross section of a BT for river rapids. Author's proposal. 1 runner without guide apparatus; 2 bulb laterally squeezed to house a 3-stage step up spurgear 3 for the alternator 4; 5 stay tower; 6 stay cable; 7 tie rod in the rocky river ground (if existing); 8 adjustment screw; 9 curved stay vane to nullify the whirl past the runner.
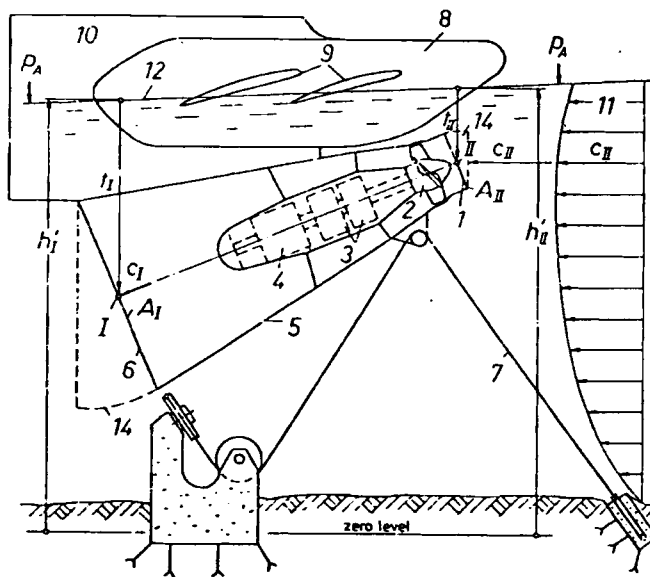
Fig. 10.2.27. Longitudinal section of a BT for river rapids with a 2-stage step up planetary-gear 3 for the alternator 4 in the bulb. 5 draft tube; 6 exit; 7 adjustable stay cables; 8 float; 9 aerofoils; 10 stabilizing fin; 11 inlet velocity profile; 12 river level. 1 intake, 2 runner, 14 eventual bends at inlet and outlet. At depth t_i and river level altitude h_i' given ($i = I, II$), the altitude of point i becomes $h_i = h_i' - t_i$. Proposal of author. Only possible in rocky bed.

432

in his own workshop, the maker does not depend on foreign suppliers in case of failure. But it can be done also by means of a planetary gear bringing the input and output shafts in line (Fig. 10.2.27), facilitating a streamlined hub.

In the case of a directly coupled generator (Fig. 3.4.29) it seems advisable, to pass the shaft through the bend of the draft tube, on which as it were the generator now rides.

The mooring of these sets must be so flexible as to allow the set to follow the river level (Fig. 10.2.26). The design of such a turbine has to start from the head, given by

$$Y = gH = [1 - (A_{II}/A_I)^2] c_{II}^2/2,$$ (10.2–15)

where c_{II} is the flow-averaged velocity at the intake II, A_{II} the cross sectional area of the latter, A_I the same of the exit I. Assume c_{II} to be uniformly distributed over A_{II}. Continuity gives the discharge as

$$Q = (\pi/4) D_{II}^2 c_{II}.$$ (10.2–16)

10.2.6.2. The optimum diameter

Since ground excavation here is no problem, the turbine runner is to be optimized with respect to efficiency. Inserting the above head and discharge with the abbreviation $\vartheta = A_{II}/A_I$ in the formula for $D_{op\,\eta}$ (10.2–4) gives

$$D_{op\,\eta} = 1,155 \{2(1 - \eta_D)/[K_0\,\varepsilon\,\omega\,c_{II}^2(1 - \vartheta^2)]\}^{1/7} \{\pi c_{II} D_{II}^2/[4(1 - N^2)]\}^{3/7}.$$ (10.2–17)

Combining both the terms with c_{II} in this relation and introducing the diameter ratio $\imath = D_{op\,\eta}/D_{II} = D/D_{II}$ then

$$D_{op\,\eta} = (1,155^7/\alpha^6) \{\pi/[4(1 - N^2)]\}^3 [2(1 - \eta_D) c_{II}]/[\omega\,\varepsilon\,K_0(1 - \vartheta^2)].$$ (10.2–18))

10.2.6.3. The installed power

H from (10.2–15) and Q from (10.2–16) yields the resulting power, shaft efficiency η, of i sets as

$$P_r = \varrho\eta Q\,i\,gH = \pi\,i\,\varrho\,D_{II}^2\,c_{II}^3\,\eta(1 - \vartheta^2)/8.$$ (10.2–19)

In general the diameter of the exit is known from the depth of the river. With the ratio $\vartheta = A_{II}/A_I$ between 0,5 to 0,1, an efficiency due to diffusion could be defined as $\eta_{ret} = 1 - \vartheta^2$, being between 0,75 to 0,99. Once ϑ is set, the inlet diameter follows from A_I known and $A_{II} = \vartheta A_I$. The power of one set is $P = P_r/i$.

Expressing P_r by (10.2–19), putting now $D_{II} = D_{op\,\eta}/\alpha$ with $D_{op\,\eta}$ from (10.2–18), the optimum angular velocity reads

$$\omega = \left[\frac{\pi\varrho\eta}{8(1 - \vartheta^2)}\right]^{1/2} \left[\frac{1,155}{\alpha}\right]^7 \left[\frac{\pi}{4(1 - N^2)}\right]^3 \frac{2(1 - \eta_D)}{\varepsilon K_0} \frac{c_{II}^{5/2}}{P^{1/2}}.$$ (10.2–20)

An example may illustrate the application of the above relations: Given $P_r = 10$ MW $= 10 \cdot 10^6$ W, $c_{II} = 8$ m/s (corresponding to a head of $H = 3,36$ m); $\vartheta = 0,1$; $N = 0,39$; $K_0 = 0,745$; $\eta_D = 0,85$; $\varepsilon = 0,03$; $\varrho = 10^3$ kg/m^3; $\eta = 0,85$; $D_I = 6,3$ m; $\alpha = 1,2$.

From this with $\vartheta = (D_{II}/D_I)^2$ the inlet diameter is obtained as $D_{II} = 2$ m. Then from $P = \pi\varrho D_{II}^2 c_{II}^3 \eta(1 - \vartheta^2)/8$, the output of one set: $P = 688 \cdot 10^3$ W $= 0,668$ MW. Hence the number of sets by $i = P_r/P = 14,5$, in round figures $i = 15$ sets. Inserting P in

(10.2 - 20) gives $\omega = 16.2$ rad/s and $n = (30/\pi)\omega = 155$ rpm. Hence the runner blade speed $u = 0.5\,\omega\,\varkappa\,D_{f1} = 19.4$ m/s. With the head the coefficient of blade tip speed $K_u = 2.43$. This rather high value corresponds to low head. The flow results from Cap. 10.2 as $Q = 25.2$ m³/s, whence with $gH = 31.8$ m²/s² the type number $n'_q = \omega\,Q^{1/2}/(gH)^{3/4} = 4.67$, or n_s about 1000 (see Table 10.2.1). Further $D = 2.4$ m; $c_m = 6.5$ m/s; $\beta_1 = 18.4$. Rotational speed realized: $n = 156$ for a grid with 60 Hz.

10.2.7. Some remarks about the runner chamber and distributor

The schematic elevation (Fig. 10.2.28) shows the proportions of the runner chamber. For the lower head range up to $H = 30$ m the throat ring has a semi-spherical form. Hence at least past the plane of the blade axis, the runner blade has a constant clearance. This arrangement facilitates an assembly and dismantling of the rotor.
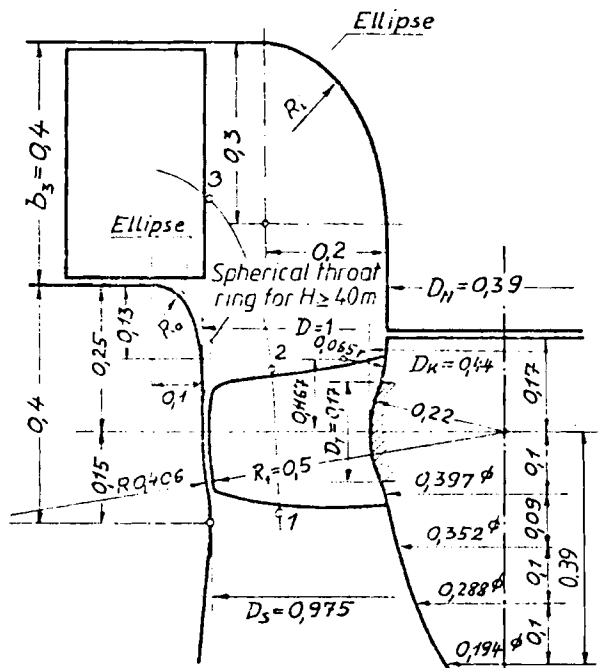
Fig. 10.2.28. Elevation of a KT with 4 to 5 blades.

For heads above 40 m, a spherical throat ring above the blade axis is preferred. This requires a separate insert of the throat ring which has to be removed before dismantling the runner, (Fig. 10.2.3).

In a welded design, the elliptic profile of the flow deflection shield on the head cover may be approximated by a polygon. To prevent stall and hence cavitation and unsteady flow at the outmost cylindrical runner vane section, the elliptic profile of the gate base ring cannot be approximated by such a welded polygon construction, even if this is made sometimes.

The flow before the runner through the vaneless space is determined by the gate position and the geometry of the distributor. This is treated in the following for the general case of a conical distributor under the assumption of axisymmetric flow but accounting for the streamline-linked loss.

10.2.8. Flow prediction in the vaneless space and distributor

I. The flow in the vaneless space between the gate and runner:
The following assumptions are made: Steady axisymmetric flow along the skeletons of the

434

gate vanes. Streamface-linked loss and moment of momentum. The loss is accounted for by assuming the gradient of absolute flow energy in an axisymmetric flow lamina of depth b with hydraulic diameter $2b$ to be $|\text{grad } Y_a| = \zeta c^2/(4b)$, where ζ is a loss coefficient, and c the absolute velocity at the station considered.

From the equation of motion grad $Y_a = c \times \text{curl } c$, the component in the n-direction, normal to the stream face becomes

$$(\zeta/4 b) c^2 n^0 = (c \times \text{curl } c)_n n^0,\tag{10.2-21}$$

where n^0 is the unit vector in n-direction. This leads to the following relation for c_m and c_u

$$dc_m^2/dn + c_m^2(2/R - \zeta/4 b) = -(1/r^2) d(c_u r)^2/dn + \zeta(c_u r)^2/(2 b r^2),\tag{10.2-22}$$

where the moment of momentum $c_u r$ due to a stream face is assumed to be known from a flow pattern preliminarily set and then improved, and the c_m distribution at the gate exit in n-direction (treated later on). R is the radius of curvature of the streamface in the meridian. The solution of the last equation is given by

$$c_m(n) = exp\left[-(1/2)\int_0^n f_1(x)\,dx\right]\left\{c_{ma}^2 + \int_0^n f_2(x)\,exp\left[\int_0^x f_1(y)\,dy\right]dx\right\}^{1/2},\tag{10.2-23}$$

where

$$f_1(n) = 2/R - \zeta/(4 b),\tag{10.2-24}$$

$$f_2(n) = -(1/r^2) d(c_u r)^2/dn - \zeta(c_u r)^2/(2 b r^2).\tag{10.2-25}$$

The values r, R and $c_u r$ are streamline bound and therefore functions of n. They are found by trial and error from a reasonable streamline pattern. $c_{ma} = c_m$ $(n = 0)$ results from the given flow by means of continuity

$$Q = 2\pi\int_0^{n_i} r c_m\,dn,\tag{10.2-26}$$

where n_i is due to the hub.

II. The flow within the vaned conical distributor: As a geometrical feature, the angle α is introduced in a plane normal to the gate axis between the vane skeleton and circumference. The gate stem makes an angle μ_0 with the axis of the turbine. At an arbitrary station, the meridional streamline makes an angle μ with the radius (Fig. 10.2.29). The assumed flow along the vane requires

$$c_u = c_m \cos(\mu - \mu_0) \cot\alpha.\tag{10.2-27}$$

Inserting this in (10.2-22) brings

$$dc_m^2/dn + (f_4/f_3) c_m^2 = 0,\tag{10.2-28}$$

where

$$f_3(n) = 1 + \cos^2(\mu - \mu_0) \cot^2\alpha,\tag{10.2-28}$$

$$f_4(n) = 2/R - (\zeta/4 b)[1 + 2\cos^2(\mu - \mu_0) \cot^2\alpha]$$
$$+ (1/r^2) d[r \cos(\mu - \mu_0) \cot\alpha]^2/dn.\tag{10.2-29}$$

ζ, r, μ and α are functions of n and linked to the flow pattern preliminarly set, and then improved by trial and error. Approximately $1/R = 0$, $\mu - \mu_0 = 0$, $\alpha = \text{const}$, $r = r_a$ $\sim n\sin\mu_0$. The solution of (10.2-28) is given by

435
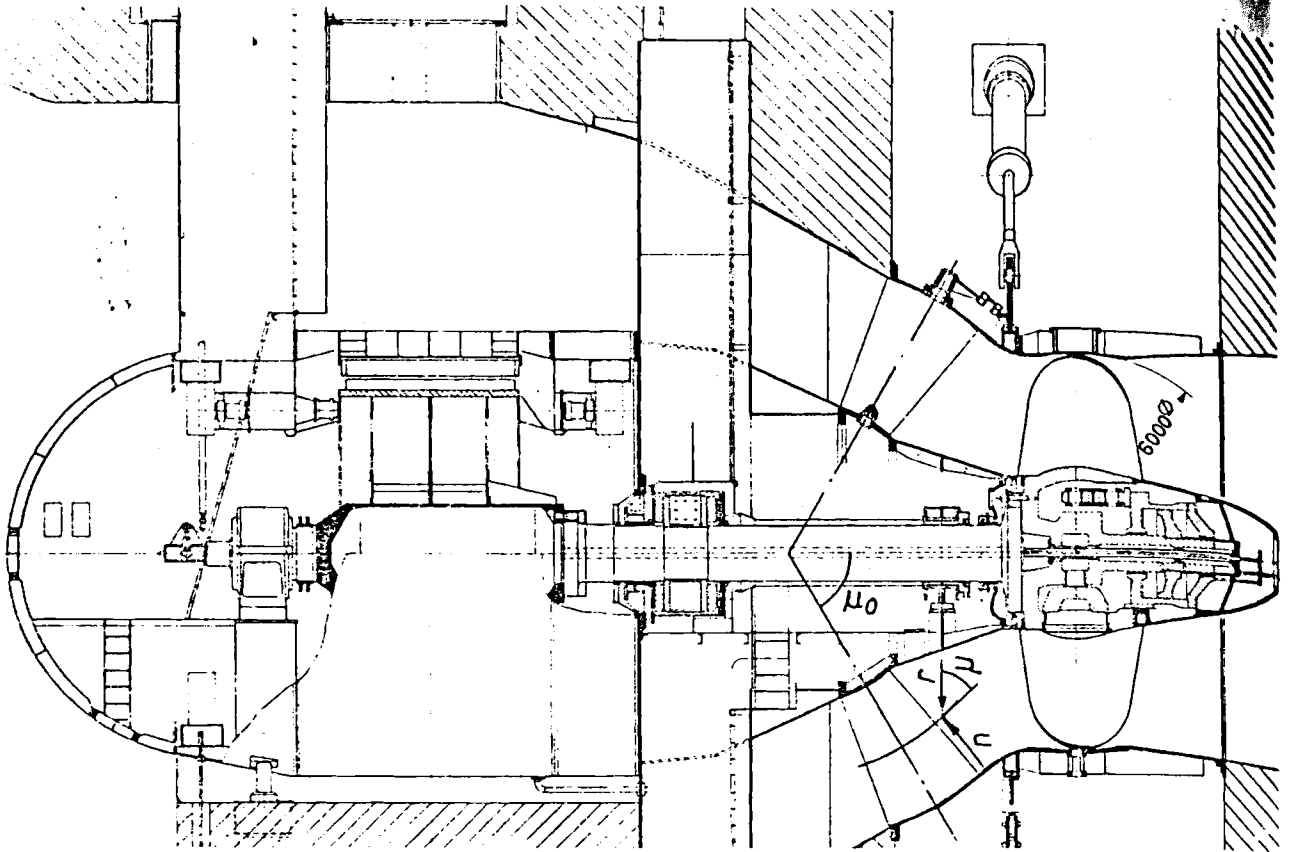
Fig. 10.2.29. Elevation of the BT at Altenwörth, Danube, Austria (owner Österreichische Donau-kraftwerke AG). $H_m = 13,57$ m; $n = 103,4$ rpm; $P_m = 41,2$ MW (Voith design). For mounting a special hatch of the alternator. 3 guide bearings. Conical guide apparatus with closing weight. $D = 6$ m. (Drawing courtesy Voith).

$$c_m(n) = c_{ma} \exp\left\{ -\tfrac{1}{2}\int_0^n [f_4(x)/f_3(x)]\,dx \right\},$$ (10.2-30)

where $c_{ma} = c_m$ ($n = 0$) is obtained from the known flow Q by continuity of the form (10.2-26).

Example: Axial distributor with $\mu = \mu_0 = \pi/2$, $\alpha = \text{const}$, $\zeta = 0$, $dn = -\,dr$. Now $f_3 = 1 + \cot^2\alpha = 1/\sin^2\alpha;\ f_4 = -\,(2/r)\cot^2\alpha;\ f_4/f_3 = -\,(2/r)\cos^2\alpha$ and

$$-\int_0^n (f_4/f_3)\,dn = -\,2\cos^2\alpha \ln(r/r_a) = 2\ln(r_a/r)\cos^2\alpha.$$

Hence $c_m = c_{ma}(r_a/r)^{\cos^2\alpha}$ and $c_u = c_{ma}\cot\alpha\,(r_a/r)^{\cos^2\alpha}$. Continuity yields

$$c_{ma} = Q(1 + \sin^2\alpha)/\{2\pi r_a^2[1 - (r_i/r_a)^{1+\sin^2\alpha}]\}.$$

A 3-dimensional calculation of the flow from the guide vane to the runner was presented by Protic [10.146]. In order to reduce the loss and to obtain a peripherally uniform influx, a model of the flow in a semi-spiral casing was developed by Corniglion [10.147]. An experimental analysis of the flow in the axial region of the runner was given by Bettochi [10.148].

436

10.2.9. Tidal power turbines, layout

I. General remarks: The low head due to the tides predetermines the axial turbine in its design as a BT, ST or a TT (see Fig. 10.2.15) to harness tidal power. For the case of double action plants with one basin (Fig. 10.2.30, 1 b), this is done by a machine capable of direct and reversed turbining, and – if necessary – also of direct and reversed pumping, see Fig. 1.6.2.

Therefore the special features of such an axial tubular pump-turbine for direct and reversed flow in both the modes of operation are considered.

Imagine a turbine of the bulb type (Fig. 10.2.15). The flow enters the runner from the side of the bulb with a whirl produced in the stay and mainly in the guide vanes of a conical distributor. In this case of a so-called direct flow whilst turbining, the draft tube operates as a diffuser. Obviously this works at a higher efficiency as a turbine than under reversed flow, when the gate operates as a diffuser.

This direct turbining usually is combined with a flow from the reservoir to the ocean [10.149]. If the basin is situated at the mouth of a river, then in consequence of the latter's energy, larger work is done, combined with a higher efficiency.

When reversedly turbining, the inlet whirl of the rotor vanishes, as the draft tube is not equipped with vanes. Then the channels between the guide vanes operate, even if under modest pressure recovery, as a diffuser. For the design of gates, it is important that in emergency they close tight.
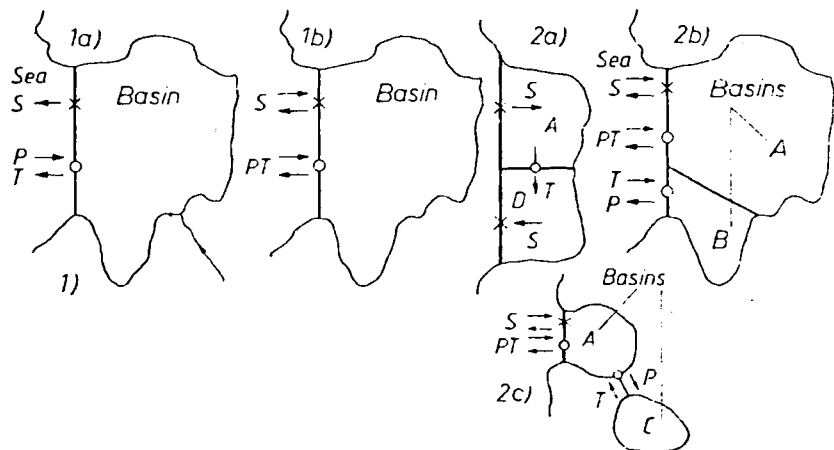
Fig. 10.2.30. Various tidal schemes with constant geometry ducts at intake and flow off. Notations: S → spillage (sluicing) in certain direction →; S ⇄ spillage (sluicing) in both directions; T → turbining in certain direction →; P → pumping in certain direction →; PT ⇆ pumping and turbining in both directions. (In each case, pumping can be omitted.) 1 Schemes with 1 basin: 1a single effect (action); if the basin has an inflow, T: basin-sea; P: sea-basin; S: basin-sea. If the basin with or without an inflow: P, T, S in arbitrary direction; 1b double effect (action): T, P, S subsequently in direction sea basin and vice versa. 2 schemes with 2 basins; 2a single effect (action): No P; S, T in the same direction (A head water pond, D tailwater pond). 2b between the sea and the basin A double effect with S, P, T subsequently in the direction sea basin and vice versa. Moreover between the sea and the basin B single effect T and P. Pool B emptied by P. Then for peak load T at relatively high head. 2c between the sea and the pool A double effect with S, P, T subsequently in the direction sea-basin and vice versa. Upper pool C (requiring mountains near coast) filled by surplus energy through P. For peak load T pool C to A (or sea). ⊙ power house.

Therefore nearly untwisted vanes are needed. For the different operations and the corresponding gate positions, the stroke of the gate servomotor must be rather long. However this can be obtained easily on a stationary part.

Contrary to the above, the rotor with its overhung design needs a blade adjustment mechanism with the smallest possible stroke. Therefore it seems advisable to operate the pump-turbine under all its modes of operation with nearly one and the same position of the rotor blades.

For a lack of sufficient time between the different operations, due to speeds, reversed to each other, the rotor vanes should also be capable of operating as a hydraulic brake. Thus a pitch to chord ratio below 1 should enable a turnover of the blades through the closed position.

II. Some peculiarities of the velocity triangles during direct and reversed turbining and pumping: Contrary to the use made so far in this book, the rotor edge towards the reservoir is denoted by subscript 2 and the opposite edge with 1.

1) Direct turbining: Flow from the distributor to the draft tube. Vane angle at overgate about 70°. On the rotor inlet, a whirl in the sense of speed u. Relative flow at rotor inlet more inclined to the circumference than at the exit. Zero whirl at the rotor exit ($c_{u_1} = 0$). Hence (Fig. 10.2.31.1) a forward curved rotor vane is required. Flow from basin to ocean.

2) Direct pumping: Flow from basin to ocean. Gate angle of 90° facilitates a vanishing whirl at the rotor inlet. At the rotor exit, whirl is in the sense of rotation. Since this gives a bad pressure recovery, also a gate angle of more than 90° may be applied, which causes a whirl at the rotor inlet contrary to its speed but avoids the whirl at the outlet. Rotation in the sense of case 1). Compared with case 1) the rotor requires backward curved vanes (Fig. 10.2.31.2).

3) Reversed turbining: Flow from ocean to basin and from draft tube to gates. Rotation reverses its sense compared with 2). Therefore fast braking is required at the end of the foregoing operation 2) by turning the blades through its zero position in a plane normal to the axis. The gates now opened by about 90° operate as a part of diffuser. For the generation of torque, the whirl at the rotor exit must be opposite to the latter's speed, since $c_{u_1} = 0$. Now backward curved vanes required as in case 2) (Fig. 10.2.31.3).

4) Reversed pumping: Flow from ocean to basin. Zero whirl at rotor inlet. Hence at the rotor exit, whirl is in the direction of rotation. Gates, now operating as a part of a diffuser, make an angle about 90° with the circumference. Forward curved rotor vanes are required (Fig. 10.2.31.4), as in case 1).

To reverse the speed for transition from 4) to 1), a turnover of rotor vanes for braking is required. Fig. 1.6.2 shows the timing of the operations 1 to 4 needed for a one pool double effect tidal power plant, e.g. the French "Rance".

Concluding, the following requirements can be stated for the design of a tubular pump turbine, for direct and reversed flow, in both the modes of operation, for such a tidal power plant:

a) The stroke of the gate must enable a gate-position of about 90° with the circumference. The gate vane must be rounded at both its ends, since they may both serve as entrance (Fig. 10.2.31.5 a).
b) The rotor vane adjustment must enable a vane position of about 20° with the circumference for normal operation and a position of -10° for braking (Fig. 10.2.31.5 b).
c) The required camber of the rotor blade is the same for direct turbining and reversed pumping, namely that due to forward curved blades. For the other two operations

438

Fig. 10.2.31. Required position, camber and rounded inlet edges for the gates and the rotor blades at the following 4 modes of operating: 1 direct turbining (basin-sea); 2 direct pumping (basin-sea); 3 reversed turbining ocean-basin; 4 reversed pumping ocean-basin. 5 compromises to be made for all the 4 modes of operating mentioned previously: a large stroke of gate and gate blade rounded on both ends; b rotor blade double cambered and rounded on the both ends. For hydraulic braking: pitch/chord ratio smaller 1.
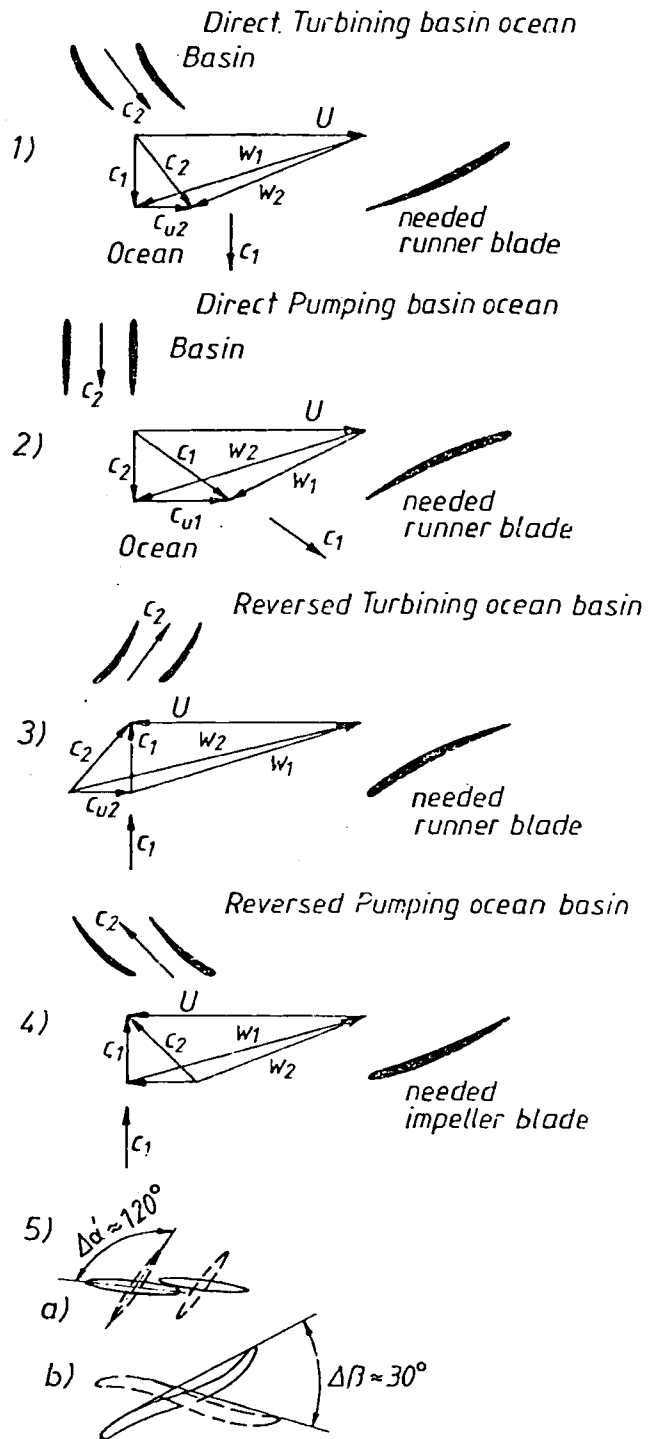
namely reversed turbining and direct pumping, the opposite camber is required. To overcome this discrepancy, double-cambered blades are realized as a compromise with both ends rounded, in the Rance tidal power plant [10.149], Fig. 10.2.31.5.

Another compromise would be the use of non-cambered skeletons. Tests made by Ravindran [10.150] showed clearly the superiority of this double-cambered solution compared with non-cambered solution with one blade end sharpened.

Since the suction face of the rotor blade is oriented towards the draft tube during the

operations 1) and 4) and oriented towards the gates during the operations 2) and 3), both the faces of the rotor blade must be finished smoothly so as to function as a suction face.

d) The guide bearings of the set have to enable lubrication in both senses of rotation.
e) Since the axial thrust changes its direction when the head water changes from the basin to the ocean, the set needs two thrust bearings for both axial flow directions.
f) The distributor with its adjustable gates must operate as a diffuser in the case of the reversed turbine and direct pump flow. Therefore both ends of the distributor vanes must be profiled carefully. Because of the rather poor pressure recovery of a distributor as a diffuser the efficiency of a machine operating that way is lower than that of a machine operating the other way with a draft tube as a diffuser.

Hence best efficiency can be achieved only, when the flow direction is retained. This can be done either by complicated bifurcations and valves at both ends of the machine (also draft tubes which may be turned on hinges have been proposed, surely not reliable) or by a single action working cycle (Fig. 10.2.32). In the largest tidal power unit of Annapolis Canada (Fig. 10.2.22) designed by Sulzer Escher Wyss the single action was preferred of using a Straflo turbine with rim generator, [10.32].
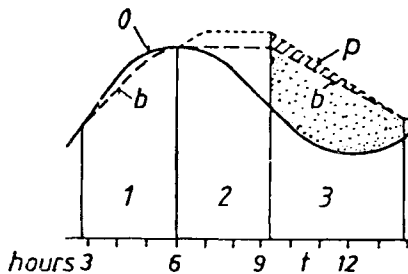
Fig. 10.2.32. The sequence of operating modes in a tidal power plant with 1 basin and single effect (action): 1 filling; 2 waiting plus eventual pumping; 3 turbining. 0 level sea; b level basin; p level basin with pumping. Utility lifted by some sets suited to return flow. (Drawing courtesy EdF).

III. The energy gain by additional pumping: Imagine the head during pumping changes parabolically with time according to $H_P = k t^2$. When H_P has reached a value H_{P0} after a period t_P, turbining starts. Whence $k = H_{P0}/t_P^2$. Assuming an electricity rate k_e, efficiency η_P, and accounting for unit flow Q_{11P} whilst pumping, the expenditure during pumping becomes

$$K_P = (k_e/\eta_P) Q_{11P} \varrho (H_{P0} g)^{3/2} t_P D^2 .$$ (10.2-31)

When the plant turbines without pumping during the period t_T, the following profit is made by the sale of energy at a constant turbine efficiency η_T and electricity rate k_e with a unit flow Q_{11T} under turbining at a head H_{T0}

$$K_T = k_e \eta_T Q_{11T} \varrho (H_{T0} g)^{3/2} t_T D^2 .$$ (10.2-32)

Then generating the same time t_T with a head increased by ΔH, as a consequence of pumping would increase the profit by

$$\Delta K_T = (3/2) k_e \eta_T Q_{11T} \varrho (H_{P0} g)^{3/2} t_T (1 - \Delta H/H_{P0}) D^2 .$$ (10.2-33)

For profitable pumping the ratio $\Gamma = \Delta K_T/K_P$ must be larger than one. Hence

$$\Gamma = \Delta K_T/K_P = (3/2) \eta_P \eta_T (Q_{11T}/Q_{11P})(t_T/t_P)(1 - \Delta H/H_{P0}) > 1 .$$ (10.2-34)

Assuming $Q_{11T}/Q_{11P} = 1,3$; $\eta_T = 0,9$; $\eta_P = 0,8$; then the condition $\Gamma > 1$ leads to $(t_P/t_T)(1 - \Delta H/H_{P0}) > 0,72$. This gives for $\Delta H/H_{P0} = 0,2$ the time ratio $t_T/t_P > 0,9$. This proves the rule that to make a profit by pumping, the duration of turbining should be equal or larger than that of pumping.

440

IV. Problems with two basins: A type of plant not made to date may be between two reservoirs (Fig. 10.2.30.2 a). The one is kept at high level by connecting it with the ocean during a time period from somewhat before high tide up to high tide. The other is kept at low level by connecting it with the ocean during a period from somewhat before low tide up to low tide. This is effected by sluice gates.

Even if the flow is now more continuous, this arrangement also shows the general disadvantages of tidal power. The first is the linkage of power production to the lunar position when there is no storage capacity, and hence the impossibility to cover peak load demand. The second is the rather low head and hence large and expensive sets.

This situation can be improved, when the topography permits it. by building a second basin C above the basin of a one basin plant in the neighbourhood of the latter (Fig. 10.2.30.2 c). Imagine this second reservoir, whose time-averaged level elevation above the first is H_P to be filled during a period t_P, when the electricity rate k_{eP} is low, by a flow Q_P at a pump efficiency η_P. Hence the expenditure of this filling $K_P = k_{eP} \varrho Q_P g H_P t_P / \eta_P$.

This stored energy may be used to cover peak load demand, electricity rate k_{eT}, during the period t_T, under a time-averaged head H_T, flow Q_T, efficiency η_T. Hence the earning by the sale of energy $K_T = k_{eT} \varrho Q_T g H_T t_T \eta_T$. Imagine the live storage volume of the upper basin $\Delta V = Q_P t_P = Q_T t_T$. Then the surplus made during both the last operations

$$S = K_T - K_P = \varrho \Delta V g (k_{eT} H_T \eta_T - k_{eP} H_P / \eta_P).$$

In the utmost favourable case, pumping is during high tide and turbining during low tide. Then $H_T = H_P + \Delta H$, ΔH being the tidal stroke. Then the maximum surplus becomes

$$S_{max} = \varrho \Delta V g H_P k_{eT} \eta_T [1 - (k_{eP}/k_{eT})/(\eta_P \eta_T) + \Delta H/H_P]. \qquad (10.2-35)$$

The base load produced by this plant with live storage volume ΔV_1 brings under the tidal stroke ΔH at least

$$E_{min} = \varrho \Delta V_1 g \Delta H k_{eP} \eta_T. \qquad (10.2-36)$$

Hence the ratio of maximum surplus by means of an additional basin for pumped storage to minimum earning with a tidal cycle without storing capacity becomes

$$S_{max}/E_{min} = (\Delta V/\Delta V_1)(H_P/\Delta H)(k_{eT}/k_{eP})[1 - (k_{eP}/k_{eT})/(\eta_T \eta_P) + \Delta H/H_P]. \qquad (10.2-37)$$

Example: $k_{eT}/k_{eP} = 2$; $H_P/\Delta H = 10$; $\Delta V/\Delta V_1 = 10$; $\eta_P = 0.85$; $\eta_T = 0.9$; $S_{max}/E_{min} = 89.3$. However, this procedure suffers from a lack of availability of the plant.

A special form of the multi-pool scheme is the two-pool scheme proposed by *Shaw* in his paper on: "Some considerations of a possible new role for tidal power", presented at the international conference on the utilization of tidal power in Halifax, 1970 (see Fig. 10.2.30).

Here the smaller pool, basin B, is pumped empty with surplus energy, so that for peak load production, water can be passed through the turbines from sea to basin at a relatively high head. A large pool, basin A, is operated in single or double effect in the same way as described above.

V. Plant with a central generator: The usually small tidal range requires even for the highest tidal range, e.g., Rance, a runner tip diameter of 5 m for 10 MW output. Therefore, *A. Fischer* has proposed one central generator should be driven by a large number

of (may be up to 100) turbines by means of hydrostatic gear to save first cost. Here each turbine generates a pressurized oil flow by a multipiston bevel disk pump.

The flow resulting from all the turbines of one group propels the rotor of the central generator.

This can be done, e.g., by a multipiston bevel disk positive displacement motor. By adjustment of the bevel disk in the central generator, the gear ratio between turbine and alternator can be changed under constant alternator speed.

Thus the adjustable bevel disk allows an adaptation of the turbine's optimum speed to the head, which varies continuously in a tidal power plant. The improved efficiency has to compensate the cost and loss of energy due to the gear. Moreover such a gear enables an economically high speed for the alternator, which would be cheaper than a slowly rotating direct coupled one.

VI. Plant with turbines for sluicing operation: A further increase in energy production can be achieved if the turbines may run also in the sluicing operation to fill or to empty the basin, when the water levels of the sea and the basin are nearly the same.

VII. Economic considerations: In his paper "Choice of hydroelectric equipment for tidal energy" presented at the Korean tidal power symposium, Seoul in 1978, H. Miller reported that the direct costs of different Fundy Bay schemes are distributed as follows:

a) Electromechanical equipment 46,7%,
b) Power house 21,6%,
c) Sluiceways 13,7%,
d) Dikes 16,3%, e) Fixed site cost 1,7%.

Hence the hydroelectric equipment, directly influences about 50% of the costs, and indirectly about 35%, since the power house and sluiceways depend largely on the machine's sluicing capacity.

For the single pool single effect scheme, an optimally designed turbine can be used. However, within the usual range of operation $H/H_{op} = 0,2$ the pump efficiency of the turbine goes down to 50% of the turbine's bep efficiency. If therefore there is no pumping a fixed blade propeller would suffice.

This reduces the machine price by about 12%, together with lower maintenance costs. Since sufficient discharge is always available, the turbine can always operate at its bep.

When compared with the single effect scheme, the double effect scheme, as a compromise, results in a lower mean efficiency and in a lower energy output per tidal cycle. Accordingly a larger number of units is required. This decreases the benefit-cost ratio. Hence, the latest results of studies on Fundy Bay have reconfirmed the single effect schemes to be the most economical.

All attempts to eliminate, e.g., by added pumped storage, the intermittent energy production, are unsatisfactory, since they require:

1) Increase of investment,
2) more complicated hydroelectric equipment,
3) higher maintenance costs,
4) shorter working life.

Therefore tidal power can be economic when it solely converts the available tidal energy directly into electric energy.

VIII. The superiority of straflo design compared with bulb design: Again following Miller, simplicity and compactness are requirements to make use of caisson construction, which has proved so successful in the building of dikes. These requirements are not fulfilled by the vertical Kaplan turbine or the tubular S-turbine.

442

The use of bulb turbines for tidal power to date originated from the fact, that the large Straflo turbine needed was not available, and that the bulb turbine can fulfil some of the requirements of a tidal power machine. However bulb turbines have some limitations.

Consider the generator output

$$P = K D_R^2 L n,$$

where K is the compactness factor, D_R the rotor tip diameter, L the rotor length, and n the speed. The slim bulb, hydraulically required, makes the generator rotor diameter D_R considerably smaller than the turbine runner diameter. Therefore, the generator length L, and the compactness factor K must be increased, which both increases the temperature. This may require complicated water-cooling in a badly accessible generator even at smaller outputs (about 10 MW).

The small rotor diameter results also in a low inertia of the set. This contradicts the requirements of stable regulation, especially when the plant supplies a grid by itself. Moreover a large inertia reduces the consequences of power swing, a tidal unit is subjected by wave-induced pressure fluctuations. It would help also to reduce the fluctuating loading on the critical connections of the poles and windings due to this power swing. These problems yield a lower limit for the runner diameter, which lies, according to recent studies on Fundy Bay, at 7500 mm.

In the compact bulb, it is difficult to carry out extensive repairs, especially on the stator. Therefore the generator should be removable through a special hatch on the top of the bulb (Fig. 10.2.11). Removing the generator through the turbine pit requires removal of the whole unit, which alone takes about 6 months for units of the size needed.

In the Straflo turbine all the disadvantages mentioned above have been eliminated, namely

1) 50% larger generator diameter than for a BT; effectively cooled generator,
2) no limitation to size of turbine and generator,
3) 3 to 4 times as much inertia makes the generator more stable and stabilizes the regulation,
4) turbine and generator in the same vertical plane require only 1 erection pit,
5) good accessibility to generator.

A comparison by *Miller* between a straflo turbine plant having 18 units, 25 MW each, and a bulb turbine plant, having 30 units, 15 MW each, results in the following: At a width of 421 m for the Straflo plant, the bulb plant has a width that is 1,27 times larger, and a price of hydro electric equipment, that is 1,5 times larger than the respective values of the Straflo plant. Hence the Straflo turbine seems to be the tool to utilize tidal power at reduced cost.

10.2.10. Runner design, simple procedure

I. Runner vane design by cascade theory: For given velocity triangles with their coefficients Ku, Kw_1, Kw_2, $K \Delta c_u$ from 10.2.5.3, the maximum lift coefficient at the hub $\zeta_{AG} = 1,4$, with the vane number z from Table 10.2.1, the known hub diameter D_N, the pitch chord ratio from relation (10.2-13) gives the chord L_i at the hub.

Runner diameter D, vane number z, the hence given tip pitch and the pitch to chord ratio: from Table 10.2.1 yields the chord L_a at the runner tip. Since the inlet edge and rear edge of the runner vane should be as straight as possible for reasons of stable flow and vane strength, the pitch chord ratio and hence the chord is given for an arbitrary cylindrical section, for which the velocity triangles are also known. The relation (10.2-13) yields the lift coefficient in the cascade ζ_{AG}.

Then from Table 6.2.1 the cascade coefficients C_1, C_2, C_3, C_4 are determined as functions of t/L and the angle β_0 which may be approximated to β_{∞} from the triangles, as the angle $w_{\infty} = (w_1 + w_2)/2$ makes with the circumference. Then from (6.2–47) the physical angle of attack $\delta_0 = \zeta_{AG}(C_4/C_1)$ is obtained.

Now the vane skeleton must be set. This may be done with respect to pressure distribution (cavitation sensitivity) or the hydrodynamic torque about the pivot of the blade. Then determination of the angles ϑ_i the skeleton makes with its chord at Birnbaum's 3 stations (Cap. 6.2–37). Hence K_1, K_2, K_3 and then the zero lift angle of attack $\delta(F_A = 0)_G$ are obtained by (6.2–4). Thus the angle the chord of the cylindrical section makes with the circumference $\beta_c = \beta_{\infty} + \delta(F_A = 0)_G$.

The skeletons then are built up so that the centre of gravity of each cylindrical section coincides with the blade axis.

For blades with a usual standard profile such as those of the basic Göttinger series or the basic *NACA* series [10.151] the centre of gravity is aproximately a distance 0,4 L from the profile's leading edge.

Hence there is no bending stress at the blade's pivot due to centrifugal load of the blade. The real thickness of the blade must be determined at first on the base of the blade on the hub.

Here the bending moment as the relevant load caused by the hydrodynamic lift may be approximated as

$$M_{bh} = (\pi/4\,z)\,\eta_i \varrho\, gH\, D^3\,[1/3 - (N/2)(1 - N^2/3)].\tag{10.2–38}$$

N being the hub to tip diameter ratio, z the vane number. The root cross section of the blade on the hub disk is nearly a rectangle, whose length equals the diameter D_T of the blade disk (Fig. 10.2.33). Roughly $D_T = 0,4\,D/z$. This gives the sectional modulus of this cross sectional area as $h_{mi}^2 D_T/6$, where h_{mi} is the maximum blade thickness at the hub section.

With the carefully set admissible bending stress σ_{ad} (which is strictly speaking only about 30% of the stress acting there, as a consequence of centrifugal load-induced torque, torque due to hydrodynamic lift, to mention the most important ones), the maximum blade thickness is

$$h_{mi} = [6\,M_b/(\sigma_{ad} D_T)]^{1/2}.\tag{10.2–39}$$

According to *Barp* and *Keller* [10.152], in blades of alloyed chromium steel, the assessment of σ_{ad} has to account for fatigue effects. To reduce the latter a fillet is provided along the corner between the disk and the blade. Moreover a rounded cut out should be provided at the corner between the disk and blade in the plan view.

This cut out has to be closed by an insert bolted on the blade to prevent leakage between pressure and suction face of the blade.

The thickness distribution of the real profile of a given cylindrical section based on a certain series, e.g., *NACA* is set so as to strain the chosen model profile normal to its centre line at any station proportional to the ratio of calculated maximum thickness, to maximum thickness of the model profile.

The maximum thickness required at an arbitrary cylindrical section h_m, drops continuously with the radius from its maximum h_{mi} on the hub towards a value h_{ma} at tip diameter, tolerable for leakage and tip clearance cavitation erosion. To reduce the latter, an anti-cavitation fin may be welded along a part of the blade's tip (see Fig. 10.2.25). The fin is usually worn off by tip clearance cavitation and therefore in general not provided.

444

Fig. 10.3.21. Hill diagram of a FT with $n_q = 70$ in the bep, obtained by tests on a model with $D = 0,455$ m runner diameter. With relative velocity w and angle β with circumference at runner inlet at different operating points according to the measurements of *Schlemmer*, in a mean flow plane [5.18]. Beginning and increase of surging in the runner indicated by arrows A: suction face, shroud; B: suction face, hub; C: suction face, shroud unsteady flow, pressure face shroud, and hub; E: suction face, shroud.

tum drops nearly linearly from the leading inlet edge (there having a magnitude $c_{u2} r_2 = (gH \, \eta_u - c_{u1} r_1 \, \omega)/\omega$) towards the value $c_{u1} r_1$ at the outlet edge of the rotor. The above tests also show the derivative of angular momentum along a normal n to the meridional streamlines $(\partial (c_u r)/\partial n)$ to be vanishing small at the bep and away from the leading edge of the runner vane, see below.

For the case of the bep $c_{u1} = 0$. Hence the whirl at a certain station with the radius r,

$$c_u = [gH \, \eta_{u \, op} - \varDelta Y_a(s_m)]/(r \, \omega), \qquad (10.3-20)$$

where $\varDelta Y_a(s_m)$ is an arbitrary steadily falling function vs the meridional stream path s_m, measured from the inlet edge and being $gH \, \eta_{u \, op}$ at the outlet.

Such an arbitrary drop of the flow energy Y_a within the runner in the streamwise direction can be set only along one elementary turbine. The relation (6.5-4) for the distribution of the meridional velocity as a function of the distribution of angular momentum normal to the streamlines shows that only in the case of a loss free flow and $\partial (c_u r)/\partial n = 0$, the distribution of the meridional velocity in the n-direction (normal to the meridional streamlines) becomes independent of the $c_u r$ distribution normal to the streamlines.

Assuming hence this simple case, then two things have to be satisfied:

a) The $c_u r$ distribution along the other elementary turbines has now to account for the one prescribed $c_u r$-course such as to have always $\partial (c_u r)/\partial n = 0$. See also tests [5.18].

b) According to (6.5-4), the c_m distribution now remaining, follows the law $dc_m/dn + c_m/R = 0$, where R is the radius of curvature of the streamline in the meridian. The last mentioned differential equation for c_m is that of a potential flow in the meridian. Hence strictly speaking the graphical method described in Cap. 5.2 has to be employed to obtain the more correct distribution of the meridional velocity instead of the rough estimate with the factor ζ. But this holds good only for a design with $\partial (c_u r)/\partial n = 0$.

475
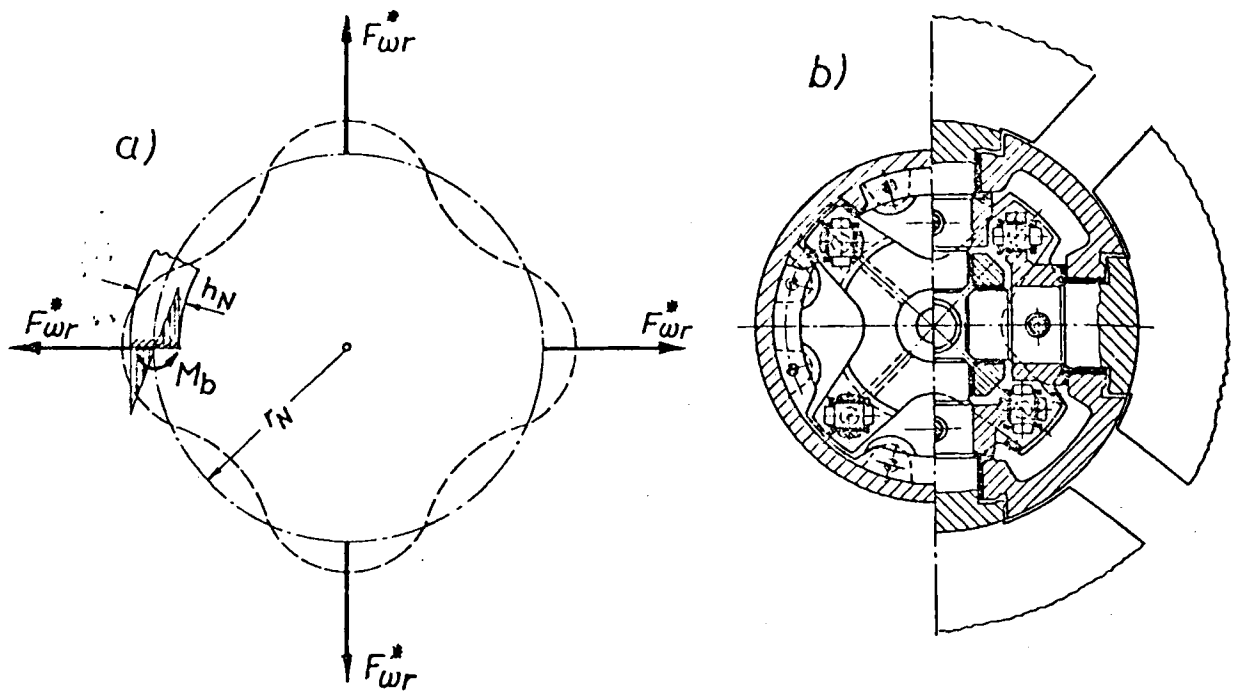
Fig. 10.2.34. Loads on the hub of a KT. a) Deformation of the hub under the centrifugal load of blades and their linkage at runaway. Highest bending moment in the meridional section of the blade axis, needing a certain sectional modulus. b) Cross section of the hub. An inclination of the links requires axial guide bars in the hub for the guide cross to transmit a tangential force on the hub, thus twisting the latter.
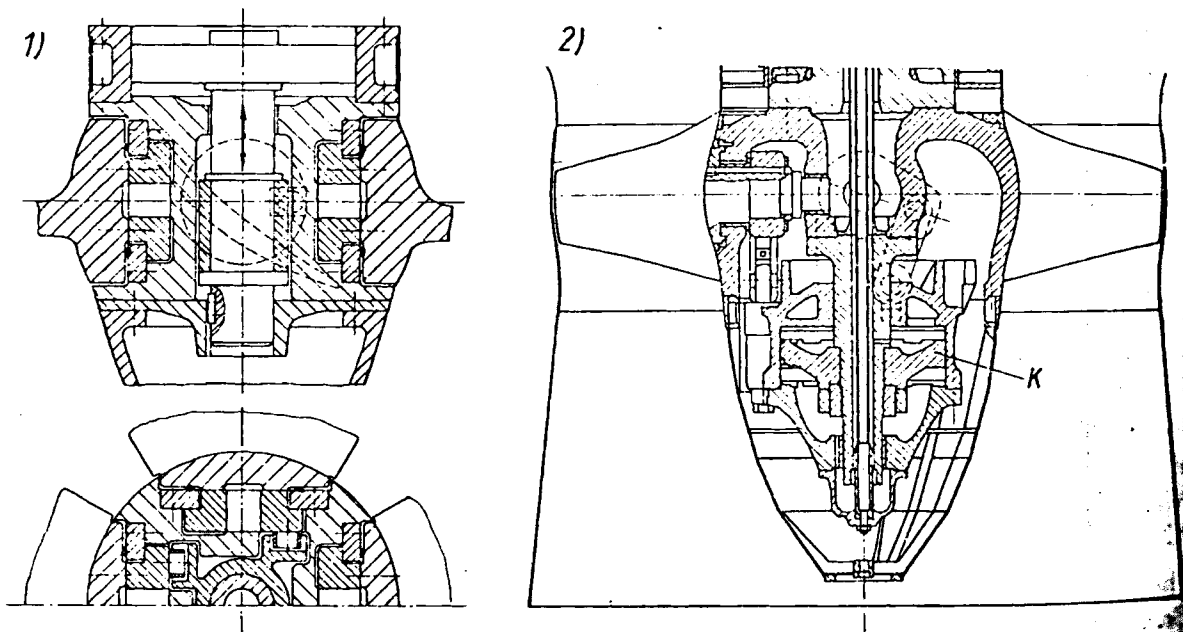
Fig. 10.2.35. Various blade drives. 1) Block and link mechanism. First applied by Englesso (KaMeWa) in Swedish plant at Lilla Edet in 1925. Compact design, but more wear than in case 2 Servomotor above the blades moves the cross head. Hub wall additionally loaded by oil pressur Large distance of the rotor's centre of gravity from the centre of the next guide bearing. 2) Cro pin drive with lever and link here from servomotor cylinder with a piston bolted to the hub. Hu wall relieved from oil pressure. Rotor centre shifted more towards the bearing centre than in ca 1). In the case of a BT cylinder is easily accessible. Disadvantage: cylinder wall additionally p loaded by the adjusting force of links. Here KT Ribarroja, Spain (Design Sulzer Escher W $H = 34$ m; $n = 125$ rpm; $P = 67$, 8 MW; z 6 blades. (Drawing b) courtesy Sulzer Escher Wys
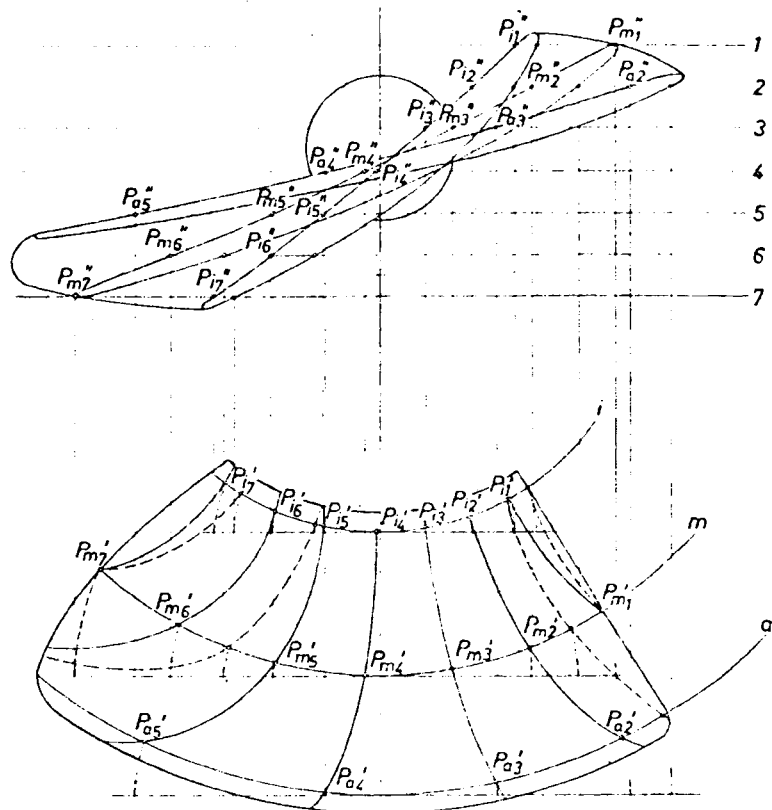
surface along a pattern section. To obtain one point of this section proceed as follows: Drop a perpendicular from point P''_{m2} of the rolled out cylindrical section in its elevation onto the plan. There is a tangent, which touches the circle of this cylindrical section at its intersection with the blade axis. Then roll up the straight section of this tangent between its point of contact and the projection of P''_{m2} onto it on the circle of the cylindrical section. This gives the point P'_{m2} of the pattern section in the plan.

In the elevation the formation of points along a certain pattern section is on a perpendicular to the turbine axis. In the plan this formation of points makes a curved line.

To obtain a smooth surface of the blade it seems advisable to make an amplified drawing and to connect the points obtained by curves with a curvature that varies continuously (spline curves).

10.3. The project and construction of Francis turbines (FT) with hints at Pelton turbines (PT)

10.3.1. General remarks

Mixed flow (semi axial) turbines, named after J. B. Francis (who only described the behaviour of a forerunner of the actual Francis turbine (FT), a simple radial centripetal turbine, based on a patent of S. Howd, USA) form the backbone of hydro electricity generation in the world. These turbines, with their head range of $(3)40\,\mathrm{m} < H$ $\cdot\,500(750)\,\mathrm{m}$ predominate in the range of available net head, which possesses the largest portion of usable potential.

447

Therefore at present FTs attain the largest output, as seen in the examples of Fig.
Fig. 3.4.16, and the Figures 10.3.1 to Fig. 10.3.8, which attains now a value of ro
800 MW or 1 100 000 hps. This is the largest output a one-stage turbomachine.
Contrary to the axial turbine with its percentage reaction up to 80(90)%, the FT
a reaction machine, has a percentage reaction of about 50%.

In former days it was and is still found in micro plants, heads down to 3 m. 20 years
the behaviour of a FT model with 4 MW under 650 m head was tested by Ulith [10.
at Parthenen, Austria (owner: Vorarlberger Illwerke). W. Meier [10.153] made a serio
study of the construction of a FT in a spherical casing for 1000 m head, which show
work as a pump-turbine (see Fig. 10.3.9). The 4 turbines with the highest head of this typ
in service operate in Rosshag, Austria $H_m = 670$ m, $P = 58$ MW, $n = 750$ rpm
Fig. 10.3.10, designed by Escher Wyss and Andritz, Austria. At the moment Sulzer Esche
Wyss have an order for two 180 MW FTs for the Austrian plant Häusling [10.193] in the
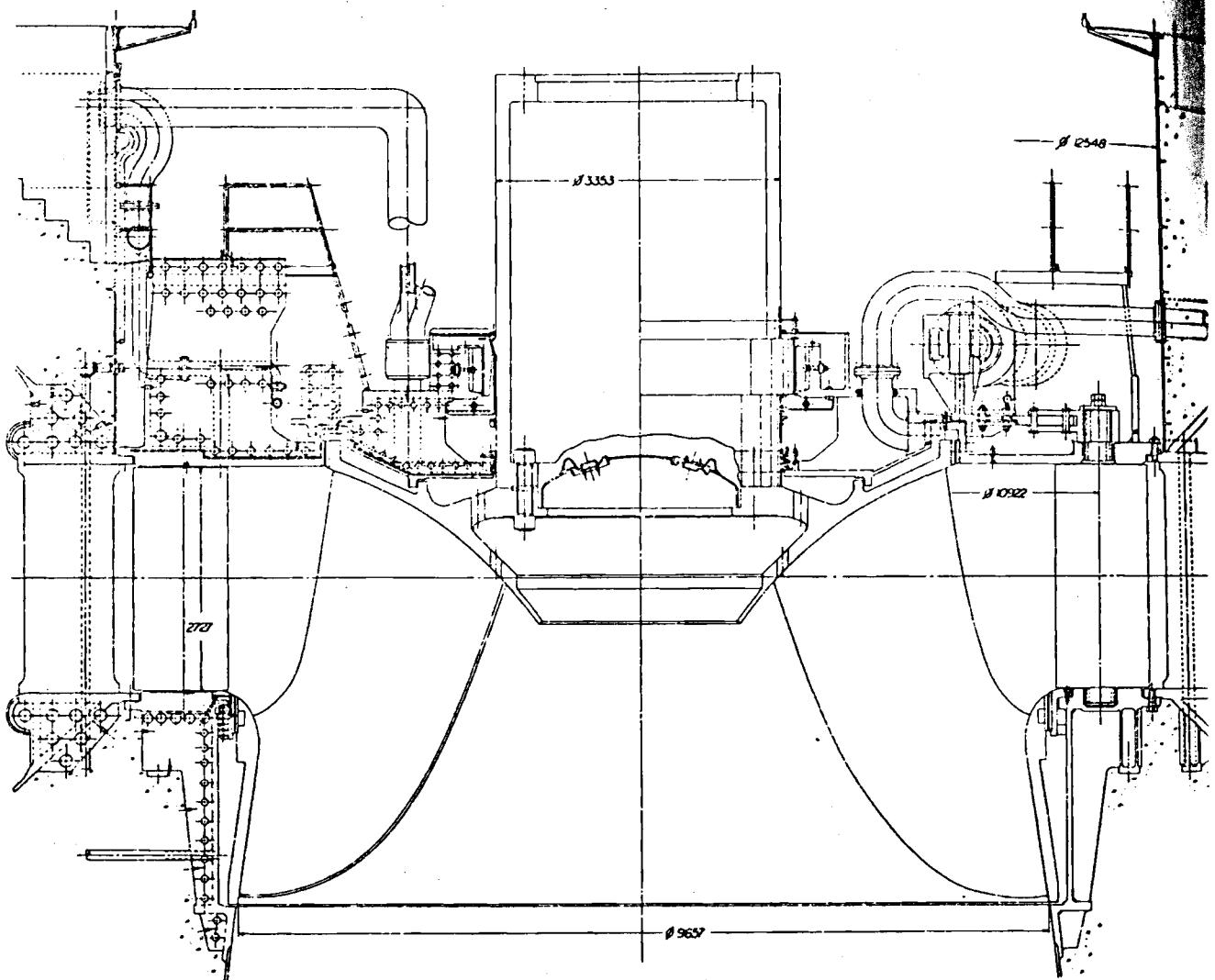
Fig. 10.3.1. Distributor section of the FT Grand Coulee, Columbia River, Washington, USA (owner US Bureau of Reclamation). 3 sets. $H = 87$ m; $n = 85,7$ rpm; P_m (against originally expected and rated 700 MW) = 837 MW = (1,123 million hp!). To date with respect to output and mass (runner weight 450 t) the largest turbine in the world. More information in 2.3.2. (Drawing courtesy Allis Chalmers Corporation, Milwaukee, Wisconsin, USA.)

448

Fig. 10.3.2. Elevation of the distributor section of a FT at Krasnojarsk, Yennissci, USSR (owner State Power Board USSR) (Design LMZ). Runner welded, 14 blades, stress relieved in LMZ and then transported by ship to the site, weight 250 t. Shaft welded, guide bearing water lubricated. Axial thrust (weight of alternator rotor 2000 t) via truncated cone on the head cover. Spiral casing with 2 pressure flanges. $H = 100$ m; $n = 93.8$ rpm; $P = 12 \cdot 507$ MW. (From G. A. Bronowski a. J. Galperin: Some special features in the construction of Krasnoyarsk turbines. Energomasino stroenije 8 (1965) no 3 p. 32.
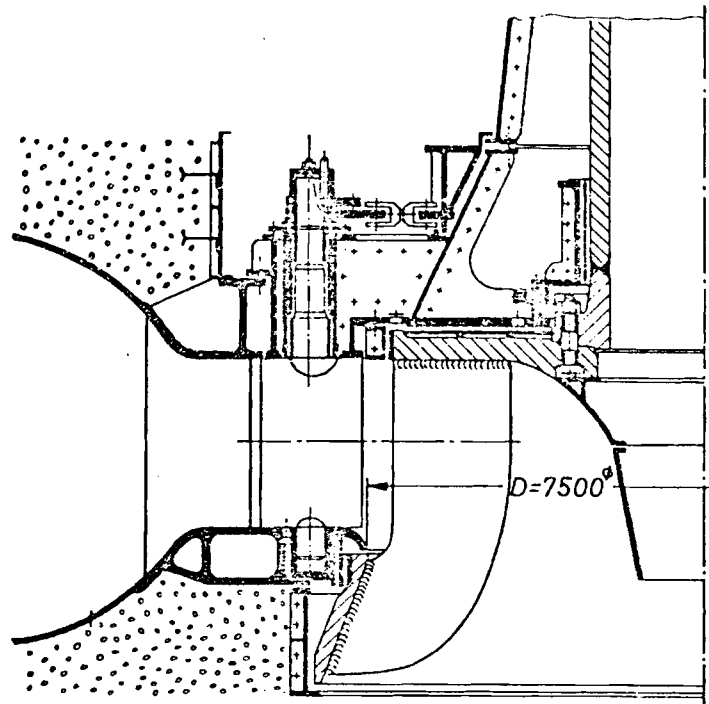
Zillertaler Alps (owner Tauernkraftwerke AG, Salzburg), with a record maximum head of 744 m (see Fig. 10.3.11) [1.76]. Rated heads about 850 m are considered seriously.

In FTs, the specific speed according to Cap. 9.2 and defined by $n_s = n(\text{rpm})\sqrt{P(\text{kW})}/H(\text{m})^{5/4}$ varies from 55 to 350. The trend, to shift n_s of a certain type to higher head, is reflected in increasing nPH. In Häusling, this product attains the value of $79 \cdot 10^9$ rpm kW m. The Francis turbine with the actually highest nPH ($= 92 \cdot 10^9$) is in the 4 pumped-storage tandem sets Wehr, Federal Republic of Germany with the working data $H_m = 645$ m, $n = 600$ rpm, $P = 257$ MW, see Fig. 10.3.12, built by Sulzer Escher Wyss.

Problems arising in the upper head range may be summarized by their causes as follows: Grid-linked, widely-staged high speed, stresses in the alternator rotor at runaway, effective cooling of the alternator, excavation cost due to deep submergence, strength of turbine rotor, spiral casing, stay vanes and distributor and hence small hydraulic channel radius, wear in the distributor, the runner labyrinths and the runner vanes due to sand erosion, cavitation, and high velocities relative to the walls there, noise and fatigue effects due to vibrations, load change and water hammer [10.43; 10.44].

Modern trends of FT design are given in [10.33].

10.3.2. Comparison of Francis (FT) and Pelton (PT) turbines

In some cases a decision must be made whether a FT or a PT should be installed [10.63]. In the case of large units the specific speed n_s (Cap. 9.2) may be used as guide. After Zanobetti [10.34] the bep efficiency of a FT in the range $n_s < 145$ (n_s from now on taken with P[kW]) according to Cap. 9.2 may be approximated by

$$\eta_{op} = \eta_{opm} - 0.7 \cdot 10^{-7}(145 - n_s)^3, \tag{10.3-1}$$

449
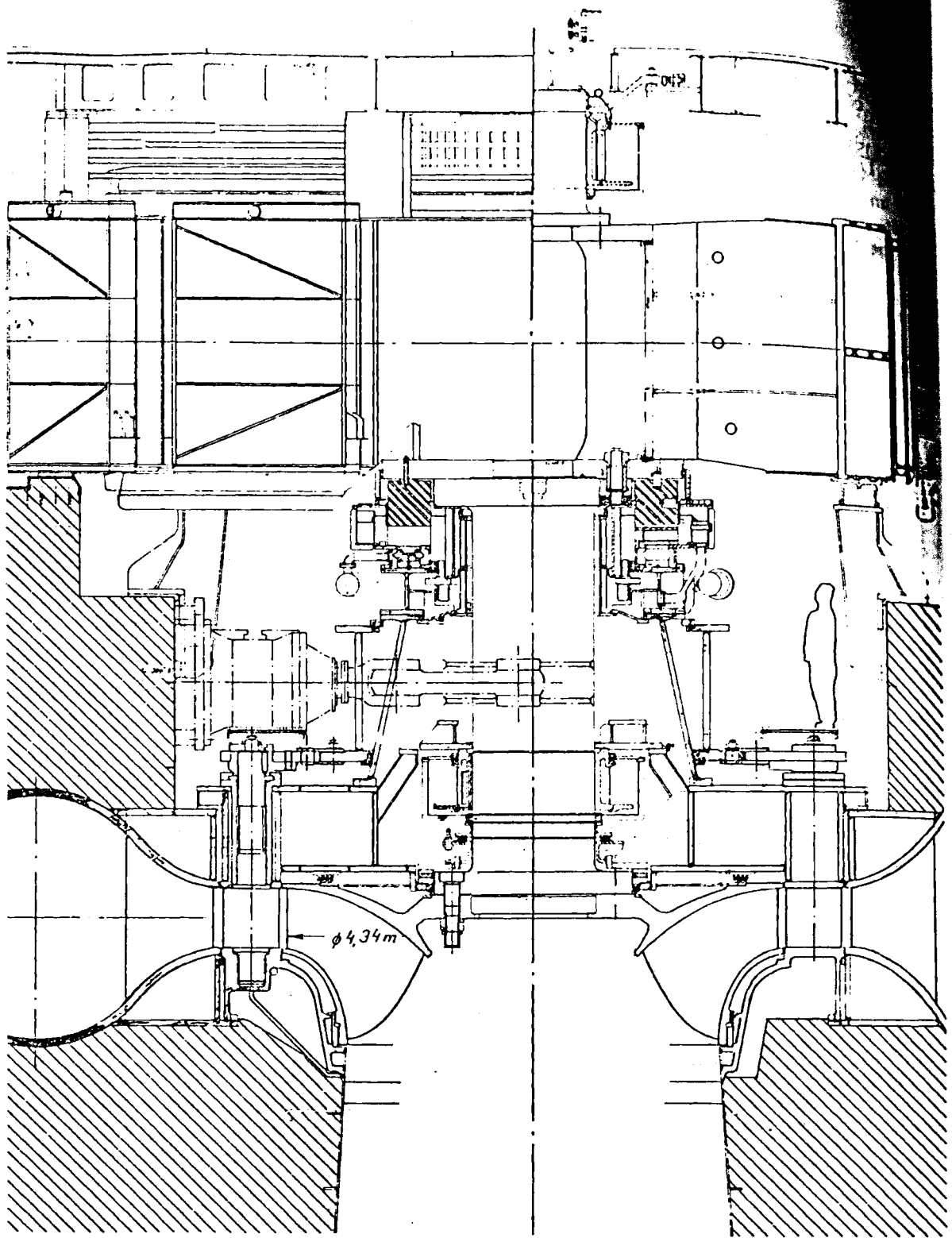
Fig. 10.3.3. Elevation of the high head FT Churchill Falls, Churchill River, Labrador, Canada (owner Churchill Falls Corporation) 11 sets, 6 of them (see figure) built by Marine Engineering Ltd, Montreal, Canada under licence of Neyrpic, Grenoble France, 5 of them built by Dominion Engineering Ltd, Montreal. The latter differ mainly in the runner blading, e.g., in having non skewed inlet edges of the runner vanes, a design exciting more vibrations on the turbine. $H_r = 312$ m; $n = 200$ rpm; $P_r = 483$ MW. Runner $D = 4,34$ m. To date, with a unit power per weight of 0,53 kW/kg the most compact built hydro turbine. See also 2.4.1. (Drawing courtesy Neyrpic, Grenoble, France.)

450
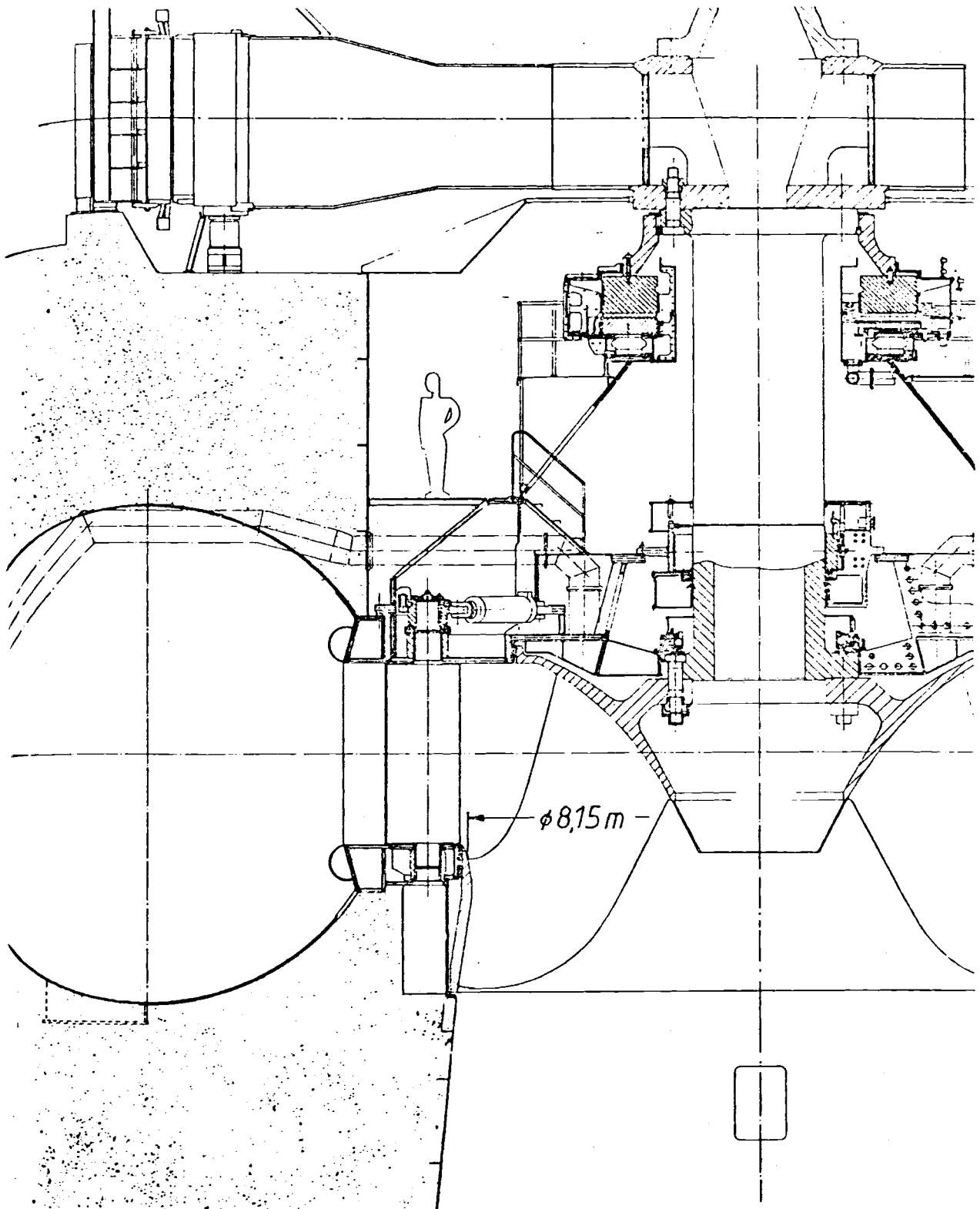
Fig. 10.3.4. Elevation of the FT Tucuri, Tocantin, Brazil (owner Electronorte). (Design Neyrpic) 6 sets, $H_r = 67,6$ m; $n = 81,8$ rpm; $P_r = 369$ MW. Thrust bearing pads hydrostatically supported (Fig. 10.5.8); gates with single servomotors (see Fig. 11.2.10b). Parallel plate spiral casing, see also [10.128]. (Drawing courtesy Neyrpic, Grenoble, France.)

451
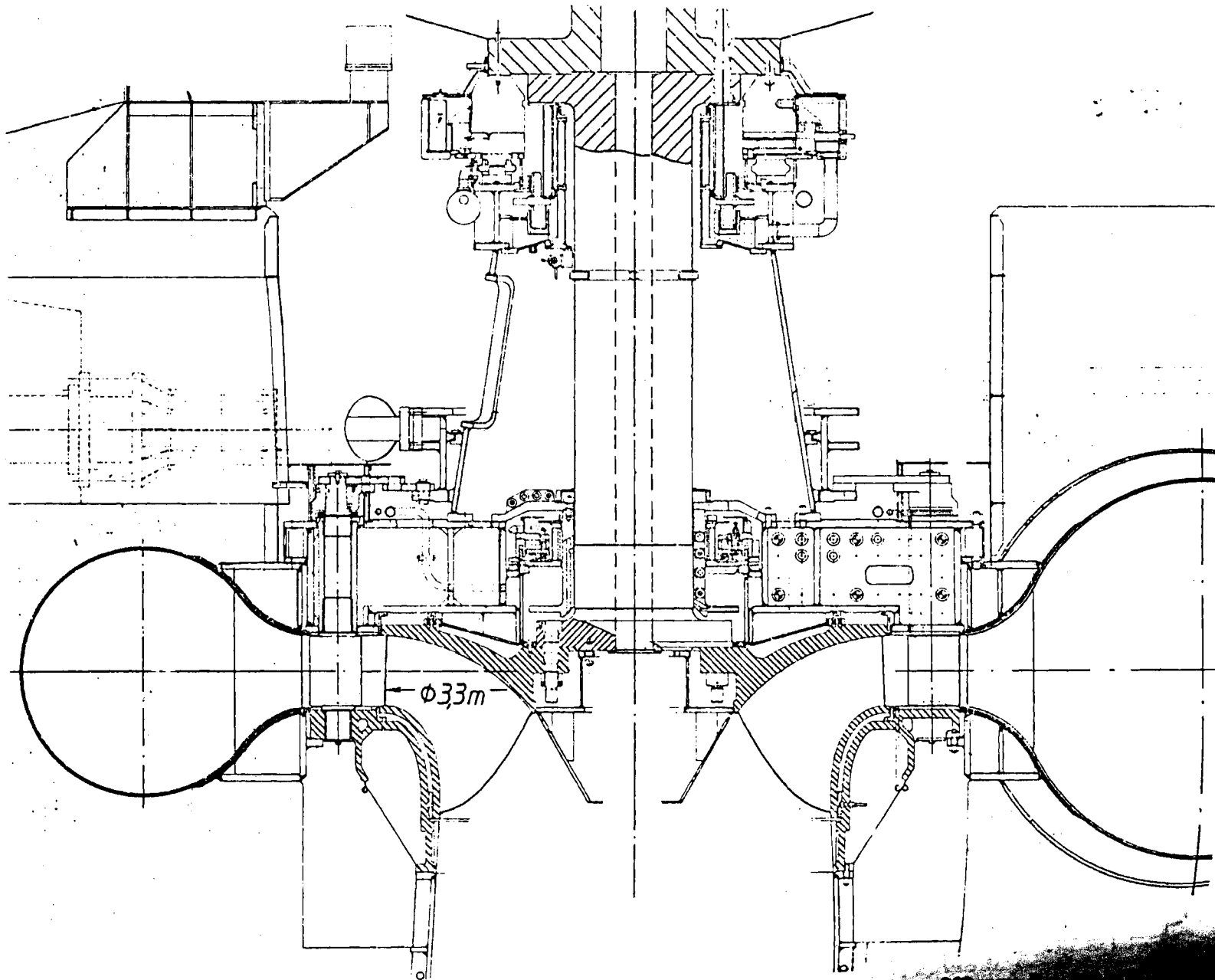
Fig. 10.3.5 Elevation of the FT Brommat II, France. (Owner EdF). (Neyrpic design $H_s = 255$ m; n = 250)

where η_{opm} is the best attainable efficiency, depending on size and the state of the art (for very big machines currently η_{opm} up to 0,95). After the last relation the bep efficiency of a large FT with $n_s = 51$ becomes $\eta_{op} = 0,89$. Experience shows that the bep efficiency of a large PT only just exceeds $\eta_{op} = 0,91$. This is mainly caused by the shallow rectangular cross section the jet has when leaving the bucket.

But the problem exists if a certain n_s, fixed by the operating data H, Q, n of a plant can be achieved by a PT design. From Cap. 9.2 a vertical PT with 6 jets and the suitable jet diameter ratio $d_0/D = 1/11,5$ attains $n_s = 49$. On the other hand from (10.3-1) a FT of $\eta_{op} = 0,91$ would need $n_s = 77$. Obviously a gap exists between the lowest possible $n_s = 77$ of a FT and the highest possible $n_s = 49$ of a PT both having 91 % bep efficiency.

To obtain an idea how the jet diameter ratio d_0/D influences the bep efficiency, the following figures mentioned by Mataix [10.1] may serve as guide: $D/d_0 (\eta_{op})$: 6,5(0,82); 7,5(0,86); 10(0,89); 20(0,9). These values are valid for a medium sized machine with only one nozzle per wheel. With a rising number of jets, the efficiency drops at the same jet diameter ratio.

According to Sulzer Escher Wyss an overlap exists between FT and PT in the $H(Q)$ plane (Fig. 10.3.16). This has an upper limit at $H = 750$ m and a lower limit described by: $\ln H (m) = 4,1 + 0,54 \ln Q (m^3/s)$; H and Q rated figures.

It may be mentioned that the cross flow turbine originated by Michell and Banki, now actually made by the West German firm Ossberger (see Figs. 3.4.8; 3.4.9; 3.4.10) may overlap this gap at the lower head and flow range. Below the above limits the FT rules out the PT by the lower cost of its set or by lower operating cost.

Reasons: For a certain head the bucket speed coefficient of a PT being $Ku = 0,42 \ldots 0,52$ is below that of a FT with $Ku = 0,7 \ldots 1,1$ (upper limit for lower head). Moreover the unit discharge Q_{11} (Cap. 9.2) of a PT is much smaller than that of a FT. For a certain head and output this leads to an increase of speed by 30 to 50% of a FT over a PT. Hence torque and size of set of a FT is smaller than that of a PT. Accordingly also the distance of adjacent sets and the power house required becomes smaller for a FT than for a PT.

On the other hand a FT may require more expenditure than a PT due to its submergence. This argument in favour of a PT may disappear in the case of an underground station. For low heads and large wheel diameters the head loss due to the free height above the tail water level may favour a FT, where the free height is used in the diffuser. The PT must have this free height to avoid disc friction and excessive windage loss (Cap. 5.5).

Further reasons affecting the decision between PT and FT, see also [10.63]:

a) In high head plants with strongly erosive sandy water (with quartz sand) the consequences of excessive wear, e.g., in the labyrinths of a FT may be worse than those in the nozzle and on the needle of a PT, since the first enlarges considerably the clearance of the labyrinth gaps and hence the leakage loss especially in high head FTs with their rather small runner breadth to diameter ratio b/D (Figs. 10.3.9; 10; 12), a loss which does not exist in a PT.

b) The FT has a more pronounced efficiency peak vs load P at bep than a PT and hence is more suitable for constant base load demand. Contrary to this the PT has the flattest efficiency vs load curve. Thereby a PT may be preferred if the plant frequently has to supply varying peak load and hence often operates in the part load range.

For example the supply of traction power in West Germany, Switzerland and Austria, which have a special grid with $16\frac{2}{3}$ Hz for this purpose, is often effected by PT sets.

c) The parts needing frequent repair and replacement in a FT operated by highly erosive sandy water are the labyrinth rings, the guide vanes, the wear rings of the distributor and

453
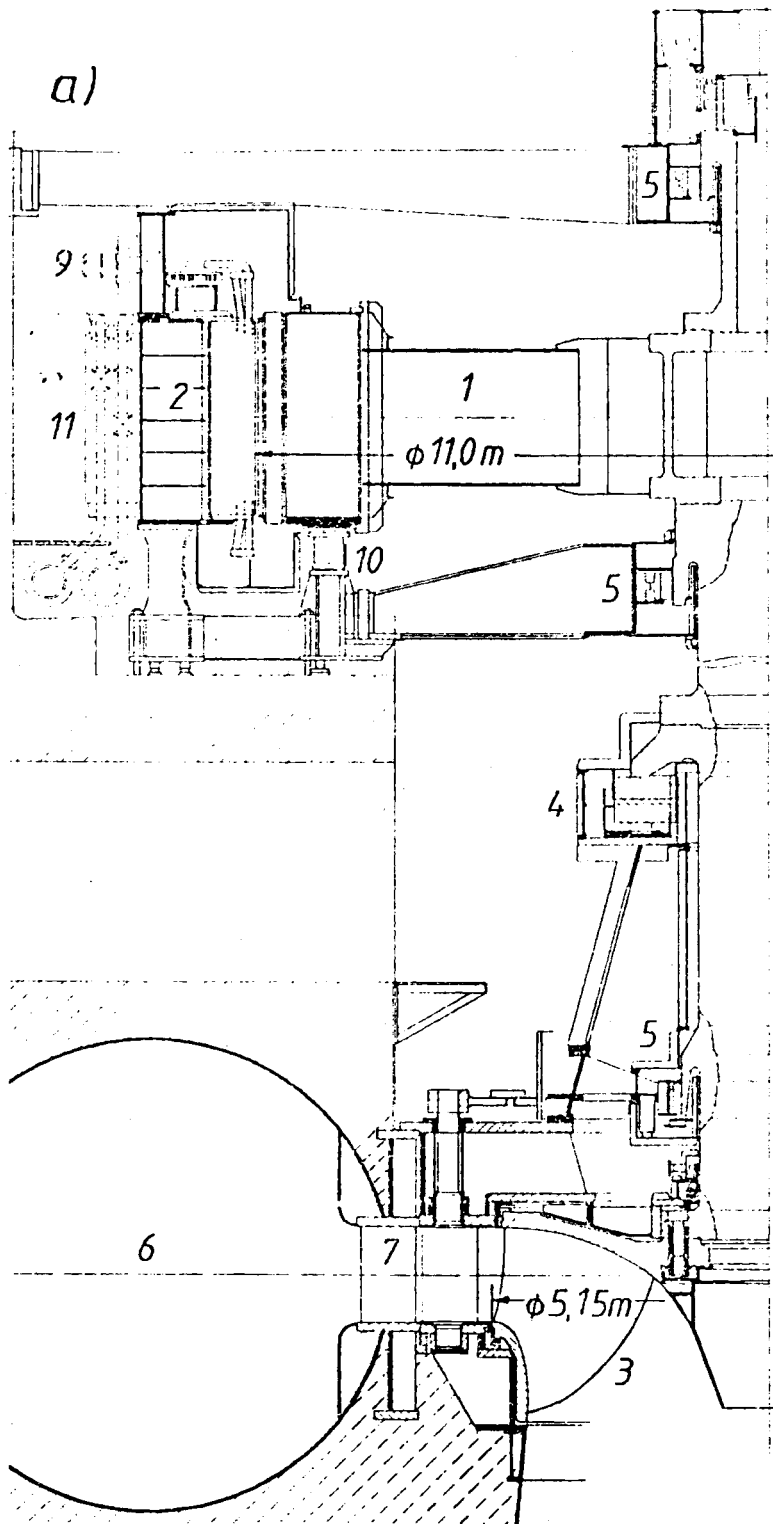
Fig. 10.3.6. a) Elevation of a FT set, Karakaya, Euphrat, Turkey (owner State Water Authorit Turkey). 6 sets (FT design Sulzer Escher Wyss, Generator design BBC, both Switzerlanc $H_r = 150$ m; $n = 150$ rpm; $P_r = 306$ MW; $P_m = 340$ MW; runner $D = 5,95$ m. Alternator rote weight 652 t: fly-wheel moment $GD^2 = 51 \cdot 10^3$ tm^2; $n_{ru} = 280$ rpm. To date the most powerf turbine built in Switzerland. 1 alternator rotor; 2 alternator stator; 3 FT; 4 thrust bearing; 5 3 guic bearings; 6 spiral casing (parallel plate design); 7 stay vane; 8 slip ring; 9 generator termin: 10 jacking and braking cylinder; 11 air cooler. Anti surge aeration through throat ring, shaft centi and bolts. From Brown Boveri Review [11.65] b) Details of FT (Drawing courtesy Sulzer Esch Wyss).

1

5

4

5

6 7

$\phi 5,15\,m$

3

0   0

455

a)

ϕ6500

ϕ5260

ϕ4235

1150

▽ ±0

▽ 340

456
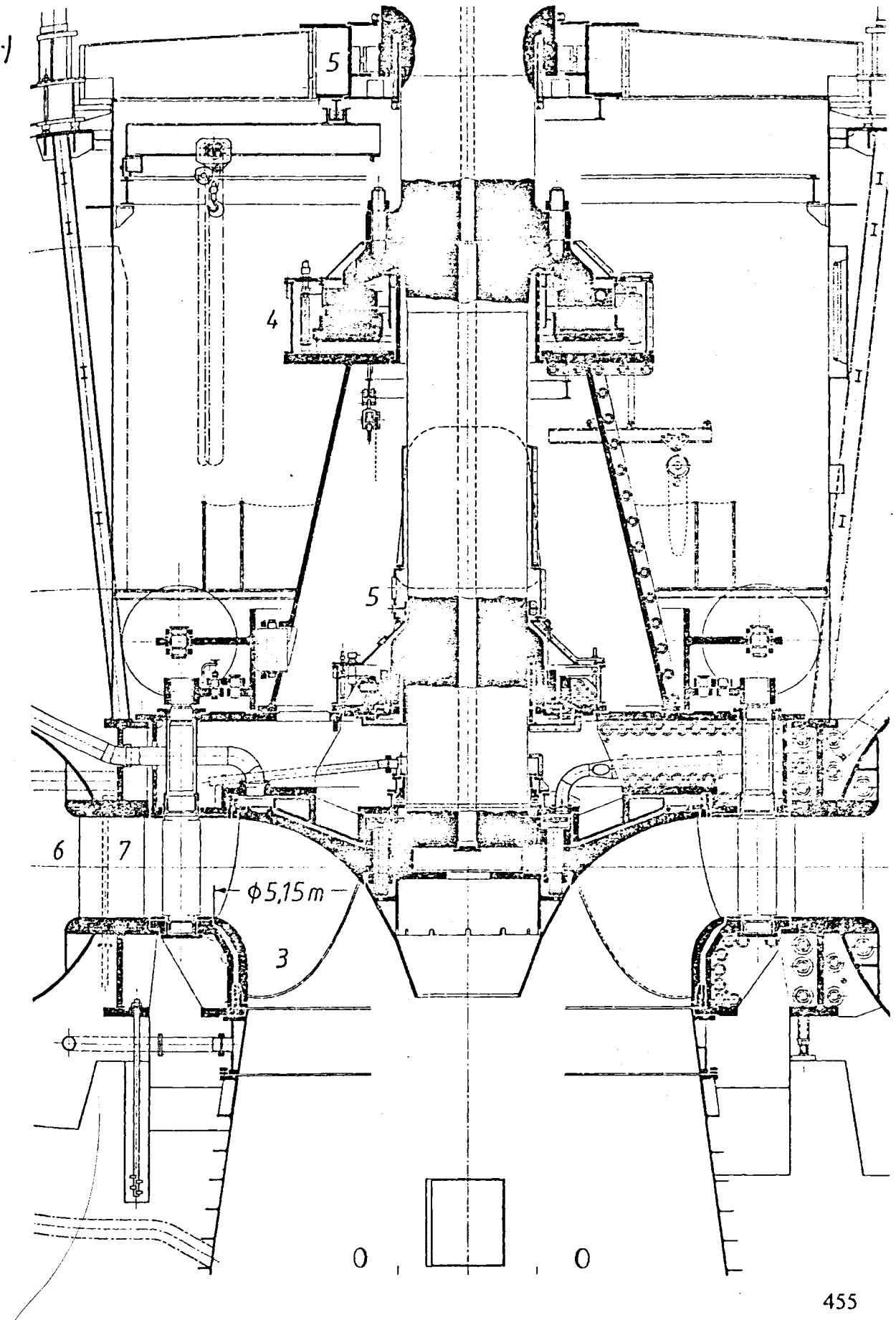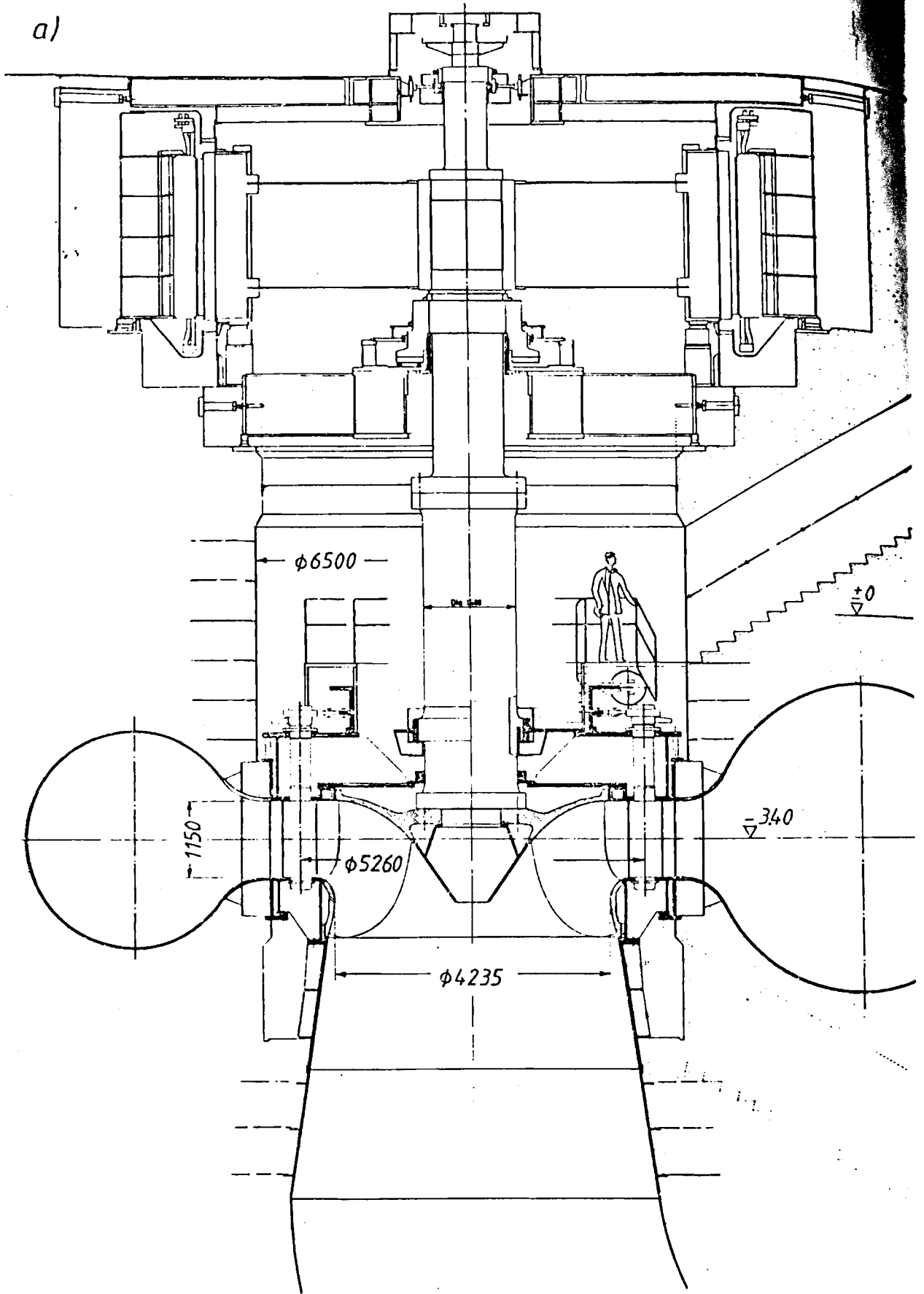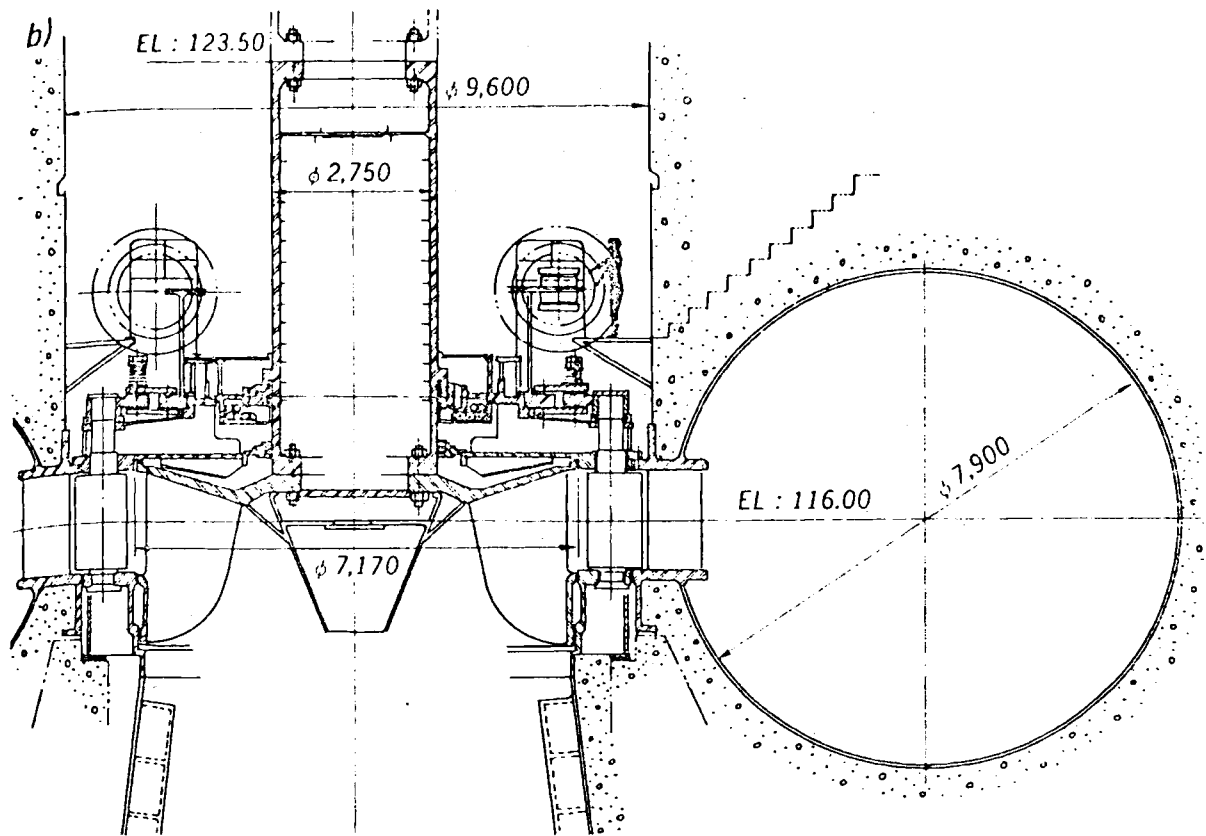
Fig. 10.3.7. b) Sectional drawing of vertical shaft FT at Guri, 2nd power house, Rio Caroni. Venezuela (owner Corporacion Venezolana de Guayana, Republic of Venezuela) built by Hitachi Ltd, Japan. $H = 111$ to 146 m, $P = 476$ to 730 MW continuous, temporary output 767 MW. $n = 112.5$ rpm. After previous designs, commissioned between 1968 and 1977 with outputs of $P = 218$ to 400 MW at heads of $H = 115$ m to 136 m, these 10 units, commisioned 1981 are at present the most powerful FTs built in Japan. Simplified design with parallel plate spiral casing. conical hub, slag-welded shaft. The runner is a one-piece casting of 13 % Cr — 1 % Ni stainless steel. to date the largest of this kind in the world of 7,17 m outermost diameter, and a weight of 130 tons. For these machines the head of the Guri plant has been increased from 111 m to 146 m by increasing the crest height of the concrete gravity dam. The submergence equals that of the previous designs. According to the author's impression on site, the 400 MW FTs showed bad cavitation pitting after one year of full load operation under the smaller head of 111 m. (Drawing courtesy Hitachi, Ltd. Japan.)

Fig. 10.3.7. a) Sectional drawing of vertical shaft FT at Hårspranget, Lule river, Sweden (owner Swedish state power board) 4th unit built by KaMeWa AB, Kristineham, Sweden. $H = 103$ m. $P = 182,8$ MW, $n = 166,7$ rpm. Runner throat diameter $D_1 = 4,235$ m. For highest reliability the stay vanes were inserted into corresponding holes of the stay ring welded from steel plates, and then connected with the wetted face of the stay ring on both sides by means of a corner weld. When commissioned in 1952 the average annual production of 2020 GWh of Hårspranget made a contribution of more than 20% of Sweden's electricity production. With an extension in 1974 to 80 the production of Hårspranget was raised to 2240 GWh and the installed capacity to 945 MW. The last and 5th unit then installed by KaMeWa had an output of $P = 450$ MW ($n = 83.3$ rpm) with an axial thrust of 1910 tons, and was since that time the most powerful hydro turbine in Europe. The water way consists (as usual in Sweden) of a vertical penstock to the underground power station and a very long horizontal tailrace tunnel with an upstream gate. A 400 kV AC transmission line with a length of 945 km, the first of its kind in the world was built in 1952 from Hårspranget to central Sweden. Due to the isolated location (north of the Arctic Circle) and the need for experienced and skilled employees a complete town with the necessary social services had to be built at site. The town consisted of houses for 1200 employees and their families in all 2200 people. as well as shops, hospitals, post and police station, other social services such as sport and leisure facilities and church. (Drawing courtesy KaMeWa AB, Kristineham, Sweden.)
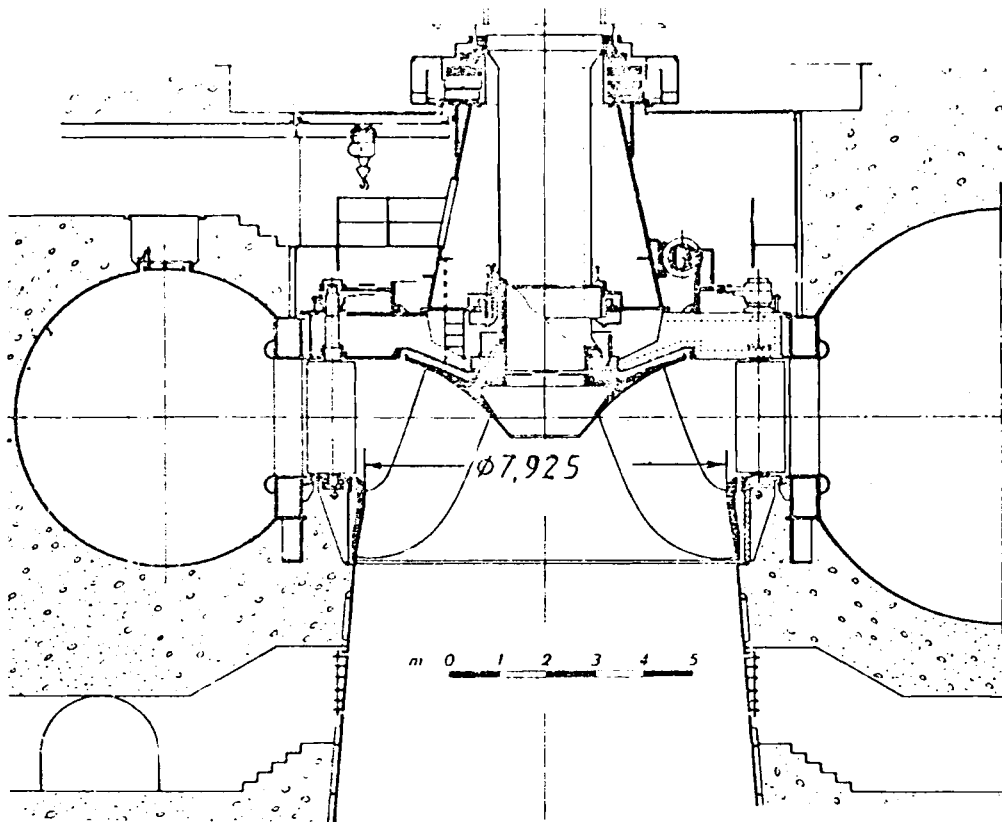
Fig. 10.3.8. Elevation of the FT Itaparica, rio São Francisco, Brazil (owner Companhia Hidroeléctrica do São Francisco) 10 sets (design Hydroart, Milan). $H_r = 53,2$ m; $n = 81,8$ rpm; $P_r = 264$ MW. Spiral casing parallel plate type of steel plates welded on site, inlet diameter 9.5 m. Runner made up by welding with separate carbon steel blades, 7.925 m diameter, weight 180 tons. Thrust bearing: 1600 tons load, via truncated cone on the head cover, with high pressure oil injection. (Drawing courtesy Hydroart, Milan, Italy.)

the runner vane channels, especially the inlet edge of the runner vanes. In a PT such damage is restricted to the mouth of the nozzle, the point of the needle and the cutting edge and the jet cutout of the bucket. As these members are much easier to get at any revision is much easier in a PT.

The dismantling and exchange of a PT's wheel need much less time than that of a FT runner. Also the repairs of a PT, e.g., the welding and the building up welding and grinding of a bucket of a PT is much easier to carry out and to check than the corresponding repair on a FT runner.

d) In the case of very small output the application of a FT would lead to rotational speeds above the upper limit of a two-pole alternator. The reduction gear then needed would raise the price of a FT set, whence a PT with its reduced speed is preferably employed.

Some special remarks concerning Pelton turbines:

The Pelton turbine, not especially treated here, is usually considered a safe machine. But it certainly has some problems. One problem, namely sand erosion occurs mainly on needle and nozzle and can be attributed to the high velocities there. It increases roughly with the 2nd to 3rd power of the head, and with the occurrence of hard ingredients in the water such as quartz.

In some cases sand erosion cannot be eliminated even by means of sand separators at the

458

Fig. 10.3.9. Project of a high
head Francis pump-turbine
for H = 1000 m. Machine in
spherical tank; cylindrical
gates. From W. Meier et al.:
Single- and multi-stage
pump-turbines for high
head storage plants. Paper
ASME Pump turbine
schemes. Fluids Engineering
Conf., Niagara Falls, New
York 1979. [10.153] (Draw-
ing courtesy Sulzer Escher
Wyss.)
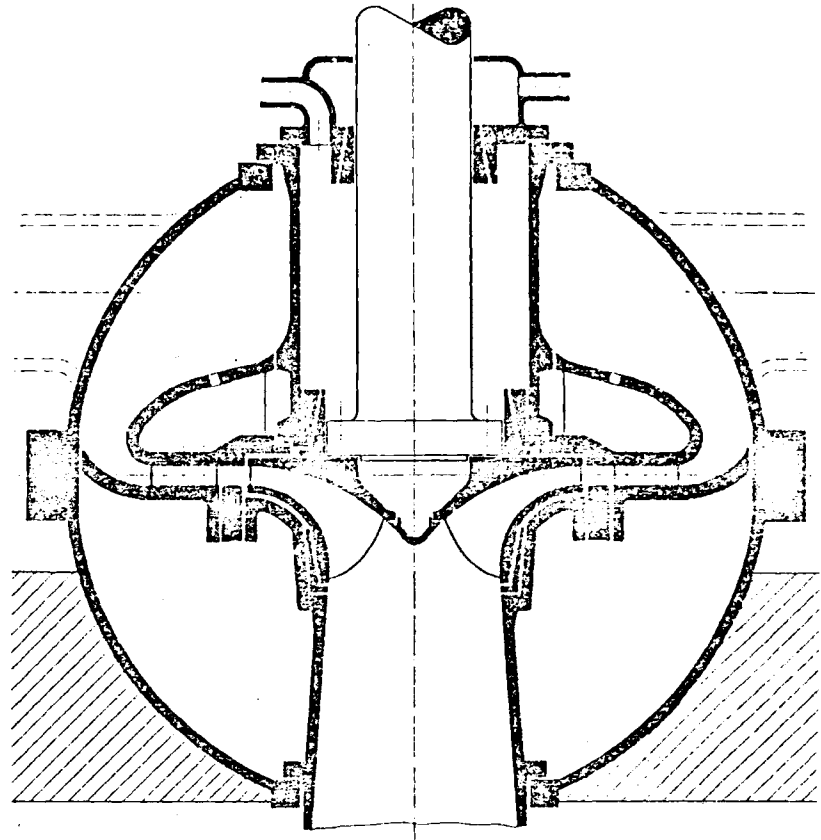
intake. In this case the sand particles are so small as to be kept suspended by Brownian motion of the surrounding liquid e.g., glaciated rock.

Another problem is the erosion by a droplet impact. It corresponds essentially to that by cavitation. Moreover droplets increase disk friction, when they impinge on the wheel with a slip in the tangential direction (Cap. 5.5).

An erosive droplet impact preferably occurs on the back of the buckets, close to the cut out. This originates from the wheel's overtaking slow droplets. Such detrimental droplets result from:

1) slow fluid particles at the outer edge of the jet, especially when the bucket cut out is too narrowly spaced,

2) droplets that are discharged from neighbouring buckets in the case of more than one jet,

3) droplets that are reflected from a casing wall too near to the wheel.

4) droplets reflected from a tailwater surface which is not sufficiently away from the bottom of the wheel.

All the latter factors increase their detrimental influence decisively with the flow rate and somewhat with the head, but also when the bucket's cut out edges are too close to the edge of the jet.

Therefore the free height of a Pelton wheel and the spacing of its casing should be increased with the number of jets, and with the jet to wheel diameter ratio.

Because of the two bends in series and in different planes, upstream of the nozzle within the main of a PT with vertical shaft, the formation of a streamwise vorticity in the main

459
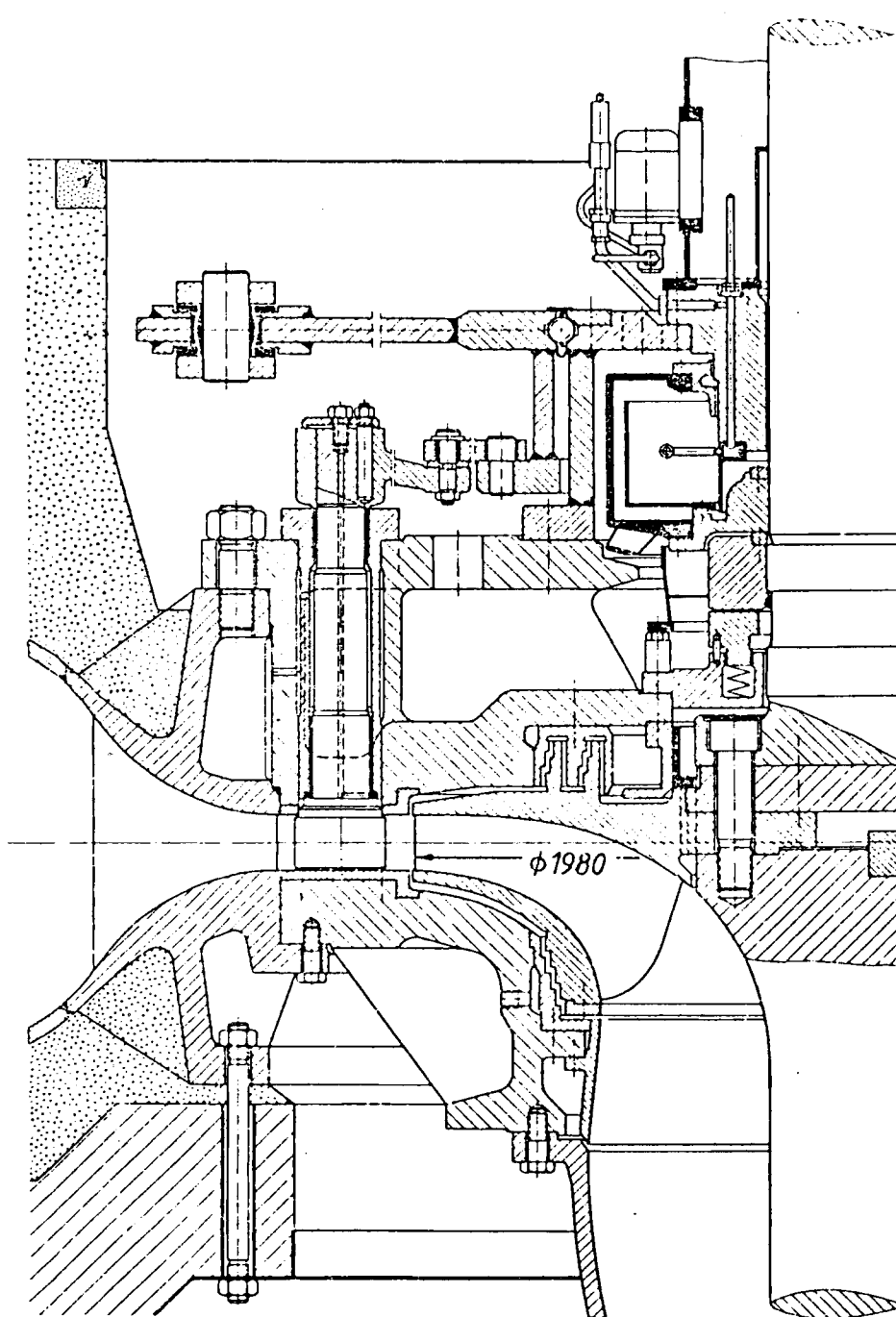
Fig. 10.3.10. Elevation of a FT in the peak load and pumped storage plant Rosshag, Zemm, Tyrol, Austria (owner Tauernkraftwerke AG, Salzburg) 4 sets (FT design Sulzer Escher Wyss and Maschinenfabrik Andritz, Graz, Austria). Shaft end passing the draft tube bend, during pumping engaged with the 2-stage single flow storage pump by a gear coupling and torque converter (design Voith). $H_n = 672$ m; $n = 750$ rpm; $P_r = 58.2$ MW. Spiral casing welded plate design, welded on cast stay vane ring. Gate with stem in 2 bearings, overhung design. Integrally cast runner of stainless steel Cr/Ni with staged and staged comb labyrinths. Labyrinth teeth in the comb labyrinth on the shroud with larger clearance towards the shaft for damping the bending oscillations of the latter. Due to a bad weather, dammaging the sand trap of a tunnel feeder, the distributor has been badly eroded. Henceforth its walls were lined with resistant material. On the one hand the through-shaft to storage pump decreases the efficiency only slightly (small value of Kc_{m1}^2), on the other hand it stops the formation of surging draft tube vortex. (Drawing courtesy Maschinenfabrik Andritz and Sulzer Escher Wyss.)

460
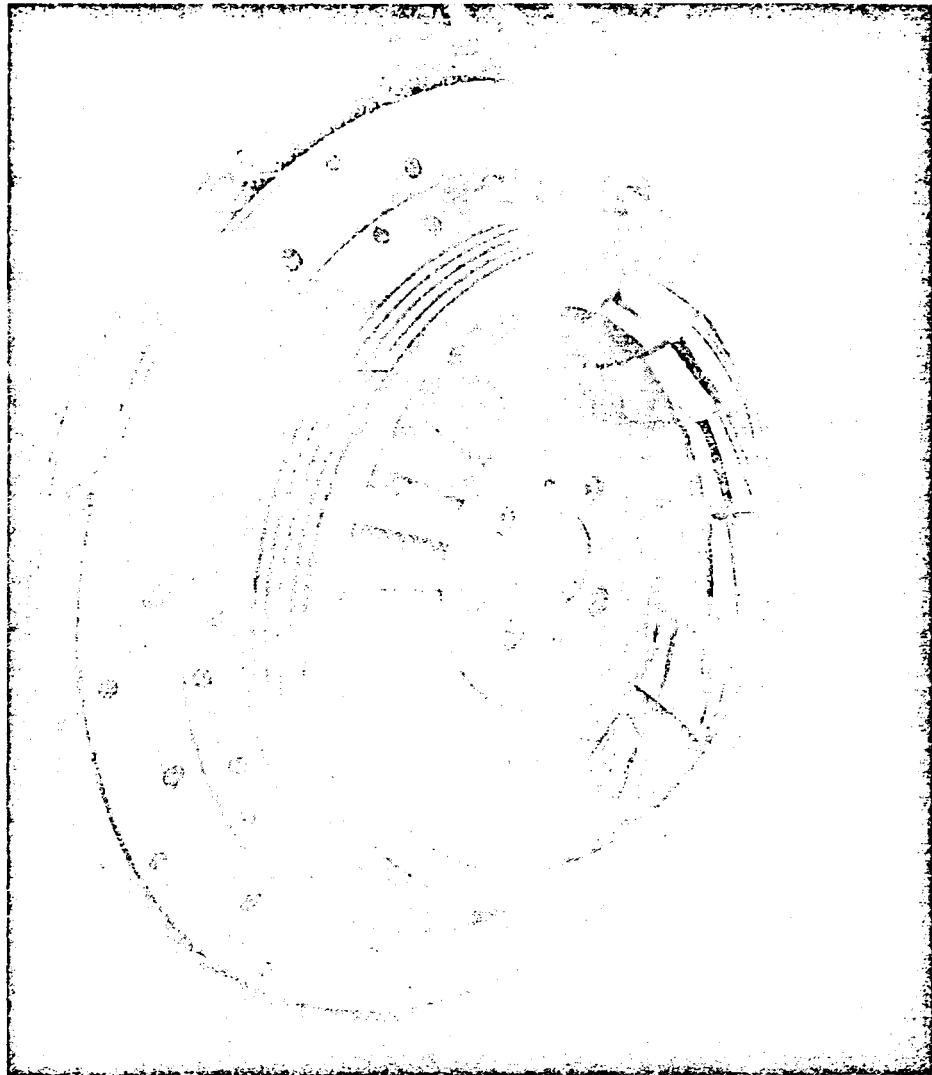
Fig. 10.3.11. Model runner of the FT at Häusling, Ziller, Tyrol, Austria (owner Tauernkraftwerke AG, Salzburg) 2 sets peak load and pumped storage plant, FTs built by Sulzer Escher Wyss, Switzerland. Data of prototype: $H = 620$ to $744 \, m$; $n = 600 \, rpm$; $P = 180 \, MW$. Runner: $D = 2{,}767 \, m$. To date the FT with the highest head in the world. $n \cdot H \cdot P$ amounts only 80% of that of Wehr (Fig. 10.3.12), but is 380% that of Rosshag. The product $n \cdot H \cdot P$ of Wehr is 160% that of Grand Coulee III, and 330% that of Churchill Falls. Scroll casing of rolled steel plates with high yield point, spot-welded on integrally cast 10-vane stay ring of stainless steel. Pseudo parallel plate design as in Fig. 1.6.4 b. (Photograph courtesy Sulzer Escher Wyss and Andritz.)

flow of the nozzle is favoured (Cap. 7.2). Thereby the acceleration of flow in the nozzle strains the streamwise vortex filaments. This increases the kinetic energy of the latter, lost for shaft work. Therefore efforts should be made in the design to minimize this effect by avoiding too strong a curvature of the main in planes inclined to each other and by adequate flow admission (Cap. 3.4).

The above mentioned loss in the nozzle of an impulse turbine seems to be the reason for its negative scale effect in the overload range (Cap. 5.5). Hence a prototype's efficiency may drop below that of the model, but curiously usually only at overload.

The cross flow on the bucket (Cap. 5.5) as another source of this loss behaviour should

461
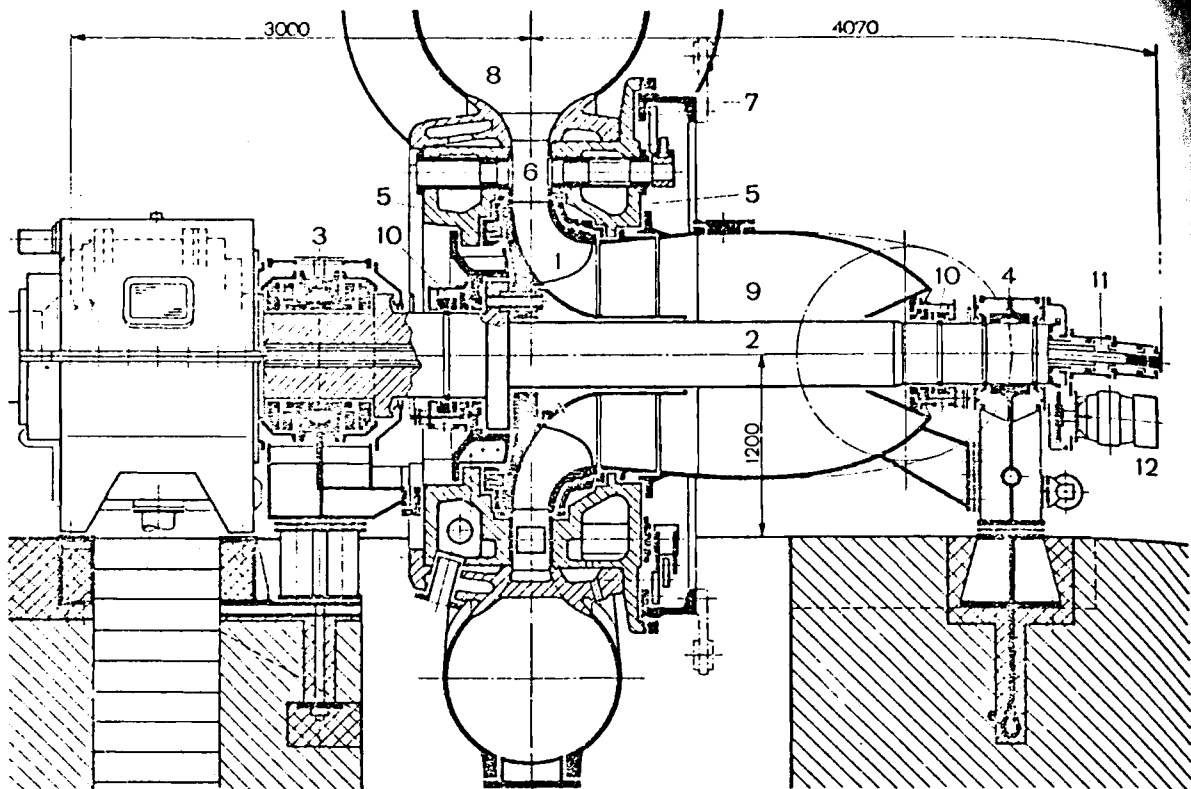
Fig. 10.3.12. Horizontal high head FT of the ternary pumped storage plant Wehr, Wehra, West Germany (owner Schluchsee AG, Freiburg). 4 sets with FTs built by Sulzer Escher Wyss and 4 2-stage double flow storage pumps with torque converters built by Voith (see Fig. 1.6.4 a). Horizontal shaft, detachable during pumping by means of an overriding clutch. FT for $H_m = 645$ m; $n = 600$ rpm; $P_m = 257.5$ MW. Runner: $D = 2,685$ m. To date the FT with the largest $H \cdot n \cdot P$. Alternator with air-cooled rotor and water-cooled stator. Initial troubles with stator laminations heated too much, and hairline cracks in the stay vane part hint at a limiting hydro-electric design in 1972. The varying span of the stay vanes requires a careful stress calculation also with respect to fatigue effect, see Grein [10.127]. Because of the high velocities, wear of wetted parts encountered by careful material selection. Runner 1 and rotary labyrinth rings: integrally cast of Cr/Ni 13/4 steel. Stationary exchangable lining around runner in regions of high velocity: cast of Cr/Ni 13/1 steel. Components in the regions of lower velocity: Cast iron, Ni, Mo-alloyed. Gate vanes: Forged Cr/Ni 13/4 steel; protective layer on the gate vane channel wall of Cr/Ni by built up welding. Spiral casing 8 fine grain steel, welded from plates of 3600 bar yield point. Stay ring: Cr/Ni 17/4 cast steel; stay vane surface: metal spray layer of Ni-Al-13 Cr steel. Through shaft 2 lined with hard chromium layer, necessary to decouple turbine during pumping by means of a special self shifting synchronizing overriding clutch, type SSS. Because of the pump, minimum submergence about 70 m. Tailrace tunnel 1,5 km long with 2-chamber surge tank. Maximum working pressure-90 bar. Fly-wheel moment so that start up time $T_a = 7,8$ s. Relative overspeed after load rejection 50%. From special issue. Schluchseewerk 3, 4 bearings, 5 covers, 6 gate, 7 gate ring, 9 draft tube, 10 shaft seal, 11 clutch adjustment. (Drawing courtesy Sulzer Escher Wyss, Switzerland.)

be kept in limits. Therefore the initial curvature of the bucket cross section close to the inlet edge should be as small as possible.

In a limiting design, in consequence of stress concentration and wear near the cutting edge of a bucket, the unit output per bucket can be increased only by blunting the edge at the cost of efficiency.

Modern trends in the design of PTs are given in [10.62]. Recent designs are shown in the Figs. 10.3.13 to 15.
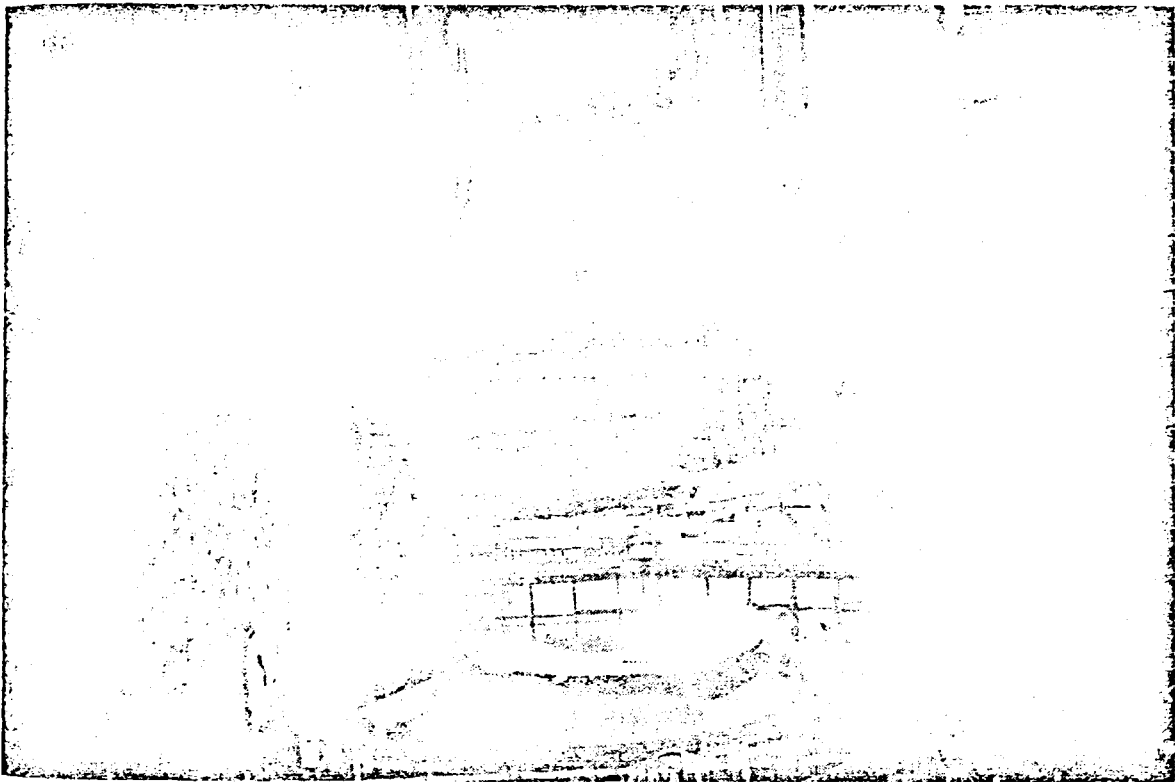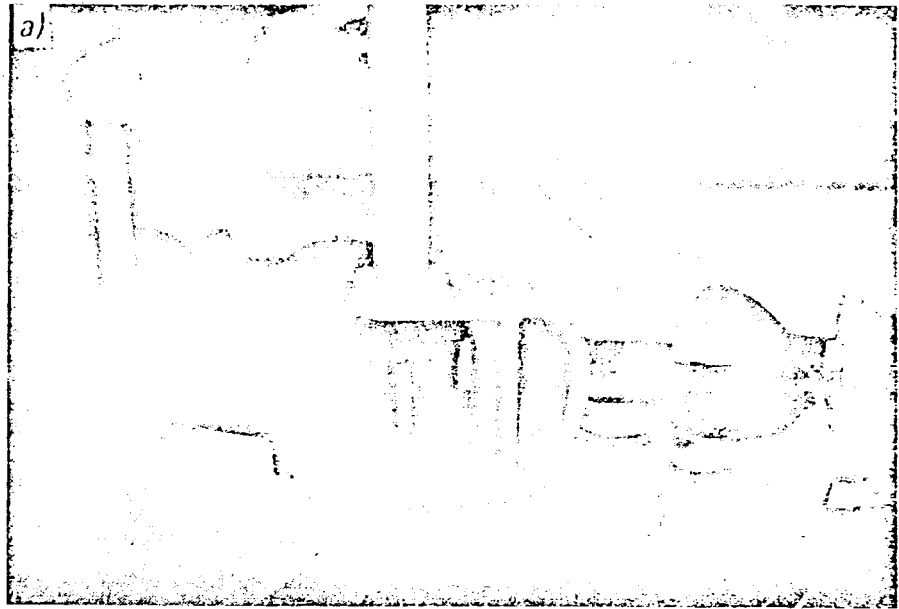
Fig. 10.3.13. a) Wheel pit of the Pelton turbines of Sy Sima plant, Norway. 5 nozzle vertical PT in operation since spring 1981 and since that time the world's most powerful Pelton turbine. $H = 885$ m; $n = 300$ rpm; $P_r = 315$ MW; $P_m = 350$ MW, built by Kvaerner Brugg A/S, Oslo, Norway. b) From the same manufacturer, 2 Pelton turbines of the Lang Sima plant under erection, in operation since 1980. They are vertical 5-nozzle units with $H_m = 1151$ m; $n = 428$ rpm; $P_m = 305$ MW (rated value $H_r = 1006$ m. $P_r = 260$ MW). In this plant, at highest head the $n \cdot H \cdot P$ is 160% that of Sy Sima plant, and 175% that of Wehr. Note the bridge of jet deflector, bucket cut-out, bucket edge, and stiffening ribs on the back of bucket. (Photograph courtesy Kwaerner Brugg S/A, Oslo, Norway.)

463

$\phi 3,445\,m$
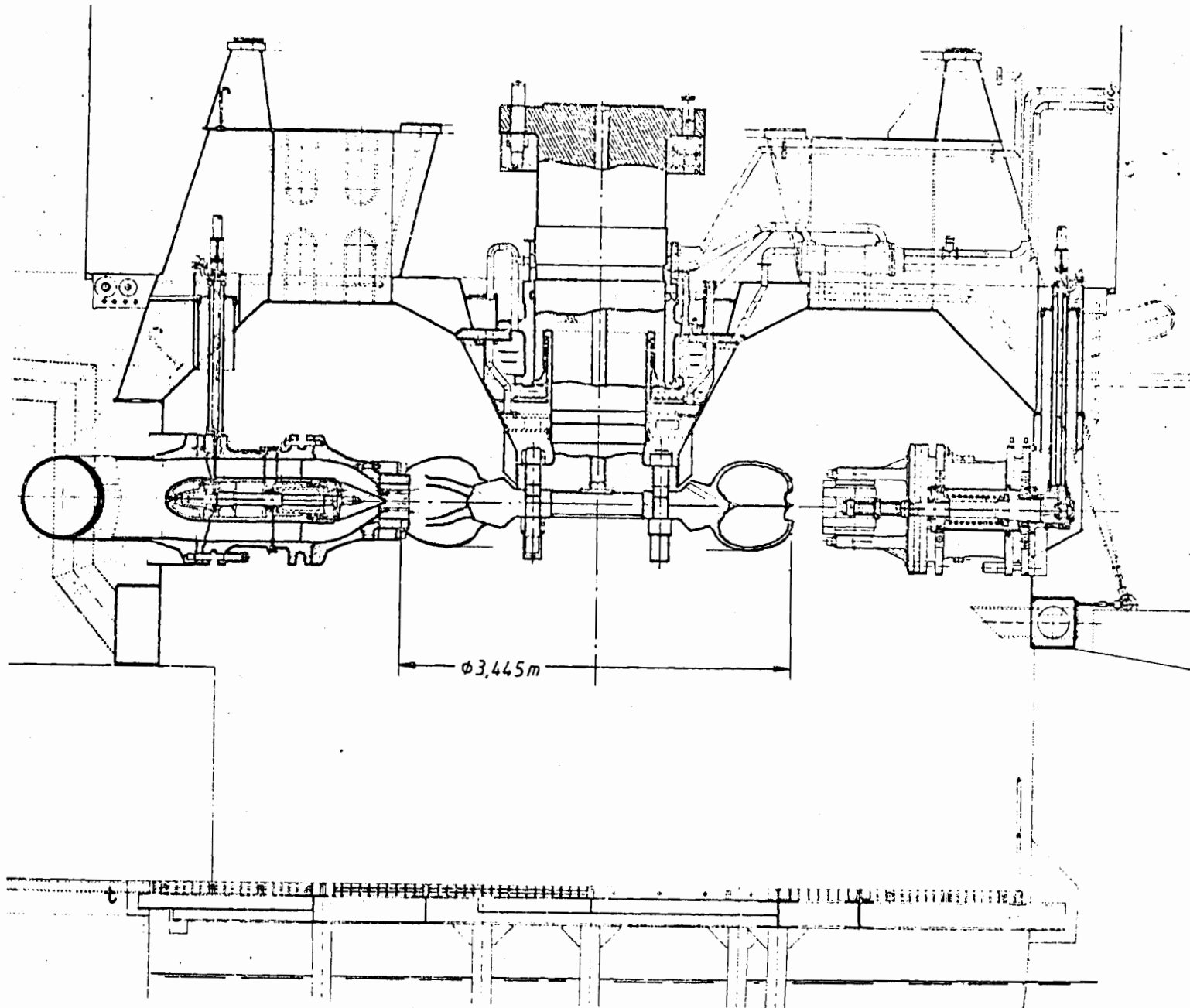
Fig. 10.3.14. Elevation of 5 jet vertical PT L'Eau d'Olle, France (Owner EdF). Plant is the upper stage of scheme fed from the reservoir created the barrage Grand'Maison, an earth-fill gravity dam, crest height 140 m, width 550 m, live storage volume *1.85 hm³. 4 PTs built*
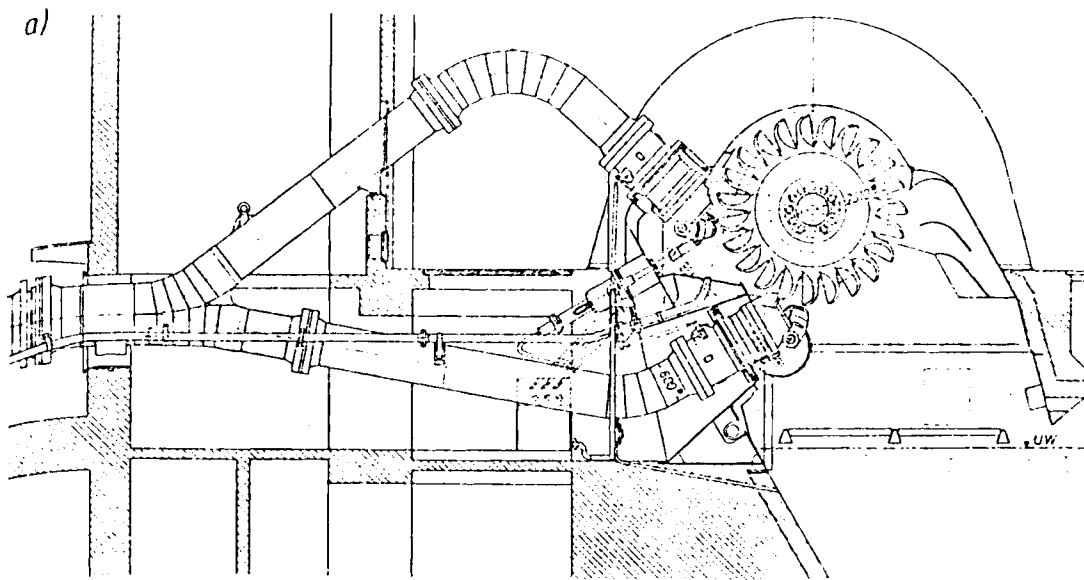
Fig. 10.3.15. a) Cross section through one of the 5 horizontal shaft sets with 2-wheel, 2-nozzle PT at Prutz, Kaunertal, Austria (owner Tiroler Wasserkraftwerke, Innsbruck) built by J. M. Voith. H = 890 m, n = 500 rpm, P = 78,8 MW. Small deflection angle of y-fitting and small curvature of the pipe at the ends of the y-branches diminish disturbances of uniformity in the flow admission to the nozzles (so called "tongs design"). Wheel of integrally cast stainless steel, D = 2,31 m, needle servo motor in the nozzle pipe with feedback linkage of both the nozzles joined together, which gives a certain position of the jet deflector via a cam to a given needle position. Both jet deflectors operated via linkage by a common servo motor. Small brake nozzle between the 2 main nozzles, jet splitter on the top of lower nozzle to minimize jet disturbance from the other jet. Casing equipped with guide plates to deflect jet towards the tailwater in the case of runaway. Occasionally badly sanderoded by fatigue-conditioned failure of the surge tank lining. (Drawing courtesy J. M. Voith.)
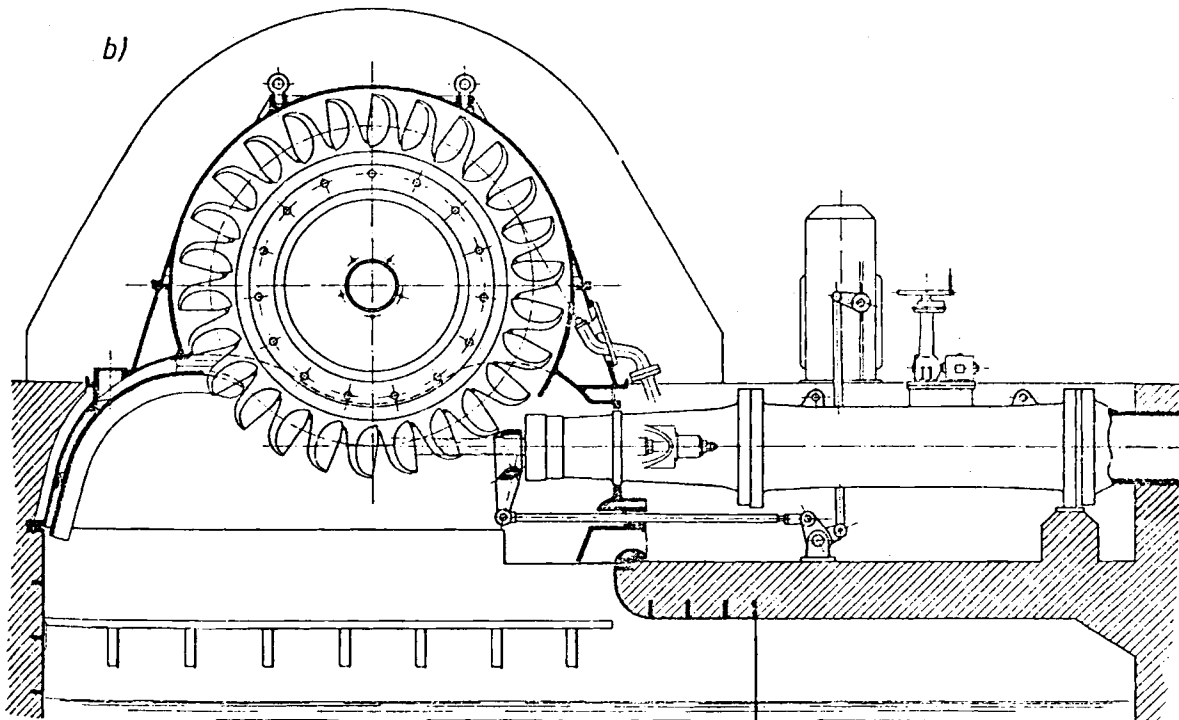
Fig. 10.3.15. b) Cross section of 1-wheel, 1-jet horizontal shaft PT Salanfe Miéville. Switzerland built by Vevey-Charmilles Engineering Works, Switzerland. Straight admission pipe, needle servomotor in the nozzle pipe, jet presser, brake nozzle. Because of the high head, small jet wheel diameter ratio. H = 1447 m, n = 500 rpm, P = 35,2 MW. This is the 3 rd highest head of the world used by a PT. The PTs with the highest heads in the world, namely Chandoline, Grande Dixence. Switzerland (H = 1740 m, P = 36,6 MW) and Reisseck, Austria (H = 1765 m. P = 22,8 MW) are also of the 1 wheel 1 nozzle type and were built also by Vevey Charmilles Engineering Works. Switzerland. (Drawing courtesy Vevey Charmilles Engineering Works.)

10.3.3. The limits of a FT in the lower head range

According to the experience of Sulzer Escher Wyss, there exists also a zone of overlap with the Kaplan turbine (KT). This range has approximately an upper limit at a head of about 70 m. Some KT plants with an upper head limit above this figure are usually located at the base of a dam storing their tailwater and needing no essential excavation for submergence.

In the range of low flows between 1,5 and 2,2 m³/s up to a head of 23 m, the upper head limit H(m) of this zone reads (Fig. 10.3.16): $ln H = 1,33 + 2,42 ln Q$, Q in m³/s. In the head range between 23 m to 67 m and the flow range between 2,2 m³/s to 13 m³/s this limit is given by: $ln H = 2,55 + 0,672 ln Q$.

In the head range below 70 m and a flow above 27 m³/s the limit between FT and KT follows from $ln H = 0,668 ln Q$.

These formulas reflect only the actual state of the art. This changes in course of time so as to raise the output and head limit for a KT in the future. This holds especially for lower flows between 13 to 350 m³/s. The causes for this evolution may be traced to the following reasons:

First the low-head FT with highest specific speed has a strongly hook-formed $\eta(P)$ graph
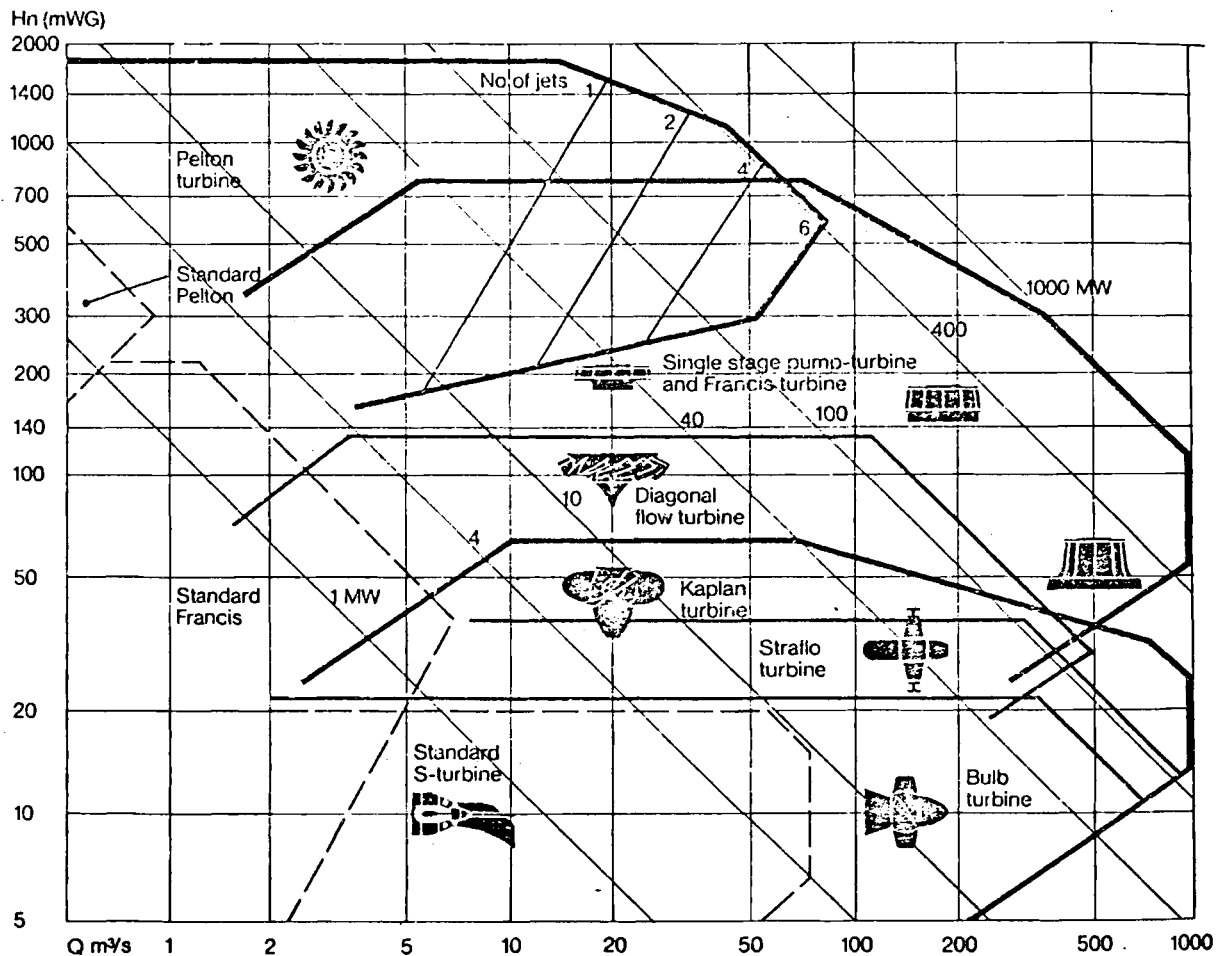
Fig. 10.3.16. Range of application for the various hydro turbomachines on a $Q(H)$-graph according to Sulzer Escher Wyss.

466

with a pronounced η peak at bep, whereas a KT especially the double regulated one, has a flatter curve around the bep. Thereby the KT can be adapted better to a changing demand of power. This item must be put aside in a plant with a large number of sets.

Furthermore the KT operating with constant speed can be adapted much better than a FT to head variations at nearly constant efficiency. Further the runner of a FT with $n_s > 350$ is axially too elastic and is mechanically not suitable for elevated heads, whereas a KT runner of this n_s-range is no problem. Finally the level of bep efficiency of a FT runner with highest specific speed $n_s \geq 350$ of this type is rather low.

Examples of large and medium FTs in this range of n_s are shown in Fig. 10.3.8 and Fig. 10.3.17.

10.3.4. Efficiency of a FT as a function of specific speed

After a systematic survey carried out on 340 FTs, Zanobetti found the efficiency at bep to depend as follows on the specific speed n_s in the range $145 < n_s < 340$ [10.34]:

$$\eta_{op} = \eta_{op\,m} - 0{,}35 \cdot 10^{-2}(n_s/145 - 1)^2. \tag{10.3-2}$$

For $\eta_{op\,m}$ see (10.3-1). Hence for a given head the designer should tend to set n and $P_{1/1}$ so as to obtain $n_s = 145$. At full load with an efficiency drop $\Delta\eta$ of about 2% the efficiency according to Zanobetti [10.34] becomes

$$\eta_{1/1} = \eta_{op\,m\,1/1} - 0{,}0413\,(n_s/145 - 1)^{1{,}75}. \tag{10.3-3}$$

Finally the same author found the efficiency at 50% of full-load output $P_{0.5\,1/1}$ to be expressed by

$$\eta_{0.5} = \eta_{0.5\,op} - 0{,}0521\,(n_s/145 - 1)^{1{,}592}. \tag{10.3-4}$$

In the above $\eta_{op\,m\,1/1} = 0{,}935\,(0{,}925)$ and $\eta_{0.5\,op} = \eta_{op\,m\,1/1} - 0{,}04$. The relations demonstrate clearly that the efficiencies η_{op}; $\eta_{1/1}$; $\eta_{0.5}$ decrease when n_s increases above 145. Note that these values apply to very large units. Hence for a FT with $n_s = 420$: $\eta_{op} = 0{,}92$; $\eta_{1/1} = 0{,}87$; $\eta_{0.5} = 0{,}72$. This figure makes clear the limits of n_s due to a FT.

A rather bad feature of a FT, also occurring on a KT with fixed runner vanes, is the pressure surge in the draft tube, when the machine operates away from the bep (Cap. 5.5, 8.2 and 9.8) and if its runner is of the overhung design.

Contrary to a KT the FT has a more moderate submergence in consequence of its smaller cavitation index (see Table 9.2.1).

Also the runaway speed the set has to withstand, which increases with rising n_s from 1,4 to 2 times the normal speed, is considerably smaller for a FT than for a KT. This appears in the dangerous case of off-cam operation at low heads up to 3,5 times the normal speed [8.132].

10.3.5. The design of a Francis turbine

The design of a FT starts from H, Q given the topography and the hydrograph. The speed n must be compatible with the grid frequency and the integer number of pole pairs of the alternator but set, if possible, so as to get a specific speed $n_s = 145$, where $n_s = n(\text{rpm})\,(P_{1/1}\,(\text{kW}))^{1/2}/H\,(\text{m})^{5/4}$. As outlined in Cap. 9.2, for reasons of limited submergence and runner strength, a certain n_s is assigned to H, a relation which corresponds to the
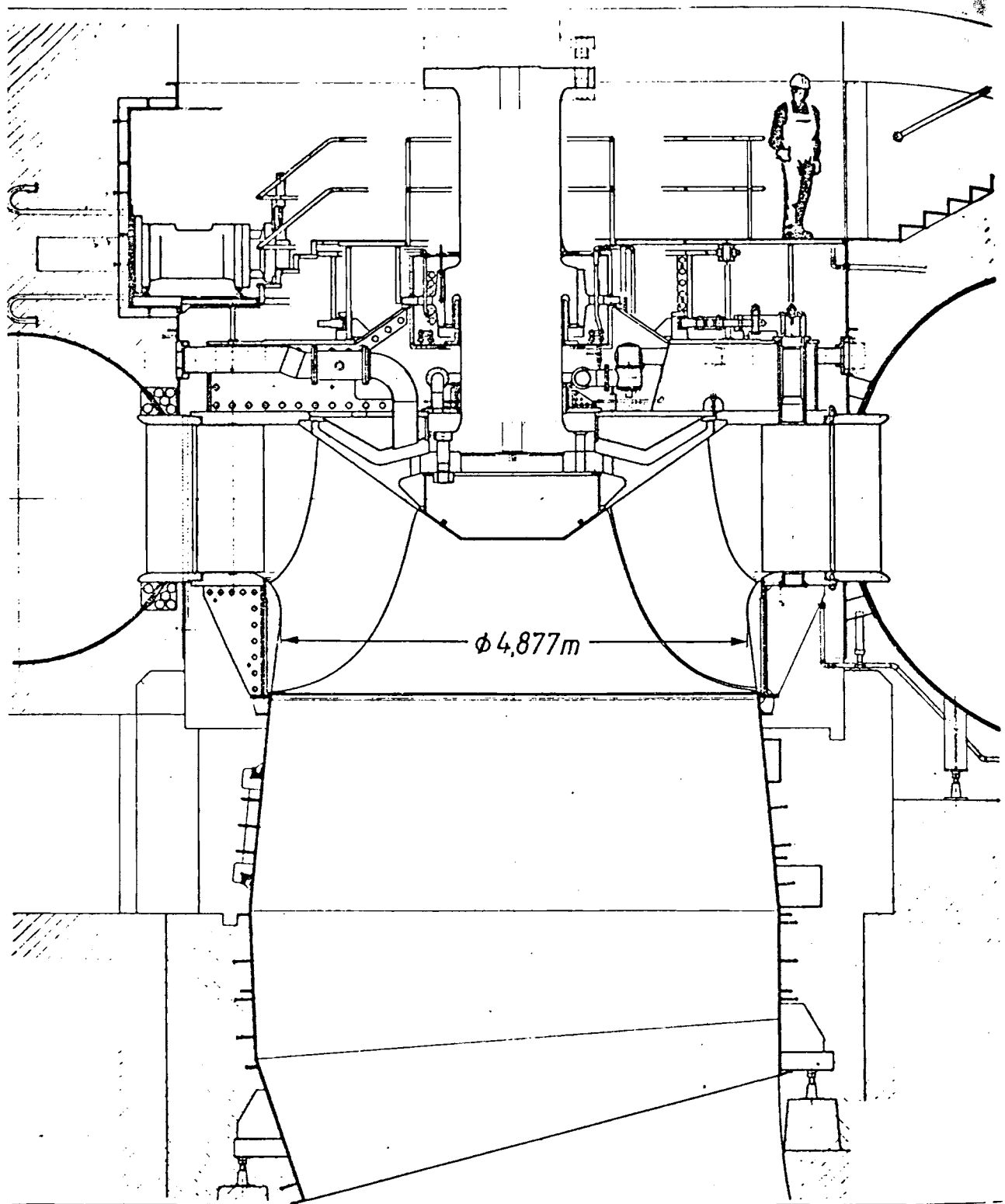
Fig. 10.3.17. Elevation of the FT at Hartwell, Ohio, USA, built by Voest Alpine, Linz, Austria. $H = 51,8$ m; $n = 112,5$ rpm; $P = 80$ MW. Runner $D = 4,877$ m. Simplified design of the runner hub. Bell-shaped guide bearing, machined from shaft, submerged in the oil pan to facilitate lubrication whilst starting up. Parallel plate spiral casing, head cover and bottom ring split into halves for transportation, bolted together on the site. Gate lever with a shear pin as breaking device, if a foreign body is squeezed between adjacent gates. (Drawing courtesy Voest-Alpine, Linz, Austria.)

468

state of the art, which in the future will move to assign higher n_q (n_s) values to a certain head.

Setting n_s above the actual limit for H, means firstly higher submergence and hence excavation cost. Then the runner is more highly stressed, so as to require a stronger material or to need a more careful stress calculation [10.52], e.g., by finite element method [10.139]. This holds especially for larger and hence more elastic units as seen in Fig. 10.3.17 and 10.3.8.

Table 10.3.1. Empirical values for a Francis turbine runner as a function of the specific speed $n_q = n Q^{1/2} H^{-3/4}$, n rpm, Q m³/s, H m.
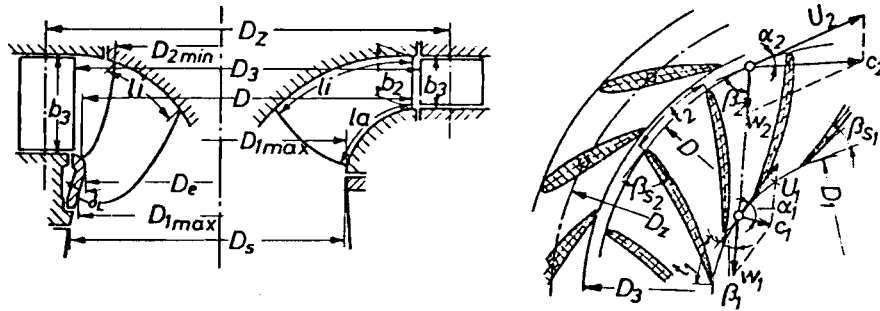
n_q	rpm	17	29	43	57	70	85	100
max H	m	700	520	300	180	120	80	64
$Q_{11\,1/1}$	m³/s	0,123	0,230	0,466	0,715	0,948	1,166	1,280
n_{11}	rpm	61	62,5	65,3	70	75,5	82,5	92,2
max n_{11}	rpm	106	107	117	131	146	161	180
$Q_{11\,1}/Q_{11\,1/1}$		0,81	0,81	0,82	0,84	0,87	0,88	0,88
$\eta_{i\,1}$		0,88	0,885	0,90	0,905	0,905	0,905	0,90
$\eta_{i\,1/1}$		0,845	0,855	0,87	0,88	0,885	0,88	0.875
$c_{11}^2/2gH$		0,024	0,033	0,049	0,065	0,082	0,098	0,115
σ		0,045	0,055	0,075	0,1	0,14	0,195	0,27
D_{2i}/D		1,0	1,0	0,98	0,92	0,85	0,775	0,695
D_3/D		1,04	1,052	1,054	1,02	1,03	1,03	0,99
D_s/D		0,6	0,68	0,825	0,955	1,06	1,12	1,15
b_3/D		0,055	0,1	0,167	0,23	0,288	0,326	0,327
l/D		0,36	0,32	0,28	0,26	0,25	0,26	0,28
l_a/D		0,27	0,22	0,17	0,14	0,13	0,14	0,15

$\eta_{i\,1}$ efficiencies for model runners of 0,3 to 0,6 m $\varnothing$ under a head of 5 to 60 m
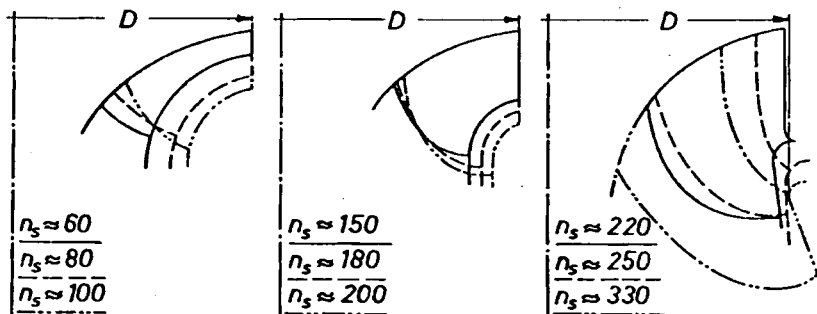
For a given specific speed n_s or n_q, the rated unit discharge $Q_{11\ 1/1}$ and unit speed n_{11} are obtained from Table 10.3.1. Hence the runner diameter alternatively (for control)

$$D = n_{11}\, H^{1\cdot 2}/n, \qquad D = [Q_{1/1}/(Q_{11\ 1/1}\, H^{1/2})]^{1/2}. \qquad (10.3\text{–}5)$$

As a third control the blade tip speed coefficient Ku may also be optimized with respect to a maximum surplus during the useful life of the turbine, following the lines of Cap. 4.4. Once n(rpm) and $\omega = \pi n/30$ are known, then

$$D = (2/\omega)\, Ku_{op}(2\, gH)^{1/2}. \qquad (10.3\text{–}6)$$

Once D is known and the figures D_{2i}/D, D_3/D, b_3/D, l_a/D, l_i/D, D_s/D are taken from Table 10.3.1 as a function of n_q, the elevation of the runner, inclusive of the gate's outlet edge and draft tube inlet may be plotted, aided by the contours of the runner given in the above table as a function of n_s. (For $\eta_{1/1} = 0{,}9$: $n_s = 2{,}97\, n_q$.)

It must be emphasized that the contour is more or less set at will and reflects the experience of a special maker.

In the following some design features (as a function of H or n_s) may be mentioned, found in the survey of modern trends in the design of FTs by *de Siervo* and *de Leva* [10.33]

$$n_s = 3470\, H^{-0{,}625}, \qquad Ku = 0{,}323 + 2{,}2 \cdot 10^{-3}\, n_s. \qquad (10.3\text{–}7)$$

The outer diameter of the runner outlet edge D_{1a} follows from the rated output $P_{1/1}$ and a coefficient usually referred to as the coefficient of the largest runner outlet diameter C_1, a figure which for machines above a n_s about 200 corresponds to what is called the runner throat coefficient

$$D_{1a} = C_1 (P_{1/1})^{1/2}. \qquad (10.3\text{–}8)$$

This rule follows the experience that the flow through a device or machine under a certain head is usually dictated by the size of its narrowest passage. C_1 may be traced to the similarity laws (Cap. 9.2), according to which, with $D = D_2$, $D_{1a} = D_1$, the speed may be expressed by $n = C\, Ku(D_1/D_2)\, H^{1/2}/D_1$ with C as a dimension-linked constant. Eliminating n from this by means of the definition of $n_s = n(P_{1/1})^{1/2}/H^{5/4}$ gives

$$C_1 = C\, Ku\,(D_1/D_2)/(n_s\, H^{3/4}). \qquad (10.3\text{–}9)$$

Since the values Ku, n_s, H and D_1/D_2 depend on n_s, C_1 also is a function of n_s. According to *Zanobetti*'s review [10.34]

$$C_1 = 0{,}075 + 0{,}855 \cdot 10^{-2}\, n_s. \qquad (10.3\text{–}10)$$

For the output, according to Cap. 9.2: $P = P_{11}\, D^2\, H^{3/2}$. Hence by logarithmic differentiation and putting $dP = P - P_{1/1}$ and $dH = H - H_{1/1}$: $P/P_{11} = -0{,}5 + 1{,}5\, H/H_{1/1}$. After *Zanobetti* for the machines reviewed

$$P/P_{1/1} = -0{,}433 + 1{,}44\, H/H_{1/1}. \qquad (10.3\text{–}11)$$

The span of the gate depends according to *de Siervo* [10.33] on n_s as

$$b_3/D_1 = 0{,}188 + 0{,}5 \cdot 10^{-3}\, n_s. \qquad (10.3\text{–}12)$$

The axial depth 'a' of runner (Fig. 10.3.18) as the distance of the outmost point on the runner outlet edge from the distributor's centre line, according to *de Siervo* and *de Leva*, is given by [10.33]

$$
\begin{aligned}
a/D_1 &= -0{,}05 + 42/n_s, & (50 < n_s < 110)\\
a/D_1 &= 1/(3{,}16 - 0{,}0013\, n_s), & (110 < n_s < 350).
\end{aligned}
\qquad (10.3\text{–}13)
$$

470

Fig. 10.3.18. Elevation of FT set with the parameters to calculate earth excavation, and characteristic relations for the lay-out of a FT.
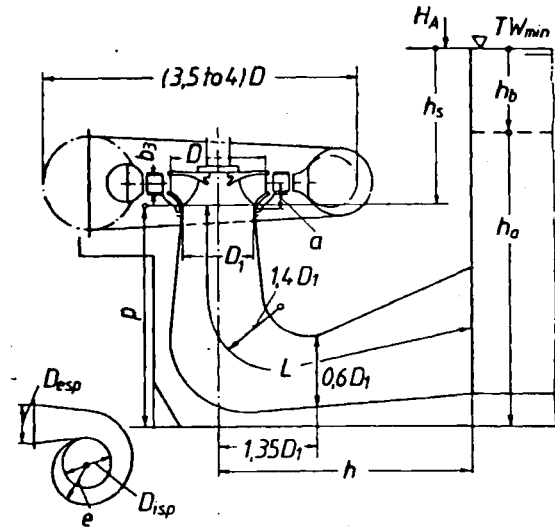
The distance of the centre lines due to adjacent sets is after [10.34] in relation to D_1

$$A/D_1 = 17.7\, n_s^{-0.272}. \tag{10.3-14}$$

Hence $A/D_1 = 5.06$ and 3.75, at $n_s = 100$ and 300.

The submergence (or the suction head h_s) of the runner outlet follows by the well-known relation of Cap. 8.3 by means of a cavitation index from Table 10.3. From *de Siervo* [10.33] the cavitation index σ reads as a function of n_s

$$\sigma = 7.54 \cdot 10^{-5}\, n_s^{1.41}. \tag{10.3-15}$$

This approximates the values recommended by *D. Thoma*.

- Draft tube: Depth of draft tube bottom below the runner outlet (Fig. 10.3.18), from *de Siervo* [10.33]

$$p/D_1 = 1.54 + 203.5/n_s. \tag{10.3-16}$$

The same author recommends for the horizontal length h of an elbow draft tube (Fig. 10.3.18) taken from its centre line

$$h/D_1 = n_s/(- 9.28 + 0.25\, n_s). \tag{10.3-17}$$

Depth of draft tube bottom below the deepest point of the runner outlet edge 2.5 to 3 D_1. Length of draft tube cone 0.8 D_1. Horizontal distance of bend outlet from the turbine axis about 1.35 D_1 (Fig. 10.3.18). Height of bend outlet section 0.6 D_1. Radius of curvature of the bend's centre line 1.4 D_1.

- Spiral casing: Mean velocity in the spiral intake at full load flow $Q_{1/1}$ for $n_s = 60$ to 350 [8.132]:

$$c_{esp\ 1/1} = (0.15 \text{ to } 0.25)(2\,gH)^{1/2}.$$

Hence inlet diameter D_{esp} of spiral casing by continuity. Internal diameter of spiral casing at stay vane inlet for a non-parallel plate stayring: $D_{isp} = (1.4 \text{ to } 2.4)\, D_{esp}$ at $n_s = 77$ to 240. The last value is subjected to large changes. This follows from the ratio of stay vane number to gate vane number and from the gate vane number itself. For large machines both vane numbers are equal. Moreover the gate number increases from say 8 for very small units to 28 for very large ones.

471

Finally the diameter is influenced by the fact whether the spiral casing is of the parallel plate design after Piguet (Fig. 10.3.4) [3.128] or the classical design (Fig. 10.3.5). The latter is more space consuming, and stresses the stay vanes, its crown and bottom cover more than in the first design but if offers a more smooth intake for the stay vanes.

As a general rule attention has to be paid to the strength of the spiral, stay vane rings and stay vanes, head and bottom cover and distributor vanes under the following relevant loads especially developed at closed gates: Water load under test pressure, which is usually 1,5 times the highest working pressure composed of the static pressure plus the highest admissible pressure surge due to water hammer.

Load of the thrust bearing, when this is supported by a truncated cone on the head cover. Membrane stress from the shell of the spiral casing usually calculated so as to assume the top most quasi cylindrical section through the spiral casing wall as free of shear parallel to the machine axis. Besides the junction between spiral casing wall and the stay vane rings (usually casings) also transfers bending moments The strength of the stay vane ring is the core of a FT design.

By adopting Piguet's contracted spiral casing with parallel plates of the stay vane ring, the calculation becomes more reliable and transparent, since the stay vanes are then of constant span over their streamwise length, and are attacked more centrally by the membrane pull from the spiral casing wall.

The bending moment in the junction of a spiral casing is a consequence of the closure of an imaginary gap that would exist if the load-induced deformations of the stay ring and spiral casing were considered independent of each other. This gap would exist along the circular junction of stay ring and spiral casing. In reality it is closed mainly by the action of an internal bending moment around a tangent of this circle. This causes a bending stress in the meridional direction, which has to be superimposed on the meridional membran stress due to internal pressure of the spiral casing. In a welded design, for reasons of fabrication, this highly stressed junction is implemented by a weld seam. Manhole and pedestal of the spiral casing, or the concrete propping it, must not overstress it.

Moreover there are fatigue problems in the spiral casing, the stay rings, and the stay vanes of sets which often change their mode of operation [10.124 to 10.131].

The stress calculation of the gate and its drive in closed position under squeezing adjacent gates needs the same care with respect to strength [10.59; 10.89; 10.122]. Here the "submergence" of the gate drive (see Figs. 10.3.1 or 10.4.17) into the head cover (if possible) avoids jamming of the gate stem by deformation of head cover, enables statically determined support of the gates (two bearing arrangement) and eliminates the fatigue problem at the transition between stem and blade of the gate. The latter follows from the fact that in a two bearing arrangement, this section with its strongly varying sectional modulus is not subjected to axial bending stresses (acting parallel to the stem), whose flux would there experience a strong contraction connected with notch effects [2.23]. However such a design is restricted to heads below 450 m (the FTs of Grand Coulee III built by Allis Chalmers can be considered to be an exemplary construction of this type). (See Cap. 2.3.)

The head cover of huge and high head machines must be stiff so as to avoid deformation causing fouling of the runner within the labyrinths and exciting runner vibrations by variation of the labyrinth's gap clearance [8.132].

The circumferential development of the cross sectional area of the spiral casing tube follows from the intention to distribute the flow to the runner uniformly over the circumference, with an angular momentum near to that required by the runner.

To reduce the loss in the case of highest heads, usually the angular momentum within the spiral tube is smaller than required by the runner. To save space in the case of low-head plants with semi-spiral casings, the angular momentum in the duct of the latter is larger than required. Because of the relatively small kinetic energy in the ducts of the guide apparatus there, this does not influence the efficiency. At any rate, the change to angular momentum required is effected by the stay and guide vanes.

Dimensioning of the cross sections is based on the assumption that at least in the first three quarters of the circumference a velocity distribution is generated that corresponds

472

to that of a free vortex. Hence the distance e of the outmost spiral wall from the machine axis depends as follows on the azimuthal distance φ from the radius due to the inlet section of the spiral case near its tongue: $\varphi(e/D_{esp})$ 90°(1,8...2,5); 180°(1,7...2,3); 270°(1,5...1,9); 360°(1,3...1,4).

For heads below about 30 m also semi-spiral casings are applied. Inlet width: $2,9 \cdot D$. Eccentricity: related to the axis of the turbine: $0,2 \cdot D$. Maximum height: $1,4 \cdot D$. Maximum lateral distance of the spiral chamber wall from the axis: $1,4 \cdot D$, [10.147].

10.3.6. Design of the runner vane, simplified method

1) Division of the runner vane channel into i elementary turbines ($i = 2$ for small n_s, $i = 5$ for high n_s, according to Fig. 10.3.19), having the same flow $\Delta Q = Q_{op}/i$. Q_{op} follows from the ratio $Q_{11\,op}/Q_{11\,1/1}$ in Table 10.3.1. Continuity for an elementary turbine, local span Δb, local distance from axis r, local meridional velocity c_m, local contraction coefficient φ (due to vane and boundary layer), requires

$$\Delta Q = 2\pi \Delta b\, r\, c_m\, \Phi = \text{const}. \qquad (10.3-18)$$

The procedure is best satisfied along a normal to the preliminarily set meridional streamlines in the n-direction. Strictly speaking introduction of c_m requires knowledge of the c_m distribution, Cap. 10.6 or 6.4. A simplified mean value of $c_{m,M}$ follows from
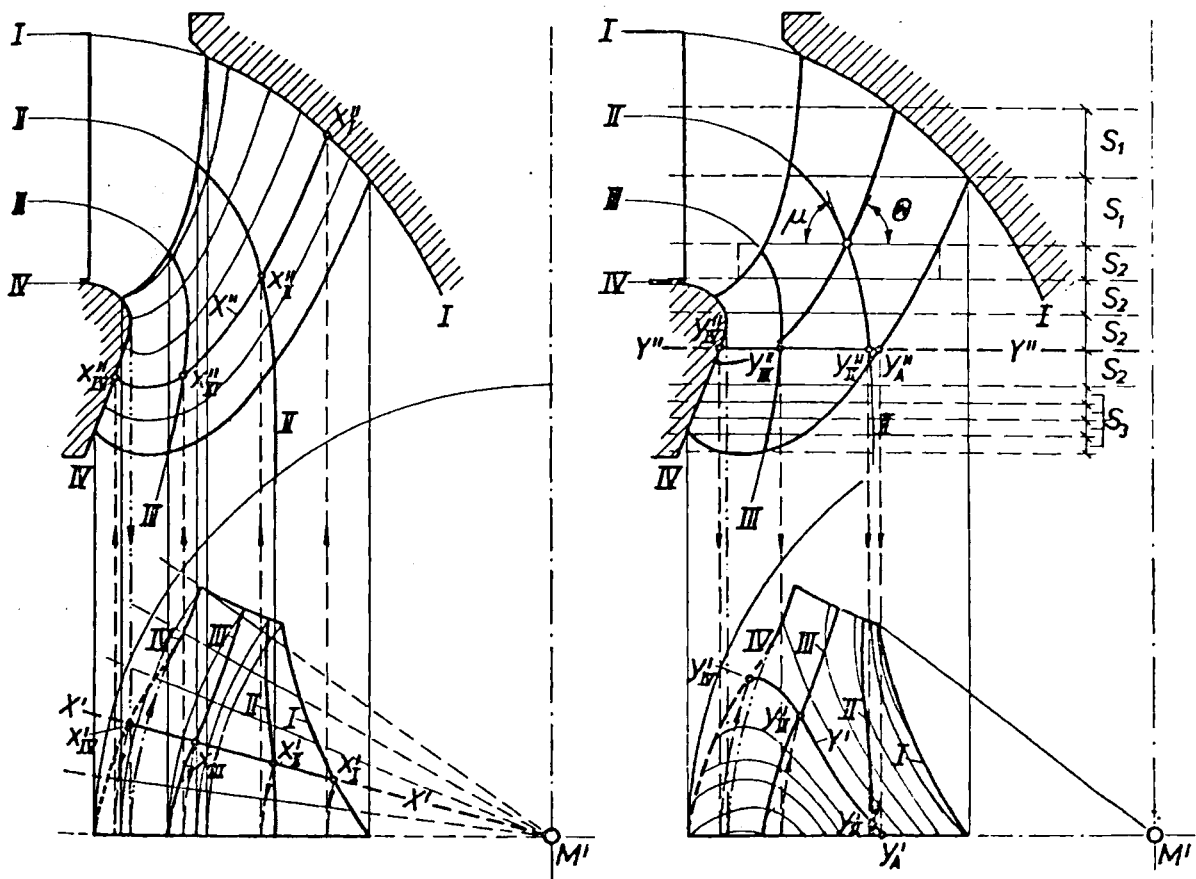
Fig. 10.3.19. Elevation and plan of an arbitrary FT (here with $n_q = 100$) with elementary turbines, radial and pattern sections and angles.

473

$c_{m.M} = Q_{op}/(2\pi r_M\,b\,\Phi)$, where b is the local breadth of rotor, r_M the mean distance of this breadth from axis. Then $c_m = \xi\,c_{m.M}$. More rigorously ξ is obtained from the potential flow pattern in the meridian, gained by the graphical method after Cap. 5.2; roughly with $n_q = 60\ldots330$, on the shroud $\xi = 1\ldots1,8$ and on the hub $\xi = 1\ldots0,5$. The contraction coefficient Φ may be preliminarily estimated between 0,9 and 0,7.

Strictly speaking Φ depends on the real vane thickness h, the angle β' between the pattern making vane section and the periphery, the angle Θ between the radial vane section and radius, the radius r and the vane number z as follows [8.132]

$$\Phi = 1 - [h\,z/(2\pi r)](1 + \cot^2\beta'/\sin^2\Theta)^{1/2}.$$

(10.3–19)

Strictly speaking h contains also the displacement thickness of the boundary layers on both the vane faces. Roughly h corresponds to the vane thickness resulting from the stress calculation given later on.

In general the vane number z is odd to avoid excitation of torsional vibrations at the instant the rotor vane cuts a wake from the gate, whose number is in general even. The number of runner vanes may vary from $z = 7$ to 17 for heads of 20 to 700 m.

2) Assumption of the streamwise change of angular momentum: After tests on Francis turbines by *Bär* [5.17] and *Schlemmer* [5.18] (Figs. 10.3.20 and 10.3.21), carried out at Lehrstuhl und Labor für Hydraulische Maschinen und Anlagen TU München, West Germany, in a streamwise direction at a working point near the bep, the angular momen-
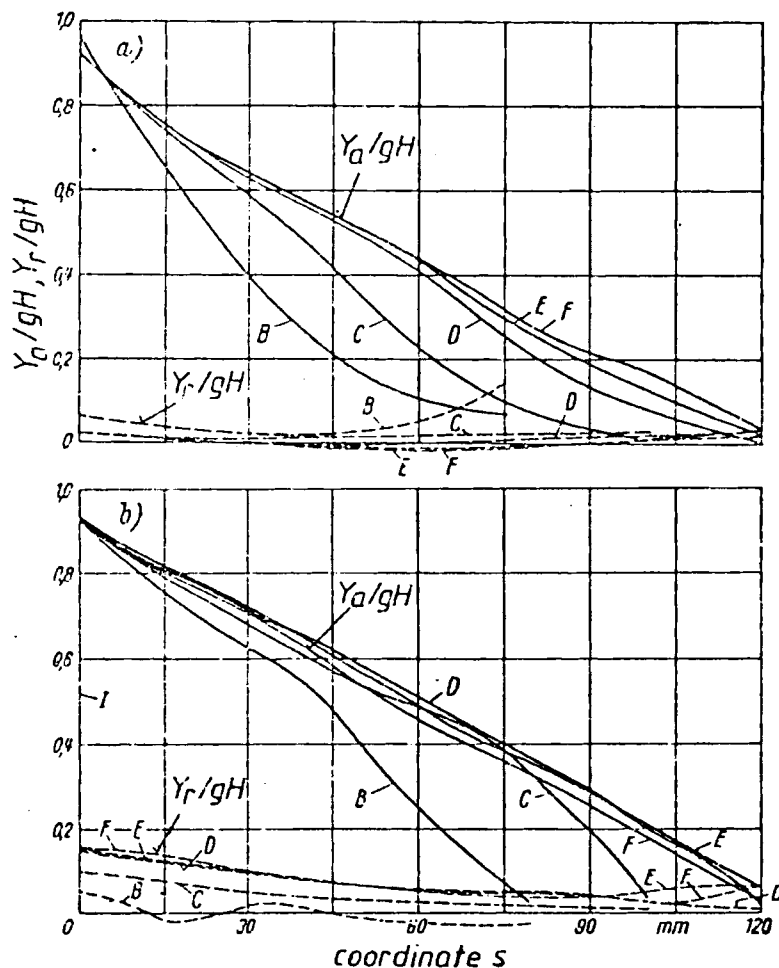
Fig. 10.3.20. Test results, showing the graph of the absolute flow energy Y_a and rothalpy Y_r, both related to specific head gH vs unrolled meridional stream line length s for various elementary turbines of a FT with $n_q = 70$ at bep according to the hill diagram of Fig. 10.3.21. B elementary turbine close to the shroud; F ditto close to the hub. Accordingly lines C, D, E belonging to the mean meridional streamlines of the elementary turbines from the shroud to the hub. From *E. Bär*: Messung des relativen Strömungsfeldes in Wasser an der Laufschaufel einer schnelläufigen Francisturbine. Forschung Ing. Wesen **36** (1970), no 2. p. 54/64.

coordinate s

474

Fig. 10.3.21. Hill diagram of a FT with $n_q = 70$ in the bep, obtained by tests on a model with $D = 0.455$ m runner diameter. With relative velocity w and angle β with circumference at runner inlet at different operating points according to the measurements of Schlemmer, in a mean flow plane [5.18]. Beginning and increase of surging in the runner indicated by arrows A: suction face, shroud; B: suction face, hub; C: suction face, shroud unsteady flow, pressure face shroud, and hub; E: suction face, shroud.

tum drops nearly linearly from the leading inlet edge (there having a magnitude $c_{u2} r_2 = (gH\,\eta_u - c_{u1}\,r_1\,\omega)/\omega)$ towards the value $c_{u1}\,r_1$ at the outlet edge of the rotor. The above tests also show the derivative of angular momentum along a normal n to the meridional streamlines $(\partial(c_u r)/\partial n)$ to be vanishing small at the bep and away from the leading edge of the runner vane, see below.

For the case of the bep $c_{u1} = 0$. Hence the whirl at a certain station with the radius r,

$$c_u = [gH\,\eta_{u\,op} - \Delta Y_a(s_m)]/(r\,\omega), \qquad (10.3-20)$$

where $\Delta Y_a(s_m)$ is an arbitrary steadily falling function vs the meridional stream path s_m, measured from the inlet edge and being $gH\,\eta_{u\,op}$ at the outlet.

Such an arbitrary drop of the flow energy Y_a within the runner in the streamwise direction can be set only along one elementary turbine. The relation (6.5–4) for the distribution of the meridional velocity as a function of the distribution of angular momentum normal to the streamlines shows that only in the case of a loss free flow and $\partial(c_u r)/\partial n = 0$, the distribution of the meridional velocity in the n-direction (normal to the meridional streamlines) becomes independent of the $c_u r$ distribution normal to the streamlines.

Assuming hence this simple case, then two things have to be satisfied:
1) The $c_u r$ distribution along the other elementary turbines has now to account for the one prescribed $c_u r$-course such as to have always $\partial(c_u r)/\partial n = 0$. See also tests [5.18].
2) According to (6.5–4), the c_m distribution now remaining, follows the law $c_m/dn + c_m/R = 0$, where R is the radius of curvature of the streamline in the meridian. The last mentioned differential equation for c_m is that of a potential flow in the meridian. Hence strictly speaking the graphical method described in Cap. 5.2 has to be employed to obtain the more correct distribution of the meridional velocity instead of the rough estimate with the factor ζ. But this holds good only for a design with $\partial(c_u r)/\partial n = 0$.

475
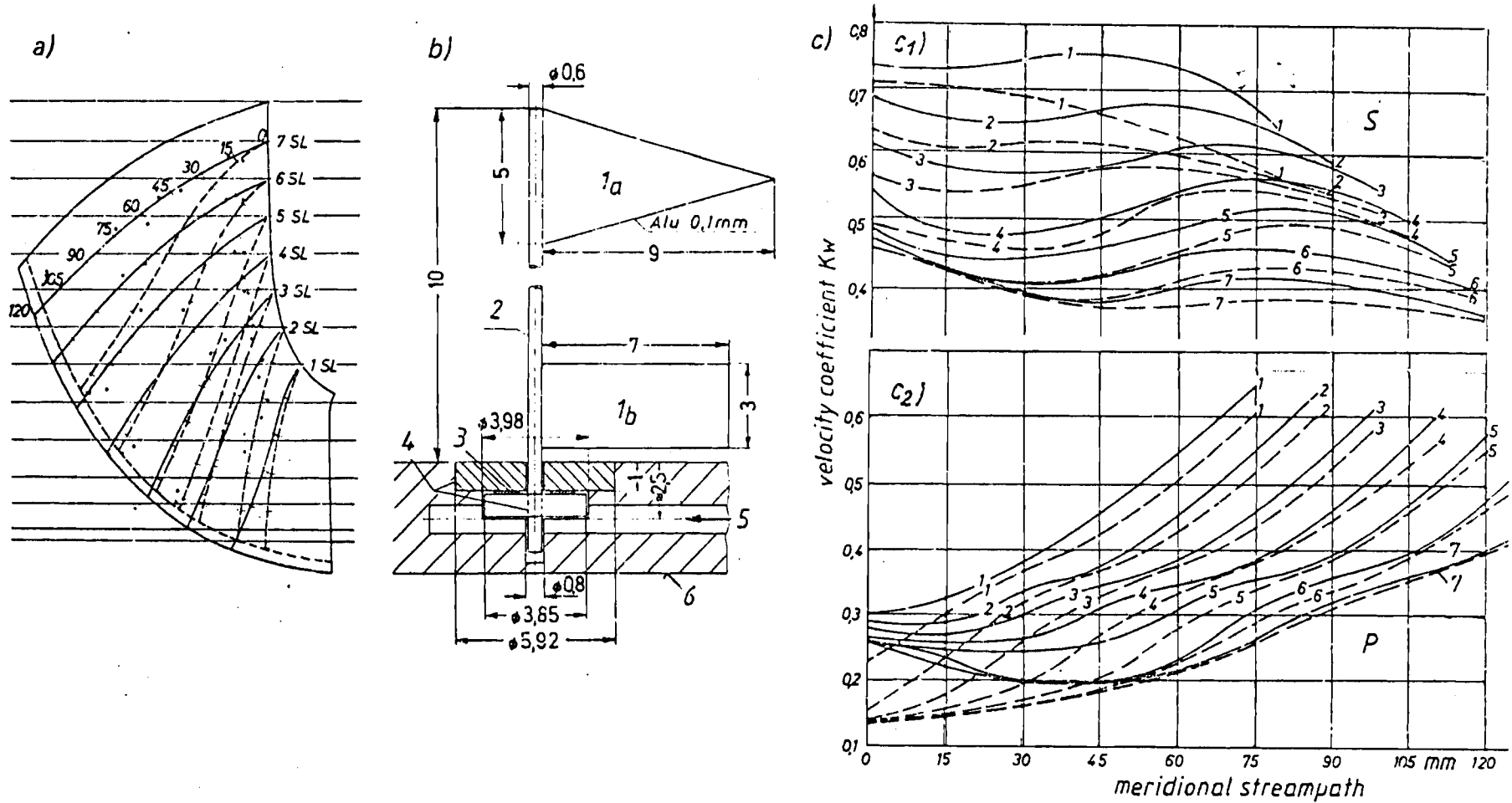
Fig. 10.3.22. Relative flow in a FT runner according to the test carried out by *Schlemmer* [5.18]. a) time-averaged meridional streamlines at the bep (point 3 in the hill diagram of Fig. 10.3.21) on pressure face (------) and on the suction face (——) indicated by b) microflags 1 a or 1 b on a rod 2, with a friction collar 3, on a piston 4, loaded by pressurized air 5; the whole inserted in a runner vane 6. By means of the friction collar, the time-averaged direction of the flag and thus of the relative flow could be retained after the runner was stopped and the separately inserted vane (Acryl glass) was dismounted. c) coefficients of the relative velocity measured at bep. c1) K_w vs unrolled meridional streamline (see a)) on the suction face S: —— in 7,5 mm distance from the vane face, ——— in 1,7 mm distance from it. c2) K_w ditto on the pressure face P. From *Schlemmer* [5.18].

This hint may be sufficient, as it shows how the method works. Assume in the following that the above conditions are satisfied and the absolute flow field is given. This flow field and the resulting relative flow field is assumed to be a pitch-averaged flow field and to be along the runner vane.

3) Calculation of the flow angle β: Once the whirl velocity c_u, the meridional velocity c_m and the peripheral blade speed $u = \omega r$ are known at any station of the runner, then from the velocity triangle of the channel centre line (Fig. 5.21 f), the angle β between relative velocity w and circumference results from (w, c_m, c_u now valid at centre line)

$$\beta = \arctan\left[c_m/(u - c_u)\right]. \tag{10.3-21}$$

Hence the relative velocity along the channel centre line follows from

$$w = c_m/\sin \beta.$$

The corresponding relative velocities on the suction and pressure face at the same parallel circle, radius r, follow from the relations (5.2-32 to 34). The latter facilitates a prediction of the cavitation index σ according to Cap. 8.2.3.

Fig. 10.3.22 shows the coefficient of relative velocity from measurements along the suction and pressure face of a Francis turbine with medium specific speed [5.17].

4) Calculating and setting of the pattern making and radial vane sections: This procedure is characterized by the intention to make the curvature of the relative streamline along the vane as small and as steadily varying as possible and by an effort to avoid any change in sign of the curvature in streamwise direction.

After (6.5-13), the angle β' between the pattern making section and periphery, the known angle β, the known angle μ of the meridional streamline and radius and the angle Θ of the radial vane section with the radius are related to each other by

$$\tan \beta' = \tan \beta \sin(\Theta + \mu)/\sin \Theta. \tag{10.3-22}$$

At the outlet edge, which usually is in a meridian, Θ is known. Along the other radial vane sections, the angle Θ may be set at will and depends mainly on the circumferential extension of the vane in the plan (Fig. 10.3.19). Usually the inlet edge makes a dihedral angle and is not normal to the axisymmetric streamface.

This reduces the excitation of torsional vibrations at the instant the runner vane's inlet edge cuts a wake from the gate's outlet edge, which is parallel to the turbine axis. By the skewed inlet edge, the rotor vane cuts the wake only at a certain station and not along its whole span as would be for a vane with its leading edge within a meridian.

Once the angles Θ, μ and β are known at any station, β' then follows from (10.3-22). Thus the vane skeleton is fixed point by point. Note that the flow so far is assumed axisymmetric and along the vane skeletons. Any prediction of the real flow along the vane, needs the methods described in Cap. 6.2 and 10.6.

To obtain a reasonable form of the rotor vane channel by the previously mentioned method, the radial vane sections have to be set for a uniformly curved vane (see Fig. 10.3.19).

The required thickness h of the vane, normal to the skeleton, follows from the stress calculation of the next section. With h, β', Θ, the vane thickness in the peripheral direction h_u results from (Cap. 10.3.9)

$$h_u = h(1 + \cot^2 \beta'/\sin^2 \Theta)^{1/2}. \tag{10.3-23}$$

Adding h_u 2 on both the faces of the skeleton along its pattern section in circumfere... direction yields the pattern section due to the real suction face and pressure face of the vane.

10.3.7. Simple stress calculation of a runner vane

Assume a runner vane to be intersected by numerous adjacent cylindrical sections. Imagine that all the blade slices so obtained are turned into one meridian. Thus the blade is transformed into a radial rib with the same thickness h_u as the real blade in the peripheral direction [8.132].

This rib is considered as a beam loaded normally by the hydraulic load component in the tangential direction. The beam is clamped at both of its ends on the hub and shroud respectively so as to be displaceable parallel to itself at the shroud's end, see [10.154].

The centrifugal load is neglected, as it acts against the hydraulic load. Its omission has to be accounted for by an adequate choice of safety factor.

The decisive peripheral force at start up is derived from the known full load torque $M_{1/1} = P_{1/1}/\omega$.

According to the torque vs speed characteristic, the starting torque is x_1 times the full load torque (x_1 being 1,3 to 2 for $n_s = 330$ to 60). The tangential force due to this starting torque is assumed to act on the rib, restricted as above, on the known pressure centre of the rotor vane, on a station a distance l_{hi} from its clamped end at the hub (Fig. 10.3.23 a). This gives the fixed end moment there

$$M_b = x_1 \, x_2 \, P_{1/1} \, l_{hi}/(\omega \, z \, r_{ss}),$$
(10.3-24)

where r_{ss} is the radius on which the tangential hydraulic load acts on the rib, x_2 accounts for the different kinds of support possible at the shroud's end of the beam. More exactly,
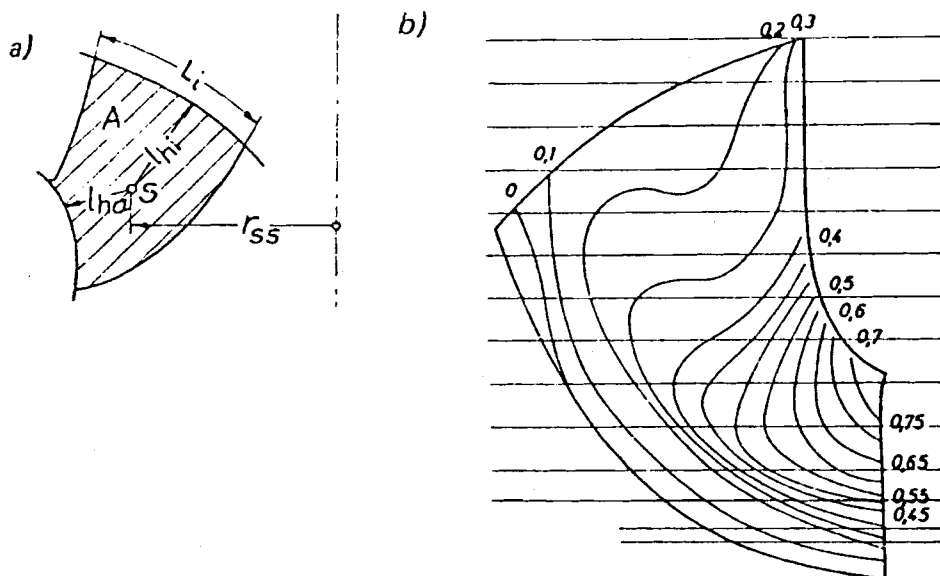
Fig. 10.3.23. Stressing of a FT runner. a) Circular projection of runner vane onto a meridian with its centre of pressure S for the peripheral hydrodynamic load. S derived from the measurement of the differential pressure $(p_p - p_S)(\varrho g H)$ between the pressure and suction face, shown in b). b) Distribution of the differential pressure Δp in the bep of a FT $n_q = 70$ (see Fig. 10.3.21). From Schlemmer [5.18].

478

the values l_{hi} and r_{ss} follow from the measurement of the runner vane's differential pressure (Fig. 10.3.23 b). For a runner with shroud $\alpha_2 = 3/4$, without a shroud $\alpha_2 = 1$. The innermost vane section of meridional length L_i (Fig. 10.3.23) and maximum peripheral thickness h_{um} has a sectional modulus of about

$$W_b = \alpha_3 h_{um}^2 L_i, \qquad (10.3-25)$$

where $\alpha_3 \approx 1/6$ for vanes of constant thickness and $\alpha_3 \approx 1/12$ for streamlined vanes. From the last two relations the bending stress in the clamping section of the vane on the hub

$$\sigma_b = M_b/W_b. \qquad (10.3-26)$$

σ_b has to be set with respect to the neglected centrifugal load. Then the above yields the maximum vane thickness in the peripheral direction h_{umi} at the hub. For a streamlined profile along the arc L_i on the hub, the distribution of the real peripheral vane thickness starts from its maximum h_{mi} [4.11]. The real vane thickness h, normal to the vane then follows from h_u by means of (10.3-23) as β' and Θ are known..

10.3.8. Simple stress calculation of the hub

The cross section of the hub half has its centre of gravity in a distance r_c from the axis (Fig. 10.3.24). With m_c and m_s as the masses of hub and the z vanes, the mean tensile stress in the tangential direction within a meridional section, area A, at runaway speed ω_{ra} becomes

$$\sigma_{\omega u} = \omega_{ra}^2 (r_c m_c + \alpha_4 z r_{ss} m_s)/(2 \pi A), \qquad (10.3-27)$$

where $\alpha_4 \approx 1/2$ for a runner with shroud and 1 for a runner without a shroud. A bending stress σ_{bu} has to be added to the tensile stress $\sigma_{\omega u}$. This results from a bending moment about the radial neutral axis of the cross section A. This bending moment M results from a tangential moment caused by the centrifugal loads of the vanes about the centre of gravity of A being $\alpha_4 m_s z r_{ss} \omega_{ra}^2 l_\omega$ (Fig. 10.3.24) and a similar counteracting moment caused by the axial thrust on the hub being $F_a l_a$. This gives the bending stress [10.35]

$$\sigma_{bu} = [e/(2 \pi I)] (\alpha_4 m_s z r_{ss} \cdot r_{ss} \omega_{ra}^2 l_\omega - F_a l_a), \qquad (10.3-28)$$

where I is the area moment of inertia of the face A about its radial neutral axis intersecting the centre of gravity, and e, the largest axial distance a point on the boundary of the section A has from the neutral axis (Fig. 10.3.24).
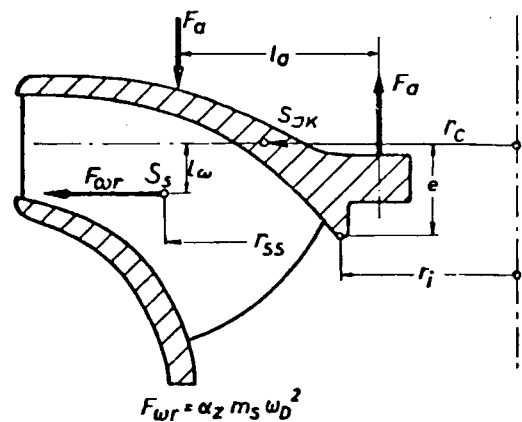
Fig. 10.3.24. Loads acting on the hub of a Francis runner, causing a bending stress about the radial neutral axis through the centre of gravity S of a meridional hub section. For safety $l_a F_a/2\pi$ (the moment due to axial thrust on the hub) should be calculated for the case of a blocked leakage flow.

479

To be on the safe side, the torque of the axial thrust about the circle of radius r_c, $F_a l_a$ should be calculated for the dangerous case of a blocked leakage flow at the hub. Then the axial thrust can be approximated by $F_a = \pi p_2 (D^2 - D_1^2)/4$ and its moment arm by $l_a = D/\pi - d_a/2$, where D_1 is the throat diameter as the approximate diameter of the labyrinth of the runner, and d_a the diameter of the bolt circle at the shaft flange.

For a runner split into 2 pieces, the bolts attaching the halves to each other have to transmit a tangential load that corresponds to that from the resulting tangential stress according to (10.3-27 and 28). Attention has to be paid to the fact that the bolts can only be stressed in the zones of tensile stress within the partition flange.

10.3.9. Derivation of the relation (10.3-23)

Consider a. vane surface element in a cylindrical coordinate system (Fig. 10.3.25). Obviously the tangential plane of the vane face is determined by the pattern section with its angle β' with the circumference and a radial section with its angle Θ with the radius. Imagine the plane to be moved
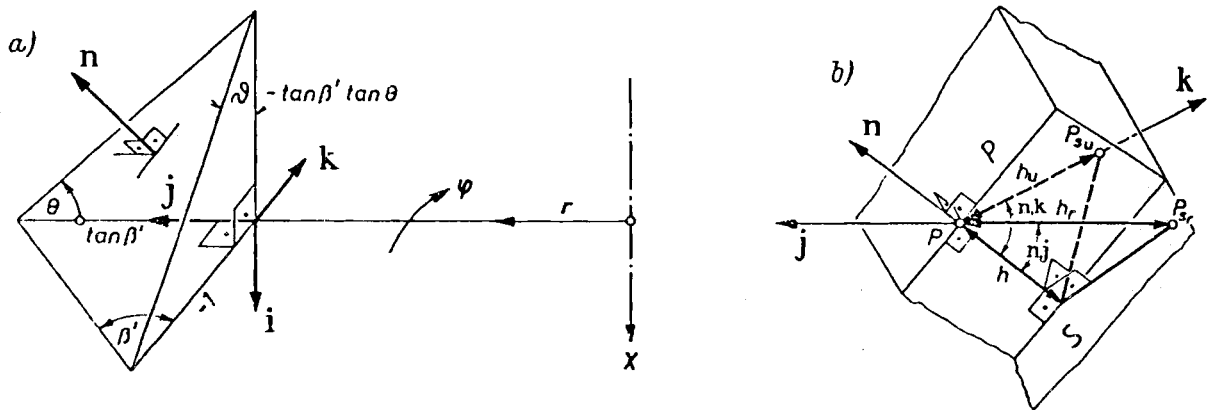
Fig. 10.3.25. Geometry of a runner vane element of constant thickness. a) Infinitesimal runner vane element, normal vector n, with a cylindrical coordinate system, where x rotor axis, r radius, φ tangential direction. b) Relation between the real vane thickness h, normal to the vane face, and the tangential vane thickness h_u making the angle (n, k) with each other, where k unit vector in tangential direction.

parallel to itself in the peripheral direction k by a distance $- 1$. Then the vane surface is described by the function: $- x \cot \beta' \cot \Theta + r \cot \beta' - r \varphi = 1$. Hence the normal vector of the vane: $n = - \cot \Theta \cot \beta' i + \cot \beta' j - k$. Thus the peripheral component of the unit normal vector:

$$\cos(k, n^0) = 1/(1 + \cot^2 \beta'/\sin^2 \Theta)^{1/2}. \qquad (10.3-29)$$

Obviously (Fig. 10.3.25 b), the peripheral thickness h_u of the vane as a function of the real thickness in the direction n^0

$$h_u = h/\cos(k, n^0). \qquad (10.3-30)$$

10.4. Optimization of pump-turbines in terms of efficiency and cavitation also applicable to impeller pumps[13])

10.4.1. Introduction

As mentioned in Chapter 2, to date pumped storage is mainly effected by pump-turbines. In the following, directions are given for the optimization of the main dimensions of a pump-turbine when its working data head gH and flow Q are known. These directions may be also used for the optimization of an impeller pump in a ternary set. For the latter see [10.69 to 10.72], [10.166 to 10.170].

The design of pump-turbines is based on the fact that a pump impeller can also be made to function as a turbine runner even though with somewhat less efficiency than a well-built turbine runner specially designed for the purpose. According to experience, a pump impeller engineered on optimum lines would reveal an outside diameter 40% greater than that of a turbine runner having the same type number. Even so, it is possible in principle to replace the pump and turbine of the ternary set in pumped storage plants by one reversible pump-turbine (binary set) [10.75], [1.50] and [8.132].

The first pump-turbines (with relatively low capacity) were installed during the early 1930's at the German Baldeney (2 MW) and Brazilian Pedreira (4 MW) facilities. The idea of the pump-turbine was not reverted to until after World War II in the USA where the first pump-turbine to be installed on a larger scale was that at the Flat Iron facility in 1950. With the two Taum Sauk pump-turbine sets (head 780 ft (240 m)) put into service in 1964, the USA achieved a spectacular breakthrough in penetrating the 250 MW limit, see [10.155; 10.156]. A new dimension has since been attained on the sector of US pump-turbine development in the form of the four 392 MW sets now in operation at the Racoon Facility along with the six 457 MW Bath County sets scheduled for service in 1979 (Fig. 10.4.1). Mentioned should also be the wourld's highest head pump-turbine (H = 600 m) in the Yugoslavian Bajina Basta plant built by Toshiba, Japan [10.85].

For highest heads the non adjustable multistage PuT was developed, see Fig. 10.4.2 and Fig. 3.4.37. The 2-stage PuT with adjustable gates facilitates a better adaptation to varying loads whilst turbining, Fig. 3.4.36. *W. Meier* proposed an adaptation of a PuT to the varying modes of operation by changing the number of stages, see Fig. 10.4.3.

European countries whose hydro-mechanical industries were able to point satisfactory results from the use of ternary sets installed at pumped storage plants, e.g., Italy, West Germany, Austria and France were slow to follow the US example, especially after having experienced some difficulty on their first large-scale pump-turbines at the point of transition from turbine to pump operation. Fig. 10.4.4 to 6 show examples of recent European pump-turbines [10.92; 10.157].

The following are a few of the "milestones" recorded in the field of pump-turbine development in West Germany.

In 1965 the first large-scale pump-turbines were commissioned for the Rönkhausen facility, Fig. 10.4.7, by Sulzer Brothers and Escher Wyss when the latter was an independent firm [10.75; 10.158; 10.159]. Another order came from the Vianden pumped storage plant in 1967 (already equipped with nine 100 MW ternary sets) for an additional 200 MW pump-turbine Vianden built by Sulzer Escher Wyss and Voith, Fig. 10.4.8 [10.160; 10.161]. The guide vanes on these sets are

---
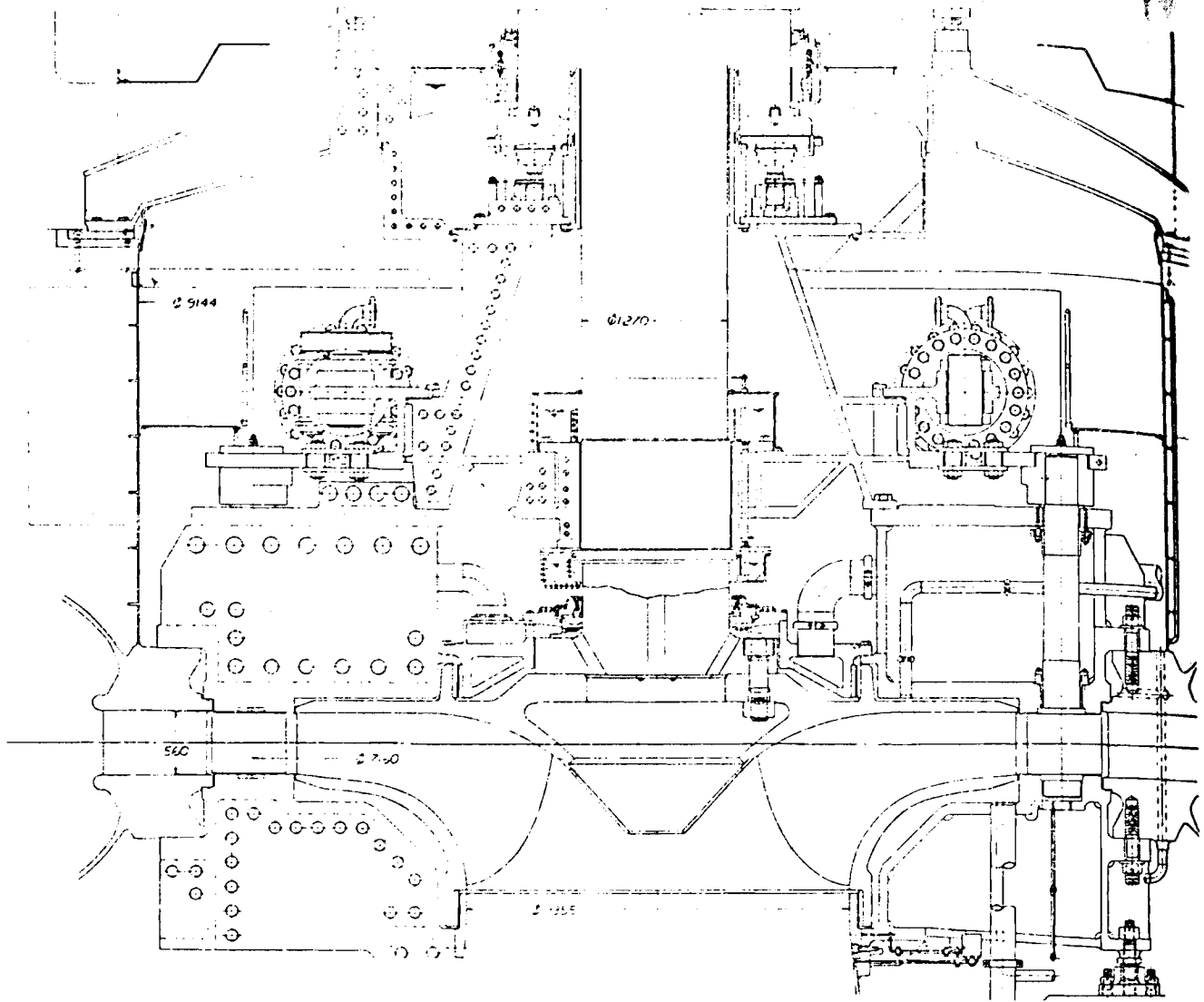
Fig. 10.4.1. Distributor section of PuT Bath County, Virginia, USA (owner Virginia Electric & Power Company). 6 sets. $H_r = 329$ m; $n = 257$ rpm; $P_r = 457$ MW. To date the largest pump-turbine with respect to size and output. Parallel plate spiral casing with a stay ring of cast steel and rolled steel plates welded on site. Welded, high head cover split into pieces for transporting and then bolted together. Thickness of the shroud and the hub reduced towards the rotor tip diameter to minimize the disc friction. Integrally cast rotor with exchangeable seals. Thrust collar machined from the shaft, bell-shaped, thus submerging the mean guide bearing in oil, to facilitate starting under fluid friction. Lower guide bearing lubricated by flinger shell with Pitot tube. Axial thrust derived into the stay vanes via a very stiff head cover and a truncated cone. The latter supports gate operating ring driven by a pair of servomotors propped on the turbine pit. The spiral casing attachment point to the stay ring is selected for each section separately to provide optimum balance of the moments due to head cover, spiral casing and water pressure. The stay vane centre of gravity is shifted to the outer edge, thus compromising its hydraulic performance to relieve this outer edge from tensile stress due to the membrane pull from the spiral casing. In the discharge ring design, only the inner sole ring, attached to the draft tube wall, and the outer sole ring, anchored by an articulation to the foundation, are transferring vertical loads from the discharge ring to the foundation [10.89]. (Drawing courtesy Allis Chalmers Corporation, Milwaukee, Wisconsin, USA.)

482
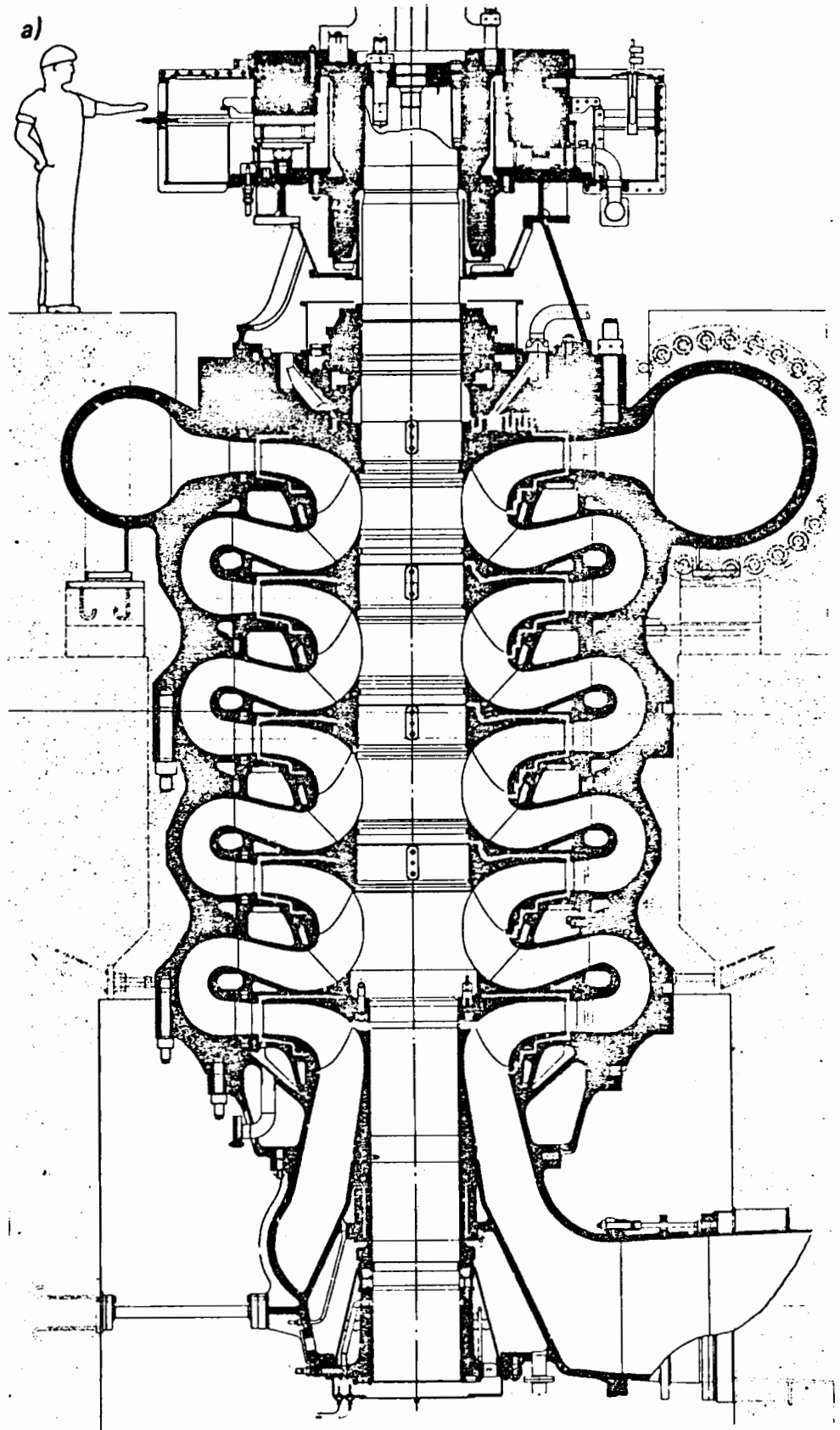
Fig. 10.4.2. a) Elevation of 5-stage non adjustable pump turbine La Coche, France, St Helene (owner EdF). Built by Neyrpic, France and Vevey Engineering Works, Switzerland. $n = 600$ rpm. Turbining: $H = 930,6$ m; $P = 80$ MW; pumping: $H = 943,9$ m; $P = 80$ MW. Multistage comb labyrinths. (Drawing courtesy Neyrpic, Grenoble, France.)
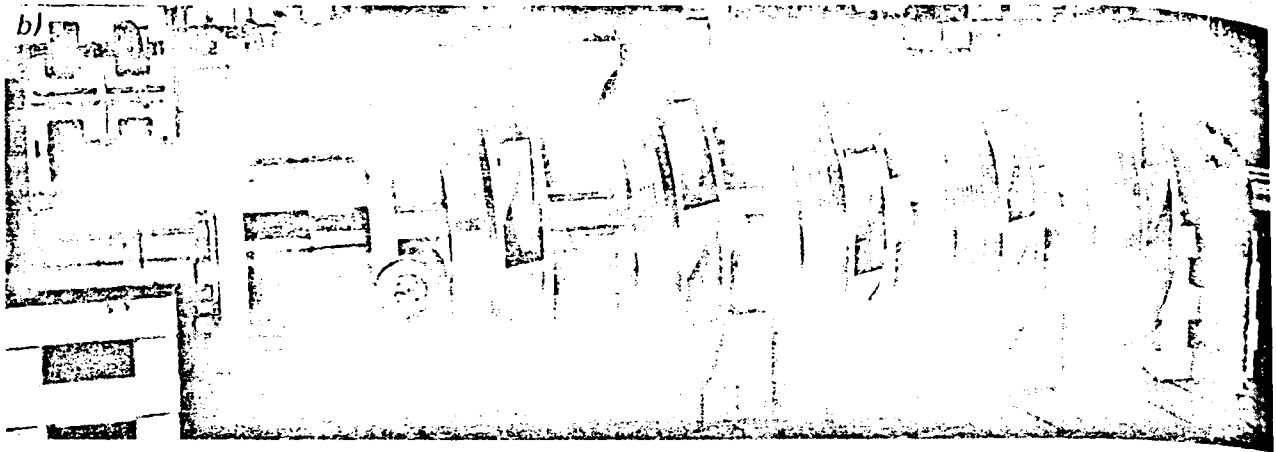
Fig. 10.4.2. b) Runner and shaft in Vevey Engineering Works. Note the skewed outer edges of the rotor vane faces to reduce the excitation of torsional vibrations and diffuser blade stall by means of wakes. (Photograph courtesy Vevey-Charmilles Engineering Works, Switzerland.)

operated by individual servomotors, and the motor-generator set is also capable of speeding up the water-filled pump-turbine into pumping action from the stationary phase with closed valve.

In 1972 two 75 MW pump-turbines were purchased from Voith for the Langenprozelten facility (Fig. 10.4.9) a power station serving to generate single phase traction power for the Federal Railway of West Germany. For the purpose of speeding up the pump-turbine into pumping action, provision was made in this case for a 27 MW Francis turbine designed on simple lines by Sulzer Escher Wyss to function as a starting turbine [10.162; 10 163].

In 1972 the 250 MW Rodund pump-turbine, Fig. 10.4.10 [10.164], was ordered from Voith to complement existing ternary sets in service at the Austrian Lünersee and Rodund 1 pumped storage plants. The head in this case amounts to 1140 ft (350 m).

According to [277] the further development of bep delivery head H_{op} and maximum input P_m of PuTs, ordered from Voith in the year indicated, is shown by the following plants: Coo, Belgium, 1975, H_{op} = 268 m, P_m = 206 MW; Kühtai, Austria, 1976, H_{op} = 409 m, P_m = 122 MW, Obravac, Yugoslavia, 1979, H_{op} = 548 m, P_m = 123 MW.

Modern trends in the design of pump-turbines are given in [10.76; 10.77; 10.80; 10.81]. Quite a number of papers have already been written on the subject of existing pump-turbines or pumped-storage sets of which only a brief selection can be cited here [10.103; 10.106; 10.157; 10.162; 10.165; 10.166; 10.167; 10.168; 10.169; 10.170].

Normally such treatises are concerned with the distinguishing features of a certain plant. This being the case, there appears to be some necessity to approach the subject of pump-turbine design from a more general theoretical angle based on practical results.

The principal objective of this chapter is to draw attention to a decisive factor, namely that of the costs rising from excavation work and mechanical losses occurring during the period of operation.

The key to the optimum design of the impeller (the actual centerpiece of a pump-turbine) is a new process applied to computing the type number of a semi-axial pump-turbine. Type number is functionally related to empirical loss coefficients (aerodynamics also being drawn upon for purposes of analogy), cavitation factors, operating characteristics such as flow rate and head, as well as known geometrical dimensions of the impeller and diffuser.

484
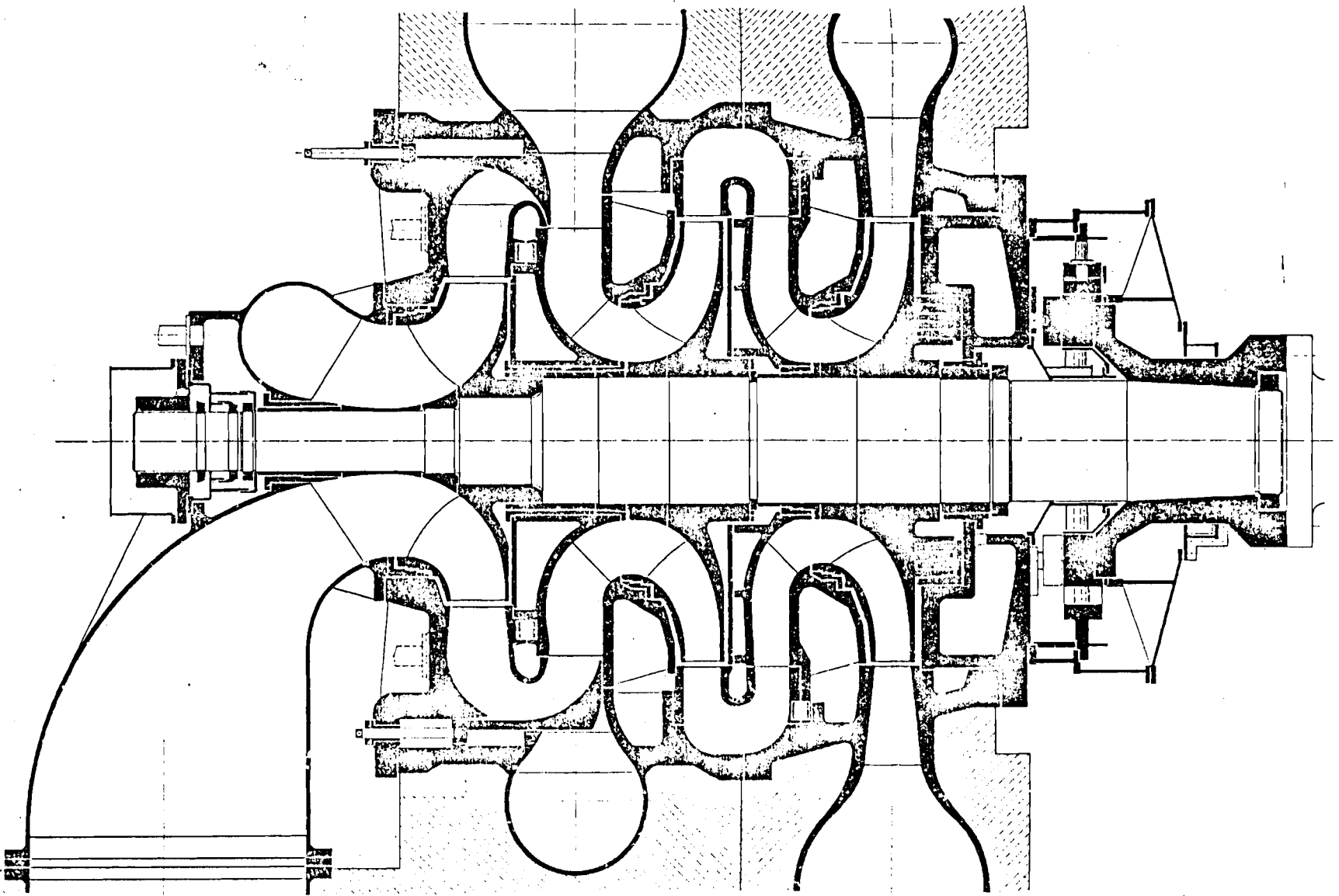
Fig. 10.4.3. Elevation of a so called "variastage pump-turbine", according to a proposal by *W. Meier* to adapt the machine during its various modes of operating to the data of the plant. Thus 2 stages during turbining (left side), then spiral-shaped draft tube, 3 stages during pumping (right side) (see ref. Fig. 10.3.8). Adjustment by cylindrical gate. (Drawing courtesy Sulzer Escher Wyss.)
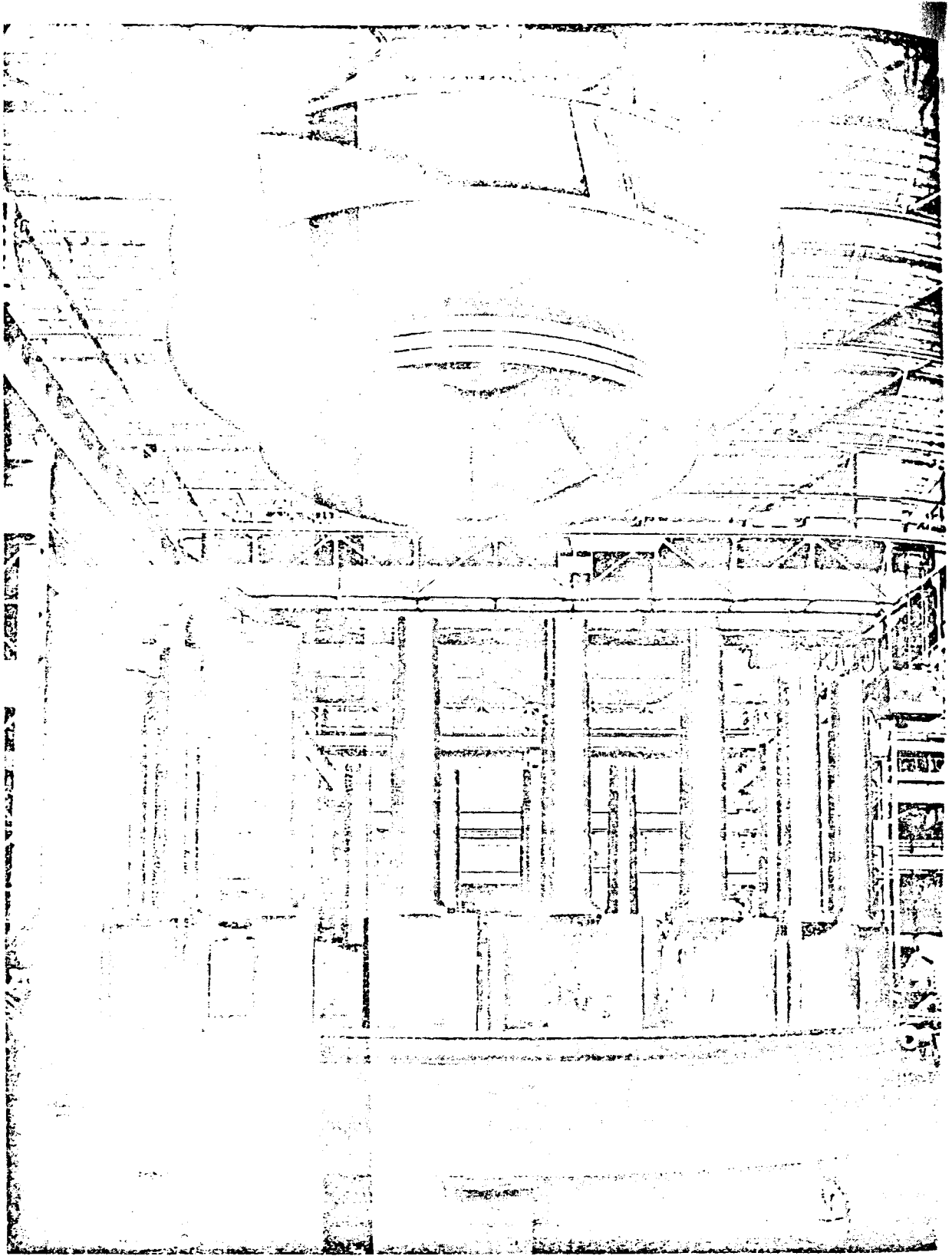
Fig. 10.4.4. Workshop assembly of the Caplijna pump-turbine (owner State Power Board of Yugoslavia) in the Hydroart shops, Milan, Italy. 2 sets whose PuTs are designed by Hydroart for a circular pit power house. $n = 300$ rpm. Turbining: $H = 237$ to 203 m; $P = 250$ to 202 MW Pumping: $H = 210$ to 260 m; $P = 218,8$ to 157,8 MW. Rotor: Integrally cast Cr/Ni 13/4 stainless steel, $D = 4.6$ m: weight 30 tons. Start up into pumping by connecting the AC grid, non-attenuated with the alternator. (Photograph courtesy Hydroart Milan, Italy.)
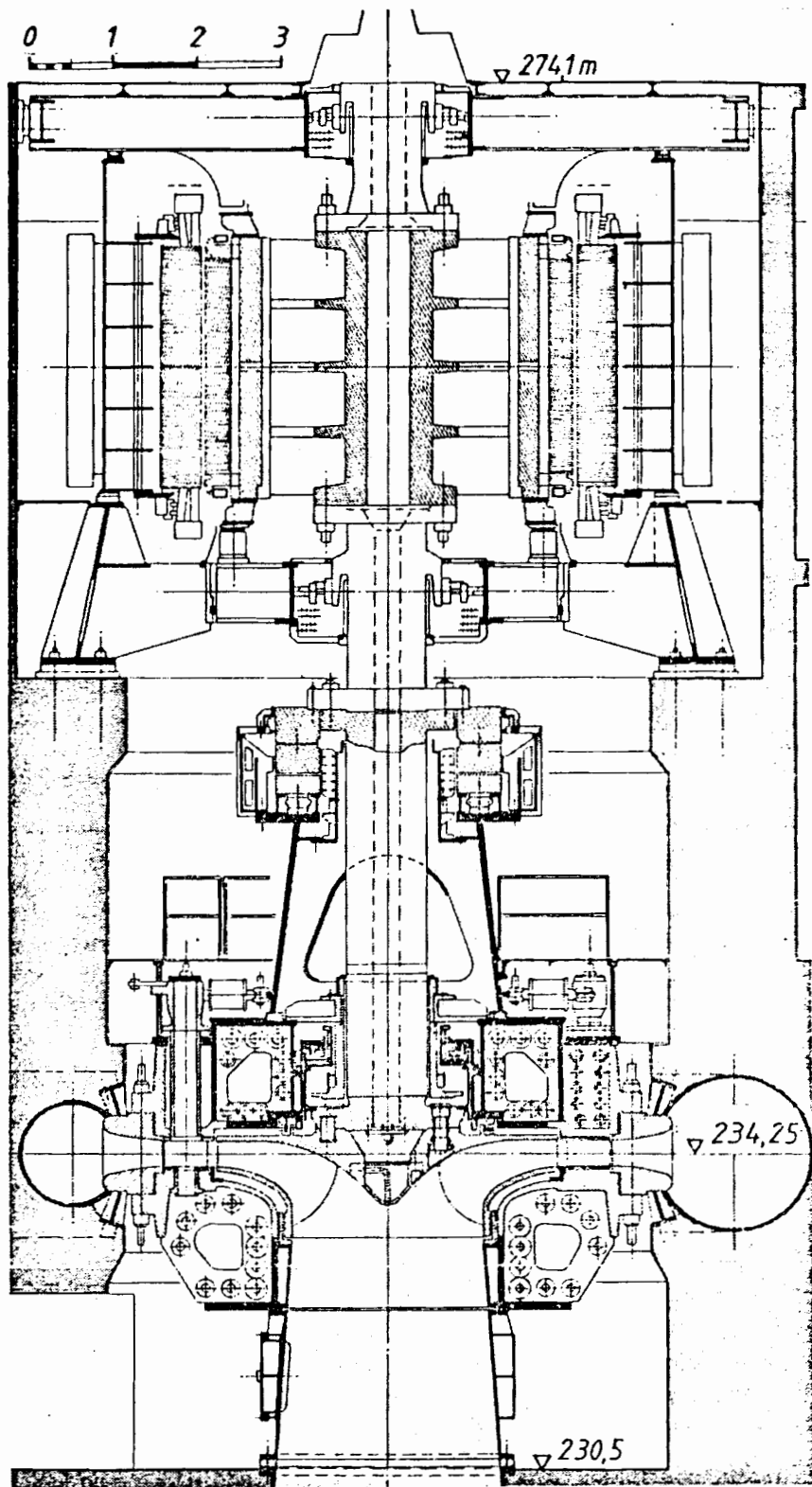
Fig. 10.4.5. Elevation of the pump-turbine set Montezic, Truyère, France (owner EdF). 4 sets built by Neyrpic, France. $n = 428$ rpm. Turbining: $H = 419$ to $378,9$ m; $P = 230$ to 193 MW. Pumping: $H = 388$ to 426 m; $P = 219$ to 202 MW. $n_{r_a} = 685$ rpm. Gate with single servomotors. Submergence under minimum tailwater level about 52 m. Maximum submergence 100 m. Fly-wheel moment $GD^2 = 2400$ m^2 tons. Rotor $D = 4,01$ m. Power absorbed of the dewatered rotor at synchronous speed $11,65$ MW. (Drawing courtesy Neyrpic, Grenoble, France.)

487

Fig. 10.4.6. Elevation of Dinorwic pump-turbine, Wales, Great Britain (owner: British power board). Design of Boving, London, on the base of model tests carried out at KaMçWa (Sweden), a joint venture of the Axel Johnson group. 6 units commissioned 1975 with the following data: $n = 500$ rpm, turbine mode, $H = 536$ m. $P = 317$ MW, pump mode, $H = 545$ m, $Q = 50$ m³/s, hence $nPH = 85,5 \cdot 10^6$ is the largest of all pump-turbines. The most powerful European pumped storage plant. Runner $D_1 = 2,03$ m, material stainless steel casting (13% Cr, 4% Ni). Efficiency as turbine 92,5%, as pump 91,7% (guarantee values for prototype) 24 gates, all rotating parts water lubricated except the guide apparatus which is automatically grease lubricated. 1 welded steel plate spiral casing, with a smooth transit to the guide plates of the guide vanes, 2 rotor, 3 bottom cover, 4 top cover, 5 guide vane, 6 guide apparatus, operated by a pair of servomotors, supported on the wall of the pit, via gate operating ring, links and levers, the latter having a friction emergency device, 7 shaft, 8 shaft seal. Compressed air is supplied via hydraulically operated valves in the interconnecting pipe work to the pump-turbine which rotates in air when neither generating nor pumping. This allows a quick start time for either operation. (Drawing courtesy KaMeWa and Boving.)
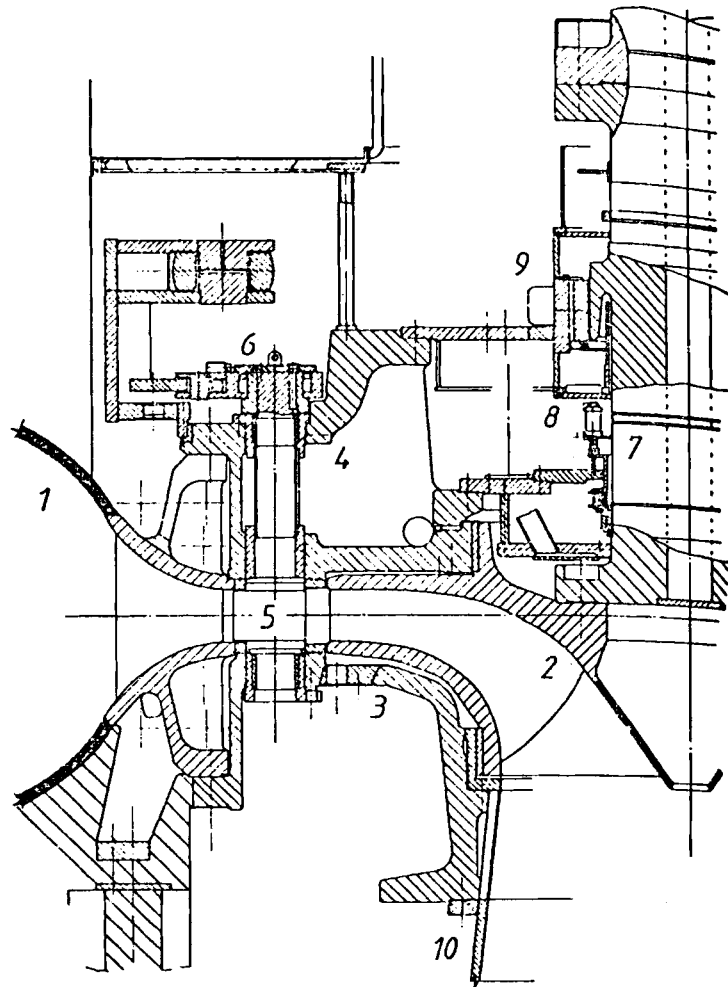
10.4.2. Optimum outside diameter of impeller on pump-turbines in terms of efficiency

Let us begin by making a study of impeller losses. In principle, the design of a pump-turbine is always required to proceed from a pump impeller. Only a pump impeller which, owing to the backward-bent vanes, reveals nonstalling relative flow and thus too, high efficiency η_P when pumping, is capable of functioning as a turbine achieving quite a satisfactory degree of efficiency η_T even in the case of reversed flow. Usually η_T is greater than η_P, but sometimes also η_P is the higher value. For example, the pump-turbine Leitzach (owner Stadtwerke München), $P = 50$ MW; $n = 333,3$ rpm; $H = 126$ m; built by Sulzer Escher Wyss, attains in service $\eta_P = 0,928$ and $\eta_T = 0,909$. (Start of operation in 1984).

The resulting costs K_r of a centrifugal pump (or pump-turbine) can be approximated in the following way as a function of the impeller outside-diameter D:

$$K_r = k_1 \cdot D^m + k_2 \cdot D^3 + k_3 \cdot D^{23/5} + k_4 \cdot D^{-2} + k_5. \tag{10.4-1}$$

488

Pump-turbine I (Escher Wyss)   Pump-turbine II (Sulzer)
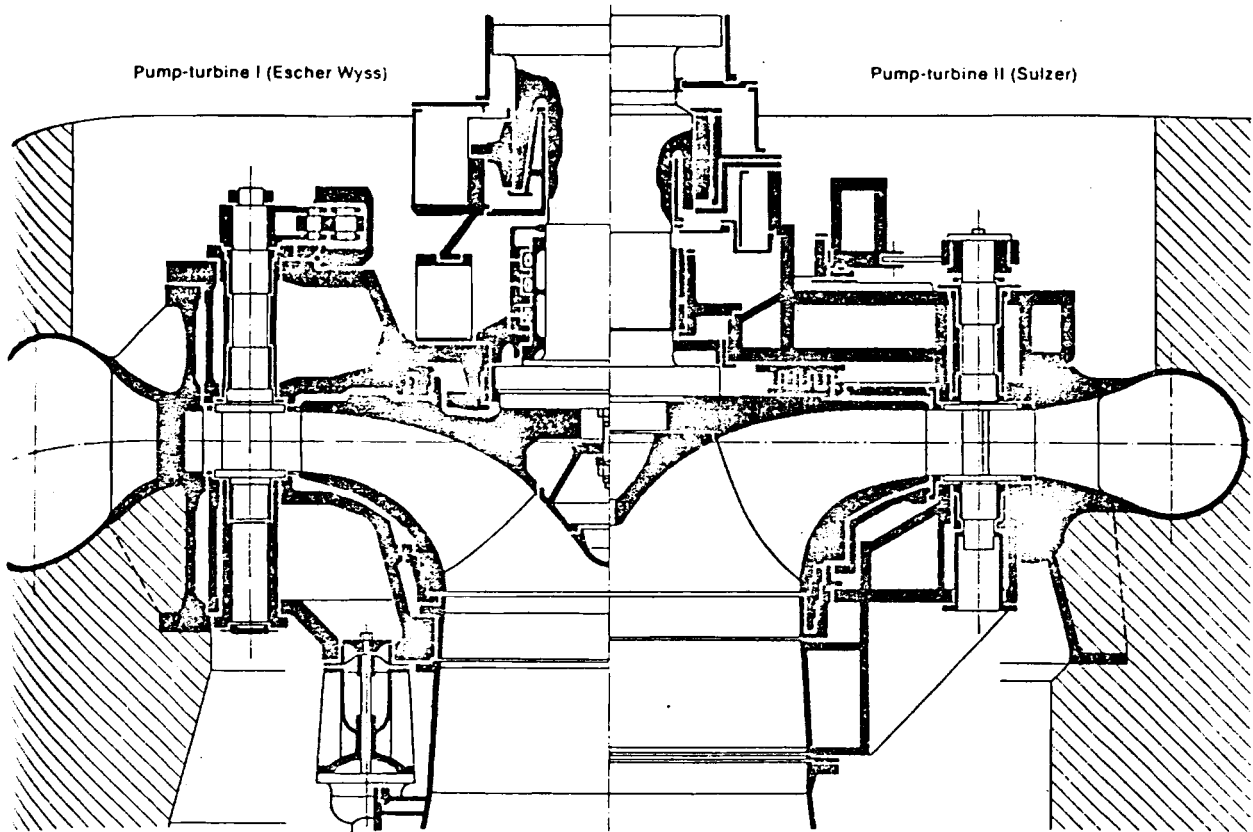
Fig. 10.4.7. Sectional drawing of pump-turbine Rönkhausen, Federal Republic of Germany (owner Elektrizitätswerke Mark). Left half (I): built by Escher Wyss by then (1966) an independent firm; right half (II) built by Sulzer Brothers; $H = 277,1$ to $253,6$ m; $n = 500$ rpm; submergence 16 m; internal diameter of spherical valve: 1,8 m; rotor vane number: 7; distributor (diffuser) vane number: 16. In the following the data of I left without, and of II right within brackets. Turbine mode: 74,8(79) to 63,8(70,8) MW; pump mode: 59,1(58,8) to 66,2(62,4) MW; static runaway speed $n_{ra} = 690(687)$ rpm; dynamic runaway speed $n_{rad} = 780(790)$ rpm. Air injection rate during turbine mode: at I under 0 to 30 MW, 1000 m³/h through the water guide plate upstream of the rotor; under 65 to 74 MW; 520 m³/h through the water guide plate upstream of the rotor, and through the draft tube wall: at II under 0 to 50 MW; 150 m³/h through the draft tube wall. Rotor tip diameter 2,76(2,8) m. Starting up pumping: rotor dewatered by pressurized air, after synchronization gates opened by a few millimeters until a water ring is formed, then release of the air through a vent valve. (Drawing courtesy Sulzer Escher Wyss.)

The 1st term of equation (10.4-1) having $m = 2,2$ to $2,4$ indicates the costs of manufacture composed of processing costs (proportional D^2) and material costs (proportional D^3). The 2nd term combines the building and excavation costs for a large semi-axial machine having an extensive head and negative suction head. For example, on the pump-turbines newly installed at the Austrian Kühtai facility, which registers a head of 1460 ft (450 m), the suction head is at -144 ft (-48 m). This being the case it was essential to locate the power station in a pit having a depth about 330 ft (100 m).

The 3rd term is used to indicate disc friction losses occurring on the outer surfaces of the shrouds of the impeller. These losses necessitate an increase in power consumption so that additional costs are incurred throughout the entire service life of the machine which, given the average yearly number of running hours along with the average power costs per kWh, are capable of being computed.

The 4th term represents diffuser losses which, like the disc friction losses (3rd term), tend to force up the costs of energy as a function of decreasing diameter D. The final term describes losses that are not directly associated with the impeller external diameter D, as for instance leakage losses.
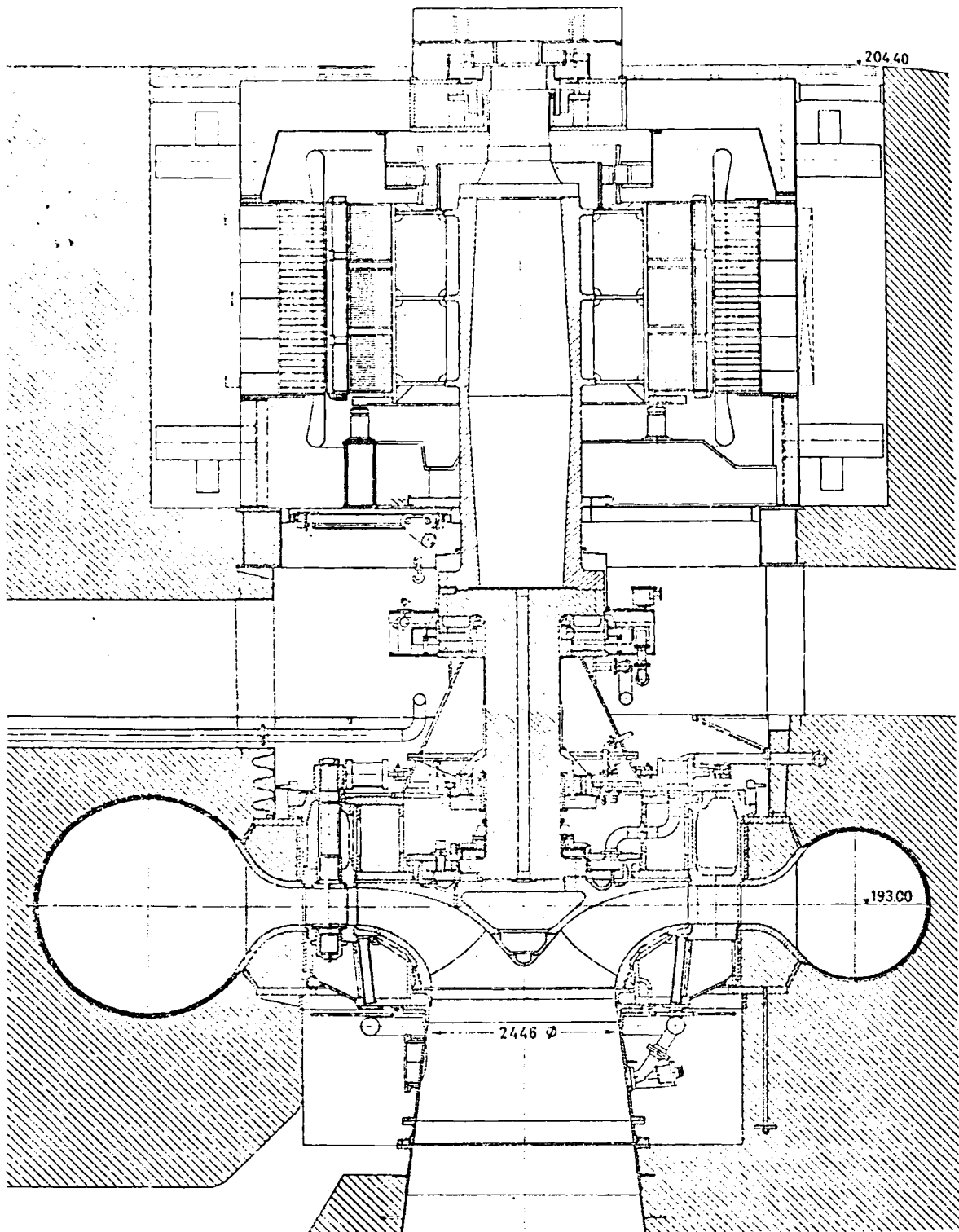
Fig. 10.4.8. Elevation of the pump-turbine set Vianden, 2. Luxemburg. (Owner Societé d'Électricité d'Our) PuT built by the collaboration of Voith and Sulzer Escher Wyss. $n = 333.3$ rpm. Turbining: $H_m = 286$ m; $P_m = 195.8$ MW; Pumping: $H = 271$ to 294 m; $P = 215$ to 202.5 MW. Rotor: $D = 2.446$ m. Gates operated by single servomotors. Axial thrust derived into the stay vanes via a truncated cone and the head cover. Initial foul of misaligned gates with rotor. Alternator facilitating an asynchronous start of pumping with a filled machine (Drawing courtesy Voith.)
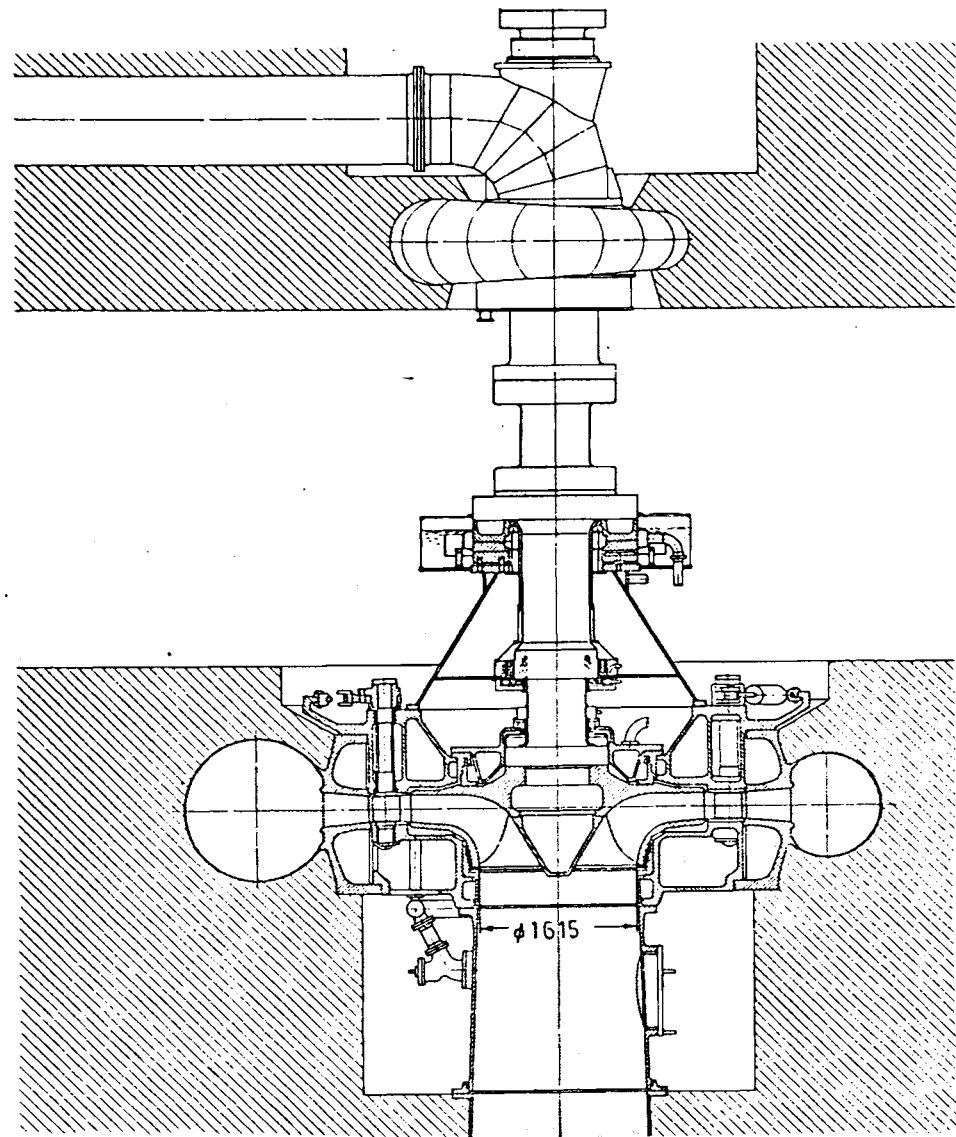
Fig. 10.4.9. Elevation of the pump-turbine Langenprozelten, West Germany (owner Rhein Main Donau AG, München and Deutsche Bundesbahn) 2 sets built by Voith. For the generation of single phase AC with 16 2/3 Hz used for traction power. Since the power installed in this grid is limited, start up of the water filled machine into pumping service is done by a simple 30 MW booster FT on shaft. $n = 500$ rpm; turbining: $H = 278{,}6$ to 305 m; $P = 73{,}5$ to 78 MW. Pumping: $H = 289{,}5$ to $317{,}7$ m; $P = 78{,}9$ to $74{,}6$ MW. Rotor $3{,}01$ m. Spiral casing inlet $1{,}6$ m. (Drawing courtesy Voith.)

According to experience gained by the writer with hydraulic turbomachines primarily used to generate peak-load power, 1% efficiency loss on these machines – in terms of the life expectancy of the machines – exceeds the production costs of a complete machine set including its percentage of excavation costs. Since centrifugal pumps normally reveal losses ranging from 8 to 12%, it follows that the last three terms from equation (10.41) are going to be more than 6 to 10 times greater than the first two terms.

For the purpose of optimizing D with respect to minimum costs, the first two terms as well as the final term in equation (10.4–1) may therefore be ignored. Moreover, in the relevant 3rd and 4th terms, the cost factor pertaining to the electric power during the operating time of the machine is assumed as constant. Thus we obtain the optimum

491
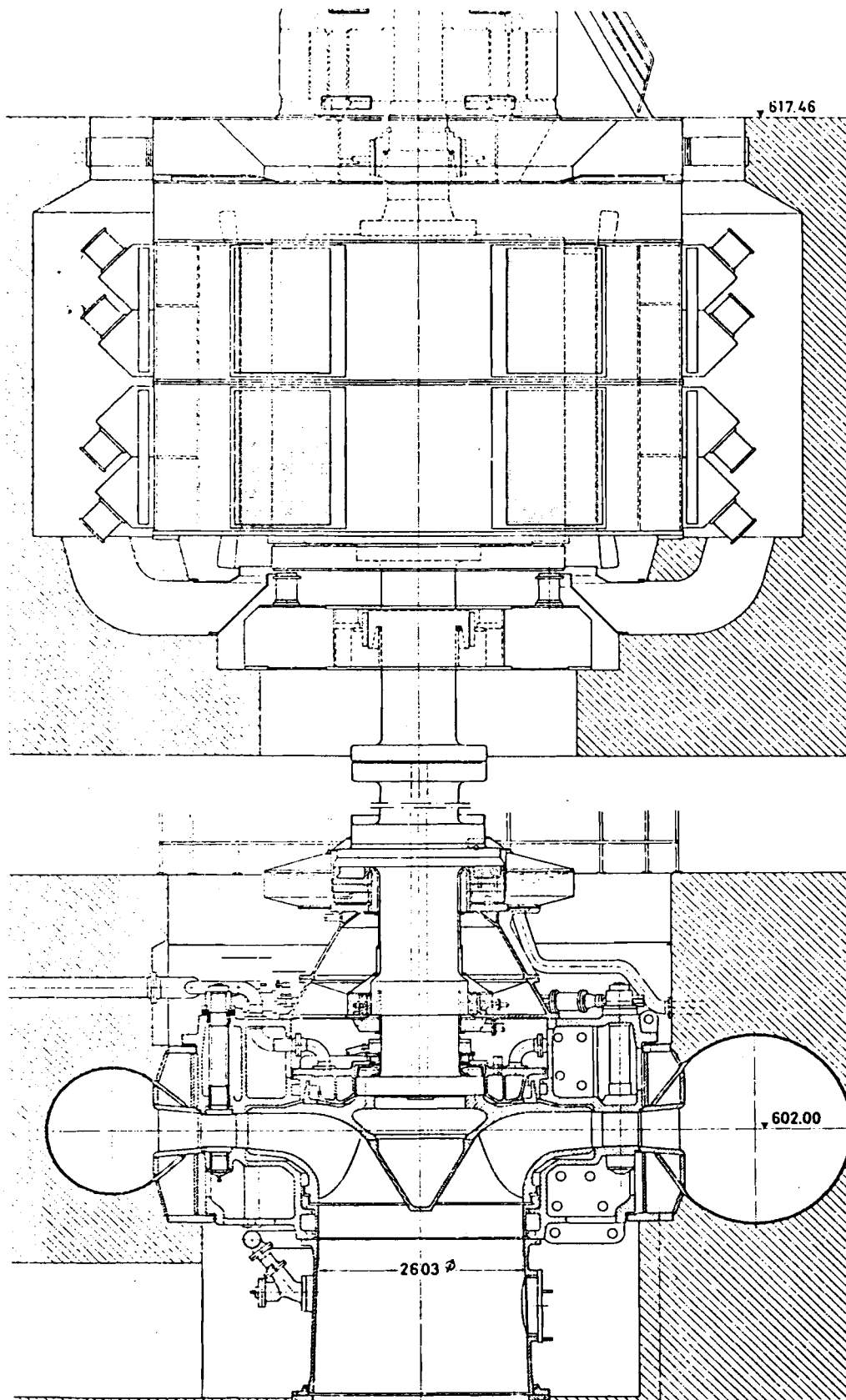
Fig. 10.4.10. Elevation of the pump-turbine set Rodund 2, Ill. Austria (Owner Vorarlberg Illwerke AG, Bregenz) built by Voith. $n = 375$ rpm, turbining: $H = 348$ m; $P = 270,9$ MW. Pumping: $H = 346$ m: $P = 246$ MW. Start of pumping with empty rotor by electric pony motor. Rotor $D = 4,35$ m. Shaft shortened. (Drawing courtesy J. M. Voith.)

492

diameter D by differentiation of the costs K_r according to D from the equation

$$d(h'_{vR} + h'_{vD})/dD = 0.$$ (10.4-2)

In the above h'_{vR} = specific disc friction losses, and h'_{vD} = specific diffuser losses.

On the basis of test results using rotary discs [5.63] and using Fig. 10.4.11, the specific disc friction losses h'_{vR} are computed as follows from the geometrical dimensions and operating data:

$$h'_{vR} = 0.256 \cdot 10^{-2} \cdot v^{1/5} \cdot \left[1 + 1.4\left(\frac{f}{D} - 0.01\right)\right]$$

$$\cdot \left(1 + 5\frac{\Delta b}{D}\right) \cdot \omega^{14/5} \cdot D^{23/5}/(gHQ).$$ (10.4-3)

In the above, v = kinematic viscosity of the fluid, f = average clearance between the impeller shrouds and housing, Δb = resulting wall thickness of both shrouds at the outside diameter, ω = angular velocity, g = gravity acceleration, H = head, and Q = flow rate in the design point.

The following applies to specific diffuser losses h'_{vD} based on the assumption of non-swirl impeller influx and employing the designations contained in Fig. 10.4.11

$$h'_{vD} = (D_2/D_3)^2 [(2 gH)/(\eta_u \omega)^2](\zeta_D/\cos^2 \alpha_3) \cdot D^{-2}.$$ (10.4-4)

Fig. 10.4.11. Sectional diagram of rotor, housing, and guide vanes applying the quantities Δb, f, D_2/D_3 and α_3.

In the above, $D_2 = D$ = outside diameter of the impeller, D_3 = inlet diameter of the vaned diffuser, ζ_D = diffuser loss factor, α_3 = angle between the diffuser vane skeleton structure and periphery at the diffuser inlet, η_u = peripheral efficiency including flow losses inside the diffuser, impeller and suction pipe.

The following introduces further the nondimensional type number n'_q

$$n'_q = \omega \cdot Q^{1/2}/(gH)^{3/4}.$$ (10.4-5)

By expressing the angular velocity ω in the equations (10.4-3) and (10.4-4) by n'_q according to equation (10.4-5) and afterwards carrying out the differentiation according

493

to equation (10.4 2) employing values $h'_{r R}$ and $h'_{r p}$ from equations (10.4 3) and (10.4-4), we arrive at the following relationship applicable to the optimum outside impeller diameter D_{op}:

$$D = D_{op} = C \cdot Q^{17/33} / [v (gH)^8]^{1/33} .$$

(10.4-6)

In the above, C represents a nondimensional parameter which in turn is dependent on nondimensional operating data and geometrical relationships:

$$C = \left\{ \frac{340 \dfrac{\zeta_D}{\eta_u^2 \cdot \cos^2 \alpha_3} \cdot \left(\dfrac{D_2}{D_3}\right)^2}{\left[1 + 1.4\left(\dfrac{f}{D} - 0.01\right)\right]\left(1 + 5\dfrac{\Delta b}{D}\right)} \right\}^{5/33} \cdot n_q'^{-8/11} .$$

(10.4-7)

It should be noted that f/D, $\Delta b/D$ and D_2/D_3 are given quantities, even if they contain $D = D_2$. The same applies to ζ_D, η_u and α_3, these likewise being given.

From equations (10.4 6), and (10.4-7) it will be observed that D_{op} is largely dependent on the type number n_q' which is defined in eq. (10.4-5).

The type number n_q' itself is likewise capable of being optimized as a function of geometrical data, loss and cavitation coefficients. This is described in greater detail in the following section.

10.4.3. New formula for the type number of a semi-axial centrifugal pump impeller

10.4.3.1. Optimum diameter of the impeller eye with respect to internal losses

10.4.3.1.1. Impeller loss

Further computation is based on the following simple assumptions (see also Fig. 10.4.12)

$$c_{m1} = c_{m2} = c_m = const,$$

(10.4-8)

$$w_1 = w_2 = w = const.$$

(10.4-9)

$$\beta_1 = \beta_2 = \beta = const,$$

(10.4-10)

$$c_{u1} = 0.$$

(10.4-11)

In the above, c = absolute speed, w = relative speed, β = angle between relative speed and circumference, c_u = circumferential component of c, and c_m = meridian component of c. Index 1 indicates the impeller inlet and index 2 the impeller outlet. All quantities are mean values ascertained between, both shroud and hub, and the vane pressure and suction faces. The vanes are assumed as being perpendicularly arranged on the impeller shroud and hub.

The loss of input inside the impeller passage is computed to the following: $P_r = w \cdot F_r$, in which case F_r = resistance force inside the impeller passage parallel to w.

Along the vanes a constant force per unit of length F_0 is intended to act perpendicularly to the vane unit as outlined in Fig. 10.4.12. The circumferential component of this force, which acts upon a vane unit of radial extension dr, is computed as follows: $dF_u = F_0 \cdot dr / \cos \mu$. μ represents the mean angle between a mean meridian flowline and the radius. Thus the peripheral input is obtained necessary for the propulsion of an impeller

494

diameter D by differentiation of the costs K_r according to D from the equation

$$d(h'_{vR} + h'_{vD})/dD = 0.\tag{10.4-2}$$

In the above h'_{vR} = specific disc friction losses, and h'_{vD} = specific diffuser losses.

On the basis of test results using rotary discs [5.63] and using Fig. 10.4.11, the specific disc friction losses h'_{vR} are computed as follows from the geometrical dimensions and operating data:

$$h'_{vR} = 0.256 \cdot 10^{-2} \cdot v^{1/5} \cdot \left[1 + 1.4\left(\frac{f}{D} - 0.01\right)\right]$$

$$\cdot\left(1 + 5\frac{\Delta b}{D}\right) \cdot \omega^{14/5} \cdot D^{23/5}/(gHQ).\tag{10.4-3}$$

In the above, v = kinematic viscosity of the fluid, f = average clearance between the impeller shrouds and housing, Δb = resulting wall thickness of both shrouds at the outside diameter, ω = angular velocity, g = gravity acceleration, H = head, and Q = flow rate in the design point.

The following applies to specific diffuser losses h'_{vD} based on the assumption of non-swirl impeller influx and employing the designations contained in Fig. 10.4.11

$$h'_{vD} = (D_2/D_3)^2 \, [(2gH)/(\eta_u \omega)^2](\zeta_D/\cos^2\alpha_3) \cdot D^{-2}.\tag{10.4-4}$$

Fig. 10.4.11. Sectional diagram of rotor, housing, and guide vanes applying the quantities Δb, f, D_2/D_3 and α_3.

In the above, $D_2 = D$ = outside diameter of the impeller, D_3 = inlet diameter of the vaned diffuser, ζ_D = diffuser loss factor, α_3 = angle between the diffuser vane skeleton structure and periphery at the diffuser inlet, η_u = peripheral efficiency including flow losses inside the diffuser, impeller and suction pipe.

The following introduces further the nondimensional type number n'_q

$$n'_q = \omega \cdot Q^{1/2}/(gH)^{3/4}.\tag{10.4-5}$$

By expressing the angular velocity ω in the equations (10.4-3) and (10.4-4) by n'_q according to equation (10.4-5) and afterwards carrying out the differentiation according

493

to equation (10.4 - 2) employing values $h'_{v,R}$ and $h'_{v,D}$ from equations (10.4 - 3) and (10.4 - 4), we arrive at the following relationship applicable to the optimum outside impeller diameter D_{op}:

$$D = D_{op} = C \cdot Q^{17/33}/[v(gH)^8]^{1/33}. \tag{10.4-6}$$

In the above, C represents a nondimensional parameter which in turn is dependent on nondimensional operating data and geometrical relationships:

$$C = \left\{ \frac{340 \dfrac{\zeta_D}{\eta_u^2 \cdot \cos^2 \alpha_3} \cdot \left(\dfrac{D_2}{D_3}\right)^2}{\left[1 + 1{,}4\left(\dfrac{f}{D} - 0{,}01\right)\right]\left(1 + 5\dfrac{\Delta b}{D}\right)} \right\}^{5/33} \cdot n_q'^{-8/11}. \tag{10.4-7}$$

It should be noted that f/D, $\Delta b/D$ and D_2/D_3 are given quantities, even if they contain $D = D_2$. The same applies to ζ_D, η_u and α_3, these likewise being given.

From equations (10.4 - 6), and (10.4 - 7) it will be observed that D_{op} is largely dependent on the type number n_q' which is defined in eq. (10.4 - 5).

The type number n_q' itself is likewise capable of being optimized as a function of geometrical data, loss and cavitation coefficients. This is described in greater detail in the following section.

10.4.3. New formula for the type number of a semi-axial centrifugal pump impeller

10.4.3.1. Optimum diameter of the impeller eye with respect to internal losses

10.4.3.1.1. Impeller loss

Further computation is based on the following simple assumptions (see also Fig. 10.4.12)

$$c_{m1} = c_{m2} = c_m = const, \tag{10.4-8}$$

$$w_1 = w_2 = w = const, \tag{10.4-9}$$

$$\beta_1 = \beta_2 = \beta = const, \tag{10.4-10}$$

$$c_{u1} = 0. \tag{10.4-11}$$

In the above, c = absolute speed, w = relative speed, β = angle between relative speed and circumference, c_u = circumferential component of c, and c_m = meridian component of c. Index 1 indicates the impeller inlet and index 2 the impeller outlet. All quantities are mean values ascertained between, both shroud and hub, and the vane pressure and suction faces. The vanes are assumed as being perpendicularly arranged on the impeller shroud and hub.

The loss of input inside the impeller passage is computed to the following: $P_r = w \cdot F_r$, in which case F_r = resistance force inside the impeller passage parallel to w.

Along the vanes a constant force per unit of length F_0 is intended to act perpendicularly to the vane unit as outlined in Fig. 10.4.12. The circumferential component of this force, which acts upon a vane unit of radial extension dr, is computed as follows: $dF_u = F_0 \cdot dr/\cos\mu$. μ represents the mean angle between a mean meridian flowline and the radius. Thus the peripheral input is obtained necessary for the propulsion of an impeller

494

Fig. 10.4.12. Simplified layout of the impeller
and one vane.
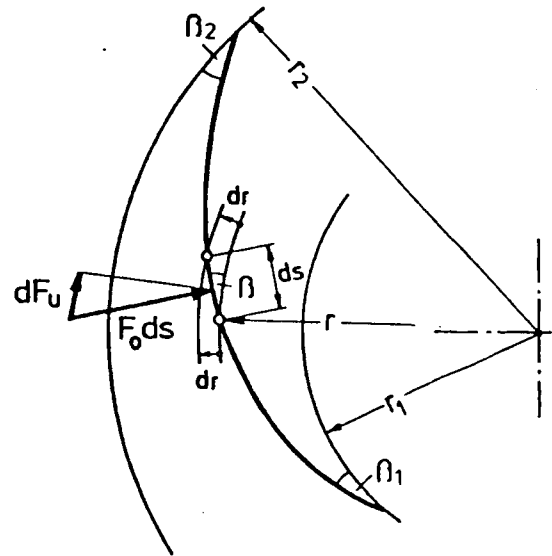
vane with angular velocity ω:

$$P_u = \omega \int_1^2 r\, dF_u = (\omega/2)(F_0/\cos\mu)(r_2^2 - r_1^2).$$ (10.4-12)

In the above, r = radius, r_2 = mean radius at the impeller outlet and r_1 = mean radius at the impeller inlet.

As β is constant according to equation (10.4-10), the following applies approximately to the resulting force F perpendicular to the impeller vane:

$$F = F_0 \cdot L \approx F_0 \cdot (r_2 - r_1)/(\cos\mu \cdot \sin\beta).$$

L signifies the mean vane length.

The resistance force F_r inside the vane passage can be split up into the component F_{rv} originating from the opposite vane surfaces, and the component F_{rsh} from the shroud and hub surfaces. F_{rv} and F_{rsh} should be related to each other in proportion to the respective wetted surfaces. Afterwards it is possible to represent F_r in the form $F_r = F_{rv} + F_{rsh} = \Omega \cdot F_{rv}$, in which case Ω, with constant β (eq. (10.4-10)), is determined approximately thus:

$$\Omega = 1 + \pi \sin\beta (r_1 + r_2)/(z\, b_M).$$ (10.4-13)

In this case, z = number of vanes and b_M = mean breadth of the impeller passage. If, by analogy to areofoil-wing theory, we were to introduce a gliding angle ε,

$$\varepsilon = F_{rv}/F,$$ (10.4-14)

the specific impeller loss would be computed to the following:

$$h'_{vL} = P_r/P_u = (2\,\varepsilon\,\Omega/\sin\beta) \cdot \{w/[\omega\,(r_1 + r_2)]\}.$$ (10.4-15)

For the purpose of converting eq. (10.4-15) use is made of the following relationships: Observing eqs. (10.4-8) to (10.4-10), $\sin\beta = c_m/w = c_{m1}/w_1$. From eq. (10.4-11) – by application of Pythagoras to the velocity triangle at the inlet – there results $w_1^2 = \omega^2 r_1^2 + c_{m1}^2$. We proceed further to introduce the "hub to tip ratio" $N_1 = r_{1i}/r_{1a}$, in which case r_{1i} = radius of the inlet edge on the hub and r_{1a} = radius of the inlet edge on the shroud (i.e. radius of the impeller eye, see Fig. 10.4.13).

495
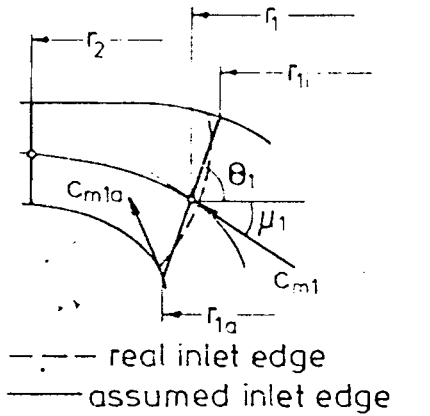
Fig. 10.4.13. Actual and assumed rotor inlet in pumping order.

— ·— — real inlet edge

———— assumed inlet edge

Assuming the inlet edge to be straight, relation $r_1 = (r_{1a}/2)(1 + N_1)$ will apply.

In addition we define a flow coefficient φ_{1a}

$$\varphi_{1a} = c_{m1a}/(\omega r_{1a}),$$ (10.4-16)

in which case c_{m1a} = meridian velocity at the inlet edge on the shroud. Thus the specific impeller loss h'_{rL} can, following conversion of equation (10.4-15), eventually be represented as follows:

$$h'_{rL} = \xi \Omega(\omega r_{1a} c_{m1})[(1 + N_1)^2 + 4 \cdot (c_{m1}/c_{m1a})^2 \varphi_{1a}^2]/[(1 + N_1)(1 + r_2/r_1)].$$ (10.4-17)

10.4.3.1.2. Diffuser loss

Observing eq. (10.4-8) and $c_{m3} = (D_2/D_3)c_{m2}$, the specific diffuser loss h'_{rD} is computed as follows:

$$h'_{rD} = \zeta_D \sin^2 \alpha_3 \cdot [c_{m1}^2/(2 g H)] \cdot (D_2/D_3)^2.$$ (10.4-18)

In the above, all characters have the same meaning as in eq. (10.4-4).

10.4.3.1.3. Optimum diameter of the impeller eye in respect to internal loss

c_{m1} can be quoted (assisted by the continuity equation) as a function of the diameter of the impeller eye D_{1a}. If a straight inlet edge is assumed in accordance with Fig. 10.4.13 along with c_{m1} being the mean meridian speed within the inlet area, the continuity equation applied to the impeller inlet will read thus:

$$c_{m1} = (4 \pi) \{(Q \cos \Theta_1)/[(1 - N_1^2) \sin(\mu_1 + \Theta_1)]\} D_{1a}^{-2}.$$ (10.4-19)

In the above, Q = flow rate in the design point, Θ_1 = mean angle between the radius and axial vane section within the area of the inlet edge, and μ_1 = angle between the radius and a mean meridian flowline at the inlet.

If we now proceed to insert c_{m1} from eq. (10.4-19) into eqs. (10.4-17) and (10.4-18) and also substitute for r_{1a} in eq. (10.4-17) the expression $D_{1a}/2$, we shall, by adding eqs. (10.4-17) and (10.4-18), obtain the resulting impeller and diffuser loss h'_{vD} as a function of the diameter of the impeller eye D_{1a}.

h'_{rr} can be represented in the form:

$$h'_{rr} = h'_{rL} + h'_{rD} = K_1 \cdot D_{1a}^3 + K_2 \cdot D_{1a}^{-4}.$$ (10.4-20)

496

K_1 and K_2 are design-conditioned constants if r_2/r_1, N_1, c_{m1}/c_{m1a}, D_2/D_3 and φ_{1a} are assumed as given. As is known, the flow coefficient φ_{1a} defined in eq. (10.4–16) is computed, as a matter of convenience for reasons pertaining to cavitation, according to the equation:

$$\varphi_{1a} = \tan \beta_{1a} = \{\lambda/[2(1 + \lambda + \zeta)]\}^{1/2}.$$ (10.4–21)

(See [6.8]). In this case λ = the pressure number for the critical point with respect to cavitation on the vane surface, ζ = suction-pipe loss factor.

The optimum diameter of the impeller eye $D_{1a\,op\,\eta}$, as regards efficiency, at which the resulting losses h'_{vr} are minimized, is finally obtained from the condition $dh'_{vr}/dD_{1a} = 0$ as follows:

$$D_{1a\,op\,\eta} = 1{,}156 \left\{ \frac{(1 + r_2/r_1)(1 + N_1)(D_2/D_3)^2 \cdot \zeta_D}{\sin^2 \alpha_3 [(1 + N_1)^2 + 4 \cdot (c_{m1}/c_{m1a})^2 \cdot \varphi_{1a}^2] \varepsilon \omega \Omega g H} \right\}^{1/7}$$

$$\cdot \left\{ \frac{Q \cos \Theta_1}{(1 - N_1^2) \sin(\mu_1 + \Theta_1)} \right\}^{3/7}.$$ (10.4–22)

10.4.3.2. Optimum diameter of the impeller eye with respect to cavitation

The normal negative suction head h_s is computed to $h_s = B' - NPSH$, in which case B' = barometric pressure head minus the critical pressure head and $NPSH$ = net positive suction head of the pump. In order to minimize excavation costs, i.e., the amount of h_s, the net positive suction head $NPSH$ is required to be minimized. Proceeding from non-swirl influx (eq. (10.4–11)) the following relationship applies to the net positive suction head according to [8.132] and Cap. 10.2.5.1

$$2g \cdot NPSH = \lambda u_{1a}^2 + (1 + \zeta + \lambda) c_{m1a}^2.$$ (10.4–23)

In the above, $u_{1a} = \omega \cdot D_{1a}/2$. By means of this, the net positive suction head $NPSH$ is obtained – after introducing c_{m1} from eq. (10.4–19) into eq. (10.4–23) – (the ratio c_{m1}/c_{m1a} being given) as a function of the impeller inlet diameter D_{1a}. $NPSH$ may be represented in the following form:

$$2g \cdot NPSH = K_3 \cdot D_{1a}^2 + K_4 \cdot D_{1a}^{-4}.$$ (10.4–24)

K_3 and K_4 are design-conditioned constants, at least at the bep.

The optimum diameter of the impeller eye with regard to cavitation $D_{1a\,op\,NPSH}$ at which the net positive suction head $NPSH$ and thus too, the excavation costs are minimized, is then computed from the condition $dNPSH/dD_{1a} = 0$ to the following:

$$D_{1a\,op\,NPSH} = 2 \left[\frac{2(1 + \lambda + \zeta)}{\lambda} \right]^{1/6} \cdot \left[\frac{Q \cdot \cos \Theta_1 \cdot (c_{m1a}/c_{m1})}{\omega \pi (1 - N_1^2) \sin(\mu_1 + \Theta_1)} \right]^{1/3}.$$ (10.4–25)

10.4.3.3. Optimum type number with respect to efficiency and cavitation

By equating the diameters obtained from (10.4–22) and (10.4–25), $D_{1a\,op\,\eta} = D_{1a\,op\,NPSH}$, the natural optimum $n'_{q\,op\,\eta\,NPSH}$ of the type number n'_q defined in equation (10.4–5), is obtained. $n'_{q\,op\,\eta\,NPSH}$ is a function of the pump geometry (expressed by quantities Ω, r_2/r_1, Θ_1, μ_1, N_1, α_3), the velocity ratio c_{m1}/c_{m1a}, loss factors (such as ζ_D, ε) and cavitation-

conditioned quantities (such as λ, ζ, φ_{1a}), see also (10.2-10):

$$n'_{q\,op\,\eta\,NPSH} = 2{,}4 \left\{ \frac{\sin^2 x_3\,[(1 + N_1)^2 + 4 \cdot (c_{m1}/c_{m1a})^2\,\varphi_{1a}^2]\,\varepsilon\Omega}{(1 + r_2/r_1)(1 + N_1)(D_2/D_3)^2\,\zeta_D} \right\}^{3/4} \qquad (10.4-26)$$

$$\cdot \left\{ \frac{(1 - N_1^2)\sin(\mu_1 + \Theta_1)}{\cos\Theta_1} \right\}^{1/2} \cdot \left\{ 2\left(1 + \frac{1 + \zeta}{\lambda}\right)\left(\frac{c_{m1a}}{c_{m1}}\right)^2 \right\}^{7/8}.$$

For the purpose of optimizing the impeller outside diameter in accordance with equations (10.4-6) and (10.4-7), this optimum type number is required to be introduced into the formula applicable to C (eq. (10.4-7)).

An impeller designed on these lines represents a distinct optimum with regard to efficiency and costs of excavation.

10.4.4. The discharge ratio as a function of the speed ratio

Applying the customary speed coefficient

$$K u_2 = \omega\, r_2/\sqrt{2gH}, \qquad (10.4-27)$$

(cf. [6.8]) we proceed to defining the speed ratio thus:

$$x = K u_{2P}/K u_{2T}. \qquad (10.4-28)$$

In the above, $K u_{2P}$ = speed coefficient applied to the process of pumping and $K u_{2T}$ = speed coefficient pertaining to turbining.

Also required to be defined is the discharge ratio at rated flows Q_P and Q_T

$$q = \frac{Q_P}{Q_T} = \frac{\Phi_{2P} \cdot c_{m2P}}{\Phi_{2T} \cdot c_{m2T}} = \frac{\Phi_{2P}\varphi_{2P}}{\Phi_{2T} \cdot \varphi_{2T}} \cdot x \cdot \chi^{1/2}. \qquad (10.4-29)$$

In the above, Q = flow rate (discharge), Φ_2 = contraction factor at the pressure edge, c_{m2} = meridian speed at that point, $\varphi_2 = c_{m2}/u_2$, in which case $u_2 = \omega \cdot r_2$ = peripheral speed at the impeller outside diameter, $\chi = H_P/H_T$ = head ratio. Index P denotes the pumping process and T referes to the turbining operation at rated points.

From the velocity triangles at the pressure edge (Index 2) it is possible to read off the following relationships applicable to the meridian speeds c_{m2P} (pumping process) and c_{m2T} (turbining process) in accordance with Fig. 10.4.14.

$$c_{m2P} = [u_{2P} - (1 + p_P^*)\,c_{u2P}^*]\tan\beta_2, \qquad (10.4-30)$$

$$c_{m2T} = [u_{2T} - (1 + p_T^*)\,c_{u2T}^*]\tan\beta_2. \qquad (10.4-31)$$

In the above, β_2 = vane angle at the pressure edge, p^* = slip factor at that point, c_{u2}^* = peripheral component of the absolute speed at the pressure edge (Index P/T: pumping/turbining process).

By means of these data in conjunction with Euler's fundamental equation governing turbomachinery (Cap. 5.3) applying in accordance with equation (10.4-11), it is possible to quote the discharge ratio q as a function of the speed ratio x as follows:

$$q = \frac{\Phi_{2P}}{\Phi_{2T}} \cdot x \cdot \chi^{1/2} \frac{[1 - (1 + p_P^*)/(2\,K u_{2P}^2\,\eta_{uP})]}{[1 - (1 + p_T^*)\,x^2\,\eta_{uT}/(2\,K u_{2P}^2)]}. \qquad (10.4-32)$$

498

Fig. 10.4.14. Impeller outlet triangle during pumping operation (P) and inlet triangle during turbining operation (T). Rotor vane indicated by hatched line. Values without star correspond to the relative flow along the vane.
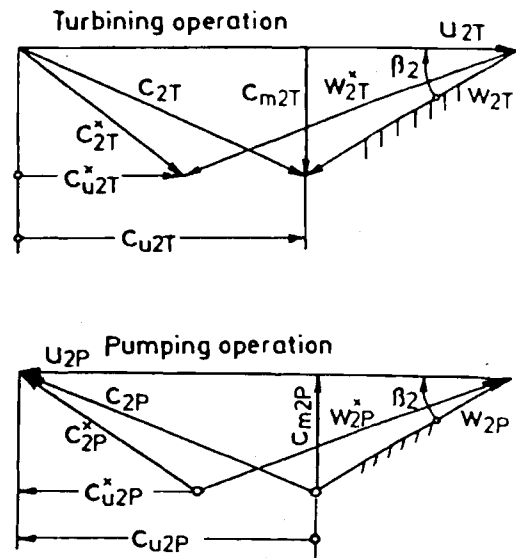
In the above, η_u = peripheral efficiency (hydraulic efficiency) in the turbining (Index T) and pumping (Index P) state.

Kku_{2P} may be computed from the speed relationship between the type number n_q and the speed coefficient $K u_{2P}$. Taking into account eq. (10.4–19), this relationship reads as follows:

$$K u_{2P} = \pi^{-1/3} \cdot 2^{-1/2} \cdot \varphi_{1a}^{-1/3} \left(\frac{r_2}{r_{1a}}\right) \cdot \left(\frac{c_{m1a}}{c_{m1}}\right)^{1/3}$$

$$\cdot \left[\frac{\cos \Theta_1}{(1 - N_1^2)\sin(\Theta_1 + \mu_1)}\right]^{1/3} \cdot n_q'^{2/3}. \tag{10.4–33}$$

The optimum value for n_q' is known from eq. (10.4–26) $(n_{q\,op\,\eta\,NPSH}')$.

10.4.5. Example for the computing optimum values of impeller diameter, type number and discharge ratio as compared with corresponding quantities of an actual pump-turbine

As an example let us study a pump-turbine with the following data:

10.4.5.1. Data

1) Impeller Geometry:

$$r_2/r_{1a} = 1,69; \quad N_1 = 0,6; \quad f/D = 0,01; \quad \Delta b/D = 0,02; \quad \beta_2 = 27°;$$
$$\alpha_3 = 20°; \quad \text{no. of vanes } z = 7; \; D_2/D_3 = 0,94; \quad b_M/(r_1 + r_2) = 0,2;$$
$$\Theta_1 = 60°; \quad \mu_1 = 70°.$$

Thus, from eq. (10.4–13), $\Omega = 2,019$.

Assuming the inlet edge to be straight, $r_2/r_1 = 2(r_2/r_{1a})/(1 + N_1) = 2,113$ will apply.

499

2) Operational-conditioned Characteristic Quantities:

$$\eta_{uP} = 0.92; \quad \eta_{uT} = 0.96; \quad \zeta_D = 0.19; \quad \varepsilon = 0.01; \quad \zeta = 0.05;$$

$$\lambda = 0.25; \quad \Phi_{2P} = 0.9; \quad \Phi_{2T} = 1.0; \quad p_P^* = 0.2; \quad p_T^* = 0.2;$$

$$v = 14 \cdot 10^{-6} \,\mathrm{sq\,ft/s} \,(= 1.3 \cdot 10^{-6}\,\mathrm{m^2/s}); \quad c_{m1a}/c_{m1} = 1.2.$$

3) Main Operating Data of Pump-Turbine:

$$H_P = 1130 \,\mathrm{ft}\ (346\,\mathrm{m}), \quad H_T = 1100\,\mathrm{ft}\ (336\,\mathrm{m}),$$

$$Q_P = 2400 \,\mathrm{cu\,ft/s}\ (67.2\,\mathrm{m^3/s}), \quad Q_T = 3210\,\mathrm{cu\,ft/s}\ (90\,\mathrm{m^3/s}),$$

$$\chi = H_P/H_T = 1.030.$$

The data quoted under 1) and 3) agree with those on the Austrian Rodund 2 pump-turbine as far as the latter were available on simple lines. This pump-turbine has a rotational speed of $n = 375$ rpm in both modes of operation, the outside diameter of the impeller measuring $D = 14.26\,\mathrm{ft}\ (4.35\,\mathrm{m})$.

10.4.5.2. Results

By means of these figures we obtain $\varphi_{1a} = 0.310$ from eq. (10.4–21) and thus the vane angle of the inlet edge on the rim $\beta_{1a} = \arctan \varphi_{1a} = 17.2°$.

From eq. (10.4–26) we obtain $n'_{q\,op\,\eta\,NPSH} = 0.728$, thus from eq. (10.4–7) $C = 2.365$, from eq. (10.4–6) $D_{op} = 14.23\,\mathrm{ft}\ (4.34\,\mathrm{m})$.

From eq. (10.4–33) we obtain $K u_{2P} = 1.044$.

D_{op}, $n'_{q\,op\,\eta\,NPSH}$ and $K u_{2P}$ agree well with the actual values of the Rodund 2 pump-turbine, which amount to $D = 14.26\,\mathrm{ft}\ (4.35\,\mathrm{m})$, $n'_q = 0.724$; $K u_{2P} = 1.037$.

From eq. (10.4–17) we compute $h'_{vL} = 0.044$, and from eq. (10.4–18) $h'_{vD} = 0.036$. These values require a peripheral efficiency $\eta_{uP} = 1 - h'_{vL} - h'_{vR} = 0.92$, which agrees with the assumed $\eta_{uP} = 0.92$ if loss in the suction line is omitted.

The actual speed ratio in accordance with eq. (10.4–28) reads $\kappa = 0.985$. Thus from eq. (10.4–32) we obtain $q = 0.738$, which agrees well with the actual value $q = 0.747$.

10.4.6. Special operational features of pump-turbines

Compromises Resulting from Shell Diagram and Practical Requirements:

Outlined in Fig. 10.4.15 is the so-called "shell (hill)-diagram" (the curves with identical efficiency are "shell-shaped") plotted for a pump-turbine in both modes of operation in the Ψ, φ-plane. Ψ indicates the pressure coefficient, $\Psi = 2gH/(\omega_0 r_2)^2$ and φ the flow coefficient, $\varphi = c_{m2}/(\omega_0 r_2) = Q/(A_2 \omega_0 r_2)$. ($\omega_0$ = angular velocity (design point), and A_2 = cross sectional area at the impeller pressure edge.)

Evidently applicable to the optimum points in pumping and turbining modes of operation according to Fig. 10.4.15 are the following relationships

$$\Psi_{op\,P} < \Psi_{op\,T}, \tag{10.4–34}$$

$$\varphi_{op\,P} < \varphi_{op\,T}. \tag{10.4–35}$$

i.e. the optimum point of the turbine zone is located further away from the origin of coordinates than the optimum point of the pump zone. Compared with the pump zone,
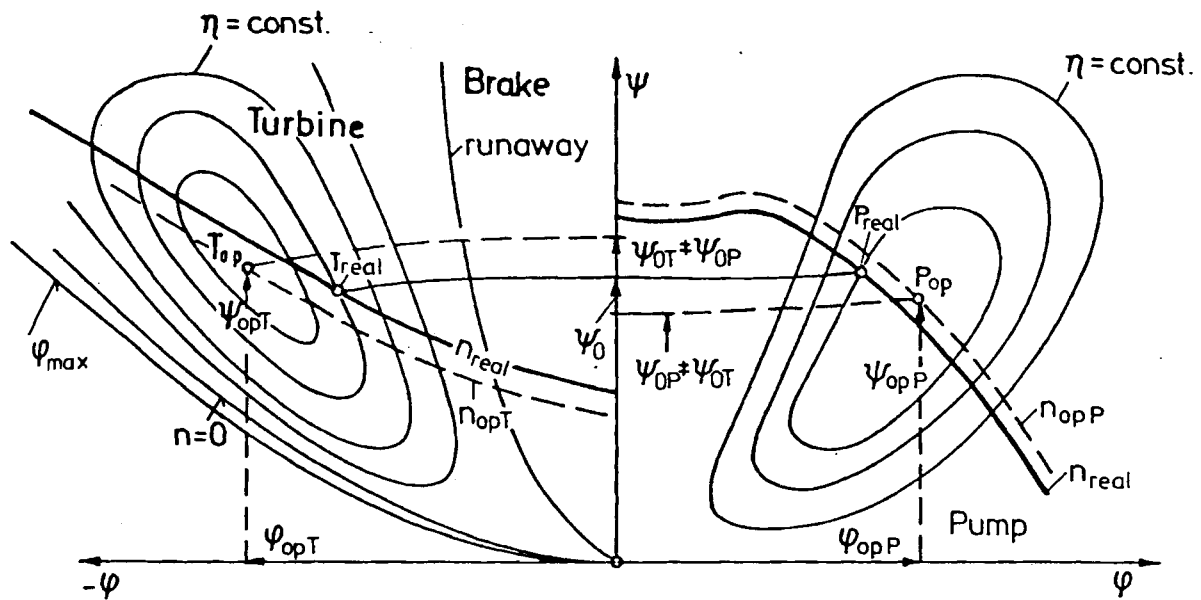
Fig. 10.4.15. Hill(shell)diagram in the pump and turbine working order, schematic.

the turbine section in the Ψ, φ-diagram is more closely limited by the runaway parabola (where torque is zero) and the parabola of maximum discharge (this is the envelope of the curves with identical rotational speed at maximum flow rate). From Fig. 10.4.15 it will be gathered that the curves of constant machine speed n cross through the peak of the constant efficiency curves over a greater length in the turbine zone than in the pump zone. This means that a deviation from the optimum point, maintaining constant rotational speed when pumping, involves a greater drop in efficiency than when turbining.

In addition, by deviating from the optimum point when pumping, maintaining constant rotational speed, the machine lands in an operating zone in which it is highly sensitive to cavitation. This would necessitate increasing the negative suction head.

On a facility purely designed as a pumped storage plant the pressure coefficient Ψ_0, belonging to the average level-difference between the head and tailrace level, is normally the same in the pumping and turbining modes of operation.

If, as is usually the case, provision is made for the same adapted rotational speed n_{real} for both modes of operation, the above circumstance calls for two courses of action to be taken (see Fig. 10.4.15).

First, it is necessary for selection of the constant rotational speed n_{real} to be lower in the pumping mode and higher in the turbining mode than the speed due to the bep.

Secondly, owing to the same pressure coefficient $\Psi_0 = \Psi_{oP} = \Psi_{oT}$ in both modes of operation, the actual turbine operating point T_{real} must be transferred into the partial-load region (see Fig. 10.4.15) where efficiency is lower and swirl occurs inside the suction pipe. This is mainly necessary in order to warrant optimum conditions as regards cavitation when pumping.

From Fig. 10.4.15 it will also be noted that, even in the case of a two-speed motor-generator set (rarely used), which permits optimum rotational speeds $n_{op\,P}/n_{op\,T}$ in both modes of operation, not both optimum points P_{op} and T_{op} are attained if the level-difference (and thus too, the pressure coefficient Ψ_0) is the same in pumping and turbining modes of service.
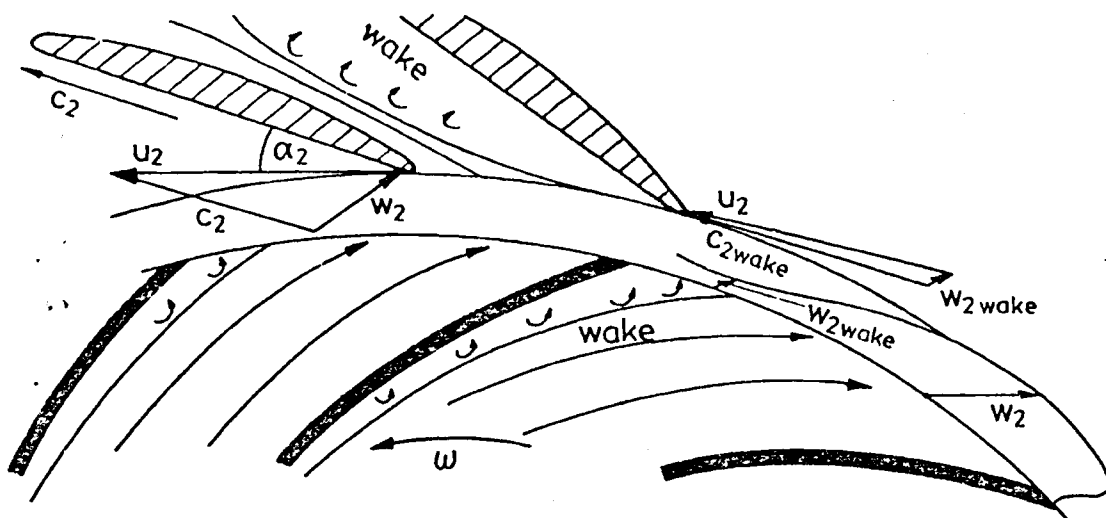
Fig. 10.4.16. Effect of wakes behind the impeller vanes at pumping at the inlet zone of gate.

The discharge ratio q must (aside from the hydraulic optimum value) be determined with due consideration to the average duration of the base- and peak-load period in the course of a working cycle. Furthermore, attention must be paid to balancing the water quantities in the turbining and pumping modes of operation, also taking into account the processes of inflow and outflow during the storage cycle provided the system is supplied by a river.

Maximum turbine efficiency is attained only at the beginning of turbining in the storage cycle owing to the presence of the maximum level-difference and thus too, the highest pressure coefficient Ψ (see Fig. 10.4.15). Maximium output will then be yielded.

10.4.7. Sources of troubles and remedies

10.4.7.1. Normal pumping

In the course of pumping, wakes occur on the impeller outlet (see Fig. 10.4.16). This produces a periodically highly varying angle of attack, on the guide vanes. If a wake passes a guide vane, the unfavourable angle of attack generates a momentary stall past the leading inlet edge of the vane (see Fig. 10.4.16).

As a result of this the vane channel is temporarily blocked. At the same time a torque, subject to periodic change, acts upon the guide vane in the opening direction.

If this causes rupture to a safety member (provision for which is usually made on gates actuated using a central servomotor), the guide vane may strike against the adjacent vane with its end projecting into the impeller. This causes destruction of the vane's ends and possibly to the coupling bolts as well when gate lever stroke limiters are not provided.

Such damage can be prevented by arranging for each of the guide vanes to be actuated by an individual servomotor, these motors being subjected to synchronous control.

The individual servomotor must provide a torque sufficient to drive a vane even in case the vane is temporarily in a misaligned position, see [10.106].

In the course of pumping, care should be taken not to regulate the gate. It will be best to block the guide vanes. If, for example, the upper vane pin is provided with a friction

502
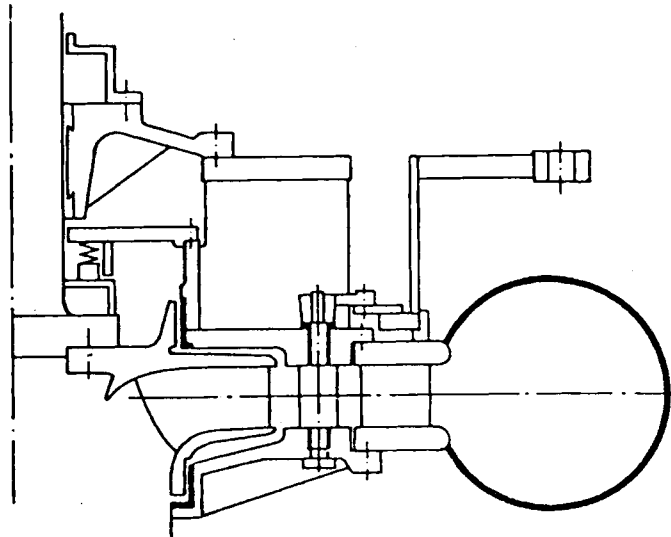
collar, this collar can be pressed against the housing (by pressure applied to the front side of the lower trunnion) so as to block the vane.

Employing short upper vane stems (corresponding to Fig. 10.4.17), the means of driving which are in the head cover, it is possible to prevent dangerous torsional vibrations from lever, stem and vane.

10.4.7.2. Abnormal operating conditions

The transitional operating conditions specified below and capable of occurring following load rejection while turbining or failure of the pump drive, might possibly involve extremely varying forces and moments acting on the guide vanes and thus too, heavy vibrations of the machine shaft and cover [10.75; 10.157].

a) Slight opening of the gate when pumping at full rotational speed.

b) Pump brake operation at low reversed flow ($\varphi < 0$), lower rotational speed and slight opening of the gate: In this case the jet, partially deflected outwards by the runner vanes, exercises a fluctuating closing moment on the guide vanes.

c) Centripetal turbine ($=$ Francis turbine) operation with extensive reversed flow ($\varphi < 0$) and reversed (negative) sense of rotation.

d) Runaway of turbine ($\varphi < 0$): when accelerating a radial machine up to the point of runaway, the flow will be throttled owing to centrifugal forces, this causing water hammer. Runaway whose operating point on the Ψ, φ-diagram (Fig. 10.4.15) is located on the runaway parabola $\Psi_{ra} = \text{const} \cdot \varphi_{ra}^2$, is a dangerous condition owing to a high rotational speed being present without normal speed control. While occurrence of the operating conditions described under a) through d) may be "permanent" in a case of emergency, the following two conditions occur only temporarily in the transitional process.

e) Turbine brake operation above the runaway speed with reversed flow ($\varphi < 0$): this zone, located on the Ψ, φ-diagram (Fig. 10.4.15) between the runaway parabola and ordinate, is passed through when the flow rate is reduced due to closure of the gate, while the speed is almost equal owing to the inertia of the rotating parts.

f) Reversed pumping ($\varphi > 0$) with reversed (negative) sense of rotation: this condition occurs, proceeding from the turbining process, when water hammer is caused due to
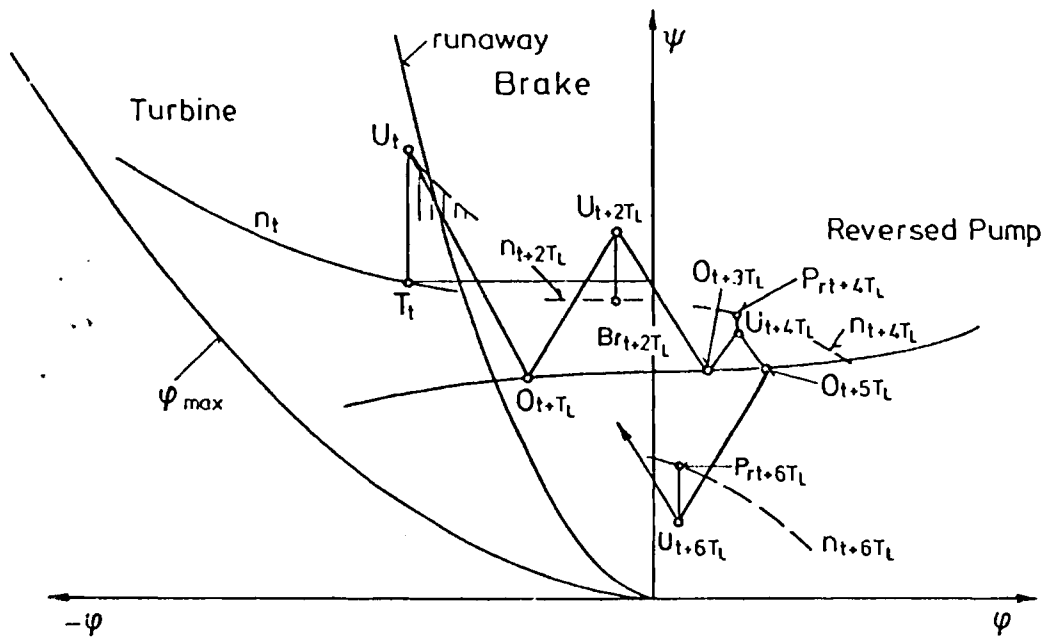
Fig. 10.4.18. Water hammer characteristics in the turbine, brake and reversed pump flow regime. For notation see Fig. 8.36.

closure of the gate, and the rotational speed decreases only slowly owing to inertia. Fig. 10.4.18 indicates, for example, the water hammer characteristics in the event of the load being switched off at a point of time t in the turbining mode of operation and the gate continuing to close. Registered in Fig. 10.4.18 are the conditions at the upper and lower end of the pressure pipe (O_{t+nT_L} or U_{t+nT_L}) as well as on the pump-turbine (T_{t+nT_L}, Br_{t+nT_L}, Pr_{t+nT_L}) this being done at the times indicated in the index $t + nT_L$ ($n = 0, 1, 2 \ldots$). $T_L = L/a$ = transit time of the pressure waves in the pipeline (L = pipe length between O and U, a = sonic speed, T = turbining, Br = braking, Pr = reversed pumping).

10.4.7.3. Beginning of pumping

Up to 80% of the full-load input is required to speed up a water-filled radial type centrifugal pump with closed valve.

Hence, speeding up into pumping action of the pump-turbine presents a problem. The technical challenge and objective in this case is to attain as short a start-up time as possible employing the smallest auxiliary set possible. To arrive at this solution numerous methods have already been devised, a few of which are mentioned below.

The pump-turbine can be accelerated by the main motor-generator set directly provided this is capable of functioning as an asynchronous motor. Owing, however, to the low permissible motor temperature (80 °C), this necessitates the use of short-circuited full iron pole pieces as for example at the Vianden 2 facility [10.161] lowering alternator efficiency.

On radial pump-turbines with extensive head, the required start-up power has, in most cases, so far been reduced by filling the impeller with air. However, this solution extends the start-up time and transfers the ensuing problems to the subsequent filling process.

During the process of filling, the turbulent, vortex-affected two-phase mixture with its compressible air-pockets may stimulate dangerous machine-shaft vibrations with frequencies below the sys-

504

chronous rotational speed. These vibrations may be influenced by the design of the impeller seals as well as by the virtual mass of fluid linked with the vibrating impeller. Such problems need to be carefully examined with regard to each individual machine and solved by applying model tests.

Carrying out the process of filling from the suction pipe may, for one thing, force up the impeller temporarily besides causing some inlet shock to occur.

The upward-force effect can be prevented if (as on the Taum Sauk facility) compressed water is briefly allowed to act on the double-scaled crown thus pressing the impeller downwards [10.155].

The inlet shock can be avoided if, by means of a jet, a simulated vortex is briefly produced in the draft tube mouth. No inlet shock occurs when filling from the gate owing to the speed coefficient normally incorporating the value $K u_2 = 1$.

Usually both methods of filling are combined. The air-pockets in the centre of the suction pipe and at the top of the spiral housing must at all events be removed carefully and quickly since these may produce shaft vibration as well as causing the drive power to fluctuate. As a means of preventing faults from occurring, the following recommendations should be observed: Gates, the cover, bearings and shaft should be constructed as solid, stiff designs. Opening of the air-exhaust valves and gate must proceed in accordance with appropriate principles of timing. Speeding up the dewatered rotor needs about 5 % of the rated input. It can be done by a pony motor or a thyristor-controlled stator field. The latter is used in the Leitzach-pump-turbine (see Cap. 10.4.2).

10.4.8. Experimental research on Francis pump-turbines

By *Zu-Yan Mei*, Professor, Department of Hydraulic Engineering Tsinghua University, Beijing, China.

I. Introduction

This section summarizes the research work carried out to investigate the hydraulic performance of Francis type pump-turbines at the department of Hydraulic Engineering at the Tsinghua University, Beijing, in the past several years. It is an English summary of Tsinghua University Scientific report QH-79006 1979.

The research project was conducted with the prospect of application to three pumped-storage power stations under planning with operating heads of 50 m, 100 m and 300 m respectively. Development and testing of reversible runners were performed in cooperation with one industrial research institute and two manufacturers of hydraulic turbines.

Testing work was carried out at the Hydraulic Machinery Laboratory mainly on the closed-cycle cavitation test stand with an maximum test head of 15 m while a few runners were tested on the open-flume test circuit under 7 m head. A total of some 30 runners with diameters of 300, 350 and 400 mm were tested.

II. Design of reversible runners

As no reversible pump-turbines of the Francis type has been designed and manufactured in the country and very little related experience accumulated, all design considerations had to be based on analysis of scattered information collected on machines in operation in foreign countries from openly published material.

In Table 10.4.1 are listed the expected performance characteristics of the three series of machines (50 m, 100 m and 300 m). The first two series of pump-turbines were intended for use in combination with conventional power generation units while the last series was to be for pure pumped-storage service.

505

Table 10.4.1. Expected performance characteristics of radial pump turbines. After *Mei*

Head range		Pump design point				Turbine design point			Turbine limit point		
		Q_{11}	n_{11}	n_s	σ	Q_{11}	n_{11}	n_s	Q_{11}	n_{11}	n_s
50 m	I	0,45	100	245	0,28	0,50	85	205	0,62	85	230
	II	0,50	100	260	0,30	0,56	85	220	0,70	85	250
100 m	I	0,32	92	190	0,20	0,38	82	175	0,44	82	190
	II	0,35	94	205	0,22	0,42	84	185	0,48	84	200
300 m	I	0,11	82	100	0,09	0,13	74	92	0,15	74	100
	II	0,13	84	110	0,10	0,16	76	105	0,19	76	115
	III	0,15	84	118	0,11	0,18	76	112	0,21	76	120

The runner layouts were at first done by graphical procedure or by integration by hand calculators. A one-dimensional computer program was later developed to enable generation of many more variants for comparative study. Still later a quasi-three dimensional flow analysis program was put to use to check on the merits of hand-drawn and computered-aided designs. More models were required to be tested in the early part of the programme, but fewer were needed as better means became available to evaluate the designs before model testing.

The reversible runner was considered first for its performance in the pumping mode. Only supplementary calculations were made to check the flow condition in the turbine mode to be within tolerable limits according to conventional hydraulic turbine design practice. Two or three specific speed options were considered for each of the three series of runners. Some model runners, especially the ones on which new design ideas were tried, were made of epoxy resin for easier and more speedy fabrication.

III. Characteristics of reversible runners

1. Pump operation

In Table 10.4.2 are given for some runners the pertinent design index figures, the relative dimensions and blade angles as designed, and the optimum point performance results. From the test data the unit flow Q_{11} and unit speed n_{11} were calculated for the bep (subscript o). These compared with the designed values (subscript d) gave the ratios listed in Table 10.4.3. As can be seen for the 100 m and 300 m series, both discharge and speed exceeded the expected values by 5% to 20% which indicates the fact that adjustments in design constants are necessary. Fig. 10.4.19 shows a typical pump characteristic curve for a 50 m series runner (No. 12) showing clearly the influence of guide vane opening on performance.

2. Turbine operation

The expected performance in turbine operation was derived in the following way: Take the turbine optimum unit flow Q_{11T} as 1,1 to 1,2 times that of pump Q_{11P}, and the limiting value $Q_{11\,Tmax}$ as 1,15 to 1,2 times $Q_{11\,T}$. With these ratios it was expected that water quantities in both directions would be nearly balanced and the power in both modes of operation computed on this basis would be in good match. However, not all runners met these expectations. Some runners showed Q_{11T} only close to Q_{11P} or even

Table 10.4.2. Design and test data for some rotors of pump turbines. After *Mei*.

Head Range	Runner	Design Parameters Q_{11} (m³/s)	n_{11} (r/m)	n_S	Basic Dimensions D_d (mm)	$\bar{D}_s$	$\bar{b}_d$	Method of Blade Design *	Blade Data Z'	β_d	β_s	φ	Pump bep Q_{11} (m³/s)	n_{11} (r/m)	η (%)	σ_1	Turbine bep Q_{11} (m³/s)	n_{11} (r/m)	η (%)	Ratios $\dfrac{Q_{11T}}{Q_{11P}}$	$\dfrac{n_{11P}}{n_{11T}}$
50 m	9	0,50	107	275	275	0,765	0,20	Conf. Map.	7	20°	24°	95°	0,56	97	85,6	0,19	0,49	82	87,4	0,89	1,19
	12	0,47	108	260	300	0,735	0,183	Hand Integr.	6	23°	25°	102°	0,47	97	87,0	0,26	0,48	86	86,8	1,02	1,13
	13	0,47	108	260	300	0,735	0,183	Conf. Map	6	19°	25°	100°	0,50	100	86,5	0,28	0,465	82,5	84,8	0,93	1,21
	15	0,44	100	245	300	0,70	0,183	Conf. Map.	6	23°	27°	110°	0,45	94	88,5	0,19	0,36	79	87,3	0,80	1,19
100 m	51	0,32	92	190	300	0,70	0,175	Hand Int.	6	18,3°	23,4°	116°	0,32	92	85,0	–	0,33	80	86,0	1,03	1,15
	54	0,37	92	204	300	0,70	0,175	Hand Int.	6	21°	31°	105°	0,39	93	85,0	–	0,45	89	86,3	1,15	1,04
	56	0,32	92	190	300	0,70	0,18	Hand Int.	6	18,5°	27°	110°	0,41	98	83,5	–	0,42	84,5	86,6	1,01	1,16
	66	0,32	92	190	300	0,70	0,18	Computer	6	18,3°	27°	138°	0,37	99	82,0	–	0,40	87,5	87,5	1,10	1,13
300 m	TC-10	0,13	84	110	400	0,50	0,10	Conf. Map.	6	28,8°	30°	122°	0,156	85	81,6	0,07	0,17	77	84,7	1,09	1,10
	FT-1	0,13	84	110	400	0,50	0,10	Hand Int.	6	23°	25°	141°	0,17	89	82,0	0,09	0,17	75,3	82,5	1,00	1,18
	A 143	0,15	84	118	400	0,60	0,10	Hand Int.	6	21°	21°	169°	0,16	87	81,4	0,04	0,155	75	84,2	0,97	1,15
	20	0,125	83	107	400	0,50	0,10	Conf. Map.	6	22°	37°	136°	0,175	91	81,8	0,123	0,17	77,5	83,5	0,97	1,16
	26	0,13	84	110	400	0,50	0,10	Computer	6	22°	27°	142°	0,16	87	81,6	0,124	0,14	74	84,2	0,90	1,18
	31	0,11	82	100	400	0,50	0,10	Computer	6	22°	30°	127°	0,167	89	80,6	–	0,18	77,5	82,6	1,09	1,14
	39	0,16	85	120	400	0,55	0,10	Hand Int.	6	21°	22°	152°	0,18	89	81,3	–	0,165	76,5	83,5	0,92	1,16

Conf. Map.: Conformal Mapping; Int.: Integration

Table 10.4.3. Comparison of design and tested parameters of radial pump turbines.
After *Mei*

	50 m Series	100 m Series	300 m Series
Q_{11o}/Q_{11d}	0,9--1,1	1,0--1,2	1,1--1,4
n_{11o}/n_{11d}	0,9--1,0	1,0--1,05	1,0--1,1
n_{so}/n_{sd}	0,9--1,0	1,05--1,1	1,1--1,3
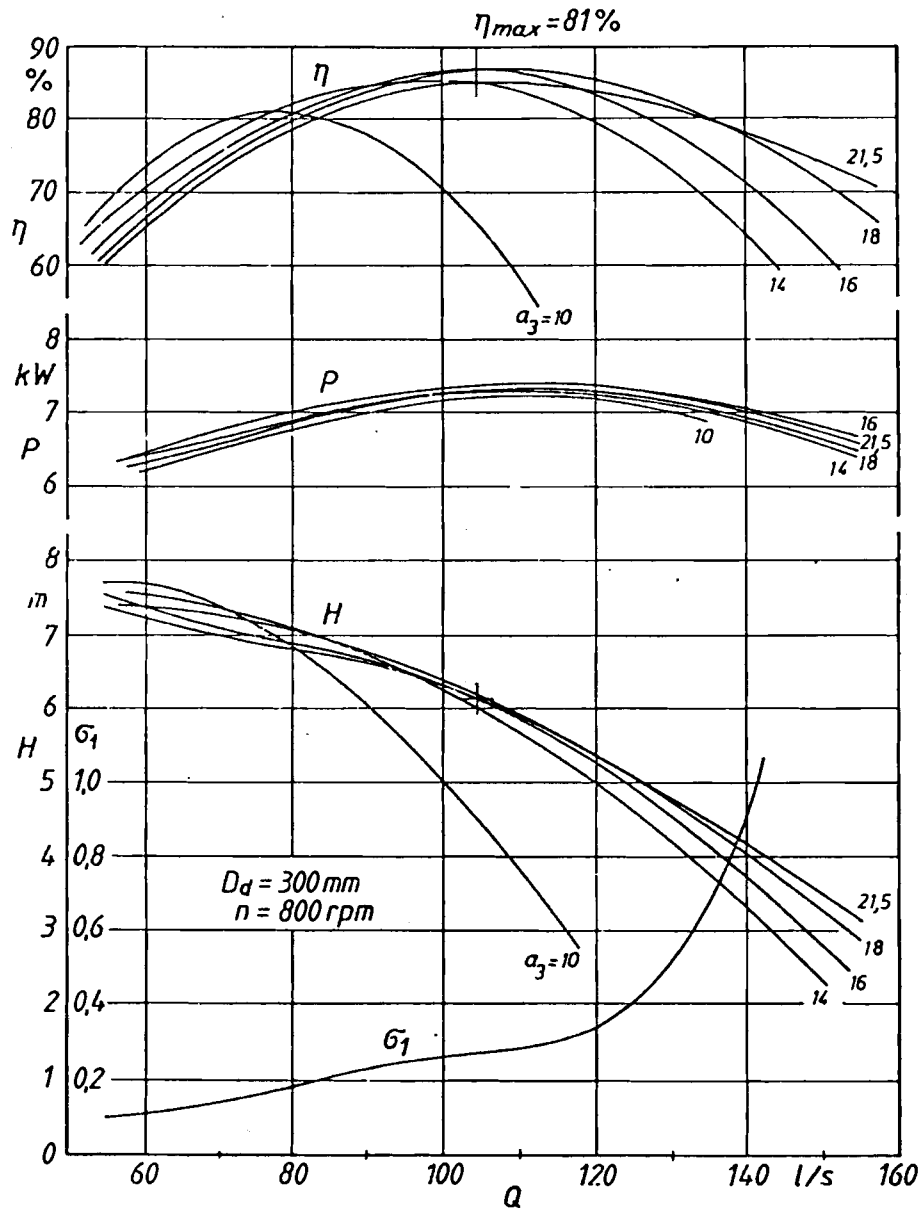
Fig. 10.4.19. Characteristic curves of a radial pump-turbine in pump mode. Above, efficiency η vs flow Q, middle, power P vs flow Q, below, head H vs flow Q, and cavitation index σ vs flow Q, after *Mei*.

508
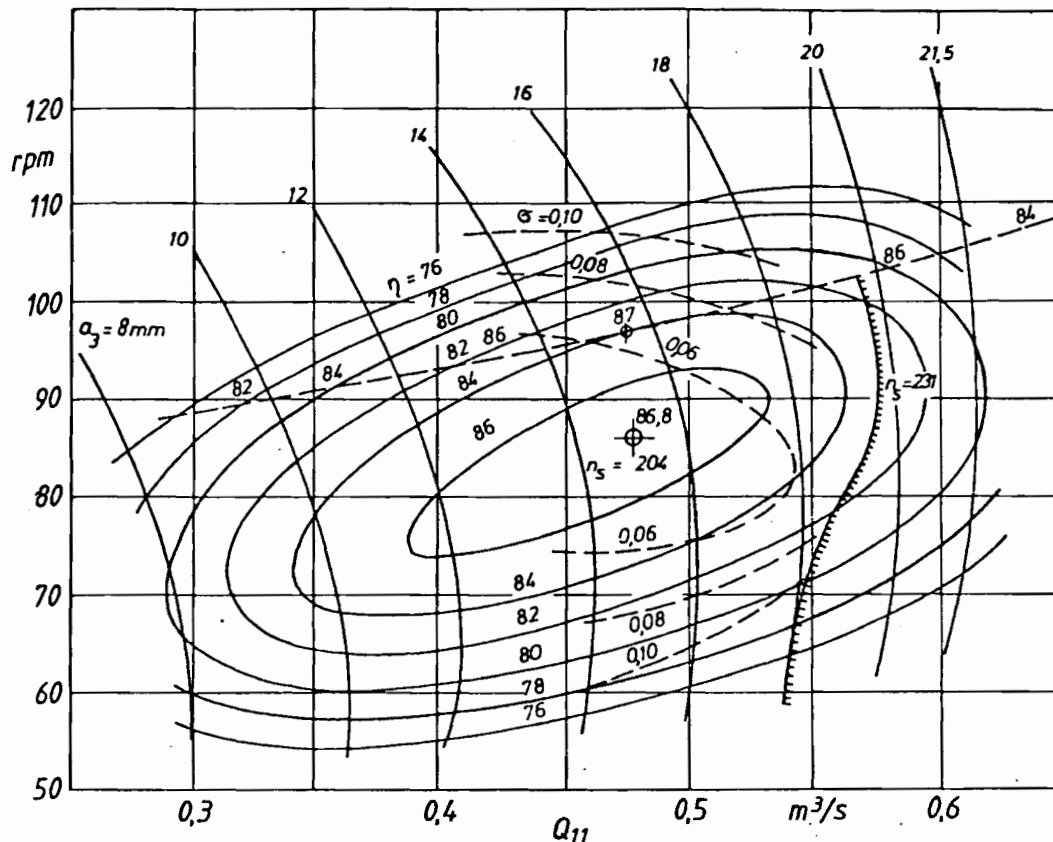
Fig. 10.4.20. Hill diagram of a radial pump-turbine in turbine mode. Hatched line indicates the H vs Q line of pump operation. After *Mei*.

smaller. Improvements were made in later designs to enlarge the spatial opening on the low pressure edge and more flow was obtained in the turbine mode. The above could also be due to insufficient guide vane height as the 50 m models were tested in a casing originally designed for other parameters.

Fig. 10.4.20 gives the turbine characteristic curve for runner No. 12 and shows the critical σ values to be much lower than those for pump operation. The pump H, Q-envelope curve (along which the pump will be recommended to operate) is plotted on the turbine hill chart for comparison. Because of the intrinsic difference in optimum regime of the two operating modes and the priority given usually to pump operation, the turbine performance will always have to be away from its best efficiency region. Runners with hill contour more skewed from the horizontal have better capability of providing better turbine performance.

3. Relation between operating points of two modes

Studies were made of the ratio of n_{11} and Q_{11} at bep of the two modes of operation. Plots of the ratios for the many runners tested are given in Fig. 10.4.21. It is apparent that good runners can be designed for different combinations of ratios if they fall within the band inclining downward from left to right. For application to pure pumped-storage plants, values around $n_{11P} = 1,1\, n_{11T}$ and $Q_{11T} = 1,15\, Q_{11P}$ are ideal as recommended by Fuji Electric.

509
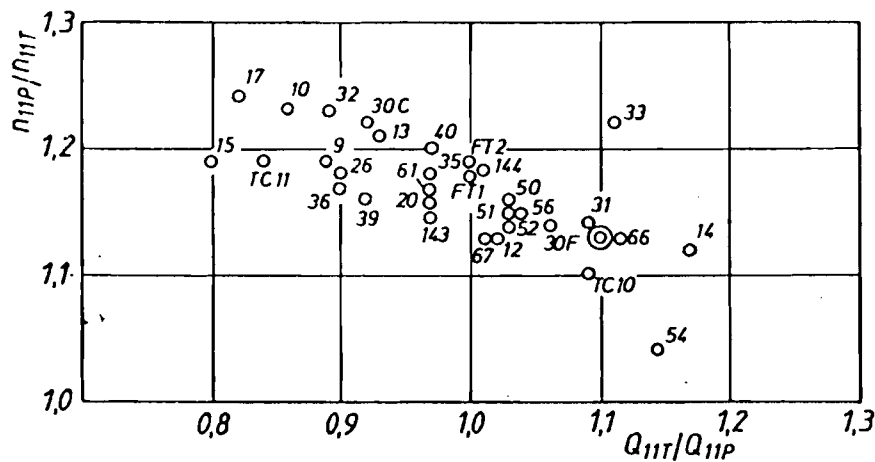
Fig. 10.4.21. Speed ratio $x = Ku_p/Ku_T$ as defined by (10.4–28) vs inversed discharge ratio $q^{-1} =$ $Q_T/Q_P = Q_{11T}/Q_{11P}$ as defined by (10.4–29), for several radial model pump-turbines, after *Mei*. The numbers indicate different types of pump-turbine, whose special design features are not mentioned here. The purpose of this graph is to hint at the linkage of x and q to each other as given by the relation (10.4–32).

IV. Conclusions

1. From the tested performance of a large number of model runners, it can be concluded that reversible runners designed by centrifugal pump procedures can give good performance in both the pump and turbine modes, provided adequate adjustments of design constants obtained through careful studies are made. Nevertheless, the flatness of the $H - Q$ curve remains to be a disadvantage for applications to power stations with large head variations.

2. The turbine operation is satisfactory in the majority of cases even though very little consideration was given to this mode of operation in the design. The *Francis* type reversible runner has a fairly flat hill contour so that it gives good performance in the high load region.

3. In order to achieve full utilization of the motor-generator and also to better balance the water quantity on a short time basis, there exists a best ratio between unit flows in both modes of operation. This ratio is an index as important as any performance figure for each of the individual operations (see Cap. 10.4.4).

10.5. Shaft, bearings, accessories of hydro power sets

10.5.1. Layout of the shaft

10.5.1.1. General remarks

Any shaft has to transmit the rated torque under rated speed and the design-linked starting torque, usually 1,4 to 2 times the rated torque. As a general rule the set should withstand runaway conditions. Its lowest critical speeds with respect to flexural and torsional vibrations should not coincide with the operating speeds possible under varying head including runaway.

10.5.1.2. Flexural vibrations

As a model to compute the lowest critical speed due to flexural vibrations, a two mass configuration is considered (see Fig. 10.5.1). It accounts only for the rotating masses of the turbine runner m_L and the generator rotor m_R, to which an adequate portion of the shaft's mass should be added, depending upon the method of supporting the shaft. Oil film and bearing assumed to be inelastic. Thus the flexibility of the shaft does not depend on the plane of its deformation and is determined only by the dimensions of the shaft and its material properties [8.132]. Added fluid mass of runner is neglected.
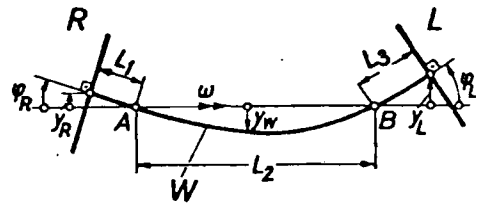
Fig. 10.5.1. Scheme of a shaft W with 2 masses. R (rotor alternator) and L (runner) in overhung design with two guide bearings. y radial deflection of the shaft centre line e.g., under a centrifugal load when rotating.

The following preliminary calculation fits for any arrangement of guide bearings, but neglects the influence of axial thrust. The arrangement shown of two guide bearings (Fig. 10.5.2), practised at heads up to about 300 m has the advantage of a statically determined bearing load. Here the usual arrangement of thrust bearing between the guide bearings does not influence remarkably the shaft deflection. In a design with vertical shaft, a tension in the shaft, caused by a thrust bearing at the upper end, stiffens the shaft and hence increases the critical speed compared with the value attained when neglecting the thrust. Contrary to this, a thrust bearing towards the lower end of a vertical shaft weakens somewhat this radial stiffness of shaft, and hence depresses the critical speed calculated without this influence.

For the computation of the natural frequencies, assume an arbitrary radial deflection y_L and y_R of the mass points m_L and m_R representing hence the runner and generator rotor. They might be in consequence of weight (horizontal shaft) or in consequence of an unbalance.

Neglecting the elasticity of the oil films and assuming the elasticity of the shaft and its guide bearing to be independent of the orientation of the deflection, the following *Maxwell* numbers are attributed to the system as constant parameters: α_{LL} is the radial deflection of shaft at station m_L by the radial unit force on m_L, α_{RR} the same at station m_R, $\alpha_{LR} = \alpha_{RL}$ the radial deflection of shaft at station m_L, or m_R by the radial unit force on m_R or m_L.

Moreover the alternator stator might exert a radial magnetic pull K_m on the rotor m_R, when deflected by $y = 1$. Under a deflection y_R and y_L a centrifugal load $y_R \omega^2 m_R$ and $y_L \omega^2 m_L$ acts on m_R and m_L. Assuming all the deflections in one plane which rotates with ω, then the deflection y_L of the runner results from $y_L = \alpha_{LL} m_L y_L \omega^2 + \alpha_{RL} y_R (m_R \omega^2 + K_m)$. Hence follows the following linear and homogeneous system for both the deflections y_R, y_L

$$(1 - \alpha_{RR} m_R \omega^2 - \alpha_{RR} K_m) y_R - \alpha_{RL} m_L \omega^2 y_L = 0, \qquad (10.5-1)$$

$$-(\alpha_{RL} m_R \omega^2 + \alpha_{RL} K_m) y_R + (1 - \alpha_{LL} m_L \omega^2) y_L = 0. \qquad (10.5-2)$$

After *Cramer's* rule, a finite radial deflection at critical speed ω_{cr} requires the main

511
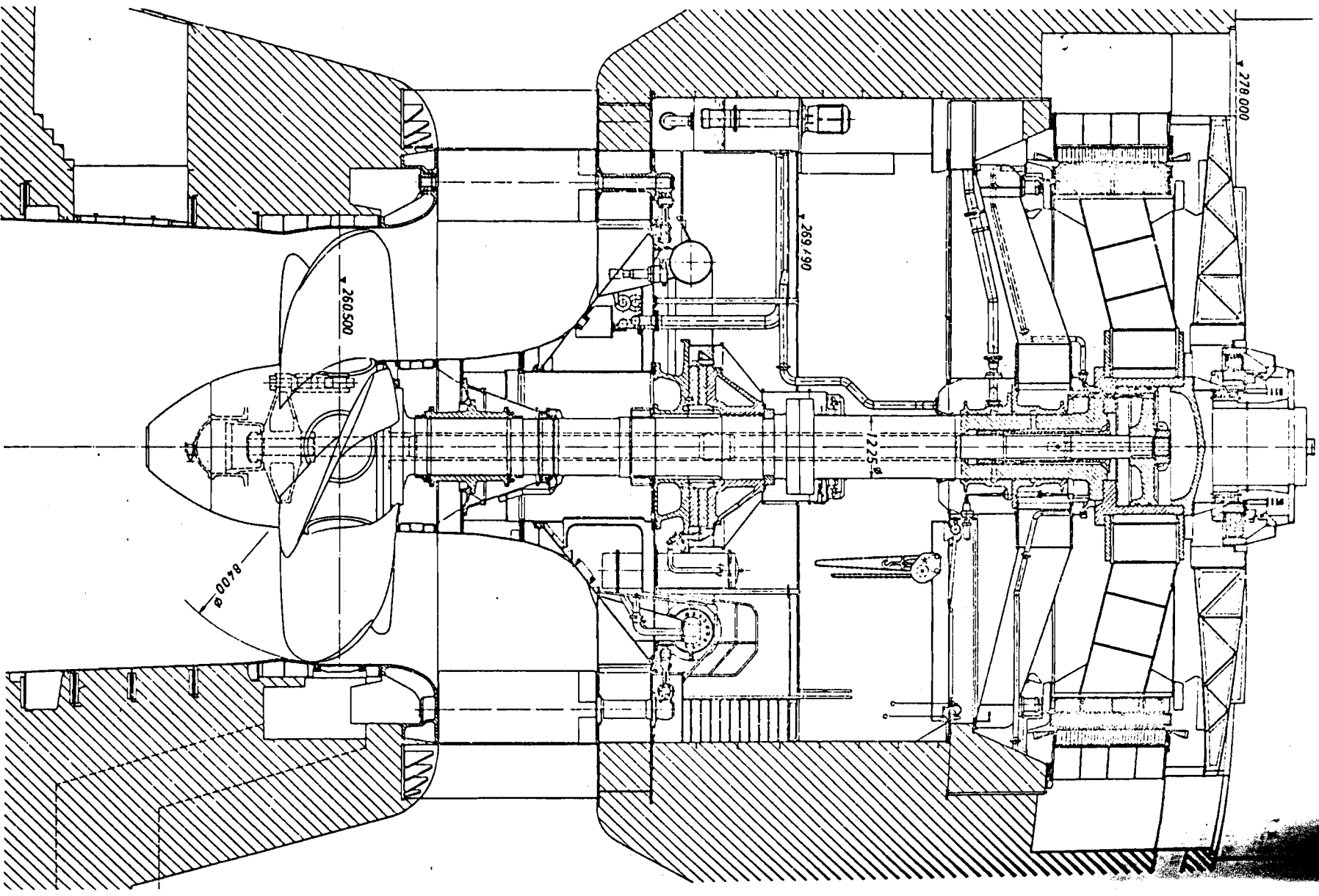
Fig. 10.5.2. Sectional view of the KT, Aschach, Danube, Austria (owner Österreichische Donau-kraftwerke AG). 2 guide bearings, 2 rotor masses of turbine runner and alternator rotor with overhung design. Thrust bearing between the guide bearings does no essentially influence the shaft deflection. Design Voith. (2 sets of Aschach built by Escher Wyss and Andritz are of similar design.) Data: $H = 15$ m, $n = 68.2$ rpm; $P_r = 66$ MW; $P_m = 75$ MW. Runner 5 blades $D = 8.4$ m (largest runner diameter of KT in Western Europe) 12 welded stay vanes, concreted at lower end, carry the welded crown of the stay ring, concreted on its outer part. A welded head cover supports the thrust bearing by means of a welded connection of a ring plate, a truncated cone and a cylindrical shell. This also carries the lower guide bearing, the gate operating ring and its 2 pairs of toroidal servomotors exerting only a couple on the ring. Removable inserts facilitate dismantling of the individual gates. Runner with 5 blades of 13% chromium steel, 2 part shaft, runner servomotor in the hub of the alternator rotor. Upper guide bearing also used as oilhead. Throat ring welded and embedded in the concrete. Draft tube lining welded on the throat ring with stiffening rings and iron ties. Revision of the runner through a door in the concrete of the semi-spiral cone. (Drawing courtesy Voith.)

determinant of this system to vanish. Hence: $a\omega_{cr}^4 - 2b\omega_{cr}^2 + c = 0$ with

$$a = m_R m_L (\alpha_{RR}\alpha_{LL} - \alpha_{RL}^2), \quad c = 1 - \alpha_{RR}K_m,$$
$$b = (1/2)(m_L\alpha_{LL} + m_R\alpha_{RR} + m_L\alpha_{RL}^2 K_m - m_L\alpha_{RR}\alpha_{LL}K_m). \tag{10.5-3}$$

Thus the two critical angular velocities of the system

$$\omega_{cr\,min}^{max} = \{b/a \pm [(b/a)^2 - c/a]^{1/2}\}^{1/2}. \tag{10.5-4}$$

Care must be taken, that $\omega_{cr\,min}$ is about 15% above the highest runaway speed $\omega_{ra\,max}$ (rare exceptions see below).

To obtain the critical speed of flexural vibrations in the case of more than two masses, the system has to be divided into two mass systems. Applying to them the above procedure and accounting for the compatibility of deflection at the station of a certain mass now assigned to two systems, the procedure results in a linear system with the same number of unknown critical speeds as are masses The same can be done with torsional vibrations which are treated in the following section.

10.5.1.3. Torsional vibrations

Torsional vibrations are excited by the alternator with a frequency equal and twice that of the grid. At short circuit they appear with largest intensity, especially in the case of short circuit between adjacent phases.

They may appear also under hydraulic transients, at start and stoppage of a set, in consequence of rotating stall, cavity-induced vibrations, e.g., a precessing and cavitating draft tube vortex.

Also here the natural frequency of the system must not coincide with the exciting one.

As a special case consider a tubular turbine with planetary gear, as used on the West German Mosel, Figs. 10.5.3; 10.2.16. The natural frequencies follow from the equation of motion for the individual parts of the gear, e.g., turbine shaft, generator shaft, sun wheel, planet pinion. Whence [10.171]

$$\omega_{1\,2cr} = \{(A + B)/2 \pm [(A + B)^2/4 - C]^{1/2}\}^{1/2}, \tag{10.5-5}$$

at which

$$A = c_{ef}(J_{er} + J_f)/(J_{er}J_f), \quad B = c_{ba}(J_{er} + i^2 J_a)/(J_{er}J_a),$$
$$C = c_{ba}c_{ef}(J_{er} + i^2 J_a + J_f)/(J_{er}J_a J_f), \tag{10.5-6}$$
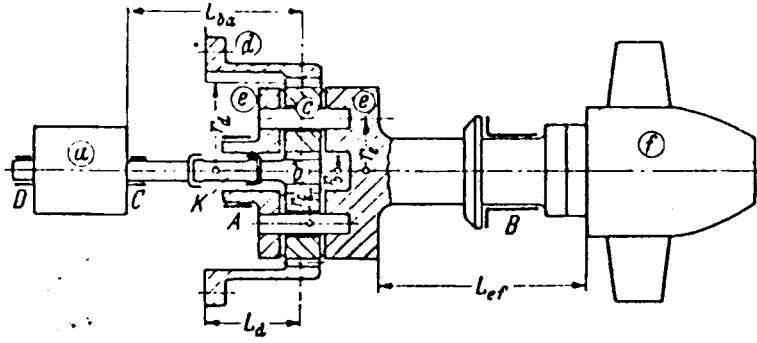
Fig. 10.5.3. Schematic elevation of the rotary parts in a bulb turbine with planetary gear. f runner, a alternator rotor, b sun wheel, c pinion cage, c planet pinion, K curved teeth coupling.

where c_{ef} is the torsional spring rate of the turbine shaft, c_{ba} the same of alternator shaft, J the moment of inertia whose indices indicate by c due to the planet pinion, by a due to alternator rotor, by f due to runner, by e due to the pinion cage. With m_b being the resulting mass of the planetary wheels, r_e the radius of their centre line, and i the gear ratio: $J_{cr} = J_c + m_b r_e^2 + [i/(i - 2)]^2 J_c + (i^2/2) J_a$.

Since a short circuit may induce high load amplitudes, it seems advisable also to note some load amplitudes as a function of the exciting torque under short circuit

$$M_k = M_0 (\sin \omega_0 t - (1/2) \sin 2\omega_0 t), \tag{10.5-7}$$

ω_0 being the cyclic frequency of the grid. M_0 becomes largest for a single phase short circuit under Δ voltage. With

$$\Delta \omega_k = (k\omega_0)^2 J_a J_{er} J_f ((k\omega_0)^2 - \omega_{1cr}^2) ((k\omega_0)^2 - \omega_{2cr}^2), \tag{10.5-8}$$

the following torque amplitudes are obtained: M_R at the generator rotor shaft, M_L at the turbine runner shaft, M_c at the gear casing, being in the worst case

$$M_R = \sum_{k=1}^{2} [(c_{ba} J_f J_{er} k M_0 \omega_0^2)/\Delta \omega_k] [c_{ef}(J_{er} + J_r)/(J_{er} J_f) - (k\omega_0)^2],$$
$$\tag{10.5-9}$$

$$M_L = \sum_{k=1}^{2} (i c_{ba} c_{ef} J_f k M_0 \omega_0^2)/\Delta \omega_k, \qquad M_c = M_R - M_L.$$

In the eventual case of resonance under short circuit, the decay of the exciting current is important, since then any load amplitude increases vs time.

10.5.1.4. Excitation of shaft vibrations by runner seal

In mixed flow machines, a wrong layout of runner labyrinths may excite flexural vibrations. The best remedy there is the provision of the so-called damper design in connection with comb labyrinth on the hub (Fig. 10.3.10). Here the outside located gap of a runner labyrinth tooth has a relatively smaller clearance than the adjacent inside located gap. Imagine that the runner is displaced radially outward. This squeezes the outer gap, increases the pressure there and widens the inner gap simultaneously reducing the pressure there. This centres the shaft again.

According to *Lomakin* [10.172], in axial machines, a shaft deflection reduces locally, clearance and leakage, which increases the tangential force there. Hence the deflection is turned by 90° thus initiating a circular shaft vibration.

514

10.5.2. Influence of bearings on shaft vibration

10.5.2.1. General remarks

The rotor of the turbine and generator and the shaft are excited usually by rotating forces due to mechanical, hydromechanical and electrical unbalance of the rotor masses, in consequence of misalignment during assembly, imperfect balancing or short circuit. The elastic system of shaft and rotor masses, which is elastically supported and damped by the bearings, responds to these excitations by shaft oscillations with finite amplitude of different kinds [10.121].

Flexural vibrations as the most obvious type of vibrations are considered now separately. I.e., for the generator to work properly, vibration must not accelerate to levels at which it might damage the components, or reach such an amplitude as to cause wear or wiping off the bearing's white metal. The rotary system must be properly insulated from the stationary one, so as to avoid subjecting it to excessive stresses. These differing requirements tend to be in contrast, as a bearing system, which limits shaft vibration tends to put greater forces on the foundations and vice versa.

The basic element of damping and elasticity between rotor and the foundation is the oil film in the bearings. As already stated, the general way to limit vibration amplitude, is to design the machine so, that its lowest critical speed is greater than any possible operating speed (runaway). Hydraulic units have considerable shaft stiffness and the masses are limited by electrical, mechanical and governing requirements.

So any method of increasing the critical speed depends on the possibility of reducing the elasticity of the guide bearings. In a very stiff system small values of the amplitude of shaft vibrations can involve significant unbalanced stresses which can exert high forces on the foundations.

For these reasons the traditional criterion of creating a large difference between critical speed due to shaft stiffness and the rotor masses and the working speed cannot be considered as an absolute guarantee of safety.

It is necessary to make a thourough analysis of the dynamic response of the rotor which takes into account three parameters: unbalance, vibration amplitude and the feature of the bearings. Since the bearing box and its support are usually rather stiff, as a minimum requirement of a good bearing design, the features of the bearings are reduced to that of the lubricating film in the gap between seat and shaft.

10.5.2.2. The spring rate of the film of lubricant

As a model consider two plane faces parallel to each other, at distance y, with an area A. The clearance is filled with a lubricant of bulk modulus E_L, the boundaries might be completely leak proof. Expressing the spring-induced force by $F = K \Delta y$, where K is the spring rate and Δy the compression of clearance, and using the relation (8.3−5) as the equation of state of the lubricant, the spring rate reads

$$K = E_L A/y. \tag{10.5-10}$$

Hence the stiffness of an oil film increases with decreasing clearance y. Thus an oil film loaded by an unbalance, by which the oil is squeezed out of the gap, becomes suddenly more stiff than an unloaded film existing in a well balanced system.

10.5.2.3. The damping coefficient of the lubricant's film

Imagine an oil-filled gap, length l in the flow direction, width b, clearance y. Both the walls of this gap might be squeezed by a damping force F_d with the clearance rate $\dot{y}$. Hence by definition the damping coefficient $d = F_d/\dot{y}$.

This squeezing actuates a pressure Δp which presses the oil out of the gap in the streamwise direction, length l, with the average speed c. To balance the wall shear stress τ: $\Delta p \sim \tau l/y$. Newton's law requires $\tau \sim \eta c/y$. Continuity requires $c \sim \dot{y}l/y$. With Δp, the damping force becomes

$$F_d \sim \Delta p l b \sim \tau l^2 b/y \sim \eta c l^2 b/y^2 \sim \eta \dot{y} l^3 b/y^3 \sim d\dot{y}.$$

Reducing $\dot{y}$ yields the damping coefficient of the film

$$d = \mathrm{const}\, \eta\, l^3 b/y^3. \tag{10.5-11}$$

b might be the axial length of a journal bearing and l the circumferential length of its loaded face, y the clearance of its gap. Hence the damping coefficient of a bearing with an unbalanced load, squeezing the oil out of the gap, increases with decreasing clearance, whereas the damping coefficient of a balanced system is nearly zero.

10.5.2.4. Control of bearings

Regular working of a large hydroelectric unit requires a continuous measurement of amplitudes due to shaft vibration to be installed, e.g., at the bearings of the rotor. Such a measuring set consists of vibration transducers, signal amplifier and an indicator and recording device with an appropriate alarm and locking signal. In this way it is possible to intervene quickly in the case of alteration in the dynamic balance of the unit, caused by anomalies (short circuit, bearing wear) and also to forecast the need for any normal or emergency maintainance, [10.121].

10.5.3. Bearing design and arrangement

10.5.3.1. General remarks

In consequence of their size and load, particularly in the axial direction the bearings of larger sets are only of the sliding type. Moreover the *Michell* tilting pad bearing type is used exclusively for the axial load, composed of hydraulic axial thrust and the weight of rotating parts in the case of vertical shafts. For shaft diameters above about 1,5 m this bearing type is also preferred for the radial (guide) bearing.

Any bearing has to transmit a certain heat flow through its casing into the supporting structure towards the foundations. This originates partly from the waste heat of the alternator (in the case of a bearing due to the latter) and partly from the bearing itself.
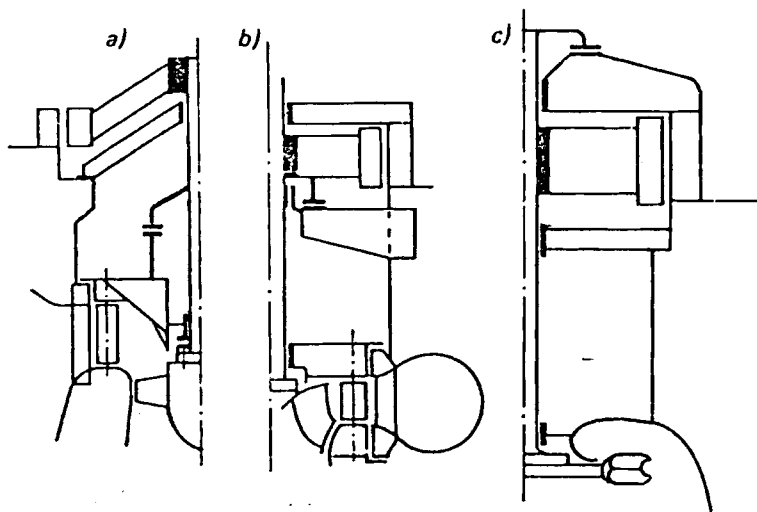
Fig. 10.5.4. Principal bearing arrangements. a) 2 Radial bearings, both the rotors of overhung design, thrust bearing on the head cover. b) 3 Radial bearings, thrust bearing on the pit. Variants: middle or upper radial bearing omitted. c) 3 Radial bearings, thrust bearing on the generator stator.

Several designs have been proposed to avoid additional stresses in this structure due to thermal expansion. One solution consists in radial arms transmitting any radial expansion via strongly prestressed springs into the concrete of the pit wall.

Another solution uses arms which are slightly inclined to the radius, so-called "skew spokes", [10.173]. Thus heat expansion of these arms is converted into a central rotation of the bearing casing about its axis. Thereby the skew spokes are subjected to bending.

With the largest heat expansion of the bearing's support, the clearance of a radial bearing must not fall short of the prescribed threshold.

Fig. 10.5.4 shows typical bearing arrangements of hydro turbo generators with vertical shaft. To this typical bearing arrangements of horizontal sets have to be added. See Figs. 3.4.1; 3.4.19; 3.4.20; 3.4.22; 3.4.23; 3.4.28; 3.4.33; 10.2.10 to 10.2.18.

10.5.3.2. Guide bearings

Usually two guide bearings are used, as their load is statically determined. Overhung design is preferred at the turbine runner especially in reaction turbines. This keeps the draft tube bend free of any obstruction by the shaft. In some ternary pumped-storage sets the runner can be disconnected either from the alternator-motor (Fig. 3.4.38) or from the pump (Fig. 3.4.39). This requires two guide bearings on both sides of the runner. This holds also for rarely found double flow FTs with a twin runner supplied by one spiral casing.

The relatively big alternator rotor has an overhung design only up to heads of about 250 m and for vertical sets. In this head range the umbrella or semi-umbrella type of alternator rotor prevails (Fig. 10.5.4 a). Above this head the alternator rotor is supported at both ends (Fig. 10.5.4 b).

In the high-head range the two and three bearing arrangement is used. In smaller low head sets with submerged turbine also three or more bearings are found, to make the generator easily accessible and to place it above the tail race level.

The lubrication of the bearing requires the existence of wedge-formed clearances between shaft and bearing sleeve in the order of $0.5 \cdot 10^{-4}$ times the shaft diameter [10.174]. To take out-of-balance loads like the magnetic pull the radial support of the bearing must be of solid design in all radial directions.

10.5.3.3. Thrust bearing design, brake

Vertical sets, especially of higher head, with axial thrust downward oriented, need only one thrust bearing (Fig. 10.5.2). Horizontal sets need two (Figs. 10.2.10; 10.5.5). For the brief and small reversed axial thrust in vertical sets during transients in KTs, a thrust collar is provided. This is usually on the lower extremity of the bell-shaped part of the shaft that is immersed in an annular oil tank, to facilitate lubrication of guide bearing during starting (see Fig. 10.5.6).

The clearance of the surge face pad on the lower front of the guide bearing casing must be in the order of the axial deflection which may be experienced under axial thrust.

For heads up to 320 m (Fig. 10.5.4) the thrust bearing is underneath the alternator and then supported either by a spider on the pit wall or a supporting truncated cone on the head cover (Figs. 10.5.4 a; 10.5.4 b). In small sets and under highest heads, e.g., in PTs the thrust bearing rests on the generator stator by means of a spider (Fig. 10.5.4 c).
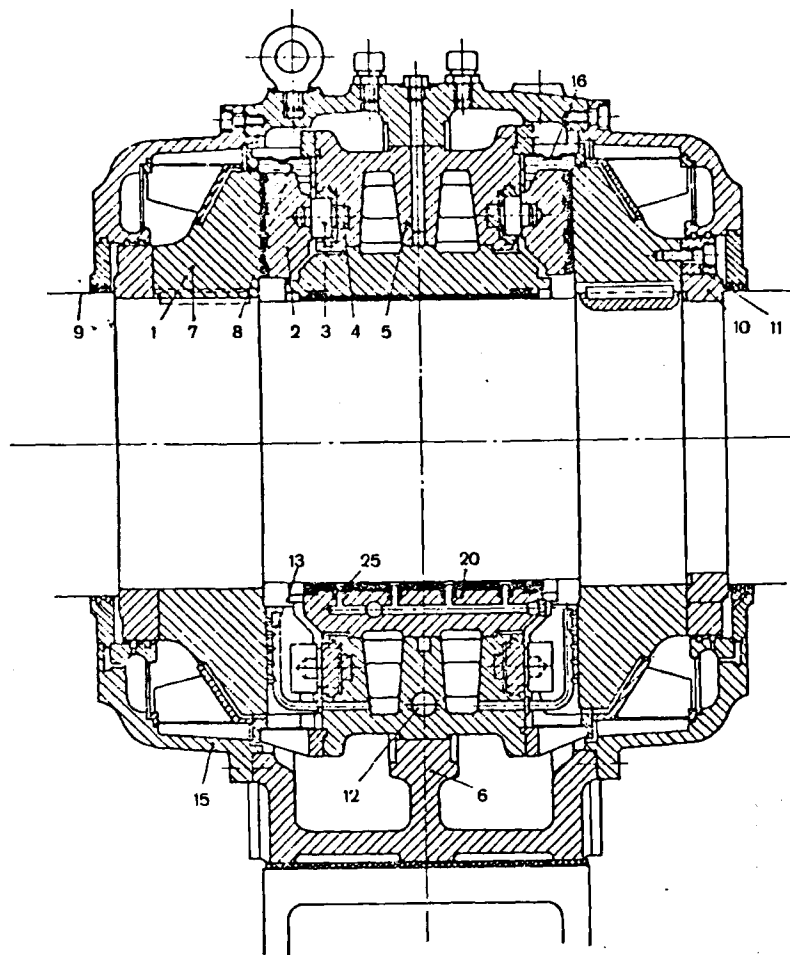
Fig. 10.5.5. Guide bearing with two axial (thrust) bearings for e.g., a FT with horizontal shaft. Oil circulation of the thrust bearing by a pump feeding a ring pipe 12, with radial branches, blowing out the oil against the rotating thrust collar 1. For a starting lift by pressurized oil from the bore 25. 1 rotating thrust collar, 2 tilted pad, 3 prop with calotte to support pad, callote pressed in mild iron ring, 5 spacer cage of pads, 6 pedestal of bearing, cast iron, 7 driver for 1, 8 oil level, 9 shaft, 10 split support ring, 11 fastening ring for 10, 12 pipe connection for fresh oil, 13 injection pipe, 15 oil pan, 16 overflow edge, 20 bearing sleeve, 25 bore for pressurized oil during start.

For an overhung alternator rotor the accessibility of the thrust bearing may be facilitated by a removable ring, connecting the upper end of the shaft with the upper front face of the rotor (Fig. 10.2.1). This ring then serves as a thrust collar, which transmits the axial thrust from the shaft to the tilted segments.

For a revision, both the rotors must be supported by other devices, e.g., the generator brake, then used as jack. Then after removing the connecting bolts and the ring the tilted pads become easily accessible.

Each pad may be supported by springs or it rests on a radial edge or a spherical calotte which presses in a ring of mild steel (Fig. 10.5.7). The pad may be supported also by a pressurized plunger piston in an elastic toroidal shell, supplied from a common oil pressure vessel, under the controlled pressure of all the pads together, Fig. 10.5.8 [10.134].

At heads above about 1000 m, a water-lubricated hydrostatic thrust bearing, at the lower end of the shaft, reduces the tip diameter of this bearing and the corresponding disk friction loss [10.135]. This follows from the head-conditioned pressure, high if compared with the mean value of about 35 bar, which is attainable in the gap of a tilted pad, (see Fig. 10.5.9).

In large units the elastic and thermal deformation of the pad face from its desired plane form is sometimes automatically compensated by means of a special construction [10.133]. Thus the centre of pressure distribution at the shoe is always retained.

518

Fig. 10.5.6. Oil lubricated lower bell-type guide bearing of a KT. Small collar for the transitory uplift during a stoppage. Cooling by the working fluid (water) on the water deflection shield. Inlet of the suction pipe near to the cooling surface. Oil circulation by the combined action of viscosity, shaft rotation and inclined groves S (after Sulzer Escher Wyss).
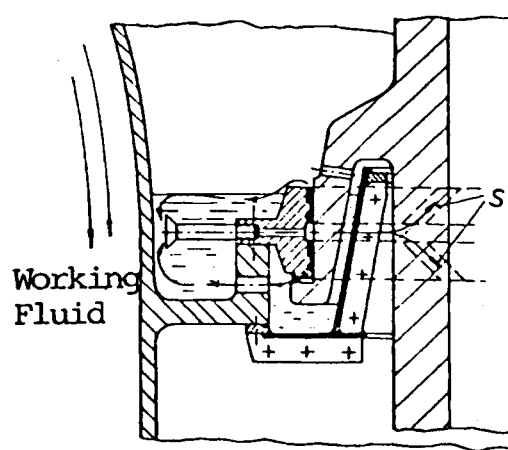
Before the start, each pad is fed through a flexible hose by pressurized oil, to ensure fluid friction from the beginning of operation. To limit the period of mixed friction during running down, each set has a brake device. This is of particular importance for peak load or pumped storage sets with their frequent load change or their cyclic service of generating and pumping.

The present tendency is to limit the proper mechanical braking to the final phase of deceleration, below 10% of the rated speed. The brake is on the spider below the alternator rotor and presses its oil operated piston against the lower front face of this rotor. This mechanical braking is preceded either by hydraulic or electric short circuit braking. In this way problems of dust, wear, overheating of sliding surface and vibrations are minimized [11.69]. The brake is designed to cope with emergency situations which would arise up to 50% of rated speed. In Fig. 10.5.10 brake and jacking device are arranged separately.

To eliminate any dust and wear during braking at the pump-turbine set of Kühtai, Austria, any mechanical braking has been cancelled in favour of an electrodynamical stoppage. Usually then the oil-operated mechanical brake is left for the emergency case, and as jacking device during revision for the rotating parts [10.175].

Under rated speed the oil is circulated either by flinger bore holes in the thrust collar or by a separate pump. The latter feeds a ring pipe with radial passages, from which the oil spouts against the lower front face of the rotating thrust collar. Then it is drawn into the oil wedge on the pad. After the pad the heated oil is wiped off by a stripper.
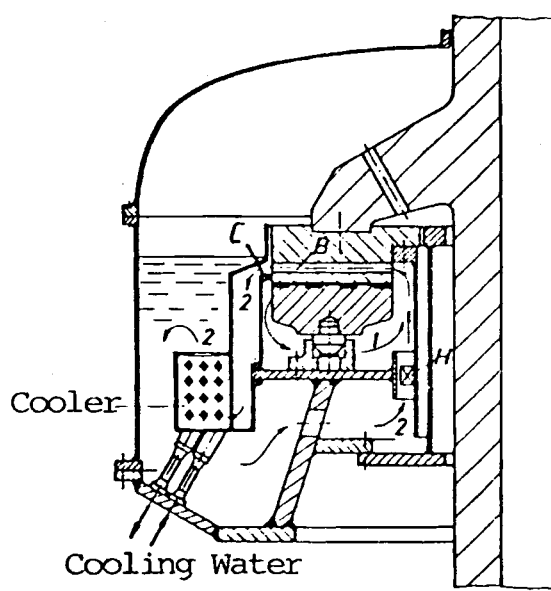
Fig. 10.5.7. Elevation of an axial thrust bearing with tilted segments, oil lubricated. Cooler in a non – pressurized oil tank. Circulation by axial booster pump H, radial bore B and baffle C past outlet from B. Oil flow through the bearing and the lubricating gap 1 in shunt to the oil flow passing the cooler 2. Air separation from the oil after the cooler on the free level of the oil tank. (After Sulzer Escher Wyss.)

519
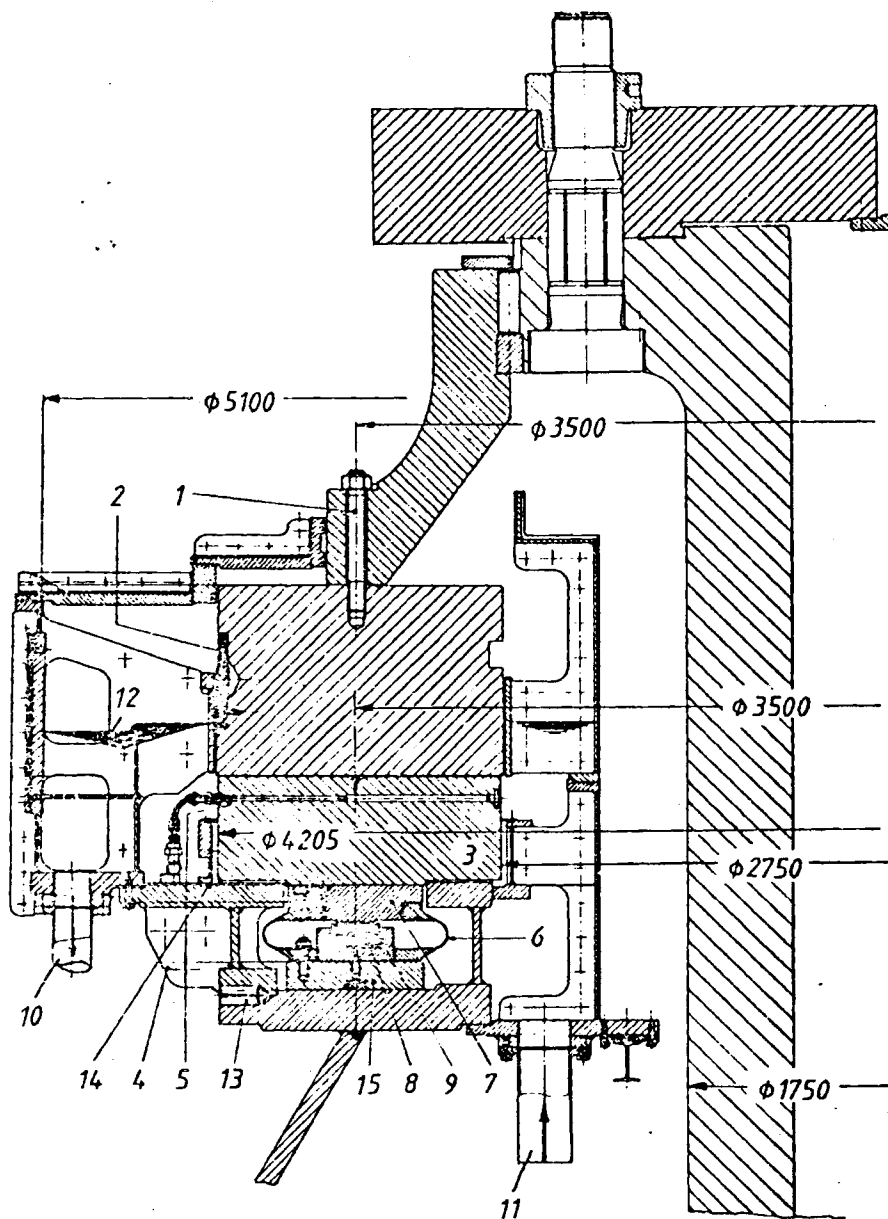
Fig. 10.5.8. Elevation of the thrust bearing of large FT. Plant Tucurui, Tocantin, Brazil (owner Electronorte) built by Neyrpic. See Fig. 10.3.4. External diameter of casing 5,1, tilted pad external diameter 4,205 m, internal diameter 2,75. Shaft diameter 1,75 m. Axial thrust 2410 tons. Oil: 8,5° Engler at 50 °C. Cooling water 90 m³/h. Oil volume 5,3 m³, auxiliary oil volume 4,3 m³. Tilted pad supported by a hydrostatically loaded piston 7 usually carried by pressurized oil in a toroidal axially flexible vessel 6, communicating with each other. In emergency the pad carried by the calotte 8. The toroidal vessel enables also a slight radial deflection, if the pad floats. Oil from cooler enters at the inner edge 11 of the bottom ring, is then centrifuged by the thrust collar 2 either between the pads directly, or through the lubricating gap into the outer part of the case. 1 Fastening of the thrust collar 2, 3 tilted pad, 4 joint, 5 oil injection for jacking at start up, 6 toroidal shell, 7 upper support disk of the pad, 8 calotte, 9 bottom support disk of the pad, 10 oil exit to the cooler, 11 oil inlet from the cooler, 12 oil level, 13 radial splint, 14 guide cage for the pad, 15 bottom plate of the pad with a pipe for pressurized oil from a balancing chamber. (Drawing courtesy Neyrpic, Grenoble, France).

520
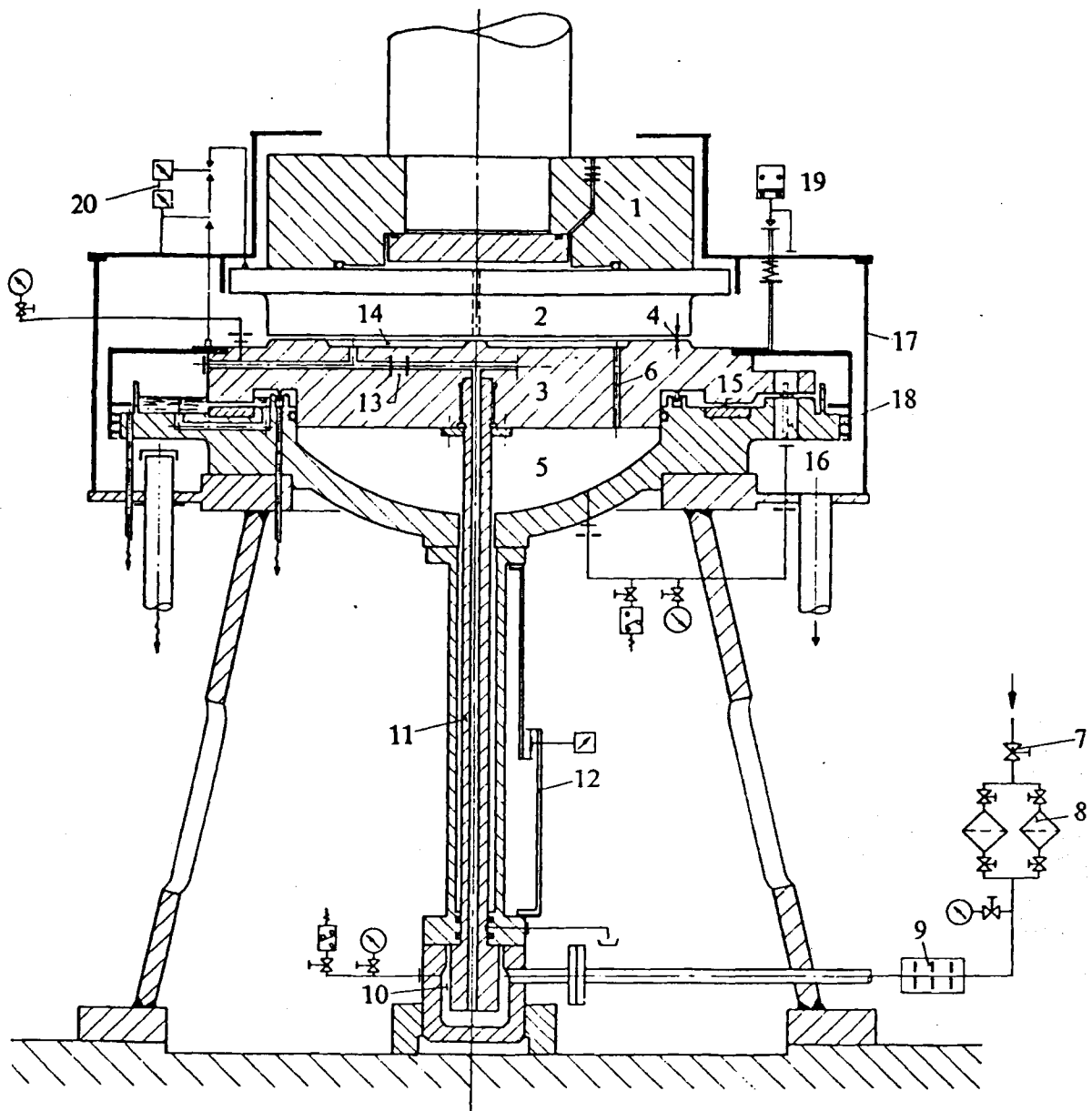
Fig. 10.5.9. Thrust bearing with hydrostatic water lubrication in one of the 6-stage storage pumps of San Fiorano pumped storage plant, (owner ENEL, Italy) with ternary sets built by Sulzer Escher Wyss de Pretto. $H_m = 1483$ m, $P_m = 105,8$ MW (see also Fig. 1.6.8). 1 thrust collar, clamped on the shaft, with discharge orifice, 2 rotary thrust disk attached to 1, 3 stationary support of 2, 4 radial gap to relieve pressure chamber 14, 5 pressurized, sealed, and water filled calotte, 6 bore to balance the pressure in 5 and 14, 7 valve for the admission of pressurized water from the penstock, 8 filter, 9 flow control, 10 water head, 11 admission pipe for the pressurized water, 12 strain gauge to indicate water load, 13 throttle, 14 pressure chamber, 15 gap between stationary parts 3 and 5, 16 leakage pan, 17 casing, 18 comb labyrinth, 19 transducer, 20 clearance indicator.

10.5.4. Lubricants and their cooling

In general oil is used as a lubricant, in some cases also grease water emulsion or (in the USSR) purified water. The oil lubrication of the bearing next to the water side needs protection against water pollution in the form of a shaft seal (Fig. 10.5.11). This requires a leakage sump between the oil collector and the shaft seal, whose level must be controlled by a float and a pump.
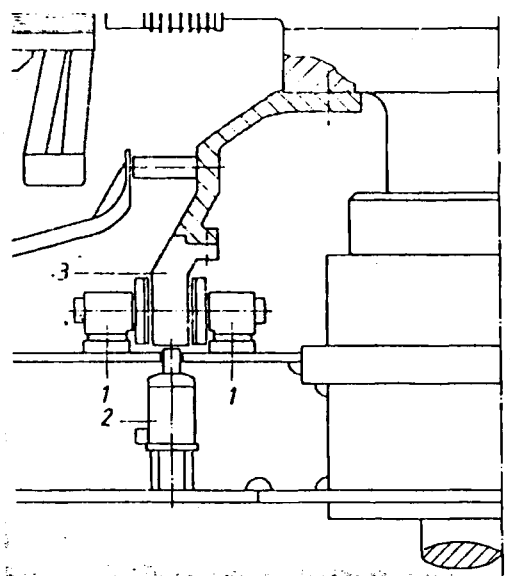
521

– Cooling of the lubricant oil: For the guide bearings next to the runner, e.g., in a KT, the oil may be cooled by the working fluid, i.e. along the water deflection shield (Fig. 10.5.6). Here the cooling is the more effective the closer the oil circuit intake is to the cooled wall. In other bearings more distant from the discharge a special cooler must be provided. This may be inside or outside the oil tank. The oil flow and its temperature at inlet and outlet of the cooler must be controlled. In the case of excessive temperature the set is stopped automatically. Through the cooler passes a flow which is a multiple of that, drawn into the wedge-formed gap of the bearing. This lubricating oil flow circulates in a shunt to the cooled oil flow so as to mix intensively at the joints with the latter. The circulation through the cooler may be via special pumps. Usually it is done by flinger bores in the thrust collar (Fig. 10.5.7) or a flinger shell (Fig. 10.3.10). The conversion of the high oil speed into pressure, needed to overcome the friction in the cooler, may be effected by baffles or a *Pitot* tube (Fig. 10.3.10). The circulation of the cooling flow in the guide bearings also may be effected by viscous shear stress on the rotating shaft in connection with a helical groove within the bearing sleeve (Fig. 10.5.6).

10.5.5. Runaway and its problems

10.5.5.1. General remarks

In the case of runaway the specific head gH is converted through dissipation into waste heat. Hence

$$c_D = (2gH/\zeta_D)^{1/2}, \tag{10.5-12}$$

where c_D is a characteristic absolute velocity of the turbine and ζ_D a coefficient. At runaway the torque becomes zero and hence by *Euler*'s equation also the difference of angular momentum between the rotor inlet and outlet $c_{u2}r_2 - c_{u1}r_1$. In a KT this condition reads $\Delta c_u = 0$. Thus both the velocity triangles coincide here under runaway. Let c_D be the absolute velocity of this runaway triangle. Hence at a certain c_D, the peripheral blade speed is the larger the smaller the angle β the blade makes with the circumference. Thus the highest possible runaway speed in a KT occurs at overgate and small blade angle at cam-off operation. This may be caused by the longer opening time the runner servomotor has compared with that of the gates (Cap. 11.2). Such a situation may occur, when the control loops of gate and runner are connected in series in which

522

Fig. 10.5.11. Shaft seal with graphite ring pressed against a chromed sleeve by a ring spring. Conical joint between outer and inner ring causes slippage of both the rings against each other and thus an axial tightness of the ring chamber. Lubrication and cooling by the admission of purified blockage water 1 between the upper and the lower seal ring chamber. Left: standstill seal pressed down before a revision of the shaft seal.
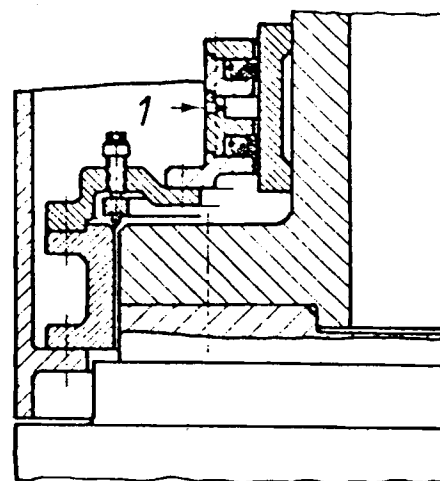
case the tachometer first actuates the gate servomotor. Therefore a connection of both the loops in parallel is preferred, e.g. by the *French* firm Neyrpic (Cap. 11.2).

10.5.5.2. Protection of the set against runaway

Contrary to practice with thermal turbo generators, the hydro turbo set in general has to withstand the runaway speed n_{ra} of its turbine. This is a multiple (1,4 to 3,3) of the rated speed, depending on the design (see Table 9.2.1). The first safety precaution is the speed governor of the set (if any at all). At least each set has an emergency shut down device for the case a certain overspeed (about 1,3 the rated one) is surpassed [11.21], [1.5].

Since the closing time of gates is limited by water hammer-induced pressure surge in the penstock, the set may reach rather high overspeed during emergency shut down. When this device fails, e.g., by jamming, the then unloaded set may attain its runaway speed.

As a general rule, it may be stated, that sophisticated devices for avoiding runaway (such as jet deflectors in impulse Ts or braking runner blades swinging out in axial Ts) are impracticable and not reliable in larger sets [10.68; 8.132].

In micro power stations runaway may be the state in which the set passes the time between its working periods. In such plants the peripheral blade speed may be small, so as to have more an idling period instead of runaway, useful to ensure the lubrication of bearings.

Sometimes in double regulated KTs the runner servo motor may be short-circuited by an overspeed-actuated valve. Thereafter the blades can follow their inbuilt opening tendency to ensure the lowest possible runaway speed (see above). This implies that the outermost components of the alternator rotor like the poles are overstrained so as to need rewinding. But the core of the set has to withstand runaway until the bulkheads are inserted [10.176].

In smaller units with step up gear for the alternator the latter may be protected against runaway by loosening the clutch then used to attach the gear casing to the ground. Remember that any gear needs a connection to the foundations so as to lead the difference in torque between the input and output shaft into the ground. When this connection is interrupted then the gear functions as a coupling. Thereby the alternator rotor is protected against runaway speed. Such a device has been proved successfully in the bulb turbine at Ossbergshausen on Agger, West Germany, with a planetary gear *Krupp-Stoeckicht*, [10.177].

The high head PT sets at Silz in Tyrol, Austria, of the Sellrain scheme are an exceptional example of the situation, that the lowest critical speed falls short of the runaway speed. Here a thickening of the shaft sufficient to raise the critical speed above the runaway speed would have required the use of rather expensive material in the alternator rotor because of the resulting increased diameter. In

such a case, care must be taken, that under all imaginable operations the runaway speed never coincides with the critical speed. The latter is only passed during running down or speeding up.

In two recently built sets with Isogyre pumpturbines, Grimsel, Switzerland, Fig. 3.4.3, and Malta, upper stage, Austria, Fig. 1.6.7, [11.70; 10.116], the lowest critical speed falls short of runaway speed. This may be a reasonable practice, if the runaway speed deviates from the lowest critical speed under all possible modes of operation.

However, for the Malta set this is not assured, as the sets operate with a large variation in head and runaway speed so as to need, by the way, also a change pole alternator. Hence the critical speed occasionally may coincide with the runaway speed. In this case all the emergency shut down devices, like governor, overspeed governor, valves and gates must operate safely.

10.6. The computation of flow in a Francis runner

10.6.1. Flow prediction for given runner and working data

10.6.1.1. Introduction

This section is considered to be supplementary to the simplified runner design of a FT in Cap. 10.3.6, which may be used as a preparation. In the following the problem is treated of the distribution of relative velocity in a given runner vane channel under given flow rate with respect to face to face and shroud to hub distribution even with regard to loss and a slight twist of the streamface within the runner channel.

10.6.1.2. Assumptions

Consider the runner of a FT (Fig. 10.6.1) with given geometry under known working data gH, Q and $n(\omega)$ around the bep. The flow does not stall and is steady. The absolute flow is irrotational. Thus the axisymmetric flow pattern in the meridian gained by the net work method due to potential flow, Cap. 5.2, is taken as a first approximation. From this stepwise approximation may be made to the real streamline pattern.

The phenomena at the ends of a vane are neglected. Hence the flow is along the vane surface. The flow is treated on a surface with coordinates a and φ (Fig. 10.6.2). The azimuthal direction φ is peripherally orientated. It coincides with the sense of the angular velocity ω of the runner. The a-lines are oriented from the shroud towards the hub and follow at least on the runner vane face the direction of the latter. They make an angle $\pi/2 - \nu$ with the periphery (Fig. 10.6.2 a). They coincide (Fig. 10.6.1.2) on the runner inlet and outlet with the axisymmetric surfaces 2 and 1, touching the inlet and outlet edge 2 and 1 of the runner vane. The other axisymmetric surfaces that contain the a-lines vary continuously in streamwise direction between these faces 2 and 1 at the extremity of the rotor vane passage.

The projections of the a-lines in the local meridian, denoted by a', make an angle ϑ with the local radius r (Fig. 10.6.1.1). The a, φ-face has the advantage, that it neither intersects the axisymmetric faces 2 and 1 touching the extremities of the runner vanes, nor the runner vane itself, when proceeding along a direction from shroud to hub or when proceeding in the φ-direction from the suction face to the pressure face of the vane. With this system the blockage of the flow passage by the vane and its boundary layers must be accounted for by an adequate contraction coefficient.

524
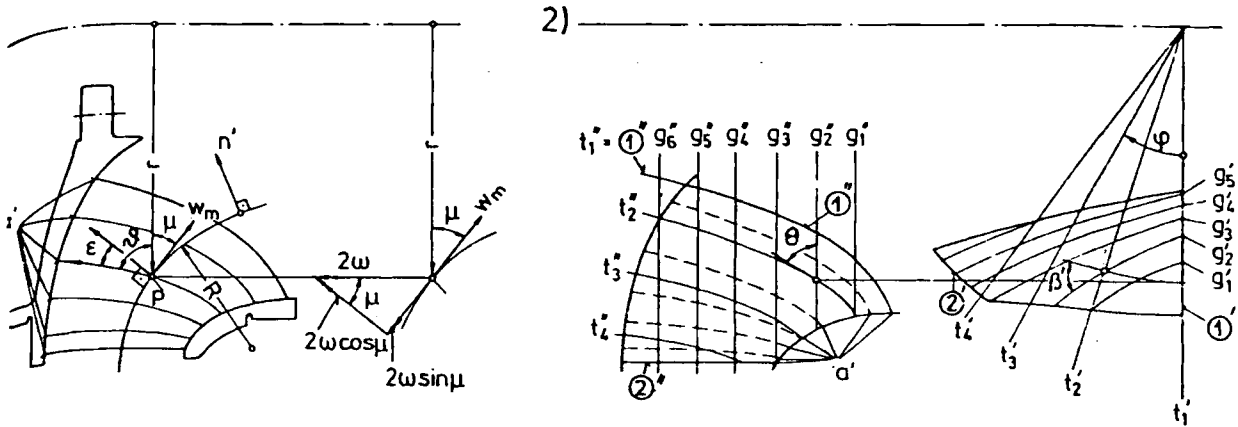
Fig. 10.6.1. 1) Runner of a Francis turbine showing a meridional streamline. of curvature $1/R$, at radius r, with angle μ to the latter. Lines a' coincide with the vane inlet and outlet edge, and make an angle ϑ with r. Right: components of the relative eddy. 2) Runner vane with pattern sections g_i in a plane normal to the axis and radial sections t_i in meridional planes. The line a' is a circular projection of line a onto the meridian in its neighbourhood. For an infinitesimal change this projection of a can be replaced by a rectangular projection of a onto its adjacent meridian.

With the usual n', φ-system, whose n'-lines are in the meridian and normal to the axisymmetrically assumed streamfaces, consideration of the phenomena at the ends of the vane (e.g., flow about the leading inlet edge of vane, formation of wake at the rearward edge of the vane) would be required. Since the inlet edge of a runner vane in general does not coincide with a meridian (Fig. 10.6.1.2), the angle Θ, which a radial vane section makes with the radius, does not coincide at the inlet with the angle ϑ, the line a' makes with the radius.

At or near the outlet edge 1, the radial vane sections and the lines a' usually coincide and hence also Θ and ϑ. Tests of *Schlemmer* [5.18] show approximately

$$\partial(c_u r)/\partial a = 0, \qquad\qquad\qquad (10.6-1)$$
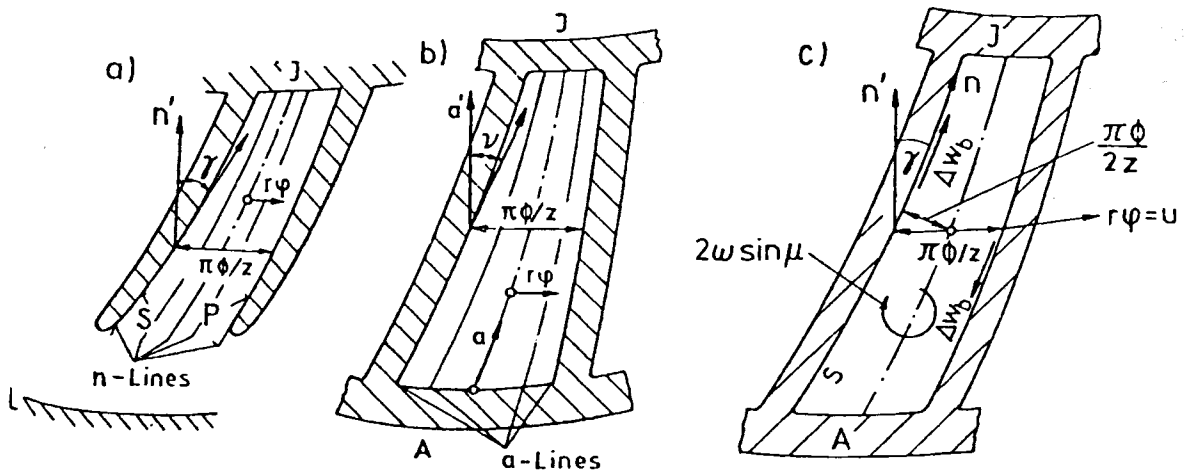
Fig. 10.6.2. a) Channel cross section of a runner seen in the direction of the meridional streamlines on the n', u-face and n, u-face respectively ($u = r\varphi$), depicted in a plane of drawing. γ longitudinal dihedral angle, S suction face, P pressure face, I hub, A shroud, L bottom cover(ring) of the guide apparatus. b) Complete cross section of a runner vane channel in a, u-face, depicted in a plane face. c) Approximate calculation of Δw_h in a runner channel section (n', u-plane) from the meridional component of the relative eddy. J hub, A shroud.

525

where c_u is the whirl component of absolute flow and r the distance from the rotor axis. Comparative calculations show, that the last relation may be substituted for the strict equation of motion needed for the shroud to hub distribution of velocity. This is advantageous since the strict relation contains the curvature $1/R$ of the meridional streamline and the convective acceleration $\partial w/\partial s$ of relative flow as unconvenient terms.

The streamface is preliminarily assumed to be axisymmetric. Later on the twist of the streamface is accounted for as a correction of the second order and this is in agreement with tests of *Schlemmer* [5.18]. The loss is introduced as a stream-line-linked term.

10.6.2. List of symbols used: (Fig. 10.6.3 to 6)

$a_n = \partial a/\partial n$; a'-coordinate in the meridian making an angle ε with a normal to the stream face and an angle ϑ with the radius r, a' is the projection of a onto the meridian, with which it makes an angle v; a-coordinate along the trace of the vane surface, which makes an angle $\pi/2 - v$ with the circumference; n'-coordinate in the meridian normal to the streamline, which makes an angle γ with line n along the vane (longitudinal dihedral angle); n-coordinate along the vane trace in a surface normal to the axisymmetrical streamface; e-internal energy term; $f = n'$ $\tan \gamma$; s_m-coordinate along the meridional streamline; s_u-coordinate or length in the peripheral direction, u-peripheral coordinate or $f + s_u$; $u_n = \partial u/\partial n$; w_n-relative velocity component normal to w caused by the twist of the streamface by the meridional component of relative eddy; β'-angle of pattern section with the periphery; γ-longitudinal dihedral angle of vane trace n in the n, φ-face with n'; β-acute angle of relative velocity w with the periphery; ε-angle between a' and n' in the meridian; Θ-angle of the radial vane section with the radius; ϑ-angle of a' and r in the meridian; μ-angle of the meridional streamline with the radius; v-angle of a' with a in the a, φ-face; φ-azimuth; χ-angle of a with n'; ψ-angle of s_m with a; Φ-contraction coefficient.

Suffices: 1-suction edge of runner vane; 2-pressure edge of runner vane; M-channel centre line; u-peripheral direction; s_m-due to the direction of the meridional streamline; u^0-unit vector in the u-direction; i-the ith step.

10.6.3. Computation of relative velocity distribution

10.6.3.1. In the peripheral φ-direction

Once the angles β' of the pattern section, Θ of the radial section, μ of the meridional streamline are known for a flow along the vane surface, then the angle β of the relative flow with the periphery follows from (6.5–13) as

$$\beta = \arctan[\sin \Theta \tan \beta'/\sin(\Theta + \mu)]. \tag{10.6-2}$$

To simplify the derivation of the velocity distribution, which obviously is not influenced by the orientation of the runner shaft, the latter is assumed as vertical.

Consider a unit mass of fluid of circumferential length $r d\varphi$ (Fig. 10.6.3.1). At the rotating frame of reference, the following forces act on this mass in the peripheral φ-direction

a) $-(1/\varrho) \partial p/(r \partial \varphi)$ due to the tangential pressure gradient
b) $2\omega \cos \mu w \sin \beta$ due to the Coriolis force in the streamface
c) $w^2 \sin \beta/R_t$ due to streamline curvature $1/R_t$ in the streamface
d) $w \partial w/\partial s \cos \beta$ due to the convective acceleration $\partial w/\partial s$ in the direction of the relative streamline (s).

526
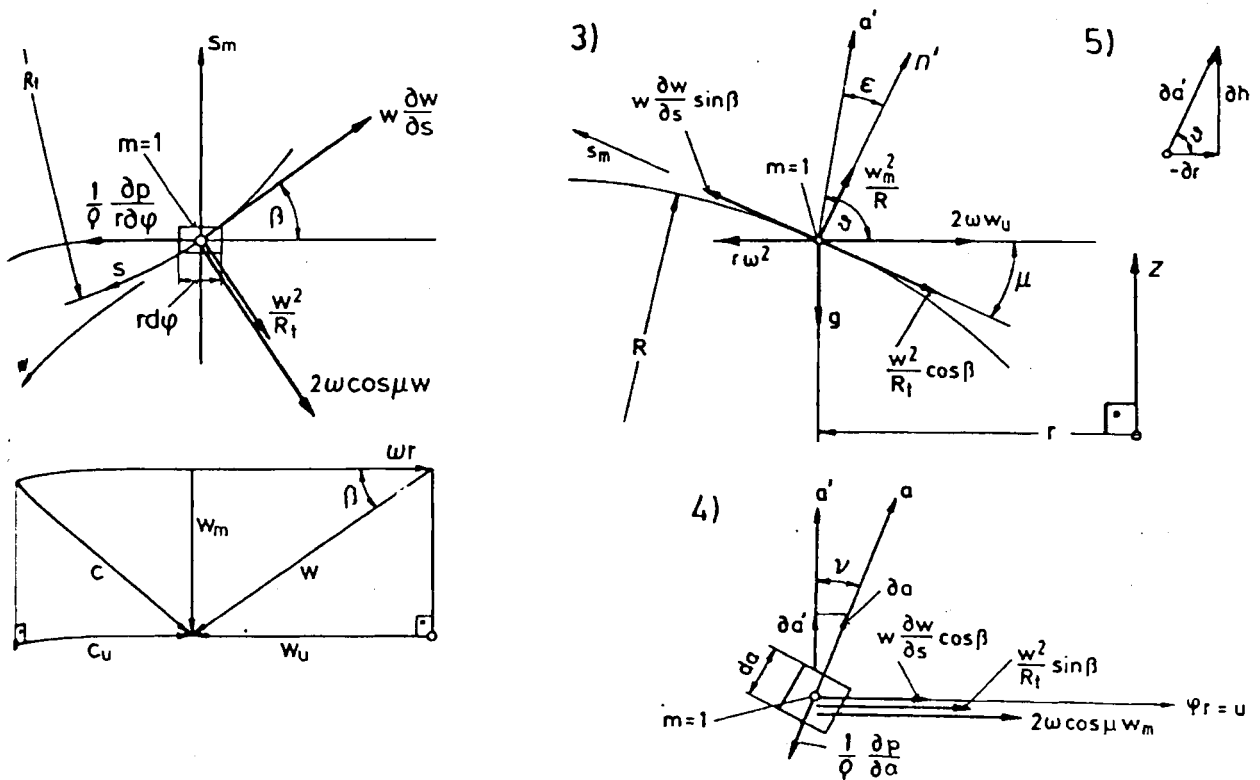
Fig. 10.6.3. Forces on a fluid element: 1) Forces on unit fluid mass, length $r\,d\varphi$, in φ-direction. 2) Velocity triangle. 3) Force on unit fluid mass, length da in a-direction in r, s_m-plane. 4) Ditto in a, φ-plane. 5) Relation between ∂h and ∂r.

Hence the equation of motion in the φ-direction

$$- (1/\varrho)\,\partial p/(r\,\partial\varphi) + w\cos\beta\,\partial w/\partial s + w^2\sin\beta/R_t + 2\omega\cos\mu w\sin\beta = 0.$$

$$(10.6-3)$$

With a streamline-linked loss term 'e' the "rothalpy" reads

$$p/\varrho + gh + w^2/2 - r^2\omega^2/2 + e = 0.$$

$$(10.6-4)$$

Eliminating $(1/\varrho)\,\partial p/(r\,\partial\varphi)$ in $(10.6-3)$ by $(10.6-4)$ gives

$$\partial w = - [w\sin\beta/R_t + \cos\beta\,\partial w/\partial s + 2\omega\cos\mu\sin\beta + \partial e/(w\,r\,\partial\varphi)]\,r\,\partial\varphi.$$

$$(10.6-5)$$

By discretizing the differentials into finite steps this facilitates a stepwise solution of the $w(\varphi)$ distribution along a strip, height $da\cos\varepsilon\cos v$, for which the flow dQ is given. In the last relation, the term $\partial w/\partial s$ is preliminarily obtained from the local velocity triangles with w_1, w_2 and the length L of the local channel centre line by $\partial w/\partial s = (w_1 - w_2)/L$. Finally this term is found by trial and error from the $w(\varphi)$ distribution along adjacent pitches arranged in the relative streamwise direction.

For a flow with forward curved streamlines the curvature $1/R_t$ of the relative streamline in the streamface results from

$$1/R_t = - \cos\mu\cos\beta/r - d\beta/ds.$$

$$(10.6-6)$$

The term $d\beta/ds$ follows at first from the local velocity triangles of the streamface considered with their angles β_1, β_2 and the channel length L by $d\beta/ds = (\beta_1 - \beta_2)/L$. Then it

527

may be improved by (10.6–2), from which

$$d\beta/ds = [\cos^2\beta/\sin^2(\Theta + \mu)]$$

$$\cdot \{[\sin(\Theta + \mu)\cos\Theta - \cos(\Theta + \mu)\sin\Theta]\tan\beta' \, d\Theta/ds$$

$$+ [\sin(\Theta + \mu)\sin\Theta/\cos^2\beta'] \, d\beta'/ds$$

$$- \sin\Theta \tan\beta' \cos(\Theta + \mu) \, d\mu/ds\}. \tag{10.6-7}$$

In the assumed flow along the vane, the derivatives of the angles Θ, β', μ (here signified by x) with respect to s follow by $dx/ds = (\partial x/\partial r)\,dr/ds + (\partial x/\partial z)\,dz/ds$, where z is the coordinate along the machine axis. The values $\partial x/\partial r$, $\partial x/\partial z$ here follow from the given pattern and radial sections of the vane and the streamline pattern. The derivatives dr/ds, dz/ds result from Figs. 10.6.3.1 and 10.6.3.3 by

$$dr/ds = (dr/ds_m)\,ds_m/ds = -\cos\mu \sin\beta;$$

$$dz/ds = (dz/ds_m)\,ds_m/ds = -\sin\mu \sin\beta.$$

With these relations and (10.6–7), the curvature term $1/R_t$ is reduced to known figures like $\partial\mu/\partial r$, $\partial\mu/\partial z$, $\partial\beta'/\partial r$, $\partial\beta'/\partial z$, $\partial\Theta/\partial r$, $\partial\Theta/\partial z$ from the elevation and plan of the vane design with its pattern and radial vane sections.

The loss term $\partial e/(w\,r\,\partial\varphi)$ may be converted into $k\,\partial w/(r\,\partial\varphi)$ by introducing $e = kw^2/2$, with k as an empirical coefficient.

10.6.3.2. In the shroud to hub ($= a$) direction

Consider a unit mass of fluid of length da in the direction a (Fig. 10.6.3.3). In the following the centrifugal force $\omega^2 r$ due to rotation and the gravity g are omitted, since they cannot influence the desired velocity distribution. Then in the rotating frame of reference, the following forces act on this mass in the shroud to hub (a)-direction:

a) $- (1/\varrho)\,\partial p/\partial a$ due to the pressure gradient in the a-direction

b) $2\omega\,(w_u \cos\vartheta \cos v + w_m \cos\mu \sin v)$ due to the radial and tangential components of Coriolis force, where $w_u = w\cos\beta$, $w_m = w\sin\beta$

c) $(w^2/R_t)(\sin\beta \sin v - \cos\beta \cos v \sin\varepsilon)$ due to the tangential and meridional components of centrifugal force under a forward curved streamline with the curvature $1/R_t$ in the axisymmetric streamface.

d) $w(\partial w/\partial s)\,(\cos\beta \sin v + \sin\beta \cos v \sin\varepsilon)$ from the tangential and meridional components of body force due to the convective-acceleration in the streamwise direction of the relative flow.

e) $(w_m^2/R)\cos\varepsilon \cos v$ from the component of centrifugal force due to the curvature $1/R$ of the meridional streamline.

The equation of motion resulting from these forces after substituting the pressure gradient term a) from the "rothalpy" (10.6–4), differentiated with respect to a, but ignoring $r^2\omega^2/2$ and the gh term, yields the following relation for the distribution of w in the a-direction

$$\partial w = - \langle w\{\sin^2\beta \cos v \sin(\vartheta + \mu)/R - (\cos\mu \cos\beta/r + d\beta/ds)$$

$$\cdot [\sin\beta \sin v + \cos\beta \cos v \cos(\vartheta + \mu)]\}$$

$$+ 2\omega(\cos\beta \cos\vartheta \cos v + \sin\beta \cos\mu \sin v) \tag{10.6-8}$$

$$+ (\partial w/\partial s)[\cos\beta \sin v - \sin\beta \cos v \cos(\vartheta + \mu)] + \partial e/(w\,\partial a)\rangle\,\partial a.$$

528

To obtain this, use was made of (10.6–6) and the following relation from Fig. 10.6.3.3

$$\varepsilon = \vartheta + \mu - \pi/2.$$

10.6.3.3. Method of solution with exact $w(a)$ distribution

For a practicable stepwise solution, the last relation has to be discretized in the form

$$\Delta w = - (w_M A + B) \Delta a, \tag{10.6-9}$$

where w_M is the relative velocity along the channel centre line whereas A and B follow from (10.6–8). There again the term $\partial e/(w \partial a)$ may be brought into the form $k \partial w/\partial a$.

The computation starts within a strip of tangential length $r(a) \Delta \varphi$ crossing the a, φ-face considered in a direction along the centre line from shroud to hub. The chosen angular increment $\Delta \varphi$ must be much smaller than the unobstructed pitch $2\pi \Phi r/z$ of the channel. ϕ being the contraction coefficient due to the thickness of the vane and its boundary layers.

It seems advisable to estimate w_M on the basis of the potential flow pattern on the shroud at $a = 0$. Whence $w(a)$ can be determined stepwise and in the first instance by (10.6–9) along the aforementioned strip in the a'-direction. The flow passing this strip results from continuity as

$$\Delta Q = \Delta \varphi \int_{a=0}^{a_i} r(a)\, w_M(a) \cos v(a) \cos \varepsilon(a)\, da, \tag{10.6–10}$$

where a_i is the coordinate a at the hub. Next compare ΔQ with the flow ΔQ_t passing this strip by means of an axisymmetric potential flow using the mean contraction coefficient ϕ_M between shroud and hub and the given flow Q. Thus

$$\Delta Q_t = z \Delta \varphi Q/(2\pi \Phi_M). \tag{10.6–11}$$

It is assumed that the more correct flow through this strip corresponds to the last value. To improve the results, all the velocities w_M, preliminarily computed have to be multiplied by the quotient $\zeta = \Delta Q_t/\Delta Q$. Hence the second approximation of the velocity along the centre line w_{M2} results from the first approximation w_{M1} by $w_{M2} = \zeta w_{M1}$.

Once w_M is determined finally by the above method, the distribution of w in the φ-direction may be implied on the base of (10.6–5) now written as

$$\Delta w = - (w_M C + D) r \Delta \varphi. \tag{10.6–12}$$

With the aid of this stepwisely obtained $w(a, \varphi)$-distribution, check by means of the continuity relation

$$Q_k = \int_{a=0}^{a_i} \int_{\varphi=0}^{2\pi\Phi(a)/z} r(a)\, w(a, \varphi) \sin \beta(a) \cos v(a) \cos \varepsilon(a)\, da\, d\varphi, \tag{10.6–13}$$

if the flow Q_k through a channel corresponds to the prescribed value Q/z. In general Q_k may deviate from Q/z. Then $\xi = Q/(z Q_k)$ may differ from 1. Hence the second approximation of velocity (now including also the $w(\varphi)$ distribution and hence denoted by $w_{2\varphi}$) is obtained from the first approximation $w_{1\varphi}$ by $w_{2\varphi} = \xi w_{1\varphi}$.

Obviously any step changes the original flow pattern and the flow-linked values such as k, $R = \partial \mu/\partial s_m$. Moreover the entry in the above calculation of the $w(a)$ distribution requires the values A and B as function of a. For this purpose some geometrical relations are required treated in the next section.

10.6.3.4. Relations needed for the coefficients A and B

To determine A and B in (10.6-9), the angle v and its functions $\sin v$ and $\cos v$ are needed as functions of the known angles β', μ, Θ, $\beta(\beta', \Theta, \mu)$, ϑ and hence as functions of the argument a. To obtain this, consider Fig. 10.6.4.1. The relations required result from relations between infinitesimal distances in the directions of a', a, n', n. Therefore the considerations are restricted to the following infinitesimal increments u, f, s_u, s_m, n', n, a', a (Fig. 10.6.4.1). With reference to the author's paper [10.46], the relations are resumed in the sequence of their mutual linkage. They are partly obvious from Fig. 10.6.4.1

$$u = f + s_u, \quad s_u = s_m \cot \beta, \quad f = n' \tan \gamma, \quad a' = n'/\cos \varepsilon, \quad s_m = n' \tan \varepsilon,$$

$$\sin \varepsilon = -\cos(\vartheta + \mu), \quad \cos \varepsilon = \sin(\vartheta + \mu). \tag{10.6-14}$$

Hence v as function of ε and the longitudinal dihedral angle γ

$$\tan v = \tan \gamma \cos \varepsilon + \cot \beta \sin \varepsilon, \tag{10.6-15}$$

$\sin v = \tan v \ (1 + \tan^2 v)^{-1/2}$; $\cos v = (1 + \tan^2 v)^{-1/2}$. Obviously (Fig. 10.6.4.1), when $\overline{OA} = 1$:

$$s_m = \tan \varepsilon, \quad u = \overline{BO} \tan v = \tan v/\cos \varepsilon, \quad y = (\sin^2 \varepsilon + \tan^2 v)^{1/2}/\cos \varepsilon,$$

$$\overline{OC} = (1 + y^2)^{1/2} = 1/(\cos \varepsilon \cos v), \tag{10.6-16}$$

whence:

$$\cos \chi = 1/\overline{OC} = \cos \varepsilon \cos v, \quad \cos \psi = s_m/\overline{OC} = \sin \varepsilon \cos v, \tag{10.6-17}$$

where χ and ψ are the angles the line a makes with s_m and n' respectively (Fig. 10.6.4.1). Hence the unit vectors a^0, n'^0 and u^0 needed for a_n and u_n below read with respect to the tripod s_m^0, n'^0, u^0

$$a^0 = \cos v \sin \varepsilon s_m^0 + \cos v \cos \varepsilon n'^0 + \sin v u^0,$$

$$n^0 = 0 \cdot s_m^0 + \cos \gamma n'^0 + \sin \gamma u^0, \tag{10.6-18}$$

$$u^0 = 0 \cdot s_m^0 + 0 \cdot n'^0 + 1 \cdot u^0,$$
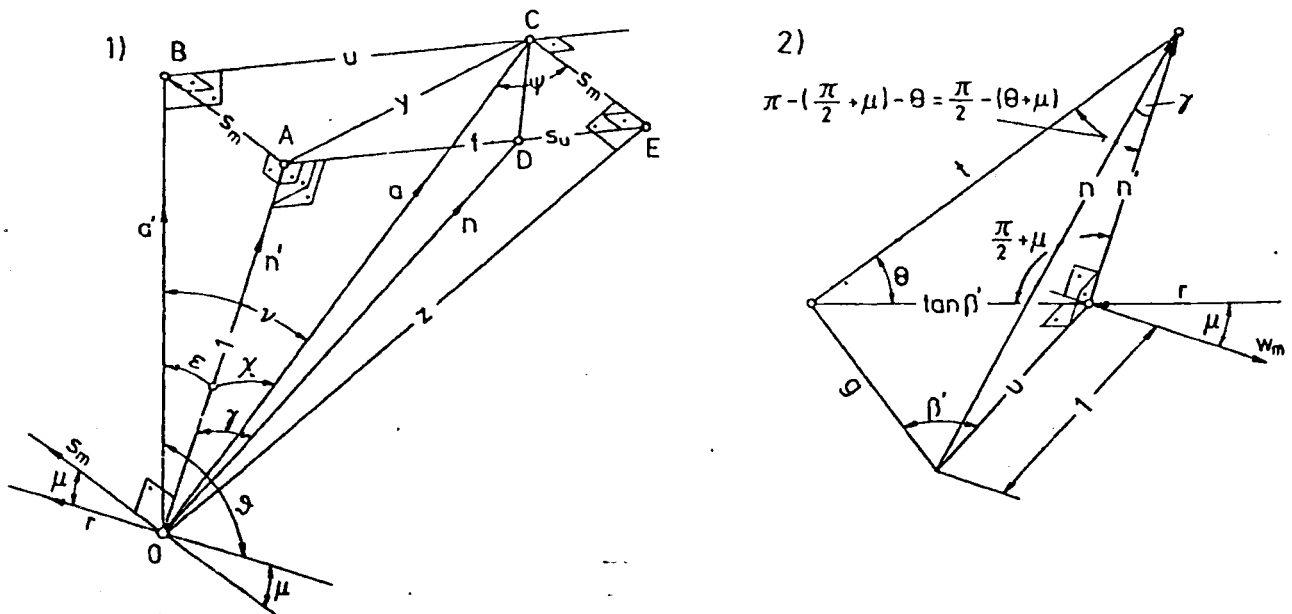
Fig. 10.6.4. Geometrical relations of the infinitesimally assumed quantities:
1) Between u, s_m, f, r, y, z, a, n, a', n', ψ, γ, χ, ε, ϑ, μ.
2) Between γ of n, φ-face with μ, Θ, β' a) $n' = \cot \gamma$. b) $n' = \tan \beta' \sin \Theta/\cos(\Theta + \mu)$.

530

whence $\partial a/\partial n$ and $\partial u/\partial n$ as scalar products

$$\partial a/\partial n = a_n = \cos(a, n) = a^0 n^0 = \cos\gamma\cos\nu\cos\varepsilon + \sin\nu\sin\gamma,$$

$$\partial u/\partial n = u_n = \cos(u, n) = u^0 n^0 = \sin\gamma, \qquad (10.6-19)$$

from Fig. 10.6.4.2 $\cot\gamma = \tan(\Theta + \mu)\tan\beta$.

10.6.4. Simplified relation for shroud to hub distribution

Equation (10.6-1) may be converted by means of the relation obvious from the velocity triangles (Fig. 10.6.3.2)

$$c_u = \omega r - w\cos\beta, \qquad (10.6-20)$$

by means of the evident relations (Fig. 10.6.3.3 and 5)

$$\partial r/\partial s_m = \cos\mu, \qquad \partial r/\partial n' = -\sin\mu, \qquad (10.6-21)$$

$$\partial s_m/\partial a = \cos\psi \Rightarrow \sin\varepsilon\cos\nu, \qquad (10.6-22)$$

$$\partial n'/\partial a = \cos\chi = \cos\varepsilon\cos\nu, \qquad (10.6-23)$$

both the last of which result from (10.6-17), and by means of the following relation, from (10.6-21) through (10.6-23) and $\varepsilon = \vartheta + \mu - \pi/2$:

$$dr/da = (\partial r/\partial s_m)\,ds_m/da + (\partial r/\partial n')\,dn'/da = -\cos\nu\cos\vartheta, \qquad (10.6-24)$$

into the following differential equation

$$\partial w = -\,[w(\tan\beta\,d\beta/da + \cos\nu\cos\vartheta/r) + 2\omega\cos\nu\cos\vartheta/\cos\beta]\,\partial a. \quad (10.6-25)$$

The structure of this equation is the same in principle as that of relation (10.6-8). But for the absence of the curvature term $w\sin^2\beta\cos\nu/R$ and the term $\partial w/\partial s$ due to convective acceleration, the last relation is much simpler than (10.6-8). This relation contains the expression $d\beta/da$. This can be related to the values $d\Theta/da,\ d\beta'/da,\ d\mu/da$ known from the geometry of the vane, as will be shown later, in a manner analogous to that applied to $d\beta/ds$ in (10.6-7). The assumed flow along the vane prohibits any derivative in the φ-direction. Hence

$$d\Theta/da = (\partial\Theta/\partial r)\,dr/da + (\partial\Theta/\partial z)\,dz/da, \qquad (10.6-26)$$

$$d\beta'/da = (\partial\beta'/\partial r)\,dr/da + (\partial\beta'/\partial z)\,dz/da, \qquad (10.6-27)$$

$$d\mu/da = (\partial\mu/\partial r)\,dr/da + (\partial\mu/\partial z)\,dz/da, \qquad (10.6-28)$$

where z is the upwardly oriented coordinate along the runner axis. The derivatives $\partial\Theta/\partial r$, $\partial\Theta/\partial z$ may be obtained from the radial vane sections in the elevation, the derivatives $\partial\beta'/\partial r$, $\partial\beta'/\partial z$ from elevation and plan of the pattern sections and the derivatives $\partial\mu/\partial r$, $\partial\mu/\partial z$ from the pattern of the meridional streamlines. The coefficients $\partial r/\partial a$ and $\partial z/\partial a$ in the last relations are evident from Figs. 10.6.3.3 and 4 as

$$dr/da = (dr/da')\,da'/da = -\cos\vartheta\cos\nu, \qquad (10.6-29)$$

$$dz/da = (dz/da')\,da'/da = \sin\vartheta\cos\nu. \qquad (10.6-30)$$

531
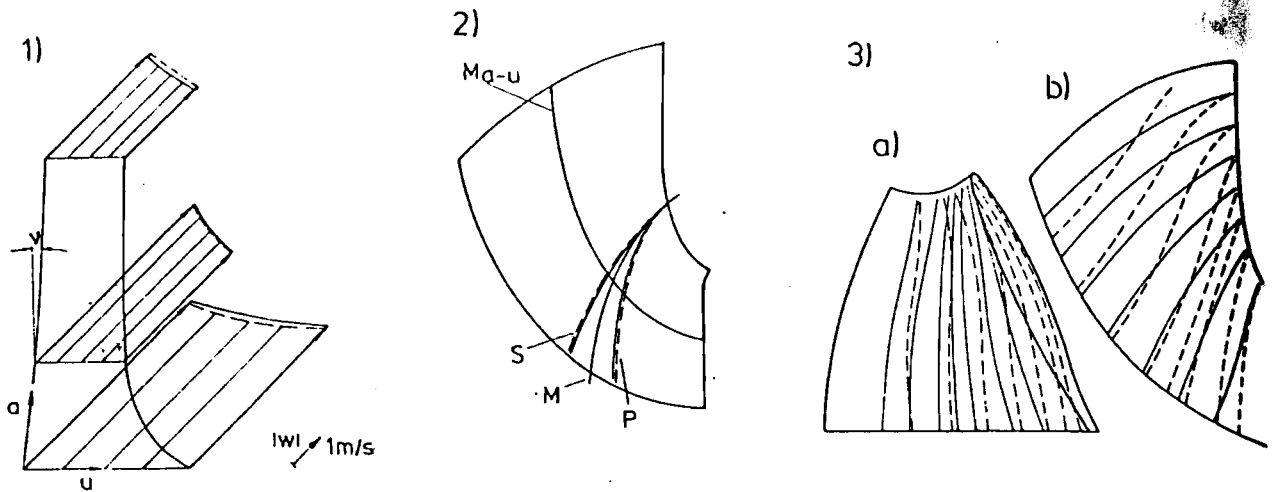
Fig. 10.6.5. 1) Computed relative velocity from the suction face S to the pressure face P, and from the shroud A to the hub J in an unrolled mean a, u-plane ($u = r\varphi$), obtained by the exact relation (10.6-8) —— and by the approximate relation (10.6-25) ——. 2) Twist of the mean stream surface, computed by (10.6-34) through the exact relation (10.6-25) —— and the approximate relation (10.6-25) ——. S suction face; P pressure face, M mean stream surface, $M_{a-u} =$ mean a, u-face. 3) Measured meridional streamlines along the outer edge of the boundary layer on the suction and the pressure face (see Fig. 10.3.22) after *Schlemmer* [5.18]. Measurements and calculations for bep of a FT with $gH = 35,8 \text{ m}^2/\text{s}^2$, $Q = 0,324 \text{ m}^3/\text{s}$, $\omega = 31,6 \text{ rad/s}$; $D = 0,455 \text{ m}$.

Fig. 10.6.5.1 shows the distribution of w in the a, φ-face for certain data Q, gH, ω, alternatively computed with the relations (10.6–25) and (10.6–8). A similar procedure was made with the twist of stream faces treated in 10.6.5. The results differ slightly.

10.6.5. The twist of the stream face in the runner channel

Schlemmer's tests in the author's lab at TU München showed that even at bep the orientation of the relative velocity in the flow near to the outer edge of the boundary layer of a runner vane hints at a twist starting from the runner entrance and causing a deviation from the axisymmetric streamface assumed, (Fig. 10.6.5.3) [10.46]. An attempt was made in the pertinent doctoral thesis [5.18] to explain the effect. As the velocity was measured outside the boundary layer, the reason for the effect seems to be the meridional component of the relative eddy (Fig. 10.6.6). This holds especially, as in this case the measured twist was in the same sense as this relative eddy component.

The consequences are now considered under the assumption, that according to the tests, the twist is small so that it may be superimposed on the axisymmetric flow as an effect of the second order. Consider an elementary parallelogram in an n', φ-face normal to the streamface. One pair of its sides is orientated in the tangential direction and the other pair parallel to the vane trace n. This makes the longitudinal dihedral angle γ with n' normal to the streamface (Fig. 10.6.6.1).

According to the assumption of an absolute irrotational flow, the meridional component of the relative eddy is $2\omega \sin\mu$ and normal to the parallelogram. It influences first the relative whirl component w_u. Also a small velocity w_n must be introduced in the direction n and normal to w. This varies in the tangential direction. *Stokes'* theorem gives

$$- \partial w_n/(r\,\partial\varphi) - \partial(w r \cos\beta)/(r\,\partial n) = 2\omega \cos\gamma \sin\mu. \qquad (10.6-31)$$

532
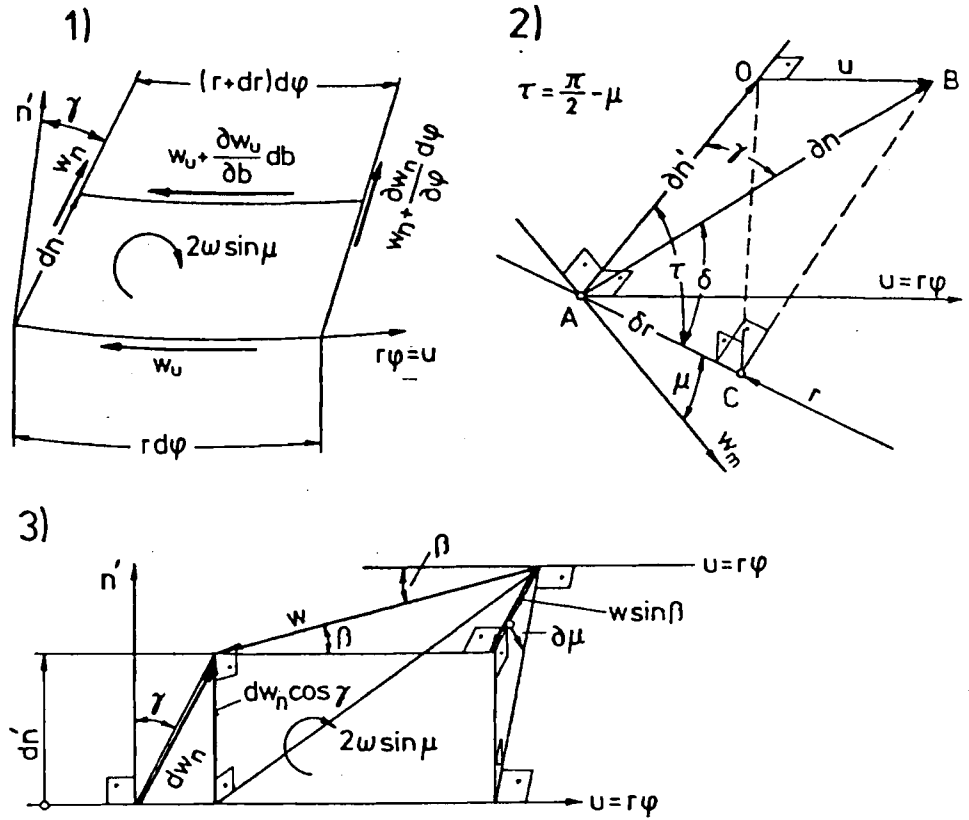
Fig. 10.6.6. Relations in context with the twist of the stream surface. 1) Quasi parallelogram in a n', φ-plane with the meridional component of the relative eddy $2\omega\sin\mu$. 2) Derivation of $\partial r/\partial n$: $\overline{AC} = \cos\delta$, $\overline{OA} = \cos\gamma$, $\overline{AC} = \overline{OA}\sin\mu$, hence $\cos\varepsilon = \cos\delta\sin\mu$, and $\partial r/\partial n = -\cos\delta = -\cos\gamma\sin\mu$. 3) to the relation between dw_n, w and $\partial\mu$ (increment of twist in tangential direction).

The derivative of the second term gives the terms $\partial\beta/\partial n$, $\partial w/\partial n$ and $\partial r/\partial n$. Obviously (Fig. 10.6.6.2) $\partial r/\partial n = -\cos\gamma\sin\mu$. In the following attention is focussed on the phenomena in the a, φ-face. Hence the derivatives $\partial w/\partial n$ and $\partial\beta/\partial n$ have to be referred to the tilted coordinates a and $r\varphi$. Thus

$$\partial w/\partial n = (\partial w/\partial a)\,\partial a/\partial n + (\partial w/r\,\partial\varphi)\,\partial u/\partial n = (\partial w/\partial a)\,a_n + (\partial w/r\,\partial\varphi)\,u_n,$$

$$\partial\beta/\partial n = (\partial\beta/\partial a)\,\partial a/\partial n + (\partial\beta/r\,\partial\varphi)\,\partial u/\partial n = (\partial\beta/\partial a)\,a_n + (\partial\beta/r\,\partial\varphi)\,u_n.$$

$$(10.6-32)$$

The expressions $a_n = \partial a/\partial n$ and $u_n = \partial u/\partial n$ in these relations follow from (10.6-19). As seen in Fig. 10.6.6.3 the increment of dw_n can be related to the increment of the angle $d\mu$. Hence

$$dw_n\cos\gamma = w\sin\beta\,d\mu.$$

$$(10.6-33)$$

Using the relations (10.6-32), (10.6-33) it follows from (10.6-31)

$$\partial w/\partial a + (\partial w/r\,\partial\varphi)\,u_n/a_n - w\{\tan\beta[1/(a_n\cos\gamma)]\,\partial\mu/(r\,\partial\varphi) + \partial\beta/\partial a$$

$$+ (u_n/a_n)\,\partial\beta/(r\,\partial\varphi) + \cos\gamma\sin\mu/(a_n r)\} = -2\omega\cos\gamma\sin\mu/(a_n\cos\beta).$$

$$(10.6-34)$$

After (10.6-8) or (10.6-25) the term $\partial w/\partial a$ can be expressed in terms of w, $\partial w/\partial s$ (known from iteration), ω, R, r, v, ϑ, μ, β, $\partial\beta/\partial s$ and $\partial e/\partial a$. After (10.6-5) the term $\partial w/(r\,\partial\varphi)$ in the

last relation can be related to w, β, R_f or according to (10.6–6) to β, r, μ, $\partial\beta/\partial s$ by (10.6–7). Hence with the assumption $\partial\beta/(r\,\partial\varphi) = 0$, (10.6–34) is a differential equation for the computation of the twist $\partial\mu/(r\,\partial\varphi)$ of the stream face.

From Fig. 10.6.5.3a it is seen that at bep according to measurements $\Delta\mu \sim 10°$. After writing down (10.6–33) for $\beta = 30°$ and $\gamma = 20°$, the quotient $\Delta w_n/w$ becomes ~ 0.1. For a simple check of this result assume the channel section in the a, φ-face to be a narrow parallelogram. Here the eddy $2\omega \sin\mu$ produces mainly a velocity along the long side. By definition of curl (Cap. 5.2) with $\omega r = w/\lambda$ nearly: $\Delta w_n/w = 4\pi\Phi \cos\gamma \sin\mu/(z\lambda)$. For $z = 15$ vanes; $\Phi = 0.7$; $\lambda = 1.5$; $\gamma = 20°$: $\Delta w_n/w = 0.12$ in fair agreement with the above.

Measurements of the relative and partially the absolute flow field also in a Francis turbine were carried out by *Bär* [5.17] and *Schlemmer* [5.18] by means of time-averaging instruments. Dynamic measurements of relative and partly absolute flow in a Francis turbine were carried out by *Furtner* [9.141], *Mollenkopf* [9.46], and *Gerich* [9.133].

10.6.6. The state of knowledge in predicting the relative flow

Experimental and numerical investigations of the behaviour of a reversible pump-turbine runner at design point and off design point were carried out by *Ventrone, Mirandola* and *Navarro* [10.178].

Carnevale et al. [10.179] made a theoretical and experimental analysis, *Korcian* [6.44] an experimental investigation on a semi-axial pump, whose flow pattern may be approximately equated to that in a Francis pump-turbine in pumping mode.

A theoretical approach of quasi-three-dimensional flow in a semi-axial machine was presented by *Eremeef* and *Philibert* [10.180]. A further theoretical approach of ideal steady relative flow in Francis turbines was treated by *Voetter* [10.181]. A critical comparison between $2d$ and $3d$ calculations, and corresponding non-dynamical, and time-averaged dynamic measurements of the relative flow in a certain FT was presented by *Pfoertner* [6.22], and his conclusions were in favour of $2d$ methods.

Another impulse to calculate the steady three dimensional ($= 3d$) ideal flow in stationary or rotating ducts came from *Wu* [10.182]. He uses the obvious fact, that any streamline can be considered as the intersection of two types of flow planes, represented by the streamfunctions Ψ_1 and Ψ_2, from which, e.g. Ψ_1 may be adaptable to the runner blade faces and Ψ_2 to the faces of shroud and hub. Thus

$$w = \operatorname{grad}\Psi_1 \times \operatorname{grad}\Psi_2. \qquad (10.6\text{--}35)$$

This vectorial equation is identical with three scalar equations. They read, in the case of cylindrical coordinates z, r, φ as

$$w_r = \frac{\partial\Psi_1}{r\,\partial\varphi}\frac{\partial\Psi_2}{\partial z} - \frac{\partial\Psi_1}{\partial z}\frac{\partial\Psi_2}{r\,\partial\varphi}, \qquad w_u = \frac{\partial\Psi_1}{\partial z}\frac{\partial\Psi_2}{\partial r} - \frac{\partial\Psi_1}{\partial r}\frac{\partial\Psi_2}{\partial z},$$

$$w_z = \frac{\partial\Psi_1}{\partial r}\frac{\partial\Psi_2}{r\,\partial\varphi} - \frac{\partial\Psi_1}{r\,\partial\varphi}\frac{\partial\Psi_2}{\partial r}. \qquad (10.6\text{--}36)$$

Putting these components of relative velocity into the equations of motion for the rotating frame of reference yields three quadratic differential equations for the unknown stream functions Ψ_1, Ψ_2. In the case of an irrotational absolute flow, the equation of

motion simplifies to curl $w = -2\omega$. The axial component of this vectorial equation reads

$$\partial w_u/\partial r + w_u/r - \partial w_r/(r\partial\varphi) = -2\omega. \tag{10.6-37}$$

Inserting w_r and w_u from (10.6–36) gives the following quadratic partial differential equation for the stream functions Ψ_1 and Ψ_2:

$$\frac{1}{r}\frac{\partial\Psi_1}{\partial z}\frac{\partial\Psi_2}{\partial r} - \frac{1}{r}\frac{\partial\Psi_1}{\partial r}\frac{\partial\Psi_2}{\partial z} + \frac{\partial^2\Psi_1}{\partial r\partial z}\frac{\partial\Psi_2}{\partial r} + \frac{\partial\Psi_1}{\partial z}\frac{\partial^2\Psi_2}{\partial r^2} - \frac{\partial^2\Psi_1}{\partial r^2}\frac{\partial\Psi_2}{\partial z} - \frac{\partial\Psi_1}{\partial r}\frac{\partial^2\Psi_2}{\partial r\partial z}$$

$$- \frac{\partial^2\Psi_1}{r^2\partial\varphi^2}\frac{\partial\Psi_2}{\partial z} - \frac{\partial\Psi_1}{r\partial\varphi}\frac{\partial^2\Psi_2}{r\partial\varphi\partial z} + \frac{\partial^2\Psi_1}{r\partial\varphi\partial z}\frac{\partial\Psi_2}{r\partial\varphi} + \frac{\partial\Psi_1}{\partial z}\frac{\partial^2\Psi_2}{r^2\partial\varphi^2} = -2\omega. \tag{10.6-38}$$

The other components of curl $w = -2\omega$ yield similar relations for the stream functions. They facilitate the elimination of one stream function so as to have ultimately one partial differential equation for one of the stream functions Ψ_1 and Ψ_2.

The development of improved computer hardware stimulated the creation of corresponding computer programs. The progress in numerical turbomachinery analysis was shown in a review by *Japikse* [10.183]. It can be considered as a prerequisite of a computer-aided blading of hydroturbomachinery, a trend of the future.

Starting from *Wu*, *Bosman* et al. demonstrate the feasibility of obtaining flow details through turbomachine blade passages by working iteratively with existing two-dimensional computer programs, which solve alternately blade to blade and shroud to hub streamsheets [10.184].

Novak et al. [10.185] present a system, which is also modeled after the work of *Wu*, and which comprises two coordinated computer programs, one providing solutions on axisymmetric blade-to-blade surfaces and the second on streamsheets roughly parallel to the blades.

In this context, the method of *Adler* and *Krimerman* has to be mentioned [10.186]. They used a finite element method, to solve modified *Wu* equations. The method allows for non-axisymmetric blade-to-blade surfaces and uses iteratively the results known from the families of face-to-face and hub-to-shroud calculations.

All known streamsurface methods suffer from the constraint, that the surfaces cannot pass across the edges of the blade passage and that the blade-to-blade surfaces which are split at the inlet edge shall meet in corresponding points at the outlet. After *Bosman* [10.187] the stream surface techniques become totally inadequate when applied to centrifugal impellers and radial turbines, where deviations of the blade-to-blade surfaces from surfaces of revolution are large enough to make the distinction between the families of blade-to-blade and shroud-to-hub faces impossible.

Since according to [10.187] there seems to be no easy way to overcome the limitations, the usefulness of streamsurface methods for the prediction of real flow effects in turbomachines is questionable.

In the last few years another strong trend has been towards fully 3 dimensional methods, which solve the fluid dynamic equations with respect to velocity and pressure.

As an example for recent finite element methods the procedure proposed by *H. Pfoertner* [10.188] may be mentioned. He solves the equations of motion (Cap. 5.3) and continuity (see 5.2) for an incompressible 3-dimensional flow. The computational domain used (see Fig. 10.6.7) consists here of one blade passage with its adjacent regions upstream and downstream of the rotor channel.

This domain is automatically divided into tetrahedron elements by two steps (see Fig. 10.6.7).

1) Preliminary division into bricks with 8 nodes given by the 3 families of bladewise, streamwise and pitchwise oriented surfaces.
2) Subdivision of the bricks into 5 or 6 tetrahedra, so as to obtain elements which are as near as possible to regular tetrahedra.
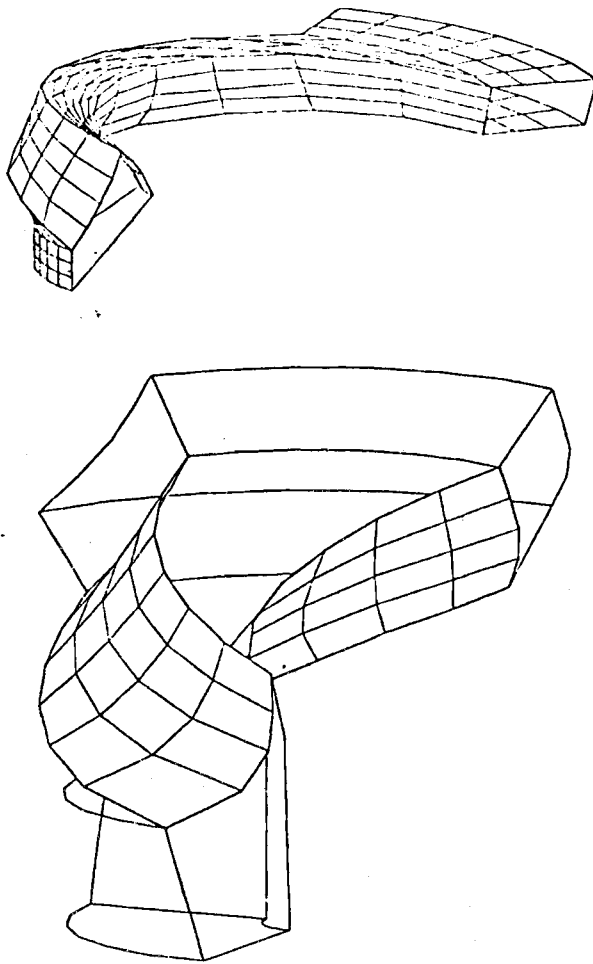
Fig. 10.6.7. Computational domain for 3-dimensional finite element calculations of relative flow in pump rotors after *Pförtner* [10.188].

Inserting a reasonable initial state in the momentum equation and continuity yields residuals in each tetrahedron. Integrating the weighted residuals of the element's volume and summing up all the elements gives a resulting residual. A procedure follows which makes the latter as small as possible. Thus the continuity and momentum equation are best satisfied.

The minimization is effected by a so-called conjugate gradient algorithm. Together with a gradient projecting technique, the latter is used to satisfy the boundary condition [10.188]. These projection techniques allow the formulation of linear relations between all the nodal variables as, e.g. all the velocity components in a peripheral oriented surface. This procedure can be used to satisfy additional side conditions such as a satisfaction of continuity over the whole passage or a useful condition for the outlet plane. Hence it is possible to prescribe a desired attenuation of any pitch-periodic non-uniformity on the distribution of the velocity components downstream of the rotor.

This method of *Pfoertner* has been successfully applied to a variety of geometric configurations such as radial and semi-axial pump impellers, Francis turbine runners, conical guide vanes for bulb turbines etc.

Ribaut [10.189] treats the three dimensional divergent and rotational flow in turbomachines. Using potential theory a quasi three dimensional method is developed, which yields high numerical accuracy. The method includes the influence of the casing and blade boundary layers on the cascade circulation. The use of two vortex sheets, representing the boundary surface, allows the calculation of stalled flows and secondary vorticity. The velocities of computed divergent flow agree fairly well with the measurements.

A careful analysis of the meridional component of relative eddy in mixed flow machines was given by *R. Lewis* and *G. Fairbairn* [10.190].

10.7. Computer aided design of hydroturbines

10.7.1. Introduction

Computer aided design (CAD) is utilized by industry to modernize the design process. The drawing board is replaced by a video display unit. Simultaneously rules are drawn up for designing a hydroturbomachine. In this manner the design is made more repeatable.

10.7.2. General goals

The immediate aim is to reduce costs by increasing the designer's productivity. Nearly as important is the reduction of the design period. The designer can examine numerous permutations of the design on the screen. This coupled with the computer's ability to quickly execute complex calculations permits an improvement of a typical design's quality.

The user no longer is forced to carry out monotonous tasks, such as dimensioning and hatching. Thus the quality of the workplace can be bettered.

Some CAD programs can produce (eliminating the conventional drawing) a punched tape for the numerical control of machine tools. Ultimately, they could lead to the automated factory.

10.7.3. Hardware for a CAD system

The object which is to be designed is represented on a screen instead of on paper. As the screen is smaller than most paper formats, the user can usually define a window and move and magnify it. Suitable terminals are manufactured in numerous different varieties and sizes, with and without colour [10.191].

Commands are keyed in using a typewriter keyboard. Graphic information (i.e., the drawing) is usually entered with a light-pen or graphics tablets. Sometimes a workstation is equipped with a printer to produce lists.

To reduce costs and to enable the exchange of information, several stations are served by a single computer. Most systems have their own minicomputer and are not connected to a firm's main-frame computer. Experience has shown that in the latter case response times are excessive. In the near future low cost microcomputers should be utilized, as their power is starting to rival that of the minis.

The computer requires at least one relatively fast mass memory device to permanently store data (i.e. drawings). Disk storage units are mainly used. A slower, but more reliable storage medium should be used to safeguard the data, tape units are popular for this application.

Drawings are made on paper by a plotter, which can operate on a mechanical or electrostatic basis.

10.7.4. Software for the CAD system

Without programs every computer is useless. Software can be divided into three major categories: system software, applications software written by outside suppliers and application software written by the user.

Systems software usually is written by the computer manufacturer and enables the machine to perform tasks on a very basic level, i.e., input and display data. Applications software permits the machine to perform complex tasks, which are immediately useful.

In the CAD field applications software written by outsiders usually can be classified as so-called drafting systems. These enable the designer to draw general mechanical designs. It is not important

537

if a bearing or a hydropower plant is being designed. Some software suppliers combine hardware and software to make a turnkey CAD system.

Obviously the user buys the software he needs when it is readily available, as the purchase price is below the cost of writing the programs. On the other hand, software suitable for narrow fields (e.g. hydroturbines) simply is not available. The user will usually combine commercially available drafting software with specialized software of his own. Ref. [10.192] offers suggestions on obtaining further information on CAD hardware and software.

10.7.5. Profile of a commercial computer aided design program for Francis turbines

For several years the Voith company has been developing the Franzl system of programs. The stated goal was to automate the most often repeated parts of the mechanical design. Franzl should not be confused with CAD-programs that serve solely as drafting sy:.:ms. The Voith system combines calculation, selection and drafting procedures. Thus Voith officials prefer calling the program a computer design system.

Franzl is utilized as a tool in the proposal and preliminary design stages of a project. These stages are often repeated and are relatively expensive and time consuming. Using a design handbook the program attempts to offer a solution based upon one of 40 model turbines. The number and scope of the model turbines are continually increasing.

Typically the program asks the user to key in major parameters, e.g., guide vane pitch diameter, specific speed and so on. Five modules successively treat the hydraulic outline, the shaft and coupling flange, the runner, the stay rings and the turbine covers.

The program then prints the input data and calculated parameters such as physical dimensions, stresses, weights, pressures, bearing forces, resonance frequencies etc. If satisfied, the designer may have a section drawn on a graphics screen. The section can also be drawn by a plotter.

The end result is a basic hydraulic outline, which the designer uses as a starting point for further design work. In this manner the problem of the blank sheet is avoided.

If dissatisfied with the output, the designer can actively intervene and change parameters in the various modules. Several program modules are either existent or in planning stages to use the data produced by Franzl. These include draft tube design, automatic cost calculation and an interface to a pure drafting system. Thus a Francis turbine could be designed from start to finish on a computer. The Franzl system is described in further detail in [10.36].

Matsuda and Nagafuji [10.139] describe the use of an automatic design program, developed in Japan in conjunction with a numerical control machining process which allows for a fast and economic manufacture of rotor models. This enables the design and performance development of turbines and pump-turbines to be carried out within a short period with little manual work. In this program a rotor is automatically designed by putting in all the necessary design parameters. It is also possible to check the effect of any of the input data on the performance characteristics by changing selected elements and comparing the experimental results of the rotor with the standard ones.

The output of this design provides full information of the rotor blade surface coordinates. A program has been developed for automatic generation of the data required for a numerically controlled machining of a model rotor. To represent in detail the three-dimensional shape of the rotor, the drawings are plotted in radial and pattern making sections.

There are two methods of making a model runner. The one is maching the blades from a solid disk. The other is finishing the runner from a piece which has been cast to form the rough blade shape.

538

The total system of n.c. machining, according to [10.139] is implemented on 3 levels. On level 1, both front and back surfaces of the blade are divided into a fine mesh and the coordinate values on the mesh are typed out on a list or punched out on the cards and also are plotted out on cards for checking whenever required. Level 2 consists of a n.c. system developed for machining the runner on a milling machine with 5 degrees of freedom. It requires a complicated part programming. It is provided with a library in which a number of routines corresponding to the various shapes of work-pieces are prepared. The cards, lists and plots are turned out by this system and they are used to check in advance the interference between tool and work-piece which are likely to occur during cutting. All the data from level 2 are processed in level 3 and converted to the sequential instructions of the n.c. machine. The control tape finally obtained on level 3 is fed into the machining control unit and the n.c. process is carried out.

10.7.6. Conclusions

Because of the high cost of program development and hardware engineering managers should carefully weigh the advantages of a computer aided design system. Perhaps instead of introducing a complete system, which treats all stages of the design, a partial automation would be more suitable. Only those stages that are often repeated, and contain many monotonous tasks or those that could stand the introduction of complex calculations would be computerized.

On the other hand in times of increasing competition, there may be no choice left. The ability to produce designs quickly of the highest quality may become a major advantage.

11. Regulation of hydro power sets, the generator

11.1. Introduction

The constant speed requirement of the usual hydro turbo set supplying an AC grid by means of a synchronous generator (the alternator) needs speed regulation, sometimes in connection with load distribution and load regulation. On the one hand the control loop used for this purpose includes the governor with a device for metering the speed deviation and sometimes also for metering the acceleration, and its servomotor for the load adjustment of the turbine.

On the other hand, the control loop includes also the plant or the controlled system. This consists of the hydro turbo set with the turbine and the alternator, its piping and the electric grid connected with it.

The different mechanical, hydraulic and electronic designs for metering the deviation of speed and their features merit some considerations. The rather large controlling forces of gates and runner vanes require oil-operated servomotors. Their valves are actuated from the speedometer via relays by sleeve valves with their special linkage including feedback, and interlinking devices for different control loops at double regulated machines.

The governor needs devices to adjust the speed droop as a characteristic of the set, to limit the gate opening, to set the damping of possible oscillations in the control loop, and to synchronize the set.

In this context the conditions for dynamic stability of the control loop have to be considered. They include the inertia of the set mainly due to its alternator and the characteristics due to certain loads of the supplied grid. Also the characteristics of the turbine and of the pipe system with respect to water hammer and its boundary conditions have to be accounted for.

For a proper operation, the individual time constants for start up and shut down of the structural members of the plant such as penstock and set, have to be tuned to each other, and also with respect to limit overspeed by fly-wheel effect.

The references [11.1 to 11.5] give a material survey of control due to hydro power, [11.6] brings a historical survey. The control of hydro power plants in general is treated in [11.7; 11.8], its stabilizing problems in [11.9 to 11, 13]. A classification of the governors is made in [11.14], the load control, also with electronic devices, in [11.15 to 11.19], the related power swing in [11.20].

Water level control is treated in [11.21; 11.22], self regulation in [11.23], the control of speed and voltage in [11.24]. The dynamic behaviour of the controlled system is generally investigated in [11.25], by means of frequency response curves in [11.26; 11.27], by stochastic signals in [11.28]. The natural frequencies of the controlled system are considered in [11.29; 11.30], with respect to the boundary conditions of penstocks in [11.31; 11.32], and with respect to rock-bored penstocks in [11.33].

540

Governing under transient load is reported in [11.34], the relevant damping factors are introduced in [11.35], non-linear solutions in [11.36], the simulation of a hydro power system in [11.37]. Governors for small plants are described in [11.38], optimization of control by electronic governing is considered in [11.39], electric equipment of the turbine governor in [11.40], motor and generator of the speedometer in [11.41], control by means of positive displacement pumps in [11.42], electro hydraulic governors in [11.43], an electronic governor head in [11.44], a computerized governor control in [11.45], use of micro computers in [11.46], use of module techniques in [11.47] and that of microprocessors in [11.48].

The locking spring is introduced as a safety device in [11.49], recording instruments are presented in [11.50], the determination of the runner vane/gate vane interrelation in [11.51], the emergency closing device in [11.52], a runaway speed limiter for Kaplan turbines in [11.53], the regulating work in [11.54], the prediction of fly-wheel mass in [11.55], the optimization of Pelton turbine governors in [11.56], the water column effect in speed control in [11.57], the safe control of a by-pass outlet in [11.58], and the starting up of a set in [11.59].

In the field of control the technical terms in the follow text following mainly from the English equivalents of the German Standards for automatic speed control technology DIN 19229 DK 621-53. Traditional denotations of some terms (if any at all) are occasionally added in brackets for the orientation of the "old fellows".

The following text has been kindly revised by my colleague Professor Dr. *H. Schmidt* with respect to the proper use of control conceptions.

The common treatment of regulation and generator in one chapter was made to keep consecutive chapters in balance with respect to their length.

One joint fact between both members is the need for frequency control, when the generator feeds an *AC* grid as usual, another can be seen in the circumstance that, at excitation unaltered, the alternator output increases linearly with frequency, and thus may change by regulation.

Usually the electric machine of the set is a generator of AC, an alternator. In pumped storage and tidal power plants with special pumping, the alternator is also used as motor. The alternator requires a special consideration. Contrary to the turbo generators of thermal sets, its number of pole pairs has to be adapted to the relatively small and widely varying head.

This requires a salient pole design instead of the usual drum rotor, standardized for the usual thermal turbo set.

Moreover the construction of the electric machine has to match the strongly varying features of the hydraulic set, e.g., withstanding runaway, forming a structural unit together with turbine and generator especially in the case of a rim generator shrunk onto the runner, and a critical operation with respect to shaft vibration. Thus the design of shaft and adjacent bearings is concentrated on the effort to shift the lowest critical speed to a margin above runaway.

At higher heads, the relative heavy electric rotor poses problems of low critical speed and sufficient cooling.

In pumped storage plants and tidal power plants with double effect, and equipped with a pump-turbine, the generator, then also used as motor, has to reverse its rotation between the different modes of operation. Pole changing between pumping and turbining, starting up the filled or emptied machine into pumping either by synchronous operation (back-to-back connections of neighbouring sets or thyristor-controlled frequency), asynchronous operation, or by a pony motor, pose problems of fatigue and heating in the conductor.

Concerning the references on the set's electric machine, a survey is presented in [11.60; 11.61]. Recent large designs of Brazilian plants are treated in [11.62], and large salient pole machines in [11.63]. Individual constructions of alternators and generators are considered in [11.64 to 11.66], induction generators in [11.67], motor generators of pumped storage plants in [11.68 to 11.70], stochastic loads on the rotor in [11.71], resonance of torsion and bending vibrations in [11.72], current-induced forces in [11.73], and resulting stresses in [11.74].

Cooling is treated in [11.75; 11.76], different exciting systems in [11.77; 11.78], the insulation problem in [11.79], the uprating of old machines in [11.80], recent Japanese technology in [11.81], and recent West German technology in [11.82].

The following text has been kindly revised with respect to the proper use of electric conceptions by Mr. K. V. Willy, deputy director at Siemens Erlangen, West Germany.

11.2. Regulation of hydro power sets, governors, accessories

11.2.1. The governor, its purposes, its design

11.2.1.1. Survey of control, different kinds, why speed control

In water power plants the alternator output usually has to be adapted to the power demand of the grid. For this purpose the output or such other values, which depend on it, e.g., the speed, have to be measured continuously and to be adjusted to the demand. The direct measurement of output exists in load control, which is usually combined with speed control (Fig. 11.2.1 a) [11.16; 11.17; 11.19].
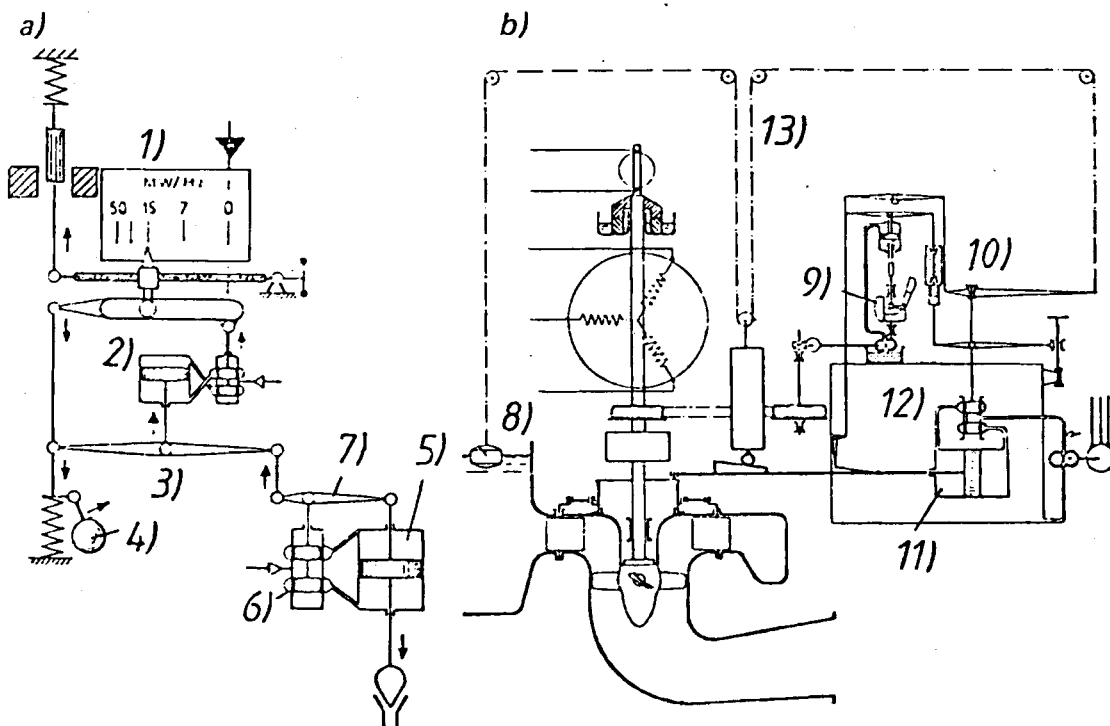
Fig. 11.2.1. Speed control in connection with that of other quantities. a) Combined power and speed control 1 Wattmeter; 2 pilot servomotor; 3 combination lever; 4 speedometer; 5 main servomotor; 7 feedback. b) Combined speed and head control. 8 float on the head water pond; 9 speedometer; 10 combination lever; 11 servomotor; 12 valve; 13 feedback.

The load control by speed is possible since both the values are assigned to each other by the proportional band necessary for load distribution of individual plants and sets.

Speed control is also useful for the checking of voltage and proper operation of a multitude of machines supplied from the grid the set is connected with. The stability of frequency in the usual AC grid supports the control of load factor by reactance. In favour of the speed control, the fact exists that even the isolated set, disconnected from the electric grid, e.g., by short circuit, may be controlled preliminarily by its speed rise, [11.3; 11.4].

In smaller sets ($P < 20$ MW) connected with an AC grid an increasing tendency exists, to omit the speed control. There in the case of emergency, e.g. short circuit, an overspeed limiter has to shut down the set after disconnection from the grid. During normal operation of such sets its speed is retained by the electromagnetic forces between alternator rotor and the rotating magnetic field of the stator and the rotor damper winding.

In rare cases of smaller plants in remote areas, fed from reservoirs with varying headwater level, also the head may control the flow (Fig. 11.2.1 b) by follower control [11.22].

11.2.1.2. Control loop, governor, controlled system

The speed control is effected by a closed control loop, in which a governor is connected in series with the controlled system. This consists of the turbine, its water ways, the generator and its electric grid. The latter is subjected to disturbances by continously varying demand of load.

The input of the governor is the speed of the set, its output the position of a servomotor for the adjustment of a turbine's distributor (gate, needle valve, jet deflector). The governor consists of a speed measuring device, that actuates a sleeve valve (Fig. 11.2.2 a), which in turn controls the oil flow for the servomotor, that adjusts the opening of the turbine.

In the case of a proportional (speed) governor the deviation of actual speed from a rated value is measured by a tachometer, which thereby operates the sleeve valve via amplifiers. In the case of a proportional-integral governor with acceleration feedback (acceleration governor), an accelerometer simultaneously measures the derivative of speed, which then together with the speed deviation actuates the sleeve valve (Fig. 11.2.2 b).

The load vs speed characteristic of the governor and its set is represented by the proportional band (permanent speed droop). It is realized by certain devices in the feedback linkage of servomotor (see Cap. 11.2.1.4). Moreover the governor contains also devices for speed adjustment and synchronization of the set, for limiting the load and for stabilizing governor oscillations (dash pot, accelerometer).

The steady state gain as the output/input ratio of the governor at steady state is expressed now by the ratio of servomotor opening to speed deviation. In the usual case of a large AC grid with nearly constant frequency this ratio tends to become rather large. Only when the set supplies a grid by itself or during synchronization, the steady state gain is smaller.

11.2.1.3. Working together of turbine and grid, self control

Under settled speed the equilibrium on the shaft of a set requires that the torque of the turbine is balanced by the grid-conditioned torque of the generator. Hence the settled speed of a set adapts itself to the point A at which the torque vs speed characteristic of the turbine intersects the corresponding grid-conditioned torque vs speed characteristic of the generator (Fig. 11.2.3), provided this point of intersection is dynamically stable.
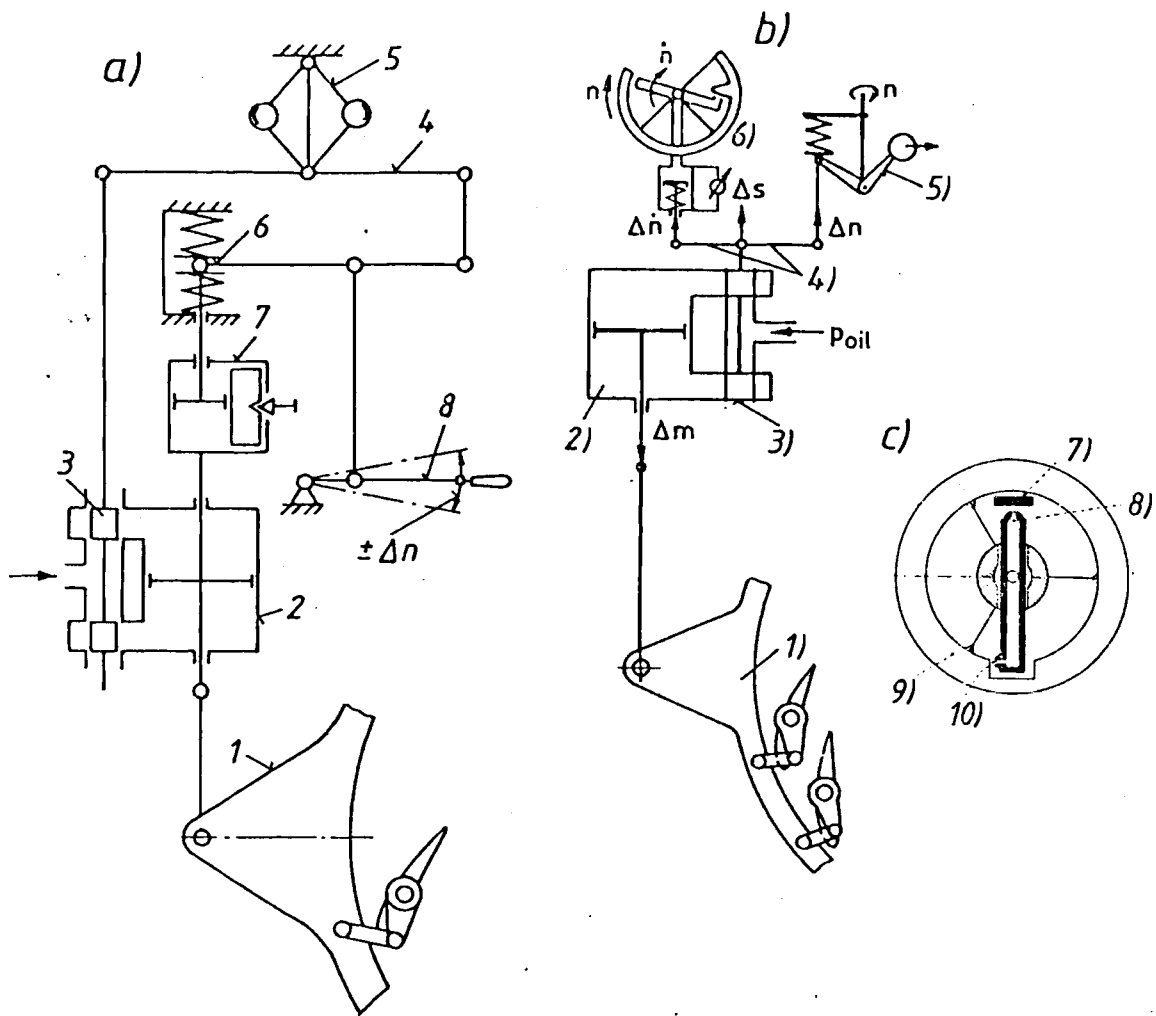
Fig. 11.2.2. Schematic diagrams of a speed governor on mechanical basis: a) Proportional integral governor with elastic feed back. 1 gate regulating ring; 2 servomotor; 3 sleeve valve; 4 combination lever; 5 speedometer (tachometer); 6 isostatic device (springs that return the point 6 of the dash pot piston always to the same station); 7 dash pot with adjustable throttle in short circuit; 8 speed-adjustment for the rated speed. b) Proportional integral governor with an acceleration feedback: 1 gate regulating ring; 2 servomotor; 3 sleeve valve; 4 combination lever; 5 speedometer (tacho-meter); 6 accelerometer (detail see c)). c) Combined hydraulic tachometer and accelerometer (Design Vevey-Charmilles Engineering Works): 7 spring-suspended fly-weight with a baffle plate; 8 speed metering nozzle; 9 flywheel with a baffle plate; 10 acceleration-metering nozzle.
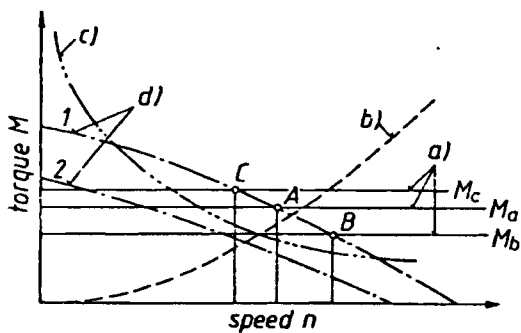
Fig. 11.2.3. Speed self control of a set with generator supplying a grid by itself under various kinds of load torque vs speed: a load by machine tools; change of the load from the torque M_a to M_b or M_c shifts the point of stable operation from A to B or C. b load by turbomachines (blowers, compressors, impeller pumps); c pure resistor load (electric bulbs, electric heating, electrolytic cells); d turbine torque vs speed under different openings 1 and 2.

From 9.2 it is known that the torque vs speed characteristic of a turbine decreases always vs the speed.

In contrast, the slope of the generator torque characteristic depends on the grid load, whereas the turbine characteristic can be changed (by means of the gate position). The generator characteristic results from the accidental grid load. This causes the main disturbance to the control loop considered.

Assuming the intersection point of both the characteristics to be stable and neglecting inertia effects, the momentary speed of a set would result from the accidental position of the intersection point of both characteristics. Now the essential task of the speed governor of a leading plant is to have a settled speed at the intersection point that is assigned to the load according to the proportional band (permanent speed droop) of the set, i.e., adapting the gate position to the randomly varying grid load.

Fig. 11.2.3 shows typical curves of grid-load-induced generator torque vs speed. Curve a) is due to machine tools, curve b) is due to pumps and blowers, curve c) is due to resistor load (bulbs, electrolytic cells etc.). This figure reveals also the so-called automatic regulation or self control of the grid by a change of load, M_a to M_c or M_b, that results ultimately in a new stable operation point C or B. This is characterized by a slope of the load torque vs speed that drops steeper than that of the turbine torque vs speed [11.23].

Contrary to this automatic regulation of a load due to machine tools or pumps and blowers, a load due to resistors usually has no self control (automatic control). At any rate the set requires the assistance of a speed governor for not obtaining indefinitely increasing or decreasing speed in case of disturbances.

11.2.1.4. The tasks of speed control

I. Frequency control: This holds especially when the alternator supplies a grid by itself and has a set proportional band $\delta_P = (n_{max} - n_{min})/n_M$ (permanent speed droop). In this n_{max}, n_{min}, n_M are the maximum, minimum and mean speed, or grid frequency in the working scope of the set. By the proportional band a speed is assigned to a certain load so as to have full load at minimum speed n_{min} and zero load at maximum speed n_{max}.

According to Fig. 11.2.4a, in consequence of a certain proportional band δ_P of the individual sets, a certain frequency change Δn effects different changes ΔP_1, ΔP_2 to the output of these sets 1 and 2. Together with the speed adjustment (III) a non-vanishing proportional band enables also synchronization of an isolated set. By virtue of the then existing slope of the set's load vs speed characteristic it is possible to effect a translation of the latter by actuating the speed adjustment device such as to shift the point of zero load from zero speed with the set at rest to synchronous speed needed for synchronization, [11.2], Fig. 11.2.4b.

In a large AC grid the frequency varies only within a rather small band of up to 1 or 2%. For base load plants δ_P is rather large, namely 0,04 ... 0,05. This guarantees a rather constant output when the frequency varies within a certain band.

Contrary to this in a peak load plant $\delta_P = 0,01 \ldots 0,02$. This facilitates a rather sensibile variation of output in the case of a modest frequency change. In other words this low δ_P enables the control of frequency especially by a powerful peak load plant 3. The frequency load coordination by the proportional band is also important for a certain load distribution in the plants of a certain grid (Fig. 11.2.4c).

A certain δ_P may be effected mechanically or electromechanically. The first by a cam which, in the steady state position of the sleeve valve, assigns a certain servomotor
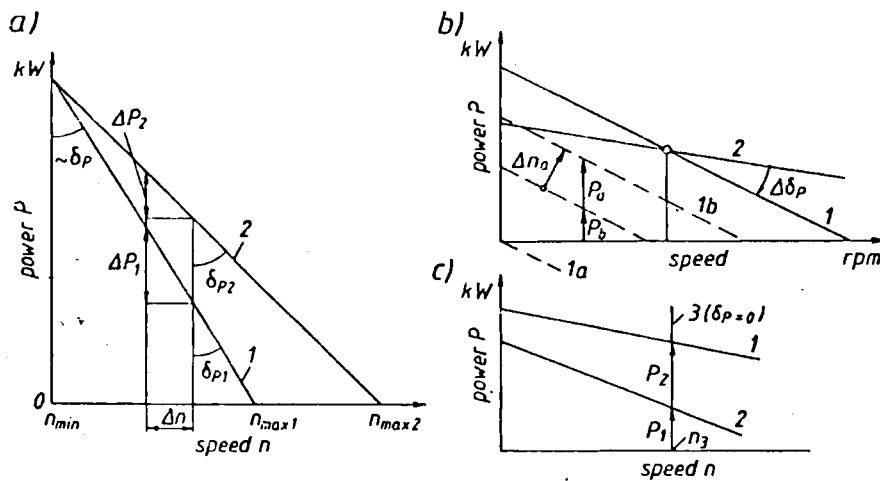
Fig. 11.2.4. Proportional band (permanent speed droop) δ_P, its ends and variations: a) δ_P inverse gradient of P vs n, set 1 with a small δ_{P1} for peak load, high load change ΔP_1 under a certain Δn. Set 2 with a large δ_{P2} for base load, smaller load change ΔP_2 under the same Δn. b) Change of P vs n: 1 by translation of the characteristic parallel to itself, retaining δ_P, by actuating the speed adjusting device, 1a start up a set to synchronization, when disconnected from the grid, 1 b changing the load of a set, if connected with large grid. 2 by turning the characteristics and actuating cam for δ_P. c) Load distribution by different speed droops δ_P. Speed $n = n_3$ determined by a large station with $\delta_{P3} = 0$. Hence different speed droops δ_{P1} and δ_{P2} of the stations 1 and 2 determine their loads P_1, P_2.

position and hence a certain gate position to a certain position of the flyball collar (in the case of a fly ball pendulum as a speed metering device) (Fig. 11.2.5). It also can be set at will by changing the slope of a cam.

Fig. 11.2.5. Schematic diagram of a hydromechanic speed governor, to visualize the implementation of the permanent speed droop (proportional band), the temporary speed droop, and their change, and the opening limiter for a single regulated FT. 1 speedometer (fly-ball pendulum), actuating the pilot valve 8, and actuated by the dash pots 2,5. the latter adjustable by the link and the throttle 4. 8 actuates the pilot servo motor 6 with a spring-induced closing tendency. Feedback of 8 by the adjustable cam 7 for the permanent speed droop. 10 speed adjustment; 11, 14 oil supply; 12 main sleeve valve actuating main servomotor 13; 16, 17 electric drive for the speedometer; 21 opening limiter.
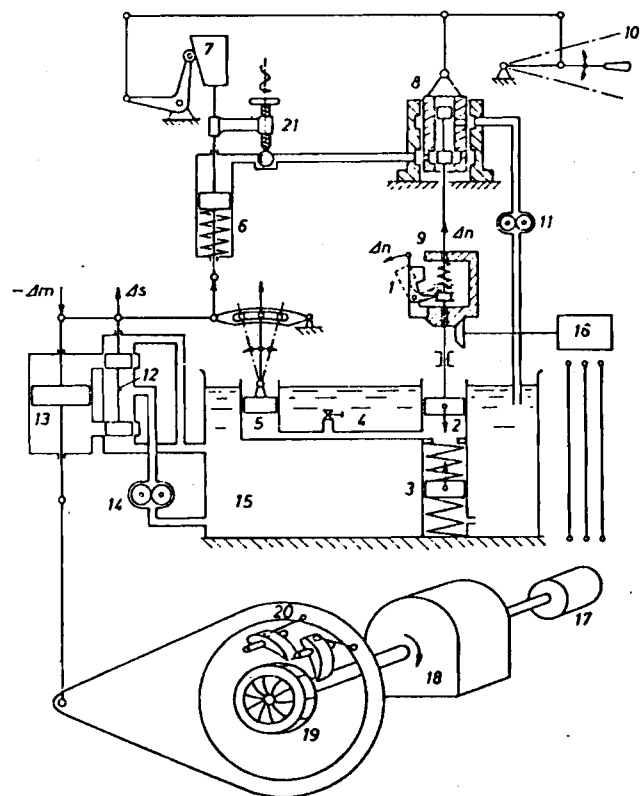
II. Emergency device to limit overspeed: This device consists usually of an astatic over-speed pendulum attached to the shaft, whose position results from the balance of centrifugal and spring loads so as to actuate an emergency oil supply for the servomotor in the case of a certain overspeed, which may (in case of a KT) require elevated forces to shut down the set [11.52].

III. Speed adjustment device for synchronization, rated frequency and load: The function of this device in the case of synchronization was described under item *I* as it requires a non-vanishing speed droop. Its function under synchronization also enables the setting of a rated frequency when the set supplies a grid by itself.

To understand its third function, namely the setting of load within the scope of a proportional band, the technical implementation of this device has to be considered (Fig. 11.2.5). It may be best visualized in the case of a mechanical governor. Here during steady state operation, when the sleeve valve of the servomotor covers the oil admission ducts in the zero position, the feedback lever hinged on this valve rod assigns a certain position of the fly ball collar and hence a certain speed to a certain servomotor piston position and thereby to a certain load.

This coordination is changed by actuating the speed adjustment so as to vary the distance between the hinge of the fly ball collar (in case of a fly ball governor) and that of the combination lever (actuating the valve either from the feedback or the speedometer) at valve position unaltered [1.50].

Then under steady state conditions with the valve position retained and the servomotor position retained in the case of a set supplying a grid by itself, the actuation of speed adjustment results in a change of the fly ball collar's position and thereby in a change of rated speed. When the speed is retained in the case of a huge grid (3rd case), then in the steady state position of a valve the above speed adjustment ultimately yields a change of servomotor position and thus a load change.

The latter method is that practised in the Austrian Vorarlberg Illwerke, one of the main peak load suppliers of the Rheinisch Westfälische Electricity board whose consumer centre is about 1000 km distant from the Austrian plant. At the switching station of *Brauweiler* near Cologne the electric commands are transmitted to the electric speed adjusting servomotors of the far remote peak load suppliers.

IV. The adjustment of fixed load, load limiter: This device dismisses temporarily the speed control (Fig. 11.2.5) by setting at will an upper load limit. This mechanism limits the stroke of the distributor servo motor by a device, that relieves the oil pressure on the opening side of the servomotor's piston at the moment the latter exceeds a certain position [1.50].

V. Guarantee of dynamic stability of speed control: This is obtained by a device, which allows changing at will be attenuation of oscillations of values due to the control loop of the governor. At any rate the governor has to meet this disturbance so as to attenuate speed and load oscillations [11.9 to 11.13].

In a proportional-integral governor with acceleration feedback the acceleration, as a prediction of speed development, is used as stabilizing feedback by shifting the valve of the gate servomotor into its steady state position before the speed deviation that also actuates the valve, has reached its desired value.

Because of the oil flow's continuity, the displacement of the servomotor is 90° phase shifted relative to the instantaneous speed deviation and hence 180° to the acceleration. Hence a feedback by this displacement on the lever that actuates the valve, also stabilizes, as acceleration does. Now the one end of the valve-actuating lever (Fig. 11.2.2 a) is shifted by the servomotor, the other by the tachometer.

To exclude in this case an excessive proportional band, this feedback acts only transitorily. This is effected by a dash pot (Fig. 11.2.2 a) in the feedback rod between servomotor piston, and its hinge on the combination lever. It behaves like a stiff linkage between servomotor and valve-actuating

547

lever, when damping is needed, when a speed disturbance causes a rapid motion such as in the case of sudden load change.

In the case of a slow motion, the dash pot acts as an elastic member. This is made possible by the now relevant leakage, squeezed through the dash pot's by-pass, by the spring load on the dash pot's piston. This load always returns the hinge of the servomotor on the combination lever to the same position. This elastic feedback is also known as isostatic regulation.

Hence in stabilized steady state, when the valve is also at the zero position, the load does not influence the speed in the sense of a proportional band. Such a correlation between P and n exists only during regulation and is attributed to a transient proportional band δ_r (temporary speed droop). To obtain stable regulation, δ_T has to be 0,3 to 3 (values larger than 0,5 are obtained only electrically), that means 10 to 100 times larger than the usual proportional band (permanent speed droop) is.

For short lasting, very strong load fluctuations, sometimes the feedback is eliminated at will by temporarily opening the by-pass of the dash pot.

11.2.2. Design of speed and acceleration metering members

11.2.2.1. Mechanical and hydromechanical members

In the first case mentioned a fly ball pendulum, driven by an electric motor, is used, which is fed by a special pendulum alternator on the shaft of the set or by the main stator current. Instead of a fly ball, a pump of the impeller or positive displacement type may also be used as a tachometer. It produces a speed-dependent oil flow, whose impact pressure on a baffle plate actuates a pilot valve of the servomotor (Fig. 11.2.2 b).

Fig. 11.2.2 c shows a rather compact design of a combined tachometer and accelerometer. It func- -tions as follows: The radial rotating tube is fed by oil whose pressure actuates the servomotor's valve by a spring-loaded piston. This pressure results from two influences. A speed-conditioned component comes from the distance the spring-suspended fly mass (which acts as a baffle plate) is from the radial outlet of the rotating tube.

The acceleration-conditioned influence of oil pressure results from the peripheral distance, the tangential orifice in the radial tube is from a radial baffle on the inert fly-wheel ring, which is spring-suspended in the tangential direction.

11.2.2.2. Electronic governor

The application of electronics is limited to the speed metering or the acceleration metering devices. The measurement of speed deviation from a rated value, may be effected by means of an electronic valve or semiconductor devices like transistor. In the case of the electronic valve, two oppositely oriented anodic currents are controlled by the grid of this valve. The resulting current actuates a pilot valve by a solenoid [11.5].

One of the currents is from a shunt of the main alternator and is proportional to the set's momentary speed. The other is proportional to a reference frequency of an oscillatory circuit, adjustable at will, see Fig. 11.2.6. Now this is effected by semiconductor devices.

At present, data processing from pilot plants by microprocessors is coming. The concept of an electronic governor head is based on the following principles [11.47; 11.48].

a) The use of proven governor design philosophies has already given excellent results in electronic governors of certain manufacturers, e.g. PD speed and speed rate governing and PI power output governing with temporary feedback.

548

Fig. 11.2.6. Scheme of an electro hydraulic speed governor with electronic head (ASEA) for metering the speed deviation from the rated value, by comparing the rated frequency of an oscillator with that of the alternator. To date the electronic valve is replaced by transistor. (Drawing courtesy KaMeWa, Kristineham, Sweden.)
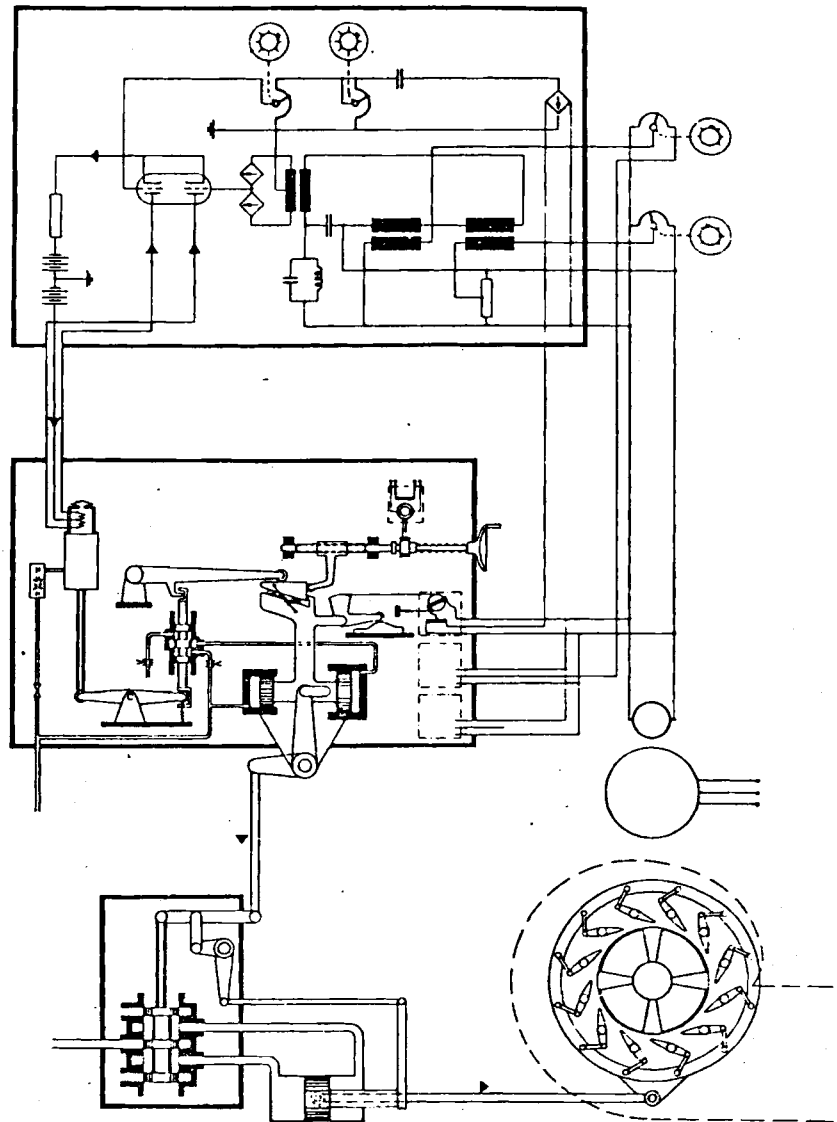
b) The application of this governing mode by means of a micro processor provides a number of advantages over analogue systems, for example:

1) the display of actual governor parameter values,
2) the modification of them during operation,
3) a better stability, thanks to the elimination of component drift,
4) the automatic testing of the internal elements,
5) the ease of adaptation to particular operating conditions, such as: water level control, connection to a master computer, etc.

On the other hand, governors equipped with this microprocessor head are provided with already well-tried measuring and control devices (transducers, servovalves etc.). Moreover this device can thus be adapted to existing plants.

Operating principles of the system: All the modules of the system are interconnected by a bus through which they can exchange data. The microprocessor module controls the operation of the bus as a function of the program of system. Each module is identified by an address by which it can be referred to in the system.

549

By means of a sequence which is repeated very rapidly, the microprocessor successively questions the various input sections such as servovalve amplifiers, indicators or relays. This sequence also includes the testing of important elements and affords the possibility of modifying parameters without disturbing the operation of the control loop. A small terminal allows the adjustment of parameters. The values displayed are the real values of parameters with an accuracy of $\mp 1\%$ of the last digit.

The block diagram in Fig. 11.2.7 shows *Vevey* electronic and electrohydraulic governor. It refers to all elements of the governing system, the turbine being under no load conditions and unsynchronized. The number in the first column indicates the line on which an element is located. The second column specifies the energy sources necessary for each unit of the governing system. The middle column gives the appropriate diagram. The 4th column indicates the external controls on the governor and the servo-valves. The last column lists the elements, [11.48].

The following text will be limited to elements of general interest and those which are suited to the Kaplan turbine considered.

Dead band device: This permits the introduction of an insensitivity into the speed governing loop, which is adjustable. Experience has shown that certain operators of machines block their governors by the gate opening limiter. If they have a conveniently sensitive governor, they thus avoid their set continually attempting to correct the frequency variations, although the effect of such corrections very often has no influence. These incessant movements can be prejudicial to the mechanical performance and life of the governing elements.

But with this method of working at the gate opening limiter, if there is any incident in the grid, e.g., tripping of an interconnection, the outputs of all the units blocked at the gate opening limiter and supplying the part of grid, whose frequency is decreasing, remain constant. Furthermore, the units supplying the other part of the network, whose frequency is increasing, only begin to close after a certain delay. The result is that the disturbance in the network may spread. The dead band has been designed precisely to prevent such incidents. When in operation, it only permits the speed governing signals to pass if its level reaches a previously chosen threshold.

Numerical speed transducer: Its moving part is a magnet on the shaft. The stationary parts are a pair of detectors, the magnets pass in front of them. Let us assume that the magnet passes successively in front of the detectors. The time elapsed between these two impulses received is compared with a reference time by means of an accurate quartz clock.

Electronic governor settings: The various settings all include, as a basic element, an angular position electrical transducer. On the one hand it consists of magnets, that are uniformly distributed in the peripheral direction on the rotary part, on the other hand it consists of stationary detectors, arranged around the rotary part.

Gate position transducer: This is of the same type used for the settings.

Temporary feedback for the runner blades and wicket gates: The electronic governor is fitted with two independent temporary feedbacks, acting separately on the gate and on the runner blade positions, in the following manner: the gate position transducer and the runner blade position transducer (line 33) in Fig. 11.2.7 enable a feedback signal of the reaction speed of the servomotor in question to its controlling servo-valve to be injected separately through the corresponding summators (line 23). Each device has two step selectors; the first enables the temporary speed droop δ_T to be fixed and the second the time constant of the damping device. This is done independently for the gates and the runner blades.

Interaction between the wicket gates and the runner blades: The interaction device (line 32) which carries out the interaction law between the runner blade and the gate openings, which depends on the head, receives information of the gate opening and of the operating head. From these data, it supplies a signal corresponding to the required runner blade opening. This signal is compared in the summator (line 39) with the signal from the runner blade position transducer (line 33) giving a signal which represents the interaction deviation.

550

		Speed pick-up head	Generator	Turbine		Description and function of governing elements

Top labels: Speed pick-up head — n: speed; Generator — P: power; Turbine

Right-hand column "Description and function of governing elements":

- External orders
- Power transducer
- Adaptation of external orders
- Choice of feedback: power or opening
- Numerical speed transducer
- Settings: C_n: speed; C_P: power; C_{YL}: opening limiter; C_{YD}: start, opening adjustment
- Disconnection of C_n and C_{YD}
- Summators
- e_n or b_n: permanent speed droop, adjustable
- Adjustable dead band device; Operation relay
- Accelerometer T_a, adjustable
- Summator
- Summator
- Trigger $C_{YL} - C_{YD}$
- Summator
- Summator
- Gate opening limiter gain
- Summator
- Trigger n, P - C_{YL}, C_{YD}
- Summator
- Summator
- Output amplifiers, T_s adjustable
- Battery
- D.C. - A.C. inverter
- Stabilized D.C. supply
- A.C. supply
- Servo-valves; Runner blade opening solenoid valve; Wicket gate closing solenoid valve
- Oil supplies
- Servomotors: Runner blades: stroke Y_B; Wicket gates: stroke Y_A
- Interaction device
- Position transducers
- Feedback effect gate on blade: r_{AB}
- Interaction error alarm
- Temporary speed droop b_t, adjustable
- Time constant of damping device T_d, adjustable
- Summator

Bottom labels: Runner blades, Wicket gates

Fig. 11.2.7. Governing system block with an electronic head for double regulated KT or BT with the signal processing diagram of the Swiss firm Vevey Engineering Works. (Drawing courtesy Vevey Engineering Works.)

551
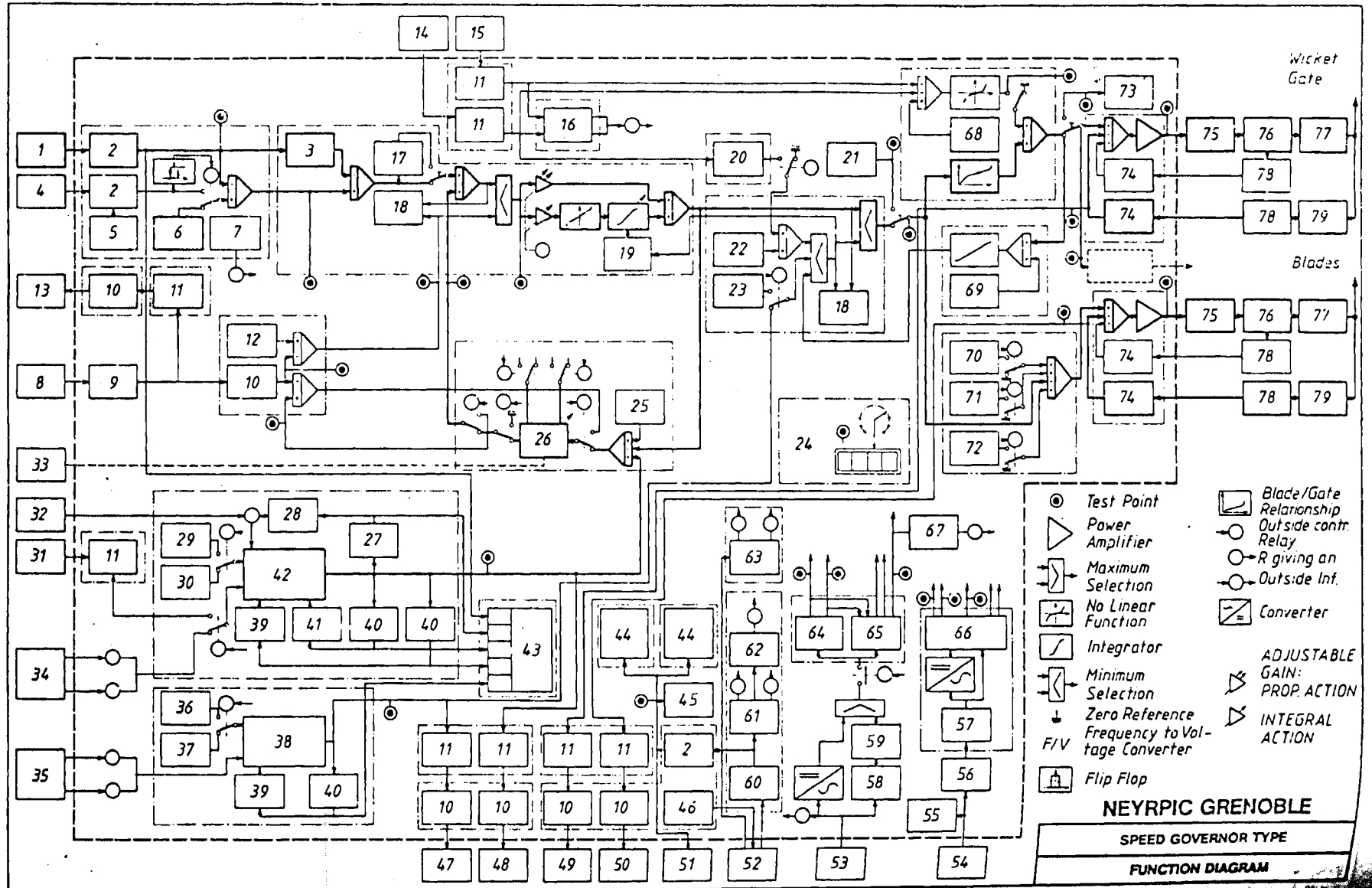
Fig. 11.2.8. Function diagram of an electronic speed governor for a double regulated Kaplan turbine, with control loops of the gates and runner in parallel of the French firm Neyrpic. For understanding, see nomenclature of symbols found on the next page.

Fig. 11.2.9. Electrohydraulic valve used by the firm Vevey Engineering Works. 102 coil; 103a, 103b leaf springs; 104 paddle; 105 spring; 108 piston; 113a, 113b nozzles; 117a, 117b diaphragms; 130 valve. (Drawing courtesy Vevey Engineering Works, Switzerland.)
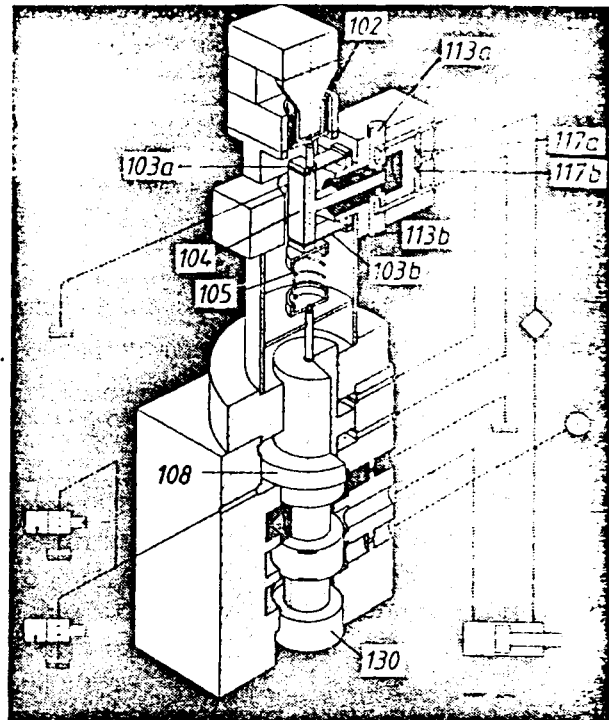
Before entering the summator (line 23), the level of this signal can be chosen by the step selector (line 35). The output signal from this summator acts on the elements controlling the runner blade position, moving them in the direction which achieves the required interaction. Since a permanent and important error of interaction can be the cause of running disturbances and possible damage to certain parts of the turbine, an interaction error detector (line 36) gives an alarm if a considerable deviation lasts for several minutes.

1: Unit voltage transformer 2: F/V converter 3: accelerometer 4: network voltage transformer 5: slippage frequency adjustment 6: reference frequency 7: frequency measurement failure 8: VT & CT system 9: power transducer 10: adaptation & filter 11: galvanic separator 12: load limit setting 13: unit power remote indication 14: downstream level 15: upstream level 16: upstream level downstream level signal loss detection 17: frequency deadband for test 18: limited unit information 19: clipping 20: adaptor 21: blade manual control 22: bias voltage for cavitation limit 23: starting bias voltage 24: voltmeter and switch for maintenance 25: speed no load bias voltage 26: permanent speed droop 27: load/frequency device at zero 28: return to zero reset 29: slow speed 30: fast speed 31: 1st analog input 32: order to return to zero 33: speed droop remote control 34: control of the load/frequency device 35: control of the opening limiter 36: slow speed 37: fast speed 38: digital opening limiter 39: order + inhibition 40: maximum travel detection 41: order − inhibition 42: digital load/frequency device 43: flip flops 44: 8 speed switches 45: frequency local indicator 46: isolated power supply 47: opening limiter remote indication 48: load/frequency device remote indication 49: wicket gate remote indication 50: blades remote indication 51: frequency remote indication 52: proximity sensors 53: power house AC auxiliaries 54: power house battery 55: relay supply 56: protective filter 57: oscillator 58: battery charging 59: Cd Ni battery 60: adaptation 61: stop & creeping detection 62: stop deflection failure 63: detection of rotating direction 64: electronic supply 65: oscillator 66: supplies for remote indications and speed switches 67: supply failure 68: rated head 69: maximum opening limit 70: 1st bias voltage 71: 2nd bias voltage (to close) 72: 3rd bias voltage (to open) 73: wicket gate manual control 74: rectifier filter 75: actuator 76: distributing valve 77: servo motor 78: variometer 79: linear cam (Drawing courtesy Neyrpic, Grenoble).
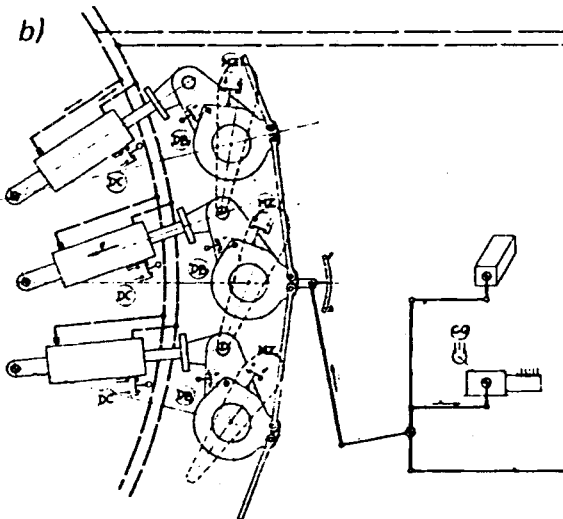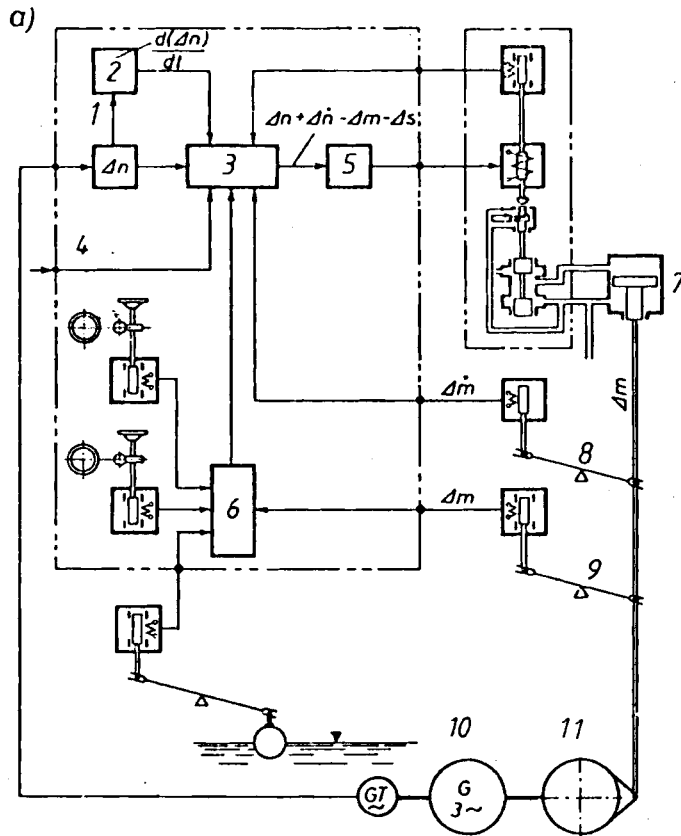
Fig. 11.2.10. Electro hydraulic control schemes for single regulated turbines, e.g., FTs. a) Scheme of information flux and design of a proportional integral speed governer with acceleration feedback (accelero-tachometric governor) used by the Italian firm Hydroart, Milan. 1 -speedometer (electronic); 2 accelerometer (electronic); 3 mixer; 4 signal transmitter; 5 amplifier; 6 mixer; 7 gate servomotor; 8, 9 feedback; 10 alternator; 11 turbine. (Drawing courtesy Hydroart, Milan.) b) Special features in the case of gates regulated by a single servo motor, according to a design of the French firm Neyrpic and implemented, e.g., on the Francis turbines of Tucuri, Brazil (see Fig. 10.3.4). Gate linkage for synchronism, common feed back. (Drawing courtesy Neyrpic, Grenoble.)

554

Fig. 11.2.11. Simplified. scheme for the speed control of a double regulated KT with hydro mechanic governor, and control loops for the gates and the runner vanes in series, assigned to each other by the cam 5. Devices for the temporary speed droop (dash pot) omitted. 1 speedometer; 2 control valve; 3 pressurized oil; 4 gate servomotor; 5 cam; 6 oil head; 7 gate operating ring; 8 runner servomotor; 9 spider; 10 alternator rotor, 11 turbine runner.
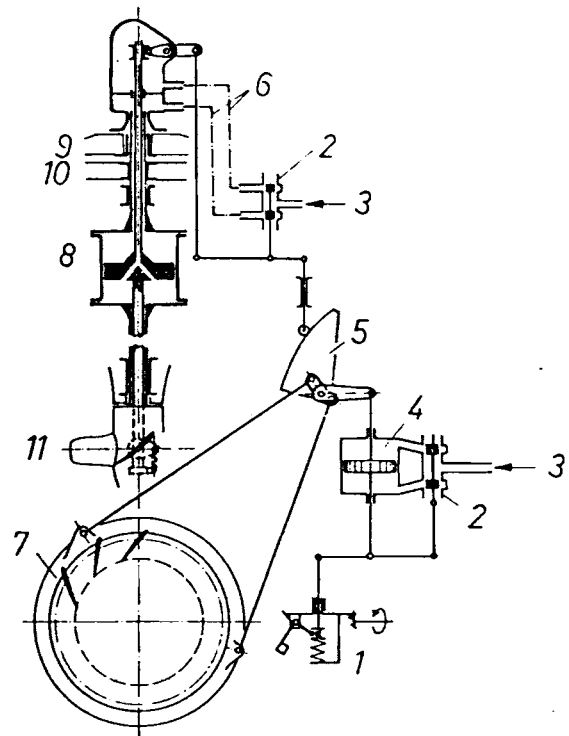
Fig. 11.2.8 shows signal flux and function diagram of a double regulated KT of the French firm Neyrpic. Here the synchronized actuation of runner and gate servomotor from speedometer and accelerometer is preferred. Here also metering devices and relays are electronic as far as reasonably possible.

In this connection wide use is made of solenoid valves, see Fig. 11.2.9. Such a valve transforms the electric current, supplied by one of the electronic governor's output amplifiers, into a proportional and accurate stroke of a hydraulic distributing valve. The latter controls, e.g., a servomotor.

The servo-valves all have cylindrical distributing valves provided with one pair of regulating edges if the usual differential type servomotor is controlled. Depending on the oil flow to be controlled, the Swiss firm Vevey uses servo valves having two or three stages of amplification.

The electro hydraulic first stage (see Fig. 11.2.9) is to transform an electric current into the motion of a small double acting servomotor 108. The latter is controlled by two symmetrical oil distributors, working without friction. These comprise two diaphragms 117a, 117b, two nozzles 113a, 113b, a paddle 104, suspended by two leaf springs 103a, 103b. Due to this suspension the paddle can move vertically without friction. Its travel is only a few tenth of a millimeter, corresponding to the clearance between the paddle and the nozzles.

In an arbitrary position, the paddle is subjected to three vertical forces, namely: that of the spring 105, that due to prestressing of the leaf springs, 103a, 103b and that resulting from the passage of an electric current through the coil 102. The value and the direction of this force is a function of the intensity and the polarity of the current. The steady state position of this electromagnetic force is nil.

In the case of an upward displacement of the paddle 104, induced by a current in the solenoid 102, the flow of oil from the nozzle 113a decreases while the flow through the other nozzle 113b increases. Hence the volume of the oil in the upper chamber of servomotor 105 increases and that in the lower chamber decreases. The piston therefore moves downwards. The result is that the upward force on the paddle 104 applied by the spring 105 is reduced. The motion stops when the variation of this force balances that due to the coil. The paddle then returns to its initial position, midway between
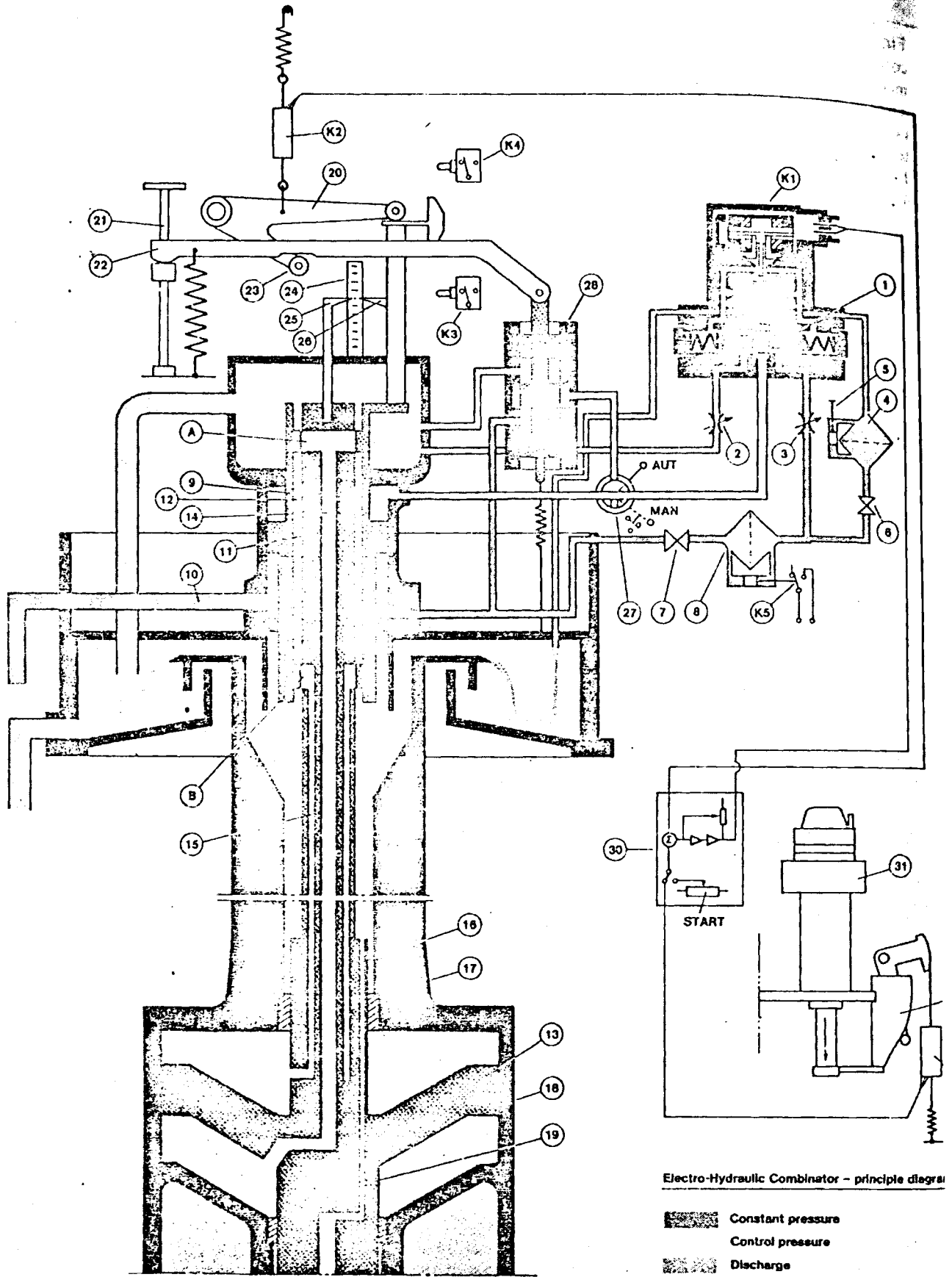
Electro-Hydraulic Combinator – principle diagram

Constant pressure

Control pressure

Discharge

556

Fig. 11.2.12. Electro hydraulic runner blade adjustment by a cam according to KaMeWa AB. Sweden, with the control loops of gates and runner vanes in series. The input quantity to this servo system is primarily the wicket gate position. The combinator cam 29 which determines the relationship between blade angle and wicket gate opening is in this case connected to the pilot servomotor of the actuator 31. In case large variations in head are encountered, the single cam is changed to a three dimensional saddle with lateral adjustment to ensure that correct setting can be achieved for every head. A third possibility is to introduce a digital processor instead of the cam or saddle.

The combinator 29 operates a transmitter K 6, which converts the corrected mechanical guidance into an electric signal. The position of the regulating sleeve 9 of the combinator is also via lever 20 transformed in the same way by transmitter K 2. Both these electrical command signals are compared and amplified in the electric error detector 30, and its output signal is fed to the transducer K 1. Pilot valve 1 actuates the regulating sleeve 9 in a direction that tends to eliminate the difference in voltage between transmitters K 2 and K 6. The regulating sleeve 9 is a valve for the runner servomotor 13. Regulating piston 11 is rigidly connected to the servomotor piston 13. If sleeve 9 and piston 11 do not assume identical positions, port A and B will be opened either A to discharge and B to pressure or vice versa depending on the sign of the error signal. Thus oil will be passed through concentric ducts 14 and 15 in the shaft of the runner servomotor 13 in such a way that the valve ports will be closed again (feedback). Thus the servomotor piston 13 copies exactly the movements of sleeve 9.

Maximum closing and opening speeds are set by means of the throttle valves 2 and 3 respectively. Reset to a larger blade angle to start, to obtain a greater torque from the turbine, is made entirely by electrical means in the error detector30. Parallel to the electro-hydraulic control there is a manual control (a general necessity for all important regulating devices in the case of emergency). If the 3-way valve 27 is turned from Auto to Manual, the hand control valve 28 takes over the control of sleeve 9. Desired runner blade angle can then be set by hand screw 21. As opposed to systems, in which the last servo stage is located in the runner hub 18, the system described offers the advantage that the true position of the blades can be checked. On a common scale 24 the position of both the regulating sleeve 9 and the runner servomotor 13, (i.e. the blade angle), are displayed. Legend K 1 electro hydraulic transducer, K 2 runner blade position transmitter, K 3 limit switch fully closed, K 4 limit switch fully opened, K 5 dirt indicating switch, K 6 gate position transmitter. 1 pilot valve piston; 2 throttle valve, closing time; 3 throttle valve, opening time; 4 filter for transducer; 5 dirt indicator; 6 shut-off valve; 7 shut-off valve; 8 filter for transducer and pilot valve; 9 combined regulating sleeve/differential piston; 10 pressure oil pipe; 11 regulating piston; 12 pressure chamber; 13 runner servomotor piston; 14 oil duct to underside of item 13; 15 oil duct to upper side of item 13; 16 oil duct for static pressure to the runner hub; 17 turbine shaft; 18 Kaplan runner hub; 19 runner servomotor piston rod; 20 bell crank lever; 21 hand screw; 22 balance lever; 23 roller; 24 scale; 25 pointer for runner blade angle; 26 pointer for regulating sleeve/differential piston position; 27 three-valve; 28 hand control valve; 29 combinator cam; 30 electronic error detector; 31 actuator. (Drawing courtesy KaMeWa, AB, Kristineham, Sweden.)

◄───

the nozzles 113a and 113b. The final travel of the piston 108 is proportional to the exciting current in the coil.

The permanence of the magnetic field passing in the coil, the travel of which is very small, and the negligible hysteresis of the spring characteristic of 105 ensure an accurate correlation between the movement of the distributing valve 130 and the current in the coil 102.

Conclusion: The advantage of an electric governor consists in its high accuracy and in the fact that the number of controlling and controlled parameters accompanying and supporting the speed control and surveillance of the set is nearly unlimited. Examples may be temperatures of bearing and alternator, blockage of by-pass outlet, flow of lubricant, response of breaking elements in the gate drive, water-hammer-induced pressure surge, energy exchange of a neighbouring grid, etc. [11.39; 11.44; 11.46 to 11.48].

Moreover an electric governor facilitates the control of power stations in remote areas from a far distant panel.

Fig. 11.2.10a shows an example of electronic data processing for a gate-regulated FT from the Italian firm Hydroart. Fig. 11.2.10b shows special features in the control of a FT with single servomotors for the gates of the French firm Neyrpic.

Fig. 11.2.11 shows a simplified scheme of a double regulated KT with the control loops for gates and runner blades in series, in which all damping devices such as dash pots have been omitted. Fig. 11.2.12 shows the control scheme of a double regulated KT implemented by the Swedish firm KaMeWa AB.

Fig. 11.2.13 shows a control scheme of a double regulated PT with the control loops of nozzle valve and jet deflector in parallel implemented by the French firm Neyrpic.

11.2.3. Simple treatment of the dynamic behaviour of governors

11.2.3.1. Nomenclature and assumptions

I. Symbols: Δ-deviation from steady state (due to speed Δn and position of servomotor piston Δm) or zero position (due to valve Δs), positive in the sense of speed rise (Δn, Δs) or opening (Δm); n_M-mean speed, m_M-stroke of servomotor piston, s_M-stroke of valve piston equal to width of ports; related values: speed $x = \Delta n/n_M$; servomotor $m = \Delta m/m_M$, valve $s = \Delta s/s_M$; δ_T-transient proportional band (temporary speed droop), being 0,3 ... 4(7) for stabilization of disturbances. T_s-regulating time (closing = opening), the servomotor piston needs to cover its stroke s_M at full opened valve port ($s = 1$) and constant piston speed $\dot{m}$. T_a-start up time of set, needed to accelerate the unloaded set by its rated torque from rest to rated speed n_M at constant acceleration. T_i-reset (isostatic) time, the $1/ln\,2$ fold time that an abruptly full-deviated dash pot piston for the elastic feedback needs to cover its half stroke. T_b-rate (acceleration) time, the accelerometer requires to cover the speed range $n_{max} - n_{min}$ at valve full-opened and at constant acceleration, (see Fig. 11.2.3).

II. Assumptions: 1) No overlap and leakage of valve in its zero position. 2) Servomotor piston covers its stroke s_M in regulating time T_s at partial opening of valve $s = \delta_P =$ proportional band. 3) For a proportional governor with stiff feedback, the valve deviation s depends linearly on deviation of speed x and its integral m; here at steady state $x(s = 0) = -\delta_T$ (temporary speed droop). For a proportional integral governor with acceleration feedback, s depends linearly on x and its derivative $\dot{x}$. 4) No automatic control, torque vs speed graph of turbine and generator are parallel to each other. 5) The excess of the turbine's torque over that of generator is proportional to the servomotor deviation m. No water hammer. In the following a dot above a quantity indicates its rate.

11.2.3.2. Proportional governor, servomotor with stiff feedback (speed governor)

Respecting 1) and 3) give the valve deviation

$$s = \delta_T m + x. \tag{11.2-1}$$

1) and 2) yield the speed $\dot{m}$ of piston, regulating time T_s, by

$$s = -\delta_P T_s \dot{m}. \tag{11.2-2}$$

4) and 5) yield the set's equation of motion, start up time T_a, by

$$m = T_a \dot{x}. \tag{11.2-3}$$
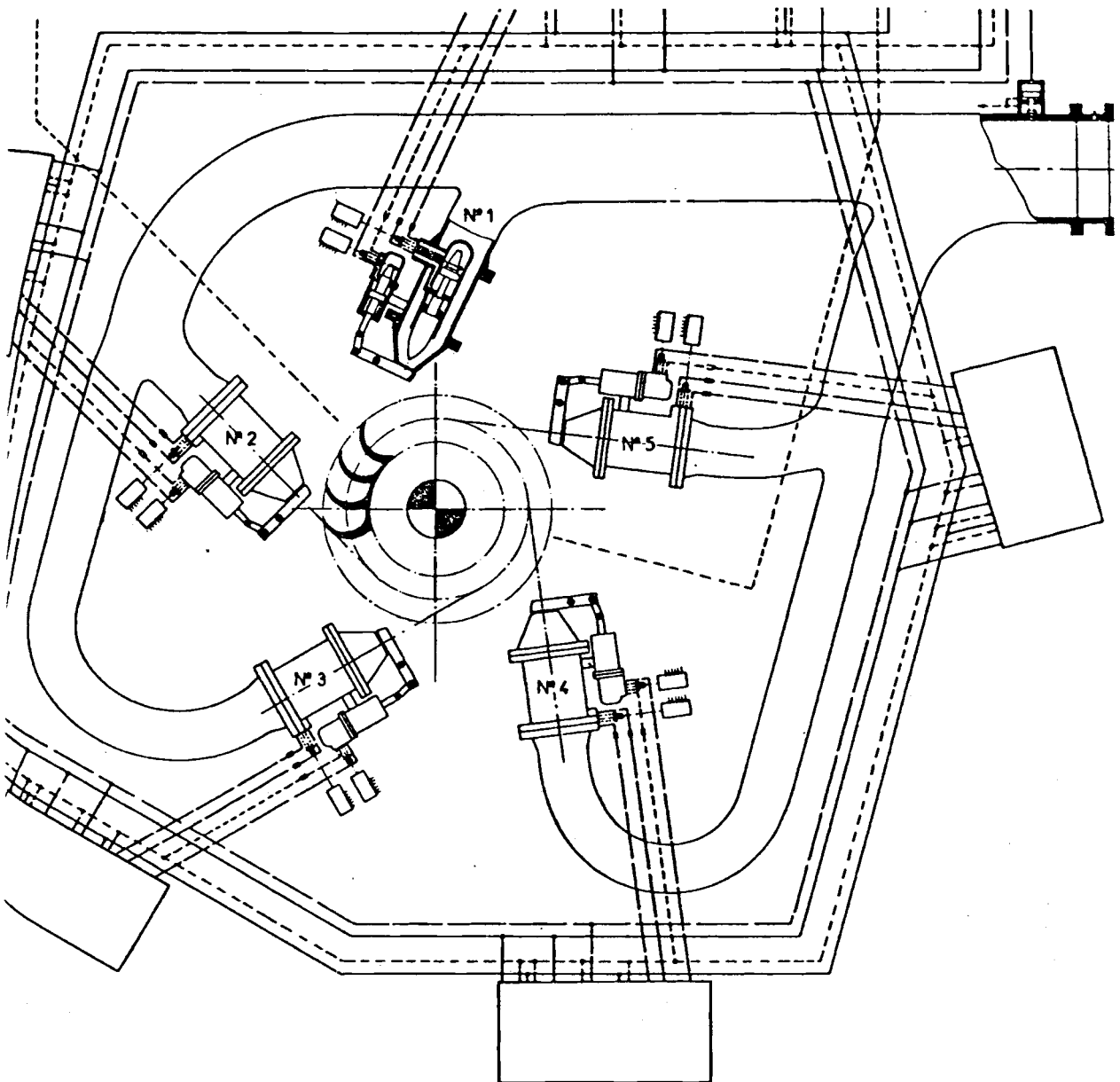
Fig. 11.2.13. Control scheme of a double regulated Pelton turbine with control loops of the jet deflector and the needle valve in series, as now used by Neyrpic. —— oil circuit pressurized and at constant pressure ——— oil circuits under variable pressure ----- oil suction line without pressure. Design of a 5-nozzle vertical shaft PT in the French Plant L'Eau d'Olle (see Fig. 10.3.14). (Drawing courtesy Neyrpic, Grenoble, France.)

Inserting (11.2–3) in (11.2–1), then (11.2–2) with respect to (11.2–3) in (11.2–1) yields the differential equation of the closed control loop

$$\delta_P T_s T_a \ddot{x} + \delta_T T_a \dot{x} + x = 0. \tag{11.2–4}$$

Its natural oscillation $x = x_0 e^{\alpha t}$ has the natural frequency

$$\alpha = [- \delta_T \pm i(\delta_T^2 - 4 T_s \delta_P / T_a)^{1/2}]/(2 T_s \delta_P). \tag{11.2–5}$$

After this the feedback-linked term $-\delta_T/(2\,T_s\delta_P)$ damps oscillations with rising temperature, droop δ_T as set, e.g., by a lever ratio of a linkage.

11.2.3.3. Proportional integral governor with acceleration feedback (acceleration governor, PD governor)

With the rate time T_b, respecting 3), the valve deviation reads

$$s = T_b\dot{x} + x. \qquad (11.2-6)$$

Expressing s by (11.2-2) and then $\dot{m}$ by (11.2-3) gives the differential equation of the closed control loop, start up time T_a, by

$$T_a T_s \delta_P \ddot{x} + T_b \dot{x} + x = 0. \qquad (11.2-7)$$

Here the natural oscillation has a damping term $-T_b/2\,T_a\,T_s\delta_P$ that increases with the rate (acceleration) time T_b.

11.2.3.4. Proportional integral governor, servomotor with elastic retarding feedback (PI governor)

Let l be the related deviation of the spring-loaded and dash-pot-linked hinge of the valve actuating lever. Then the spring load becomes $\sim l$. It is balanced by the hydraulic load on the dash pot, which, in the case of laminar flow, is proportional to the speed difference between the servomotor ($\dot{m}$) and the dash pot ($\dot{l}$).

Accordingly with T_i as the reset (isostatic, isodrome) time,

$$l = (\dot{m} - \dot{l})\,T_i. \qquad (11.2-8)$$

Now m in the relation (11.2-1) has to be replaced by l. Hence

$$s = \delta_T l + x. \qquad (11.2-9)$$

From this $\dot{l} = (\dot{s} - \dot{x})/\delta_T$. This in (11.2-8) gives $l = T_i(\dot{m} - \dot{s}/\delta_T + \dot{x}/\delta_T)$. Putting this and s from (11.2-2) in (11.2-9) the differential equation of the governor, input x, output m, reads

$$\delta_P T_i T_s \dot{m} + (\delta_P T_s + \delta_T T_i)\,\dot{m} + T_i \dot{x} + x = 0. \qquad (11.2-10)$$

In practice the regulating time T_s is much smaller than T_i. Moreover δ_P is about 1/10 th of δ_T. Therefore the terms with $\delta_P T_s$ are omitted in the last equation. Hence the simplified, practice-oriented differential equation of the governor

$$\delta_T T_i \dot{m} + T_i \dot{x} + x = 0. \qquad (11.2-11)$$

Inserting here m from (11.2-3) the differential equation of the closed control loop, start up time T_a, reset time T_i, reads

$$\delta_T T_i T_a \ddot{x} + T_i \dot{x} + x = 0. \qquad (11.2-12)$$

Here the natural frequency has a damping term $-1/(2\delta_T\,T_a)$, that is inverse to the transient proportional band δ_T.

11.2.4. Other time parameters, tuning

I. Start up time of penstock: Because of its inertia, the now assumed inelastic water column in an assumed stiff penstock of length L, needs a period T_{sp} to be speeded up

560

under the head H to its velocity c_r, due to the rated load. Accounting also for the speed linked head drop by the pipe loss, assumed to be $\zeta c^2/2$, then T_{sp} follows from the energy theorem by (artanh $\equiv$ tanh^{-1})

$$T_{sp} = L\{2/[gH(1 + \zeta)]\}^{1/2}\,\text{artanh}\{c_r[(1 + \zeta)/(2gH)]^{1/2}\}. \qquad (11.2-13)$$

For the usual case $c_r/(2gH)^{1/2} \ll 1$, this becomes

$$T_{sp} = c_r L/(gH). \qquad (11.2-14)$$

II. Opening time of distributor, T_0: Obviously this has to last longer than the start up time of the penstock. Hence $T_{sp} \leqq T_0$.

III. Reflection time, closing time: Any shut down of a turbine on a penstock causes water hammer, propagating with velocity a along the penstock, length L. At the latter's upper end the wave is negatively reflected and returns to the machine after the reflection time T_r has elapsed

$$T_r = 2L/a. \qquad (11.2-15)$$

According to Cap. 8.3, decreasing the pipe velocity within the period T_r by Δc, i.e. by closing the distributor, generates a pressure rise at the lower pipe end

$$\Delta p = \varrho a \Delta c. \qquad (11.2-16)$$

The closing rate of the distributor is usually decelerated in a stepwise manner towards the closed position. This has to be done as described in Cap. 8.3 with respect to reflected water hammer waves, the rotary inertia of the set, and the characteristics of the hydro turbomachine in the regime concerned, as a function of distributor opening and speed.

A fairly dimensioned timing of the closure is signified by the fact, that the maximum pressure increase, set before and mentioned in Cap. 8.3 is never surpassed but used as often as possible.

Usually the relative pressure rise due to water hammer is prescribed by $\Delta H/H = 0,1$ to 1 for $H = 1000$ m to 10 m. To keep the pipe loss under rated load below 1 % of the head, the rated pipe speed is chosen in the range $c_r = 0,1\,(2gH)^{1/2}$. Making the velocity change Δc in (11.2-16) equal to this c_r, then

$$\Delta H/H = 0,1\sqrt{2}a/(gH)^{1/2}. \qquad (11.2-17)$$

An example $H = 500$ m, $a = 1000$ m/s with the result $\Delta H/H = 2,02$ demonstrates that at least in the relevant high head range, a closure within the reflection time would yield unacceptably high water hammer pressure surges. Hence in high head plants, the time T_r may be considered as the lowest limit for the closing time T_s.

It is known that any closure extending beyond T_r benefits from the then occurring attenuation of pressure surge by the negative water hammer waves reflected at the upper end of the pipe. Strictly speaking this holds only for the period T_r after the time elapsed $t = T_r$.

The whole may be understood as a hint that any estimate of the closing time does not negate the inclusion of a water hammer calculation.

Generally any waterhammer destabilizes the loop of the governor in so far as it creates a pressure rise upstream of a closing valve and hence counteracts the intended reduction of flow. Problems of governor stability together with water hammer are dealt with in the following Cap. 11.3.

Hence any closing time T_s that is predicted, from the set's moment of inertia Θ, its full load torque $M_{1/1}$ and a desirable limit of overspeed $\Delta \omega$, e.g. at short circuit, by application of the equation of motion

$$T_s = A\omega\,\Theta/(\gamma\,M_{1/1}),\qquad\qquad (11.2\text{--}18)$$

requires an empirical correction factor γ. The similarity requires $M_{1/1} \sim \omega^2 D^5$, $\Delta\omega \sim \omega$. Assuming γ and T_s to be constant, the above yields $\Theta \sim D^5\omega$. This reflects the known fact, that the required moment of inertia increases with the speed ω.

IV. Start up time of set: Imagine the set with a moment of inertia Θ is to be speeded up at its rated torque $M_{1/1}$ to the rated speed ω. Hence the start up time of the set

$$T_a = \omega\,\Theta/M_{1/1}.\qquad\qquad (11.2\text{--}19)$$

Note that in any formula with Θ the effect of added water mass should be accounted for, but usually is not. The start up time T_a of the set should exceed the start up time of the penstock after (11.2–14), according to $T_{sp} \leqq T_a$. To develop the rated torque at start up the opening time of distributor T_0 has to fall short of the start up time of the set according to $T_0 \leqq T_a$. The above can be reconciled with $T_{sp} \leqq T_0$ under II by $T_{sp} \leqq T_0 \leqq T_a$.

11.2.5. Special regulating devices

I. *Kaplan* turbines: Here usually the control loop of the distributor is connected in parallel to the control loop of the runner (Figs. 11.2.7 and 8). A design with both the control loops in series (Fig. 11.2.12), but also different regulating times of the loops favours a cam-off operation (Cap. 10.5). Both the loops, are connected by a cam (see Fig. 11.2.12). Sometimes to reduce swell waves in navigable rivers a swell-reducing cam is used in case of sudden load rejection (Cap. 3.1).

To avoid the consequences of reversed water hammer after water column separation, KTs are usually equipped with an aeration valve on the head cover, operated by the gate ring in the case of quick shut down (see also Cap. 8.2).

II. *Francis* turbines: Here sometimes with sets on long penstocks a by-pass outlet is used to reduce water hammer, see Cap. 8.3. Aside the bep also ventilation is used.
III. *Pelton* turbines: Here a sudden load drop is encountered by a deflection of the jet by means of a jet presser or cutter. The closed control loops of the jet deflector and needle valve may be connected in parallel, preferably, (Fig. 11.2.13) or in series (to date rarely built). Both the loops are connected by a cam. This provides for a ready position of jet deflector under steady state operation close to the outer edge of the jet. See Cap. 8.3 [1.50], [11.2]. Quickly actuating the jet deflector allows dismissal of the cam (Cap. 8.3).

11.3. Stability of control with respect to water hammer, autoregulation of grid, and turbine characteristic

11.3.1. Introduction to the problem

Let us consider a set, that supplies a grid by itself. This set is controlled either by a PI or a PD governor. It is equipped with a single regulated reaction turbine, i.e., a FT or a KT of the propeller type. The following characteristics of the turbine are known as functions of the gate opening (for which the servomotor position m is taken) and the rotary speed n: a) Internal efficiency $\eta(m, n)$. b) Unit flow $Q_{11}(m, n)$. Q_{11} and n allow easy inclusion of head oscillations.

The turbine is supplied from a long penstock with elastic response (water hammer), which may be single-staged or double-staged, the upper end of which is fed from a large vessel

(surge tank or reservoir) at constant pressure. The turbine is attached to a generator that supplies an electric grid with a known auto regulating load characteristic due to machine tools, pumps and blowers, or resistors, [10.57].

Here the problem arises with respect to dynamic stability of the closed control loop (consisting of the governor and the controlled system turbine, penstock, grid) how to set the reset time T_i of a PI governor or the rate time T_b of a PD governor, and the start up time T_a of the set, when the characteristics of turbine and grid, the proportional band δ_P, the temporary speed droop δ_T are known or set, a certain damping coefficient is desired, and the natural period of the system's oscillation should not coincide with the reflection time of the pipe.

11.3.2. Assumptions

The natural frequency of a closed control loop, excited by disturbances from the grid, the pipe system or a change of gate position or speed, is considered at a time elapsed that is a multiple of the pipe reflection time (11.2–13). The amplitudes of all the deviations considered are infinitesimally small compared with their reference values. All disturbances are nondimensional, the time constants real times.

11.3.3. Dynamically equivalent types of governors

First a proportional integral governor with acceleration feed back (PD governor) is considered, whose measuring element is of the tacho-accelerometric type. According to Cap. 11.2.3.1 the figures used for the deviation of speed, Δn, servomotor piston, Δm, and valve piston, Δs, respectively, are

$$m = \Delta m/m_M, \quad (11.3-1); \qquad x = \Delta n/n_M, \quad (11.3-2); \qquad s = \Delta s/s_M, \quad (11.3-3)$$

in which m_M is the stroke of servomotor piston, s_M that of the valve, n_M the rated speed.

According to (11.2–6) the valve deviation s is induced by a speed deviation x and its acceleration $\dot{x}$. Expressing the valve deviation s by the speed $\dot{m}$ of the servomotor piston, according to (11.2–2), the differential equation of the governor, proportional band (permanent speed droop) δ_P, reads

$$- \delta_P T_s \dot{m} = T_b \dot{x} + x, \tag{11.3-4}$$

in which T_s is the regulating (closing) time, and T_b the rate (acceleration) time, according to Cap. 11.2.3.1.

Next the simplified differential equation for a proportional integral (PI) governor (servomotor with elastic retarding feedback), according to (11.2–11) is considered. Rearranged as

$$- \delta_T T_i \dot{m} = T_i \dot{x} + x, \tag{11.3-5}$$

in which T_i is the reset (isostatic) time and δ_T the transient proportional band (temporary speed droop) (see Fig. 11.2.3). Obviously both the governors have a similar dynamic behaviour when the product of proportional band and regulating time $\delta_P T_s$ vanishes against the reset time T_i. According to a proposal of G. Fabritz [11.2], the equivalence of both the governors exists when the corresponding coefficients in both relations are set equal, according to

$$T_i = T_b \quad \text{and} \quad \delta_P T_s = \delta_T T_i. \tag{11.3-6}$$

Note that the regulating time T_s here is due to the PD governor.

11.3.4. The controlled system (turbine, grid, penstock)

11.3.4.1. General remarks on the electric grid

With reference to Cap. 11.2.1.3, the grid-induced generator torque M_G (rated value M_N) vs speed n (in rps) reads as follows

$$M_G = (n/n_N)^u M_N,$$ (11.3-7)

in which $u = 0$ for a load due to machine tools, $u = -1$ for a load due to resistors (under the assumption of constant voltage at the generator terminals) and $u = 2$ for a load due to blowers and impeller pumps [11.23; 11.57].

11.3.4.2. Linkage of turbine characteristic and grid

With $Q_{11}(m, n)$ as the unit discharge and $\eta(m, n)$ as the shaft efficiency, both depending on gate position m and speed n the torque of the turbine, head H, diameter D, reads

$$M_T = (2\pi)^{-1} \eta(m, n) \, Q_{11}(m, n) \, D^2 (Hg)^{3/2} \varrho n^{-1}.$$ (11.3-8)

During unsteady operation, the equation of motion requires

$$\Delta M_T - \Delta M_G = 2\pi [d(\Delta n)/dt] \, \Theta,$$ (11.3-9)

in which Δ indicates deviation from steady state, and Θ the moment of inertia of the set. Dividing this relation by the rated torque $M_N = P_N/(2\pi n_N)$, P_N rated output, n_N rated speed, using the identity $(1/n_N) \, dn/dt = (1/n_N) \, d(\Delta n)/dt = \dot{x}$ and accounting for the start up time of the set according to

$$T_a = (2\pi)^2 \, \Theta n_N^2/P_N,$$ (11.3-10)

the relation (11.3-9) reads

$$(\Delta M_T - \Delta M_G)/M_N = \dot{x} \, T_a.$$ (11.3-11)

Introducing the load degree $\lambda = M_T/M_N$, accounting for (11.3-7) and taking the increment Δ as infinitesimally small then

$$\Delta M_G/M_N = \lambda(\Delta M_G/M_T) \approx \lambda \Delta M_G/M_N \approx \lambda d M_G/M_N \approx \lambda u x.$$ (11.3-12)

Employing the nondimensional infinitesimally small head deviation $h = \Delta H/H$, H rated head, after (11.3-7) with $dm = \Delta m$, $dn = \Delta n$, $dH = \Delta H$ and introducing the figures,

$$K_{Qn} = (n_N/Q_{11})(\partial Q_{11}/\partial n)_m, \quad K_{Qm} = (m_M/Q_{11})(\partial Q_{11}/\partial m)_n,$$ (11.3-13)

$$K_{\eta n} = (n_N/\eta)(\partial \eta/\partial n)_m, \quad K_{\eta m} = (m_M/\eta)(\partial \eta/\partial m)_n,$$ (11.3-14)

the term $\Delta M_T/M_N$ in (11.3-11) becomes

$$\Delta M_T/M_N = \lambda[(K_{\eta m} + K_{Qm})m + (K_{\eta n} + K_{Qn} - 1)x + 3h/2].$$ (11.3-15)

Then using the self control parameter,

$$K_e = 1 + u - K_{\eta n} - K_{Qn},$$ (11.3-16)

and accounting for (11.3-12), (11.3-15), and relation (11.3-7), the equation of motion of the set, with respect to turbine characteristic and grid load, takes the form

564

$$\lambda[(K_{\eta m} + K_{Q m})\, m - K_e x + 3h/2] = \dot{x}\, T_a. \tag{11.3-17}$$

11.3.4.3. Intervention of penstock

With the related deviation of flow $q = \Delta Q/Q_N = \Delta c/c_N$, and head $h = \Delta H/H$ (Q_N = rated flow, H = rated head, c_N = rated pipe velocity) the coordinate $\zeta = z/L$ along the pipe axis, beginning at the upper end, and assuming a vanishingly small velocity in the pipe, the equation of onedimensional motion in the z-direction and the continuity of a fluid element filling the pipe section read (see Cap. 8.2)

$$\partial h/\partial \zeta + T_{sp}\partial q/\partial t = 0, \quad \text{and} \tag{11.3-18}$$

$$\partial h/\partial t + (K/T_L)\, \partial q/\partial \zeta = 0, \tag{11.3-19}$$

in which T_{sp} is the start up time of the penstock, $T_{sp} = c_N L/(gH)$ from (11.2−14), L the penstock length, H the head, $T_L = L/a$ the travel time of a pressure wave, to cover the penstock length L with the velocity a, and K the following penstock parameter,

$$K = T_{sp}/T_L = a c_N/(gH), \tag{11.3-20}$$

being the ratio of pressure surge due to water hammer, induced by cutting off the speed c_N, to the pressure of the rated head H.

11.3.4.4. Boundary conditions of water hammer in a simple pipe

For the two governing equations due to water hammer (11.3−18) and (11.3−19), the following solution is introduced

$$h = h_1^* e^{r\zeta} e^{pt} \quad (11.3-21) \qquad \text{and} \qquad q = q_1^* e^{r\zeta} e^{pt}, \tag{11.3-22}$$

in which h_1^* and q_1^* are unknown amplitudes. Inserting the last two relations into the equation of motion and continuity gives

$$r h_1^* + T_{sp} p q_1^* = 0, \qquad p h_1^* + (Kr/T_L)\, q_1^* = 0. \tag{11.3-23}$$

By *Cramer's* rule, the interesting case $h_1^* \neq 0$, $q_1^* \neq 0$ requires

$$\begin{vmatrix} r & T_{sp} \cdot p \\ p & Kr/T_L \end{vmatrix} = 0 \quad \text{or} \quad r = \pm \sqrt{T_{sp} T_L/K}\; p = \pm p T_L. \tag{11.3-24}$$

With the complete solution of (11.3−18), (11.3−19)

$$h = h_1 e^{p T_L \zeta} e^{pt} + h_2 e^{-p T_L \zeta} e^{pt}, \tag{11.3-25}$$

$$q = q_1 e^{p T_L \zeta} e^{pt} + q_2 e^{-p T_L \zeta} e^{pt}, \tag{11.3-26}$$

the unknown constants follow from the boundary conditions.

At the upper end of the penstock ($\zeta = 0$): $h(\zeta = 0) = 0$. Hence $h_1 = -h_2$,

$$h = 2h_1 e^{pt} \sinh p T_L \zeta. \tag{11.3-27}$$

Due to the constancy of pressure at the upper end, $\partial h/\partial t$ vanishes at $\zeta = 0$. Hence from (11.3−19): $q_1 = q_2$. Hence (11.3−26)

$$q = 2q_1 e^{pt} \cosh p T_L \zeta. \tag{11.3-28}$$

Putting h and q from (11.3−28), (11.3−27) in (11.3−18) gives

$$h_1/q_1 = -T_{sp}/T_L = -K.$$

(11.3-29)

Eqs. (11.3-27) and (11.3-28) give the desired relation between relative surge of pressure head h and relative increment of flow q on the turbine's end of penstock ($\zeta = 1$) as

$$h = -K \tanh(p\,T_L) \cdot q.$$

(11.3-30)

11.3.4.5. Relation for the controlled system

To obtain the desired relation $h(x, m)$, q in the last equation has to be expressed in terms of m and x. With the load degree $\lambda = P_T/P_N$, the efficiency parameter $K_\eta = \eta_N/\eta$ (η_N-efficiency at rated load), and the similarity law

$$Q = Q_{11}(n, m)\, D^2 (gH)^{1/2},$$

(11.3-31)

the following approximation for infinitesimally small ΔQ,

$$q = \Delta Q/Q_N = \lambda K_\eta \Delta Q/Q \approx \lambda K_\eta\, dQ/Q = \lambda K_\eta\, d \ln Q \tag{11.3-32}$$

$$= \lambda K_\eta\, d \ln[Q_{11}(n, m)\, D^2 (gH)^{1/2}] = \lambda K_\eta[dQ_{11}/Q_{11} + (1/2)\, dH/H]$$

$$= \lambda K_\eta[(n_N/Q_{11})(\partial Q_{11}/\partial n)_m\, dn/n_N + (m_N/Q_{11})(\partial Q_{11}/\partial m)_n\, dm/m_M + dH/2H],$$

the approximations $dn = \Delta n$, $dm = \Delta m$, $dH = \Delta H$ and $m = \Delta m/m_M$, $h = \Delta H/H$, and (11.3-13), the following intermediate result $q(x, h)$ is obtained

$$q = \lambda K_\eta(K_{Qn}x + K_{Qm} \cdot m + h/2). \tag{11.3-33}$$

Putting this relation into (11.3-30) gives the desired relation $h(m, x)$

$$h = -[\lambda K_\eta K(K_{Qn}x + K_{Qm}m) \tanh p\,T_L]/[1 + (K K_\eta \lambda/2) \tanh(p\,T_L)]. \tag{11.3-34}$$

From (11.3-17)

$$h = (2/3)[(T_a/\lambda)\, \dot{x} - (K_{\eta m} + K_{Qm})\, m + K_e x]. \tag{11.3-35}$$

Eliminating h in the last two relations gives the desired $m(x)$ relation of the controlled system, consisting of turbine (K_{Qn}, K_{Qm}, K_η, λ), penstock (T_L, K) and grid (K_e), as

$$(2/3)[(T_a/\lambda)\, \dot{x} - (K_{\eta m} + K_{Qm})\, m + K_e x][1 + (\lambda K_\eta K/2) \tanh(p\,T_L)]$$

$$= -\lambda K K_\eta(K_{Qn}x + K_{Qm}m) \tanh(p\,T_L). \tag{11.3-36}$$

11.3.5. Relation for closed control loop, stability parameters

Eliminating m and its derivative from (11.3-36) and (11.3-5) gives the differential equation for the closed loop

$$\frac{2 T_a}{3\lambda}\left[1 + \frac{1}{2} K_\eta K \lambda \tanh(p\,T_L)\right] \ddot{x} + \left\{ K_\eta K \lambda \left[K_{Qn} - \frac{K_{Qm}}{\delta_T}\right] \tanh(p\,T_L) \right.$$

$$+ \frac{2}{3}\left[\frac{K_{\eta m} + K_{Qm}}{\delta_T} + K_e\right]\left[1 + \frac{1}{2} K K_\eta \lambda \tanh(p\,T_L)\right] \right\} \dot{x} \tag{11.3-37}$$

$$+ \left\{\frac{2}{3} \frac{K_{\eta m} + K_{Qm}}{\delta_T T_i}\left[1 + \frac{1}{2} K K_\eta \lambda \tanh(p\,T_L)\right] - \frac{K_{Qm} K_\eta K \lambda}{\delta_T T_i} \tanh(p\,T_L)\right\} x = 0.$$

Imagine a closed control loop with the natural oscillation

$$x = A e^{(d + i\omega)t}, \tag{11.3-38}$$

in which d is the damping factor and ω the circular frequency. Inserting this in the foregoing relation yields an equation, whose imaginary and real parts have to be satisfied simultaneously. Assuming the circular frequency to be prescribed so as to avoid coincidence with the pipe's reflection time, and the damping factor prescribed also, the start up time T_a of the set and reset time T_i of the governor or after $(11.3-6)$ its rate time $T_b = T_i$ follow from the linear system of T_a and T_i^{-1}

$$T_a A + T_i^{-1} B = C, \qquad T_a D + T_i^{-1} E = F, \tag{11.3-39}$$

in which the coefficients A, B, C, D, E, F depend on the known or prescribed values $d, \omega, \delta_T, K_\eta, K_{Qm}, K_{Qn}, K_{\eta m}, K_{\eta n}, K, K_e, T_L$ by the following relations

$$A = \frac{2}{3\lambda} \left\{ (d^2 - \omega^2) \left[1 + \tan^2(\omega T_L) \tanh^2(d T_L) + \frac{\lambda}{2} K K_\eta \frac{\tanh(d T_L)}{\cos^2(\omega T_L)} \right] \right.$$
$$\left. + K d\omega \lambda K_\eta \frac{\tan(\omega T_L)}{\cosh^2(d T_L)} \right\}, \tag{11.3-40}$$

$$B = \frac{2}{3} \frac{K_{\eta m} + K_{Qm}}{\delta_T} \left[1 + \tan^2(\omega T_L) \tanh^2(d T_L) + \frac{\varrho}{2} \lambda K_\eta \frac{\tanh(d T_L)}{\cos^2(\omega T_L)} \right]$$
$$- \frac{\lambda K K_\eta K_{Qm}}{\delta_T} \frac{\tanh(d T_L)}{\cos^2(\omega T_L)}, \tag{11.3-41}$$

$$C = -\frac{2}{3} d \left[\frac{K_{\eta m} + K_{Qm}}{\delta_T} \right] \left[1 + \tanh^2(d T_L) \tan^2(\omega T_L) \right]$$
$$+ \frac{\lambda K_\eta K}{3} \left[\omega \frac{\tan(\omega T_L)}{\cosh^2(d T_L)} - d \frac{\tanh(d T_L)}{\cos^2(\omega T_L)} \right] \left[\frac{K_{\eta m} - 2 K_{Qm}}{\delta_T} + K_e + 3 K_{Qn} \right], \tag{11.3-42}$$

$$D = \frac{4}{3} \frac{\omega d}{\lambda} \left[1 + \tan^2(\omega T_L) \tanh^2(d T_L) + \frac{K}{2} \lambda K_\eta \frac{\tanh(d T_L)}{\cos^2(\omega T_L)} \right]$$
$$+ \frac{1}{3} K K_\eta (d^2 - \omega^2) \frac{\tan(\omega T_L)}{\cosh^2(d T_L)}, \tag{11.3-43}$$

$$E = \frac{K_\eta K \lambda (K_{\eta m} + K_{Qm})}{3 \delta_T} \frac{\tan(\omega T_L)}{\cos^2(d T_L)} - \frac{\lambda K_\eta K K_{Qm}}{\delta_T} \frac{\tan(\omega T_L)}{\cosh^2(d T_L)}, \tag{11.3-44}$$

$$F = -\frac{2}{3} \omega \left[\frac{K_{\eta m} + K_{Qm}}{\delta_T} + K_e + 3 K_{Qn} \right] [1 + \tan^2(\omega T_L) \tanh^2(d T_L)]$$
$$- \frac{1}{3} K K_\eta \lambda \left[\frac{K_{\eta m} - 2 K_{Qm}}{\delta_T} + 2 K_{Qn} \right] \left[d \frac{\tan(\omega T_L)}{\cosh^2(d T_L)} + \omega \frac{\tanh(d T_L)}{\cos^2(\omega T_L)} \right]. \tag{11.3-45}$$

The system (11.3 39) yields the starting time T_a, and hence the required moment of inertia of the set and the isostatic time of the governor needed to satisfy the set stability conditions (when d and ω are prescribed) as

$$T_i = \frac{AE - DB}{AF - DC},$$ (11.3-46)

$$T_a = \frac{CE - BF}{AE - BD}.$$ (11.3-47)

11.3.6. Special $h(q)$ relations at the lower penstock end

I. For incompressible fluid and a rigid duct: From (11.3-22), $T_L = L/a$, (11.3-20), (11.3-30) $h = - T_{sp}[\tanh(p\,T_L)/(p\,T_L)]\,q$. Hence for vanishing T_L which corresponds to an incompressible fluid in a rigid pipe, the relation (11.3-30) tends to

$$h = - T_{sp}\,q,$$ (11.3-48)

in which T_{sp} is the start up time of the penstock: $T_{sp} = Lc_N/(gH)$.

II. Double staged penstock: This task was solved by the author [11.57]. Assuming the upper reach of the penstock to have the parameters T_{Lo}, K_o, according to (11.3-20), at the lower reach to have T_{Lu}, K_u, accounting for the boundary conditions of constant pressure at the upper end, continuity at the joint of both the reaches and the fact that the pressure acts there into both the reaches with the same value, the desired $h(q)$ relation at the lower end of the whole penstock reads

$$\frac{h_u}{q_u}(\zeta_u = 1) = - K_o \tanh(p\,T_{Lo}) \frac{1 + \sinh(p\,T_{Lu})\,e^{pT_{Lu}}\left[1 + \dfrac{K_u}{K_o}\coth(p\,T_{Lo})\right]}{1 + \sinh(p\,T_{Lu})\,e^{pT_{Lu}}\left[1 + \dfrac{K_o}{K_u}\tanh(p\,T_{Lo})\right]}.$$ (11.3-49)

For the case of a vanishing lower pipe section, connected with vanishing time T_{Lu}, the terms in the square brackets become zero. Hence $\displaystyle \lim_{T_{Lu}=0} h_u/q_u = h_o/q_o(\zeta_o = 1) =$ $- K_o \tanh(p\,T_{Lo})$ as it must be, see (11.3-30).

11.3.7. Example

A Francis turbine set is given with $P_N = 150\ \text{MW}$; $n = 500\ \text{rpm}$; $H = 300\ \text{m}$; $a = 800\ \text{m/s}$; $L = 1000\ \text{m}$; $\delta_T = 0.3$; $c_N = 3.5\ \text{m/s}$; $K_e = 0$; $K_{\eta m} = 0$; $K_\eta = 1$; $\lambda = 0.8$; $K_{Qn} = 0$; $K_{Qm} = 0.8$. Hence $T_L = L/a = 1.25\ s$; $K = 0.95$; $T_{sp} = 1.19\ s$. The damping factor d is set so as to have during one period an attenuation of amplitude 0.4 of its initial value. Hence $d = - \omega\,ln2.5/(2\pi) = - 0.146\,\omega$. To avoid resonance between pipe oscillation and governor oscillation, the circular frequency is set to have no coincidence in its period T with the wave reflection time $T_r = 2L/a = 2.5\ s$ of the pipe. The ratio $T/T_r = 5.6$ is set at will. Thus $\omega\,T_L = 0.56$; $dT_L = - 0.082$. Hence $T_a = 5.55\ s$; $T_i = 2.58\ s$. This yields by (11.3-10) the moment of inertia of the set as $\Theta = 203 \cdot 10^3\ \text{kg m}^2$ [11.23; 11.57].

568

11.3.8. Theory of motion and resonance in the pipe system

I. Periodic motion in the penstock, surge tank and pressure tunnel: In (11.3–38) a harmonic motion of the control loop of a hydro turbine set has been assumed. This requires also a harmonic motion in the penstock. The natural period of a pipe starting from a large vessel (head pond, surge tank) equals twice the reflection time $T_r = 2L/a$ of a pressure pulse, which covers the pipe length L with the celerity a. Hence the period $T = 4L/a$.

In the following the period of the combined pipe system consisting of penstock, surge tank and pressure tunnel is considered. It is well-known that every time a valve at the lower end of a penstock is closed, periodic motion in the pipe line will result. It is here assumed that this so-called "pendulation" was produced some time before the instant under consideration and that a sinusoidal motion occurs at the valve.

A horizontal pipe line is assumed (see Fig. 11.3.1) with an ideal onedimensional flow. Pipe diameter and celerity are uniform along the pipe. (Gravity is neglected, as superimposable later on.) As is well-known, the wave equation, e.g. for the pressure pulse [5.3]

$$\partial^2 p/\partial x^2 - (1/a^2)\,\partial^2 p/\partial t^2 = 0, \tag{11.3–50}$$

has a solution

$$p = F_1(x + at) + F_2(x - at), \tag{11.3–51}$$

Fig. 11.3.1. Scheme of the usual pipe system. 1 penstock, 2 surge tank, 3 tunnel.
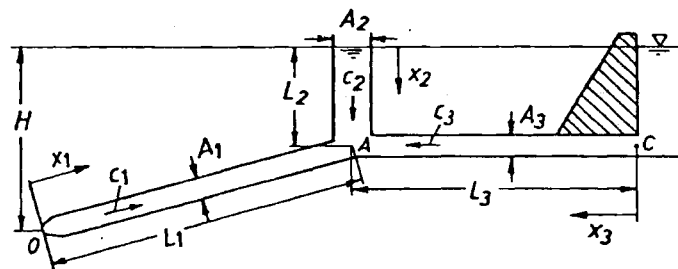
where F_1 and F_2 are arbitrary functions of the arguments '$x + at$' and '$x - at$', respectively. This reflects the fact, that any pressure distribution $p(x)$ along the pipe axis is propagated as a whole and without deformation, at a velocity a, either in $+x$ or $-x$-direction.

A sinusoidal motion is described by $p = A_1 \sin m(x + at) + A_2 \sin m(x - at)$. To satisfy the boundary condition of a constant pressure p_0 at the upper end, the amplitudes A_1 and A_2 must be identical: $A_1 = A_2 = A$. Moreover the eigenvalue m must be an integer multiple n of $\pi/2$. Assuming $n = 1$, a simple transformation leads to the following pressure p and velocity c at any point with the abscissa x (originating from the lower end of the pipe), at time t (standing wave)

$$p = p_0 + 2A \cos \frac{\pi x}{2L} \sin 2\pi \frac{t}{T}, \tag{11.3–52}$$

$$c = \frac{2A}{a\varrho} \sin \frac{\pi x}{2L} \cos 2\pi \frac{t}{T}.$$

Note that the latter relation satisfies a disappearance of the velocity at the lower end $x = 0$ due to the closed valve.

More generally, with $m = 2\pi/T$ as the cyclic frequency of the oscillation, pressure and velocity read as follows

$$p = p_0 + 2A \cos m \frac{x}{a} \sin mt, \qquad (11.3-53)$$

$$c = \frac{2A}{a\varrho} \sin m \frac{x}{a} \cos mt. \qquad (11.3-54)$$

The most important case to be examined is the resonance occurring in a system of pipe lines. The discussion will be illustrated assuming a system of three pipe lines, joining at point A (Fig. 11.3.1). The valve is supposed to be located at point 0, at the bottom of pipe 1 (the penstock). Pipes 2 and 3 are open at their upper ends, where waves are totally reflected with change of sign. Such a system would represent a conventional arrangement of pressure tunnel (pipe 3), surge tank (pipe 2) and pressure pipe or penstock (pipe 1) in a hydropower station.

The theoretical period of pipe 1, length L_1, is $T_1 = 4L_1/a_1$. According to *Jaeger* [8.85], the apparent period of the system is $T = T_1(1 + \varepsilon)$, its cyclic frequency $m = 2\pi/T_1(1 + \varepsilon)$.

With the above the pressure in pipe 1 becomes $p_1 = 2A \cos m x/a_1 \sin mt$. For the other pipes, the coordinate x starts at the upper end. To ensure a vanishing variable pressure term there, the pressures at the stations x in pipe 2 and pipe 3 are chosen as follows: $p_2 = 2B \sin mx/a_2 \sin mt$, $p_3 = 2C \sin mx/a_3 \sin mt$. Both also satisfy the wave equation (11.3–50). Identity of pressure for all the three pipes at the point of bifurcation A is expressed by

$$A \cos m L_1/a_1 = B \sin m L_2/a_2 = C \sin m L_3/a_3. \qquad (11.3-55)$$

From the pressures p_2 and p_3 the equation of motion $\partial p/\partial x + \varrho \partial c/\partial t = 0$ yields the velocity at the bifurcation A

$$c_2 = - [2B/(\varrho a_2)] \cos m L_2/a_2 \cos mt, \qquad (11.3-56)$$

$$c_3 = - [2C/(\varrho a_3)] \cos m L_3/a_3 \cos mt. \qquad (11.3-57)$$

Since all the coordinates x_i are oriented towards the point A, continuity requires (see also [5.3])

$$c_1 A_1 = - c_2 A_2 - c_3 A_3, \qquad (11.3-58)$$

where A_1, A_2, A_3 are the respective cross sectional areas of the pipes. Using (11.3–55) through (11.3–57), $c = c_1$ from (11.3–54) with $m = m_1$, $a = a_1$, $x = L_1$, continuity yields

$$(A_1/a_1) A \sin m L_1/a_1 = (A_2/a_2) B \cos m L_2/a_2 = (A_3/a_3) C \cos m L_3/a_3. \qquad (11.3-59)$$

Dividing the last equation by $A \cos m L_1/a_1$ and its equivalents according to (11.3–55), and introducing the cyclic eigenfrequency

$$m = 2\pi/T = \pi a_1/[2L_1(1 + \varepsilon)], \qquad (11.3-60)$$

yields, according to *Jaeger* [8.85], the following relation for ε which facilitates the calculation of the period T of the system by means of $T = 4L_1(1 + \varepsilon)/a_1$

$$\tan \frac{\pi}{2} \frac{1}{1 + \varepsilon} = \frac{A_2 a_1}{A_1 a_2} \cot \frac{\pi}{2} \frac{L_2 a_1}{L_1 a_2} \frac{1}{1 + \varepsilon} = \frac{A_3 a_1}{A_1 a_3} \cot \frac{\pi}{2} \frac{L_3 a_1}{L_1 a_3} \frac{1}{1 + \varepsilon}. \qquad (11.3-61)$$

During surge tank oscillations the length L_2 varies between given limits. Since the period of these oscillations is much longer than that of the water hammer considered, L_2 may be assumed as constant. As shown by *Jaeger* [8.85] the usual wide low surge tank $(A_2/A_1 > 5, L_1/L_2 > 30)$, and neglecting the now vanishing cot term results in the following small ε:

$$\varepsilon = (A_1/A_2)(L_2/L_1). \tag{11.3-62}$$

The condition for a cot function to be equally negligible is that

$$\frac{\pi}{2}\frac{L_3 a_1}{L_1 a_3} = \frac{\pi}{2}(1 + 2K), \tag{11.3-63}$$

where K is an integer. L_3/a_3 and L_1/a_1 are the time periods, a pressure pulse needs to cover the tunnel 3 or the penstock 1. Since $1 + 2K$ is an odd number, the last condition indicates that the pressure tunnel allows only odd harmonics of the penstock. When this condition exists, the resonance of the fundamental of the pipe is possible and the maximum pressure at point A, intersection of the surge tank, is given by

$$\Delta p = A \cos\frac{\pi}{2(1 + \varepsilon)}. \tag{11.3-64}$$

Strictly speaking this differential pressure also influences surge tank oscillations. These are superimposed on the water hammer oscillations. The latter are short period oscillations. Frequently they have died down before the long period oscillation of the surge tank starts. Contrary to water hammer which originates from compressibility and energy, the surge tank motion results from inertia force and gravity. Note that the construction of the tunnel and the surge tank also has to withstand the case of an eventual resonance with respect to fatigue effects on the lining.

II. Surge tank oscillation: In the analysis which follows and which relates only to surge tanks fed by tunnels under pressure, it has been assumed, that the tunnel walls are inelastic and that the water is incompressible. This means that the water along the whole length L of the tunnel behaves like an incompressible solid. Mathematically $\partial c/\partial x = 0$ or $c = \text{const}$ for the whole tunnel length.

The following additional assumptions are made:

1) The velocity head $c^2/2g$ in the tunnel is negligible.
2) The mass of the water in the surge tank is negligible.
3) The value of the frictional resistance of the water in the tunnel is the value for steady flow. Its head loss is proportional to c^2 or ζc^2. Then the equation of motion for the level of the surge tank, a distance z from its position at zero flow Q (in the penstock), reads in the form of a difference equation

$$(L/g)\,\Delta c/\Delta t + z_M \pm \zeta c_M^2 = 0. \tag{11.3-65}$$

To this comes the continuity

$$c_M A_t = Q_M + A_{sM}\,\Delta z/\Delta t, \tag{11.3-66}$$

where Δt is the time interval considered, A_{sM} the mean horizontal cross sectional area of the surge tank during Δt, A_t the mean value of the cross section of the tunnel in cases where this section is variable, $z_M = z_i + \Delta z/2$, $c_M = c_i + \Delta c/2$, $Q_M = (Q_i + Q_{i+1})/2$. The index i denotes the time t_i at the beginning of the interval Δt considered. Equation (11.3-66) yields

$$\Delta z = (A_t/A_{sM})\,c_i\,\Delta t + (A_t/2A_{sM})\,\Delta c\,\Delta t - (Q_M/A_{sM})\,\Delta t.$$

Substitution of Δz in equation (11.3-65) leads to the following second degree equation for Δc

$$a(\Delta c)^2 + b\Delta c + f = 0,$$ (11.3-67)

$$a = \mp \zeta/4,$$ (11.3-68)

$$b = [L(q\Delta t) + A_t \Delta t/(4 A_{sM}) \pm \zeta c_i].$$ (11.3-69)

$$f = z_i + A_t c_i \Delta t/(2 A_{sM}) - Q_M \Delta t/(2 A_{sM}) \pm \zeta c_i^2.$$ (11.3-70)

Frequently, according to *Jaeger* [8.85] the first term $a(\Delta c)^2$ is small compared with the other two, and sufficiently accurate results may be obtained from

$$\Delta c = -f/b - (a/b)(f/b)^2.$$ (11.3-71)

Usually the course of the flow $Q_i(t)$ follows from the regulation of the turbine. The crucial events for a surge tank are start and shut down of the whole plant and this in a rapid sequence as it may happen in peak load plants. Hence the cross sectional area or the design of the surge tank has to be fixed so that in any case the amplitudes of its oscillations are kept within prescribed limits.

11.4. The electric machine (generator, alternator, motor)

11.4.1. Survey

11.4.1.1. General remarks

The speed of a hydroturbine results from its head, flow and specific speed. The head follows from the topography of the site and yields also the specific speed, after a side glance at the flow rate. On the other hand, the speed of the usual alternator results from its grid frequency. In high-speed machines of higher head, these electrically permitted speeds are staged rather widely. Thus the design of a hydroturbine has to follow the speed requirements of its alternator.

This situation is somewhat contrary to that of a thermal turbo-set, which has a more or less standardized speed subsequent to its standardized stages of pressure drop and output, to which the design can be adapted at will, and which leads to a more or less standardized alternator of drum armature design.

From the preceding remarks it could be concluded that this problem of mutual adaptation of hydraulic and electric machine could be eliminated by generating an AC with a desired frequency, which afterwards by means of thyristor techniques, were to be converted to that of the existing grid.

As the following might show, also then some problems would remain, to adapt both machines to each other.

Especially at higher head, the high density of water results in a high power/mass ratio of the turbine runner. This is contrary to the low power/mass ratio of the electric rotor, which results from the modest force density in consequence of the low magnetic flux density and the limited current density. The latter issues from the temperature limits imposed by the insulating material.

As a result, the generator rotor often has a rather large weight and a corresponding diameter compared to the turbine runner. On the one hand, the large fly-wheel mass combined herewith is needed to stabilize the speed control, or to limit the overspeed after a sudden load rejection during a prescribed closing time of the turbine's main valve. Since a certain closing speed results from the admissible pressure surge due to water hammer of the piping, a relatively large generator rotor would compensate troubles originating from the hydraulics.

572

On the other hand the exposure of the rotor to runaway in consequence of too long a closing time (or even by possible failure of the shut down device), in connection with its large diameter and its limited material strength, imposes a restriction on the rated speed of the generator. Hence for a generator with limiting output and somewhat elevated rated speed, the output decreases considerably with rising speed.

Because of the high specific heat of water, and the large flow rate, the water turbine shows no problems caused by temperature rise due to waste heat as a consequence of its losses.

Contrary to this, the sensitivity of the insulation with regard to high temperature, a low specific heat of conductor and iron and the surrounding air, in connection with the small heat transfer coefficient from metal or insulating material to air makes effective and economic cooling of the generator a crucial problem when the machine is of the limiting output type.

To keep its mass in economic limits, the alternator requires here internal cooling by water, being thus "converted" almost to a hydraulic machine. The problem is aggravated by the large diameter (size) of the alternator. This makes its surface/volume ratio very small. Since any emission of waste heat has to pass the now limited surface of the generator, any effective cooling is impeded.

The following example may highlight the situation. Consider a design of a set with limiting output equipped with a high-head Francis turbine and horizontal shaft. Putting aside the problems of critical speed, bearing arrangement and varying the shaft diameter, it is easily possible to double the output of the turbine runner by means of a back to back arrangement with a double flow runner having the same diameter as before. Restricted heat flow and limited temperature would not allow a similar measure for the generator.

The evident feature of hydro turbo generators contrary to that of thermal turbo sets is the wide variety of speeds and the resulting salient pole design of its armature. In the low head range, the overhung construction with umbrella or semi-umbrella design of the rotor is another speciality. In the "Straflo" design for lowest heads, the discharge of water passes the bore of the stator, thus cooling it effectively.

11.4.1.2. Output as a function of speed

Because of physical limitation imposed by the mechanical properties of materials, the maximum output of a hydroelectric machine with limiting output is related to its rotational speed n (rpm), e.g., 15 MW at 1500 rpm, 250 MW at 600 rpm, up to a maximum of 1000 MW at 120 rpm according to the estimates of *Foster* [11.61].

Consequently, at sites with large potential power, the speed of the turbines has been chosen in the 100 to 375 rpm speed range to reduce the number of sets (Cap. 4.3) for the same installed capacity.

The maximum output/speed characteristic for air and water-cooled generators is given in the Fig. 11.4.1. This is based on a turbine runaway speed of 180% of the rated speed and normally accepted safety factors. Moreover a difference is made between conventional generators and motor generators of pumped storage sets with either pump-turbines (binary sets) or separate pump and turbine (ternary or tandem sets).

11.4.1.3. Water cooling

Water cooling can increase the output limit at a given speed by about 60% or, alternatively, for a given combination of rated output and speed, a physically smaller machine can be installed. This would also present a change in the losses in the machine, particularly a reduction in no load losses. Depending on their evaluation the extra cost, if any, of water cooling can be offset by the capitalization of the reduction in loss.

A number of direct-water-cooled hydroelectric machines have already been installed. Of these some are only to gain operational experience in the technique involved (e.g., Bavona or Tonstad), while
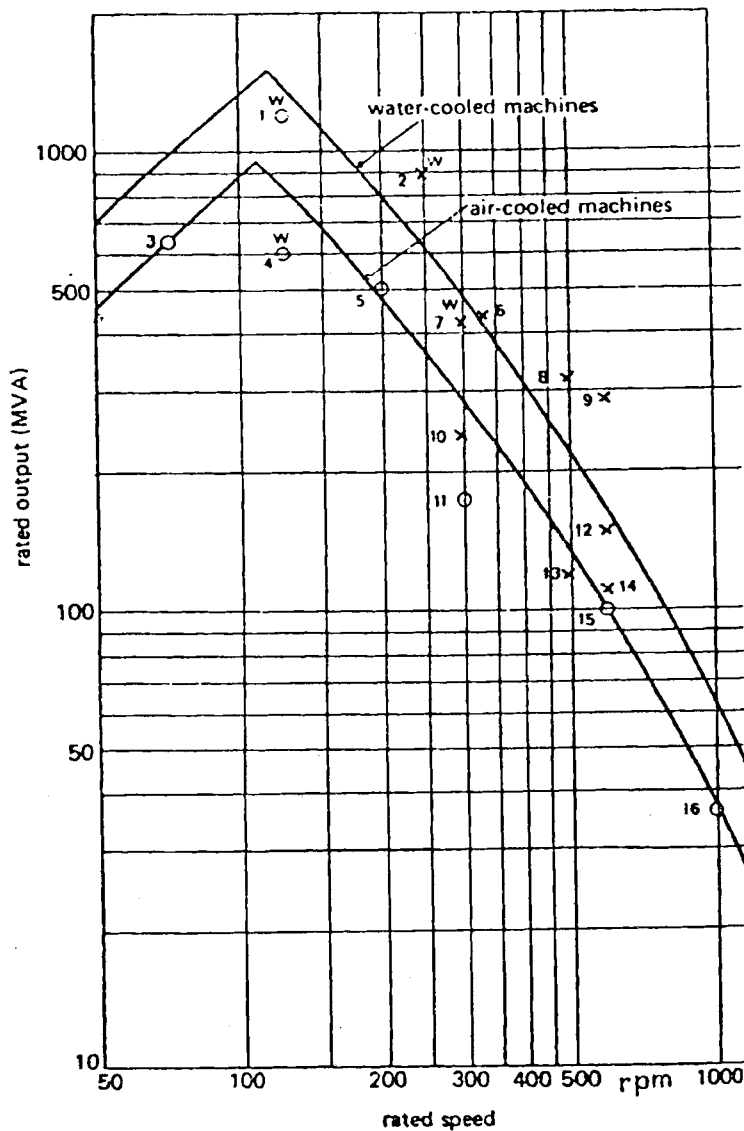
Fig. 11.4.1. Output limits for hydroelectric generators based on the assumption that the overspeed ratio equals 1.8, and the maximum stator core length equals 4 m. 1 Lower Lena (projected), USSR; 2 6 Craig Royston (projected) UK; 3 Grand Coulee USA; 4 Krasnoyarsk, USSR; 5 Churchill Falls, Canada; 7 Racoon Mountain, USA; 8 Dinorwic, UK; 9 Hornberg, Germany; 10 Capljina, Yugoslavia; 11 Dehar, India; 12 Parabky-Zar, Poland; 13 and 14 Cruachan, UK; 15 Tierfehd, Switzerland; 16 Filisur, Switzerland; w water-cooled; x motor generator; o true generator.

others were built because, the combination of speed and output are beyond the capacity of an air-cooled machine, e.g., Wehr ($P = 254$ MW, $n = 600$ rpm), Krasnoyarsk ($P = 507$ MW, $n = 107$ rpm), Silz ($P = 265$ MW, $n = 500$ rpm), Malta main stage ($P = 208$ MW, $n = 500$ rpm), Itaipú ($P = 730$ MW, $n = 90,2$ rpm or 93,2 rpm respectively).

11.4.1.4. Pumped storage motor-generators

The advent of the successful reversible Francis type pump-turbine has provided impetus for some powerful sets. In these schemes the net head affects the choice of speed. The mechanical design is eased because of the lower overspeed ratio, namely 1,5 for a high head pump-turbine compared with 1,8 for a Francis turbine. This originates from the relatively smaller radial extension of a high head Francis turbine rotor.

The specific output per pole has reached about 35 MVA per pole. Direct water cooling will further increase this value.

High efficiency machines are required and there is the possibility of abnormal wear, compared with conventional hydrogenerators, on all components due to their frequent

operation which may entail starting and stopping 10 times a day. With a reversible set the following additional factors affect the generator design: hydraulic machine characteristics, dual rotation, methods of starting the units in the pumping mode.

The present insulation design provides a built-in overload capacity, which can sometimes be used by operating the turbine at a gate opening greater than the specified one. Pumped storage involves frequent mode changes, starts and stops, and even reversal of rotation and in aggregate these will amount to several thousand significant load changes per annum. The epoxy-resin-based insulation system is designed to withstand this rapid cyclic duty.

11.4.1.5. Special machines for low head   -

The rim generator of Straflo turbines (Cap. 10.2) could prove to be the economic means of generating electric power from the tides at selected sites, including several river estuaries, in the UK. Ratings of up to 50 MVA at 60 rpm have been considered. Such generator would have a rotor diameter of 12 m. This design combines excellent cooling by the discharge passing the rotor bore with an easy accessibility of the alternor. Highest possible natural fly-wheel mass ensures stable regulation.

11.4.1.6. Operating regimes

In the past, very many hydroelectric installations were built as base load stations, but with the changing pattern of generating capacity in an interconnected system, attention is being given to re-assessing the role of these existing machines. In many cases it would be more economical to operate the sets as peak-load stations with the added security of quickly available standby capacity. To achieve this, would mean increasing the installed capacity by 25 to 50 per cent and running at reduced load factor φ; see also [11.61].

Increasing the rating of the station could be achieved in a number of ways among which uprating the existing generators is immediately attractive. Replacing the existing bitumen based stator windings by modern epoxy windings would permit a substantial increase in permissible rating both by increasing the volume of copper in the machine and by providing an insulation system of much improved thermal conductivity.

11.4.1.7. Computerized design

Computer techniques for the electromagnetic and mechanical design calculations are increasingly being developed and these enable more detailed design studies to be carried out before the final design is established [11.60].

11.4.2. Alternator, electric features

The alternator consists of a rotor as a carrier of a magnetic field with a magnetic flux Φ. This is obtained by a certain number p_p of pairs of DC excited poles uniformly distributed around the circumference of the rotor.

The rotor is driven by the hydroturbine. This has a speed n [rpm], resulting from its head H and its essentially head-conditioned unit speed n_{11} (see Cap. 9.2) and a nominal diameter D_T (from now on instead of D which henceforth denotes the diameter of the alternator rotor) of the turbine runner. Thereby the magnetic field of the poles, uniformly distributed around the circumference, induces in the z_p windings of the p_p pairs of poles an effective internal voltage (in volts)

$$E = C_0 n z_p p_r \Phi,$$

where C_0 is constant $= 0{,}517 \cdot 10^{-9}$, and Φ the effective magnetic flux in Maxwell, harmonically varying around the circumference.

The grid frequency f, the number of pole pairs p_P, and the speed n or the angular velocity of set ω are related by

$$f = n p_P / 60 = \omega p_P / (2\pi).$$

(11.4–2)

In rare cases with large variations of head and thereby widely changing optimum speed n, the speed and the number of pole pairs either in the rotor or in the stator of alternator may be changed at will in two steps, especially when the machine is a motor-generator of a pump-turbine used for turbine and pump operation, see Cap. 11.4.7.

When the alternator is loaded with its current I, then the internal voltage E differs from the effective voltage U at the alternator terminals by the following voltage drops to be subtracted vectorially (Fig. 11.4.2): 1) $2\pi f (X_\sigma + X_a) I$, due to the synchronous reactance and with 90° lead against the current I, where X_σ is the reactance due to the stray field of the stator and X_a that due the armature reaction, 2) $I R$ due to ohmic resistance R of alternator circuit (usually unimportantly small) in phase with the current I ($v = 2\pi f$).
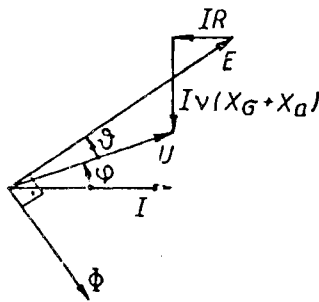
Fig. 11.4.2. Vector diagram of an alternator. Θ effective magnetic flux; U effective voltage at the generator terminals; I effective current; X_a reactance due to the armature reaction; X_σ reactance due to stray field of the stator; φ phase shift angle; E effective inner voltage.

Obviously (Fig. 11.4.2) a phase shift φ between U and I results from this. The internal voltage E depends on the magnetic flux Φ and hence can be regulated by variation of the exciting current I_{ex}. This is DC and supplied by the exciter, usually a stationary device, but sometimes a rotary machine at the shaft's end [11.77; 11.78].

From the vector diagram (Fig. 11.4.2) it is seen, that in the case of parallel operation of alternators, the angle ϑ between E and U depends on the current I. If ϑ is too large, the alternator may fall out of step, which must be avoided by regulation.

The phase angle φ between U and I and hence the power factor $\cos\varphi$ depend on the excitation current. Therefore the latter has to be regulated as a function of the load.

Usually three phase current is generated, occasionally also single phase current for traction power. In the case of a three phase alternator, the terminal output results from the current I and either the star voltage U_s or the delta voltage U_Δ by

$$P = 3 U_s I \cos\varphi = \sqrt{3}\, I U_\Delta \cos\varphi.$$

(11.4–3)

Besides regular operation sometimes the idling generator is used to balance the reactance power on the line by so-called 'condenser' or 'phase shifter' operation, which the emptied hydraulic machine has to withstand [10.138]. As a "spinning reserve" also standby operation is practised.

The terminal voltage U has to be kept constant by regulation of the exciter. The operating voltage ranges from 3 to 26 kV at frequencies of $16\frac{2}{3}$, 50 or 60 Hz. For smaller machines standardized

voltages are recommended. Optimum magnetic and electric utilization of the machine is achieved. when the voltage can be freely selected. According to experience, the voltage increases with the output P. This can be approximated by a logarithmic law $P/P_0 = ln(U/U_0)$, where P_0 and U_0 are the output and voltage of a certain plant.

Excepting traction power with its grids of 16⅔ and 25 Hz, the frequency of AC grids is standardized at 50, or 60 Hz. Therefore regulation of an alternator to cover a certain load demand implies constant terminal voltage under nearly constant speed according to (11.3–2) and the proportional band (permanent speed droop) of the governor (see 11.2).

11.4.3. Design features with respect to critical speed

I. General remarks: The design of alternator rotor, its shaft and bearings is influenced by the effort, to shift the critical speed to the desired high level (usually above runaway) at reduced cost. Therefore low head sets with low runaway speed show in general the two bearing design with an overhung arrangement of turbine runner and alternator rotor. In order to reduce the distance of the rotor's centre of gravity from the guide bearing centre, the umbrella or semi-umbrella design (Fig. 10.2.1.3) is preferred.

The shortening of this distance also under higher head, when the large rotor mass then does not allow this design, is one of the decisive needs for a high critical speed. Moreover such a speed requires also a small mass of alternator rotor. As the latter is always larger than that of turbine runner, the design has to be focussed on this small distance between rotor and its adjacent guide bearings.

The dominating mass of alternator rotor is a typical feature of hydroturbine sets especially in the high head range. It requires corresponding machine tools, partly fabrication on site, a stress relief oven there, or transportation facilities with sufficient loading gauges, also cranes at the shop and site respectively, depending on the construction and the mode of rotor fabrication (in shop or on site) as well as on the existence of a satisfactory erection bay.

II. Fly-wheel effects: The big rotor mass suits the large moment of inertia often required for stable speed control and for limitation of overspeed after sudden load rejection. This holds especially for smaller and high-speed units.

The fly-wheel effect of the rotor also effects the torsional vibration and thus the dimensioning of the shaft in some cases. The shaft diameter should then be selected so that no danger occurs in the case of short circuit or faulty synchronization and the critical torsion speed range is avoided when the torque varies.

If the synchronous machine can be dimensioned for optimum electrical and magnetic utilization, without mechanical overstressing, the rotor has the so-called natural fly-wheel effect.

If a fly-wheel effect greater than the natural one is required, it is necessary to increase the bore diameter so far as mechanical stresses permit (so-called fly-wheel type rotor).

If it is desired to retain the bore diameter corresponding to the natural fly-wheel effect, the required $m_R R^2$ can be achieved by an additional fly-wheel with a diameter larger than that of the stator bore. For reasons of accessibility in vertical sets, this fly-wheel is installed underneath the bore. It is then no longer possible to install and dismantle the complete rotor (+ fly-wheel) through the stator bore.

The physical origin of the large rotor mass in relation to that of the turbine runner, especially striking at high-head machines, results on the one hand from the modest strength of the magnetic field in iron even under saturation. On the other hand it results from the limited admissible density of current in the conductor, to avoid heat stresses and damage of insulation by waste heat. As a result the force between rotor and stator is combined with a rather low pressure (1 to 2 bar) of the conductor bars on the radial walls of the notches. This could be overcome by cryogenics.

Against that the hydraulic reaction turbine at a head H has a differential pressure about $\varrho g H$ on the rotor vanes, yielding up to 70 bars. Moreover the propelling force on the runner is extended over the whole vane-filled space of the rotor, whereas in the alternator rotor it is limited to the surface near the gap between rotor and stator.

III. Shaft diameter due to critical speed and rotor mass: The shaft diameter is usually determined by the need, to set the lowest critical speed ω_{cr} due to flexural vibrations somewhat above the runaway speed ω_{ra} (see also Cap. 10.5). According to the similarity laws (Cap. 9.2)

$$\omega_{ra} = 2^{3/2} i \, Ku (gH)^{1/2}/D_T, \tag{11.4-4}$$

where D_T is from now on the runner diameter of the turbine, Ku its rated blade speed coefficient, and i its runaway to rated speed ratio (a type-conditioned figure).

The critical speed ω_{cr} is mainly determined by the imaginary deflection f of the horizontally assumed shaft under the weight m_a of the alternator rotor, according to

$$\omega_{cr} = \text{const} (g/f)^{1/2}. \tag{11.4-5}$$

The mass of the rotor, density ϱ_R, axial length L, diameter D (from now on), with L/D as a design feature, may be expressed by

$$m_a \sim \varrho_R D^3 (L/D). \tag{11.4-6}$$

With a distance between the centre of the bearing and the rotor proportional to L, an area moment of inertia of the shaft, diameter d_{sh}, proportional to d_{sh}^4, the shaft deflection becomes

$$f \sim g \varrho_R (D/d_{sh})^4 (L/D)^2 L^2/E, \tag{11.4-7}$$

where E is Young's modulus of the shaft. Inserting this in (11.4-5), gives the lowest order critical speed

$$\omega_{cr} = \text{const} (d_{sh}/D)^2 (D/L) (E/\varrho_R)^{1/2}/L. \tag{11.4-8}$$

Introducing the mass of the turbine runner, diameter D_T, axial depth L_T, density ϱ_R, in the same way as that of the alternator rotor after (11.4-6), the ratio of the 2 rotor masses reads

$$\mu^* = m_a/m_T = (L/D) (L_T/D_T)^{-1} (D/D_T)^3. \tag{11.4-9}$$

Safe operation requires

$$\omega_{cr}/\omega_{ra} = \text{const (in general)} \geq 1. \tag{11.4-10}$$

Inserting (11.4-4) and (11.4-8) in (11.4-10) and expressing D/D_T from (11.4-9) brings the shaft to rotor diameter ratio

$$d_{sh}/D = \text{const} (i \, Ku)^{1/2} (\varrho_R gH/E)^{1/4} (L/D)^{5/6} (L_T/D_T)^{1/6} \mu^{* \, 1/6}. \tag{11.4-11}$$

The upper limit of d_{sh}/D depends on the rotor type (Cap. 11.4.7).

11.4.4. Dimensioning the alternator rotor

I. Diameter of the alternator rotor: Calculating the diameter D has to start from the turbine-conditioned runaway speed ω_{ra} being i times the rated speed ω (hence in terms of angular velocity). Thus $\omega_{ra} = i\omega$. Rotor dimensioning may start from the admissible stress σ_{ad} of a critically stressed element, usually on the outermost diameter D. Accounting for fatigue and notch effects by a factor k, then in a limiting design

$$D = 2[(\sigma_{ad}/\varrho_R)/k]^{1/2}/(i\omega), \tag{11.4-12}$$

where ϱ_R is the mean rotor density.

578

Then the diameter D_T of the turbine runner follows from the head H and the flow Q, the hence given type number n_q (Cap. 9.2), the resulting angular velocity ω and blade speed coefficient Ku by means of

$$D_T = 2^{3/2} Ku(gH)^{1/2}/\omega.$$

(11.4–13)

To facilitate, in the case of a vertical set, dismantling and assembly of the runner (for reasons of submergence at the bottom of the set's pit) by lifting it through the bore of the alternator stator, the following condition must be satisfied (if ignoring step up gears.)

$$D > D_{Tm},$$

(11.4–14)

where D_{Tm} is the maximum runner diameter. This is usually satisfied if designs of very low head are exempted. On the other hand D and with it the outmost stator diameter should allow a convenient placing of two adjacent alternators within a distance given by the lateral width required by the spiral chamber or its equivalent (see Cap. 4.2).

II. The iron length L of the alternator rotor: On the one hand this results from the rotor's required moment of inertia Θ. Expressing this by $\Theta = k_1 \varrho_R L D^4$, with k_1 as a design-linked parameter, accounting for the start up time of set T_a required (Cap. 11.3), with the parameter k_3 due to the torque vs speed graph and the shaft efficiency η_T of the turbine, the equation of motion of the starting set gives for the iron length L of a rotor, which has the so-called natural fly-wheel effect, the following expression

$$L = P_T T_a/(\varrho_R k_1 \omega^2 D^4) = k_3 \varrho Q g H \eta_T T_a/(\varrho_R k_1 \omega^2 D^4).$$

(11.4–15)

With the requirements of magnetic flux and current coverage of the alternator, the latter's output $P_a = P_T \eta_G$, its speed $n = 30\omega/\pi$, the pole pair number p_p, the rotor length however becomes

$$L = P_a/(C p_p D^2 n) = \pi P_a/(30 p_p D^2 \omega C).$$

(11.4–16)

The parameter C (kW/(m^3 rpm)) depends on such features as the permissible temperature rise ΔT, the terminal voltage and an iron filling factor for bundle lamination of the stator [11.83]. In the case of water cooling C may be raised by about 60%.

ω, f and p_p in (11.4–2), L in (11.4–15) and (11.4–16) and ω in (11.4–12), (11.4–13), (11.4–15), (11.4–16) must be compatible with each other in a limiting design.

11.4.5. Alternator output as a function of working data

I. The output: By means of the similarity laws (Cap. 9.2), the flow Q reads: $Q = Q_{11} D_T^2 (gH)^{1/2}$, where Q_{11} is the unit flow and D_T the runner diameter of the turbine. Introducing this in (11.4–15) gives the iron length L, which the turbine needs for a certain start up time T_a of the set due to a stable regulation. Putting this in (11.4–16), and using for the number of pole pairs p_p the relation (11.4–2), the generator output becomes

$$P_a = 60 f C \eta_T (gH)^{3/2} \varrho k_3 Q_{11} T_a (D_T/D)^2/(k_1 \varrho_R \omega^2).$$

(11.4–17)

It should be noted that C has the dimension kg/(m/s^2) (in practice kW min/m^3).

Accounting for (11.4–8) and (11.4–4), the required distance of the lowest critical speed due to flexural vibrations of the set from its runaway speed according to (11.4–10) yields

$$(D_T/D)^2 = 8 i^2 Ku^2 (D/d_{sh})^4 (L/D)^4 g H \varrho_R/E.$$

(11.4–18)

This in (11.4–17) gives the alternator output the form (Q_{11} due to rated flow)

$$P_a = 480 \eta_T k_3 Q_{11} i^2 K u^2 (D/d_{sh})^4 (L/D)^4 (T_a/k_1) (\varrho/E) (g H)^{5/2} f C/\omega^2. \quad (11.4-19)$$

By the similarity laws (9.2) the specific head gH can be reduced to the runner blade speed coefficient Ku: $gH = (\omega D/2)^2/(2 Ku^2)$. The strength of the generator rotor under runaway requires according to (11.4-12) the following linkage of the circumferential rotor tip speed $\omega D/2$ and the admissible stress σ_{ad}: $(\omega D/2)^2 = \sigma_{ad}/(k \varrho_R i^2)$, where ϱ_R is the rotor density and i the runaway to rated speed ratio. Both the last relations give

$$gH = [\sigma_{ad}/(k \varrho_R)]/(2 i^2 Ku^2). \quad (11.4-20)$$

Putting this in (11.4-19) the alternator output becomes

$$P_a = \frac{85 \eta_T Q_{11} k_3}{k_1 i^3 Ku^3} \left(\frac{D}{d_{sh}}\right)^4 \left(\frac{L}{D}\right)^4 \left(\frac{\sigma_{ad}}{k \varrho_R}\right)^{5/2} \frac{\varrho Cf T_a}{E \omega^2}. \quad (11.4-21)$$

In a limiting design, now considered, D/d_{sh} and L/D are more or less constant. For a reaction turbine the speed coefficient Ku and the runaway to rated speed ratio i rise slightly with the type number n'_q (Cap. 9.2). It is seen, that P_a is proportional to the line frequency f and the design factor C. The latter can be raised by 60% in the case of a water cooling. Hence the output of an alternator, keeping everything else constant, is mainly inversely proportional to the squared speed ω.

In a real design, this holds only from a certain minimum speed on. Below the latter, the output depends otherwise on the speed ω of the set. Strictly speaking in a limiting design, $P = P(\omega)$, (see Fig. 11.4.1). Hence by means of the similarity laws, the type number n'_q can be expressed as follows as a function of the angular velocity and the head

$$n'_q = \omega (P(\omega))^{1/2}/[(\eta_T \varrho)^{1/2}(gH)^{5/2}]. \quad (11.4-22)$$

In the case of a large reaction turbine, the submergence links a given head gH to a certain type number n'_q (Cap. 9.2). At given ϱ, η_T, n'_q and gH the last relation can be considered as a limiting relation for the speed ω. The latter must be adapted to the line frequency f by means of (11.4-2). Then the output follows by means of $P(\omega)$ according to (11.4-21).

II. The output as a function of the mass ratio μ^* (11.4-9) and cooling: Inserting (11.4-20) in (11.4-11) gives

$$(d_{sh}/D)^4 \sim (\sigma_{ad}/(k E)) (L/D)^{10/3} (L_T/D_T)^{2/3} \mu^{*\,2/3}. \quad (11.4-23)$$

This in (11.4-21) shows that the output is inverse to μ^*

$$P_a = \text{const} \frac{\eta_T Q_{11} k_3}{k_1 i^3 Ku^3} \left(\frac{\sigma_{ad}}{k \varrho_R}\right)^{3/2} \left(\frac{L}{D}\right)^{2/3} \left(\frac{L_T}{D_T}\right)^{-2/3} \frac{\varrho}{\varrho_R} \frac{Cf T_a}{\omega^2} \mu^{*-2/3}. \quad (11.4-24)$$

The latter relation is valid only for an alternator whose outermost parts operate with a stress-limited peripheral velocity at runaway. Below a certain speed ω and for a rotor whose tip diameter is limited by manufacture and portability, the limit of alternator output does not depend in inverse proportion on the speed of the set (see Fig. 11.4.1).

With the specific loss h'_i, the heat flow $h'_i P_a$ has to cross a surface $\sim DL$ by means of a heat transfer coefficient α at a temperature difference ΔT. Hence the squared diameter of the alternator rotor

$$D^2 = \text{const}[h'_i P_a/(\alpha \Delta T)] D/L. \quad (11.4-25)$$

The generator/turbine rotor mass ratio μ^*, (11.4-9), can be reduced to L/D, D^3, L_T/D_T and D_T^3. Expressing D by (11.4-25), D_T by (11.4-13), the mass ratio μ^* reads

580

$$\mu^* = \text{const} \frac{D_T}{L_T} \left(\frac{D}{L}\right)^{1/2} \left(\frac{h_t' P_a}{\alpha \Delta T}\right)^{3/2} \frac{\omega^3}{K u^3 (gH)^{3/2}}. \tag{11.4-26}$$

Inserting this in the relation (11.4–24), the alternator output of a limiting design, at given head gH, reads as follows

$$P_a = \text{const} \left(\frac{\eta_T Q_{11} k_3}{k_1 i^3 Ku}\right)^{1/2} \left(\frac{\sigma_{ad}}{k \varrho_R}\right)^{3/4} \left(\frac{\varrho}{\varrho_R}\right)^{1/2} \left(\frac{Cf\, T_a g H \alpha \Delta T}{h_t'}\right)^{1/2} \left(\frac{L}{D}\right)^{1/2} \omega^{-2}. \tag{11.4-27}$$

Thus the alternator output increases by raising a) the overheating ΔT (limited by insulation material), b) the resulting heat transfer coefficient α. Hence, 60% increase in output by water cooling reflects 150% growth in α. Since the heat transfer coefficient between coolant and metal for water is about 100 times that of air, the above demonstrates a predominantly diminishing influence of the heat conduction term in the iron and copper on the value α.

General consideration: From (11.4–16) and (11.4–2) the output of an alternator with a grid frequency f can be expressed by

$$P_a = \text{const}\, C D^2 L f.$$

For homologous machines $L \sim D$ and at a given grid frequency, the generator output becomes proportional to its volume, namely $P_a \sim D^3$. The alternator's power loss is mainly proportional to its output and mainly converted into heat flow $\dot{Q}_{al}^*$. Hence $\dot{Q}_{al}^* \sim D^3$.

At a given permissible temperature difference ΔT between the alternator and the coolant entering, and at a given heat transfer coefficient α, this heat flow has to pass the alternator's surface A. Hence $\dot{Q}_{al}^* \sim \alpha A \Delta T$. With the proportionalities $A \sim D^2$ and $\dot{Q}_{al}^* \sim D^3$, the resulting heat transfer coefficient required becomes
$$\alpha \sim D/\Delta T.$$

Thus cooling of an alternator becomes more difficult with increasing physical dimension of the machine.

11.4.6. Cooling in practice

I. General survey: The purpose of cooling is temperature control of zones with heat loss (conductor, magnetic materials), and its components which may be damaged by excess heat [11.75].

Overheating is established by a series of temperature rises. In the following this may be shown in the case of air cooling. The temperature of stator winding can be divided into the following factors:

1) air from coolers to air entering the ventilation ducts,
2) air entering the ventilation ducts to the iron,
3) iron stator copper winding.

The first is due to the heat carried in the air before reaching the stator ventilation. The second is a function of the heat transfer coefficient from iron to air, that is on the velocity of the coolant and the shape of the ventilation ducts. The third cause of temperature rise results from construction techniques.

To establish as accurately as possible the intensity of these types of heat exchange, complete knowledge of coolant flow is necessary, i.e.

1) A fluid flow calculation to evaluate the pressure required for coolant circulation.
2) Heat flow calculation.
3) Fan or impeller pump system design.

II. The coolant circuit for air cooling: The circuit design depends on various features of the machine. With air as a coolant alternators can be divided into the following groups.

1) High speed generators (small diameter, low pole numbers).

2) Slow generators (large diameter, large pole numbers).

3) Reversible motor-generators for pump-turbines and non reversible motor-generators for ternary pumped storage sets.

In air-cooled machines a distinction is also made between axial and radial ventilation, where the first is preferably employed in the group 1) and the latter in group 2). Both methods of cooling can be used in an open or closed system.

With axial ventilation (Fig. 11.4.3.1), the air is supplied predominantly by a radial fan. The bore and parts of the outer surface of the active iron are cooled directly. This also applies to the pole winding in the gaps between the poles. Heat is removed from the stator winding indirectly over the length of the axial slot, whereas the end windings are cooled directly but have different temperatures corresponding to the temperature rise of the air within the axial slot.

With radial cooling (Fig. 11.4.3.2), the air is blown symmetrically into the gaps between the poles from both sides by axial fans. The centrifugal effect of the rotating poles diverts the air in the radial direction and into the cooling air ducts of the stator iron. The stator end windings lie directly in the cooling flow from the fan.

With larger bore diameters the air can also flow radially through the rotor (group 2). Additional vanes may be provided in the spaces between the rotor rings to assist the flow.

III. Cooling systems: Open systems for smaller ratings withdraw the cooling air from the turbine hall (Fig. 11.4.3.3) and discharge it into the machine pit. In the case of greater
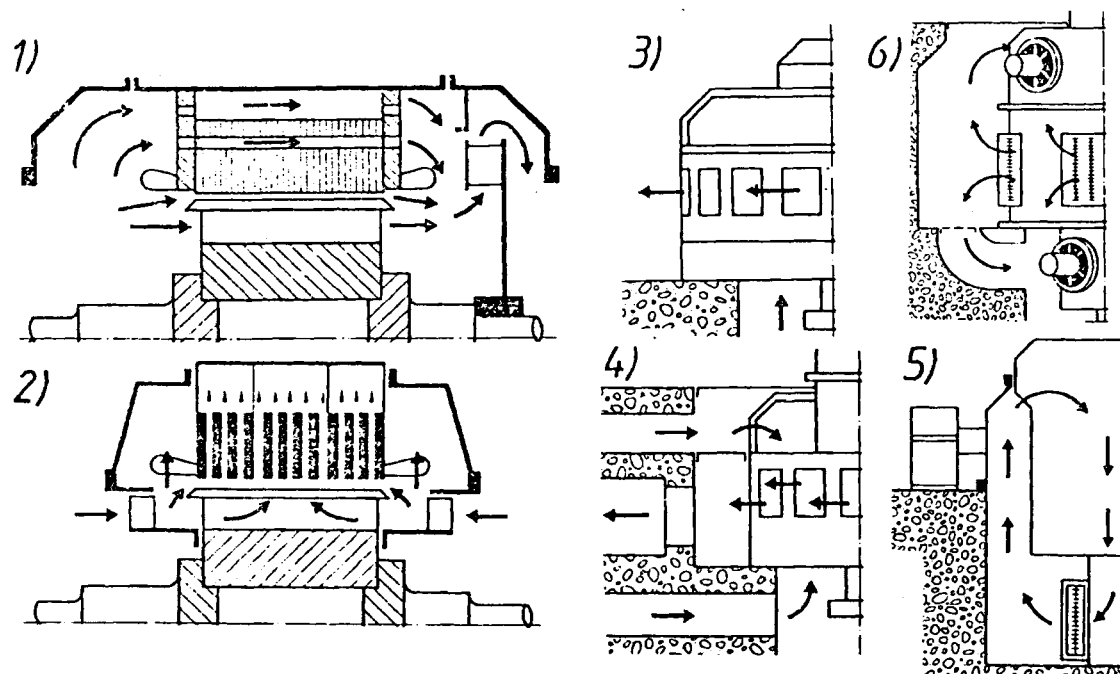
Fig. 11.4.3. Air cooling systems: 1 Cooling with axial ventilation by a radial flow fan; 2 cooling with radial ventilation by 2 axial fans; 3 open system, cooling air is drawn in from the turbine hall and expelled into the generator hall; 4 cooling air supplied from and discharged to the atmosphere; 5 re-cooling of ventilating air by water/air heat exchangers; 6 air supplied by a separate motor fan unit for reversible units. (Drawing from Brown Boveri and Cie: Synchronous machines for hydro-electric power plants. Special issue publication No CH-T 130082 E.)

582

power loss the cooling air is preferably drawn from the atmosphere via filters and ducts and subsequently discharged (Fig. 11.4.3.4). The air can be discharged through openings in the warm air duct and used for heating the power house if necessary.

The *closed system* is used when the atmosphere is polluted and for high output machines. The air circulates in a closed circuit and is re-cooled by water/air heat exchangers (Fig. 11.4.3.5). It is possible to maintain an almost constant operating temperature by metering the quantity of cooling water or mixing warm water with the cold water according to the load on the machine. The heat exchangers are either flanged to the stator frame or let into the foundation cooling ducts.

Synchronous machines for reversible operation (group 3) and pole changing two-speed machines are ventilated separately. The cooling air is supplied by motor driven fan units (Fig. 11.4.3.6).

Further efforts to increase the specific output and improve the utilization of the machines have led to the application of liquid cooling. The economic advantage of liquid cooling is dependent on the evaluation of losses. Its application is particularly justified for high outputs and high speeds. Moderate values of fly-wheel effect (bulb generators) permit full utilization of the advantages of liquid cooling.

IV. Water cooling of the stator: In the stator winding bars are inserted, consisting of transposed conductor elements (according to *Roebel*'s principle) hollow conductors for
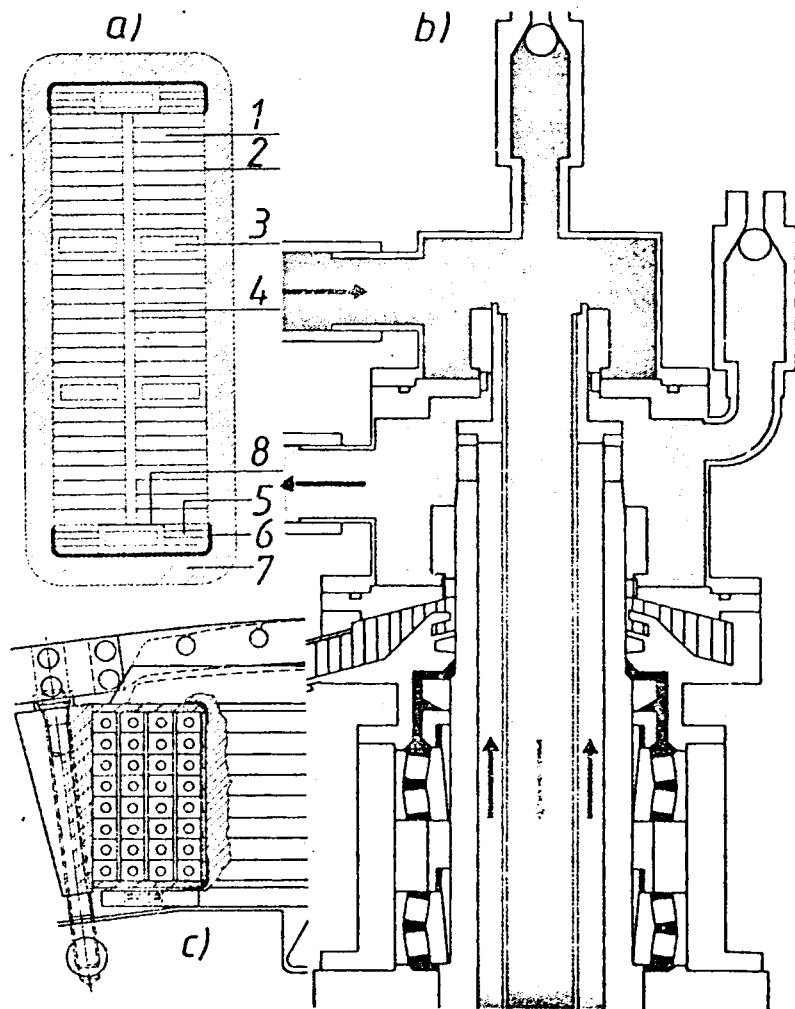
Fig. 11.4.4. Devices for a water-cooled system: a) Section through a water-cooled Roebel bar; 1 solid conductor element; 2 insulation of a conductor element; 3 cooled conductor element (hollow conductor); 4 half insulation; 5 filling; 6 semi-conductive potential coating; 7 main insulation; 8 bend underlay. b) Transfer unit (water head) for feed and discharge of the cooling water to and from the rotor winding. c) Rotor coil with square, hollow copper conductor. (Drawing courtesy Brown, Boveri & Companie Ltd. Baden, Switzerland.)

the cooling water (Fig. 11.4.4 a). The cooling water is supplied to the stator winding bars and removed by a closed circuit system of pipes or a ring main system arranged outside the windings in the stator frame. The insulation between the stator windings and the cooling system is provided by Teflon hoses.

The iron losses of the stator lamination are likewise removed by cooling water.

V. Water cooling of the rotor: The cooling water is fed to the rotor winding and removed via a transfer unit on the end of the shaft (Fig. 11.4.4 b). Concentric stainless steel tubes in the shaft bore carry the treated cooling water via flexible connections to the manifolds mounted on the rotor. The water then flows via insulating hoses into the hollow conductors of the pole windings (Fig. 11.4.4 c). The liquid cooling system consists of two circuits. The first circuit supplies treated, i.e., de-ionized, oxygen-free water to the stator and rotor winding system. The other circuit supplies untreated fresh water to the stator end plates and the back of the stator iron.

The conductivity of the treated water, the relative humidity inside the stator frame and the circulation of the liquid are monitored continuously.

Fig. 11.4.5 a shows the sectional drawing of the fully water-cooled alternator at Tonstad, Norway, built by BBC, to prove the reliability of this design. Fig. 11.4.5 b shows a perspective sectional drawing of the alternator Itaipú, Rio Paraná, Brazil, at present one of the largest water-cooled alternators in the world, built by BBC and Siemens. But here, only the stator is water cooled.

11.4.7. Rotor construction

The output, runaway speed, and the required fly-wheel effect largely determine the construction of rotors. Assembly and transport limitations are often additional criteria which affect rotor construction. The shaft dimensions are determined by the critical flexural and torsional speed, which must be in adequate distance from the interfering excitation frequencies. Fig. 11.4.6 shows different bearing arrangements.

I. Rotor body: Rotors for small number of poles and small bore diameters are constructed as solid forgings (Fig. 11.4.7.1). The shaft and central body form one unit. In rotors with a larger number of poles and larger bore diameters the heavy central section is replaced by a cast or forged hollow body with shaft ends flanged on to both sides (Fig. 11.4.7.2). Rotors for large capacities and medium number of poles are preferably constructed as disk rotors (Fig. 11.4.7.3). The central body is formed of several rolled steel plates centred in relation to each other by spigots or mating rings and compressed by prestressed clamping bolts. The shaft ends are also flanged to the rotor body by means of clamping bolts.

The central section can be replaced by a cast steel spider with several shrunk-on forged steel rings (Fig. 11.4.7.4). Rotors for larger diameters and medium to low speeds are constructed with laminated rims. They have a continuous shaft with a shrunk-on spider, or shaft ends flanged to the latter (Fig. 11.4.7.5). The spider consists of a cast, forged or welded hub with attached arms, which can be onscrewed or are welded to the hub depending on transport limitations. The rim consists of segments of steel laminations each several millimeters thick. The punched segments overlap each other and are compressed by clamping bolts to form a ring resistant to bending. With the usual overlapping of one pole pitch, at the joint between the individual segments, the critical cross-section for the strength analysis deviates less from the full ring cross-section, the greater is the number of pole pitches in a segment.

584
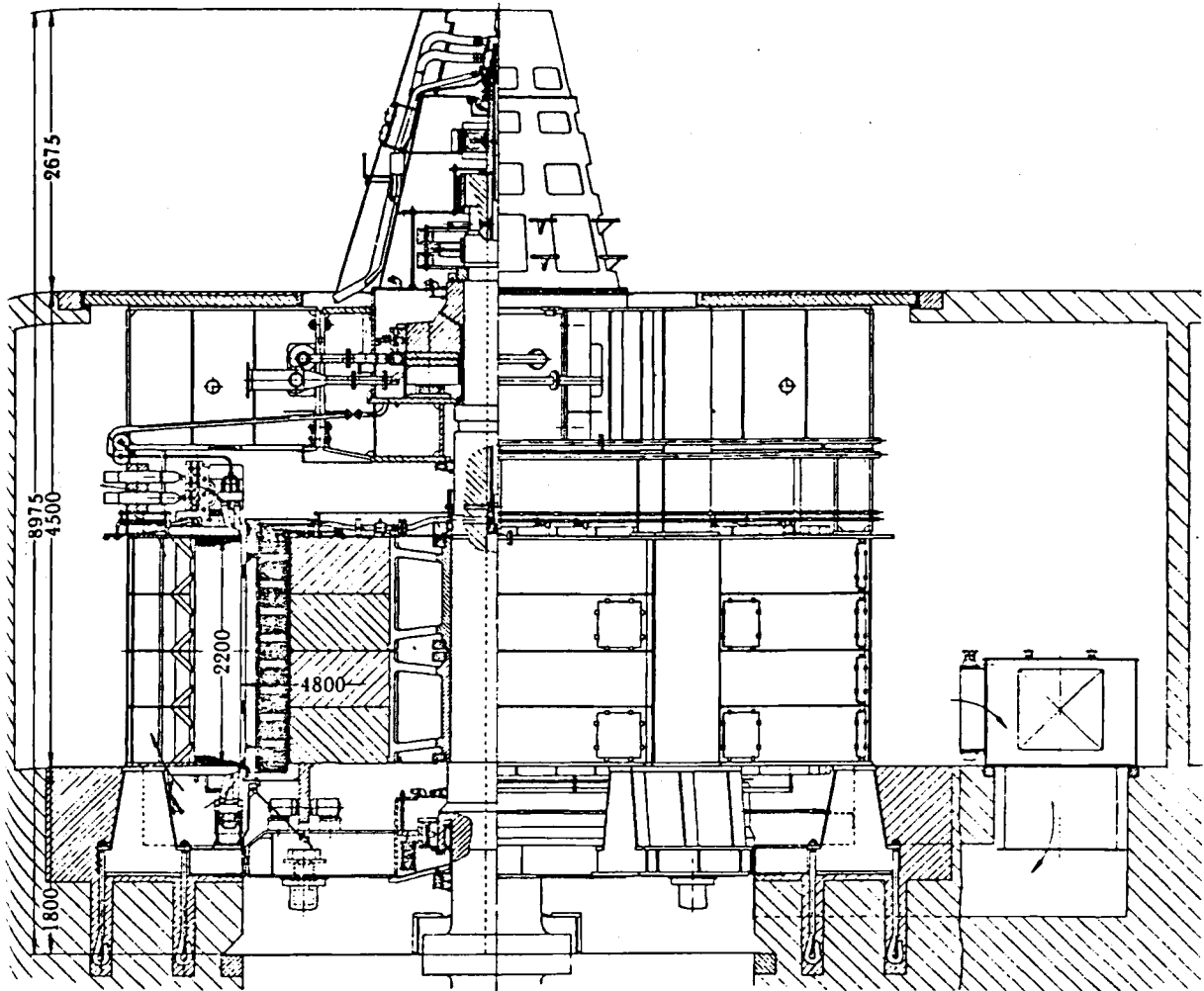
Fig. 11.4.5. a) Longitudinal section of a fully water-cooled alternator at Tonstad, Norway (owner Sira Kvina Kraftselskap), operating satisfactorily since 1968. Contrary to plants like Wehr, needing water-cooling, this alternator was equipped with it, to test the method. (Design Brown Boveri and Cie, Baden, Switzerland) $P = 190$ MVA; $n = 375$ rpm; $n_{ra} = 600$ rpm; terminal voltage 12 kV; rated current $I = 9140$ Amp; cos $\varphi = 0,85$; fly-wheel moment 3000 m^2 tons; exciter current 2630 Amp; exciter Voltage 220 V; total weight 480 tons. Relative losses: stator winding 43%; rotor winding 25%; bearing 13,9%; stator iron 5%; water cooler 10%. From [11.76]. (Drawing courtesy Brown, Boveri & Company Ltd, Baden, Switzerland).

To observe the required dimensional tolerances of the lamination segments, the contour, bolt holes, pole fixing grooves and keyways are punched out in one operation. Torque transmission between laminated rings and the spider requires accurate keying, which ensures tangential guidance even with a floating ring.

The rings of large low-speed machines are built up on the fully mounted spider in the power stations. Laminations to a height of a few centimeters are applied only to check the spacing between the bolt holes and pole securing grooves and to locate the keyways on the arms of the spider.

II. Poles: Poles are solid or laminated depending on the mechanical stresses and the type of operation. As a result of the relatively low ohmic resistance the additional losses in solid poles, made of forged or cast steel, are higher than those in laminated poles. The additional losses are essentially the eddy current losses caused by the higher field harmon-
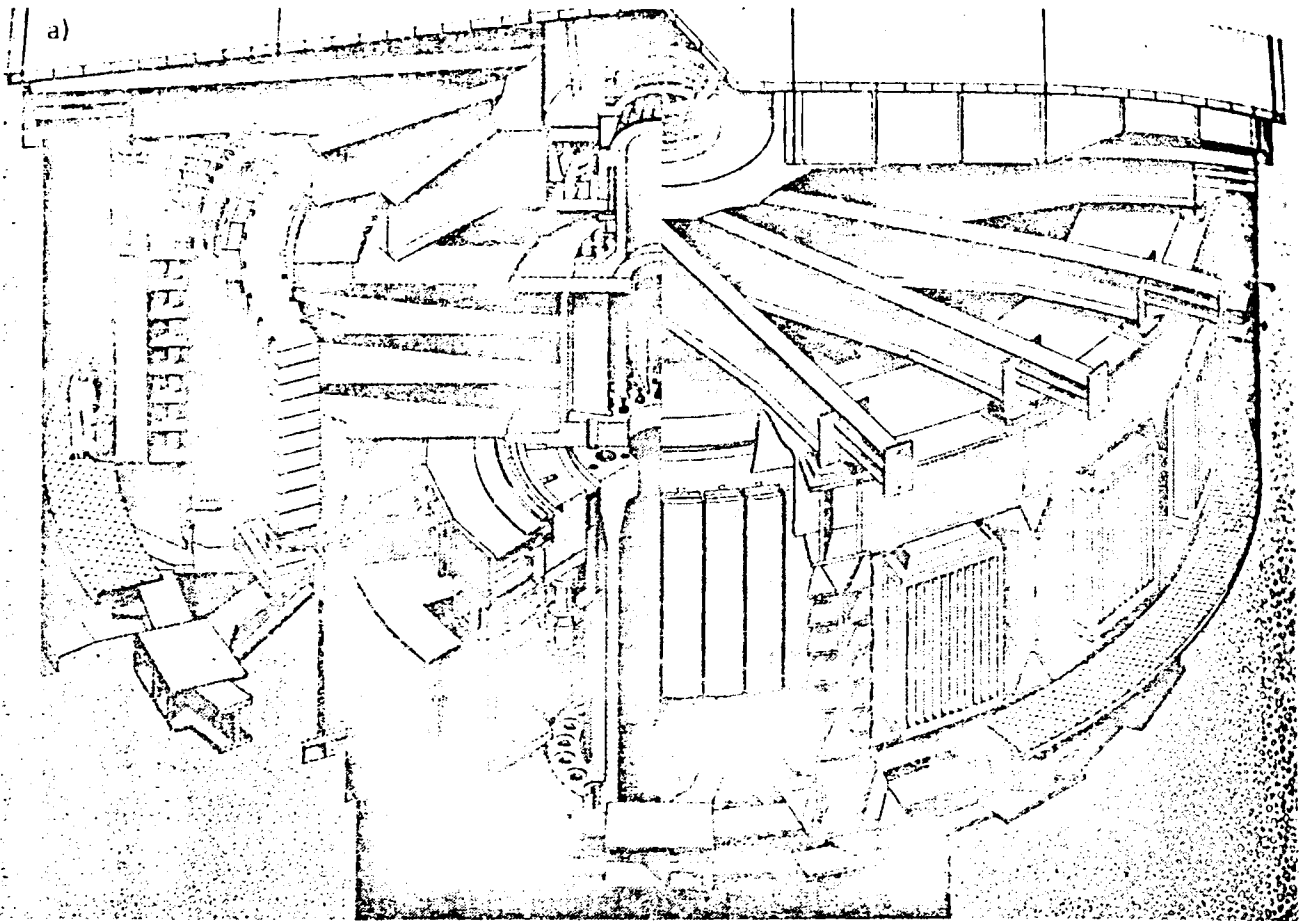
Fig. 11.4.5. b) Perspective sectional view of Itaipú alternator, Rio Paraná, Brazil, Paraguay (owner Itaipú Binacional) 18 units fabricated by Consorcio Itaipú Electromecanico (CIEM), comprising on the electric side the European firms, Alsthom Atlantique, France, Brown Boveri, West Germany and Switzerland, Siemens Limited, West Germany, and their Brazilian subsidiary firms Industria Electrica Brown Boveri S.A., and Siemens S.A. in Lapa. To date with respect to output one of the largest alternators for hydropower sets. Water-cooled stator. Data for the Paraguayan (Brazilian) machine: frequency 50(60) Hz, rated capacity 823,6(766,0) MVA, power factor 0,85(0,95), rated speed 90,9(92,3) rpm, runaway speed 170 rpm, rated terminal voltage 18 kV $\pm$ 5%, outside stator diameter 19,7 m, stator bore diameter 16 m, thickness of stator bundle lamination 3,5(3,26) m. Thrust bearing load 4240(4200) tons, rotor weight 1961(1945) tons, total weight 3343(3342) tons. Starting operation 1983/84. Rated head H_r = 118,4 m. Power transmission at 50(60) Hz with 500 kV AC, $\pm$ 600 kV DC (500 or 765 kV AC). Note skewed spider arms!

In this context, a comparison with the fully water-cooled alternators of Krasnoyarsk designed by LMZ, SU, and put into service in 1966 may be of interest. Here rated head H_r = 101 m, rated capacity 600 MVA. n = 93,8 rpm, stator bore diameter 16 m, rotor weight 2000 tons, axial thrust 3400 tons. From this it is seen that at nearly the same peripheral speed, rotor diameter, and rotor weight, the electric output of an alternator with a water-cooled stator has been increased by about 37% compared with a fully water-cooled alternator built about 20 years earlier.

The gap clearance of 29 mm results in a gap/rotor diameter ratio of 1,8 · 10⁻³. Because of the radial thermal expansion of the heated rotor working, this ratio has to be about 5 times larger than in the runner seal of the water turbine, where it is dictated by the clearance of the adjacent guide bearing and the flexibility of the shaft. From H. Gabler; Itaipú, Wasserkraftwerk der Superlative. ETZ 103 (1982) no 10, p. 522/528. (Drawing courtesy Siemens, Erlangen, West Germany.)

586
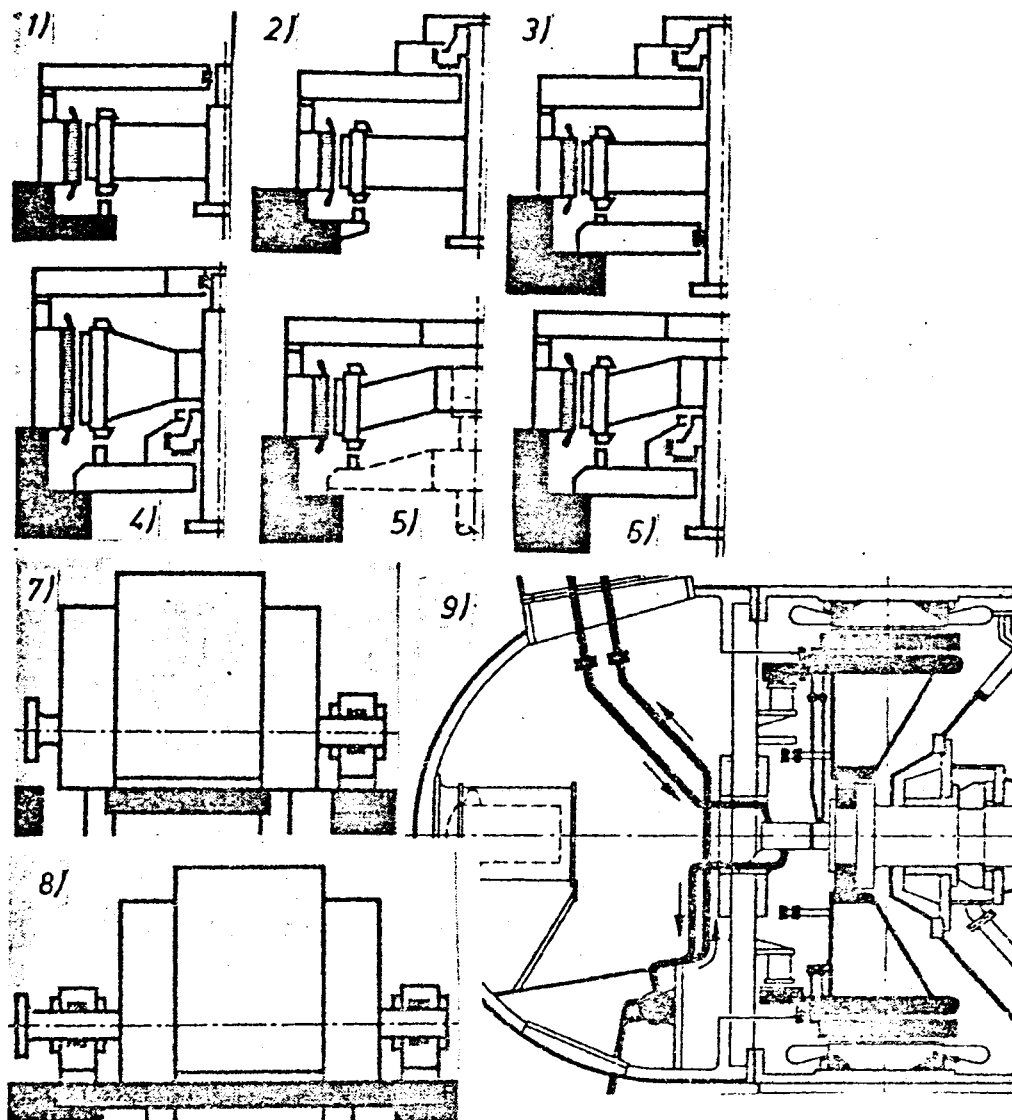
Fig. 11.4.6. Typical arrangements of bearings in hydroelectric generators. 1 one guide bearing above generator rotor (= gr); 2 combined guide and thrust bearing above gr; 3 combined guide and thrust bearing above gr, guide bearing below gr; 4 guide bearing above and combined guide and thrust bearing below gr; 5 overhung design with guide bearing below gr; 6 overhung design with combined guide and thrust bearing below gr; 7 horizontal shaft with guide bearing at one side of gr; 8 ditto with guide bearings at each side of gr; 9 alternator of bulb turbines of Lechwerke with water-cooled rotor. Lech plant of BAWAG, München, West Germany. P = 4,45 MVA, n = 167 rpm. (Drawing courtesy Siemens, Erlangen.)

ics produced by the armature current, and the pulsation losses generated by the main field and the slots.

Solid poles act like the conductor bars of a squirrel cage winding, so that heavy currents can flow in them in the case of asynchronous operating conditions, e.g., starting up to pump of the water-filled pump of a large synchronous generator motor.

Laminated poles have a higher ohmic resistance in the longitudinal direction, but their damping effect on torsional vibrations is also reduced. Hence the laminated pole must be provided with a damper winding for the required operating stability. Flexible connections between the ring-formed

587
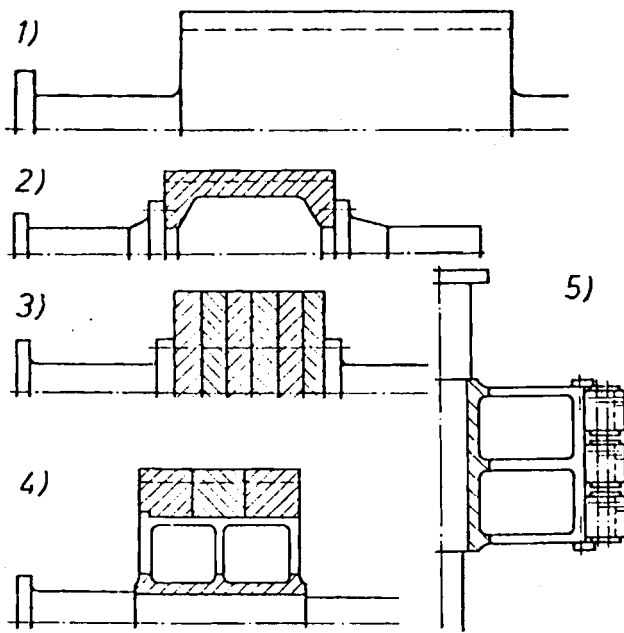
Fig. 11.4.7. Construction of the rotor. 1 solid forged body; 2 cast or forged hollow body in central section; 3 body made of several rolled steel discs (disc rotor); 5 laminated rim rotor consisting of a spider and one or more rims formed by overlapping steel lamination segments. (Drawing from special issue BBC, see Fig. 11.4.3.)

damper bars in front of the rotor and the ring segments permit compensation of varying thermal expansion of the individual bars.

The method of securing the poles to the rotor body depends on the stressing by the centrifugal force at the runaway speed. With low peripheral speeds and small bore diameters the poles are bolted on to the rotor rings or rotor rim from the air gap side. With larger bore diameters and peripheral speeds the poles can be bolted on from the hub side. The poles can then be dismantled axially to allow overhaul of the pole or stator winding without dismantling the machine.

Single or multi-claw mountings are required for medium and high peripheral speeds, e.g., 2 T-head claws which engage in corresponding keyways in the rotor body. The claws are pressed against the rotor body by wedging at both ends. Carefully designed radii of curvature in notches and claws help to reduce the stress peaks caused by the unavoidable notch effect.

III. Field coils: The individual turns of the field coils consist of hard drawn copper sections cut to appropriate length and width and hard soldered at the joints. To increase the cooling surface area individual turns may have a greater conductor width, so that the outer coil surface forms a finned cooling element. The insulation between the turns consists of glass asbestos or plastic films and is baked with the copper under pressure (corresponding to the centrifugal force at the runaway speed).

The end windings are terminated by an insulating frame made of glass reinforced plastics. In addition to high mechanical strength this frame must have sliding properties to compensate for the relative expansion of the field coils relative to the pole pieces. The winding is secured by steel frames bolted to the pole piece. Cup springs inserted in the frame keep the windings pre-stressed.

IV. Pole changing: Occasionally pump-turbine sets have two speeds, since optimum hydraulic efficiencies are achieved if the pump speed is about 20% above the turbine speed. Pole changing can be achieved by the following methods:

a) The rotor poles are of identical construction and their number corresponds to the lower speed. For the higher speed, poles are switched out or two adjacent poles are energized in the same direction (Fig. 11.4.8.1).

b) Poles with different widths are distributed unevenly around the periphery (Fig. 11.4.8.2). By switching over groups of poles and possibly disconnecting individual

588
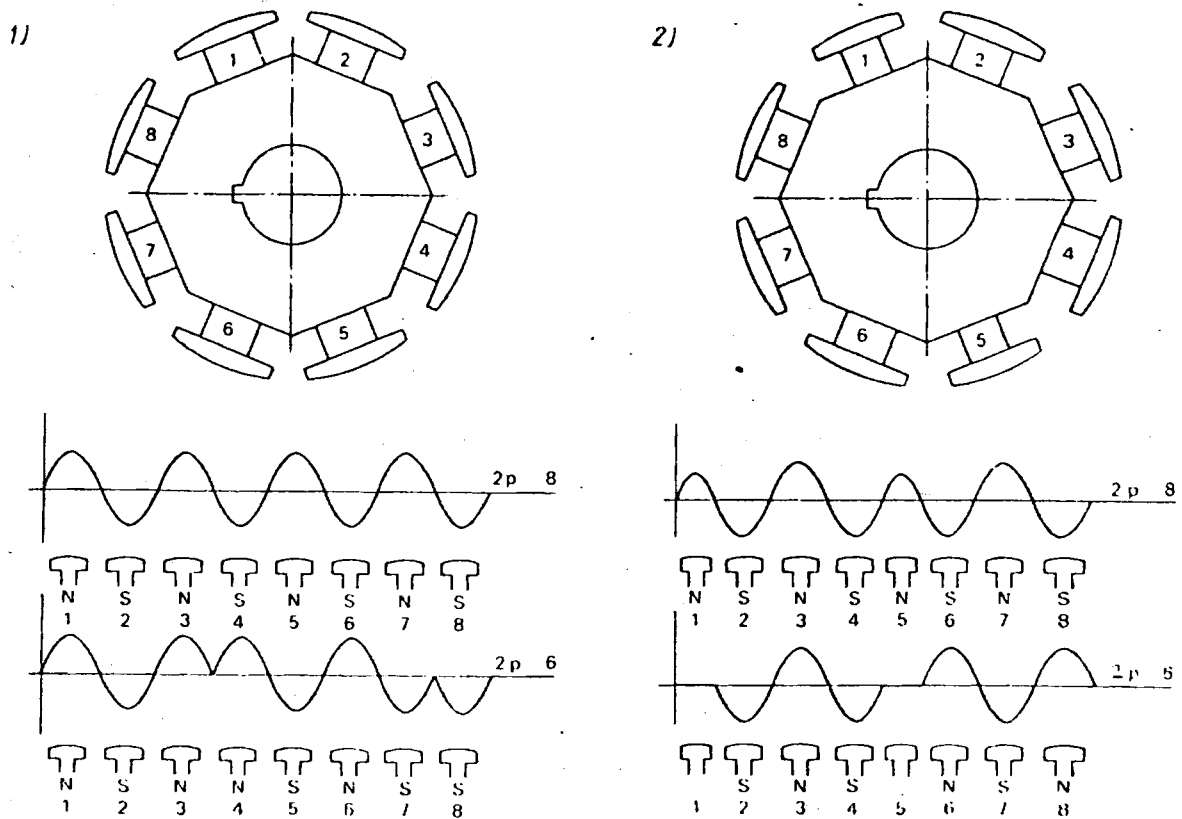
Fig. 11.4.8. 1) left: Pole arrangement and pole field pattern for changeover from 8 to 6 poles with identical construction and uniform spacing of the poles. 2) Right: Pole arrangement and pole field pattern for changeover from 8 to 6 poles with different construction and irregular spacing of the poles. After BBC publication on "Synchronous machines for hydro-electric power plants". No CH-T 130082 E.

poles, two different numbers of poles can be achieved, the smaller one giving a substantial increase in the flux density of the fundamental wave. At the same time the fields due to other harmonics are weaker than in case a). Brown Boveri have combined the advantages of simple pole arrangement in a) with the functional superiority of b) by making the pole shoes asymmetrical and displacing them in such a way that their flux distribution produces the best possible conditions for both speeds.

Moreover the stator of the BBC machines has two separate windings, in which every second coil of one pole number is assigned to the interposed coil of the other pole number.

With machines based on this concept, very smooth running is achieved up to the largest outputs.

11.4.8. Stator construction

I. Stator frame: This is a welded structure designed and dimensioned to withstand the stresses of the rated torque, and in the case of a fault, e.g., short circuit, of the much greater impulsive torque, of the dead weight of the stator, of the axial thrust on the rotating parts

(in the case of a vertical set with thrust bearing on the head cover of the stator), of magnetic forces and due to thermal expansion.

Stators in horizontal machines transmit these forces through supporting feet to the base plates into the foundations. The stators of vertical machines are supported on the foundations by means of brackets or by bearer rings, particular attention being paid to the forces involved. Hence, with rising temperature the stator can expand axially freely.

Single phase machines cause a special problem with regard to stator support as a result of the torque badly pulsating at twice the system frequency. Here a stator spring suspension may reduce the transmission of the jolting forces.

The stator is supported by spring units each comprising a number of leaf springs, whose ends are clamped in holders. The lower holder is connected to the stator by a suspension rib, the upper holder to the foundation ring via a supporting rib. The leaf springs are subjected to the stator weight with the result that the danger of buckling is eliminated. Thus the stator can oscillate freely peripherally.

The concrete support of the stator has to be reinforced by stay wires which are tensioned in the axial and peripheral direction, to avoid fatique effects in the case of short circuit. For this emergency case the stator frame has to resist any buckling by twist.

Fig. 11.4.6 shows different arrangements of stator.

II. Stator iron: The active iron is formed of 0,5 mm thick laminations of low-carbon, silicon-alloyed iron. A thin electrically insulating coating of varnish resistant to high temperatures is applied to both sides. Maximum care is taken when installing the laminations to prevent local overheating due to short-circuited laminations. The overlapping segments are guided by wedge-shaped bars of prismatic cross-section.

The type of connection between the stator iron and frame ensures that the bore tolerance is observed up to the largest diameters and enables the stator frame to absorb the thermal expansion of the iron core.

The laminations are compressed by hydraulic jacks. On completion of the pressing operation, pressure is applied to the wedge-shaped bars used for guiding the laminations. Designed as bolts threaded at both ends, these wedge-shaped bars project beyond the end plates and are tensioned by nuts. Clamping fingers transfer the pressure to the stator teeth, so that tooth vibration of the end laminations and possible damage to the stator winding insulation are prevented.

For radial flow of the cooling air the iron is subdivided into individual packets of laminations in the axial direction. The cooling ducts are formed by spacers of steel spot-welded to the end lamination. The number and arrangement of the spacers are selected so that the pressure is distributed as uniformly as possible over the segment area and the resistance of the cooling air flow is moderate. It is advantageous to glue the lamination segments of the stator iron for certain operation conditions and machines of a specific type.

In bulb turbines for example, this leads to mechanical bracing of the stator, because the iron acts as an integral part of the frame. In pole changing machines the gluing permits the absorption of jolting forces caused by the upper harmonics.

III. Stator winding: The reliability of the stator winding is determined primarily by the quality of its insulation. An effective insulating system consists of a continuous tape insulation impregnated with synthetic resin in vacuo and subsequently cured. A glass fabric strip is used as a carrier material for the insulating fleece and a special solvent-free epoxy resin is the impregnating agent.

The larger machines usually have a double-layer bar in open slots. The bar cross section consists of several conductor elements transposed on the *Roebel* principle (Fig. 11.4.4.1). These elements are covered with glass filament and glued with epoxy resin under pressure to form a compact bar. The insulation taping is subsequently applied to the bar strengthened in this way. Great care is taken to ensure firm permanent wedging of the conductors inside the slots and similarly effective support of the end windings.

590

Some speculations on regulation and future tendencies: At reaction turbines with fixed runner blades (to-date the majority of hydro turbines), an adaptation to the varying power demand causes a changing angle of incidence of the relative flow and hence an inlet shock at runner inlet edge. This decreases either the efficiency from its bep value with vanishing inlet shock or it creates cavitation past the inlet edge of the rotor vane. Moreover in such a machine a deviation from the bep causes whirling flow past runner exit and hence draft tube surges.

Both troubles originate from the velocity triangles in consequence of constant blade velocity due to speed regulation. Inlet shock and exit whirl disappear when the speed of the set is regulated appropriately. Such a speed regulation may be implemented, if the alternator of the set supplies a high voltage DC power transmission line, provided its thyristors and wave filters for harmonics are insensitive to the speed variation considered.

At heads up to 300 m and constant gate, the turbine flow is not influenced by speed change. Thus water hammer must not be accounted for. Nevertheless the range of speed regulation has to be limited since some loss components, e.g., disk friction and ventilation rise with speed. Moreover the speed range has to be set so that, due to common practice at hydro power sets, the lowest critical bending and torsion speed are above the upper limit of the working speed. Also material strength of the rotors limits the speed by stresses originating from centrifugal load. The large inertia of alternator rotor due to its iron and conductor mass required and its long start-up time is a considerable hindrance to fast variable speed regulation. Material with higher magnetic flux density and conductors with higher permissible current density (realized by applying cryogenic engineering) could assist in overcoming these troubles.

Operations with continuously varying speed would require an appropriate regulation of generator terminal voltage. The layout has to start from the ratio of upper and lower speed limit. On the hydraulic side this depends on the turbine design and should not exceed the value of 1,5, on the electric side this could reach 3. The upper limiting speed results from the critical speed and material strength at runaway with a glance at frequency-induced losses. The lower limit derives from too large cross sectional areas the magnetic flux then requires.

To eliminate the inlet shock and exit whirl when the turbine works away from its bep, also an operation with constant gate opening is thinkable. Ignoring the case with a number of sets sufficient to work around the bep by switching them on and off, a constant flow operation could be imagined when the excess of electricity generated, produces by-products, e.g., hydrogen electrolytically. However, this process, with about 90% efficiency and its low voltage, can in no way compete with up-to-date high voltage power transmission. Further the recuperation of energy thus chemically stored in hydrogen is also linked to low voltage and hence uneconomical.

The high combustion temperature of hydrogen makes it useless for room heating. Problems of lacking material strength and resulting low service life also prohibit the application of hydrogen in internal combustion machines. Hence to day the combustion of hydrogen could only be used for welding or chemical processes. In future it may be used for power generation at highest temperature, e.g., magnethydrodynamic process. At present, all this cannot compete with hydro-electric power generation in respect to efficiency. Hence such a detour in energy transmission is only justified if energy is affluent and the by-products gained in this process are scarce thus increasing the resulting economy of the installation.

Growing size of units, welded and hence more elastic construction, economic use of high yield point, or wear-resistant material with limited useful life, fatigue effects, transients like regulation, change of operating mode, water hammer and cavitation, will give priority to the prediction of the proto-type's dynamic response and wear with respect to the phenomena mentioned above. This requires model tests on the machine, its components and their material.

Any prediction of this kind has to consider material properties of the set, its foundation including the power house, its liquid-filled gaps in bearings and labyrinths, the properties and geometry of its piping, the properties of the working fluid as, e.g., free air content (also that due to cavitation), the modes of operating and regulating the set, and the power spectrum of exciting frequencies and their response. This power spectrum, as a function of free air content, has been measured, e.g., on a model Francis turbine of high specific speed by Walter [9.34].

591

On the basis of dynamic prototype tests, the prediction of the elastic response of penstock and tunnel as a function of the penstock/tunnel length ratio has been facilitated by the calculations of Hudovernik and Lein [112; 111a; 76b]. Predicting the shaft vibration of a prototype pump-turbine on the basis of model tests and calculations, has been reported by Ulith [236]. A prediction of system oscillation and remedies against it has been shown by Grein [99; 9.52].

However, a prediction of all the dynamic prototype phenomena occurring in a hydro-electric turbomachine set, with its known material, piping and electric grid, will remain a task, whose solution is reserved to the future.

12. List of References

[1.1] *Cotillon, J.:* L'hydroélectricité dans le monde. Houille Blanche 33 (1978) no 1/2, p. 71/86.

[1.2] *Lyra, F. H.:* Planning and construction sequence at Itaipú. Water Power 34 (1982) no 5, p. 27/30.

[1.3] *Garstka, W. U.:* Hydro and water resources of the USA. Water Power 31 (1979) no 4, p. 33/37.

[1.4] *Weigong, C.:* China's potential for hydrodevelopment. Water Power 33 (1981) no 4, p. 18/21.

[1.5] *Smil, V.:* A new era for China's hydro power. Water Power 33 (1981) no 4, p. 23/25.

[1.6] *Smil, V.:* Exploiting China's hydropotential. Water Power 28 (1976) no 3, p. 19/26.

[1.7] The Editor: Yangtze Gorge scheme could yield 110 TWh/year. Water Power 33 (1981) no 4, p. 38/42.

[1.8] *Gubin, F. F.:* Gidroelektričeskie stanzii. Moskva: Energia 1972.

[1.9] *Borovoi, A. A. and L. P. Michailow:* 60 years of Soviet hydro power. Water Power 31 (1979) no 3, p. 21/25.

[1.10] *Lefoulon, R.:* Thirty years development on the Rhine. Water Power 28 (1976) no 5, p. 48/52 and no 6, p. 45/48.

[1.11] *Götz, A. and G. Schiller:* The hydropotential of Austria. Water Power 35 (1983) no 2, p. 27/30.

[1.12] *Vischer, D.:* Surface water an exclusive feature of our planet? IAHR J. 21 (1983) no 1, p. 45.

[1.13] *Wurzer, E. and M. Eichler:* Die Erhebung des Wasserkreislaufes in Österreich. Österr. Wasserwirtsch. 31 (1979) p. 221.

[1.14] *Brendl, O.:* Wasser ist Leben. Österr. Wasserwirtsch. 32 (1980) p. 229.

[1.15] *Amyot, P. et al.:* Quebec's power needs for the eighties. Water Power 28 (1976) no 7, p. 27/30.

[1.16] The Editor: Inga scheme. Water Power 16 (1964) no 9, p. 380.

[1.17] *Bloss, W. H. et al.:* Survey of energy resources 1980. 11th world energy conference Munich 1980. Univ. Hannover Fed. Inst. for Geoscience and natural resources. 1980.

[1.18] *Slebinger, V.:* Statistics of all existing waterpower resources. Trans. 4th Worldpower Conf. London. 1952.

[1.19] *Langager, H. C.:* Hydro studies in Greenland. Water Power 35 (1983) no 2, p. 43/45.

[1.20] *Gillette, R. W.:* Small and low head hydro in USA. Water Power 33 (1981) no 11, p. 25/29.

[1.21] *Weber, G. W.:* Uprating Switzerland's hydroplants. Water Power 30 (1978) no 2, p. 39/44.

[1.22] *Goldsmith, K.:* The role of Swiss Hydro in Europe. Water Power 32 (1980) no 6, p. 31/33.

[1.23] *Weber, G.:* Exploiting the Rhine above Lake Constance. Water Power 33 (1981) no 5, p. 44/45.

[1.24] *Koh, N. P.:* Small hydro power plants in China. Water Power 32 (1980) no 7, p. 31/32.

[1.25] *Fällström, P. G.:* Turbine developments on the Lule River. Water Power 34 (1982) no 3, p. 27/35.

[1.26] *Angelin, S. and H. Borström:* Hydro development in Sweden. Water Power 32 (1980) no 6, p. 35.

[1.27] *Aalto, A. and A. Jouhki:* The changing role of hydro in Finland. Water Power 33 (1981) no. 5, p. 40/43.

[1.28] *Morariu, S.:* Computer-aided evaluation of Peru's hydro power. Water Power 34 (1982) no 1, p. 34/39.

[1.29] *Oramas, G.:* The hydroelectric resources of Columbia. Water Power 30 (1978) no 3, p. 41/45.

[1.30] *Bichon, A.:* Exploiting France's hydro resources. Water Power 32 (1980) no 6, p. 38/42.

[1.31] *Domercq, J.:* Spain's remaining hydro-electric potential. Water Power 32 (1980) no 6, p. 33/37.

[1.32] *Jeganathan, T. V.:* Hydropower development in India. Water Power 33 (1981) no 3, p. 43/46.

[1.33] *Datta, M.:* Hydropower in India. Water Power 28 (1976) no 7, p. 14/19.

[1.34] *Eißfeldt, G.:* Kleine Wasserkraftanlagen. Seminar Techn. Akad. Wuppertal 1981.

[1.35] *Goubet, A.:* Les petits installations hydroélectriques dans les pays industrialisées. Houille Blanche 36 (1981) no 4/5, p. 230/235.

[1.36] *Francou, J.:* Les petits installations hydroélectriques dans les pays en voie de développement. Houille Blanche 36 (1981) no 4/5, p. 237/242.

[1.37] *Cuinat, R. and Ph. Roussel:* Environment et petites usines hydroélectriques. Houille Blanche 36 (1981) no 4/5, p. 244/247.

[1.38] *Rouyer, J. P. and C. Le Plomb:* Recuperation d'énergie hydraulique: petites installations d'énergie associées aux grands projets hydraulique. Houille Blanche 36 (1981) no 4/5, p. 260/268.

[1.39] *Kössler, E.:* Installed and planned mini hydro. Water Power 34 (1982) no 1, p. 35/38.

[1.40] *Gordon, J. L. and A. C. Penman:* Quick estimating techniques for small hydro potential. Water Power 31 (1979) no 31, p. 46/51.

[1.41] *King, R. M.:* Mini hydro developments for small areas. Water Power 31 (1979) no 1, p. 38/41.

[1.42] *Cotillon, J.:* Micro power: an old idea for a new problem. Water Power 31 (1979) no 1, p. 42/48.

[1.43] *Nair, R.:* Development potential for low head hydro. Water Power 34 (1982) no 1, p. 49/56.

[1.44] *Warnick, C. C.:* Hydro potential of irrigation schemes. Water Power 31 (1979) no 4, p. 38/41.

[1.45] *Tomasino, M.:* Predeterminazione della protate a breve termine dei corsi d'acqua. ENEL relazione di studio e ricerce no 129, 1972.

[1.46] *Plate, E.:* Die Zerlegung einer Ganglinie in Trend, periodischer und Zufallsanteil. 4. Fortbildungslehrg. f. Hydrologie DVWW. Univ. Karlsruhe 1972.

[1.47] *Press, H.:* Anwendung elektronischer Rechenverfahren in Hydrologie, Wasserwirtschaft und Wasserbau. Berlin: Verl. Ernst 1968.

[1.48] *Murray, N. and K. Weissbeck:* Computer program for a river hydro development. Waterpower 32 (1980) no 3, p. 30/39.

[1.49] *Press, K.:* Hilfstafeln zur Lösung wasserwirtschaftlicher und wasserbaulicher Aufgaben. Berlin: Verl. Ernst 1981.

[1.50] *Raabe, J.:* Hydraulische Maschinen und Anlagen vol. 4 Wasserkraftwerke. Düsseldorf: VDI Verl. 1970.

[1.51] *Moser, J.:* 100 Jahre Wasserturbinen. EW-Mitt. (1942/43) p. 101.

[1.52] *Press, H.:* Stauanlagen und Wasserkraftwerke vol. 1 Talsperren 1958, vol. 2 Wehre 1959, vol. 3 Wasserkraftwerke. Berlin: Verl. Ernst 1967.

[1.53] *Mosonyi, E.:* Wasserkraftwerke, vol. 1 Niederdruckanlagen. Düseldorf: VDI-Verl. 1966.

[1.54] *Mosonyi, E.:* Wasserkraftwerke, vol. 2 Hochdruckanlagen, Kleinstkraftwerke, Pumpspeicheranlagen. Düsseldorf: VDI-Verlag 1966.

[1.55] The Editor: The ups and downs of wave energy. Water Power 31 (1979) no 1, p. 54/55.

[1.55a] *Simeons, C.:* Hydro power, The Use of Water as an Alternative Source of Energy. Oxford, New York, Paris, Frankfurt. Pergamon Press 1980.

[1.56] The Editor: A steady output from a variable source. Water Power 31 (1979) no 3, p. 49/50.

[1.57] *Shaw, T. L.:* The status of tidal power. Water Power 30 (1978) no 6, p. 29/34.

[1.58] *Lory de, R. P.:* Integrating Fundy tidal power. Water Power 31 (1979) no 9, p. 37/40.

[1.59] *Douma, A. G. D. Steward, and W. Meier:* Straflo Turbine Annapolis-Royal, erstes Gezeitenkraftwerk in der Bay of Fundy. EW-Mitt. 54/55 (1981/82), no 1, p. 37.

[1.60] *Sharma, H. R.:* India embarks on tidal power. Water Power 34 (1982) no 6, p. 32.

[1.61] *Subrahmanyam, K. S.:* Tidal power in India. Water Power 30 (1978) no 6, p. 42/44.

[1.62] *Benn, T.:* Tidal power, problems and benefits. Water Power 30 (1978) no 6, p. 27.

[1.63] *Angelini, A. M.:* The role of pumped storage in Western Europe. Water Power 32 (1980) no 6, p. 62/66.

[1.64] *Okada, M. et al.:* High head pumped-storage plants in Japan. Water Power 31 (1979) no 10, p. 48/52.

[1.65] *Stürzinger, P.:* The role of pumped storage in Switzerland. Water Power 30 (1978) no 2, p. 29/31.

[1.66] *Rochat, P. and J. L. Motier et al.:* Pumped storage for Swiss railways. Water Power 32 (1980) no 2, p. 54/57; no 3, p. 39/46.

594

[1.67] *Hernan, B.:* Dinorwic pumped-storage station for standby and stability. Water Power 29 (1977) no 7, p. 27/38.

[1.68] *Meier, W., J. Müller, H. Grein and M. Jaquet:* Pumpturbinen und Speicherpumpen. EW-Mitt. (1971) no 2, p. 3.

[1.69] *Magnago, G., G. Bortolan:* Pumpspeicherwerke der ENEL. EW-Mitt. (1972). special issue.

[1.70] *Hausmann, G. and G. Vulliod:* The "Isogyre" Pump-turbine. Charmilles Techn. Bull. no 14 (1975) p. 15/25.

[1.71] *Vulliod, G. and M. Bossert:* Das System Isogyre. Sympos. Wien (1981) Österr. Ing. u. Architekt. Ver.

[1.72] *Fauconnet, M.:* The Isogyre evolves. 7th IAHR Symp. Vienna (1974) Trans. XI 1, p. 1/12.

[1.73] *Widmann, R. and W. Finger:* Die Oberstufe, Entwicklung des Projektes und Planung. Energie Wirtsch., Zeitschr. für die Anwendung der Energie in Wissenschaft, Technik u. Wirtschaft, Wien (47/48), Sonderausgabe: Kraftwerksgruppe Malta p. 35/47.

[1.74] *Hautzenberg, H.:* Die Kraftwerksgruppe Malta, Energie Wirtsch., Zeitschr. für die Anwendung der Energie in Wissenschaft, Technik u. Wirtschaft, Wien (47/48), Sonderausgabe: Kraftwerksgruppe Malta p. 10/20.

[1.75] *Grüner, J.:* Die Kraftwerskette Bertoldsheim-Ingolstadt an der oberen Donau. Voith Forsch. u. Konstr. 20, no 3.

[1.76] *Widmann, R.:* Die Kraftwerksgruppe Zemm-Ziller (The Zemm-Ziller group of power stations.) Österreich. Wasserwirtsch. 35 (1983) no 5/6, p. 126/137.

[1.77] Yearbook of World Energy Statistics, United Nations, New York, 1981.

[2.1] *Liberatore, S. N.:* Financing large hydro projects with IDB. Water Power 31 (1979) no 8, p. 23/26.

[2.2] *Bevril, T. W.:* The role of international lending agencies. Water Power 31 (1979) no 8, p. 27/30.

[2.3] *Warncock, J. G.:* Project financing: precept and practice. Water Power 31 (1979) no 8, p. 36/39.

[2.4] *Schubert, H.:* Kommerzielle Aspekte bei Großanlagengeschäften. Voith Inf. Wasserturbinen (1975) no 2.

[2.5] *Bertinelli, E.:* Bonding and insurance: a contractor's view. Water Power 31 (1979) no 8, p. 40/44.

[2.6] *Stigler, H.:* Ausgewählte Gesichtspunkte zur energiewirtschaftlichen Bewertung bei Kleinwasserkraftwerken. Österreich. Wasserwirtsch. 33 (1981) p. 265.

[2.7] *Mitchell, A. G.:* Pricing electric power from small hydroplants. Water Power 32 (1980) no 7, p. 42/46.

[2.8] *Tschermutter, P.:* Nutzen-Kosten Analyse und Rentabilitätsbereiche bei Kleinwasserkraftwerken. Österr. Wasserwirtsch. 33 (1981) p. 259.

[2.9] *Nachtnebel, H. P.:* Bewertung der Kleinkraftwerke. Österr. Wasserwirtsch. 33 (1981), p. 254.

[2.10] *Picard, J.:* Les aspect socio-économique de la valeur de l'eau. Houille Blanche 32 (1977) no 2/3, p. 237/242.

[2.11] *Mayer, R.:* Ausbau der Neckarwasserstraße 1948 bis 1958. Die Wasserwirtsch. (1958) no. 3.

[2.12] *Rümelin, B.:* La liaison Main-Danube favorise la navigation et l'économie de l'eau. Houille Blanche 36 (1981) no 2/3, p. 93/98.

[2.13] *Fenz, R.:* Die Rhein-Main-Donau Wasserstraße und der österreichische Donauausbau. Österr. Wasserwirtsch. 30 (1978) p. 1.

[2.14] *Méchin, Y. and D. Normand:* Example d'application de la gestion optimale des réservoirs à buts multiple. Houille Blanche 32 (1977) no 2/3, p. 259/264.

[2.15] *Press, H.:* Kulturlanderhaltung und Kulturlandgewinnung durch wasserwirtschaftliche und wasserbauliche Maßnahmen. Berlin: Parvey Verlag 1959.

[2.16] *Coste, F. et al.:* Aspects referred to the hydromechanical equipment, manufacturing and characteristics hydroenergetics and navigation system "Portile de Fier" Danube. 7th IAHR Symp. Vienna (1974) Trans. VI, 1, p. 1/11. Delft: IAHR.

[2.17] *Borovoi, A. A. and L. P. Mikhailov:* The Nurek multipurpose development. Water Power 30 (1978) no 12, p. 53/55.

[2.18] *Mosonyi, E. and W. Buch:* Die Grundlagen der Wirtschaftlichkeitsanalyse und Kostenverteilung. 4. Fortbildungslehrgang Hydrologie. DVWW Univ. Karlsruhe 1972.

[2.19] *Mosonyi, E.:* Die neueste Entwicklung in der Wasserkraftnutzung und Pumpspeicherung. Fachtagung Haus der Technik, Essen. Nov. 1981.

[2.20] *Sirman, W. R.:* Turbines for the Grand Coulee hydro powerplant. Water Power 29 (1977) no 4, p. 37/47.

[2.21] *Pfafflin, G. E.:* 700 MW Francisturbines for Grand Coulee. 7th IAHR Symp. Vienna (1974). Trans. IV, 3, p. 1/11. Delft: IAHR.

[2.22] *Engström, F.:* Hydraulic turbine for the 3rd power plant at Grand Coulee dam. 7th IAHR Symp. Vienna (1974). Trans. IV, 2, p. 1/10. Delft: IAHR.

[2.23] *Chacour, S.:* Design technique for giant hydraulic turbines. Paper Canadian Electr. Ass., Hydr. power sect. March 17–20. (1975), Vancouver p. 1/7.

[2.24] Allis Chalmers, York Pa, USA: Site manufacture of Grand Coulee 700 MW Francis turbine. Prospectus.

[2.25] *Akhtar, A. et al.:* Field welding of large turbine runners. Water Power 31 (1979) no 9, p. 40/46.

[2.26] *Cotrim, J. R. et al.:* The bi-national Itaipú hydro power project. Water Power 29 (1977) no 10, p. 40/42; no 11, p. 44/52.

[2.26] *Moraes de, J. et al.:* Turbines for Itaipú. Water Power 33 (1981) no 12, p. 36/41; 34 (1982) no 1, p. 28/33.

[2.28] *Caric, D. M. et al.:* The Itaipú hollow gravity dam. Water Power 34 (1982) no 5, p. 30/44.

[2.29] *Hardt, E.:* Fertigung eines Spiralgehäuses und eines Turbinenlaufrades für eine Francisturbine. DVS Berichte 76 (1983), p. 52/58.

[2.30] *Chavarri, G.:* Guri power complex, design. Am. Power Conf. Chikago (1979) pap. no 1.

[2.31] *Carrera, E.:* Guri power complex, installation and operation. Am. Power Conf. Chicago (1979) pap. no 3.

[2.32] *Beltran, H. et al.:* Guri power complex. The 10000 MWs of hydraulic turbines for the Guri project. Am. Power Conf. Chicago (1979) pap. no 5.

[2.33] *Carrera, E. S. et al.:* Guri power complex. Generators. Am. Power Conf. Chicago (1979) pap. no 6.

[2.34] *Palacios, P. H.:* Guri power complex, planning. Am. Power Conf. Chicago (1979) pap. no 2.

[2.35] *Bronowski, G. A. and M. J. Galperin:* Some special features in the design of the Krasnojarsk turbines (Orig. Russian) Energomasinostroenije 8 (1965) no 3, p. 32.

[2.36] Anonymous: The Bratsk 230 MW turbines. Water Power 15 (1963) no 8, p. 324/325.

[2.37] *Smith, H.:* The Russians. The N.Y.Times Book Co., New York 1976.

[2.38] *Steche, O.:* Brehms Tierleben. 4rth edition, 13 volumes, vol. 3 Fische, p. 139 Bibliographisches Institut Leipzig 1914.

[2.39] *Heynes, G. et al.:* Layout of the HVDC terminal stations Cabora Bassa and Apollo. Int. Conf. on large high voltage Electro-systems Paris (1974) pap. 14–04 p. 1/10.

[2.40] *Klein, M. et al.:* Cabora Bassa. A gigantic HVDC project unfolding in Africa. IEEE-Spectrum 11 (1974) no 10, p. 51/58.

[2.41] *Fosca, V.:* The Turim Magurele-Nicopole hydro station for the Danube. 7th IAHR Symp. Vienna (1974). Trans. VI, 1, p. 1/11.

[2.42] *Stchegolev, G. S. et al.:* Construction and operation of the Jerdap-Iron gates hydro scheme. Water Power 29 (1977) no 8, p. 48/51.

[2.43] *Warncock, J. G.:* Churchill Falls, a project profile. Water Power 31 (1979) no 9, p. 52/57.

[2.44] *Netsch, H. and A. Giacometti:* Axial flow induced vibrations in large high head machines. Water Power 34 (1982) no 8, p. 21/27.

[2.45] *Francou, J.:* L'amenagement hydroélectrique d'Inga sur Zaire. Houille Blanche 32 (1977) no 2/3, p. 121/132.

[2.46] *Bader, W.:* Großzügige Wasserstraßenplanungen im Donauraum. Wasserwirtschaft 65 (1975) no 4, p. 95/101.

[2.47] *Fenz, R.:* Heutige und geplante Wasserkraftnutzung an der Donau. Wasser und Energiewirtschaft 65 (1973) no 3/4, p. 101/114.

[2.48] *Fenz, R. and W. Roehle:* Der Ausbau der mittleren und unteren Donau. Jahrbuch der Hafenbautechnischen Gesellschaft 35 (1975/76), p. 231/236.

[2.49] *Roehle, W.:* Das Donaukraftwerk am Eisernen Tor. Wasser und Energiewirtschaft 65 (1973) no 3/4, p. 115/125.

[2.50] *Bachmann, J.:* Standardizing small turbines. Water Power 32 (1980) no 7, p. 40/42.

[3.1] *Lucas, K. C.:* The mortality to fish passing throug hydraulic turbines as related to cavitation and performance characteristics; pressure change, negative pressure and other factors. Proc IAHR Symp. Sendai, Japan (1962). Tohoku Univ. Inst. High Speed Mech., p. 307/336.

[3.2] *Roger's, A.:* Rescueing Dinorwic's fish. Water Power 32 (1980) no 10, p. 24/26.

[3.3] *Bisak, E. K., C. Taubmann, and P. Fischer:* Improvement in transport of floating debris. Water Power 28 (1976) no 11, p. 41/45.

[3.4] *Dexter, R. B. and E. B. Zeigler:* Penstock intake vortex and related turbine operation model studies. Symp. ASCE-IAHR-ASME, Fort Collins Co, (1978), Proc. Vol. I, p. 425/436.

[3.5] *Bleuler, W.:* Schützen. EW-Mitt. 36 (1963) no 2/3, p. 27.

[3.6] *Meystre, N.:* 100 Jahre Schweizer Druckrohrleitungen für Wasserkraftwerke. EW-Mitt. 52 (1979) no 2, p. 16.

[3.7] *Pirchl, H.:* Verteilleitung Castaic. EW-Mitt. 47 (1974) no 2, p. 42.

[3.8] *Meystre, N.:* Verteilleitung für die Zentrale Sils. EW-Mitt. 32 (1959) no 2/3, p. 76.

[3.9] *Wood, M. M. et al.:* Dams and their tunnels. Water Power 32 (1980) no 2, p. 27/33; no 3, p. 47/50; no 4, p. 37/44; no 5, p. 42/48.

[3.10] *Anderson, A.:* Surge tank solutions using programmable pocket calculators. Water Power 30 (1978) no 7, p. 50/58.

[3.11] *Yu-Tek Li:* Surge tank analysis, a graphical solution. Water Power 28 (1976) no 5, p. 28/32.

[3.12] *Martin, C. S.:* Method of characteristics applied to calculation of surge tank oscillations. Int. conf. on pressure surges. Univ. Kent, Canterbury (1972), paper E1, p. 1/12.

[3.13] Hütte: Taschenbücher d. Ingenieurs, Bauhütte Bd. II. Grundbau, Verkehrsbau, Wasserbau. Berlin: Verlag Ernst 1970.

[3.14] *Glattfelder, A. H. et al.:* Zur Begrenzung von Wasserschloßtransienten in hydraulischen Anlagen. EW-Mitt. 53 (1980) no 1/2, p. 20.

[3.15] *Jaeger, Ch.:* Theory of resonance in hydro power systems. Water Power 15 (1963) no 4, p. 14.

[3.16] *Calame, J. and D. Gaden:* Theorie des chambres d'équilibre. Paris: La Concorde et Ganthier Villars. 1926.

[3.17] *Brekke, H.:* Induced hydraulic resonance analysis on a Francis-turbine power plant with an air-cushioned high pressure tunnel system. Trans 7th IAHR Symp. Vienna (1974), p. 1, II 3, p. 1/13.

[3.18] *Frank, J.:* Nichtstationäre Vorgänge in den Zuleitungs- und Ableitungskanälen von Wasserkraftwerken. Berlin: Verlag Springer 1957.

[3.19] *Baustädter, K.:* Das Pfeilerkraftwerk aus heutiger Sicht. Österr. Wasserwirtsch. 31 (1979) p. 149.

[3.20] *Penman, A. D. M.:* Measuring earth pressures in embankment dams. Water Power 31 (1979) no 6, p. 29/34.

[3.21] *Severn, R. T.:* The aseismic design of concrete dams. Water Power 28 (1976) no 1, p. 41/46.

[3.22] *Fetzer, C. A.:* Seepage of earth and rockfill dams on rock foundations. Water Power 29 (1977) no 8, p. 38/44.

[3.23] *Anonymous:* The Assuan dam hydroelectric scheme: Water Power 13 (1961) no 12, p. 463; 14 (1962) no 1, p. 4; no 2, p. 49.

[3.24] *Gill, A.:* Blankets for dams on pervious foundations. Water Power 32 (1980) no 9, p. 47/50.

[3.25] *Singhota, J. S. and R. S. Sachdeva:* Prevent seepage through India's Bhakra dam. Waterpower 28 (1976) no 10, p. 26/31.

[3.26] *Jaeger, Ch.:* The Vajont rock slide I and II. Water Power 17 (1965) no 3, p. 110; no 4, p. 142.

[3.27] *Jaeger, Ch.:* The Malpasset report. Water Power 15 (1963) no 2, p. 55/61.

[3.28] *Blind, H.:* Inspection galleries in earth and rockfill dams. Water Power 34 (1982) no 4, p. 25/31.

[3.29] *Blind, H.:* A German view of dam safety. Water Power 34 (1982) no 3, p. 21.

[3.30] *Gallico, A.:* Foundation drainage of arch dams. Water Power 28 (1976) no 4, p. 54/59.

[3.31] *Bonaldi, P., M. Fanelli, and G. Guiseppetti:* Displacement forecasting for concrete dams. Water Power 29 (1977) no 9, p. 42/50.

[3.32] *Jaeger, Ch:* Assessing problems of underground structures. Water Power 28 (1976) no 1, p. 29/36.

[3.33] *Fanelli, M. and G. Giuseppetti:* Safety monitoring of concrete dams. Water Power 34 (1982) no 11, p. 31/33.

[3.34] *Fanelli, M:* Automatic observation for dam safety. Water Power 31 (1979) no 11, p. 106/110; no 12, p. 41/48.

[3.35] *Hansen, D. and L. H. Roehm:* The response of concrete dams to earthquakes. Water Power 31 (1979) no 31, p. 27.

[3.36] *Housner, G. W. et al.:* Earthquake considerations in dam design. Water Power 31 (1979) no 7, p. 31/37.

[3.37] *Scott, R. F. and A. M. Abdel-Ghaffar:* Forced vibration tests of an earth dam. Water Power 30 (1978) no 10, p. 41/45.

[3.38] *Leps, T. M., A. S. Strassburger, and R. L. Mechan:* Seismic stability of hydraulic fill dams. Water Power 30 (1978) no 10, p. 27/36; no 11, p 43/52.

[3.39] *Johnson, F. A. and P. Illies:* A classification of dam failures. Water Power 28 (1976) no 12, p. 43/45.

[3.40] *Herzog, M. A. M.:* Failure mechanism in dams subject to earthquakes. Water Power 32 (1980) no 8, p. 28/30.

[3.41] *Seed, H. B., F. I. Makdisi and P. de Alba:* The performance of earth dams during earthquakes. Water Power 32 (1980) no 8, p. 17/27.

[3.42] *Biswas, A. K. and M. R. Biswas:* Hydro power and the environment. Water Power 28 (1976) no 5, p. 40/43.

[3.43] *Cunietti, M., A. Marazio and F. Vermese:* Considerations gènerales sur le controle du comportments des barrages moyennement procédes géodésiques. L'Energia Elettrica 50 (1973) no 3, p. 1/14.

[3.44] *Germond, J. P.:* Insuring dam risk. Water Power 29 (1977) no 6, p. 36/39.

[3.45] *Moffat, A. I. B. and A. C. Price:* The rolled dry lean concrete dam. Water Power 30 (1978) no 7, p. 35/41.

[3.46] *Joshui, C. S.:* Optimum profiles of gravity dams. Water Power 34 (1982) no 9, p. 35/36.

[3.47] *Glebow, V. D. and V. S. Kuznetsov:* Embankment dams with polyethylene and steel membranes. Water Power 35 (1983) no 1, p. 25/28.

[3.48] *Pircher, W. and H. Schwab:* Austria's Finstertal rockfill dam. Water Power 32 (1980) no 6, p. 43/47.

[3.49] The Chinese Committee an large dams: Dam construction by the Chinese people. PO Box 366 Beijing. People's Rep. of China.

[3.50] *Stini, J.:* Die baugeologischen Verhältnisse der österreichischen Talsperren. Wien: Springer Verlag 1955.

[3.51] *Mermel, T. W.:* Major dams of the world. Water Power 33 (1981) no 5, p. 55/64.

[3.52] *Mermel, T.W:* International activity in dam construction. Water Power 28 (1976) no 4, p. 66/69.

[3.53] *Schnitter, N. J.:* The evolution of the arch dam. Water Power 28 (1976) no 10. p. 34/40; no 11, p. 19/21.

[3.54] *Özis, U., Y. Kocak:* The first arch dam in Turkey. Water Power 29 (1977) no 4, p. 30/36.

[3.55] *Schlosser, J. et al.:* Der Bau der Kölnbreinsperre. Energiewirtschaft. Sonderdruck: Kraftswerksgrupe Malta p. 57/66.

[3.56] *Fanelli, M. et al.:* Il calculo delle dighe a volte. ENEL. Relazione di studie e ricerca (1978), no 340.

[3.57] *Legas, J.:* First prestressed arch dam in the USA. Water Power 28 (1976) no 2, p. 21/24.

[3.58] *Eiselmayer, M. and R. Widmann:* Zum Schwingungsverhalten von Gewölbemauern. Österr. Wasserwirtsch. 31 (1979) p. 154.

[3.59] *Flögl. H.:* Der Einfluß des Kriechens und der Elastizitätsänderung des Betons auf den Spannungszustand von Gewölbesperren. Wien: Springer-Verlag 1954.

[3.60] *Barrows, H. K.:* Water Power Engineering. New York: publishers MacGraw Hill. 1927.

[3.61] *El Yussif, F. Y.:* Dimensioning multiple arch dams. Water Power 29 (1977) no 7, p. 47/49.

[3.62] *Hartung, F. and K. Csallner:* The angular dam-a study of a new form of dam. 11th ICOLD, Madrid. Q 43 R 2.

598

[3.63] *Mackintosh, J. B.:* American advances in earth dam construction. Water Power 16 (1964) no 5, p. 219.

[3.64] *Schober, W.:* Staudammforschung – ein Schwerpunkt am Institut für Bodenmechanik, Fels-mechanik und Grundbau der Universität Innsbruck. Österr. Wasserwirtsch. 31 (1979) p. 107.

[3.65] *Ganser, O. and A. Niel:* Sicherheit und Kontrolle von Talsperren. Österr. Wasserwirtsch. 32 (1980) p. 152.

[3.66] *Mundt, G.:* Hochwassergefahr und Hochwasserabwehr am unteren Inn. Österr. Wasser-wirtsch. 32 (1980) p. 160.

[3.67] *Knaus, J.:* Besondere Erfahrungen und konstruktive Konsequenzen aus Modellversuchen für Entlastungsanlagen an deutschen Talsperren. Wasserwirtsch. 70 (1980) no 3. p. 1/4.

[3.68] *Herbrand, K. and H. Scheuerlein:* Examples of model tests dealing with special problems and design criteria at large capacity spillways. Proc. 13th ICOLD. New Delhi (1979). Q 50, R 10. p. 161/176.

[3.69] *Neiger, F.:* Donaustauräume und Hochwasserschutz. Österr. Wasserwirtsch. 32 (1980). p. 163.

[3.70] *Fahlbusch, F. E.:* Optimum design flow for spillway. Water Power 31 (1979) no 11, p. 79/84.

[3.71] *Knaus, J.* Computation of maximum discharge at overflow rockfill dam. 13th ICOLD. New Delhi (19799). Q 50, R 9, p. 143/160.

[3.72] *Hartung, F. and J. Knauss:* Barrages with gateless built-in diversion devices for constant discharge under extreme variationes of afflux. 12th ICOLD. Mexico (1976). Q 47, R 1, p. 732/740.

[3.73] *Hartung, F.:* Gestaltung von Hochwasserentlastungsanlagen bei Talsperrendämmen. Was-serwirtsch. 62 (1972) no 1/2, p. 1/13.

[3.74] *Hack, H. P.:* Air entrainment in dropshafts with annular flow by turbulent diffusion. Proc. 17th IAHR congr. Baden-Baden (1977). Vol. 1, p. 505/514.

[3.75] *Hartung, F.:* Gates in spillways of large dams. Trans. 11th ICOLD. Madrid (1973). Q 41, R 77.

[3.76] *Hartung, F.:* Gedanken zur Gestaltung von Klappenwehren. Wasserwirtsch. 9 (1975) p. 238/243.

[3.77] *Mussard, F.:* Grundablaßschützen EW-Mitt. 25/26 (1952/53) p. 147.

[3.78] *Naudascher, E.:* Flow-induced structural vibrations. IUTAM-IAHR Symposium Karlsruhe 1972. Berlin, New York: Springer-Verlag 1972.

[3.79] *Naudascher, E. and D. Rockwell:* Oscillator modell approach to the identification and assess-ment of flow-induced vibrationes in a system. IAHR J. 18 (1980) no 1, p. 59/81.

[3.80] *Rockwell, D. and E. Naudascher:* Review-self exciting oscillations of flow past cavities. Trans. ASME 100 (1978) p. 152/164.

[3.81] *Peters. K.:* Flatterschwingungen an Überfallstrahlen. Mitt. Hydr. Inst. TH München 10 (1940) p. 40/55.

[3.82] *Petrikat, K.:* Schwingungsanfachende Kräfte im Wehrbau. MAN Forschungsheft 1953.

[3.83] *Josserand, A., D Milan, and G. Berthollon.:* Vibrations des vannes des aménagements hydro-eléctriques. Connaissances actuelles, exemples industrielles. Houille Blanche 35 (1980) no 7/8, p. 476/483.

[3.84] *Binder, M. M. et al.:* Problèmes généraux de la dissipation d'énergie dans les organes et circuits hydrauliques. Houille Blanche 35 (1980) no 7/8, p. 424/430.

[3.85] *Kulkarni, V. N. and J C. Patel:* Ski jump spillway for India's Ukai dam. Water Power 33 (1981) no 9, p. 44/48.

[3.86] *Herbrand, K.:* The spatial hydraulic jump. IAHR J. 11 (1973) p. 205/218.

[3.87] *Häusler, E.:* Der Kolk unter der Kariba Staumauer. Tiefbau 10 (1972) p. 953/962.

[3.88] *Häusler, E.:* Zur Kolkproblematik bei Hochwasser-Entlastungsanlagen an Talsperren mit freiem Überfall. Waserwirtsch. 70 (1980) no 9, p. 1.

[3.89] *Hartung, F. and E. Häusler:* Scours, stilling basin and downstream protection under free overfall jets at dams. Trans 11th ICOLD. Madrid (1973), Q 41, R 3.

[3.90] *Herbrand, K. and J. Knauss:* Computation and design of stilling basin with abruptly or gradually enlarged boundaries. Trans. 11th ICOLD, Madrid (1973). Q 41, R 4.

[3.91] *Sharma, H. R. and E. R. S. Goel:* Inlet and control valves for hydro power projects. 11th IAHR symp. Amsterdam (1982). proc. vol 1, 12 p 1/9.

[3.92] *Casacci, S.,P. Hudson and J. Bose:* Vannes cylindriques de protection des turbomachines hydrauliques. Houille Blanche 35 (1980) no 7/8, p. 30/31.

[3.93] *Strub, W. R. et al.:* Ring gates for La Grande 2 turbines. Water Power 31 (1979) no 9, p. 30/31.

[3.94] *Grein, H.:* Experimentelle Untersuchungen als Grundlage zur konstruktiven Gestaltung von Absperrorganen in Wasserkraftanlagen. Symp. Absperrorgane, Essen, Haus der Technik 1981.

[3.95] *Polder, G.:* 50 Jahre Escher Wyss Kugelschieber. EW-Mitt. 48 (1975) p. 1

[3.96] *Wiedler, K.:* Die Pumpenkugelschieber von Vianden. EW-Mitt. 38 (1965) no 1, p. 29.

[3.97] *Grein, H. and J. Osterwalder:* Hydraulic forces acting on the upstream and downstream pipelines and the casing of butterfly valves during closing. ASCE-IAHR-ASME Symp. Fort Collins, Co (1978) Proc. Vol. II p 423/438.

[3.98] *Osterwalder, J. and K.-J. Peschges:* Cavitation investigation of butterfly valves. 8th IAHR Sympos. Leningrad (1976), II - 4, p. 148/159.

[3.99] *Meystre, N.:* Sicherheitsdrosselklappen. EW-Mitt. 36 (1963) no 1, p. 13.

[3.100] *Meystre, N.:* Drosselklappen-Grundablaßschütze, Druckleitungen. EW-Mitt. 27/28 (1954/55) p. 59.

[3.101] *Barp, B. and H. Grein:* Die Doppeldecker-Drosselklappe. EW-Mitt. 42 (1969) no 1, p. 11.

[3.102] *Schwarz, H. J.:* Design trend in the construction of high pressure outlet gate. Swiss Dam Techniques. Publ. 42 (1970).

[3.103] *Peschges, K.-J.:* Experimentelle Untersuchungen zum Kavitations und Betriebsverhalten einer linsenförmigen Drosselklappe. Dr.-Ing. thesis TH Darmstadt 1978.

[3.104] *Strohmer, F.:* Investigating the characteristics of shut-off valves by model tests. Water Power 29 (1977) no 7, p. 41/46.

[3.105] *Osterwalder, J.:* Der Escher Wyss Kugelschieber. Versuche bei hohen natürlichen Gefällen zur Beurteilung des Verhaltens bei Rohrbruch und Freilauf. EW-Mitt. 31 (1958) no 2, p. 7.

[3.106] *Malquori, E. and F. Milanese:* Pump-service valves in Italian pumped storage stations, characteristics and performance. 11th IAHR Symp. Amsterdam 1982. Proc. Vol 1,11, p. 1/15.

[3.107] *Keller, C. and I. Vuskovic:* Strömungsversuche an Sicherheitsorganen von Wasserkraftanlagen. EW-Mitt (1942/43) S. 91.

[3.108] *Osterwalder, J. and Ch. Wirth:* Experimentelle Untersuchungen des Ausflußverhaltens rohrbruchähnlicher Querschnitte. Wasserwirtsch. 72 (1972) no 9, p. 324/329.

[3.109] *Richter, K.:* Die Festigkeit von Kugelschiebern. EW-Mitt. 41 (1968) no 3, p. 14.

[3.110] *Wagensonner, H.:* Planung und Ausführung der maschinenbaulichen und elektrischen Ausrüstung des Kaunertalkraftwerkes. Elektrotechn. u. Masch. bau. 80 (1971) no 5, p. 181/228.

[3.111] *Chausson, P.:* Four large vertical shaft Charmilles Pelton turbines. Charmilles Techn. Bulletin. no 141 975, p. 7/14.

[3.112] *Mederer, E.:* Gründungsmaßnahmen für das Kraftwerk Silz. Österr. Wasserwirtsch. 31 (1979) p. 186.

[3.113] *Osterwalder, J.:* Tail water depression of multi jet impulse turbines. Water Power 18 (1966) no 9, p. 358/362.

[3.114] *Grein, H. and H. K. Höller:* Peltonturbinen im Gegendruckbetrieb. EW-Mitt. 54 (1981) no 1, p 32/36.

[3.115] *The Editor:* Small but thriving (From Michell to Ossberger) Water Power 31 (1979) no 1, p. 54/55.

[3.116] *Deriaz, P.:* Comparative study of Kaplan und Deriaz turbines. Electr. Rev. 165 (1959) no 14, p. 633.

[3.117] *Kovalev, N. N. and W. S. Kviatkovsky:* (Orig. Russian) Kotloturbinostroenije, Leningrad 1964.

[3.118] *Ronicke, N. and J. J. Victory:* Francis turbines for small scale application. Water Power 34 (1982) no 1, p. 61/65.

[3.119] *Petit, Ch.:* Microcentrales hydroélectriques d'une puissance inférieurs à 100 kW. Houille Blanche 36 (1981) no 4/5, p. 249/257.

[3.120] *Etienne, J. and P. Chadenson:* Les minigroupes hydroélectriques (100 à 1000 kW). Houille Blanche 36 (1981) no 4/5, p. 269/274.

[3.121] *Rabaud, J. and G. Picolier:* Les groupes pour petites centrales de production (1000 à 8000 kW) Houille Blanche 36 (1981) no 4/5, p. 276/282.

[3.122] *Miller, H.:* The straight flow turbine turns full circle. Water Power 29 (1977) no 1, p. 31/35.

600

[3.123] *Cotillon, J.:* Advantages of bulb units for low head developments. Water Power 29 (1977) no 1. p. 21/26.

[3.124] *Cederberg, B.:* Hydroturbines geared for higher power. Water Power 33 (1981) no 9, p. 40/41.

[3.125] *Borciani, G. and G. Giberti:* Research on multi-stage reversible model pump-turbines for the Chiotas-Piastra project. 7th IAHR symp. Vienna (1974). Trans. XI 3. p. 21/24.

[3.126] *Meier. W. and M Jaquet:* Single and multistage pump-turbines for high-head storage plants. ASME Fluids Engineering Conference on Pump Turbine Schemes. Niagara Falls, New York (1979), paper.

[3.127] *Kovalev, N. N.:* Hydroturbines (orig. Russian) Israel Scientific Translation, Jerusalem. 1965.

[3.128] *Chaix, B.:* Comparaison du point de vue hydrauliques entre la bâche spirale de type Piguet et une bâche conventionelle. Charmilles Inform. Techniques no 7 (1958) p. 31/34.

[3.129] *Surber, A.:* Die druckausgeglichene Dehnungsmuffe von Vianden. EW-Mitt. 38 (1965) no 1, p. 24.

[3.130] *Gordon, J. L.:* Estimating hydro power house crane capacity. Water Power 30 (1978) no. 11, p. 25/26.

[3.131] *Zakayow. D.:* Circular underground powerhouse for USA's Kerchhoff. Water Power 33 (1981) no 9. p. 21/24.

[3.132] *Shingota, J. S. et al:* The design of penstock Wyes for the Bari hydrostation. Water Power 29 (1977) no 6, p. 42/46.

[3.133] *Novotny. V.:* Spherical branch-off pipes for pumped storage plants. Water Power 32 (1980) no 9. p. 42/47.

[3.134] *Christ, A. and W. v. Allmen:* Strömungstechnische Erkenntnisse über Abzweigstücke von Verteilleitungen. EW-Mitt. 53 (1980) no 1/2, p. 20.

[3.135] *Süss, A. and J. Hassan:* Verminderung von Materialaufwand und Energieverlusten bei Verteilleitungen von Wasserkraftanlagen. EW-Mitt. 30/31 (1957/58) p. 25.

[3.136] *Wiederkehr, R.:* Zur Berechnung von Zylinderschalen. EW-Mitt. 33 (1960) no 1/2/3, p. 159.

[3.137] *Wiederkehr, F. and P. Ritter:* Die Einflußzahlen der Zylinderschale veränderlicher Wandstärke. EW-Mitt. 33 (1960) no 1/2/3, p. 162.

[3.138] *Dolder, G.:* Escher Wyss Verteilleitung mit biegefreier Innenverstärkung für hydraulische Anlagen. EW-Mitt. 39 (1968) no 2, p. 26.

[3.139] *Meystre, N. and W. Stauffer:* Bruchverhalten von Rohrleitungen für Druck und Verteilleitungen, die in gewissen Gebieten frühzeitig plastisch verformt werden. EW-Mitt. 44 (1971) no 1, p. 15.

[4.1] *Rossmann, H.:* Möglichkeiten und Grenzen wasserwirtschaftlicher Planung. Österr. Wasserwirtsch. 32 (1980) p. 57.

[4.2] *Nemet, A.:* Mathematisches Modell hydraulischer Anlagen. EW-Mitt. 47 (1974) no 1, p. 3.

[4.3] *Hartung, F.:* Hydraulische und mathematische Modelle an Flüssen. Wasserwirtsch. 60 (1970) no 1/2, p. 1/10.

[4.4] *Altieri, D.:* Tailwater levels for maximum power. Water Power 28 (1976) no 9, p. 36/39.

[4.5] *Ramsahoe, S. I.:* Flow duration curves in tropical equatorial regimes. Water Power 34 (1982) no 12, p. 66/69.

[4.6] *Sheldon, L. H.:* Cost analysis of hydraulic turbine. Water Power 33 (1981) no 6, p. 24/28.

[4.7] *Bahamonde, R.:* Economic criteria in selecting the number of units for a hydro plant. Waterpower 33 (1981) no 7, p. 43/45.

[4.8] *Gingold, P. R.:* The optimum size of small run-off-river plants. Water Power 33 (1981) no 11, p. 50/53.

[4.9] *Keller, C. and H. Bleuler:* Der theoretisch günstigste Durchmesser für Axialturbinen. EW-Mitt. 10 (1937) p. 112.

[4.10] *Pantell, K.:* Das Laufrad der Kaplanturbine und seine Kennlinie. Wasserkraft u. Wasserwirtsch. München, Berlin (1934) p. 251.

[4.11] *Raabe, J.:* Beiträge zur Berechnung von Kaplanturbinen. Ing. Arch. 27 (1959) no 1, p. 1/30.

[4.12] *Pfleiderer, C.:* Die Kreiselpumpen für Flüssigkeiten und Gase. Berlin: Springer-Verlag 1961.

[4.13] *Gordon. J. L.:* Estimating hydro stations costs. Water Power 33 (1981) no 9, p. 31/33.

[4.14] *Yang, K. H.:* Design trend of hydro plants in the USA. Water Power 32 (1980) no 2. p. 32/36.

[4.15] *Raabe, J.:* The optimization of speed coefficient Ku for hydraulic reaction turbines with special emphasis to mixed flow type. Paper 3 ro Colloqio Turbomáquinas, The University of Valencia. 1982.

[4.16] *Seus, G. and W. Bauch:* Entwurfsoptimierung von Stauräumen an Wehren. Water Power 24 (1972), p. 284/289.

[4.17] *Seus, G. J. and O. Ushu:* Über die adaptive Steuerung von Hochwasserrückhaltebecken-Systemen. Wasserwirtsch. 68 (1978) no 1/2, p. 1/8.

[4.18] *Klaghofer, E.:* Ein Beitrag zur Bestimmung der Verdunstung von einer freien Wasseroberfläche. Österreich. Wasserwirtsch. 32 (1980) p. 38.

[4.19] *Mosonyi, E.:* Leakage and seepage from upper reservoirs. Water Power 33 (1981) no 1, .p. 35/39.

[4.20] *Mühlemann, E. H.:* Hydraulische Maschinen für Pumpspeicheranlagen und Vergleiche von Kosten, Wirkungsgraden und Anfahrzeiten. EW-Mitt. 45. (1972) no 1, p. 3.

[4.21] *Panichelli, S. et al.:* Pumped storage plant evaluation planning studies. Water Power 33 (1981) no 1, p. 55/59.

[4.22] *Zobel, R.:* Versuche an einer hydraulischen Rückstromdrossel. Mitt. Hydr. Inst. TH München, Vol. 8 (1936) p. 1/47.

[4.23] *Seeber, G.:* Das Wasserschloß des Kaunertalkraftwerkes der TIWAG. Schweiz. Bauzeitg. 88 (1970) no 1, p. 1/8.

[4.24] *Tagwerker, J:* Häufigkeit von Wasserschloßschwingungen und ihre Auswirkungen auf die Betriebsfestigkeit von Stollenpanzerungen. Österr. Wasserwirtsch. 32 (1980) p. 105.

[4.25] *Peruginelli, A.:* Flow in horseshoe section tunnels. Water Power 28 (1976) no 7, p. 20/26.

[4.26] *Rössert, R.:* Hydraulik im Wasserbau. München: Oldenbourg-Verlag 1981.

[4.27] *Nir, Z.:* Partition lines in Moody's diagram. Water Power 31 (1979) no 3. p. 29/34.

[4.28] *Purdy, G, C.:* Energy loss of draft tube exits and in penstock. Water Power 26 (1974) no 10, p. 53/54.

[4.29] *Müller, W. and H. Stratmann:* Rohrleitungsverlust und Druckleitungen von Wasserkraftanlagen. Techn. Rundschau Sulzer 3 (1964).

[4.30] *Maksimovic, C.:* Reducing drag by polymers for hydro constructions. Water Power 30 (1978) no 6, p. 53/58.

[4.31] *Parmakian, J.:* Minimum thickness for handling steel pipes. Water Power 34 (1982) no 6, p. 18/19.

[4.32] *Surber, A.:* Experimentelle Untersuchung zur Bestimmung der geeigneten Druckschachtpanzerung eines Großkraftwerkes. EW-Mitt. 32 (1959) no 1, p. 3.

[4.33] *Mait, P. F. et al.:* Prestressed concrete pressure tunnels. Water Power 30 (1978) no 3, p. 23/31.

[4.34] *Sarkaria, G. S.:* Economic penstock diameter. Water Power 31 (1979) no 11, p.70/72.

[4.35] *Mühlemann, E. H. and G. Dolder:* Druckleitungen und Druckschächte für hydroelektrische Anlagen, insbesondere in der Schweiz. EW-Mitt. 44 (1971) no 2, p. 33.

[4.36] *Povh, D.:* Hochspannungsgleichstromübertragung. Siemens Eng. Techno E-124/1921.

[4.37] *Hengsberger, J R. et al.:* An oil cooled HVDC thyristor valve for outdoor installation. Int. Conf. on large high voltage el. Systems. Paris 1970.

[4.38] *Beriger, C. et al.:* Design of water cooled thyristor valve for extension of Manitoba Hydro-HVDC System. Int. Conf. on Large high voltage el. systems. Paris (1976). pap. 14–05, p. 1/9.

[4.39] *Causse, L. and A. Lacoste:* Prospects concerning the development of power transmission methods by way of underground cables in France. Int. Symp. High Voltage Technology. Techn. Univ. Munich (1972), p. 535/541.

[4.40] *Eidinger, A. and C. D. Flössel:* High power transmission with gas-insulated pipe-type cables-a comparison with lines and cables. Intern. Symp. High Voltage Technology, Techn. Univ. Munich (1972). p. 542/549.

[4.41] *Scheffler, E.:* The "wellmantel"- a welded and corrugated tube-as a component for new kinds of high power cables. Intern. Symp. High Voltage Technology, Techn. Univ. Munich (1972), p. 579/586.

[4.42] *Peschke, E. F.:* Bulk power transmission by cables. Intern. Symp. High Voltage Technology, Techn. Univ. Munich (1972), p. 558/565.

602

4.43] *Roemer, L. E., S. R. Robinson and D. C. Thorn:* Non-destructive test procedures for underground power cables. Internat. Symp. High Voltages Technology, Techn. Univ. Munich (1972), p. 573/578.

4.44] *Girkmann, K. and E. Königshofer:* Die Hochspannungsfreileitungen. 2. Auflage 1952. Wien: Springer-Verlag.

4.45] *Rieger, H. and R. Fischer:* Der Freileitungsbau. 2. Auflage. Berlin, Heidelberg, New York: Springer-Verlag 1975.

5.1] *Euler, L.:* Théorie plus complete des machines qui sont mise en mouvement par la réaction de l'eau. Hist. del'académie Royales des Sciences. t. 10. Berlin 1754.

5.2] *Kaufmann, W.:* Technische Hydro- und Aeromechanik, 3rd edition. Berlin: Springer-Verlag 1963.

5.3] *Truckenbrodt, E.:* Fluidmechanik, Bd. 1 und 2. 2. Auflage Berlin, New York: Springer-Verlag 1980.

5.4] *Schlichting, H.:* Grenzschichttheorie 3. Auflage Karlsruhe: Verlag Braun 1958.

5.5] *Lamb, H.:* Hydrodynamics. Cambridge Univ. Press publishers 1932.

5.6] *Streeter, V. L:* Fluid Mechanics. New York: McGraw Hill publishers 1951/66.

5.7] *Hinze, I. Q.:* Turbulence. New York: McGraw Hill publishers 1959.

5.8] *Albring,W.:* Angewandte Strömungslehre. Leipzig: Steinkopf-Verlag 1962.

5.9] *Gerber, H.:* Experimentelle Methoden zur Ermittlung von Potentialströmungsbildern. EW-Mitt. 1 (1928) p. 171.

5.10] *Raabe, J.:* Die rechnerische Behandlung des relativen Strömungsfeldes bei diagonalen Turbomaschinen. Masch. Markt 66 (1960), no 10, p. 6, no 12, p. 6.

5.11] *Betz, A.:* Einführung in die Theorie der Strömungsmaschinen. Karlsruhe: Verlag Braun 1959.

5.12] *Stanitz, J, D. and V. D. Prian:* A rapid approximate method for determining velocity distribution on impeller blades of centrifugal compressors. NACA TN. 2421 1951.

5.13] *Scholz, N:* Aerodynamik der Schaufelgitter. Karlsruhe: Verlag Braun 1965.

5.14] *Grammel, R.:* Die hydrodynamischen Grundlagen des Fluges. Braunschweig: Vieweg-Verlag 1917.

5.15] *Kutta, W.:* Auftriebskraft in strömenden Flüssigkeiten. Ill. astr. aeron. Mitt 1902.

5.16] *Joukovsky, N.:* Über die Konturen der Tragflächen der Drachenflieger. Z. f. Flugtechn. u. Motor Luftschiffahrt 1910.

5.17] *Bär, E.:* Messung des relativen Strömungsfeldes in Wasser an der Laufschaufel einer schnellläufigen Francisturbine. Dr.-Ing. thesis TU München 1969.

5.18] *Schlemmer, G.:* Messung des absoluten und relativen Strömungsfeldes einer schnelläufigen Francisturbine mit Berücksichtigung der Wirbelzopferscheinungen im Saugrohr. Dr.-Ing. thesis. TU München 1973.

5.19] *Petermann, H.:* Einführung in die Strömungsmaschinen. Berlin, New York: Springer-Verlag 1974.

5.20] *Riemerschmidt, F.:* Der Einfluß der Zähigkeit des Wassers auf die hydraulischen Eigenschaften einer kleinen Francistrubine. Mitt. d. Hydr. Inst. TH München vol 5 (1932) p. 20/46.

5.21] *Navier, M.:* Mémoire sur les lois du mouvement des fluides. Mem. de l'Acad. d. Sci 6, 389 (1827).

5.22] *Stokes, G, G.:* On the theories of the internal friction of fluids in motion. Trans. of the Cambr. Phil. Soc. 8 (1845).

5.23] *Prandtl, L.:* Über Flüssigkeitsbewegung bei sehr kleiner Reibung. III Int. Math. Kongr. Heidelberg 1904. NACA TM 452 (1928).

5.24] *Blasius, H.:* Grenzschichten in Flüssigkeiten mit kleiner Reibung. Z. Math u. Phys. 56 1 (1908)

5.25] *Hagen, G.:* Über die Bewegung des Wassers in engen zylindrischen Rohren. Pogg. Ann. 46, 423 (1839).

5.26] *Poiseuille, J.:* Récherches expérimentelles sur le mouvement des liquides dans les tubes de très petit diamètre. Comptes Rendue 11 961 at 1041 (1840) 12, 112 (1841).

5.27] *Nikuradse, J.:* Strömungsgesetze in rauhen Rohren. Forsch. Ing. Wes. Heft 361 (1933).

5.28] *Strscheletzky, M.:* Neuere Erkenntnisse über Wandgrenzschichten in hydraulischen Strömungsmaschinen. Voith Forsch. u. Konstr. 25 (1979) no 6 u. 27 (1981) no 6.

[5.29] *Reynolds, O.:* Phil. Trans. Roy. Soc. T. 186 A p 123.

[5.30] *Reichhardt, H.:* Messungen turbulenter Schwankungen. ZAMM 18 (1938) p. 358.

[5.31] *Blasius, H.:* Das Ähnlichkeitsgesetz bei Reibungsvorgängen in Flüssigkeiten. Forsch. Ing. Wes. (1913) 13

[5.32] *Prandtl, L.:* The mechanics of viscous fluids. In Durand: Aero dynamic theory. III Berlin: Springer-Verlag 1935, p. 142.

[5.33] *Coles, D. E.:* The law of the wake in the turbulent boundary layer. J. Fluid. Mech. I (1956) p. 191/226.

[5.34] *Lorentz H. A.:* Abhandlungen über theoretische Physik I. 43. Leipzig 1907.

[5.35] *Tollmien, W.:* Über die Entstehung der Turbulenz I. Mitt. Nachr. Ges. Wiss. Göttingen, Mth. Phys. Klasse 21 (1929).

[5.36] *Tollmien, W.:* Göttinger Monographie über Grenzschichten. Teil B 3 (1946).

[5.37] *Tollmien, W.:* Ein allgemeines Kriterium der Instabilität laminarer Geschwindigkeitsverteilungen. Nach. Ges. Wiss. Göttingen. Math. Phys. Klasse, Fachgeb. I 1 (79) 1935.

[5.38] *Schubauer, G. B. and H K. Skramstad:* Laminar boundary layer oscillations and stability of laminar flow. Nat. Bur. of Stand. Res. pap. 1772 (1943).

[5.39] *Truckenbrodt, E.:* Neuere Erkenntnisse über die Berechnung der Strömungsgrenzschicht mittels einfacher Quadraturformeln. Teil I, Ing. Arch. 43 (1973) p. 9/25; Teil II, Ing. Arch 43 (1974) p. 136/144.

[5.40] *van Driest, E. R.:* J. Aeronautical Sci. (1956) p. 1007.

[5.41] *Renau, L. R., J. P. Johnston and S. J. Kline:* Performance and design of straight two dimensional diffusers. Rep. PD-8. Thermo sci Div. Dep. Mech. Engg. Stanford Univ. California 1964.

[5.42] *Schraub, F. A. and S. J. Kline:* A study of turbulent boundary layer with and without longitudinal pressure gradients. Rep. MD-12 Thermo. sci. Div. Dep. Mech. Eng. Standford Univ. California 1955.

[5.43] *Barna, S. et al.:* Experiments on tandem diffusers with boundary layer suction applied in between. Symp ASCE-IAHR-ASME, Fort Collins Col. (1978), vol. I. p. 341/352.

[5.44] *Jesionek, K. J. and R. Wyszinski:* Effect of entrance conditions on the performance of curved subsonic diffusers. Symp. ASCE-IAHR-ASME Fort Collins Col. (1978) vol. I. p. 291/300.

[5.45] *Ghose, S. and S. J. Kline:* A numerical method for calculating the performance of two dimensional diffusers operating in the transitory stall regime, including prediction of optimum recovery. Symp. ASCE-IAHR-ASME. Fort Collins Col.(1978) vol. I. p 193/210.

[5.46] *Smith, C. R. and J. L. Layne:* An experimental investigation of flow unsteadiness generated by transitory stall in plane wall diffusers. Symp. ASCE-IAHR-ASME Fort Collins Col. (1978). Vol. I. p. 167/176.

[5.47] *Walley. R. L. and S. J. Kline:* A procedure for computation of fully stalled flows in two dimensional passages. Symp. ASCE-IAHR-ASME Fort Collins Col. (1978) Vol. I. p. 177/191.

[5.48] *Ashjace, J., J. P. Johnston and S. J. Kline:* Subsonic turbulent flow in plane wall diffusers. Dep. Mech. Engg. Stanfort Univ. Rep. PD-21 1980.

[5.49] *Strscheletzky, M.:* Über Grenzschichtablösung und freie Begrenzung in inkompressiblen Flüssigkeiten bei sehr kleiner Reibung. VDI Tagg. Strömgs. masch. Freiburg (1963). VDI Berichte no 75.

[5.50] *Bardina, J., S. J. Kline and J. H. Ferziger:* Computation of straight diffusers at low Mach number incorporating an improved correlation for turbulent attachment and reattachment. Stanford Univ. Thermo sci Div. Dep. Mech. Engg. Report PD-22 1982.

[5.51] *Wirasinghe, N E. A.:* Effect of swirl on conical diffuser performance. Symp. ASCE-IAHR-ASME Fort Collins Col. (1978) Vol. I. p. 223/234.

[5.52] *Strscheletzky, M.:* Gleichgewichtsformen der rotationssymmetrischen Strömungen mit konstantem Drall in geraden zylindrischen Rotationshohlräumen. Voith Forsch. u. Konstr. 5 (1959) no 1.

[5.53] *Dziallas, R.:* Francisturbinen bei Teil- und Überlast. Symp. Hydr-Strömungsmasch. Freiburg (1963) VDI Berichte no 75 p. 53/64.

[5.54] *Palde, U. J.:* Model and prototype turbine draft tube surge analysis by the swirl momentum method. 7th IAHR symp. Vienna (1974), trans III 3, p. 1/13.

[5.55] *Dörfler, P.:* Mathematisches Modell der zopferregten Teillastschwingungen von Francisturbinen. EW-Mitt. 59 (1980) no 1/2, p. 101.

604

[5.56] *Fischer, K.:* Untersuchung der Strömung in einer Zentrifugalpumpe. Mitt. d. Hydr. Inst. TH München (1931) vol. 4, p. 7/27.

[5.57] *Moon, J. M.:* Effect of Coriolis force on the turbulent boundary layer in rotating fluid engines. MIT gas turbines lab. (1962) Report 69.

[5.58] *Strscheletzky M.:* Wirkung und Steuerung der Sekundärströmung in hydraulischen Turboströmungsmaschinen. Voith Forsch. u. Konstr. 5 (1959) no 1.

[5.59] *Raabe, J.:* Über die Anwendung des Hamiltonschen Prinzips zur Berechnung von Trägheitsablösungen im umlaufenden Schaufelkanal einer Turbomaschine. Stroiniski Vestnik 21 (1975) no 9/10, p 1/14.

[5.60] *Wasielewski, R.:* Verlust in glatten Rohrkrümmern mit kreisrundem Querschnitt bei weniger als 90° Ablenkung. Mitt. Hydr. Inst. TH München 6 (1932) p 35/67.

[5.61] *Agerwal, P. K. and G. K. Viktorov:* The third two dimensional problem of three dimensional blade systems of hydraulic machines. Trans ASME J. Fluid Engg. 103 (1981) p. 33/51.

[5.62] *Raabe, J:* Der Relativwirbel als Verlustfaktor und Störungsursache für die Rotationssymmetrie der Stromflächen bei axialen Turbomaschinen. Masch. Markt 64 (1958) no 3, p. 7.

[5.63] *Föttinger, H.:* Über die Flüssigkeitsreibung umlaufender Scheiben, Zylinder und Zellenkörper. ZAMM 17 (1937) no 6, p. 356.

[5.64] *Domm, U. and H. Zilling:* Axial thrust in centrifugal pumps. Trans. IAHR Symp. Braunschweig (1966). VDI Fachgruppe Energietechnik paper J 23.

[5.65] *Greenspan, H. P.:* The theory of rotating fluids. Cambridge: Univ. Press 1969.

[5.66] *Sproule, R. S. and P. Koeller:* Reduction of fluid friction losses in rotary machines EIC-64-HYDEL, (1964) vol. 7, no C-6.

[5.67] *Osterwalder, J. and H. Geis:* Radseitenverluste einer Hochdruck-Francisturbine radialer Bauart. Masch. Markt 31 (1983) p. 669/672.

[5.68] *Wagner W.:* Experimentelle Untersuchungen an radial durchströmten Spaltdichtungen. Dr.-Ing. thesis TU Braunschweig 1972.

[5.69] *Kosyna, G.:* Untersuchung an radial durchströmten Dichtspalten mit ebenen Spaltwandungen unter Berücksichtigung von Parallelitätsfehlern. Dr.-Ing. thesis TU Braunschweig 1976.

[5.70] *Raabe, J.:* Approach to prediction of turbulent leakage through coaxial gaps as function of boundary layer, relative flow distribution on wall, swirl and shear stress due to disk friction and pipe flow. 11th IAHR symp. Amsterdam (1982). Proceed. Vol. 3,78. p. 1/5.

[5.71] *Stampa, B.:* Experimentelle Untersuchungen an axial durchströmten Ringspalten. Dr.-Ing thesis. TU Braunschweig 1968.

[5.72] *Keller, C.:* Labyrinthströmungen bei Turbomaschinen. EW-Mitt. 8 (1935) p. 160.

[5.73] *Eichler, O. and M. Wiedmann:* Untersuchung gestufter Spaltabdichtungen für hydraulische Strömungsmaschinen. VDI-Ber. Nr. 424 (1981) p. 53/62.

[5.74] *Raabe, J.:* The negative efficiency scale effect in Peltonturbines and its causes. Trans. IAHR Symp. Tokyo (1980) p. 689/702.

[6.1] *Traupel, W.:* Thermische Turbomaschinen Bd. 1, 3. Aufl. Berlin, New York: Springer-Verlag 1977.

[6.2] *Martensen, E.:* Berechnung der Druckverteilung an Gitterprofilen in ebener Potentialströmung mit einer Fredholmschen Integralgleichung. Arch. Rat. Mech. Anal. 3 (1959) p. 235/270.

[6.3] *Jacob, K.:* Erweiterung des Martensen-Verfahrens auf Einzel und Gitterprofile mit eckiger Hinterkante oder sehr kleinem Abrundungsradius. Aerodyn. Vers. Anst. Göttingen Ber. 67 A 21 1967.

[6.4] *Isay, W. H.:* Zur Berechnung der Strömung durch axiale Schaufelgitter. ZAMM 33 (1953) p. 321.

[6.5] *Traupel, W.:* Die Berechnung der Strömung durch Schaufelgitter. Sulzer Techn. Rundschau no 1 (1945) p. 45.

[6.6] *Birnbaum, W.:* Die tragende Wirbelfläche als Hilfsmittel zur Behandlung des ebenen Problems der Tragflügeltheorie. ZAMM 3 (1923) p. 290.

[6.7] *Schilhansl. M.:* Näherungsweise Berechnung von Auftrieb und Druckverteilung in Flügelgittern. Jahrb. d. wiss. Ges. f. Luftft. München: Oldenbourg-Verlag 1927.

[6.8] *Raabe, J.:* Hydraulische Maschinen und Anlagen. vol. 1 Grundlagen der hydraulischen Strömungsmaschinen. Düsseldorf: VDI-Verl. 1968.

[6.9] *Weinig, F.:* Die Strömung um die Schaufeln von Turbomaschinen. Leipzig: Barth-Verlag 1935.

[6.10] *Schlichting, H.:* Berechnung der reibungslosen, inkompressiblen Strömung durch ein vorgegebenes Schaufelgitter. VDI-Forsch. Heft Nr. 447; Düseldorf: VDI-Verlag 1955.

[6.11] *Raabe, J.:* Ein Beitrag zur Bestimmung der auftriebslosen Anströmrichtung bei endlicher Profildicke im Flügelgitter einer axialen Turbomaschine. Masch. Markt 65 (1959) no 3, p. 7.

[6.12] *Strscheletzky, M.:* Zur konformen Abbildung von Stromflächen in rotationssymmetrischen Hohlräumen. Voith Forsch. u. Konstr. 14 (1966) no 2.

[6.13] *Vötter, M.:* Numerische Berechnung des räumlichen Strömungsfeldes in hydraulischen Turbomaschinen. VDI Forschungsheft 535 (1969) p. 28/40.

[6.14] *Bauersfeld, W.:* Die Grundlagen der Berechnung schnellaufender Kreiselräder. VDI-Z 66 (1922) p. 461.

[6.15] *Inoue, M. T., T. Ihui, Y. Kamada and M. Tashiro:* A quasi 3 dimensional design of diagonal flow impeller by use of cascade data. 10th IAHR symp. Tokyo (1980). Proceed. p. 403/414.

[6.16] *Byrd, P. F. and M. D. Friedmann:* Handbook of Elliptic Integrals for Engineers and Physicists. Berlin, New York: Springer-Verlag 1953.

[6.17] *Schilling, R.:* Numerical calculation of the quasi 3D incompressible inviscid flow in turbomachines. 11th IAHR symp. Amsterdam (1982), proc. Vol. 3, 79, p. 1/13.

[6.18] *Borel, L.:* Étude pseudo-tridimensionelle des écoulement fluides autours des aubes de turbomachine. Vevey. Bulletin Technique 1978/79/80/81.

[6.19] *Hirsch, C. H. and G. Warzée:* A finite element method for the axisymmetric flow computation in a turbomachine. Int. J. f. num. Math. of Engg. 10 (1976) p. 93/113.

[6.20] *Keck, H.:* Finite-Elemente-Berechnung von Strömungen in hydraulischen Turbomaschinen. EW-Mitt. 53 (1980) no 1/2, p. 92.

[6.21] *Höller, H. K and H. Keck:* The complete finite element flow computation in a bulb turbine from inlet thrashrack to runner outlet. 10th IAHR symp. Tokyo. proc. p. 595/608.

[6.22] *Pfoertner, H.:* Laufradströmung in einer Francisturbine-Vergleich experimenteller Ergebnisse mit numerisch berechneten Strömungsfeldern. Tagg. Hydr. Strömungsmasch. Braunschweig (1981) VDI-Berichte 424. p. 121/129.

[6.23] *Martelli, F. and G. Manfrida:* Finite element calculation of blade-to-blade flow in pumps. Houille Blanche 37 (1982) no 7/8, p. 665/671.

[6.24] *Murai, H.:* Theory on blades of diagonal flow pumps. Sendai, Rep. Inst. High Sp. Mech. Japan 20 (1968), p. 177/195; p. 197/211.

[6.25] *Daiguji, H. and H. Shirahata:* Upstream cascade effects in diagonal cascade flow analysis. 10th IAHR Symp. Tokyo (1980), proc. p. 571/582.

[6.26] *Adler, D. and H. Ihlberg:* A simplified method for calculation of the flow field at the entrance of a radial or mixed flow impeller. ASME (1971) publ. 70-FE. 36.

[6.27] *Lotz, M. and J. Raabe:* Blade oscillations in one stage axial turbomachinery. ASME J. of basic engineering (1968) p. 485/493.

[6.28] *Lotz, M.:* Erregung von Schaufelschwingungen in axialen Turbomaschinen durch die benachbarten Schaufelgitter. Dr.-Ing. thesis, TU München 1965.

[6.29] *Castorph, D.:* Messung des instationären Strömungsfeldes in einer Kaplanturbine mit elektrischen Miniatursonden. Forsch Ing. Wes. 41 (1975) no 6, p. 191/199.

[6.30] *Kemp, N. H. and W. R Sears:* Aerodynamik interference between moving blade rows. J. Aeron. Sci 20 (1953) p. 585.

[6.31] *Lienhart, W.:* Berechnung der instationären Strömung durch gegeneinander bewegte Schaufelgitter und deren Schaufelkraftschwankung. VDI-Forsch. Heft 562 Düsseldorf 1974.

[6.32] *Lienhart, W.:* Aerodynamische Erregungskräfte von Schaufelschwingungen in axialen Turbomaschinen infolge der Interferenz benachbarter Schaufelgitter. Ing. Arch. 48 (1979) p. 239/258.

[6.33] *Lahm, G.:* Experimentelle Bestimmung der Schaufelkräfte durch stationäre und instätionäre Druckmessungen an interferrierenden Doppelgittern. Dr.-Ing. thesis TU München 1981.

[6.34] *Castorph, D. and G. Lahm:* Untersuchung zur Nachlaufströmung einer Axialturbinenstufe. VDI-Berichte 361 (1980) p. 11/16.

[6.35] *Castorph, D. and G. Lahm:* Vereinfachtes Modell zur Abschätzung der Rückwirkung bei interferrierenden Schaufelgittern in Axialturbinen. Wärme 88 (1982) no 6, p. 95/99.

606

[6.36] *Castorph, D. and M. Hubensteiner:* Einfluß der stromauf- und stromabwärts liegenden Gitter auf die instationären Schaufelkräfte eines mittleren Turbinengitters. VDI-Berichte Nr. 487 (1983) p. 79/87.

[6.37] *Krammer, P.:* Potentialtheoretische Berechnung der instationären Schaufelkräfte in Turbomaschinen mit Simulation von Nachlaufdellen. Dr.-Ing. thesis TU München 1983.

[6.38] *Fanelli, M. and F. Siccardi:* Réponse d'une turbomachine hydraulique a des fluctuations des paramètres dynamiques de circuit. Houille Blanche 35 (1980) no 1/2, p. 115/122.

[6.39] *Raabe, J.:* The calculation of the meridional velocity distribution in a mixed flow impeller with respect to spatial shape and losses. Int. Conf. on pumps and turbines. East Kilbride, Glasgow (1976) paper 1–3.

[6.40] *Kubota, N. and Y. A. Sami:* Influence of meridian profile of mixed flow impeller on pump characteristics. 10th IAHR symp. Tokyo (1980) proc. p. 379/390.

[6.41] *Pfleiderer, C. and H. Petermann:* Strömungsmaschinen. Berlin: Springer-Verlag 1964.

[6.42] *Adler, D.:* Three dimensional flow effects on the slip factor of centrifugal impellers. Israel J. of Technology 9 (1971) no 6, p. 587/593.

[6.43] *Anton, J.:* Contribution a l'étude des machines hydrauliques, radial reversibles. Révue Roumaine de sciences techniques. Série de Mécanique appliqueé 18 (1973) no 2, p. 191/202.

[6.44] *Korcian, J.:* Dreidimensionale, quasistationäre Messung des relativen Strömungsfeldes im Schaufelkanal eines langsamläufigen Kreiselpumpenlaufrades. Dr.-Ing. thesis. TU München 1982.

[6.45] *Raabe, J.:* Hydraulische Maschinen und Anlagen, vol 3 Pumpen. Düsseldorf: VDI-Verl. 1970.

[6.46] *Furuya, O.:* Nonlinear theory for partially cavitating cascade flow. 10th IAHR Symp. Tokyo 1980, proc. p. 221/241.

[6.47] *Siebrecht, W.:* Beitrag zur Regelung der Kreiselpumpen und Untersuchungen über die theoretische und wirkliche Förderhöhe. VDI-Forschungsheft 321. (1929).

[6.48] *Stepanoff, A. J.:* Radial und Axialpumpen. Berlin: Springer-Verlag 1959.

[6.49] *Stodola, A.:* Dampf und Gasturbinen. Berlin: Springer-Verlag 1924.

[6.50] *Busemann, A.:* Das Förderhöhenverhältnis radialer Kreiselpumpen mit logarithmisch spiraligen Schaufeln. Zeitschrift Angew. Math u. Mech. 8 (1928) no 5, p. 372.

[6.51] *Eck, B.:* Ventilatoren, Berlin: Springer-Verlag 1957.

[6.52] *Noorbakhsh, A.:* Etudes experimentale de pomps centrifuges. Inst.v.Karman de dynamique de Fluids. Publication no 46, Rhode St. Genese, Belgique 1974.

[6.53] *Murakami, M, K. Kikuyama and E. Asukura:* Velocity and pressure distribution in the impeller passages of centrifugal pumps. ASME, J. Fluids Engng. 102 (1980) no 4.

[6.54] *Osterwalder, J. and Chr. Ettig:* Determination of individual losses and scale effect by model tests with a radial pump. Institution Mech. Eng. Conf. Stirling (1977) paper C 185/77.

[7.1] *Oseen, C. W.:* Arkiv för Mat, Astron., och Fys. 7 (1911), p. 1/11.

[7.2] *Helmholtz, v. H.:* Über Integrale der hydrodynamischen Gleichungen, welche den Wirbelbewegungen entsprechen. J. reine u. angew. Math. 55 (1858) p. 25/55.

[7.3] *Thomson, W. (Lord Kelvin):* On vortex motion. Roy. Soc. Edinbg. 25 (1869) p. 217/260.

[7.4] *Hawthorne, W. R.:* rotational flow through cascades. Quarterly J. Mech. a. Appl. Mathem. vol. 8 (1955) p. 266/278.

[7.5] *Squire, H. B. and K. G. Winter:* The secondary flow in a cascade of airfoils in a nonuniform stream. J. Aero Science 8 (1951) p. 271.

[7.6] *Railly, J. W. and J. H. G. Howard:* Velocity profile development in axial flow compressors. J. Mech. Engng. Sci. 4 (1962) no 2, p. 166/176.

[7.7] *Raabe, J.:* Teoria para algunos tipos de flujo secundario en turbomáquinas. Quaderns d'enginyeria. 2 Barcelona (1980) no 1, p. 1/24.

[7.8] *Johnston, J. P.:* On the three-dimensional turbulent boundary layer generated by secondary flow. Trans ASME Ser. D. March 1960.

[7.9] *Raabe, J.:* Ein Beitrag zur Berechnung der Grenzschicht mit Sekundärströmung an doppelt gekrümmten Laufschaufeln eines halbaxialen Rades bei stationär turbulenter Strömung eines Newtonischen Fluids. Festschrift z. 60. Geburtstag von E. Truckenbrodt. München (1977). Eigenverlag Lehrstuhl für Strömungslehre der TU München p. 295/319.

[7.10] *Falkner, V. M.:* The resistance of a smooth flat plate with turbulent boundary layer. Aircraft Engng. 15 (1943) p. 65.

[7.11] *Coles, D.:* The problem of the turbulent boundary layer. ZAMP 5 (1954) no 5, p. 181/202.

[7.12] *Faulders, C. R.:* An interferometer study of the boundary layer on a turbine nozzle blade. ASME 76 (1954) p. 61/68.

[7.13] *Squire, H. B.:* On the stability of three-dimensional distribution of viscous fluid between parallel walls. Proc. Roy. Soc. A 142 (1933).

[7.14] *Arakawa, C., T. Tagori and M. Shirakura:* Anaylsis of three dimensional turbulent boundary layer on the rotating blade of axial flow. pump. 10th IAHR Symp. Tokyo (1980), proc. p. 341/351.

[7.15] *Reichardt, H.:* Über eine neue Theorie der freien Turbulenz. ZAMM 21 (1941) p. 257.

[7.16] *Ueda, T., T. Kubota and Y. Kimoto:* Performance prediction of pumpturbine in generating mode. 10th IAHR Symp. Tokyo (1980), proc. p. 703/714.

[7.17] *Raabe, J.:* Prediction of internal loss of semi axial impeller for an incompressible fluid, based on turbulence and velocity distribution of main and secondary flow within the boundary layer, known from test results. Irst Int. Conf.-Centrifugal Compressor Technology. IIT Madras India (1978). A 4 p. 1/12.

[7.18] *Raabe, J.:* The prediction of disk friction loss for shroud and gap of arbitrary geometry with respect to leakage, nonsubmerged boundary layers of stationary and rotating wall, slip, secondary flow, turbulence level, Reynoldsnumber and roughness. Proc. 8th Nat. Conf. Fluid Mech. a. Fluid Power, Coimbatore India (1978). paper A 27 NC FM FP p. 137/141.

[7.19] *Keller, C.:* Über Energieverlust bei rasch laufenden Turbomaschinen infolge unregelmäßiger Laufradströmung. EW-Mitt. 8 (1935), p. 40.

[7.20] *Nakkasyan, A. and I. L. Ryhming:* Calculation of three dimensional boundary layers with isotropic and anisotropic turbulent viscosities. Houille Blanche 37 (1982) no 7/8, p. 633/640.

[7.21] *Nikuradse, J.:* Gesetzmäßigkeiten der turbulenten Strömung in glatten Rohren. (1932) Beilage zur Forschg. Ing. Wes. Ausg. B, Bd. 3. Nr. 356.

[7.22] *Vasiliev, O. F. and V. I. Kvon:* Friction forces of unsteady flows in open channels and pipes. Proc. 14th IAHR Congr., Paris, 1971.

[7.23] *Prandtl, L.:* Führer durch die Strömungslehre, Braunschweig, Vieweg-Verlag 1965.

[7.24] *Kolmogorov, N.:* Equations of turbulent motion of an incompressible turbulent fluid. Izv. Akad. Nauk SSSR Ser. Phys. VI (1942) no 1/2.

[8.1] *Numachi, F. (Editor):* Cavitation and Hydraulic Machinery. Proceed. IAHR Symposium Sendai, Japan (1962). Inst. High Speed Mech. Tohoku Un.

[8.2] *Chahine, G. L.:* Etude locale du phénomène de cavitation-analyse de facteurs régissant la dynamique des interfaces, École nationale. supérieure de techniques avancées. Rapport de récherche 116. 1979.

[8.3] *Grein, H.:* Kavitation, eine Übersicht. Technische Rundschau Sulzer. Forschungsheft 1974.

[8.4] *Raabe, J.:* Cavitation effects in turbomachinery-European experiences. Cavitation state of knowledge. ASME Conf. Evanstone (1979). p. 168/194.

[8.5] *Karelin, V. J.:* Kavitacionnye Javlenija v centrobešnyx i osevyx nacocax. Moskva: Mašinostronenie 1975.

[8.6] *Knapp, R. T., J. Daily and G. F. Hammitt:* Cavitation. New York: MacGraw Hill publishers 1970.

[8.7] *Raabe, J.:* Cavitation in pumps, its causes and remedies. Int.Tech. Seminar of Indian Pump Manufacturers Ass. (1976) Silver Jubilee. Symp. Bombay, p. 185/207. Poona: Kirloskar Press, Veev Savakar Nagar.

[8.8] *Dziallas, R.:* Beitrag zur Beurteilung des Kavitationsverhaltens von radialen Kreiselpumpen. Voith Forsch. u. Konstr. 15 (1967) no 3.

[8.9] *Thuss, W.:* The submergence of pumped-storage sets for cavitation requirements with special consideration of high delivery heads per stage. 6th IAHR Symp. Rome (1972) paper J 1.

[8.10] *Osterwalder, J. and W. Lecher:* Ein neuer Prüfstand für Kennlinienmessung und Kavitationsbeobachtung an Wasserturbinen und Pumpen. EW-Mitt. 29 (1956) no 2, p. 21.

[8.11] *Outa, E. et al.:* Low frequency oscillations of centrifugal pump discharge due to cavitation choking at an inlet contraction. 10th IAHR Symp. Tokyo (1980), proc. p. 313/323.

608

[8.12] *Pearsall, J. S. and G. Scobie:* Pumps for low suction pressures. Symp. on pumping problems. NEL (1970) pap 2.

[8.13] *Osterwalder, J. and W. Lecher:* Einfluß des Versuchsgefälles auf den Kennlinienverlauf einer Francisturbine im Kavitationsbereich. EW-Mitt. 36 (1963) no 1, p. 28.

[8.14] *Ulith, P.:* Kavitationsgrenzen in Francisturbinen. Voith Inf. 3. 1981.

[8.15] *Borciani, G. and R. Thalmann:* Influence de la cavitation sur les caractéristiques moyennes et instantanées des turbines et des pompeturbines. Houille Blanche 37 (1982) no 2/3, p. 197/208.

[8.16] *Eichler, O. and E.-U. Jaeger:* Assessment of the cavitation behaviour of Kaplan turbines on the basis of the comparison between model tests and field experiences. IAHR Symp. – Leningrad (1976) pap. II-1.

[8.17] *Ishii, Y.:* The two types of the runaway state of propeller turbine under cavitation. Proc. IAHR Symp. Sendai (1962). (See [8.1]) p. 247.

[8.18] *Yamazaki, T.:* Cavitation erosion on the back of Pelton turbine bucket. Proc. IAHR Symp. Sendai 1962) (See [8.1]) p. 219.

[8.19] *Reali, M:* Carbon Dioxide vapour as a potential stability agent of gaseous nuclei in water air solution. IAHR Symp. on water column separation. Obernach (1981). Proc. p. 55/70.

[8.20] *Harvey, E. N. et al.:* On cavity formation in water. J. Appl. Phys. 18 (1947) p. 162

[8.21] *Brand, F.:* Ein physikalisches Verfahren zur Bestimmung von gelösten und ungelösten Gasen in Wasser. Voith Forsch. u. Konstr. 27 (1980) no 7.

[8.22] *Osterwalder, J. and K. Kümmel:* Influence of nuclei spectrum on incipient cavitation. 6th Conf. Fl. Machinery. Budapest (1979). Vol. 2 p. 788/798.

[8.23] *Keller, A. and R. Prasad:* Influence on the history of water on cavitation inception. Cavitation and Polyphase flow forum ASME. Fort. Collins, Co. 1978.

[8.24] *Gates, E. M. and M. L. Billet:* Cavitation nuclei and inception. 10th IAHR Symp. Tokyo (1980). Proc. p. 3/25.

[8.25] *Murai, H., W. Watanabe and K. Katagiri:* Supression of cavitation inception in water by additives. 10th IAHR Symp. Tokyo (1980) proc. p. 65/76.

[8.26] *Lecoffre, Y.:* Controle de la nucléation d'une eau en moyens d'essais. 8th IAHR Symp. Leningrad (1976) proc. p. 173/186.

[8.27] *Oldenziel, D. M., R. H. J. Hansen, A. P. Keller, Y. Lecoffre and R. L. van Renesse:* Comparison of instruments for detecting of bubble and particles in water during cavitation studies. 11th IAHR symp. Amsterdam (1982) proc. Vol. 1, 6 p. 1/8.

[8.28] *Keller, A.:* The influence of cavitation nucleus spectrum on cavitation inception, investigated with scattered light counting method. J. Basic Engng. (1972) p. 917/925.

[8.29] *Gast, P.:* Experimentelle Untersuchungen über den Beginn der Kavitation an umströmten Körpern. Dr.-Ing. thesis. TH Darmstadt 1971.

[8.30] *Raabe, J.:* Theoretical considerations about the physical background of the polytropic power n belonging to a quickly expanding mixed gaseous and vaporous spherical cavity. Cavitation and polyphase forum ASME Fort. Collins Col. 1978.

[8.31] *Chincholle, L. and A. Sevastianov:* Étude du mouvement d'une bulle de gaz dans un liquide à l'intérieur d'un diffuseur. Houille Blanche 31 (1976) no 5, p. 355/360.

[8.32] *Matsumoto, Y. and M. Shirakura:* Formation and collapse of cavitation bubble. 10th IAHR Symp. Tokyo (1980). Proc. p. 79/90.

[8.33] *Fujikawa, S. and T. A. Akamatsu:* On the mechanism of cavitation bubble collapse. 10th IAHR Symp.Tokyo (1980) proc. p. 91/102.

[8.34] *Plesset, M. S. and A. Prosperetti:* Vapour bubble dynamics and heat transfer in nuclear boiling. IAHR-SHF Symp. Cavitation, Grenoble (1976) proc. p. 89/99.

[8.35] *Oldenziel, D. M.:* Gas transport into cavitation bubble during explosion. IAHR SHF Symp. Cavitation, Grenoble (1976) proc. p. 77/88.

[8.36] *Raabe, J.:* The scale effect of cavitation inception due to tensile stress, heat conduction and gas diffusion. IAHR-SHF Symp. Cavitation, Grenoble (1976) proc. p. 101/109.

[8.37] *Chahine, G. L.:* Pressure field generated by the collective collapse of cavitation bubbles. 11th IAHR Symp. Amsterdam (1982) proc. Vol. 1, 2 p. 1/14.

[8.38] *Chahine, G. L. and A. G. Bovis:* Pressure field generated by non spherical bubble collapse. ASME Conf.Cavitation Erosion etc. Boulder Co (1981) p. 27/40.

[8.39] *Walter, A. and J. Raabe:* Theoretical considerations and experiments about the motion of a small bubble in a vertical laminar flow. Conf. Appl. Mech. Fluid Engng. and Bio Engng. New Haven (1977). 6-D.

[8.40] *Fritz, C. G., C. A. Ponder, Jr. and D. H. Blount:* Bubble coalescence in a longitudinally vibrated liquid column. ASME Symp. Cavitation etc. Chicago (1965) p. 148/161.

[8.41] *Hammitt, F. G.:* Collapsing bubble dammage to solids. Cavitation state of knowledge. ASME conf.(1969) Evanstone p. 87/102.

[8.42] *Plesset, M, S.:* Bubble dynamics. Symp. Cavitation in real liquids. Warren Michigan. Amsterdam, New York: Elsevier (1964) p. 1.

[8.43] *Scriven, L. E.:* On the dynamics of phase growth. Chem. Engng. Sci. 10 (1959) p. 1.

[8.44] *Poritsky, H.:* The collapse or growth of a spherical bubble or cavity in a viscos fluid. US Nat. cong. o. Appl. Mech. (1952) p. 813/821.

[8.45] *Keller, A. P.:* Tensile strength of liquids. IAHR Symp. on water column separation, Obernach (1981) proc. p. 129/152.

[8.46] *Rayleigh, Lord:* On pressure developed in a liquid during collapse of a spherical cavity. Phil. Mag. 34 (1917) p. 914.

[8.47] *Keller, A.:* Cavitation inception measurements and flow visualization on axisymmetric bodies at two different free stream turbulence levels and test procedures. Int. Symp Cavitation Inception ASME New York (1979) p. 63.

[8.48] *Billet, M. L., J. W. Holl and B. R. Parkin:* Scale effect on cavitatiting flow due to surface roughness and laminar separation. 10th IAHR Symp. Tokyo (1980) proc. p. 39/52.

[8.49] *Holl, J. W.:* Inception of cavitation on isolated surface irregularities. Trans. ASME J. Ser. D. Basic Engng. 82 (1966) no 1, p. 169.

[8.50] *Numachi, F., R. Oba and I. Chida:* Effects of surface roughness on cavitation performance of hydrofoils. Rep. Trans ASME Ser. D (1965) p. 495.

[8.51] *Arndt, E. A.:* Pressure fields and cavitation 7th IAHR Symp. Vienna (1974) Trans p. 1 XI p. 1/20.

[8.52] *Billet, M. L. and J. W. Holl:* Scale effects on various types of cavitation. Int. Symp. cavitation inception ASME New York (1979).

[8.53] *Billet, M. L.:* The effect of secondary vorticity on the magnitude of vortex cavitation. Int. Symp. Cavitation inception ASME New York (1979) p. 153/162.

[8.54] *Plesset, M. S.:* The tensile strength of liquids. Cavitation state of knowledge. ASME conf. (1969) Evanstone p. 15/25.

[8.55] *Arndt, R. E. and J. W. Daily:* Cavitation in turbulent boundary layers. Cavitation state of knowledge, ASME conf. (1969) Evanstone p. 64/86.

[8.56] *Arakeri, V. H. and A. Acosta:* Viscous effects in the inception of cavitation. Int. Symp. Cavitation inception, ASME New York (1979) p. 1/10.

[8.57] *Holl, J. W., M. L. Billet and D. S. Weir:* Thermodynamic effects on developed cavitation. ASME conf. Cavity flow Minneapolis (1975) p. 101/110.

[8.58] *Bonnin, J.:* Similarity of non-equilibrium two-phase flow in turbomaschinery. Symp ASCE-IAHR-ASME. (1978) Fort Collins Col proc. Vol I p. 35/48.

[8.59] *Henry, P., Y. Lecoffre and P. Y. Larroze:* Effets d'échelle en cavitation. 10th IAHR Symp. Tokyo (1980) proc. p. 131/141.

[8.60] *Holl, J. W.:* Cavitation hysteresis: ASME Symp. Cavitation etc. Chicago (1965) p. 250.

[8.61] *Raabe, J.:* Scaling of limited cavitation when ultimate size of bubble is proportional to dimension of apparatus. Int. Symp. on cavitation incepton ASME New York (1979), p. 39/49.

[8.62] *Kato, H.:* On the prediction method of cavitation erosion from model tests. IAHR-SHF Symp. cavitation, Grenoble (1976) proc. p. 171/180.

[8.63] *Kaveshnikov, A. T., and N. P. Rosanow:* Cavitation erosion from investigations with equivalent materials. IAHR-SHF Symp. Cavitation Grenoble (1976) proc. p. 181/188.

[8.64] *Raabe, J.:* The prediction of celerity (velocity of sound) for some types of two phase flow. IAHR Symp. on water column separation, Obernach (1981) proc, 3.2 p. 181/196.

[8.65] *Pighini, U. and G. Di. Chirico:* Further approach in defining the material resistance to cavitation attack. IAHR-SHF Symp. Grenoble (1976) proc. p. 462/471.

[8.66] *Simoneau, J. L. and L. Chincholle:* L.Effect d'activation anodique de la cavitation érosive. 11th IAHR symp. Amsterdam proc. Vol. 3, 72 p. 1/15.

[8.67] *Kato, H. et al.:* A comparison and evaluation of various cavitation erosion test methods: ASME conf.Cavitation erosion etc. Boulder Co (1981) p. 83/94.

[8.68] *Rao, P. V. and B. C. S. Rao:* Some erosion studies and scale effects with rotating disk device. ASME conf. Cavitation erosion etc. Boulder Co (1981) p. 119/133.

[8.69] *Plesset, M. S.:* An experimental method for evaluation of resistance to cavitation erosion. Proc. IAHR Symp. Sendai (1962) (See [8.1]) p. 62.

[8.70] *Fay, A.:* Computation of jet formation in wake cavities. IAHR-SHF Symp. Cavitation Grenoble (1976) proc. p. 419/426.

[8.71] *Sotnikov, A, A. and N. I. Pylayev:* Some design means of reducing cavitation damage in hydraulic turbines in service. 8th IAHR symp. Leningrad (1976) proc. p. 136/147.

[8.72] *Quintela, A, C.:* Flow areation to prevent cavitation. Water Power 32 (1980) no 1, p. 17/22.

[8.73] *Schur, S. M. A. and S. P. Hutton:* Hydrodynamic similitude for cavitation erosion. ASME conf. Cavitation erosion etc. Boulder Co (1981) p. 15/26.

[8.74] *Sotnikov, A. A. and N. I. Pylayev:* Comparison of cavitation erosion in model and full scale hydraulic turbine. 10th IAHR symp. Tokyo (1980) proc. 143/154.

[8.75] *Raabe, J.:* Theoretical approach of erosion rate vs speed and cavity size in wall-attached cavitation. ASME conf. cavitation erosion etc. Boulder Co (1981) p. 41/52.

[8.76] *Osterwalder, J. and W. Lecher:* Kavitation und Materialerosion. EW-Mitt. 33 (1960) no 1/2, p. 179.

[8.77] *Ren-Gung, G., X. Zhang and Z. Mei:* Determination of model turbine critical cavitation by means of radio active isotope. 11th IAHR Symp. Amsterdam (1982) proc. Vol. 1 23 p. 1/11.

[8.78] *Martin, C. S., H. Medlarz, D. C. Wiggert and C. Brennen:* Cavitation inception in spool valves. Int.Symp.Cavitation inception ASME New York (1979) p. 219/231.

[8.79] *Chahine, G. L.:* Asymptotic theory of collective bubble growth and collapse. IAHR symp. on water column separation Obernach (1981). proc. 1.1 p. 13/47.

[8.80] *Furness, R. A. and S. P. Hutton:* Experimental and theoretical studies on two dimensional fixed cavities. ASME conf. cavity flow, Minneapolis (1975) p. 111/118..

[8.81] *Michel, J. M., S. Biset and J. P. Franc:* The cavitation developing on continuous-curve walls: the physics of detachment. Houille Blanche 37 (1982) no 7/8 p. 559/570.

[8.82] *Lush, P. A. and P. I. Peters:* Visualization of the cavitating flow in a Venturi type duct using high speed cine photography. 11th IAHR symp. Asmsterdam (1982). proc. Vol. 1, 5. p. 1/13.

[8.83] *Oba, R.,K. Sato, Y. Ito, S. Yasu, K. Uranishi and J. Higuchi:* Vented cavity formation in a hydraulic turbomachinery. Rep. Inst. High Speed Mech. Tohoku Univ. Vol. 46 (1983) p. 59/74.

[8.84] *Jaeger, Ch.:* Technische Hydraulic. Basel: Birkhäuser-Verlag 1949.

[8.85] *Jaeger, Ch.:* Fluid Transients. Glasgow London: Blackie publishers 1977.

[8.86] *Martin, C. S.:* Transformation of pump-turbine characteristics for Hydraulic transients analysis. 11th IAHR Symposium Amsterdam (1982) proc. V. 2.30. p. 1/15.

[8.87] *Graeser, J. E., J. E. Prenat and W. Walther:* Caractéristiques de machines hydrauliques et de vannes dans les calcules de régimes transitoires. 11th IAHR symp. Amsterdam (1982) proc. V. 2,31, p. 1/13.

[8.88] *Tschumy, A.:* Analysing the transient phase of the Malta scheme's pump-turbines. Water Power 33 (1981) no 5, p. 27/33.

[8.89] *Brekke, H. and K. B. Bugaarden:* A study on governing problems caused by transients in high pressure tunnel systems. 10th IAHR Symp. Tokyo (1980), proc. p. 463/477.

[8.90] *Veremenko, I. S., I. D. Kuzmin and L. T. Margulis:* Studies of transient processes and cavitation, characteristics of the Dniepr HEP-II propeller turbines. Symp. ASCE-IAHR-ASME Fort Collins Co (1978), proc. vol. I, p. 109/118.

[8.91] *Grein, H. and M. Jaquet:* Einige Ergebnisse von Druckschwingungsmessungen an Speicherpumpen und Pumpturbinen. EW-Mitt. 47 (1974) no 1, p. 20.

[8.92] *Tschumy, A. and Ch. Wavre:* Transient state calculation in large complex pump-turbine power schemes. Charmilles Techn.Bull. no 14 (1975) p. 27/34.

[8.93] *Zolotov, L. A and V M. Klabukov:* Optimum control of transient parameters in hydro power installations. 10th IAHR Symp. Tokyo (1980) proc. p. 455/462.

[8.94] *Seybert, T. A., W. S. Gearhart and H. T. Falvey:* Studies of method to prevent draft tube surge in pump-turbines. Symp. ASCE-IAHR-ASME Fort Collins Co (1978), proc. vol. I, p. 109/118.

611

[8.95] *Grein, H.:* Vibration phenomena in Francisturbines, their causes and prevention. 10th IAHR Symp. Tokyo (1980) proc. p. 527/539.

[8.96] *Purdy, C. C.:* Reducing power swing of Tarbela's turbine. Water Power 31 (1979) no 4, p. 23/27.

[8.97] *Fanelli, M and M. Reali:* A theoretical determination of the celerity of water hammer waves in a two phase mixture. ENEL paper Direzione studio e ricerca 1974 no 2442 MF/MR, ENEL Symp. on water column separation Vallombrosa 1974.

[8.98] *Martin, S. C.:* Pressure pulse propagation in two component slug flow. Symp. ASCE-IAHR-ASME Fort Collins Co (1978), proc. Vol. I, p. 13/24.

[8.99] *Bernardinis, de, B., G. Federici and F. Siccardi:* Transients with liquid column separation: Numerical evaluation and comparison with experimental results. ENEL symp. on water column separation Vallombrosa 1974.

[8.100] *Fanelli, M.:* Considerazioni sule fenomeni di risonanza idraulica nelle aduzzioni in pressione. ENEL relazione di studio e ricerche no 087, 1976.

[8.101] *Hudovernik, W. und G. Lein:* Frequenzganguntersuchungen im Triebwasserweg von Hochdruckwasserkraftanlagen. Österr. Zeitschr. Elektrizts.-Wirtsch. 22 (1969) no 12, p. 637/648.

[8.102] *Fanelli, M.:* Les phénomènes de résonance hydraulique: Houille Blanche 30 (1975) no 4 p. 3/23.

[8.103] *Fanelli, M.:* Nota sulla riposta dinamica di condotti in pressione a celerità variabile linearmente lungo il percorso. ENEL relazione di studio e ricerche no 197, 1974.

[8.104] *Ehrhart, R. W.:* Auto oscillations in the Hyatt plant's penstock system. Water Power 31 (1979) no 4, p. 38/41.

[8.105] *Krivčenko, G. I., K. A. Kvyatkovskaya and K. A. Lynbitskyi:* Some special conditions of unit operation in hydro power plant with long penstocks. 8th IAHR symp. Leningrad proc. p. 465/475.

[8.106] *Wiggert, D. C.:* The effect of gaseous cavitation on fluid transients Symp. ASCE-IAHR-ASME Fort Collins Co (1978), proc.V. I, p. 49/61.

[8.107] *Brekke, H.:* Frictional damping of pressure oscillations in high head power plants. 11th IAHR Symp. Amsterdam (1982), proc. Vol. 2, 45 p. 1/15.

[8.108] *Wylie, E. B. and V. L. Streeter:* Column separation in horizontal pipe line. Symp. ASCE-IAHR-ASME Fort Collins Co (1978), proc Vol. I p. 3/13.

[8.109] *Pejovic, S., L. Krsmanovic, A. Gajic and D. Obradovic:* Kaplan turbine incidents and reversed water hammer. Water Power 32 (1980), no 8, p. 36/40.

[8.110] *Ramsahoye. S. I.:* Calculating load rejection surges. Water Power 30 (1978) no 3, p. 28/33.

[8.111] *Guarga. R.:* About the necessity to perfect the theory of resonance in pressurized piping systems. 11th IAHR symp. Amsterdam (1982), proc. Vol. 2, 46 p. 1/13.

[8.112] *Parkin, B. R. and R. W. Kermeen:* The role of convective diffusion and liquid tension stresses during cavitation inception. See [8.1] p. 17.

[8.113] *Chincholle, L:* L. étude de l'écoulement d'une émulsion. Houille Blanche (1967) no 5, p. 515.

[8.114] *Föttinger, H.:* Untersuchung über Kavitation und Korrosion bei Turbinen, Turbopumpen und Propellern. Hydraulische Probleme VDI-Verlag 1926.

[8.115] *Numachi, F., R. Oba and J. Chida:* Cavitation tests on hydrofoil profiles designed for accelerating flow cascade. See [8.1] p. 143.

[8.116] *Plesset, M. S.:* On physical effects in cavitation damage , in Grammel (editor), Deformation and Flow of Solids, Berlin, Springer Verlag 1956 p. 218/235.

[8.117] *Thiruvengadam, A.:* Research facilities and techniques. Symp. Cavitation, Research Facilities and Techniques. ASME (1964) p. 157.

[8.118] *Piltz, H. H:* Werkstoffzerstörung durch Kavitation. Literaturbericht Düsseldorf: VDI-Verlag 1966.

[8.119] *Florjancic, D.:* Experimentelle Untersuchungen an einer Pumpe zur Feststellung der Änderung der Saugfähigkeit durch Oberflächenrauhigkeit, durch Mischvorgänge am Laufradeintritt und durch Heißwasserförderung. Dissertation ETH Zürich. Nr. 4406.

[8.120] *Thoma, D.:* Die Kavitation in Wasserturbinen. Hydraulische Probleme Berlin: VDI 1926 p. 65.

[8.121] *Strasberg, M.:* The influence of air-filled nuclei on cavitation inception. David Taylor Basin. Rep. 1078, 1957.

612

[8.122] *Stepanoff, A. J.:* Cavitation in centrifugal pumps with liquids other than water. Trans ASME ser.A J. Engng. Power 83 (1961) p. 79.

[8.123] *Numachi, F:* Über die Kavitationsentstehung mit besonderem Bezug auf den Luftgehalt des Wassers. Techn. Rep. Tohoku Imperial University no 12 (1938) p. 422.

[8.124] *Rippken, J. F and R. M. Olson:* A study of the influence of gas nuclei on cavitation scale effects in water tunnel tests. Univ. of Minnesota (1958) Rep. no 58.

[8.125] *Meyer, E. and E. Skudozyk:* Über die akustischen Eigenschaften von Gasblasenschleiern in Wasser. Acustica 3 (1953) p. 434.

[8.126] *Oshima, M and K. Kawagushi:* Experimental study of axial and mixed flow pumps. See [8.1] p. 397.

[8.127] *Kasai, T and Y. Takamatu:* Cavitation aspects and suction performance of centrifugal pumps. See [8.1] p. 417.

[8.128] *Stepanoff, A, J.:* Pumps and Blowers, two phase flow. New York: Wiley publishers 1965.

[8.129] *Schöneberger, W.:* Untersuchungen über Kavitation in radialen Kreiselpumpenlaufrädern. Dr.-Ing. thesis TH Darmstadt 1966.

[8.130] *Lecher, W.:* Über den Einfluß von Gefälle und Luftgehalt auf Kavitationsphänomene. EW-Mitt. 33 (1960) no 1/2 p. 42.

[8.131] *Campmas, P.:* Stabilité du régime de fonctionnement des turbines Francis. IAHR Symp. Nice 1960.

[8.132] *Raabe, J:* Hydraulische Maschinen und Anlagen, vol. 2 Wasserturbinen Fragen der Konstruktion und des Betriebsverhaltens. Düsseldorf: VDI-Verlag 1970.

[8.133] *Schnyder, O.:* Über Druckstöße in verzweigten Leitungen mit besonderer Berücksichtigung von Wasserschloßanlagen. Wasserkrft. u. Wasserwirtsch. (1930) p. 173.

[8.134] *Bergeron, L.:* Variation de régime dans les conduites d'eau. Société Hydrotechnique de France 1937.

[8.135] *Kirmse, R. and J. Raabe:* Measurements in pulsatile water flow in a straight circular tube using Laser-Doppler velocimeter. 8th IAHR Symp. Leningrad (1976) p. 330/346.

[8.136] *Hartner, E.:* Turbulenzmessung in pulsierender Rohrströmung. Dr.-Ing. thesis TU München 1983.

[8.137] *Richardson, E. G. and E. Tyler:* Proc. Phys. Soc. London 42 (1929), p. 1.

[8.138] *Joukovsky, N:* Mem. Imperial Academy, Sci. of St. Petersburg 1898.

[8.139] *Allievi, L:* Teoria generale del moto perturbato dell' acqua nei tubi in pressione. Ann. soc. Ing. Arch. Italiano 1903.

[9.1] *Eichler, O.:* SI-Einheiten und Kenngrößen bei hydraulischen Maschinen. Voith Forsch. u. Konstr. 27 (1980) Nr. 2432 + e.

[9.2] *Lecher, W.:* Ähnlichkeitsgesetze für hydroelastische Schwingungen EW-Mitt. 40 (1967) no 2, p. 23.

[9.3] *Grein, H.:* Einige Bemerkungen über die Oberflächenrauhigkeit der benetzten Komponenten hydraulischer Maschinen. EW-Mitt. 48 (1975) no 1 p. 1.

[9.4] *Henry, P.:* Influence de la rugosité sur le rendement d'un modéle reduit de turbine Francis. 10th IAHR Symp. Tokyo (1980), proc. p. 677/687.

[9.5] *Hutton, S. P., S. M. A. Schin and P. A. Lush:* Surface roughness, measured for assessing cavitation erosion. 11th IAHR Symp. Amsterdam (1982). proc. Vol. 3, 71, p. 1/13.

[9.6] *Clement, J. P. et al.:* Incertitudes à prendre en compte sur les courbes H(Q) et P(Q) à débit partiel des pompes et de pompe-turbines. Houille Blanche 37 (1982) no 2/3, p. 121/130.

[9.7] *Beducci, G., E. Berra, G. Borciani and G. Rossi:* Comissioning and efficiency measurement in modern hydroelectric generating and pumping units, comparison with laboratory measurements. 11th IAHR Symp. Amsterdam (1982) proc. Vol. 3, 58, p. 1/15.

[9.8] *Casacci, S., M. Wegner, P. Henry and J. F. Graeser:* Examen expérimental de la stabilité des turbines Francis sur modéle et sur prototype à charge partielle. 11th IAHR Symp. Amsterdam (1982) proc. V. 2, 41, p. 1/13.

[9.9] *Seydel, J. and G. David:* Mise en service d'une turbine pompe de 230 MVA, essais et mesures, comparaison avec le modéle. 10th IAHR Symp. Tokyo (1980) proc. p. 663/675.

[9.10] *Brand, F.:* Die Messung des Wirkungsgrades von hydraulischen Maschinen nach dem thermodynamischen Verfahren. Voith Forsch. u. Konstr. 7 (1961), no 1577-d + e.

[9.11] *Brand, F.:* Die Geschichte des thermodynamischen Verfahrens zur Messung des Wirkungsgrades von hydraulischen Maschinen. Technikgeschichte 39 (1972) no 3.

[9.12] *Vaucher, R.:* Thermodynamische Wirkungsgradmessungen an hydraulischen Maschinen. EW -Mitt. 32 (1959) no 2/3, p. 39.

[9.13] *Tako et al.:* Field test result of hight head pump-turbines for Numapara pumped-storage power station. Hitachi rev. 23 (1974) no 6, p. 241/246.

[9.14] *Jarriand, P., J. Lathuile and G. Caillot:* Essais industriels sur le comportment d'une turbine-pompe mono-étage de haute chute. Houille Blanche 35 (1980) no 1/2, p. 95/104.

[9.15] *Takase, M. et al.:* Field test results of large capacity pump-turbines to USA. Hitachi Rev. 23 (1974) no 8, p. 305/310.

[9.16] *Arorio, L. and M. Rosnati:* Special measurements on a 170 MW pump turbine. 8th IAHR ·symp. Leningrad (1976) proc. p. 73/84.

[9.17] *Picollier, G.:* Turbomachines hydrauliques. Essais industriels et métodes de calcul. Houille Blanche 32 (1977) no 7/8, p. 657/670.

[9.18] *March, P. A.:* Flow measurements at Racoon mountain. Water Power 34 (1982) no 10 p. 42/44.

[9.19] *Brekke, H.:* Experiences from large Pelton turbines in operation. 11th IAHR Symp. Amsterdam (1982) proc. Vol. 2, 55. p. 1/11.

[9.20] *Meier, W.:* Ergebnisse von Abnahmeversuchen an Speicherpumpen. EW-Mitt 35 (1962) no 2 p. 3.

[9.21] *Osterwalder, J.:* Abnahmeversuche an Modellwasserturbinen. EW-Mitt. 33 (1960) no 1/2/3 p. 35.

[9.22] *Klein, J.:* Problems of model testing for high head pump-turbines. 7th IAHR Symp. Vienna (1974), Trans. part 1 I, 3, p. 1/15.

[9.23] *Dziallas, R.:* Bisherige Praxis in Modellturbinenuntersuchungen an Stelle von Abnahmemessungen. Bull ASE 50 (1959) no 3 p. 617/621.

[9.24] *Dziallas, R.:* Versuchsstände und Versuchseinrichtungen in den Versuchsanstalten Brunnenmühle und Hermaringen. Voith Forsch. u. Konstr. 4 (1958) no 2.

[9.25] *Ulith, P.:* Der Hochdruck-Kreislauf in der Versuchsanstalt Brunnenmühle. Voith Forsch. u. Konstrukt. 22 (1975), no 2.

[9.26] *Offenhäuser, H.:* Der 1,5 MW Versuchsstand der hydraulischen Versuchsanstalt Brunnenmühle. Voith Forsch. u. Konstrukt. 22 (1975) no 3.

[9.27] *Grein. H, W. Gygax and A. Engel:* Ein neuer Prüfstand für Untersuchungen an Freistrahlturbinen. EW-Mitt. 41. (1968) no 2 p. 3.

[9.28] *Lecher, W., M. Jaquet and H. Grein:* Ein neuer Prüfstand für Modellversuche an hydraulischen Turbomaschinen, insbesondere für Pumpen und Pumpturbinen. EW-Mitt. 44 (1971) no 1 p. 26.

[9.29] *Chenal, R:* Hydraulic laboratory: New all-purpose test rig for scale models of hydraulic machinery. Vevey, Bulletin Technique (1980/81) p. 3/32.

[9.30] *Bovet, Th. and P. Henry:* Le nouveau stand d'essai universel pour machines hydrauliques à réaction. EPUL, Lausanne, Inst. de Machines Hydrauliques 1970.

[9.31] *Scobie, G. and J. D. Lighthead:* The NEL variable pressure water turbine test rig. NEL Fluid mech. Divison. East Kilbride 1971.

[9.32] *Angelin, S.:* The hydrodynamic laboratory at Älvkarleby. The power board of Sweden. Blue white series 23.

[9.33] *Höller, H. K:* Wasser und Gasversuch an einem neuen Universalprüfstand für hydraulische Turbomaschinen, insbesondere für Pumpen und Pumpturbinen. EW-Mitt. 47 (1974) no 2 p. 3.

[9.34] *Walter, A.:* Messungen des Frequenzverhaltens einer Francisturbine in Wasser verschiedenen Luftgehaltes und Luft verschiedener Dichte. Dr.-Ing. thesis TU München 1979.

[9.35] *Osterwalder, J.:* Luftversuchs-Prüfstände für hydraulische Maschinen. EW-Mitt. 33 (1960) no 1/2/3 p. 19.

[9.36] *Pfenninger, A.:* Aufwertungsversuche durch Druckvariation EW-Mitt. 12 (1939) p. 41.

[9.37] *Casacci, S., P. Jarriaud and N. Roche.:* Étude théorique et experimentale préparatoire au projets de pompes-turbines bi-étages réglables pour chutes supérieures a 1000 m. 11th IAHR symp. Amsterdam proc. Vol. 3,59, p. 1/24

614

[9.38] *Ambühl, H. and P. Bachmann:* Bestimmung der Verlustanteile einzelner Stufenkomponenten in einer mehrstufigen Pumpturbine radialer Bauart. EW-Mitt. 53 (1980) no 1/2, p. 82.

[9.39] *Rebernik, B.:* Hydraulic investigation on water intakes for pumped storage plants. 7th IAHR symp. Vienna. Trans part. 1 I 2 p. 1/12.

[9.40] *Grein, H. and P. Bachmann:* Flow Pattern between the adjustable guide vanes of a large specific speed pump-turbine. Int. Conf. pumps and turbines etc. East Kilbride (1976) pap. 1–5.

[9.41] *Amblard, H. and R. Philibert:* Quelque résultats de récherches concernants des canaux de rétour des turbines-pompes multiétages. 11th IAHR symp. Amsterdam (1982) proc. Vol. 3, 64 p. 1/12.

[9.42] *Stoffel, B. and P. Krieger:* Experimental investigations on the energy balance of radial centrifugal pump impeller at part load conditions. 11th IAHR symp. Amsterdam (1982) proc vol. 1, 19 p. 1/15.

[9.43] *Dziallas, R.:* Einige Betriebszustände außerhalb des normalen Arbeitsbereiches einer Kaplanturbine, VDI-Berichte 75 (1964).

[9.44] *Lazzaro, B. and G. Rossi:* Experimental analysis of the main factors affecting the power of a hydraulic machine operating as a pump at zero discharge. 11th IAHR symp. Amsterdam (1982) proc. Vol 3, 63 p. 1/11.

[9.45] *Gerich, R. and J. Raabe:* Measurements of the unsteady and cavitating flow in a model Francis turbine of high specific speed. ASME conference Cavity flow. Minneapolis (1975) p. 29/32.

[9.46] *Mollenkopf, G.:* Messung der instationären und kavitierenden Strömung im Saugrohr einer Francisturbine. Dr.-Ing. thesis TU München 1970

[9.47] *Cassidy, J. J.:* Experimental study and analysis of draft tube surging. Bureau of reclamation. Rep. Hy-591, 1969.

[9.48] *Fischer, R. K. and R. K. Donelson:* Theoretical and experimental investigation of operating characteristics of a Francis turbine in off design regions. 11th IAHR symp. Amsterdam (1982), 84, p. 1/12.

[9.49] *Doerfler, P.:* System dynamics of the Francis turbine half load surge. 11th IAHR symp. Amsterdam. (1982) 39 p. 1/15.

[9.50] *Ulith, P., E. U. Jaeger and M. Strscheletzky:* Contribution to clarifying the inception of nonstationary flow phenomena in the draft tube of high specific speed Francis turbines operating at part load. 7th IAHR symp. Vienna (1974), III, 4 p. 1/18.

[9.51] *Ulith, P. and R. K. Fisher:* Vergleich der Saugrohrdruckschwankungen von Francisturbinen an geometrisch ähnlichen Modellen und Prototypen. Voith Forsch. u. Konstrukt. 28 (1982) no 7.

[9.52] *Glattfelder, A. H., H. Grein and P. K. Dörfler:* Systemschwingungen in Wasserkraftwerken. EW-Mitt. 54/55 (1981/82) no 1 p. 27.

[9.53] *Klein, J., F. Strohmer and D. Enzenhofer:* Investigation on Vibrations of a large penstock, on the sources of their excitation and on getting them under control 8th IAHR symp. Leningrad (1976) I–3 p. 29/46.

[9.54] *Zolotov, L. A., V. M. Klabukow and A. N. Zaitsev:* Effect of hydraulic unbalance on the dynamic characteristics of large turbines. 7th IAHR symp. Vienna (1974), V,3, p. 1/7.

[9.55] *Brand, F.:* Geräuschprobleme in Wasserkraftwerken. Voith Forsch. u. Konstrukt. 12 (1964), no 1685.

[9.56] *Rossi, G. and V. Zanetti:* Attempts of synthesis of radial thrust measurements. 11th IAHR symp. Amsterdam (1982), 52, p. 1/11.

[9.57] *Siebert, G. and O. Eichler:* Allgemeine Einrichtungen und Besonderheiten der Kreisläufe in der hydraulischen Versuchsanstalt Brunnenmühle. Voith Forsch. u. Konstrukt. 22 (1975) no 2125.

[9.58] *Eichler, O., G. Heimann and F. Brand:* Automatische Meßwerterfassung und Meßwertverarbeitung der hydraulischen Versuchsanstalt Brunnenmühle. Voith Forsch. u. Konstrukt. 22 (1975) no 2126 + e.

[9.59] *Brand, F.:* Elektronische Geräte zur Drehzahlmessung an Prüfständen. Voith Forsch. u. Konstrukt. 4 (1958) no 12.

[9.60] *Brand, F.:* Akustisches Verfahren zur Messung von Strömungsgeschwindigkeiten. Voith Forsch. u. Konstruktion 12 (1973) no 6.

[9.61] *Schweizer, F.:* Dehnungsmeßtechnik für Kaplan Modellturbinen. EW-Mitt. 43 (1970) p. 38.

[9.62] *Osterwalder, J.:* Die Differenzdruckmethode als Mittel der Durchflußüberwachung bei hydraulischen Maschinen. EW-Mitt. 33 (1960) no 1/2/3 p. 21.

[9.63] *Brand, F. and H. Selbach:* Laser measurements for Kaplan runners. Waterpower 35 (1983) no 2, p. 21/23.

[9.64] *Durst, F. and M. Zare:* Laser Doppler measurements in two phase flows. IAHR-SHF Symp. Cavitation etc. Grenoble 1976, proc. p. 409/418.

[9.65] *Furtner, N., E. Göde, P. Jermann and H. Durrer:* Zweidimensionale Messung des instationären Strömungsfeldes in und am rotierenden Laufrad einer horizontalen Axialmaschine mit dem Laser-zwei-Focus Verfahren. 3. int. Seminar Wasserkraftanlagen. Techn. Universität Wien 1984, paper.

[9.66] *Kirmse, R. E.:* Investigations of pulsating turbulent pipe flow. J. of Fluids Engng. 100 (1979) p. 436/442.

[9.67] *Resnik, A. and A. Goulas:* Laser Doppler measurements inside an axial pump impeller at off design conditions. 11th IAHR Symp. Amsterdam (1982). 18, p. 1/15.

[9.68] *Kinori, B. Z.:* Scaling problems of hydraulic models. Waterpower 31 (1979) no 2, p. 28/31.

[9.69] *Raabe, J.:* The negative scale effect in Pelton turbines and its causes. 10th IAHR Symposium. Tokyo (1980). Proc. p. 689/702.

[9.70] *Osterwalder, J.:* Efficiency scale up for hydraulic turbomachines with consideration of surface roughness. J. Hydr. Res. 16 (1978) no 1, p. 55/76.

[9.71] *Hutton, S. P. and A. Fay:* Scaling up head, flow, power curves for water turbines and pumps. 7th IAHR Symp. Vienna (1974). trans 1, X, 4, p. 1/19.

[9.72] *Kühnel, W.:* Untersuchung der Druckverteilung am Kopf konischer Vektorsonden. Hydroturbo (1976). Int. Conf. Hydr. Mach. Brne.CVTS, Dum. Techniky, Brne. CKD Blansko. F 2 p.

[9.73] *Matsunaga, S. et al.:* Three dimensional flow measurements in a diagonal flow pump. 11th IAHR symp. Amsterdam proc. 15, p. 1/12.

[9.74] *Kühnel, W. and J. Raabe:* Einfluß der Schaufelzahl bei sonst gleichbleibenden Gitterparametern auf die Durchströmung axialer Turbinenlaufräder. Masch.Markt 72 (1966) no 28, p. 13;73 (1967) no 82 p. 16;70 (1964) no 72, p. 20.

[9.75] *Bär, E.:* Messung des relativen Strömungsfeldes in Wasser an der Laufschaufel einer schnellläufigen Francisturbine. Forsch. Ing. Wesen 36 (1970) no. 2, p. 54/64.

[9.76] *Wegener, M. and P. Y. Larroze:* Comparaison entre écoulement calculés et observés dans les roues Francis. 11th IAHR Symp. Amsterdam (1982) proc. 81, p. 1/13.

[9.77] *Campmas, P. and J. Tehel:* Analyse d'écoulement réel à travers les turbines Francis en vue de la modification de leur performance. 11th IAHR Symp. Amsterdam (1982) proc. 81, p. 1/14.

[9.78] *Chen, Y,N.:* 60 Jahre Forschung über die Karmansche Wirbelstraße. Ein Rückblick. Schweiz. Bauztg. 91 (1973) no 4. p. 2/20.

[9.79] *Kubota, T. and Y. Kimoto:* Effect of inlet shape of runner blades on hydraulic characteristics of Francisturbines with variables heads. 11th IAHR Symp. Amsterdam (1982) proc. 54, p. 1/11.

[9.80] *Kubota, T. and S. Yamada:* Effect of cone angle at draft tube inlet on hydraulic characteristics of Francis turbines. 11th IAHR Symp. Amsterdam (1982) proc. 53, p.1/14.

[9.81] *Castorph, D. and J. Raabe:* Measurement of unsteady pressure, unsteady relative and absolute velocity field of a Kaplan runner by means of an electronic multi miniature probe as a basic contribution to research on unsteady runner load. 7th IAHR Symp. Vienna (1974) Trans. part. 1, I, 2. p. 1/13.

[9.82] *Furtner, N. and J. Raabe:* The dynamic measurement of the unsteady flow near and within the boundary layer of the runner vane face of water-operated axial and semi-axial model turbines. 10th IAHR Symp. Tokyo (1980) proc. p. 327/340.

[9.83] *Schlemmer, G., R. Gerich and J. Raabe:* Measurements of quasi-steady and unsteady flow field in Francis turbines of high specific speed carried out before the runner, in the runner and in the draft tube. 6th IAHR Symp. Rome (1972) Trans. part. 1 H 3 p. 1/13.

[9.84] *Pawlowski, J.:* Die Ähnlichkeitstheorie in der physikalisch technischen Forschung. Berlin: Springer Verlag 1971.

[9.85] *Camerer, R.:* Vorlesungen über Wasserkraftmaschinen. Leipzig Berlin: Engelmann-Verlag 1914.

[9.86] *Schmidt, E.:* Einführung in die technische Thermodynamik. 10. Aufl. Berlin: Springer-Verlag 1963.

616

[9.87] *Willm, G. and P. Campmas:* Mesure du rendement des turbines hydrauliques par la méthode thermométrique Poirson. Houille Blanche 9 (1954) no 7 p. 449.

[9.88] *Borel, L.:* Thermodynamic method of measuring turbine efficiency. Bull. Techn. Vevey (1966) p. 1.

[9.89] *Gabaudan, J., P. H. Thomas and J. Gallian:* Évolution de la méthode thermodynamique de détermination du rendement des machines hydrauliques. Houille Blanche 21 (1966) no 4, p. 433.

[9.90] *Alming, K. and J. Överli:* The isothermal factor for different water qualities. Water power 28 (1976), no 8. p. 52/56.

[9.91] *Hutton, S.:* Water metering and water meters. Nat. Engng. Läb. (NEL), Kilbride Fluid rep. 94.

[9.92] *Gyr, G.:* New miniature current meter. Water Power 17 (1965) no 9, p. 348.

[9.93] *Anonymous:* 10th IAHR congress. Water Power 16 (1964) no 3, p. 122.

[9.94] *Thoma, D.:* Über den Genauigkeitsgrad des Gibsonschen Wassermeßverfahrens. Mitt. d. Hydr. Inst. d. TH München (1926), no 1 p. 59.

[9.95] *Knapp-Böttcher, C.:* Geschwindigkeit und Mengenmessung mittels Ultraschall. Dissertation ETH Zürich 1958.

[9.96] *Moody, L. F.:* Efficiency and power step up. Proc. ASCE (1939), p. 1584.

[9.97] *Ackeret, J.:* Theoretische Betrachtungen zur Kaplanturbine. EW-Mitt. 4 (1931) p. 73.

[9.98] *Hutton, S. P.:* Über die Voraussage des Verhaltens von Wasserturbinen auf Grund von Modellversuchen. Schweiz. Bauztg. 77 (1959) p. 371.

[9.99] *Hutton S. P. and A. Fay:* Scaling up head, flow, power curves for water turbines and pumps. 7th IAHR Symp. Vienna (1974) Trans 1, X,4, p. 1/19.

[9.100] *Osterwalder, J.:* Model testing for Kaplan turbine design, including studies on efficiency scale effects. Waterpower 19 (1967) no 3, p. 103.

[9.101] *Osterwalder, J.:* Modellversuche und Aufwertungsstudien an Wasserturbinen. Schweiz. Bauztg. 87 (1969) no 49, p. 951/955.

[9.102] *Rütschi, K.:* Zur Aufwertung des Wirkungsgrades bei Pumpen und Trubinen. Schweiz. Bauztg. 69 (1951), no 38, p. 525/527.

[9.103] *Mühlemann, E.:* Zur Aufwertung des Wirkungsgrades von Überdruckwasserturbinen. Schweiz. Bauztg. 65 (1948) p. 331.

[9.104] *Fay, A.:* Theoretische Grundlagen der Modellgesetze und Umrechnung der Meßergebnisse an Überdruckturbinen. Acta Tecnica Hungarica Budapest (1980) no 3/4.

[9.105] *Osterwalder, J. and L. Hippe:* Studies on efficiency scaling process in series pumps. J. Hydr. Research 20 (1982) p. 175/201.

[9.106] *Strscheletzky, M:* Neuere Erkenntnisse über viskose Unterschichten an rauhen Wänden. Fortschritts-Ber. VDI-Zs. (1976) R.7. no 43, p. 105.

[9.107] *Osterwalder, J.:* Analyse der Verlustquellen bei Francis und Kaplanturbinen und Beispiele für deren Minderung. EW-Mitt. 37 (1964) p. 3.

[9.108] *Wissenschaftl. Gesellschaft für Luftfahrt:* Aerodynamische Meßtechnik, TH Aachen (1962) Ber. no 5.

[9.109] *Conrad, O.:* Geräte zur Messung von Strömungseinrichtungen. Arch. für techn. Messen (1950) Lieferung 172 V 116-2.

[9.110] *Jahn, R.:* Messungen des absoluten und relativen Strömungsfeldes einer mit Wasser betriebenen Kaplanturbine. Dr.-Ing. thesis TU München 1970.

[9.111] *Fleischner, P.:* Strömungsvorgänge in hydraulischen Turbomaschinen. Masch. Markt. 76 (1970) no 43, p. 937/943.

[9.112] *Fister, W. and J. Kozut:* Untersuchung zur Weiterentwicklung von radialen Turboverdichtern. GHH Technischer Ber. 1969, no 1, p. 2/14.

[9.113] *Fister, W.:* Verdichter. BWK, 22 (1970) no 4, p. 192/195.

[9.114] *Gallus, H. E., H. Künne and S. Subramanian:* Experimentelle und theoretische Untersuchungen zur Energieumsetzung in einem Radialverdichterlaufrad. Mitt. no 81-05 Inst. für Strahlantriebe und Turboarbeitsmaschinen RW TH Aachen, 1981.

[9.115] *Klein, J.:* Reynoldszahl und Machzahleinfluß auf den Wirkungsgrad einer schnelläufigen Francis-Modellturbine im Gasbetrieb. Dr.-Ing. thesis TU München 1984.

[9.116] *Castorph, D.:* Messung des instationären Strömungsfeldes in einer Kaplanturbine mit elektronischen Miniatursonden. Dr.-Ing. thesis TU München 1974.

[9.117] *Schlichting, H.:* Berechnung der reibungslosen, inkompressiblen Strömung für ein vorgege-benes, ebenes Schaufelgitter. VDI-Forschungsheft 447. (1955).

[9.118] *Finke, E.:* Beitrag zur Berechnung der Strömung und der Schaufelform bei axialbeauf-schlagten Strömungsmaschinen mit geringer Schaufelzahl. Dr.-Ing. thesis TH Karlsruhe 1951.

[9.119] *Touchy, W.:* Beitrag zur Berechnung des Geschwindigkeitsfeldes in axial und halbaxial beaufschlagten Strömungsmaschinen mit geringer Schaufelzahl mit Berücksichtigung des Wand-einflusses. Dr.-Ing. thesis TH Karlsruhe 1956.

[9.120] *Jochem, H.:* Beitrag zur Untersuchung des Einflusses der Schaufelfächerung bei der Berech-nung axialer Schaufelgitter. Dr.-Ing. thesis TH Karlsruhe 1960.

[9.121] *Rahmo, R.:* Vergleichende Untersuchung der räumlichen Durchströmung von Laufrädern axialer hydraulischer Turbomaschinen. Dr.-Ing. thesis TU München 1960.

[9.122] *Strscheletzky, M.:* Hydrodynamische Grundlagen zur Berechnung der Schiffsschrauben. Karlsruhe: Braun Verlag 1950.

[9.123] *Glauert, H.:* Grundlagen der Tragflügel und Luftschraubentheorie Berlin: Springer Verlag 1929.

[9.124] *Pantell, K.:* Die Laufradberechnung von Kaplanturbinen. Wasserkraft und Wasserwirtsch. München, Berlin (1933) p. 241.

[9.125] *Betz, A.:* Tragflügel und hydraulische Maschinen. In H. Geiger und K. Scheel: Handbuch der Physik, Bd. VII p. 256, Berlin: Springer Verlag 1927.

[9.126] *Imbach, H:* Die Berechnung der inkompressiblen, reibungsfreien Unterschallströmung durch räumliche Gitter aus Schaufeln auch großer Dicke und starker Wölbung. Dissertation ETH Zürich (1964). no 3402.

[9.127] *Kühnel, W.:* Einfluß der Schaufelzahl bei sonst gleichbleibenden Gitterparametern auf die Durchströmung axialer Turbinenlaufräder mit drallfreier Zuströmung. Dr.-Ing. thesis TU Mün-chen 1969.

[9.128] *Hahn, K.:* Die Untersuchung der Strömung durch eine Flügelradturbine bei verschiedenen Schaufelzahlen. Dr.-Ing. thesis TH Karlsruhe 1933.

[9.129] *Fabritz, G.:* Wasserkraftmaschinen. In Hütte, Maschinenbau Teil II A p. 865/922. Berlin: Ernst Verlag 1954.

[9.130] VDI-Durchflußmeßregeln. DIN 1952 Düsseldorf: VDI-Verlag 1948.

[9.131] *Marcinowski, H.:* Versuchsstand zur Untersuchung von Axialgebläsen. Das Versuchswesen der Maschinenfabrik. J. M. Voith, Heidenheim 1949.

[9.132] *Szabó, I.:* Mathematik. In Hütte, Theoretische Grundlagen I p. 1/236 Berlin: Ernst-Verlag 1955.

[9.133] *Gerich, R.:* Die Untersuchung über die instationäre Strömung in einer schnelläufigen Fran-cisturbine mit besonderer Berücksichtigung des Teillastverhaltens. Dr.-Ing. thesis TU München 1974.

[9.134] *Kazacov, J. Ja.:* Die nichtstationäre Umströmung eines mehrreihigen zweidimensionalen Profilgitters einer hydraulischen Maschine in einer Schicht mit veränderlicher Dicke (Russian) Energomasinostroenije 16 (1970) p. 6.

[9.135] *Furtner, N.:* Instationäre Messung der schaufelnahen Relativströmung in Laufrädern von Axial und Halbaxialturbinen. Dr.-Ing. thesis. TU München 1978.

[9.136] *Rotta, J. C.:* Fortran IV Programm für Grenzschichten der kompressiblen, ebenen, achsen-symmetrischen Strömungen. DFVLR Ber. AVA-FB 7 113, Göttingen, Mai 1970.

[9.137] *Sexl, Th.:* Über den von E. G. Richardson entdeckten Annulareffekt. Z. Phys. 61 (1930) p. 349. or W.Tollmien: Handbuch der Experimentalphysik IV Teil 1 (1931) p. 281.

[9.138] *Lecher, W. and K. Baumann:* Francisturbines at part load with high back pressure. IAHR Symp. Lausanne (1968) B 4.

[9.139] *Ulith, P.:* A contribution to influence the part load behaviour of Francisturbines by aeration and σ-value. IAHR Symp. Lausanne (1968) B.11.

[9.140] *Durst, F., A. Melling and J. J. Whitelaw:* Principles and practice of LDA. Acad. Press Lon-don 1976.

[9.140a] *Turton, R. K.:* The Laser Doppler velocimeter applied to hydraulic machines. 7th IAHR Symp. Vienna (1974). Trans part 1 I, 1, p. 1/11.

618

[10.1] *Mataix, C.:* Turbomáquinas hidráulicas: ICAI Madrid, 1975.

[10.2] *Nechleba, M.:* Water turbines, their design und equipment. Artia Prague 1956.

[10.3] *Krivcenko, F. I.:* Nacocy i Gidroturbiny (Pumps and Water turbines). Moskva: Energia 1970.

[10.4] *Kviatkovskij, V. S:* Diagonalnye Gidroturbinye (Diagonal Water turbines). Moskva: Mašinostrocnie 1971.

[10.5] *Kovalev, N. N:* Hydroturbines (translated from Russian) Israel Progr. Scientific Transl. Jerusalem 1970.

[10.6] *Mühlemann, E.:* Große Kaplanturbinen. EW-Mitt. 42 (1969) no 1 p. 3.

[10.7] *Osterwalder. J.:* Kaplanturbinen für hohe Gefälle. EW-Mitt. 25/26 (1952/53) p. 11.

[10.8] *Gerber, H.:* Die Kaplanturbinen für die Großkraftwerke Donzère Mondragon an der Rhône und Assuan am Nil. EW-Mitt. 25/26 (1952/53) p. 1.

[10.9] *Wucherer, J and R. Vaucher:* Hochdruck Kaplan-Turbinen. EW-Mitt. 29 (1956) no 1 p. 5.

[10.10] *Obrist, H.:* Die 90 000 PS Kaplanturbinen für das Kraftwerk Pirttikoski. EW-Mitt. 32 (1959) no 2/3 p. 46.

[10.11] *Siervo de, F. and F. de la Leva:* Modern trends in selecting and designing Kaplanturbines. Water Power 29 (1977) no 12 p. 51/56;30 (1978) no 1, p. 52/58.

[10.12] *Jaeger, E.-U.:* Einfluß von voll- und halbkugeligen Laufradringen bei Kaplan Turbinen auf Wirkungsgrad und Kavitationsverhalten. Voith Forsch u.Konstrukt. 19 (1969) no 3.

[10.13] *Jaeger, E.-U. and M. Göhringer:* Blade spindle torques on the runner blades of Kaplan turbines, particularly under runaway conditions with regard to the cavitation effect. 11th IAHR Symp. Amsterdam (1982) proc. 50 p. 1/9.

[10.14] *Ceravola, O., M. Ubaldi, P. Zunino and A. Satta:* Flow field analysis in a Kaplan turbine. Comparison between theoretical calculations, velocity measurements, and cavitation observations. Houille Blanche 37 (1982) no 7/8 p. 579/587.

[10.15] *Barp, B., F. Schweizer and E. Flury:* Betriebsspannungen an Kaplanturbinen EW-Mitt. 46 (1973) no 2, p. 10.

[10.16] *Ancona, I. and A. Compte:* Calculation of the flow field in a Kaplan turbine and of the stresses in the blades. Houille Blanche 37 (1982) no 7/8 p. 589/597.

[10.17] *Grein, H., B. Barp and K. Höller:* Stresses on blades of Kaplan and bulb turbines due to the hydrodynamic forces 7th IAHR symp. Vienna (1974). Trans III, 2, p. 1/12.

[10.18] *Cotillon, J:* World's bulb turbines. Water Power 33 (1981) no 9, p. 42/43.

[10.19] *Thuß, W.:* Rohrturbinen als axiale Pumpturbinen. Voith Forsch. u. Konstrukt. 12 (1964) no 1682.

[10.20] *Parzany, K. and G. Rauchschindel:* Die Rohrturbinen an der Mosel Energie 18 (1966) no 4 p. 153/161.

[10.21] *Fentzloff, H. E.:* Ermittlung der wirtschaftlichsten Bauweise für ein Niederdruckkraftwerk mit Rohrturbinen. EW-Mitt. 38 (1965) no 2. p. 19.

[10.22] *Höller, K and H. Miller:* Rohrturbinen und Straßloturbinen für Niederdruckkraftwerke. EW-Mitt. 40 (1977) no 2, p. 3.

[10.23] *Hollenstein, M. and W. Soland:* Die Rohrturbinen für das Kraftwerk Racine. EW-Mitt 54/55 (1981/82) no 1, p. 13.

[10.24] *Eichler, O. and H. Wulz.:* Untersuchung über die Gestaltung von Einläufen bei Rohrturbinen. Voith Forsch. u. Konstrukt. 27 (1981) no 2430 + e.

[10.25] *Zintner, O:* Betriebserfahrungen mit Rohrturbinen. EW-Mitt. 25/26 (1952/53) p. 30.

[10.26] *Lacoste, A.:* Exploitation et entretien des groupes bulbes. Houille Blanche 32 (1977) no 7/8 p. 583/596.

[10.27] *Strohmer, F., D. Enzenhofer and J. Witzmann:* Comparison of the computed stresses and natural frequencies of a large bulbe turbine with the measured values of a prototype unit. 10th IAHR symp. Tokyo (1980) proc. p. 727/736.

[10.28] *Becke, L.:* Modellversuch zur Entwicklung einer neuen Pumpturbine (Granadilla). EW-Mitt. 53 (1980) no 1/2 p. 63.

[10.29] *Barp, B.:* Umbau des Kraftwerkes "Am Gießen" in Zürich-Höngg. EW-Mitt. 52 (1979) no 2, p. 39.

[10.30] *Meier, W. and H. Miller:* Die Entwicklung zur Straflo Turbine. Bulletin SEV/VSE 69 (1978) no 17, p. 943/947.

[10.31] *Coumarcs, X, and Y. van Pachterbeke:* Economics of straflo units for run-off-river stations. Water Power 33 (1981) no 5, p. 48/52.

[10.32] *Whiteaker, J. C.:* Annapolis points the way for Fundy. Water Power 34 (1982) no 7 p. 23/25.

[10.33] *Siervo de, F. and F. de Leva:* Modern trends in selecting and designing Francisturbines. Water Power 28 (1976) no 8, p. 28/35.

[10.34] *Zanobetti, D.:* Characteristics of Francisturbines. Water Power 11 (1959) no 3, p. 96/103.

[10.35] *Raabe, J.:* The natural limits for the output of a mixed flow water turbine. Hydroturbo (1976) Int. Conf. Hydr. Mach., Brno, CVTS. Dumtechniky, Brne CKD Blansko El p. 1/13.

[10.36] *Grosse, G.:* Rechnergestütztes Entwerfen von Wasserkraftanlagen am Beispiel der Francisturbine, Voith Forsch. u. Konstrukt. 28 (1982) no 8.

[10.37] *Schirm, J..* Die Francis Turbinen von Vianden. EW-Mitt 38 (1965) no 1, p. 7.

[10.38] *Podlesack, J. and W. Geromiller:* Die Francisturbinen, Notschlußdrosselklappen und Kugelschieber im Pumpspeicherwerk Säckingen. EW-Mitt. 44 (1971) no 1, p. 3.

[10.39] *Ruud, F.O.:* Initial operation of 600 MW turbines at Grand Coulée third power plant. 8th IAHR Symp. Leningrad (1976) proc. p. 502/516.

[10.40] *Kawano, M, T. Ohkumi and H. Ikeda:* 730 000 kW Hydraulic turbines for Guri second powerhouse etc. Hitachi Rev. 28 (1979) no 4 p. 177/182.

[10.41] *Baumann, K.M. J. and J. Podlesack:* The Francisturbines of the Infiernillo and la Angostura Hydro electric stations in Mexico. Escher Wyss news 45 (1972) no 1 p. 1/60.

[10.42] *Ulith, P.:* Versuche an einer Francis Modellturbine bei 650 m Fallhöhe. Voith Forsch. u. Konstrukt. 15 (1967) no 6.

[10.43] *Gysi, G. and F. Schneebeli:* Hochdruck-Francis- und Freistrahlturbinen. EW-Mitt. 25/26 (1952/53) p. 24.

[10.44] *Gysi, G.:* Hochdruck-Francis Spiralturbinen und ihr Verhalten im Betrieb. EW-Mitt. 32 (1959) no 2/3 p. 14.

[10.45] *Fachbach, H.:* Die Strömung in einer schnelläufigen Francisturbine. Dissertation TH Graz 1970.

[10.46] *Raabe, J.:* Berechnung der dreidimensionalen Strömung eines reibungsfreien Fluids durch ein Turbomaschinenlaufrad mit doppelt gekrümmten Schaufeln. VDI Tagung, Hydraulische Strömungsmaschinen. Braunschweig (1981). VDI-Berichte 424 p. 109/120.

[10.47] *Nagafugi, T. and H. Mori:* A flow in Francis turbine runner. 10th Symp. IAHR Tokyo (1980) Trans p. 583/594.

[10.48] *Fisher, R. K., U. Palde and P. Ulith:* Comparison of draft tube surging and homologous scale models and prototype Francis turbines. 10th IAHR Symp. Tokyo (1980), proc. p. 541/556.

[10.49] *Henry, P., M. Wegner and J. E. Graeser:* Analyse experimentale de la stabilité hydraulique. Symp. SHF Fonctionnement des turbomachines a débit partiel. Paris (1981). Sess. 18 p. 1/20.

[10.50] *Nishi, M., T. Kubota, S. Matsunaga and Y. Senov:* Study on swirl flow and surge in an elbow draft tube. 10th IAHR Symp. Tokyo (1980), proc. p. 557/567.

[10.51] *Graf, K., H. Ries and E. Kraft:* Fabrikation geschweißter Francisturbinen-Laufräder. EW-Mitt. 43 (1970) no 2, p. 33.

[10.52] *Angehrn, R., K. Keller and B. Barp:* A comparison of theoretical stress calculations with experimentally verified stresses on Francis turbine runners of high specific speed. 8th IAHR Sym. Leningrad (1976), proc. p. 97/108.

[10.53] *Malquori, E. and F. Milanese:* Planning, design and operating of hydraulic machinery in the Italian energy system. 10th IAHR Symp. Tokyo (1980) proc. p. 417/428.

[10.54] *Moysa, N:* Maintenance experience with large Francis hydroelectric turbines. 7th IAHR Symp. Vienna (1974), trans IV, 5 p. 1/9.

[10.55] *Kohler, K. and H. Kirchner:* Design details of large hydraulic turbines. 7th IAHR Symp. Vienna (1974) Trans. V, 1 p. 1/9.

[10.56] *Flödl, G., P. Spitaler and F. Strohmer:* Problems in the design of Francis type turbines and single stage reversible pump-turbines due to the tendency to large dimensions, outputs, net heads and total dynamic heads. 7th IAHR Symp. Vienna (1974). Trans V, 2 p. 1/4.

[10.57] *Bernhard, H. J. and R. V. Mathews:* The design of guide vane apparatus for large turbines und pump-turbines. 7th IAHR Symp. Vienna (1974), Trans. XI, 4, p. 1/13.

[10.58] *Casacci, S. et al.:* Conception et construction des turbomachines hydrauliques de grandes dimensions. Houille Blanche 32 (1977), p. 591/616.

[10.59] *Bernhardsgrütter, W.:* Einzelservomotoren für Leitschaufeln großer Francis und Kaplanturbinen. EW-Mitt. 38 (1965) no 3 p. 41

[10.60] *Grein, H., H. Henninger and H. Podlesack:* Versuche zur Ermittlung der günstigsten Anfahrmethode einer Francisturbine bei Anwendung einer Überholkupplung zwischen Turbine und Motorgenerator. EW-Mitt. 42 (1969) no 1, p. 33.

[10.61] *Moulin, G., M. Wegner, R. Eremeef and Vonh-Phong:* Méthodes de tracé des turbomachines hydrauliques. Houille Blanche 32 (1977) no 7/8, p. 617/628.

[10.62] *Siervo de, F. and A. Lugaresi:* Modern trends in selecting and designing Peltonturbines. Water Power 30 (1978) no 12, p. 40/48.

[10.63] *Weingart, Ch.:* Francis oder Freistrahlturbinen? EW-Mitt. 25/26. (1952/53), p. 54.

[10.64] *Hoz, M. and U. Scherrer:* Die zwei vertikalachsigen Freistrahlturbinen des Kraftwerks Tysso II/Norwegen. EW-Mitt. 43 (1970) no 2, p. 3.

[10.65] *Vulliod, G.:* Développments récents dans le cadre d'études pour l'augmentation de puissance de turbine Pelton vertical multijet. Vevey Bulletin Techniques (1983) p. 15/22.

[10.66] *Angehrn, R., I. Schweizer and K. Starkermann:* Zur Spannungsanalyse in Peltonbechern. EW-Mitt. 53 (1980) no 1/2, p. 153.

[10.67] *Angehrn, R. and M. Dubas:* Experimental stress analysis on a 260 MW Pelton turbine. 11th IAHR symp. Amsterdam (1982), proc. 48. p. 1/10.

[10.68] *Poshi, B. A. and M. S. Konnur:* Reducing the runaway speed of a Pelton turbine: Waterpower 29 (1977) no 11, p. 39/42.

[10.69] *Meier, W.:* Getrennte hydraulische Maschinen oder reversible Pumpturbinen für Pumpspeicherwerke. EW-Mitt. 39 (1966) no 3, p. 31.

[10.70] *Randegger, E.:* Die Speicherpumpen von Vianden. EW-Mitt. 36 (1965) no 1 p. 15.

[10.71] *Cardinal von Widdern, H.:* Die Wahl der richtigen Kupplung für Pumpspeichermaschinensätze. EW-Mitt. 35 (1962) no 1, p. 23.

[10.72] *Baumann, K. M. J.:* Das Konstruktionskonzept der Einwellen Dreimaschinensätze des Pumpspeicherwerkes Waldeck II. EW-Mitt. 44 (1971) no 2, p. 24.

[10.73] *Abraham, K. H. and G. Lottes:* Constructional problems in large pumped storage plants. Water Power 33 (1981) no 1, p. 31/35.

[10.74] *Jaquet, M.:* Einige spezielle Probleme bei der Entwicklung von Pumpturbinen. EW-Mitt. 47 (1974) no 2, p. 20.

[10.75] *Meier, W.:* Pumpenturbinen. EW-Mitt. 35 (1962) no 2, p. 6.

[10.76] *Swiecicki. I.:* Trends in pump-turbine design. Water Power 29 (1977) no 1, p. 45/47.

[10.77] *Schweiger, F. and J. Gregori:* Developments in pump-turbines. Water Power 34 (1982) no 10, p. 22/25.

[10.78] *Dziallas, R.:* Radiale umkehrbare Pumpturbinen. Voith Forsch. u. Konstrukt. 12 (1964) no 1.

[10.79] *Yokoyama, T. et al:* Latest Technology for hydraulic pump-turbine. Hitachi Rev. 28 (1979) no 4, p. 171/176.

[10.80] *Siervo de, F. and A. Lugaresi:* Modern trends in selecting and designing reversible Francis pump-turbines. Water Power 32 (1980) no 5 p. 33/42.

[10.81] *Kaufmann, J. P.:* The dimensioning of pump-turbines. Water Power 29 (1977) no 8, p. 34/37.

[10.82] *Zagars, A. and J. M. Hagood. Jr.:* Bath County a 2100 MW development in the USA. Water Power 29 (1977) no 10, p. 25/33.

[10.83] *Lenssen, G.:* Vianden pumped storage scheme-design criteria for the 10th set. Escher Wyss News (1972) no 1, p. 1/9.

[10.84] *Giersig, K.:* Rodund pumped storage scheme commissioned. Water Power 29 (1977) no 4 p. 21/24.

[10.85] *Tsunoda, S., K. Howada and A. Yamakami:* The world's highest head pump-turbines. Water Power 35 (1983) no 4, p. 17/21.

[10.86] *Fischer, R. K. and J. R. Regnau:* Advances in pump-turbine design. Water Power 35 (1983) no 4, p. 21/26.

[10.87] *Tanaka, H.:* The development of high head single stage pump-turbines. 10th IAHR symp. Tokyo (1980) proc. 429/440.

[10.88] *Ando, J., T. Watanabe and K. Fukumasu:* Research and development of large capacity high head Francis type pump-turbines. 7th IAHR symp. Vienna. Trans. XI, 2 p. 1/12.

[10.89] *Chacour, S. A. and R. S, Grubb:* Conceptional design of pump-turbines for Bath County. Water Power 33 (1981) no 1, p. 44/50.

[10.90] *Vucetic, J.:* Pump-turbine power plant operating problems. 10th IAHR symposium Tokyo (1980) proc. p. 479/488.

[10.91] *Casacci, S., N. Roche and P. Jarriand:* High head pump-turbines, French experiences. Water Power 35 (1983) no 2 p. 31/40.

[10.92] *Plichon. J. N. et al.:* Le problème des Pompes-turbines vue par le maître d'oevre. Houille Blanche 32 (1977) no 719 p. 575/582.

[10.93] *Raabe, J.:* Optimization of pump-turbines. Proc. ASCE J. Engng. Div 107 (81) p. 41/63.

[10.94] *Thuß, W.:* Mögliche Grenzen der Umsetzung großer Fall und Förderhöhen in einer Lauf-radstufe von Pumpspeichermaschinen aus der Sicht der Strömungsvorgänge. Voith Forsch. u. Konstrukt. 21 (1973) no 2431.

[10.95] *Grein, H. and M. Jaquet:* Einige hydraulische Aspekte beim Anfahren von Speicherpumpen und Pumpturbinen großer Leistung. EW-Mitt. 48 (1975) no 1, p. 3.

[10.96] *Swift, W. L. and W. G. Whippen:* A study of effects of dynamic loads in reversible pump turbines. 8th IAHR symp. Leningrad (1976), proc. p. 296/308.

[10.97] *Tschumy, A.:* Le calcul des régimes transitoires dans les installations de turbinage-pompages complexes et de grandes dimensions. 7th IAHR symp. Vienna (1974), Trans. p. II, 4, p. 1/11.

[10.98] *Miyashiro, H and K. Takada:* Axial hydraulic thrust caused by pump starting. J. of Basic Engng. (1972) p. 629/635.

[10.99] *Boussuges, P., H. Amblard and C. Lathuile:* Vibrations des directrices des turbomachines à l'emballement. Houille Blanche 37 (1982) no 2/3, p. 247/256.

[10.100] *Casacci, S. and P. Jarriaud:* Analyse de éssais industriels des turbines pompes hors des zones de fonctionnement normal et lors transitoires. Houille Blanche 37 (1982) no 2/3, p. 185/196.

[10.101] *Yamaguchi, Y. and M. Suzuki:* Stress and pressure fluctuations in high head pump-turbines. Hitachi Rev. 27 (1978) no 4. p. 209/214.

[10.102] *Yamabe, M:* Hysteresis characteristic of Francis pump-turbines when operated as turbine. ASME paper No 70-FE-D. New York 1971.

[10.103] *Casacci, S., P. Boussuges, P. Jarriand, R. Philibert and P. Guiton:* Contribution à l'étude des vibrations des organes de vannage des turbines-pompes. Houille Blanche 32 (1977) no 7/8, p. 629/646.

[10.104] *Bedñucci, M. and M. Giberti et al.:* Interactions entre vannes de machine et organes de régulation des groupes hydroéiectriques réversibles. Houille Blanche 35 (1980) no 7/8, p. 467/483.

[10.105] *Boussuges, P., J. Jarriand and H. Amblard:* Analyse des forces pulsatoires agissant sur les particels tournantes des turbines-pompes. Houille Blanche 35 (1980) no 1/2, p. 77/86.

[10.106] *Grein. H. and P. Bachmann:* Hydraulique torque on misaligned guide vanes. Water Power 28 (1976) no 2, p. 37/40.

[10.107] *Baumann, K. M. J. and H. Grein:* Francis-Anfahrturbinen des Pumpspeicherwerkes Langenprozelten (BRD). EW-Mitt. 52 (1979) no 2, p. 35.

[10.108] *Klemm, P. and W. Thuß:* Hydraulic force fluctuations and shaft vibrations in pump-turbines. 8th IAHR symp. Leningrad (1976) proc. p. 318/329.

[10.109] *Krämer, E.:* Determining the hydraulic lateral forces in pump-turbines. Water Power 33 (1981) no 1, p. 50/54.

[10.110] *Zanetti, V:* La poussée radiale dans les machines hydrauliques experiencée de laboratoire. Houille Blanche 32 (1982) no 2/3, p. 237/246.

[10.111] *Oishi, A. and T. Yokoyama:* Development of high head single and double stage reversible pump-turbines. 10th IAHR symp. Tokyo (1980). proc. p. 441/452.

[10.112] *Borciani, G.:* Un nuovo tipo di machine idraulica. La reversible multistadie. Idrotecnica 2 (198) marzo-aprile p. 79/88.

[10.113] *Bortolan, G. and M. Peron:* Multistage pump-turbine for Chiotas and Edolo. Water Power 34 (1982) no 9, p. 41/45.

[10.114] *Moore, A. E.:* Design of diffusing and turning passages. ASCE-IAHR-ASME symp. Fort Collins Col. (1978). proc. vol. I, p. 247/253.

622

[10.115] *Hausmann, G. and G. Vulliod:* The isogyre pump-turbine. Charmilles Techn. Bulletin. 14 (1975) p. 15/26.

[10.116] *Müller, H. and G. Wörther:* Die maschinellen und stahlwasserbaulichen Anlagen der Kraftwerksgruppe Malta. Energiewirtschaft. Sonderdr. Kraftwerksgruppe Malta p. 137/145.

[10.117] *Thuß, W.:* Einfluß des umgebenden Mediums auf Eigenschwingungen von Laufrädern. Voith Forsch. u. Konstrukt. 27 (1980), no 2431.

[10.118] *Angehrn, R.:* Berechnungsverfahren für das Querschwingungsverhalten an Rotoren. EW-Mitt. 53 (1980) no 1/2, p. 173.

[10.119] *Barp. P.:* Dynamic behaviour of large pump-turbine rotors. Water Power 28 (1976) no 1, p. 48/51.

[10.120] *Eichler, O.:* Vibration phenomena on hydraulic axial turbines. IAHR/IUTAM. Karlsruhe (1979) pap.B-3.

[10.121] *Bellochio, M. and G. Prini:* Flexural vibrations and design criteria Ansaldo Rev. no. 10 (1981), p. 19/22.

[10.122] *Grein, H.:* Rechnergestützte Entwicklung und Konstruktion von Maschinenkomponenten am Beispiel der Leitschaufeln. EW-Mitt. 53 (1980) no 1/2 p. 107.

[10.123] *Osterwalder, J.:* The loss analysis as means for dimensioning the volute inlet diameter of water turbines. Proc. 4th conf. Fluid machinery, Budapest (1972), paper.

[10.124] *Salzmann, F. and A. Süss:* Festigkeitsuntersuchungen an Spiralgehäusen. EW-Mitt. 15/16 (1942/43) p. 164.

[10.125] *Bovet, Th.:* Calcul de la résistance mécanique des bâches spirales de turbines Francis à haute chute. Charmilles, Inf. Techn no 7 (1958) p. 19/30.

[10.126] *Casacci, S. and J. Bosc:* Calcul à la flexion des coques coniques. Paris: Dunod éditeur 1959.

[10.127] *Grein, H.:* Spiral casing stress in pumped storage plants. Water Power 30 (1978) no 2, p. 48/49.

[10.128] *Zöllinger, M.:* Festigkeitsberechnung von Parallelplattenspiralen. EW-Mitt. 53 (1980) no 1/2 p. 32.

[10.129] *Chen, Y. N.:* Water pressure oscillations in the volute casing of storage pumps. Sulzer Technical rev. 534, 1–14. 621.671.22.

[10.130] *Grein, H.:* Ermüdungsbrüche in Stützschaufeln. EW-Mitt. 51 (1978) no 1, p. 33.

[10.131] *Casacci, S., B. Lourdeaux and M. Wegner:* Compartment dynamiques des avant-distributeurs de grandes turbines Francis. 11th IAHR Symp. Amsterdam (1982) proc. 49, p. 1/13.

[10.132] *Okano, K. et al.:* Recent development in thrust bearing for large-capacity high-speed hydrogenerator. Hitachi Rev. 28 (1979) no 4, p. 189/198.

[10.133] *Starcevic, C. M:* Die Entwicklung von großen Traglagern für vertikale Wasserkraftgeneratoren. BBC Mitt. 67 (1980) p. 152/153.

[10.134] *Galetto, R.:* Tilting pad thrust bearings with balancing hydraulic chamber. Rivista ASGEN (1967) no 2, p. 53/61.

[10.135] *Christ, A. and M. Peron:* Hydrostatische Axiallager für Speicherpumpen EW-Mitt. 53 (1980) no 1/2 p. 40.

[10.136] *Waldhüter, W.:* Self-lubricating bearings for hydro station equipment. Water Power 32 (1980) no 6, p. 51/54.

[10.137] *Mayer, E.:* Theorie und Praxis der Gleitringdichtungen. Konstruktion 27 (1975) p. 169/175.

[10.138] *Ceravola, O., M. Fanelli and B. Lazzaro:* The behaviour of the free level below the runner of Francis turbines und pump-turbines in operation as synchronous condenser. 10th IAHR symp. Tokyo (1980) proc. p. 765/775.

[10.139] *Matsuda, I. and T. Nagafuji:* Computerized design for turbines. Water Power 31 (1979) no 10, p. 31/35.

[10.140] *Barp. B.:* Die Methode der finiten Elemente als Konstruktionshilfsmittel im Großmaschinenbau. EW-Mitt. 45 (1972) no 1, p. 22.

[10.141] *Keck, H.:* Finite-Element-Berechnung von Strömungen in hydraulischen Turbomaschinen. EW-Mitt. 53 (1980) no 1/2 p. 92.

[10.142] *Bachmann, J.:* Standardizing small turbines. Water Power 32 (1980) no 7, p. 40/42.

[10.143] *Webster, J.:* The effect of changing jet and wheel size on the performance of inclined-jet hydraulic impulse turbines 7th IAHR symp. Vienna (1974), Trans. IX 5, p. 1/10.

[10.144] *The Editor:* Rance tidal power scheme. Water Power 19 (1967) no 1, p. 7.

[10.145] *Duhoux, L.:* Fermeture de la Rance: déroulement des travaux et analyses des observations. Houille Blanche 19 (1964) no 4, p. 491.

[10.146] *Protic, Z. and M. Babic:* A three dimensional calculation method for computation of flow from guide vane to the runner inlet of Kaplan turbines. 11th IAHR symp. Amsterdam (1982), trans. 80, p. 1/13.

[10.147] *Corniglion, J., P. Vinh and M. Couston:* A model of the flow in fronto (semi) spiral tanks. Houille Blanche 36 (1982) no 7/8, p. 571/578.

[10.148] *Bettochi, R., G. Cantore, L. Magri and M. Ubaldi:* Experimental analysis of the flow in the axial region of propeller turbine admission ducts. Houille Blanche 36 (1982) no 7/8, p. 599/606.

[10.149] *Christaller, H.:* Der Bau des Gezeitenkraftwerkes an der Rance. Wasserwirtsch. 55 (1965) no 3, p. 65.

[10.150] *Ravindran, M.:* Design and flow investigations on a fully reversible pump-turbine. Ph. D.-thesis, deapartment of mechanical engineering. Indian Institute of Technology. Madras: 1978.

[10.151] NACA report TR 460,580,610.

[10.152] *Barp, B., A. Keller and H. Höller:* Some results of fatigue tests on steel containing 13% Chromium, 7th IAHR Symp. Vienna (1974). Trans. VII 1, p. 1/11

[10.153] *Meier, W. and M. Jaquet:* Single and multistage pump-turbines for high head storage plants. ASME Pump Turbine Schemes Fluids Engineering. Conf. Niagara Falls. Transactions New York p. 29/37.

[10.154] *Rühl, K. H.:* Festigkeitslehre: Stabartige Tragwerke p. 867/940 in Hütte I, Theoretische Grundlagen. Berlin: Ernst-Verlag 1954.

[10.155] *Raabe, J.:* Studienreise Wasserkraft durch USA and Mexico. Energie, München 17 (1965) no 7 p. 277/285.

[10.156] *Raabe, J.:* Wasserkraftmaschinen, Jahresübersicht. BWK Düsseldorf 18 (1966) no 4, p. 183/188.

[10.157] *Boussuges, P., L. Megnint and H. Amblard:* Turbines pompes de hautes chutes. Houille Blanche 32 (1977) no 7/8, p. 647/655.

[10.158] *Gersdorff, v, B. and G. Lottes:* Das Pumpspeicherwerk Rönkhausen. Elektrizitätswirtschaft 66 (1967) 24, p. 725/734.

[10.159] *Kraft, W.:* Das Kraftwerk des Pumpspeicherwerks Rönkhausen. Siemens Zeitschrift Erlangen 42 (1968) no 6, p. 475/486.

[10.160] *Voith, J. M.:* Pumpspeicherwerke. Special Issue.

[10.161] *Wehinkel, L.:* Der Endausbau des Pumpspeicherwerks Vianden. Special publication Rheinisch Westfälische Elektrizitätswerke Essen, Federal Republic of Germany 1965.

[10.162] *Grüner, J.:* Das Pumpspeicherwerk Langenprozelten. Maschinen, elektrische Einrichtungen und Stahlwasserbau. Elektrizitätswirtsch. 74 (1975) no 24, p. 868/877.

[10.163] *Voith, J. M.:* Probebetrieb Langenprozelten Maschine 2 beendet. Voith Information Geschäftsbereich Wasserturbinen und Pumpen. (1974) no 3.

[10.164] *Innerhofer, G., A. Eder and R. Gstettner:* The Rodund II pumped storage scheme. Water Power 26 (1973) no 11, p. 413/427.

[10.165] *Abraham, K. H.:* Construction progress at the Waldeck II plant. Water Power 25 (1973) no 12 p. 464/466.

[10.166] *Jaeger, H. and H. Muehloecker:* Entwurf und Bemessung der Hauptmaschinensätze des Pumpspeicherwerks Waldeck II. Elektrizitätswirtsch. 7 (1971) no 24, p. 685/691.

[10.167] *Landsberger, R. and H. Doelz:* Die Kraftwerksgruppe Edersee: Die Entwicklung des Pumpspeicherwerks Waldeck II. Energiewirtsch. Tagesfragen Essen 22 (1972) no 10, p. 515/525.

[10.168] *Meyer, J.:* Kraft aus Wasser p. 97/98. Bern: Staempfli u. Cie.-Verlag 1975.

[10.169] *Pfisterer, E.:* Die Hornbergstufe der Schluchsee AG, Wasserwirtsch 63 (1973) no 1, p. 12/21.

[10.170] *Voith, J. M.:* Storage pumps and spherical valves in the Säckingen pumped storage plant. Special issue Voith, Heidenheim, Brenz.

[10.171] *Raabe, J.:* Die mechanischen Auswirkungen des Kurzschlusses bei Rohrturbinen mit Planetengetrieben. Konstruktion 14 (1962) no 2 p. 58/64.

624

[10.172] *Lomakin, A. A.:* Die Berechnung der kritischen Drehzahl und der Bedingung für die Stabilität des Läufers von hydraulischen Hochdruckmaschinen unter Berücksichtigung der Kräfte, die in den Dichtungen entstehen. Energomasinostroenije 4 (1958) no 4, p. 1/5.

[10.173] *Kellenberger, W.:* Der optimale Winkel für die Abstützung von vertikalen Wasserkraftgeneratoren mit schrägen Armen oder Blattfeder. BBC Mitt. 67 (1980) no 2. p. 108/116.

[10.174] *Niemann, G.:* Gleitlagertechnik. In Hütte Maschinenbau IIA p. 60/76. Berlin: Ernst-Verlag 1954.

[10.175] *Baltisberger, K.:* Bremsverfahren bei Synchronmaschinen. BBC Mitt. 1967 no 9, p. 1/9.

[10.176] *Raabe, J:* Ein Beitrag zur Begrenzung der Durchgangsdrehzahl von Kaplanturbinen. Wasserwirtsch. 52 (1962) no 10, p. 273/278.

[10.177] *Hutarew, G:* Die Turbine des Wasserkraftwerks Ossbergshausen an der Agger. Wasserwirtsch. 47 (1957) no 6, p. 137.

[10.178] *Ventrone, G., A. Mirandola and G. Navarro:* Récherche experimentale et numérique sur le comportment d'une roue réversible au point de tracé et hors du point de tracé Houille Blanche 37 (1982) no 7/8 p. 607/613.

[10.179] *Carnevale, E., S. Giusti and G. Angelo:* Analyse théorique experimentale de le'écoulement réel dans les pompes asso-radiales. Houille Blanche 37 (1982) no 7/8, p. 553/557.

[10.180] *Eremeef, L. R. and R. Philibert:* Modelization quasi-tridimensionelle de l'écoulement dans les turbomachines hydrauliques. Houille Blanche 37 (1982) no 7/8, 543/551.

[10.181] *Vötter, M.:* Beiträge zur numerischen Berechnung des räumlichen Strömungsfeldes in hydraulischen Turbomaschinen. Dr.-Ing. thesis TU München 1968. See also VDI-Forschungsheft Nr. 535. Düsseldorf: VDI-Verlag 1969.

[10.182] *Wu, Chung-Wua:* A general theory of three-dimensional flow in subsonic and supersonic turbomachines of axial radial and mixed flow type. Trans. ASME, 74 (1952) p. 1363/1380.

[10.183] *Japikse, D.:* Review: Progress in numerical turbomachinery analysis. Trans. ASME. J. of Fluids Engng. (1976) p. 592/606.

[10.184] *Bosman, C. and M. A. T. El-Shaarawi:* Quasi-three-dimensional numerical solution of flow in turbomachines. Trans. ASME J. of Fluids Engng (1977) p. 132/140.

[10.185] *Novak, R. A. and R. M. Hearsey:* A nearly three-dimensional intrablade computing system for turbomachinery. Trans. ASME. J. of Fluids Engng. (1977), p. 154/166.

[10.186] *Krimerman, Y. and D. Adler:* The complete three-dimensional calculation of the compressible flow field in turbo impellers. Journ. Mech. Engng. Science 20 (1978), no 3, p. 149/158.

[10.187] *Bosman, C. and J. Highton:* A calculation procedure for three-dimensional time dependent, inviscid, compressible flow through turbomachine blades of any geometry. Journ. Mech. Engng. Series 21 (1979), no 1, p. 39/49.

[10.188] *Pfoertner, H.:* Berechnung der Relativströmung in Kreiselpumpenlaufrädern mittels finiter Elemente. Dr.-Ing. thesis TU Munich not yet terminated.

[10.189] *Ribaut, M.:* On the calculation of three dimensional divergent and rotational flow in turbomachines. Trans. ASME J. of Fluids Engng. (1977) p. 187/196.

[10.190] *Lewis, R. I and G. W. Fairbairn:* Analysis of the through-flow relative eddy of mixed-flow turbomachines. Int. J. Mech. Sci. 22 (1980) p. 535/549.

[10.191] *Krouse, J. K.:* Graphic terminals for CAD/CAM. Machine Design, (1981) Aug. 6.

[10.192] *Chasen, S. H.:* Guide lines for Acquiring CAD/CAM information. Computer and Mechanical Engng. ASME Aug. 1982.

[10.193] *Meier, W. and N. Meystre:* Moderne Maschinen für hydraulische Kraftwerke. Techn. Rundschau Sulzer (2/1982) no 2, p 4/8.

11.1] *Fabritz, G.:* Die Regelung der Kraftmaschinen unter besonderer Berücksichtigung der selbsttätigen Wasserturbinenregelung. Wien: Springer-Verlag 1940.

11.2] *Fabritz, G.:* Regelung von Wasserkraftmaschinen. In Hütte IIa, p. 922 Berlin: Ernst-Verlag 1954.

11.3] *Nechleba, M:* Theory of indirect speed control. London, New York, Sidney 1964.

11.4] *Hutarew, G.:* Regelungstechnik: Kurze Einführung am Beispiel der Drehzahlregelung von Wasserturbinen. Berlin, New York: Springer-Verlag 1961.

11.5] *Kühnel, W.:* Gerätetechnischer Aufbau der Regler. In H. Kirchbach: Taschenbuch der Hydraulik in Industriebetrieben p. 574/597. Stuttgart: Franckh-Verlag 1961.

[11.6] *Rudquist, O.:* Turbine control, an historical survey. Water Power 28 (1976) no 9, p. 27/29.

[11.7] *Causon, G. J.:* Governing a hydro-electric system. 7th IAHR symp. Vienna 1974. Trans. X, 2, p. 1/13.

[11.8] *Berhardsgrütter, W.:* Regulierungen großer Wasserturbinen. EW-Mitt. 15/16 (1942/43) p. 151.

[11.9] *Seeberger, F.:* Das Stabilitätsproblem der Wasserturbinenregelung. EW-Mitt. 21/22 (1948/49) p. 43.

[11.10] *Truxal, J. G. (editor):* Control Engineer's Handbook. New York: MacGraw Hill publishers 1958.

[11.11] *Fanelli, M.:* Problemi di stabilita dei sistema idraulica. ENEL Relazione di Studie e Ricerca, no 384, 1981.

[11.12] *Howe, J. C.:* Predicting the stability of regulation. Water Power 33 (1981) no 7, p. 32/35.

[11.13] *Fasol, K. H.:* Bemerkung zur Stabilitätsprüfung in Wasserkraftwerken. Schweiz. Bauzeitg. 88 (1970) no 16, p. 863/864.

[11.14] *Stein, Th.:* Systematik der Reglerarten. EW-Mitt. 13 (1940) p. 59.

[11.15] *Seeberger, F.:* Ein neuartiger Regler für konstante Maschinenleistung. EW-Mitt. 25/26 (1952/53), p. 101.

[11.16] *Stein, Th.:* Lastverteilung durch primäre Leistungsregler. EW-Mitt. 15/16 (1942/43) p. 158.

[11.17] *Hirt, M. and F. Seeberger:* Wirkungsweise und Betriebsergebnisse des Escher Wyss Leistungsreglers. EW-Mitt. 21/22 (1948/49) p. 37.

[11.18] *Hirt, M.:* Neuartige Systeme zur Leistungsverstellung in Anpassung an die verschiedenen Betriebe EW-Mitt. 25/26 (1952/53).

[11.19] *Woodward, J. L. and J. T. Boys:* Electronic load governor for small hydro plants. Waterpower 32 (1980) no 7, p. 37/39.

[11.20] *Rocka, G. and A. Sillos:* Power swing produced by hydro power units. 11th IAHR Symp. Amsterdam (1982), proc. 44, p. 1/15.

[11.21] *Horn, H. E. and J. Bergseng:* Water level control for small hydro plants. Water Power 33 (1981) no 11, p. 50/53.

[11.22] *Wiederkehr, W.:* Regulierung einer Wasserturbine nach der zufließenden Wassermenge und Nachsteuerung des Niveaus bei Teilbelastung. EW-Mitt. 25/26 (1952/53) p. 103.

[11.23] *Stein, Th.:* Einfluß der Selbstregelung und Abklingzeit auf den Materialaufwand von Wasserturbinen. EW-Mitt. 19/20 (1946/47). p. 90.

[11.24] *Dube, B.,M. Cuenod, H. Netsch and J. Ch. Gille:* Réglage de tension et de fréquence dans un groupe hydroélectrique. Automatic Control, Theory a. Applications 1 (1972) no 1, p. 2/9.

[11.25] *Fasol, K. H.:* On some recent methods for investigation of the dynamic behaviour of turbine governors, turbine-units, and large hydraulic systems. 7th IAHR Symp. Vienna (1974) Trans X, 1 p. 1/12.

[11.26] *Matthias, H. B.:* Beitrag zur dynamischen Untersuchung axialer Wasserturbinen nach der Frequenzgangmethode. Dr-Ing. thesis. Univ. Stuttgart 1971.

[11.27] *Hutarew, G.:* Tests on turbine governing systems. Water Power 15 (1963) no 4, p. 157; no 5, p. 197.

[11.28] *Netsch, H.:* Bestimmung der Impulsantwort und des Frequenzganges von Regelelementen mittels stochastischer Störsignale kleiner Amplitude-Anwendung an Wasserturbinenreglern. Regelungstech. no 6, p. 197/206.

[11.29] *Junghanns, K.:* Calcul des fréquences naturelles hydrauliques et ses problèmes. 8th IAHR symp. Leningrad (1976) proc. 421/430.

[11.30] *Jaeger, Ch.:* Theory of resonance in hydro power systems: Water Power 15 (1963) no 4, p. 14.

[11.31] *Zolotov, L. A., V. M. Klabukov, V. M. Vladimirsky, S. G. Dimitriev and A. N. Zaitsev:* Influence of boundary conditions on dynamic loads in penstock and hydraulic elements. 8th IAHR symp. Leningrad (1976) proc. 269/282.

[11.32] *Arake, M. et al:* Analysis of total pump-turbine system including pipe lines. Hitachi Rev. 24 (1975) no 5, p. 217/224.

[11.33] *Fanelli, M.:* Hydraulic resonance in rock-bored penstocks. Water Power 25 (1973) no 9, p. 42/48.

[11.34] *Benkö, G. B.:* Governing turbines for transient loads. Water Power 33 (1981) no 4, p. 38/42.

626

[11.35] *Arcidiano, V. and E. Ferrari:* Analysis of factors affecting the damping of low-frequency oscillations in multimachine systems. ENEL relazione di studie e ricerca (1976) no 302.

[11.36] *Blair, P. and W. Wozniak:* Non-linear solution of hydraulic turbine governor system. Water Power 28 (1976) no 9, p. 23/26.

[11.37] *Fasol, K. H. and M. Hoppe:* Simulating and improving hydroplant control. Water Power 34 (1982) no 5, p. 73/78.

[11.38] *Forberg, J.:* Governors for small hydroelectric plants. Water Power 31 (1979) no 1, p. 26.

[11.39] *Agnew, P. W. and G. W. Bryce:* Optimizing turbine operation by electronic governing. Water Power 29 (1977) no 1, p. 36/38.

[11.40] *Tuszynski, J.:* Electric equipment for turbine governor, Water Power 28 (1976) no 9, p. 30/33.

[11.41] *Süss, A.:* Elektrischer Pendelantrieb von Drehzahlreglern für Wasserturbinen mittels Doppelmotor. EW-Mitt. 25/26 (1952/53) p. 91.

[11.42] *Schlegel, M., K. Mendler and F. Riescher:* Regelung von Kaplan und Rohrturbinen mit elektrisch angetriebenen Steuerpumpen. EW-Mitt. 54 (1981) no 1 p. 43/50.

[11.43] *De Lorenzo, J. and W. Keil:* Neuer elektro-hydraulischer Regler im Wasserkraftwerk Meitingen am Lech. Voith Forsch. u. Konstrukt. 20 (1974) no 6 and 7.

[11.44] *Seigne, M. and M. Philippe:* The Charmilles electronic governor head RE-301. Charmilles Techn. Bull.no 14 (1975) p. 39/48.

[11.45] *Sandberg, T., O. Karlson, B. Forden and S. Hartwig:* Computerized governor control for bulb and Kaplan turbine. Water Power 31 (1979) no 7, p. 43/46.

[11.46] *Kopacek, P. and E. Zauner:* Governing turbines by microcomputers. Water Power 34 (1982) no 9, p. 26/27.

[11.47] *Wührer, W.:* Wasserturbinenregelung mit Elementen der elektronischen Modultechnik, EW-Mitt. 49 (1976) no 2, p. 3.

[11.48] *Mouron, J.:* Microprocesseurs appliqués au réglage des machines hydrauliques. Vevey Bullet. Techn. (1983) p. 23/25.

[11.49] *Süss, A.:* Wasserturbinenregler mit Schließfeder mit anpaßbarer Federcharakteristik. EW-Mitt. 25/26 (1952/53) p. 98.

[11.50] *Wiedler, K.:* Untersuchungen von Reglervorgängen in Wasserkraftanlagen mittels neuer Registrierinstrumente. EW-Mitt. 33 (1960), no 1/2/3, p. 51.

[11.51] *Gerber, H.:* Die Bestimmung des günstigsten Zusammenhanges zwischen Leitapparat und Laufrad von Kaplanturbinen. EW-Mitt. 8 (1935) p. 107.

[11.52] *Kohler, A.:* Not-Schließvorrichtungen für Kaplanturbinen zum Schutz gegen Durchgehen. EW-Mitt. 36 (1963) no 2/3 p. 48.

[11.53] *Voaden, G. H.:* A new runaway speed limiter for Kaplan turbines. Trans. ASME Ser. A., J. Engng. Power 83 (1961) no 1, p. 19.

[11.54] *Gerber, H.:* Untersuchungen über die Regulierarbeit von Wasserturbinen. EW-Mitt 15/16 (1942/43) p. 158.

[11.55] *Seeberger, F.:* Die Bestimmung der Schwungmassen für stabile Regelung von Wasserturbinen mittels Kataraktreglern. EW-Mitt. 25/26 (1952/53) p. 93.

[11.56] *Yokoikawa, T. et al.:* Improvement on stability and response speed of Peltonturbine governor. Hitachi Rev. 23 (1974), no 7, p. 283/290.

[11.57] *Raabe, J.:* Stabilitätsbetrachtungen an Wasserturbinenreglern unter Berücksichtigung des Druckstosses, erläutert am Beispiel einer Francisturbinenanlage. Masch. Markt 67 (1961) no 12, p. 15.

[11.58] *Biland, O.:* Eine neue Druckreglersteuerung. EW-Mitt. 25/26 (1952/53) p. 105.

[11.59] *Bernhardsgrütter, W.:* Praktische Winke für die Inbetriebsetzung von Wasserturbinen. EW-Mitt. 25/26 (1952/53).

[11.60] *Walker, J. H.:* Large Hydro Generators. Oxford: Univ. Press 1981.

[11.61] *Foster, E. N.:* The design of generators for hydro power. Water Power 29 (1977) no 1, p.48/49.

[11.62] *Fiesenig, K. and G. Rais:* Generatoren für große Wasserkraftwerke in Brasilien. BBC Mitt. 67 (1980) p. 94/99.

[11.63] *Kranz, R. D.:* Große Schenkelpolmaschinen. BBC Nachr. CH-T 130053D p. 3/7.

[11.64] *Holenström, E.:* The 320 MVA generator for Ritzem. Water Power 30 (1978) no 8, p. 28/31.

[11.65] *Howaldt, W. et al.:* Karakaya, ein Wasserkraftwerk in der Türkei. BBC Mitt 67 (1980) p. 100/107.

[11.66] *Barozzi, A. and M. Silei:* Large low speed generators for the Itaparica power plant. Ansaldo Rev.no 10 (1981) p. 5/11.

[11.67] *Perkira, L.:* Induction generators for small hydro plants. Water Power 33 (1981) no 11, p. 30/34.

[11.68] Baltisberger, K. et al.: Motorgeneratoren für Pumpspeicheranlagen BBC Druckschr. no. CH-T 130-143 D p. 3/14.

[11.69] *Costigliolo, G. and M. Bavosi:* From Lago Delio to Presenzano high speed unit for power generating und pumping plants. Ansaldo Rev. no 10 (1981) p.30/34.

[11.70] *Gyenge, J. and W. Regez:* Die Motorgeneratoren für das Pumpspeicherwerk Grimsel II Ost. BBC no CH-T 130 263 D.

[11.71] *Schwirzer, T.:* Dynamic stressing of hydro electric units by stochastic hydraulic forces on the turbine runner. Water Power 29 (1977) no 1, p. 39/44.

[11.72] *Kellenberger, W.:* Erzwungene Kombinationsresonanzen der rotierenden Welle, Kopplung von Biegung und Torsion. BBC Mitt. 67 (80) p. 117/121.

[11.73] *Brandl, P.:* Stromkräfte in den Stirnverbindungen von Drehstromwicklungen, BBC Mitt. 67 (1980), p. 128/134.

[11.74] *Nigam, P. S., O. P. Jani and M. B. Kauch:* Generator stresses in hydro power plants. Water Power 28 (1976) no 1, p. 44/47.

[11.75] *Arrigo, F. and F. Montebruno:* Cooling of Kaplan, Inga and Argus river generators. Ansaldo Rev. no 10 (1981), p. 5/10.

[11.76] *Baltisberger, K. and K. Gamlesoeter:* Experience gained with fully water-cooled salient pole machines. BBC Rev. 58 (1971) no 1, p. 18/24.

[11.77] *Peer, F. et al:* Static excitation equipment for Itaipú. Water Power 34 (1982) no 9, p. 25/26.

[11.78] *Peneder, F. and H. Herzog:* Moderne Erregungseinrichtungen für Hydrogeneratoren BBC Mitt. 67. (1980) p. 141.

[11.79] *Schuler, R.:* Isoliersysteme für Hydrogeneratoren: Stand der Technik und Betriebserfahrungen. BBC Mitt. 67 (1980) p. 135/140.

[11.80] *Gasperini, J. R. and P. F. Johrde:* Uprating hydrogenerators: mechanic and electrical factors. Water Power 32 (1980) no 1, p. 25/28.

[11.81] *Suzuki, T. N. and N. Suzuki:* Latest technology for hydrogenerators. Hitachi Rev. 28 (1979) no 4, p. 183/188.

[11.82] *Spirk, F.:* Heutiger Stand und mögliche Entwicklungen von Wasserkraftgeneratoren. Beitrag, Tagung: Die Neueste Entwicklung in der Wasserkraftnutzung und Pumpspeicherung. Haus der Technik e.V. Essen, Nov. 1981.

628

13. List of further Literature in alphabethic order of the authors

[1] *Aitken, P. L.:* Dams and salmon in Scotland, Waterpower 32 (1980) no 10, p 31/32.

[2] Allis Chalmers: Site manufacture of Grand Coulée 700 MW Francis turbine runners. Special issue 54 P 101 15.

[3] *Alwers, E., K. Baltisberger, and R. Grabitz:* Asynchronous starting of synchronous machines for pumped storage schemes. BBC Rev. 2/3 (1972) p. 1/8.

[4] *Anderson, H. H.:* Efficiency mayorisation formula for fluid machines. 7th IAHR Symp. Vienna (1974) trans IV, no 3, p. 1/12.

[5] *Araki, M., and T. Kuwabara:* Analysis of total pump-turbine system including pipe lines. Hitachi Rev. 24 (1975), no 5, p. 217/224.

[6] *Bachmann, P.:* Fortschritte und Erfassen und Auswerten von Kräften und Meßmomenten an Rotoren hydraulischer Modellturbomaschinen. EW Mitt. 53 (1980). no 1/2. p. 82.

[7] *Bagliani, G.:* Energy problems: hydraulic equipment for pumping plants. Bulletin U.I.I. 1972, p. 15/36. (U.I.I. = Ufficio Impianti Idroelettrici).

[8] *Baltisberger, K.:* Bremsverfahren bei Synchronmaschinen. BBC Mitt. (1967) no. 9, p. 3/9.

[9] *Battegay, C. L. and C. von Widdern:* Rohrturbinen. EW Mitt 35 (1962) no 3 p. 3.

[10] *Bleuler, W.:* Druckrohrleitungen. EW Mitt. 25/26 (1952/53) p. 158.

[11] *Blind, H.:* Funktion von Kontrollgängen bei Staudämmen. Wasserwirtschaft 71 (1981) p. 115/116.

[12] *Bose, B., M, Canay and J.-J. Simond:* Frequenzanlauf für Pumpspeicherwerke-Möglichkeiten und Optimierung. BBC Mitt. 70 (1983) p. 295/302.

[13] *Bohn, J. G.:* The influence of surface irregularities on cavitation, a collation and analysis of new and existing data with application to design problems. Technical memorandum file, (1972) no 72–223. The Pensylvania State University, Ordnance Research Laboratory, Navy Department, Naval Ordnance, Systems Command.

[14] *Boller, Ch.:* Spherical stop valves. Charmilles, Technical Bulletin (1975), no. 14, p. 35/38.

[15] *Bonapace, B., H. Drobir and E. Kresnik:* Die Unterwasserschächte des Pumpspeicherwerks Kühtai der Kraftwerksgruppe Sellrain-Silz. Österr. Wasserwirtsch. 31 (1979).

[16] *Bonny, L.:* Influence de la compressibilité de l'huile sur le fonctionnement d'amplificateur hydromécanique. Bulletins Techniques Vevey (1976) p. 53.

[17] *Bonny, L. and J. J. Hemmeler:* Test d'un régulateur de turbine Pelton avec simulation approximative du coup de bélier d'onde. Bulletins Techniques Vevey (1977) p. 39.

[18] *Borciani G. A. and F. del Brenna:* Stress analyses of some components of hydraulic machines through model and prototype testing. Bulletin Ufficio Impianti Idroellettrici (1972) p. 53/62.

[19] *Borel, L.:* Stabilité de réglage des turbines Kaplan. Bulletins Techniques Vevey (1963/64) p. 66.

[20] *Borel, L. and J. Berberides:* Simulation d'une installation hydraulique equipée d'une turbine Kaplan. Bulletins Techniques Vevey (1965), p. 22.

[21] *Borel, L.:* Méthode thermodynamique pour la détermination du rendement des machines hydrauliques. Bulletins Techniques Vevey (1966), p. 1/46.

[22] *Borel, L. and M. Mamin:* Installation de pompe turbine en régime transitoire. Bulletins Techniques Vevey (1966) p. 47.

[23] *Borel, L.:* Chiffres characteristiques adimensionelles en turbomachines. Bulletins Techniques Vevey (1976), p. 38.

[24] *Borel, L. and J. Chappuis:* Méthode d'étude pseudo-tridimensionelle du diffuseur-distributeur d'une pompe-turbine. Bulletins Techniques Vevey (1972), p. 24.

[25] *Borel, L.:* Application pratique de la méthode thermodynamique pour la détermination du rendement des machines hydrauliques. Bulletins Techniques Vevey (1973) p. 25.

[26] *Borel, L.:* Étude pseudo-tridimensionelle des écoulements fluides autour des aubes de turbomachine, premier partie: Bulletins Techniques Vevey (1978) p. 79, deuxième partie; ditto (1979), troisieme partie; ditto (1980/81) p. 79.

[27] *Bortolotti, B.:* Récent realisation Vevey en turbine hydraulique. Quelque observations générales en matière d'introduction. Bulletins Techniques Vevey (1960) p. 11/18.

[28] *Bortolotti, B. and E. Schobinger:* Cents ans de turbines Vevey. Bulletins Techniques Vevey (1963/64) p. 26/58.

[29] *Bortolotti, B. and E. Moret:* La pompe-turbine de la centrale de Vouglans d'Électricité de France. Chapitre I. Dimensionement et conception de la machine. Bulletins Techniques Vevey (1976) p. 3/26.

[30] *Bortolotti, B.:* Participation de Vevey a l'amenagement hydro-électrique "Hongrin-Leman". Chapître I. Régulateurs de vitesse. Bulletins Techniques Vevey (1969), p. 42.

[31] *Bradshaw, P., D. H. Ferriss and N. P. Atwell:* Calculations of boundary layer development using the turbulent energy equation. Journ. Fluid Mech. 28 (1967) p. 593.

[32] *Bradshaw, P.:* The analogy between streamline curvature and buoyancy in turbulent shear flow. Journ. Fluid Mech. 36 (1969) part 1, p. 177/191.

[33] *Bradshaw, P.:* A note on reverse transition. Journ. Fluid. Mech. 35 (1969) part 2, p. 387/390.

[34] *Brand, F.:* Die Verwendung eines elektronischen Impulszählers für die Drehzahlmessungen bei Turbogetrieben. Voith Forsch. u. Konstrukt. 6 (1959) special issue 1522.

[35] *Brand, F.:* Das thermodynamische Verfahren zur Messung des Wirkungsgrades von Wasserturbinen und Pumpen. VDI-Berichte no 75 (1964), special issue Voith 1664.

[36] *Brand, F.:* Die Entwicklung des thermodynamischen Meßverfahrens in den vergangenen 50 Jahren. Voith Forsch. u. Konstrukt. (1967) no 19.

[37] *Brand, F.:* Das Ultraschallverfahren zur Messung von Strömungsgeschwindigkeiten. Vortrag vor dem Arbeitsausschuß Meßmethoden in der Wasserwirtschaft (1969). Voith special issue 2048 d + o.

[38] *Brand, F.:* Automatische Meßwerterfassung und Meßwertverarbeitung an Versuchsständen der hydraulischen Versuchsanstalt Brunnenmühle. Voith Forsch. u. Konstrukt. 22 (1974) no 6.

[39] Brown, Boveri u. Cie (BBC): Automatische Steuerung für Wasserkraftwerke. Druckschrift Nr D SI 80 484 D.

[40] *Caglar, M.:* A contribution to the variation of flow parameter pumping highly viscous fluids. Proc. 7th conf. on fluid machinery (1983), no 13, p. 116/121. Akademiai Kiado, Budapest.

[41] *Canay, M.:* Asynchronanlauf einer großen 230 MVA Synchronmaschine im Pumpspeicherwerk "Vianden 10". BBC Druckschrift Nr. CH-T 130023 D.

[42] *Canay, M.:* Anlaufprobleme im Pumpspeicherwerken und deren mathemathische Behandlung. Elektrizitätsverwertung 6 (1974) p. 231/237.

[43] *Casacci, S.:* Advances in low-head machines. Water Power 13 (1961) no 4. p. 152/157.

[44] *Ceravola, O.:* Alcuni probleme relative alle turbine Pelton. L'Energia Elettrica 47 (1970) no 12, p. 1/9.

[45] *Chappuis, J. and R. Chenal:* Quelque mesures récentes du rendement de turbomachines hydrauliques au moyen d'un thermomètre a quartz. Bulletins Techniques Vevey (1971) p. 14.

[46] *Chaubert, A.:* Les turbines de la central de Zongo. Bulletins Techniques Vevey (1956) p. 1.

[47] *Chaubert, A.:* Sollicitations du pivot butée d'un groupe hydroélectrique a axe vertical comportant une pompe. Bulletins Techniques Vevey (1967) p. 25.

[48] *Chaubert, A.:* La pompe-turbine de la centrale de Vouglans d'Électricité de France. Chapitre trois. Mise on route et essais de réception. Bulletins Techniques Vevey (1976) p. 27/40.

[49] *Chaubert, A.:* Mesure de l'épaiseur du film d'huile sur un pivot. Bulletins Techniques Vevey (1963/64) p. 21/50.

[50] *Chen, Y. N. et al.:* Guide vane vibrations caused by water and blower noise. Journ. of Enginrg. for Industry 98 (1976), no. 1, p. 948/955, no. 3, p. 956/964.

630

[51] *Chenal, R.:* Laboratoire d'hydraulique, nouveau stand d'essai universel pour modeles réduits de turbomachines hydrauliques. Bulletins Techniques Vevey 40 (1980/81) p. 3/32.

[52] *Cheng, E. and M. J. Prosser:* Intake design to prevent vortex formation. Symp. ASCE, IAHR, ASME Fort Collins Col USA (1978), proc. vol I p. 393/402.

[53] *Christ, A.:* Freistrahlströmung nach einer beliebig geformten Spaltblende. EW Mitt. 50 (1977) no 2, p. 28.

[54] *Cita, A.:* Abacus for the choice of the speed adoptable for a hydraulic turbine on the basis of the maximum normal discharge to be delivered by the turbines and for the corresponding mean operating head under which the turbine shall work. Bulletin Ufficio Impianti Idroelettrici (1972), p. 7/14.

[55] *Clark, R. H.:* Re-assessing the feasibility of Fundy tidal power. Water Power 30 (1978) no 6, p. 35/41.

[56] *Corbellini, G.:* Slide valve hydraulic amplifier for the control of hydraulic turbine wicket gates. Ufficio Impianti Idroelettrici (1972), p. 79/88.

[57] *Coxon, R. E.:* Dam and third parties. Water Power 29 (1977) no 6, p. 33/36.

[58] *Coxon, R. E.:* Dam hazards, risks and liabilities. Water Power 31 (1979), no 11, p. 68/70

[59] *Csallner, K. and E. Häusler:* Abflußinduzierte Schwingungen an Zugsegmenten, Ursachen, Sanierung und allgemeine Erfahrungen. Versuchsanst. für Wasserbau der TU München/ Obernach Ber. 45 (1981), p. 1/49.

[60] *Csallner, K.:* Strömungstechnische und konstruktive Kriterien für die Wahl zwischen Druck und Zugsegment als Wehrverschluß. Versuchsanstalt f. Wasserbau der TU München/Obernach. Ber. 45 (1981), no I, p. 1/49.

[61] *Dammner, F., H. Haschka and H. Schild:* Ein Wochenfahrplan für den hydrothermischen Verbundbetrieb. Elektrotechn. u. Maschinenbau 88 (1971) no 8, p. 333/336.

[62] *Dörr, M.:* Laufradkontrolle bei Francisturbinen. Voith Information (1975) no 1.

[63] *Dolder, G.:* Fünfzig Jahre Escher Wyss Kugelschieber. EW Mitt. 48 (1975) no 1, p. 19.

[64] *Dreher, W.:* Kranzgenerator für Straflo-turbine in Kraftwerk Höngg. BBC Mitt. 70 (1983) p. 280/282.

[65] *Duran, H., R. Querubin, G. Cuervo and A. Renjifo:* A model for planning hydrothermal power systems. Proc. 9th PICA conf., New Orleans (1975) p. 235/241.

[66] *Durgin, W. W., and G. E. Hedler:* The modelling of vortices and intakes structures. Symp. ASCE, IAHR, ASME, Fort Collins Co, USA (1978), proc. vol. I, p. 381/391.

[67] *Dziallas, R.:* Ermittlung der Winkelübertreibung einer Radial-Wasserturbine, VDI-Zeitschr. 79 (1935) no 47, p. 1426/1427.

[68] *Dziallas, R.:* Schwingungen einer Kreiselpumpe mit labiler Kennlinie, Berlin: VDI-Verl. 1940.

[69] *Dziallas, R.:* Über Verluste und Wirkungsgrade bei Kreiselpumpen. Wasserkraft und Wasserwirtsch. 38 (1943), no. 5, p. 106/111.

[70] *Dziallas, R.:* Kavitationsbeobachtungen an radialen Kreiselpumpen mit räumlich gekrümmten Schaufeln, VDI-Zeitschr. 89 (1945), no. 3/4, p. 41/45.

[71] *Dziallas, R.:* Hydraulische Auslegung von Kaplanturbinen. Voith Forsch. u. Konstrukt. 1 (1955) no 3.

[72] *Dziallas, R.:* Auslaufversuche. Arch. Techn. Messen (ATM) 163 (1955) no. 1, p. 25/26.

[73] *Dziallas, R.:* Maschinen für Pumpspeicherkraftwerke. Energie 12 (1960), no. 3, p. 113/115.

[74] *Dzialllas, R.:* Francisturbinen bei Teil- und Überlast. VDI-Berichte no. 75 (1965), p. 53/61.

[75] *Eichler, O., J. Widman and H. Wulz:* Untersuchung über die Gestaltung von Einläufen bei Rohrturbinen. Österr. Ing. Zeitschrift 10 (1974) p. 326/332.

[76] *Etter, S.:* Bestimmung von Korrekturfaktoren für ein Ultraschalldurchflußmeßverfahren in Rohrleitungen mit Störungen. Dissertat. Universität Stuttgart 1982.

[76a] *Etter, S., and G. Lein:* Regelung von Wasserturbinenanlagen mit langem Zuleitungskanal. Schweizer Ingenieur and Architekt, 102 (1984), no. 3.

[76b] *Etter, S., and G. Lein:* Regelungstechnische Messungen an Regeleinrichtungen von Wasserturbinen. Schweizer Ingenieur und Architekt, 102 (1984), to be published in the middle of the year 1984.

[77] *Fanelli, M., A. Marazio and R. Ruso:* Premiers résultats d'un procède d'évolution continue de déplacement appliqué au control de barrages en exploitation. 10 iéme congrés des grands barrages, Montreal (1970). Paper Q28/R37, p. 675/709.

[78] *Fanelli, M.:* Hydraulic problems in hydro power (excluding machinery). ENEL (= Ente Nazionale Elettricità) (1980), relazione di studi e ricerca no. 380.

[79] *Feldmann, J. M.:* How many lives is a kilowatt worth? Water Power 32 (1980), no 10, p. 37/41.

[80] *Fiesenig, K., M. Starcevic and A. Fust:* Foz do Areia, neue Konzepte beim Bau großer Wasserkraftgeneratoren. BBC Mitt. 70 (1983) p. 258/267.

[81] *Fister, W.:* Druckverteilungsmessungen an umlaufenden Schaufeln. VDI-Forschungsheft 448 (1955) Ausgabe D vol. 21.

[82] *Fister, W.:* Versuche zur Erfassung der Strömungsverhältnisse in Radiallaufrädern. Forschungsbericht Nr. 63-01 der Aerodynamischen Versuchsanstalt Göttingen. Triebwerksaerodynamik der Turbomaschinen, vol II Radialmaschinen 1963.

[83] *Fister, W.:* Sichtbarmachung der Strömung in Radialverdichterstufen, besonders der Relativströmung in rotierenden Laufrädern durch Funkenblitze. Brennstoff Wärme Kraft (BWK) 18 (1966) no. 19.

[84] *Fister, W. and J. Eikelmann:* Rechnergestützte Konstruktion und Fertigung von Radiallaufrädern und räumlich verwundenen Schaufeln. Fachgemeinschaft Pumpen im VDMA. Pumpentagung Karlsruhe 1978.

[85] *Fister, W. and H. Heiderich:* Rechnerische Verformungs und Spannungsermittlung von Radialpumpenlaufrädern unter Berücksichtigung von Fluid- und Fliehkräften. Fachgemeinschaft Pumpen im VDMA. Pumpentagung Karlsruhe (1978).

[86] *Fister, W. and J. Eikelmann:* A contribution to the design of radial compressor impellers with double curved blades. The 6th conf. on fluid machinery, Budapest 1979.

[87] *Fister, W. and J. Eikelmann:* A procedure for the computer-aided construction of radial compressor impellers with high flow coefficient. 55th specialists meeting on centrifugal compressors. Flow Phenomena and Performance (AGARD) Brüssel May 1980.

[88] *Fister, W., G. Zahn and F. W. Adrian:* Theoretische und experimentelle Untersuchungen ar Rückführkanälen hydraulischer Strömungsmaschinen. Pfleiderer Gedächtnistagung Hydrauli sche Strömungsmaschinen TU Braunschweig. VDI-Berichte 442, p. 173/192.

[89] *Fister, W., G. Zahn and J. Tasche:* Theoretical and experimental investigations about vaneles return channels of multistage radial flow turbomachines. ASME-Turbomachinery gas turbine conference (1982) London, paper.

[90] *Fister, F. and W. Adrian:* Experimental researches of flow in hydrodynamic torque converters Porc. 7th conf. on fluid machinery (1983), no 24, p. 210/224. Akademiai Kiado, Budapest.

[91] *Fleischner, P.:* The flow through a system of profile cascades. Porc. 7th conf. on fluid mach nery (1983), no 25, p. 225/233 Akademiai Kiado, Budapest.

[92] *Füzy, O. and A. Sebestyen:* Generalization of the downwash condition for the dynamic cas Proc. 7th conf. on fluid machinery, (1983) no. 29, p. 256/263, Akademiai Kiado, Budapest.

[93] *Füzy, O. and A. Sebstyen:* Simulation of the dynamic behaviour of pumps. Proc. 7th conf. c fluid machinery (1983), no. 31, p. 264/273, Akademiai Kiado, Budapest.

[94] *Gaal, V., F. Riezinger and A. Magyar:* Klein-Wasserkraftwerke, ein Beitrag zur Lösung d Energieproblems. BBC Mitt. 70 (1983) p. 289/294.

[95] *Galetto, R.:* Thrust bearings. Ansaldo Rev. 10 (1981) p. 36/37.

[96] *Gerber, H.:* Geschwindigkeitsverteilungen in großen kreisrunden Querschnitten. Incrnatior current meter group (1960). Report no. 37.

[97] *Götz, O.:* Rationelles Messen im hydraulischen Laboratorium. EW Mitt. 33 (1960) no. 1/2 p. 31.

[98] *Graeser, J. E.:* Turbines Francis. Bulletins Techniques Vevey (1960), p. 20/29.

[99] *Grein, H.:* Schwingungserscheinungen in Francisturbinen, Ursachen und Gegenmaßnahm EW Mitt. 54 (1981) no 1, p. 37/42.

[100] *Grgić, A.:* Mechanical brakes for hydro electric generator sets. BBC publication no CI 130103E.

[101] *Grigić, A.:* The application of mechanical brakes to hydroelectric generator sets. BBC publ tion no CH-T 130113E.

[102] *Grossmann, G.:* Rechenreinigungsmaschinen EW Mitt. 2 (1929) p. 73.

[103] *Gruber, J. and E. Litvai:* An investigation of the effects caused by fluid friction in ra impellers. Proc. 3rd conf. on fluid machinery (1969) p. 241/247, Akademiai Kiado, Buda

632

[104] *Guidez, J., C. C. Girard and P. Jarriand:* Influence d'une fluide annulaire sur la vitesse critique d'une arbre en rotation. Houille Blanche 35 (1980) no 1/2, p. 87/94.

[105] *Häfele, J.:* Statistik über die Entwicklung der Wasserturbinen. EW Mitt. 15/16 (1942/43) p. 120.

[106] *Hack, P. L.:* Lufteinzug in Fallschächten mit ringförmiger Strömung durch turbulente Diffusoren. Versuchs. Anst. f. Wasserbau TU München/Obernach. Ber. 36. (1977).

[107] *Häusler, E.:* Unkonventionelle neuere Stauhaltungswehre an bayerischen Flüssen als gleichzeitige Sohlsicherungsbauwerke. Versuchs Anst. f. Wasserbau d. TU München/Obernach. Ber. 41, (1979) p. 104/143.

[108] *Halleen, R. M. and J. P. Johnston:* The influence of rotation on flow in a long rectangular channel. An experimental study. Rep. MD–18, Mech. Engg. Dept. Stanford University 1967.

[109] *Herbrand, K.:* Spezielle Probleme bei Hochwasserentlastungsanlagen. In: Talsperrenbau und bauliche Probleme der Pumpspeicherwerke. Hamburg: Parey (1980) p. 99/121.

[110] *Herz, W.:* Kopierfräsen für Kaplanschaufeln. EW Mitt. 25/26 (1952) p. 19.

[111] *Hirano, K. and T. Kuwabara:* Recent control system for hydropower plants. Hitachi Review 28 (1979) no. 4, p. 193/198.

[111a] *Hochstatter, J. and G. Lein:* Druckpendelungen im Leitungssystem von Wasserkraftanlagen mit Wasserschloß. Schweizer Ingenieur und Architekt. 98 (1980) no. 6, p. 92/95.

[111b] *Hochstatter, J.:* Entwicklung eines berührungslosen optischen Meßverfahrens zur Bestimmung der Konzentrationsverteilung von Gasblasen in ebenen und rotationssymmetrischen Zweiphasenströhmungen. Dissertation Universität Stuttgart 1979.

[112] *Hudovernik, W. and G. Lein:* Frequenzuntersuchungen im Triebwasserweg von Hochdruck-Wasserkraftanlagen. Österr. Zeitschr. f. Elektrizitätswirtsch. 22 (1969) Nr. 12, p. 637/648.

[113] *Hutton, S. P.:* An alternative to the Fay pipeflow analogy for scaling up water turbine efficiency. Proc. 7th conf. on fluid machinery (1983), no 43, p. 379/385, Akademiai Kiado, Budapest.

[114] *Ito, H., K. Moriguchi, T. Fujii and S. Higuchi:* Actual stress of high head pump-turbine runner. Hitachi Rev. 24 (1975) no. 7, p. 293/300.

[115] *Jacobsen, S.:* Buckling of pressure tunnel steel linings with shear connections. Water Power 30 (1978) no 6, p. 58/62.

[116] *Jonston, J. P.:* The effects of rotation on boundary layers in turbomachine rotors. Rep. MD–24, Mech. Engg. Dept. Stanford University 1970.

[117] *Kaufmann, J. P.:* La centrale hydro-électrique de Taboo. Bulletins Techniques Vevey (1979), p. 35.

[118] *Kawano. M, T. Ohkuni and H. Ikeda:* 730 000 kW hydraulic turbines for Guri second power house. Corporacion Venezolana de Guayana a Republic of Venezuela. Hitachi Rev. 2 (1979) no. 4, p. 177/182.

[119] *Keller, A.:* Langzeitige Werkstoffversuche unter mechanischer Spannung. EW Mitt. 42 (1969), no. 1, p. 30.

[120] *Kercan, V. and J. S. Taylor:* The use of surface approximation in processing of water turbine test results. Porc. 7th conf. on fluid machinery (1983), no. 46, p. 404/412, Akademiai Kiado, Budapest.

[121] *Kiessling, H.:* Die Kraftswerksgruppe Fragant. Österreich. Wasserwirtsch. 31 (1979) p. 136.

[122] *Kimura, Y. and T. Yokoyama:* Planning of reversible pump-turbine. Hitachi Rev. 22 (1973) no. 8, p. 328/334.

[123] *Kissel, W.:* Der Verdrehwinkel eines Raumkrümmers. EW Mitt. 30 (1957) no. 1, p. 28.

[124] *Klemm, D.:* Untersuchung der Vorgänge beim Ausblasen und Füllen einer Pumpturbine. Voith Forsch. u. Konstrukt. 27 (1981) no. 2.

[125] *Klemm, D. and W. Thuss:* Hydraulic radial force fluctuations and shaft vibrations in pump turbines. paper IAHR symp. Leningrad 1976.

[126] *Klemm, D.:* Untersuchung der Vorgänge beim Ausblasen und Füllen einer Pumpturbine. Voith Forsch. u. Konstrukt. 27 (1981) no. 2.

[127] *Kleinert, J. H., G. Will and S. Nagork:* Investigation on the flow and energy conversion in the impeller and in the casing of a centrifugal pump. Proc. 7th conf. on fluid machinery (1983), no. 49, p. 430/438, Akademiai Kiado, Budapest.

[128] *Kopshoff, H. and H. Schorr:* Berechnung des optimalen Einsatzplanes einer Flußspeicherkette. Österreich. Zeitschr. f. Energiewirtschaft 21 (1968) no. 3, p. 110/118.

[129] *Kosmowski. J. and K. H. Steinheimer:* Effects of operating conditions on centrifugal pumps when conveying liquids with gas contents. Proc. 7th conf. on fluid machinery (1983), no. 52, p. 458/466, Akademiai Kiado, Budapest.

[130] *Knauss, J.:* Neuere Beispiele für Blocksteinrampen an Flachlandflüssen. Vers. Anstalt f. Wasserbau d. TU München/Obernach Ber. 45, (1981) no. IV, p. 1/18.

[131] *Kranich, L., J. Wucherer and W. Meier:* Rheinkraftwerk Albbruck-Dogern Ag (Überholungsarbeiten an den Kaplanturbinen und Generatoren) EW Mitt. 43 (1970) no. 2, p. 14.

[132] *Krivchenko, G. T. et al.:* High head water outlet with vortex gate. 7th IAHR Symp. Vienna (1974). Trans. VI, 3 p. 1/12.

[133] *Kurokawa, J. et al.:* Determination of the flow characteristics in volutes. 10th IAHR Symp. Tokyo (1980). Proc. p. 623/634.

[134] *Laue, R. G. T.:* Earth quake hazards. Water Power 30 (1978) no. 10, p. 36/38.

[135] *Lecher, W.:* Ähnlichkeitsgesetze für hydroelastische Schwingungen. EW Mitt. 35 (1962), no. 2, p. 32

[136] *Leemann, P., A. Rüegg:* Kugelschieber. EW Mitt. 25/26 (1952/53), p. 169.

[137] *Lein, G.:* Rechnerische Untersuchungsmethoden für die Steuerung und Regelung von Wasserkraftmaschinen. Voith Forsch. u. Konstrukt. 15 (1967) no. 17, p. 1.

[138] *Lein. G.:* Graphische Druckstoßberechnung für Pumpen und Turbinendruckrohrleitungen. Voith Forsch. u. Konstrukt. 4 (1958) no. 5, p. 1.

[139] *Lein, G.:* Steuerungen von Kaplanturbinen zur Verhinderung von Schwall und Sunkwellen. Voith Forsch. u. Konstrukt. 15 (1967).

[140] *Lettle, R.:* Montagebeginn in Cabora Bassa. Voith Mitteilungen (1973) no. 2.

[141] *Lewis, R. J.:* Simultaneous analysis of boundary layer and potential flow. Proc. 7th conf. on fluid machinery (1983), no. 58, p. 505/515, Akademia Kiado, Budapest.

[142] *Liess, C.:* Die Ermittlung dynamischer Radialkräfte in hydraulischen Maschinen. Voith Forsch. u. Konstrukt. 38 (1982) no. 3.

[143] *Liess, C.:* Die Bestimmung der charakteristischen Rauheitshöhe für Oberflächen mit mechanischer Rauheit. Voith Forsch. u. Konstrukt. 28 (1982) no. 13.

[144] *Mac Millan, O. J. and J. P. Johnston:* Performance of low aspect ratio diffusers with fully developed turbulent inlet flows. Report PD-14. Mech. Engg. Dept. (1978). Stanford University.

[145] *Magyar, A., J. Schwanda and II. Vögele:* Rohrturbinen-Generatoren für die Anlagen Guijo de Granadilla und Bischofshofen. BBC Mitt. 70 (1983) p. 283/288.

[146] *Meier, W.:* Bestimmung der Energielinie im Unterwasser von Kaplanturbinen. EW. Mitt. 41 (1968), no. 3, p. 10.

[147] *Merenda, A.:* Évolution de l'activité de Vevey en matière de turbines hydrauliques. Bulletins Techniques Vevey (1962), p. 3/26.

[148] *Merenda, A.:* L'équipment des basses chutes, Bulletins Techniques Vevey (1965) p. 8.

[149] *Mez, F. and K. Gamlesaeter:* Voll wassergekühlte Schenkelpolmaschinen mit 4472 MVA Gesamtleistung. BBC Mitt. 70 (1983) p. 253/257.

[150] *Moore, J.:* The development of turbulent layers in centrifugal machine. Report no. 99 M.I.T. Gas Turbine Laboratory.

[151] *Moret, Ed. and P. Helfer:* Conception et réalisation des bâches spirales de la centrale de Schiffenen. Bulletins Techniques Vevey 1963/64 p. 59.

[152] *Moser. J.:* Die Turbinen des Rheinkraftwerkes Albbruck Dogern. EW Mitt. 9. (1936), p. 63.

[153] *Motlik, J.:* Czechoslovakia's Largest pumped storage plant. Water Power 34 (1982), no. 10, p. 36/39.

[154] *Motta, S. G. and J. A M. Costa:* Draft tube emergency closure gates at Porto Colombia power plant. 7th IAHR Symp. Vienna (1974). Transact. part 1, II 1, p. 1/12.

[155] *Murugesam, K.:* Analysis of Francis turbine runner blade channel flow. National Aeronautic Laboratory, Bangalore, India (1-1978) Technical memorandum 304.

[156] *Murai, H and S. Tezuka:* Experimental research on reverse flow charcteristics of high specific speed pump and its generating mechanism. Proc. 7th conf. on fluid machinery (1983) no. 65, p. 581/590. Akademiai Kiado, Budapest.

[157] *Naudascher, E. et al.:* Unified analysis of grid turbulence. Proc. ASCE, Journ. Engineering Mech. Div. Ap. (1976), p. 121/141.

[158] *Neiger, F.:* Donaustauräume und Hochwasserschutz. Österreich. Wasserwirtsch. 32 (1980) p. 163.

[159] *Nemet, A.:* Mathematische Modelle hydraulischer Anlagen. EW Mitt. 47 (1974) no. 1, p. 3.

[160] *Nessen-Lapp, von W.:* Parameter excited, coupled rotor vibrations on a horizontal Francis turbine. 8th IAHR Sympos. Leningrad (1976) proc. p. 47/58.

[161] *Neuhauser, E.:* Modellversuche über die Wirkung von Schwallwellen am Staudamm Gepatsch. Österreich. Wasserwirtsch. 31 (1979) p. 191.

[162] *Ng, C. K. and T. B. Ferguson:* A note on the blockage of cylindrical probes. Proc. 7th conf. on fluid machinery (1983) no. 67, p. 601/604. Akademiai Kiado, Budapest.

[163] *Noskievič, J.:* Energy proportions in cavitation wear of material. Proc. 7th conf. on fluid machinery (1983), no. 68, p. 605/614. Akademiai Kiado Budapest.

[164] *Obretenov, V. S. and V. M. Kichev:* Experimental study of some dynamic characteristics of a low speed Francis turbine. Proc. 7th conf. fluid machinery (1983) no. 71, p. 633/642. Akademiai Kiado, Budapest.

[165] *Obrist, H.:* Ausgeführte Kaplanturbinen. EW Mitt. 15/16 (1942/43) p. 138.

[166] *Obrist, H.:* Speicherpumpen. EW Mitt. 35 (1962) no. 1, p. 3.

[167] *Obrist, H.:* Eine Spezialkupplung für Speicherpumpen. EW Mitt. 25/26 (1952/53) p. 135.

[168] *Odaglia, G.:* Brazil: Hydroelectric units constructed by COESMA. Ansaldo Rev. 10 (1981) p. 44/47.

[169] *Oishi, A. and T. Yokoyama:* Development of high head single and double stage reversible pump-turbines. 10th IAHR Symp. Tokyo (1980). Proc. p. 441/452.

[170] *Okano, K., Y. Furukawa and K. Kawaike:* Recent development in thrust bearings for large-capacity high-speed hydrogenerators. Hitachi Rev. 28 (1979), no. 4, p. 189/192.

[171] *Ortlieb, J.:* La cavitation sur modèles reduits en laboratoire. Bulletins Techniques Vevey (1965), p. 18.

[172] *Osterwalder, J. and K.-J. Peschges:* Cavitation investigations on butterfly valves. 8th IAHR Symp. Leningrad (1976) proc. p. 148/159.

[173] *Osterwalder, J.:* Entwicklung kavitationssicherer Venturidüsen zur Wassermengenmessung. EW Mitt. 33 (1960) no. 1/2/3 p. 42.

[174] *Osterwalder, J. and W. Lecher:* Ein neuer Prüfstand für Kennlinenmessungen und Kavitationsbeobachtungen an Wasserturbinen und Pumpen. EW Mitt. 29 (1956) no. 2, p. 21.

[175] *Osterwalder, J.:* Die Differenzdruckmethode als Mittel zur Druchflussüberwachung bei hydraulischen Maschinen. EW Mitt. 33 (1960) no. 1/2/3 p. 21.

[176] *Osterwalder, J.:* Modellversuche und Aufwertungsstudien an Wasserturbinen. Schweizerische Bauzeitung, 86 (1968), no. 26, p. 455/460.

[177] *Osterwalder, J.:* Belüftung von Freistrahlturbinen bei Gegendruckbetrieb. Schweizerische Bauzeitung 85 (1967), no. 31, p. 575/578.

[178] *Osterwalder, J.:* Analyse der Verlustquellen bei Francis und Kaplanturbinen und Beispiele für deren Verminderung. EW Mitt. 37 (1964) no. 3, p. 3/11.

[179] *Paranjpe, P.:* Auslegung der Spiralenquerschnitte von hydraulischen Maschinen EW Mitt. 40 (1967), no. 1, p. 36.

[180] *Pejovic, S. and A. Gajic:* Reverse water hammer in Kaplanturbines. 10th IAHR Symp. Tokyo (1980) proc. p. 489/499.

[181] *Pejovic, S. and H. A. Lenk:* Verfahren zur Berechnung einer räumlichen nicht rotationssymmetrischen Strömung in Turbomaschinen. Konstruktion 20 (1968), no. 11, p. 450/459.

[182] *Picollier, G.:* Turbomachines hydrauliques. Essais industrielles et méthodes de calcul. Houille Blanche 32 (1977), no. 7/8, p. 657/670.

[183] *Pighini, U. and G. de Francesco:* Cavitation tests on copper beryllium alloys. Proc. 7th conf. on fluid machinery (1983) no. 74, p. 658/667. Akademiai Kiado, Budapest.

[184] *Pfenninger, A.:* Propellerpumpen EW Mitt. 25/26 (1952/53) p. 78.

[185] *Protič, Z. and M. Popovic:* Investigations of the behaviour of the guide vane torque on a reversible pump-turbine model in pumping operation. 10th IAHR Symp. Tokyo (1980), proc. p. 749/762.

[186] *Potter, M. C. and M. D. Chawla:* The stability of boundary layer flow subject to rotation. Ph. D. thesis by M. D. Chawla. Michigan State University 1969.

[187] *Raabe, J.:* A theoretical approach to the relation between cavity length and NPSH in an impeller pump of given head-NPSH graph under pulsating cavitation. Proc. 7th conf. on fluid machinery (1983), no. 77, p. 687/695. Akademiai Kiado. Budapest.

[188] *Racher, F.:* Régleur électronique Vevey. Bulletins Techniques Vevey (1962) p. 7.

[189] *Reichert, K., G. Schaffer, R. Marenheim and F. Wettstein:* Optimal control of hydro-electric power plants-problems, concepts, solutions. BBC publication no CH-T 130099E.

[190] *Reichert, K.:* Betriebsführungskonzepte elektrischer Energiesysteme. Bull. SEV. 66 (1975) no. 20, p. 1116/1122.

[191] *Rössert, R.:* Beispiele zur Hydraulik im Wasserbau 3. Aufl. München: Oldenbourg-Verlag 1968.

[192] *Roth, K.:* Stabilité de réglage d'un groupe hydro-électrique. Bulletins Techniques Vevey (1959), p. 29.

[193] *Rouvé, G.:* Anströmverhältnisse in Niederdruckanlagen. EW Mitt. 40 (1966) no. 2, p. 36.

[194] *Seeber, G.:* Entwicklung und derzeitiger Stand der neuen österreichischen Tunnelbauweise. Österreich. Wasserwirtsch. 31 (1979) p. 114.

[195] *Seus, G. J., E. F. Joeres and H. M. Engelmann:* Lineare Entscheidungsregeln und stochastische Restriktionen bei Bemessung und Betrieb von Speichern. Ber. 42 d. Versuchs. Anst. f. Wasserbau d. TU München/Obernach 1979.

[196] *Seus, G. J. and W. Bauch:* Enwurfsoptimierung von Stauräumen an Wehren. Wasserwirtschaft 62 (1972) no. 2, p. 1/6.

[197] *Shaw, T. L.:* Tidal power: closing the gap. Water Power 28 (1976) no. 5, p. 48/52.

[198] *Siebert, G.:* Niederdruck-Kreislauf in der hydraulischen Versuchsanstalt "Brunnenmühle". Voith Forsch. u. Konstrukt. 22 (1975) no. 3

[199] Siemens. Electrical machines for hydroelectric power station deliveries since 1903. Special issue no E 111/1502-380.

[200] *Simmler. H.:* Zur Geschiebeabwehr bei Wasserfassungen. Modellversuche und Ergebnisse Österreich. Wasserwirtsch. 31 (1979), p. 99.

[201] *Simond, J.-J. and G. Neidhöfer:* Verfahren zur genauen Berechnung von Kurvenform und Schwingungsgehalt der Spannung bei Schenkelpolmaschinen. BBC Mitt. 67 (1980), p. 122/127

[202] *Sisak, E.:* A universal aerodynamic diagram of the family of single aerofoils. Proc. 7th conf on fluid machinery (1983), no. 92, p. 823/828. Akademiai Kiado, Budapest.

[203] *Spronle. R. S. and P. Koeller:* Efficiency improvement by high pressure shroud aeration o turbines and pumps demonstrated on a 75 000 hp turbine. Internal report Dominion Engineering Works Limited. Montreal Canada 1966.

[204] *Süss, A.:* Francisturbinen von 115 000 PS. EW Mitt. 15/16 (1942/43) p. 124.

[205] *Surber, A. and F. Schweizer:* Festigkeitsuntersuchungen an Bauteilen hydraulischer Anlager EW Mitt. 33 (1960). no. 1/2/3 p. 168.

[206] *Szalay. K.:* Perfomance monitoring for dam safety. Water Power 32 (1980) no. 9, p. 21/2(

[207] *Schavae, G., O. Jeschek, H. Geymayer and S. Dekitsch:* Wasserkraftwerk Sölk. EW Mit 54/55 (1981.82), no. 1, p. 23.

[208] *Scheuerlein. H.:* Optimization of water resources and water conservation, essential requir ments for human survival. 3rd world congress on water resources, Mexico City (1979). Vol. p. 1486/1495.

[209] *Scheuerlein, H.:* Wasserentnahme aus geschiebeführenden Flüssen. (1979) Ber. 41, Vers. An: f. Wasserbau d. TU München/Obernach.

[210] *Schilling. R.:* Strömungsberechnung bei hydraulischen Maschinen, Voith, Informati((1982). no. 1.

[211] *Schilling. R., O. Eichler, D. Klemm and H. Offenhäuser:* Investigation of the fluid flow with the return passages of multistage centrifugal pumps. Proc. 7th conf. on fluid machinery (198 no. 85, p. 761/769. Akademiai Kiado, Budapest.

[212] *Schmitz. G.:* Instationäre Eichung mathematischer Hochwasserablaufmodelle auf der Ba eines neuen Lösungsprinzips für hyperbolische Differentialgleichungen. Ber. 46 d. Versuc Anst. f. Wasserbau der TU München/Obernach 1981.

[213] *Schohinger. E.:* Turbines Kaplan. Bulletins Techniques Vevey (1962), p. 13/19.

[214] *Schobinger, E.:* Les turbines C.A.F.L. Vevey de la centrale de Vouglans d'Électricité France. Bulletins Techniques Vevey (1969), p. 26.

636

[215] *Schraub. F. A., S. J. Kline, J. Henry, P. W. Rundstadler and A. Littell:* Use of hydrogen bubbles for quantitative determination of time depentent velocity field in low speed water flow. Trans ASME (Scr. D) 87 (1965), p. 429/444.

[216] *Schramm, G., G. Schilg and W. Hahn:* Detection of the service life of turbine components. Proc. 7th conf. on fluid machinery (1983), no. 86, p. 770/778. Akademiai Kiado, Budapest.

[217] *Starkermann, K. and M. Zollinger:* Festigkeitsberechnung von Parallelplattensprialen. EW Mitt. 53 (1980), no. 1/2 p. 158.

[218] *Stoffel, B. and P. Krieger:* Experimental investigations on the energy balance of radial centrifugal impeller at part load conditions. 11th IAHR Symp. Amsterdam proc. Vol. 1. no. 19. p. 1/15.

[219] *Steller, K. and J. Kirejczyk:* Diagnostics of cavitation in the hydraulic machinery. Transactions of the Institute of Fluid Flow machinery. Polish Academy of Science. Warszawa-Poznan (1983), p. 3.

[220] *Steller, K.:* Prediction of cavitation damage in hydraulic turbomachinery. Proc. 7th conf. on fluid machinery (1983). no. 96, p. 856/866. Akademiai Kiado, Budapest.

[221] *Stefani, H.:* Betrachtung der Wirkungsweise von Wirbelfallschächten. Die Bautechnik 7 (1968) p. 221/226.

[222] *Strohmer, F. and G. Horacek:* Model test on a semiaxial pump-turbine. Proc. 7th conf. on fluid machinery (1983). no. 96, p. 856/866. Akademiai Kiado, Budapest.

[223] *Strscheletzky, M.:* Die Eulerschen Differentialgleichungen der Bewegung und das kinetische Gleichgewicht von Strömungen inkompressibler Flüssigkeiten mit freien Begrenzungen. Voith Forsch. u. Konstrukt. 9 (1962) no. 1.

[224] *Strscheletzky, M.:* Ein Beitrag zur Theorie des hydrodynamischen Gleichgewichts von Strömungen. Voith Forsch. u. Konstrukt. 2 (1957) no. 1.

[225] *Strscheletzky, M., P. Ulith and E.-U. Jaeger:* Contribution of clarifying the inception of nonstationary flow phenomena in the draft tube of high specific speed Francis turbines operating in part load. IAHR Symp. (1974) Vienna. Special issue Voith 2264.

[226] *Strscheletzky, M.:* Ein Beitrag zur Berechnung der Umströmung von festen Leitflächen. Voith Forsch. u. Konstrukt. 4 (1958) no. 16.

[227] *Tognola, S.:* Weiterentwicklung von Hochdruckspeicherpumpen. EW Mitt. 33 (1960), no. 1/2/3 p. 58.

[228] *Tognola, S.:* Luftversuche für Speicherpumpen. EW Mitt. 33 (1960) no. 1/2/3 p. 22.

[229] *Tognola, S.:* Modellversuche für Pumpturbinen. EW Mitt. 35 (1962). no. 2, p.12.

[230] *Toyokura, T., N. Kitamura and K. Kida:* Studies on the improvement of high specific speed pump performance at low flow rates. Bulletin of ISME 8 (1965), no. 29, p. 78.

[231] *Toyokura, T. et al.:* Study on turbine flow through guide vanes and stay vanes for a reversible pumpturbine. 10th IAHR Symp. Tokyo (1980), proc. p. 353/364.

[232] *Treske, A.:* Experimentelle Überprüfung numerischer Berechnungsverfahren von Hochwasserwellen. Ber. 44 d. Versuchs. Anst. f. Wasserbau der TU München/Obernach (1980).

[233] *Tschada, H.:* Betriebserfahrungen mit den Bachfassungen des Kaunertalkraftwerkes. Österreich. Wasserwirtsch. 31 (1979) p. 210.

[234] *Tschumy, A. and Cl. Wavre:* Transient state calculations in large and complexe pump-turbine power schemes. Charmilles Technical Bulletin no. 14, (1975) p. 27/34.

[235] *Ulith, P., R. K. Fisher, jun. and U. Palde:* Comparison of draft tube surging of homologous scaie model and prototype Francis turbines. IAHR Symp. (1980) Tokyo.

[236] *Ulith, P. and D. Klemm:* Das hydraulische Verhalten von einstufigen Pumpturbinen für verschiedene spezifische Drehzahlen und Fall- und Förderhöhenbereiche. 2. internationales Seminar Wasserkraft (1982) Wien. Voith special issue t 2537.

[237] *Ulith, P.:* Cavitation limits in Francis turbines. Voith Information 3, (1981).

[238] *Ulith, P. and H. Kirchner:* Dynamische Beanspruchung. Voith Information 2, (1978)

[239] *Vasilyev, Yu. S., I. S. Samurukov, B. A. Solotov, D. S. Schavelev and M. F. Skladnev:* The selection of hydro power plant parameters considering hydraulic instability of the flow. Proc. 8th IAHR Symp. Leningrad (1976) p. 362/371.

[240] *Vaucher, R.:* Rückblick auf eine vierjährige Anwendung der thermodynamischen Methode bei Wirkungsgradmessungen an hydraulischen Maschinen. EW Mitt. 36 (1963) no. 2/3. p. 52.

[241] *Vaucher, R.:* Neue hydraulische Versuchseinrichtungen. EW Mitt. 41 (1968), no. 2, p. 3.

637

[242] *Vischer, D.. et al.:* Optimale Bewirtschaftung von Speicherseen. Wasser und Energiewirtschaft 66 (1974), no. 3, p. 97/104.

[243] *Vogel, A.:* Die Geschichte der gemauerten Talsperren: Teil I. Österreich. Wasserwirtsch. 33 (1981) p. 167.

[244] *Voska, A. and A. Pfenninger:* Moderne Speicheranlagen. EW Mitt. 25/26. (1952/53) p. 117.

[245] *Vuskovič, I.:* Über Rotationsverluste hinter Laufrädern von Turbomaschinen. EW Mitt. 14 (1941), no. 1, p. 14.

[246] *Vuchkova, I. V.. V. S. Obretenov and V. K. Mitsova:* Computer aided synthesis of an impeller optimum version in improving water turbines. Proc. 7th conf. on fluid machinery (1983) no. 106, p. 939/947. Akademiai Kiado, Budapest.

[247] *Wachter, J. and B. Wöhrl:* Aufwertung des Wirkungsgrades von Turbomaschinen bei radialer Bauart in Abhängigkeit von Reynoldszahl und Geometrie. VDI Berichte – 424 (1981), p. 19/28.

[248] *Wada, Y., Y. Yamaguchi, N. Yokoi and S. Tanabe:* Analysis of flow in pump-turbine runner. "FLANPT" and ists application. Hitachi Rev. 22 (1973) no. 10, p. 404/410.

[249] *Weber, D.:* Experimentelle Untersuchung an axial durchströmten ringförmigen Spaltdichtungen für Kreiselpumpen. Konstruktion 24 (1972).

[250] *Weiss, J.:* Installation d'une turbine Kaplan à Serières. Bulletins Techniques Vevey (1941) no. 2, p. 8.

[251] *Werle, H.:* Visualizations hydrodynamique de l'écoulement dans une maquette de trubomachine axial. Houille Blanche 37 (1982) no. 2/3. p. 175/184.

[252] *Wippermann, R.:* Beitrag betreffend das Verhalten von Meßflügeln bei Schräganströmung. International current meter group. Report no. 34. (1965).

[253] *Wolfram, F.:* Leistungsverhältnis von Pumpturbinen Voith Information (1975), no. 3.

[254] *Wulz, H.:* Freistrahlturbinen-hydraulische Neuentwicklungen. Voith Information (1979), no 1.

[255] *Yamaguchi, Y.:* Water level depression in Francis type reversible pump-turbines. 10th IAHR Symp. Tokyo (1980), proc. p. 777/787.

[256] *Yamaguchi, Y. and T. Takoh:* An experimantal research on the transient phenomena of a pumped storage power station. Paper ASME conference on gas turbine and fluid engineering. New Orleans 1976.

[257] *Yamaguchi. Y. and M. Suzuki:* Stress and pressure fluctuations in high head pump-turbines. Hitachi Rev. 27 (1978), no. 4, p. 209/214.

[258] *Yokohama, T., M. Suzuki and S. Higuchi:* Latest technology for hydraulic pump-turbine. Hitachi Rev. 28 (1979), no. 4, p. 171/176.

[259] *Yoshizawa, T.:* Trends in hydroelectric generating equipment technology. Hitachi Rev. 28 (1979), no. 4. p. 167.

[260] *Zanetti, V. and G. Rossi:* Synchronous condenser operation and running up in air of a medium characteristic speed pump-turbine: model tests. ASCE-IAHR Symp. Fort Collins Co. USA (1978), paper.

13.1 Supplement of further Literature in alphabetic order of the authors

[261] *Antonini, A. and A. Giadrossi:* Design and testing of a radial flow reversible hydraulic machine. Symp. Turboinštitut Lubljana (1984), paper, p. 149.

[262] *Barlit, V.:* Computerized calculation and experimental investigation of flow in mixed-flow high-head hydraulic turbine runner. Symp. Turboinštitut Lubljana (1984), paper, p. 825.

[263] *Beier, H.:* Umweltfreundliche Gestaltung von Staubecken in flachen Talräumen – dargestellt am Beispiel der Altmühlüberleitung. Wasserwirtschaft 74 (1984) no. 3, p. 103.

[264] *Benišek, M, I. Vuškovič, B. Ignatovič and M. Nedeljkovič:* The energetic characteristic scale-up calculation of the smaller to the bigger tube model turbine with the evident distinction of the hydraulic design of inlet water passages. Symp. Turboinštitut Lubljana (1984), paper, p. 279.

[265] *Bizjak, L.:* Turbo machines characteristics. Symp. Turboinštitut Lubljana (1984), paper, p. 310.

[266] *Bouras, C., R. Comolet and J. Fusil:* Flow and volume metering using the vortex effect in both permanent and non permanent flow. Symp. Turboinštitut Ljubljana (1984), paper, p. 398.

[267] *Brekke, H.:* A general study on the design of vertical Pelton turbines. Symp. Turboinštitut Ljubljana (1984), paper, p. 383.

[268] *Chaix, B.:* Labyrinth seals: Advantages and limitations of research on a two-dimensional model. Symp. Turboinštitut Ljubljana (1984), paper, p. 528.

[269] *Czibere, T.:* Theoretical principles of hydrodynamic computation of turbomachines. Symp. Turboinštitut Ljubljana (1984), paper, p. 1.

[270] *Da-kai, L., L. Shen-cai and Y. De-quan:* The effect of the flap on cavitation of hydro-machine. Symp. Turboinštitut Ljubljana (1984), paper, p. 73.

[271] *Fanelli, M., G. Angelico and P. Escobar:* An experimental research on the response of a turbomachine to steady pulsating conditions. Symp. Turboinštitut Ljubljana (1984), paper, p. 706.

[272] *Florjančič, D.:* Pumps in feedwater circuits of thermal and nuclear power stations. Symp. Turboinštitut Ljubljana (1984), paper, p. 447.

[273] *Gerloni de, M., R. Grossi. O. Ceravola and B. Lazzaro:* "Skifia" general steady hydraulic behaviour tests on the physical model of the whole pumped storage power plant. Symp. Turboinštitut Ljubljana (1984), paper, p. 229.

[274] *Höller, K. H., H. Grein and M. Hollenstein:* Layout, design. erection and operating experience of low head turbines. Symp. Turboinštitut Ljubljana (1984), paper, p. 244.

[275] *Imhoff, K. R.:* Talsperren und Umwelt. Wasserwirtschaft 74 (1984), no 3, p. 94.

[276] *Kamemoto, K. and R. Suzuki:* Modification and application of a mean camberline singularity method for thick wings having rounded trailing edges. Symp. Turboinštitut Ljubljana (1984), paper, p. 105.

[277] *Klemm, D.:* The dynamic behaviour of the Obrovac pump turbines in comparison with some other pump-turbines. Symp. Turboinštitut Ljubljana (1984), paper, p. 346.

[278] *Kössler, E. and W. Panhauser:* Ecological small hydro power plants. Symp. Turboinštitut Ljubljana (1984), paper, p. 793.

[279] *Korcian, J. and J. Raabe:* Measurement of the 3-dimensional relative flow inside the impeller of a low speed centrifugal pump at different points of performance. IAHR Symp. Stirling Aug. 1984, paper, p. 594.

[280] *Koutny, A.:* On the problem of material selection for hydraulic machine parts subject to intensive cavitation erosion. Symp. Turboinštitut Ljubljana (1984), paper, p. 654.

[281] *Krzyzanowski, J., G. Beckman and B. Weigle:* Comments on liquid impact erosion. Symp. Turboinštitut Ljubljana (1984), paper, p. 670.

[282] *Linse, D.:* Die Gründungsfuge von Staumauern-Beanspruchung und konstruktive Ausbildung. Wasserwirtschaft 74 (1984), no 3, p. 142.

[283] *Matthias, H. B. et al.:* Project, design and installation of small hydro power plants. Symp. Turboinštitut Ljubljana (1984), paper, p. 767.

[284] *Pejović, S., A. Gajić and D. Obradović:* Calculations of hydraulic oscillations. Symp. Turboinštitut Ljubljana (1984), paper, p. 750.

[285] *Raabe, J.:* On the re-evaluation of diffuser loss in case of a water turbine draft tube. Hydro-turbo. Olomouce (1985), paper.

[286] *Raabe, J.:* A new aspect of efficiency scale effect of a rotor in the light of an experiment. Symp. Turboinštitut Ljubljana (1984), paper, p. 294.

[287] *Rey, R., R. Noguera, B. Brachemi and F. Massouh:* Generalized representation of hydraulic and geometric performances of axial pumps and fans. Symp. Turboinštitut Ljubljana (1984), paper, p. 499.

[288] *Rißler, P.:* Neuere Untersuchungsmethoden für die Gründung von Absperrbauwerken. Wasserwirtschaft 74 (1984), no 3, p. 153.

[289] *Schiechtl. H.:* Umweltgestaltung bei Wasserkraftanlagen am Lech. Wasserwirtschaft 74 (1984), no 3, p. 118.

[290] *Schmidt, M.:* Die Umwelteinflüsse von 300 Jahren Talsperrenbau im Westharz. Wasserwirtschaft 74 (1984), no 3, p. 109.

[291] *Schwab, H.:* Analyse der Kontrollmessungen im Staudamm Finstertal. Wasserwirtschaft 74 (1984), no 3, p. 172.

[292] Seidel, H. P.: Landschaftsgestalterische und ökologische Fragen beim Bau der Rhein-Main-Donau-Wasserstraße. Wasserwirtschaft 74 (1984), no 3, p. 114.

[293] Starke, J.: Boundary layer control for axial flow compressor or pump; what is the real gain. Symp. Turboinštitut Lubljana (1984), paper, p. 91.

[294] Steller, K. and J. Steller: On prediction of cavitation and its erosive effects in hydraulic turbomachinery. Symp. Turboinštitut Lubljana (1984), paper, p. 627.

[295] Strobl, Th. and R. Weber: Abdichtung des stark klüftigen Sandsteingebirges an der Brombachtalsperre. Wasserwirtschaft 74 (1984), no 3, p. 158.

[296] Tanaka, T.: A visualizing study of cavitation condition with respect to blade camber in a high specific speed turbomachinery. Symp. Turboinštitut Lubljana (1984), paper, p. 570.

[297] Tong, D.: Research on scaly pitting of hydraulic machinery. Symp. Turboinštitut Lubljana ·(1984), paper, p. 619.

[298] Ulith, P. and F. Wolfram: The economical solution of low head turbine application from a hydraulic point of view. Symp. Turboinštitut Lubljana (1984), paper, p. 258.

[299] Vischer, D. and A. Huber: Wasserbau. Berlin: Springer-Verlag (1982).

[300] Widmann, R.: Grundlagen für den Entwurf der Bogenstaumauer Zillergründl. Wasserwirtschaft 74 (1984), no 3, p. 147.

[301] Wittke, W. and K. Gell: Wechselwirkung zwischen Staumauer und Untergrund. Wasserwirtschaft 74 (1984), no 3, p. 137.

[302] Wittke, W.: Felsmechanik-Gundlagen für wirtschaftliches Bauen im Fels. Berlin: Springer-Verlag (1984).

[303] Beyrich, D. and J. Grüner: Automation of a chain of run-of-river power stations. IAHR Symp. Stirling (1984), pap., p. 469.

[304] Brekke, H.: A study on the dynamic behaviour of power plants in the low frequency region based on frequency response test. IAHR Symp. Stirling (1984), pap., p. 212.

[305] Doerfler, P.: On the role of phase resonance in vibrations caused by blade passage in radial hydraulic turbomachines. IAHR Symp. Stirling (1984), pap., p. 228.

[306] Emler, J., H. Keck and Lai Min Er: Performance prediction of axial turbine runners treating the trailing edge problem by a combined numerical experimental approach. IAHR Symp. Stirling (1984), pap., p. 90.

[307] Franc, J. P. and J. M. Michel: Developed cavitation and boundary layer. IAHR Symp. Stirling (1984), pap., p. 20.

[308] Grein, H, R. Angehrn, M. Lorenz and A. Bezinge: Inspection periods of Pelton runners. IAHR Symp. Stirling (1984), pap., p. 422.

[309] Henry, P., J. E. Graeser, J. E. Prenat and M. Wegner: Scale effect concerning hydraulic quasi-stationary oscillations on a turbine model and test circuit. IAHR Symp. Stirling (1984), pap., p. 356.

[310] Le Tutor, J. and J. Bosc: Hydro-electric power plant built entirely in a shipyard. IAHR Symp. Stirling (1984), pap., p. 506.

[311] Muciaccia, F., G. Rossi and V. Zanetti: Study on model of the dynamic behaviour of a hydraulic machine. IAHR Symp. Stirling (1984), pap., p. 341.

[312] Paterson, I. S. and C. S. Martin: Effect of specific speed on pump characteristics and hydraulic transients in abnormal zones of operation. IAHR Symp. Stirling (1984), pap., p. 151.

[312] Schilling, R. et al.: Prediction of Kaplan turbine cavitation by finite differences and singularity methods. IAHR Symp. Stirling (1984), pap., p. 107.

[314] Simoneau, R.: The optimum protection of hydraulic turbines against cavitation erosion. IAHR Symp. Stirling (1984), pap., p. 56.

[315] Strohmer, F. and G. Horacek: Sluice operation of bulb turbinesmodel tests and operation criteria. IAHR Symp. Stirling (1984), pap., p. 457.

[316] Wegner, M. and J. M. Roman: control of erosion and instability effects induced by cavitation erosion in Francis turbines. IAHR Symp. Stirling (1984), pap., p. 77.

640

14. Subject index

647

650

660

670

15. Author index